SCC 2016

8th International RILEM Symposium on Self-Compacting Concrete

Flowing toward Sustainability

Washington DC, USA

15-18 May 2016

Edited by Kamal H. Khayat

Conference Chair

K.H. Khayat, Missouri University of Science and Technology, USA, Chair
S.P. Shah, Northwestern University, USA, Co-Chair

Honorary Advisory Committee

G. De Schutter, Chair of SCC 2007, Ghent, Belgium
K.H. Khayat, Chair of SCC 2010, Montreal, Canada
H. Okamura, Chair of SCC 2001, Tokyo, Japan
N. Roussel, Chair of SCC 2013, Paris, France
S.P. Shah, Chair of SCC 2005 and SCC2008, Chicago, USA
A. Skarendahl, Chair of SCC 1999, Stockholm, Sweden
O. Wallevik, Chair of SCC 2003, Reykjavik, Iceland

Steering Committee

S. P. Shah, Northwestern University, Chair
K. Wang, Iowa State University, Co-Chair
B. Blair, LafargeHolcim
J. Daczko, BASF Construction Chemicals
R. Detwiler, PCI
D. Feys, Missouri University of Science and Technology
J. Garbini, RMC Research & Education Foundation
K.H. Khayat, Missouri University of Science and Technology, Chair
D. Lange, University of IL – Urbana-Champagne
L. Lemay, NRMCA
D. Marsh, Concrete Products Magazine
C. Ozyildirim, Virginia Transportation Research Council
W. Palmer, Hanley Wood Business Media
W. Phelan, The Euclid Chemical Company
A. Schindler, Auburn University
A. Sherman, Missouri University of Science and Technology
G. Spitzmiller, Missouri University of Science and Technology
S. Vanikar, Federal Highway Administration (FHWA)
W. Weiss, Oregon State University

International Technical Committee

O. Wallevik, ICI, Iceland, Chair
C. Shi, Hunan University, China, Co-Chair
J. Aldred, AECOM, Australia

M. Alexander, University of Cape Town, S. Africa
A. Duran Herrera, Universidad Autónoma de Nuevo León, Mexico
Robert Flatt, ETHZ, Switzerland
R. Gettu, IIT-Madras, India
T.A. Hammer, SINTEF, Norway
Z. Li, The Hong Kong University of Science and Technology, China
M. Ouchi, Kochi University, Japan
Johann Plank, Technical University of Munich, Germany
Zhengwu Jiang, Tongji University, China
A. Schindler, Auburn University, USA
M. Sonebi, Queen's University, Belfast, UK
J. Walraven, Delft University, The Netherlands
A. Yahia, Université de Sherbrooke, Canada
F. Yazbeck, Readymix Abu Dhabi, UAE
P. Yan, Tsinghua University, China

Scientific Committee

G. De Schutter, Ghent University, Belgium, Chair
N. Roussel, IFSTTAR, France, Co-chair
H. Abdelgader, Tripoli University, Libya
M. Al Kazzas, Sodamco, Lebanon
C. Bédard, The Euclid Chemical Company, Canada
H. Bessaies, IFSTTAR, France
P. Billberg, SWEROCK, Sweden
C. Brumaud, ETHZ, Switzerland
J. Daczko, BASF Construction Chemicals, USA
T. K. Erdem, Izmir Institute of Technology, Turkey
L. Ferrara, Politecnico di Milano, Italy
C. Ferraris, National Institute of Standards and Technology, USA
R. Flatt, ETHZ, Switzerland
M. Geiker, Technical University of Denmark
S. Grünewald, Hurks Beton / TU Delft, the Netherlands
J. Hu, University of Nebraska-Lincoln, USA
S. Kawashima, Columbia University, USA
M. Khrapko, CBE Consultancy, New Zealand
J.H. Kim, Ulsan National Institute of Science and Technology, Korea
E. Koehler, Titan America, USA
M. Konsta-Gdoutos, Democritus University of Thrace, Greece
A. Leemann, EMPA, Switzerland
W. Long, Shenzhen University, China
D. Ludirdja, Trumix LLC, USA
P. Lura, EMPA, Switzerland
W. Mansour, Readymix Abu Dhabi, UAE

C. Mazzotti, University of Bologna, Italy
G. Morcous, University of Nebraska-Lincoln, USA
F. Müller, IMP Bautest AG, Switzerland
J. Myers, Missouri University of Science and Technology, USA
H. Nassif, Rutgers, The State University of New Jersey, USA
Serina Ng, Sintef, Norway
A. Perrot, Université de Bretagne Sud, France
A. Schindler, Auburn University, USA
W. Schmidt, BAM Berlin, Germany
K. Sideris, Democritus University of Thrace, Greece
K.R. Sompura, Sika Corporation, USA
C. Talbot, The Euclid Chemical Company, USA
L.N. Thrane, Danish Technological Institute, Denmark
F. Toussaint, Pôle technologique Lafarge, France
N. Tregger, W. R. Grace, USA
M. Vachon, Sika, Canada
Jon E. Wallevik, ICI, Iceland
K. Wang, Iowa State University, USA
M. Zhang, National University of Singapore, Singapore
W. Zhu, University of the West of Scotland, Paisley, UK

Conference Secretariat

A. Sherman, USA

Table of Contents

Theme 1: Mix Design for SCC

Theme 6: Mechanical and Physical Properties of SCC

Theme 7: Durability of SCC

Theme 8: Fiber-Reinforced SCC

Theme 9: Structural Performance of SCC

Theme 10: Sustainability

Theme 11: Case Studies

Preface

Dear Colleagues,

We are pleased to organize the Eighth International RILEM Symposium on Self-Compacting Concrete and the Sixth North-American Conference on the Design and Use of Self-Consolidating Concrete, from May 15-18, 2016, in Washington, D.C. This conference is held simultaneously with the 11th Annual International Concrete Sustainability Conference of the National Ready Mix Concrete Association (NRMCA). SCC 2016 (*Flowing toward Sustainability*) is designed to bring researchers and practitioners together to exchange the latest knowledge and tools used in building sustainable concrete structures with SCC. The RILEM series of symposia started in 1999 in Stockholm, followed by Tokyo in 2001, Reykjavik in 2003, Chicago in 2005, Ghent in 2007, Montreal in 2010, and Paris in 2013 with a steadily increasing number of papers, participants, and interests from across the globe. Due to the growing success of SCC, regional conferences have been organized, such as the North-American Conference on the Design and Use of SCC held in Chicago in 2002, 2005, 2008, and 2013 and in Montreal in 2010; the International Symposium on Design, Performance and Use of SCC held in Changsha in 2005, Beijing in 2009, and Xiamen City in 2014; as well as the 2nd International Conference on Advances in Concrete Technology in the Middle East: SCC held in Abu Dhabi in 2009. These regional conferences and symposia were very successful and reached a far more international audience than anticipated.

Nearly 170 papers were submitted to SCC2016, from 32 countries, covering a wide range of timely and original subjects from around the world. Topics covered in these Proceedings include SCC mix design, materials, test methods, rheology and workability, production and placement, production and placement, mechanical and physical properties, durability, structural performance, fiber reinforcement, sustainability, and case studies. These papers reflect the most recent advances in research, design, and implementation of SCC worldwide. Nearly 120 papers are presented during three parallel sessions in addition to 35 papers discussed during the poster session at the conference.

We would like to thank our sponsors for their support of the joint conference. Special thanks go to the Honorary Advisory Committee, the Steering Committee, and the International Technical Committee for their advice and help in promoting the conference.

We would like to thank the organizers of the joint conferences: the Center for Infrastructure Engineering Studies (CIES) at Missouri University of Science and Technology (Missouri S&T), the US DOT Tier-1 Center for Research on Concrete

Applications for Sustainable Transportation (RE-CAST), the NRMCA, as well as RILEM and ACI.

Kamal Henri Khayat
SCC2016 Conference Chair
Missouri S&T
May 2016

Effect of Sand-Powder Ratio on Properties of Self Compacting Concrete

Murtada Khalid A. Osman[1] and Osama Mohammed Ahmed Daoud[2]

[1] Post Graduate student, Building and Roads Research Institute (BRRI), University of Khartoum
[2] Assistant Professor, Head of Building Materials and Structures, Building and Roads Research Institute (BRRI), University of Khartoum

Abstract Experimental studies done on the effect of Dolomite Quarry dust as partial replacement of Sand on powder type - Self Compacting Concrete. The quarry dust is a by-product of blasting and quarrying activities of aggregate quarry of QARGADA Mountain in the Blue Nile State, Sudan. The rock powder contained about 55% fines less than 0.15 mm. The main components were calcium magnesium carbonate contaminated with high amount of amorphous silica. Crushed aggregates with max size of 20 mm and natural sand were used. The total powder comprised of cement and 25 % Type F fly ash. The Quarry dust replaced the fine aggregate by zero, 6%, 12%, 18% and 24% of the total sand content. The flowability, passing ability were minimally affected. However; Viscosity and static and segregation of SCCs were affected. The static segregation increased as the quarry dust increased. The Static segregation negatively affected when the sand was replaced by more than 18% by these stone powders (sand-powder ratio less than 1.0). When the sand content was decreased by 6%, 12%, and 18% of the total sand, the sand powder ratio decreased from 1.4 up to 1.0. Spilt tensile strength and elastic modulus of concrete were significantly affected as so as the compressive and flexural strength. The compressive strength was increased when the dolomite stone dust incorporated as replacement of fine aggregates by 12 percent of the total sand content (1.1 sand powder-ratio). However, when the sand content decreased by more than 12 percent, the compressive strength was decreased. The Spilt Tensile and the flexural strength were affected similarly. The elastic modulus of concrete was beneficially affected when the sand-powder ratio decreased from 1.4 to 0.9. The Young's modulus of elasticity of SCC positively increased from 38.00 GPa to 42.0 GPa. Therefore, the actual sand ratio to the total aggregate shall be kept near to 0.5 or fine-coarse aggregate ratios greater than 0.82 without incorporating the finer particle in stone dust depending on the particle size distribution of both fine and coarse aggregate.

Keywords: *Self Compacting Concrete, Sand-Powder Ratio, Dolomite Quarry dust.*

Introduction

Self Compacting or Consolidating Concrete (SCC) is a highly flowable, non-segregating concrete that spreads into place, fills formwork, and encapsulates even the most congested reinforcement, all without any mechanical vibration. The concrete homogeneous and has the same engineering properties and durability as traditional vibrated concrete.

The fresh rheological characteristics, strength and durability of SCC can be improved with the addition of powders which can be separated into two groups as inert or pozzolanic. The usage amount and the type of cementitious or inert powders depend on the physical and chemical properties of these powders which affect the performance of fresh paste such as particle shape, surface texture, surface porosity and rate of superplasticizer adsorption, surface energy (zeta potential), finest fraction content, Blaine fineness and particle size distribution.

Alternative materials as aggregates in concrete, numerous types of by-product such as recycled concrete aggregate, quarry dust, fly ash and slag, as well as several types of manufactured aggregates have been studied by many researchers [1] [9]. Other additions originating from industrial waste materials are being tested for use as filler in SCC, such as granite filler or marble dust. Such use of industrial by-products in SCC can provide economic benefits and prevent environmental pollution [2].

Literature Review

Several researchers investigated the incorporation of quarry dust as partial replacement material to sand in concrete or SCC. For nornal vibrated concrete, Ahmed et al investigated the influence of very fine sand less than 75 micron or passing No. 200 sieve, from natural and crushed stone sources, on the performance of fresh and hardened concrete [3, 4]. Tests were conducted on two series of concrete mixes. One series (Series A) consisted of mixes having a constant slump of 100 ± 15 mm and the other series (Series B) contained mixes with a water-cement ratio of 0.70. The very fine sand passing No. 200 sieve was removed by sieving over a No. 200 sieve.

In Series A (constant slump) tests showed that the compressive strength of constant-slump concrete decreases linearly with increasing percentage of fines. The flexural and bond strengths were also affected similarly. Series B tests (concrete with constant water-cement ratio) showed that incorporation of fines in concrete resulted in significant reduction in slump. The compressive strength of crushed

stone sand concrete indicated an increase in strength by the incorporation of fines. However, the compressive strength of concrete using natural sand was not affected significantly by the incorporation of fines.

Malhotra et al also studied the problem of incorporation of limestone dust as partial replacement for sand in concrete. The results of the tests, conducted by the authors, were almost the same as given by Ahmed et al. The results indicated that at water-cement ratios of 0.53 and 0.70, compressive strength of concrete incorporating 15% and 20% limestone dust were higher than that of the concrete with no fines. Authors suggest two reasons for the increase in strength, although no experiments were performed to confirm these observations [7, 4]. Due to the filler effect of the dust, air content of the concrete mix was reduced, thus increasing the density of the mix and the strength. Factors such as the accelerated hydration of cement paste and the formation of carbo-aluminates contribute to an increase in strength.

Hanifi Binici et al [5] found that the compressive strengths of concrete increases with increasing of percentage of marble dust additions of seven concrete mixtures were produced in three series with control concrete. These control mixes were modified to 5, 10 and 15% of Marble Dust and Limestone Dust in place of fine sand aggregate. Same to Ilangovana et al [6] of that the strength of Quarry Rock Dust concrete is comparatively 10 to12 percent more than that of similar mix of Conventional Concrete and provided a strong support for the use of Quarry Rock Dust as fine aggregate in Concrete Manufacturing.

However, several researchers found that the incorporation of quarry dust as partial replacement material to sand in concrete resulted in a reduction in the compressive strength, and this was more evident when the replacement proportion was increased [10].

In SCC, Tarun R. Naik et al [13] studied the use of quarry fines for partial replacement of sand. For evaluating the effect of quarry fines in SCC, 35% replacement of cement with fly ash was selected as the reference “Mixture 18” for this series of mixtures. Limestone-quarry fines were used to replace 10%, 20%, 30%, 40%, and 50% of the sand used in reference SCC by mass. w/c ratio of 0.35 was used. A proprietary copolymer HRWRA that complies with the requirements of ASTM C 494 for Type F, High Range Water Reducing Admixture (HRWRA), and Viscosity-Modifying Admixture (VMA) were used.

Tarun R. Naik et al found that, regardless of the replacement level of sand with quarry fines, the requirement of VMA remained approximately the same as the reference probably because the quarry fine is angular and finer material replacing rounded and coarser natural sand. However, the requirement of HRWRA decreased gradually as the replacement level of sand with quarry fines increased.

Tarun R. Naik et al reported that when sand was replaced with limestone quarry fines, compressive strength generally increased but sometimes decreased to some extent. Overall, the 3-day and 7-day strengths were higher, and the 28-day strength was lower compared with Reference. Replacing sand with 30% quarry fines has highest 28-day strength. The 28-day strength of concrete made with partial replacement of cement with Class C fly ash combined with partial replacement sand with quarry fines, was equivalent to that of the Control "Mixture 15R" made without Class C fly ash or quarry fines.

M. Shahul Hameed and A. S. S. Sekar investigated the properties of green Self Compacting Concrete containing quarry rock dust and marble sludge powder as fine aggregate [8]. The fineness module of marble sludge powder and quarry rock dust were compare with that fine sand of 2.2 to 2.6 with coefficient of gradation from 1 to 3 achieving requirement of fine sand coefficient of grading less than 6. Marble sludge powder was obtained in wet form directly taken from deposits of marble factories and dried before the preparation of sample and sieved from 1 mm.

Mix A is the controlled concrete using river sand and Mix B is the green concrete using industrial waste (50% quarry rock dust and 50% marble sludge powder) as fine aggregate. The water/cement ratio for both two mixes was 0.55% by weight. Water reducing admixture was used to improve the workability and its dose was fixed as 250 ml/50kg of cement. A superplasticizer based on refined lingo Sulphonates, was used to get and preserve the designed workability. Mix proportion (by weight) use in the mixes of conventional concrete and green concrete were fixed as 1:1.81:2.04, 1:1.73:2.04 after several trials.

Hameed and Sekar [8] reported that Green Concrete induced higher workability and it satisfies the self-compacting concrete performance. The Slumpflow increased with increasing of marble sludge powder content, but the V-funnel time decreased. The results showed that, the 7days and 28 days compressive strength of green concrete are about 6.5% and 9.5% higher than controlled concrete respectively. Similarly, the 7days and 28days of split tensile strength are 14.62 and 18.66% higher than controlled concrete respectively. However, the 3days compressive and split tensile strengths of green concrete were lower by 12.36% and 10.41% respectively when compared with control concrete.

J. K. Su et al [14] studied the effect of sand ratio on the elastic modulus of self-compacting concrete. Self Compacting Concretes with various S/A ratios (fine aggregate volume/total aggregate volume) were cast and tested. Slump flow test, slump test, and box test were carried out to evaluate concrete flowability.

Cement paste were made of cement (specific gravity: 3.15), slag (specific gravity: 2.2), fly ash (specific gravity: 1.66), and water. Superplasticizer was adjusted to keep required slump and slump flow. Natural sand (specific gravity: 2.63) was used as fine aggregate and crushed limestone (specific gravity: 2.60) with a

maximum size of 10 mm was used as coarse aggregate. Six different S/A ratios (S/A = 0.3, 0.4, 0.45, 0.475, 0.5, 0.525, and 0.55) were considered in the mix proportions. The aggregate volume fraction was 0.6 for all mixes. The water/binder ratio was 0.4.

J. K. Su et al found that, the flowability of SCC and the filling height increase with an increase in S/A ratio. When S/A is higher than 0.475, the concrete can pass the box test. And the filling height and slump flow increase with an increase in the S/A ratio. J. K. Su et al suggested that Particle packing characteristics play a significant role on the concrete flowability. According to the test results, J. K. Su et al suggested that the S/A ratio (fine aggregate volume/total aggregate volume) for SCC is to be 0.475.

From the experimental results, the elastic modulus of concrete is not significantly affected when the S/A ratio increases. When (elastic modulus of fine aggregate) is 2 times of (elastic modulus of coarse aggregate), the elastic modulus of concrete increases from 28.00 GPa to 29.66 Gpa when the S/A ratio increases from 30% to 47.5%. When Efa is half of Eca, the elastic modulus of concrete decreases from 22.54 Gpa to 21.00 Gpa when the S/A ratio increases from 30% to 47.5%.

J. K. Su et al found that elastic modulus of concrete is influenced by the elastic properties and the volume fraction of aggregate. The elastic modulus of concrete is influenced mainly by the elastic properties of matrix, fine aggregate and coarse aggregate. However, when the elastic moduli of fine aggregate and coarse aggregate are not much different and the total volume of aggregate is constant, the elastic modulus of SCC is not significantly affected by S/A ratio.

Experimental Program

Powder type Self Compacting Concretes were prepared for this study with crushed aggregates and natural sand was used. Ordinary Portland Cement OPC was used for casting cubes according to ASTM C 150 [18], for all concrete mixes. Summary of the various tests conducted on cement are as under given below in Table 1.

Table 1. The physical properties of cement

Consistency of standard paste		29.25%
Setting time	Initial setting time	2:20
	Final setting time	4:00
Compressive strength	2 Days	23 Mpa
	28 Days	48 Mpa

The coarse aggregates used in SCC mixes, was crushed basalt obtained from TORYIA Mountain in Khartoum State, with maximum size of 20 mm. Crushed

and natural coarse sand used as fine aggregates. The results of various tests conducted on the coarse and fine aggregates according to ASTM C 136 [17] , ASTM C 128 [16], ASTM C 117 [15], ASTM C 33 [22], British Standard BS 812: Section 103.2: 1989 [29], BS 812: Part 101: 1984 [30], and BS 812: Part 2: 1995 [31] are given below:

Table 2. Physical Properties of Coarse Aggregates

Characteristics	Blended	5~10	10~20
Type	Crushed	Crushed	Crushed
Specific Gravity	2.66	-	-
Total Water Absorption	0.56	-	-
Fineness Modulus	6.83	-	-
Loose Density (kg/m³)	-	1546.0	1516.1
Rod Density (kg/m³)	-	1625.5	1650.5

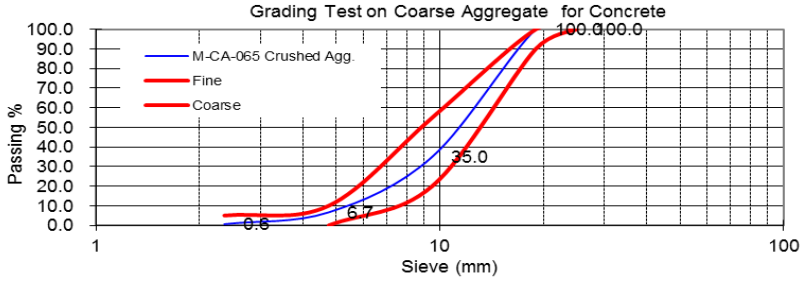

Figure 1. Particle Size Distribution (PSD) of Blended Aggregates

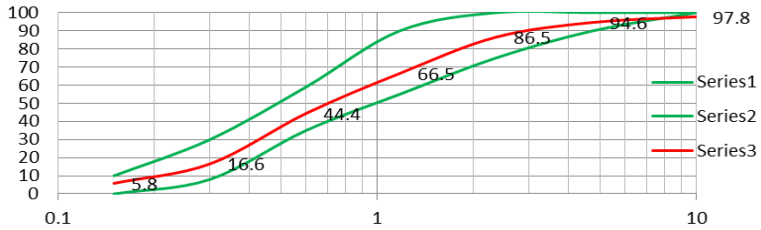

Figure 2. Particle Size Distribution (PSD) of Natural Sand

Type F Fly ash was used according to ASTM C 618 [25]. Results of fly ash are shown in Table 3. The chemical compositions of Fly Ash is presented in Table. The X-ray diffraction showed that, Fly ash is contained a higher content of Sillimanite (Di-aluminum Silicate Oxide) (Al_2SiO_5) and Silicon Oxide (Quartz).

Table 3. The characteristics of Fly Ash

Sample No.	M.C %	Density gm./cm^3	Difference of Initial Setting Time	Fineness %	Soundness %	Water Requirement %	Strength Activity Index %	
							28 days	90 days
1	0.1	2.16	27	10.3	0.5	92	100	101

Table 4. The chemical composition of Fly Ash

Ingredient	CaO	Sio2	Al_2O_3	Fe_2O_3	MgO	SO3	K2O	Na2O	L.O.I.	T.D.S
Percent %	3.6	53.58	34.04	3.498	0.9602	0.453	0.17	N.D	1.7	1.998

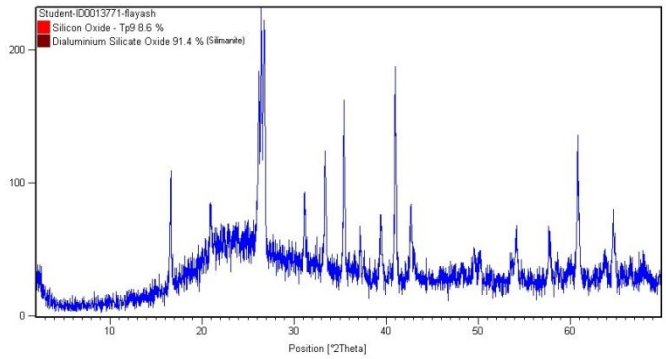

Figure 3. The Powder X-Ray Diffraction of Fly Ash

The Quarry dust used in this study was a Dolomite-Marble Quarry Dust. It is a by-product obtained directly from the crushing, blasting process during quarrying activities for marble aggregates quarry in the Blue Nile State. The Dolo-Marble Dust is white, angular, and very fine powder with an amounts of fine crushed sand. The particle distribution and chemical compositions of this material are shown in Figure 4. The chemical composition which was tested and the x-ray diffraction in Table 5 and Figure 3 respectively.

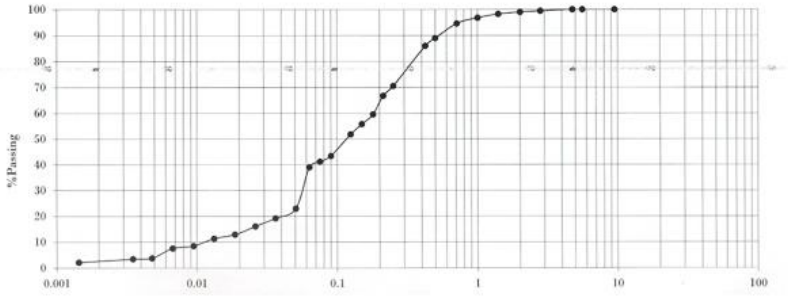

Figure 4. The Particle Size Distribution (PSD) of Quarry Dust

Table 5. The chemical composition of the Marble Quarry Dust

Ingredient	CaO	Sio2	Al_2O_3	Fe_2O_3	MgO	SO3	K2O	Na2O	L.O.I.	T.D.S
Percent %	32.00	29.55	1.89	0.37	16.89	1.97	N.D	N.D	16.74	N.D

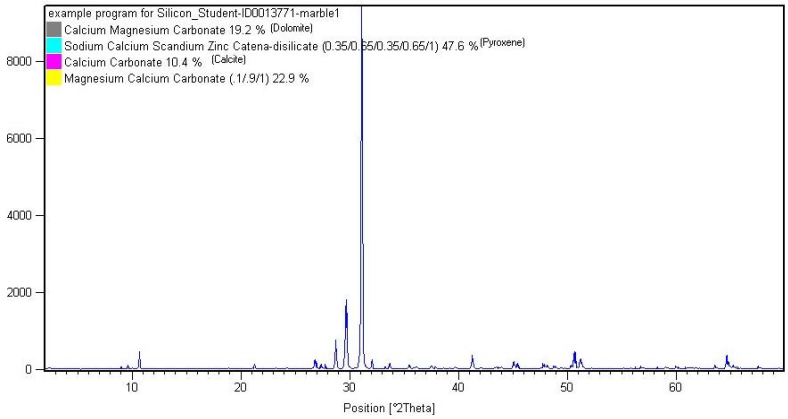

Figure 5. The Powder X-Ray Diffraction (XRD) of the Marble Powder

A highly effective superplasticizer with a slight set retarding effect for producing free-flowing concrete in hot climates was used as substantial water reducer agent for promoting high early and ultimate strengths. It Complies with ASTM-C-494 Type G as a high range water reducing admixture with retarder.

Sikament® -R2004 is dark brown liquid based on modified Synthetic dispersion type instantly dispersible in water with density of 1.195 Kg/l at20°C. The dosage will be between approximately 0.6% - 2.5% by weight of cement.

The Trails were carried out to establish the correct dosage required for SCC mixtures.
Sikament® -R2004added directly to the mixing water prior to its addition to the aggregates or separately to the fresh mixes. When Sikament® -R2004 added separately to the fresh mixes, further mixing took place for at least one minute per cubic meter as the manufacturer's recommendations.

A Certain amount of tests followed the development of SCC mix to ensure the highest level of control. The mixture developed was tested for the target fresh properties. If the properties were not achieved, adjustments to the mixture proportions were made. If the fresh target achieved, then testing for the mixing robustness and for the required hardened properties was conducted.

An experimental study was undertaken to investigate some properties of quarry dust and discussed those properties in order to use the quarry dust as partial replacement for sand in Self Compacting Concrete (SCC). The Dolo-Marble rock dust was used as partially replacement material to sand in SCC. The Marble Dust contained about 55% powder material finer than 0.15 μm. This percent of fine powder will increase the powder content in Self Compacting Concrete which affected the sand-powder ratio.

The influence of partially replacement of fine aggregates with Dolo-Marble dust at varying percentages in the properties of fresh and hardened concrete was investigated. The Dolo-Marble Dust replaces the fine aggregates by 50, 100, 150, and 200 Kg, or 6%, 12%, 18%, 24% respectively of the total sand. The mix proportions is presented in Table 6.

Table 6. Mix proportions for Utilization of Marble Quarry Dust as partial replacement of sand

ID	Cement (kg/m^3)	Fly Ash (kg/m^3)	Marble Dust (kg/m^3)	Powder Content (kg/m^3)	Water (kg/m^3)	W/P ratio	Sand-Powder ratio	Coarse aggreg. (kg/m^3)	Sand (kg/m^3)	FA/CA ratio	SP/P %
Cont. SCC	450	150	0	600	205	0.34	1.4	830	834	1	2
QD 50	450	150	50	625	205	0.32	1.3	830	784	0.94	1.7
QD 100	450	150	100	650	205	0.29	1.1	830	734	0.88	1.45

QD 150	450	150	150	675	205	0.27	1.0	830	684	0.82	1.35
QD 200	450	150	200	700	205	0.24	0.9	830	634	0.76	1.35, 1.40*

*In Q200, different dosages of Superplasticizer were used.

Results and Discussion

The investigation on properties of quarry dust and discussed those properties in order to use the quarry dust as partial replacement for sand in Self Compacting Concrete (SCC). The Dolo-Marble rock dust was used as partially replacement material to sand in SCC. The influence of partially replacement of fine aggregates with Dolo-Marble dust at varying percentages in the properties of fresh and hardened concrete was investigated.

From Table 7 and Figure 6 It was found that, the all of the self compactability parameters especially the mix stability of SCC were adversely affected when the sand is replaced by more than 18% of these stone powders or less than 0.82 fine-coarse aggregate ratios with actual sand ratio near to 0.496. The SCC mixture after this percent is difficult to be controlled and more sensitive to the small change in constituent material especially the superplasticizer demand as QD 200.

Table 7. The influence of partial replacement of fine aggregates with Dolo-Marble dust in the properties of fresh of Self Compacting Concrete

MIX ID	Sand-Powder ratio	SLUMP FLOW (mm)	T50 (sec)	V-FUNNEL (sec)	T50 min V-FUNNEL (sec)	T50J (sec)	J-ring diameter (mm)	Bj(mm)	Segregation (%)	HRWRA (%)	REMARK
Control SCC	1.4	800	5	10	11	7	775	8	2.6	2	OK
QD 50	1.3	815	4.4	19	22.5	7	755	7	3.3	1.7	OK

QD 100	1.1	-	-	-	-	-	-	-	78.7	1.7	Too much Segregation
QD 100	1.1	800	7	11.3	13	9	755	10	11.9	1.35	OK
QD 150	1.0	785	5.3	14.8	19	8	775	8.8	4.4	1.4	OK
QD 200	0.9	640	5.3	15.1	20	10	545	22.5	23.7	1.4	Not OK, Trial mix was repeated
QD 200	0.9	820	4.9	12	14.9	7	765	7	22.5	1.35	Too Much segregation

When 1.4% superplasticizer demand was used in QD 200, different self-compactability results of unstable SCC mixture was recorded. High segregation with low Slumpflow and high retained amount of concrete in J-ring Test was measured. Then the trial was repeated with approximately superplasticizer dosage of 1.35%, and tested.

Generally, the superplasticizer demand was decreased corresponding with the replacing of the fine aggregates as shown in Figure 6, while the Slumpflow also was slightly increased correspondingly until the Optimum replacement and then was insignificantly affected. The V-funnel time was also affected similarly.

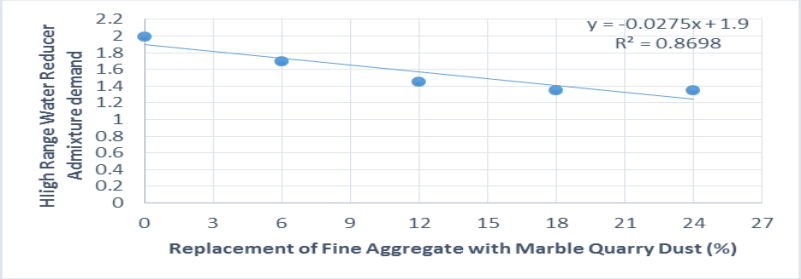

Figure 6. Superplasticizer demand against Percentage of replacement of Sand with Marble Quarry Dust

When more very fine particles from the quarry rock duct were presented in SCC mixture instead of valley sand, the lubrication effect was increased. The stone dust has about 97% particles less than 1 mm and 55% powders less than 0.15 mm, whereas the silica river sand has about only 60% passing 1 mm and very small

amount passing 0.15 mm. Therefore, the workability was increased and the superplasticizer dosage was decreased accordingly.

On the other hand, when very fine stone powder replaced the fine aggregates, the effect of Superplasticizing of mineral admixture increased and caused an increase in workability of SCC. The pores were filled by fine gains of stone dust with active amorphous silica substituting for water in the pores, the water layer in between is greater and it became free, then the fluidity of mix increased significantly. Thus, the dosage of superplasticizer demanded was decreased. It same to Tarun R. Naik et al [13]. However, In Tarun R. Naik et al studies the VMA required remain approximately constant because the quarry fine is angular and finer material replacing rounded and coarser natural sand to maintain the viscosity of SCC.

Figure 7 shows that, the effect of sand-powder ratio on viscosity and static segregation of SCC. The static segregaration was affected according to the increase and decrease of viscosity of mix and sand-powder ratio..

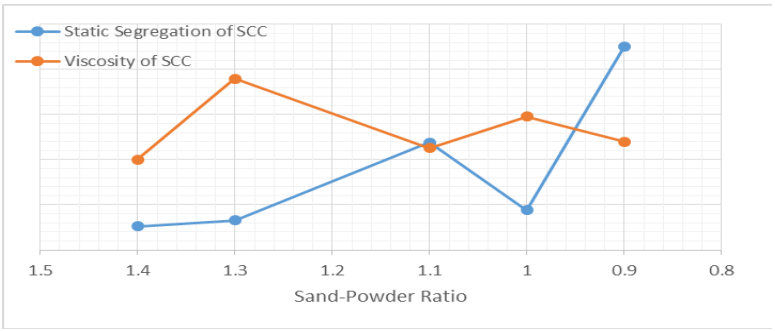

Figure 8. Effect of Sand Powder ratio on Viscosity and Static segregation of SCC

In order to study the effect of sand powder ratio or the fine aggregate/coarse aggregate ratio on the hardened properties of Self Compacting Concrete including the Young's Elastic Modulus using longitudinal resonant method [20], SCCs with various replacement of sand with Dolo-Marble dust were casted and tested.

From Table 8 the elastic modulus of concrete was beneficially affected when the sand-powder ratio decreased from 1.4 to 0.9 with the small decreasing in the actual sand to total aggregate ratio, the elastic modulus of concrete increased from 38.00 GPa to 42.0 GPa. The compressive strength increased when the dolomite stone dust incorporated as replacement of fine aggregates by 12 percent of the total sand content.

Young's elastic modulus of SCC was influenced by the elastic properties and the volume fraction of aggregate. It was significantly influenced mainly by the elastic properties of matrix and fine aggregate (i.e. replacement of silica sand with dolomite quarry fines), beside the total volume of aggregate. When the sand-powder ratio decreased from 1.4 to 0.9, elastic moduli and the total volume of aggregate was decreased, the elastic modulus of SCC was significantly affected. It same to J. K. Su et al [14].

Table 8. Compressive Strength, Split Tensile, Flexural Strength, and Modulus of Elasticity of concrete for SCC incorporating Dolo-Marble dust as partially replacement of Sand

ID	Sand-Powder ratio	Sand / coarse aggregate ratio %	Actual sand ratio %	Water-Powder ratio	Strength (MPa)	E-Modulus (GPa)	Splitting Tensile (MPa)	Flexural Strength (MPa)
Control SCC	1.4	1.0	0.501	0.342	50.7	38.60	2.6	10.4
QD 50	1.3	0.94	0.500	0.327	55.7	39.30	2.9	8.6
QD 100	1.1	0.88	0.498	0.313	56.0	40.80	2.4	8.8
QD 150	1.0	0.82	0.496	0.300	52.9	39.80	2.9	9.8
QD 200 (1.35% SP)	0.9	0.76	0.495	0.289	47.9	42.00	2.7	7.9
QD 200 (1.4% SP)	0.9	0.76	0.495	0.289	47.85	40.87	2.6	7.6

However, when the sand content was decreased by more than 12 percent, the compressive strength decreased. The Spilt Tensile and the flexural strength were not significantly affected when the dolomite stone dust incorporated as replacement of fine aggregates.

Conclusions

Experimental studies conducted to investigate some properties of the same quarry dust in order to use the quarry dust as partial replacement for sand. The Dolo-Marble dust was contained only about 55% particles finer than 0.15 mm.

It was found that, the flowability, passing ability were minimally affected. However; Viscosity and static and segregation of SCCs were affected. The static segregation increased as the quarry dust increased. The Static segregation negatively affected when the sand was replaced by more than 18% by these stone powders (sand-powder ratio less than 1.0). The SCC mixture after this percent was difficult to control and it was more sensitive to small change in constituent materials especially the superplasticizer demand.

The elastic modulus of concrete was beneficially affected when the fine/coarse aggregate decreased from 1.4 to 0.9. The elastic modulus of concrete positively increased from 38.00 GPa to 42.0 GPa.

The compressive strength was positively increased when the dolomite stone dust incorporated as replacement of fine aggregates by 12 percent of the total sand content (1.1 sand-powder ratio). However, when the sand content decreased by more than 12 percent, the compressive strength was decreased. The Spilt Tensile and the flexural strength were similarly affected.

Numerous researches investigated the incorporation of different powders type with different fineness as partial replacement material to sand in concrete or SCC. These replacement illustrated as percent of sand only. However; the properties of SCC affects by content and type of powders significantly. When these replacements presented as sand-powder ratio can give well understanding of how much of content of sand to powder ratio influence the properties of on properties of SCC.

References

[1] Rafat Siddique, *Effect of Fine Aggregate Replacement with Class F Fly Ash on The Mechanical Properties of Concrete*, Cement and Concrete Research 33 (2003), Thapar Institute of Engineering and Technology, Civil engineering Dept, Deemed University, Patiala 147004, India, 16 September 2002, p 539 – 547.

[2] Ilker Bekir Topçua, Turhan Bilira, and TayfunUygunog˘lu, *Effect of Waste Marble Dust Content As Filler On Properties of Self-Compacting Concrete*, Construction and Building Materials 23 (2009) 1947–1953.

[3] Ahmed, Ahmed E. and El-Kourd, Ahmed A., *Properties Of Concrete Incorporating Natural And Crushed Stone Very Fine Sand*, Technical Paper, ACI Materials Journal, July-August 1989, PP 417 - 424.

[4] Doraiswamy Sentil Kumarand W. R. Hudson, *Use of Quarry Fines For Engineering And Environmental Applications*, special research report for The National Stone Association, Center for Transportation Research, BUREAU of Engineering Research, The University of Texas at Austin, October 1992.

[5] Hanifi Binici, Hasan Kaplan and SalihYilmaz, *Influence Of Marble And Limestone Dusts As Additives On Some Mechanical Properties Of Concrete*, Scientific Research and Essay Vol. 2 (9), pp. 372-379, September 2007.

[6] Ilangovana R., N. Mahendranaand K. Nagamanib, *Strength And Durability Properties of Concrete Containing Quarry Rock Dust as Fine Aggregate*, ARPN Journal of Engineering and Applied Sciences, VOL. 3, NO. 5, OCTOBER 2008.
[7] Portland Cement Association, *Thickness Design for Soil-Cement Pavements*", Engineering Bulletin, Portland Cement Association (PCA), Stokie, Illinois, 1970.
[8] Shahul M. and A S. S. Sekar, *Properties of Green Concrete Containing Quarry Dust And Marble Sludge Powder As Fine Aggregate*, APPN journal of Engineering and Applied Sience, Vol. 4, No 4, June 2009.
[9] Selvamony C., M. S. Ravikumar, S. U. Kannan and S. Basil Gnanappa, *Investigations on Self-Compacted Self-Curing Concrete Using Limestone Powder and Clinkers*, Sathyabama University, CSI Institute of Technology, India.
[10] Raman S. N., M. F. M. Zain, H. B. Mahmud, and K. S. Tan, *Suitability of Quarry Dust as Partial Replacement Material for Sand in Concrete*, University of Kebangsaan and Malaya, Malaysia
[11] Joseph F. Lamond and James H. Pielert, *Significance of Tests and Properties of Concrete and Concrete-Making Materials*, ASTM International, Bridgeport NJ, April 2006.
[12] Turgut, Turk and Bakirci, *Segregation control of SCC with a modified L-box apparatus*, Magazine of Concrete Research, 2012, 64(8), 707–716, http://dx.doi.org/10.1680/macr.11.00144.
[13] Tarun R. Naik, Rudolph N. Kraus , Yoon-moon Chun , Fethullah Canpolat, and Bruce W. Ramme, *Use of Limestone Quarry By-Products For Developing Economical Self-Compacting Concrete,* Report No. CBU-2005-14, Presented and Published at the CANMET/ACI (SDCC-38) Three-Day International Symposium on Sustainable Development of Cement and Concrete, October 5-7, 2005, Toronto, CANADA
[14] J. K. Su, S. W. Cho, C. C. Yang, and R. Huang, *Effect of Sand Ratio on The Elastic Modulus of Self-Compacting Concrete*, Journal of Marine Science and Technology, Vol. 10, No. 1, pp. 8-13 (2002)
[15] ASTM C 117 *Standard Test Method for Materials Finer than 75-μm (No. 200) Sieve in Mineral Aggregates by Washing*
[16] ASTM C 128 *Standard Test Method for Density, Relative Density (Specific Gravity), and Absorption of Fine Aggregate*
[17] ASTM C 136 *Standard Test Method for Sieve Analysis of Fine and Coarse Aggregates*
[18] ASTM C 150 *Standard Specification for Portland Cement*
[19] ASTM C 191 *Standard Test Method for Setting of Hydraulic Cement by Vicat Needle*
[20] ASTM C 215 *Standard Test Method for Fundamental Transverse, Longitudinal, and Torsional Resonant Frequencies of Concrete Specimens*

[21] ASTM C 293 *Standard Test Method for Flexural Strength of Concrete (Using Simple Beam with Center-Point Loading)*
[22] ASTM C 33 *Standard Specifications for Concrete Aggregates*
[23] ASTM C 494 *Standard Specifications for Chemical Admixtures for Concrete*

[24] ASTM C 496 *Standard Test Method for Splitting Tensile Strength of Cylindrical Concrete Specimens*
[25] ASTM C 618, *Standard Specification for Coal Fly Ash and Raw or Calcined Natural Pozzolan for Use in Concrete*
[26] ASTM D 75 *Standard Practice for Sampling Aggregates*
[27] British Standard *BS 1881 : Part 116 : 1983 Testing Concrete, Method For Determination of Compressive Strength of Concrete Cubes*
[28] British Standard *BS 1881: Part lll: 1983, Testing concrete, Method of Normal Curing of Test Specimens (20 ºC method)*
[29] British Standard *BS 812: Section 103.2: 1989 Testing Aggregates: Method for Determination of Particle Size Distribution, Sedimentation Test*
[30] British Standard, *BS 812: Part 101: 1984 Testing Aggregates: Guide To Sampling And Testing Aggregates*
[31] British Standard, BS 812: Part 2: 1995 Testing Aggregates: Methods For Determination of Density
[32] EN 12350 Part 10: 2010 Self-compacting concrete — L box test
[33] EN 12350 Part 11: 2010 Self-compacting concrete — Sieve segregation test
[34] EN 12350 Part 12: 2010 Self-compacting concrete — J-ring test
[35] EN 12350 Part 8: 2010 Self-compacting concrete — Slump-flow test
[36] EN 12350 Part 9: 2010 Self-compacting concrete — V-funnel test

Effects of Mix Design Parameters on Consolidation Behavior of Fresh Cement-Based Materials

Arnaud Perrot[1] and Damien Rangeard[2]

[1] LGCGM, INSA de Rennes, Rennes, France
[2] LIMATB, Université de Bretagne Sud, Lorient, France

Abstract The consolidation behavior of fresh cementitious materials is a key factor that governs water retaining ability of concrete and therefore its bleeding behavior. Moreover, consolidation theory provides a tool able to predict heterogeneous profile of W/C within formwork. Recent studies have shown that bleeding rate of cement-based materials is monitored by the material permeability and that the amount of available free water can be computed using concrete compressibility. Both parameters can be combined to compute the consolidation coefficient which describes the whole consolidation process. The aim of this study is to describe the effect of mix-design parameters such as aggregates volume fraction, water reducing admixtures and a supplementary cementitious material on the consolidation behavior of fresh cement-based materials. We provide the evolution of both permeability and compressibility of concrete for the three studied mix design parameters. Finally, involved physical phenomena that explain the observed trends are given.

Keywords: *Fresh concrete, Consolidation, Bleeding, Permeability.*

Introduction

Consolidation theory is commonly used in civil engineering to predict soil settlement during construction and to evaluate durability of the structures [1]. Recent studies have shown that bleeding and settlement of concrete in formwork can be predicted using the consolidation theory and the consolidation coefficient (Cv $m^2.s^{-1}$) [2-5]. Bleeding is an important issue in concrete technology and is a frequent topic of research. Authors have investigated a way of predicting the bleeding amount [5-8]. Also, other authors have focussed on the effects of mix design parameter such as superplasticizers or viscosity enhancers on the bleeding behaviour of cement-based materials [9-12]. It is worth to note that bleeding may lead to heterogeneity of mechanical characteristics [13]. The previously mentioned

studies highlight the need for an accurate determination of *Cv* for fresh cement-based materials.

Cv is directly linked to consolidation kinetics and enables the prediction of settlement for a given stress path, at a given time. Its accurate determination is also required for reliable modelling of the hydro-mechanical material behaviour. The consolidation coefficient depends on both the liquid migration velocity that is in turn linked to the granular skeleton permeability and the grain network compressibility that governs the settlement amplitude. Rangeard et al. [14] have proposed a method for the determination of *Cv* for cement-based materials using both permeability measurements and compressibility tests. The authors proposed a relationship that links the consolidation coefficient to the compressibility index and the permeability for a given void ratio *e* (i.e. the ratio of the liquid volume over the solid volume which can be linked to the *W/C* ratio). This methodology is used in this paper to study the effect of mix-design parameters such as aggregates volume fraction, water reducing admixtures and silica fume on the consolidation behavior of fresh concrete. We provide the evolution of both permeability and compressibility of concrete for the three studied mix design parameters. Those parameters evolutions enable the computation of coefficient of consolidation for concretes formulation.

Theoretical Background

The hydro mechanical behavior of geo suspensions can be studied using classical consolidation theory developed by Terzaghi [15]. The one dimensional consolidation theory analysis (along the direction z) conducted by Terzaghi highlights that a unique parameter *Cv*, the consolidation coefficient, is able to describe the spatial and temporal evolution of the void ratio e (Eq (1)). The void ratio *e* is defined as the ratio of void volume (constituted by air and/or liquid volume) to solid volume (volume of solid particles). In case of saturated cementitious material (neglected entrapped air), the void ratio is directely linked to water to cement mass ratio *W/C* ($W/C = e / (\rho_c/\rho_w)$, with ρ_c and ρ_w the specific density of cement and water).

$$\frac{\partial e}{\partial t} = \frac{Cv}{(1+e^2)} \cdot \frac{\partial^2 e}{\partial z^2} \tag{1}$$

The consolidation coefficient is directly linked to the material permeability *k* and to the material deformability as shown by Eq (2).

$$Cv = \frac{k}{m_v g \rho_w} \tag{2}$$

where m_v is the coefficient of volume change with effective stress σ' defined in Eq (3).

$$m_v = -\frac{\partial e}{(1+e)\partial\sigma'} \tag{3}$$

This coefficient of volume change m_v can be expressed from the compressibility index λ which linearly links the void ratio evolution to ln σ' (Eq 4).

$$e = -\lambda \ln\sigma' + N_\lambda \tag{4}$$

Then the expressiom of m_v according to λ writes :

$$m_v = \frac{\lambda}{(1+e)\sigma'} \tag{5}$$

Where N_λ is the value of e for σ' = 1kPa. Considering that the water flow is one dimensional and laminar, the permeability k is derived from Darcy's law, and depends on the material porosity. The prediction of the permeability of a material according to its microstructure has been an important source of research, and many models have been proposed [16-19]. For fresh cement pastes, previous studies have shown that the empirical relationship proposed by Taylor [20] allowed a good representation of the measured evolution of k with void ratio [12, 21]:

$$e = C_k \log_{10} k + K_e \tag{6}$$

According to the expressions of material compressibility and permeability, the general expression of the consolidation coefficient vs. void ration is given in eq 7.

$$Cv = \frac{(1+e)}{\lambda\gamma_w}.\exp\left(\frac{N_\lambda - e}{\lambda} + \frac{(e-Ke)\ln(10)}{Ck}\right) \tag{7}$$

Materials and Methods

In this study, the same device is used for determining permeability and compressibility of tested materials. The device consists in an oedometer device placed under a compression press. The permeability tests are conducted using the constant head method with bottom up water flow. The device allowed the determination of the permeability coefficient for different values of the void ratio on the same specimen. Details of the experimental equipment and test procedure

can be found in previous studies [12, 21]. The compressibility parameters are derived from constant strain rate test. This test procedure is faster than the traditional step by step loading, inadequate for material such as fresh cement paste where the testing time is limited due to hydration effect and setting time. Two suspending pastes were used: a kaolin and a cement paste. The cement paste used is a CEM I with a 3.15 specific density and a Blaine specific surface area of 339 $m^2.kg^{-1}$. The average particle size, D_{50}, is 10 μm. The kaolin clay used was a Powdered Polwhite BB from Imerys® (kaolins de Bretagne, Ploemeur, France) with a specific gravity of 2.65 and a Blaine specific surface area of 10^5 $cm^2.g^{-1}$. The mean grain size is close to 9 μm.

The effect of three kinds of mix-design parameters on permeability and compressibility of cement pastes are tested: the effect of aggregates volume fraction, the effect of a water reducing admixture, and the effect of supplementary cementitious material. The inclusions used to represent the aggregates are glass beads. Two particles size distributions were used: the first being a 2 mm diameter monodisperse distribution and the second having a 0.5-0.7 mm diameter distribution. For the two distributions, volume contents ranging from 0% to 60% were used. This allowed the investigation of a large range of volume fraction, from 0, i.e. a pure cement paste suspension, to a volume fraction corresponding to the maximum packing of aggregates. The high range water reducing agent (HRWRA) used in this study is a polycarboxylate type polymer. It consists in a liquid solution with 20% of dry material, designed to be added to the mix with a mass ratio of agent to cement (A/C) ranging from 0.5% to 4.0%. The filler used is a silica fume with an average diameter of 0.1 μm and a Blaine specific area of 25 000 m^2/kg.

Results and Discussion

Effect of inclusions

The effect of solid inclusions on the permeability have been studied for two suspending pasts (kaolin and cement paste) and for two particle size distributions (2mm and 0.5-0.7 mm). The evolution of the dimensionless permeability (value of permeability normalized by the permeability value of the suspending paste) with inclusion volume fraction is presented in figure 1. We note that the dimensionless permeability does not depend on both the suspending paste and the distribution size of solid inclusions. Considering impermeable inclusion, the permeability of the composite material k is linked to the length of the flow path, i.e. the tortuosity τ, and to the permeability of the suspending paste. Using the tortuosity expression proposed by Neale and Nader for an isotropic packing of spherical particle, Perrot et al. [22] have proposed a model providing the permeability of a mortar in function on the permeability of the suspending medium k_{sp} and the inclusion volume fraction, as shown by eq (8).

$$k = k_{sp}\frac{1-\phi^{2/3}}{\tau} \qquad \text{with} \qquad \tau = \left(\frac{3-\phi}{2}\right)^{1/2} \tag{8}$$

This relationship have been validated for glass beads (figure 1) and for sand [22]. As shown on figure 2, the compressibility index decreases with the addition of aggregate (glass beads in the present study). This decrease is linked to two phenomena: the reduction of the volume of compressible material (i.e the cement paste) and the friction between inclusions that increases with their volume fraction.

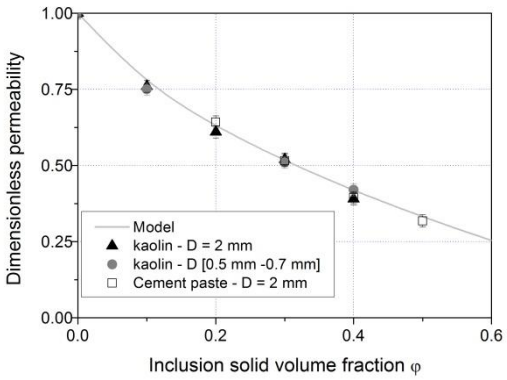

Figure 1. Influence of aggregate volume fraction on dimensionless permeability for two particle size distributions of aggregates and two suspending pastes.

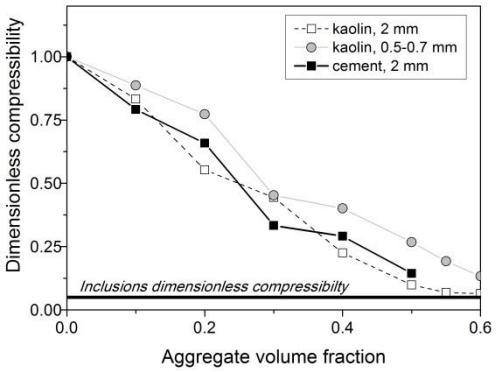

Figure 2. Influence of aggregate volume fraction on dimensionless compressibility for two particle size distributions of aggregate and two suspending pastes.

It is worth noting that the λ value of tested mortars tends toward the one of the dry inclusions as their solid volume fraction tends toward the packing fraction. This

means that for inclusion volume fraction close to the inclusions packing fraction, the compressibility is governed by inclusions frictional interactions.

Effect of superplasticizer

The addition of a polycarboxylate-based admixture reduces the permeability of the cement-based mixes as shown on figure 3. The decrease of permeability with admixture content can be due to both a change in the cement grain assembly and a change in the interstitial liquid phase viscosity due to the presence of non-adsorbed polymers. However, for the tested materials, it has been shown that the viscosity increase can be neglected [12]. Polycarboxylate induces a strong steric hindrance which allows the separation of the cement grains. Then, for the tested mixes, the average distance between grains at the contact points can be multiplied by four when the HRWRA is used at the saturation dosage [23]. The admixture changes an assembly of densely flocculated grains into a better dispersed grains assembly which presents the smallest number of accessible capillaries for the water flow. Without any admixture, dense aggregates of flocculated cement grains are formed, creating a wider percolated network throughout the sample. Figure 3 shows that the permeability diminution is about a decade with the addition of 3 % of admixture whatever the W/C ratio is. This implies a better stability of concrete with large amount of superplasticizer, such as SCC as the bleeding rate is reduced.

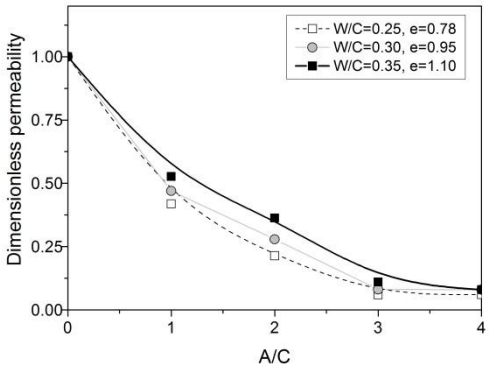

Figure 3. Influence of HRWRA content on permeability.

The compressibility curves of the tested self-consolidating pastes exhibit two linear segments as proposed by [12] and as shown on figure 4. In the first segment, the compressibility index λ_1 is high and the material behaves as a highly flowable mixture. In the second segment (compressibility index λ_2), the material becomes stiffer and the consolidation regime changes. Both segments cross at critical stress σ'_c and void ratio e_c. It is important to note that the compressibility index values λ_1 and λ_2 are not affected by the HRWRA dosage (figure 5). However, the coordinates of the crossing point (σ'_c, e_c) depend on the HRWRA dosage (figure 6).

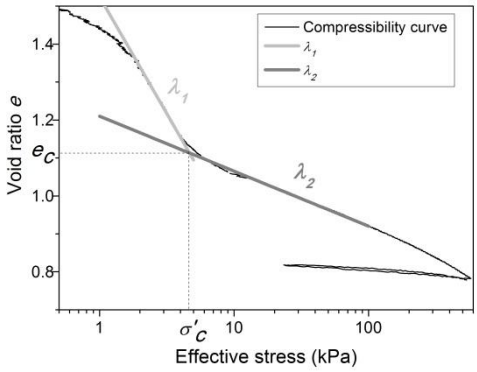

Figure 4. Definition of compressibility index (λ_1 and λ_2) and critical stress (σ'_c) and critical void ratio (e_c) from a compressibility curve.

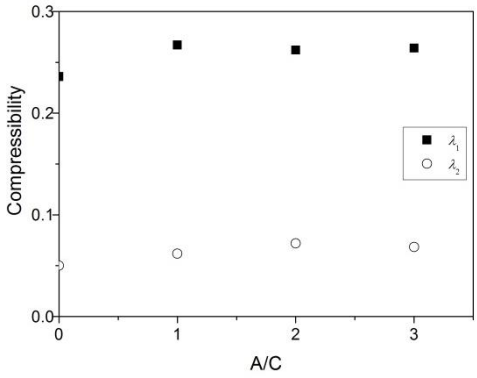

*Figure 5.*Compressibility coefficient evolution with HRWRA content.

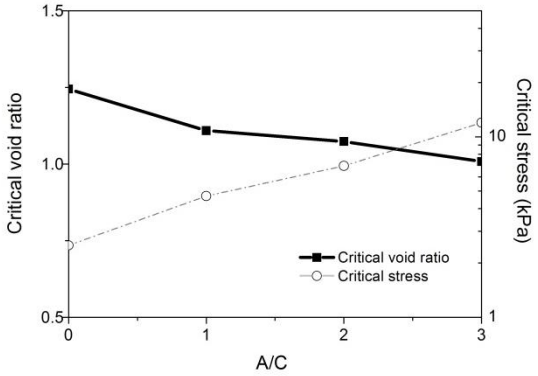

Figure 6. Influence of HRWRA on critical stress and void ratio.

The critical void ratio decreases with the dosage and traduces a change in the cement grains microstructure. This can be linked to the change in the cement grains percolation threshold as shown by Perrot et al. [23].

Effect of silica fume

Permeability measurements have been performed for silica fume contents of 20% and 40%. In order to compare the effect of addition content on permeability, a value of k is extrapolated for a same void ratio of 1.0. The procedure of extrapolation, which assumed that the evolution of k with void ratio follows the Taylor relationship [20], can be find in detailed in Perrot et al. [12]. The obtained evolution of k with content of silica fume is presented in figure 7. It is worth noting that the addition of silica fume induces a dramatically decrease in permeability. This effect can be imputed to the large difference between particle size distributions between cement and silica fume ($D_{50cement}/D_{50silicafume}$ = 100). Indeed, the silica fume particles are place in the porosity of the cement grain's skeleton, and greatly limit the water flow throw in the cement grains skeleton.

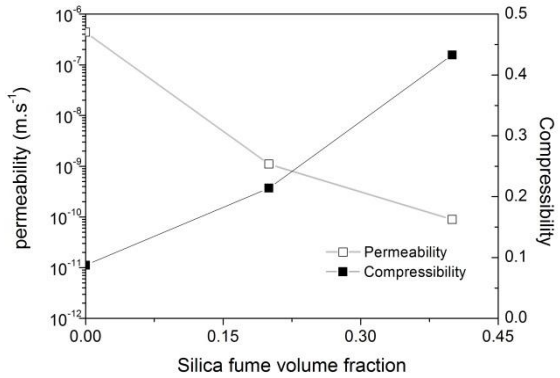

Figure 7. Silica fume content influence on permeability and compressibility of cement paste.

For the compressibility measurement tests, the materials have been prepared in order to obtain the same workability (yield stress of 50 Pa measured using a Vane geometry with a stress growth protocol as in [7]). Regarding to the high specific surface or the silica fume, the initial water content, and so the initial void ratio of the samples, are largely dependent on silica fume content (e = 0.9 for 0% of silica fume, e = 2,2 for 40% of silica fume). The obtained compressibility, which is dependent on initial void ratio, is largely affected by this fact, and exhibits an increase with the silica fume content. In order to better analyse the silica fume effect, further investigations are provided for silica fume content lower than 10%.

Conclusions

The effects of several parameters on the consolidation behaviour of fresh concrete have been investigated in this study. Firstly, the effect of solid inclusions has been studied by measuring the evolutions of both permeability and compressibility with aggregate volume fraction in cement and kaolin pastes. The main result shows that the decrease in permeability does not depend on the type of inclusions, and of the suspending paste. A simple model providing the permeability of a mortar regarding to the permeability of the cement paste and the inclusion volume fraction have been validated from experimental measurements. The compressibility of the material is also reduced with the inclusions volume fraction, and tends toward the compressibility of the dry inclusions assembly (elastic behaviour). Secondly, an addition of a superplasticizer induces a decrease in permeability with the admixture content. This reduction is linked to a finer porous network due to a better dispersion of cement grains with the superplasticizer. The permeability diminution is about a decade with the addition of 3% of admixture, inducing better stability of concrete. The investigation of the compressibility curve shows that the compressibility behaviour is firstly governed by a high compressibility corresponding to the compression of macro-flocculated cement grains, and then the compressibility become lower, traducing the compaction of a denser assembly of cement grains. The critical void ratio which corresponds to this change in compressibility decreases with the content of superplasticizer and traduces a change in the cement grains microstructure. Finally, the effect of an addition of silica fume is studied. The very high difference between particles size leads to an important decrease of permeability with the silica fume content. The decrease in permeability is more than two decades with the addition of 20% of silica fume. Due to the important increase of the initial void with the silica fume content, the mixes exhibit increase in compressibility with silica fume content. Further investigations are necessary for silica fume in dosages below 20% to study its effect on mixtures in the same initial state.

References

[1] Terzaghi, K. Peck, R.B. and Mesri G. (1996) *Soil mechanics in engineering practice*, John Wiley and Sons, Third Edition.

[2] Morris, P.H. Dux, P.F. (2010) Analytical solutions for bleeding of concrete due to consolidation, *Cement and Concrete Research*, Vol. 40, p. 1531-1540.

[3] Josserand, L. de Larrard ,F. (2004) A method for concrete bleeding measurement, *Materials and Structures*, Vol. 37, p. 666-670.

[4] Assaad, J.J. Harb, J. (2011) Surface settlement of cementitious-based materials determined by oedometer testing, *Materials and Structures*, Vol. 44, p. 845-856.

[5] Yim, J.Y. Kim, J.H. Kwak, H.Y. Kim, J.K. (2013) Evaluation of internal bleeding in concrete using a self-weight bleeding test, *Cement and Concrete Research*, Vol. 53, p. 18-24

[6] Josserand, L. de Larrard, F. (2004) A method for concrete bleeding measurement, *Materials and Structures*, Vol. 37, p. 666-670.
[7] Perrot, A. Lecompte, T. Khelifi, H. Brumaud, C. Hot, J. Roussel, N. (2012), Yield stress and bleeding of fresh cement pastes, *Cement and Concrete Research*, Vol. 42, pp. 937-944.
[8] Miltiadou-Fezans, A. Tassios, T.P. (2013) Stability of hydraulic grouts for masonry strengthening, Materials and Structures, Vol. 46, p. 1631-1652.
[9] Wainwright, P.J. Ait-Aider, H. (1995) The influence of cement source and slag additions on the bleeding of concrete, *Cem Concr Res*, Vol. 25, p. 1445-1456.
[10] Khayat, K.H. (1998) Viscosity-enhancing admixtures for cement-based materials — An overview, Cement and Concrete Composites, Vol. 20, p. 171-188.
[11] Mikanovic, N. Jolicoeur, C. (2008) Influence of superplasticizers on the rheology and stability of limestone and cement pastes, *Cem Concr Res*, Vol 38, p. 907-919.
[12] Perrot, A. Rangeard, D. Picandet, D. and Mélinge, Y. (2013) Hydro-mechanical properties of fresh cement pastes containing polycarboxylate superplasticizer , *Cem Concr Res*, Vol. 53, p. 221-228.
[13] Giaccio, G., Giovambattista, A. (1986), Bleeding: evaluation of its effects on concrete behaviour, *Mater. Struct.*, Vol. 19, pp. 265–271.
[14] Rangeard, D. Perrot, A. Picandet, V. Mélinge, Y. and Estellé, P. (2015) Determination of the consolidation coefficient of low compressibility materials, *Materials and Structures*, Vol. 48, p. 1475-1483.
[15] Terzaghi, K. (1943); *Theoretical Soil Mechanics*, John Wiley and Sons, New York
[16] F. Tavenas, F., Leblond, P., Jean P., Leroueil, S. (1983), The permeability of natural soft clays, *Canadian Geotechnical Journal*, Vol. 20, pp. 629–660.
[17] Carman, P.C. (1956), Flow of Gases through Porous Media, New York Academic, NewYork,
[18] Carman, P.C. (1939), Permeability of saturated sands, soils and clays, *Journal of Agricultural Science*, Vol. 29, pp. 263–273.
[19] Chapuis, R.P., Aubertin, M. (2003), On the use of the Kozeny–Carman equation to predict the hydraulic conductivity of soils, *Canadian Geotechnical Journal*, Vol. 40, pp. 618–628.
[20] Taylor, D.W. (1948), Fundamentals of soil mechanics, Wiley, New York.
[21] Picandet, V., Rangeard, D., Perrot, A., Lecompte, T. (2011), Permeability measurement of fresh cement paste, *Cem Concr Res*, Vol. 41, pp. 330-338.
[22] Perrot, A., Rangeard, D., Picandet, V., Serhal, S. (2015), Effect of coarse particle volume fraction on hydraulic conductivity of fresh cement based material, *Materials and Structures*, Vol. 48(7), pp. 2291-2297.
[23] Perrot, A. Lecompte, T. Khelifi, H. et al. (2012) Yield stress and bleeding of fresh cement pastes. *Cem Concr Res*, Vol. 42, p. 937 – 944.

Micro-Proportioning of SCC with Crushed Aggregate: PART I Filler Particle Characterization and Properties

Rolands Cepuritis[1,2], Stefan Jacobsen[1], Sverre Smeplass[1,3], Ernst Mørtsell[1,4] and Børge J. Wigum[2,5]

[1]Department of Structural Engineering, Norwegian University of Science and Technology, NO-7491 Trondheim, Norway
[2]Norcem AS (HeidelbergCementGroup), R&D Department, Setreveien 2, Postboks 38, NO-3950 Brevik, Norway
[3]Skanska Norge AS, Drammensveien 60, PO Box 1175, N-0107 Oslo, Norway
[4]NorBetong AS (HeidelbergCementGroup), Heggstadmyra 6, NO-7080 Heimdal, Norway
[5]Department of Geology and Mineral Resources Engineering, Norwegian University of Science and Technology, Sem Sælands vei 1, NO-7491 Trondheim, Norway

Abstract In concrete micro-proportioning, the fine particle size distribution (PSD) is adjusted by controlling and varying the PSD of different aggregate fine fractions smaller than about 0.125-0.250 mm (also cement and pozzolana may of course be included). It has been performed concrete micro-proportioning with the fine part of the crushed sand (≤ 0.250 mm) divided into several fractions by air classification that were re-combined to obtain a desired PSD of the fines. In practice this can be done either at the RMC plant or at the crushed aggregate quarry. Here in PART I it is presented the particle properties of crushed sand made from rock types of 10 different quarries in Norway, and in PART II it is studied how micro-proportioning with crushed fines can be used to control concrete rheology. The 10 materials represent a wide range of local geological variety used for concrete aggregate production. This included igneous (intrusive and extrusive), metamorphic and sedimentary rocks that are both monomineralic and polymineralic. The results presented here include X-ray micro-computed tomography (μCT), coupled with spherical harmonic (SH) analysis to mathematically describe the full 3-D shape of particles and investigations with the 2-D Dynamic Image Analysis (DIA) approach as an alternative fast and industrial method for shape measurements. The study also investigates the applicability of methods, such as laser diffraction, X-ray sedimentation and BET for PSD and specific surface measurements of the crushed aggregate fines.

Keywords: *Micro-proportioning, Crushed fines, Shape, PSD, Specific surface.*

Introduction

Rapid depletion of natural sand and gravel resources for concrete production in many countries and densely populated regions in the world has lately led to several new developments and innovations in the field of crushed sand production. A new technology developed in Norway during the last years has been concrete production with the micro-proportioning concept. This approach is based on experimental findings [1], [2], [3], [4], [5], [6], [7] showing that not all concrete aggregate fractions have equal influence on the fresh concrete rheological properties. In particular, it can be demonstrated [5], [8], [9] that accurate control of the volume and composition of crushed sand fines from a wide variety of bedrock allows to control the rheological properties of the cement paste matrix, and thus concrete mix through an approach that is introduced here as concrete micro-proportioning. Here concrete micro-proportioning means to recombine 3 crushed fines fractions < 0.250 mm produced with vertical shaft impact (VSI) crusher and air classification to control fresh concrete properties. The concrete micro-proportioning aims for cost- and resource effective concrete production by offering two parallel, complementary paths to control concrete rheology: chemical admixtures and mineral powders.

Self-Consolidating Concrete (SCC) is known to be much more dependent on obtaining the right properties and volume of the cement paste matrix than the Conventional Vibrated Concrete (CVC). On the other hand, SCC should be produced in a way so that the production costs are not excessively high to keep the competiveness of this product compared to CVC, as this has been one of the historic problems that is still keeping the market share of this technically advanced material quite limited [10]. As the concrete production with the micro-proportioning approach allows for a very careful and precise selection of both volume and composition of the cement paste matrix phase, this approach is technologically very suitable for production of economic and robust SCC mixes.

In order to utilise the concrete micro-proportioning approach one needs to very precisely describe the physical characteristics of the crushed aggregate fines. However, standard methods to carry out the characterization that would be adapted by the aggregate and concrete production industries are not available, and different researchers have previously used widely different measurement methods. It is, however, also well-established from studies within the geological sciences on analysing natural sediments of similar grain size distributions [11] that different methods for characterisation of particle properties can give very different results for one and the same material. This in particular concerns determination of the specific surface, particle size distribution (PSD) and shape of the fine crushed sand aggregate particles. Here in Part I it is presented the characterisation of crushed

fines and how to use this for micro-proportioning. Then in Part II it is studied the effect on rheology. Full details are given in [12].

Materials and Methods

Crushed sand fines

A total of 30 different fine powder samples were produced (

Table *I*) from 10 different rocks by combining high-speed (70 m/s) VSI crushing and static air classification: three particle size ranges (4 to 25 µm, 20 to 60 µm and 40 to 250 µm microns) for each rock type. The particle size ranges are defined by their d_{10} to d_{90} equivalent diameters (where 10 % and 90 % of the particles pass). Mineralogical composition of the crushed powders was determined by quantitative X-ray diffraction (XRD) analysis on the 4 µm to 25 µm size fractions (Table II) [13].

Methods

Four different methods were used to determine PSD of the crushed fines. These are wet-method laser diffraction (LD), X-ray sedimentation technique (XS), X-ray microcomputed tomography (µCT) combined with spherical harmonic (SH) analysis and Dynamic Image Analysis (DIA). An approximate specific surface area can be calculated from the result of any of these PSD measurements by assuming some defined particle shape (typically spherical). A fifth method, nitrogen (N_2) adsorption BET method analysis, was used only for direct specific surface area measurements. In addition, the results obtained from the DIA, which is a two-dimensional (2-D) method, and µCT coupled with SH analysis, which is a three-dimensional (3-D) method, were analysed together to evaluate the applicability of the 2-D DIA method as a fast quality test in production.

These measurement methods are well-known techniques that have been widely used for characterising other materials. For details see [11], [14] for LD and XS methods, [15], [16], [17], [18] for µCT, [14], [16] for DIA and [19] for the BET method.

Results

The studies [13] revealed that for crushed aggregate fines passing 125 µm or 63 µm sieves, generally about 50 % of the surface area is concentrated among particles below about 5 µm of equivalent sphere size since specific surface is inversely proportional to particle size [20]. Particles smaller than 1 µm of equivalent sphere diameter were detected in some of the materials; however, their total amount was difficult to determine reliably. Since such a large amount of the specific surface area comes from small particles, this suggests that only the PSD

measurement methods that allow precise measurements of particles below about 5 µm and down to at least 1 µm are suitable for crushed aggregate fines over the entire expected particle size range. Only two of the methods considered, namely XS and LD, could detect particles in this size range. As discussed in [13], the XS method seemed to be the best for this purpose due to fewer uncertain input parameters. The LD method could introduce an error of up to about 30 % in the approximated specific surface area values (calculated by dividing the obtained PSD into a finite amount of bins and assuming equivalent spherical or other diameters of particles that correspond to the mean size of each bin) due to its inputs. The uncertainties are mainly arising from the imaginary part of the index of refraction needed for Mie theory analysis.

Table I. Crushed rock fines used for the study [13].

Rock type designation	Rock name	Water absorption[a]	Mean fines density[b]	Crushed rock fines fraction designation		
				Fine	Medium	Coarse
		[%]	[g/cm^3]	4 µm to 25 µm	20 µm to 60 µm	40 µm to 250 µm
T1	**Mylonitic quartz diorite**	0.4	2.77	T1-1	T1-2	T1-3
T2	**Gneiss/ granite**	0.4	2.71	T2-1	T2-2	T2-3
T3	**Quarzite**	0.2	2.67	T3-1	T3-2	T3-3
T4	**Anorthosite**	0.7	2.93	T4-1	T4-2	T4-3
T5	**Limestone**	0.2	2.72	T5-1	T5-2	T5-3
T6	**Limestone**	0.6	2.76	T6-1	T6-2	T6-3
T7	**Dolomite**	0.2	2.85	T7-1	T7-2	T7-3
T8	**Basalt**	0.9	2.93	T8-1	T8-2	T8-3
T9	**Aplite**	0.7	2.65	T9-1	T9-2	T9-3
T10	**Granite/ gneiss**	0.3	2.74	T10-1	T10-2	T10-3

[a] Water absorption was determined on the 0.063 mm to 2 mm size fraction particles obtained after the VSI crushing experiments by the "pycnometer method for aggregate particles between 0.063 mm and 4 mm" according to EN 1097-6.
[b] Density of each crushed fines sample was measured by helium pycnometry. The presented value is the mean for the three fractions of the same rock type. The density values of the fines of different size fractions from the same rock type in general varied only in the order of 0.01 g/cm^3.

The studies [13] have also used the µCT SH results to investigate the error introduced in the calculations of specific surface from particle size distributions, as determined, for example, with the XS method. The results of these investigations indicated that for crushed fines produced by VSI crushing from rocks of vastly

different mineralogy (see Table II), the underestimation error introduced due to assuming spherical shape for surface area approximation is of surprisingly similar magnitude, 20 % to 30 % for all 30 fractions studied (10 rock fines with 3 fine fractions each). This finding is important and simplifies specific surface area determination for our crushed aggregate fines and probably also for general concrete proportioning purposes and quality control at aggregates quarries using VSI and air classification.

Table II. Mineralogical composition of the used rock types determined with quantitative XRD [13].

Rock type	**Mylonitic quartz diorite**	**Gneiss/ granite**	**Quartzite**	**Anorthosite**	**Limestone**	**Limestone**	**Dolomite**	**Basalt**	**Aplite**	**Granite/ gneiss**
Rock type designation	**T1**	**T2**	**T3**	**T4**	**T5**	**T6**	**T7**	**T8**	**T9**	**T10**
Tested fraction	4 µm to 25 µm									
Mineral or group of minerals	Mass %									
Quartz	27.9	20.9	90.0	6.5	2.3	2.5	1.1	8.9	36.2	17.8
Carbonate minerals	4.4	-	3.6	10.6	97.7	95.0	95.0	8.3	-	5.0
Epidote minerals	8.4	-	-	24.4	-	-	-	7.6	-	-
Feldspar minerals	37.7	63.9	3.9	33.1	-	0.4	0.6	26.5	58.2	58.8
Sheet silicates (micas[a])	1.3	3.7	1.5	-	-	1.1	-	5.2	2.7	5.5
Sheet silicates (other)	6.7	4.4	-	20.4	-	0.4	0.7	0.0	0.0	3.7
Chlorite	11.3	1.4	1.0	2.6	-	0.6	1.6	20.2	1.7	0.5
Inosilicate minerals	1.0	3.9	-	2.3	-	-	1.1	11.0	1.2	8.7
Iron oxide minerals	-	-	-	-	-	-	-	3.5	-	-
Other minerals	1.3	1.9	-	0.2	-	-	-	8.8	-	-

[a] Biotite and muscovite.

Investigations on the crushed aggregate fines [21] also suggest that the specific surface area measurements by the N_2 adsorption based BET method is strongly affected by the mineralogical composition of the crushed fines. This is because the gas adsorption-based BET measurements include not only the external but also the open internal specific surface area. Thus, even though the possibilities of using the BET specific surfaces as a performance parameter in fresh SCC has been

demonstrated for limestone fillers [20], it could not be used when comparing crushed fines of a different mineralogical composition for their effect on the rheological properties in cementitious suspensions. It is possible, from the evidence presented in [12], [13], [21] that adsorption between the mica mineral layers and also in certain other minerals like chlorite, and weathering of the particle surfaces affect surface area as measured by BET. Thus these are not correctly reflecting the external specific surface that is relevant for rheology.

With respect to the filler particle shape, it has been demonstrated that the µCT SH method allows obtaining analytical, differentiable mathematical shape for surface of the crushed aggregate fines particles in form of the spherical harmonic functions [21], [22], for grains as small as about 3 µm of volume equivalent spherical diameter (VESD) (see Figure 1). By using those functions one can compute any geometrical quantity of the particle which can be defined by integrals over the volume or over the surface or any other algorithm using points on the particle surface or within the particle volume [22]. It has also been demonstrated [21] that by this method analysing samples up to about 250 000 particles for the crushed aggregate powder size fraction of 20 µm to 125 µm and up to about 5500 particles in the size range $\leq$ 20 µm was accomplished. This allowed analysing enough particles to obtain a statistically representative result even for comparably long fine particle size fractions. One drawback of the µCT and SH method is the time consumption, which including the sample preparation could reach up to about 24 hours and the comparable cost of the µCT scanning equipment. Thus the 2-D DIA method was investigated [23], [24] as an alternative much faster way allowing a quick analysis (about 5 minutes) of a comparable number of crushed aggregate powder particles by using less costly equipment and virtually no special sample preparation. However, the method can only provide limited amount of information about the 2-D particle shape. Thus, it could be better applicable for the everyday quality control at the crushed concrete sand production quarries and concrete production units where less fundamental knowledge is needed, but speed and costs is important. The results [23], [24] showed that the 2-D DIA method exhibits problems correctly measuring the shape of particles smaller than about 40 µm due to too large pixel size used and possibly some particle flocculation. However, for particles larger than the 40 µm the 2-D method allowed ranking the shapes of the same size VSI crushed aggregate fines in the same order as the much more fundamental 3-D µCT and SH method. The results [23], [24] also demonstrated that for a given sample of VSI crushed aggregate fines, of the same rock type, uniform particle form characteristics, in terms of particle aspect ratios, were found for the entire size range of 3 µm to 250 µm. This means that it should be possible to find mean shape description parameters that can model the influence of the particle shape of the whole sample on the rheological properties of filler modified cement paste and concrete. This also means that the 2-D DIA shape investigations can actually be applied in everyday aggregate and concrete production to get an indication of the shape variations of the crushed fines > 40 µm size.

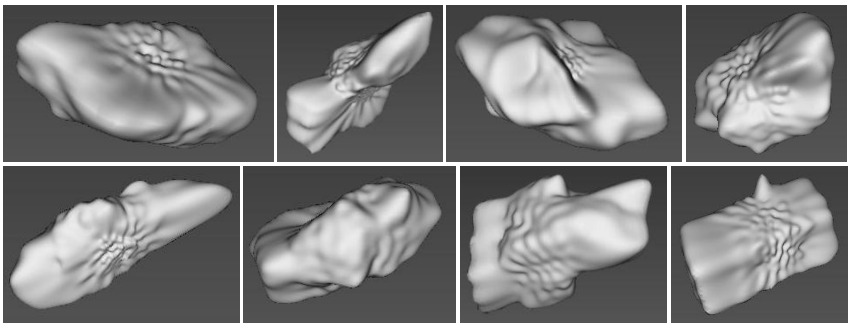

Figure 1. VRML images of random particles based on the results from µCT scanning and spherical harmonic analysis (T5-1 crushed fines fraction; 10 µm < VESD < 20 µm; 1.6 < Length/Width < 2.4) [13].

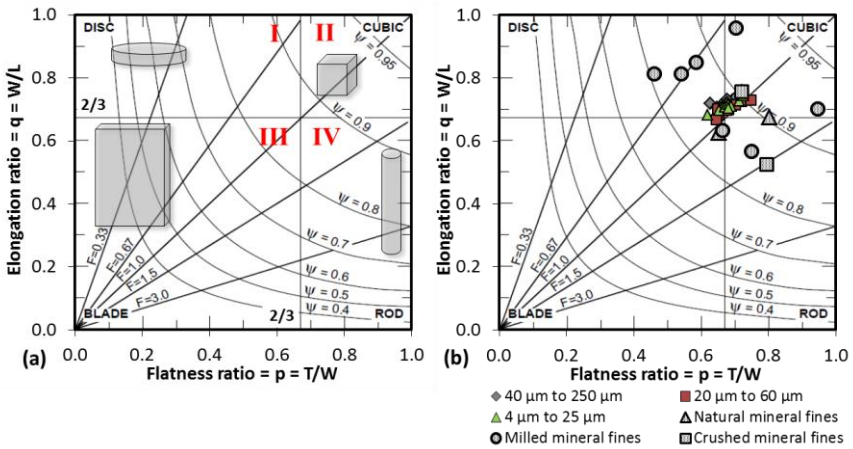

Figure 2. Zingg's diagram [26], showing the relationship between the axial ratios Width/Length = W/L and Thickness/Width = T/W, Krumbein's intercept sphericity Ψ_I [27] and Aschenbrenner's shape factor F [28]; (a) general particle shape classification chart, after [29]; (b) relationship between the mean axial ratios of the particles from this study and mean axial ratios obtained from some previous studies [17], [18], [21] on similar-sized mineral particles. Figure adopted from [23].

The results [23], [24] showed that, in contrast to what is typically assumed [25], VSI crushing is able to affect the shape of crushed concrete aggregate fines down to a particle size of about 3 µm, independent of the very different mineralogical composition of the 10 rock types included in this study. This indicates that it is indeed possible to improve the shape of fines, where improvement means to make the particles more equi-dimensional. The results [23], [24] also showed that surprisingly similar particle shapes in terms of the classification system typically used by sedimentary petrologists (Zingg's diagram [26]) were found for all the VSI

crushed particles analysed (see Figure 2) independent of the parent rock physical propeties and mineralogy (see Table II).

Conclusions

The following main conclusions can be drawn from the results obtained in the study with respect to characterization and properties of the crushed sand fines to be used for the production of SCC:

- XS method seems to be the most suitable for determining PSD and specific surface of the fines;
- Good indication of the relative specific surface of the crushed sand fines can be obtained by approximations from the PSD measurements;
- BET specific surface area cannot be used when comparing crushed fines of a different mineralogical composition for their effect on the rheological properties in cementitious suspensions, because it is not correctly reflecting the external specific surface that is relevant for rheology;
- µCT SH method is best suitable for fundamental characterization of the shape of the crushed aggregate fines, and it has been showed to be applicable for grains as small as about 3 µm of VESD;
- By the 2-D DIA method, a good but limited indication of the actual 3-D shape of the irregularly shaped crushed aggregate fines larger than 40 µm of equivalent diameter can be acquired and used for simple quality control in hard rock quarries;
- VSI crushing seems to be able to successfully normalise shape (equi-dimensionality) of crushed sand fines down to the particle size of about 3 µm VESD.

References

[1] A. Heath, A manual of lime and cement, London: William Clowes and Sons, 1983.

[2] L. Edwards, “Proportioning the materials of mortars and concretes by surface area of aggregates,” *In: ASTM, Proceedings of the 21st annual meeting, 18, Part II*, pp. 235-302.

[3] L. Murdock, “The workability of concrete,” *Magazine of Concrete Research*, vol. 12, no. 36, pp. 135-144, 1960.

[4] M. Wills, “How aggregate particle shape influences concrete mixing water requirement and strength,” *Journal of Materials*, vol. 2, no. 4, pp. 843-865, 1987.

[5] E. Mørtsell, “Modelling the effect of concrete part materials on concrete consistency. PhD,” Norwegian University of Science and Technology (In

Norwegian), 1996.

[6] K. Day, Concrete Mix Design, Quality Control and Specification. 3rd edition, Oxon: Taylor & Francis, 2005.

[7] R. Cepuritis, S. Jacobsen, B. Pedersen and E. Mørtsell, "Crushed sand in concrete – effect of particle shape in different fractions and filler properties on rheology," *Manuscript submitted to Cement and Concrete Composites.*

[8] R. Cepuritis, S. Jacobsen and T. Onnela, "Sand production with VSI crushing and air classification: Optimising fines grading for concrete production with micro-proportioning," *Minerals Engineering,* vol. 78, pp. 1-14, 2015.

[9] R. Cepuritis, S. Jacobsen, S. Smeplass, E. Mørtsell, B. Wigum and S. Ng, "Influence of crushed aggregate fines with micro-proportioned particle size distributions on rheology of cement paste," *Manuscript submitted to Construction and Building Materials.*

[10] R. Cepuritis, "Yield stress and slump-flow of SCC: Short review and application," *Nordic Concrete Research,* vol. 46, pp. 1-15, 2012.

[11] J. Syvitski, Principles, Methods, and Application of Particle Size Analysis, Cambridge: Cambridge University Press, 1997.

[12] R. Cepuritis, "Development of Crushed Sand for Concrete Production with Micro-proportioning. PhD thesis submitted for evaluation," Norwegian University of Science and Technology, Trondheim, 2016.

[13] R. Cepuritis, E. Garboczi, C. Ferraris, S. Jacobsen and B. Sørensen, "Measurement of particle size distribution and specific surface area for crushed concrete aggregate fines," *Manuscript submitted to Cement and Concrete Composites.*

[14] T. Allen, Powder Sampling and Particle Size Determination, Amsterdam: Elsevier, 2003.

[15] M. Taylor, E. Garboczi, S. Erdoğan and D. Fowler, "Some properties of irregular 3-D particles," *Powder Technology,* vol. 162, pp. 1-15, 2006.

[16] E. Garboczi and H. Azari, "National Cooperative Highway Research Program 20-07 (243): Development of Glass Beads Utilised in Traffic Markings," Transportation Research Board, Washington, 2010.

[17] E. Garboczi, "Three dimensional shape analysis of JSC-1A simulated lunar regolith particles," *Powder Technology,* vol. 207, pp. 96-103, 2011.

[18] E. Garboczi, X. Liu and M. Taylor, "The 3-D shape of blasted and crushed rocks: From 20 μm to 38 mm," *Powder Technology,* vol. 229, pp. 84-89, 2012.

[19] G. Fagerlund, "Determination of specific surface by the BET method," *Materials and Structures,* vol. 6, no. 3, pp. 239-245, 1986.

[20] O. Esping, "Effect of limestone filler BET(H2O)-area on the fresh and hardened properties of self-compacting concrete," *Cement and Concrete Research,* vol. 38, no. 7, pp. 938-944, 2008.

[21] R. Cepuritis, B. Wigum, E. Garboczi, E. Mørtsell and S. Jacobsen, "Filler from crushed aggregate for concrete: Pore structure, specific surface, particle shape and size distribution," *Cement and Concrete Composites,* vol. 54, pp. 2-16, 2014.

[22] E. Garboczi, "Three-dimensional mathematical analysis of particle shape using x-ray tomography and spherical harmonics: application to aggregates used in concrete," *Cement and Concrete Research,* vol. 32, pp. 1621-1638, 2002.

[23] R. Cepuritis, E. Garboczi, S. Jacobsen and K. Snyder, "Comparision of 2-D and 3-D shape analysis of concrete aggregate fines from VSI crushing," *Manuscript submitted to Powder Technology.*

[24] R. Cepuritis, E. Garboczi and S. Jacobsen, "Three dimensional shape analysis of concrete aggregate fines produced by VSI crushing," *Manuscript submitted to Cement and Concrete Composites,* 2015.

[25] B. Lagerblad, H.-E. Gram and M. Westerholm, "Evaluation of the quality of fine materials and filler from crushed rocks in concrete production," *Construction and Building Materials,* vol. 67, pp. 121-126, 2014.

[26] T. Zingg, "Beitrag zur Schotteranalyse," *Schweiz. Mineralog. und Petrog. Mitt.,* vol. 15, pp. 39-140, 1935.

[27] W. Krumbein, "Measurement and geological significance of shape and roundness of sedimentary particles," *Journal of Sedimentary Petrology,* vol. 11, pp. 64-72, 1941.

[28] B. Aschenbrenner, "A new method of expressing particle sphericity," *Journal of sedimentary petrology,* vol. 26, pp. 15-31, 1956.

[29] V. Janoo, "Special Report 98-1. Quantification of Shape, Angularity, and Surface Texture of Base Course Materials," US Army Corps of Engineers - CRREL, Hanover, 1998.

[30] E. Hämäläinen, "Manufactured sand success with Velde Pukk in Norway," *Metso's customer magazine for the mining and construction industries - results: minerals&aggregates,* vol. 2, pp. 6-7, 2010.

[31] K. Aslaksen Aasly, S. Danielsen, B. Wigum, S.-H. C. R. Norman and T. Onnela, "Review report on dry and wet classification of filler materials for concrete. State-of-the-art. COIN Project report 52 – 2014," SINTEF, Oslo, 2014.

Mix Design Procedure for Low-Powder Self-Consolidating Concrete: Eco-SCC

Behrouz Esmaeilkhanian[1], Kamal H. Khayat[2] and Ólafur H. Wallevik[3]

[1]Department of Civil Engineering, Université de Sherbrooke, 2500, boul. de l'Université, Sherbrooke, Qc, CANADA, J1K 2R1. (819) 821-8000 Ext. 63916, behrouz.esmaeilkhanian@usherbrooke.ca
[2]Missouri University of Science and Technology, Université de Sherbrooke, 224 Engineering Research Laboratory 500 W. 16th St. Rolla, MO 65409, USA. (573) 341-6223, khayatk@mst.edu
[3]ICI Rheocenter, Reykjavik University & Innovation Center Iceland, Keldnaholt, IS-112 Reykjavik, Iceland, wallevik@ru.is

Abstract Reducing the powder content of self-consolidating concrete (SCC) while maintaining a satisfactory performance is an efficient approach to decrease the environmental impact of SCC as well as the production cost. However, producing a low-powder SCC, Eco-SCC, is challenging since all self-consolidating characteristics mainly depend on a high powder volume which is not the case for Eco-SCC. In the current study, a comprehensive design approach for attaining SCC of low carbon footprint (Eco-SCC) is proposed. The method is based on the optimization of the volumetric proportions of sand and coarse aggregate according to an ideal particle gradation curve. The paste composition is obtained from rheology-based optimizations in such a way to reduce water demand. The water content is adjusted to provide the necessary minimum paste volume. Silica fume, fly ash, and finely ground limestone filler are employed as powder materials. The recommended design procedure is found to be effective for producing Eco-SCC. Mixtures with total powder content of approximately 300 kg/m^3 are shown to exhibit adequate workability characteristics and compressive strengths between 25 and 35 MPa at 28 days.

Keywords: *Ecological self-consolidating concrete, Mix design, Particle-size optimization, Rheology, Workability.*

Introduction

The emission of CO_2 during cement clinker production is an environmental issue associated with concrete [1-6]. The production of 1 kg of cement releases between

0.66 to 0.82 kg of CO_2 into the atmosphere [2]. Given the sheer volume of concrete produced annually [3], the contribution of CO_2 emission due to cement production to the global warming is significant [1-3, 7]. Thus, reduction of the environmental impact of concrete has become an important subject of research in recent years giving rise to different types of ecologically friendly concrete. Ecologically-friendly concrete, or Eco-concrete, can be produced by either minimizing the use of portland cement or by maximizing the concrete mechanical properties to reduce section dimensions as well as increasing durability to enhance service life [6].

SCC is a sustainable material due to its ease of placement, and when properly designed, it can produce a highly durable concrete [8]. Achieving the desired fresh properties of SCC usually necessitates the use of a high binder content dwindling the ecological and economical aspects of such concrete. In this respect, SCC with low cement and total binder contents, called here Ecological-SCC, can be of great interest since it embodies the advantages of both self-consolidation and reduction of CO_2 emissions as well as reducing materials cost. Hunger [9] successfully applied the method proposed by Brouwers and Radix [10] to design Ecological SCC. The volumetric proportions of all granular materials were optimized so that the grading curve of solid materials correlates well with the Funk and Dinger (FD) ideal curve [11] which reads:

$$P(d) = \frac{d^q - d_{min}^q}{d_{max}^q - d_{min}^q} \quad (q \neq 0) \tag{1}$$

where P(d) is a fraction of the total solids being smaller than size d, and q is the distribution modulus. The water content was obtained from the choice of water to powder ratio (*w/p*). Such design process was user-friendly and required few input data. Ghezal and Khayat [12] applied the response surface methods to experimental data to develop a mix design method for SCC mixtures with low cement content. Optimum SCC formulations with 280 kg/m³ of type GU cement and 95 kg/m³ of limestone filler yielded adequate workability and mechanical properties for the SCC intended for commercial and housing construction with targeted compressive strength of 20 MPa at 28 days.

In 1998 Wallevik and Nielsson [13] presented SCC mix-design with less than 320 kg/m^3 cementitious materials and without additional filler, applying so-called rheological approach and using the particle lattice effect. Fidjestol et al. [14] reported “Eco-mix” SCC with low carbon footprint, based on this approach having about 150 kg/m^3 cement and 270 kg/m^3 fly ash. Eco-SCC was introduced by Wallevik et al. [15, 16] for which the total powder content was limited to 315 kg/m^3. About 7000 m^3 of this concrete was casted in at the Karahnuka hydropower plant in 2005. This concept significantly reduces the CO_2 emissions compared to normal SCC or conventional concrete (CC) for applications where strength class of C25/35 and normal durability characteristics suffice. Mueller [17] developed

further the rheology-based approach for the design of this type of Eco-SCC. Rheographs were proposed as a basis of mixture optimization. The matrix volume, particle size distribution (PSD), and matrix-aggregate interaction were proposed as key design factors for this design approach.

In the current work, an attempt was made to combine various recommendations for the design of Eco-concrete [9, 10, 15, 17], and to propose a step-by-step design method to produce low-binder Eco-SCC with minimal trial experiments. The focus here was on the fresh properties with compressive strength being the only measured hardened characteristic. Optimization of volumetric proportions of sand and coarse aggregate were carried out based on the principle of ideal grading curve as the stability of Eco-SCC is mainly provided by the lattice effect which is directly related to PSD [15, 17]. In other words, for two adjacent particle size classes, the volume fraction of the finer class should be always equal or larger than the coarser one in order to improve the lattice effect. The devised procedure yielded in the production of Eco-SCC with satisfactory workability and compressive strength.

Materials and Testing

Type GU portland cement (C) was employed. Class F fly ash (FA), and silica fume (SF), and fine limestone filler (LF) were used. A polycarboxylate-based SP with a dry content of 31.4%, and a compatible polycarboxylate-based viscosity-modifying admixture (VMA) with a dry content of 42.1% were used. Three classes of crushed limestone coarse aggregates of 5-10 mm (CA1), 5-14 mm (CA2), and 5-20 mm (CA3) were employed. The CA1 aggregate had a saturated surface dry (SSD) density of 2.78 g/cm^3 and water absorption of 0.55%. These values were 2.74 g/cm^3 and 0.63% for the CA2 aggregate and 2.76 g/cm^3 and 0.49% for the CA3 aggregate. Natural river sand with a SSD density of 2.66 g/cm^3 and water absorption of 1.01% was employed for the fine aggregate. The PSD of all solid materials is shown in Figure 1. The packing densities of sand and coarse aggregate were evaluated using a dry method. A sample of the granular material, previously oven-dried at 110 °C for 24 hours, was poured in a cylindrical container and undergone 1 min of simultaneous vibration and 10 kPa pressure. Knowing the mass of the sample and its final bulk volume, the density of the material was calculated. The ratio of the computed density to the real density of the material was considered as the packing density. The packing density of the combinations of materials was calculated by means of the compressible packing method (CPM) [18].

The concrete mixtures were mixed in a drum mixer with 100 L capacity. The mixing procedure started with homogenizing the sand and coarse aggregate in the mixer, then introducing half of the water and mixing for 1 min. All the powder materials were then added, and mixing was resumed for 30 s. Without turning the

mixer off, the second half of the water with SP diluted in it was added and mixing continued for 2.5 min. The mixture was left at rest for 2 min, after which it was remixed for another 3 min.
Testing included the determination of slump flow (ASTM C1611), T_{50}, and VSI, J-ring (ASTM C1621), V-funnel (PCI TR-6-03), unit weight and air content (ASTM C231), and column segregation (ASTM C1610). Compressive strength (ASTM C39) was measured at 7, 28, and 56 days using 100 × 200 mm cylindrical specimens.

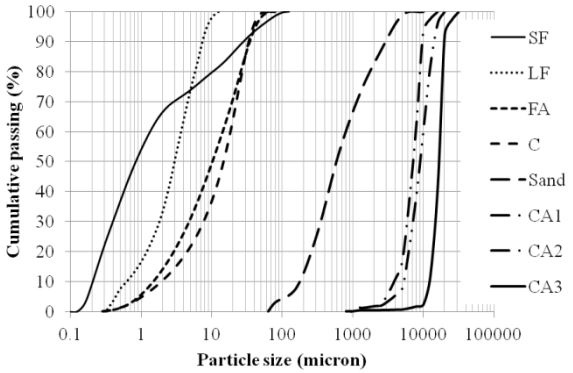

Figure 1. Particle size distribution of solid materials

Proposed Design Method

The proposed design process can be summarized in four main steps: (1) The maximum binder volume is fixed at 10% of the total concrete volume (100 l/m^3), which corresponds to 315 kg/m^3 for a concrete made with portland cement with a specific gravity of 3.15. The water volume is set to 20% of the total concrete volume for non-air-entrained Eco-SCC to ensure a minimum matrix volume to meet self-consolidation requirements as well as the robustness of mixtures [17]. For air-entrained mixtures, this volume can be reduced to around 17% (2). The volumetric proportions of sand and coarse aggregate are optimized in accordance with an ideal grading curve fitting the FD model. The distribution modulus (q) of the FD model is set to 0.26 for the employed materials as explained below. (3) Powder composition is determined in a way to decrease the water demand for a given workability level based on rheological measurements on pastes containing SCMs and fillers as cement replacement. The limits imposed by hardened properties (such as minimum compressive strength or durability aspects) are also considered before making the final choice of powder composition. (4) The SP saturation point is determined for the selected powder composition using the

method described subsequently. The initial SP content used in the Eco-SCC mixtures should be around 85% of this value.

Regarding q in the FD equation, it should be determined in a manner so that the resulting optimized combination of sand and coarse aggregate has both a high packing density and enhanced passing ability. Concerning the latter, a lower total volume of coarse aggregate and a lower volume of coarse aggregate near the MSA reduces the risk of blocking. For the available materials here, a q value of 0.26 provides a high packing density while limiting the total coarse aggregate volume (33% of total concrete volume) and the volume fraction of the coarsest aggregate class, CA3 (a CA1 to CA3 volumetric ratio of 1.46).

Rheological measurements are carried out on pastes with constant SP contents and *w/p* to ensure self-consolidation and stability. Samples are mixed in a Hobart mixer. Powder is added to the water with the SP diluted in it, and the mixture is mixed for 2 min at low speed. The mixer bowl and vane are scarped for 30 sec after which the mixing is resumed for 3 min at medium speed. A ConTec Viscometer 6 rheometer is employed for the measurements which start with a 45 s pre-shearing period at 0.7 rps rotational velocity. This maximum speed is then reduced step-wise over 14 intervals, each with a constant speed, to the minimum velocity of 0.025 rps. The Bingham model is used to calculate the yield stress and plastic viscosity of the tested sample.

Figure 2 presents the evolution of rheological properties with different cement replacement rates for the SCMs and the filler studied. Replacing cement with SF up to 7.5% increases yield stress but slightly decreases viscosity. Replacement of cement with FA-F decreases yield stress but increases viscosity. Substituting cement with LF up to 30% reduces both yield stress and viscosity. Thus, replacement rates (volume based) of SF, FA, and LF are limited to 5%, 50%, and 10%, respectively. Such values ensure desirable rheological properties as well as acceptable hardened performance.

The saturation point is measured by means of the Marsh cone test [19]. The Marsh cone (with an orifice diameter of 4.75 mm) is filled with 1200 mL of grout, and the flow time needed for 700 ml of grout to flow out is recorded. Tests are carried out on grouts made with *w/p* representing that of concrete. Solid materials finer than 125 μm are considered as powder except for the fine portion of sand. The same procedure as the rheological measurements is used to prepare the samples in a Hobart mixer.

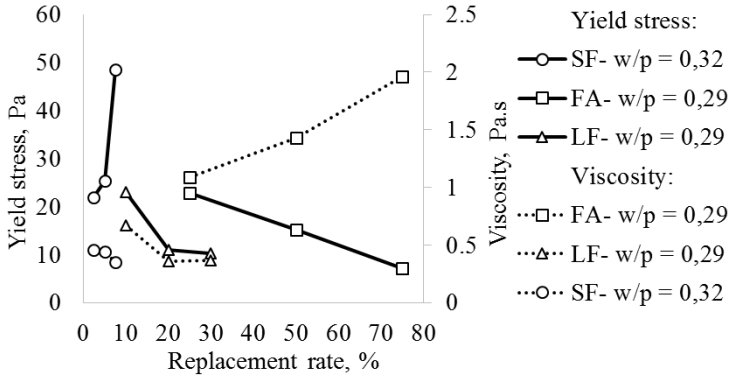

Figure 2. Effect of SCMs or filler on rheological properties of pastes

Optimized mixtures

Four optimized Eco-SCC mixtures obtained from the proposed design procedure were studied. Table I presents the mixture proportions of the optimized mixtures. Table II shows the properties of these mixtures. Regarding the slump flow value (sf), all mixtures were in the acceptable SCC range although the SP demand varied between the mixtures. For the same range of slump flow, mixtures 50%SF and 5%SF+10%LF showed a lower SP demand. The particle packing density of sand and coarse aggregate ($\alpha_{S\text{-}CA}$) was similar for all mix designs. In terms of passing ability characterized by the spread between the slump flow and the J-ring flow (sf-Jr), all mixtures met the requirement specified by ASTM C1621 (maximum difference $\leq$ 50 mm). The V-funnel flow times were relatively low (from 2 sec to 3.5 sec) as expected for this type of concrete. The four Eco-mixtures exhibited acceptable stability level (Si) with 5%SF+30%FA and 5%SF+10%LF being slightly more stable. The air content ranged between 1.5% and 4%. The 28-day compressive strength is within the targeted range of 25 to 35 MPa. Thus, all mixtures designed by the aforementioned procedure met the requirements for SCC in the fresh state and showed acceptable compressive strength. The next section investigates the influence of design variations on some of the optimized mixtures.

Table I. Mixture proportioning of optimized Eco-SCC

	Mixture			
	5%SF	5%SF+30%FA	50%FA	5%SF+10%LF
C, kg/m^3	302	218	169	274
SF, kg/m^3	12	11	-	15
FA, kg/m^3	-	75	131	-
LF, kg/m^3	-	-	-	30
Total powder, kg/m^3	314	304	300	319

Sand, kg/m^3	925	922	916	911
CA1, kg/m^3	541	540	536	533
CA3, kg/m^3	368	367	364	362
Water, kg/m^3	204	198	195	203
SP (liquid), kg/m^3	2.25	2.19	1.91	2.03

Table II. Optimized Eco-SCC mixtures properties

		Mixture			
		5%SF	5%SF+30%FA	50%FA	5%SF+10%LF
sf, mm		660	650	630	645
T_{50} sec		0.8	1.4	3.0	1.1
VSI		2	1	1	1
sf-Jr, mm		45	25	55	45
Vf_t, sec		2.0	2.5	3.5	2.0
Si, %		14.5	9.0	15.0	10.0
f'_c, MPa	7 day	27	24	17	26
	28 day	36	36	26	40
	56 day	39	39	30	40
$\alpha_{S\text{-}CA}$		0.833			

Variations in Optimized Mixtures

An investigation was undertaken to evaluate the effect of the variation of coarse aggregate grading on the performance of Eco-SCC mixture. Two mixtures were made based on the 5%SF+30%FA concrete with one of them having the CA3 fraction replaced with the same volume of CA2. This concrete was referred to as mixture N-5%SF+30%FA. In the other mixture, named N-5%SF+30%FA-14, the CA1 and CA3 fractions were replaced by the CA2 aggregate on a volume basis. The data presented in Table III indicate that for both mixtures, the deviation of coarse aggregate grading from the ideal curve had a significant impact on segregation resistance due to the lack of adequate lattice effect. For mixture N-5%SF+30%FA, the SP demand increased by 15% compared to the reference mixture. For the N-5%SF+30%FA-14 mixture, the V-funnel flow time increased, which can indicate an increase in the viscosity. This can be the reason of the slight increase in the slump flow – J-ring difference. The change in aggregate composition, on the other hand, had limited impact on compressive strength.

Table III. Properties of mixtures with varied coarse aggregate grading

	Mixture	
	N-5%SF+30%FA	N-5%SF+30%FA-14
SP, kg/m^3	2.51	2.20

sf, mm		660	670
T_{50} sec		0.8	1.4
sf-Jr, mm		30	70
Vf_t, sec		3.5	5.5
Si, %		20.5	20.0
f'_c, MPa	7 day	23	24
	28 day	34	36
	56 day	37	39
$\alpha_{S\text{-}CA}$		0.818	0.824

Mixtures 50%FA and 5%SF+30%FA were selected for the study of air-entrained mixtures. A 3% increase in the air content was assumed. In 50%FA, the same volume of water (30 l) was deducted from the mixing water to reach the air-entrained mixture, A-50%FA (*w/p* = 0.53). For the 5%SF+30%FA mixture, 21 l was removed since the mixture was not sufficiently workable. The latter mix design is referred to as A-5%SF+30%FA (*w/p* = 0.57). The air content of the mixtures was between 7% and 9%. From Table IV, an increase in the SP demand of 40% and 20% for the A-50%FA and A-5%SF+30%FA mixtures, was observed, respectively. The stability level of the A-5%SF+30%FA mixture compared to the original mixture was considerably lower. The compressive strength of the air-entrained mixtures was similar to those of the corresponding reference mixtures.

The effect of SF on stability was also investigated using two Eco-SCC mixtures based on the 5%SF+30%FA mixture. In the first one, called 35%FA, SF was replaced with the same volume of FA. The other mixture, named 35%FA+VMA, was the same as 35%FA but contained high relative dosage of VMA. The results, summarized in Table IV, demonstrated that eliminating 5% of SF from the 5%SF+30%FA mixture resulted in an unstable mixture. The incorporation of VMA significantly improved the stability of 35%FA+VMA mixture. The VMA use resulted in an increase in viscosity, which is reflected by a considerably higher V-funnel flow time. Using VMA also increased the SP demand by 70%. Both the 35%FA and 35%FA+VMA mixtures exhibited the same strength classes.

Table IV. Properties of air-entrained mixtures and mix designs used to investigate the effect of SF and VMA on performance

	Mixture			
	A-5%SF+30%FA	A-50%FA	35%FA	35%FA+VMA
SP, kg/m^3	2.56	2.61	1.92	3.71
VMA, kg/m^3	-	-	-	1.67
sf, mm	630	655	695	650
T_{50} sec	1.9	2.9	1.4	1.4
sf-Jr, mm	25	35	5	40
Vf_t, sec	3.5	4.0	3.0	11.0

Si, %		17.5	18.0	25.0	9.5
f'_c, MPa	7 day	23	19	21	20
	28 day	34	27	29	26
	56 day	38	31	33	31

Conclusions

A mix design procedure is proposed to develop low-binder Eco-SCC. The concept of optimization is based on ideal grading curve and requires limited effort for trial batches. The FD curve with a *q* value of 0.26 is shown to be an effective design criterion for Eco-SCC. Concrete mixtures with low powder content (300 kg/m^3) designed according to the proposed mix design method are shown to exhibit adequate passing ability, filling ability, and stability as well as compressive strength. It is found that deviation of PSD of coarse aggregate from the optimized PSD results in significant reduction in stability due to the compromising of the aggregate particle lattice effect. In addition, air-entrained mixtures with air content of 7% to 9% and low *w/p* of 0.53 to 0.57 exhibit similar behavior as the reference non-air-entrained mixtures with *w/p* of 0.65. Silica fume may be eliminated provided that an appropriate dosage of VMA is incorporated to enhance stability.

References

[1] Yang, K., Song, J. and Song, K. (2013), Assessment of CO_2 reduction of alkali-activated concrete, *J Clean Prod*, vol. 39, no. 0, p. 265-272.

[2] Turner, L.K. and Collins, F.G. (2013), Carbon dioxide equivalent (CO_2-e) emissions: A comparison between geopolymer and OPC cement concrete, *Constr Build Mater*, vol. 43, no. 0, p. 125-130.

[3] Flatt, R.J., Roussel, N. and Cheeseman, C.R. (2012), Concrete: An eco material that needs to be improved, *Journal of the European Ceramic Society*, vol. 32, no. 11, p. 2787-2798.

[4] Proske, T., Hainer, S., Rezvani, M. and Graubner, C. (2013), Eco-friendly concretes with reduced water and cement contents — Mix design principles and laboratory tests, *Cem Concr Res*, vol. 51, no. 0, p. 38-46.

[5] Damineli, B.L., Kemeid, F.M. and Aguiar, P.S. (2010), John VM. Measuring the eco-efficiency of cement use, *Cement and Concrete Composites*, vol. 32, no. 8, p. 555-562.

[6] Habert, G. and Roussel, N. (2009), Study of two concrete mix-design strategies to reach carbon mitigation objectives, *Cement and Concrete Composites*, vol. 31, no. 6, p. 397-402.

[7] Aitcin, P. (2000), Cements of yesterday and today - concrete of tomorrow, *Cem Concr Res*, vol. 30, no. 9, p. 1349-1359.

[8] Figueiras, H., Nunes, S., Coutinho, J.S. and Figueiras, J. (2009), Combined effect of two sustainable technologies: Self-compacting concrete (SCC) and controlled permeability formwork (CPF), *Constr Build Mater*, vol. 23, no. 7, p. 2518-2526.
[9] Hunger, M. (2010), An integral design concept for ecological Self-Compacting Concrete, *PhD Thesis*, Eindhoven University of Technology, Netherlands.
[10] Brouwers, H.J.H. and Radix, H.J. (2005), Self-Compacting Concrete: Theoretical and experimental study, *Cem Concr Res*, vol. 35, no. 11, p. 2116-2136.
[11] Funk, J.E. and Dinger, D.R. (1994), *Predictive process control of crowded particulate suspensions: applied to ceramic manufacturing*, Kluwer academic publ. Boston.
[12] Ghezal, A. and Khayat, K.H. (2002), Optimizing self-consolidating concrete with limestone filler by using statistical factorial design methods, *ACI Mater J*, vol. 99, no. 3, p. 264-272.
[13] Wallevik. O. and Nielsson, I. (1998), Self-compacting concrete – A rheological approach, In: *International Workshop on SCC, JSCE Concrete Engineering Series no. 30*, p. 136-159, Kochi, Japan.
[14] Fidjestol, P., Wallevik, O., Nielsson, I. and Holton, I. (2003), Topic concrete: rationale, "development and laboratory performance of an environmentally friendly concrete for piling application", In: *3rd Int. Symposium on SCC*, p. 920-931, Rilem, Reykjavik.
[15] Wallevik, O.H., F.V. Mueller, B. Hjartarson and Kubens, S. (2009), The green alternative of self-compacting concrete; Eco-SCC, In: *HV 2.29*, p. 12, iBausil, Germany.
[16] Mueller, F.V. and Wallevik, O.H. (2009), Effect of maximum aggregate Size in air-entrained Eco-SCC", In: *Rilem SCC-China*, p. 7, Beijing.
[17] Mueller, F.V. (2012), Design criteria for low binder self-compacting concrete, Eco-SCC', *PhD Thesis*, Reykjavik University, Iceland.
[18] de Larrard, F. (1999), *Concrete mixture proportioning: a scientific approach*, London: E & FN Spon, London.
[19] Hanna, E., Luke, K., Perraton, D. and Aitcin, P. (1989), Rheological behaviour of Portland cement in the presence of a superplasticizer, In: *Proceedings of the 3rd international conferences on superplasticizer and other chemical admixture in concrete*, p. 171-188, Ottawa.

Adaptation of SIMPLEX Method for Studying Rheology of SCC Cement Pastes using Mixture Experimental Design

Givanildo Alves de Azeredo[1], Guilherme Urquisa Leite[2] and Aline Figueiredo Nóbrega de Azeredo[3]

[1] Professor at Federal University of Paraíba - Brazil
[2] Master Student at Federal University of Paraíba - Brazil
[3] Professor at IFPB – Brazil

Abstract Mixture methods for self-compacting concrete (SCC) are an important step in the development of this type of concrete, since it must comply with specific performance in both fresh and hardened states. For many researchers the performance of SCC is mainly related to the properties of the cement paste. These properties are result from the proportion among the constituent materials. The use of a mixture experimental design seems to incorporate the assumptions necessary to understand the relationship between the proportion of the constituents and the paste characteristics. In this way, a specific mixture experimental design is proposed to map, in a simplex experimental region, the ideal proportions among the constituents to obtain a paste with a suitable rheology to be used in the production of SCC.

Keywords: *Mixture experimental design, Rheology, SCC, Cement paste, SIMPLEX.*

Introduction

The self-compacting concrete (SCC) originated in Japan in the late 80s by the need to obtain more durable structures, due to problems in buildings attributed to molding steps of structural elements [1]. It fills the forms completely, without the need for external vibration or the occurrence of segregation of components. This promotes time gain and labor savings, in addition to the reduction of noise [2,3]. SCC served then as a topic for many researches, particularly regarding the dosage. Many researchers believe that the paste governs self-compacting properties of concrete (liquid phase). Once a cement paste possesses the appropriate

characteristics, in sufficient quantity, it provides the concrete with the self-compacting status [2,4-7].Herschel-Bulkley fluid fits well the rheological behavior of concentrated suspensions such as SCC and cement pastes [6, 8]. However, many experts consider that Bingham model is suitable to describe with sufficient precision such behavior [6, 8].
In order to gain time and savings in buying materials, the experimental design is a useful tool, allowing the acquisition of results statistically verified [9-11,12].
In a mixture experimental design, the properties vary with the relative proportions of the components [13, 14]. In the mixture, if x_i is the proportion of material *i* and *n* is the total number of components, it gives the Eqn. (1):

$$\sum_{i=1}^{n} x_i = 1 \quad (1)$$

$$0 \leq x_i \leq 1 \quad (2)$$

A simplex with dimension n-1 represents an experimental region of a mixture (Fig. 2) [15]. Sometimes, technical or economic reasons do not allow the use of Eqn. (2). Thus, lower (Li) and upper (Ui) limits can be set for the proportions of these components. Eqn. (2) becomes then as follows, shown in Eqn. (3):

$$0 \leq L_i \leq x_i \leq U_i \leq 1 \quad (3)$$

New limits imply that the experimental region studied will become a sub-set of the original simplex [14, 15]. This research aims at defining an experimental mixture design using a pseudo simplex method, proposed by [16].

Experimental Procedure

Design of experiments

Eqns. (4), (5), (6) and (7) show lower and upper limits for each component. Those for cement are a function of limits of other components. Upper limits of limestone filler and superplasticizer defined lower limit of cement and lower limits of limestone filler and superplasticizer defined upper limit of cement.

$$L_i \leq x_i \leq U_i \quad (1)$$

$$0{,}008 \leq x_{SP} \leq 0{,}02 \quad (5)$$

$$0{,}2 \leq x_F \leq 0{,}4 \quad (6)$$

$$0{,}58 \leq x_c \leq 0{,}792 \quad (7)$$

where x_i is the proportion of material *i* in the mixture; L_i and U_i represent the lower and upper limits of the proportion of material *i* in the mixture, respectively; x_{SP}, x_F and x_C are the proportions by weight of superplasticizer, filler and cement in the

mix, respectively. Figure 1a) shows the complete simplex region while Figure 1b) represents the sub-region simplex restricted by the upper and lower limits of the components.

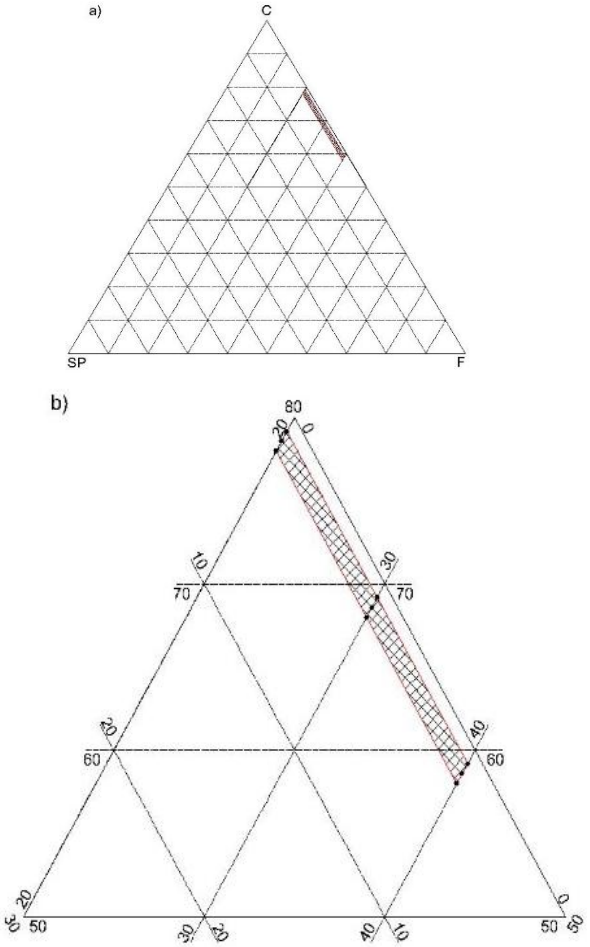

Figure 1. Simplex of the paste with lower and upper limits in all components: a) Complete simplex region; b) Details of limited regions by imposing limits. Source: Author

Cornell [14, 15] also states that when the range variation of the proportion in one component is at very low order, such as the superplasticizer (Figure 1a)), there is a risk of generating co-linearity among the terms of the model that takes into account such proportion as a variable. This study developed a special procedure named pseudo-simplex method in order to carry out this planning.

Pseudo-Simplex Method

This method applies three components to the mixture where upper limits or upper and lower limits are applied to two of these components and the third one is restricted by the mixing definition, conditioned to the remaining amount of material to complete 100%. In addition, binary mixture occurs in only one point among the components B and C. This means that the proportion of component A is zero in only one point at most. When one observes these conditions, a sub-region parallelogram-shaped from the original simplex represents the experimental region. Figure 2 shows a drawing of this sub-region.
The method [16] suggests creating four pseudo-components from the union of the original components in the proportions that represent the vertices of the sub-region formed by the limitations in the B and C material (Figure 2). Therefore, for that, there are the following proportions:

$$C_1 = U_B\ of\ B + L_C\ of\ C + (1 - U_B - L_C)\ of\ A \quad (8)$$
$$C_2 = L_B\ of\ B + U_C\ of\ C + (1 - L_B - U_C)\ of\ A \quad (9)$$
$$C_3 = L_B\ of\ B + L_C\ of\ C + U_A\ of\ A \quad (10)$$
$$C_4 = U_B\ of\ B + U_C\ of\ C + L_A\ of\ A \quad (11)$$

where C_j are composites composed by materials components A, B and C, with j=1,2,3,4; U_i and L_i are the upper and lower limits of proportion of material *i* in the mix, with *i*=A,B,C.

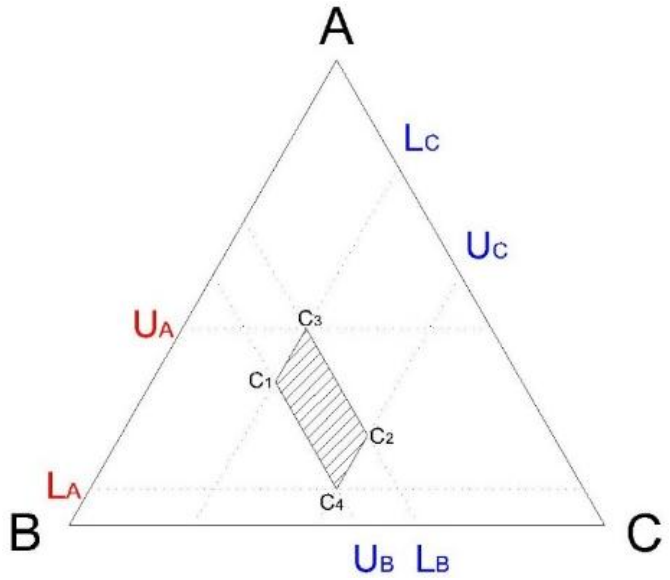

Figure 2. Simplex for a 3-component mixture (A, B and C) with upper and lower limits. Source: Author

From these composites, union of two simplex regions formed by mixtures C_1 + C_2 + C_3 and C_1 + C_2 + C_4 form a region like a diamond. C_3 and C_4 composites are at opposite ends of diamond vertices and the lines that define the binary mixture between C_1 and C_2 match in both simplexes.
The use of this method implies that two equations describe the response, one for each mixture of three composites. Therefore, it is necessary to define a routine that indicates when using each equation in terms of the initial components of mixture. Any binary mixture that occurs between pseudo-components C_1 and C_3 results in a composite that has the percentage equal to the lower limit of the material C (L_C), while the percentage of material B increases as proportion of C1 increases.
Thus, if one wishes to correlate, graphically, the responses to the real components, R_B is a reference value that measures the relative distance from the C_2C_3 side to the line that is parallel to it, limited by lower and upper limits of material B. On the other hand, R_C measures the relative distance from C_1C_3 side to the line that is parallel to it, limited by lower and upper limits of material C. Such values come from Eqn. (12):

$$R_i = \frac{x_i - L_i}{U_i - L_i} \tag{122}$$

where: x_i is the percentage of the material i in the mix with $i = B, C$.
The Ri value ranges from 0 and 1. When $x_i = L_i \rightarrow R_i = 0$, and when $x_i = U_i \rightarrow R_i = 1$.
Therefore, considering these observations, one can define a criterion for choosing equations that describe simplex response related to C_1+ C_2+ C_3 or C_1+C_2+C_4 mix. This method allows working with two simplex entire regions, instead of a sub-region of simplex. In addition, the risk of co-linearity decreases.

Conclusions

The method guarantees good analysis of three components that constitute the mixture with no risk of co-linearity. Visually, it brings a great advantage when observing the influence of material whose content level is very low. Also, defining experimental points in a region already limited by required lower and upper levels optimizes the chance of obtaining the better mixes for the production of SCC cement pastes. Finally, as the experimental design of mixtures is very useful in the production process, and still not usually used in concrete production, the method proposed here contributes to the state of art concerned.

Acknowledgements

We would like to thank to Dolomil and Grace Brazil LTDA plants, for donating the filler and admixtures used in this research. The authors acknowledge also the CAPES, that provided scholarship to the Master student.

References

[1] Okamura, H.; Ouchi, M. (2003), Self-compacting concrete. *Journal of advanced concrete technology*, v. 1, n. 1, p. 5-15.
[2] Azeredo, G.; Diniz, M. (2013), Self-compacting concrete obtained by the use of kaolin wastes. *Construction and Building Materials*, v. 38, p. 515-523.
[3] Shindoh, T.; Matsuoka, Y. (2003), Development of combination-type self-compacting concrete and evaluation test methods. *Jour. of Advan. Conc. Techn.*, v. 1, n. 1, p. 26-36.
[4] Bui, V. K.; Montgomery, D. (1999). In: Mixture proportioning method for self-compacting high performance concrete with minimum paste volume. *International rilem symposium on self-compac. concrete*, 1, Stockholm, p. 373-384.
[5] Gomes, P. C. C.; Gettu, R.; Agulló, L. (2003). In: Uma nova metodologia para obtenção de concretos auto-adensáveis de alta resistência com aditivos minerais. *V Simpósio EPUSP sobre Estruturas de Concreto*, p. 1-14.
[6] Sedran, T.; De Larrard, F. (1999). In: Optimization of self-compacting concrete thanks to packing model. International rilem symposium on self-compacting concrete, 1, Stockholm.
[7] Wu, Q.; An, X. (2014), Devel. of a mix design method for SCC based on the rheological characteristics of paste. *Const. and Build. Mat.*, v. 53, p. 642-651.
[8] Chen, J. J.; Kwan, A. K. H. (2012), Superfine cem. for improve. Packi. density, rheol. and streng.of cem.paste. *Cem. and Concr. Compos.*, v. 34, n. 1, p. 1-10.
[9] Rodrigues, M. I.; Lemma, A. F. (2009). In: Planejamento de experimentos e otimização de processos. 2. ed. Campinas. 358 p.
[10] Montgomery, D. C.; Runger, G. C. In: Applied statistics and probability for engineers. 6. ed. Hoboken: John Wiley & Sons, 2014. 832p.
[11] Olubanwo, A. O.; Karadelis, J. N. (2015), Applied mixture optimization techniques for paste design of bonded roller-compacted fibre reinforced polymer modified concrete (BRCFRPMC) overlays. *Materials and Structures*, p. 1-20.
[12] Mebrouki, A.; Belas, N.; Bendani, K.; Bouhamou, N. (2009), A self compact. cement paste formul. using mixture design. *Jour. of app. Scien.*, v. 9, p. 4127-4136.
[13] Scheffe, H. (1963)The Simplex-Centroid Design for Experim. with Mixt.. *Jour. of the Royal Statist. Socie.*. Series B (Methodological), v. 25, n. 02, p. 235-263.
[14] Cornell, J. (2011). In: A Retrospective View of Mixture Experiments. Quality Engineering, v. 23, n 04, p. 315-331.
[15] Cornell, J. (2002). In: Experiments with mixtures: designs, models, and the analysis of mixture data. John Wiley & Sons.
[16] Leite, G. U. (in progress). In: Uso do planejamento experimental de misturas na obtenção de concretos auto-adensáveis. Dissertação de Mestrado. Programa de Pós-Graduação em Engenharia Civil e Ambiental (PPGECAM).

Optimization of Mix Proportioning for Self Compacting Concrete using Particle Packing Theories

K.L.Radhika[1,2], P. Rathish Kumar[3], M. Sri Rama Chand[2] and B. Prasad[4]

[1]Assistant Professor, Department of Civil Engineering, UCE, OU, Hyderabad
[2] Research Scholar, Department of Civil Engineering, NIT, Warangal
[3]Associate Professor, Department of Civil Engineering, NIT, Warangal
[4] Graduate Student, Department of Civil Engineering, NIT, Warangal

Abstract: It is universally agreed that by controlling the aggregate phase, paste quality and quantity the basic requirement for producing SCC mixes can be achieved. Reduction in the voids content in the aggregates and the content of cement paste which is required to cover aggregate surface, workability improves, voids are reduced and thereby the strength and durability properties of SCC can be enhanced. This can be achieved by improving the pore structure possible by designing the concrete mix using Particle Packing Models (PPM).The main objective of the present investigation is focused on optimizing a mix proportioning method based on PPM to satisfy the requirements of SCC. It was noted from the detailed experimental study that the Compressible Packing Model (CPM) based optimization of mix design methodology is best suitable for designing SCC as it considers the important parameters like wall effect and loosening effect which are important in deciding the aggregate portion of SCC. It can be concluded based on this study that it is possible to obtain an economical and more reliable mix design methodology using CPM model.

Keywords: *Self compacting concrete, Compressible packing model, Loosening effect, Wall effect, Perturbed volume.*

Introduction

Particle packing theory is not only important in the concrete industry but also other fields such as ceramic industry, geotechnological industry, food processing industry etc. are benefitted with this theory. The very first investigation on particle packing was done by Dinger D R & Funk J E, [1]. If we assume the monosized particles which are spherical in shape, its packing density depends upon the structure formed by them. According to White H E & Walten S F [2], if the smaller sphere shaped particles are induced to fill the voids between the larger sphere the PD of the system has been increased. Further studies has been extended to make use of two or more sized spheres by R K Mc Geary [3] where in a blend of spheres with size ratio of 3.5:1 with an individual packing density of 0.63 each, improves the PD to 0.70.To access the voids in between the larger grains, the smaller should have a diameter equal to 15.4% of the larger grain having size ratio of (6.5:1). It concluded that by increasing the number of grain sizes, the PD could be increased. According to Dinger D R & Funk J E [1], since nature does not provide monosized grains and the main problem being that the smaller sized grains cannot be provided in its place between the larger particles, it is required to develop many more models which leads to real particle size distribution. With this basic concepts there are many models developed by different researches over the past several years to calculate the real packing density of polysized mix grains [4 -15]. A number of computer - based mix proportioning methods have also been developed over the last few years [16 -18].These allow the engineer to determine the optimum combination of mix proportions that will provide a maximum packing density and minimise the void content. These computer based mix design methods adopted of the mathematical models available which can be used to determine the maximum packing density with minimum voids resulting from different combinations of materials.

Research Significance

Particle packing models are based on the concept that voids between larger particles would be filled by the smaller particles there by reducing the volume of the voids and increasing the packing density. Concrete being one of the most important construction materials, it is not so comparable with the demands of sustainable development because manufacturing of cement generates a large amount of carbon dioxide and therefore cement consumption produces a huge carbon footprint. Particle packing models which are used to estimate the packing

density/void ratio of the solid combination can provide tool to improve the performance of concrete by reducing the voids and maximizing the solids. Concrete proportioning being the packing problem all existing methods recognize this problem by suggesting the measurement of the packing parameter of some component or by approximating an 'ideal' grading curves. Therefore, there is a requirement to select the appropriate model which satisfies the specified requirement for SCC. With this requirement an attempt has been made to select an appropriate packing model for proportioning of aggregate which suits the requirements.

Optimization of Aggregate Proportions

In the present investigation the main focus is to make use of the concept of particle packing theory for aggregate mix proportioning. Different models like Modified Toufar model, J D Dewar model, Compressible packing model are available in the literature to predict the optimized aggregate proportions for maximum packing density and minimum void ratio. The models mentioned are used to determine the maximum packing density for poly sized aggregate materials. In the present work, individual mono sized aggregate materials: Four coarse aggregate groups'20mm-16mm', '16mm-12.5mm', '12.5mm-10mm' and '10mm-4.75mm', four fine aggregate groups '4.75mm- 2.36mm', '2.36mm-1.18mm', '1.18mm-0.6mm' and '0.6mm-0.15mm' are used for blending. Table I shows the physical properties of mono sized aggregate proportions.

Table I. Physical properties of mono sized aggregate proportions

Aggregate Size (mm)	20-16	16-12.5	12.5-10	10-4.75	4.75-2.36	2.36-1.18	1.18-0.6	0.6-.15
Mean Aggregate Size	17.89	14.14	11.18	6.89	3.35	1.67	0.84	0.424
Initial Weight Ws, kg	7.5	7.3	7.38	7.21	7.9	8.04	7.91	7.71
Bulk density (kg/m^3)	1414	1376	1392	1360	1490	1516	1492	1454
Specific Gravity	2.65	2.65	2.65	2.65	2.42	2.42	2.42	2.42

Φ	0.534	0.520	0.525	0.513	0.616	0.627	0.616	0.601
	Height of the Container-300mm				Diameter of the container-150mm			

Modified Toufar Model

This technique can be used to design multi-source aggregate blend volume proportions by maximizing the packing degree of the combined gradation. The individual aggregate properties required to be inputted for this particle packing model are the particle size distribution, relative density (in SSD condition), and loose bulk density (in SSD condition). For poly dispersed blending, a stepwise binary blending process is used where the two aggregate materials with the highest diameter ratio are first blended (Goltermann et al, 1997). The process of blending is carried separately for coarse aggregate materials and fine aggregate materials and the maximum packing density for poly dispersed mixes is obtained by binary blending of CA and FA. The Final optimized aggregate proportions for poly dispersed mixes are shown in Table II.

Table II. Optimized aggregate proportions for poly dispersed mixes (MTM)

Size	CA/FA	20 - 16	16 – 12.5	12.5 – 10	10 - 4.75	4.75 – 2.36	2.36 – 1.18	1.18 – 0.6	0.6 – 0.15	Ø
20mm	40/60	0.14	0.06	0.08	0.12	0.22	0.14	0.12	0.12	0.807
16mm	40/60	-	0.16	0.10	0.14	0.22	0.14	0.12	0.12	0.798
12.5mm	35/65	-	-	0.23	0.12	0.24	0.13	0.15	0.13	0.791

Theory of Particle Mixtures (JD Dewar Method)

In Dewar's model, the voids ratio, U and the log mean size, d_m of each single material are used to calculate the voids ratio of a particular combination of materials. For poly dispersed blending, a stepwise binary blending process is used where the two finest materials are first blended. Similar to MTM, here also the aggregate materials are primarily divided into coarse and fine, and blending operations are continued step by step Table III shows the optimized aggregate proportions by JD Dewar method.

Table III. Optimized aggregate (NA) proportions for poly dispersed mixes (JDDM)

Size	CA/FA	20 - 16	16 – 12.5	12.5 – 10	10 - 4.75	4.75 – 2.36	2.36 – 1.18	1.18 – 0.6	0.6 – 0.15	Ø
20mm	35/65	0.12	0.07	0.09	0.07	0.36	0.15	0.06	0.08	0.777
16mm	31/69	-	0.10	0.12	0.09	0.38	0.16	0.08	0.07	0.769
12.5mm	28/72	-	-	0.16	0.12	0.39	0.17	0.09	0.07	0.762

Compressible Packing Model

Compressible Packing Model (CPM) has been developed by De Larrard. The model requires the particle size distribution (PSD) to be measured for all constituent materials. PSD is expressed as the fraction retained in each size group, y_i, % by volume. The mean size of a clustered size class, d_i is calculated as the log mean and arranged in a sequence such that $d_i > d_{i+1}$. Wall effect, container effect and loosing effect are considered in this method for better packing. The calculation of the aggregate proportions for a poly-disperse mixture along with the Virtual Packing Density is calculated as explained by the author's paper elsewhere [19]
The final mix proportions of 20mm, 16mm and 12.5mm nominal size aggregates are obtained for minimum virtual packing density. Table IV shows the aggregate proportions for poly disperse mixture.

Table IV. Aggregate proportions for a poly disperse mixture

CA/FA	20-16	16-12.5	12.5-10	10-4.75	4.75-2.36	2.36-1.18	1.18-0.6	0.6-0.15	γ_{min}
40/60	0.04	0.04	0.12	0.2	0.03	0.06	0.21	0.30	0.872
40/60	-	0.05	0.05	0.3	0.03	0.06	0.21	0.30	0.870
40/60	-	-	0.05	0.35	0.03	0.06	0.21	0.30	0.870

Comparison of Various particle packing models for graded aggregates

A comparison is made on optimum aggregate proportions obtained from various particle packing models. From the percentage weight retained on IS Sieves, the percentage passing is calculated for 20mm, 16mm, 12.5mm graded coarse aggregates and fine aggregates using Compressible Packing Model, Modified

Toufar Method and JD Dewar Method. Table V shows the percentage passing for graded aggregates of different sizes. From the percentage passing values, it can be observed that the percentage passing values calculated by MTM and JD Dewar shows high coarser content, but CPM suggests high finer fraction.

Table V. Percentage passing for graded aggregates of nominal size 20, 16 & 12.5mm

IS Sieve Designation	CPM			Modified Toufar Method			J D Dewar Method		
	20	16	12.5	20	16	12.5	20	16	12.5
40mm	100	-	-	100	-	-	100	-	-
20mm	100	100	100	100	100	100	100	100	100
16mm	90	100	-	65	100	-	66	100	-
12.5mm	80	87.5	100	50	65	100	46	68	100
10mm	50	75	87.5	30	35	34	20	29	43
4.75mm	0	0	0	0	0	0	0	0	0
2.36mm	-	-	-	-	-	-	-	-	-

Table VI shows the percentage passing for fine aggregate obtained through optimum aggregate proportions. The amount of aggregate passing on top sieves of fine aggregate is higher with CPM whereas, the amount of aggregate passing is less for other methods.

Table VI. Percentage passing for fine aggregate

Sieve Size	CPM Method	ModifiedToufar Method	J DDewar Method
10 mm	100	100	100
4.75 mm	100	100	100
2.36 mm	95	63	45
1.18 mm	85	40	22
0.60 mm	50	20	11
0.30 mm	-	-	-
0.15 mm	0	0	0

Suitable Particle Packing Model for Self Compacting Concrete

Self Compacting Concrete requires more fine content than ordinary vibrated concrete for better flowability, passing ability and segregation resistance. The aggregate proportions suggested by Modified Toufar method and J D Dewar method are suitable for vibrated concretes, because the proportions of aggregate shows coarser fractions and the methods itself are designed for vibrated concretes. But, the Compressible Packing Model suggests less coarse fractions in maximum size sieves and gives appropriate proportions for Self Compacting Concrete. Hence, for Self Compacting Concrete, the suitable Particle Packing Model is Compressible Packing Model.

Experimental Work

An experimental program is conducted to determine the suitability of compressible packing model. It was decided by designing mix proportions for different grades of SCC (M20, M40 and <60) taking optimized aggregate proportions. From the optimized aggregate proportions obtained by CPM, Packing factors are calculated experimentally for different graded sizes of aggregate. Packing factor affects the aggregate content in SCC mix proportions and is defined as the ratio of mass of aggregate of tightly packed state to that of loosely packed state [19]. Nan Su Mix design methodology [19] is adopted here to obtain the mix proportions. The mixes for three grades of SCC (M20, M40 and M60) are shown in Table VII.

Table VII. Mix proportions for self compacting concrete

Mix	CA/FA	PF	Cement Kg/m^3	Fly Ash Kg/m^3	Fine Aggregate Kg/m^3	Coarse Aggregate Kg/m^3	Water Kg/m^3	SP Kg/m^3
M20	40/60	1.234	220	180	1088.4	696.00	197	2.2
M40	40/60	1.210	350	150	1067.22	682.00	190	3.5
M60	40/60	1.190	470	135	1049.6	671.00	186	5.6

Materials used in the experimentation

Cement used in the investigation was 53 Grade Ordinary Portland cement [20]. The specific gravity of cement was 3.14 and specific surface area of 225 m^2/g having initial and final setting time of 40 min and 560 min respectively. River sand was used as natural fine aggregate; whereas crushed granite was used as natural coarse aggregate. The physical properties of aggregates are already represented in Table 1.

In the present investigation, poly carboxylic ether based water-reducing admixture confirming ASTM C494 was used as super plasticizer for improving flow or workability.

Fresh Property Tests

The final selection of mix design was mainly based on their relation to one or more of the key properties of SCC (filling ability, passing ability, and resistance to segregation) as well as on reproducibility and repeatability. Various Fresh properties- slump flow, L-box, J-ring, and V-funnel tests were carried out on Self Compacting Concrete of different grades. The fresh property test results of M20, M40 and M60 SCC are shown in Table VIII and it was observed that all the three grades of SCC satisfies EFNARC specifications [21].

Table VIII. Fresh Properties of different grades of SCC

Mix	Slump Flow (mm)	T_{50cm} (sec)	V-Funnel (sec)	V_{5min} (sec)	L - box H_2/H_1	J-Ring (mm)
M20	653	4.3	10.53	13.15	0.85	9
M40	691	3.01	8.96	11.08	0.91	8
M60	685	3.12	8.97	10.68	0.93	6

Hardened Property Tests

Compressive strengths of different grades of SCC were determined by casting cube specimens (150mm × 150mm × 150mm) were tested under axial compression using 300 Tonne Compressive Strength Testing Machine under a load rate of 140 Kg/cm^2 as per IS:516-1999 [22]. Similarly, Split tensile strength and flexural strength of concretes were determined by casting cylinders (150mm diameter& 300mm height)and prisms (500mm × 100mm × 100mm). Three specimens were tested after 28 days curing period for each type of concrete and the average strength value was noted.

Results and Discussion

Mechanical Properties of SCC

Table IX shows the test results of M20, M40 and M60 grade of SCC after 28 days curing period. Compressive Strength values show that all grades of SCC have attained their target strengths after 28 days curing period.

Table IX. Mechanical Properties of SCC

Grade of Concrete	Compressive Strength (MPa)	Split Tensile Strength (MPa)	Flexural Strength (MPa)
M20	31.27	2.15	3.13
M40	51.27	4.12	4.44
M60	72.56	6.25	5.46

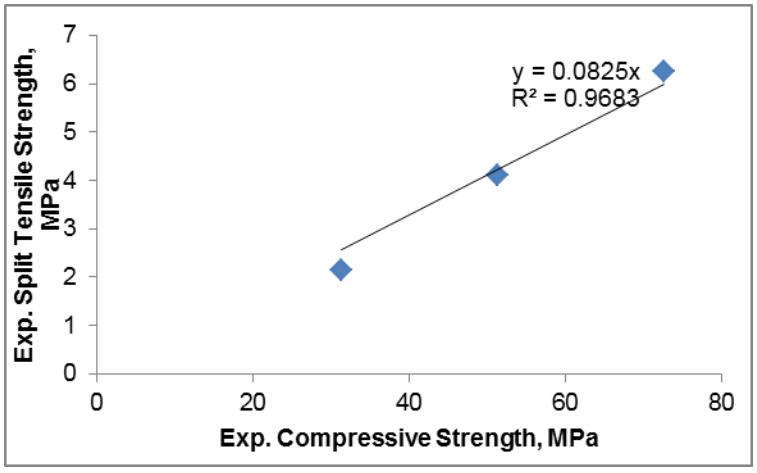

Figure 1. Compressive strength vs split tensile strength

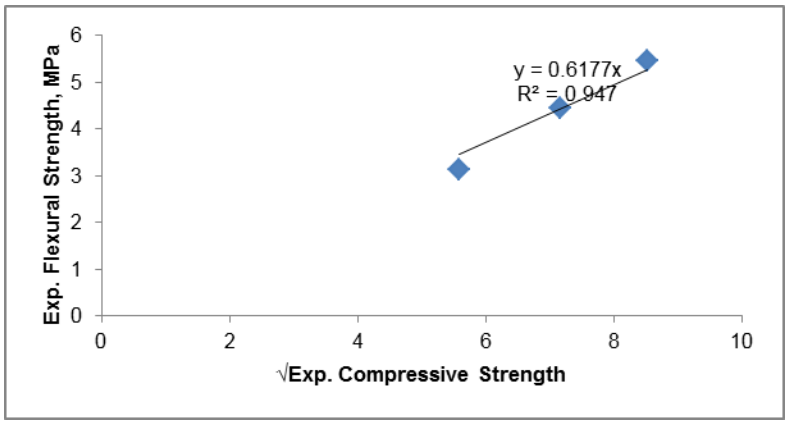

Figure 2. Compressive strength vs flexural strength

Conclusions

- Modified ToufarModel and J.D.Dewar Methods were basically established for vibrated concrete using binary, ternary and poly blending. In the present study these methods are used for poly dispersed groups and for SCC.
- Compressible Packing Model (CPM) is suitable for all grades of SCC, because it covers a wide range of factors like shape and size of the aggregate, loosening effect and wall effect along with the compaction effort which are not considered in other particle packing models.
- It was observed that as strength of the concrete increases, the packing factor decreases.
- It can be noted that all the fresh properties were satisfied for all three grades of SCC as per EFNARC specifications.

References

[1] Dinger D R & Funk J E ,(1994)Particle Packing Part 1-5,Interceram, Vol 41 no.1,2,3 -1992, Vol-42 no.3, 1993 and Vol 43 no. 2.

[2] White H E & WaltenS F (1936), Particle packing and Particle shape, Journal of the American Ceramic Society 20.

[3] R K Mc Geary (1961) Mechanical packing of spherical particles, Journal of American Ceramic Society, Vol 44, Issue 10,,pp 513-522.

[4] Furnas C. C. (1929), Flow of gasses through beds of broken solids, *Bureau of Mines Bulletin* 307.

[5] Aim R. B. and Goff, P. L. (1967) Effet de paroi dans les empilements desordonnes de spheres et application a la porosite de melanges binaries, Powder Technology 1, pp 281-90.

[6] Andresen P J and Johansen V(1991), Particle packing and concrete properties, Material Science of concrete : II , Skalny J and Mindess S (Edited),The Americal Ceremic Society,Inc.,Westyerville,Ohio, pp 111-147.

[7] Senthil Kumar V, Manu Santhanam,(2003) Particle packing theories and their application in concrete mix proportioning : A Review, Indian Concrete Journal , pp1324-1331.

[8] Stovall T, De Larrard F, Buil M,(1986) Linear packing density model for grain mixtures, Powder Technology 48, pp 1-12.

[9] Dewar J D, (1986) Ready-mixed concrete mix design, *Municipal Engineering* 3 Feb , pp 35-43.

[10] Goltermann P, Johansen V, Palbfl L, (1997) Packing of aggregate: An alternative tool to determine the optimal aggregate mix', ACI Materials Journal, Vol 94, No.5, pp 435-443).

[11] Franqois De Larrard,(1989) Ultrafine particle for making very high strength concretes',Cement and Concrete Research Vol 19, No 1, pp 161-172).

[12] Mangulkar M N , Jamkar S S, (2013) Review of Particle Packing Theory Used for Concrete Mix Proportioning, Journal of Scientific and Engineering Research, Vol 4, Issue 5.

[13] Radhika K L, P. Rathish Kumar, Rao S V, Krishna Rao M V, Manikanta. K "Mix Design Methodology for fibrous self compacting concrete based on Compressible Packing Model (CPM)", International Journal of Cement Wapno Beton, Vol.5, MARZEC-KWIECIEN 2012, ISSN-1425-8129, pp310-323

[14] Jones M R,Zheng and M D Newlands (2002) Comparison of Particle Packing Models for Proportioning Concrete constituents for minimum void ratio, Material and Structures, Vol 35, 2002, pp 301-309).

[15] De Larrard,(1999)Concrete Mixture Proportioning: A Scientific Approach', (E & FN Spon.

[16] Dewar.J.D.(1999) Computer Modelling of Concrete Mixtures, E & FN Spon.

[17] Europack (1995) Idorn, G. M, Europack V1.1 User Manual, Idorn G M Consult A/S.

[18] MixSim98 (1998) Questjay Limited, 'MixSim98-Operating Manual', Draft Version 5, Questjay Limited.

[19] Nan Su, Kung-Chung Hsu, His-Wen Chai,(2001) A simple mix design method for self-compacting concrete, Cement and Concrete Research, pp 1799-1807.

[20] IS: 12269, Indian Standard Code, Specifications for 53 Grade Ordinary Portland cement, Bureau of Indian Standards.

[21] Specifications and guidelines for Self Compacting Concrete, Published by EFNARC in February 2005.

[22] IS:516–1956(Reaffirmed 1999), Indian Standard Method of Tests for Strength of Concrete, Bureau of Indian Standards.

Mixture Compositions and Fresh Properties of Self-Compacting Concrete: Analysis of 25 Years of Research

Pieter Desnerck[1], Bart Craeye[2, 5], Veerle Boel[3] and Petra Van Itterbeeck[4]

[1] Concrete and Composites Structures Group, University of Cambridge, UK
[2] DUBiT Research Group, Odisee University College, BELGIUM
[3] Department of Structural Engineering, Ghent University, BELGIUM
[4] Belgian Building Research Institute (BBRI), BELGIUM
[5] EMIB Research Group, University of Antwerp, Belgium

Abstract Since its development in the late 1980's, numerous research projects have investigated the properties and performance of self-compacting concrete. Whereas early investigations focussed on the fresh properties, workability, mix design, durability and rheology, aspects such as structural behaviour, mechanical properties and flow modelling have gained more interest nowadays.
When looking into literature regarding self-compacting concrete, a wide range of materials can be noticed as well as a lot of different mix design approaches and targeted workability properties. For researchers, practitioners and designers new to the field, it can be hard to consolidate all this information as there is not one single way forward or approach to be taken.
In order to get a clear overview of the ranges in which properties and the materials used to produce self-compacting concrete may vary, an extensive database was developed containing results from over 250 papers published the last 25 years. Results for powder-type, VMA-type as well as combination-type SCC are gathered in the database.
The current paper looks into a statistical analysis of the mix proportioning of the different types of SCC, discussing amongst others the binder composition, aggregate type and origin, additions and additives used, as well as the ratios between the constituents (water-to-binder, water-to-cement, sand-to-aggregates, etc.). Furthermore, the achieved ranges of fresh properties (slump flow, V-funnel, L-box, sieve stability, etc.) are discussed. In this way a comprehensive overview is provided of SCCs produced for research purposes worldwide.

Keywords: *self-compacting concrete, database, fresh properties, mix composition, constituents*

Introduction

Self-compacting concrete (SCC) (1), also referred to as self-consolidating concrete, was developed in the late 1980's. In comparison with conventional vibrated concrete, SCC can be considered a new type of concrete with a different approach to mix design and rheological characteristics. Above that, SCC can be seen as a new approach to casting concrete, enabled by adjusted fresh concrete properties.

For more than 20 years, SCC has been applied in the construction industry. In this period, a lot of research has been performed in the field of the applicability, mix design, pump-ability, durability, rheology, etc. of SCC. In the nineties, little attention was devoted to the mechanical properties of the material and to its structural performance. Recently, an increasing amount of research has been dedicated to these mechanical properties as well (2).

In 2008 a RILEM Technical Committee was created focussing on the mechanical behaviour of SCC (RILEM TC-MPS 228). The main purpose of this committee was to create a state-of-the-art report (3) on the mechanical and structural behaviour of SCC. It was found that research projects often included data on compressive strength, tensile strength, and Young's modulus, although the main focus was on other aspects of the concrete, as mentioned above. Some authors, e.g. Domone (4) and Holschmacher (5), have presented surveys on the mechanical properties of SCC based on available literature at that time. Due to a scarce amount of available test results, these studies were based on a limited set of data. In this way they did not include, neglected or generalised the influence of some major parameters for the mechanical behaviour, such as type of aggregate or cement class. Therefore, it was decided, in the framework of the RILEM committee work, to develop an extensive database with results on fresh and hardened properties of SCCs reported between 1990 and 2013, originating from numerous journal and conference papers.

This database has been analysed in respect to compressive strength, tensile strength, Young's modulus, etc. The main focus of this paper, however, will be on the mix proportioning and fresh properties as included in the database. For information and analysis of the data with respect to the mechanical properties, reference is made to the RILEM report (3) or previously published papers (e.g. (6)).

Description of the Database

With results for a wide range of SCC types (Powder-type , VMA-type and Combination-type SCC) (1) taken from over 250 papers, an extensive dataset is available for thorough investigation of the mix proportioning and fresh properties of SCC's.

The database is structured around the concrete mixtures. From each paper the different mixtures are taken and implemented. Information is gathered (if available in the paper or by personal contacts with the authors) on the water content, cement content and type (Portland, binary types, etc.), addition content and type (limestone, fly ash, blast furnace slag, silica fume), viscosity modifying agent

(VMA) content, superplasticiser content and type (poly-carboxylic, etc.), air entrainment content, aggregate content, maximum aggregate size, etc. Besides that, details of the constituents' density, class (e.g. crushed/uncrushed in case of the aggregates), origin (e.g. sandstone, basalt, quartz, etc.), the solid content of the admixtures, etc.

Linked to each concrete mixture is information on the origin of the data being the reference information of the paper/publication, the fresh concrete properties, the compressive strength (of the concrete and of standard cement samples), the tensile strength (direct, splitting and/or bending tensile strength), the Young's modulus and the curing regime.

The overall structure of the database (in terms of general data categories) is schematically presented in Figure 3.

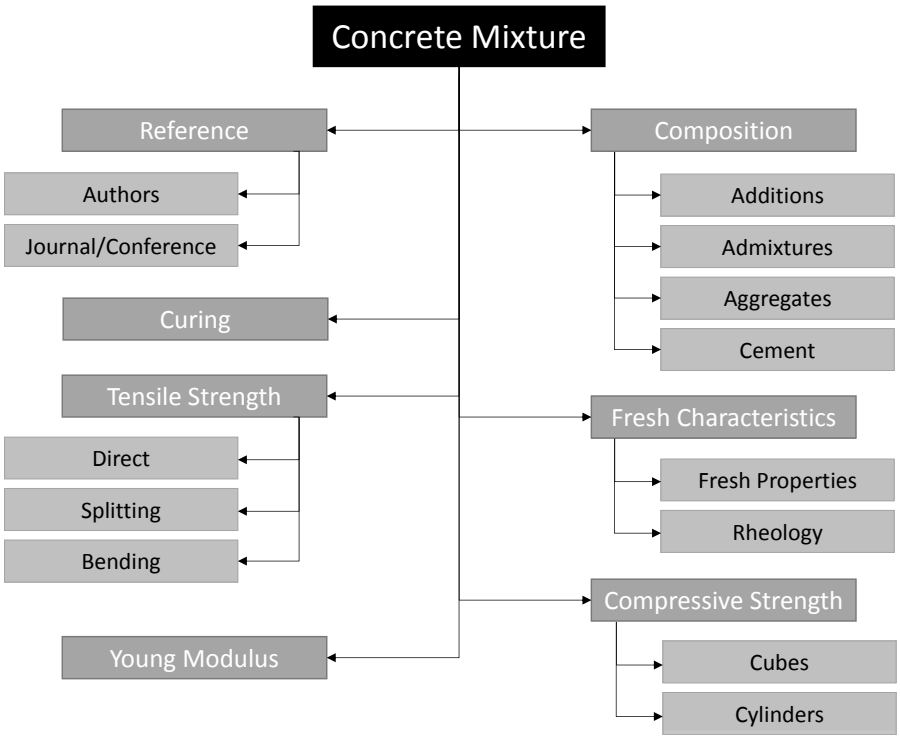

Figure 3. **Structure of the SCC database**

There are more than 1800 mixtures in the database that cover a wide range of SCC types. Based on the implemented data, the influence of some parameters which could be of major interest to users, designers, etc. are derived, including W/C, W/B, W/P, S/A, addition content, etc. Most of the time these parameters were

mentioned in the papers as well, but it was found that different researchers calculate them in different ways (e.g. accounting the binary and ternary binders only partially in W/B) making it hard to compare them one-to-one. Therefore it was decided, by the authors, to calculate these parameters based on the mix composition according to a fixed set of definitions. The following designations were put forward (as agreed upon by the RILEM TC-MPS 228):

Addition: A fine-grained inorganic material. Two types are included [EN206]: inert or nearly inert addition (Type I) and pozzolanic or latent hydraulic addition (Type II).
Admixture: A material, other than water, aggregate, hydraulic cement, and fibre reinforcement, used as an ingredient of a cementitious mixture to modify its freshly mixed, setting, or hardened properties and that is added to the batch at the beginning of or during its mixing.
Binder: A cementitious material, either a hydrated cement or reaction product of cement or lime and reactive siliceous material; the kind of cement and curing conditions governing the characteristics of the product formed. Also materials such as asphalt, resins, and other materials forming the matrix of concrete, mortar, and sanded grout.
Cement-Powder ratio (C/P): The ratio of the mass of cement to the mass of powder.
Fillers: Finely divided inert materials, such as limestone powder, silica, or colloidal substances, sometimes added to Portland cement, paint or other materials to reduce shrinkage, improve workability, or act as an extender or material used to fill an opening in a form.
Powder: Includes cement, fillers, and additions.
Sand-Aggregate ratio (S/A): The ratio of the mass of sand to the mass of aggregates.
Water-cement ratio (W/C): The ratio of the mass of water, exclusive only of that absorbed by the aggregate, to the mass of cement in concrete, mortar, or grout.
Water-cement ratio, corrected (W/C_{corr}): The ratio of the mass of water, exclusive only of that absorbed by the aggregate and including the water content in the admixtures, to the mass of cement in concrete, mortar, or grout

Based on these definitions, the different parameters were calculated in a consistent way for all the different mixtures.

To be able to quantify the self-compacting properties of the mixtures reported in literature, results of fresh concrete property tests such as slump-flow (SF), V-funnel, L-Box, U-Box, sieve segregation, etc. were collected.

Analysis of the Data

General Observations

The gathered data represents results from tests conducted in over 35 countries. Most research reported in international publications is done in Europe and North-America, but results are reported from Algeria, India, South-Korea, Japan, Brazil, Iran, etc. as well. The geographical distribution of the analysed papers is shown in Figure 4.

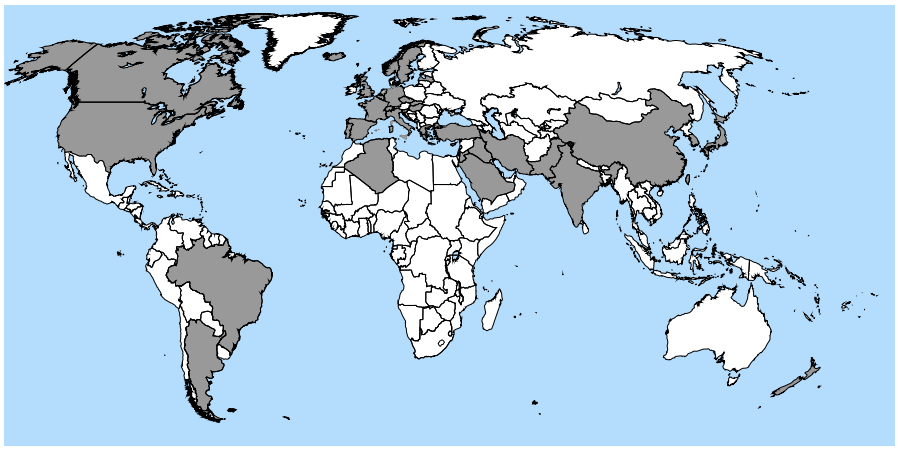

***Figure 4*. Geographical distribution of the analysed papers**

As the database contains results from over 250 papers, it can provide insights on the ranges of SCC properties. SCC can be developed according to the powder-type , VMA-type or combination type SCC approach (1). This is seen in the database as well. Based on the amount of mixtures in which a VMA is used, the powder-type approach was chosen in 83% of the cases, whereas the VMA- or combination-type SCC mixtures were utilised in 17% of the reported research papers

The reported slump-flow values (see Table III and discussion later on) range from 320 to 933 mm. The majority of the test results (95.1%) are within the range of 550 to 850 mm defined by EN 206-1 (7) for SCC.

The authors believe that concrete mixtures with slump-flow values of 320 mm or above 900 mm cannot be classified as self-compacting. Therefore, in the analysis, only concrete mixtures with slump-flow values within the limits defined by EN206-1(550 to 850 mm) are considered.

Fresh Properties

In most studies, the fresh properties of the mixtures are characterized by means of the slump flow, the V-funnel, L-box, etc. The most commonly reported fresh property is by far the slump-flow (Figure 5). The ranges of fresh properties of the so claimed SCCs are listed in Table III. For the V-funnel measurements, different dimensions of the outlet can be used. However, in papers the authors do not often include the applied apparatus type. Therefore, all V-funnel measurements are combined regardless of the dimensions of the apparatus.

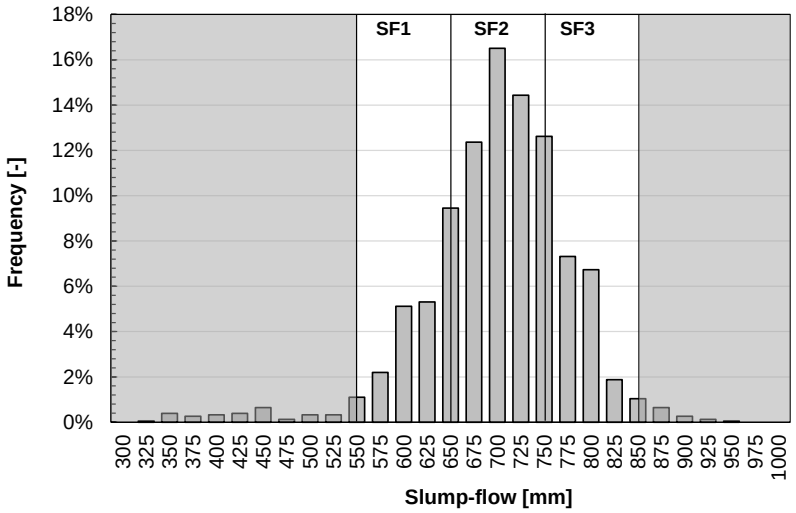

***Figure 5*. Histogram of reported SF-values for SCC (based on 1551 mixtures)**

***Table III*. Range of reported fresh properties for SCC**

Property		# meas.	Min.	10% centile	Mean	90% centile	Max.
Slump-flow	[mm]	1545	320	600	690	780	933
V-funnel	[s]	741	1.0	3.5	9.3	16.0	57.2
L-box	[-]	563	0.20	0.73	0.86	0.97	1.12
Sieve stability	[%]	141	0.20	2.24	8.35	15.51	29.30
Air content*	[%]	488	0.4	1.3	3.2	6.1	12.8

*This includes mixtures in which air entrainment agents were used

Besides these common fresh properties, tests to determine the t_{500}, U-box value, J-ring value, column segregation and VSI are reported as well. Although these tests

seem more common in North-America and less used in other parts of the world and were hence less often reported.

Mix Composition

Table IV presents an overview of some of the major mixture properties of the different SCC mixtures. Besides the maximum and minimum values, the mean values are provided as well as 10% and 90% centile values.

***Table IV*. Applied ranges of mixture properties for SCC (1474 mixtures out of 214 reported studies)**

Property		Min.	10% centile	Mean	90% centile	Max.
Cement content	[kg/m^3]	83	250	360	490	700
Binder content	[kg/m^3]	150	300	420	550	750
Powder content	[kg/m^3]	275	410	535	625	1272
Sand content	[kg/m^3]	135	600	800	940	1190
Coarse aggr. content	[kg/m^3]	283	650	820	1035	1740
Water content	[kg/m^3]	77	160	185	220	434
Paste volume	[l/m^3]	151	320	370	425	709
W/C	-	0.19	0.38	0.54	0.80	2.73
$(W/C)_{corr}$	-	0.20	0.39	0.55	0.81	2.81
W/B	-	0.15	0.33	0.46	0.63	1.33
W/P	-	0.14	0.27	0.36	0.45	0.65
C/P	-	0.15	0.50	0.69	0.95	1.00
S/A	-	0.10	0.37	0.50	0.60	0.81
Max. grain size	mm	5	10	16	20	25

The cement, sand, and coarse aggregate contents generally vary over a wide range, covering almost the entire range found for vibrated concrete (VC). All types of cement are applied in SCC mixtures: CEM I, CEM II, CEM III (according to European standards (8)), Type I, Type II, CEM Type GU (according to ASTM Standards (9)), etc.

The higher powder content needed for SCC is obtained by increasing the cement content or more often by increasing the amount of additions (powder-type SCC). The addition can be composed of one or more types. As addition material, inert as well as pozzolanic materials are widely used. The most used materials are limestone filler, fly ash, blast furnace slag, and silica fume. Less common fillers but nonetheless used in some cases, are marble powder, glass powder, rice husk ash, metakaolin, volcanic ash, and granite powder.

In

Table V the main addition type is mentioned with the frequency of occurrence. As SCC is often composed of larger amounts of fines compared to vibrated concrete, the powder content is higher as well. According to the database common powder contents for SCC mixtures are situated in the range of 410 to 625 kg/m³.

***Table V*. Origin of main addition materials (based on 1352 mixtures)**

Addition Class	Amount		Addition Class	Amount
Basalt	0.2%		Natural pozzolan	0.2%
Fly Ash	35.1%		Quartz	1.8%
Granite	0.3%		Rubble powder	0.2%
Kiln Dust	0.1%		Silica	9.2%
Limestone	40.7%		Slag	9.0%
Metakaolin	0.7%		Vegtal Ash	2.4%

Values of the water-to-cement ratio (W/C) are mentioned in Table IV as well as the corrected water-to-cement ratio $(W/C)_{corr}$. The $(W/C)_{corr}$ considers the water content that is included in the superplasticiser, as in some mixtures superplasticiser content can be as high as 14 l/m³, which could lead to a significant contribution to the overall water content.

With respect to the W/C, values between 0.19 and 2.73 are found with a mean value of 0.54. The highest reported W/C is relatively high, but it has to be emphasized that, in those cases also other types of binders are added to the mixtures.

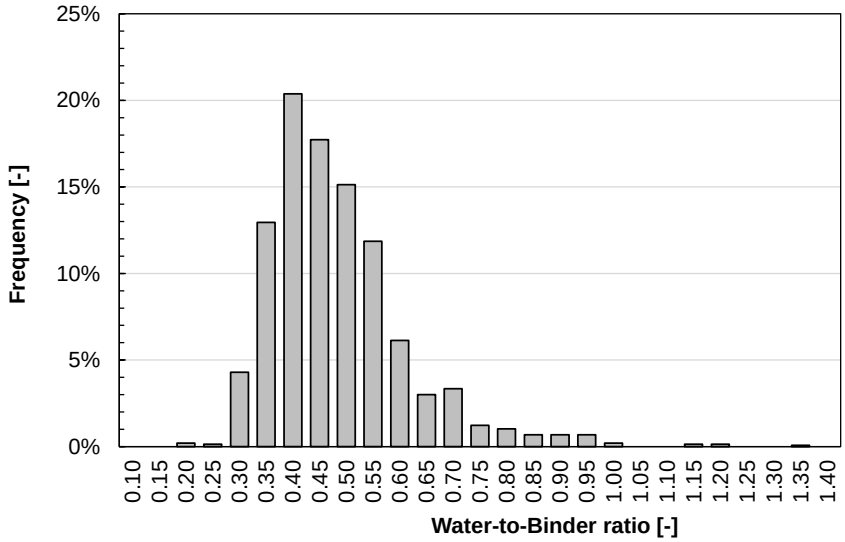

Figure 6. **Histogram of the applied W/B in SCC (based on 1474 mixtures)**

The W/B for the investigated SCC ranges from 0.15 to 1.33 with a mean value of 0.46. The majority of the mixtures were composed with a W/B between 0.33 and 0.63 (Figure 6).

Another important property of SCC is the paste volume. The total paste volume of a SCC mixture is, in most cases, higher than that of a VC mixture. The applied paste volumes (excluding air) in SCC mixtures can be seen in Figure 7. Values of 150 l/m³ up to 710 l/m³ were calculated based on the mixture composition with a mean value of 370 l/m³, whereas for VC the mean value is situated around 290 l/m³ (1).

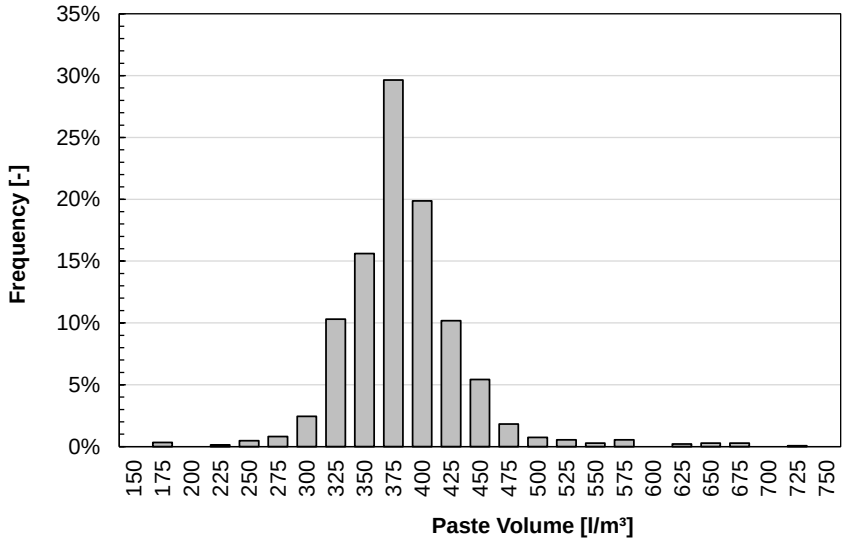

Figure 7. **Histogram of applied paste volumes in SCC (based on 1474 mixtures)**

Conclusions

Numerous studies have reported properties of SCC in the past. For the sake of providing a general view of obtained results, an extensive database was developed and analysed, rather than reviewing individual studies.

With respect to the mix composition, most researchers seem to opt for the powder-type approach using additions ranging from fly ash and blast furnace slag, over limestone to less common types such as granite or basalt. The applied water-to-binder ratio varies largely with the majority of mixtures showing W/B-values in a range of 0.33-0.63. Paste volumes on the other hand show an average of 370 l/m^3.

The most common test for evaluating the fresh properties of SCC is by far the slump flow test (values are reported for over 90% of the investigated mixtures). Other tests often used are the V-funnel test and L-box test. Measures to evaluate the stability such as the sieve stability test or column segregation test are less common.

Further analysis of the data is ongoing to provide a more detailed analysis of general mixture composition trends, the relationships between composition and fresh properties, the achieved mechanical properties and the agreement with existing codes and provisions for conventional concrete.

Acknowledgements

This work was initiated by the activities of the RILEM technical committee 228 on ‘Mechanical Properties of Self-Compacting Concrete’ (TC-228 MPS). The contribution and dedication of all committee members is greatly acknowledged.

References

1. De Schutter G, Bartos P, Domone P, Gibbs J. Self-Compacting Concrete. Caithness, UK: Whittles Publishing; 2008. 296 p.
2. Roussel N. Proceedings of the 1st international conference on rheology and processing of construction materials and of teh seventh international conference on self-compacting concrete. Paris, France: RILEM Publications SARL; 2013.
3. RILEM TC 228-MPS. Mechanical Properties of Self-Compacting Concrete. State-of-the-Art Report of the RILEM Technical Committee 228-MPS on Mechanical Properties of Self-Compacting Concret. Khayat K, De Schutter G, editors. Springer; 2014.
4. Domone P. A review of the hardened mechanical properties of self-compacting concrete. Cem Concr Compos. 2007;29(1):1–12.
5. Holschemacher K, Klug Y. A database for the evaluation of hardened properties of SCC. Lacer. 2002;123–34.
6. Craeye B, Van Itterbeeck P, Desnerck P, Boel V, De Schutter G. Modulus of elasticity and tensile strength of self-compacting concrete: survey of experimental data and structural design codes. Cem Concr Compos. Elsevier Ltd; 2014;54:53–61.
7. European Committee for Standardization. EN 206-1 - Concrete: Specification, performance, production & conformity. Brussels, Belgium; 2013. 98 p.
8. European Committee for Standardization. EN 197-1:2011 - Cement - Part 1: Composition, specifications and conformity criteria for common cements. Brussels, Belgium; 2011. 38 p.
9. ASTM International. C150/C150M-11 Standard Specification for Portland Cement. 2011. 1-9 p.

SCC Cement Pastes Designed by a Pseudo-Simplex Method

Givanildo Alves de Azeredo[1], Guilherme Urquisa Leite[2] and Aline Figueiredo Nóbrega de Azeredo[3]

[1] Professor at Federal University of Paraíba - Brazil
[2] Master Student at Federal University of Paraíba - Brazil
[3] Professor at IFPB - Brazil

Abstract The self-compacting concrete (SCC) has been treated as a great evolution in concrete technology. Mixture methods are an important step in the development of this type of concrete, since it must comply with specific performance in both the fresh and hardened states. For many researchers the performance is related mainly to the properties of the cement paste. These properties are functions of the proportion between the constituent materials. The use of a mixture experimental design seems to incorporate the assumptions necessary to understand the relationship between the proportion of the constituents and the paste characteristics. The mini-slump test was used and the responses were T_{115} and Flow. The results showed great correlation (R^2 in the order of 0.95).

Keywords: *Mixture experimental design, Rheology, SCC, Cement Pastes, Mini-slump test*

Introduction

Since its beginning, the SCC production means a very important development in concrete technology [1]. It fills the forms completely, without the need of external vibration or the occurrence of segregation of components. This promotes time gain and labor savings, in addition to the reduction of noise [1]. One can say it is a consensus that the paste governs self-compacting properties of concrete. Once a cement paste possess the appropriate characteristics, in sufficient quantity, it offers to the concrete the self-compacting status [2-4].
In general, it takes many trials to characterize the appropriate paste for the production of SCC. Thus, the experimental design is an extremely useful tool, allowing the reduction of the number of experiments, however maintaining the

quality and representativeness of data [5]. Increasingly, experimental design has been integrated into the civil engineering domain [6], through either factorial design [6, 9] or mixtures planning [7, 9].

Mixtures design are those experiments whose properties vary with the relative proportions of the components [10]. A simplex with dimension n-1 represents an experimental region of a mixture [11]. Sometimes, it does not make sense vary from 0 to 1 the proportion of one or more components. Thus, lower and upper limits (Li) and (Ui) can be set for the proportions of these components, as shown in Eqn. (1):

$$0 \leq L_i \leq x_i \leq U_i \leq 1 \quad (1)$$

The pseudo-simplex method, proposed by Leite [12], is based on this concept represented by Eqn. (1). This research aims at studying the rheology of cement pastes through mini-slump tests, using an experimental mixture design in order to understand the relationship between the proportions of components and the flow and cohesion characteristics of the paste.

Materials and Experimental Procedure

Materials

Local availability and cost defined selection of materials. Portland cement CP II-E used, according to NBR 11578:1991 (Brazilian standard), is a blended Portland cement that receives the addition of ground granulated blast-furnace slag, between 6% and 34%. Limestone filler used presents particles smaller than 80μm donated by Dolomil plant, located in the city of Campina Grande.

The superplasticizer used was the ADVA CAST ™ 525 supplied by Grace Brazil LTDA, carboxylate based on. It presents liquid aspect and does not contain chloride. Its pH is between 3.00 and 5.50 and its specific gravity is 1.06 g/cm³. The water comes from the city of João Pessoa.

Design of experiments (Pseudo-simplex method)

The paste studied in this work consists of cement, filler, water and superplasticizer. A mixture of four components thus represents the experimental design. However, water/cement ratio 0.4 was set constant. Thus water is no more a variable of the design but linked to the amount of cement in the mixture. Therefore, the mixture of cement, filler and superplasticizer represents the experimental design.

Eqn. (2), (3), (4) and (5) show lower and upper limits for each component. Those for cement are function of limits of other components. Upper and lower limits of limestone filler and superplasticizer defined lower and upper limits of cement, respectively.

$$L_i \leq x_i \leq U_i \quad (2)$$
$$0{,}008 \leq x_{SP} \leq 0{,}02 \quad (3)$$
$$0{,}2 \leq x_F \leq 0{,}4 \quad (4)$$
$$0{,}58 \leq x_c \leq 0{,}792 \quad (5)$$

where x_i is the proportion of material *i* in the mixture; Li and Ui represent the lower and upper limits of the proportion of material *i* in the mixture, respectively; x_{SP}, x_F and x_C are the proportions by weight of superplasticizer, filler and cement in the mix, respectively.

In this way, this pseudo-simplex method was conceived [12]. This method applies three components to the mixture where upper limits or upper and lower limits are applied to two of these components and the third one is restricted by the mixing definition, conditioned to the remaining amount of material to complete 100% [11].

Experimental Procedure

For planning the cement paste, a special cubic model in simplex-centroid is considered. It needs at least seven different tests at each simplex in order to determine all coefficients values of the model, as shown in Eqn 6. However, each simplex got three different tests more in order to have fewer model parameters than different experiments, allowing doing an analysis of variance (see Figure 1). Moreover, for each test, two replications were carried out which allows the analysis of variance considering pure error and lack of fit. Table I shows the experimental points in accordance with the actual components and pseudo-components, presented in Figure 1.

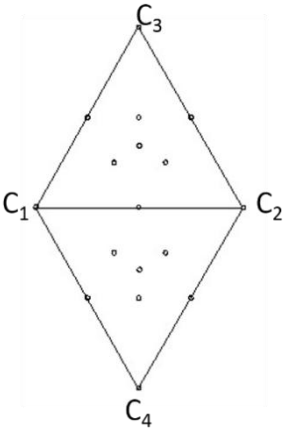

Figure 1. Two pseudo-simplex scheme composed by pseudo-components C_1, C_2, C_3 and C_4 formed by A, B and C materials [12]. Source: Author

For seventeen (17) different proportions, mini-slump tests were carried out three times each. Fifty-one (51) is the total number of experiments. Answers T_{115} and the flow are measured. According to [3] and already verified in [13], the suitable paste for producing SCC presents the following characteristics: T_{115} = 3 ± 1s; Flow = 180 ± 10mm.

Statistical analysis were performed with the Statistica 8.0 software from StatSoft Inc.®, where the responses were plotted in four simplex (two for T_{115} and two for flows) and were joined then, separately. Eqn. (6) defines the planning simplex-centroid:

$$y=b_1x_1+b_2x_2+b_3x_3+b_{12}x_1x_2+b_{13}\,x_1x_3+b_{23}x_2x_3+b_{123}x_1x_2x_3 \quad (6)$$

where b_i, b_{ij} and b_{ijk} are the coefficients of Eqn. [6] and x_i is the proportion of composite material *i* in the mix.

Table I. Experimental points of paste study (see Figure 1)

Experimental Points		Pseudocomponents				Actual Components		
		C1 Proportion	C2 Proportion	C3 Proportion	C4 Proportion	Cement (A) Proportion	SP (B) Proportion	Filler (C) Proportion
Simplex 1 (C_1+C_2+C_3)	1	100%	0%	0%	0%	78.000%	2.000%	20.000%
	2	0%	100%	0%	0%	59.200%	0.800%	40.000%
	3	0%	0%	100%	0%	79.200%	0.800%	20.000%
	4	50%	50%	0%	0%	68.600%	1.400%	30.000%
	5	50%	0%	50%	0%	78.600%	1.400%	20.000%
	6	0%	50%	50%	0%	69.200%	0.800%	30.000%
	7	33%	33%	33%	0%	72.133%	1.200%	26.667%
	8	50%	25%	25%	0%	73.600%	1.400%	25.000%
	9	25%	50%	25%	0%	68.900%	1.100%	30.000%
	10	25%	25%	50%	0%	73.900%	1.100%	25.000%
Simplex 2 (C_1+C_2+C_4)	11	100%	0%	0%	0%	78.000%	2.000%	20.000%
	12	0%	100%	0%	0%	59.200%	0.800%	40.000%
	13	0%	0%	0%	100%	58.000%	2.000%	40.000%
	14	50%	50%	0%	0%	68.600%	1.400%	30.000%
	15	50%	0%	0%	50%	68.000%	2.000%	30.000%
	16	0%	50%	0%	50%	58.600%	1.400%	40.000%
	17	33%	33%	0%	33%	65.067%	1.600%	33.333%
	18	50%	25%	0%	25%	68.300%	1.700%	30.000%
	19	25%	50%	0%	25%	63.600%	1.400%	35.000%
	20	25%	25%	0%	50%	63.300%	1.700%	35.000%

The experimental procedure started weighing 500g materials, excluding the weight of water which was always equal to 40% of the weight of cement (w/c = 0.4). After that, the dry materials cement and limestone filler were mixed by hand. Then, half amount of water was added to start the wetting process of grain surface. Finally, superplasticizer was added to the mixture. All materials were mixed by hand; up to obtain a homogeneous mix. The entire mixing procedure lasted five minutes.

Results

Mixture experimental design was used to evaluate the fluidity characteristics and viscosity of a cement paste through the mini-slump test. The observed responses were the T_{115} and the final diameter (Flow). T_{115} is the time interval between the moment the slump is lifted and the time the paste reaches a diameter of 115mm. Table II presents the test results.

Table II. Results from mini-slump test

Experimental Points		T_{115}			Flow		
		1	2	3	1	2	3
Simplex 1 (C_1+C_2+C_3)	1	1.02 s	0.85 s	0.88 s	20.50 cm	20.48 cm	20.78 cm
	2	15.22 s	16.54 s	16.63 s	15.00 cm	14.93 cm	15.50 cm
	3	0.85 s	0.88 s	0.91 s	19.37 cm	19.38 cm	19.10 cm
	4	2.57 s	2.83 s	2.81 s	18.30 cm	18.20 cm	18.30 cm
	5	1.19 s	0.91 s	1.05 s	19.70 cm	19.80 cm	19.75 cm
	6	1.32 s	1.53 s	1.43 s	18.40 cm	18.60 cm	18.50 cm
	7	1.42 s	1.36 s	1.39 s	19.90 cm	19.88 cm	19.68 cm
	8	1.36 s	1.39 s	1.43 s	20.53 cm	20.40 cm	20.08 cm
	9	1.97 s	1.93 s	1.93 s	19.33 cm	19.03 cm	19.03 cm
	10	1.35 s	1.35 s	1.26 s	19.95 cm	19.80 cm	19.83 cm
Simplex 2 (C_1+C_2+C_4)	11	1.02 s	0.85 s	0.88 s	20.50 cm	20.48 cm	20.78 cm
	12	15.22 s	16.54 s	16.63 s	15.00 cm	14.93 cm	15.50 cm
	13	3.93 s	6.00 s	5.89 s	17.80 cm	17.30 cm	17.23 cm
	14	2.57 s	2.83 s	2.81 s	18.30 cm	18.20 cm	18.30 cm
	15	2.78 s	2.34 s	2.91 s	18.30 cm	18.90 cm	19.00 cm
	16	11.29 s	15.80 s	13.55 s	14.75 cm	14.50 cm	15.00 cm
	17	1.93 s	2.07 s	1.93 s	19.50 cm	19.85 cm	19.45 cm
	18	1.32 s	1.43 s	1.25 s	20.20 cm	20.35 cm	19.88 cm
	19	2.11 s	2.10 s	1.93 s	19.28 cm	19.88 cm	20.18 cm
	20	1.89 s	1.80 s	1.83 s	19.88 cm	19.75 cm	20.73 cm

For the variable T_{115}, Pareto chart shows in Figure 2, for the equation corresponding to C_1+C_2+C_3 SIMPLEX, that coefficients are statistically significant, except AC. The model can then be simplified to the one presented in Eqn. 7. For equation corresponding to C_1+C_2+C_4 SIMPLEX, the coefficients A and AC are also not statistically significant. The model can then be simplified to the one presented in Eqn. 8.

$$y=b_1x_1+b_2x_2+b_3x_3+b_{13}\,x_1x_3+b_{23}x_2x_3+b_{123}x_1x_2x_3 \quad (7)$$

$$y=b_2x_2+b_3x_3+b_{13}\,x_1x_3+b_{23}x_2x_3+b_{123}x_1x_2x_3 \quad (8)$$

The ANOVA Table showed in Figure 3 show that despite a good correlation model ($R^2 > 0.95$) for C_1+ C_2 + C_3 mix, they exhibit a significant lack of fit which may indicate that perhaps a model with more terms, for example the full cubic one,

could better represent the variation of property. For C_1+ C_2 + C_4 mix, it behaves similarly. Authors consider the special cubic model sufficient for this research.

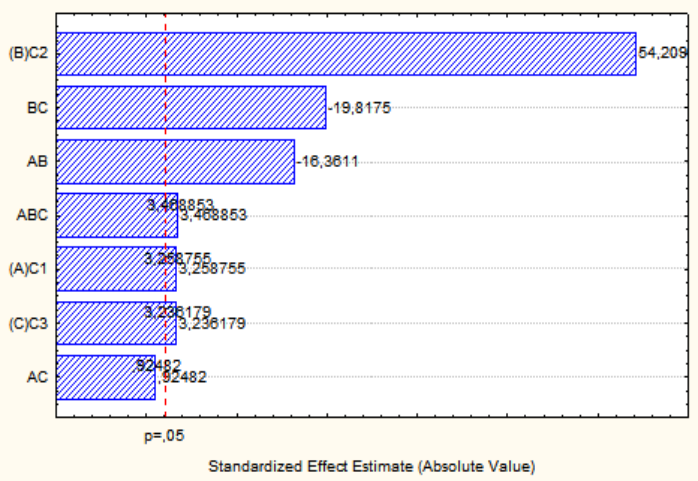

Figure 2. Pareto chart for the coefficients of mixing C_1+C_2+C_3 for the special cubic model (T115)

	Overall Fit of Model; Var.: T115 (simplex-centroid design) 3 Factor mixture design; Mixture total=1,, 30 Runs (Some terms were excluded from the respective full models)				
Source	SS	df	MS	F	p
Model	584,9514	5	116,99030	445,5279	0,000000
Total Error	6,3021	24	0,26260		
Lack of Fit	4,9238	4	1,23090	17,8614	0,000002
Pure Error	1,3783	20	0,06890		
Total Adjusted	591,2535	29	20,38810		

Figure 3. ANOVA of special cubic model for mixing for mix $C_1 + C_2 + C_3$ (T_{115}) neglecting AC effect

Concerning Flow variable, Pareto chart showed that the AC coefficient is not statistically significant. Therefore, removal of such coefficients would not cause great losses in the correlation model. The values of the coefficients A, B and C were quite significant, while the interaction coefficients are insignificant. The coefficient A is the most significant and is related to the proportion of C_1, which regulates the amount of SP in the mixture. This can be attributed to the fact that the fluidity characterized by paste flowing is directly related to the proportion of SP.

The ANOVA Table presented in Figure 4 shows that the model considered for C_1 + C_2 + C_3 mixture does not present significant lack of fit. Considering C_1 + C_2 + C_4 mixture, ANOVA Table presented in Figure 5 shows that the model shows lack of fit statistically significant, which may indicate that such a model may require a

greater number of terms to better represent the flow of the paste. For this work, the special cubic model was considered sufficient by the authors.

Overall Fit of Model; Var.: Flow (3 factor simplex-centroid design)
3 Factor mixture design; Mixture total=1,, 30 Runs
(Some terms were excluded from the respective full models)

Source	SS	df	MS	F	p
Model	65,67249	5	13,13450	373,5624	0,000000
Total Error	0,84384	24	0,03516		
Lack of Fit	0,30271	4	0,07568	2,7970	0,053949
Pure Error	0,54113	20	0,02706		
Total Adjusted	66,51634	29	2,29367		

Figure 4. ANOVA for the special cubic model mixture of C_1+C_2+C_3 (Flow) ignoring the AC effect

According to [3], the paste that has a high probability of obtaining the SCC is one that presents T115 = 3 ± 1s and Flow = 18 ± 1 cm. Thus, the high probability area to obtain SCC is defined by the intersection of the zone presenting 2≤T115≤4s and the zone presenting 17≤Flow≤19cm.

Overall Fit of Model; Var.: Flow (3 factor simplex-centroid design)
3 Factor mixture design; Mixture total=1,, 30 Runs
(Some terms were excluded from the respective full models)

Source	SS	df	MS	F	p
Model	111,8694	4	27,96734	94,73643	0,000000
Total Error	7,3803	25	0,29521		
Lack of Fit	5,3223	5	1,06446	10,34461	0,000052
Pure Error	2,0580	20	0,10290		
Total Adjusted	119,2497	29	4,11206		

Figure 5. ANOVA for special cubic model of mixture $C_1 + C_2 + C_4$ (Flow) neglecting AC effect

Conclusion

The method proposed in this research proved useful to apply and provided results statistically significant or not. Therefore, the experimental design of mixtures can be used to obtain sufficient and precise results for the production of SCC cement pastes. The experimental design allowed the mapping of flowing time T_{115} and Flow of cement pastes composed by superplasticizer and limestone filler, and w/c constant equal to 0.4, having as coordinates the proportions of the materials. This allows speed and economy in the SCC production.

Acknowledgements

We would like to thank to Dolomil and Grace Brazil LTDA plants, for donating the filler and admixtures used in this research. The authors acknowledge also the CAPES, that provided scholarship to the Master student.

References

[1] EFNARC (2002) - *European Fed. for Specialist Const. Chem. and Conc. Systems*. Specification and guidelines for self-compacting concrete.
[2] Bui, V. K.; Montgomery, D. (1999). In: Mixture proportioning method for self-compacting high performance concrete with minimum paste volume. *International rilem symposium on self-compac. concrete*, 1, Stockholm, p. 373-384.
[3] Gomes, P. C. C.; Gettu, R.; Agulló, L. (2003). In: Uma nova metodologia para obtenção de concretos auto-adensáveis de alta resistência com aditivos minerais. *V Simpósio EPUSP sobre Estruturas de Concreto*, p. 1-14.
[4] Wu, Q.; An, X. (2014), Devel. of a mix design method for SCC based on the rheological characteristics of paste. *Const. and Build. Mat.*, v. 53, p. 642-651.
[5] Rodrigues, M. I.; Lemma, A. F. (2009). In: Planejamento de experimentos e otimização de processos. 2. ed. Campinas. 358 p.
[6] Ahmad, S.; Zubair, A.; Maslehuddin, M.. (2014), Effect of the Key Mixture Param. on Shrinkage of Reactive Powder Concrete. *The Scient. World Jour.*, v. 2014.
[7] Olubanwo, A. O.; Karadelis, J. N. (2015), Applied mixture optimization techniques for paste design of bonded roller-compacted fibre reinforced polymer modified concrete (BRCFRPMC) overlays. *Materials and Structures*, p. 1-20.
[8] Abouhussien, A.; Hassan, A. (2014), Application of statistical analysis for mixture design of high-strength self-consolidating concrete containing metakaolin. *Journal of Materials in Civil Engineering*.
[9] Bouziani, T. (2013), Assessment of fresh properties and compressive strength of self-compacting concrete made with different sand types by mixture design modelling approach. *Construction and Building Materials*, v. 49, p. 308-314.
[10] Scheffe, H. (1963)The Simplex-Centroid Design for Experim. with Mixt.. *Jour. of the Royal Statist. Socie.*. Series B (Methodological), v. 25, n. 02, p. 235-263.
[11] Cornell, J. (2002). In: Experiments with mixtures: designs, models, and the analysis of mixture data. John Wiley & Sons.
[12] Leite, G. U. (in progress). In: Uso do planejamento experimental de misturas na obtenção de concretos auto-adensáveis. Dissertação de Mestrado. Programa de Pós-Graduação em Engenharia Civil e Ambiental (PPGECAM).
[13] Azeredo, G.; Diniz, M. (2013), Self-compacting concrete obtained by the use of kaolin wastes. *Construction and Building Materials*, v. 38, p. 515-523.

A Rational Method for the Design of Self-Compacting Concrete Mixes

Alyhya W. S.[1], Abo Dhaheer M. S.[1], Al-Rubaye M. M.[1], Karihaloo B. L.[1] and Kulasegaram S.[1]

[1] School of Engineering, Cardiff University, Cardiff CF24 3AA, UK

Abstract Methods for proportioning self-compacting concrete (SCC) mixes have not kept pace with their production techniques. This paper reports on a rational method, supplemented by design charts, for proportioning SCC based on the desired target plastic viscosity and compressive strength of the mix. A series of SCC mixes that contained different volumetric ratios of paste to solid phases were prepared using the design charts. These mixes were extensively tested in the fresh state using the slump cone, J-ring, L-box and V-funnel, and in the hardened state. These tests proved conclusively the validity of the mix proportioning method in the sense that all the mixes satisfied the self-compacting criteria and achieved the desired target plastic viscosity and cube compressive strength.

Keywords: *Self-compacting concrete; Plastic viscosity; Compressive strength; Mix proportioning*.

Introduction

The proportioning of self-compacting concrete (SCC) mixes requires a balance between their flow and passing ability on the one hand and the resistance to segregation on the other. The early mix proportioning approaches were all based on trial and error. However, the recent extensive research on the rheological properties of SCC has greatly improved the proportioning of SCC mixes.

A rigorous method for proportioning SCC mixes based on their plastic viscosity has been proposed by Karihaloo and Ghanbari [1] and Deeb and Karihaloo [2]. It exploits the expression for the plastic viscosity of an SCC mix developed by Ghanbari and Karihaloo [3]. This expression is the product of the known plastic viscosity of the paste and contributions of each of the solid phases. Whilst the method for proportioning SCC mixes proposed in [1, 2] is rigorous, it produces a

bewildering array of satisfactory mixes but does not give any practical guidelines on how to choose the most appropriate mix. Moreover, the method was developed on the basis of reference mixes of a range of known cube compressive strength, but the latter was not explicitly imposed as a design criterion.

In two recent papers [4, 5] the authors have overcome the above shortcomings of this method for proportioning SCC mixes. Practical guidelines in the form of design charts have been provided for choosing the mix proportions that achieve the target plastic viscosity in the range 3 to 15 Pa s and the target cube compressive strength in the range 30 to 80 MPa. Details of the construction of design charts are given in [4]. Several mixes with differing paste to solids ratios by volume were selected using these guidelines and prepared in the laboratory in order to confirm the simplicity and usefulness of this method. An overview will be given in this presentation.

Target compressive strength

The compressive strength of a concrete mix is mostly determined by the water to binder ratio (*w/cm*) under given curing conditions. A regression analysis was performed on the data collected from many published sources and the compressive strength of SCC could be best fitted by an Abrams-type relation ($R^2 = 0.94$);

$$f_{cu} = \frac{195}{12.65^{(w/cm)}} \tag{1}$$

where f_{cu} is the 28-day equivalent cube compressive strength (MPa) and *w/cm* is the ratio of water to cementitious materials. The large scatter in the surveyed data is a reflection of the differences in the curing conditions, the cement type, the type of cement replacement material and replacement levels up to 30%, the amount of coarse aggregate and the maximum size of coarse aggregate. The values have been adjusted for the size of the cube test specimens to that of 100 mm cubes.

Target plastic viscosity

Fresh SCC behaves like a Bingham fluid described by two rheological parameters - yield stress and plastic viscosity. The yield stress of SCC is low (tens of Pa) in comparison with vibrated concrete and it remains so over a wide range of plastic viscosity. Thus the most important parameter in most applications is the plastic viscosity which changes with the plastic viscosity of the paste and the mix composition, although in some instances the yield stress can be equally important.

The plastic viscosity of a homogeneous viscous fluid, such as a paste can be measured rather accurately with a viscometer which is not possible for a non-homogenous viscous fluid such as an SCC mix. There is a large scatter in the plastic viscosity of the same SCC mix measured with different rheometers. Ghanbari and Karihaloo [3] therefore proposed a procedure for estimating the plastic viscosity of an SCC mix knowing the plastic viscosity of the paste. In this procedure, SCC is regarded as a two-phase suspension in which the solid phase is suspended in a viscous liquid phase. The increase in the plastic viscosity of the liquid phase as a result of the addition of the solid phase (filler, fine and coarse aggregates) is estimated in stepwise manner until all the solid phases have been added. Thus the plastic viscosity of an SCC mix with *n* solid phases is (Eqn. 2):

$$\eta = \eta_{paste} \times f_1(\phi_1) \times f_2(\phi_2) ..... \times f_n(\phi_n) \tag{2}$$

Einstein was the first to develop an expression $f_i(\phi_i)$ for dilute suspensions containing rigid or hollow spheres with no hydrodynamic interactions (Eqn. 3):

$$f_i(\phi_i) = 1 + [\eta]\phi_i \tag{3}$$

where $[\eta]$ is equal to 2.5 for rigid spherical particles and to 1 for spherical air bubbles that are packed randomly in a hexagonal arrangement. Subsequent investigations have proved that the numerical factor 2.5 is quite accurate even for rigid ellipsoidal particles with an aspect ratio less than 3.

However, at higher concentrations of the solid phase (volume fraction >10% up to the maximum possible volume fraction, ϕ_m), the hydrodynamic interactions between the particles and the Brownian motions cannot be ignored. In this situation, Krieger–Dougherty formula has been found to be appropriate for cement–based suspensions (Eqn. 4):

$$f_i(\phi_i) = \left(1 - \frac{\phi_i}{\phi_m}\right)^{-[\eta]\phi_m} \tag{4}$$

ϕ_m is 0.74 for hexagonal close packing, 0.63 for random hexagonal packing, and 0.524 for cubic packing. The particle size distribution significantly affects ϕ_m. In most SCC mixes, the volume fractions of the filler, fine and coarse aggregates exceed 10%, so that their contribution to the known plastic viscosity of the paste is given by the Krieger-Dougherty formula. The volume fraction of the trapped air bubbles is however low, around 2%, such that Einstein equation with the numerical

factor equal to 1 is appropriate. This 2% increase due to trapped air can be included in the plastic viscosity of the paste. Note that the packing density increases with the addition of solid phases. When the first solid phase is added to the paste, the packing is loose so that it may be assumed as cubic. When however, the last solid phase is added to the suspension, the packing becomes very dense so that hexagonal close packing can be assumed. This however restricts the order in which the ingredients have to be added to make the mix, i.e. limestone powder first, followed by fine aggregate and coarse aggregate last.
It should be noted that if a rheometer capable of measuring the plastic viscosity of heterogeneous SCC mix accurately became available then the above micromechanical relation may be used to check the accuracy of the measurements. It should also be mentioned that the LP filler is treated as a second phase in the paste despite its size being similar to the grain size of cement and ggbs because the plastic viscosity of the paste with LP filler has not been reported in the literature.

Basic steps of the proposed mix design method

The basic steps of the proposed mix design method are summarised below.

1. Select the desired plastic viscosity of the mix within the range of 3-15 Pa s, remembering that the slump cone t_{500} time increases with increasing plastic viscosity of the mix. The EFNARC guidelines [6] will be helpful in the choice of the desired plastic viscosity depending on the application;
2. Calculate the ratio of water to binder (*w/cm*) that produces the target cube characteristic strength from the regression equation (Eqn. 1) given above;
3. Choose the water content in the range of 150-210 kg/m^3, following EFNARC guidelines [6], and calculate the mass of cementitious materials (*cm*) in kg/m^3. The amount of ggbs is assumed to be 25% of binder (*cm*). It is known that the replacement of 25% cement (c) by ggbs has little effect on the paste viscosity;
4. Assume a trial superplasticizer (SP) dosage as a per cent of the binder mass in the range of 0.4-0.8 % for the MasterGlenium SP used in this work. For this SP the manufacturer's recommended dosage is 0.2-1.2 kg /100 kg of binder;
5. Estimate the plastic viscosity of the paste from the *w/cm* and SP/*cm* ratios. It is known that SP/*cm* has little impact on the paste viscosity; the major impact is on the yield stress;
6. Calculate the mass of the solid phase ingredients (filler, fine aggregate and coarse aggregate) according to their volume fractions, as will be explained in the examples below;
7. Check if the total volume of the produced mix is equal to 1 m^3. If not, scale the ingredient masses to achieve a total volume of 1 m^3;
8. Calculate the plastic viscosity of the mix using Eqn. (2) and compare it with the desired one (step 1). If the difference is within ±5%, adopt the mix proportions.

If not, choose a different combination of the volume fractions of the solid phase ingredients (step 6) and repeat steps 7-8.

Examples of the use of design charts

In order to demonstrate how easy it is to use the design charts, let us assume we wish to design an SCC mix with a target cube compressive strength of 50 MPa.

1. Suppose further that the desired target plastic viscosity of mix is 7 Pa s;
2. For the desired target strength= 50 MPa → *w/cm* = 0.53 (Eqn. 1);
3. Calculate the cementitious material content (*cm*);
   For η = 7 Pa s → *cm*/ η = 56 (bottom curve; Figure 1)
   cm = 7 × 56 = 392 kg/m^3;
   c= 0.75 × 392 = 294 kg/m^3, ggbs = 0.25 × 392 = 98 kg/m^3;
   As *w/cm* = 0.53 → *w* = 0.53 × 392 = 207.8 l/m^3
4. Assume a trial superplasticizer dosage (SP) as a per cent of mass of cementitious materials (say 0.60%) which equals to 2.35 kg/m^3;
5. The plastic viscosity of the paste, η_{paste} according to its *w/cm* and SP/*cm* ratios is equal to 0.23;
6. Calculate the solid phase ingredient contents (*LP*, *FA* and *CA*);
   For η = 7 Pa s → (*cm*+*LP*)/ η = 77 (second curve from bottom; Figure 1);
   (*cm*+*LP*) = 7 × 77 = 539 kg/m^3 → *LP* = 539 – 392 = 147 kg/m^3
   (*cm*+*LP*+*FA*)/ η = 184 (second curve from top; Figure 1)
   (*cm*+*LP*+*FA*) = 7 × 184 = 1288 kg/m^3 → *FA*=1288 – 539= 749 kg/m^3
   (*cm*+*LP*+*FA*+*CA*)/ η = 300 (top curve; Figure 1)
   (*cm*+*LP*+*FA*+*CA*) = 7 × 300 = 2100kg/m^3→ CA =2100 – 1288 = 812 kg/m^3
7. Calculate the total volume of the mix;

$$Volume = \frac{c}{\rho_c} + \frac{ggbs}{\rho_{ggbs}} + \frac{w}{\rho_w} + \frac{SP}{\rho_{SP}} + \frac{LP}{\rho_{LP}} + \frac{FA}{\rho_{FA}} + \frac{CA}{\rho_{CA}} + 0.02 = 1m^3$$

   From the above masses, we can calculate the volume fractions, giving ϕ_{LP}, ϕ_{FA} and ϕ_{CA} to be equal to 0.142, 0.396 and 0.289, respectively.
8. Check the plastic viscosity using Eqn. (2);

$$\eta = \eta_{paste} \times \left(1 - \frac{\phi_{LP}}{0.524}\right)^{-1.9} \times \left(1 - \frac{\phi_{FA}}{0.630}\right)^{-1.9} \times \left(1 - \frac{\phi_{CA}}{0.740}\right)^{-1.9} = 7.05 \text{ Pa s}$$

This differs from the target viscosity by 0.7%, i.e. within the acceptable difference ± 5 %. Thus the above mix proportions are acceptable.

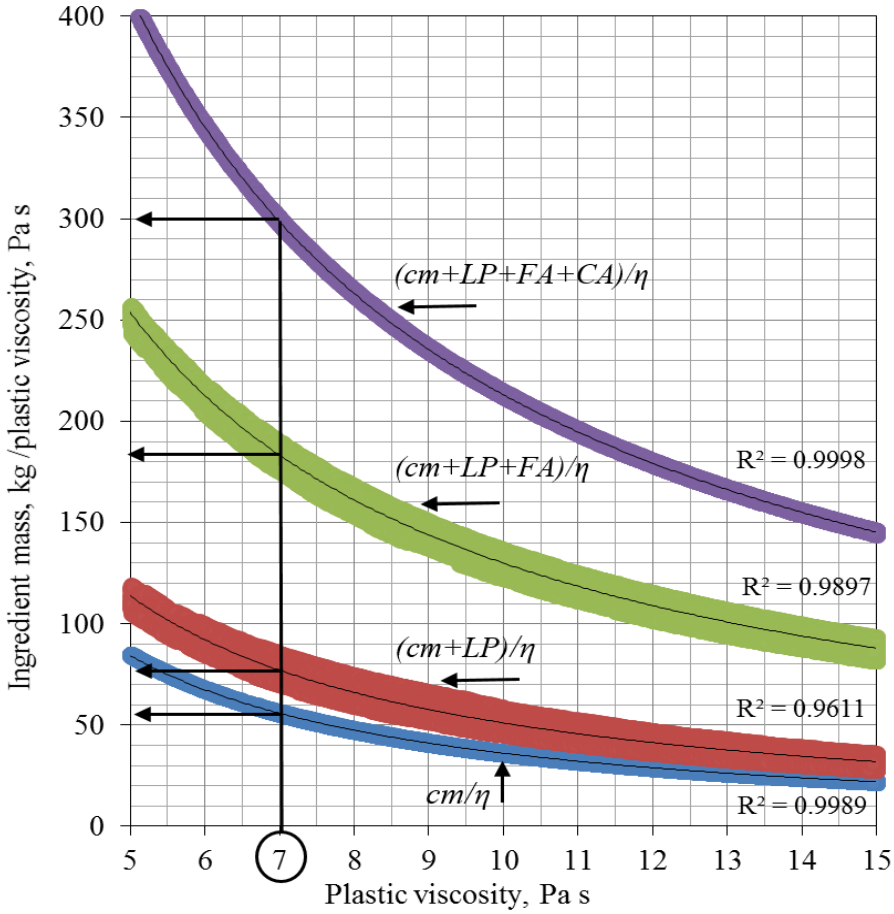

Figure 1. Ingredient mass (kg) normalised by mix plastic viscosity vs plastic viscosity for 50 MPa mix

As a second example, let us design a mix with cube compressive strength 80 MPa.

1. Assume the desired target plastic viscosity to be 11 Pa s;
2. For the desired target strength = 80 MPa → *w/cm* = 0.35 (Eqn. 1);
3. Calculate the cementitious material content (*cm*);
   For η = 11 Pa s → *cm*/ η = 43 (bottom curve; Figure 2)
   cm = 11 × 43 = 473 kg/m^3;
   c= 0.75 × 473 = 355 kg/m^3, ggbs = 0.25 × 473 = 118 kg/m^3;
   As *w/cm* = 0.35 → *w* = 0.35 × 473= 165.6 l/m^3
4. Assume a trial superplasticizer dosage (SP) as a per cent of mass of cementitious materials (say 0.60%) which equals to 2.84 kg/m^3;

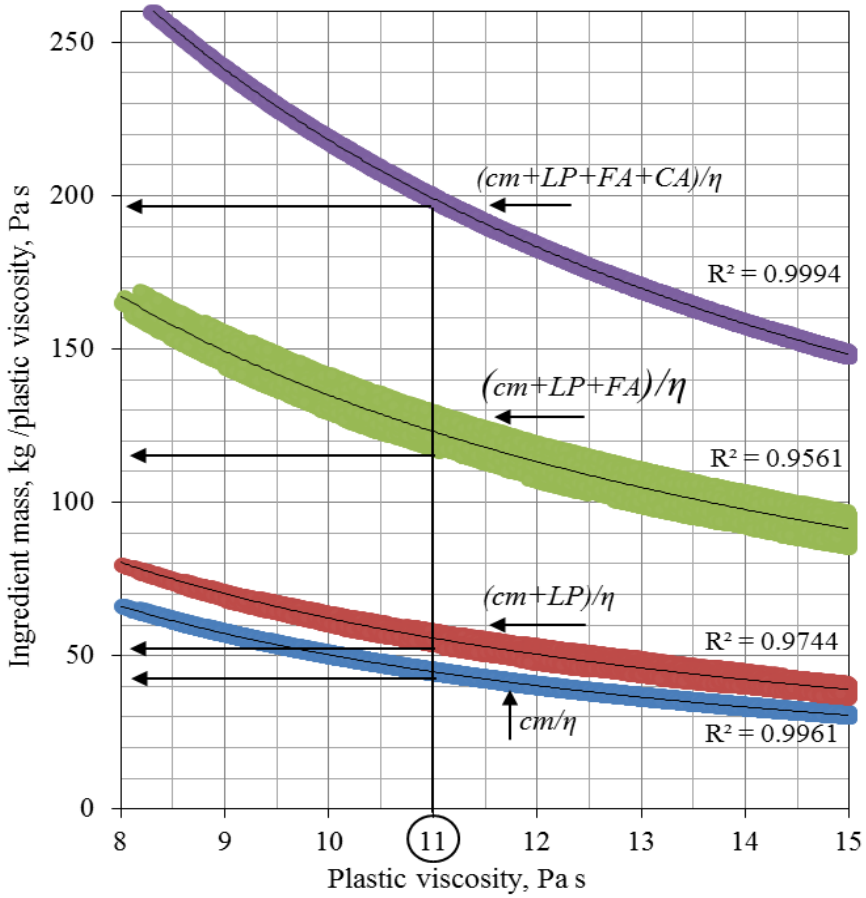

Figure 2. Ingredient mass (kg) normalised by mix plastic viscosity vs plastic viscosity for 80 MPa mix

5. The plastic viscosity of the paste, according to its *w/cm* and SP/*cm* ratios is equal to 0.37;
6. Calculate the solid phase ingredient contents (*LP*, *FA* and *CA*);
   For η = 11 Pa s → (*cm*+*LP*)/ η = 52 (second curve from bottom; Figure 2);
   (*cm*+*LP*) = 11 × 52 = 572 kg/m^3 → *LP* = 572 – 473 = 99 kg/m^3
   (*cm*+*LP*+*FA*)/ η = 116 (second curve from top; Figure 2)
   (*cm*+*LP*+*FA*) = 11 × 116 = 1276 kg/m^3 → *FA* = 1276 – 572 = 704 kg/m^3
   (*cm*+*LP*+*FA*+*CA*)/ η = 196 (top curve; Figure 2)
   (*cm*+*LP*+*FA*+*CA*) = 11 × 196 = 2156 kg/m^3→ *CA* = 2156 – 1276 = 880 kg/m^3
7. Calculate the total volume of the mix;

$$Volume = \frac{c}{\rho_c} + \frac{ggbs}{\rho_{ggbs}} + \frac{w}{\rho_w} + \frac{SP}{\rho_{SP}} + \frac{LP}{\rho_{LP}} + \frac{FA}{\rho_{FA}} + \frac{CA}{\rho_{CA}} + 0.02 = 0.98 m^3$$

Adjust the material masses in order to have a yield of 1 m^3. From the adjusted masses, we can calculate the volume fractions, giving ϕ_{LP}, ϕ_{FA} and ϕ_{CA} to be equal to 0.103, 0.400 and 0.321, respectively.

8. Check the plastic viscosity using Eqn. (2) for the mix after been adjusted;

$$\eta = \eta_{paste} \times \left(1 - \frac{\phi_{LP}}{0.524}\right)^{-1.9} \times \left(1 - \frac{\phi_{FA}}{0.630}\right)^{-1.9} \times \left(1 - \frac{\phi_{CA}}{0.740}\right)^{-1.9} = 11.21 \text{ Pa s}$$

This differs from the target viscosity by 1.9%, i.e. within the acceptable difference ± 5 %, so the above mix proportions are acceptable.

Mix design validation

Mix proportions and materials

The verification of the proposed SCC mix design method using the design charts was carried out by testing many mixes of differing cube compressive strength. Twenty one different mixes of strength 30, 40, 50, 60, 70, and 80 MPa and different target plastic viscosity were prepared and subjected to the slump flow, J–ring, L–box and V–funnel tests in the fresh state to ensure that they met the flow and passing ability criteria without segregation. Standard cubes (100 mm) were then cast, cured in water and tested for compressive strength at 7, 28 and 90 days of age. The ingredients used in the test mixes were chosen using the procedure described above and charts for relevant compressive strength from [1].
Locally available type II cement and ground granulated blast furnace slag (ggbs) were used. The superplasticizer used was a polycarboxylic ether-based type with specific gravity of 1.07. Crushed limestone coarse aggregate with a maximum size of 20 mm was used, while the fine aggregate was river sand. Limestone powder as filler with a maximum particle size of 125 μm was used A part of the river sand was replaced by an equivalent volume of the coarser fraction of limestone filler in the size range 125 μm - 2 mm. Such a replacement is environmentally friendly and economic, thus enhancing the sustainability of the SCC mixes.

Tests on fresh SCC

Tests were conducted to determine the t_{500} and $t_{v-funnel}$ times of the fresh mixes. The time taken by the fresh SCC mix to reach a 500 mm diameter spread in the slump cone flow t_{500} was determined from time sequencing a video recording of the test with an accuracy of a thousand of a second, while the time taken by the fresh SCC mix to flow out of the funnel (daylight appearing when viewed from above) was

recorded as $t_{v\text{-}funnel}$ flow time. All tested self-compacting mixes showed no signs of segregation or bleeding on thorough visual inspection.
The time needed to reach 500 mm diameter spread is related to the plastic viscosity of the mix. This is clearly seen in Figure 3 for a given target flow spread. It is worth remembering that it is very difficult if not impossible to measure plastic viscosity accurately. It is well known [7-9] that for one and the same mix different types of rheometer give different values of Bingham parameters (plastic viscosity and yield stress).

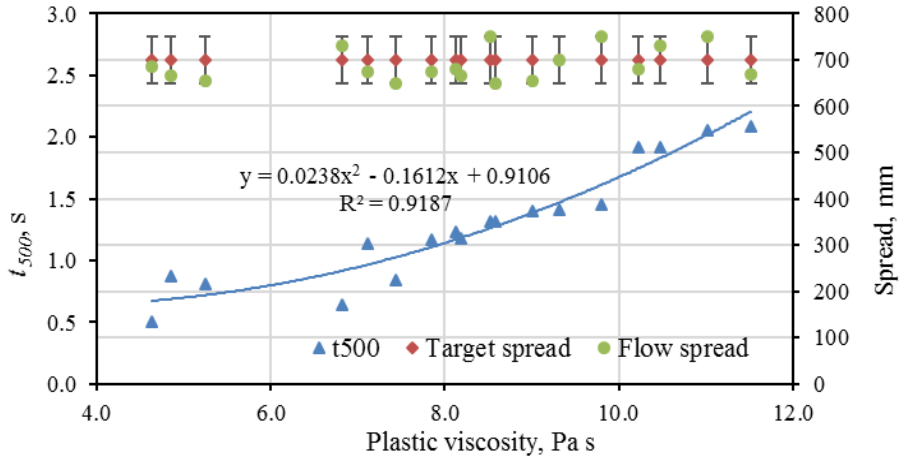

Figure 3. Plastic viscosity and t_{500} Relationship for target flow spread 700±50mm

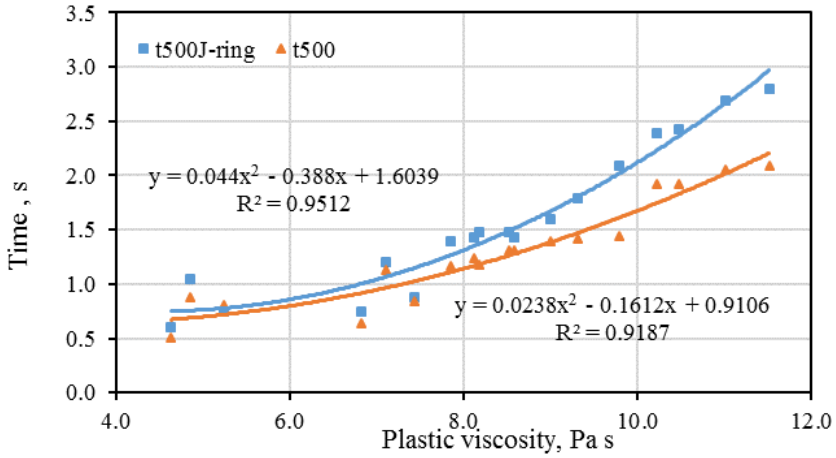

Figure 4. Plastic viscosity versus t_{500} and t_{500J}

All the test mixes that satisfied the flow-ability criterion and showed no signs of segregation were subjected to the passing and filling ability test using the J–ring

and L–box to ensure that they were able to pass through the narrow gaps that exist between reinforcing bars in real reinforced concrete structural elements.

The relationship between the parameters t_{500} of J-ring and slump flow of SCC was also taken into consideration in this study. The best-fit curve of t_{500} against the plastic viscosity is plotted graphically alongside with the t_{500J} in Figure 4. It was found that the difference between these times is more pronounced at higher plastic viscosities (9-12 Pa s) only. A possible explanation for this is that the mixes become sticky taking more time to pass through the obstacles in the J-ring.

References

[1] Karihaloo, B. L. and Ghanbari, A. (2012), *Mix proportioning of self–compacting high–and ultra–high–performance concretes with and without steel fibres*. Magazine of Concrete Research, 64, 1089–1100.

[2] Deeb, R. and Karihaloo, B. L. (2013), *Mix proportioning of self–compacting normal and high–strength concretes*. Magazine of Concrete Res, 65, 546–556.

[3] Ghanbari, A. and Karihaloo, B. L. (2009), *Prediction of the plastic viscosity of self–compacting steel fibre reinforced concrete*. Cement and Concrete Research, 39, 1209–1216.

[4] Abo Dhaheer, M. S., Al-Rubaye, M. M., Alyhya, W. S., Karihaloo, B. L. and Kulasegaram, S. (2015), *Proportioning of self–compacting concrete mixes based on target plastic viscosity and compressive strength: Mix design procedure.* Journal of Sustainable Cement-based Materials, doi:10.1080/21650373.2015.1039625

[5] Abo Dhaheer, M. S., Al-Rubaye, M. M., Alyhya, W. S., Karihaloo, B. L. and Kulasegaram, S. (2015), *Proportioning of self–compacting concrete mixes based on target plastic viscosity and compressive strength: Experimental validation*. Journal of Sustainable Cement-based Materials, doi:10.1080/21650373.2015.1036952

[6] EFNARC, (2005). *The European guidelines for self-compacting concrete–specification, production and use*. [Online] Available at: www.efnafrc.org.

[7] Banfill, P., Beaupre, D., Chapdelaine, F., Larrard, F., D., Domone, P., L., J., Nachbaur, L., Sedran, T., Wallevik, O., H., and Wallevik, J., E. (2000). *Comparison of concrete rheometers*: International tests at LCPC, Paris; pp 157.

[8] Feys, D., Heirman, G., De Schutter, G., Verhoeven, R., Vandewalle, L., and Van Gemert, D. (2007). *Comparison of two concrete rheometers for shear thickening behaviour of SCC.* Proceeding of the 5th International RILEM Symposium on Self-Compacting Concrete, Eds: G. De Schutter and V. Boel. Paris: RILEM Publications SARL, P. 365 – 370.

[9] Wallevik, O., H., and Wallevik, J., E., (2011). *Rheology as a tool in concrete science: The use of rheographs and workability boxes*. Cement and Concrete Research, 41(12): p. 1279-1288.

Effect of Particle-Size Distribution and Lattice Effect on Stability of Self-Consolidating Concrete

Behrouz Esmaeilkhanian[1], Paco Diederich[1], Kamal H. Khayat[2], Ammar Yahia[1] and Ólafur H. Wallevik[3]

[1]Department of Civil Engineering, Université de Sherbrooke, 2500, boul. de l'Université, Sherbrooke, Qc, Canada, J1K 2R1
[2]Missouri University of Science and Technology, Université de Sherbrooke, 224 Engineering Research Laboratory 500 W. 16th St. Rolla, MO, 65409
[3]ICI Rheocenter, Reykjavik University & Innovation Center Iceland, Keldnaholt, IS-112 Reykjavik, Iceland

Abstract Particle size distribution (PSD) can affect the stability of a granular skeleton suspended in a fluid through particle lattice effect (PLE). The PLE refers to the modification of the sedimentation behavior of one particle or a group of particles in the presence of neighboring particles. For highly flowable concretes which are sensitive to segregation, the PLE may be a key solution to stabilize the system. In the present work, the stability of several groups of polydisperse spherical glass marbles suspended in a model mortar constituted of limestone filler paste and fine spherical marbles is investigated. Test results show that for a given size-class, increasing the volume fraction leads to better stability due to a higher PLE. Furthermore, the main contribution of PLE to the enhancement of the stability of the suspension seems to be achieved via the stabilization of the fine particles by increasing their volume fraction. The highest level of stability is obtained when the volume fraction of fine particles is larger than or equal to that of coarse particles. The experimental validations carried out on self-consolidating concrete (SCC) mixtures show similar trends to those of model suspensions.

Keywords: *Particle lattice effect, particle-size distribution, particle stability, rheology, self-consolidating concrete*

Introduction

Self-consolidating concrete (SCC) should achieve high filling ability, high passing ability, and sufficient segregation resistance. Attaining the first two properties can jeopardize the stability of the mixture since it necessitates a lower yield stress and

viscosity of paste i.e., a lower capacity to keep the aggregate suspended [1]. Thus, knowing that the particle-size distribution (PSD) of aggregate is a parameter affecting the stability of a suspension [2], it is advantageous to utilize the potential of PSD in this respect to maximize the stability of the granular system.

The stability of particles in a suspension, with focus on concrete stability, was addressed by some researchers. Saaks et al. [3] developed a mix design procedure for SCC based on controlling segregation of particles in paste. Assaad et al. [4] demonstrated the importance of rheological properties of SCC (with slump flows between 615 and 715 mm), that were directly related to the rheology of the paste, on the segregation resistance of concrete. Aissoun et al. [5] found that PSD played a significant role in the segregation resistance of highly flowable concrete (HFC). Ramge et al. [6] suggested a segregation potential classification for particles of different shapes, densities, and diameters. One phenomenon that can affect the sedimentation of particles in a fluid is the particle lattice effect (PLE).

The PLE refers to the phenomenon that induces a difference between the sedimentation behavior of an individual particle and that of a group of particles. Inter-particle interactions and modifications in the activated shear area (or flow patterns) around the particles inside the suspending fluid are the two principal phenomena at the origin of the PLE [6, 7]. Roussel [8] related the minimum distance between similar particles in a yield stress fluid to the properties of the fluid and the characteristics of the granular skeleton. Hence, knowing the yield stress of the fluid and assuming that in the segregated zone the particles are positioned at the minimum distance relative to each other, the volume fraction of aggregate in this area could be calculated. This theory is useful when comparing the influence of PLE on the segregation of a group of similar spheres to that of a single sphere. Bethmont et al. [7, 9] found that the resisting force of a single particle to the flow of fluid around it is always lower than that of a group of particles, thus indicating the existence of the PLE. It was observed that the PLE was a function of the total volume of particles and the rheological properties of the paste. In case of SCC mix design, the type of PLE that is important is the one originating from the interaction between several size-classes of aggregate in the mixture i.e., the finer more stable particles can restrict or stop the settlement of the coarser ones [10]. Wallevik et al. [11] mentioned that such PLE can increase if in a granular skeleton the volume fraction of a certain size-class is equal or larger than the consecutive coarser size-class.

The aforementioned review demonstrated the importance of the granular skeleton in improving stability of a suspension of particles in a yield stress fluid. However, no distinction is made between the contributions of PSD and PLE to the segregation resistance of suspended particles. Moreover, the hypotheses put forward by Bethmont et al. [7] and Wallevik et al. [11] need to be assessed thoroughly to verify applicability and limits. The objective of the present study is to determine experimentally the influence of PLE on the segregation of spherical

particles in a yield stress fluid. Spherical glass particles of different sizes are used to produce several polydisperse PSDs. A suspension of limestone filler paste and 3 mm spherical marbles is employed as suspending fluid. The mode of action of PLE and its relation to PSD are discussed. The applicability of the results to SCC mixtures is examined. Six SCC mixtures with slump flow values typical of a wide range of common SCC mixtures (620 to 800 mm) are prepared. Such mixtures have similar PSDs to those of the polydisperse combinations in model materials. Good correlations between the model materials and the SCC mixture results were observed.

Experimental Program

Model Materials

Fine limestone powder with a maximum particle size of 100 μm along with a polycarboxylate-based high-range water reducing admixture (HRWRA) was used in the composition of limestone filler paste (LP). Glass marbles with a density of 2530 ± 20 kg/m^3 and nominal radii of 3, 5, 10, 14, and 19 mm were employed as solid inclusions. The Model Mortar (MM) comprised of 45.5% of 3 mm marbles and 54.5% of the LP. The water to powder ratio *(w/p)* and HRWRA content of the LP were adjusted to obtain the desired properties for MM as given in Table I. The total volume of coarse marbles, i.e., 5, 10, 14, and 19 mm classes were kept constant (30% of total mixture volume) in all studied suspensions.

LP was prepared in a paddle mixer in batches of 4.5 l. Water and HRWRA were introduced in the mixer first. The powder was then added into the mixer and mixed for 120 s at slow speed. The mixer was stopped afterwards for 90 s. During the first 30 s, any paste collected on the sides of the mixer bowl was scraped down into the mixture. The sequence was finalized by a 180 s mixing period at medium speed. From the same batch of LP, two samples were extracted for the segregation test and characterization of the properties of the MM. To prepare the MM, LP was poured in a container before 3 mm marbles were added into the recipient and hand stirred for 30 s. Afterwards, the coarse marbles were introduced into the MM receptacle (paste + 3 mm marbles) and hand stirred for an additional 30 s. [12]. For rheological measurements on the MM, the MM sample was directly prepared in the rheometer bowl at the same time as the preparation of segregation test sample.

Table I. Properties of Model Mortar (MM)

	Yield stress, Pa		Viscosity, Pa.s	Density, kg/m^3
	Dynamic	Static		
Model Mortar (MM)	11.1 ± 0.6	13.8 ± 1	3.4 ± 0.1	2075 ± 10

Once the segregation test and rheological measurement samples were ready, the segregation sample was cast into the testing mold over a period of 30 s in a way to minimize the free fall height i.e., the sample container rest on the edge of the mold during the filling procedure. The mold was a rectangular column with a cross section measuring 150 mm by 150 mm and a height of 400 mm. The rheology sample was hand stirred while the testing sample was placed into the mold after which it was transported to the rheometer. The sample was left at rest inside the mold for 30 min. After this period, four plates were inserted into the side wall of the mold alongside the height to divide the sample into five sections of 60 mm high (the total sample height inside the mold was maintained at 300 mm for all tests). The sample within each section was then collected and sieve-washed to retrieve the marbles. The marbles were dried and weighed to determine the segregation index (SI) and the lack of lattice index (LLI) as explained subsequently. The SI reflects the homogeneity of entire particles over the height of the mold and is derived from Eq. (1):

$$SI\ (\%) = \frac{\sqrt{\frac{\sum_{i=1}^{5} (m_i - \bar{m}_i)^2}{4}}}{\bar{m}_i} \times 100 \tag{1}$$

where m_i is the total coarse marble mass in the i^{th} section, and $\bar{m}_i$ is the average of m_i over the five sections. Hence, SI represents the coefficient of variation of m_i in the five sections of the mold.

The LLI quantifies the state of distribution of each size-class over the height of the mold and thus is defined as:

$$LLI\ (\%) = (v_1 \times LLI_1 + \ldots + v_5 \times LLI_5) \times 100 \tag{2}$$

where v_j is the volume fraction of size-class j, and LLI_j is the lack of lattice index of the same class given by:

$$LLI_j\ (\%) = \frac{\sqrt{\frac{\sum_{i=1}^{5} \left(\frac{m_{i,j}}{M} - \frac{\overline{m_{i,j}}}{M}\right)^2}{4}}}{\frac{\overline{m_{i,j}}}{M}} \times 100 \tag{3}$$

where $m_{i,j}$ is the mass of size class 'j' in section 'i', and M is the average mass of all coarse marbles over the five sections i.e., one fifth of the total mass of coarse marbles in the test sample. Hence, a higher LLI for a given size-class means a more heterogeneous distribution of that class over the height of the testing box.

SCC Mixtures

Six SCC mixtures were tested to examine the applicability of the results obtained from the model suspensions. A Type GU portland cement and a fine limestone powder were employed as powder materials. Natural siliceous river sand with a saturated surface dry (SSD) density of 2.68 g/cm^3 and water absorption of 0.9% was used in all mixtures. Crushed limestone coarse aggregate with SSD density of 2.75 g/cm^3 and water absorption of 0.49% were sieved to produce the three desired particle size classes, i.e., 5-10 mm, 10-14 mm, and 14-19 mm.

There were two classes of mixtures in regards to fluidity. Thus, for each PSD, one fluid SCC (F) and one thick SCC (T) mixtures were tested. The only difference between the two mixtures is the HRWRA content. The name of each mixture starts with the letter 'F' or 'T' representing the fluidity class followed by three numbers standing for the volumetric proportions between different size-classes of coarse aggregate. For example, F-40-50-10 stands for a fluid mixture containing 40% 5-10 mm, 50% 10-14 mm, and 10% 14-19 mm classes (percentage of total coarse aggregate volume, which is fixed to 30% in all mixtures). Table II presents the material proportions of the investigated SCC mixtures.

SCC mixtures were prepared in a 100-l rotating drum mixer. The mixing sequence comprised of homogenizing coarse aggregate and sand for 2 min before adding half of the water and mixing for 1 min. The powder materials were introduced afterwards, and mixing was resumed for 30 s, after which the remaining water with the HRWRA diluted in it was added into the mixer and mixed for an additional 2.5 min. The mixture was then left at rest for 2 min before the final 3 min of mixing. Immediately after the end of mixing, the fresh properties were characterized by means of slump flow (C1611/C1611M), J-Ring (C1621/C1621M), and V-funnel (with an opening of 75 × 75 mm). Rheological measurements were also carried out.

Table II. Material proportions of studied SCC mixtures

	F-40-50-10	F-25-50-25	F-10-50-40	T-40-50-10	T-25-50-25	T-10-50-40
Cement, kg/m^3			375			
Limestone filler, kg/m^3			55			
Water, kg/m^3			193.5			
Sand, kg/m^3		945			955	
HRWRA, L/m^3		2.6			2.3	
5-10 mm, kg/m^3	336	210	84	336	210	84
10-14 mm, kg/m^3	420	420	420	420	420	420
14-19 mm, kg/m^3	84	210	336	84	210	336

The column segregation test was performed to quantify the segregation and the lattice effect for each mixture. The testing apparatus was comprised of a column measuring 660 mm in height and 200 mm in diameter. The column was divided into four separable sections measuring 165 mm each. The SCC sample was cast into the column over a period of 2 min, after which the column was left at rest for 15 min. Then, the concrete sample in each section was collected starting from the top. After determining the weight of each SCC sample, the sample was washed over a 5 mm sieve to retain the coarse aggregate [4]. The ratio between the mass of the coarse aggregate and the total mass of the concrete sample for each section (relative mass of coarse aggregate) was determined, and the SI was calculated using Eq. (1). Here m_i corresponded to the relative mass of coarse aggregate in the i^{th} section, and $\bar{m}_i$ was the average of m_i over the five sections. In order to determine the LLI and the LLI_j using Eqs. (2) and (3), the coarse aggregate collected from each section was sieved, and the mass of each size class, i.e., 5-10 mm, 10-14 mm, and 14-19 mm were recorded. These values were then normalized by the mass of the SCC sample in the respective section before being used in Eq. (3).

Rheological Measurements

Model Mortar (MM). Rheological measurement on the MM was carried out using a ConTec Viscometer 6 rheometer, which is a coaxial cylinder rheometer with an outer rotating cylinder. The radii of outer and inner cylinders were 0.06 and 0.05 m, respectively. The measuring procedure for dynamic properties consisted of pre-shearing the sample for 30 s with a rotational speed of 0.3 rps, after which the speed was reduced to 0.025 rps over seven steps. The Reiner-Riwlin equation corresponding to the Bingham model was employed to transform the torque-speed data to calculate yield stress and viscosity. The procedure for determining the static

yield stress consisted of applying a constant rotational speed of 0.3 1/min during 20 s to a sample that was at rest for 5 min prior to testing. The peak value of shear stress was reported as the static yield stress. Both dynamic and static testes were repeated at the end of the segregation test i.e., after 30 min, and no significant variation in the rheological properties was observed

SCC mixtures. A ConTec Viscometer 5 rheometer, similar to ConTec Viscometer 6, was employed to characterize the rheological properties of SCC mixtures. The radii of outer and inner cylinders were 0.15 and 0.1 m, respectively. The measuring configuration involved a 30 s pre-shearing period at 0.4 rps before the speed was decreased stepwise to 0.025 rps (7 steps). The Bingham model was used to calculate yield stress and viscosity of mixtures.

Results

Effect of PSD on PLE and Segregation of Particles Suspended in MM

Figure 1 presents the variation of SI and PLE with volume ratio between 5 mm and 19 mm marble classes in a polydisperse granular skeleton suspended in the MM. The studied PSDs include: 10%5mm25%10mm25%14mm40%19mm, 25%5mm25%10mm25%14mm25%19mm, and 40%5mm25%10mm25%14mm10%19mm. Consequently, the volume fraction and the volume ratio between the two middle classes are kept constant in all tests. The total volume of 5-19 mm marbles and 3 mm marbles are 30% and 25% of the total mixture volume, respectively, in all tests. The SI and PLE are only calculated for 5 mm and coarser marbles. It is observed that by replacing the 19 mm particles with 5 mm particles, the segregation and lack of lattice first reduce and then remain constant. The improvement of stability originates from a higher stability of 5 mm and 10-14 mm marbles. Considering that the volume of 10-14 mm class is constant, the lower segregation of this class with increase in volume of 5 mm particles is due to a better PLE provided by 5 mm marbles. The stability of 19 mm particles is not significantly affected among the studied PSDs. It is noted that in the case of the used mortar, the most stable mixture is already obtained when the volume of 5 mm marbles is equal to that of each individual coarser class.

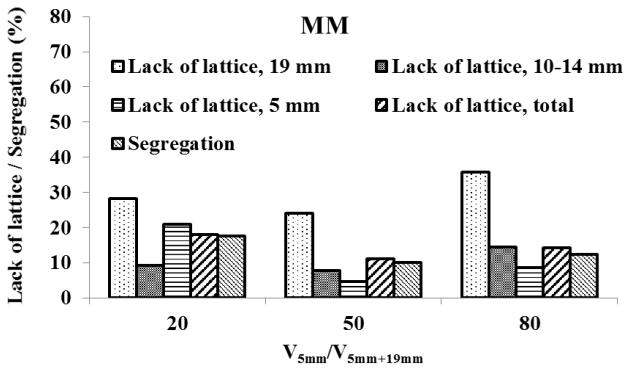

Figure 1. Influence of volume ratio between 5 mm and 19 mm particle classes on SI and PLE of polydisperse granular skeletons suspended in the MM

Influence of Coarse Aggregate PSD on Stability and PLE of SCC

Table III presents the fresh properties of the investigated SCC mixtures except for the segregation test. The results of the segregation tests are summarized in Figure 2.

Table III. Fresh properties of studied SCC mixtures

	F-40-50-10	F-25-50-25	F-10-50-40	T-40-50-10	T-25-50-25	T-10-50-40
Slump Flow, mm	710	710	800	620	640	680
Slump flow - J-Ring, mm	30	70	110	50	80	60
V-funnel, s	3.2	4.2	6.7	4.8	6.9	9.5
Yield stress, Pa	22	26	37*	44	42	35
Viscosity, Pa.s	18	18	10*	20	22	14

* Segregation may affect the results

It is seen that the trends of SI and PLE obtained for both fluid and thick SCC mixtures are similar to the ones attained for marbles suspended in the MM (see Figure 1). Regardless of the fluidity level, decreasing the volume of 5-10 mm class from 40 to 25% of total coarse aggregate volume, does not affect the SI and PLE of the SCC mixtures. Further reduction of this class to 10% causes an increase in the SI and LLI of the mixtures. In the latter case, the increase in segregation level is more drastic for the fluid concrete than the thick one. It is noted that apart from the mixtures with 10-40-50 PSD type, all other SCC mixtures exhibit the same level of stability.

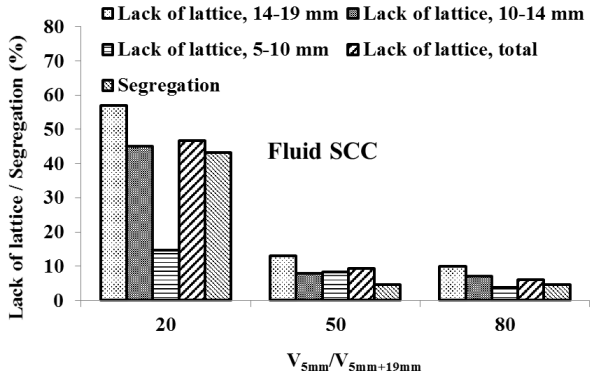

(a)

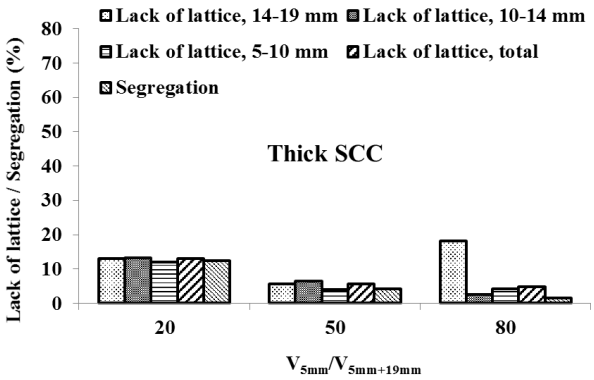

(b)

Figure 2. Effect of the variations of PSD on the segregation and PLE of SCC mixtures

Discussions

Stability vs Rheology for SCC

For each fluidity class (F or T), varying the PSD of coarse aggregate from 40%5-10mm50%10-14mm10%14-19mm to 25%5-10mm25%10-14mm25%14-19mm does not remarkably alter the stability and rheological properties of the SCC mixtures as seen in Table III. The only property which is notably influenced is the passing ability characterized by the difference in diameters of slump flow and J-Ring tests. In the latter case, the mixtures with 40%5-10mm50%10-14mm10%14-19mm PSD exhibit a better passing ability. Using a grading of 10%5-10mm50%10-14mm40%14-19mm adversely alters all properties, and the resulting mixtures do not meet the self-consolidation criteria.

The importance of maximizing the PLE is obvious in Figure 2 where for 40-50-10 and 25-50-25 PSDs, the stability level of the respective SCC mixtures does not vary by a considerable increase in the fluidity of the mortar. More specifically, for the two mixtures that meet all the fresh properties requirements of self-consolidation, i.e. T-40-50-10 and F-40-50-10, the yield stress is reduced by half from T-40-50-10 to F-40-50-10 while the SI remains rather similar. Thus, employing an appropriate PSD with a high level of PLE provides the possibility of improving the passing ability and the filling ability of SCC without compromising the stability of the mixture.

Conclusions

The stability of a series of model suspension systems made with spherical glass particles of different sizes and combinations was investigated. The influence of PSD on segregation and PLE of model mixtures was determined. The applicability of the results to SCC was evaluated. Based on the outcome of the presented research work, the following conclusions are warranted:

- The increase in volume fraction of any size class of a granular skeleton can improve stability of that class via a more effective PLE. This

phenomenon is the main contribution of the PLE to the stability of the mixture. However, if this size-class is segregating, an increase in the PLE would not be sufficient to mitigate segregation. When the volume of the stable class of the granular skeleton becomes large relative to that of the unstable ones (a ratio greater or equal to 2/3 by volume), the stable particles can provide a low degree of support for coarser unstable particles, which is another manifestation of the PLE originating from inter-particle interactions.

- An appropriate PSD constitutes of a continuous granular skeleton in which the volume fraction of each class increases with the decrease in the size in order to improve the PLE. When such PSD is employed in a SCC mixture, the fluidity of the mixture can be significantly increased without jeopardizing the stability of the mixture.

References

[1] Khayat, K. H. (1999), "Workability, testing, and performance of self-consolidating concrete," *ACI Mater. J.*, vol. 96, no. 3, pp. 346–354.

[2] de Larrard, F. (1999), *"Concrete mixture-proportioning – a scientific approach", modern concrete technology series*, No. 9. London: E & FN SPON.

[3] Saak, A. W., Jennings, H. M. and Shah, S. P. (2001), "New methodology for designing self-compacting concrete," *ACI Mater. J.*, vol. 98, no. 6, pp. 429–439.

[4] Assaad, J., Khayat, K. H. and Daczko, J. (2004), "Evaluation of static stability of self-consolidating concrete," *ACI Mater. J.*, vol. 101, no. 3, pp. 207–215.

[5] Aïssoun, B. M., Hwang, S.-D. and Khayat, K. H. (2015), "Influence of aggregate characteristics on workability of superworkable concrete," *Mater. Struct.*.

[6] Ramge, P., Proske, T. and Kuhne, H.-C. (2010), "Segregation of coarse aggregates in self-compacting concrete," In: *Design, Production and Placement of Self-Consolidating Concrete, RILEM Bookseries 1*, vol. 1, no. 1, pp. 113–125, Khayat, K. H. and Feys, D. (Eds.)

[7] Bethmont, S. (2005), "Segregation mechanism in self-consolidating concrete (SCC): experimental study of granular interactions, " (in French), Ph.D. Thesis, Ecole Nationale des Ponts et Chaussées.

[8] Roussel, N. (2006), "A Theoretical frame to study stability of fresh concrete," *Mater. Struct.*, vol. 39, no. 1, pp. 81–91.

[9] Bethmont, S., D'Aloia Schwartzentruber, L., Stefani, C., Tailhan, J. L. and Rossi, P. (2009), "Contribution of granular interactions to self compacting concrete stability: Development of a new device," *Cem. Concr. Res.*, vol.

39, no. 1, pp. 30–35.

[10] Wallevik, O. H. (2003), "Rheology—a scientific approach to develop self-compacting concrete," In: *Proceedings of the 3rd International RILEM Symposium on Self-Compacting Concrete*, pp. 23–31.

[11] Wallevik, O. H., Mueller, F. V, Hjartarson, B. and Kubens, S. (2009), "The green alternative of self-compacting concrete, Eco-SCC," In: *XVII IBAUSIL Weimar, Vol. 1*, pp. 1105–1116.

[12] Mahaut, F., Mokéddem, S., Chateau, X., Roussel, N. and Ovarlez, G. (2008), "Effect of coarse particle volume fraction on the yield stress and thixotropy of cementitious materials," *Cem. Concr. Res.*, vol. 38, no. 11, pp. 1276–1285.

Robustness of Powder-Type SCC with Fly Ash and Limestone Crushed Aggregates

Gálvez-Moreno, D.[1], Durán-Herrera, A.[1], González-López, J.R.[1] and Khayat, K.H.[2]

[1]Universidad Autónoma de Nuevo León, Facultad de Ingeniería Civil. Pedro de Alba S/N, San Nicolás de los Garza, 66400, Nuevo León, México.
[2]Missouri University of Science and Technology, 1870 Miner Cir, Rolla, MO 65409, USA.

Abstract To ensure stable fresh properties of a Self-consolidating concrete (SCC) a balance between cohesiveness, deformability, segregation resistance and passing ability should be provided. Therefore, it is desirable to produce robust mixtures able to absorb small fluctuation of ingredients inherent to the nature of materials or variations from the production process, without significantly changing fresh or hardened concrete properties. In this research, a powder type SCC with slump flow of 720 mm and zero static segregation (measured with the segregation column) was produced by replacing 20% of cement volume by fly ash. The SCC was prepared using limestone crushed aggregate and limestone powder (< 125 µm) contained in the fine aggregate as a paste constituent to improve segregation resistance. The variables studied were small variations in mixing water, superplasticizer content and sand gradation. The effect of such variations on slump flow, V-funnel, J-Ring, segregation column, rheological parameters and compressive strength at 28 d was determined comparing the obtained results with confidence intervals at 95% constructed by repeating the reference mixture five times, so natural variations produced during mixing, testing or while proportioning materials due to scale precision, environmental factors and labor were taken into account within the confidence intervals. The results obtained showed that Powder-type SCC is more sensitive to changes in sand gradation and mixing water than to superplasticizer variations.

Keywords: *SCC, robustness, rheology, concrete, self-consolidating concrete, portable rheometer.*

Introduction

Self-consolidating concrete (SCC) is a high performance concrete that can flow under its own weight without significant segregation [1]. The robustness of SCC describes the tolerance of its fresh and hardened properties to variations caused by small fluctuations in constitutive materials properties, dosages, production procedures or mixing conditions [2, 3]. To ensure robust mixtures capable to tolerate small variations present at any ready-mixed plant to reduce the number of batches that fail to meet the jobsite acceptance criteria, standard procedures/methodologies can be established for the optimization of any mixture design; so, for SCC mixtures it becomes convenient to identify which variables will have the strongest negative impact in the self-consolidating properties of a given mix design in order to establish strategies that can ensure mixture stability in fresh stage and engineering properties in hardened stage. In this study, the influence of variations of mixing water, superplasticizer content and fine aggregate grading on the properties of a powder-type SCC were evaluated and a robustness index was evaluated for each variable to assess which one has the higher impact on the SCC properties.

Materials and methods

Materials

The cementitious materials used were a Type III portland cement (OPC) which meets ASTM C150-09 requirements and a Class F fly ash (FA) obtained from a carboelectric power plant located at Nava, Coahuila, Mexico. The FA fulfills the chemical composition, fineness, strength activity index and loss of ignition requirements of ASTM C618-08. The OPC and FA used had density of 3.13 and 2.06 g/cm^3, respectively. Locally available crushed limestone was used as fine and coarse aggregates. The maximum nominal size of coarse aggregate was 19 mm. The fine aggregate was sieved and sorted by sizes in order to reproduce the lower, average and upper grading limits established by ASTM C33-09 (G-L1, G-L2 and G-L3, respectively). The fine aggregate original grading was also evaluated (G-BM). Table VI shows the density and absorption of coarse and all fine aggregate gradings evaluated.

The particle-size distributions (PSD) of all granular materials used is shown in Figure 8. It is evident that the FA is coarser than the typically reported in literature. Nonetheless, it should be noted that it can improve the packing density by providing particles which have an intermediate size between the fine aggregate and cement. The selected PCE superplasticizer meets all the requirements of ASTM

C494-10 for Class A and F chemical admixtures and had a density and solid content of 1.09 g/cm^3 and 43%, respectively.

Table VI. Fine and coarse aggregates physical properties.

Material	Fine aggregate				Coarse aggregate
	G-BM	G-L1	G-L2	G-L3	
Density (g/cm^3)	2.62	2.60	2.59	2.37	2.69
Absorption (%)	1.58	1.55	2.41	2.57	0.4

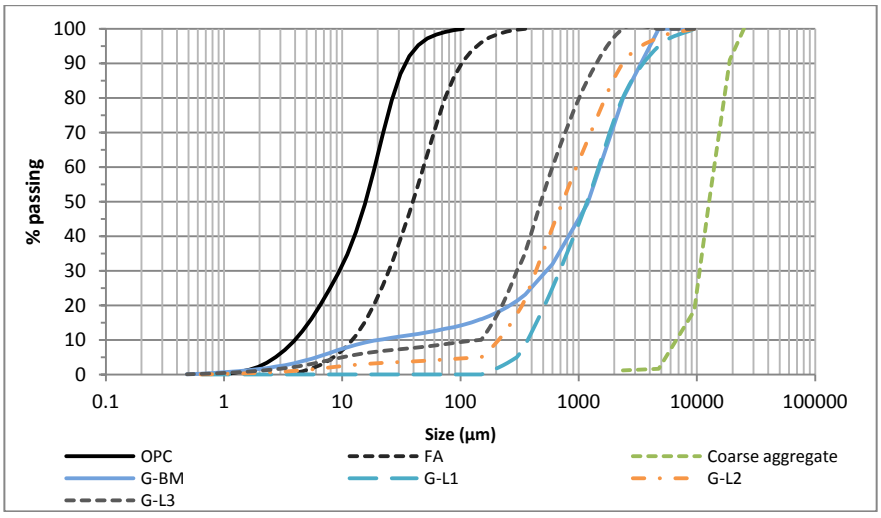

Figure 8. Particle size distributions of the materials employed in this study.

Methods

A powder-type SCC mixture was designed with a w/p of 0.29, slump flow of 720 ± 20 mm and zero segregation (measured accordingly with ASTM C1610-14) using 20% fly ash as cement volume replacement. All particles < 125 µm were considered as part of the powder volumetric fraction. The reference mixture materials proportion is shown in Table VII. The repeatability of the reference mixture was assessed by repeating five batches of 80 liters which were made in a conventional drum mixer. Their properties were measured by slump flow, v-funnel, J-ring, segregation column and compressive strength as specified in ASTM C1611-09, EFNARC 2005 [2], ASTM C1621-09, ASTM C1610-14 and ASTM C39-09,

respectively. The rheological properties were determined using a portable vane rheometer. The rheometer testing protocol consisted in 20 s pre-shearing period followed by 10 rotational frequency downward steps, which started at 0.5 rps and stopped at 0.03 rps. Every step had a 5 s fixed time and only the data from the last 4 s of each step was considered for further analysis. Due to the produced SCC showed a shear-thickening behavior, the data analysis was carried out independently of the results provided by the rheometer software to determine the modified Bingham model (MBM) rheological parameters, and the rheology tests results were transformed from relative to fundamental physical units using proper transformation [4]. When a non-linear rheological model is used, it is not possible to define the plastic viscosity as the slope of the flow curve because the slope changes constantly depending on the shear rate applied. To solve this, the differential viscosity is reported at a shear rate value of 3.1 s^{-1}, since this is the mean shear rate obtained from all the rheological tests conducted with the rheometer. In addition, due to the wide gap between the diameters of inner and outer cylinders, plug flow effect was considered and corrected for by means of an iterative method.

After that, confidence intervals of 95% were calculated using the average and standard deviation of the five measurements of each test method. Therefore, all small changes regarding to mixture proportions, mixing procedure, mixing energy, temperature and aggregate humidity, among others, are taken into account inside the confidence intervals. Therefore, if there is a change in the observed behavior outside the confidence intervals in a given property due to an intentional deviation in mixing water, superplasticizer content or fine aggregate gradation, the probability that the measured change is significant, would be high [5].

Table VII. Reference powder-type SCC mixture proportion.

Materials	**Dry materials without absorption water (kg/m^3)**
Water	178
SP (total solution)	1.7
Cement	384
Fly ash	63
Limestone powder (fine aggregate particles < 125 μm)	178
Coarse aggregate	518
Fine aggregate (Particles > 125 μm)	1,000
Air (2.5%)	-

Robustness assessment

In order to assess the robustness of the mixture, the maximum variation range (MVR) of ± 6% in mixing water and SP (total solution) was investigated. Accordingly to EFNARC, a well-proportioned SCC should tolerate a change of ±10 liters of mixing water, which represents approximately ±6% of water content of a typical SCC [6]. The influence of fine aggregate grading was evaluated by reproducing the upper (G-L3), lower (G-L1) and average (G-L2) grading limits of ASTM C33-09. Since the original grading of fine aggregate (G-BM) included 15.09% of limestone powder due to the crushing process (expressed as 6.8% of total mixture volume), the grading variations were expressed as changes in the water-to-powder volume ratio (Vw/Vp) (Figure 9). As the fine aggregate becomes coarser, the amount of limestone powder < 125 µm was reduced gradually to fit the ASTM C33-09 grading limits. Therefore, for comparing the influence of changes in fine aggregate grading with the influence of changes in water and SP content, the variation range (VR) was normalized to 12 points as shown in Figure 10 and Figure *11*.

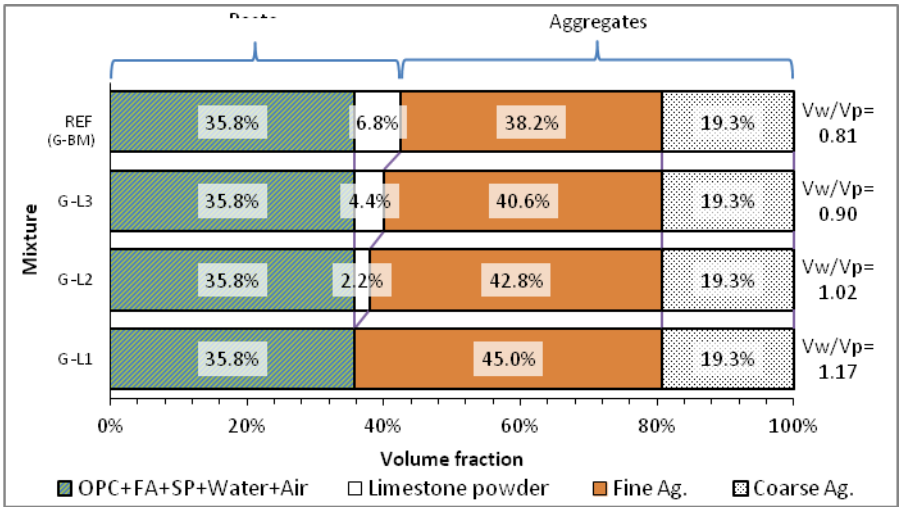

Figure 9. Changes at mixture volumetric fractions produced due to fine aggregate grading variations

The measured changes were plotted together with the confidence intervals. The tolerance ranges (TR) were defined as the variation limits where the observed trend remained within the confidence intervals, as shown in Figure 10 and Figure *11*. The robustness index (RI) for each variable was calculated according to eqn. (1). The higher RI value, the more tolerance to changes in the variable assessed can be expected within the variation ranges tested.

$$RI = \frac{\Sigma_{TR}}{MVR * NCT} x100 \quad (1)$$

where:

$RI =$ Robustness index
$TR =$ Tolerance range of each conducted test
$MVR =$ Maximum variation range
$NCT =$ Number of conducted tests

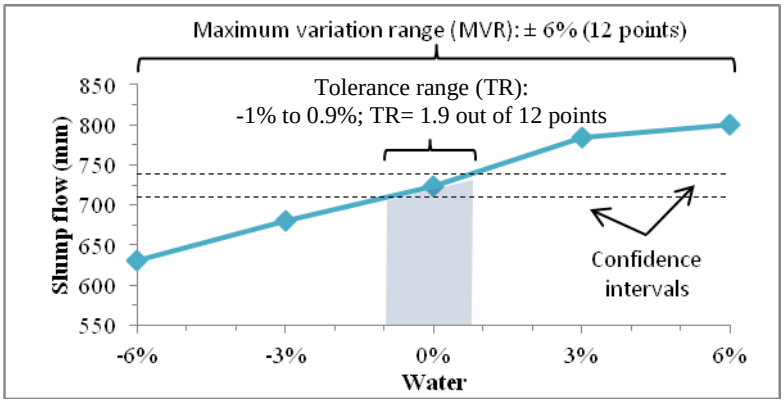

Figure 10. Robustness assessment due to mixing water variation

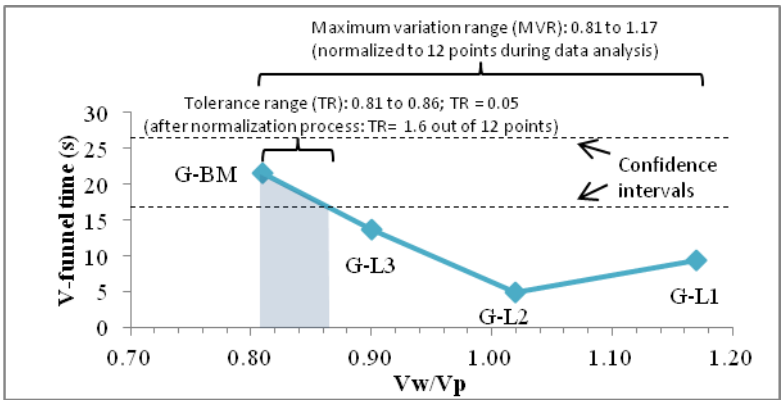

Figure 11. Robustness assessment for fine aggregate grading variation (expressed as changes in Vw/Vp)

Results and discussion

Reference mixture repeatability

Table *VIII* shows the results obtained from the repeatability of the investigated mixture. As can be seen, the slump flow and the segregation resistance targeted were achieved (720 mm ± 20mm and zero segregation). The mean V-funnel time was very high due to the high viscosity needed to drag and keep the coarse aggregate in suspension during flow. Accordingly with ASTM C1621-09, the passing ability can be assessed as the difference between the slump flow values performed with and without the J-Ring. It can be observed in Table III that test can be classified as extreme. Nonetheless, an extreme blockage condition would be a problem only if this mixture design was intended to be used in highly reinforced concrete structures. On the other hand, the compressive strength at 28 d was superior to what it was expected, taking into consideration that only 384 kg of cement/m^3 of concrete were used. This can attributed to the high particle packing achieved by the powders used (fly ash and fine aggregate microfines). Table III shows the calculated rheological parameters. Due to the high intensity of shear-thickening (expressed as c/μ) behavior exhibited by the reference mixture, the differential viscosity was high in comparison to the most of SCC mixtures reported in literature (15 to 120 Pa.s) [7]. However, because of its high fluidity, the selected powder-type SCC had a good workability under low shear rates. Regarding the segregation column test, the measured value of five repetitions was 0%, making it impossible to calculate confidence intervals. So, the threshold for determining when an induced variation is significant was adopted as 10% as suggested by ACI 237-07 [1].

Table VIII. Measured mixture properties

Mixture	Slump flow (mm)	V-funnel (s)	J-ring Blockage (mm)	Compressive strength @ 28 d (MPa)	Segregation column (%)	Modified Bingham model rheological parameters			
						Yield stress (Pa)	Viscosity coefficient, μ (Pa.s)	Differential viscosity $\dot{\gamma}$= 3.1s^{-1} (Pa.s)	c/ μ
R1	730	18.0	115	48.9	0	23.2	25.2	81.8	0.361
R2	720	18.0	100	49.5	0	22.8	30.9	89.7	0.306
R3	740	20.9	125	53.1	0	25.3	26.4	103.3	0.468
R4	720	26.3	50	48.4	0	29.9	23.1	124.2	0.704
R5	710	25.1	55	51.9	0	25.5	27.5	138.9	0.652
Reference mixture confidence intervals									
Avg.	724	21.7	89	50.4	0	25.3	26.6	107.6	0.498
Std.Dev	11	3.9	35	2.0	-	2.8	2.9	23.8	0.175
+95% C.I.	738	26.5	132	52.9	-	28.9	30.2	137.1	0.716
-95% C.I.	701	16.9	46	47.9	-	21.8	23.0	78.1	0.281
Mixing water									
-6WR	630	67.4	108	46.7	0		-	-	-
-3WR	680	45.9	110	44.7	0	28.2	54.3	210.15	0.461
+3WR	785	5.4	73	51.2	10.0	25.2	10.9	37.4	0.390
+6WR	800	9.3	18	52.3	41.3	17.0	15.1	41.4	0.280
Superplasticizer									
-6SP	630	26.3	120	53.3	0.0	24.2	36.9	124.7	0.383
-3SP	685	21.9	75	53.1	0.0	27.5	24.5	91.1	0.436
+3SP	780	14.9	75	48.2	3.1	27.6	14.4	70.1	0.632
+6SP	830	9.6	70	46.5	11.5	24.9	17.3	61.3	0.401
Fine aggregate grading									
G-L3	600	13.8	55	48.4	8.3	43.8	66.9	66.9	-
G-L2	695	4.9	35	47.5	9.4	25.0	25.4	25.4	-
G-L1	838	9.5	98	40.0	40.8		-	-	-

Table *VIII* also shows the results obtained after the variations in mixing water, superplasticizer and fine aggregate grading were implemented. Increasing the water content (from -6 to 6%), allows to the solid particles to move easier through the mixture during flow or at rest conditions because there is less friction between them, increasing the slump flow and passing ability while reducing the v-funnel time and segregation resistance. These results are in agreement with the rheological parameters evaluated, the more water is added, and the lower yield stress, viscosity and shear-thickening response will be obtained. It was not possible to obtain the rheological parameters of mixture -6WR because the water reduction produced a highly stiff SCC, thus hindering the correct measurement of rheological properties. Increasing the SP content from -6 to 6% led gradually to a higher slump flow and lower v-funnel time and segregation resistance. Due to the dispersant effect of the SP, as the SP dosage increases there is more water available to add fluidity to the mixture which originally remained trapped inside the agglomerated solid particles. Mixtures G-L3 and G-L2 showed a Bingham plastic rheological behavior due to the lack of the sufficient amount of fine particles, which could trigger the shear-thickening effect [7]. It is also worth noticing that a reduction of the limestone powder, included in the fine aggregate, increased the static segregation, making it impossible to measure the rheological parameters of mixture G-L1 due to the lack of stability. It was expected to get an increase in compressive strength at lower w/p and higher SP content, but this was not the case due to the high amount of entrapped air because the lack of self-venting. The high viscosity of the produced powder-type SCC hinders the ability of releasing the entrapped air during mixing or casting once that the SCC is at flow or rest conditions. The more entrapped air the concrete have, the lower the compressive strength that it will develops [9, 10].

As can be seen in

Table *IX*, the most sensitive test for evaluating robustness was the slump flow, which is the one with the smaller tolerance range for all the studied variables. The V-funnel was highly sensitive to changes in mixture viscosity. Since a Vw/Vp increment (due to an increase in mixing water or a reduction in the volumetric fraction of powder content in fine aggregate) will reduce the friction between solid particles, a reduction in viscosity was expected. On the other hand, the V-funnel test was not sensitive enough to variations in superplasticizer content, since superplasticizer will mostly have effect into the yield stress [7]. Accordingly to the data analysis of the rheological measurements, the SP did not have a significant effect on yield stress, which is opposite to the behavior observed at the slump flow test results. After observing this particularity, the rheometer was examined and an issue in the torquemeter cell was detected, so the yield stress measurements were not taken into account for further analysis. Since viscosity depends on the relationship of torque readings at different rotational frequencies, this issue did not have an effect on viscosity measurements, and they were in good agreement with the recorded v-funnel times. Lastly, the RI for each of the studied variables was calculated using eqn. 1, the analysis indicates that the investigated powder-type SCC is more sensitive to changes in fine aggregate grading, than mixing water and superplasticizer.

Table IX. Robustness index

	Test methods	Mixing water			Superplasticizer			Fine aggregate grading (as Vw/Vp)		
		Tolerance		TR	Tolerance		TR	Tolerance		TR (normalized)
		-	+		-	+		-	+	
1	Slump flow	1.00	0.90	1.90	1.10	0.80	1.90	0.81	0.82	0.33
2	J-Ring Blockage	6.00	4.40	10.40	6.00	6.00	12.00	0.81	0.98	5.67
3	V-funnel time	0.80	0.80	1.60	6.00	2.00	8.00	0.81	0.86	1.67
4	Segregation column	6.00	3.00	9.00	6.00	5.40	11.40	0.81	1.02	7.00
5	Differential viscosity	1.00	1.20	2.20	6.00	2.50	8.50	0.81	0.88	2.17
6	c/μ	3.00	6.00	9.00	6.00	6.00	12.00	0.81	0.81	0.00
7	Compressive strength at 28 d	1.20	6.00	4.80	2.90	3.50	6.40	0.81	1.03	7.33
	Cumulative tolerance range (Σ_{TR})			*38.9*			*60.2*			*24.17*
	Robustness index (RI):			***46%***			***72%***			***29%***

Conclusions

Based on the selected powder-type SCC mixture assessed in this research work, the following conclusions can be drawn:

- The powder-type SCC is highly sensitive to changes in Vw/Vp because its stability relies on the viscosity provided by the use of high amount of powder and powder combinations.

- The variation of ± 6% of superplasticizer content is the less sensitive variable among mixing water and fine aggregate grading. This is because in powder-type SCC, part of the fluidity is given by the high paste volume, instead of high amounts of superplasticizer, thus increasing the tolerance to fluctuations in superplasticizer content.

- Small fluctuations in mixing water, superplasticizer and fine aggregate grading can lead to important changes in the rheological properties of powder-type SCC, which could compromise its flowability, passing ability, filling ability and segregation resistance as well as its compressive strength.

- The shear thickening behavior can be reduced or even eliminated by increasing the Vw/Vp.

References

1. ACI Commitee 237 (2007). “Self-Consolidating Concrete”. ACI 237-07, ACI Manual of Concrete Practice, Detroit, MI, USA.
2. BIBM, CEMBUREAU, ERMCO, EFCA, and EFNARC (2005) “European Guidelines for Self Consolidating Concrete: Specification, Production and Use”
3. Naji, S., Hwang, S. D., & Khayat, K. H. (2011). Robustness of self-consolidating concrete incorporating different viscosity-enhancing admixtures. ACI materials journal, 108(4).
4. Feys, D., Wallevik, J. E., Yahia, A., Khayat, K. H., & Wallevik, O. H. (2013). Extension of the Reiner–Riwlin equation to determine modified Bingham parameters measured in coaxial cylinders rheometers. Materials and structures, 46(1-2), 289-311.
5. Feys, D., Asghari, A., Ghafari, E., Hernandez, A. M. L., Van Der Vurst, F., & De Schutter, G. (2014). Influence of Mixing Procedure on Robustness of Self-Consolidating Concrete (No. NUTC R333).
6. Rigueira, J. W., García-Taengua, E., & Serna-Ros, P. (2009). Self-consolidating concrete robustness in continuous production regarding fresh and hardened state properties. ACI Materials Journal, 106(3).
7. Wallevik, O. H., & Wallevik, J. E. (2011). Rheology as a tool in concrete science: The use of rheographs and workability boxes. Cement and Concrete Research, 41(12), 1279-1288.
8. Wagner, N. J., & Brady, J. F. (2009). Shear thickening in colloidal dispersions. Physics Today, 62(10), 27-32.
9. Łaźniewska-Piekarczyk, B. (2014). The methodology for assessing the impact of new generation superplasticizers on air content in self-consolidating concrete. Construction and Building Materials, 53, 488-502.
10. Kostrzanowska-Siedlarz, Aleksandra, and Jacek Gołaszewski. "Rheological properties and the air content in fresh concrete for self consolidating high performance concrete." Construction and Building Materials 94 (2015): 555-564.

Influence of Mix Design Parameters on Dynamic Segregation of Self-Consolidating Concrete

Aida Margarita Ley Hernández and Dimitri Feys

Department of Civil, Architectural & Environmental Engineering, Missouri University of Science and Technology, Rolla, MO, United States.

Abstract Dynamic segregation is a phenomenon that occurs when concrete is flowing. It refers to the tendency for coarse aggregate to separate from the suspended matrix while being cast into the formwork. Self-Consolidating Concrete (SCC) is a highly flowable concrete that can spread into place under its own weight and achieve good consolidation in the absence of vibration. Due to the high flow capacity of SCC, it is more vulnerable to suffer stability problems compared to conventional vibrated concrete. In this research project the main purpose is to investigate dynamic segregation of self-consolidating concrete (SCC) using the tilting box. Changes in superplasticizer content, paste volume, aggregate distribution, w/cm and the width of the T-box have been investigated. The results show that dynamic segregation of SCC is dependent on the paste volume, the sand-to-total-aggregate ratio and the width of the formwork, in addition to the rheological properties of the concrete.

Keywords: *self-consolidating concrete; dynamic segregation; rheology; mix design; workability.*

Introduction

Self-consolidating concrete (SCC) is a highly flowable concrete that can spread into place by its own weight and achieve good consolidation in the absence of mechanical vibration without showing defects due to segregation and bleeding[1]. As a consequence of this high flowing ability SCC is more vulnerable to segregation, which means that the concrete must remain homogenous during production, transport and placement[2]. Stability problems such as dynamic and static segregation, may lead to a lower compressive, tensile and flexural strength. In addition, it may cause a weaker interface between the aggregate and the cement paste and can adversely

affect the bond behavior between steel and concrete. One of the least investigated aspects of SCC is dynamic segregation, which occurs when the coarse aggregates settle while concrete is flowing generally in horizontal direction while being cast into the formwork[3]. Dynamic segregation is controlled by the rheological properties of the paste; aggregates properties, such as density, size and volume fraction; the flowing velocity of concrete and the frictional force provided by flowing surface[4]. In order to evaluate dynamic segregation, a limited number of test methods have been developed. A new test method (T-box test) was recently proposed to simulate dynamic segregation during flow[5].
The main objective of the study is to better understand the mechanisms influencing dynamic segregation of SCC using the T-box test. In this way, practical guidelines can be developed to assure dynamic stability of SCC dependent on the casting conditions.

Experimental program

Materials and Mix Design

The investigated SCC mixtures were produced with ordinary type I/II Portland cement that meets the ASTM C150/C150M-15, having a Blaine specific surface of 386 m^2/kg and a specific gravity of 3.11. The specific gravity, fineness modulus and absorption of the fine aggregate, which was a natural Missouri river sand, were 2.61, 2.72 and 0.4%, respectively. The coarse aggregate is a crushed limestone with a maximum aggregate size of 12.5mm. The specific gravity and absorption of the coarse aggregate are 2.55 and 3.61 % respectively. Pea gravel was also used with a maximum aggregate size of 9.5mm with a specific gravity of 2.4 and absorption of 3.6%. A polycarboxyl-ether based superplasticizer (SP) with a specific gravity of 1.085 and a solid content of 39% was incorporated in all mixtures. To enhance the stability of SCC a welan-gum based viscosity modifying admixture (VMA) was used with a specific gravity of 1.207 and a solid content of 44%. The mix design is based on Coreslab Structures' reference SCC, and has a w/cm= 0.4 and a paste volume of 335 l/m^3 (excluding the air content). Although an air-entraining agent is typically used in practice, no air-entrainer was employed in the mixtures.

The following variations were induced to investigate the effect on dynamic segregation:

- The w/c was changed ± 0.05 to 0.35 and 0.45.
- The paste volume was varied with 25 l/m^3, or 2.5% of the concrete volume
- The sand-to-total aggregate ratio was altered by ± 0.05, from 0.51 (ref) to 0.46 and 0.56.

- The total amount of SP was modified to increase or decrease the slump flow.

Mixing procedure

All SCC mixtures were prepared in 100 L batches in a drum mixer with capacity of 150 L. The mixing sequence consisted on homogenizing the fine and coarse aggregate for 1 min, after that half of the water was added and mixed for 30s. The cement was then added along with the rest of the water. After approximately 1 min, the SP and VMA were incorporated. The mixture was continually mixed for 2 min. After a rest period of 3 min, the concrete was mixed for 2 additional minutes, after which it was determined either visually or by slump flow test if more SP was needed to achieve the target slump flow.

Testing procedure

Following the confirmation that the target slump flow was achieved (i.e 700 ± 200mm), the time needed for the concrete to spread 500mm (T_{50}) was noted and the visual stability index had to be 0 or 1. For all ten mixtures, the following properties were also measured: V-funnel flow time, air content, sieve stability, tilting box test and concrete rheology. Compressive strength specimens (three 100 x 200 mm cylinders) were cast upon completion of the testing procedure. All specimens were demolded at 24h and cured under water for 28 days.

To investigate the dynamic segregation of concrete, the width of the tilting box (T-box), developed by Esmaeilkhanian, et al.[5] was modified to evaluate the effect of different formwork dimensions. The T-box consists on a rectangular channel of 1 m, which can tilt from a horizontal to an inclined position. The tilting height of the box is 140 mm. The box width was 400 mm, which can be divided into one section with a width of 100 mm, and one with 200 mm width. Before testing, fresh concrete is placed reaching a height of 80 mm in the tested sections, while the box was maintained in horizontal position. The box is then tilted during 1 second, and brought back to horizontal during another second. Cycle time can be varied during the test, but in this testing program, the cycle time is kept constant at 2s. The 100 and 200 mm channel widths were used in this work.

At the end of the 120 cycles, which corresponds theoretically to a flow distance of 9 m, a sieve- washing technique was used. Samples were taken from the tilt-up and tilt-down sections, from both the 100 and 200 mm width. Standard 4 x 8” cylinders were filled with concrete, washed over a #4 sieve (4.75 mm opening), and dried to measure the amount of coarse aggregates in each of the sample sections. The amount of aggregate in each section corresponds directly to dynamic segregation.

The Volumetric Index (VI) is defined according to (eq. 1), where V_{td} is the relative coarse aggregate volume in the tilt-down section and V_{tu} is the relative coarse aggregate volume in the tilt-up section.

$$VI(\%) = 100\frac{V_{td} - V_{tu}}{average(V_{td}, V_{tu})} \quad (1)$$

Results and Discussion

Workability characteristics

Table I summarizes the results for workability, dynamic segregation and concrete rheology measurements carried out for all the mixtures.

Table X Workability, dynamic segregation and rheology for the tested mixtures.

Mixtures		**Workability** Slump flow (mm)	T 50 (s)	V-Funnel (s)	Air Contet (%)	Sieve stability (%)	**Dynamic segregation** VI in 100 mm (%)	VI in 200 mm(%)	**Concrete Rheology** Yield stress (Pa)	Plastic Viscosity (Pa s)
Ref		720	1.5	3.4	6.5	7.0	13.6	21.9	21.6	16.6
w/cm	0.35	690	1.3	11	6.5	4.8	1.3	5.4	7.3	33.5
	0.45	690	1.1	2.3	2.0	8.9	7.3	17.6	20.5	9.6
±SP	-10%	658	0.9	3.8	6.0	7.0	4.4	13.5	14.4	15.5
	+10%	740	0.9	3.1	4.5	10.7	12.6	48.7	8.6	12.6
Paste Volume	-25 l/m^3	690	0.8	4.5	7.0	6.2	9.4	13.8	18.0	18.9
	+25 l/m^3	695	0.9	4.5	5.5	10.8	14.1	31.8	11.4	14.7
s/a	46%	700	0.9	4.1	6.0	7.6	17.5	23.1	14.2	13.9
	56%	695	0.7	3.9	6.5	7.2	23.3	44.1	14.6	17.4

Effect of water-to-cement ratio

To investigate the effect of the water-to-cement ratio on the dynamic segregation resistance of SCC mixtures, two mixtures were prepared, tested and compared to the reference. The w/cm varied ± 0.05 to 0.35 and 0.45, where SP content was adjusted to maintain a slump flow of 700 ± 20 mm. The coarse/fine aggregate ratio, paste volume and VMA content were kept constant. Figure 1, shows that decreasing w/cm from 0.4 to 0.35 significantly increases V-funnel time and plastic viscosity, thus increasing the ability to avoid the aggregate to separate from the suspending matrix. When the mixture has a lower plastic viscosity, increasing yield stress can enhance dynamic stability. Increasing w/cm also results in higher sieve stability, making the mixture more susceptible to have static segregation.

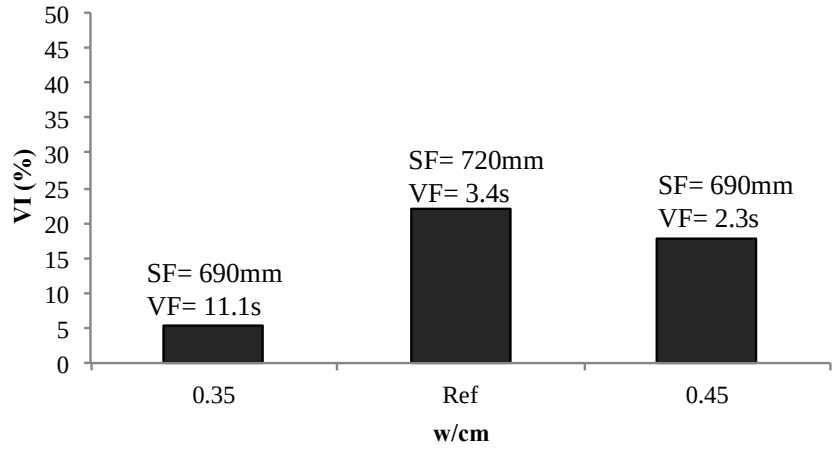

Figure 12. Influence of water cement ratio on dynamic segregation.

Effect of SP dosage

Figure 2, shows the effect of SP dosage on the ability of SCC mixtures to maintain a uniform distribution of large coarse aggregate particles. The mixtures were prepared with a constant w/cm of 0.4. The VMA content, paste volume and the coarse/fine aggregate ratio were kept constant. The SP content was altered by 10% compared to the reference mixture. The variation of the SP content significantly affects the slump flow and static stability, and has a negligible effect on the V-Funnel flow time. A similar trend can be observed in the rheological properties, but in this case the yield stress measured of the reference mixes was higher than other values. The separation of the concrete constituents while being cast it is more prominent with the decreasing of yield stress and plastic viscosity[6].

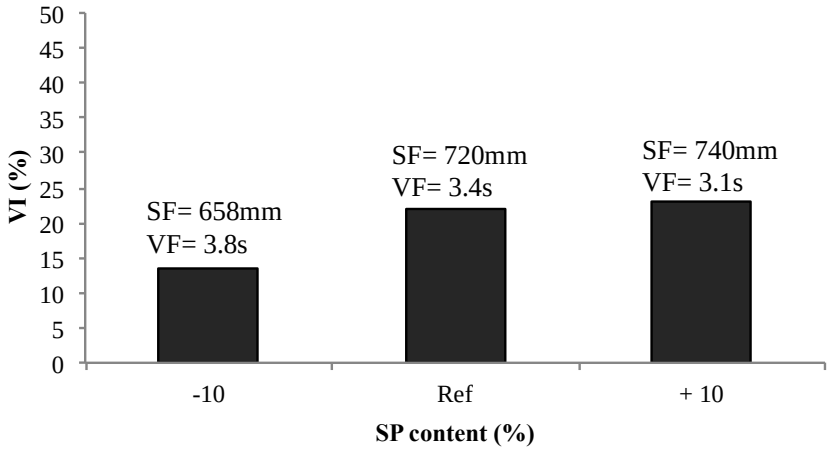

Figure 13. Influence of superplastizicer content on dynamic segregation.

Effect of paste volume

Two additional SCC mixtures were prepared to evaluate the effect of the paste volume on dynamic stability. The variations of the paste volume were ± 25 l/m^3 from the reference with a constant w/cm of 0.4. Coarse/fine aggregate ratio and VMA content were also constant while SP content was adjusted to achieve a slump flow of 700 ± 20 mm. Figure 3 shows that mixtures with higher and lower paste volume have very similar workability properties such as V-funnel time and slump flow and the same trend was observed on the rheological properties. On the other hand, a higher dynamic segregation had been observed when increasing the paste volume. For this reason it can be concluded that the paste volume has a marked effect on dynamic segregation in addition to the known effects of the plastic viscosity and yield stress. By increasing the paste volume, the amount of aggregates in the concrete decreases, leading to a greater inter-particle spacing and a higher potential for settlement.

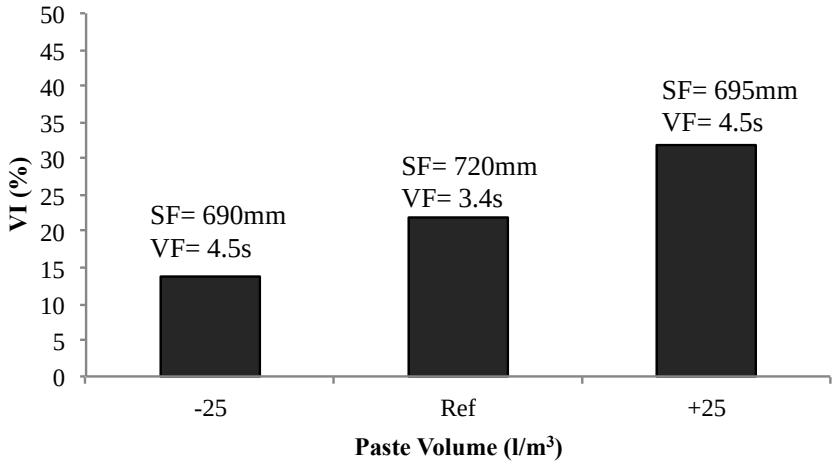

Figure 14. Influence of paste volume on dynamic segregation.

Effect of Sand/total aggregate ratio

The effect of sand-to-total-aggregate ratio (s/a) on segregation of SCC needed to be quantified. For this purpose, two SCC mixtures were prepared and tested with a variation in sand-to-total-aggregate ratio of ± 5% from the reference with a constant w/cm of 0.4. VMA content and paste volume were kept constant while the SP content was adjusted to achieve a slump flow of 700 ± 20 mm. Results of the volumetric index (VI) are shown in Figure 4, which indicates a high risk of dynamic segregation in SCC mixtures that have a relatively low yield stress in combination with a high sand-to-total-aggregate ratio. This effect can be explained in similar way as an increase in paste volume: an increase in s/a decreases the total amount of coarse aggregates, leaving more space for these to move. When the s/a decreases, the results do not follow the same tendency, as the VI is approximately equal to the reference mixture. It is important to emphasize that to prevent the coarse aggregate settlement in the mixture, it is necessary to have an appropriate amount of sand, which in the same way needs finer particles to stabilize and so forth[7]. This effect is called lattice effect and explains why the coarse aggregates stay in suspension in a cement paste. It is expected that a decrease in the s/a caused the mixture to have a reduced lattice effect, explaining why the VI does not decrease with decreasing s/a.

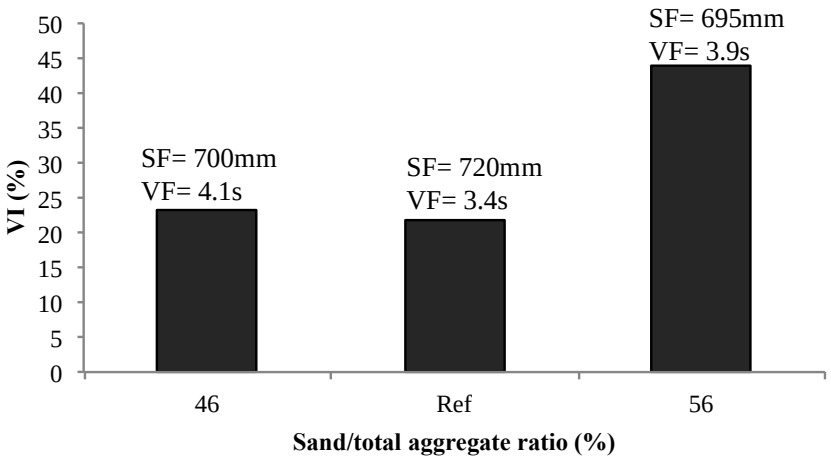

Figure 15. Influence of sand-to-total aggregate ratio on dynamic segregation.

Figure 5, shows the effects on the variations of the width of the box for all the mixtures tested, comparing the volumetric index in the 100 mm channel to the results in the 200 mm part. It can be concluded that the segregation index is approximately half in the 100 mm channel compared to the 200 mm channel. According to Esmaeilkhanian et al.[5] increasing the flow velocity decreases dynamic segregation, which can be a possible reason for this observation since higher flow velocities occur in the narrower channels.

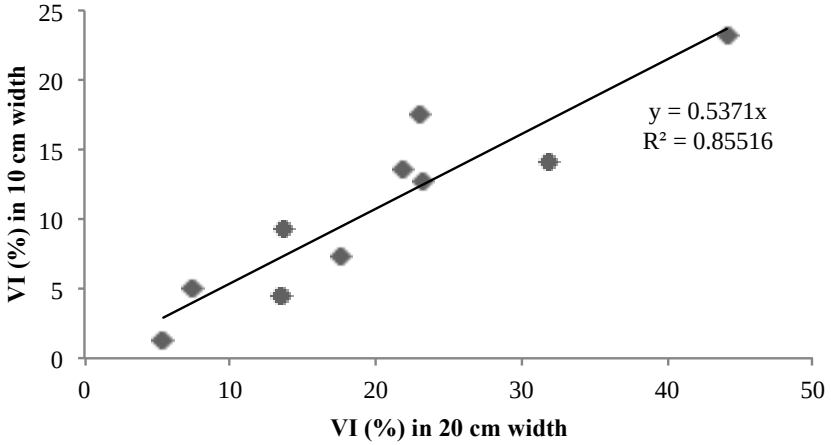

Figure 16. Dynamic segregation in 100 mm compared to 200 mm width channel.

Conclusions

A modified T-box was used to evaluate the effects of w/cm, SP content, paste volume, sand-to-total aggregate ratio, workability characteristics and rheological properties on the dynamic segregation of SCC. The following conclusions can be drawn:

The variations on w/cm and SP dosage confirm that rheological properties of concrete have a high influence on dynamic segregation. Increasing viscosity significantly reduces dynamic segregation. Decreasing yield stress increases the risk of separation of the particles from the suspended matrix. To avoid dynamic segregation, yield stress and plastic viscosity must be well-balanced.

The paste volume has a significant effect on dynamic segregation. An increase in paste volume can ease the shear-induced aggregate movement in the suspension with higher inter-particle spacing.

Varying the sand-to-total-aggregate ratio (s/a) also has an influence on dynamic segregation. Reducing s/a can destabilize the mixture due to a reduction in lattice effect.

Reducing the width of the tilting box from 200 mm to 100 mm significantly reduces dynamic segregation. It will be further investigated whether an enlargement of the box to 400 mm will have a similar effect.

References

1. Khayat, K. H. (1999). Workability, testing, and performance of self-consolidating concrete. *ACI Materials Journal*, *96*(3).
2. Panesar, D. K., & Shindman, B. (2012). The effect of segregation on transport and durability properties of self-consolidating concrete. *Cement and Concrete Research*, *42*(2), 252-264.
3. Shen, L., Jovein, H. B., & Wang, Q. (2015). Correlating Aggregate Properties and Concrete Rheology to Dynamic Segregation of Self-Consolidating Concrete. *Journal of Materials in Civil Engineering*, 04015067.
4. Shen, L., Struble, L., & Lange, D. (2009). Modeling static segregation of self-consolidating concrete. *ACI Materials Journal*, *106*(4).
5. Esmaeilkhanian, B., Feys, D., Khayat, K. H., & Yahia, A. (2014). New test method to evaluate dynamic stability of self-consolidating concrete. *ACI Materials Journal*, *111*(3).
6. Esmaeilkhanian, B., Khayat, K. H., Yahia, A., & Feys, D. (2014). Effects of mix design parameters and rheological properties on dynamic stability of self-consolidating concrete. *Cement and Concrete Composites*, *54*, 21-28.
7. Wallevik, O. H. (2003, August). Rheology—a scientific approach to develop self-compacting concrete. In *Proceedings of the 3rd international RILEM Symposium on Self-Compacting Concrete* (pp. 23-31).

Design and Properties of Low-binder Self-Compacting Concrete

Zuo Wen-qiang[1], Xu Wen[2], Tian Qian[2], Zhang Qian-qian[2], Wang Peng-gang[2] and Li Wei[1]

1. School of Materials Science and Engineering, Southeast University, Nanjing 211189, China;
2. State Key Laboratory of High Performance Civil Engineering Materials, Jiangsu Research Institute of Building Science Co., Ltd., Nanjing 210008, China

Abstract Self-Compacting Concrete (SCC) has been widely studied and used in modern society. However, low binder SCC seems to be more economical and benefit for the environment. This study presents a series of studies on designing and testing the properties of low-binder SCC including its rheological properties by applying common used Slump Cone and the co-axial cylinders viscometer. Harden properties such as compression strength and autogenous shrinkage were also analyzed. It shows that through replacing moderate amount of cement by ground limestone filler, the rheological and hardened properties can meet the requirement as common SCC does. It is feasible to use ground limestone filler and fine sand to modified the gradation of all the solid components, and with a moderate addition of fine sand, one type of high fluidity concrete can be obtained. However, the fine sand can induce a large amount of air into the mixture and increase the yield stress as well as reduce the viscosity which may unfortunately decrease the compression strength of the hardened concrete. Finally, the autogenous shrinkage test is also conduct and not apparently affected by the variation of inert powder or aggregates.

Keywords: SCC, Low-binder, Fine sand, Ground limestone filler, Yield stress.

Introduction

In recent decades, Self-Compacting Concrete (SCC) has been widely studied and utilized in various cases of construction such as steel/concrete composite, thin section pre-cast units and underwater construction [1-5]. According to P.L. Domone's study [5], common SCC usually has a binder content around 500 kg/m3, which is rather high comparing to conventional vibrated concrete (CVC) [2].This high binder content will not only cause significantly shrinkage and temperature

problems but consume large amount of cement which would induce high carbon dioxide emission [6-7].It also shows that the strength class of C25/C30 in Europe accounts for 88% of all the commercial concrete in European Union, while in China, only 15.7% of the ready-mix concrete has the strength class higher than C40 [8],which provides a broad prospect for designing SCC with low-binder content although the low binder content high water volume would cause a low strength development [6]. However, although the definition of low-binder SCC still being unclear, but from the mix designing point of view, the binder content below 350~400kg/m^3 will be boldly considered as the low-binder SCC in this paper.

This paper mainly focus on studying the designing method of low-binder SCC as well as its rheological properties by applying common used Slump Cone and the co-axial cylinders viscometer for concrete [6,9]. Harden properties such as compression strength and autogenous shrinkage were also analyzed at the last part of the study.

Materials and Methods

Materials description

In this study, cement, silica fume and ground limestone filler were used as the powder materials, while river sand and crushed basalt were used as aggregates.

Powder materials. Ordinary Portland Cement named PII 52.5 obtained from Xiao Yetian Cement Co., Ltd. (Jiangsu, China) was used. The apparent density of cement is 3150kg/m^3, and its strength properties are listed in Table 1. Silica fume with density of 2200 kg/m^3 was used as supplementary cementitious materials (SCMs) and ground limestone with density of 2700 kg/m^3 was used as powder filler in this study. The Particle Size Distribution (PSD) of these three types of powder tested by *HELOS-SUCELL Laser Particle Size Analyzer* is shown in Figure 1.

Table I Chemical and mineral composition of cement

Chemical composition (% by mass)							
SiO_2	Al_2O_3	CaO	MgO	Fe_2O_3	SO_3	NA_2O_{eq}	Ignition Loss
21.10	6.16	64.8	1.94	4.41	2.52	0.48	2.59
Mineral composition (% by mass)							
		C_3S	C_2S	C_3A	C_4AF		
		52.50	21.40	6.40	13.10		

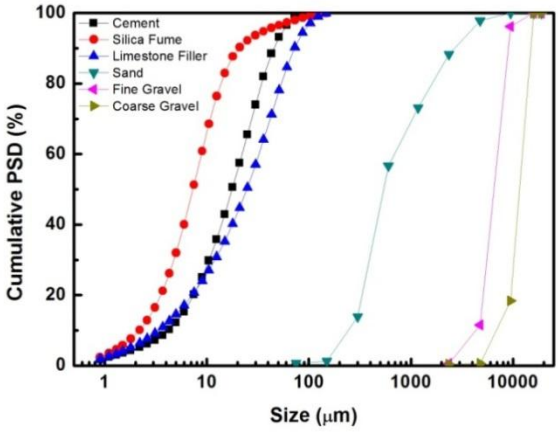

Figure 1. Particle Size Distribution of powder and aggregates

Aggregates. River sand with apparent density of 2630 kg/m^3 was used as fine aggregate and two types of crushed basalts with different particle grading were used as coarse aggregates. The apparent density of the coarse aggregates is 2780 kg/m^3. In order to modify the grading of solid particles, sieved sand with particle size between 0.075mm-0.300mm was used. The grading curves of sand and coarse aggregates are shown in Figure 1.

Water and admixtures. The tap water was used. The polycarboxylate-type of water-reducing agent was used as admixture with solid content of 15% and water-reducing ratio of 20% according to the Chinese standard of GB 8077-2012 .

Test methods

Slump cone was used to test the slump and slump flow (with and without J-ring)of each fresh concrete mixture according to the Chinese standard of GB/T 50080-2002 and JGJ/T 283-2012, respectively.The co-axial cylinders viscometer for concrete named Viscometer 5 was used to test the rheological parameters, the detailed descriptions and working principles of this apparatus was shown in literature [10].

Compression strength of each concrete cubes was tested according to the Chinese standard of GB/T 50081-2002 at the age of 3d, 7d and 28d. Drying shrinkage was tested according to the Chinese standard of GB/T 50082-2009.In addition, the autogenous shrinkage was tested by casting fresh concrete into bottom-sealed PVC tubes with height of 400 mm and diameter of 100 mm. The top of the PVC tubes was sealed by paraffin wax right after the initial set of the concrete.

Mix proportion design

The mix proportion design of this study is listed in Table 2.Six mixtures with the same binder content (300 kg/m^3) but different ground limestone content or fine sand content (particle size between 0.075-0.300mm) was studied. The paste volume, water to binder ratio and water to powder ratio are also listed in Table 2.

Table 2. Mix proportion design of low-binder SCC (for 1 cube meters)

Mix Design	Ref	LS75	LS150	LS225	LS75_ FS75	LS75_ FS150
CEM PII 52.5/kg	279	279	279	279	279	279
Silica Fume/kg	21	21	21	21	21	21
Water/kg	150	150	150	150	150	150
Limestone Filler/kg	0	75	150	225	75	75
Fine Sand/kg	0	0	0	0	75	150
Sand/kg	996	956	918	878	910	866
Fine Gravel 5-10mm/kg	299	287	275	263	273	260
Coarse Gravel 10-16mm/kg	697	669	643	615	637	606
Superplasticizer/kg	6	7.5	9	10.5	7.5	7.5
Air/%	1.6	1.8	2.0	2.8	4.5	6.8
m_{water}/m_{binder}	0.50	0.50	0.50	0.50	0.50	0.50
m_{water} / m_{Powder}	0.50	0.40	0.33	0.29	0.40	0.40
m_{Powder}/kg	300	375	450	525	375	375
V_{Paste}/%	26.4	29.4	32.4	35.9	32.1	34.4

The gradation curve of all the solid components of each mix proportions are shown in Figure 3, together with the Modified Andreasen & Andersen equation with q=0.27 according to the systematic study of Eco-SCC in previous research [6, 11].

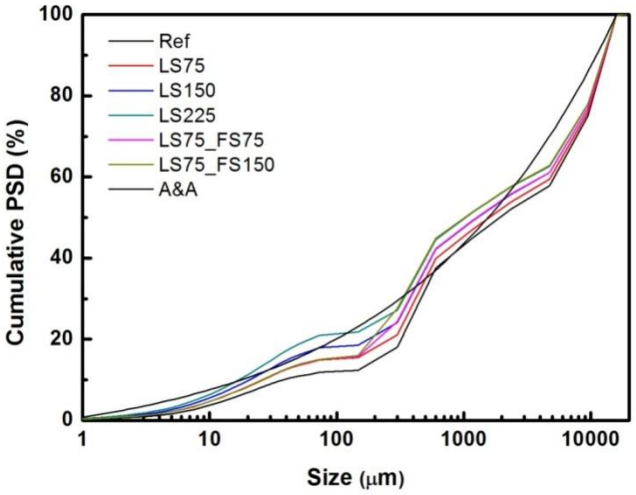

Figure 2. PSD of all the solid components and A&A equation

Results and Discussion

Workability and segregation resistance

The Slump and slump flow of different mixtures are shown in Figure 3 and Figure 4, respectively. It can be seen clearly from Figure 3 that the slump value increases nearly linear with the addition of ground limestone filler as well as the paste volume (see Table 2) for non-fine sand mixtures while the slump flow values also present same trend (see Figure 4). For mixtures with 75kg/m^3 limestone filler but different fine sand content, the two values vary irregularly with the varied content of fine sand. The slump values are 125 mm, 240 mm and 210 mm and the slump flow are 230mm, 520mm and 380mm for LS75, LS75_FS75 and LS75_FS150 respectively, which indicates that there exist a moderate amount (around 75 kg/m^3 for this specific case) of fine sand replacing the ordinary sand and aggregate to make the mixture more flowable than ordinary mix proportion with constant low content of binder. However, the presence of excessive content of fine sand (150 kg/m^3 of fine sand replacing the ordinary sand and aggregate here) may induce too much air into the mixture, which has a adverse influence for the fluidity of concrete.

In order to evaluate the segregation resistance and passing ability, J-ring was used. As Figure 4 shows, only three mixtures (namely LS150, LS225 and LS75_FS75) have apparent flowability by using J-ring. Besides, through visual inspection, the

mixtures of LS150 and LS225 both have a good cohesiveness and no obvious segregation nor bleeding was observed while slight bleeding and obvious air bubbles were observed for the mixtures of LS75_FS75 and LS75_FS150. This can be attributed to insufficient powder content that cannot absorb all the water in the mixture as well as the air entraining effect of fine sand.

However, the results of workability for different mixtures above can be linked to the relative content of matrix volume and the gradation curve of solid components [6]. As figure 2 shows, LS225 and LS75_FS75 are more close to the Modified Andreasen& Andersen equation which indicates the particle cumulation of the two mixtures are more dense [4, 6] which need less volume of paste to fill the void of the solid skeleton thus increase the volume of the lubricant layer between aggregates.

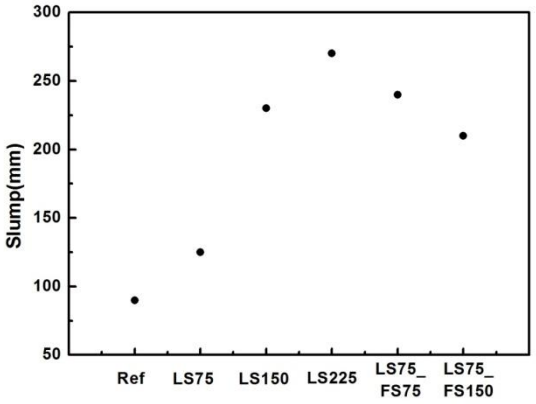

Figure 3. Slump of different mixtures

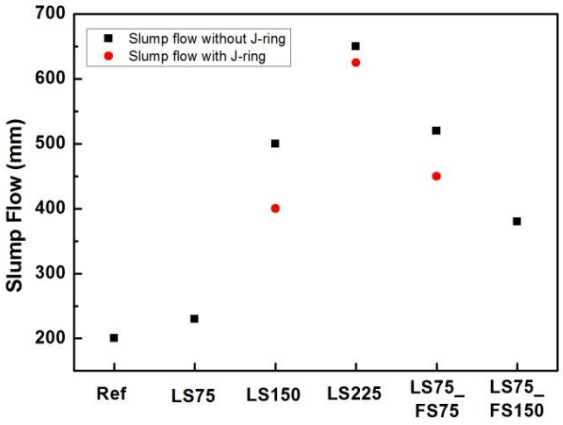

Figure 4. Slump flow of different mixtures

Rheological properties

The rheological values of flowable mixtures are shown in Figure 5. It can be seen that the yield stress τ_0 slightly varies with varying content of powder while it increases dramatically with decreasing powder content and increasing fine sand content. The former two mixtures contain high volume of powder, which are more like common SCC with low yield stress and high plastic viscosity. However, by replacing a fraction of powder with the same amount of fine sand, the mixture turn to the type of high-yield stress high flowability concrete as proposed in [12] and Figure 6. This is mainly due to the increasing amount of fine sand enhances the interaction of aggregate particles and affects the lattice effect [1].

Furthermore, high volume of powder needs high dosage of superplasticizer to release water for enhancing flowability, which in parallel resulting in high viscosity of the mixtures. It should be noted that the addition of fine sand meanwhile increases the air content in the mixture from 1.8 for LS75 to 4.5 and 6.8 for LS75_SF75 and LS75_SF150, respectively, as shown in Table 2. A moderate increase of air content in turn can increase the volume of matrix which is benefit for the flowability of SCC [6]. However, high content of fine sand replacing the ordinary sand and aggregate may leads to excess amount of air as well as increase the total specific surface area of aggregate which needs higher matrix volume to cover and form the lubricating layer that in turn reduces the flow of the mixture and results in a higher yield stress as well as lower viscosity.

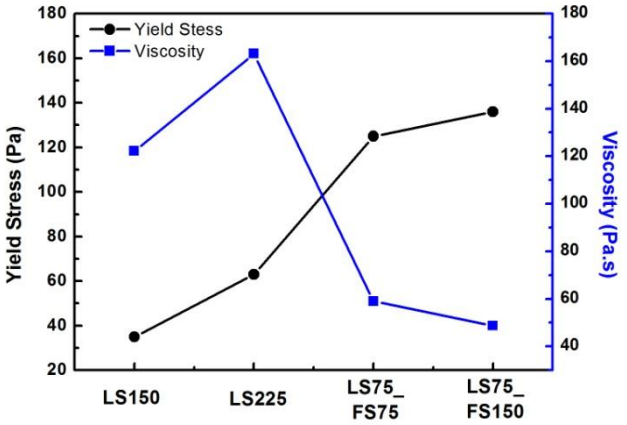

Yield stress and plastic viscosity of flowable mixtures

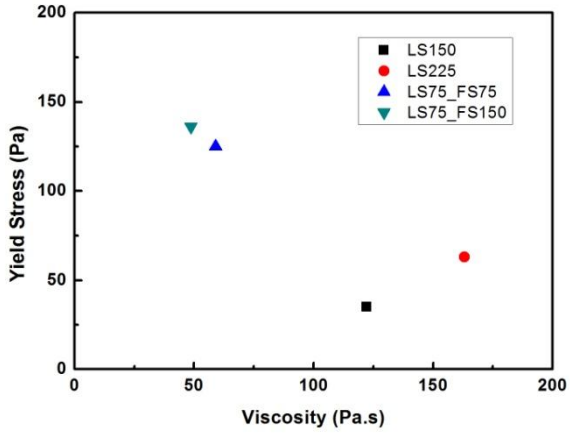

Figure 6. Relationship between yield stress and plastic viscosity for flowable mixtures

Mechanical properties of low-binder SCC

Three ages of compression strength of hardened concrete cubes were tested and the results are shown in figure 7. The addition of ground limestone filler slightly decreases the early age strength of concrete. However, the 7d and 28d compression strength shows no difference with reference group. Nevertheless, adding fine sand

into concrete mixtures significantly decreases the strength both for the three ages, around 10MPa and 20MPa for the mixture of LS75_SF75 and LS75_SF150, respectively. It is mainly due to the high air content which increases the porosity of harden concrete samples and the lower filling ability which leads to insufficient compaction when casting. Finally, the relative low compression strength was tested.

However, as mentioned above, the compression strength of all the mixtures (above 40MPa at the age of 28d) always meets the requirement of most practical engineering. Therefore, through reasonable control of the air content, the mechanical properties would never be the main problems.

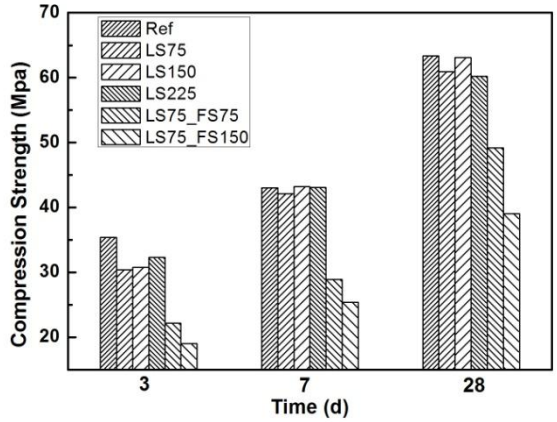

Figure 7. Compression strength of early age mixtures

Shrinkage properties of low-binder SCC

As shown in figure 8, the autogenous shrinkage values of different mixtures have little differences between each other, which shows that the addition of inert powder such as ground limestone filler or variation of aggregate gradation such as adding fine sand into mixtures does not affect the autogenous shrinkage significantly. As a matter of fact, the main reason for autogenous shrinkage is the self-desiccation effect induced by hydration of cement after the formation of solid skeleton [14, 15]. At sealed condition, the shrinkage of cementitious materials most relates to the content of cement as well as the active pozzolanic materials, however this factor are set as constant in this study.

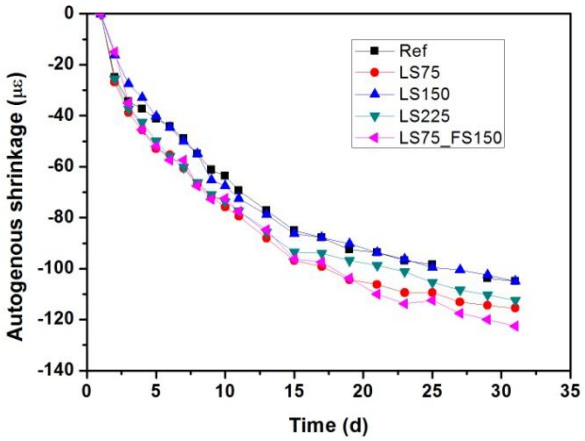

Figure 8. Autogenous shrinkage of early age mixtures

Conclusions

This paper studied a series of low-binder concrete mixtures on its workability by testing the values of slump and slump flow as well as the rheological parameters by using the co-axial cylinders viscometer for concrete. Harden properties such as compression strength and autogenous shrinkage were also analyzed.

- It is valid to add ground limestone filler and fine sand into concrete mixtures to modified the gradation of all the solid components and making it more relative to the Modified Andreasen& Andersen equation.

- By adding 150 to 225 kg/m^3 ground limestone filler into mixtures, the rheological properties are more close to the common SCC which has a high plastic viscosity and low yield stress.

- With a moderate addition around 75kg/m^3 of both fine sand and limestone filler in this specific low binder content mixture which can obtain one type of high fluidity concrete with high yield stress and low viscosity. However, comparing with the mixture with the same content of limestone filler instead, the Bingham parameters are much different.

- The presence of fine sand may however induce a large amount air into the mixture which may decrease the compression strength of the strength of hardened concrete. In addition, the autogenous shrinkage is not apparently affected by the variation of inert powder or aggregates.

References

[1] Nicolas Roussel, Anael Lemaître, et al. (2010),*Cement and Concrete Research*, vol.40, p.77-84.
[2] Fabien Mahaut, Samir Mokéddem, et al. (2008),*Cement and Concrete Research*, vol.38 p.1276-1285.
[3] Joumana Yammine, Mohend Chaouche, et al. (2008),*Cement and Concrete Research*,vol.38, p. 890-896.
[4] H.J.H.Brouwers,, H.J. Radix. (2005), *Cement and Concrete Research*, vol.35, p. 2116-2136.
[5] P.L. Domone. (2006), *Cement & Concrete Composites*,vol. 28, p. 197-208.
[6] Mueller FV. (2012), Design criteria for low-binder self-compacting concrete. ECO-SCC. PhD thesis. Reykjavik University, Iceland.
[7] J.Y. Yang, P.M. Wang, etal. (2014), Journal of Jiamusi University (Natural Science Edition),vol.32, p.1-4. (In Chinese)
[8] L. Lin. (2012), *Ready-mixed Concrete (Beton Chinese Edition)*, vol. 6, p. 40-43.
[9] Florian V. Mueller, Olafur H. Wallevik, et al. (2014), *Cement & Concrete Composites*, vol.54, p. 117-125.
[10] G. Heirman, L. Vandewalle, et al. (2008) *J. Non-Newtonian Fluid Mech.*vol.150, p. 93-103.
[11] Florian V. Mueller, Olafur H. Wallevik and Kamal H. Khayat. Considerations for designing low-powder Self-Compacting Concrete, Eco-SCC. International Symposium on Environmentally Friendly Concrete – ECO-Crete 13.-15. August 2014. Reykjavik, Iceland.
[12] Olafur Haraldsson Wallevik, Jon Elvar Wallevik. (2011),*Cement and Concrete Research*,vol.41, p. 1279-1288.
[13] Gaurav Sant, Barbara Lothenbach, et al. (2011),*Cement and Concrete Research*, vol.41, p.218-229.
[14] Ole Mejlhede Jensen, Per Freiesleben Hansen. (2001), *Cement and Concrete Research*, vol. 31, p. 1859-1865.

Investigation on the Mechanisms Governing the Robustness of Self-Compacting Concrete at Paste Level

Farid Van Der Vurst[1], Karel Lesage[1], Steffen Grünewald[1,2], Lucie Vandewalle[3], John Vantomme[4] and Geert De Schutter[1]

[1] Ghent University, Department of Structural Engineering, Magnel Laboratory for Concrete Research, Technologiepark-Zwijnaarde 904, 9052 Ghent, Belgium
[2] Delft University of Technology, Faculty of Civil Engineering and Geosciences, Concrete Structures Group, Stevinweg 1, 2628 CN Delft, The Netherlands
[3] KU Leuven, Department of Civil Engineering, Kasteelpark Arenberg 40 – PO Box 2447, 3001 Heverlee, Belgium
[4] Royal Military Academy, Civil Engineering Department, Av. de la Renaissance 30, B-1000 Brussels, Belgium

Abstract In spite of the many advantages, the use of self-compacting concrete (SCC) is currently widely limited to application in precast factories and situations in which external vibration would cause large difficulties. One of the main limitations is the higher sensitivity to small variations in mix proportions, material characteristics and procedures, also referred to as the lower robustness of SCC compared to vibrated concrete. This paper investigates the mechanisms governing the robustness at paste level. Phenomenological aspects are examined for a series of paste mixtures varying in water film thickness and superplasticizer-to-powder ratio. The impact of small variations in the water content on the early-age structural buildup and the robustness of the paste rheology is investigated using rotational and oscillating rheometry.

Key words: *Self-compacting concrete, SCC, Robustness, Sensitivity, Rheology, Storage Modulus.*

Introduction

Self-compacting concrete (SCC) is a high performance concrete, characterized by the absence of the need of external compaction. As a result, less construction errors are made and significantly less man effort is required. However, despite the many

benefits of SCC, the use in actual structures is mainly limited to precast concrete products and situations requiring a high flowability or in which external compaction would result in large difficulties. One of the major limitations for the use of SCC is its lower robustness compared to vibrated concrete, which is its sensitivity to small changes in the material properties, material proportions, or production methods.
This lower robustness imposes a more rigorous quality control demand on material properties and mix proportioning, skilled and experienced staff, and a better understanding of the mix design. Regarding the mix design, the following trends have been observed:

- A surplus of fines in the aggregate grading curve results in a higher robustness of SCC [1, 2]. The surplus of fines prevents the coarse aggregate particles from dominating the rheology.
- In SCC having a high plastic viscosity, the robustness against small variations in the water content increases as the amount of powder in the mixture is high [2, 3]. For SCC with a low plastic viscosity, an opposite trend is observed [3].
- An increase of the water-to-powder ratio increases the robustness of the V-funnel flow-time against variations in the water content [3, 4]. However, Kwan and Ng [1] have shown that a lower water-to-powder ratio increases the robustness of the slump flow against variations in the superplasticizer content. More fundamental research on this topic is necessary.
- The choice of superplasticizer [5, 6] and VMA [4, 6, 7] also affects the robustness. The addition of a VMA in the mix design can increase or decrease the robustness of the mixture [2-4, 7].
- A possible link between the thixotropy and robustness has been suggested [8, 9]. Low alkali cement is also reported to be less robust than high alkali cement [10]. Low alkali cement contains less SO_4^{2-} and C_3A, which results in a lower heat of hydration and less structural buildup [11].

Although many other parameters and influences can cause the rejection of a SCC batch [12-14], this experimental program focusses on variations in the water content. Variations in the water content have the largest impact on the rheology in concrete plants since the dosage of admixture and powders is measured very precisely and variations in the properties and grading curve of sand and gravel have a relatively smaller impact [15]. According to the European guidelines [16], a good SCC mix design should allow variations of 5 to 10 l/m³ in the water content, which corresponds with about 3 to 6% of the water content. The ACI 117-90 and EN 117-90 codes allow variations up to 3% of the water content during the industrial production of concrete.

In this study, the Water Film Thickness (WFT) of all mixtures was evaluated. According to Li and Kwan [17], the water in fresh concrete can be divided into two

parts: the filling water which fills the voids in between the solid particles, and the excess water which forms a water film on the surface of the solid particles and contributes to the fluidity of the fresh concrete. The WFT can be calculated using Equations 1-3 (Table I: Definition of parameters). The maximum packing density ϕ_{max} is calculated based on the maximum possible density of the paste obtained by variations in the water content.

$$WFT = \frac{u_w - u_{min}}{A_s} \quad \text{(Eq. 1)}$$

$$u_{min} = \frac{1-\phi_{max}-\varepsilon_a(\phi_{max})}{\phi_{max}} \quad \text{(Eq. 2)}$$

$$u_w = \frac{1-\phi-\varepsilon_a(\phi)}{\phi} \quad \text{(Eq. 3)}$$

Table I. Definition of the parameters used in Equations 1 to 3

Symbol	Unit	Name	Meaning
WFT	[m]	Water Film Thickness	Thickness of the excess water layer covering the solid particles.
ϕ	[%]	Packing density	The volume of solids divided by the bulk volume
ϕ_{max}	[%]	Maximum packing density	The maximum possible packing density possible for this mixture under varying water content.
$\varepsilon_a(\phi)$	[%]	Air content	The volume of air divided by the bulk volume.
u_w	[%]	Water ratio	The volume of water divided by the volume of solids.
u_{min}	[%]	Minimum voids ratio	The water ratio corresponding with the maximum packing density.
A_s	[m²/m³]	Specific surface area of the solids	The total surface of al solids in one volumetric unit.

When performing tests on paste, the shear forces during mixing and testing have a different order of magnitude compared to the concrete level [18, 19]. This causes differences in the flocculation of fines [20], the hydration speed [21], the thixotropic behavior [22], and relationships are difficult to establish between workability tests on paste and concrete. The investigated parameters might also affect the robustness of the stability against segregation. As a result, extrapolations from paste level to concrete level should be treated with great prudence.

Experimental setup

In order to investigate the influence of the water film thickness and paste fluidity on the robustness of the rheology against small variations in the water content, nine self-compacting pastes, varying in water-to-powder volumetric ratio (0.85, 0.90, and 0.95) and superplasticizer dosage (0.118%, 0.159%, and 0.200% of the cement weight) were tested. In order to cover a wider range of WFT, four additional mixtures were tested with water-to-

Table II. Chemical composition of the cement and limestone filler

	Cement I 52.5 N [%]	Limestone filler [%]
CaO	63.01	0.00
$CaCO_3$	0.00	98.8
SiO_2	18.55	0.11
Al_2O_3	5.83	0.04

powder / superplasticizer dosage combinations of respectively 0.75/0.200%, 0.80/0.200%, 1.00/0.159%, and 1.00/0.118%. The cement-to-powder ratio (by weight) was always kept at 0.6 . The material properties and grading curves of the cement and limestone are summarized in Figure 2 and Table II. Tap water and a polycarboxylate (PCE) superplasticizer with a concentration of 35% were also used in the experiments. The specific surface of the cement and limestone were calculated based on the particle size distribution which is given in Figure 1.

Fe_2O_3	4.09	0.04
MgO	1.22	0.32
K_2O	0.60	0.00
Na_2O	0.53	0.01
SO_3	2.97	0.02
Cl^{2-}	0.086	<0.008
L.O.I.	1.24	-
Insolubl e rest	0.94	-
Density	3116 kg/m³	2674 kg/m³
Specific surface	339 m²/kg	434 m²/kg

Table III summarizes all mix compositions. For each mix composition, two additional mixtures were fabricated in order to evaluate the robustness against small variations in the water content. One with 3% more water, and one with 3% less water. Each mixture was made according to the mixing and testing procedure given in Table IV in a Hobart mixer.

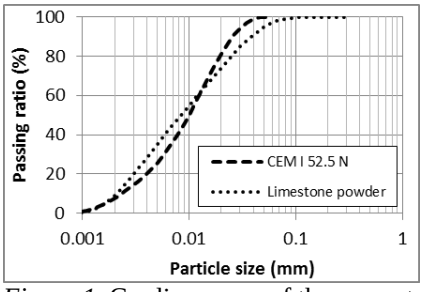

Figure 1. Grading curve of the cement and limestone powder

Table III. Mix proportions of the 14 reference self-compacting paste mixtures

Mix nr	Water-to-powder ratio	Super-plasticizer dosage	Cement	Limeston e powder	Water	Super-plasticizer dosage
	[-]	[%]	[kg/m³]	[kg/m³]	[kg/m³]	[kg/m³]
1	0.85	0.118	948	632	459	1.12
2	0.90	0.118	923	615	474	1.09
3	0.95	0.118	899	600	487	1.06
4	1.00	0.118	877	585	500	1.03
5	0.85	0.159	948	632	459	1.51
6	0.90	0.159	923	615	474	1.47
7	0.95	0.159	899	600	487	1.43
8	1.00	0.159	877	585	500	1.39
9	0.75	0.200	1002	668	429	2.00
10	0.80	0.200	974	650	444	1.95
11	0.85	0.200	948	632	459	1.90
12	0.90	0.200	923	615	474	1.85
13	0.95	0.200	899	600	487	1.80

Table IV: Mixing and testing procedure

Time	Duration	Step	Mixing speed
0 min	1 min	Mixing of cement, limestone powder and water	140 rpm
1 min	1 min	Adding the superplasticizer	140 rpm
2 min	1 min	Mixing	285 rpm
3 min	2 min	A thin layer of paste is scraped from the mixing arm and the walls and bottom of the mixing bowl	0 rpm
5 min	1 min	Mixing	285 rpm
6 min	11 min	Rest	0 rpm
17 min	1 min	Remixing	285 rpm
18 min	2 min	Rest	0 rpm
20 min	3 min	Rotational rheometry: determination of the Modified Bingham parameters	-
25 min	45 min	Start oscillatory rheometry: measurement of G' buildup	-
29 min	1 min	Remixing	285 rpm
30 min	5 min	Measuring the density and air content	-

The Modified Bingham parameters [23] (Equation 4 and Table V) of each paste were determined using rotational rheometry in an Anton Paar MCR 201 rheometer with a wide gap concentric cylinder configuration. The inner cylinder has a radius of 20 mm, a height of 60 mm and it is covered with a sand-blasted surface; the outer cylinder has a radius of 35 mm and is provided with ribs to prevent wall slip. The rotational velocity profile, illustrated in Figure 2, consists of a preshear step, a stepwise decreasing rotational velocity profile, and the determination of a segregation point. When the torque measured during a rotational velocity step was not in equilibrium, this data point was not used for the analysis. A plug flow correction was performed when plug flow occurred [24].

$$\tau = \tau_0 + \mu \cdot \dot{\gamma} + c \cdot \dot{\gamma}^2 \qquad \text{(Eq. 4)}$$

Table V: Symbols used in the Modified Bingham equation (Eq. 4)

Symbol	Unit	Meaning
τ	[Pa]	Shear stress
$\dot{\gamma}$	[s^{-1}]	Shear rate
τ_0	[Pa]	Yield stress
μ	[Pa.s]	Modified Bingham linear term
c	[$Pa.s^2$]	Modified Bingham second order term

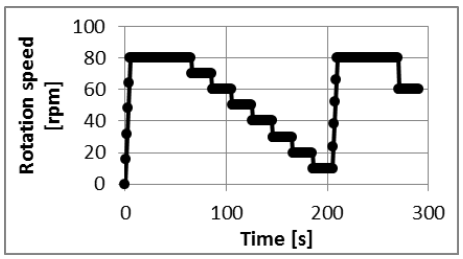

Figure 2. Rotational velocity profile applied in rotational rheometry

Oscillatory rheometry was used to monitor the structural buildup of the paste sample at rest. The storage modulus G' evolution was measured using an Anton Paar MCR 201 rheometer with a vane in cylinder setup. In these experiments, a vane with a diameter of 15 mm and a height of 40 mm vibrates within a small angle and a frequency of 1 Hz in an outer cylinder with a radius of 35 mm. After destroying the structure in a 2 minutes time sweep with a strain of 50% (above the critical strain), the structural buildup inside the paste was monitored in a time sweep with a small strain of 0.1% (below the critical strain) for 20 minutes using the storage modulus G' [25-27]. A typical example of a measurement is shown in Figure 3.

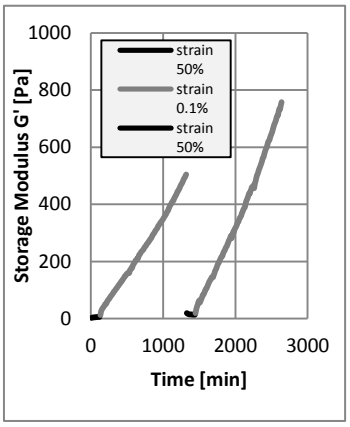

Figure 3. Monitoring of the Storage Modulus G' using oscillatory rheology

Results and Discussion

The measured properties of the 13 reference mixtures are listed in Table VI. The range of covered WFT values is illustrated in Figure 4 and are based on the maximum packing densities of the powder measured in wet condition. A smaller dosage of superplasticizer leads to a higher maximum packing densities and smaller WFT values at a similar water-to-powder ratio. A clear link between the WFT and the rheology of the mixture can be observed in Figure 5.

Table VI. Properties of the reference self-compacting paste mixtures

Mix nr	Water-to-powder ratio	Super-plasti-cizer dosage	Max. pack-ing density	Air cont-ent	WFT	Yield stress	MB linear term	MB 2nd order term	Increase in G' (1)	Increase in G' (2)
	[-]	[%]	[%]	[%]	[µm]	[Pa]	[Pa.s]	[Pa.s²]	[Pa]	[Pa]
1	0.85	0.118	0.577	1.0	0.188	16.38	1.59	0.0000	1073	1873
2	0.90	0.118	0.577	0.8	0.198	7.05	0.85	0.0005	711	1218
3	0.95	0.118	0.577	0.5	0.276	2.55	0.39	0.0024	717	1665
4	1.00	0.118	0.577	0.5	0.304	2.17	0.30	0.0012	514	1220
5	0.85	0.159	0.589	0.4	0.209	2.68	0.41	0.0048	322	365

6	0.90	0.159	0.589	0.5	0.236	2.23	0.32	0.0034	306	364
7	0.95	0.159	0.589	0.2	0.308	0.62	0.28	0.0018	302	411
8	1.00	0.159	0.589	0.2	0.340	0.49	0.14	0.0031	225	521
9	0.75	0.200	0.603	0.6	0.151	8.71	0.68	0.0086	701	1007
10	0.80	0.200	0.603	0.5	0.209	3.22	0.28	0.0066	265	462
11	0.85	0.200	0.603	0.3	0.267	0.77	0.32	0.0047	206	202
12	0.90	0.200	0.603	0.1	0.289	0.00	0.22	0.0031	256	504
13	0.95	0.200	0.603	0.3	0.355	0.00	0.18	0.0022	382	2836

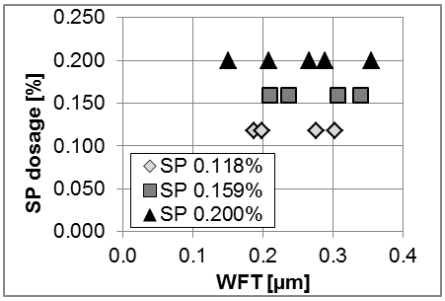

Figure 4. The range of WFT covered in this experimental program

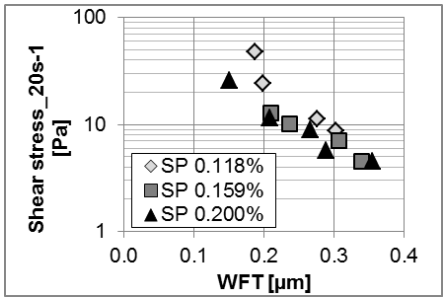

Figure 5. Influence of the WFT on the rheology

The robustness against small variations in the water content is tested by changing the water content with ±3%. Table VII summarizes the impact on the rheological characteristics. Because the variations in the test results should be compared by the value of the reference mixture, all changes are expressed as percentages.

Figure 6 illustrates an increasing water-to-powder ratio or superplasticizer dosage increases the robustness of the shear stress at a shear rate of 20 s^{-1} ($\tau(20\ s^{-1})$. A similar trend can be observed using the shear stress inclination at 20 s^{-1} ($\frac{d\tau}{d\dot{\gamma}}(20\ s^{-1})$. The effect on the yield stress seems to be independent of water-to-powder ratio (similar slopes are obtained).

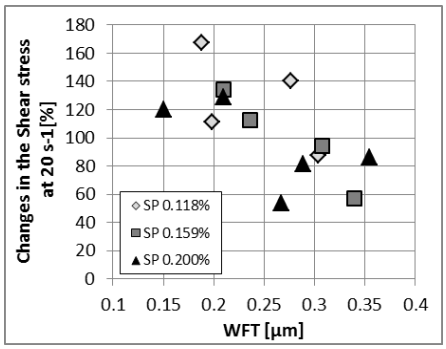

Figure 6. The influence of the WFT and

superplasticizer dosage on the robustness of the rheology

Table VII. Robustness of the reference mixtures against small changes in the water content

Mix nr	Water-to-powder ratio	Superplasticizer dosage	WFT	Changes in the shear stress at 20s-1	Changes in the yield stress	Changes in the shear stress inclination at 20s-1
	[-]	[%]	[µm]	[%]	[%]	[%]
1	0.85	0.118	0.188	167	176	160
2	0.90	0.118	0.198	111	126	105
3	0.95	0.118	0.276	140	201	115
4	1.00	0.118	0.304	87	118	73
5	0.85	0.159	0.209	134	257	77
6	0.90	0.159	0.236	112	196	91
7	0.95	0.159	0.308	94	313	75
8	1.00	0.159	0.340	57	121	51
9	0.75	0.200	0.151	120	118	95
10	0.80	0.200	0.209	128	199	89
11	0.85	0.200	0.267	53	245	48
12	0.90	0.200	0.289	81	248	57
13	0.95	0.200	0.355	86	90	73

Figure 7 shows the changes of the rheology in a rheogram. A logarithmic scale is used to illustrate the graphs because the impact of a change in the rheological parameters depends on the value of the parameter itself. A change of 0.1 Pa on the yield stress has a more pronounced impact on a mixture with a yield stress of 0.2 Pa than on a mixture with a yield stress of 50 Pa. Based on the concept of robustness area described by Billberg and Westerholm [7] on concrete rheograms, a definition of robustness is proposed. Assuming a rectangle surrounding the changes in rheology on the logarithmic graphs in Figure 8 illustrates the sensitivity of pastes to small changes in the water content, the definition of the robustness value is defined as one divided by the area of the rectangle in a logarithmic scale (Equation 5). The higher R is, the more robust is a paste system.

$$R = \frac{1}{log\left(\frac{\tau_{0,max}}{\tau_{0,min}}\right) * log\left(\frac{\mu_{max}}{\mu_{min}}\right)} \quad \text{(Eq. 5)}$$

This definition of the robustness allows to compare the combined changes relative to the original values of the two parameters describing the rheological behavior of the paste. Table VIII summarizes the robustness value R of all mixtures. The table also summarizes the increases in storage modulus G' during the first and second 20 minutes of structural buildup during the oscillatory rheometry (G'_1 and G'_2).

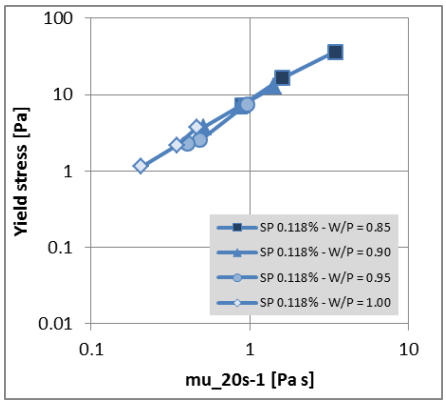

Figure 7a. Robustness of the rheology illustrated in a rheogram (SP 0.118%)

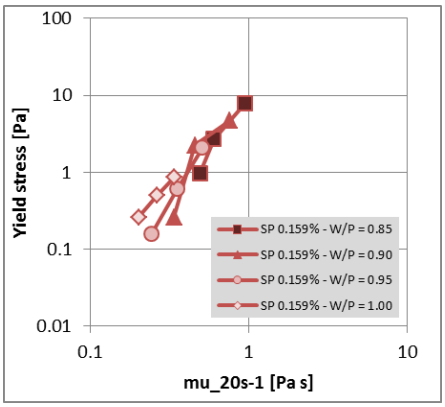

Figure 7b. Robustness of the rheology illustrated in a rheogram (SP 0.159%)

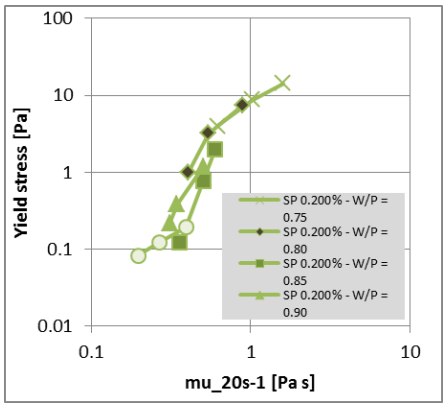

Figure 7c. Robustness of the rheology illustrated in a rheogram (SP 0.200%)

Table VIII. The robustness evaluation of all reference mixtures

Mix nr	Water-to-powder ratio	Superplasticizer dosage	WFT	Yield stress	Inclination of the shear stress at 20s-1	Increase in G'_1	Increase in G'_2	Robustness value R
	[-]	[%]	[µm]	[Pa]	[Pa]	[Pa]	[Pa]	[-]
1	0.85	0.118	0.188	16.38	1.59	1073	1873	2.44
2	0.90	0.118	0.198	7.05	0.87	711	1218	4.28
3	0.95	0.118	0.276	2.55	0.49	717	1665	5.22
4	1.00	0.118	0.304	2.17	0.35	514	1220	5.59
5	0.85	0.159	0.209	2.68	0.60	322	365	3.81

6	0.90	0.159	0.236	2.23	0.46	306	364	2.29
7	0.95	0.159	0.308	0.62	0.35	302	411	2.81
8	1.00	0.159	0.340	0.49	0.26	225	521	8.69
9	0.75	0.200	0.151	8.71	1.03	701	1007	4.40
10	0.80	0.200	0.209	3.22	0.54	265	462	3.38
11	0.85	0.200	0.267	0.77	0.50	206	202	3.66
12	0.90	0.200	0.289	0.00	0.35	256	504	6.45
13	0.95	0.200	0.355	0.00	0.27	382	2836	8.99

Based on the robustness definition, the following trends and influence factors are observed:

- Figures 8 and 9 illustrate the correlation between the robustness and the water-to-powder volumetric ratio (SP 0.118%: $R^2 = 0.91$; SP 0.159%: $R^2 = 0.45$; SP 0.200%: $R^2 = 0.68$) or a higher WFT ($R^2 = 0.47$). The relation between the water-to-powder ratio and the robustness depends on the superplasticizer dosage. Similar trends can be found based on the ratio of the packing density to the maximum packing density ϕ/ϕ_{max} of the mixtures ($R^2 = 0.42$).
- No clear influence of the yield stress τ_0, inclination of the shear stress at 20 s^{-1} $\frac{d\tau}{d\dot{\gamma}}(20\ s^{-1})$, or the shear stress at 20 s^{-1} $\tau(20\ s^{-1})$ on the robustness is observed.

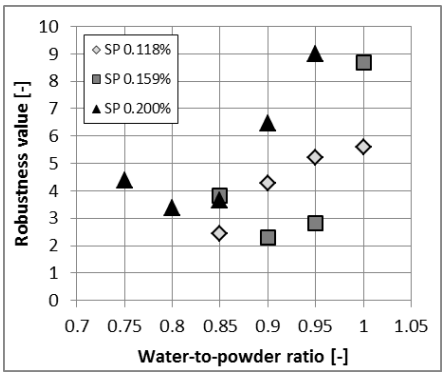

Figure 8. The influence of the water-to-powder ratio on the robustness value

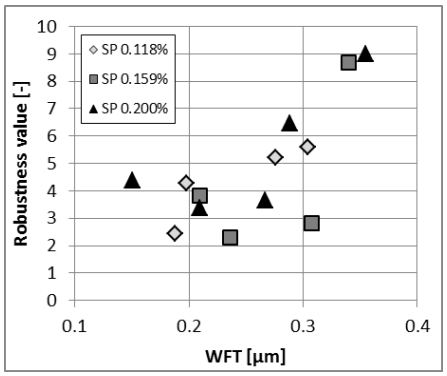

Figure 9. The influence of the WFT on the robustness value

- In Figure 10, the relation between the sensitivity of the rheology and the structural buildup as measured by the storage modulus G' buildup at rest is illustrated. Mixtures with a higher G' buildup rate were more sensitive to changes in the shear rate and the inclination of the shear rate of mixtures (Table VIII). However, no relation between the structural buildup and the robustness value can be established.

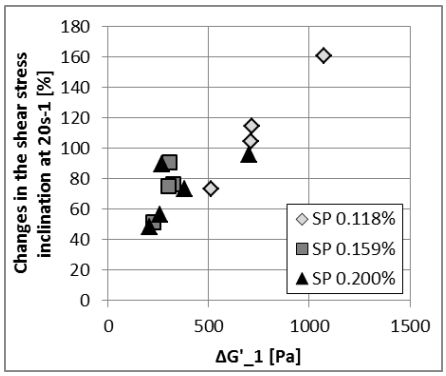

Figure 10. Influence of the structural buildup on the robustness of the shear stress at 20 s^{-1}

The observed relation between the water-to-powder ratio or WFT and the rate of structural buildup is valid on paste level. Because the pastes were mixed in the absence of the ball-bearing effect of aggregates and in a Hobart mixer, the hydration reaction rate differs from a paste mixed inside a concrete mixture.

Conclusions

Based on an extensive experimental program, some possible mechanisms governing the robustness of the paste rheology against small variations in the water content have been investigated. Thirteen mixtures varying in water-to-powder volumetric ratio and superplasticizer dosage were subjected to variations of ±3% of their water dosage. Higher water-to-powder ratios resulted in a higher water film thicknesses (WFT), and in more robust mixtures. A higher superplasticizer dosage resulted in a higher WFT and also more robust mixtures. A higher early age structural buildup as measured by the increase in storage modulus G' at rest resulted in less robust mixtures. No clear influence of the viscosity of the mixtures was observed.

References

[1] Kwan AKH, Ng IYT. Optimum superplasticiser dosage and aggregate proportions for SCC. Magazine of Concrete Research. 2009;61(4):281-92.

[2] Bonen D, Deshpande Y, Olek J, Shen L, Struble L, Lange DA, et al. Robustness of self-consolidating concrete. In: De Schutter G, Boel V, eds. *5th International RILEM Symposium on Self-Compacting Concrete*. Ghent, Belgium: RILEM Publications SARL 2007:33-42.

[3] Van Der Vurst F, Grünewald S, Feys D, Vandewalle L, Vantomme J, De Schutter G. Interaction between Rheology and Robustness of Fresh Self-Compacting Concrete. in press. 2016.

[4] Billberg PH. Influence of powder type and VMA combination on certain key fresh properties of SCC. In: Wallevik O, Khrapko M, eds. *9th International Symposium on High Performance Concrete*. Rotorua, New Zealand: New Zealand Concrete Society 2011.
[5] Haldenwang R, Fester VG. The influence of different superplasticisers on the flowability and reproducibility of a SCC mix. In: Wallevik O, Khrapko M, eds. *9th International Symposium on High Performance Concrete*. Rotorua, New Zealand: New Zealand Concrete Society 2011.
[6] Naji S, Hwang S-D, Khayat KH. Robustness of self-consolidating concrete incorperating different viscosity-enhancing admixtures. ACI Materials Journal. 2011;108(4):432-8.
[7] Billberg P, Westerholm M. Robustness of fresh VMA-modified SCC to varying aggregate moisture. NCR Journal. 2008;38(7):103-19.
[8] Bonen D, Deshpande Y, Olek J, Shen L, Struble L, Lange DA, et al. Chapter 1. Robustness of SCC. In: Lange DA, ed. *Self-consolidating concrete*. Urbana, IL, U.S.A.: The Center for Advanced Cement Based Materials (ACBM) 2007:4-22.
[9] Bouras R, Chaouche M, Kaci S. Influence of viscosity-modifying admixtures on the thixotropic behaviour of cement pastes. Applied Rheology. 2008;18(4):45604-1 - -8.
[10] Nkinamubanzi P-C, Aïtcin P-C. Cement and superplasticizer combinations: Compatibility and robustness. Cement, Concrete and Aggregates. 2004;26(2):102-9.
[11] Ferron RPD. Formwork pressure of self-consolidating concrete: influence of flocculation mechanism, structural rebuilding, thixotropy, and rheology. *Department of Civil and Environmental Engineering*. Evanston, IL, USA: Northwestern University 2008:Doctoral thesis.
[12] Nunes S, Milheiro-Oliveira P, Sousa Coutinho J, Figueiras J. Rheological characterization of SCC mortars and pastes with changes induced by cement delivery. Cement & Concrete Composites. 2011;33(1):103-15.
[13] Feys D, Asghari A, Ghafari E, Ley Hernandez AM, Van Der Vurst F, De Schutter G. Influence of mixing procedure on robustness of self-consolidating concrete. Center for Transportation Infrastructure and Safety 2014.
[14] Yamada K, Yanagisawa T, Hanehara S. Influence of temperature on the dispersibility of polycarboxylate type superplasticizer for highly fluid concrete. In: Skarendahl A, Petersson Ö, eds. *First International RILEM Symposium on Self-Compacting Concrete*. Stockholm, Sweden: RILEM Publications 1999:437-48.
[15] Rigueira JW, García-Taengua E, Serna-Ros P. Self-consolidating concrete robustness in continuous production regarding fresh and hardened state properties. ACI Materials Journal. 2009;106(3):301-7.
[16] BIBM - CEMBUREAU - EFCA - EFNARC - ERMCO. The European Guidelines for Self-Compacting Concrete - Specification, Production and Use. 2005.
[17] Li LG, Kwan AKH. Concrete mix design based on water film thickness and paste film thickness. Cement and Concrete Composites. 2013;39(5):33-42.

[18] Yang M, Jennings HM. Influences of mixing methods on the microstructure and rheological behavior of cement pastes. Advanced Cement Based Materials. 1995;2(2):70-8.
[19] Williams DA, Saak AW, Jennings HM. The influence of mixing on the rheology of fresh cement paste. Cement and Concrete Research. 1999;29(9):1491-6.
[20] Takada K, Walraven JC. Influence of mixing efficiency on the properties of flowable cement pastes. In: Ozawa K, Ouchi M, eds. *Second International Symposium on Self-Compacting Concrete*. Tokyo, Japan 2001:545-54.
[21] Juilland P, Kumar A, Gallucci E, Flatt RJ, Scrivener KL. Effect of mixing on the early hydration of alite and OPC systems. Cement and Concrete Research. 2012;42(9):1175-88.
[22] Assaad J, Khayat KH. Assessment of thixotropy of self-consolidating concrete and concrete-equivalent-mortar - effect of binder composition and content. ACI Materials Journal. 2004;101(5):400-8.
[23] Feys D, Wallevik JE, Yahia A, Khayat K, Wallevik OH. Extension of the Reiner-Riwlin equation to determine modified Bingham parameters measured in coaxial cylinders rheometers. Materials and Structures. 2013;46(1-2):289-311.
[24] Wallevik JE. Rheology of particle suspensions - Fresh concrete, mortar and cement paste with various types of lignosulfonates. *Department of Structural Engineering*. Trondheim, Norway: The Norwegian University of Science and Technology (NTNU) 2003:Doctoral thesis.
[25] Roussel N, Ovarlez G, Garrault S, Brumaud C. The origins of thixotropy of fresh cement pastes. Cement and Concrete Research. 2012;42(1):148-57.
[26] Lesage K. Interactions between cement and combined concrete admixtures - The influence on cement paste rheology. *Department of Civil Engineering*. Leuven, Belgium: University of Leuven 2014:Doctoral thesis.
[27] Betioli AM, Gleize PJP, Silva DA, John VM, Pileggi RG. Effect of HMEC on the consolidation of cement pastes: isothermal calorimetry versus oscillatory rheometry. Cement and Concrete Research. 2009;39(5):440-5.

Theme 2: Materials for SCC

Bleeding in Cement Paste: Induction, Acceleration and Consolidation Phases

Nadia Massoussi and Nicolas Roussel

Université Paris Est, IFSTTAR, Laboratoire Navier, France

Abstract We focus in this paper on the bleeding phenomenon and its kinetics at the scale of cement paste. Our experimental results on simple systems suggest that this kinetics can be divided into three regimes: a dormant period (which could, if fully understood, be of major interest from an industrial point of view), an accelerating period (during which the apparent permeability of the paste increases due to the formation and percolation of water extraction channels) and a consolidation regime (during which the permeability of the sample decreases because of the water extraction itself until gravity is not able to further consolidate the sample and extract any additional water). As a consequence, the bleeding cannot be simply considered as the consolidation of a porous material as observed until now in literature but is of an obvious heterogeneous nature leading to the formation of water extraction channels or preferred paths within the paste.

Keywords: *Fresh propertie, Bleeding, Consolidation, Stability.*

Introduction

In recent years, the understanding of the rheological behavior of homogeneous cementitious materials has made significant progress. However, concrete or mortar stability (*i.e.* the ability of the mixture to stay homogeneous) and the physical phenomena at the origin of this stability are still poorly understood. Concrete or mortar stability can be divided into two major features: the stability of the coarse aggregates or sand particles suspended in the cement matrix (which can reverse into so-called segregation), and the stability of the cement grains suspended in water (which can reverse into so-called bleeding). Although there exist some analysis of aggregates stability [1], bleeding is still treated empirically and the methods allowing for its proper measurement are only weakly developed and/or understood. Relatively few scientific publications are available on this topic. The most complete state of the art is gathered in the thesis of Josserand [2], in which

the main conclusion is that bleeding of cementitious materials [2-5] can be seen as a soil-consolidation-like process.
We focus in this paper on this specific gravity-induced phase separation process and its kinetics at the scale of cement paste. Our experimental results on simple systems suggest that bleeding cannot be simply considered as the consolidation of a porous material but is of an obvious heterogeneous nature leading to the formation of water extraction channels within the paste. As a consequence, its kinetics can be divided into four regimes: a dormant period (which could, if fully understood, be of major interest from an industrial point of view), an accelerating period (during which the apparent permeability of the paste increases due to the formation and percolation of water extraction channels), a constant rate period (water continues to percolate through these channels) and finally a consolidation state (which eventually lead to the total extraction of the free water in the system). Only the last two have been observed until now in literature.

Materials and Protocol

A Portland CEM I type cement of specific density 3.14 is used in this study. Its specific surface measured using a Blaine apparatus is 3390 cm^2/g. Its maximum solid fraction is estimated at around 59% [6] and its chemical composition is given in the following table:

Table I. Cement chemical compoistion

SiO_2	Al_2O_3	Fe_2O_3	CaO	Mgo	Na_2O	K_2O	SO_3	Cl	CAO
21.04 %	3.34%	4.14%	65.43 %	0.83%	0.22%	0.35%	2.31%	0.02%	0.69%

The water to cement mass ratio is fixed at 0.6 in order to measure a significant bleeding. Water is mixed with cement during 3 minutes using a Turbo test Rayneri VMI mixer at 840 rpm. Just after mixing, the mixture is poured into a transparent test tube. The total time needed to fill the beaker does not exceed one minute. After filling, the tube is sealed with a plastic film to prevent any water evaporation. Progressive water extraction from the sample is recorded using numerical image acquisition and automated analysis. The acquisition period of the extracted water layer thickness is one second during the first hour then one minute for the following three hours.

Results and Discussion

In theory, if we consider that we are facing the homogeneous consolidation of a deformable porous media, we expect from Darcy's Law that the amount of water that has left the sample after a time t shall be proportional to $\Delta\rho.g.kt/\mu_0$ where μ_0 is

the viscosity of the interstitial fluid, $\Delta\rho$ is the density difference, K is the permeability (which could decrease with time and consolidation). We can however also consider that the final compaction state below the extracted water layer shall be the same no matter the initial filling height. As a consequence, the final amount of water that has left the sample shall be proportional to the initial volume of material tested.

From the above basic scaling, we therefore expect that water flow rate shall not depend on the initial filling height whereas the final amount of water that has left the sample shall be proportional to the initial height. As a consequence, bleeding shall start similarly no matter the initial height but stop before for the lowest initial heights.

This is what we get on long time scales as shown in Fig. 1 in which the experimental results obtained for three different initial sample heights are plotted.

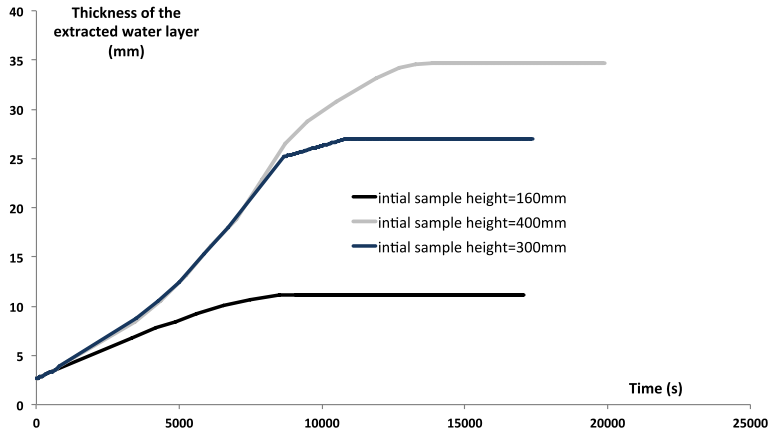

Figure 1. Thickness of the extracted water layer as a function of time for three different initial sample heights.

On long time scales, bleeding rate decreases as expected and the final amount of extracted water is as expected proportional to the initial height of material that suggests that the compaction state is the same for all samples. On intermediate time scales, the extraction rate is the same for all samples also as expected from the above basic scaling. We conclude therefore, similarly to other authors, that bleeding, on these long time scales, can be seen as a soil-consolidation-like process. The permeability of the sample decreases because of the water extraction itself until gravity is not able to further consolidate the sample and extract any additional water.

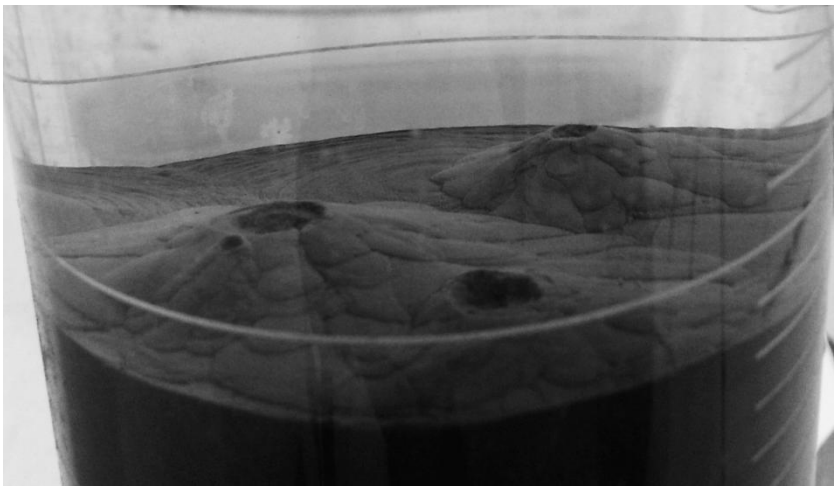

Figure 2. Water extraction channels visible at the upper surface of the sample. Initial height is 40cm. These channels are not visible for the 14cm initial height.

Two features suggest however that the physics behind bleeding is more complex. The first one is shown in Fig. 2, in which some extracting water channels can be spotted at the surface of the sample for the highest sample initial height. This suggests that the consolidation process is not the one of an homogeneous porous media and involves some strong localization of the water extraction, which can lead to some erosion and transport of the finest particles within the sample. These particles are then carried out to the surface to form the heterogeneities shown in Fig. 2.

The second feature suggesting that the physics behind bleeding is more complex than initially expected is shown in Fig. 3, in which the focus is given to short time scales by redrawing Fig. 1 in log scale.

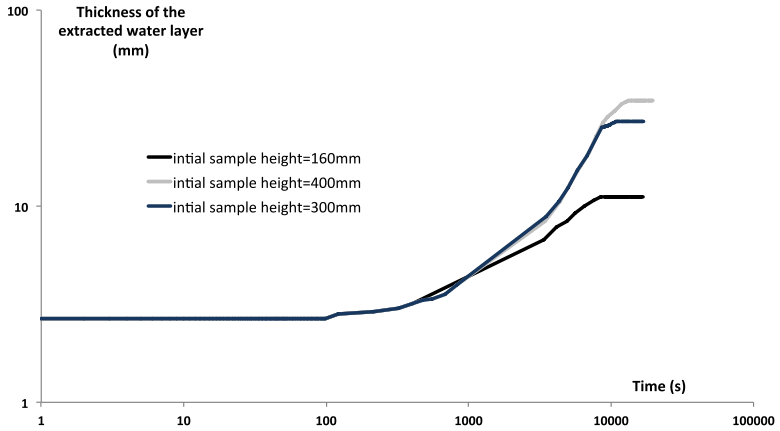

Figure 3. Thickness of the extracted water layer as a function of time for three different initial sample heights

We see in Fig. 3 that, below 1000 s (*i.e.* around 15 minutes), there exists a regime of very low water extraction rate. We will call this regime the dormant period. The water layer thickness in this regime is the one that already existed at the end of the pouring phase. This extremely low water extraction rate can be associated to a very low permeability. This suggests that the apparent permeability of the sample involved in the constant extraction rate following the dormant period is higher than the initial permeability of the sample suggesting that something has changed within the sample.

Considering this and the water extraction channels in Fig. 2, we suggest therefore that bleeding of cement pastes result from the formation of water extracting channels or water extraction preferred paths, which lead to an increase in the permeability of the paste resulting into an increase in water extraction rates and to a fast consolidation of the material surrounding these channels, which would consequently lead to a decrease in apparent permeability. If the size of these channels or preferred water extraction paths becomes larger than a few 100 micrometres, they can then be visually spotted. Even when they cannot be visually spotted, they do exist within the paste and are at the origin of the water extraction rate increase that can be seen in Fig. 3 for the lowest sample initial height, which visually seem to stay homogeneous during the entire duration of the test. The fact that its permeability starts from a low initial value to increase to a higher one in the accelerating regime suggests however that these channels or preferred paths do form in the paste.

Conclusions

We focus in this paper on the bleeding phenomenon and its kinetics at the scale of cement paste. Our experimental results on simple systems suggest that this kinetics can be divided into three regimes: a dormant period (which could, if fully understood, be of major interest from an industrial point of view), an accelerating period (during which the apparent permeability of the paste increases due to the formation and percolation of water extraction channels) and a consolidation regime (during which the permeability of the sample decreases because of the water extraction itself until gravity is not able to further consolidate the sample and extract any additional water). As a consequence, the bleeding cannot be simply considered as the consolidation of a porous material as observed until now in literature but is of an obvious heterogeneous nature leading to the formation of water extraction channels or preferred paths within the paste.

Acknowledgements

The authors would like to acknowledge the financial support of both Soletanche Bachy © and FNTP. The authors acknowledge FNTP committee reviewers for their constructive comments to the text.

References

[1] Roussel N., A theoretical frame to study stability of fresh concrete, Materials and Structures, Volume: 39 Issue: 1 Pages: 81-91, 2006.
[2] Josserand L., Ressuage des bétons hydrauliques, thesis report (in French), LCPC, 2004.
[3] Loh C.K., Tan T.S., Yong K.Y., Wee T.H., An experimental study on bleeding and channelling of cement paste and mortar, Advances in cement research, 10, n°1, pp 1-16 , January, 1998.
[4] Powers T.C., The properties of fresh concrete, J. Wiley & Sons, Inc. pp 533-652, New York, U.S.A,1968.
[5] Giaccio G., Giovambattista A., Bleeding :Evaluation of its effects on concrete behaviour, Materials and structures ,RILEM, v112 pp 265 - 71, july-august, 1968.
[6] Hot J., Bessaies-Bey H., Brumaud C., Duc M., Castella C., Roussel N., Adsorbing polymers and viscosity of cement pastes, Cement and Concrete Research, Volume 63, Pages 12-19, 2014.

Adsorption Characteristics of PCEs and its Effect on Rheological Properties of Cement Paste

Jin Young Yoon[1] and Jae Hong Kim[1]

[1] Ulsan National Institute of Science and Technology, Republic of Korea

Abstract Polycarboxylate ether (PCE) is the main component of superplasticizer and it has been widely used in construction industry for decades. The role of PCE is to improve workability of freshly mixed concrete by dispersing cement particles through electrostatic and steric repulsion. The use of PCE changes hydration rate and rheological properties of cement paste in early ages. The aim of this research is to analyse affinity of PCE on cement paste and its effect on rheological properties of cement-based materials. The affinity of PCE is related to their adsorption ability. Total amount of adsorbed carbon to cement are characterized by using a Total Organic Carbon (TOC) equipment. According to different types of PCE, the degree of adsorption and its effect on rheology were evaluated. This presentation will discuss the tendency of the PCE effects related to mix proportion of cement-based materials.

Keywords: *PCE, TOC, Rheological properties, ICP, Compatibility.*

Introduction

The use of polycarboxylate based superplasticizers (PCE) allow a reduction of water content and improving workability by dispersing cement particles in mortar or concrete [1]. The structures of PCE are generally composed of negatively charged backbone with (poly)carboxylate and grafted side chains mainly composed of (poly)ethylene oxide. The charged backbone adsorbs on the surface of the cement particles and the graft chains extend for developing steric repulsion among the cement particles. [1,2]. As a results, the addition of PCE achieves a reduction of the amount of necessary water to obtain required workability of the freshly mixed concrete. The addition of PCE to a fresh concrete allows high flow properties required for high-performance concrete and SCC [3]. However, the number of and the length of side chains and their grafting density are flexible according to a PCE production process. It induce a different repulsive inter-particle force which prevents the formation of agglomerates.

Therefore, it is important to understand how much amount of PCE adsorbed on cement particles and its effect on the rheological properties of cement-based materials. In this study, the adsorption characteristics of PCE were studied based on Total Organic Carbon (TOC) measurement. Moreover, the relationship between the amount of adsorbed PCE and workability of cement paste was investigated with different dosage of PCE and water-to-cement ratio (w/cm) of cement paste.

Experimental Program

Materials

In this study, commercially available ordinary Portland cement was used. The specific density and Blaine specific surface area of cement were 3,150 kg/m^3 and 335 m^2/kg, respectively.

A total of 6 PCE samples were used in this study. 3 PCEs, labelled by LA, LB and LC, were formulated for the purpose of high-range water reducing. The others labelled by LD, LE, and LF help to maintain the consistency of cement-based suspensions. All samples were diluted with deionized water, and their total solid content (TSC) became 21%. The FT-IR result is given in Fig. 1.

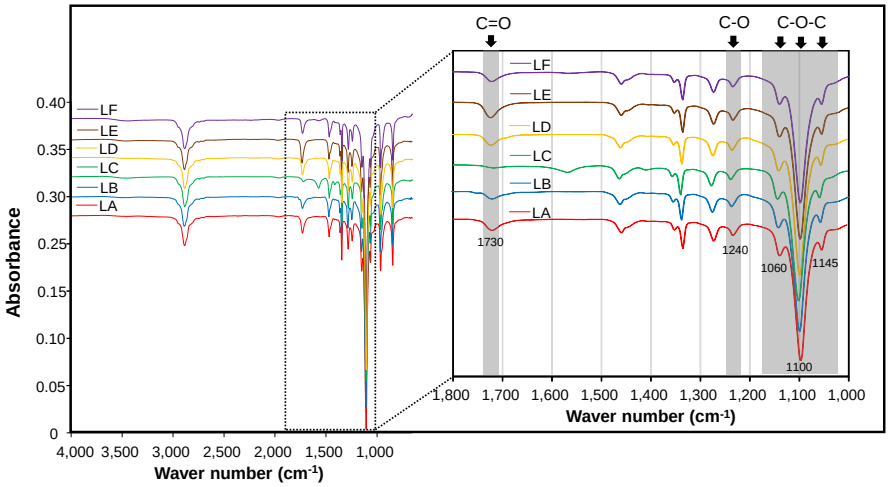

Figure 1. FT-IR spectra of PCEs

Sample preparation

The different w/cm of cement pastes, 0.33, 0.4 and 0.53, were prepared. The dosages of PCE were controlled to obtain consistency of the cement pastes. The consistency of cement paste was measured by the use of mini slump cone test. A

flow cone is filled with a cement paste. After the cone was lifted, the average diameter of the spread was recorded. The mini slump flow test was repeated at interval of 30 minutes. Fig. 2 shows the dimension of mini slump cone.
The extraction of mixing water from cement paste was conducted in accompany with the mini slump flow test. The extracted water was used for measuring total organic carbon (TOC) inductively coupled plasma (ICP). Both expected to indicate the amount of absorbed carbon on cement grains and dissolved ion contents in the pore solution, respectively.

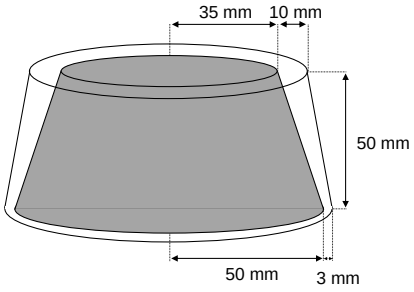

Figure 2. The dimension of mini slump cone

Figure 3. TOC analyzer

The mass of adsorbed PCEs on a cement particles was measured by a TOC analyser as shown in Fig. 3. The amount of total adsorbed carbon is calculated from the difference between the amount of the PCEs in mixing water and pore solution:

$$C_{ad(t)} = C_i - C(t) \tag{1}$$

where $C_{ad}(t)$ means adsorbed carbon of PCEs on cement, Ci is initial carbon contents in mixing water and $C(t)$ is measured TOC in pore solution at time of t. The adsorption ratio of PCEs is calculated as

$$C_{ad,\%}(t) = \frac{C_i - C(t)}{C_i} \tag{2}$$

Experimental Results and Discussion

Adsorption of PCEs

In this study, the adsorption characteristics of 6 PCEs on cement paste were investigated under different w/cm of cement paste and dosage of PCEs. Fig. 4 shows the adsorption of PCEs over time, where w/cm of the cement paste was controlled. The water reducing PCEs of LA, LB and LC showed the highest adsorption ratio the initial measurement when 0.05% dosage was added for each case. The PCE dosage is expressed by solid contents compared to the cement mass

contents. The adsorption of two consistency maintaining PCEs (LE and LF) increased with time when they were incorporated on 0.05% or 0.11%. When the amount of added PCEs increased in Fig 3 (c) and (d), the adsorption ratio of PCEs tended to be converged with time. It is expected that the adsorption of PCEs has a limit regardless of w/cm of cement paste.

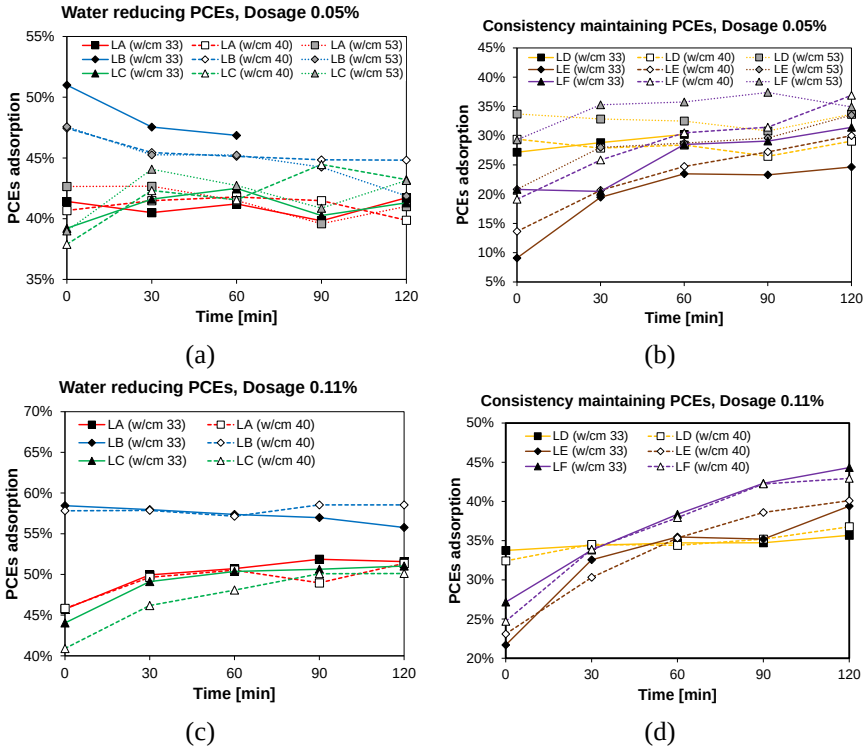

Figure 4. The relationship between PCEs adsorption and w/cm of cement paste.

The relationship between different dosages of PCEs under the same w/cm of 0.33 cement paste is focused. Fig. 5 presents the adsorbed amount of PCEs when w/cm is 0.33. When mixing is finished, the water reducing PCEs showed higher adsorption as shown in Fig. 5 (a). The allowable dosage in terms of non-segregation or no-bleeding is limited until 0.12%. On the other hand, the consistency maintaining PCEs showed lower adsorption at the initial measurement (0 min), but they could be added until 0.21%. The consistency maintaining PCEs have continuously got adsorbed and after 2 h their adsorbed amount were similar to that of the water-reducing PCEs.

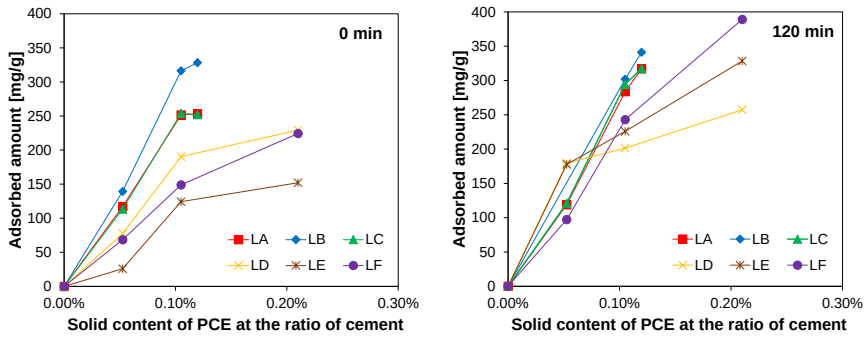

(a) (b)

Figure 5. The adsorbed amount of PCEs with w/cm of 0.33 cement paste after mixing 0 min and 120 min

Consistency of cement paste

Fig. 6 shows the mini slump flow of cement paste as a function of PCE dosage, where w/cm of cement pastes was identical (0.33).Higher dosage of PCEs brought higher mini slump flow as expected. Except for LB, the performance of the water reducing PCEs was greater than the consistency maintaining PCEs at the same dosage level. For all samples, regardless of PCEs type, their stability became problematic when the mini slump flow was higher than 40 cm.

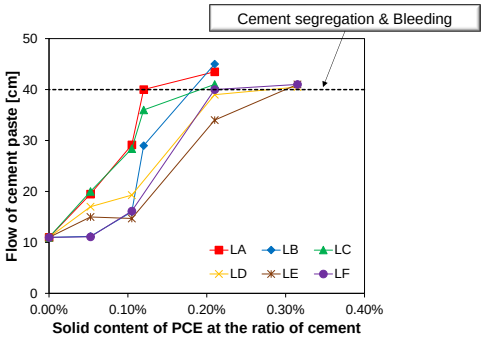

Figure 6. Flow of cement paste of w/cm 0.33 as a function of dosage of PCEs after mixing 0 min

Fig. 7 shows change in the mini slump flow, where the legend mean the type of dosage followed by its dosage. For example, LA21 indicates the addition of LA PCE with 0.21%. In Fig. 4, a large amount of water reducing PCEs were initially adsorbed and sustained, but for the consistency maintaining PCEs its adsorption slowly increases from the initial small amount. The mini slump results corresponded to the adsorption results. When the dosage of PCEs were less than

0.11%, PCEs of LA and LC added cement paste have much higher workability compared to the others at 0 to 30 min in Fig. 7 dotted line. However, the mini slump flow of PCEs of LE and LF added cement paste are slowly increased after mixing 30 to 60 min which is properly corresponded to additional adsorption of PCEs in Fig. 4.

According to the PCE type, the time for occurring paste stability problem is also different. The cement segregation and bleeding is severely occurred with the addition of PCEs with 0.21% of LA, LB and LC. In case of consistency maintaining PCEs of LD, LE and LF, cement segregation occurred with dosage of 0.32% at 0 min. When the dosage of LE and LF is 0.21%, there was no stability problems at 0 min, but the cement segregation occurred after mixing 30 min due to additional adsorption of PCEs. Since LD PCE had no additional PCEs adsorption, there was no stability problems for LD21.

In general, the cement paste with LB has comparatively lower consistency despite of higher PCE adsorption. The LD added cement paste does not show any additional consistency improvement with time.

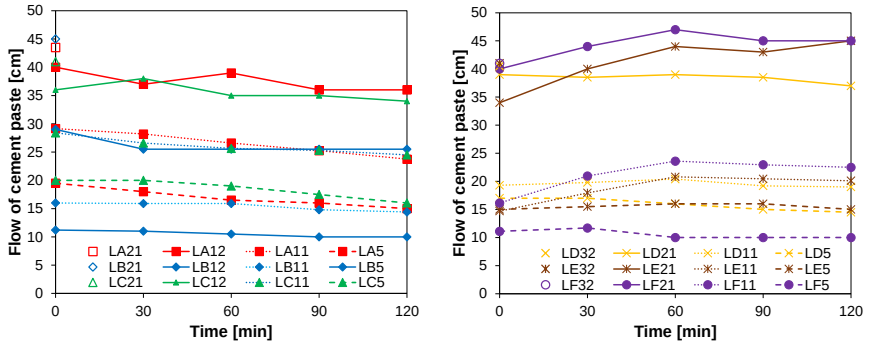

(a) (b)

Figure 7. Time dependent workability change of w/cm 0.33 cement paste with different PCEs dosage

Atomic concentration in pore solution

The ICP spectrometry was conducted using extracted water from the cement paste proportioned by w/cm=0.33. The ICP focused the effect of PCEs on the cement hydration: Related atoms Ca, Al, S and Na. The PCEs of LA and LF were chosen as a representative of water reducing and consistency maintaining PCEs, respectively.
The Na concentration curve shows that the overall ion dissolution rate is similar regardless of the use of PCEs. The dissolution rate of LA11 is slightly higher and that of LF11 is lower than no-PCE case.

The Ca concentration is related to formation of C-S-H and ettringite. Generally, the C-S-H phase formation occurs after mixing 6 hours, but ettringite is formed faster after mixing [4]. At early age of cement hydration, the dissolution of Ca ion is dominant. . In the Fig. 8 (b), the Ca ion concentration is slightly increased for LF11 samples after mixing 30 min. This is corresponded to the trend of both adsorption of PCEs and mini slump test. In other words, the surface area of cement particles which directly contact with water is increased and Ca ion dissolution is also increased.

The Al concentration is very small compared to the other ions concentration. LA11 samples has higher Al concentration compared to the others. It might be related to a higher specific surface area of cement particles when LA11 was incorporated. LA PCE caused better adsorption and consequent dispersion of cement particles in the TOC analysis. In LF11 and no PCE added cement paste, Al atom might be consumed during paste mixing. The reaction rate of C_3A is instantaneous at the early age [5]. On the contrary, higher amount of Al in LA11 sample with more reactive sites on dispersed cement particles. They were still remained at the end of the mixing and gradually consumed with time.

The consumption tendency of S ion is related to additional adsorption of LF PCE. The previous study reported that delayed added PCEs enhances the adsorption on dissolved S ion on reactive sites of C_3A [5]. The additional adsorption of LF PCE would have similar behaviour with this mechanism and it interrupts consuming S ion for 30-120 min. In case of LA11 samples, it has higher reactive sites compared to no PCE added cement paste and it continuously consumed S ion.

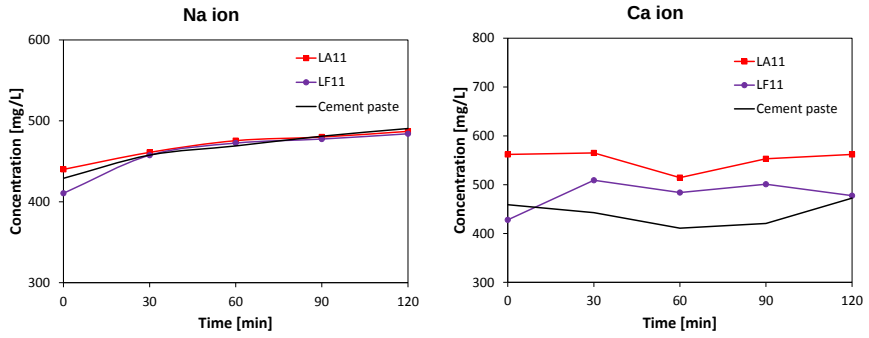

(a) (b)

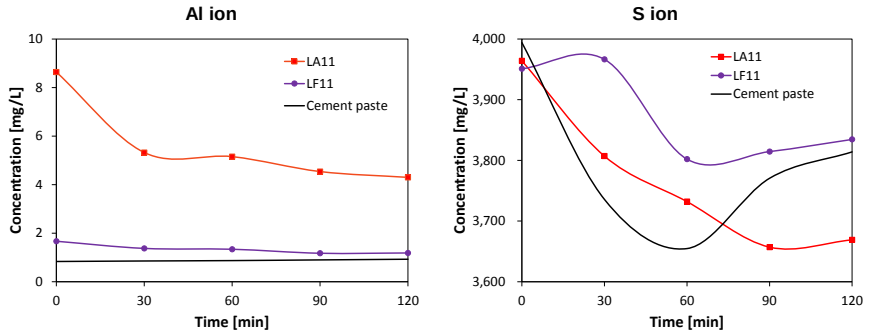

(c) (d)

Figure 8. Ion concentration change of w/cm 0.33 cement paste with different PCEs

Conclusions

In this study, the adsorption characteristics of various types of PCEs on cement paste were investigated. When a small amount of PCE (0.05% dosage) was incorporated, the adsorption ratio of PCE are not perfectly converged. However, the adsorption ratio is converged with a large amount of PCEs (0.11%). Therefore, the adsorption ratio of PCE under a different w/cm of cement paste are the same when sufficient amount of PCE was supplied.

Water reducing PCEs tended to adsorb cement particles at very early age and it was sustained, but the adsorption amount of consistency maintaining PCEs slightly increased with time. The adsorption trend corresponds with the mini slump flow of the cement paste sample. When water reducing PCEs were used, the flow at the early age was very high and it decreased as time goes. The use of consistency maintaining PCEs continuously increased paste slump.

However, LB PCE brought very low consistency among the water reducing PCEs. The adsorption and consistency results of LD (a consistency maintaining PCE) shows a performance like water reducing PCEs.

Finally, the early age cement hydration rate was compared by the use of ICP spectrometry. The addition of a water reducing PCE (LA) increased the specific surface area and reactive sites of cement particles which improved dissolution of Ca, Al and S ion. On the other hand, the consistency maintaining PCE (LF) were adsorbed on cement particles slowly. They adsorbed on reactive sulphate ion and it interrupted the consumption of sulphate ion.

Acknowledgementss

This research was supported by the Global Ph.D Fellowship Program through the National Research Foundation of Korea (NRF) funded by the Ministry of Education (No. 2014H1A2A1018466).

References

[1] J. Plank, B. Sachsenhauser. (2009). Experimental determination of the effective anionic charge density of polycarboxylate superplasticizers in cement pore solution. Cem. Concr. Res, Vol. 39, pp. 1-5.
[2] K. Yoshioka, E. Tazawa, K. Kawai, T. Enohata. (2002). Adsorption characteristics of superplasticizers on cement component minerals. Cem. Concr. Res, Vol 32, pp. 1507-1513.
[3] L. Ferrari, J. Kaufmann, F. Winnefeld, J. Plank. (2010). Interaction of cement model systems with superplasticizers investigated by atomic force microscopy, zeta potential, and adsorption measurements. J. Colloid Interface Sci. Vol. 347, pp. 15-24.
[4] P.K. Mehta, P.J.M. Monteiro. (2013). Concrete: Microstructure, Properties, and Materials. McGraw Hill Professional
[5] I. Aiad, S. Abd El-Aleem, H. El-Didamony. (2002). Effect of delaying addition of some concrete admixtures on the rheological properties of cement pastes. Cem. Concr. Res, Vol 32, pp. 1839–1843

Effects of Silica Fume and Metakaolin on Rheology and Structural Breakdown Properties of Self-Consolidating Concrete

Reza Saleh Ahari[1] and Tahir Kemal Erdem[2]

[1]Tabriz Branch, Islamic Azad University, Tabriz, Iran
[2]Izmir Institute of Technology, Izmir, Turkey

Abstract The study herein was intended to evaluate the effect of using several amounts of silica fume (SF) and metakaolin (MK) on T_{50} flow time, V-funnel flow time, torque plastic viscosity, apparent yield stress, structural breakdown and compressive strength of self-consolidating concrete (SCC) mixtures. Moreover, influence of elapsing time on these parameters was investigated in a standstill condition. The results showed that mixtures containing SF showed lower torque plastic viscosity, V-funnel flow time and T_{50} flow time values in comparison with mixtures containing only portland cement (PC). However the opposite tendency was observed when MK was incorporated with PC. The yield stress and breakdown area of SF and MK blended mixtures were higher than that of the control mixtures. Moreover, addition of SF has a more significant effect on the mixture viscosity compared to incorporation of MK at the same level of replacement. After a resting time of 50 min., apparent yield stress and breakdown area values increased significantly with time while torque plastic viscosity values changed only in a limited range.

Keywords: *Plastic viscosity, Yield stress, Breakdown, Silica fume, Metakaolin.*

Introduction

Rheology and structural breakdown of self-consolidating concrete (SCC) have been recognized as important tools to be tailored to achieve a multifold set of engineering properties required for successful accomplishment and performance of the intended application [1-4]. Many parameters such as w/b ratio [5], binder type and content [6], aggregate characteristics and content [7], type and dosage of high-range water-reducing admixture (HRWR) [8] can affect the rheological properties and structural breakdown behavior of SCC. Besides, the dosage and characteristics

of supplementary cementitious materials (SCM) are important parameters in this regard [2,9].

Several studies [2,3,10-14] reported that utilization of very fine SCM such as silica fume (SF) and metakaolin (MK) in concrete not only improves the hardened properties of concrete, but also helps to adjust the rheological and thixotropic properties as well as stability of the fresh concrete for a given application. In other words, rheological parameters can be tailored according to the desired performance in a variety of civil engineering applications by the utilization of these SCM, which increases the interest in the use of MK and SF to produce SCC.

In a recent study, Hassan et al [11] proposed that with utilization of MK and SF in SCC, both plastic viscosity and yield stress increased as percentage of MK was increased. At constant slump flow, plastic viscosity of SF mixtures was similar to that of the control mixture without any SCM. In a another investigation Mouret and Cyr [15] reported that cement paste with MK exhibited high plastic viscosity while cement paste with SF showed lower plastic viscosity than reference cement paste.

Assaad [12] reported that mixtures containing a binary cement (PC+SF), showed lower plastic viscosity and higher breakdown area values than corresponding plain SCC mixtures. Rahman et al [16] reported that the utilization of SF in SCC did not influence the thixotropy significantly. Ferron et al. [17] determined the structural buildup of SCC cement pastes containing silica fume (SF) at a rest time up to 90 min and found that in a standstill condition structural buildup of SF blended mixtures increased with time.

Although a number of studies about the effects of using SF and MK on the fresh and hardened properties of SCC have been found in the literature, the effect of using these SCM on the rheological properties were discussed only in limited number of studies [11,12,15-17].

The study herein was intended to evaluate the effect of SF and MK on rheological and structural breakdown properties of SCC. T_{50} flow time, V-funnel flow time, torque plastic viscosity, apparent yield stress, structural breakdown and compressive strength of the mixtures were investigated in a constant slump flow value. Moreover, influence of elapsing time on these parameters was investigated in a standstill condition.

Experimental Methods

Materials

The cement used was an ordinary portland cement (PC), CEM I 42.5 R.. The properties and particle-size distribution of PC, SF and MK are presented in Table I and Fig. I. In addition, the micrographs of SF, MK and PC inspected by a scanning

electron microscope (SEM) are shown in Fig. II. Crushed limestone aggregate with maximum particle size of 15 mm and 4 mm, respectively for coarse and fine aggregate, were employed. The bulk specific gravity of the coarse and fine aggregates were 2.64 and 2.61, respectively, and their absorption capacities were 0.21% and 0.67%, respectively. A polycarboxylate ether-based high-range water-reducer (HRWR) was incorporated in all mixtures.

Table I. Properties of PC, SF and MK

	PC	SF	MK
CaO, %	64.06	0.25	0.3
SiO_2, %	17.74	87.92	51.1
Al_2O_3, %	4.76	0.4	39.1
Fe_2O_3, %	3.17	0.35	2.15
MgO, %	1.28	3.97	0.7
SO_3, %	2.94	0.21	0.08
K_2O, %	0.8	0.81	1.78
Na_2O, %	0.45	1.79	0.11
Free lime, %	2.21	—	—
Other minor oxides, %	0.64	1.43	0.88
Loss on ignition, %	1.95	2.87	3.8
Specific gravity	3.13	2.29	2.54
Blaine Fineness,cm^2/g	3310	—	—
Surface area B.E.T.,cm^2/g	—	245100	154100
Residue 45 μm, %	4.2	—	0.4

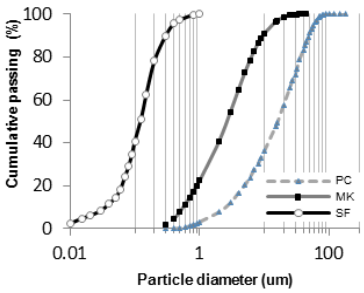

Figure 1. Particle size distributions of PC, SF and MK

Mixtures proportions

As summarized in Table II, one control mixture without any SCM and 7 SCC mixtures with SF or MK were designed to have a constant w/b of 0.44 and total binder content of 454.5 kg/m^3. Replacement of PC with SF and MK was made on the total mass basis of the binder. For all SCC mixtures the fine aggregate-to-total aggregate ratio, by mass, was set at 0.53. The HRWR dosages used in the mixtures were adjusted to secure an initial slump flow of 650 ± 10 mm. The mixtures were designated according to the type and the amount of cementitious materials included. For example, 8SF shows the mixture containing 8% SF.

Testing procedure

The measurement of fresh SCC properties was started as soon as mixing of all materials was finished. The slump flow values and time required for the concrete to spread to a diameter of 500 mm (T_{50}) were recorded. The rheological parameters (torque plastic viscosity and apparent yield stress) were evaluated using a coaxial cylinder concrete rheometer (Con Tec 4SCC) with a four-bladed vane impeller. Following the rheology tests, structural breakdown tests were performed. In order to determine the effect of passing time, the rheological parameters were measured at 0 and 50 minutes after mixing.

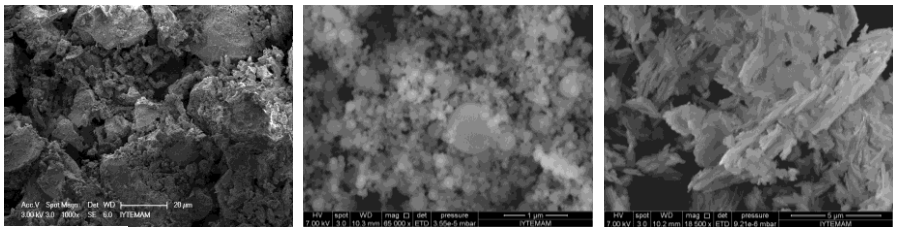

(a) (b) (c)

Figure 2. SEM images of a) PC, b) SF and c) MK.

Table II. Mix proportions of mixtures (kg/m^3).

Mixture ID	Water	PC	SF	MK	HRWR	Aggregates, (SSD)	
						Fine	Coarse
Control	200	454.5	—	—	5.75	883	783
4SF	200	436.5	18	—	6.7	880	778
8SF	200	418.5	36	—	7.5	875	774
12SF	200	400	54.5	—	8	870	771
4MK	200	436.5	—	18	6.18	881	781
8MK	200	418.5	—	36	6.5	878	779
12MK	200	400	—	54.5	6.7	876	776
18MK	200	373	—	81.5	7.5	873	773

Evaluating torque plastic viscosity and apparent yield stress. Rheometer measurements were made at five different revolution speeds of 0.70, 0.55, 0.40, 0.25 and 0.10 rps. Measuring sequence started from the highest speed to the slowest speed (down-curve). Each speed continued 8 seconds. However, the torque values obtained only during the last 6 seconds were used in calculating the average torque value corresponding to that speed. Bingham model was constructed by adding a linear trendline to the torque vs. rotation speed data. The intersection point of the trend line with the torque axis corresponds to apparent yield stress (g) and the slope of the trendline is determined as torque plastic viscosity (h).

Evaluating structural breakdown. Structural breakdown of the mixtures were evaluated by the method recommended by Lapasin et al [18]. In this method, after five minutes of rest in the bowl of the rheometer, the mixture was subjected to a

constant rotational speed of 0.2 rps for 10 seconds. Then, after another five-minute rest period, the mixture was subjected to a constant rotational speed of 0.4 rps for 10 seconds. The same procedure was repeated for speeds of 0.6 and 0.8 rps. For each speed, the time-dependent change in torque was recorded, and then the initial torque (T_i) and equilibrium torque (T_e) values were determined (Fig.IIIa). Then, initial torque values and equilibrium torque values were plotted against rotational speeds (Fig.IIIb). Second order polynomial functions were fitted to the data (Fig.IIIb). The area between the initial torque curve and equilibrium curve, calculated by integration, was used to quantify the structural breakdown.

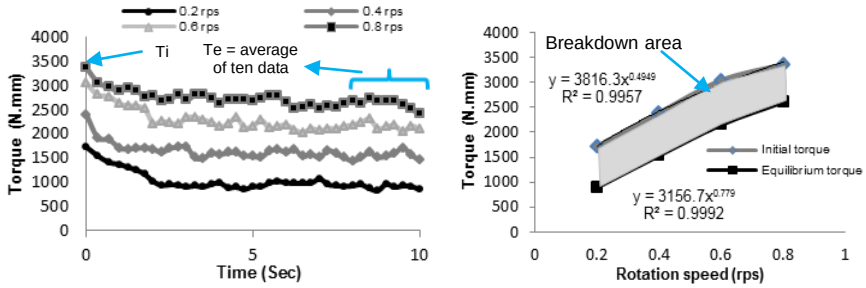

(a) (b)

Figure 3. Breakdown area method a) breakdown curves, b) area calculation

Results and Discussion

Compressive strength

Fig. IV present the 28-day compressive strength of SCC mixtures containing SF and MK at different replacement levels. It is clear from Fig. IV that both SF and MK significantly increased the compressive strength of mixtures. This behavior was more significant in SF blended mixtures. The highest compressive strength was observed in 12SF mixture whose compressive strength was approximately 46% greater than that of the control mixture. Addition of 12% SF was similar to that of 18% MK in terms of strength enhancement. The partial replacement of PC by 4% and 8% SF increased the compressive strength noticeably in comparison with MK blended mixtures for the same level of replacement. On the other hand, compressive strength development of MK incorporated mixtures was found to be more significant beyond 8% replacement of PC by MK. For example, the increase in strength of 18MK mixture was 44% while it was only 3% for 8% MK blended mixture. The contribution of SF to concrete strength was restricted beyond 8SF blended mixture.

T_{50} flow time

The T_{50} flow time after 0 and 50 min of mixing are presented in Fig.V. As shown in this Figure, incorporation of MK enhanced the cohesiveness of the mixtures due to the high surface area which resulted in higher T_{50} flow time after 0 and 50 min of rest. The binder containing 18% MK increased T_{50} flow times up to 3.4 and 6.9 seconds, after 0 and 50 min of rest respectively. On the other hand, T_{50} flow time reduced when SF was incorporated in the binder system at both time of rest. The mixture containing 12% SF, led to the greatest reduction in T_{50} flow time. The reason for this kind of treatment is probably due to smooth surfaces and spherical shape of SF particles providing additional lubrication between solid particles.

The flow time of almost all mixtures increased approximately 2 times compared to 0 min. Generally, increase in flow time of mixtures can be owing to the absorption of free mixing water of the mixtures by the admixtures, hydration reactions or the loss of the HRWR dispersing effect.

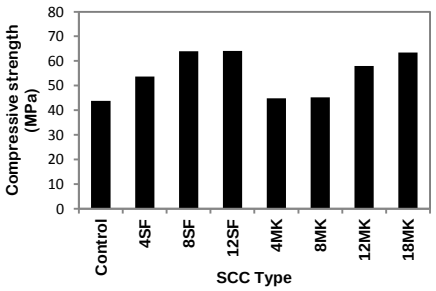

Figure 4. Compressive strength values

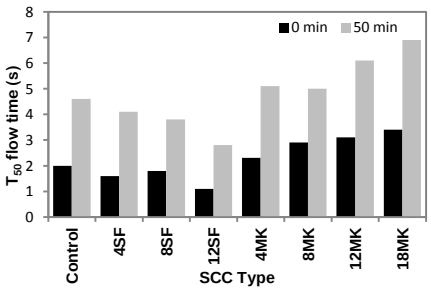

Figure 5. T_{50} flow time values

V-funnel flow time

V-funnel flow times are presented in Fig. VI. As seen in this figure these values ranged from 8 to 21 seconds at 0 min and 21 to 47 at 50 min. SF had a significant influence on V-funnel time. As the amount of SF was increased, reduction in flow time values was visible. 12% replacement of SF resulted in the greatest reduction (2 times less) in V-funnel flow time. On the other hand, adding MK increased flow time values in all of the mixtures. The binder containing 12% MK increased V-funnel times to 21 and 47 seconds, after 0 and 50 min of rest, respectively, while that of control mixture was only 16 and 33 seconds. Measurement of V-funnel time for 12% MK blended mixture was not possible after 50 min of rest.

Torque plastic viscosity (h)

The test results for torque plastic viscosity measurements are given in Fig. VII. As demonstrated in this figure, the partial replacement of PC by MK increased the h

values compared to control mixture. 18MK mixture, whose h value was approximately 17% greater than that of the control mixture, showed the highest increase in torque plastic viscosity. On the other hand, incorporation of SF reduced the h values. 12% replacement of SF with PC resulted in the greatest reduction (approximately 2.3 times less) in h. The amount of reduction was less as the percentage of SF was decreased. This behavior was contrary to the behaviors of MK: as replacement level of MK was increased, h values also increased.

Similar results were reported by the other investigations for MK bearing mixtures [11]. However, the data related with the effect of SF on the plastic viscosity of SCC is contradictory. Some of the researchers found that SF reduces the plastic viscosity (similar to the finding of this study) but the others reported that SF has not a significant effect on the viscosity of SCC [11,12,19].

The decrease in torque plastic viscosity due to the presence of SF in the SCC mixture can be attributed to the sphericity of SF particles that provides better packing than PC particles resulting in lower shear stress and lower plastic viscosity values [9,20]. Besides, owing to the difference between the specific gravity of PC and SF, mixtures containing SF had greater binder volumes causing reduction in h.

MK particles, owing to their high porosity, can absorb water and HRWR, leading to a reduction in inter-particle distance between solid particles and an increase in the level of attractive forces within solid particles that can be significant sake for obtaining high h values. Moreover, MK particles have elongated shape and irregular surface texture (Fig.IIc), and contrary to the lubrication effect of spherical shape and smooth surface (as was the case in SF), they can reduce workability of SCC mixtures thereby increase the h values.

As seen in Figure VII, mixtures containing MK showed significant increase in torque plastic viscosity values as a function of time. The highest increase was observed in 18MK mixture whose plastic viscosity was approximately 23% greater than the viscosity of this mixture at 0 min. The reason for this kind of treatment in comparison with other mixtures can be related to high porosity of MK particles.

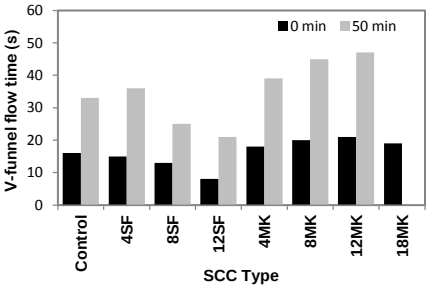

Figure 6. V-funnel flow time values

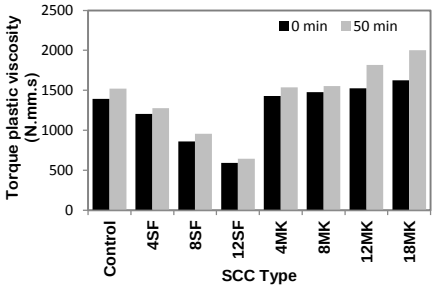

Figure 7. Torque plastic viscosity values

On the other hand, there was an enhancement between 7-11% in plastic viscosity values of SF blended and control mixtures after 50 min of a standstill condition. Increase in torque plastic viscosity with time in control and SF blended mixtures can be due to the rapid hydration of cement and interaction between SF particles with high fineness. Hydration of PC with time results in increase in the solid volume concentration, thus increasing the h values [21]. In addition, SF particles with high surface area can increase the number of interparticle links and attractive forces within solid particles with time, resulting in increase in the h values.

Apparent yield stress (g)

The results of apparent yield stress for a constant slump flow diameter of (650 mm) are given in Fig. VIII. It should be kept in mind that for constant slump flow, a wide range of difference in yield stress values is not expected in different mixtures [22]. However, the change of yield stress with utilization of SF and MK in SCC mixtures was remarkable in this study. SF blended mixtures had most significant influence on the values compared to MK blended mixtures. Highest increase was observed in 12SF mixture whose g values were approximately 3.5 times greater than of the control mixture. In addition, as shown in Fig. VIII, although 4% replacement by MK had significant effect on g values, a wide range of difference in yield stress values was not observed as percentage of MK increased. Obtaining a greater yield stress with utilization of SF and MK compared to control mixture can be related to higher surface area of these materials (Table I). Enhancing surface area increases the interaction between solid particles thereby increases g values.

Fig. VIII presents the change in g with time, as well. As seen, MK blended mixtures had significant influence on g values with passing time. The highest increase was observed in 12MK mixture whose yield stress was approximately 96% greater than that of this mixture at 0 min. The reason behind this behavior can be summarized as follow: High surface area and porosity of MK particles can absorb water and HRWR with passing time. Reduction of free water and HRWR of the mixtures can lead to higher degree of internal friction, to produce greater resistance to beginning of the flow, thereby resulting in an increase of shear stress necessary to maintain a steady-state condition.

In addition it should be noticed that in contrast to torque plastic viscosity values (change in plastic viscosity ranged between 5-23%), change in apparent yield stress with time was ranged from 43% to 96%. On the other wise it was found that in a standstill condition, passing of time had significant influence on enhancement of yield values while similar behavior was not obtained in plastic viscosity values.

Structural breakdown

In this study, two rest periods of 0-30 and 50-80 min were selected for determining the structural breakdown area. The breakdown area values are shown in Fig. IX. As seen, greater values were obtained for SCC mixtures made with MK when

compared to that of the control mixtures. The increase was more significant as the percentage of MK replacements were increased. The highest value, which was approximately 29% greater than that of the control mixture, was observed in 18MK mixture. In the case of mixtures containing SF, there was some irregularity in breakdown area values. On the other wise mixtures incorporating SF exhibit breakdown area values similar to that of the control mixture at 0-30 min.

Breakdown area calculations strongly depend on the factors that affect initial shear stress and equilibrium shear stress values determined during the tests [18]. Higher breakdown area values of the mixtures containing MK can be related to the difference in the volume of the binders. Owing to the difference between the specific gravity of cement and MK, mixtures containing MK had greater binder volumes. Higher paste volumes caused reductions in equilibrium torque values. Another reason for the increase in breakdown area values with higher percentage of MK can be attributed to the higher surface area and particle shape of MK particles: MK particles have higher surface area (Table I), increasing the number of inter-particle links and the level of attractive forces within solid particles, and they have elongated shape (Fig.IIc), increasing the internal friction. Therefore, they can increase initial torque values.

The results of change in breakdown area with time is presented in Fig IX. As shown in this Figure, mixtures containing SF and MK had significant influence in enhancement of breakdown area with passing time. The highest increase was observed in 12MK mixture whose breakdown area at 50-80 min time period was approximately 32% greater than that of the same mixture at 0-30 min. Similarly, 31% enhancement in breakdown area was observed in mixture containing %12 SF. Also a relatively high (%23) enhancement in breakdown area was observed in control mixture. This could be related to hydration of PC with time. As a result of PC hydration, concentration of solid particles and interparticle links responsible for flocculation increases with time, causing an increase in breakdown area values.

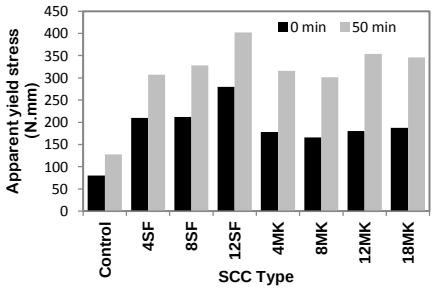

Figure 8. Apparent yield stress values

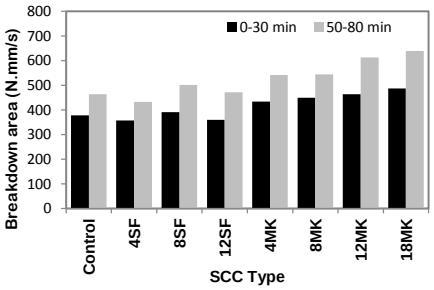

Figure 9. Breakdown area values

Increase in breakdown area values with time for the SF and MK blended mixtures can be related to the high fineness and nucleating effect of these SCM with time. In a cement-based system, thixotropy is due to colloidal flocculation or CSH bridges

between particles. Colloidal flocculation only affects thixotropy on a few seconds time scale and indeed CSH nucleation governs thixotropy behavior. High thixotropy values in the mixtures containing fine mineral admixtures is related to intercalated grains of these fine mineral admixtures with strong nucleating effect [23].

Conclusions

T_{50} flow time, V-funnel flow and torque plastic viscosity reduced when SF was incorporated in the binder system at both time of rest. As the amount of SF was increased, reduction was more significant. Contrary to the behavior of SF, MK blended mixtures resulted in higher T_{50}, V-funnel flow time and torque plastic viscosity values compared to control mixture. Adding of SF had a more significant effect on the mixture viscosity compared to incorporation of MK at the same level of replacement. Besides, mixtures containing MK showed significant increase in torque plastic viscosity values as a function of time. The yield stress values of SF and MK bearing mixtures were higher than that of the control mixtures. But MK blended mixtures had significant influence on g values with passing time. Greater breakdown area values were obtained for SCC mixtures made with MK when compared to that of the control mixtures. Contrary to the behavior of SF, mixtures incorporating SF exhibit breakdown area values similar to that of the control mixture at 0-30 min. Also, mixtures containing SF and MK had significant influence in enhancement of breakdown area with passing time and after a resting time of 50 min., apparent yield stress and breakdown area values increased significantly with time while torque plastic viscosity values changed only in a limited range.

References

[1] Saleh Ahari, R. (2014), PhD Thesis, *Ege University, İzmir*, 215, p. [in Turkish].
[2] Saleh Ahari, R., Erdem, T.K. And Ramyar, K. (2015), *Cem. Concr. Compos*., vol. 59, p. 26.
[3] Saleh Ahari, R., Erdem, T.K. And Ramyar, K. (2015), *Constr. Build. Mater*.,vol. 75, p. 89.
[4] Erdem, T.K., Khayat, K.H. and Yahia, A. (2009), *ACI Mater. J*., vol. 106, p. 154.
[5] Khayat, K.H. and Assaad, J. (2006), *ACI Mater. J*., vol. 103, n. 3, p. 186.
[6] Assaad, J. and Khayat, K.H. (2004), *ACI Mater. J*., vol. 101, n. 5, p. 400.
[7] Assaad, J. and Khayat, K.H. (2005), *ACI Mater. J*., vol. 102, n. 3, p. 145.
[8] Assaad, J. and Khayat, K.H. (2006), *ACI Mater. J*., vol. 103, n. 3, p. 186.
[9] Tattersall, G.H. and Banfill, P.F.G. (1983), *Pitman Adv. Pub. Prog.*, London.
[10] Saleh Ahari, R., Erdem, T.K. And Ramyar, K. (2015), *Constr. Build. Mater*., vol. 79, p. 326.

[11] Hassan, A., Lachemi, M. and Hossain, K. (2012), *ACI Mater. J*, vol.109, p. 657.
[12] Assaad, J. (2004), PhD Thesis, *University of Sherbrooke, Canada*.
[13] Ferraris, C.F., Obla, K.H. and Hill, R. (2001), *Cem. Concr. Res*., vol. 31, p. 245.
[14] Hassan, A.A., Lachemi, M. and Hossain, K., (2012), *Cem. Concr. Compos*., vol. 34, p. 801.
[15] Mouret, M. and Cyr, M. (2003) In: *Superplasticizers and Other Chemical Admixtures in Concrete*, Proceedings of 7 th CANMET/ACI Inter. Conference,, vol. I, pp. 241–255, Malhotra VM,. (Ed.), Farmington Hills.
[16] Rahman, M.K., Baluch, M.H. and Malik, M.A. (2014), *Constr. Build. Mater*., vol. 50, p. 710.
[17] Ferron, R.P., Gregori, A., Sun, Z. and Shah, S.P. (2007), *ACI Mater. J*., vol. 104, n. 3, p. 242.
[18] Lapasin, R., Papo, A. and Rajgelj, S. (1983), *Cem. Concr. Res*., vol. 3, p. 349.
[19] Wallevik, O.H. and Wallevik, J.E. (2011),*Cem. Concr. Res*., vol. 41, p. 1279.
[20] Bentz, D.P., Ferraris, C.F., Galler, M.A., Hansen, A.S. and Guynn, J.M. (2012), *Cem. Concr. Res*., vol. 42, p. 404.
[21] ACI, Committee 237R-07. (2007), p 30.
[22] Wallevik, J.E. (2006), *Cem. Concr. Res*., vol. 36, p. 1214.
[23] Roussel, N., Ovarlez, G., Garrault, S. and Brumaud, C. (2012), *Cem. Concr. Res*., vol. 42, p. 148.

Evaluation of Quarry Powders as Viscosity-Modifying Material in Cement Mixtures

Rudiele Aparecida Schankoski[1], Ronaldo Pilar[1], Luiz Roberto Prudêncio Jr.[1] and Raissa Douglas Ferron[2]

[1]Federal University of Santa Catarina – Universidade Federal de Santa Catarina – UFSC – Brazil
[2]The University of Texas at Austin - USA

Abstract In quarries, considerable amounts of powders are produced as by-products of stone crushers. They are collected and are a problem from the aspects of disposal, environmental pollution and health hazards. However, these fines could be utilized as viscosity modifying material in self-compacting concrete (SCC). This paper evaluates quarry powders of limestone, gneissic and dibasic origin. In the study has been used powders of different particle size distributions. Results from rheological measurements on pastes mixes incorporation limestone, gneiss and dibasic dust quarry were compared. As well as, it was used the focused beam reflectance measurement technique to evaluate the particle size evolution and identify the flocculation mechanisms in the mixture. It was found that the gneiss and diabase quarry dusts, could be used successfully in the production of SCC, because the mixture's behavior was similar to limestone filler mixtures. However, due to its shape and particle size distribution, mixes with this quarry dusts can require a higher dosage of superplasticizer to achieve similar flow properties that mixtures with limestone filler.

Keywords: *Quarry dust, Gneiss, Diabase, Limestone, Powder, SCC.*

Introduction

The quarrying for marketing aggregates used in construction produces a significant amount of environmental waste in the form of fine (quarry dust powder) material, produced in aggregate beneficiation process, especially in the manufactured fine aggregate.

In most cases, the quarries are little or no destination for these dusts, and storage of these by-product dusts a serious environmental concern. In normal concrete, the introduction of quarry dust to mixes is limited due to its high fineness. However, for SCC is necessary high content of powder materials. Limestone powder has been one of the traditional materials used in self-compacting concrete for controlling the segregation potential and deformability [1]. However, due to high demand of limestone for cement manufacturing, the use of alternative fine materials, such as quarry dust would be ideal for SCC applications.

Fillers origin of basalt, granite and marble have been tested by several authors in pastes, mortars and concretes, mainly SCC, that reporting advantages with using these alternatives materials [1-6]. Other rock formations have few or no studies about their performance as addition in cement mixtures. The objective of the research presented in this manuscript was to evaluate the use of quarry dust of diabasic origin and gneissic origin as replacer limestone filer, used as viscosity modifying material. The article at hand focuses on the rheological properties and the microstructure of fresh cement pastes, using the focused beam reflectance measurement (FBRM). In addition, the influence of particles characteristics was also taken into consideration.

Experimental Study

Materials

A commercially available Portland cement, conforming to ASTM C150 [7] Type III cement and Type F polycarboxylate superplasticizer (SP), conforming to ASTM C494 [8] were used in all of the mixtures. Three different fillers were evaluated in this work. One filler as of limestone origin (represented as L), and two industrial wastes fillers: a quarry dust powder of diabase origin (represented as D) and a quarry dust powder of gneiss origin (represented as G). The specific gravity of the fillers were 2.80, 2.82 and 2.77, for C, D and G, respectively.

The fillers were obtained directly from quarries and the average size particle diameters of the as-collected powder (represented as L0, D0, and G0 in Table I) between 33 and 38 μm. To evaluate the influence of the particle size each type of filler was ground to achieve average particle sizes equal to 16 μm to 25 μm, which is similar to average particle size ranges for typical cement. A ball mill was used to reduce the size of the particles. Depending on the hardness of the filler, more or less time was required to obtain the desired particle size.

Particle analysis

Each type of filler was examined by using scanning electron microscopy (SEM – secondary electron images) to characterize the shape of the particles [9]. These

images were analyzed using the program Image Tool Version 3.0 (IT3) software program. To characterize the particles, it was used the equation called aspect ratio (length and width ratio) [10].

Table I: Specifications of materials

Filler	Denomination	D 50 (μm)
Cement	C0: no grinding	20.00
Limestone 0	L0: no grinding	38.09
Limestone 1	L1: size 1	25.22
Limestone 2	L2: size 2	16.45
Diabase 0	D0: no grinding	33.01
Diabase 1	D1: size 1	24.22
Diabase 2	D2: size 2	16.12
Gneiss 0	G0: no grinding	34.15
Gneiss 1	G1: size 1	25.09
Gneiss 2	G2: size 2	16.56

Mix proportions and mixing preparation

The proportion of the pastes are displayed in Table II. All replacements of fillers were made on a volume basis. The demand of superplasticizer varied depending on the inert powder used and was defined for each mixture, with target mini-slump diameter of 110 ± 5 mm. The objective of this procedure was to verify if the powders would produce pastes with similar rheological properties if only the admixture content was adjusted. Each mineralogical type of filler has been studied in three different particle sizes, and using the same water/powder ratio in volume (1.0).

Each suspension was prepared following ASTM 1738 [11]. The addition of the admixture occurred during the rest period. The mini-slump flow test was performed immediately after preparing the pastes. At least two independent mixtures were conducted for each filler used to check the repeatability of results. Averaged values are provided for the tests.

Rheological Tests

Rheological tests were conducted with a commercially available rotational rheometer, Anton Paar MCR 301. It was configured with a Vane geometry (four blades). The routine followed the steps: Pre-shear of 50 s^{-1} during 60 s, followed by a 30 s rest period. After that, the flow curve test was performed by increasing and decreasing (0 to 50 to 0 s^{-1}) the shear in 9 consecutives steps of 30 s each one. However, the analyses of results just will use the rheology data for decreasing

shear rate. The Bingham model was used to determine the parameters rheology (Eqn. 1).

$$\tau = \tau_0 + \eta \times \gamma \qquad \textbf{(1)}$$

Where, τ: Shear Stress (Pa); τ_0: Yield Stress (Pa); γ: Shear rate (1/s); n: Viscosity (Pa.s).

Table II: Mixture proportions (by volume)

Paste	Cement (%)	Filler (%)	Water/Powder	Admixture (% powder by volume)
C0	100	0	1.0	0.140
L0	60	40	1.0	0.130
D0	60	40	1.0	0.045
G0	60	40	1.0	0.277
L1	60	40	1.0	0.159
D1	60	40	1.0	0.276
G1	60	40	1.0	0.279
L2	60	40	1.0	0.167
D2	60	40	1.0	0.286
G2	60	40	1.0	0.262

FBRM

The FBRM, focused beam reflectante measurement, was used to verify if the presence of different fillers altered the flocculation process of the paste. It was important to analyze the influence of fillers in the cement paste microstructure [12]. After preparing the pastes, 50 ml of the paste was placed into the container, and subjected to agitation speeds in 2 consecutives steps, each one with duration of 30 min: 40 rpm, followed 400 rpm. The laser beams scans at a fixed velocity (2 m/s).

Results

Particle Analyses Results

Figure 17 shows an example of SEM images and the aspect ratio. Depending on the degree of grinding, the particle aspect ratio was increased (L1 and D1). Aspect ratio is close to 1 for equidimensional or spherical aggregates, and have larger values for elongates and flat aggregates. Limestone particles presented the nearer values of 1. These results were expected, since very authors cite the form of particles as a disadvantage of quarry dust powder of other mineralogical origins [1, 9, 13, 14].

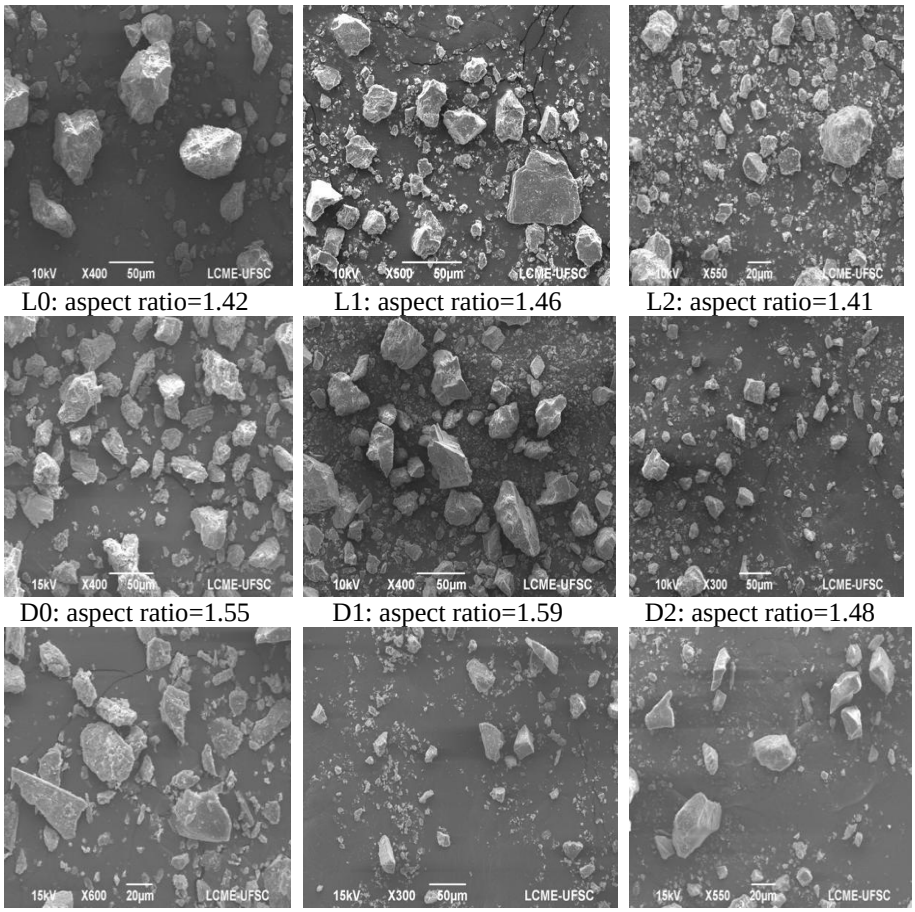

Figure 17: Images obtained by SEM

Rheological Tests Results

The flow curves can be seen in **Error! Reference source not found.**, 3 and . It is noticed that, although all pastes have the same mini-slump spread, pastes containing cement only had high yield stress. The other pastes containing fillers showed similar behavior, being very close to the pastes containing limestone. Considering all the rheology parameters, it is clear that the presence of mineral additions in cement pastes lead to better performances in fresh properties, compared to pastes containing cement only. This is in line with that reported in the literature in relation to the presence of other types of additions [15].

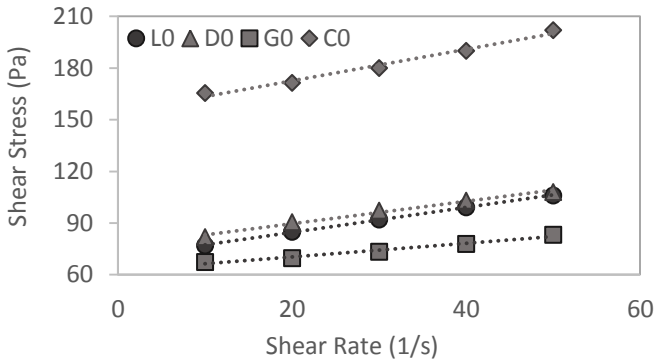

Figure 18: Flow curves: pastes reference and pastes contend filers no grinding

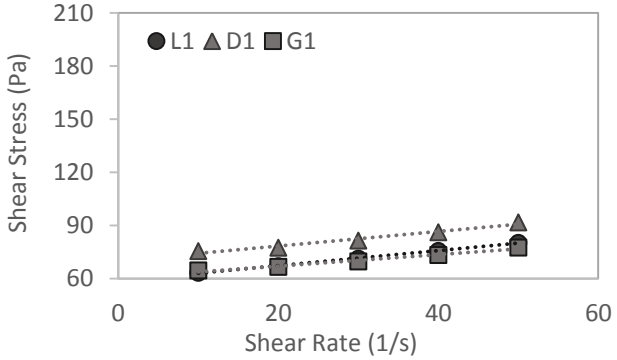

Figure 19: Flow curves: pastes contend fillers with $D_{50} \approx$ 24-25µm

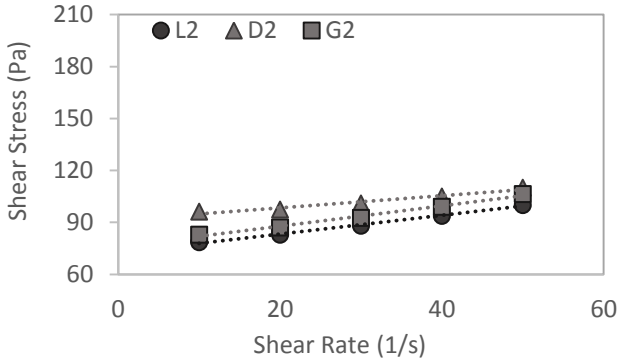

Figure 20: Flow curves: pastes contend fillers with D50 ≈16µm

The milling process of particles affected the yield stress of pastes. Pastes containing no grinding powders showed yield stress of 59, 70 and 62 Pa, for L0, D0 and G0 respectively, while pastes containing L2, D2 and G2 showed values of 72, 91 and 76 Pa, respectively. The milling process had adverse effect on the viscosity of the pastes containing limestone and diabase, with 0.63 and 0.54 Pa.s for L0 and L2; and 0.65 and 0.35 Pa.s for D0 and D2, respectively. Pastes containing gneiss, the viscosity increased from 0.33 when used G0 to 0.59 Pa.s with G2. These results indicate that the aspect ratio has no significant influence on the rheology, since the use of particles having smaller aspect ratio did not decreased the yield stress, this as well not resulted in the use lower amount of additive for the same slump-flow (see Table 4). This shows that the particle size affects the rheology, but not its shape.

Comparing the fillers with each other, it can be seen that the viscosity of the pastes containing same size particles filers were very similar (L1, D1 and G1 showed viscosity of 0.42, 0.41 and 0.40 Pa.s, respectively). The yield stress of the pastes containing limestone were lower than the values of the pastes containing the other kinds of powders but very close to the results of pastes with gneiss.

FBRM Results

Figure 21, 6 and 7 show the counts number of particle evolution of pastes. Although the mean chord length is not showing in this paper, it presented the reverse behavior that Counts per second.

The kinetics of aggregation dominates at low stirring intensity and reflects the phenomena of floc formation, when individual particles coming together to form a larger one [16]. When N=400 rpm the disaggregation process dominates, and larger flocs are broken into smaller flocs due to the high stirring intensity decreasing the aggregation efficiency [16,17].

It can be seen that regardless of the particle size (D_{50}), pastes containing filer gneissic had a higher counts, compared with other pastes, i.e., the particles of gneiss show less flocculation. Furthermore, gneiss particles have higher aspect ratio. The shape of the particles may have contributed to keeping the grains less flocculated.

The samples prepared with limestone filler displayed the fewest number of particle counts in pastes with the same D50. This suggests that its fresh state microstructure is in a condition that is more agglomerated than the samples prepared with the other quarry dusts. Pastes containing fillers gneissic had the lowest flocculation and lower viscosities. Pastes containing filler limestone showed large flocculation and higher viscosities. This is consistent with the Yim et al. [18]. They observed an

increase in the viscosity of a cement paste as its packing density increased. Han and Ferron (2015) observed that the mixtures with larger chord length size and smaller number of particle counts also had higher viscosities in rheology testing.

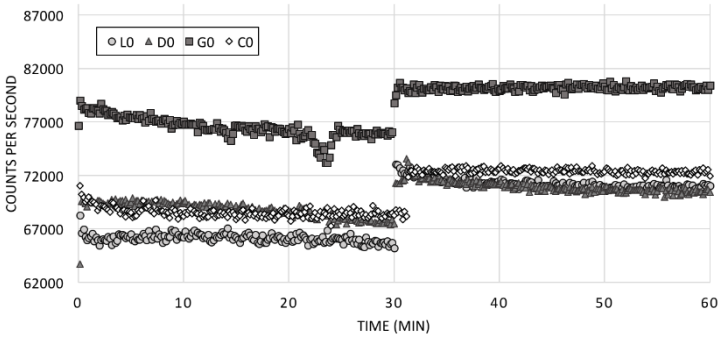

Figure 21: Counts per second: pastes with fines no grinding

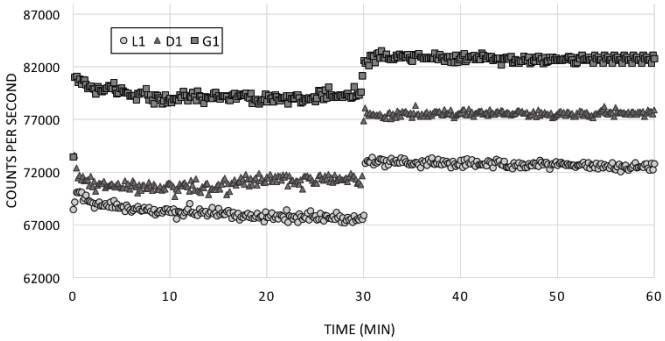

Figure 22: Counts per second: pastes contend fillers with D50 ≈ 24-25µm

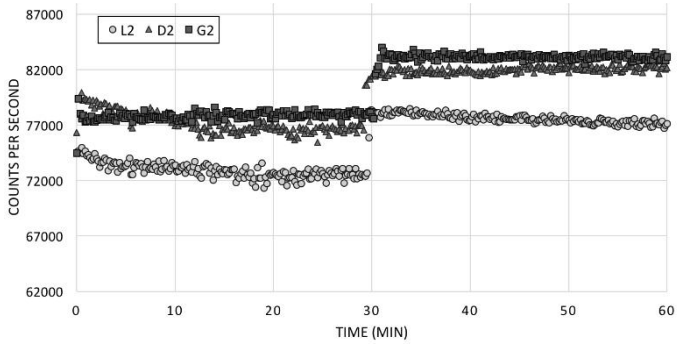

Figure 23: Counts per second: pastes contend fillers with D50 ≈ 16 µm

Conclusions

Based on the data developed in this study, the following conclusions could be drawn.

- All pastes containing only cement had the highest yield stress. Therefore, it is recommended the addition of mineral powders to improve fresh cement mixtures when the same fluidity is fixed.

- The aspect ratio of the particles influence the rheological properties of mixtures made with them. Gneiss quarry dust performed better after the milling process.

- The results of FBRM showed good correlation with the rheology results. Mixtures with larger chord length size and smaller number of particle counts (counts per second) also had higher viscosities in rheology testing.

- Cement pastes containing powders quarry (diabase and gneiss) are able to achieve the same rheological properties of the pastes containing limestone, although they may demand higher amount of superplasticizer to achieve similar rheological properties. Thus, the use of these quarry dusts can be result in a significant cost saving in regions where limestone filler is not available and is an effective use of a waste environmental.

Acknowledgements

CAPES: Coordenação de Aperfeiçoamento de Pessoal de Nível Superior. Ministério da Educação – Brazil.
99999.008308/2014-04 and 99999.008307/2014-08
LCME: Laboratório Central de Microscopia Eletrônica – UFSC.
Department of Civil Architectural and Environmental Engineering, The University of Texas at Austin.
Itambé Cements

References

[1] HO, D.W.S; SHEINN, A.M.M; NG, C.C; TAM, C.T. The use of quarry dust for SCC applications, Cem Conc Res, 32, I 4, 2002, Pg 505-511.
[2] FELEKOĞLU, B. Effects of PSD and surface morphology of micro-aggregates on admixture requirement and mechanical performance of micro-concrete, Cem Conc Comp, 29, I 6, 2007, Pg 481-489.

[3] BELAIDI, A.S.E.; AZZOUZ, L. ; KADRI, E. ; KENAI, S. Effect of natural pozzolana and marble powder on the properties of self-compacting concrete, Construction and Building Materials, 31, 2012, Pages 251-257
[4] DEHWAH, H.A.F. Mechanical properties of self-compacting concrete incorporating quarry dust powder, silica fume or fly ash, Construction and Building Materials, 26, Issue 1, Pg 547-551, 2012.
[5] ALIABDO,A.; ELMOATY,A.; AUDA, E. Re-use of waste marble dust in the production of cement and concrete, Const Build Mat, 50, 2014, Pages 28-41
[6] TENNICH, M.; KALLEL, A.; OUEZDOU, M.B. Incorporation of fillers from marble and tile wastes in the composition of self-compacting concretes, Construction and Building Materials, 91, 2015, Pages 65
[7] ASTM International. ASTM C150, Standard Specification for Portland Cement. ASTM International, West Conshohocken, PA (2012).
[8] ASTM International. ASTM C494, Standard Specification for Chemical Admixtures for Concrete. ASTM International, West Conshohocken, PA (2015).
[9] FELEKOGLU,B. A new approach to the characterization of particle shape and surface properties of powders employed in concrete industry, Construction and Building Materials, 23, I 2, Pg 1154-1162, 2009.
[10] KUO, C.-Y.; FREEMAN, R., "Imaging Indices for Quantifi- cation of Shape, Angularity, and Surface Texture of Aggregates," Transp Research Record 1721, Journal of the Transportation Research Board, Washington, D.C., 2000, pp. 57–65.
[11] ASTM International. ASTM C1738, Standard Practice for High-Shear Mixing of Hydraulic Cement Pastes. ASTM International, West Conshohocken, PA (2014).
[12] HAN, D.; FERRON, R.D. Effect of mixing method on microstructure and rheology of cement paste, Const Build Mat, 93, 2015, Pages 278-288,
[13] STEWART J.; NORVELL, J.; JUENGER, M.; FOWLER, D.W. ICAR Report 107-1 ICAR 107: Characterizing minus N° 200 fine aggregate for performance in concrete. International Center for Aggregates Research. UT. Austin, 2003.
[14] RAMOS, T.; MATOS, A.M.; SCHMIDT, B.; RIO, J.; SOUSA-COUTINHO, J. Granitic quarry sludge waste in mortar: Effect on strength and durability, Construction and Building Materials, 47, 2013, Pages 1001-1009
[15] FERRARIS, C.F.; OBLA, K.H.; HILL, R. The influence of mineral admixtures on the rheology of cement paste and concrete, Cem Conc Res, 31, Pg 245-255, 2001.
[16] FERRON, R.; SHAH, S.; FUENTE, E.; NEGRO, C. Aggregation and breakage kinetics of fresh cement paste. Cem Concr Res, 50, 2013, pp. 1–10
[17] NEGRO, C.; SÁNCHEZ, L.M.; FUENTE, E.; BLANCO, A.; TIJERO, J. Polyacrylamide induced flocculation of a cement suspension, Chemical Engineering Science, 61, I 8, 2006, Pages 2522-2532
[18] YIM, H.J.; KIM, J.H.; SHAH, S.P. Cement particle flocculation and breakage monitoring under Couette flow. Cem Concr Res, 53, 2013, pp. 36–43

Self-Leveling Paste Systems (SLPs) using Blends of CAC-OPC at Variable Mixing Water Temperature

Syed Ali Rizwan[1], Sami Ullah Khan Bangash[2], Bharat Kumar[2] and Thomas A Bier[3]

1. Professor of Civil Engineering and HoD Structural Engineering Department, NUST Institute of Civil Engineering (NICE), NUST H-12, Islamabad. Email: syedalirizwan@nice.nust.edu.pk
2. Graduate Student, NICE, NUST H-12, Islamabad. Email: sukbangash@gmail.com, lohia.bharat@gmail.com
3.Professor and Chair of Construction Materials Technology, IKGB, TU Freiberg, Germany. Email: thomas.bier@ikgb.tu-freiberg.de

Abstract Binary and ternary blends of self leveling paste systems(SLPs) containing blended CAC-OPC cement are used to make or to repair concrete systems in applications like Self-leveling underlayments (SLUs), general concrete repairs and repairs to systems resembling crater like situations arising due to some terrorist activity or aerial attacking on transportation systems in short open times. Such field placements and repairs are generally carried out where temperature and relative humidity control is not possible. Such situation was simulated in laboratory by using variable mixing water temperature (MWT) of 5°C, 23°C and 35°C. The formulations were made at respective Vicat water demands. At elevated MWT, binary blends of SLPs had higher super plasticizer dosage for the target flow. Vicat setting times of few minutes were obtained in some studied SLPs when either MWT was higher for single cement binder or when CAC content in OPC was around 15% of blended powder mass. No accelerators were used. Compressive strength of self-leveling paste systems using binary binders at 28 day's age was higher at low MWT. Though water demands of different formulations were different but flow was constant and it clearly showed the effect of MWT as responses in both fresh and hardened state were different. It may be concluded that 20-23°C seems to be the optimum MWT range for making OPC rich binary blends of SLP systems for field placements and repairs requiring very short open time.

Keywords: *self-leveling paste systems, binary blends and optimum mixing water temperature.*

Introduction

Very little literature is available on the effect of mixing water temperature on the response of concrete in fresh and hardened states. Self-leveling paste systems using OPC-CAC blends find their application in pavement repair, rapid hardening underlayments and special concrete placements. The studied systems were in range 1 of Fig 1 and can be used in field applications where fast setting is required either in masonry or concrete [1]. Blends of CAC and OPC when mixed with water exhibit different setting behavior and strength development rate than either of these when used separately. In an earlier side investigation by the authors, it became known that increase in CAC replacement of OPC shortens the setting time considerably [2]. It also obtains measurable strength values in less than an hour with lower later age strength (strength degradation) unless formulations are adjusted to counter strength degradation [3, 4]. In CAC-OPC blends when OPC is the main constituent, the occurrence of rapid setting and hardening of paste is mainly due to the rapid formation of early hydrates and especially ettringite in the presence of gypsum in OPC and CAC powders [2, 3]. The hydration of calcium silicates in such cases has little influence on the setting process, but contributes to strength development after setting. In such mixes, all phases formed in the hydration of pure OPC and CAC are available. In addition to that, straetlingite (C_2ASH_8) may also be formed throughout the hydration process [2].

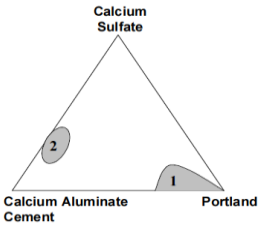

Figure 24. CAC-OPC-Gypsum Systems [1]

Research Significance:

The effect of mixing water temperature on early and late age properties of self-levelling cementitious systems has hardly been reported and this formed the basis of this investigation. This research reports results of OPC-CAC based SLPs for field applications with shorter open time where pre-packaged bags are prefered.

Experimental

Materials

Local OPC 42.5R , calcium aluminate cement ISTRA-40 and class F fly ash (FA) were used in addition to PCE based super-plasticizer Melflux 2651F to obtain flow target of 36±1 cm in a trial process, using Hagerman's cone [5, 6]. Physical and chemical properties of powders are shown in Table 1.

Table I. Physical and Chemical properties of powders used

Oxides	**OPC**	**CAC**	**FA**
SiO_2	19.61	2.58	54.94
Na_20	1.48	--	--
MgO	1.72	0.72	1.03
Al_2O_3	4.89	40.03	27.18
CaO	63.07	37.31	2.33
K_2O	0.85	0.22	2.02
Fe_2O_3	2.62	15.93	9.26
SO_3	2.92	--	0.32
Particle size D_{50} (µm)	12.01	4.88	7.12

Note: -- = not measured, OPC= Ordinary Portland cement, CAC = calcium aluminate Cement, FA= Fly-Ash

Particle Size distribution of powders used:

Laser Particle Analyser was used to obtain particle size distribution of powders used in SLPs. Ethanol was used as a dispersing agent.

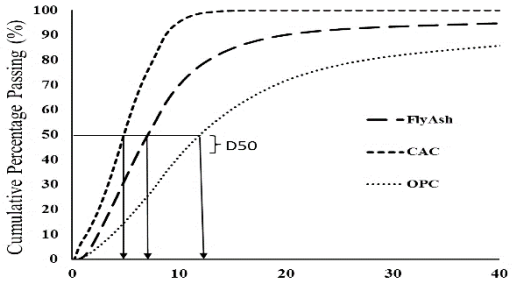

Figure 2. Particle Size Distribution with 50% passing Diameter marked for each raw material

Mix Proportions

A total of fifteen SLPs' at mixing water temperatures of 5^{O}C, 23^{O}C and 35^{O}C were studied. The formulation details are given Table 2. The letters A through E represent the description of formulation and the successive number denotes mixing

water temperature in Celsius in the column labeled as Formulation ID. CAC and FA percentages are in terms of weight of OPC replaced. Water demand was based on standard consistency of cement and SP dosage was calculated for target flow of (36±1) cm using Hagerman Cone. Water demand and SP demand are taken as percentage of total binder mass plus any secondary raw material if any. E35 formulation showed very fast setting so its flow and strength tests are not reported.

Table II. Description of Mix Proportions of different SLPs

Formulation ID	OPC (%)	CAC (%)	FA (%)	Water Demand (%)	SP demand (%)
A5	-	100	-	21	0.05
A23	-	100	-	21.4	0.06
A35	-	100	-	22	0.07
B5	100	-	-	26.3	0.205
B23	100	-	-	26.5	0.22
B35	100	-	-	27	0.225
C5	90	10	-	26.4	0.233
C23	90	10	-	26.8	0.27
C35	90	10	-	30.5	0.426
D5	85	15	-	26	0.214
D23	85	15	-	27.8	0.28
D35	85	15	-	31	0.525
E5	75	15	10	25.7	0.21
E23	75	15	10	28.5	0.282
E35	75	15	10	30.5	> 1

Mixing Regime

Self-leveling paste system (SLPs) mixtures were prepared by manually mixing powder materials (OPC, CAC, FA) and powdered SP in dry state in a plastic jar for 2 minutes. Then water was put in the Hobart bowl at specific temperature and then blended powder was fed in the bowl. Slow mixing for 15sec (145rpm) was done and then interior of Hobart mixer was cleaned. Thereafter, fast mixing (285 rpm) was done for 2minutes and 45seconds. The total mixing time in Hobart mixer was 3 minutes.

Curing and Testing

Vicat water demand is reported in terms of total powder content of formulations at prescribed mixing water temperatures of 5^{O}C, 23^{O}C and 35°C as per EN 196-3 followed by determination of Vicat setting times. EN 196-1 Standard was followed to cast, cure and perform strength tests of SLP formulations in SSD condition at 1,

and 28 day age at loading rate of 0.1 MPa/sec. Calorimetry was performed using F-Cal 8000 field Calorimeter and shrinkage was performed using modified Schwindrinne shrinkage channel measuring 4x6x25 cm^3. Specimens were cast at laboratory temperature and relative humidity in the ranges of 17-25°C and 35-55% respectively. These were covered with plastic sheet for initial 24 hours and were demolded thereafter and were immersed in water at 20°C till testing age.

Results

Water Demand

Figure 3 shows the effect of mixing water temperature on water demands of SLP formulations.

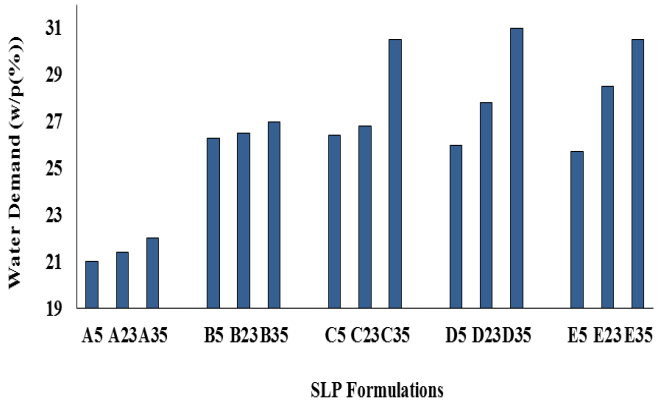

Figure 3. Effect of mixing water temperature on Water Demand of SLP formulations

Flow

Figure 4 shows SP demand of SLP systems for target flow of 36 ±1 cm on Hagerman Cone.

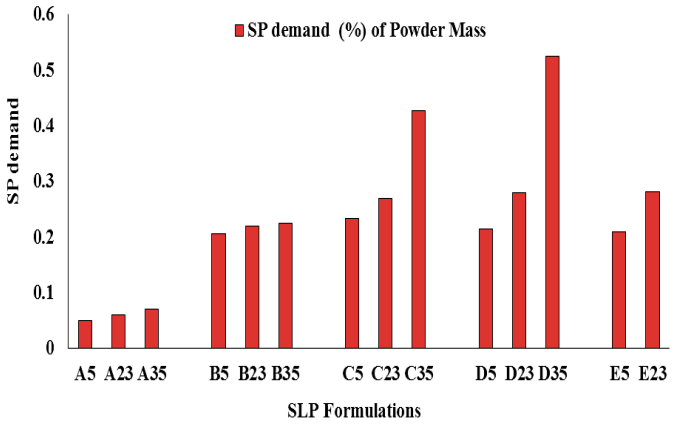

Figure4. Flow times and SP demand of SLP systems

Setting Times

Figure 5 shows Vicat setting times of SLP systems. It should be remembered that the setting times shown are at water demands of the respective formulations at the prescribed mixing water temperatures (5^{O}C, 23^{O}C and 35^{O}C).

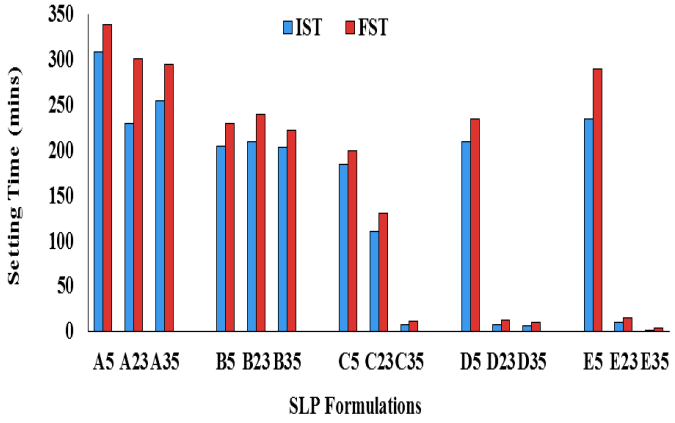

Figure 5. Effect of Mixing water temperature on initial and final setting times

Compressive Strengths

Figure 6 shows the compressive strengths of SLPS at two ages. Strengths shown are at respective water demands of the formulations made at three mixing water temperatures (5°C, 23°C and 35°C).

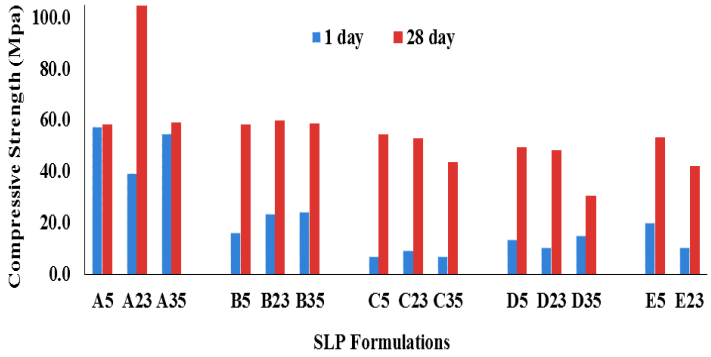

Figure 6. Effect of mixing water temperature on Compressive Strengths of SLP formulations

Calorimetry of SLPs at Three Mixing Water Temperatures

Calorimetry of SLPs was performed on semi-adiabatic calorimeter FCAL 8000 and temperature log details plotted for 24 hours as shown in Fig 7. Here, formulation C is studies for three temperature ranges and B23 – neat OPC based SLP serves as control mix.

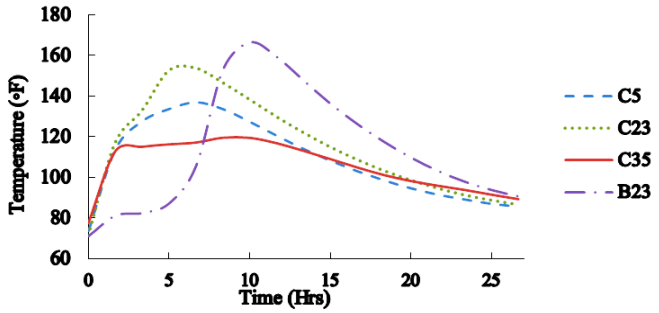

Figure 7. Effect of mixing water temperature on calorimetric response of SLP formulations

Linear Shrinkage

Early linear shrinkage measurements were performed for first twenty four hours using modified Schwindrinne shrinkage channel measuring 4x6x25 cm – under covered conditions. Formulation C was compared at three MWTs with B23 serving as control.

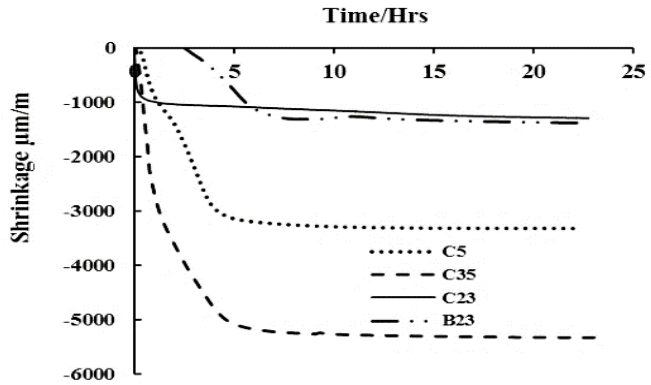

Figure 8. Effect of mixing water temperature on shrinkage of SLP formulations

Discussion

All the formulations were determined at three different mixing water temperatures. Generally water demands increased with increase in mixing water temperature in all the formulations investigated. This effect is more pronounced in C, D and E formulations : These formulations contain multiple binders with CAC and increased mixing water temperature, both acting as accelerator for OPC component, resulting in increased hydration kinetics and faster precipitation of hydration products [7, 8]. At lower temperatures, fly- ash addition to ternary blends further reduces the water demand of SLP system and also delays the setting time – (see Fig 5, sample E23). This is in line with literature which suggests that in general, addition of fly-ash reduces water demand, delays setting time and reduces early-age shrinkage [9]. It has been established in literature [9] that the optimum mixing water content of any SLPs is around the respective water demand. Setting times and SP dosages also showed predictable trends for binary SLPs : higher the temperature, more pronounced the rapid setting behavior and hence higher SP dosages and rapid setting times – see Fig 5, Formulation ID C-D at 35°C. However C and D at 5°C showed unusual trend because with increase in CAC replacement %, setting times extended and water demands/ SP dosages reduced. This suggests that at cold temperatures, CAC particles tend to enhance workability and slow down the hydration process. SP dosages for A5, A23 and A35 are also much lower compared to binary SLPs suggesting that CAC particles tend to flow well upon agitation.

28 day compressive strengths for binary SLPs was adversely affected by increasing temperature beyond 23^{O}C and also by increasing CAC replacement % - see Fig 6. Later age strengths for blends were found to be significantly less than control formulations A and B (100 % CAC and OPC SLPs). This trend has been extensively reported in literature [10]. In blended cement formulations, optimum results were at 23^{O}C beyond which later age strength decreased.
Formulation C showed greater heat released at 23^{O}C mixing water temperature while at 5^{O}C, early hydration of this formulationis rather slow and at 23^{O}C mixing water temperature, the hydration kinetics of both OPC and CAC components increased. Increasing the mixing water temperature futher to 35^{O}C, peak heat released reduced instead of increasing as most of the the hydration of aluminate phases of both cements might have taken place during mixing stage and during initialization of calorimetric procedures. The temperature generated might well have dissipated in such early processes. Another possibility is that rapid formation of hydration products at 35^{O}C around anhydrous cement grains leads to delay in Silicate Phase hydration as well as non-uniform distribution of hydrates [11]. Bulk of unreacted exothermic silicate phases might be depriving the hydration process of substantial energy release. Its also likely that rapid heat released in early stages leads to substantial water evaporation which brings cooling effect. Or it could be a combination of all these factors.

During early shrinkage, many mechanisms are operative simultaneously and the net strain at any time is the algebraic summation of strains due to these parallel operative mechanisms. It is difficult to understand early shrinkage of multibinder complex cementitious systems. Early shrinkage test of formulation C was performed at three different temperatures. At 23^{O}C, it apears that optimum internal growth of expansive hydrates seems to reduce early shrinkage.

Concluding Remarks

The results show that MWT plays a crucial role in defining the fresh and hardened characteristics of SLP systems using binary blends of CAC-OPC. It is possible to undertake special repairs using blends of CAC-OPC at variable MWTs without using any accelerator in situations where open time is very short. It can be concluded that CAC replacement of around 10% and MWT around 23^{O}C are ideal for achieving fast setting times and good later age strengths.

Acknowledgements

The authors are grateful to DAAD for providing F-Cal 8000 calorimeter and modified Schwindrine shrinkage channel apparatus to NICE/NUST under International research project " CO_2 Reduced Concrete using local secondary Raw Materials"- Kennziffer Number 54385351. Authors also express their gratitude to NUST graduate students Muhammad Ossama Waseem and Muhammad Maab Ali for providing assistance in experimental testing.

References

[1] Lambert, S. (2005),"Durability of ternary binders based on portland cement, calcium aluminate cement and calcium sulphate", pp 1, PhD Thesis, University de Lyon, France.
[2] Kırca, Ö. (2006), "Temperature effect on CAC cement based composite binders. p.25. Thesis: Middle East Technical University, Ankara, Turkey.
[3]:Hewlett, Peter.C. (2004 edition), Lea's Chemistry of Cement and Concrete. pp 734-739. Elsevier Publications.
[4] Xu, L. andWang, P. (August 2014), "Effect of CAC variety on the hydration of portland Cement in blended systems", Journal of Wuhan University of Technology,Vol 29- Issue 4, pp 751-756.
[5] SCC028, May 2005, "The European Guidelines for Self-Compacting Concrete – Specification, production and use", pp.1-68.
[6] Rizwan, S.A., Bier, T.A. (2009), "Self-compacting mortars using various secondary raw Materials," ACI Mater J.; 106(1), pp 26.
[7] Gu, P.; Beaudoin, J.J.(July 1997), "A conduction Calorimetric Study of Early Hydration of Ordinary portland cement/High Aluminate Cement." 32(1997):3875-3881. Journal of Material Science.
[8] Gu, P., Beaudoin, J.J., Quinn, E.G., Myers, R.E. (1997), "Early Strength Development and Hydration of Ordinary Portland Cement Calcium Aluminate Cement Pastes". Journal of Advanced Cement Based Materials,Vol. 6, pp. 53-58.
[9] Rizwan, S. A. (2006), "High Performance Mortars and Concretes using Secondary Raw materials", PhD thesis, Technical University Freiberg, Germany.
[10] Barnes, P., Bensted, J. (2002), "Structure and Performance of cements, 2nd Edition," CRC Press ; p.p 124.
[11] Neville, A.M. (2006), "Properties of Concrete, 4th and final edition," p.p 360.

Modelling Cement Hydration and Microstructure Development Incorporating Fly Ash, Slag and Silica Fume Based on Cellular Automaton Rules

Cheng Liu [1 2],Yunsheng Zhang [1 2]*, Deqing Xie [1 2], Lin Yang [1 2] and Ran Huang [1 2]

[1] School of Materials Science and Engineering, Southeast University, Nanjing 211189, China
[2] Jiangsu Key Laboratory for Construction Materials, Nanjing, 211189, China

Abstract Granulated slag from metal industries, fly ash from the combustion of coal and silica fume from silicon industries are important parts of self-consolidating concrete (SCC), affecting SCC's mechanical and rheological properties. Due to the multiphase, heterogeneity and reaction with cement hydration products of slag, fly ash and silica fume, the hydration process containing admixtures is much more complex compared with Portland cement, particularly the double adding or tri adding. In this paper, a new modified three dimensional digital image model, based on cellular automaton (CA) and used to simulate cement hydration incorporating one or more mineral admixtures, is proposed. This paper presents the design of the new model and the model is then verified by experimental data and finally, the microstructure development of SCC with 0.5 water-to-binder ratio and different mineral admixture substitution ratios is predicted, by focusing on the evolution of phases and the pore-size distribution. Comparing with the complicated experiment, this model can test the validity of hypotheses more easily.

Keywords: *Cement hydration, Mineral admixtures, Modelling, Microstructure, Self-consolidating concrete.*

Introduction

Self-compacting concrete (SCC) characterized by high fluidity under its own weight can be placed without vibration, easily fill small interstices of formwork and be pumped through long distances. In order to achieve the SCC of high fluidity and to prevent the segregation and bleeding transportation and placing, the formulators have employed a high Portland cement content, causing cost of such concretes remarkably increased. Therefore, the use of mineral admixtures such as

fly ash, blast furnace slag and/ or silica fume reduced the material cost of the SCCs and also affected fresh and harden properties of the concretes[1, 2]. Understanding the hydration process and microstructure development of cementitious materials is needed to allow the design of systems with improved performance, especially with mineral admixtures. Unfortunately, three-dimensional continuous and quantitative characterization of microstructure evolution is pretty difficult and complicated.

Using computer models to represent the microstructure of cementitious materials has been widely developed over the past 20 decades. Van Breugel [3] developed a cement hydration microstructure simulation model called HYMSTRUC, with a vector approach. Various mass and volume balance rules are used to accommodate microstructural changes due to dissolution and precipitation of various phases in this model. Like the vector approach, μic (pronounced "mike") microstructural modelling platform designed by Bhashank and Karen [4] is derived from an earlier model developed by Navi and Pignat[5]. This model can model the hydration of millions of cement particles based on realistic particle size distribution, considering neighborhood of each particle in consideration. In contrast to vector models described above, a 3D microstructure-based simulation tool for cement hydration, called CEMHYD3D, is originally developed by Bentz [6, 7]. It uses a lattice-based approach based on digital images and changes to the microstructure simulated through cellular automaton rules, mimicking the dissolution of solids, diffusion of dissolved species according to a random walk and nucleation and growth of hydration products. However, the hydration system with mineral admixtures is hardly or partially considered into these models.

In this paper, the modified computer model CEMHYD3D, embedding the classical pozzolanic reactions, is verified through cement hydration kinetics. Then, based on the realistic particle size distribution and chemical components of cement, fly ash, slag and silica fume, the effect of mineral admixtures on the microstructure and hydration products of cementitious materials is simulated on this modified model. Finally, through a classic introduced algorithm in modified CEMHYD3D, pore size distribution is analyzed under different mixed proportions.

Experiment

The cement selected for this study issued as a Chinese standard Graded 52.5 P I Portland cement is used. With the SEM and X-ray image technique, its chemical composition analysis was implemented before [8] and clinker phases' volume proportion is listed in Table I. Also, in order to achieve crystal phase data of mineral admixtures, the result of XRF analysis is shown in table II. Additionally, the particle size distribution of cement, fly ash and slag, measured by laser diffraction from a dilute suspension of particles in isopropyl alcohol, is provided in

Figure 1. The densities of cement, fly ash, slag and silica fume are 3.15 g/cm^3, 2.24 g/cm^3, 2.80 g/cm^3 and 2.2 g/cm^3, respectively.

Table I. Phase fractions for the cement [8].

Phase	Area fraction (%)	Bogue mass fraction (%)	Volume fraction (%)
C_3S	52.36	53.09	53.72
C_2S	27.75	24.95	24.09
C_3A	4.77	7.20	7.61
C_4AF	13.12	10.69	8.98
$CaSO_4$	-	4.06	5.06

Table II. Oxide compositions for fly ash, slag and silica fume.

Oxide	Composition (mass%)		
	Fly ash	Slag	Silica fume
CaO	5.194	31.223	-
SiO_2	55.36	37.37	94.29
Al_2O_3	25.46	17.72	-
SO_3	1.203	2.98	-
Fe_2O_3	-	0.963	-
MgO	-	4.02	-
Others	12.783	5.724	5.71

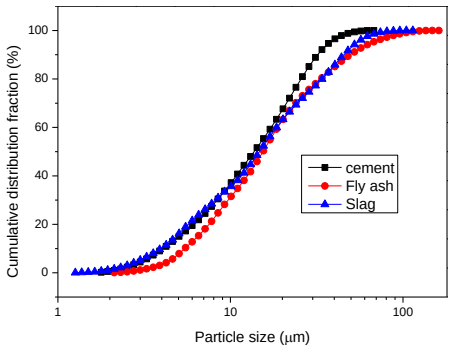

Figure 1. Measured particle size distribution for cement, fly ash and slag.

Modified CEMHYD3D model

Cellular automata (CA) were first proposed by Ulam [9, 10] and Von Neumann [11], based on ideas of Zuse [12]. Cellular automata, a basically computer

algorithm that is discrete in space and time and operates on a lattice of sites, used to model natural systems, was first introduced into the model of cement hydration and microstructure development by Bentz [6] and the model was named CEMHYD3D. This model presents the microstructure of the hydration cement by using a 100×100×100 box with 10^6 voxels of size 1 μm^3. Each voxel represents a chemical phase either fresh binder or hydration material. The initial microstructure thus consists of cement particles and water, where each particle is made up of a number of voxels.

The first step of simulation is the creation of an initial microstructure, representing cement and water. Therefore the particle size distribution and the chemical composition of cement is taken into consideration. Based on the chemical composition, the initial particles of cement are divided into the heterogeneous materials, consisting of C_3S, C_2S, C_3A, C_4AF and gypsum. The second step of simulation is the performance of the chemical reactions of clinker by the cellular automata algorithm. In order to eliminate the wall-effect of the cubic system, periodic boundaries are applied in CEMHYD3D [7] .

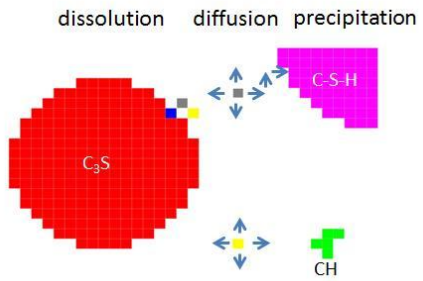

Figure 2. Main reaction mechanism of CEMHYD3D

$$C + H \rightarrow CH$$
$$1 \quad 1.07 \quad 1.96$$

$$A + 3CH + 3H \rightarrow C_3AH_6$$
$$0.26 \quad 1 \quad 0.544 \quad 1.512$$

$$S(FA, SF) + 1.1CH + 2.8H \rightarrow C_{1.1}SH_{3.9}$$
$$1 \quad 1.349 \quad 1.867 \quad 3.771$$

$$S(S) + 1.5CH + 1.5H \rightarrow C_{1.5}SH_3$$
$$0.5438 \quad 1 \quad 0.5438 \quad 1.7724$$

$$C_3AH_6 + CH + 12H \rightarrow C_4AH_{19}$$
$$1 \quad 0.22 \quad 1.44 \quad 2.476$$

$$C_6AFS_2 + 8H \rightarrow C_6AFS_2H_8$$
$$1 \quad 0.6797 \quad 1.345$$

$$M_5A + 19H \rightarrow M_5AH_{19}$$
$$1 \quad 4.18 \quad 3.947$$

Figure 3. Mineral admixture reactions (numbers below reactions indicate volume stoichiometry)

Reactions of clinker with water or other phases are simulated by discrete steps. Three processes: dissolution, diffusion and reaction, are included by each whole step, which are shown in Figure 2. The dissolution step is performed by scanning all voxels in the hydration system then checking them for their abilities to dissolves. The ability depends on which phase they belong to, their local

environment where they are located at that moment and the number of reacted phases, such as water. Each phase has a dissolution probability defined by Bentz [7] as the likelihood of each phase to dissolve. Then, the dissolved phase implements a diffused step which is a random walk to one of six directions. If the site of the walking is a pore, the dissolved phase will diffuse to this site and the original site become the pore. Otherwise, the dissolved will stay at the original site or react with the collided phase. During the diffusion process, the dissolved phase can also nuclear into the hydration product according to the probability of nucleation.

As is described above, mineral admixtures (fly ash, slag and silica fume) are introduced in CEMHYD3D by the similar reaction algorithm. In this paper, the classical pozzolanic reactions proposed by Papadakis [13] and Richardson [14] are summarized in Figure 3 and implemented as a series of cellular automata-like rules. The volume stoichiometries indicate below each reaction have been calculated based on the molar stoichiometries of the reactions and the compound molar volumes. Noticeably, C_6AFS_2 and M_5A, two phases in the modelling slag, do not exist in the real slag. But, in order to modelling the slag hydration products, hydrogarnet ($C_6AFS_2H_8$) and hydrotalcite (M_5AH_{19}), these two phases are defined in the slag for reducing the number of total modelling phase. Also, although non-crystal S of fly ash and silica fume has the same reaction with water, silica fume's S is defined to be non-dissolvable because of modelling silica fume's nucleation and filling effect.

Figure 4 shows the initial microstructure based on real particle size distribution (Figure 1) and composition of the binder (Table.1 and Table.2) with w/b 0.35 and tri-adding in the cement (50% cement, 35% slag, 15% fly ash and 10% silica fume). In these pictures, different colored voxels represent different phases. In order to distinguish the main phases in the pictures clearly, some phases with some similar features have the same color, such as silica phase (S and C_6AFS_2) has the same grey level.

In the modified CEMHYD3D, the pore-size distributions of microstructures obtained are calculated using a simplified three-dimensional voxel method. In the method [4, 15] , shown in Figure 5, used here, the microstructure is divided into much finer cubic mesh and the voxels are marked to be solid and pore based on their occupancy. The pore voxels sharing a face with a solid voxels are marked with the number 1, and in the next step, the pore voxels sharing a face with the voxels marked 1, are marked with 2, and so on until all the voxels were marked with the number of steps required to reach them from boundaries. While this method is one of many possible definitions of pore-sizes and ignores information regarding pore-topology, it can obtain quick comparative results.

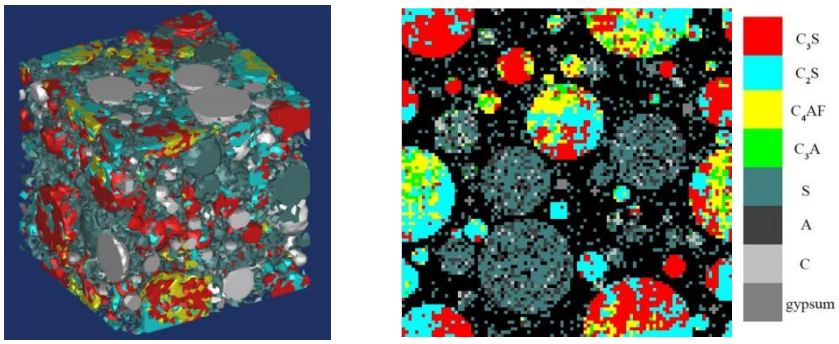

Figure 4. Initial microstructure (left: 3D right: 2D slice) with w/b 0.35 and 0.5 cement, 0.25 slag, 0.15 fly ash and 0.10 silica fume.

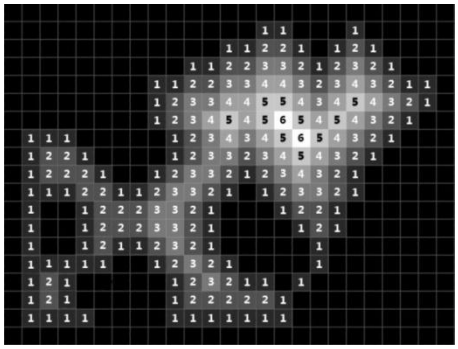

Figure 5. Erosion to identify pore-skeleton using pixels. The black parts are solids and the pores are shown in shades of grey with numbers indicating the number of steps required to reach the given pore pixels from the closest solid pixel.

Verification

The hydration product (CH), non-evaporable water and degree of hydration of binders are important parameters, measuring hydration process in cementitious material systems. Therefore, the data of adding different mineral admixtures in cement from Jia [16] is used to verify the modified CEMHYD3D.

Figure 6 shows the relationship between CH content and fly ash's ratio and non-evaporable water content and fly ash's ratio at the same fly ash's degree of hydration, respectively. From these two figures, the modelling lines both fluctuate slightly between the measured lines, indicating the modified CEMHYD3D can model cement hydration with different fly ash's content. Also, measured and model CH content (left) and non-evaporable water content (right) versus slag's ratio is illustrated in Figure 6. Like the fly ash's lines, the lines of slag have good fit with

experimental data. Even the line of CH content versus slag's content has the same decreasing trend in Figure 7.

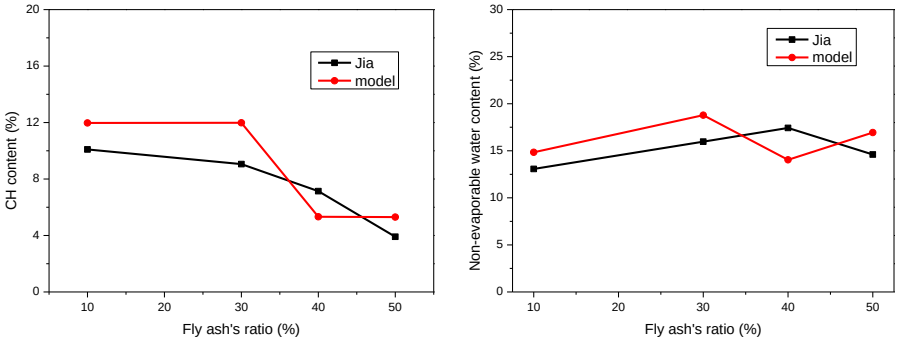

Figure 6. Measured and model CH (left) and non-evaporable (right) versus fly ash's content with w/b 0.5.

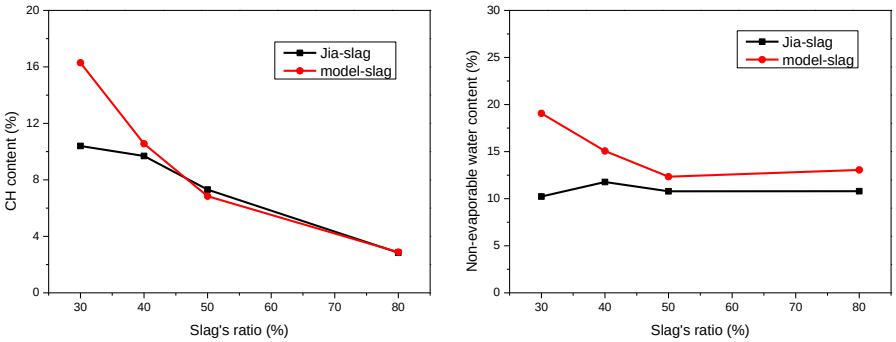

Figure 7. Measured and model CH (left) and non-evaporable (right) versus slag's content with w/b 0.5

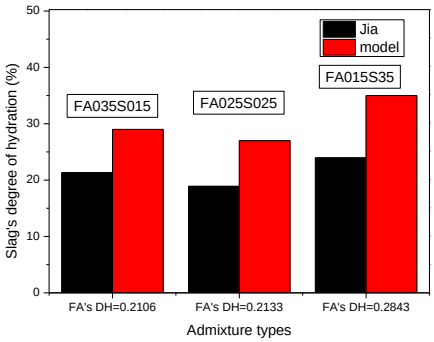

Figure 8. Slag's degree of hydration versus fly ash's degree of hydration at different mixed contents

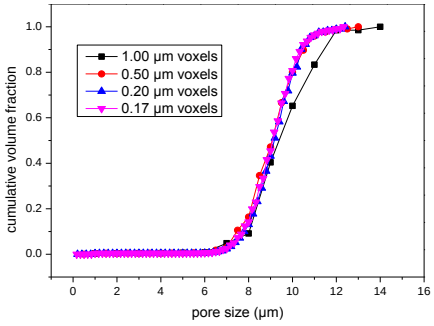

Figure 9. Pore size distribution at 50% degree of hydration at four voxel sizes: 1.0, 0.5, 0.2 and 0.17μm with w/b 0.5

The modelling cement hydration system of double adding fly ash and slag is provided in Figure 8. This figure shows the relationship between fly ash's degree of hydration and slag's at different mixed proportion. The figures for modelling slag's degree of hydration at three different mixed proportions are all higher slightly than the experimental data and have the same changing trend, declining slightly and then increasing a little. According to the model rules, this means that the modified model can well simulate the cement system with two or more mineral admixtures.

The simulation of pore-sizes is carried out at 50% degree of hydration to study the change in pore-size distribution with the voxel size. Four voxel sizes are used in the simulations, resulting in four independent resolutions. The results obtained from this analysis are shown in Figure 9. From the figure, when the voxel size is less than 0.5 μm, there is a slight difference among the lines of particle size distribution. Even the largest pore sizes have the same value at 0.2 and 0.17 μm voxels. So the 0.2 μm voxel size is chosen in this paper, considering computational efficiency and convergence.

Modelling results

Figure 10 provides the predicted volume fraction changes of clinker and hydration products at w/b 0.5 and 50% fly ash. In this figure, the volume fractions of clinker and fly ash show a decreasing trend during the hydration process, while the hydration products have an opposed trend, accordingly. The hydration rate of cement is comparatively high at the early stage, lasting 50 days, then, becomes very low. While the fly ash's degree of hydration rate is consistently low because of lower activity of fly ash. At the same time, the change of pore-size distribution with curing time during 1 year is provided in Figure 11. With the curing time increasing, the largest pore size decreases from 8 μm at 3 days to 3.5μm at 1 year and in the 56 days, the largest pore size decreases dramatically, then, stay stable around 3.5 μm. Also, compared with the change of the largest pore size, the line has the same trend to move toward to the direction of small pore. And in the 56 days, there is a significant fall of pore size.

The line curves show the degree of hydration of cement and fly ash versus time at three different mixed proportions in Figure 12. It's clear from the figure that the degree of cement is higher than that of fly ash at all three proportions. With the fly ash mixed growing, the degree of hydration of cement will also increase at the same time, while the fly ash's degree of hydration will fall. This is because when the fly ash's substitution ratio increases, the system's effective w/c will also grow, resulting in the increasing cement hydration rate and the system with low activity totally.

Figure 13 shows the effect of double adding fly ash and slag on pore-size distribution with 35% fly ash and 15% slag substitution ratio. Compared with single adding fly ash in Figure 11, the largest pore size of double adding has smaller value at early stage (14 days), while later the numbers both stay at around 0.4 μm after 56 days. Because when adding slag which has the high activity with low crystallinity, this improves slag's degree of hydration and also can promote the fly ash's degree of hydration because of the CH from slag. But with the reaction continuing, CH is consumed to a low content and eventually, the number of hydration products is almost similar which result in the same largest pore-size. Also, the tri-adding has the same reasons in Figure 14. While because of the non-dissolvable silica fume, the filling and nucleation effect contributes to smaller pore-size.

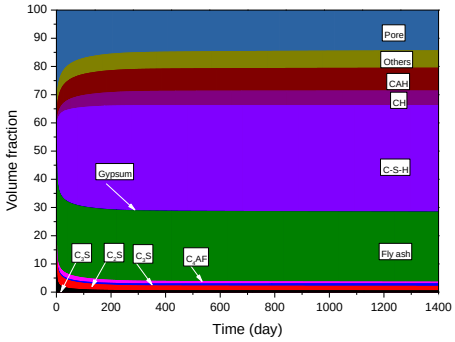

Figure 10. Predicted volume fraction changes of hydration system

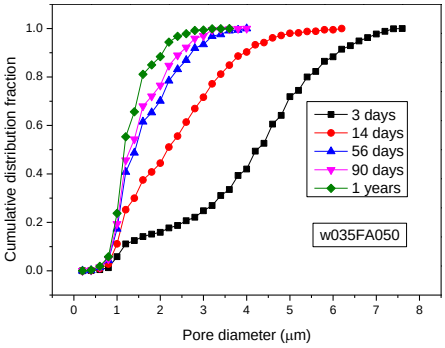

Figure 11. Predicted pore-size distribution changes with w/b 0.35 and 50% fly ash

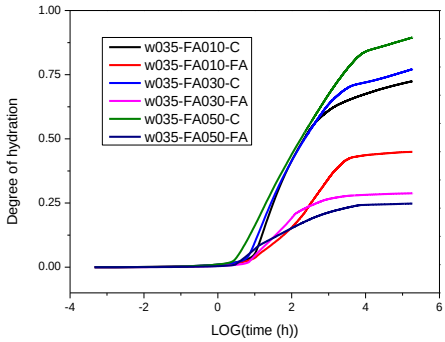

Figure 12. Predicted degree of hydration of cement and fly ash

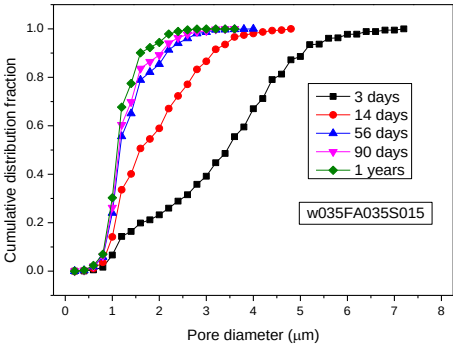

Figure 13. Predicted pore-size distribution changes with double adding fly ash and slag at 35% fly ash and 15%

slag substitution ratios

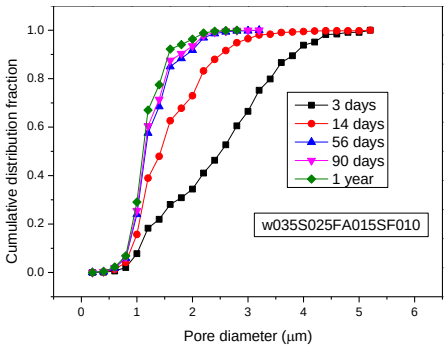

Figure 14. Predicted pore-size distribution changes with tri-adding 25% slag, 15% fly ash and 10% silica fume

Conclusions

This paper introduces mineral admixtures into the CEMHYD3D model by cellar automaton rules to predict microstructural evolution of cementitious materials. This model is verified to best fit to experimental data of cement hydration incorporating different mineral admixtures substitution ratios. Also, a simplified voxel-erosion method to characterize pore-size distribution is developed. In the modified CEMHYD3D model, the microstructural development and reaction mechanisms of 52.5 P I Portland cement and special mineral admixtures in China are studied. It can be seen that the modified CEMHYD3D model is a useful tool to predicted cement hydration incorporating slag, fly ash and silica fume.

Acknowledgements

The authors wish to thank the staff of the National Institutes of Standards and Technology (NIST) for initial CEMHYD3D model. And this work is financially supported by 973 Program (2015CB6551002) and National Natural Science Foundation of China (51178106 and 51378116).

References

[1] Gesoğlu M, Güneyisi E, Özbay E. *Properties of self-compacting concretes made with binary, ternary, and quaternary cementitious blends of fly ash, blast*

furnace slag, and silica fume[J]. Construction & Building Materials, 2009, 23(5):1847–1854.
[2] Şahmaran M, Christianto H A, İsmail Özgür Yaman. *The effect of chemical admixtures and mineral additives on the properties of self-compacting mortars*[J]. Cement & Concrete Composites, 2006, 28(5):432–440.
[3] Breugel K V. *Simulation of hydration and formation of structure in hardening cement-based materials*[J]. Cement & Concrete Research, 1995.
[4] Bishnoi S, Scrivener K L. *μic: A new platform for modelling the hydration of cements*[J]. Cement and Concrete Research, 2009, 39(4): 266-274.
[5] Navi P, Pignat C. *Simulation of cement hydration and the connectivity of the capillary pore space*[J]. Advanced Cement Based Materials, 1996, 4(2): 58-67.
[6] Bentz D P. *Three-Dimensional Computer Simulation of Portland Cement Hydration and Microstructure Development*[J]. Journal of the American Ceramic Society, 1997, 80(1): 3-21.
[7] Bentz D P. CEMHYD3D: *a three-dimensional cement hydration and microstructure development modeling package. Version 3.0. NISTIR 7232*[J]. US Department of Commerce, 2005.
[8] Liu Z, Zhang Y, Jiang Q. *Continuous tracking of the relationship between resistivity and pore structure of cement pastes*[J]. Construction and Building Materials, 2014, 53: 26-31.
[9] Ulam S. *Random processes and transformations*[C]//Proceedings of the International Congress on Mathematics. 1952, 2: 264-275.
[10] Ulam S M. *Adventures of a Mathematician (Charles Scribner's Sons, New York, 1976)*[J]. ACKNOWLEDGEMENTS We wish to thank Shimon Even, Michael J. F, 281.
[11] Von Neumann J, Burks A. *Theory of self-replicating automata*[J]. Urbana: University of Illinois Press, 1966.
[12] Kier L B, Cheng C K, Seybold P G. *Cellular automata models of aqueous solution systems*[J]. Reviews in computational chemistry, 2001, 17: 205-254.
[13] Papadakis V G. *Effect of fly ash on Portland cement systems: Part I. Low-calcium fly ash*[J]. Cement and Concrete Research, 1999, 29(11): 1727-1736.
[14] Richardson I G, Groves G W. *Microstructure and microanalysis of hardened cement pastes involving ground granulated blast-furnace slag*[J]. Journal of Materials Science, 1992, 27(22): 6204-6212.
[15] Baldwin C A, Sederman A J, Mantle M D, et al. *Determination and characterization of the structure of a pore space from 3D volume images*[J]. Journal of Colloid and Interface Science, 1996, 181(1): 79-92.
[16] Jia Y. *The hydration mechanism of the BFS and FA cement-based materials*[D]. Master thesis, Southeast, China, 2005.

Influence of Recycled Concrete Coarse Aggregate on Self-Compacting Concrete Robustness at Short and Long Times

Iris González-Taboada[1], Belén González-Fonteboa[1], Nicolas Roussel[2] and Fernando Martínez-Abella [1]

[1]School of Civil Engineering. Department of Construction Technology, University of A Coruña. Spain
[2]IFSTTAR, Laboratoire Navier – UMR 8205, France

Abstract It is well known that self-compacting concrete (SCC) is more sensitive to small changes in constituent materials and production method than vibrated concrete, i.e. it is less robust. An experimental program was carried out to evaluate the robustness of SCC containing recycled aggregate. Two series of SCC mixes with different percentages of recycled concrete coarse aggregate (0%, 20%, 50% and 100%) were studied, one series with the aggregate used in dry-state conditions and the other incorporating it in the mixer with a 3% of moisture. The analysis focused on the capacity of self-compacting recycled concrete (SCRC) to keep workability and rheological properties over time when variations in water (W = ±3%), superplasticiser (S = ±5%) and cement (C = ±3%) are imposed.
The tests results show that, since SCRC presents more difficulty to control water due to recycled aggregate higher water absorption, special care should be taken to produce SCRC. Consequently, water control is going to be even more important than in conventional SCC and more important than in traditional vibrated concrete.

Keywords: *Self-compacting recycled concrete; rheology; robustness; mixing method*

Introduction

Self-compacting concrete (SCC) is more sensitive to small changes in raw materials characteristics, mix parameters and mixing conditions than conventional vibrated concrete [1], that is, it is less robust. Robustness is defined as the capacity of a concrete to maintain its performance requirements (at the fresh and hardened states) after introducing some variations in the mixing procedure, transport, and

casting [2]. It is worth mentioning that it refers to the ability of a SCC mixture to maintain its filling ability, passing ability and segregation resistance during processing and placement [3]. The total quantity of mixing water is a key factor that affects robustness of SCC [2]. Then, reducing or increasing the amount of water is expected to have a significant influence on self-compactability. Other critical changes can occur when there is excess cement, excess fly ash, less fly ash, excess superplasticiser, excess sand, excess gravel… [4].

Self-compacting recycled concrete (SCRC) is expected to present properties in hard-state similar to those of its equivalent vibrated recycled concrete (RC) and to show, in fresh-state, a greater influence of RC and SCC singularities (specific mixing procedures [5] and a particular fresh behaviour [6], and less robustness, respectively).

Objectives

This paper focuses on the capacity of SCRC to keep workability and rheological properties over time when variations in water (W = ±3%, superplasticiser (S = ±5%) and cement (C = ±3%) are imposed independently. The objective is to show that SCRC robustness is going to be lower than in conventional SCC and to demonstrate that, however, producing a robust SCRC is feasible knowing which are the main parameters to achieve it.

Experimental Program

Materials

Table XI summarizes the basic properties of the aggregates used.

Table XI. Aggregates properties

Property	NFA	NCA	RCA
Fineness modulus (EN 933-1)	4.19	7.14	6.47
Fines percentage (EN 933-1) (%)	8.40	0.84	3.00
Moisture content (EN 1097-3) (%)	1.18	0.84	5.95
Saturated-surface-dry density (EN 1097-6) (t/m^3)	2.72	2.56	2.34
Absorption (EN 1097-6) (%)	1.00	1.12	6.96
Flakiness index (EN 933-3) (%)	-	5.41	5.33
Shape	Crushed	Crushed	Crushed

Portland cement, CEM-I 52.5 R (EN 197-1), and a limestone filler were used as powder fraction. A modified policarboxylate was used as superplasticiser. As fine

aggregate (NFA), a siliceous sand with nominal size 0-4 mm and a fineness modulus of 4.19 was used. Two types of coarse aggregates, natural and recycled, were used: a crushed granitic coarse aggregate (NCA) with nominal size 4-11 mm and a fineness modulus of 7.14, and a recycled coarse aggregate (RCA) whose size fraction was a 4-11 mm with a fineness modulus of 6.47. This RCA was obtained from real demolition debris of structural concrete. It was made up mainly of concrete and stone.

In addition to the standard absorption test (EN 1097-6), a continuous measurement of this property over time was conducted. At the usual reference time of 10 min [5], RCA absorbs water up to 80% of that at 24 h (Figure 25).

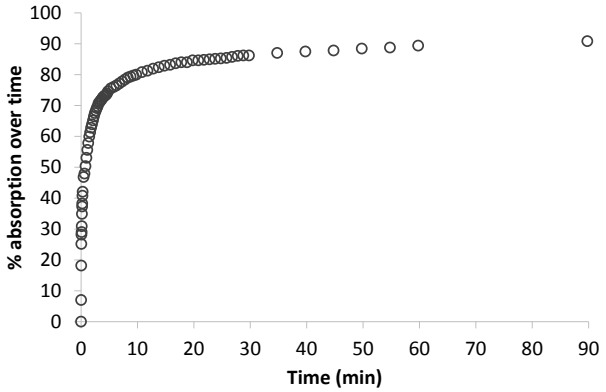

Figure 25. Evolution of reycled aggregate absorption from 0 to 90 min

Mix Proportioning

Four types of self-compacting concrete were studied (

Table ***XII***), a reference concrete and three recycled concretes replacing the natural coarse aggregate with the recycled one, with volume replacements of 20%, 50% and 100% respectively.

Table XII. Mix proportions (1 m³)

SCRC dosage	% RCA			
	0%	**20%**	**50%**	**100%**
Cement, c (kg)	400.00	400.00	400.00	400.00
Filler, f (kg)	180.00	180.00	180.00	180.00
Water, w (kg)	184.00	184.00	184.00	184.00
Natural sand (kg)	865.59	865.59	865.59	865.59
Natural coarse aggregate (kg)	768.00	614.40	384.00	0.00
Recycled coarse aggregate (kg)	0.00	140.40	351.00	702.00
Effective w/c	0.46	0.46	0.46	0.46
Superplasticiser/(c+f) (%)	1.70	1.70	1.70	1.70

All recycled concretes were produced adding an extra quantity of water during the mixing. This was calculated to compensate the recycled aggregate absorption at 10 min (i.e. 80% of that at 24 h), which was used dry (M1 method) or with a 3% of natural moisture (M3 method).

Tests Methods

The empirical and rheological tests (Table XIII) were performed at 15, 45 and 90 min since the contact cement-water (Age). This corresponds to 0, 30 and 45 min resting time (RT) respectively for rheological tests.

Table XIII. Experimental program

Test	**Parameter measured**	**Objective limits**
Slump flow	t500 (s)	[2-8]
	Df (mm)	[650-800]
V-funnel	tv (s)	[4-20]
L-box	PL	≥ 0.80
J-Ring	t500J (s)	< 8
	DJF (mm)	> 600
	PJ (mm)	≤ 10
Sieve segregation	SR (%)	≤ 15%
Stress growth test	Static yield stress	–
Flow curve test	Plastic viscosity	–

In order to use the same material several times, concrete was mixed for 30 s immediately before each empirical test. In the rheological tests, the stress growth test started as soon as the vane was immersed into the concrete. The vane was rotated at a low and constant speed (0.025 rps) and the torque value was acquired. Once the peak torque was reached, the vane was removed and concrete was

remixed with a shovel. Then, the vane was reinserted into concrete and the flow curve test started. At the end, the vane was removed and concrete was again remixed with a shovel and left at rest.

Results and Discussion

Fresh-State Results with Empirical Tests

In terms of workability characteristics, the slump flow and J-Ring tests are found to be sensitive for robustness evaluation [2]. Thus, the experience obtained during this research has suggested that using the combination of slump flow test (parameters t500 and Df) and J-Ring test (parameters t500J and DJF) lead to evaluate the filling ability and the passing ability (Table XIV), respectively.

Table XIV. Filling ability and passing ability (Y: Y; N: no)

SCRC	Age (min)	Filling ability (t500 and Df)							Passing ability (t500J and DJF)						
		Base	C+	C-	S+	S-	W+	W-	**Base**	C+	C-	S+	S-	W+	W-
0%	15	**Y**	Y	Y	Y	Y	Y	Y	**Y**	Y	Y	Y	Y	Y	Y
	45	**Y**	Y	Y	Y	Y	Y	Y	**Y**	Y	Y	Y	Y	Y	Y
	90	**Y**	Y	Y	Y	Y	Y	Y	**Y**	Y	Y	Y	Y	Y	Y
M1 20%	15	**Y**	Y	Y	Y	Y	Y	Y	**Y**	Y	Y	Y	Y	Y	Y
	45	**Y**	Y	Y	Y	Y	Y	Y	**Y**	Y	Y	Y	Y	Y	Y
	90	**Y**	Y	Y	Y	Y	Y	Y	**Y**	Y	Y	Y	Y	Y	Y
M1 50%	15	**Y**	Y	Y	Y	Y	Y	Y	**Y**	Y	Y	Y	Y	Y	Y
	45	**Y**	Y	Y	Y	Y	Y	Y	**Y**	Y	Y	Y	Y	Y	Y
	90	**Y**	Y	Y	Y	N	Y	N	**Y**	Y	Y	Y	N	Y	N
M1 100%	15	**Y**	Y	Y	Y	Y	Y	Y	**Y**	Y	Y	Y	N	Y	N
	45	**Y**	Y	Y	Y	Y	Y	N	**Y**	Y	Y	Y	N	Y	N
	90	**N**	N	Y	N	N	Y	N	**N**	N	N	N	N	N	N
M3 20%	15	**Y**	Y	Y	Y	Y	Y	Y	**Y**	Y	Y	Y	Y	Y	Y
	45	**Y**	Y	Y	Y	Y	Y	Y	**Y**	Y	Y	Y	Y	Y	Y
	90	**Y**	Y	Y	Y	Y	Y	N	**Y**	Y	Y	Y	N	Y	N
M3 50%	15	**Y**	Y	Y	Y	Y	Y	Y	**Y**	Y	Y	Y	Y	Y	Y
	45	**Y**	Y	Y	Y	Y	Y	Y	**Y**	Y	Y	Y	Y	Y	Y
	90	**Y**	N	Y	Y	N	Y	N	**N**	N	Y	Y	N	Y	N
M3 100%	15	**Y**	N	Y	Y	N	Y	N	**Y**	N	Y	Y	N	Y	N
	45	**Y**	N	Y	Y	N	Y	N	**Y**	N	N	Y	N	N	N
	90	**N**	N	N	N	N	N	N	**N**	N	N	N	N	N	N

The analysis of the filling ability shows that SCRC with low replacement percentages (20% and 50%) keeps its self-compacting behaviour until a 45 min

age, and for both mixing methods. This same comment can be made for the passing ability. At a 90 min age, this situation is only satisfied by the reference concrete and by the mix with 20% of RCA and produced with M1 method. In this case, for both properties, the mixes with 50% and 20% of RCA and produced with M1 method and M3 method respectively show difficulties to maintain their self-compacting condition when superplasticiser or water decrease. The mix with 50% of RCA and produced with M3 method is also affected negatively by the cement increase.

For the 100% replacement concrete, regarding filling ability until the 45 min age, SCRC made with M1 method only stops being self-compacting when water decreases. Its passing ability is also affected by the superplasticiser decrease. At the 90 min age, its behaviour is no longer self-compacting. In the case of M3 method, SCRC does not present robustness since its self-compacting condition is lost with the cement increase or with the superplasticiser or water decrease, even at short ages (15 min).

Fresh-State Results with Rheological Tests

This second analysis is focused on the static yield stress development until 45 min. Regarding the RCA percentage used, the mixes with a low replacement ratio are more robust than the ones produced with high replacement rate, i.e. they maintain the rheological parameters over time without almost any variations. Moreover, the mixes produced with the method M1 (dry aggregate) (Figure 26, Figure 28, Figure 30) are more robust than the ones produced with the method M3 (recycled aggregate with a 3% of natural moisture) (Figure 27, Figure 29).

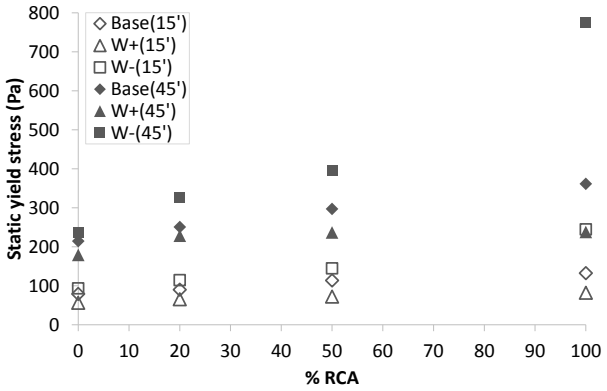

Figure 26. Static yield stress – Water variations (M1 method)

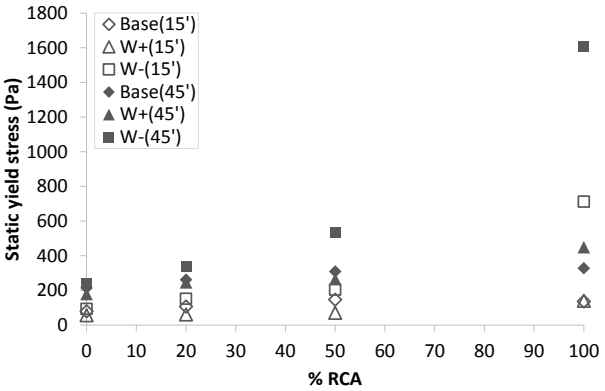

Figure 27. Static yield stress – Water variations (M3 method)

Figure 26 and Figure 27 show that the greatest influence of the water variation on self-compactability takes place when water is reduced and the replacement percentage is high, and it is more noticeable in M3 method, where the water control is more difficult due to the moisture of recycled aggregate.

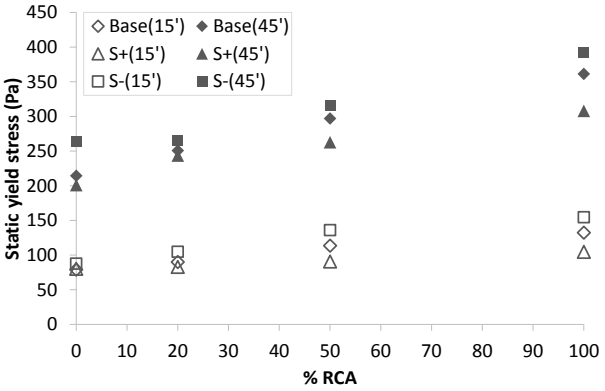

Figure 28. Static yield stress – Superplasticiser variations (M1 method)

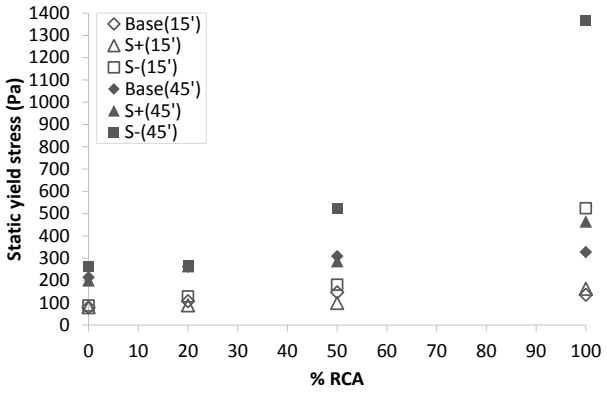

Figure 29. Static yield stress – Superplasticiser variations (M3 method)

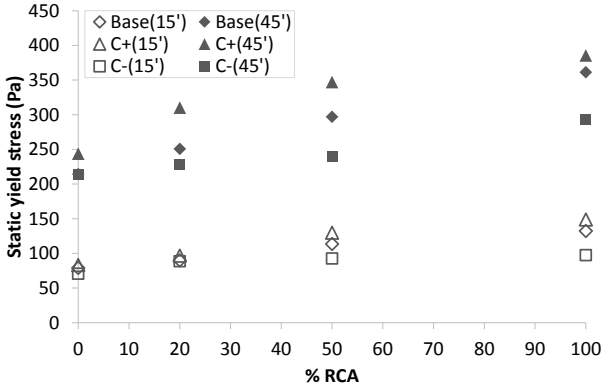

Figure 30. Static yield stress – Cement variations (M1 method)

Secondly, changes in the superplasticiser dosage do not modify yield stress significantly when dry-state recycled aggregate is used (Figure 28). Therefore, in this case, all SCRCs show a suitable rheological behaviour, similar to the conventional SCC until a mix age of 45 min. This trend can also be seen in M3 method (Figure 29), but only up to 50% of RCA.

Finally, Figure 30 shows the results of the cement modifications, which follow the same trend as those obtained with the water variations (so, only method M1 was studied). Thus, an increase in cement will be analogous to a decrease in water and vice versa. However, the water changes influence to a greater extent the SCRC behaviour.

Final discussion

The amplitude of variation (in percentage) in the static yield stress is shown for each concrete when water, superplasticiser and cement were modified (Figure 31). These values are the sensitivity parameters.

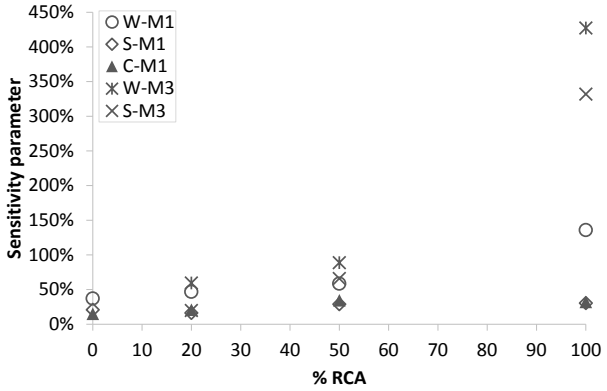

Figure 31. Sensitivity parameters (average 15 and 45 min – M1 and M3)

It can be stated that SCRC is less robust. Furthermore, in Figure 31, it is shown that the water is the key factor that affects SCRC robustness. This type of concrete is more sensitive to water changes than conventional SCC, because these have to be added to the variations produced by the evolution of the recycled aggregate water absorption. Therefore, although the mixing protocol takes into account the water absorption of RCA at 10 min, this does not solve completely the problem with water, especially over time.

In order to observe the influence of the different variations (water, superplasticiser and cement) plus the non-compensated water absorption in the SCRC robustness, different mortars with different w/c ratios were designed. (Figure 32). Figure 32 shows two different patterns of behaviour: w/c ratios higher than 0.45 will not imply significant changes in yield stress, whereas w/c ratios lower than 0.45 will lead to important changes. This can be considered a “critical w/c ratio”, since a little change in w/c ratio under this critical value will imply a great change in yield stress.

So, reducing water leads to a little decrease in effective w/c ratio but to a noteworthy increase in yield stress due to the trend under the aforementioned “critical w/c ratio”. However, increasing water does not affect so adversely (Figure 32). In the case of superplasticiser, its volume is small and, therefore, the effective w/c ratio remains practically unaffected (Figure 32).

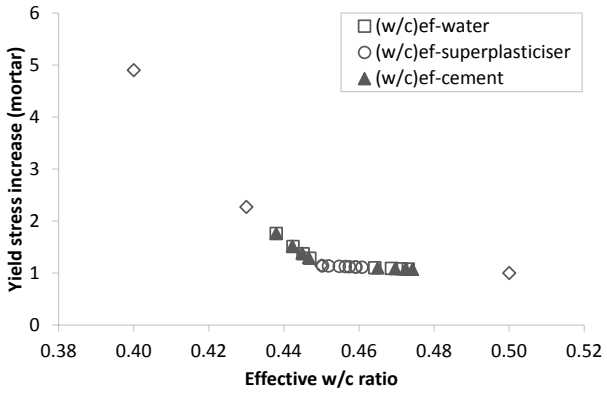

Figure 32. Effective water to cement ratio of reference mortars and concretes at 45 min age

The variations in effective w/c ratio are more important for a SCRC than for a conventional SCC. Moreover, the more recycled aggregate, the more influence on robustness will be produced. Then, it is necessary to pay special attention to water control in SCRC, even more than in a conventional SCC and, of course, more than in vibrated concrete.

Conclusions

This paper studies the robustness of self-compacting recycled concrete (SCRC) and the following conclusions can be drawn:

- The use of recycled coarse aggregate with a previous moisture content (M3 method) involves a greater difficulty to control workability than the use in dry-state conditions (M1 method), especially for high replacement percentages (50% and 100%).
- In both methods, SCRC with the 20% of RCA maintains, until the 90 min age, its self-compacting behaviour. Substitution rate of 50% guarantees the self-compacting ability until the 45 min age. Regarding 100% SCRCs, those produced with the M1 method stop being self-compacting at 45 min, being reduced this age to 15 min with the M3 method.
- The mixes with a low replacement ratio and produced with the method M1 are more robust than the ones produced with the method M3.
- Water is the key factor that affects SCRC robustness. This type of concrete is more sensitive to water variations than conventional SCC. These variations are going to be more significant with the increase of the recycled aggregate percentage and when it is used with a previous

moisture. Then, it is necessary to pay special attention to water control in SCRC, even more than in a conventional SCC and, of course, more than in vibrated concrete.

Acknowledgments

The study is part of two projects: (a) “Industrial Investigation about Concrete for a Sustainable Market” funded by the Innovation Galician Agency; (b) “Robust self-compacting recycled concretes: rheology in fresh state and mechanical properties” funded by MINECO. This work was also made possible by the financial support of INDITEX-UDC 2015 fellowships for international pre-doctoral stays.

References

[1] Nunes, S.; Milheiro, P.; Coutinho, J. S.; & Figueiras, J. (2013). Robust SCC Mixes through Mix Design. *J. Mater. Civ. Eng.*, vol. 25, pp. 183-193.

[2] Naji, S.; Hwang, S-D.; & Khayat, K. H. (2011). Robustness of Self-Consolidating Concrete Incorporating Different Viscosity-Enhancing Admixtures. *ACI Mater. J.*, vol. 108, n. 4, pp. 432-438.

[3] Shen, L.; Jovein, H. B.; Shen, S.; & Li, M. (2015). Effects of Aggregate Properties and Concrete Rheology on Stability Robustness of Self-Consolidating Concrete. *J. Mater. Civ. Eng.*, vol. 27, n. 5.

[4] Gettu, R.; Shareef, S. N.; & Ernest, K. J. D. (2009). Evaluation of the robustness of SCC. *Indian Concr. J.*, vol. 83, n. 6, pp. 13-19.

[5] González-Taboada, Iris; González-Fonteboa, Belén; Martínez-Abella, Fernando; & Pérez-Ordóñez, Juan Luis (2016). Prediction of the mechanical properties of structural reycled concrete using multivariable regression and genetic programming. *Constr. Build. Mater.*, vol. 106, pp. 480-499.

[6] Roussel, N. (2015). Rheology of Self-Compacting Concrete: from measurements to casting processes. IV Congresso Ibero-americano sobre Betão Auto-compactável – BAC2015, Oporto, 6-7 July 2015.

[7]

Developing Self-Compacting Concrete Using Local Materials of Libya

Hakim S. Abdelgader[1] and Ali S. El-baden[2]

[1] Professor, Department of Civil Engineering, University of Tripoli, Tripoli, Libya
[2] Associate Professor, Department of Civil Engineering, University of Tripoli, Tripoli, Libya

Abstract A self-compacting concrete (SCC) is the one that can be placed in the form and can go through obstructions by its own weight and without the need of vibration. Since its first development in Japan in 1988, SCC has gained wider acceptance in Japan, Europe and USA due to its inherent distinct advantages. Although there are visible signs of its gradual acceptance in the North Africa through its limited use in construction, Libya has yet to explore the feasibility and applicability of SCC in new construction. The contributing factors to this reluctance appear to be lack of any supportive evidence of its suitability with local aggregates and the harsh environmental conditions.The primary aim of this study is to explore the feasibility of using SCC made with local aggregates of Libya by examining its basic properties characteristics. This paper consists of: (i) Development of a suitable mix for SCC such as the effect of water to powder ratio, and lime stone powder (LSP) that would satisfy the requirements of the plastic state; (ii) Casting of concrete samples and testing them for compressive strength and unit weight. Local aggregates were used in this research. Results indicated that LSP substitution generally results in favorable outcomes.

Keywords: *Self-compacting concrete, powder, lime stone, silica fume, admixtures*

Introduction

Development of self- compacting concrete (SCC) is a desirable achievement in the construction industry in order to overcome problems associated with cast-in-place concrete. Also it can be pumped longer distances due to its high –fluidity and resistance to segregation [1]. The concept of self-compacting concrete was proposed in use but the prototype was first developed in Japan [2, 3]. Self-compacting concrete was developed at that time to improve the durability of concrete structures. Self-compacting concrete is cast so that no additional inner or

outer vibration to perform compaction. It flows like "honey" and it has a very smooth surface level after placing. With regard to its composition, self-compacting concrete consists of the same components as conventionally vibrated concrete, which are cement, aggregates, and water, with the addition of chemical and mineral admixtures in different proportions. Usually, the chemical admixtures used are high-range water reducer (super-plasticizers) and viscosity- modifying agents. Mineral admixtures are used as an extra fine material, besides cement, and in some cases, they replace cement. Self-compacting concrete, in principle, is not a new. Special applications such as underwater concreting have always required concrete which, could be placed without need for compaction [1]. In such circumstances vibration was simply impossible. Early self-compacting concretes relied on very high contents of cement paste and, once super-plasticizers became available, they were added to the concrete mixes. The mixes require specialized and well – controlled placing methods in order to avoid segregation, and the high contents of cement paste made them prone to shrinkage. The overall costs were very high andapplication remained very limited. In the early 1990's there was only a limited public knowledge about SCC, mainly in Japanese language. Simultaneously with Japanese developments in the SCC; research and development was continued in mix-design also. Production of SCC mixes with performance matching that of the Japanese SCC concrete was developed in Canada [4]. The motive for development of self-compacting concrete was the problem of durability of concrete structures that arose around 1983 in Japan. Due to a gradual reduction in the number of skilled workers in Japan's construction industry, a similar reduction in the quality of construction work took place. As a result of this fact, one solution for the achievement of durable concrete structures independent of the quality of construction work was to implement self-compacting concrete, which could be compacted into every corner of a formwork, purely by means of its own weight. Studies to develop self-compacting concrete, including a fundamental study on the workability of concrete, were carried out at the University of Tokyo[3]. The main reasons for utilizing self-compacting concrete can be summarized as follows:

1. To shorten construction period.
2. To assure compaction in the structure; especially in confined zones where vibrating compaction is difficult.
3. To eliminate noise due to vibration (effective especially at concrete product plants).

A mix proportioning system for SCC was proposed by Ozawa [3]. In this system, the coarse aggregate and fine aggregate contents are fixed and self-compatibility is to be achieved by adjusting the water /powder ratio (w/p) and super-plasticizer dosage. The coarse aggregate content in concrete is generally fixed at 50 percent of the total solid volume, the fine aggregate content is fixed at 40 percent of the mortar volume and the w/p ratio is assumed to be 0.9-1.0 by volume depending on the properties of the powder and the super plasticizer dosage. The required w/p ratio is determined by conducting a number of trials. Other mix designs for SCC were developed by means of trial mixes based on guidance given by either the European federation (EFNARC) or the American concrete institute (ACI) [5,6].

Bosiljkov [7] has carried out a study on SCC with poorly graded aggregate and high volume of limestone as filler (in the range of 47 to 49% of the mass of powder), a high paste content of (in the range of 891 to 906 kg/m3 of mix, i.e. 41.3 to 42.8 % by the volume of mix) due to the poorly graded coarse aggregates, the lower w/p ratio (in the range of 0.22 to 0.25 by mass), a constant optimum dosage of super plasticizer (0.6% by mass of powder), and a viscosity agent (30 to 35% by the mass of water). The results obtained indicated that finer and better-graded limestone dust significantly increases the deformability of the paste and it also appeared that the addition of filler improved the 28-day compressive strength of concrete mixes besides the required self-compacting properties.This paper describes a procedure specifically developed to achieve self-compacting concrete. In addition, the test results for acceptance characteristics for self-compacting concrete such as slump flow, J-ring, V-funnel, U-box and L-Box are presented. Further, the strength characteristics in terms of compressive strength for 28-days are also presented.

Materials used

Cement

For all mixes in this research, Ordinary Portland Cement Type I meeting (ASTM 150) manufactured by Libyan cement company was used in concrete mixes. Its specific gravity was 3.13. Its chemical composition is shown in Table I.

Limestone Powder

Lime stone powder as filler (in the range of 0 to 50% of the mass of powder) was used. It was imported from Libyan plants and its specific gravity of 2.71. The chemical composition of Limestone powderis given in the Table I, and it is denoted in this paper as LSP.

Table I. Chemical composition of cement and lime stone powder

The Compound	Percent by weight (%)	
	Cement	LSP
Calcium Oxide (CaO)	62.7	52.35
Silicon Dioxide (SiO_2)	20.60	0.45
Aluminum Oxide(AL_2O_3)	4.90	0.33
Magnesium Oxide(MgO)	3.10	1.05
Sulphur Trioxide (SO_3)	2.80	0.04
Ferric Oxide (Fe_2O_3)	2.70	0.14
Potassium Oxide(K_2O)	0.8	0.02
Sodium Oxide (Na_2O)	0.23	0.06
Loss on Ignition (L.O.I.)	-	45.15

Aggregates

locally available natural sand with 4.75 mm maximum size was used as fine aggregate, having specific gravity, fineness modulus and absorption capacity as given in Table II. Crushed stone with 19 mm maximum size having specific gravity, water absorption ,unit weight, impact value, crushing value and angularity number as given in Table II was used as coarse aggregate. Both fine aggregate and coarse aggregate conformed to BS and ASTM Standard specifications [8, 9]. Grading-curves for both fine and coarse aggregate are presented in Figure 1 and Figure 2.

Table II. Fine and coarse aggregate properties

Type of Aggregate	Property	Test Procedure	Value
Fine Aggregate	Specific gravity	ASTM C128	2.58
	Absorption capacity	ASTM C128	0.4%
	Fineness Modulus	ASTM C 33	2.72
Coarse Aggregate	Specific gravity	ASTM C 127	2.56
	Water Absorption	ASTM C 127	2.15%
	Bulk Density	ASTM C 29 / 29M	1419.45 kg/m^3
	Angularity Number	BS 812 : Part 1	6.1
	Impact Value	BS 812 : Part 3	24.13%
	Crushing Value	BS 812 : Part 3	29.3 %

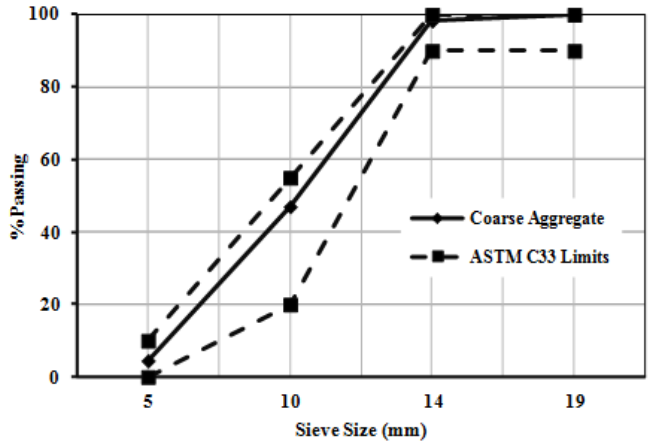

Figure 1. Grading curves of coarse aggregate

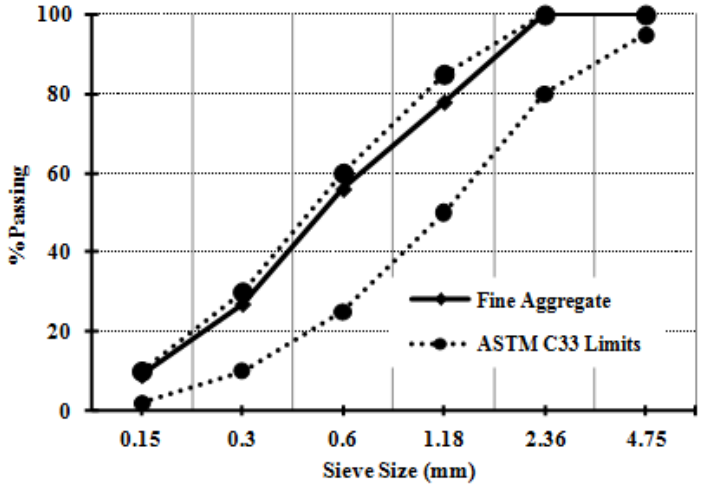

Figure 2. Grading curves of fine aggregate

Admixtures

A visco-crete 5400 based super-plasticizer complying with ASTM C- 494, Type G and F, was used.

Test Methods

Self- Compacting Concrete is characterized by filling ability, passing ability and resistance to segregation. Many different methods have been developed to characterize the properties of SCC. No single method has been found until date, which characterizes all the relevant workability aspects, and hence, each mix has been tested by more than one test method for the different workability parameters. Typical acceptance criteria for SCC as described by EFNARC [5, 10] are presented in Table III.

Table III. Acceptance criteria for SCC [5]

The method	units	values range	
		minimum	maximum
Slump flow by Abram's cone	mm	650	800
T50cm Slump flow	second	2	**5**
J-ring	mm	0	10
V-funnel	second	6	12
Time increase V-funnel at T_5 min	second	0	+3
L-box ($h_2.h_1$)	-	0.8	1.0
U-box (h_2-h_1)	mm	0	30

Mixing procedure

All Concrete batches were prepared in rotating drum mixer following the EFNARC trial guidance [5]. First, the aggregates are introduced and then one-half of the mixing water was added and rotated for approximate two minutes. Next, the cement, most manufacturers recommend at least 5 minutes mixing upon final introduction of admixtures. Once, the mix was determined to have sufficient visual attributes of SCC, the rheological tests were performed in quick succession. Typically, the order of testing employed was as follows:

- U-box (height of concrete in each compartment)
- V-funnel (time to empty).
- L-Box (T20, T40 and heights at 20 and 40cm).
- Flow Test.
- Density (Unit weight).
- Ring test.
- Air Determination (using pressure meter).
- Casting of Specimens

After the flow test was conducted, concrete's visual stability index (VSI) was determined. Criteria used for VSI rating is presented in Table IV as described by ASTM (C16111), [11].

Table IV. Visual stability index (VSI) rating criteria, [11]

VSI	Criteria
0	No evidence of segregation in slump flow patty, mixer drum or wheelbarrow
1	No mortar halo in slump flow patty, but some bleeding on the surface of concrete mix drum or wheel barrow
2	A slight mortar halo (<3/8in (10mm)) in slump patty and noticeable layer of mortar on the surface of resting concrete in mixer
3	Clearly segregating by evidence of large mortar halo(>3/8in (10mm)) and a thick layer of mortar and bleed water in the surface of resting concrete

Experimental Program

Eighteen trial mixes were prepared by varying the lime stone content and w/p ratio. Six levels of the lime stone : from 0% to 50% step 10% kg/m^3, three levels of water to powder ratio : 0.3, 0.34,0.37, and super plasticizer (1.15% by mass of powder) were used for preparing and testing the eighteen trial mixes. For each trial mix, a constant powder content: 550 (kg/m^3) and a constant fine to total aggregate ratio: 0.525 (by mass) of concrete were taken. Parameters of the trial mixes are presented in Table V.

Table V. Parameters of trial concrete mixes

Parameter Studied	No. of levels	Levels
Sand to total aggregate ratio	1	0.525
Powder content	1	550 kg/m^3
w/p ratio	3	0.3, 0.34, 0.37
LSP substitution	6	0%, 10%, 20%, 30%, 40 %, 50%

Tables VI summarize the results of rheological test performed on these 18 mixes. Mixes from 0% LSP to 10% LSP completely failed, i.e. a SCC type concrete could not be obtained within the set parameters especially within dosage limits. Mixes from 20% LSP to 30% LSP failed certain tests (U-box and/or L-Box) and were abandoned from further testing. Note that for many of these mixes, multiple batches were prepared to optimize the admixture dosages. Careful study of the data clearly reveals the importance of all two factors studied, namely, w/p ratio and LSP substitution. The success of achieving SCC type concrete is highly dependent on

these factors. LSP has general tendency to improve or enhance SCC type properties. Generally is improving the slump flow time, reducing air content, improving performance especially in U-box and L-box. It was observed that below 30% LSP for (0.3) w/p, below 20% lime stone for (0.34) w/p and below 10% lime stone for 0.37 w/p one or more attributes of SCC was not accomplished according to EFNARC acceptance criteria. For these mixes, the super-plasticizer (HRWR) dosage was incrementally increased and even exceeded beyond the recommended limits but without success. Lime stone has general tendency to improve SCC rheological properties.

Table VI. Rheological test results

Mix ID		Air	Unit weight	Slump Flow	T50	U-Box Index	L-Box Index	V-Funnel	J-Ring	VSI Index	f_c`
w/p	LSP %	(%)	(Kg/m$^{3)}$	(mm)	(Sec)			(Sec)	(mm)		(MPa)
0.3	40	5	2277	650	3	0.96	0.81	6	585	1	37.53
	50	5	2309	650	4	0.87	0.89	10	555	2	38.65
0.34	40	2	2222	660	4	0.98	0.94	5	570	1	34.22
	50	2.5	2269	730	6	1	0.85	6	610	1	31.69
0.37	20	3.5	2307	800	8	1	1	10	630	2	31.22
	30	3	2309	750	2.4	1	0.86	6	730	3	32.11
	40	4	2326	740	2	1	0.78	7	720	2	28.14
	50	4	2386	800	2	1	1	5	790	2	25.69

Results and Discussion

As shown in Figure 3 and Figure 4, the U-box index and L-Box index correlated well and was observed that mixes with U-Box index of 1 (i.e., when it self levels), it will pass other tests easily. It is the investigators opinion that U-box and L-box can adequately measure the blocking resistance of SCC and these test could be adopted “as-is” to measure blocking ability of SCC. As for slump cone test to measure the spread time (T-50) and slump spread is concerned, the test can be performed with either the slump cone inverted or traditional (upright) way. Inverted cone offers additional advantage that a single operator can perform this test.

To study if there is a difference between these two alternatives, all mixes were tested in both configurations. It was observed that these two methods provide similar results, especially for a mix that will pass the other tests such as U-box and

L-Box. From the rheological point of view, a Lime stone content of 40% should be recommended. Figure 5 show the relationship between cylinder compressive strength of 28 days and w/p ratios at lime stone percentage of 40% and 50%. Comparable results of strength observed and general typical trend of w/p ratio and strength obtained.

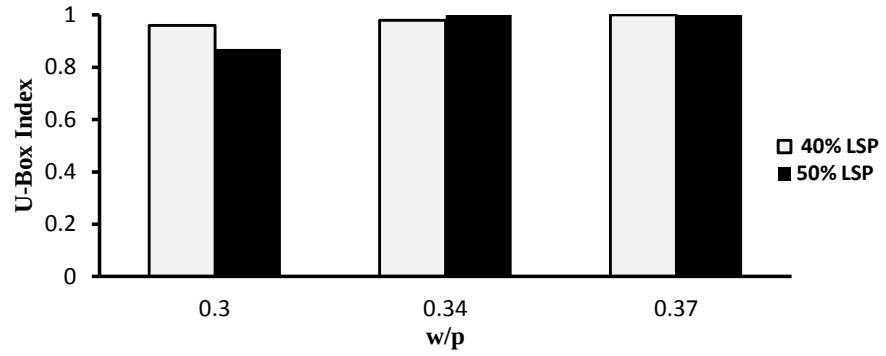

Figure 3. U-Box index and w/p ratio relationships

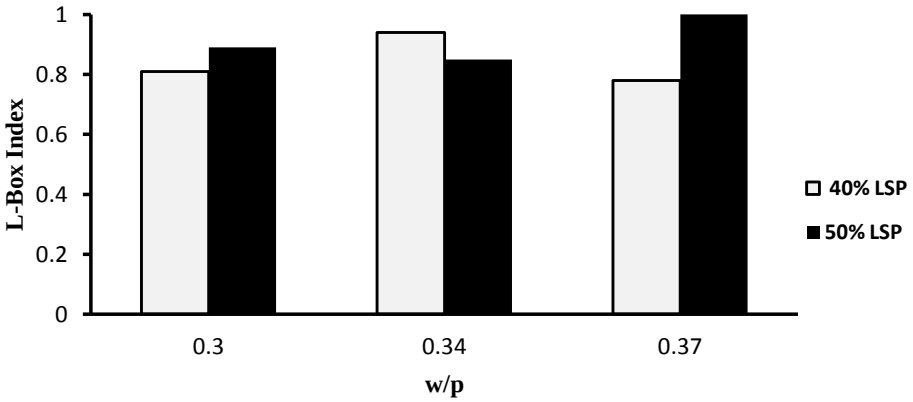

Figure 4. L-Box index and w/p ratio relationships

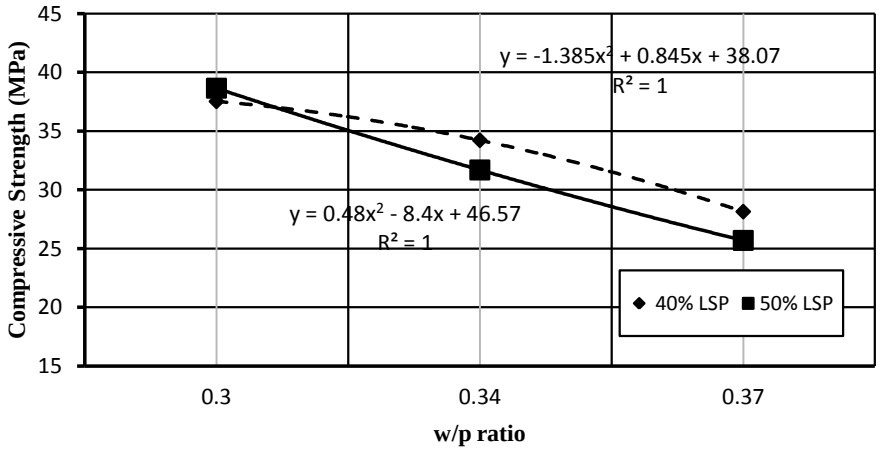

Figure 5. Compressive srength and w/p ratio relationships

Concusions

1. Lime stone substitution generally results in favorable outcomes.
2. A 40% replacement of cement with Lime stone resulted in consistently better VSI rating for the mixes studied.
3. If a concrete mix self-levels in a U-box (U-box index =1), it will generally pass all other tests. This is due to fact that in the U-box the concrete has to move against gravity versus flowing horizontally in the L-box.
4. Concrete with VSI rating of 2 or more must be rejected. Concrete with VSI of 2 or more will clearly show the halo of mortar at the periphery of the spread concrete indicating segregation potential.

References

1. Bartos, J. (2000). *Measurement of key properties of fresh self-compacting concrete*, CEN/PNR Workshop, Paris.
2. Okamura, H. (1997). *Self-Compacting High-Performance Concrete*, *Concrete Int.*, vol. 19, n.7, pp. 50-54.
3. Ozawa, K., Maekawa, K., Kunishima, M. and Okamura H.(1989). *Development of High Performance Concrete Based on the Durability Design of Concrete Structures*, Proceedings of the Second East-Asia and Pacific Conference on Structural Engineering and Construction (EASEC-2), Vol. 1, pp. 445-450.
4. Ferraris, C. F., Brower, L., Daczko J. and Ozyldirim, C. (1999). *Workability of Self-Compacting Concrete*, Journal of Research of NIST, Vol. 104, n.5, pp. 461-478.
5. EFNARC, (2005). *Specifications and Guidelines for Self-Compacting Concrete*, EFNARC, UK (www.efnarc.org), pp. 1-32.

6. American Concrete Institute (ACI), (2007). ACI-237R. *Self-Consolidating Concrete*, pp. 1- 31.
7. Bosiljkov, V.B. (2003). *SCC Mixes With Poorly Graded Aggregate and High Volume of Limestone Filler*, Cement and Concrete Research, Vol. 33, n. 9, pp. 1279-1286.
8- American Society of Testing and Materials (ASTM), (1997)-C33. *Specification for Concrete Aggregates.* American Society for Testing and Materials, Philadelphia, Pennsylvania, USA, pp. 1-29.
9. British Standard Institution: BS 882, (1992*). Testing Aggregates: Specification for Aggregate From Natural Sources for Concrete*. BSI, London.
10. Abdelgader H. S, Elbajegni S. A., and Elwefati A. M. (2014). *Mix Designs of Self Compacting Concrete Using Local Materials. CPI-Concrete Plant International* http://www.cpi-worldwide.com/en/journals/artikel/33608
11- American Society of Testing and Materials (ASTM), (2014)-C1611M. *Standard Test Method for Slump Flow of Self-Consolidation Concrete.* American Society for Testing and Materials, Philadelphia, Pennsylvania, USA, pp. 1-20.

Influences of Nano Effects on the Flow Phenomena of Self-Compacting Concrete

Wolfram Schmidt, Luciana Weba, Dorothee Silbernagl, Berta Mota, Patrick Höhne, Heinz Sturm, Jutta Pauli, Ute Resch-Genger and Gabriele Steinborn

Bundesanstalt für Materialforschung und-prüfung, 12205 Berlin, Germany

Abstract Chemical admixtures like superplasticisers or stabilising agents are of ever increasing importance for modern concrete technology. They liberate the workability of concrete from its dependency on water content, and thus, open the gate towards innovative and future oriented concrete technologies such as self-compacting concrete. Meanwhile admixtures have become common practice in concrete technology, but the understanding of these highly complex polymers in the entire concrete system lags far behind their application. Due to its complex time-dependent, multi-phase and multi-scale behaviour, flowable concrete systems are highly complicated and cannot be described comprehensively by simple models. It is therefore extremely challenging to identify the relevant parameters that predominantly control flow phenomena on different size scales, since these may occur on any scale between the nano scale (e.g. superplasticizer adsorption) and macro scale (e.g. grading of the aggregates). The present study discusses fundamental mechanisms at the interface between particle or hydrate surfaces and the fluid phase at a very early stage of concrete formation, and links these effects to macroscopic flow phenomena. Methods are discussed that appear promising interdisciplinary tools for enhancement of the understanding of the relevant interactions that are responsible for the macroscopic flow of flowable concrete.

Keywords: *Adsorption, analytics, hydration PCE, rheology*

Introduction

Coarsely dispersed flowable cementitious systems are highly complex. The reason is that modern concrete is considered to be a five component system consisting of cement, water, sand and aggregates, additions, and admixtures, which mutually interact with each other [1]. Changes in one parameter automatically yield effects on the other parameters and often a changed parameter is not automatically the root cause for the respective performance change.

Table I. Dimensions at which effects on rheological properties occur

	Effect's impact on observation scale				
	Solution and colloid	Particle-solution interface	Finely dispersed system	Dispersed particle system	Coarsely dispersed system
	< 1000 nm	-	< 200 µm	< 4-5 mm	< 8-32 mm
Effect	Ionic content, ionic strength				
	Surface chemistry				
	Surface charges and particle morphology				
	Time dependent hydration				
	Selective adsorption of polymers and ions				
	Competitive adsorption of polymers and ions				
	Different charges of particles and surface areas				
	Time dependent hydration				
	Solid volume fraction and air pore content and distribution				
	Interactions between different admixtures (e.g. starch and polycarboxylates)				
	The enormously wide band of particle sizes from nm to cm				
		Finest particle size distribution			
			Coarse particle size distribution		
			Particle lattice and density differences		

For most scientific and engineering applications, concrete has to be simplified. Often relatively "simple" Bingham behaviour can be assumed, though in the finer systems (e.g. pore solution or binder paste) the behaviour can be more complicated. This is why typical equations that describe the flow performance consider concrete as a two phase fluid consisting of a fluid and a solid phase. Based on the Einstein equation researchers have developed a number of equations to predict the viscosity of more concentrated suspensions, the mostly applied of which is the Krieger-Dougherty equation [2]. Recently, also more complex equations have been developed and applied [3-5]. All equations are based on considerations about the solid volume fraction and the fluid viscosity. In order to cope with the time dependent performance change, sometimes a thixotropy term is added [6].

However, neither the solid volume fraction nor thixotropy can fully describe the effects within a flowable concrete system at fresh state. For example, a flowable system changes its performance significantly based on the adsorption of superplasticiser, though they do not impact on the volumetric mixture composition, and thixotropy is only one out of a number of phenomena responsible for time dependent changes of the rheology. The ongoing hydration changes the morphology of the particles as well as the solution chemistry irreversibly.

For the understanding of influences that can affect the flow performance of self-compacting concrete, it is important to look at all dimensional scales at which these

effects take place and to evaluate the impact of this effect for the performance on macroscopic scale. Hence, the flow properties of concrete depend upon but are not inevitably limited to the items listed in Table 1. This paper provides an overview of several effects that need to be taken into account for better understanding of the rheology of SCC. This overview that does not make the claim to be complete is given within the framework of the interdisciplinary research project M-Flow on the influence of nano- and micro effects with impact on the macroscopic behaviour.

Effects on the nano scale with impact on the macroscopic flow performance

Cement hydration

Ordinary portland cement is a highly heterogeneous material. During the processing at approximately 1450 °C the solid impure tricalcium silicate phases and the impure dicalcium silicate phases are sintered into the interstitial aluminate and ferrite phases. During grinding gypsum is added to the clinker as set retarder. Instantly upon addition of water first complex reactions occur in parallel, the most prominent of which are the dissolution of alite and sulphate as well as the formation of first reaction products which appear in the sizes of a few to a few hundred nm, namely a gel like calcium silicate hydrate layer (C-S-H) as well as portlandite and ettringite (Fig. 1). The entire early hydration is driven by alternating dissolution and precipitation processes, in which in an alternating way the undersaturation of the pore solution is the driving force for the dissolution of the next soluble clinker phase and the resulting supersaturation of the pore solution is the driving force for the precipitation of new hydration phases, which again cause undersaturation in the solution [7]. After an intense reaction during the first minutes the process slows down significantly during the so called dormant period. The dormant period in which the cement paste is still plastic typically ends after a few hours when a massive formation of newly formed C-S-H takes place. However, also during the dormant period the hydration goes on slowly but steadily.

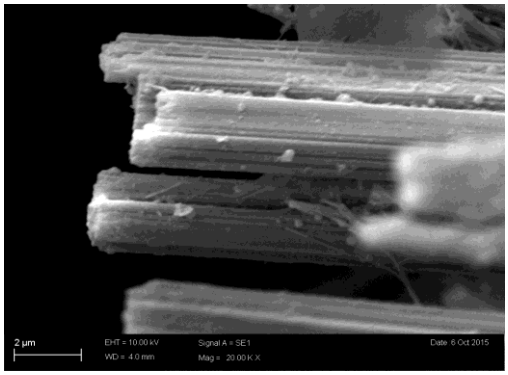

Figure 1. ESEM picture of needle like ettringite

The most prominent reaction with regard to the workability is the reaction of sulfate and calcium aluminate to form mainly ettringite (Fig. 1), which significantly changes the morphology of the particles and forms bridges between the particles into the solution. This leads to a steady loss of workability, so that typically the point in time at which concrete can be considered as no longer processible already starts within the dormant period [8]. The first ettringite crystals have lengths of 300 to 500 nm and diameters between 50 to 250 nm [9]. The ettringite crystals do not change their morphology significantly over the course of the early hydration but their formation is determined by the solubility of the set retarder and calcium aluminate availability, and thus depends strongly upon the cement's chemistry, the environmental temperature, the presence of supplementary cementitious materials (SCM) and admixtures

Superplasticizer adsorption

One of the most relevant constituents to provide flowable performance for SCC is the superplasticizer. Today, typically comb type polymers are used, the majority of which are polycarboxylate ethers (PCE). Their sizes in solution range between few and several nm. Due to complexation with calcium ions in the cementitious pore solution, their appearance in a cementitious system may vary greatly from the appearance in aqueous system. Fig. 2 shows samples of PCEs in water and pore solution compared to lignosulfonate and two types of polysaccharides.

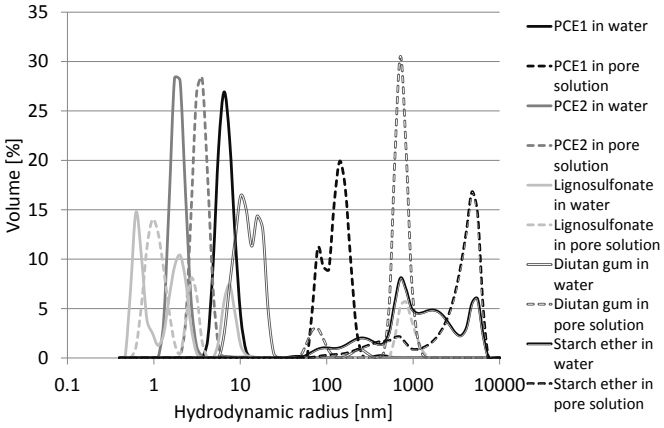

Figure 2. Hydrodynamic radii of different admixtures for SCC in water and in pore solution of a cement paste with w/c = 0.5

The mode of operation of PCE is based on the adsorption on particles, clinker phases and hydrates on the particle surfaces as well as in solution [8, 10, 11]. Compared to other superplasticizers, their charges are relatively low. Their dispersion effect is considered to be mainly steric [8]. PCEs are typically added in relatively small amounts (solid content between 0.05% and 0.2% of the total

concrete's mass) so that their effect on the solid volume fraction is negligible. Nevertheless, their influence on the flow performance is enormous. PCEs mainly affect the yield stress of SCC without significant influence on the plastic viscosity [8, 12-14]. Despite the nano scale at which the adsorption of PCE takes place, it affects the macroscopic scale significantly. Fig. 3 illustrates the wide band of dimensions that need to be observed to understand, why aggregates are homogenously transported with in concrete, or why they probably segregate.

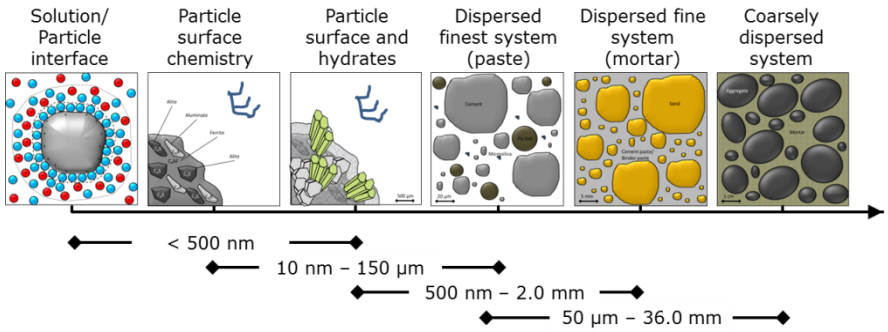

Figure 3. The ionic composition of the pore solution and PCE adsorption affect the flow of aggregates in concrete

Superplasticizer-cement hydration interaction

Since PCEs need to be adsorbed to become effective, their performance depends strongly on the cement hydration. In return, their presence also interferes with the hydration. PCEs are adsorbed on clinker and hydration phases. It is assumed that they preferably adsorb on ettringite [10] but due to the high ionic content in the pore solution it is likely that they also tend to adsorb on other phases [15]. Due to their anionic backbone, PCEs compete with sulfate ions for adsorption. The higher the charge density of PCE, the better they can be adsorbed, but due to the ongoing hydration of cement, the performance of PCE can never be uncoupled from time effects. PCEs can thus be distinguished according to their adsorption behaviour:

- Rapidly adsorbing PCEs typically provide higher charge densities. Due to the rapid adsorption, they have a good plasticizing effect, but since they are consumed quickly, the flow retention is short.
- Slowly adsorbing PCEs typically provide lower charge densities. Due to the rapid adsorption, they have a good plasticizing effect, but since they are consumed quickly, the flow retention is short.

The interaction between the cement hydration and the PCE thus also defines the great differences between normal concrete and SCC in terms of rheology. The rheology of normal concrete is mainly determined by effects induced by the ongoing formation of hydration products. For SCC, where typically high amounts of PCE are required, the rheology is also determined by the cement hydration in the

same way as normal concrete, but in parallel the ongoing hydration affects the performance of the superplasticizer. This is illustrated in Fig. 4. This cement superplasticizer interaction, which is an interaction between polymers of several nm and crystals of a few hundred nanometres is eventually responsible for the transportation of aggregates in the order of magnitude of centimetres. This means, the root cause for a rheological effect in SCC may be smaller than the finally affected constituent in the order of magnitude of 10^7 (Fig. 3).

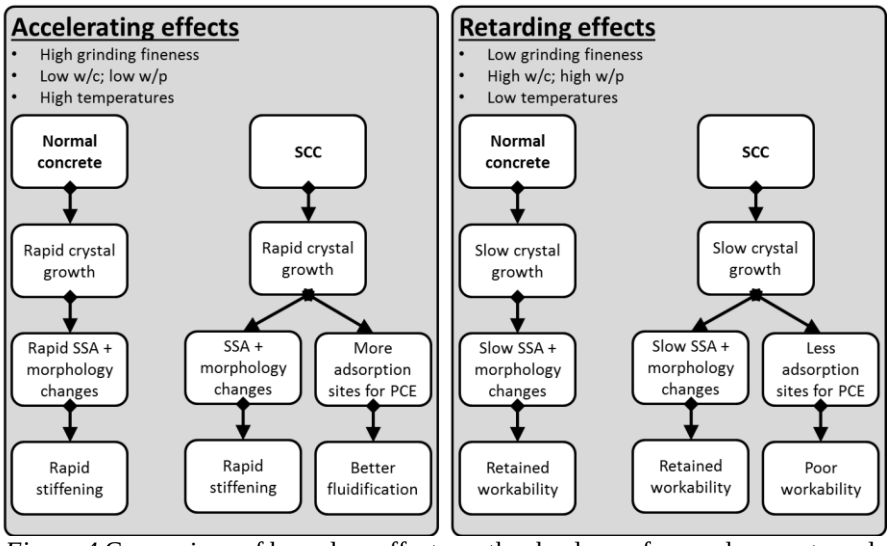

*Figure 4.*Comparison of boundary effects on the rheology of normal concrete and SCC due to the presence of PCE

Additions, SCMs and admixtures

Additions or SCMs act as fillers for voids between cement particles or replacement for cement. Hence, they can change the morphology and surface charges within the binder paste, they can offer additional adsorption sites, and depending upon their composition and solubility of phases, they can interfere with the pore solution's composition, thus strongly modify the performance of PCE within the binder paste.

Admixtures are required to tailor the concrete properties, e.g. stabilising agents, air entraining agents, or retarders. They can strongly interact with the chemistry of the fresh system and the ionic pore solution [12, 16]. In SCC often stabilising agents based on polysaccharides are added in order to enhance the robustness and to modify the viscosity. As can be found in Fig. 2, these polymers are significantly larger than PCEs. Nevertheless, they were found to affect the cement hydration characteristics at fresh state as well as the performance of PCE [8, 17] and that they mutually interact with sand particles up to diameters of 4 mm at fresh state [18].

Consequences

From Table 1 it becomes obvious that the major challenge in understanding the rheology of concrete is the fact that effects occur time dependent and on multiple scales affecting multiple phases within the system. Furthermore, the overlapping of effects increases the intricacy of understanding relevant parameters fundamentally rather than phenomenologically. Nevertheless, it is of utmost importance to increase the knowledge in the field and to master the step from pure physical model approaches with limited range of validity and a multitude of boundary limitations towards more practical, modular solutions with relevance for real applied technologies.

Experimental methods and complexity of model systems

The highest challenge is that SCC is time dependent, multi-phase system, where effects take place on multiple scales. New findings can be expected if interdisciplinary research is conducted and a variety of experimental methods is combined.

Promising approached can be expected from nuclear magnetic resonance spectroscopy, and Raman and infrared spectroscopy. These methods help understanding atom interactions and crystal structures and compositions. Fluorescence and absorption spectroscopy help to better visualise polymers and phase changes in complex systems. In combination with in-situ X-ray diffraction measurements and atomic force microscopy a clearer picture of effects and processes at particle and crystal interfaces can be created. In addition atomic force microscopy can be used to observe the nano and micro rheology. However, the most challenging task is the creation of a link to the µm and mm scales.

The link can be made by environmental scanning electron microscopy to visualise characteristic time steps during the early period of hydration. Dynamic light scattering can amend the observations by providing information about adsorption and agglomeration as well as by being able to determine zeta potential changes due to varying influences such as pH or charged polymers. Rheometers can close can close the gap between micro scale and macro scale. However, evaluation on the real scale is required.

However, for the more fundamental understanding of effects at solid fluid interfaces and for the understanding of early effects on the macroscopic rheology, it is getting obvious that model systems need to be applied. The choice of adequate model systems is challenging, since a compromise between necessary simplification and required complexity has to be found. The main challenges arise from the complexity of the pore solution. Fig. 5 gives an example on how strongly the composition of the pore solution affects the rheology. Limestone filler and OPC

were mixed with water, at volume fractions of 0.52 and 0.41, respectively. For the limestone filler dispersions water was also replaced by calcium hydroxide and pore solution extracted from OPC water systems with w/c = 0.5. The high content of cations and anions in the pore solution increases the attractive forces in the system with pore solution, however upon addition of PCE the yield stress decreases dramatically. The system with calcium hydroxide behaves partly overlaps with the cement system, but the yield stress at maximum PCE adsorption remains higher than in all other systems, which emphasizes the enormous importance of the ionic content of the dispersion.

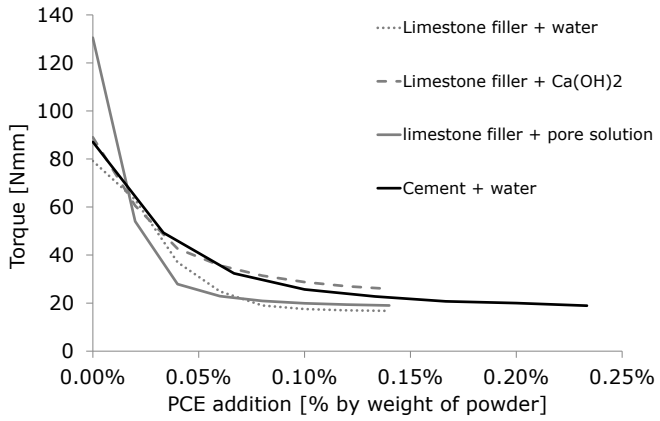

*Figure 5.*Effects of PCE on the torque of different model systems at rpm 240

Conclusions

Today, chemical admixtures like superplasticisers, e.g. based on polycarboxylates, phosphonates, or naphthalene sulphonates are extremely important for modern concrete technology as well as other rheology modifying admixtures like polysaccharides. These agents have meanwhile become common practice in concrete technology, but the understanding within the entire system lags far behind their application. This calls for more interdisciplinary research that connects researchers from natural sciences and engineering and that combines fundamental analytic research methods with applied and phenomenological research methods.

This paper provides a brief overview of the complexity of the self-compacting concrete system in its entirety, and suggests analytical method combinations that seem to be promising in future to gain depper insight into processes that take place on a nano scale but eventually influence phenomena that can be observed on macroscopic scale. Future research will provide a more comprehensive picture of concrete at a higher level of theory that is required to spark fundamental innovation

in concrete technology and to help managing the step from fundamental scientific understanding of individual effects to engineering applications.

References

[1] W. Schmidt, M. Sonebi, H. J. H. Brouwers, H.-C. Kühne, and B. Meng, "Rheology Modifying Admixtures: The Key to Innovation in Concrete Technology – A General Overview and Implications for Africa," *Chemistry and Materials Research*, vol. 5, pp. 115-120, 2013.

[2] I. M. Krieger and T. J. Dougherty, "A Mechanism for Non-Newtonian Flow in Suspensions of Rigid Spheres," *Transaction of the Society of Rheology*, vol. 34, pp. 137-152, 1959.

[3] A. Lemaitre, J. N. Roux, and F. Chevoir, "What do Dry Granular Flows Tell us About Dense Non-Brownian Suspension Rheology?," *Rheologica Acta*, vol. 48, pp. 925-942, 2009.

[4] S. Mansoutre, P. Colombet, and H. Van Damme, "Water Retention and Granular Rheological Behavior of Fresh C3S Paste as a Function of Concentration," *Cement and Concrete Research*, vol. 29, pp. 1441-1453, 1999.

[5] N. Roussel, A. Memaitre, R. J. Flatt, and P. Coussot, "Steady State Flow of Cement Suspensions: A Micromechanical State of the Art," *Cement and Concrete Research*, vol. 40, pp. 77-84, 2010.

[6] N. Roussel, "A thixotropy model for fresh fluid concretes: Theory, validation and applications," *Cement and Concrete Research*, vol. 36, pp. 1797-1806, 2006.

[7] K. L. Scrivener and A. Nonat, "Hydration of cementitious materials, present and future," *Cement and Concrete Research*, vol. 41, pp. 651-665, 2011.

[8] W. Schmidt, "Design concepts for the robustness improvement of self-compacting concrete - Effects of admixtures and mixture components on the rheology and early hydration at varying temperatures," 193, University of technology Eindhoven, The Netherlands, 2014.

[9] J. Stark, B. Möser, and A. Eckart, "Neue Ansätze zur Zementhydratation, Teil 2," *ZKG International*, vol. 54, pp. 52-60, 2001.

[10] J. Plank and C. Hirsch, "Impact of zeta potential of early cement hydration phases on superplasticizer adsorption," *Cement and Concrete Research*, vol. 37, pp. 537-542, 2007.

[11] R. J. Flatt and Y. F. Houst, "A simplified view on chemical effects perturbing the action of superplasticizers," *Cement and Concrete Research*, vol. 31, pp. 1169-1176, 2001.

[12] W. Schmidt, H. J. H. Brouwers, H.-C. Kühne, and B. Meng, "Influences of superplasticizer modification and mixture composition on the performance of self-compacting concrete at varied ambient temperatures," *Cement & concrete composites*, vol. 49, pp. 111-126, 2014.

[13] O. Wallevik, "Rheology – A New Dimension in Concrete Technology," in *16th International Conference on Building Materials - ibausil*, Weimar, Germany, 2006, pp. 1417-1430.

[14] N. Roussel, C. Stefani, and R. Leroy, "From mini-cone test to Abrams cone test: measurement of cement-based materials yield stress using slump tests," *Cement and Concrete Research*, vol. 35, pp. 817-822, 2005.
[15] D. Lowke and C. Gehlen, "Effect of Pore Solution Composition on Zeta Potential and Superplasticizer Adsorption," in *ACI Special Publication-302 Eleventh International Conference on Superplasticizers and Other Chemical Admixtures in Concrete*, V. M. Malhotra, Ed., ed, 2015, pp. 253-264.
[16] W. Schmidt, H. J. H. Brouwers, H.-C. Kühne, and B. Meng, "The working mechanism of starch and diutan gum in cementitious and limestone dispersions in presence of polycarboxylate ether superplasticizers," *Applied Rheology*, vol. 23, 2013.
[17] W. Schmidt, H. J. H. Brouwers, H.-C. Kühne, and B. Meng, "The working mechanism of starch and diutan gum in cementitious and limestone dispersions in presence of polycarboxylate ether superplasticizers," *Journal of Applied Rheology*, 2013.
[18] W. Schmidt, S. Peters, and H. C. Kühne, "Effects of Particle Volume Fraction and Size on Polysaccharide Stabilizing Agents," in *ACI Special Publication-302 Eleventh International Conference on Superplasticizers and Other Chemical Admixtures in Concrete*, V. M. Malhotra, Ed., ed, 2015, pp. 39-52.

Optimum Replacement of OPC by Fly Ash and Limestone Powder and their Blends in Self-Consolidating Paste Systems Prepared at Variable Mixing Water Temperatures

Syed Ali Rizwan[1], Abdul Wahab Safdar[2], Imran Ahmed[2] and Thomas A. Bier[3]

1. Professor of Civil Engineering and HoD Structural Engineering Department, NUST Institute of Civil Engineering (NICE), NUST H-12, Islamabad. Email: syedalirizwan@nice.nust.edu.pk
2. Graduate Students, NICE, NUST H-12, Islamabad. abdul.wahab.535@gmail.com, imran.ahmed6000@gmail.com
3. Professor and Chair of Construction Materials Technology, IKGB, TU Freiberg, Germany. Email: thomas.bier@ikgb.tu-freiberg.de

Abstract This research evaluates the properties of thirteen series of Self-Consolidating Paste Systems (SCPSs) containing binary and ternary binders. Fly Ash (FA) and Limestone Powder (LSP) were used separately as mineral admixtures and subsequently in equal mass blends to partially replace OPC within 0 - 40% mass range in SCPSs. Thereafter five optimized formulations of SCPs were subjected to variable mixing water temperature of 10°, 20° and 30°C to know its role in fresh and hardened state properties of SCPSs. FA based SCP systems showed retardation and lower early strengths within first seven days. Thereafter, pozzolanic activity of FA increased to give comparable twenty-eight day compressive strengths to that of control SCP system. Results of limestone powder based SCP systems were other way around; they had higher early strength but relatively lower twenty-eight day strengths. Blended FA and LSP complemented each other to give enhanced flow properties of SCPSs, yielding significantly higher twenty-eight days compressive strengths. It is concluded that OPC can be replaced up to 20% of its mass when limestone powder and fly ash are used separately in SCPs while their blends can repalce OPC up to 30% in SCPs. Optimum mixing water temperature seems to be around 20°C at which better results in terms of water demand, super-plasticizer demand and strength were obtained.

Keywords: *Self-Consolidating Paste, Portland Cement, Mineral Admixtures, Fly Ash, Limestone Powder, Optimum Replacement, Mixing Water Temperature.*

Introduction

Use of Self-consolidating concrete (SCC) containg mineral admixtures is an indirect way of reducing carbon dioxide footprint [1]. Excellent deformability and high resistance to segregation seem diametric properties of SCC and their balance is required for successful applications [2]. Flow and testing protocols of SCC are important and have been described in detail in literature [3].

SCP systems, in addition to cement and water, contain mineral and chemical admixtures. Secondary Raw Materials (SRMs) or Supplementary Cementitious Materials (SCMs) are the mineral admixtures which may be inert or pozzolanic materials used to partially replace cement in SCC. Some typical blends of SRMs, for example fly ash (FA) and limestone powder (LSP) can produce synergy resulting in enhanced response [4, 5, 6]. The behavior of various SRMs in self-consolidating concrete systems (SCCSs) is described [7-8] while the role of limestone powder on hydration and microstructure of SCC is given in detail elsewhere [9].

However, the role of mixing water temperature has not been extensively reported in literature and this study gives information on this dimension of SCPs and shows that fresh and hardened state properties are greatly influenced by change in mixing water temperature.

Research Significance:

This study aims at determining the optimum replacement level of OPC by FA and LSP as well as their blends in self-consolidating paste systems (SCPs). It also reports the response differences of SCPs prepared with different Mixing Water Temperatures (MWT) so that suitable formulations may be used to make successful SCC after incorporation of aggregate phase in SCPs.

Experimental

Materials:

Lafarge Ordinary Portland Cement, CEM-I 52.5 R conforming to EN 197-1, class F German Fly Ash (FA) and Limestone Powder (LSP) from Margalla Hills, Taxila Pakistan were used. A PCE based powdered super-plasticizer, Melflux 2651-F by BASF was used to achieve the target flow of (30 ± 1) cm measured by Hagerman's cone of 6x7x10 cm^3 dimensions. This target gives good flow indices and shortened flow times enabling better self-consolidation.

Physical and Chemical Characterization of Powders:

X-Ray Fluorescence (XRF) test was used for chemical analysis of the powders. *Figure 1* shows calculation of D_{50} of powders using particle size and cummulative percent passing curve. *Table I* gives the physical and chemical properties of powders.

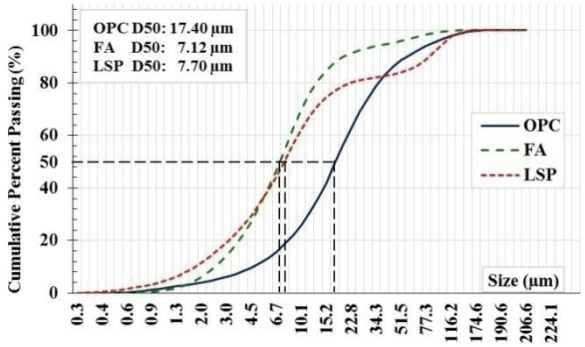

Figure 33. Results of Particle Size Distribution from Laser Scattering Method

Table I. Chemical Composition and Physical Characteristics of OPC and SRMs

Properties / ***Powders***	SiO_2	CaO	Al_2O_3	Fe_2O_3	*LOI*	*Particle Size (D_{50})*	*BET Area (m^2/g)*
OPC	18.92	63.18	5.09	2.27	2.34	17.40 µm	0.882
FA	51.44	4.03	26.13	5.55	2.71	7.12 µm	2.107
LSP	7.07	48.57	2.53	0.88	38.32	7.70 µm	1.968

SCP Mix Formulations:

A total of thirteen SCP formulations with replacement levels of cement up to 40% of its mass by different SRMs and their equal mass blends were investigated. After manual dry mix, mixing water equal to WD of the formulation was added and 60 seconds of slow mixing (145 rpm) was done. The inside of Hobart Mixer bowl was cleaned. Then finally two minutes of fast mixing (285 rpm) was made. 4x4x16 cm^3 specimens were cast, cured and tested as per DIN 196-1. *Table II* gives the details of SCP formulations.

Table II. Mix Formulations of Self-Consolidating Paste Systems studied

Mix Proportion	**ID**	**OPC (wt. %)**	**FA (wt. %)**	**LSP (wt. %)**	**Percent OPC Replacement**
CI-00-WD	Control	100	0	0	0
CI-FA10-WD	F10	90	10	0	10
CI-FA20-WD	F20	80	20	0	20
CI-FA30-WD	F30	70	30	0	30
CI-FA40-WD	F40	60	40	0	40
CI-LSP10-WD	L10	90	0	10	10
CI-LSP20-WD	L20	80	0	20	20
CI-LSP30-WD	L30	70	0	30	30
CI-LSP40-WD	L40	60	0	40	40
CI-FA5-LSP5-WD	FL10	90	5	5	10
CI-FA10-LSP10-WD	FL20	80	10	10	20
CI-FA15-LSP15-WD	FL30	70	15	15	30
CI-FA20-LSP20-WD	FL40	60	20	20	40

Results of SCP Formulations with Mixing Water at 20°C:

Figure 2 gives the Vicat water demand (WD) of powders based on water-cement (w/c) shown above control line and WD in terms of water-powder (w/p) ratio below control formulation line.

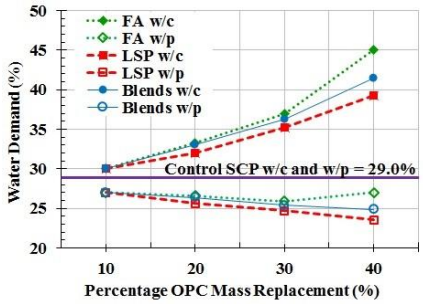

Figure 34. Water Demand (w/c and w/p) of SCP Systems at 20°C MWT

Figure 3 gives the per cent super-plasticizer (SP) demands of SCP systems at 20°C MWT for the flow target of 30±1 cm. The segregation phenomenon was visually observed instead of making V-funnel measurements.

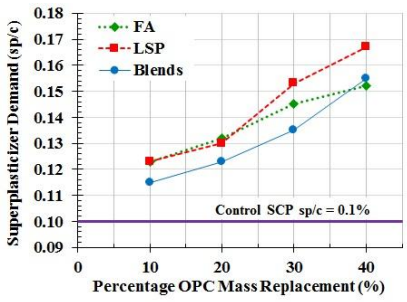

Figure 3. Super-Plasticizer Demand of the SCP Systems at 20°C MWT

Figure 4 gives the Vicat Setting Times and *Figure 5* gives the compressive strengths of SCP formulations at different ages. Data for Control Mix (CI-00) is also shown as solid horizontal lines and vertical box in Figures 4 & 5.

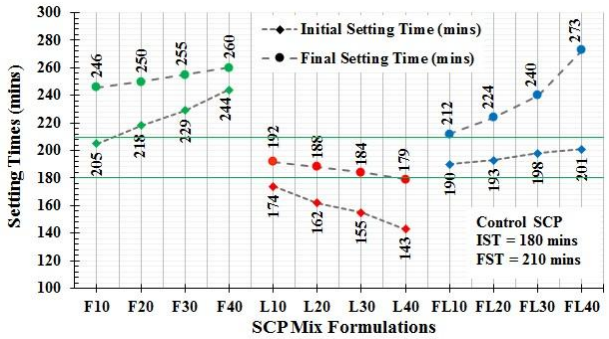

Figure 4. Initial and Final Setting Times of SCP Systems at 20°C MWT

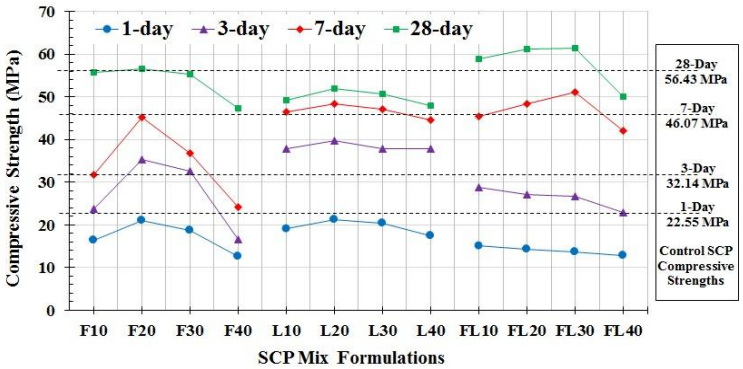

Figure 5. Compressive Strengths of SCPSs at 1, 3, 7 and 28 days of age

Response of Optimized SCPs subjected to Variable Mixing Water Temperatures

Out of thirteen, five optimized formulations giving better flowability and strength indices were subjected to further tests. *Figure 6* gives the water demand of these formulations now subjected to different mixing water temperatures following same mixing regime. *Figure 7* gives the per cent super-plasticizer demand of five SCP formulations made at different mixing water temperatures having same mixing regime. The laboratory temperature and relatively humidity were (20±2) ºC and (40±5) %, respectively.

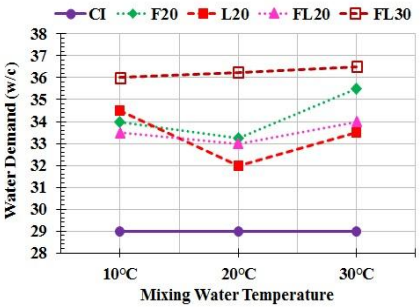

Figure 6. Water Demand (w/c) of SCPs with Variable MWT

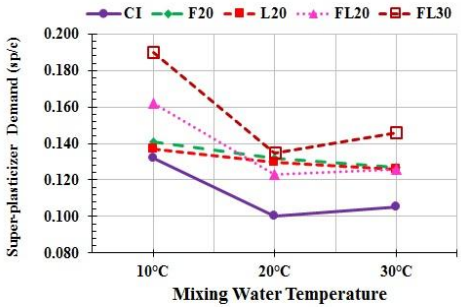

Figure 7. Super-plasticizer Demand (sp/c) of SCPSs with Variable MWT

Figure 8 gives the Vicat final setting times of five formulations made at different mixing water temperatures having same mixing regime.

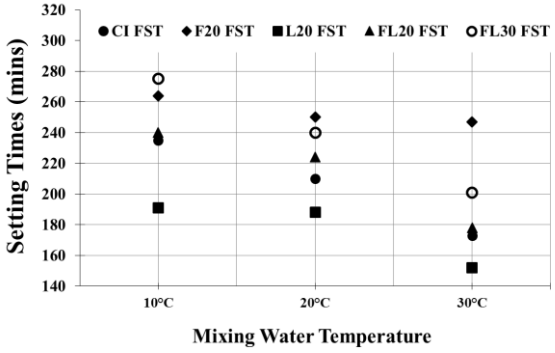

Figure 8. Final Setting Times of SCPSs with Variable MWT

Figure 9 (a, b and c) give the Calorimetric curves of five SCP formulations prepared with mixing water at 10, 20 and 30°C temperature, respectively. Field calorimter shows data from acceleration phase.

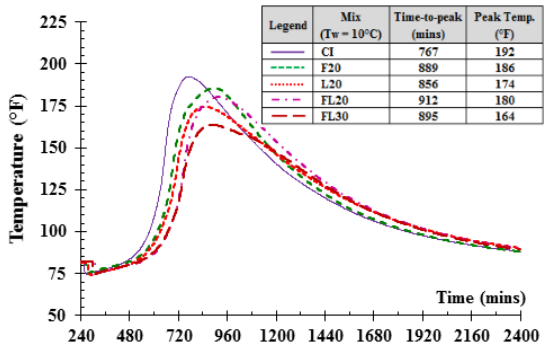

Figure 9(a). Calorimetry of SCPs with Mixing Water at 10°C

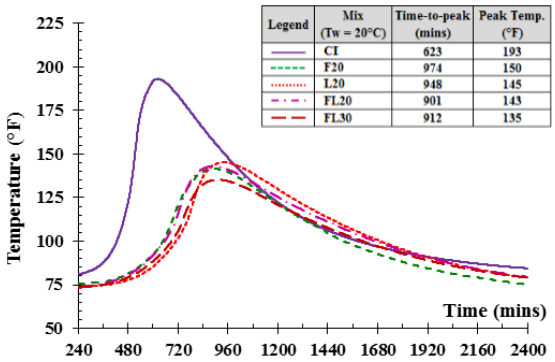

Figure 9(b). Calorimetry of SCPs with Mixing Water at 20°C

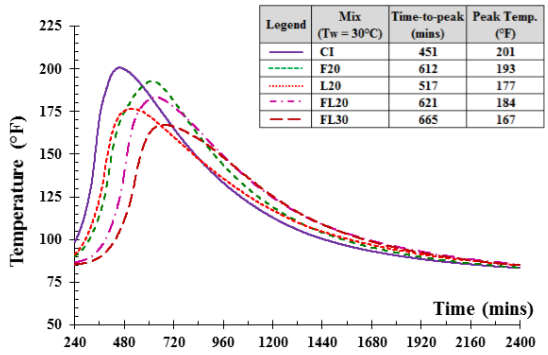

Figure 9(c). Calorimetry of SCPs with Mixing Water at 30°C

Figure 10 shows the 28-day compressive strength results of five optimized SCP systems prepared with variable mixing water temperatures.

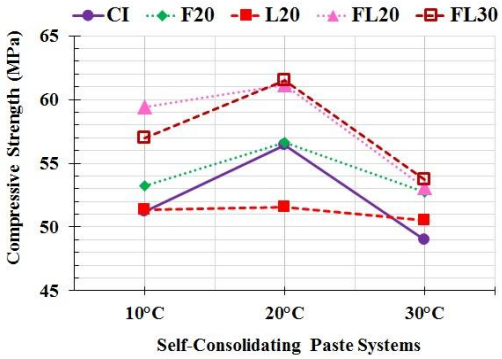

Figure 10. 28-Day compressive Strengths of SCPSs with varying MWT

Table III compares the typical strength-to-cement ratios of five highest strength yielding SCP formulations having SRMs and prepared at optimum 20°C mixing water temperature.

Table III. Strength-to-Cement Ratios of Self-Consolidating Paste Systems

Mix Formulation at 20°C	**CI**	**F20**	**L20**	**FL20**	**FL30**
% wt. OPC/SRM	100	80/20	80/20	80/20	70/30
Compressive Strength (MPa)	56.4	56.7	52.0	61.2	61.5
Strength-to-cement ratio	0.564	0.708	0.650	0.765	0.879

Schutter et al. [10] explain the effect of mineral filler type on the autogenous shrinkage of SCC. However, as construction engineers, mostly it is the overall shrinkage obtained as a result of simultaneously operating mechanisms that is of interest. Figure 11 provides the twenty four hour linear early shrinkage response of the five SCP Systems outlined in Table III using modified German Schwindrinne shrinkage channels.

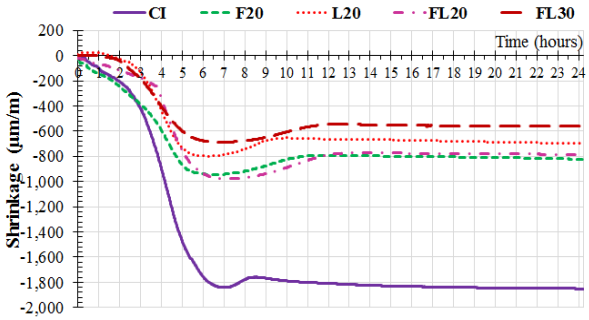

Figure 11. Early Linear Shrinkage Results of Optimized SCP Systems

Discussion

Water Demand of SCPs if calculated on the basis of w/c ratio increases with increase in cement replacement and reverse true when based on w/p ratio. This is because of lower cement in formulations having cement replacement. Moreover, both FA and LSP when replace cement give reduced overall WD due to physical packing, smaller particle sizes and morphology of such SRM particle sizes. SP demand increases with increase in cement replacement. Formulations containing LSP give higher demand especially at 30 and 40% replacement due to increased internal friction. When these SRMs are blended, the SP demand for target flow got lowered except at 40% replacement and seem to be largely governed by LSP characteristics. Generally LSP when incorporated reduces Vicat setting times due to availablility of nucleation sites upon which early preferential precipitation takes place. FA on the other hand retards setting due to its glassy, smooth surface, its carbon content and other factors [11].

Up to 28 days, FA in SCP systems generally gave reduced strength with respect to control formulation, especially at higher replacement levels. The physical filler effect of FA based SCP formulations is dominant during first seven days and optimum replacement level is around 20-30%. LSP in SCP systems reduced the strength beyond 20% repalcement level however their strength up to seven days is better than those with FA due to initial faster hydration of LSP particles. The blends of FA and LSP at 30% combined cement replacement gave optimum SCP strength. Such blends gives higher strength,more than control, beyond seven days.

When five selected SCP formulations were made at different mixing water temperatures, the Vicat WDs of repective system generally increased with increase in mixing water temperature due to accelerated hydration of C_3A and C_3S phases. At 20°C, the water demands were lowest. At both lower and higher mixing water temperatures, it increases. Almost similar trend was observed for SP demand of SCP formulations. Highest SP demand is at lower temperatures probably due to

rather slow activation of SP. Higher mixing water temperature also accelerates the setting of these formulations. Calorimetry data show the exothermic nature of hydration. With higher replacement, peak temperature lowers due to the dilution of cement. The strength comparison is made at 28-days, strength results show that optimum mixing water temperature for achieving higher strength is 20°C. In linear measurements, the most of shrinkage happens near the Final Vicat Setting Time for a typical formulation which may be during 0-5 hours in super-plasticized SCP systems. The swelling/reduction in shrinkage may be attributed to creation of expansive crystals especially Calcium Hydroxide at that particular time shown in shrinkage curves. From volume stability view point FL30 seems to be a good option.

Highest strength-to-cement ratio and least shrinkage is offered by the blended formulation having an equally mixed fly ash and limestone powder replacing thirty percent of cement mass.

Concluding Remarks

It may be said that good self-consolidating concretes can be produced using blended secondary raw materials prepared with optimum 20°C mixing with 20-30 % of OPC mass replacement. The mixing water temperature has a strong influence on both the fresh and hardened state properties of SCP systems.

Acknowledgements

The authors are grateful to DAAD for providing F-Cal 8000 Field Calorimeter, Schwindrine Shrinkage Apparatus and admixtures, used in this study, to NICE/NUST under International Research Project (Kennziffer 54385351).

References

[1] Okamura. H, Ouchi. M. (April, 2003), “Self-Compacting Concrete”, Journal of Advanced Concrete Technology, Vol. 01, No. 1, p. 5-15.
[2] Shindoh. T, Matsuoka. Y. (April, 2003) “Development of Combination-Type Self-Compacting Concrete and Evaluation Test Methods”, Journal of Advanced Concrete Technology, Vol 1, No. 1, p. 26-36.
[3] K.H. Khayat, (June, 1999) “Workability, Testing, and Performance of Self-Consolidating Concrete”, ACI Materials Journal, Title no.96-M43, p. 346-354.
[4] De Weerdt K. et al. (2011), “Synergy between fly ash and limestone powder in ternary cements.” Cement and Concrete Composites 33, p. 30-38.
[5] De Weerdt K. et al. (2011), “Hydration mechanisms of ternary Portland Cements containing limestone powder and fly ash”, Cement and Concrete Research 41(2011), p. 279-291.

[6] Rizwan, S.A, Bier, T.A (2012), "Blends of limestone powder and fly-ash enhance the response of self-compacting mortars", Construction and Building Materials, Vol.27, p. 398-403.
[7] Rizwan S.A, Bier T.A. (2009), "Self-consolidating mortars using various secondary Raw materials", ACI Materials Journal, 106 (1) p. 25-32.
[8] Lothenbach B., Scrivener K. (2011), "Supplementary Cementitious Materials", Cement and Concrete Research, Vol.41, p.1244-1256.
[9] Ye G, Liu X, De Schutter G, Poppe AM, Taerwe L. 2007. "Influence of limestone powder used as filler in SCC on hydration and microstructure of cement pastes." Cement and Concrete Composites 29 (2), p. 94-102.
[10] De Schutter, G, Craeye. B et al. (2010), "Effect of mineral filler type on autogenous shrinkage of self-compacting concrete", Cement and Concrete Research 40 p. 908-913.
[11] Rizwan, S.A and Bier, T.A., "Role of Mineral Admixtures in High Performance Cementitious Systems", 2nd All Russian International Conference on "Concrete and Reinforced Concrete-Development trends", Vol. 3, "Concrete Technology", 5-9 September 2005, Moscow, Russia. pp 727-732. ISBN 5-98580-013-x

Low-pH Cementitious Matrices to Stabilize Cemented Radioactive Wastes

Fodhil Kassimi*, Alain Bilodeau* and Nabil Bouzoubaâ*

* Canmet MINING, Natural Resources Canada, Ottawa.

Abstract The use of low-pH concrete is a relatively new technology to stabilize radioactive wastes. These latter are often stored for a very long term in deep and stable geological clayed formations. The interaction concrete-bentonite most probably leads to concrete degradation and alteration of the clay properties including dissolution of quartz and clay minerals and precipitation of calcite and zeolites in presence of concrete pore solution.

Low-pH cementitious matrices, including cement suspensions, mortars, and concretes, containing up to 60% of supplementary cementing materials as replacement of cement, were developed. The suspensions were prepared to develop a combination of supplementary cementing materials (SCM) leading to low final pH over time. The macro-encapsulation consists of using concrete to make large containers (caissons) with highly-dense steel reinforcement and used as radiation shielding to encapsulate the as-received cemented radioactive waste (CRW) in pails. The micro-encapsulation consists of grinding the CRW and re-cementing it in mortar mixtures. Both concrete and mortars were made of the low-pH SCM combination developed in the suspensions (40% GU Type cement, 50% silica fume, and 10% Class F fly ash). With this high silica content, different consistencies (conventional vibrated, semi-flowable, and self-consolidating concretes) could be obtained with good stability and the concrete mixtures had various strength levels (normal-strength and high-performance concrete up to 70 MPa) and low drying shrinkage. The mortar mixtures exhibited adequate compressive strength (up to 60 MPa), low length variation, and low leachability of cesium.

Keywords: *Consistency, low-pH mortar/concrete, micro/macro-encapsulation, radioactive cemented waste, supplementary cementing materials*

Introduction

The disposal of radioactive waste in underground repository facilities should be sustainable for very long periods until achieving negligible levels of radioactivity. The sustainability is based on many criteria such as preventing infiltration (penetration) of external elements to the stabilized radioactive waste and leaching (leacking) of the hazardous elements from the radioactive waste to the environment. This can be done using deep and stable geological structures, typically clayed formations such as bentonite [1] used as a second compact and impervious barrier for radioactive waste containment. The bentonite also has capacity to absorb large quantities of water. Nevertheless, the contact between the concrete pore solution ($13 \leq pH \leq 13.5$) and the bentonite ($8 \leq pH \leq 10$) creates degradation of both concrete and bentonite.

On one hand, the concrete hydrates include calcium silicates (C-S-H), calcium aluminates (C-A-H), and portlandite (CH). The CH crystals constitute an alkaline reserve and maintains pH above 12.5 [2]. Degradation of concrete is manifested by decalcification of the cement paste (dissolution of CH that increases porosity, decalsification of C-S-H, and precipitation of low quantity of ettringite in the pores and calcite). On the other hand, degradation of the clay barrier is manifested by loss of swelling, dissolution of quatrz and clay minerals, precipitation of calcite and other silicate minerals such as zeolites (principally analcime and phillipsite, rarely merlinoite and chabazite) especially at temepratures higher than 60°C [3]. It is also manifested by illitization of smectite and formation of illite (release of Si and Mg at the interface increasing the porosity), formation of potassium-feldspar, formation of C-S-H and M-S-H. In other words, these reactions in concrete and bentonite result in exchange by diffusion of the ions Si^{2+}, SO_4^{2-}, CO_3^{2-}, Cl^-, H^+ from bentonite to concrete, and Ca^{2+}, K^+, and OH^- from concrete to bentonite [1].

To prevent these deterioations, the pH of the cementitious materials should be lower than 11 for purpose of chemical compatibility with the repository environment (clay barrier) [4, 5]. To obtain a low-pH matrix, it is necessary to minimize the alkali content in the pore solution, reduce the ratio CaO/SiO_2 of C-S-H, and consume the CH [1]. This is because the use of Ca compound (such as CaO) increases pH [6]. This can be achieved by addition of pozzolans rich of silica (SiO_2). The pozzolanic reaction between SiO_2 and CH (liberated by hydration of cement) converts CH to a second generation of C-S-H.

Extraction of the concrete pore solution by compression to determine pH is difficult because the process requires special equipment and a high volume of concrete. The shaking of a cement suspension for a given duration is a simple alternative that can provide similar pH values to that of the compression method as long as the solid-to-liquid ratio (S/L) is comprised between 1/9 and 1 [7]. Previous researches [8, 9] investigated normal-and low-pH suspensions formulated from different cement types and combined with various mineral additives in binary and ternary mixtures. They found that development of the pH is proportional to that of

the alkalis concentrations. The pH is also affected by the water amount (S/L), shaking duration and velocity [9].

A preliminary optimization program [1] was carried out at CanmetMINING on suspensions of binary and ternary binders, using General Use type cement (GU) and calcium aluminate cement (CAC), to achieve low-pH matrices. The Class F fly ash (FA-F), silica fume (SF), ground granulated blast-furnace slag (GGBFS), and metakaolin, used separately in binary systems at different portions, contributed in decreasing the pH over the shaking time. This was due to the CH consumption by the pozzolanic reactions. However, the decrease was not significant and the pH was still above 11. The ternary combinations of SF/FA-F or SF/GGBFS provided lower pH values. Also, compared to the FA-F, the SF with GU decreased more the pH. Using the CAC, SF is more effective but FA-F increased the pH. The GU is more recommended than the CAC in ternary combinations for many reasons. SF and FA were found to reduce the pH better than GGBFS and metakaolin. The combination of 40% GU, 50% SF, and 10% FA-F was found to be the best one with a pH value of 10.5 and acceptable fluidity allowing filtration at 14 days. This paper is a continuation of this program [1] and aimed to follow up of the pH development of this low-alkalinity combination for a longer duration (28 days) and to use it in two different ways of stabilization. The first way consists of mixing this combination with crushed cemented radioactive waste (CRW) in mortar mixture (micro-encapsulation system, [10]). The second way consists of using this combination to make containers of low-pH concrete that can encapsulate "as received" pails of CRW without much processing (macro-encapsulation system [11]). The CRW is stored temporarily and the micro-and macro-encapsulation systems are proposed for final disposal, i.e. for very long periods until the waste achieves a level of negligible radioactivity.

Materials

Surrogate cemented waste

The actual CRW represents different chemical radioactive solutions that were poured robotically on certain quantities of GU Type cement without any stirring in metallic pails containing an internal layer of plastic liner. The solution-to-cement ratios were low (0.29) to ensure absorption of the whole solution by cement in absence of stirring. This method was used for several years for the stabilization/solidification and short-term storage of solutions containing radioactive and hazardous elements. CanmetMINING worked on the development of methods for the treatment and stabilization/solidification of the current CRW. The work was done using surrogate cemented wastes (SCW) similar to the actual CRW, produced with solutions containing various metals including mercury (Hg), cesium (Cs) and natural uranium (U). Some SCW was also made without Hg and U. Tables I and II show proportions and grain size distribution, respectively, of a

typical SCW used in mortar mixtures in this study. The SCW underwent the same cementing procedure as those used for the CRW described above. The surrogate solution was heated up to 90°C before pouring it on cement to mimic the conditions of the actual CRW production Immediately after pouring the solution on the cement, the pail was sealed and then covered with 5-mm thick layer of thermal isolation to prevent the heat loss during the first hours of hydration. The isolation was then removed and the curing continued at ambient laboratory temperature and humidity for several months.

Other materials

The cementitious materials used were general use Type cement (GU), silica fume (SF), ground-granulated blast-furnace slag (GGBFS) and Class F fly ash (FA-F). The physico-chemical characteristics and grain size distribution of the cementititous materials are presented in Table IIII and Figure 1, respectively. The grain-size distribution was carried out using a 'Laser Particles Sizer' and different dispersants. The different physical characteristics (grading, fineness moduli, specific gravities, and absorptions) of the normal-weight fine and coarse aggregates (FA and CA, respectively) used in the concrete mixtures are given in Table II. To ensure good workability for mortar and concrete mixtures, a polycarboxylate-based high-range water-reducing admixture (HRWRA) was employed. To secure the required air content in the concrete mixtures, a hydrocarbons liquid solution-based air-entraining admixture (AEA) was used. To obtain reasonable setting times for the concrete mixtures and avoid corrosion of the steel reinforcement, a non-chloride set accelerator admixture (SA) was incorporated. The specific gravities and solid contents of the three admixtures were 1.07, 1.007, and 1.29, and 30%, 5%, and 36%, respectively.

Table XV. Proportions of a typical SCW used in mortar mixtures

Cement	GU, kg	15.5
Solution	Quantity, L	4.5
	$Al(NO_3)_3 \cdot 9H_2O$, g	1650
	$Cu(NO_3)_3 \cdot 3H_2O$, g	35.9
	$Cs(NO_3)$, g	0.26
	$Sr(NO_3)_2$, g	0.50
	$La(NO_3)_2.6H_2O$, g	2.14
	$Fe(NO_3)_3.9H_2O$, g	1.82
	$Ni(NO_3)_2.6H_2O$, g	0.24
	$Cr(NO_3)_3.9H_2O$, g	0.59
	HNO_3 (16M), mL	100
Solution/cement		0.29

Table XVI. Grain-size distribution and physical properties of typical aggregates and SCW [12-16]

Sieve		SCW	FA	CA
No.	Size (mm)			
1”	*25.0*			100
¾”	*19.0*			100
½”	*12.5*			60
⅜”	*9.50*		100	35
# 4	*4.75*	100	97.2	0
# 8	*2.36*	82.9	85.5	
# 16	*1.18*	53.8	67.7	
# 30	*0.60*	38.3	43.6	
# 50	*0.30*	29.7	17.8	
# 100	*0.15*	25.3	5.50	
# 200	*0.075*	22.5		
# 325	*0.045*	19.5		
Fineness modulus		*	2.8	2.1
Absorption			0.80	0.40
Specific gravity		2.51	2.70	2.72

* Calculation of fineness modulus of SCW from this table gives wrong value given the difficulty of use of sieves of smaller sizes because of the presence of an un-hydrated cement portion.

Table XVII. Physico-chemical properties of cementitious materials and SCW

	Property	GU	GGBFS	FA-F	SF
Chemical properties [17]	SiO_2, %	18.88	35.38	47.9	95.2
	Al_2O_3, %	4.93	10.98	25.3	0.23
	Fe_2O_3, %	3.10	0.60	16.2	0.06
	MgO, %	2.76	11.55	0.82	0.28
	CaO, %	63.15	37.80	2.70	0.51
	Na_2O, %	0.24	0.50	0.54	0.26
	K_2O, %	0.53	0.60	1.88	0.58
	TiO_2, %	0.27	0.79	1.35	< 0.01
	P_2O_5, %	0.14	< 0.01	0.35	0.13
	MnO, %	0.07	0.74	0.02	0.03
	Cr_2O_3, %	< 0.01	< 0.01	0.03	--
	V_2O_5, %	0.03	0.01	0.05	--
	S as SO_3, %	3.82	3.89	0.87	0.25
	LOI, %	2.48	-1.25	1.88	2.91
Physical properties	Specific gravity [18]	3.15	2.9	2.45	2.2
	Blaine fineness, m²/kg [19]	447	551	321	--
	BET fineness, m²/kg [20]	--	--	--	20437
	Passing 45 µm, % [21]	94.7	99.3	82.6	100
	7-d f'_c, MPa [22]	33.3	--	--	--
	28-d f'_c, MPa [22]	43.4	--	--	--

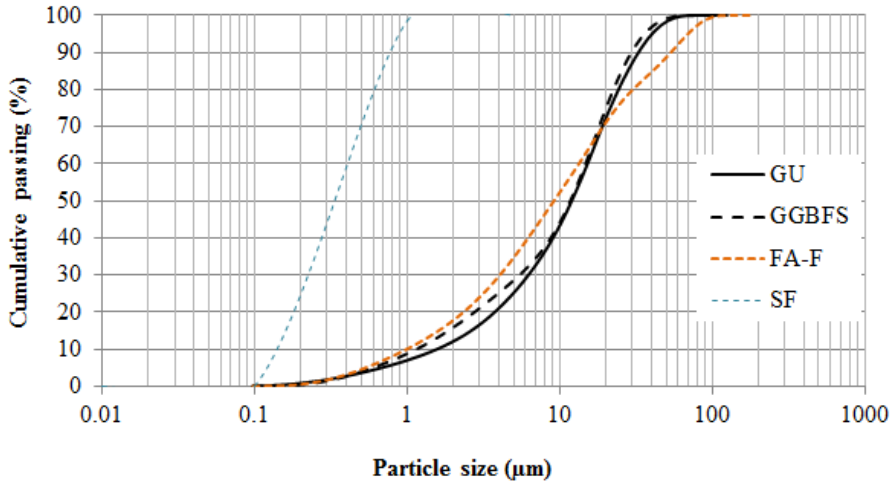

Figure 35. Grading of the cementitious materials

Cement suspensions

In the suspensions, only water, GU Type cement, SF, GGBFS (or FA-F) were used. Two cement suspensions were prepared: suspension (A) of normal pH as reference and suspension (B) of low-pH. This latter was issued from a preliminary optimization protocol [1]. The mixture proportions of the two suspensions are presented in Table IV. A solid-to-liquid ratio (S/L) of 0.50 was adopted. In the lierature [7-9], the recommended S/L is 1/9 to 1.

Table XVIII. Proportions of the cement suspensions

Suspension	GU Cement, %	SF, %	FA-F, %	GGBFS, %	Solid/liquid
(A)	53	7	--	40	0.50
(B)	40	50	10	--	0.50

Mixing, test methods, and curing

The mixing, sampling, shaking, and testing procedures were carried out in the laboratory conditions. A total volume of 1.3 L for each suspension was prepared in a Hobart mixer [23]. The water was placed first in the bowl, then the cementitious materials were added for the absorption within 30 s. The suspensions were mixed at 140 ± 5 rpm for 30 s then the mixer was stopped for 15 s to scrape the bowl sides. The mixing was continued at 285 ± 10 rpm for another 60 s.

After mixing, a number of glass flasks were filled with approximately 400 mL of each suspension, closed with rubber lids, and transferred on a multi-velocity circular-movement shaker. The velocity was fixed at 200 rpm for all the testing duration of 28 days. Hidalgo et al. [8] recommended a longer time (up to 90 days) for hydration of the mineral additives (pozzolanic reactions). In this study, the 28-day duration was sufficient to obtain the intended results (in the preliminary phase [1], the target pH was obtained in only 14 days). At each testing age of 7, 14, and 28 days, one flask was removed from the shaker and the suspension was filtred using 22-µm filters for measurements of pH and the oxides concentrations of alkalis (Na_2O, K_2O), CaO, and SiO_2 (the main elements affecting pH). From each filtered solution and at each age, one or more samples were saved into 20-mL glass vials for archive. The results are presented in Table V.

Table XIX. pH and oxide concentration of the filtered cement suspensions at different ages

Age	4 d		7 d		14 d		28 d	
Suspension	(A)	(B)	(A)	(B)	(A)	(B)	(A)	(B)
pH	--	12.34	12.34	12.22	12.82	11.30	12.39	10.11
CaO (ppm)	--	77	155	59	75	68	82	206
SiO_2 (ppm)	--	6	2	9	2	85	23	182
Na_2O (ppm)	--	522	654	317	734	182	732	219
K_2O (ppm)	--	1165	1415	683	1350	296	1220	275
Na_2O+K_2O (ppm)	--	1687	2069	1000	2084	478	1952	494
CaO/SiO_2	--	12	82	7	34	1	4	1

Test results and analysis

The following figures and analysis are based on data presented in Table V. It can be seen that the individual concentrations of Na^+ and K^+ are higher than that of Ca^{2+}, regardless of the mixture type and mixture age. This is in agreement with previous findings [24].

From Figure 2, both the suspensions (A) and (B) had similar pH at 7 days of age (12.34 and 12.22, respectively). In the case of suspension (A), the alkalis (Na_2O+K_2O) concentration of the pore solution were still stable over the shaking time (2069 ppm and 1952 ppm @ 7 and 28 d, respectively), leading to a stable pH of the pore solution at 28 d (12.39). However, in the case of the low-pH suspension (B), the pH decreased by more than two units at 28 d (10.11) with reduction in the alkalis concentrations (from 1687 to 494 ppm), that qualified (B) as a low-pH matrix (pH lower than 11). The alkali content of pore solution of high-silica ternary blends reduced significantly with decrease in pH [1]. It should be noted that the two suspensions were prepared with the same water-to-cementitious materials ratio of 0.50.

From Figure 3, the increase of SiO_2 of the pore solution of suspension (B) from 6 to 182 ppm also resulted in lowering the pH from 12.34 to 10.11 between 4 and 28 days of shaking time. Furthermore, there is a correlation between the pH and the concentration ratio CaO/SiO_2, i.e. the more stable CaO/SiO_2 is, the sharp increase in pH is and vice versa (Figure 4). This relationship is in agreement with previous findings [1]. It was also found that CaO/SiO_2 affects the alkali concentration (Na_2O + K_2O), as illustrated in Figure 5. In other words, the stability or reduction in CaO/SiO_2 of the C-S-H (availability of supplement in silica) results in reduction (consumption) of the alkali concentration which results, in turn, in reduction of the pH value of the pore solution equilibrium over time. Codina [7] reported that the

CaO/SiO_2 of C-S-H decreases leads to decrease of pH of equilibrium and increase the sorption capacity of very soluble alkaline cations those are responsible of very high pH of the pore solution.

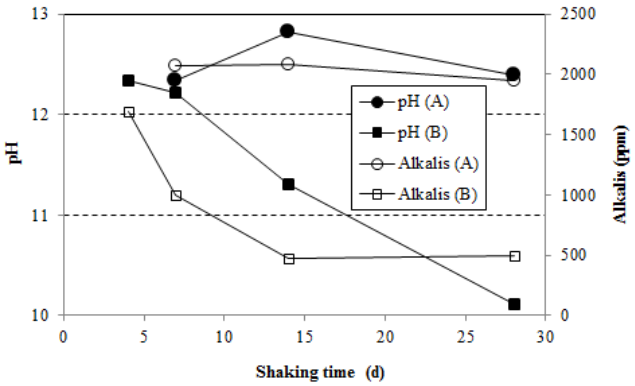

Figure 36. Development of pH with alkalis concentration

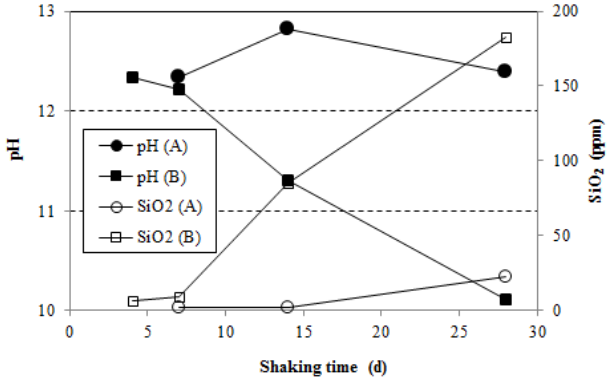

Figure 37. Development of pH with SiO_2 concentration

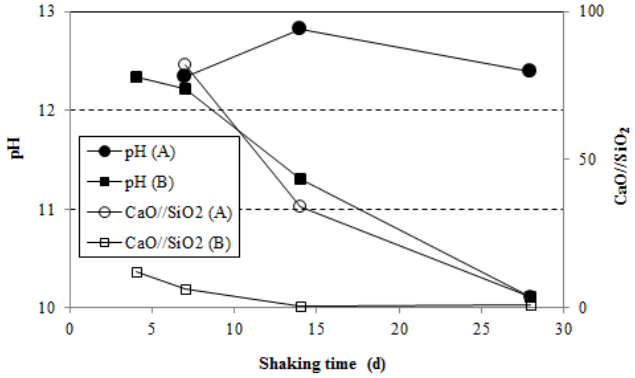

Figure 38. Development of pH with CaO/SiO_2

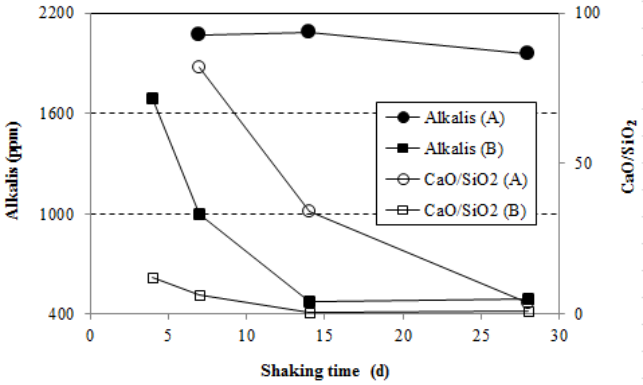

Figure 39. Correlation between development in the alkalis concentration and CaO/SiO_2

Mortar

One of the solutions proposed by CanmetMINING for the long-term stabilization is a micro-encapsulation system. This consisted firstly of grinding the solid SCW to different specified fineness suitable for mixing. The nominal maximum size of the SCW in this paper is 4.75 mm, allowing using it as fine aggregate in the mortar

mixtures. The second step of the micro-encapsulation system consisted of re-cementing the crushed SCW. The latter was mixed with water and the combination of cementitious materials used in low-pH cement suspension (B). The intent of using of such combination of cementitious materials was to prevent deterioration due to possible contact with clay formations. The new mortar mixture had a water-to-cementitious materials ratio (W/CM) of approximately 1, a relative SCW volume in the mortar mixture of 46%-47% (based on preliminary optimization [10]), and was prepared with two consistency ranges: normal and fluid (M1 and M2, respectively) by variation in the HRWRA dosage (Table VI). This was done mainly to evaluate the effect of the HRWRA dosage (thus mixture consistency) on the leachability of Cs from the cemented SCW in the hardened state. The leaching of Cs was selected as a good indicator of the leaching resistance of the mortar since this element is very mobile in the cementitious matrices compared to uranium and mercury [10]. The medium value of W/CM was considered as a compromise between the mechanical strengths and porosity from one hand, and pH and workability from the other hand.

Table XX. Proportions of the mortar mixtures

Mortar	Cement %*	SF %*	FA %*	HRWRA %**	W/ CM	V_{SCW} (%)	Solid /liquid	CM/ SCW	CM/ Solid
M1	40	50	10	0.96	1.01	47	4.1	0.32	0.24
M2				1.90	1.03	46	4.0		

* Mass portion in the cementitious materials (CM) system (GU + SF + FA-F)

** Portion in the total mortar volume

Mixing, test methods, and curing

In the following, the mixing, testing in the fresh state, sampling, demolding, curing, and testing in the hardened state were carried out in the laboratory conditions at ambient temperature of 20 ± 2 °C.

For the mixing, a total mortar volume of 1.6 L was prepared in an ASTM Hobart mixer. The mixing sequence [23] was used with some modifications. The mixing water was placed first in the bowl. The cementitious materials (GU + FA + SF) were then added to the water and mixed at a speed of 140 ± 5 rpm for 30 s. The crushed SCW was added over 30 s and the HRWRA over another 30 s while mixing with the same speed. The mixer was then stopped and the mixture was kept at a rest for 90 s (the bowl sides were scraped during the first 15 seconds). After, the mixing continued for 60 s to allow adjustment of the HRWRA dosage if needed.

In the fresh state, a flow table [25, 26] was used to assess the mortars workability. The test consisted of filling, in two equal layers, the steel cone positioned on the table with the fresh mixture and applying 20 tamps for each layer with a rubber tamper. The mixture underwent then 25 vertical drops in 15 s. Four measurements of the flow were then be taken at each 45° using a steel caliper. The flow value (in %) is the sum of the four measurements.

The compressive strength (f'_c) test was carried out on 50-mm cubes. For mortar M1of normal flowability, the cubes were filled in two layers, each layer was tamped 32 times with a rubber tamper [22]. No mechanical consolidation was applied for the high flowable mortar M2. The molds were covered with a layer of plastic sheet, then with a layer of wet tissue, and then a second layer of plastic sheet. Following this, the molds were placed in a plastic bag. This was done to simulate the curing method *in-situ* where the actual CRW will be sealed in drums. After 24 hours of curing in molds, the same wrapping method was applied on the demolded cubic samples. At each due age of 7 and 28 days, a controlled-load hydraulic press was used at 1.35 kN/s, to determine the f'_c.

Three 25×25×250-mm prisms were prepared for the length change test for each mortar mixture. The mixture M1 was cast in two layers and tamped 10 times for each layer. No consolidation was applied for M2. The prismatic specimens underwent the same sealed curing conditions as for the f'_c test specimens for the whole duration of testing. The measurements were recorded up to 182 days [27].

The extended leaching test [28] was performed on two 38×61-mm cylindrical specimens at each age of testing (28 and 91 d). The specimens were cast in small plastic vials which were closed hermetically with a plastic lid immediately after consolidation of the mortar. The specimens were kept in their closed molds (sealed curing) up to the testing day. From each mixture, a third specimen was utilized to determine the initial concentration of Cs needed for determination of the leachability index ($\bar{L}$). The test consists of immersing the specimen of known mass and dimensions in a non-reactive container (glass jar) with a given volume of deionized water. At each age of 2 hr, 5 hr, 1 d, 2 d, 3 d, 4 d, 7 d, 18 d, 46 d, and 91 d, the specimen was removed from the old water and immersed in a fresh one. The pH and electrical conductivity of the leachate were measured and a sample of the leachate was taken. The Cs concentration (in ppb) of the leachate samples at the different ages was then determined using the inductively coupled plasma mass spectrometry (ICP-MS) method. The $\bar{L}$ for the 7-d and 91-d tests was calculated in Eqns. (1) and (2), respectively [28].

$$\bar{L_\iota} = \frac{1}{7}\sum_1^7 [log(\beta/D_i)]_n \quad (1)$$

$$\bar{L_\iota} = \frac{1}{10}\sum_1^{10} [log(\beta/D_i)]_n \quad (2)$$

β: constant (1.0 cm²/s);
D_i: effective diffusivity of nuclide (element i) calculated from the test data (cm²/s), given by Eqn. (3).

$$D_i = \pi \left[\frac{a_n/A_0}{(\Delta t)_n}\right]^2 \left[\frac{V}{S}\right]^2 T \quad (3)$$

a_n: quantity of element i released from the specimen during leaching interval n (mg);
A_0: total quantity of element i in the specimen at the beginning of the first leaching interval (after the initial 30-s rinse period) (mg);
$(\Delta t)_n$: duration of the n'th leaching interval (s);
V: volume of the specimen (cm^3);
S: measured geometric surface area of the specimen (cm^2);
T: leaching time representing the mean time of the leaching interval (s) calculated in Eqn. (3).

$$T = \left[\frac{1}{2}\left(t_n^{1/2} + t_{n-1}^{1/2}\right)\right]^2 \quad (4)$$

The higher the value of $\bar{L}$ is, the better the resistance to leaching of the mortar is.

Test results and analysis

The results of the tests performed on the two mortar mixtures, including flow, f'_c, length change, and leaching, are presented in Table VII. The high 28-d f'_c values (42.9 and 59.7 MPa) were expected given the high replacement of supplementary cementitious materials, particularly SF.

Table XXI. Test results for the two mortars

Mortar	Flow %	7-f'_c MPa	28-f'_c MPa	182-d length change %	28 d [1]		91 d [1]	
					7-d $\bar{L}$	91-d $\bar{L}$	7-d $\bar{L}$	91-d $\bar{L}$
M1	116	45.6	59.7	- 0.0257	--	--	9.7	9.9
M2	[2]	31.4	42.9	--	8.9	9.8	9.2	9.4

[1] Age at which the leaching test was initiated.
[2] Mortar overflew on the flow table.

The rise in the HRWRA dosage led to the loss of approximately 30% in the f'_c, regardless of the age (Table VII). This is partially due to the small increase in W/CM from 1.01 to 1.03. On the other hand and from the same table, it seems that the leaching resistance was not significantly affected over time between tests

initiated at 28 days and 91 days of age regardless of the duration of testing. Also, the increase (approximately double) in the HRWRA dosage resulted in a slight reduction in the leaching resistance to Cs.

Concrete

The second option to stabilize the CRW involves making containers (caissons) of heavyweight low-pH concrete that can encapsulate a numbers of the 'as received' pails of CRW together without much processing. This option is called macro-encapsulation system. The concrete is used simultaneously as radiation shielding and a self-protection from the chemical incompatibility in contact with the clay environment (external barriers). As in the case of micro-encapsulation system, the use of the low-pH combination (40% GU + 10% FA-F + 50% SF) was tested to make concrete mixtures.

The design of the caisson requires a dense steel reinforcement and a flowable concrete is consequently needed for easy casting *in-situ*. This is to avoid blockage of concrete behind the steel reinforcement and prevent segregation that may occur with application of mechanical consolidation on conventional vibrated concrete (CVC) containing such type of aggregates.

This paper presents the results of a preliminary development program performed on concretes containing only normal-weight aggregates. Validation on concretes made of heavyweight aggregates will be presented in a future work. The characteristics of the aggregates used are shown in Table II. The admixtures (HRWRA, AEA, and SA) employed are also described above (Materials section). The proportions of the low-pH concretes of each consistency range (CVC, semi-flowable concrete (SFC), and self-consolidating concrete (SCC)) are presented in Table VIII.

Table XXII. Proportions of the low-pH concretes

	Content (kg/m³)						Dosage (L/m³)			W/CM	CA/FA
	Sand	19-mm CA	Water	GU	SF	FA-F	HRWRA	AEA	SA		
CVC	718	898	159	159	199	40	6.0	0.7	--	0.40	1.25
SFC	694	1041	138	149	187	38	12	0.4	--	0.37	1.50
SCC1	680	1014	135	145	182	37	35	0.3	1.3	0.37	1.50
SCC2	770	770	176	176	221	44	25	0.3	--	0.40	1.00

Mixing, test methods, and curing

The mixing, fresh testing, sampling, demolding, and curing procedures were carried out in the laboratory conditions at ambient temperature of 20 ± 2 °C. The 20-L batches were prepared in a 57-L capacity close-pan mixer with variable speeds. The pan speed was fixed at 30 rpm; however, the gear shaft attaching the agitator blades turns at an invariable speed of 68 rpm. The mixing method [29] underwent some modifications depending on the consistency level. The aggregates were first homogenized with half quantity of water and AEA for 30 s. The cementitious materials were then incorporated and mixed for 30 s. The remaining half (½) amount of water and ¾ of the HRWRA volume were added and mixed for 2 minutes. Three minutes of rest were necessary before additional mixing for 2 minutes allowing the correction of the HRWRA dosage.

For the CVC mixture, the slump [30], specific gravity [31], and air volume of the fresh mixture [32] were determined. The cone was filled in three layers and the concrete was consolidated 25 times for each layer, using a steel rod measuring 16 mm in diameter and 600 mm in length. The same protocol was followed for the air-meter bowl with tapping the sides 10 to 15 times after each layer using a 600-g rubber mallet.

For the SFC mixtures, the slump flow diameter [33], T_{40} spread time, and visual stability index (VSI) were evaluated. It is to be reminded that the qualitative measurement, VSI, ranges between 0 (for the more stable mixtures) and 3 (for the segregated mixtures). The VSI is based on three parameters: final concrete shape (circular for stable mixtures), bleeding layer around the mixture perimeter, and homogeneity degree (uniformly distributed for stable concrete and separation of particles, i.e. conglomeration of CA at the center of segregated concrete). The slump cone was filled in one layer and consolidated using a 16-mm steel rod with application of 10 internal strikes. The same protocol was used for determining the unit weight and air volume and the air-meter bowl received then 10 external strikes using a 600-g rubber mallet. The passing ability was evaluated using the modified L-box test method to determine the blocking ratio (h_2/h_1) and T_{20} or T_{40}. The h_1 and h_2 values correspond to the heights of the concrete at both ends of the horizontal leg of the device. The T_{20} and T_{40} flow times (Fig. 5.15) corresponding to the time needed for the concrete to spread 200 mm and 400 mm, respectively. Only two bars were used instead of three. The clearance between the bars and bar-wall was 59 mm, representing approximately 3.1 times of the nominal maximum size aggregate of ¾" (19 mm). The concrete was vibrated in the vertical leg of the L-box using a pencil vibrator with a diameter of 33 mm in 5-s intervals. The h_2/h_1 values were recorded after each of these vibration intervals until obtaining a minimum blocking ratio of 0.80.

For the SCC mixtures, the slump flow diameter [33], T_{50} spread time, and VSI were evaluated. The air-meter bowl was filled in one layer without any consolidation to determine the unit weight and air volume. The modified L-box described above was employed to determine h_2/h_1 and T_{70} (time spent to cross the horizontal leg of 700 mm). A V-funnel with an outflow opening of 65×75 mm was used.

Several 100×200-mm cylinders and 76×76×300-mm prisms were prepared for testing in the hardened state. For the CVC, the cylinders were cast in two layers and consolidated for less than 5 s for each layer [29]. The prisms were cast in one layer and vibrated in less than 10 s [29, 34]. For the SFC mixtures, the cylinders and prisms were cast in one layer and the vibration time was fixed between 1 and 3 s, depending upon the workability degree. In both CVC and SFC mixtures, the vibration time allowed was the time necessary to obtain a smooth surface of concrete without excessive vibration. The vibration was carried out onto a vibrating table operating at a frequency of 60 Hz and horizontal amplitude of 0.775 mm. For SCC mixtures, the cylindrical and prismatic samples were cast in one layer without any consolidation.

The sampled cylinders and prisms were kept in their molds and covered with plastic sheets and then stored in the laboratory conditions (normal temperature and humidity) until demolding. After demolding at 24 hrs, the cylinders were cured in water until the testing day at 7, 28, or 56 days for the f'_c and 7 and 56 days for splitting tensile strength (f'_{sp}). The prisms were immersed in lime-saturated water for additional six days before being transferred to a temperature-and humidity-controlled room at 23 ± 2 °C and 50% ± 4% RH until the end of testing at 182 days. The loading rates for f'_c [35] and f'_{sp} [36] were 2500 N/s and 1250 N/s, respectively.

Test results and analysis

The test results of the mixtures are presented in Table IX. In the fresh state, it was possible to make low-pH concrete with different consistencies up to slump flow value of 710 mm in spite of the high SF content (50% as replacement of cement) and medium W/CM (0.37 to 0.40). The temperature after mixing in all mixtures was approximately 21°C. The adjustment in the mixture proportions was so far mainly based on the HRWRA dosages that were generally very high, knowing that the CA/FA were higher than 1 in view to obtain high mechanical strengths. The high dosages of HRWRA were used to compensate the huge water demand caused by the high content of SF of high fineness (more than 20000 m²/kg, as indicated in Table III). The use of such high volumes of HRWRA can significantly affect the mixture cost. Even tough, there was no need to use a viscosity-enhancing admixture (VEA) because all the mixtures were stable without any sign of bleeding or segregation (VSI of 0) because all the water quantity was used to fluidize the SF

particles. In this case, the use of a VEA can lead to a reverse effect, i.e. blockage rather than resistance to blockage. However, the mixtures were generally quite viscous and that can also affect the concrete manipulation and casting. The high viscosity was evaluated through the different unconfined and confined flow rates: slump flow T_{40} or T_{50} between 4 and 18 s, V-funnel flow time between 8 and 28 s, L-box T_{40} or T_{70} between 5 and 18 s, regardless of the concrete consistency. For instance, T_{50} [33] gives an indication of the relative viscosity of the concrete mixture, i.e. longer T_{50} values correspond to increased viscosity.

The mixtures exhibited delays in setting time due to the low contents of GU cement (Table VIII). Using the set accelerator (SA) and when demolding at 24 hr of age, the mechanical strengths were however not developed sufficiently yet. In this case, a particular attention must be paid during demolding and manipulation to avoid the concrete damage. For the SFC, a minimum duration of 10 s for mechanical consolidation using the internal vibration was necessary to obtain a blocking ratio higher than 0.80 to avoid the high risk of blockage.

Table XXIII. Test results in fresh and hardened states of the typical concretes

Concrete type	Slump flow (mm)	T_{50} (s)	VSI	Density (kg/m³)	Air (%)	V-funnel (s)	L-box				Demolding (hr)	f'_c (MPa)			f'_{sp} (MPa)		182-d Dry. shr. (µm/m)
							0 s		5 s	10 s		7 d	28 d	56 d	7 d	56 d	
							h_2/h_1	T_{70} (s)	h_2/h_1	h_2/h_1							
CVC	190*	--	--	2245	7.9	--	--	--	--	--	48	27.0	47.0	57.0	3.0	4.1	-325
SFC	520	18×	0	2345	6.0	--	0.61	18§	0.71	0.82	48	28.1	51.8	60.9	3.6	5.0	-427
SCC1	650	7	0	2276	6.0	28	0.85	12	--	--	24	35.4	68.2	70.0	4.0	5.9	-442
SCC2	710	4	0	2302	5.5	8	0.95	5	--	--	34	29.2	54.9	61.2	3.7	5.2	-448

* Slump × T40 of slump flow § T40 of L-box

In spite of the low content of the Type GU cement in the mixtures (150 to 180 kg/m³), high f'_c and f'_{sp} values (57 to 70 MPa and 4.1 to 5.9 MPa, respectively, at 56 days) were obtained. This range of strengths can qualify this mixture as a high-performance concrete. The 182-day drying shrinkage values were ranging between 325 and 450 micro-strains, regardless of the consistency range. These relatively low values can indicate low cracking potential of concrete. This was possibly due to refinement of the porous network by incorporation of the SF of high fineness (D_{50} < 4 µm, as per Figure 1) used at high contents (up to 225 kg/m³) as well as the fairly low W/CM values.

Concluding remarks and recommendations

In light of the results obtained on suspensions, mortars, and concrete matrices, the following conclusions can be drawn:

- After optimization, it was found that a ternary combination of GU Type cement (40%), high content of silica fume (50%), and Class F fly ash (10%), is able to produce a low-alkalinity cementitious matrix with a pH of 10.1 at only 28 days of age.
- For the micro-encapsulation system, the developed low-pH mortar mixtures had adequate fluidity and mechanical strengths (up to 60 MPa) as well as negligible length changes (up to 340 micro-strains at 6 months) and low leachability of cesium.
- The low-pH concretes made with different consistency levels exhibited good stability without need for a viscosity-modifying agent, high 56-day mechanical properties (f'_c up to 70 MPa) and low 6-month drying shrinkage (up to 450 micro-strains). However and regarding to the high content of SF, the mixtures required high HRWRA demand to obtain the desired workability.
- This paper presented only a preliminary research on development of low-pH matrices and opens perspectives to perform extensive testing on this material needed for stabilizing the CRW. The macro-encapsulation development will consider heavyweight aggregates and more comprehensive testing program.

Acknowledgements

The authors would like to acknowledge the contribution of the technicians Cheryl Laviolette, André Demers, and Jacob Kruszewski from CanmetMINING (Natural Resources Canada) in this work. The authors wish also to thank Canadian Nuclear Laboratories for the financial support and fructuous discussions during the regular meetings. Euclid Canada, Quebec Silicium, and Lafarge Cement are also acknowledged for supplying with materials.

References

[1] Oueslati, O., Bouzoubaâ, N., Bilodeau, A. (2012) *Development and characterisation of low-pH cements for structural purposes in geological repository systems*, Internal Report, CanmetMINING, 21 p.

[2] Atkinson, A. (1985) *The time dependence of pH within a repository for radioactive waste disposal*, UKAEA Atomic Energy Research Establishment.

[3] Dauzères, A. (2010) *Experimental study and modeling of physico-chemical mecanisms of interactions concrete-clay in the context of geological storage of radioactive wastes*, PhD thesis (in French), Université de Poitiers, France, 249 p.

[4] Ramírez, S., Cuevas, J., Vigil, R., Leguey, S. (2002) *Hydrothermal alteration of "La Serrata" bentonite (Almeria, Spain) by alkaline solutions*, Applied Clay Science, vol. 21, n. 5-6, p. 257–269.
[5] Savage, D, Benhow, S. (2007) *Low-pH cements,* SKI report 2007: 32, 45 p.
[6] Pratt, A. (2011) *Cementitious compositions containing feldspar and pozzolanic particulate material, and method of making said composition*, Patent 8066813, CanmetMINING, Natural Resources Canada.
[7] Codina, M. (2007) *The low-pH concretes, proportioning, characterization, and investigation for long-term,* PhD thesis (in French), Institut National des Sciences Appliquées (INSA) de Toulouse, France, 167 p.
[8] Hidalgo, A., Garcia ,J-L., Alonso, C., Fernandez-Luco, L., Andrade, C. (2005) *Testing methodology for pH determination of cementitious materials – Application to low pH binders for use in HLNWR*, 2nd low-pH Workshop, Madrid, p. 64–76.
[9] Räsänen, V., Penttala, V. (2004) *The pH measurement of concrete and smoothing mortar using a concrete powder suspension,* Cement and Concrete Research, vol. 34, n. 5, p. 813–820.
[10] Bilodeau, A., Lastra, R., Laviolette, C., Kruszewski, J., Fiset, J.F., Bouzoubaâ, N., Chapman, M., (2013) *Micro-encapsulation of cemented radioactive waste*, Internal report, CanmetMINING, Natural Resources Canada, 202 p.
[11] Bilodeau, A., Chevrier, R., Demers, A., Bouzoubaâ, N., Chapman, M. (2013) *Development of concrete and grout for the macro-encapsulation of cemented radioactive waste*, Internal report, CanmetMINING, Natural Resources Canada, 71 p.
[12] ASTM C33/C33M-13 (2013) *Standard specification for concrete aggregates*, ASTM International, West Conshohocken, PA, USA, vol. 04.02, 11 p.
[13] ASTM C127-12 (2013) *Standard test method for density, relative density (specific gravity), and absorption of coarse aggregate*, ASTM International, West Conshohocken, PA, USA, vol. 04.02, 6 p.
[14] ASTM C128-12 (2013) *Standard test method for density, relative density (specific gravity), and absorption of fine aggregate*, ASTM International, West Conshohocken, PA, USA, Vol. 04.02, 6 p.
[15] ASTM C136-06, (2013) *Standard test method for sieve analysis of fine and coarse aggregates*, ASTM International, West Conshohocken, PA, USA, vol. 04.02, 5 p.
[16] ASTM C637-09 (2013) *Standard Specification for Aggregates for Radiation-Shielding Concrete*, ASTM International, West Conshohocken, PA, USA, vol. 04.02, 4 p.
[17] ASTM C114-13 (2013) *Standard test methods for chemical analysis of hydraulic cement*, ASTM International, West Conshohocken, PA, USA, vol. 04.01, 32 p.
[18] ASTM C188-09 (2013) *Standard test method for density of hydraulic cement*, ASTM International, West Conshohocken, PA, USA, Vol. 04.01, 3 p.

[19] ASTM C204-11 (2013) *Standard test methods for fineness of hydraulic cement by air-permeability apparatus*, ASTM International, West Conshohocken, PA, USA, Vol. 04.01, 9 p.
[20] Brunauer, S., Emmett, P.H., and Teller, E. (1938) *Adsorption of gases in multimolecular Layers*, Journal of American Chemistry Society, vol. 60, p. 309–319.
[21] ASTM C430-08 (2013) *Standard test method for fineness of hydraulic cement by the 45-μm (No. 325) sieve*, ASTM International, West Conshohocken, PA, USA, Vol. 04.01, 3 p.
[22] ASTM C109/C109M-12 (2013) *Standard test method for compressive strength of hydraulic cement mortars (Using 2-in. or [50-mm] cube specimens)*, ASTM International, West Conshohocken, PA, USA, Vol. 04.01, 10 p.
[23] ASTM C305-13 (2013) *Mechanical mixing of hydraulic cement pastes and mortars of plastic consistency*, ASTM International, West Conshohocken, PA, USA, vol. 04.01, 3 p.
[24] Ahn, J., Apted, M.J. (2010) *Geological repository systems for safe disposal of spent nuclear fuels and radioactive waste*, volume in Woodhead Publishing Series in Energy, 762 p.
[25] ASTM C230/C230M-13 (2013) *Standard specification for flow table for use in tests of hydraulic cement*, ASTM International, West Conshohocken, PA, vol. 04.01, 6 p.
[26] ASTM C1437-13 (2013) *Standard test method for flow of hydraulic cement mortar*, ASTM International, West Conshohocken, PA, USA, vol. 04.01, 2 p.
[27] ASTM C452/C452M-10 (2013) *Standard test method for potential expansion of portland-cement mortars exposed to sulfate*, ASTM International, West Conshohocken, PA, USA, vol. 04.01, 2013, 3 p.
[28] ANSI/ANS-16.1 (2003) *Measurement of the leachability of solidified low-level radioactive wastes by a short-term test procedure*, American Nuclear Society, IL, USA, 33 p.
[29] ASTM C192/C192M-07 (2013) *Standard practice for making and curing concrete test specimens in the laboratory*, ASTM International, West Conshohocken, PA, USA, vol. 04.02, 8 p.
[30] ASTM C143-13 (2013) *Standard test method for slump of hydraulic-cement concrete*, ASTM International, West Conshohocken, PA, USA, vol. 04.02, 2013, 4 p.
[31] ASTM C138/C138M-13 (2013) *Standard test method for density (unit weight), yield, and air content (gravimetric) of concrete*, ASTM International, West Conshohocken, PA, USA, vol. 04.02, 4 p.
[32] ASTM C231-231M-10 (2013) *Standard test method for air content of freshly mixed concrete by the pressure method*, ASTM International, West Conshohocken, PA, USA, vol. 04.02, 10 p.
[33] ASTM C1611/C1611M-09b (2013) Standard test method for slump flow of self-consolidating concrete, ASTM International, West Conshohocken, PA, USA, vol. 04.02, 6 p.

[34] ASTM C157/C157M-08 (2013) *Standard test method for length change of hardened hydraulic-cement mortar and concrete*, ASTM International, West Conshohocken, PA, USA, vol. 04.02, 7 p.
[35] ASTM C39/C39M-12 (2013) *Standard test method for compressive strength of cylindrical concrete specimens*, ASTM International, West Conshohocken, PA, USA, vol. 04.02, 7 p.
[36] ASTM C496/C496M-11 (2013) *Standard test method for splitting tensile strength of cylindrical concrete specimens*, ASTM International, West Conshohocken, PA, USA, vol. 04.02, 5 p.

Fresh and Hardened Properties of Self-Compacting Bacterial Concrete

H. B. Dhonde[1], A. R. Undre[2], G. S. Choudekar[3] and T. S. Dashputre[4]

[1] Associate Professor, Dept. of Civil Engg., VIIT, Pune, India 411048
[2] Postgraduate student, Dept. of Civil Engg., VIIT, Pune, India 411048
[3] Undergraduate student, Dept. of Civil Engg., VIIT, Pune, India 411048
[4] Lecturer, Dept. of Civil Engg., VIIT, Pune, India 411048

Abstract Concrete typically experiences deterioration due to formation of micro cracks, which affect its overall fitness. Conventional crack repairing techniques are generally time consuming, costly and challenging. Current research work focuses on the use of non-toxic calcite depositing bacteria - *Bacillus Subtilis* introduced in fresh concrete to self-heal cracks in hardened concrete at micro level. *B.subtilis* in presence of food and moisture initiates microbiologically induced calcite precipitation depositing stable and strong crystals of calcium carbonates in the cracks. For the first time, the effects of addition of bacteria on the fresh and hardened properties of Self-Compacting Concrete (SCC) made with Polycarboxylic Ether (PCE) High Range Water Reducer (HRWR) were examined in this preliminary work. Bacterial dosage of $5x10^9$ cells/ml of mixing water was provided in all the bacterial concretes. Various fresh and hardened properties of four types of concretes i.e. normal, normal bacterial, SCC and bacterial SCC, were investigated. The addition of bacteria affected neither the concrete's workability nor the effectiveness of HRWR in fresh SCC. Moreover, *B.subtilis* bacteria was found to function as an ideal viscosity modifying admixture in concrete, as it noticeably enhanced the stability, consistency and cohesiveness of concrete mix, especially that of SCC, without hampering workability. Bacterial concrete showed a general trend of increase in compressive and split tensile strengths. Interestingly, the normal bacterial concrete showed higher increase in strengths than the bacterial SCC. Therefore, the effects of *B.subtilis* bacteria on the hardened properties of SCC made with PCE-HRWR requires further investigation.

Keywords: *Self-compacting concrete, microbiologically induced calcite precipitation, Bacillus subtilis, self-healing, bacterial concrete*

Introduction

Concrete being weak in tension typically cracks and repairing these cracks require significant resources and cumbersome techniques. The limitations of traditional crack repairing techniques are well known, and so is the extent of this problem. Researchers are intent on finding a more feasible way of repairing cracks in concrete. One such technique is the Microbiologically Induced Calcite Precipitation (MICP), a natural process of bio-mineralization by which living microorganisms (such as bacteria) produce layers of calcium carbonate ($CaCO_3$), that subsequently fill cracks resulting in enhanced strength and durability of concrete [1-8]. Several research studies have been carried out and many more are underway to establish the use of bacteria in self-repairing cracked concrete. Self-healing bacterial concrete could be a viable way to build stronger, durable, and sustainable concrete structures in near future. Recently, a new generation of bio-admixture for Self-Compacting Concrete (SCC) was developed using this novel technology [9]. Self-healing bacterial concrete holds promise as it has transitioned from laboratory phase to insitu experimentations and application phase.

In MICP, the bacteria urease-hydrolyzes urea from the food source to produce ammonia and carbon dioxide. The ammonia released in surroundings subsequently increases pH, leading to accumulation of insoluble $CaCO_3$ which is innate and beneficial to concrete [3, 10]. Negatively charged bacterial cell acts as nucleation site by attracting and depositing Ca^{2+} cations from the surrounding media, eventually forming $CaCO_3$ on the cell wall. MICP depends on bacterial concentration and its ionic strength, availability of water, air space and nutrients, appropriate pH of the matrix, and availability of nucleation sites [8]. Some of these prerequisite conditions are intrinsic in concrete, while others are easily provided for. Most commonly used bacterial food source is calcium lactate and agar-agar urea solution. Noticeable activation of MICP is within a few days and micro cracks are completely filled within a few weeks [10, 11]. MICP is more effective in healing micro-cracks (widths < 30 μm) compared to macro-cracks [6, 12]. Nonetheless, concrete cracks upto 0.46 mm in width have been satisfactorily healed by MICP aided via the use of auxiliary filler materials under laboratory conditions [5, 10].

Common soil Gram-positive bacteria, *Bacillus subtilis* (*B. subtilis*) is highly effective in MICP when used in concrete [2, 6, 10, 12, 13]. *B. subtilis* adheres on the surface of cement particles and forms nucleation sites for MICP [10, 14, 15]. $CaCO_3$ is deposited on the peripheral bacteria wall and surrounding matrix. As the bacteria metabolizes, they develop filaments on wall element that serve as reinforcing fibers and produce crystals of $CaCO_3$ and glue that acts as a binding agent and fills the cracks [9, 12]. *B. subtilis* are non-pathogenic, non-toxic and can remain in dormant state for many years, without food. Moreover, *B. subtilis* stored at 28°C effectively bring about MICP even after months of inactivity. Larger amount of precipitated $CaCO_3$ are obtained by using higher concentrations of

bacteria in concrete [7]. Previous studies had found bacterial dosage of 0.1 to 5 x 10^6 cell/ml of mixing water (corresponding to about 0.01 to 0.5% by weight of dry cement) effective in concrete [7- 9, 16].

Highly resistant to a wide range of pressure, temperature, and acid or alkali environments, *B. subtilis* are rod shaped and circular in cross-section about 4 to 10 μm long and 0.25 to 1.0 μm in diameter, with wall element that are characterized with heavily flagellated filament like fibers used for moving in media (Fig. 1) [17]. At micro level, these filaments function similar to synthetic fiber used in fiber reinforced concrete. The cell wall may occupy 20 to 70% of the cell mass, and is found to play an important role in influencing the fresh and hardened properties of concrete [9]. As shown in *Fig. 1*, the major component of cell wall is anionic peptidoglycan, covalently attached to which are the teichoic acids and proteins [19, 20]. Peptidoglycan's chemical structure is similar to that of a Viscosity Modifying Admixtures (VMAs) such as starch, welan gum, diutan gum, and cellulose ethers used in making stable and robust SCC [9]. The negatively charged cell wall (peptidoglycan) serve as C-S-H nucleation site for additional MICP in concrete [14, 15].

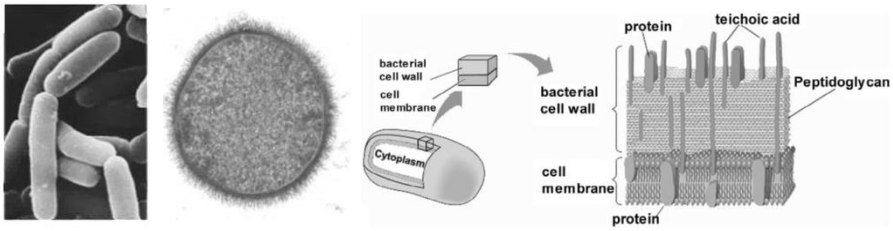

Figure 1. Microscopic details of *B. subtilis* bacterium cell [9, 18-20]

A recent study has found an important physical interaction between *B. subtilis* and concrete matrix that enhances MICP. Bacterial cell walls get detached from bacteria by the grinding action during concrete mixing and long molecules of peptidoglycan (cell walls) are obtained [6, 9]. These detached cell walls (but interestingly not the live and dead bacterial cells) were found to enhance concrete compressive and tensile strength by about 15% and decrease porosity after 28 days of curing [6, 10]. On the contrary, high concentrations of dead bacterial cells of *B. subtilis* were noted to decrease compressive strength of concrete, possibly due to the repulsion effect of negatively charged cell and wall membranes hindering formation of nucleation sites that are vital for effective MICP [6]. The addition of bacteria does not always increase concrete strength owing to the effects of added organic nutrients/food (such as components of urea, glucose, $CaCl_2$ and other media), high concentrations of dead cells, and some other unknown interactions [6]. Certain aspects of MICP are not fully understood and needs further investigation. Effects of ammonia (a by-product of MICP) on reinforcement in

concrete, quantity and quality of brittle $CaCO_3$ produced, compatibility with other chemical and powder admixtures, long-term performance, structural behaviour, and performance in real-life applications are some of the unknown factors of MICP [21].

A latest study has found bacterial SCC made with 1st generation naphthalene-sulfonate based High Range Water Reducer (HRWR) compatible with *B. subtilis*, with regard to the fresh and hardened performance [6, 9]. However, the interactions of *B. subtilis* with the most commonly used Polycarboxylic Ether (PCE) polymer based 2nd generation HRWR in SCC are unknown; especially when the physicochemical behaviour of 1st and 2nd generation HRWR in SCC are quite different, and therefore may function differently with *B. subtilis* bacteria. It is not yet understood, how the delayed absorption of PCE molecules on cement particles would affect the performance of *B. subtilis* bacteria and MICP in SCC. MICP in normal concrete has been successfully achieved, but remains to be studied in a rheologically and chemically different regime of SCC made with PCE-HRWR. SCC's unique rheology and presence of complex PCE-HRWR may affect MICP in concrete. The present study examined the effects of calcite depositing *B. subtilis* bacteria on the fresh and hardened properties of Self-Compacting Bacterial Concrete (SCBC) made with 2nd generation PCE-HRWR.

Materials and Methodology

Materials and Mix Proportions

Four concrete mixes i.e. Normal Concrete (NC), Normal Bacterial Concrete (NBC), SCC and SCBC were tested. All the concrete mixtures in this work were made using - 450 kg/m^3 of ordinary portland cement (53-Grade) confirming to IS 12269 [22]; 825 kg/m^3 of well graded Zone-I river bed sand with specific gravity of 2.7, passing through 4.75 mm sieve and retained on 0.75 mm sieve; and 901 kg/m^3 uniformly graded, crushed angular Basalt coarse aggregates of 12 mm maximum size, with specific gravity of 2.65, both aggregates confirmed to IS 383 [23]; and 180 liters/m^3 of potable water. PCE-HRWR (2nd generation) confirming to IS 9103 [24] with a dosage of 4 liters/m^3 was used to make SCC and SCBC mixes. *B. subtilis* bacterial stock solution made with glucose and agar-agar broth of 6 liters/m^3 with 5 x 10^9 cells/ml of mixing water (i.e. about 0.134% dry weight of cement) was used in all bacterial concrete mixes. Water content of the bacterial stock solution was accounted in the total designed water quantity of the concrete mix.

It was easy and cheap to produce *B. subtilis* stock culture using locally available resources under laboratory conditions. In this work, the cost of producing *B. subtilis* stock culture was about \$1/liter (i.e. \$6/m^3 of concrete), which locally was approximately 10% and 7% of NC and SCC material cost, respectively. The cost of

standard dosage of bacteria in SCC was almost half the cost of HRWR. Initially, M40 grade of SCC was proportioned as per the ACI 237 [25] guidelines. Two trial batch mixes were prepared to verify the satisfactory performance of fresh SCC. Concrete mix proportions were finalized after slight alterations based on the trials. Concrete was mixed in a 40-liter capacity motorized drum mixer. The mixing time for all mixes was 2 minutes for dry mixing (cement plus aggregates) and additional 4 minutes for wet mixing of all concrete ingredients. Desired dosage of the bacterial stock solution was dispersed in concrete during the wet mixing stage. SCC mixes were left standing for about a minute after mixing for initialization of HRWR.

Experimental Work

Fresh and hardened properties of all the four concrete mixes were determined for a concrete batch of 28-liter capacity mix. Slump tests [26], which provide a relative measure of consistency and workability of conventional concrete, were conducted for NC and NBC mix. Slump flow tests were performed as per the ASTM C1161 [25, 27] to determine the unconfined filling ability and flow potential of the SCC/SCBC mixtures. Slump flow is the mean diameter of the horizontal spread of the concrete mass (i.e. patty), after lifting the Abram's slump cone filled with fresh SCC. Additionally, Visual Stability Index (VSI) and T_{50}-Time values were recorded during the slump flow test [26]. The VSI value is a visual rating (0 to 3; in increments of 0.5) indicating apparent stability of SCC in terms of degree of segregation and bleeding evaluated by observing the slump flow patty. A VSI rating of zero designates a highly stable SCC mix whereas a value of three indicates severe segregation and bleeding, representing a very poor quality of SCC. The T_{50}-Time is the time required by SCC to spread to 500 mm diameter during the slump flow test indicating filling ability and viscosity of the mixture. A satisfactory SCC has a slump flow greater than 550 mm, VSI value between 0 to 1 and T_{50}-Time value between 3 to 7 seconds [25].

Standard 150 mm size concrete cubes and 150 mm (diameter) x 300 (height) mm cylinders were cast for each mix inside the laboratory. It should be noted that the NC and NBC mix specimens were manually compacted as per standard practice [26] whereas the SCC and SCBC mix were cast without any mechanical vibration or compaction energy. Hardened properties i.e. compressive [28] and tensile [29] strengths of the concrete specimens were tested at 28 days after casting. The specimens were air cured for one day and then water-immersion cured upto the testing day. Three specimens per mix were tested for each of the hardened properties. Additionally, non-destructive Rebound Hammer tests [30] were performed on concrete cubes and cylinders before destructive testing, to compare the relative compressive strength of different mix.

Results and Discussions

Fresh Properties

The results of various fresh properties measured for all the concrete mixes are depicted in *Table I*. Photographs of slump and slump flow tests of various concrete mixes are shown in *Fig. 2*. The slump of NBC was a true slump (*Fig. 2b*), indicating cohesive mix compared to that of NC, which was slightly larger than NBC but a shear slump (*Fig. 2a*), representing a relatively harsh/lean concrete. The relatively cohesive and better quality of slump observed in NBC may be due to the viscosity modifying effect of *B.subtilis* in concrete. Satisfactory workability and stability performance was obtained for the self-compacting concretes, except for the undesirable VSI greater than 1.0, in case of SCC mix.

Table I. Fresh Properties of various concrete mixtures

Fresh property	NC	NBC	SCC	SCBC
Slump [mm]	90	85	-	-
Slump Flow [mm]	-	-	695	695
VSI	-	-	1.5	0.5
T_{50}-Time [sec]	-	-	4	4

a) NC-Shear slump b) NBC-True slump c) SCC-Slump flow patty d) SCBC-Slump flow patty

Figure 2. Slump and slump flow tests of various concrete mixes

Although, the slump flow values of SCC and SCBC mix were exactly the same, the visual quality of both these mixes were significantly different; SCC being more

leaner (*Fig. 2c*) and SCBC being relatively viscous and cohesive (*Fig. 2d*). Furthermore, the VSI rating for SCC was 1.5, due to signs of an aggregate pile (i.e. segregation) at the center of slump flow patty and slight mortar halo (i.e. bleeding) around it (*Fig. 2c*). On the contrary, the VSI of SCBC was rated as 0.5, based on no signs of segregation and bleeding in the slump flow patty (*Fig. 2d*). The above observations suggest that the addition of bacteria in concrete does not significantly affect its workability, but noticeably enhances the consistency and cohesiveness of the concrete mix. This improvement in the general quality of concrete is more prominent in SCC than in traditional concrete. The T_{50}-Time for SCC and SCBC was same and seems not to be affected by addition of bacteria. The enhancement in concrete stability caused by addition of *B.subtilis*, without hampering the filling ability and flow potential of SCC, is similar to the effect brought out by an ideal VMA in SCC, as was also noted by other study [9].

Hardened Properties

Figure 3. Cube and cylinder test specimens of bacterial concrete

Table II. Results of hardened properties of various concrete mixes

Mix	Compressive Strength [Mpa]			f_{ct} [MPa]	k
	f_c	RH_{Cu}	RH_{Cyl}		
NC	39.87	41.62	37.37	3.45	0.546
NBC	48.96	45.36	41.48	3.73	0.533
SCC	54.84	54.53	54.36	4.25	0.574
SCBC	59.96	57.78	57.76	4.70	0.607
Strength ratio: SCC/NC	1.38	1.31	1.45	1.23	1.05
NBC/NC	1.23	1.09	1.11	1.08	0.98
SCBC/SCC	1.09	1.06	1.06	1.11	1.06

f_c – Compressive strength of cube; RH_{Cu} – Cube strength by Rebound Hammer; RH_{Cyl} – Cylinder strength by Rebound Hammer; f_{ct} – Split tensile strength; k - Tensile strength coefficient = $f_{ct}/\sqrt{fc}$

The external and internal visual appearance (color, texture and finish) of bacterial and non-bacterial concretes was similar, and without any indications of segregation, as observed in the demolded and broken specimens. Close inspection of broken specimens showed uniform distribution of intact unfractured aggregates throughout the specimens. Typical cube and cylinder specmens of bacterial concrete before and after testing are shown in *Fig. 3*. The results of different hardened properties evaluated for the various concrete mixes in this work are presented in *Table II*. The depicted results are the representative average values of three specimens tested at 28-days, of a particular mix – readers are cautioned about this preliminary and limited investigation.

All the concretes easily achieved the design strength of minimum 40 MPa except NC mix, which fell slightly short of the mark. As expected, the SCC mix was about 38% stronger than the control traditional NC mix based on the measured compressive strengths (f_c, RH_{Cu}, RH_{Cyl}), owing to the HRWR effect. The bacterial concrete mixes showed enhanced compressive and tensile strengths over the respective control mix. Interestingly, the compressive strength (f_c) of NBC mix was about 23% more than its control NC mix, while this increase was only about 9% in SCBC mix over its control SCC mix. Additionally, the indicative compressive strengths obtained by Rebound Hammer tests were also relatively lower for SCBC than NBC mix. This reduced effectiveness of *B.subtilis* in enhancing compressive strength of SCBC mix may be attributed to the possible incompatibility of PCE-HRWR with *B.subtilis* bacteria resulting in lower pH of matrix, reduced nucleation sites, and formation of comparatively more amounts of dead bacterial cells, which may have resulted in below-par MICP [6, 9]. Furthermore, due to the unique rheology of SCBC (i.e. lower yield stress and moderate-to-high viscosity, compared to normal concrete [25]) it is likely that lesser amounts of bacterial cell walls (responsible for effective MICP [6, 9]) were produced while mixing due to reduced attrition in the SCBC mix.

The split tensile strength of SCC mix was about 23% higher than corresponding control NC mix, evidently due to improvement in compressive strength of SCC upon addition of HRWR. The tensile strength of SCBC was about 11% more than its control SCC mix, while this increase was only about 8% in NBC mix over its control NC mix. The normalized split tensile strength with respective to the square-root of corresponding compressive strength for each mix i.e. the normalized split tensile strength coefficient (k), was slightly reduced in NBC mix than the other mixes. Moreover, k values for SCBC were 6%, 11% and 14% higher than the SCC, NC, and NBC mixes, respectively. This is presumed to be due to the fiber-reinforcing effect of excessive amounts of flagellated bacterial dead/live cells in

SCBC, but which may have been suppressed in NBC due to MICP on the surface of the cells.

Conclusions

Based on this limited study the following conclusions are presented;

1) The *B.subtilis* bacteria culture is easily produced in laboratory conditions using local materials and can safely and effortlessly be used in concrete. The *B.subtilis* bacteria functions as a VMA in concrete, as it noticeably enhances the stability, consistency and cohesiveness of concrete mix, especially that of SCC.

2) Mechanical test results showed a general trend of increase in compressive and tensile strengths of the bacterial concrete mixes. Compressive strength improved by about 23% and 9% in NBC and SCBC mixes, respectively. Whereas tensile strength increased by about 11% and 8% in SCBC and NBC mixes, respectively.

3) Interestingly, NBC mix showed higher increase in compressive strength than the SCBC mix due to the reduced effectiveness of bacteria in SCBC mix. This may be due to an incompatibility between PCE-HRWR and *B.subtilis*, manifested by formation of relatively large amounts of dead bacterial cells, lower pH of matrix, and reduced nucleation sites in SCBC than in NBC mix. Also, less attrition in concrete while mixing SCBC owing to its unique rheology, may have produced lower amounts of bacterial cell walls, consequently reducing the extent of MICP in SCBC compared to NBC. In contrast, higher tensile strength was observed in SCBC compared to NBC mix, presumably due to the fiber-reinforcing effect of excessive amounts of flagellated bacterial dead/live cells formed in SCBC, but which may have been suppressed in NBC due to excessive MICP on the surface of the cells. Thus, PCE-HRWR may not be fully compatible with the *B.subtilis* bacteria. Additional detailed investigation to confirm this hypothesis is required.

4) In this study, the cost of bacterial concrete was only about 10% more than conventional concrete. However, the multifunctional benefits of bacteria in concrete that effects in enhanced strength and durability, self-repair of cracks, and improved stability through bio-admixture VMA action - may outweigh the associated cost.

Acknowledgments

The support of Dr. Dhakaphalkar (Agharkar Research Institute, Ind.) for providing bacterial culture and VIIT for sponsoring the research work is greatly appreciated.

References

[1] Ramachandran, S. K., Ramakrishnan, V., and Bang, S. S. (2001), *ACI Mat. J.*, vol. 98, n. 1, p. 3-9.
[2] Ghosh, P., Mandal, S., Chattopadhyay, B.D., and Pal, S. (2005), *Cem. Concr. Res.*, vol. 35, no. 10, p. 1980-83.
[3] Jonkers, H.M., (2007), Self healing concrete: a biological approach, In: *Self healing materials:an alternative approach to 20 centuries of materials science*, van der Zwaag, S. (Ed.), Springer, Berlin, p. 195-204.
[4] De Muynck, W.D, Debrouwer, D., De Belie, N.D, and Verstraete, W., (2008), *Cem. Concr. Res.*, vol. 38, p. 1005-14.
[5] Wiktor, V., and Jonkers, H.M., (2011), *Cem. Concr Compos*., vol. 33, n. 7, p. 763-70.
[6] Pei, R., Liu, J., Wang, S., and Yang, M., (2013), *Cem. Concr. Compos*., vol. 39, p. 122-30.
[7] Wang, J.Y., De Belie, N., and Verstraete, W., (2012), *J. Ind. Microbiol. Biotechnol.*, vol. 39, p. 567-77.
[8] Stocks-Fischer, S., Galinat, J.K., and Bang, S.S., (1999), *Soil Biol. Bioche.*, vol. 31, p. 1563-71.
[9] Pei, R., Liu, J., and Wang, S., (2015), *Cem. Concr. Compos*., vol. 55, 186-95.
[10] Reddy, S., Rao, M., Aparna, P., and Sasikala, C., (2010), *Asian J. Civ. Eng. (Build. Hous.)*, vol. 11, n. 1, p. 43-55.
[11] Jonkers, H.M., Thijssen, A., Muyzer, G., Copuroglu, O., and Schlangen, E., (2010), *Ecol. Eng.*, vol. 36, n. 2, p. 230-5.
[12] Li, P., and Qu, W., (2012), *Adv. Mater. Res.*, vol. 365, p. 280-86.
[13] Plank, J., (2004), *Appl. Microbiol. Biotechnol.*, vol. 66, n. 1, p. 1-9.
[14] De Muynck, W.D., De Belie, N.D, and Verstraete, W., (2010), *Ecol. Eng.*, vol. 36, n. 2, p. 118-36.
[15] Douglas, S., Beveridge, T.J, (1998), *FEMS. Microbiol. Ecol.*, vol. 26, n. 2, p. 79-88.
[16] Calvert, P., (2012), *Cem. Concr. Res.*, vol. 38, p. 1005-14.
[17] Yu, A., Loo, J., Yu, S., Kong, S., and Chan, T., (2013), *Appl. Microbiol. Biotechnol.*, vol. 98, n. 2, p. 855-62.
[18] Weiner, A., (2006), *Bacillus subtilis* image, Weizmann Inst. Sci., Israel.
[19] Atrih, A., Bacher, G., Allmaier, G., Williamson, M.P., and Foster, S.J., (1999), *J. Bacteriol.* Vol. 181, n. 13, p. 3956–66.
[20] Vollmer, W., Blanot, D., and De Pedro, M.A., (2008), *FEMS Microbiol. Rev.*, vol. 32, n. 2, p. 149-67.
[21] Ivanov, V., Chu, J., and Stabnikov, V., (2015), Chapter 2-Basics of construction microbial biotechnology, In: *Biotechnologies and biomimetics for civil engineering*, Pacheco, T.F., et al. (Eds.), Springer, Switzerland.
[22] IS12269, *Ordinary portland cement 53-grade-specification*, BIS, 2013, Ind.

[23] IS 383, *Specification for coarse and fine aggregates from natural sources for concrete*, BIS, 2002, Ind.
[24] IS 9103, *Concrete admixtures-specification*, BIS, 2004, Ind.
[25] ACI 237R, *Self-consolidating concrete*, ACI, 2007, USA.
[26] IS 1199, *Methods of sampling and analysis of concrete*, BIS, 2004, Ind.
[27] ASTM C1611, *Standard test method for slump flow of self-consolidating concrete*, ASTM International, 2014, USA.
[28] IS 516, *Methods of tests for strength of concrete*, BIS, 2004, Ind.
[29] IS 5816, *Splitting tensile strength of concrete*, BIS, 2004, Ind.
[30] IS 13311, *Non-destructive testing of concrete: part 2: rebound hammer*, BIS, 2004, Ind.

Fly Ash-Nano SiO_2 Blends for Effective Application in Self-Consolidating Concrete

Rani Pradoto[1], Mohamad Reza Moini[1,2], Ismael Flores-Vivian[1,3], Marina Kozhukova[1], Konstantin Sobolev[1]

[1] *Civil and Environmental Engineering, Advanced and Nano Cement-Based Materials Lab,*
University of Wisconsin - Milwaukee, Milwaukee, WI 53211 U.S.A.
[2] *Collins Engineers Inc., 2033 W Howard Ave, Milwaukee, WI 53221 U.S.A.*
[3] *Universidad Autónoma de Nuevo León, Av. Universidad s/n, Cd. Universitaria, San Nicolás de los Garza, 66455, Nuevo León, Mexico*

Abstract The use of SiO_2 nanoparticles (nanosilica) in nano-engineered self-consolidating concrete (SCC) was investigated. It was observed that the addition of very small amounts of nanosilica (less than 1%) can replace a need for a viscosity modifying agent and improve the performance of SCC.
In this research, the SCC mixtures were designed with 30% and 50% of class C fly ash and produced at a cementitious content of 400 kg/m^3 and 500 kg/m^3. The SCC designed with fly ash, nanosilica, and superplasticizing (high-range water-reducing, HRWR) admixtures were investigated for fresh properties, rheological response, and compressive strength.

Introduction

Self-consolidating concrete (SCC) is a new type of concrete which is characterized by the ability to fill the formwork under its own weight without external compaction effort, while still maintaining homogeneity and low segregation [1]. Self-compacting concrete can flow under its own weight and has very low, near zero yield. Therefore, for workability characterization, slump (correlated with yield stress) is of lesser significance than it is for conventional concrete and other methods related to material flow (such as v-funnel, J-ring test) were proposed for characterization of workability [1]. To understand the workability and flow properties of SCC, the rheological response of cement pastes and mortars can be used. To maintain the workability of SCC, it is essential to provide adequate spacing between the aggregates in order to facilitate the flow and eliminate the

friction between the particles. This is achieved by the optimization of aggregates spacing, grading and proportions and using mixtures with higher volumes of cement paste. The volume of cement paste between the aggregates depends on the aggregate packing, which is known as a “compact paste”, and the cement paste surrounding the aggregates is known as “excess paste”. This excess paste allows concrete to flow and maintain a uniform dispersion [2].

The use of nanoparticles in nano-engineered concrete has been a subject of interest for many researchers. Collepardi et al. [3] investigated SCC with low heat release by combining supplementary cementing materials (SCM) such as fly ash and limestone with colloidal nanosilica. It was demonstrated that colloidal nanosilica in SCC acts as a viscosity modifying agent [3-7]. The developed SCC with nano-SiO_2 had a better performance when tested on slump flow and resistivity to segregation.

In this reported study, SCC was developed using nanosilica and fly ash blends, and the effect of nanoparticles on the fresh and hardened properties of nano-engineered SCC was investigated. The SCC mixtures were designed with different proportions of fly ash used as a cement replacement material along with nanosilica and superplasticizer.

Materials and Methods

Nanosilica is the key component of SCC affecting the flow, density and heat of hydration. The amount of nanosilica used in cement based systems is up to 2%. By replacing portland cement with a small amount of nanosilica, the workability, density, compressive strength and the rate of heat release from cement hydration can be controlled. Cembinder is a surface modified amorphous colloidal silica (nanosilica) product which was designed for concrete applications. For this study, two different colloidal nanosilica products were used. The first is Cembinder 50 which had an average particle size of 5 nm and a solid concentration of 15%. Another product is Cembinder 8 which had an average particle size of 10-100 nm and a solid concentration of 50%. The properties of nano-SiO_2 are listed in Table 24. Quercia et al. [7] analyzed the size and morphology of commercial Cembinder products using the scanning electron microscope (SEM) to determine the characteristic parameters important for the application in cement systems, Figure 1.

Table 24 Properties of nanosilica

Test Parameter	**SiO_2 Cembinder Grade**	
	50	**8**
Density, g/cm^3	1.1	1.4
SiO_2,%	15	50
pH	10.0	9.5
Viscosity, mPas	<10	<10
Average particle size, nm	5	10-100

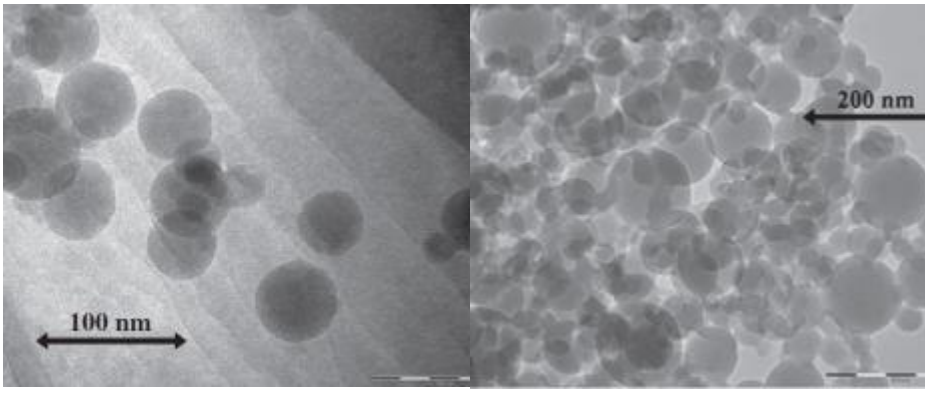

(a) Cembinder 50 (b) Cembinder 8

Figure 1. Particle shape of (a) Cembinder 50 and (b) Cembinder 8 [7]

ASTM Type I portland cement was used for this study. The chemical composition of portland cement is reported in Table 25, along with the requirements of ASTM C150 Standard Specification for Portland cement. The chemical composition of cement was tested using the X-Ray Fluorescence (XRF) technique and reported by the cement manufacturer.

Table 25. Chemical composition of portland cement

Parameter	**ASTM C150**	**Test Result**
SiO_2, %	-	19.4
Al_2O_3, %	-	5.3
Fe_2O_3, %	-	3.0
CaO, %	-	63.2
MgO, %	6.0 max	2.9
SO_3, %	3.0 max	3.3
Na_2O, %	-	0.3
K_2O, %	-	0.7
Others, %	-	0.9
Loss on Ignition, %	3.0 max	1.1
Composition		
Al_2O_3 / Fe_2O_3		1.8

C_4AF, %	-	9.1
C_3A, %	-	8.9
C_2S, %	-	9.9
C_3S, %	-	60.7
Na_2O_{equi}, %	0.6 max	0.8

ASTM Class C fly ash (from We Energies) was used in this research. The chemical composition of fly ash is reported in Table 3, along with the properties of Class F fly ash and the requirements of ASTM Specification for Coal Fly Ash and Raw or Calcined Natural Pozzolan for use in concrete (C 618). Fly ash can be used in concrete as a replacement for portland cement at levels of up to 50%. There are many advantages associated with fly ash application such as:

- Improved workability;
- Reduced heat of hydration;
- Improved ultimate compressive strength;
- Reduced porosity and permeability;
- Increased resistance to alkali silica reaction;
- Increased resistance to sulfate attack.

Table 3. Chemical composition of fly ash

Item	**Class F**	**Class C**	**ASTM C 618 limits**	
			Class F	**Class C**
SiO_2, %	46.9	32.7	-	-
Al_2O_3, %	22.9	17.6	-	-
Fe_2O_3, %	19.2	5.9	-	-
Total, $SiO_2+Al_2O_3+Fe_2O_3$, %	89.0	56.2	70 min	50 min
SO_3, %	0.3	2.0	5.0 max	5.0 max
CaO, %	3.8	27.3	-	-
MgO, %	0.8	6.6	-	-
K_2O, %	1.7	0.4	-	-
Na_2O, %	0.6	2.2	-	-
Moisture Content, %	0.1	0.8	3.0 max	3.0 max
Loss on Ignition, %	2.3	0.3	6.0 max	6.0 max

Polycarboxylate superplasticizer (PCE-SP), a commercially available high-range water reducing agent was supplied by Handy Chemicals. After a preliminary study

and testing, the optimal superplasticizer dosage was selected and used for the reported research.

Coarse, intermediate and fine (natural sand) aggregates from Southern WI were used in this project. Table 4 provides a summary of the physical characteristics of aggregates. The sieve analysis of aggregates is reported by Figure 2. It can be observed that the aggregate gradings were within the limits set by ASTM C33. Slight access of 300 µm fraction in sand can be considered as acceptable.

Table 4. Physical characteristics of aggregates

Aggregate Type		Specific Gravity			Density, kg/m^3			Water Absorption, %	Fines <75µm, %
		OD	SSD	Apparent	OD	SSD	Apparent		
C1	1”Limestone	2.730	2.765	2.829	2723	2758	2822	1.29	0.78
I1	5/8”Limestone	2.684	2.734	2.824	2678	2727	2817	1.84	0.79
F1	Torpedo Sand	2.566	2.637	2.762	2559	2630	2755	2.77	1.19

Experimental Program

The experimental matrix involved mixing and testing SCC mixtures containing a total of 400 kg/m^3 and 500 kg/m^3 of cementitious materials. The SCC mixtures were designed at a fly ash content of 30% and 50%, with nanosilica and high range water reducer (HRWR). The flowability and stability are the two most important properties of SCC. A high flowability of SCC can be achieved without changing the W/C ratio by using effective HRWR admixtures such as PCE. The improved stability can be achieved by increasing the total quantity of fine aggregates, which is affects viscosity and reduces segregation. In this study, the stability of SCC mixtures was achieved by using fly ash and nanosilica. The reference portland cement based SCC mixtures were compared with fly ash based concrete. The aggregate blend was selected using 40% of coarse aggregates, 10% of intermediate aggregates and 50% of fine aggregates, which meets the optimized gradation. All concrete mixtures were proportioned according to the ACI 211 concrete specification. The resulting concrete was evaluated for fresh properties using V-funnel test, slump flow and J-ring flow (for passing ability and stability). The hardened properties such as compressive strength at 1, 3, 7 and 28 days were also evaluated.

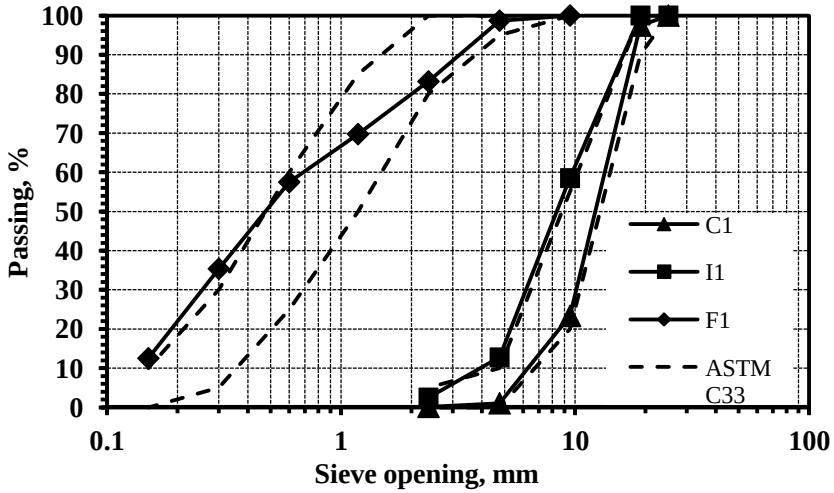

Figure 2. Particle size analysis of aggregates

Test Methods

Concrete mixtures were batched, mixed, cast, cured, and tested according to the corresponding ASTM standards. Compressive strength tests were performed on cylinders with a diameter of 102 mm (4-in.) and height of 203 mm (8-in) according to ASTM C39. These specimens were tested with an ADR-Auto ELE compression machine at a loading rate of 2.4 kN/s (540 lb/s). The maximal loads and corresponding maximal compressive stresses were recorded and reported. The test was performed at different ages of 1, 3, 7 and 28 days of normal curing. The experimental data were obtained using the required number of specimens for various tests. For each testing age and each compressive strength test, the reported results were based on testing 3 specimens. The errors and standard deviations for all results of final batches were calculated and the outliers were eliminated from the results, according to the requirements imposed by the associated standards for compressive strength tests.

Results and Discussion

The mixture proportions, as well as fresh and hardened properties of investigated SCC are reported in Table 5.

The flow time of the SCC mixtures was investigated using the V-funnel test. The V-funnel times were in the range of 4 to 15 seconds. The SCC with 50% fly ash content had the lowest flow times, and the reference SCC without fly ash had the highest flow times. It was determined that due to the spherical shape of fly ash particles, the replacement of portland cement with fly ash improves the flow as

well as the overall workability of SCC mixtures. The flow performance of SCC depends on the volume of cementitious materials and the volume of cement paste (including air) [8-10]. In spite of lower viscosity (induced by higher W/CM), the flow time for SCC with 400 kg/m^3 was longer than that of the 500 kg/m^3 mixtures. This can be attributed to higher volume of cementitious materials (and cement paste) and better separation thickness between the aggregates.

The slump flow performance of the investigated SCC was within a range of diameters, changing between 469 mm and 1015 mm. Based on ASTM C1611, the typical SCC slump flow ranges from 450 mm to 810 mm. For SCC with cementitious content of 400 kg/m^3, all the mixtures were within the range of the required standard; the SCC with 30% of fly ash and cementitious content of 500 kg/m^3 had exceptionally high slump flow of 1015 mm produced without any bleeding or segregation. These results prove that incorporating of fly ash and nanosilica dispersion can provide concrete with significantly enhanced slump flow.

Excellent correlation between the slump flow and J-ring test was observed as represented by Figure 3. Here it can be observed that the increased slump flow is directly proportional to the increase in the J-ring value for all investigated SCC.

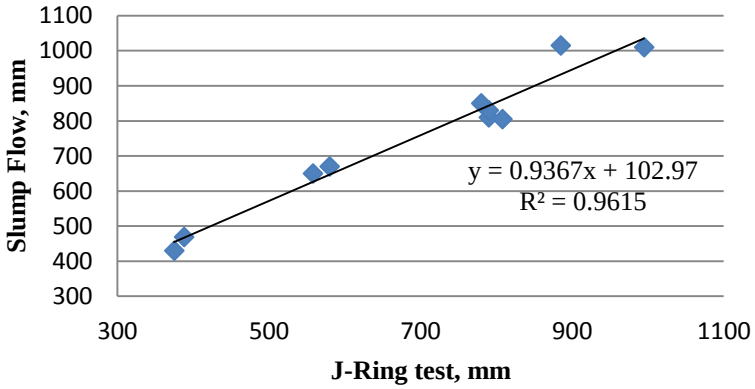

Figure 3. The correlation between the slump flow and J-ring test

The highest 28-day compressive strength of 59.6 MPa and 83.3 MPa was achieved by SCC with 30% fly ash and cementitious material content of 400 kg/m^3 and 500 kg/m^3, respectively (Figure 4). These values slightly exceed the strength of reference portland cement based SCC and are an indication that the use of nanosilica can improve the compressive strength of SCC with SCM. It can be concluded that strength improvement is due to the use of ultrafine particles of fly ash and nanosilica.

The strength of SCC with 50% fly ash was low, especially at early ages of hardening. The 28-day compressive strength of SCC with 50% fly ash at a cementitious material content of 400 kg/m^3 and 500 kg/m^3 was only 80% and 72% of reference values, respectively. However, concrete with 30% fly ash demonstrated only slightly reduced early-age strength and also exceeded the 28-day strength of reference SCC.

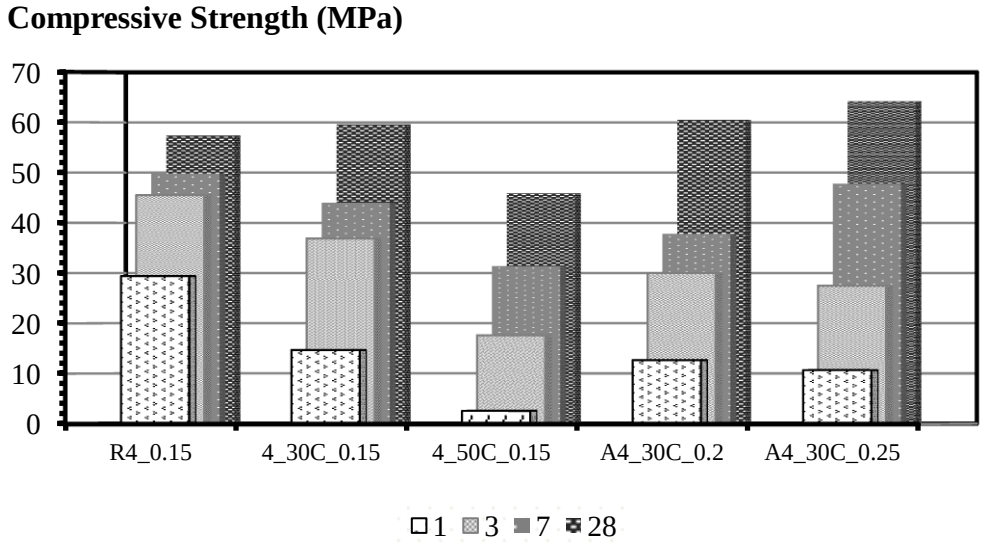

Figure 4. Compressive strength of developed SCC with nanosilica

Table 5. Performance of developed SCC with nanosilica

Mix ID	Mixture Proportions, kg/m^3				W/CM	V-funnel, s	Slump flow, mm	J-Ring, mm	Compressive Strength, MPa			
	Cement	Fly Ash	Admixtures						1 day	3 days	7 days	28 days
			PCE	Nano silica								
R4	400	0	0.938	3.427	0.375	15	469	388	29.4	45.5	49.8	57.4
4_30C	280	120	0.938	3.427	0.375	14	650	558	14.7	36.9	44.0	59.6
4_50C	200	200	0.938	3.427	0.375	4	810	790	2.6	17.6	31.4	45.9
R5	500	0	1.564	4.284	0.300	11	805	808	30.0	54.9	65.6	81.5

5_30C	350	150	1.564	4.284	0.300	10	1015	885	25.2	50.0	54.3	83.3
5_50C	250	250	1.173	4.284	0.300	4	670	580	6.0	44.3	47.9	59.0

Conclusions

The boost of performance of cementitious systems with fly ash can be achieved by the incorporation of ultrafine super-reactive particles of nanosilica resulting in the acceleration of cement hydration. The effective use of fly ash requires the application of fly ash-nanosilica-superplasticizer blends; this enables the considerable reduction of W/CM ratio and at the same time, provides excellent workability at the levels required for SCC as well as the achievement of early-age strength with 1-day compressive strength of up to 25 MPa (e.g., for mix 5_30C with cementitious material content of 500 kg/m^3).

Effective nano-engineered SCC can be designed with Class C fly ash of up to 50% in the compositions with PCE superplasticizer and nanosilica used at the dosage of 0.15% and 0.15%, respectively. The developed approach for nano-engineering of SCC and reported research results can serve as a foundation for the specification and application of sustainable concrete with high volumes of supplementary cementitious materials and enhanced performance as required for applications in modern civil and transportation infrastructure.

References

1. Chockalingam, M., (2014) Experimental Investigation on Self Compacting Concrete (SCC) using marble powder and silica fume. *International Journal and Magazine of Engineering, Technology, Management and Research* (*IJMETMR*) 1, 15.

2. Sobolev, K. and Yeginobali, A., (2005) The Development of High-Strength Mortars with Improved Thermal and Acid Resistance. *Cement and Concrete Research*, 35(3) 578-583.

3. Collepardi, M., et al. (2002) Influence of Amorphous Colloidal Silica on the Properties of Self-Compacting Concretes: *in Proceedings of the International Conference, Challenges in Concrete Construction - Innovations and Developments in Concrete Materials and Construction*. Dundee, UK, 473 - 483.

4. Nobel, A., (2011) Cembinder for the oil field industry, colloidal silica dispersions - uses and benefits: https://www.akzonobel.com/colloidalsilica/system/images/AkzoNobel_Cembinder_W_for_the_oil_field_industry_eng_tcm135-68676.pdf

5. Flores, I., Sobolev, K., Torres-Martinez, L., Cuellar, E., Valdez, P., and Zarazua, E., (2010) Performance of Cement Systems with Nano-SiO_2 Particles

Produced by Using the Sol-Gel Method. *Transportation Research Record: Journal of the Transportation Research Board*, 2141(1) 10-14.

6. Björnström, J., et al., (2004) Accelerating effects of colloidal nano-silica for beneficial calcium–silicate–hydrate formation in cement. *Chemical Physics Letters*, 392(1–3) 242-248.

7. Quercia, G., G. Hüsken, and H.J.H. Brouwers (2012) Water demand of amorphous nano silica and its impact on the workability of cement paste. *Cement and Concrete Research*, 42(2) 344-357.

8. Mehta, P.K. and P.J.M. Monteiro (2006) *Concrete, Microstructure, Properties and Materials*, New York: McGraw Hill Companies.

9. Banfill, P., (1990) Rheology of Fresh Cement and Concrete: *in Proceedings of an International Conference*, Liverpool, CRC Press.

10. Sobolev, K., et al., (2015) Laboratory Study of Optimized Concrete Pavement Mixtures, *in Final Report for WHRP 2012-2015*, UW-Milwaukee, UW-Madison, Temple University/Bloom.

Theme 3: Test Methods

Quality Control of Controlled Low Strength Materials with the Dynamic Cone Penetrometer

Samuel Pothier[1], Michel Vaillancourt[1] and Claudiane Ouellet-Plamondon[1]

[1]École de technologie supérieure, 1100 Notre-Dame West, Montreal, QC, H3C 1K3, Canada

Abstract Controlled low strength materials (CLSM) are increasingly used in urban areas to fill the trenches that constitute the technical urban underground network. CLSM replaces compacted rock stone; it is delivered with a concrete mixer and self-compacts due to its high water content. Few quality control requirements are listed in its specifications, none of which mention draining capacity and ground rigidity. Using data from four urban test sites, our study shows that the consolidation of CLSM varies with ground type, which has major implications for quality control specifications. The primary tool used to measure CLSM consolidation was the dynamic cone penetrometer, while the current standard is based on ball drop to determine suitability for load application. The dynamic cone penetrometer had more information on ground conditions than the drop ball tests. The results will be incorporated in a consolidation model to estimate the minimum time required before opening the road to car circulation.

Keywords: *Controlled low strength materials, Dynamic cone penetrometer, Trench, Ball drop, Quality control, Underground network.*

Introduction

Controlled low strength materials (CLSM) are cementitious self-compacting backfill materials delivered with a concrete mixer. When used as fill in trenches, in discrete apertures or near foundations, the cement content is kept low to allow for easy reexcavation. The maximum compression resistance should be 0.8 to 1.0 MPa for reexcavation, while structural backfill can reach 8.0 MPa [1]. CLSM requires no warehouse space, reduces building site equipment requirements, and reduces the risk of accidents, which often result from compaction without prior trench widening. Significant savings in time and cost can be achieved [2]. A bridge abutments construction using CLSM eliminates several weeks of construction time

as no pole is required in the structure. Design calculations are simple, which minimizes costs and driver impact [3].

One study suggests that the design of the CLSM mix take into account the strength and compressibility of the adjacent soils. The soil data is found using laboratory tests or dynamic penetrometer in the field. For example, two soil types encountered in southern Louisiana have an optimal compressive strength of 0.41 MPa at 28 days. However, a resistance of 0.7 MPa is required if traffic is to be re-established within 24 hours of casting [4]. A more recent study suggests incorporating the data of the receiving ground using a 3D mathematical model, from DIANA 9.1, in the design phase of CSLM. In the case of narrow trenches, a compressive strength between 2.0 and 2.5 MPa ensures maximum stability while preserving the ability to excavate [5]. However, this approach is considered too theoretical and hard to replicate with other compositions of the receiving medium [6].

Since 1989, the city of Montreal, QC has filled with CLSM trenches related to the maintenance of its public services [7]. CLSM is increasingly used in tight places, for example, deep sections in pavement cantilever, but the development of quality control is overdue and must be improved [8]. The current specifications in Montreal address the maximum compressive strength, ball drop (Kelly ball) penetration, and particle size of the mixture, but not the receiving environment or the rest time required before restoring traffic. Consolidation problems are sometimes encountered and are usually caused by a lack of permeability of the ground, precipitation, or particle size of the mixture [8, 9]. In Montreal, CLSM is used in cold weather days and can cause quality problems due to the high water content of the mixture that is in contact with frozen trench walls.

The main objective of this research project is to develop a simple method for quality control of CLSM, in the field on urban sites. Bearing capacity prediction models are built after each test is carried out, until the end of the project, to build an overall model. These models help construction managers find the optimal time to restore traffic. The permeability of the medium, the temperature of installation, the outside temperature, and the precipitation during the CLSM rest period are considered. The tool chosen to characterize trench compaction is the portable dynamic cone penetrometer; due to its simplicity, it requires no special permit, as a moisture density gauge, and accurately measures the stiffness of materials.

Methodology

The experimental part of this project is carried out in two phases. Phase 1 is carried out using CLSM made with a concrete mixer on construction sites in Montreal. Phase 2 is carried out in our laboratory with aggregates and vendor formulations. Reference mixtures are provided with sizes that approach the maximum density according to Fuller-Thompson curves. This article deals with only part of the on-site procedure. We include trials with a Kelly Ball to measure the short-term

CLSM consolidation and dynamic penetrometer tests to monitor the rigidity with time and depth. Cylinders of samples are taken for the maximum compressive strength of the mixture and soil samples are taken from the walls of the excavation before casting to estimate the permeability of the receiving environment.

Materials

CLSM mixtures A and B shown in Table 1 were used in this study. They are derived from regional suppliers and they are all compounds of rock stone, sand, cement, and water. Mixture B contains 140 kg more sand than the mixture A. The reference mixture proposed by the Quebec Concrete Association in 1993 is very similar to both A and B. The mixture used by the Ohio Department of Transportation (DOT) is also presented as the mixtures used in the United States are almost all made of fly ash, sand, water and cement [1]. Quebec mixtures should be able to drain, whereas the mixtures used by Ohio Department of Transportation behave rather like concrete [7].

Table I Composition of CLSM mixes

	Mix A	Mix B	Quebec Concrete Association	Mix from Ohio DOT
Stone	1 180 kg	1 185 kg	1 200 kg	
Sand	853 kg	992 kg	955 kg	1727 kg
Cement	25 kg	25 kg	25 kg	30 kg
Water	200 kg	220 kg	220 kg	297 kg
Air	4 %	1 %	1 %	8 %
Fly ash				148 kg

Description of the urban test sites

Mixture A was used on a 7 km electrical transmission line burial site (site 1, 2 and 3). The trenches were compacted and drained, and a massive concrete wall almost entirely lines the bottom of a trench that is 0.9 meters wide. A thickness of at least 600 mm of CLSM is cast before the concrete slab under the rolling surface. Up to 10 liters of water per cubic meter were added to mixture A on site to increase maneuverability, but a dosage greater than 100% water does not decrease the density of the fill once drained [10]. Mixture B was used on an underground electrical and telecommunications services site (Site 4). The presence of clay, silt, and organic soils decreases the permeability of the trenches in this series of tests. The trenches are large and irregularly shaped. Concrete manholes are installed under future sidewalks, between the street structure and the fill soils below.

Tests and measurements

The evolution of the stiffness of the backfill was followed using the portable dynamic penetrometer (Figure 1a) according to American Standard of Testing Materials (ASTM) D6951 [11]. The penetration is read on a ruler and recorded at regular intervals. The device has a falling weight of 7.7 kg on a stem that strikes straight into the ground. The mass can be reduced to 4.5 kg for soft ground. According to the manufacturer, one blow from the largest hammer is equivalent to two blows of the smallest hammer [12]. The first test is carried out on CLSM about three hours after casting with the smaller hammer. After 24 hours, the material is quite rigid and the 7.7 kg hammer is used to minimize the number of blows required for the test.

Testing is done midway between the trench walls or midway between a concrete manhole and the trench wall. Some tests were carried out near the walls for comparing the hardness of the material near a draining soil versus clay soil. All penetration tests performed at the same location must be close and in the same drainage conditions, but more than 300 mm apart to avoid interference [11]. The short-term consolidation of CLSM was followed with the ball drop by ASTM D6024 [13]. The 15 kg apparatus is placed gently on the fresh material (Figure 1b). Penetration and the time elapsed are both noted. The test should be repeated at least a few times, but ideally until ground stability is achieved.

a) b)

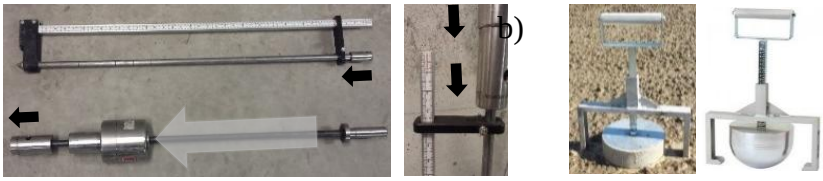

Figure 1. Mesurement of the consolidation of CLSM, a) dynamic cone penetrometer, b) ball drop (Kelly ball)

Results

Dynamic cone penetrometer

Site 1 With the results of the dynamic penetrometer, a penetrogram can be constructed to monitor the stiffness of the fill with depth. Figures 2 and 3 present the penetration data on a 600 mm trench, casted with mixture A. A penetration index (PI) of 5 means a strong consolidation of the mix, because the rod only penetrates 5 mm per hammer blow. The left to right curves illustrate the evolution of the rigidity of CLSM from 3.5 to 112 hours after casting. This figure is useful for analyzing the layers of CLSM over time. The test results at 45 hours is not

shown in Figure 2. The first layer of 100 mm is less resistant to penetration, probably because the confinement effect is smaller on the surface.

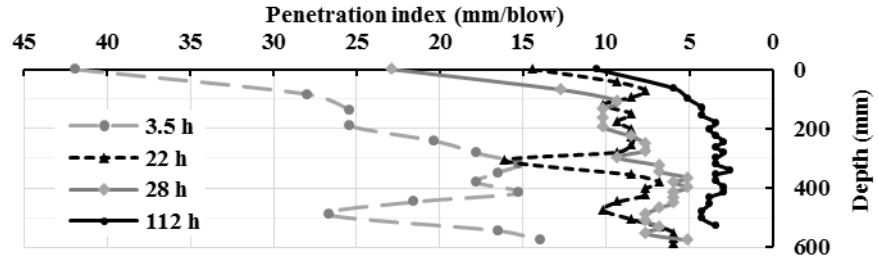

Figure 2. Consolidation of controlled low strength materials with time and depth (Site 1, mix A)

The results of Figure 2 are presented in Figure 3 as mean number of strokes to 152.4 mm (6 inches) penetration. In this way, changes in the rigidity of CLSM as a function of time can be seen as a trend and then compared with other mixtures and sites. The walls of the trench were made of dry and compact rock stone.

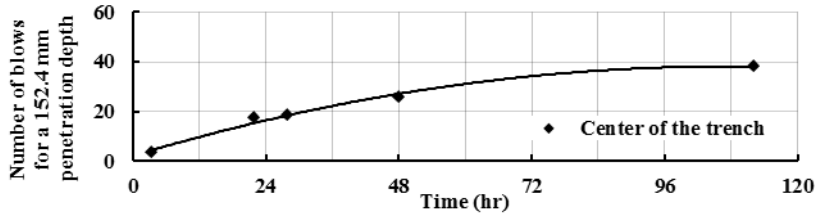

Figure 3. Evolution of the trench stiffness (Site 1, mix A)

Site 2 Figure 4 shows how the tests were conducted on a similar trench, but in brown fine sand. It was filled for 750 mm from left to right with mixture A. The bottom of the trench was made of solid concrete and the walls of the trench were compacted. The sample collected from the walls had a water content of 12.7%. The order of the tests was: A1, B1, A2, B2, and so on. The distance between the tests complies with the 300 mm requirement from the ASTM D6951 standard to prevent interference [11].

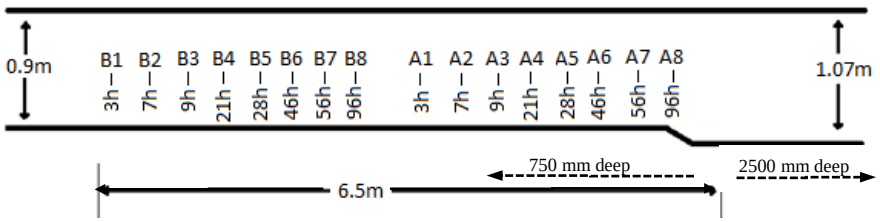

Figure 4. Measurement pattern on a trench of a construction site (Site 2, mix A)

Figure 5 shows the stiffness evolution of the portion A of the trench versus the portion B. The stiffness obtained from the A series was always less than series B: at 28 hours, it was 20 blows versus 16 blows; at 96 hours, it was 45 blows versus 33 blows. However, the wall conditions seemed uniform and the batch was made continuously: Two concrete mixers were used in this trench section, one for the bottom (300 mm) and the other to fill the trench. As a comparison, a compacted stone backfill under 20 mm vibrated in 400 mm layers corresponded to an average of 17 blows for a 152.4 mm penetration.

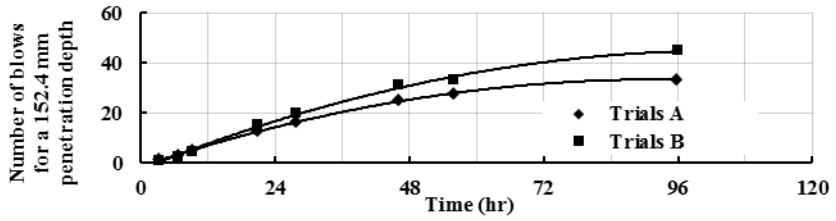

Figure 5. CLSM stiffness over time mesured with a dynamic cone penetrometer following the pattern in Figure 4 (site 2, mix A)

The most probable hypothesis to explain the differences between trial A and B is that drainage water from next castings (to the right in Figure 4) increased the water content of section A which reduced stiffness. The increase in water content following precipitation reduces the rigidity of CLSM [10]. In addition, the amount of CLSM casted in the next section was larger. The 2.5 m deep trench was casted two hours after and the water flow through sections presented in Figures 4 and 5, less than 1 m deep.

Site 3 Figure 6 collects test data made in a special trench. No samples were taken, but the observation that one of the walls was embankment dry and the other made up of silt and clay fill soils was made before the casting of the embankment. Penetration tests were therefore carried out at 100 mm from each wall in the center of the trench. Both the center of the trench and the draining wall achieved a penetration resistance at least 50% higher at all points than the clay wall. It was not possible to collect data after 48 hours, because the concrete slab under the asphalt was poured quickly to restore circulation.

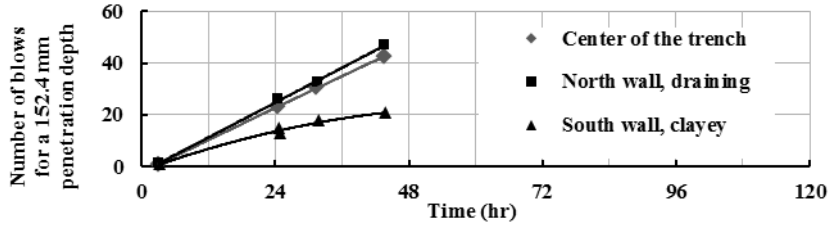

Figure 6. Stiffness of CLSM according to three draining conditions (Site 3, mix A)

Site 4 Figure 7 shows mixture B of CLSM over time for a compacted draining wall and a fill soil wall around a manhole. The CLSM in contact with the undensified wall did not develop the same short-term bearing capacity than the CLSM in contact with the draining wall of the pavement structure. More measurements comparing draining and soil walls are needed.

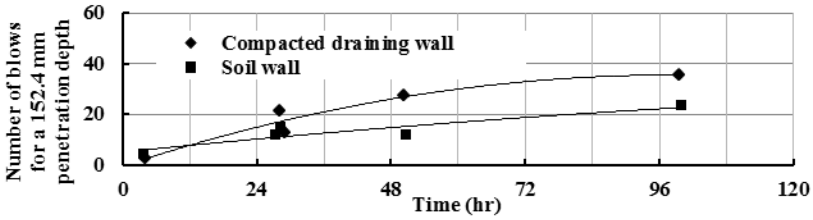

Figure 7. Evolution of the CLSM stiffness around a manhole (Site 4, mix B)

There is a correlation between the penetration index and the California bearing ratio (CBR) when using the formula recommended by ASTM D6951 [11]. The formula is good for all types of soils, except clayey soils, but it has not been verified for CLSM containing 1% cement. For example, 20 blows correspond to a CBR of 30, 30 blows to a CBR of 47, 40 blows to a CBR of 65, and 50 blows to a CBR of 83. The number of blows to 152.4 mm depression and the penetration index are the best ways to monitor the stiffness of embankments.

Figure 8 shows the evolution of the rigidity of all sites. Mixture A contains more coarse aggregates than mixture B, and it reached the highest rigidity in a draining medium after 45 hours. Conversely, mixture B, which contains a lot of sand, is drained slowly in the soil medium and reached low rigidity.

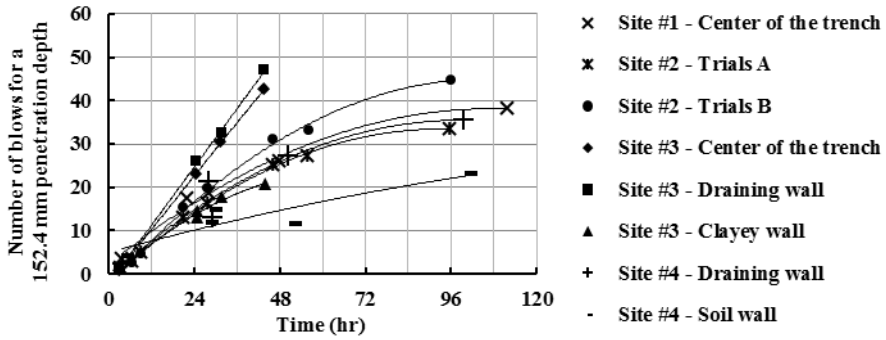

Figure 8. Stiffness evolution of the CLSM for the monitored sites

Drop ball

Figure 9 shows test results achieved with a drop ball on 4 sites. The sites 3 and 4 received several concrete mixers to fill the trench. The blue rectangles represent the identified areas of non-compliance according to the specification of the Commission des Services Électriques de Montréal (CSEM, zone 1) and according to the specifications of the City of Montreal (zone 2). In the city of Montreal, a depression of more than 25 mm after 15 minutes is unacceptable, while at the CSEM, 5 minutes is the limit. From discussions, it appeared that CSEM was unable to identify the origins of their compliance criteria. Test 4.2 in Figure 9 was conducted after the casting of a second truck in one place. It is clear that the amount of CLSM casting steps in the same place influences short term consolidation, especially if the receiving environment is not very permeable. According to the results of the penetrometer in Figure 8, the embankment at site 4 obtained the lowest final rigidity. Before reexcavating a non-compliant embankment, as suggested by the specification, a portable dynamic penetrometer test can be done to estimate the actual rigidity of the embankment. A decision can then be made based on real needs bearing capacity of the infrastructure.

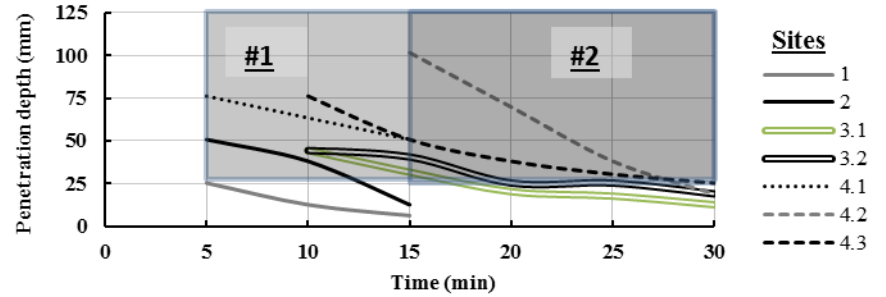

Figure 9. Evolution of the penetration depth with the drop ball test on the four sites according to two specifications

Conclusion

The penetrometer is a useful tool to monitor the quality of CLSM, but it will require several other trenches measurements to successfully validate stiffness prediction models over time and define performance. The results of this report show that the permeability of the medium clearly influences the evolution of stiffness. Well-drained embankment may have an acceptable bearing capacity between 24 and 48 hours, while the same mixture may take up to a week in undrained fill soils to achieve the same bearing capacity. The laying temperature, outside temperature, precipitation received, wet density, dry density measured sand cone are important parameters that need to be analyzed in the next step. The use of the mixture in winter conditions will be studied closely by comparing the evolution of its rigidity with normal temperature results.

Current specifications must be revised to include the penetrometer test as a criterion of acceptability of an embankment. Currently, quality control is based on the ball drop (Kelly ball), which is a good test, but only able to consolidate in the short term without considering the curing conditions of the material. Companies use mobile concrete mixers to fill trenches with CLSM, after which they immediately sink a concrete slab. A steel plate is then installed during the cure and paving is done a week later. This accelerated technical work needs to be investigated as it is not possible at present to control the fill under the slab. In addition, CLSM subsidence, which occurs during the water drainage, affects the quality of the work.

References

[1] ACI Committee 229 (2013), *Controlled low-strength materials*, ACI 229R-13, Farmington Hills, MI: American Concrete Institute.

[2] Smith, A. (1991), *Controlled Low-Strength Material*, Concrete Construction, May, p. 6.

[3] Alizadeh, V., Helwany, S., Ghorbanpoor, A. and Oliva, M. (2014) *Rapid-Construction Technique for Bridge Abutments Using Controlled Low-Strength Materials*, Journal of Performance of Construted Facilities, vol 28, p.149-156.

[4] Zhang, Z. and Tao, M. (2007), *Flowable Fill as Geotechnical Material in Highway Cross-Drain Trenches*, Geotechnical Testing Journal, No. 1.

[5] Blanco, A., Pujadas, P., Cavalaro, S. H. P., and Aguado, A. (2014), *Methodology for the design of controlled low-strength materials. Application to the backfill of narrow trenches*, Construction Building Materials, vol. 72, p. 23-30.

[6] Pujadas, P., Blanco, A., Cavalaro, S. and Aguado, A. (2015), *Performance-Based Procedure for the Definition of Controlled Low-Strength Mixtures*, American Society of Civil Engeneers, p. 7.

[7] Martin, Y. (2001), *Remblai sans retrait : optimisation de la formulation et conditions d'utilisation*, Université de Sherbrooke, p. 215.
[8] Tripathi, H. and Pierce C. (2004), *Methods for Field and Laboratory Measurement of Flowability and Setting Time of Controlled Low-Strength Materials*, Journal of ASTM International, June, Vol. 1, No 6.
[9] Association Béton Québec (2007), *Le remblai sans retrait*, Techno-béton bulletin technique, No.18.
[10] Lupien, C., Gagne, R. and Martin, Y. (2002), *Formulation optimale du remblai sans retrait*, 2e conférence spécialisée en génie des matériaux de la Société canadienne de génie civil, p. 10.
[11] ASTM D6951 (2009), *Standard Test Method for Use of the Dynamic Cone Penetrometer in Shallow Pavement Applications D6951M – 09*, West Conshohocken, PA.
[12] Kessler Soils Engineering Products (2010), *KSE Dynamic Cone Penetrometers K-100 Model*, p. 31.
[13] ASTM D6024 (2015), *Standard Test Method for Ball Drop on Controlled Low Strength Material (CLSM) to Determine Suitability for Load Application D6024M – 15*, West Conshohocken, PA.
[14] Ville de Montréal (2008), *Devis technique normalisé 6VM-30 : Remblai sans retrait*, p. 5.

New Indexes to Evaluate Self-Consolidating Concrete Robustness

Parviz Ghoddousi[1] and Amir Masoud Salehi[2]

[1]Iran University of Science and Technology
[2] Iran University of Science and Technology

Abstract One of the main obstacles for a wider use of Self-Consolidating Concrete (SCC) is high sensitivity to small changes in constituents or low robustness of this type of concrete. Evaluation of SCC robustness and its effect on compressive strength changes is the main subject of this study. An experimental program was undertaken to evaluate the robustness of SCC subjected to small variations in mixing water. Eight mixtures of SCC with various mix proportion or admixtures were tested. In order to study of robustness, the water content of each mixture was changed ±3% and ±6%. Then the workability tests including Slump flow, J ring and sieve stability, rheology parameters including yield stress and plastic viscosity and compressive strength were measured. The results indicate that one of the best tests for assessing robustness is sieve stability test. GTM index that has been developed based on sieve stability test can assess robustness and identify robust SCC. Drawing rheology parameters of each mixture with different mixing water on rheograph indicates that a quadratic function can explain the relationship between small change in mixing water and rheology parameters. A new index called curve length of rheology parameters (CL_R) that is the length of quadratic function between ±3% changes in mixing water is presented here for SCC robustness. The results show that the robustness of mixtures based on two indicators (GTM and CL_R index) is largely matched together. Also the situation of robustness in fresh state unrelated with scattering of compressive strength results.

Keywords: *Indicator of Robustness, Sieve Stability Test, Rheograph, Compressive Strength*

Introduction

A developed class of concrete materials is self consolidating concrete (SCC) that offers great potential for improved ease of placement, increased rate of construction, and reduced cost through reduced time and labor [1].

The limited practical use of SCC is partly because its properties are not completely known (mix proportion and fresh tests) and partly because its performance is highly sensitive to small changes. The term of robustness is the ability of a given mixture to maintain its fresh properties and uniformity during processing, casting, and due to small changes in the quality and quantity of mixtures ingredients. A lack of robustness can be manifested in several ways that affects workability and the other assigned properties of SCC [2-3].

There are a few approaches available to assess the robustness of SCC. The first method was suggested by the European Guidelines for SCC [4] in which a well-designed and robust SCC should tolerate a change in water content of 5 to 10 L/m^3 without falling outside the specified class of performance. Such a change in water content can correspond to approximately +6% [5].

Kwan and Ng [6], according to their researches, have suggested that the width of the acceptable range of SP dosage as well as the acceptable range of slump flow (i.e. the range of SP dosage or slump flow that satisfying all the performance requirements) may be taken as a quantitative measure of the robustness of SCC.

Naji et al. [7] have used the coefficient of variation (CV) for comparison and ranking of SCCs in terms of robustness. To evaluate the robustness of SCC, twenty properties of SCCs were measured at three levels of sand humidity. For each property (test), the CV of the responses were calculated and used to estimate the relative spread of each response. According to CV values of tests, the robustness of each SCC has been estimated.

The main aim of this research is the study of different approaches to assesse the robustness of SCC in fresh state. Moreover, the relationship of robustness and the scattering of strength results is investigated.

Experimental Works and Analysis Methods

Materials

In this study an ASTM type I Portland cement as well as limestone powder as filler were used. Crushed limestone aggregate was used as coarse aggregate with a nominal maximum size of 19.5 mm. The specific gravity and water absorption of coarse aggregate are 2.55 and 1.8% respectively. As fine aggregate, sand with nominal size of 4.75 mm was used. The Specific gravity and water absorption of sand are 2.60 and 3.9% respectively. Particle size distribution of aggregates is falling within the permissible limits stipulated in ASTM C33 [8]. A third generation polycarboxylate-based superplasticizer (SP) with a specific gravity of 1.1 was used. Also a synthetic detergent air-entraining admixture (AEA) and a

microbial polysaccharide (welan gum) as a viscosity-modifying admixture (VMA) were used in some SCCs.

Mix Proportions

A total of eight SCC mixes were designed and their workability properties, rehology parameters and compressive strength were tested. A control mix (C) was the initial target and, seven series of mixes were developed with variations of each of the principal properties (i.e. filling and passing ability and segregation resistance) or using of AEA and VMA admixture. Table I gives details of mix proportion of eight *reference* SCCs.

In order to evaluate the robustness of each mixture, in addition to the reference mixture, four mixtures were made that the water content of each mix was changed ±3% and ±6% relative to the base water content.

Table I. Proportioning of SCC mixtures

Mix Code	W/C	Water	Cement	Limestone Powder	Sand	Gravel	SP	AEA*	VMA*
		kg/m^3					%*	kg/m^3	
C	0.50	200	400	175	916	611	0.92	-	-
F(SP)	0.50	200	400	175	916	611	1.11	-	-
F(SP+W)	0.46	185	400	175	927	618	1.30	-	-
P	0.50	200	400	175	763	763	1.04	-	-
S(L)	0.50	200	400	100	960	640	0.78	-	-
S(C+L)	0.49	185	375	160	987	658	1.07	-	-
A$^+$	0.50	200	400	175	916	611	0.74	0.22	-
V$^\times$	0.50	200	400	100	960	640	0.88	-	0.33

* Percent of cement content
$^+$ Air Antraining Admixture
$^\times$ Viscosity Modifying Admixture

Mixing Procedure and Test Methods

Each batch of SCC was mixed in a gravity mixer with 60 L capacity in volume of 45 L. Each batch of SCC was mixed for 4 min and then was allowed to rest for 2 minutes. The determination of the workability specifications were started after 5 min from contact time of cement with water. The workability properties were measured by slump flow and J-ring tests according to PCI methods [9] and sieve stability test Version II according to European Guidelines for SCC [4].

The rheology parameters (yield stress, plastic viscosity) values were determined by a coaxial rheometer. This automated rheometer, which is shown in Figure 1, is a rate-controlled rheometer that was employed to carry out rheological

measurements 10 minutes after the initial contact between water and cement. It consists of a four-bladed vane that is immersed into the concrete and rotated at various speeds [10].

Figure 1. Rheometer for determining the rheology parameters

Experimental Results and Analysis

Robust SCCs Based on EFNARC

The changes in SCCs properties due to ±3% variations in mixing water has been studied to identify the robust SCC based on EFNARC criteria [4]. The robust SCC provides all of EFNARC proposed limits (table II). It should be mentioned that ±6% increase in mixing water cause to withdraw all SCCs from desired ranges.

Table II. Workability characteristics and their limits

SCC property	Test	Recommended values	
		Min.	Max.
Filling ability	Slump flow (mm)	550	850
Passing ability	J Ring (mm)	0	10
Segregation	Sieve stability (%)	5	20

The changes in slump flow, J ring and sieve stability tests in different mixing water are shown in figure 2. For identifying robust mixtures, proposed limits are shown in these charts.

As can be seen, the changes in slump flow and J ring tests are located within permissible ranges. But in F(SP), P, S(C+L) and S(L) mixtures, 3% increase in mixing water cause to pass sieve stability test from 20%. Therefore based on EFNARC procedure, mixes C, F(SP+W), A and V are robust.

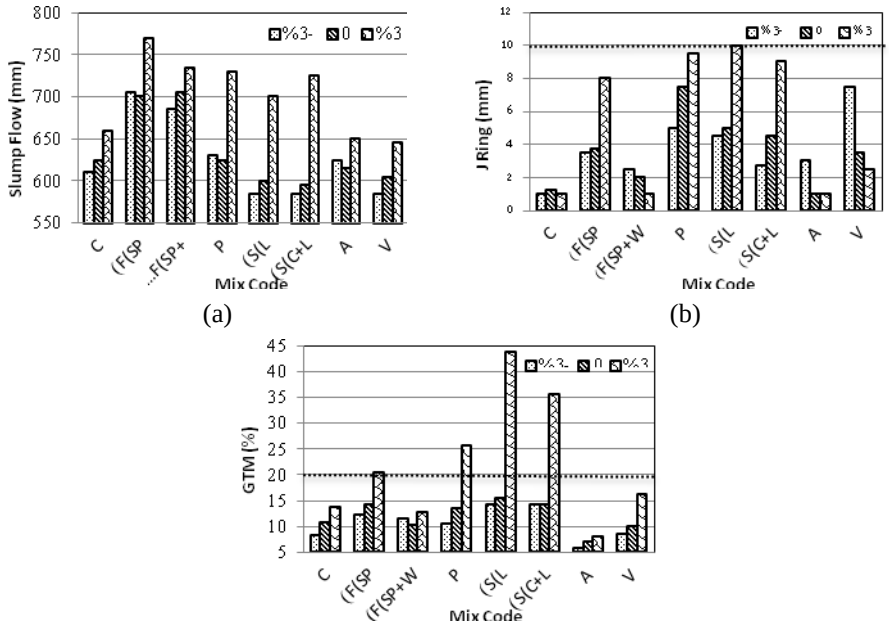

(a) (b)

(c)

Figure 2. Variations in tests in ±3% change in mixing water a) slump flow; b) J ring; c) sieve stability

Variations of Strength Based on ACI 214R-6

The dispersion of strength results are studied by recommended statistical indicator by ACI 214R-6 [11]. The coefficient of variation (CV) of strength due to change in water content is summarized in table III. According to the classification of standards control, the class of change in each concrete has been identified.

Table III. Strength results in different water variations and scattering of results

		Compressive strength (Mpa)							
		C	F(SP)	F(SP+W)	P	S(C+L)	S(L)	A	V
Change in water	-6%	47.1	40.4	46.2	41.4	36.2	42.9	30.5	38.8
	-3%	41.8	39.2	43.9	37.1	33.1	37.9	30.1	38.2
	0	41.9	37.3	43.6	34.6	32.8	34.5	28.2	36.2
	+3%	37.7	35.4	40.3	34.2	26.2	27.3	26.2	35
	+6%	37.6	33.5	37.1	33.5	23.5	24.4	24.1	33.1
CV in ±3%		5.9	5.1	4.7	4.5	12.7	16.2	7	4.4
Strength category		Fair	Good	Good	Very Good	Poor	Poor	Fair	Very Good

±6% change in water content cause to considerable change in strength and all mixes except V have located in poor class of variations. ±3% change in mixing water causes to different variations in strength of concretes. The minimum variations are corresponding to V and P mixes (very good). On the other side, S(L) and S(C+L) concretes have been sensitive to water content changes and located in poor class of strength category.

Comparing the robust of SCCs based on EFNARC criteria and category of strength variations (ACI 214R-6) in ±3% water changes indicate that the EFNARC control limits is more restricted and dominant. According to these results, if the category of strength variations is poor, then SCC based on EFNARC is not robust (S(L) and S(C+L) mixes). But if the category of strength variations is better than poor, it can not be guaranteed that SCC is robust based on EFNARC (F(SP) and P mixes).

Robustness Based on Sieve Stability Test

SCCs robustness based on EFNARC indicate that only segregation resistance of concretes that were assessed by sieve stability (GTM) test has been withdrawn from recommended ranges. Then, in this section robustness indicator is developed based on sieve stability test (GTM index). The concept of developed method to assess the robustness is shown in figure 3.

The following assumptions considered to develop an appropriate indicator:

1. Slight decrease in water content can't withdraw GTM test from boundaries.
2. The distribution of GTM test due to change in water content assumes normal distribution.
3. Upper limit of GTM test assumes 20%.
4. Acceptable number of GTM test higher than 20% is assumed 10%.

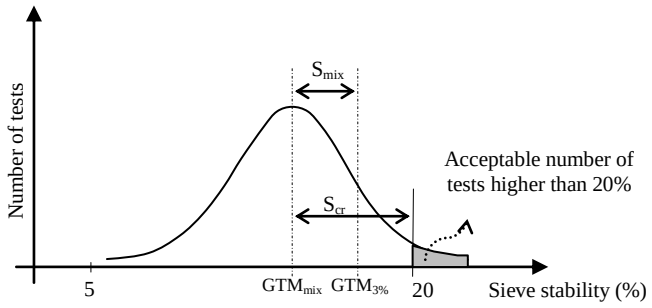

Figure 3. The concept of assessing the robustness of SCC based on GTM test

Step by step of determining GTM index is as follow:

1. Mix is made with exact amount of water and sieve stability test result is determined as mean value (GTM_{mix}).
2. Mix is made with 3% increase in water content and sieve stability test result is determined as $GTM_{3\%}$ and then standard deviation value (S_{mix}) is determined using the following equation:

$$S_{mix} = GTM_{+3\%} - GTM_{mix} \quad (1)$$

3. Critical standard deviation (S_{cr}) is calculated as following equations:

$$P(X > 20\%) \le 0.9 \rightarrow p(Z > \frac{(20 - GTM_{mix})}{S_{cr}}) \le 0.9 \rightarrow \frac{(20 - GTM_{mix})}{S_{cr}} \le 1.29$$

$$\rightarrow S_{cr} = \frac{(20 - GTM_{mix})}{1.29} \quad (2)$$

4. GTM index is determined as following equation:

$$GTM \text{ Index} = S_{mix} - S_{cr} \quad (3)$$

In table IV, step by step approach to determine GTM index of SCCs in current research is summarized. Algebraic symbols of Index is determined the status of robustness (positive algebraic sign represents robust SCC). Also in the case of positive, the higher the index, the greater safety margin of mix. Therefore, this index is a quantitative index that can be identified robust SCC.

Table IV. Evaluation of SCC robustness based on GTM index

Mix Code	Sieve stability (%)		Standard deviation (%)		GTM Index	Robustness status
	GTM_{mix}	$GTM_{+3\%}$	S_{mix}	S_{cr}	S_{cr}-S_{mix}	
A	7.1	7.95	0.85	10	9.15	√
F(SP+W)	10.28	12.7	2.42	7.53	5.11	√
C	10.76	13.66	2.9	7.16	4.26	√
V	10.14	16.2	6.06	7.64	1.58	√
F(SP)	14.32	20.5	6.18	4.40	-1.78	×
P	13.57	25.79	12.22	4.98	-7.24	×
S(C+L)	14.23	35.56	21.33	4.47	-16.86	×
S(L)	15.45	43.7	28.25	3.53	-24.73	×

The robustness of SCCs based on GTM index has been compared in figure 4. As can be seen, 4 mixes A, F(SP+W), C and V are robust and among them, mix A has the maximum robustness. On the other side, among SCCs that not robust, mix S(L) has the maximum sensitivity (minimum robustness).

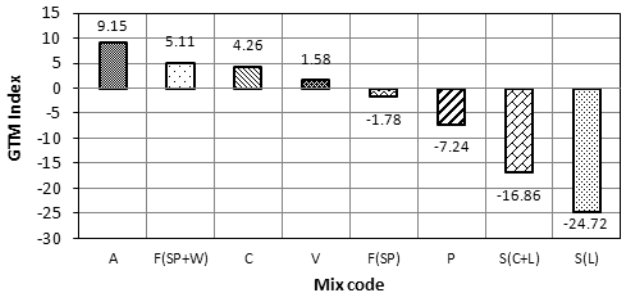

Figure 4. Robustness of SCCs based on GTM index

SCC Robustness Based on the Rheology Parameters

A good approximation of the fundamental rheological quantities for cement based material can be obtained in terms of yield stress (τ_0) and plastic viscosity (μ). A rheograph is defined as a graph that X axis is yield stress (τ_0) and Y axis is plastic viscosity (μ) [12].

To proper study of changes in rheology parameters in rheograph due to mixing water variations, it has been fitted quadratic function on rheology parameters (figure 5-a). Fitted quadratic function is as follow:

$$\tau = a\mu^2 + b\mu + c \tag{4}$$

Where τ is yield stress, μ is plastic viscosity and a, b and c are the constant coefficients. According to the fitted quadratic curves on rheology parameters, the proper and logic index for determining the robustness of SCCs is the curve length between lower and upper limit of plastic viscosity. The curve length of rheology parameters (CL_R) as an SCC robustness index has been shown in figure 5-b. The methof of determinning CL_R is based on arc length integration as follow:

$$S_{(\mu_{\min}-\mu_{\max})} = \int_{\mu_{\min}}^{\mu_{\max}} \sqrt{1+f'(\mu)^2}\, d\mu \tag{5}$$

The results of CL_R as well as results of GTM index are shown in figure 6. The borderline of robustness based on this indicator is 27.36. So SCC is robust if CL_R is lower than 27.36. According to CL_R indicator, four mixes is robust. Among these

mixes, mix C has the maximum robustness (minimum CL_R). On the other side, mixes S(L) and S(C+L) have the minimum robustness that their CL_R values are much more than other SCCs. Notable subject is relatively low robustness of mix V.

Comparing two robustness evaluation methods (GTM and CL_R) show that two methods can distinguish robust from non robust SCC equally. But relative status of robustness is different based on each method.

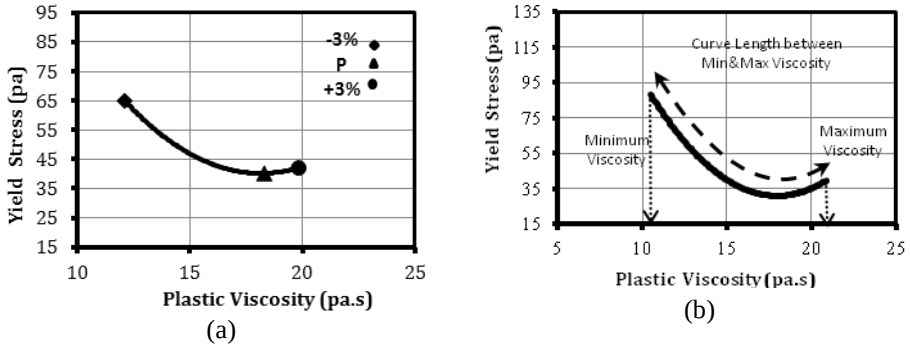

(a) (b)

Figure 5. a) Quadratic fitting on rheograph data b) Robustness index according to fitted curve length

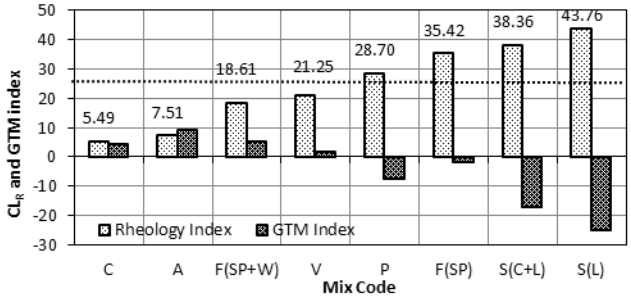

Figure 6. Robustness based on rheology parameters (CL_R) and GTM Index

Conclusion

1. Comparing the robust of SCCs based on EFNARC criteria and categoty of strength variations (ACI 214R-02) indicate that the EFNARC control limits is more restricted and dominant.
2. Checking of sieve stability changes is one of the best procedures to assess the SCC robustness. In this research, a quantitative index to identify robust SCC (GTM Index) is developed using sieve stability results in exact and 3% increase in mixing water.

3. An appropriate rheology index for assessing the robustness is the curve length of change in rheology parameters (CL_R) in rheograph among the variations of mixing water. The borderline of robustness based on this indicator is 27.36. So SCC is robust if CL_R is lower than 27.36. The results show that the robustness of mixtures based on two indicators (GTM and CL_R index) is largely matched together.
4. Comparing the scattering of compressive strength results due to ±3% change in mixing water with different robustness indexes indicate that the situation of robustness in fresh state unrelated with scattering of strength results.

References

1. Bonen, D., Deshapande, Y., Olek, J., Shen, L., Struble, D., Lange, D. and Khayat, K., (2007), "*Robustness of SCC*," The Center for Advanced Cement Based Materials (ACBM).
2. Khayat, K., (1999), *Workability, testing, and performance of self-consolidating concrete*. ACI Materials Journal, 96(3).
3. BIBM, C. and E. ERMCO, EFNARC (2005), *The European guidelines for self-compacting concrete*.
4. Rigueira, J.W., García-Taengua E., and Serna-Ros P., (2009), *Self-consolidating concrete robustness in continuous production regarding fresh and hardened state properties.* ACI Materials Journal, 106(3).
5. Kwan, A.K. and Ng I.Y., (2010), *Improving performance and robustness of SCC by adding supplementary cementitious materials.* Construction and Building Materials, 24(11): p. 2260-2266.
6. Naji, S., Hwang S.-D. and Khayat K.H., (2011), *Robustness of self-consolidating concrete incorporating different viscosity-enhancing admixtures.* ACI Materials Journal, 2011. 108(4).
7. ASTM C33, A., (2004), *Standard Specification for Concrete Aggregates*, ASTM International West Conshohocken, PA.
8. Team, P.S.-C.C.F., (2003), *Interim Guidelines for the Use of Self-Consolidating Concrete in PCI Member Plants.* PCI Journal.
9. Koehler, E.P., et al., (2006), *A new, portable rheometer for fresh self-consolidating concrete*. ACI Special Publication, 233.
10. ACI 214R-02, *Evaluation of Strength Test Results of Concrete*.

Wallevik, O.H. and Wallevik J.E., (2011), *Rheology as a tool in concrete science: The use of rheographs and workability boxes*. Cement and Concrete Research, 41(12): p. 1279-1288.

Practical Methods to Assess Segregation Risk of SCC on Site

Tor Arne Martius-Hammer[1], Sverre Smeplass[2] and Gunrid Kjellmark[1]

[1]SINTEF Building and Infrastructure
[2]Skanska Norge AS

Abstract Many of the suggested methods for testing of SCC stability are quite demanding in execution and therefore seldom used in field. Furthermore, questions have been raised about how well they represent the stability problems in situ. The aim of the present investigation was therefore to find a method to assess stability of SCC which is practical, reliable and representative for in situ stability problems. This was done by a large scale test where the stability assessed according to four selected methods was compared with the stability assessed in low wall elements (10 m long) where the SCC was cast from one end, by measuring the distribution of the coarse aggregate content. Two mixes of the same concrete were tested in order to see the comparison for both stable and unstable concretes. The one was known to give sufficient stability for wall casting, and the other one added more water reducing admixture to give rather poor stability. The results showed a good correlation between three of the methods and between these methods and the stability assessed by measuring the coarse aggregate distribution in the walls. One of these methods is a simple visual based assessment of the residue after the slump flow test.

Keywords: *Self compacting concrete, stability, test methods, comparison, on site*

Introduction

Previous work on stability of SCC, reported in [1], concluded with questioning the ability of stability test methods to mirror the stability problems in situ. The question is attempted answered in the investigation referred to here and reported in [2], with the aim to find a method to assess stability of SCC which is practical, reliable and representative for in situ stability problems. Stability is considered here as the resistance to segregation of coarse aggregate under long distance flow of SCC (dynamic stability). Segregation is experienced to be a far more important stability problem than bleeding of such concretes.

The investigation started with setting up a number of requirements for the method, such as dynamic action and easy execution. It ended up in four recommended methods and which were tested in the lab to gain experience and as basis for necessary adjustments [2].

Then, a large scale test was performed in order to compare the stability assessed according to the four methods with the stability assessed in low wall elements (10 m long) where the SCC was cast from one end, by measuring the distribution of the coarse aggregate content. Two concretes were tested; one known to give sufficient stability for wall casting, and one with expected rather poor stability, in order to see the comparison for both stable and unstable concretes.

The tests methods used were:

- Visual segregation, VSI^b
- Rheological Segregation, RSI
- Settlement Pipe Segregation Test, SPSI
- T-Box – dynamic segregation index, PDI, and dynamic segregation volumetric index, VI.

Visual segregation

The test is performed simply by observing the slump flow residue, and then characterise according to the following [3]:

0 / 0.1	Stable and homogenous concrete. Aggregates and paste flow towards the rim of the sample.
0.2/ 0.3	Stable and homogeneous concrete that flows well, but has become a shiny surface with possible black spots (usually unburned coal residue liberated from the fly ash when the hollow spheres are crushed upon grinding).
0.4 / 0.5	Has additionally a hint of a paste rim at the outer edge of the spread, but the aggregates follow the flow towards the edge. Still stable.
0.6 / 0.7	Clear rim of paste at the outer edge of the spread. Coarse aggregates tend not to flow towards the edge of the spread (are left in the middle of the spread).
0.8 / 0.9	Additional separation of water/paste at the outer rim of the spread.
1	Complete separation

Rheological Segregation

The RSI [3] is determined using a 4SCC rheometer produced by ConTec with a special rotor which simulates a dynamic separation process by pushing the coarser aggregates aside. After 60 s the rheological parameters G and H of the resulting separated slurry are measured. G relates to the yield stress and H to the viscosity.

Settlement Pipe Segregation

The method is based on the settlement column test [4] in principle, but with other geometry and sampling procedure [2]. The pipe has 3 sections. The segregation index is the ratio between coarse aggregate content (> 5 mm) in the top section and the bottom section after jolting 20 times within a 1-minute period via the turn handle of the flow table apparatus, see Fig. 1.

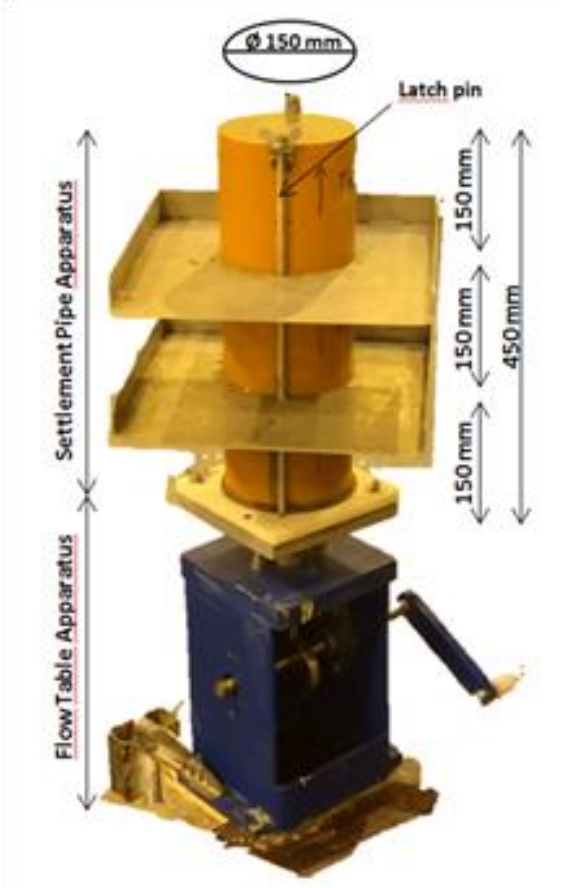

Figure 1. Test apparatus for Settlement Pipe Segregation Test

Standard Test Method for Dynamic Segregation of Self-Consolidating Concrete by T-Box

The method is described in [5]. A sample of freshly-mixed self-consolidating concrete is placed in a rectangular channel without tamping or vibration, see Fig. 2. The channel is tilted numerous times through cyclic motions. By means of a penetrometer, the penetration depth is measured on the extremity that tilts upwards before and after the tilting cycles. The difference between the initial and the final penetration depth is an indicator of dynamic segregation.

A comparison of the coarse aggregate content in tilt-up and tilt-down sections at the end of the T-Box test can also be done to provide an indication of dynamic segregation.

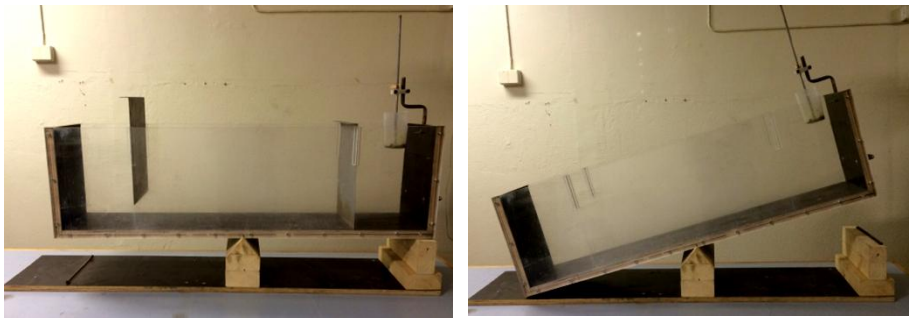

Figure 2. T-box (1.0x0.2x0.2 m) with penetrometer (right end)

Execution

Two concretes were tested, both delivered by a local ready mix company in a truck mixer. The first concrete was similar to a commonly used SCC in the region (Trondheim area). The other one was similar to the first one, but added more water reducing admixture (WRA) on site to make it fairly unstable. The recipes, along with the slump flow and t_{500}, are given in Table 1.

T*able 1. Recipe and consistency of the UNICON concrete*

Materials	**Mix A**	**Mix B**
Cement, CEM II/A-V 42.5R	364	364
Silica fume	19	19
Water	189	189
WRA ("Glenium SKY 601")	5.2	5.8
Sand/gravel, 0 – 10 mm	1162	1162
Crushed stone, 8 – 16 mm	637	637
w/c	0.53	0.53
Slump flow	700 mm	740 mm
t_{500}	0.8 sec.	<0.4 sec.

The wall formwork had dimension l/h/w = 10/0.6/0.2 m, and was made of Plywood. No reinforcement was used. The stability was assessed by measuring the coarse aggregate content, particles > 5 mm, in both ends of the wall and in two in between positions, as well as on top and bottom in all positions (i.e. a total of eight points in each wall), see Figs 1 and 3. To enable careful sampling in the bounded positions without interference from concrete outside the positions, two metal plates were pressed down in pre-cut notches in the Plywood with a mutual spacing of 0.2 m, see Fig. 3. To make action of pressing down the plates as easy as possible, the cuts were filled with silicone grease prior to casting, to avoid blocking by sand particles.

Figure 3. The wall elements with metal plates bounding the area for sampling

Prior to the tests, the slump flow was adjusted on site by adding WRA in the truck until the target of 700 and 740 mm, respectively, was achieved. Casting of the walls and testing with the four methods were done simultaneously, during approximately 60 minutes. The walls were cast directly from the truck gutter, see Fig 4. The filling took 5-6 minutes in both cases. Within half an hour after

completed casting, the metal plates were pressed down and sampling was done immediately after. Each sample of approx. 5 litres, were taken out with a shovel and filled in a bucket with known volume. The sample was weighed, then placed on a 5 mm sieve and flushed with water until the coarse aggregate appeared clean. At last, the aggregate on the sieve was packed in bags to be transported to the lab for drying and weighing.

The samples to be used in the four lab tests were taken from wheelbarrows filled directly from the truck gutter. The wheelbarrows were handled carefully to prevent segregation, and the concrete was remixed by hand before starting the lab tests. This was done to ensure homogenous and representative concrete. The procedure of each test is given in [2].

Figure 4. Casting of wall elements from truck gutter

Results

Wall tests

The surface slope over the 10 m were 0.11 m for Mix A and somewhat less for Mix B, 0.07 m, as expected because of higher slump flow, see Fig. 5.

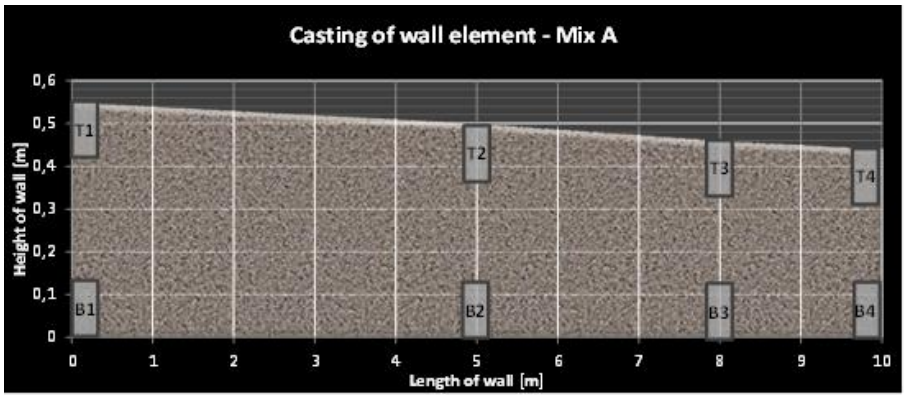

Figure 5. Slope of the concrete surfaces and locations for sampling (T1-T4, B1-B4)

The results are presented, in Fig. 6, as the measured mass of aggregate > 5 mm in the selected locations shown in Fig. 5, when dried at 105 °C to constant weight and given as kg/m3 of concrete. It is compared with the corresponding mix design aggregate content of 819 kg/m^3.

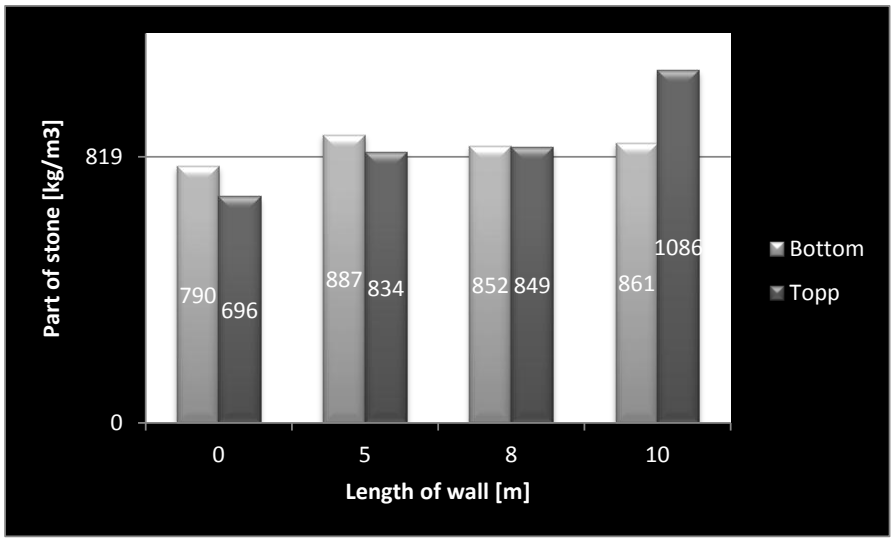

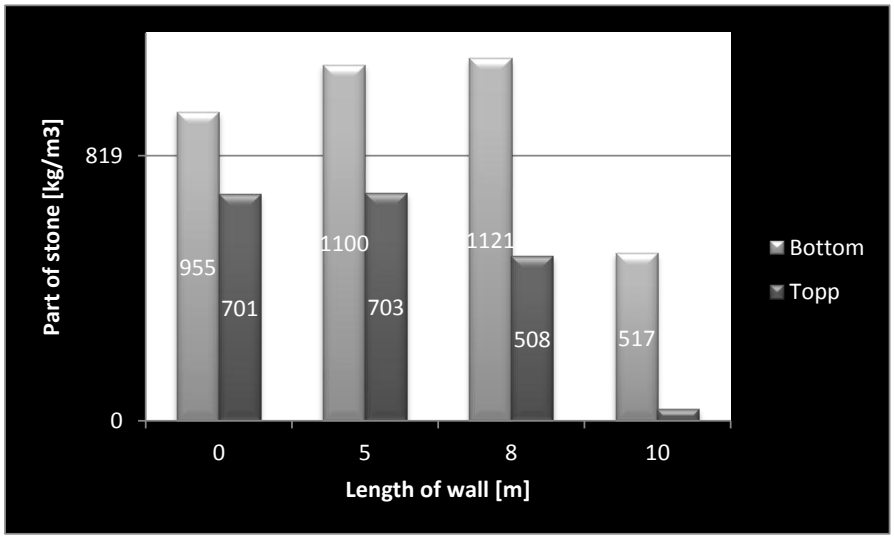

Figure 6. Coarse aggregate content in the selected locations. The coarse aggregate content taken from the mix design is 819 kg/m^3

The difference between the concretes is obvious: The coarse aggregate (stone) distribution in Mix A is quite uniform, both over the length and height, while it varies considerably in Mix B. both over the length and height. It seems that the stone followed up to 8 m (the sum of bottom and top is fairly constant), but that the vertical segregation started already at filling. In fact, the top section at the flow end of the beam did hardly contained stone. Hence, Mix A can be judged to exhibit satisfactory stability for this job, and Mix B certainly not.

Apparently, the total coarse aggregate content (bottom plus top) is lowest at the filling end highest at the flow end. Spangenberg et al [6] also found that the total stone concentration at the filling was lower than in the middle section of a similar test wall. A higher stone content especially at the top for Mix A, corresponds to the observation that stones tend to be pushed upward when the concrete met the end wall.

Stability tests

There is a very good agreement between the methods in that all results from testing Mix A indicate acceptable stability, see Table 2, and thus in accordance with the result from the wall test. And the indices are rather close to the limits of acceptance, except for the VI from the T-Box. This makes sense since a rather little increase of WRA (5.2 to 5.8 kg) caused a quite unstable concrete (Mix B). The VI is far below the acceptance criteria, and thus, indicates very good stability. Note

that this disagreement can lay in the restriction of the T-Box test as discussed below.

Also, results from testing of Mix B were in accordance with the beam test; not acceptable, except for the T-Box test results. The T-Box results were irrational: PDI (penetration indicator) of minus 6 mm and VI (content of coarse aggregate indicator) lower than that for Mix A. It lays probably in the restriction of the T-Box test, saying: "Do not perform this test on self-consolidating concrete which does not show sufficient static stability". We did not measure static stability as such, but the PDI includes an initial measurement of penetration before tilting. It showed 9.5 mm penetration, which must be considered to be quite high, and thus, indicates poor static stability (concrete A showed 2 mm, only).

Table II. Results and limits for acceptable stability (green and red indicate stable and instable concrete, respectively, according to the test methods)

Concrete	VSI[b]	RSI	SPSI	T-Box	
				PDI	VI
	≤ 0.6	≤ 0.5	≥ 0.88*	≤ 6 mm	≤ 25 %
A, SU=700, t_{500} = 0.8	0.55	0.5	0.88	4.5 mm	4.7 %
B, SU=740, t_{500} = 0.4	0.75	0.9	0.68	**-6 mm**	1.4 %

** According to the original Settlement Column Test*

Similar comparisons have been performed earlier. The EU GROWTH-project "Testing-SCC" [7], concluded that the "Sieve Segregation Test" gave the best correlation with stability assessed in situ (but yet not consistent), followed by the "Penetration Test" and "Settlement Column Segregation test" (from which our SPSI-test is modified). We considered the two others to be too execution demanding to fit our aim. VSI and RSI were not a part of the "Testing-SCC".

Final assessment - conclusion

The present reference concrete is judged to be quite sensitive with respect to stability based on the facts a) that it has a rather high SU and a low viscosity (as indicated by the low t_{500} of 0.8 sec.) as a result of a high water-powder ratio, and b) that only little extra addition of WRA made it quite unstable. Bearing this in mind, it is encouraging that three of the stability test methods showed good agreement between them, and more important, with the results from the wall tests, both when the stable and the unstable concrete is considered. The experimental results confirm that these methods may be suitable for qualification, declaration and acceptance control purposes, at least for concretes fairly similar to the present ones, i.e. most Norwegian SCCs for buildings. Similar comparison should be done with

concretes having higher viscosity, either by use of more/other fines or viscosity modifying admixtures. The latter may be the most interesting one as it is often used to repair unstable concrete on site.

Given that the three methods; **Visual Segregation Index (VSI^b), Rheological Segregation Index (RSI)** and **Settlement Pipe Segregation Index (SPSI)**, predict the stability of SCC on just as well, the questions about easy handling, time consumption and robustness remain to answer. Note that taking a representative and homogenous sample from the truck or mixer is of outmost importance for all tests (a general challenge not only for stability measurements), especially if the concrete is unstable or on the limit of being accepted as stable. Assuming that this is taken care of, the following evaluation is done:

The **VSI-test** is obviously the easiest and fastest one, also because slump flow is measured in most cases anyway. The main weakness is a possible person dependency, surely related to the execution of the slump flow test itself, but mainly to the evaluation of the stability, i.e. grading (0 to 1) according to the given description. Allowing a number of people to perform the evaluation simultaneously on the same slump flow residue, would answer this question, and perhaps form a basis for a possible modification of the description.

The **RSI-test** is relatively easy and fast, but data has to be processed in a separate computer. We assume that the device can be further developed with data processing integrated. The person dependency is considered to be unimportant.

The **SPSI-test** is the slowest and less easy one of the three. It includes also flushing, drying and weighing of the coarse aggregates. Hence, it takes quite much time to get the results. The test might be person dependent; at least it should be checked. Its strength is that the results are fairly directly to the point; the distribution of coarse aggregate. Hence, it may be suited for e.g. declaration procedures.

The **T-Box test**, seems to be too sensitive to allow reliable evaluation of concretes similar to the ones tested here. It is moreover rather demanding to operate, especially if the second option of the procedure is chosen, in that it includes flushing, drying and weighing of the coarse aggregates.

References

[1] Martius-Hammer, T.A., Smeplass, S. and de Weerdt, K. (2013): *Stability of SCC – robustness for changes in water content and sand grading.* COIN Project report 47, SINTEF Trondheim, Norway: www.sintef.no/coinweb

[2] Martius-Hammer, T.A., Smeplass, S. and Kjellmark, G. (2014): Assessemnt of SCC stability – Test methods vs in situ. COIN Project report 59, SINTEF Trondheim, Norway: www.sintef.no/coinweb

[3] Wallevik JE. (2009): *Utvikling av stabilitetsmåler for SKB.* Prosjektrapport for P653 "SKBB" DP 6. Norcem / ICI, Norway / Iceland (in Norwgian)
[4] Sonebi, M., Rooney, M. and Bartos, PJM. (2007): *Test method to evaluate the dynamic segregation resistance of fresh SCC using the settlement column test*. SCC-conference in Gent 2007.
[5] Esmaeilkhanian, B., Feys, D., Khayat, K.H., and Yahia, A. (2014): *New Test Method to Evaluate Dynamic Stability of Self-Consolidating Concrete*, ACI Materials Journal, 111 (3), May 2014, pp. 299-308.
[6] Spangenberg, N, Roussel, N, Hattel, E.V., Zirgulis, G. and Geiker, M.R. (2012): *Patterns of gravity induced aggregate migration during casting of fluid concretes.* Cement and Concrete Research 42 (2012), 1571-1578
[7] Cussigh, F, and Bonnard, V. (2004): *Testing SCC, Summary report on WP4, Site trials and full scale construction trials*. Growth Project No. GRD2-2000-30024. GTM Construction Nanterre, France, October 2004.

The Plate Test Carried Out on Fresh Self-Compacting Concrete

Sofiane Amziane[1] and Arnaud Perrot[2]

[1]LIMat B, Université de Bretagne Sud, Lorient France
[2]Clermont Université, Institut Pascal, Clermont-Ferrand, France

Abstract To monitor, these entire physical phenomenon linked to cement setting, several tools are needed from rheometer, transducer, calorimeter and others expensive and sometimes very difficult set up. The plate test can be a simple and cheap substitute for all these tools and can provide interesting information about structural build-up and setting. This device consists of a steel rough plate immersed in the cement-based materials and was initially developed to enable a simpler measurement of the yield stress increase during the dormant period. After providing and explaining the test physical background and procedure, we here try to extend the test duration to get information on both the thermal dilatation and the setting time. Due to the deformation of the material at rest and due to changes in the volume linked to thermal expansion, the plate apparent mass varies with time. The apparent shear stress value and the thermal stress of the cement paste could be deduced from this measurement.

Keywords: *setting, yield stress, structural build-up, dimensional variations*

Introduction

Despite the long tradition of characterizing cement paste time evolution by the initial and final setting time, these values are not sufficient to answer some of the more practical questions related with constructability. The answer to these questions is of paramount importance for the civil engineer to design a concrete meeting a given construction schedule. However, to answer the above questions, the flow properties of the material need to be known. In contrast with a mechanical method that will be always dependent on the geometry and the applied forces, the proposed investigation was carried out on the idea that it was possible to monitor the setting through the variation of yield stress. Roussel and other authors have shown that during the dormant period and at rest, SCC structure build-up and its

yield stress increases [1–4]. This increase is responsible for lot of practical application such as multilayer casting, 3D printing, formwork pressure decay…[1, 5–10]. The increase rate of yield stress is commonly determined using rheological measurements carried out after different resting time. Portable system has been developed to monitor the yield stress increase on site [11]. Another strategy is to use the plate test measurement [5]. The plate test device, consisting of a rough plate (or needle) immersed in the fluid sample, was developed to enable a simpler measurement of the yield stress increase of non-Newtonian suspensions such as self-compacting concrete. Due to the deformation of the material at rest along the vertical axis, shearing appears at the plate surface inducing the plate apparent mass to vary with time.

The plate test device has been first used for concrete in 2008 [12][10]. The problem is the same as the steel rebar immersion in concrete formwork [13]. The elastoplastic properties and deformation of the fresh cement paste are used. Due to local vertical deformation of the cement paste at very early age (shrinkage, dilatation, settlement), stresses are mobilized at the interface between the paste and the rough plate. This induces variation of the apparent mass of the plate or needle, as proposed by Sleiman et al. [14]. Moreover, since the plate or needle is static and the material shrinkage is slow, the dynamic effects are, therefore, negligible. The plate tests measurements has also been shown to be able to give accurate values of the setting times [14]. The paper aims to provide a correct protocol for performing a plate test measurement carried out on SCC that is able to provide the rate of increase of yield stress during the dormant period, the setting times. Moreover, we show that the plate test is able to detect the thermal dilatation due to exothermic hydration of the cement particles. We also try to give some limitations of this test that is able to provide important data when properly carried out.

Experimental program

The plate test device, a multiform apparatus

The device is composed of a needle or a plate (solid body) rigidly attached below a fixed support. The (solid body) is lowered into a frustum, containing the material. The apparent mass of the needle or the apparent mass of the sample is continuously monitored versus time by recording the balance output with a computer. The immersed tool used can be a needle with a diameter of 1.13 mm ± 0.05 mm and 40 mm long (i.e. a roughened Vicat needle) [14], can be a plate covered by sandpaper [10, 12] or also a 10mm diameter rebar [5, 13]. The distance between the needle/plate and the frustum walls is large enough that there is no influence on the stress measured due to the size of the frustum as shown by [15] and Tchamba et al.[10]. Moreover, in order to ensure that the yield stress is fully mobilized at the interface with the immersed tool, it is critical to make sure that the critical strain is overcome at the interface. This can be made by having a sufficient length of concrete under the immersed tool. Assuming a linear settlement of concrete with

sample height, figure 1 obviously describes the increase of the strain at the interface with the sample height.

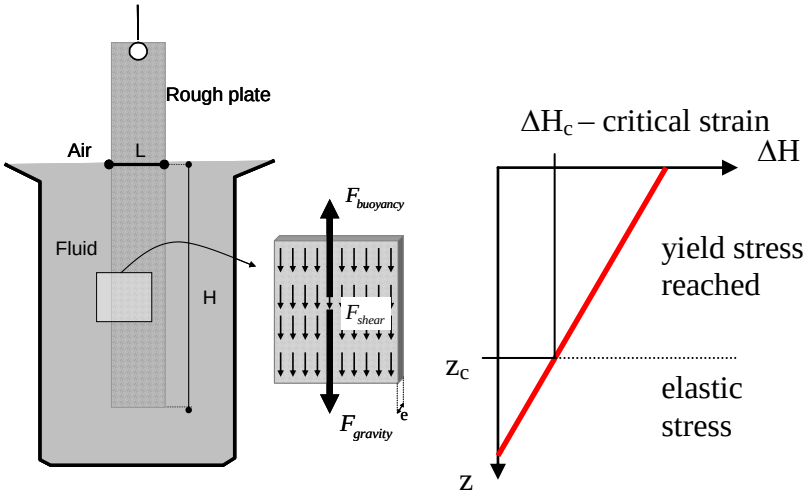

Figure 1. Evolution of the settlement ΔH within the sample. The yield stress is fully mobilized only over a critical depth z_c corresponding to a critical settlement ΔH_c for which the concrete critical strain is obtained.

It is important to note that the balance can be used to measure the immersed tool apparent mass and the sample apparent mass as shown on figure 3 for two possible test configurations. In this work, we have performed two series of tests using two different apparatus. For all tests, a thermocouple was introduced into the self-compacting materials in order to measure the thermal activity of the material during the whole test.

The first configuration consists of the static Vicat needle device used in Sleiman et al. work. The second configuration is designed to be dedicated to mortar and concrete. The measurement sequence begins with the immersion of the plate in a suspension filled vessel. Then length of the immersed portion of the tool is measured before the start of the test.

Measurement precision and reproducibility depend on the following parameters: a) immersion depth (precision: 1 mm), b) measured mass (precision: 0.1 g) and c) experimental conditions such as temperature and relative humidity. Variations between tests performed on the same material in the same experimental conditions are less than 5 %. The immersed tool surface is lightly roughened or covered with sandpaper to avoid slippage effects. In addition for the Vicat static test, we measure the material deformation with a comparator placed on the frustum material. We used a small steel grill placed between the comparator and the cement paste to reduce the error due to comparator weight. We followed the evolution of deformation with time to check if the settlement is sufficient to reach the critical

strain at the interface. A linear deflectometer, LVDT, attached by fixed support, is placed on the top surface of this frustum. This LVDT is used to monitor surface settlement. Tests are carried out during 24 hours.

Materials

The first serie of tests is performed on normal consistency cement pastes. The cement (CEM I/52.5 N) used contains mass fractions of 95 % clinker, 3.5 % gypsum and 1 % filler. The specific Blaine surface is 425 m²/kg. The cement was prepared in a 5 L mixer according to the standard ISO 9597. The second serie is performed on a self-compacting concrete. For this concrete, A CEM I 42.5 N is used at a recipe of 420 kg/m^3. A limestone filler is added (120 kg/m^3) and the naturally rounded aggregate is of granitic origin (sand + coarse aggregate 1700 kg/m^3). A poly carboxylate ether (PCE) plasticizer was used in this study. The W/C ratio is 0.385. All computed yield stress from plate tests are compared with a reference yield stress measured on a BOHLIN Gemini®200 viscometer equipped with a Vane geometry following the procedure described in [16] with an apparent shear rate of 0.001 s^{-1}.

Data analysis – general equation.

The data analysis is based on the force balance equation of a static cylinder (Fig. 1). Three phenomena are acting on the plate: gravity, buoyancy and shearing at the material/plate interface. In air, the mass plate M_0 is only due to gravity and does not change with time:

$$M_0(t) \times \vec{g} = \overrightarrow{F_{gravity}} \tag{1}$$

For an immersed plate, the mass measured corresponds to the apparent mass M(t), which can deduced from the static equilibrium of the tool in a yield stress fluid:

$$M(t) \times \vec{g} = \overrightarrow{F_{gravity}} + \overrightarrow{F_{buoyancy}} + \overrightarrow{F_{shear}} - \alpha.G.\Delta T.\vec{z} \tag{2}$$

where $F_{gravity}$ is the constant weight of the plate , $F_{buoyancy}$ is the resistance force due to buoyancy and F_{shear} is the resistance due to shearing at the material/cylinder interface, $\alpha.G.\Delta T.\vec{z}$ is a correction term taking into account the thermal dilatation which might not be negligible during the hydration period. G is an apparent shear modulus and α is the dilatation coefficient depending only hydration time. In the present case (i.e. A Vicat needle), it is important to note that the bottom end effect is neglected because the cylinder is very thick (needle) or empty (cylinder). This assumption is not valid for higher diameter value [17–19]. In this case, we advise to slightly move the plate upward in order to create an empty space between the bottom end of the immersed tool and the concrete.

It is important to note here that, as opposed to a penetrometer test (Vicat needle), the plate is perfectly static. This test is not really intrusive because the only movement is due to the changes occurring in the material. In other words the plate behaves as an additional vessels wall. In the general case, the particles in a suspension move downwards creating a higher density layer at the bottom. Equation 2 can be rewritten as follow if considerations are taken that the force applied on the cylinder change with time due to sedimentation:

$$M(t,T) = \frac{1}{g}(F_{gravity}(t) - F_{buoyancy}(t) + F_{shear}(t) - F_{dilation}(t,T)) \quad (3)$$

As a result, the mass variation induced by the plate immersion is:

$$\Delta M(t,T) = \frac{1}{g}(-F_{buoyancy}(t) + F_{shear}(t) - F_{dilation}(t,T)) \quad (4)$$

If the material remains homogeneous, the buoyancy remains constant during time.

Raw data

Consolidation diagram

The consolidation of the cement paste under its own weight is possible as long as the material has not yet stiffened and is recorded with the LVDT. Thixotropy and then structural build up gradually reduces the rate of consolidation as shown by Sleiman et al. [14] The stress recorded by the needle corresponds to the yield stress as soon as the paste settlement is more than 0.005 (just after the test began). This means that before this time, the yield stress is not mobilized wherever on the needle surface. In order to reduce and avoid this duration, we advise, another time, to slightly move the immersed needle upward. For all performed tests, the time needed to overcome the critical strain is always lower than 15 minutes.

Mass/Temperature-Time diagram.

Three stages can be identified on the diagram mass vs. time (Figure 2) recorded with the static Vicat needle device. The first stage corresponds to a low thermal activity. The mass variation is attributed to the entire phenomena occurring during the setting period (thixotropy, consolidation and plastic shrinkage). Around 5 hours, the thermal activation begins inducing the swelling of the cement paste. The "stage two" can be identified as the swelling period with an inversion of the stress at the plate. After that, stage 3 shows that the temperature goes down and the mass and the temperature tend toward a stabilized value. Moreover, we can observe that the temperature peak is simultaneous with the recorded minimum mass variation. Then, it shows that both local extrema are linked .Now that we have examined the

raw data, we can go a step further and see what information we can obtained from the plate tests measurement.

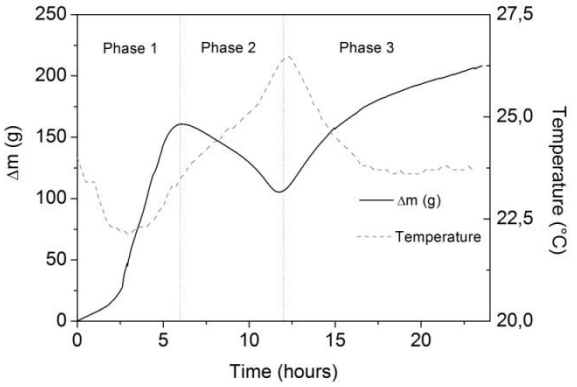

Figure 2. Mass-Temperature vs.Time diagrams recorded using the static Vicat device / different stages of behavior.

Discussion and analysis of the raw data

Rheology and structural build-up

For cement paste, in a previous study made by Sleiman et al. [14] on the static Vicat device, a focus on the dormant and setting stages was made. During these periods, the temperature variation and the sedimentation are neglected. Then, the shear stress recorded at the Vicat needle surface can be computed as follow:

$$\tau(t) = \frac{g\Delta M(t) + \rho\pi HD^2/4}{\pi DH} \tag{5}$$

Where D and H are respectively the immersed cylindrical tool diameter and immersed length and ρ is the cement paste density. During this stage, the vertical strain is higher than the critical strain and the shear stress is equal to the yield stress of the cement paste. The evolution of yield stress with time is computed from equation 5 with the results of the static Vicat test presented above. Figure 3 presents, in different ways, the comparisons of the various results obtained: yield stress, Vicat penetration and Vane test. For the yield stress method, the time at point B is defined as the setting time. It is clear for all three types measurements, the time obtained for setting times equal 2 hours and 45 minutes. The key points to describe Figure 4 are points A, B and C. These points can be used for all curves in Figure 4 to define two specific sections: Section AB (from point A to B) which shows a slow steady increase of the yield stress with time ans section BC (from point B to C) exhibiting a dramatic increase of the yield stress, indicating the change of the cement paste from a fluid to a solid state. Therefore, the method

proposed could be used not only to determine setting time, but also to monitor the process before initial set (dormant thixotropic period). The initial gradient of the yield stress vs. time, linked to the hydraulic pressure, could give an indication of the material performance. The evolution of the non-Newtonian viscosity is an indication of the flow capability of a material. The transition from a flowing material to a specimen governed by frictional forces, or almost solid, cannot be clearly determined by the change in viscosity.

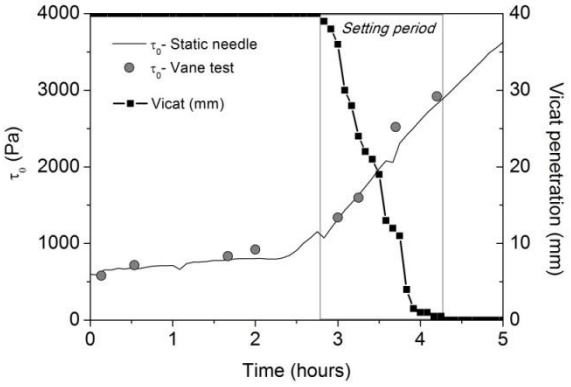

Figure 3. Zoom on stage 1 [0-5h]: Yield stress variation from plate test / Vicat penetration vs. time during dormant and setting stages of a cement paste in the static Vicat apparatus.

For cement paste tested in the Vicat Apparatus, it clearly appears that the rapid deformation of cement paste allows measuring the cement paste yield stress as the critical strain is quickly reached and overcome. As a result, the static Vicat needle is sufficient to monitor the yield stress evolution and is able to monitor the evolution of a cement-based paste during thixotropic reversible period and during setting period. In the case of concrete and mortar, due to the presence of aggregates, the level of settlement is limited. It is therefore important to check if the height of the concrete sample is sufficient. For example, it is observed that a sample height of 21 cm is too low to ensure the mobilization of the yield stress at the interface (see figure 4). A sample height is here required to obtained results that are in agreement with results provided by rheological measurements.

Modelling of the thermal expansion.

The effect of thermal expansion on measured mass can be computed assuming that the critical strain of the cement paste and the TDC remain both constant during the expansion stage. In the first stage of figure 6, the critical strain of cement paste ε_c is usually taken at 0.005 and corresponds to the breakage of CSH gel [14, 18, 21]. Then, the evolution of the shear modulus G(t) can be computed from the evolution of the yield stress with time:

$$G(t) = \tau_0(t) / \varepsilon_c \tag{6}$$

Then, the shear modulus can be computed as follow:

$$G(t) = \frac{g\Delta M(t) + \rho g V}{\varepsilon_c . S - \alpha \Delta t} \tag{7}$$

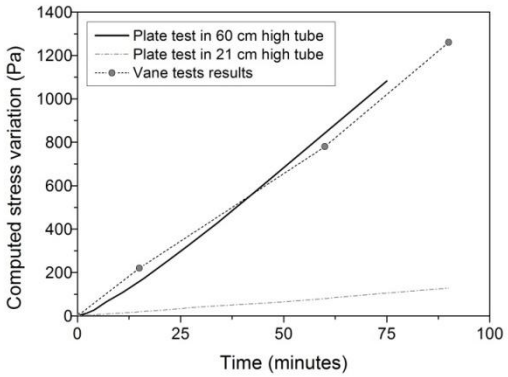

Figure 4. Stress variation computed from data of tests performed with concrete. Tests performed with two different sample heights (21 and 60 cm). Results compared with rheological vane tests measurement.

During the thermal expansion stage, the critical strain is no longer reached due to the paste swelling. Then, in the second stage, the computed modulus does not correspond to the intrinsic shear modulus but to an apparent shear modulus that depends on the test geometry. In this stage, the material is not able to flow on its own weight and part of the immersed tool interface is irreversibly broken.

$$G_{apparent}(t) = \frac{g\Delta M(t) + \rho g V}{\varepsilon_c . S - \alpha \Delta t} \tag{8}$$

Then, equation (8) is used to fit a value of a that erases the effect of thermal dilation on the evolution on the apparent shear modulus. A value of 0.005 is found and is in agreement with values found in the literature [20]. Then, the evolution of the shear modulus can be obtained during the first 24 hours (Figure 10). We can see on figure 5 that the effect of thermal expansion has to be taken into account in order to accurately describe the paste hardening. A shear modulus computed with equation (4) and (5) that does not take into account the thermal expansion is also computed. Then, the difference obtained between the shear moduli computed with and without taking into account the thermal expansion at 24 hours is due to the difference of the paste temperature at this time. It is worth noting that the difference between both shear modulus obtained with both computation follow the temperature evolution of the paste given in figure 2.

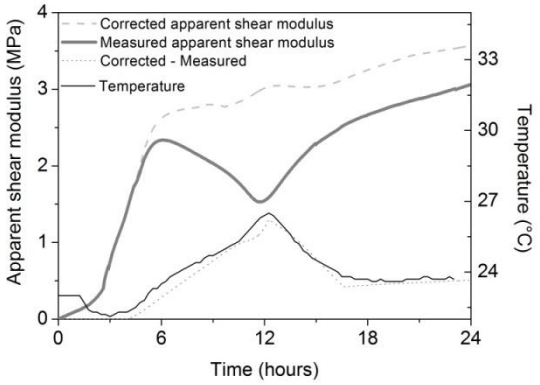

Figure 5. Evolution of the apparent shear moduli. The grey line corresponds to the measured one. The dashed line corresponds to a corrected apparent shear moduli that takes into account thermal expansion.

Conclusions

The main scope of the paper was to examine the possibility of using alternative tests to the classical methods to monitor early age behaviour of SCC from casting to hardening. It was shown that plate test method tested on SCC is very promising as they correlate well with rheological test and thermal variation measurement, providing more information with a unique test.

References

[1] Roussel, N. (2006) A thixotropy model for fresh fluid concretes: Theory, validation and applications, *Cement and Concrete Research*, Vol. 36, p. 1797 – 1806.

[2] Roussel, N. (2005) Steady and transient flow behaviour of fresh cement pastes, *Cement and Concrete Research*, Vol. 35, p. 1656 – 1664.

[3] Roussel, N. Ovarlez, G. Garrault, S. and Brumaud, C. (2012) The origins of thixotropy of fresh cement pastes, *Cement and Concrete Research*. Vol. 42, p. 148 – 157.

[4] Wallevik, J.E. (2009) Rheological properties of cement paste: Thixotropic behavior and structural breakdown, *Cement and Concrete Research, Vol.* 39, p. 14 – 29.

[5] Billberg, P.H. Roussel, N. Amziane, S. Et al. (2014) Field validation of models for predicting lateral form pressure exerted by SCC, *Cement and Concrete Composites*, Vol 54, p. 70–79.

[6] Ovarlez, G. and Roussel, N. (2006) A Physical Model for the Prediction of Lateral Stress Exerted by Self-Compacting Concrete on Formwork, *Materials and Structures*, Vol. 39, p. 269–279.

[7] Perrot, A. Pierre, A. Vitaloni, S. and Picandet, V. (2015) Prediction of lateral form pressure exerted by concrete at low casting rates, *Materials and Structures*, Vol. 48, p. 2315–2322.
[8] Perrot, A. Rangeard, D. and Pierre A. (2015) Structural built-up of cement-based materials used for 3D-printing extrusion techniques, *Materials and Structures*.Available online.
[9] Roussel N. and Cussigh F. (2008) Distinct-layer casting of SCC: The mechanical consequences of thixotropy, *Cement and Concrete Research*, Vol. 38, p. 624–632.
[10] Tchamba, J.C. Amziane, S. Ovarlez, G. and Roussel, N. (2008) Lateral stress exerted by fresh cement paste on formwork: Laboratory experiments, *Cement and Concrete Research*, Vol. 38, p. 459 – 466.
[11] Khayat, K.H. Omran, A.F.. Naji, S. Billberg, P. and Yahia, A. (2012) Field-oriented test methods to evaluate structural build-up at rest of flowable mortar and concrete, *Materials and Structures*, Vol. 45, p. 1547–1564.
[12] Amziane, S. Perrot, A. and Lecompte, T. (2008) A novel settling and structural build-up measurement method, *Measurement Science and Technology*, Vol. 19, p. 105702.
[13] Perrot, A. Amziane, S. Ovarlez, G. and Roussel, N. (2009) SCC formwork pressure: Influence of steel rebars, *Cement and Concrete Research*, Vol. 39, p. 524 – 528.
[14] Sleiman, H. Perrot,A. and Amziane, S. (2010) A new look at the measurement of cementitious paste setting by Vicat test, *Cement and Concrete Research*. Vol. 40, p. 681 – 686.
[15] Zhang, M.H. Ferraris, C. Zhu, H. Et al. (2010) Measurement of yield stress for concentrated suspensions using a plate device, *Materials and Structures*, Vol. 43, p. 47–62.
[16] Perrot, A. Lecompte, T. Khelifi, H. et al. (2012) Yield stress and bleeding of fresh cement pastes, *Cement and Concrete Research*, Vol. 42, p. 937 – 944.
[17] Boujlel, J. and Coussot, P. (2012) Measuring yield stress: a new, practical, and precise technique derived from detailed penetrometry analysis, *Rheologica Acta*, Vol. 51, p. 867–882.
[18] Lootens, D. Jousset, P. Martinie, L. et al. (2009) Yield stress during setting of cement pastes from penetration tests, *Cement and Concrete Research*, Vol. 39, p. 401 – 408.
[19] Perrot, A. Mélinge, Y. Estellé, P. et al. (2011) The back extrusion test as a technique for determining the rheological and tribological behaviour of yield stress fluids at low shear rates, *Applied Rheology*, Vol. 21, p. 53642.
[20] Loukili, A. Chopin, D. Khelidj, A. and Le Touzo J.Y. (2000) A new approach to determine autogenous shrinkage of mortar at an early age considering temperature history, *Cement and Concrete Research*, Vol. 30, p. 915–922.
[21] Roussel, N. Lemaître, A.. Flatt, R.J. and Coussot, P. (2010) Steady state flow of cement suspensions: A micromechanical state of the art, *Cement and Concrete Research*, Vol. 40, p. 77–84.

Heat Flux Measurements for the Characterization of Maturity and Stability of Mortars and Self-Consolidating Concrete

H. Kada[1], K.H. Khayat[2] C. Djelal[1], Y. Vanhove[1],

[1] *Univ. Artois, EA 4515, Laboratoire de Génie Civil et géo-Environnement (LGCgE), Béthune, F-62400, France*
[2] *Department of Civil, Architectural and Environmental Engineering, Missouri University of Science and Technology, Rolla, MO, United States*

Abstract The chemical phenomena responsible for the setting of concretes are thermo-activated processes. The degree of advancement of the reactions and the corresponding instantaneous mechanical performance of the product depend on the temperature changes undergone by the mixture. In situ, this is a function of the local weather conditions which are difficult to forecast. In this study, a novel method based on the direct determination of the changes in heat flux along a concrete specimen is proposed to monitor the hydration kinetics and the setting. Other phenomena investigated in this study include the segregation of aggregate and bleed water on the surface. This process creates a vertical heterogeneity in the distribution of water, cement grains and aggregate, leading to different local kinetics depending on the height. The local measurement of the heat of hydration can be detected using the proposed heat flux sensors to quantify the segregation.

Keywords: *Mortar, Concrete setting, heat flux, segregation.*

Introduction

Modern concrete has diverse mixture compositions characterized by complex and specific reaction processes. The progress of the chemical hydration reaction of cement, which affects microstructural development and performance of the hardened product, depends on the evolution of temperature of the mixture. This progress is a function of the mixture composition and constituent materials as well

as ambient temperature, which is difficult to predict. In-situ monitoring different elements of the construction is essential to estimate the evolution of the mechanical strength of the concrete. Different maturity techniques can be used on construction sites to evaluate the development of mechanical properties of concrete at early age [1-3]. These techniques need the detection of the start of setting to use the Arrhenius law. In the case of relatively thin structural elements, these techniques may not be suitable since temperature rise can be small or negligible, and the maturity technique may not be able to detect the start of setting.

The objective of this paper is to investigate the feasibility of using a new flux sensor system that can be attached to the surface of a concrete element (shuttering 'skin' sensor) to detect the evolution of heat flux of cement hydration and to detect strength gain and setting during the early age.

In this study, an attempt was has been carried out to evaluate the risk of segregation and bleeding of concrete using the non-destructive in-situ testing of heat flux, which represents the thermal signature of cement hydration reaction. Such hydration kinetics are affected by the local composition of the material, including the local water to cement ratio (W/C) and paste content. The basic idea is to consider the phenomenon of the segregation involving a vertical heterogeneity in the distribution of water, cement, and aggregate which can lead to different local kinetics of cement hydration. The local measurement of the heat of hydration could then lead to detect and quantify the segregation in cement-based materials. The variation in W/C can affect the onset of setting. Areas where the W/C is higher than the bulk values used in the preparation of the mixture should then lead to a delayed heat rise that can be detected with a local heat flux sensor approach.

The present study is divided into two phases. The first involves a proof-of-concept study under controlled ambient temperature conditions to verify the effectiveness of using heat flux measurements to detect homogeneous composition along a given sample. The experimental heat flux apparatus consists of sensors instrumentation integrated thermocouple and an associated data acquisition system. The study is performed on mortars prepared with W/C ranging from 0.4 to 0.7. The mortar had a slump flow spread of 140 to 320 mm. The mortar with W/C of 0.7 was unstable. In the second phase, the effect of the incorporation of chemical admixtures on mortar was investigated. Four mortar mixtures were prepared with superplasticizer dosages varying between 0.2% and 0.5%, by mass of cement. A fifth mortar was prepared with 8% silica fume substitution and a superplasticizer dosage of 0.6%. After validation of the method on mortar, the use of the heat flux sensors was applied to concrete under a non-controlled ambient in order to simulate in-situ conditions. Testing was conducted on three concrete mixtures consisting of a conventional concrete, a self-consolidating concrete, and segregating concrete.

Thermal principles and instrumentation

Theoretical aspects

In the laboratory, the ambient temperature conditions are controlled and maintained constant. The evolution of the heat flow and the temperature in the concrete are exclusively due to the hydration reaction. In-situ, the work is in interaction's energy with its microclimate environment according to random changes. In these conditions, direct measurement of work (flux, temperature), during the setting, are from two contributions, namely the internal supply of energy from the hydration process and the heat flux representing the thermal imbalance of the medium with the external environment. This is depicted in equation.1 where ϕ_r is the hydration reaction flow, ϕ_m is the measured flow, ϕ_s is the purely sensitive flux that would have brought the system into the same thermal state in the absence of internal reaction.

$$\varphi_m = \varphi_r + \varphi_s \tag{1}$$

Here, the main objective is to separate the component corresponding to the heat of hydration. This can be achieved by modeling the energy exchange with the external environment, and then isolating the hydration flux by difference.

During the setting process, an element of concrete can be represented as a linear and stationary thermal system where the principle of additivity of sources is applicable. Therefore, we seek to estimate □$_s$ that can be subtracted from the measured flux to get the reaction flux. One possible approach is to simulate the sensitive flux by performing a convolution product between temperatures of the faces of the element and step response u(t) corresponding to these solicitations.

It should be noted that the thermo-physical properties (□□□□□□□c) of concrete can be considered as constant. Thereby, the sensible flux can be considered as linear and steady.

The concrete element is considered as one-dimensional system since its thickness is small with regard to the two other dimensions (Figure.1).

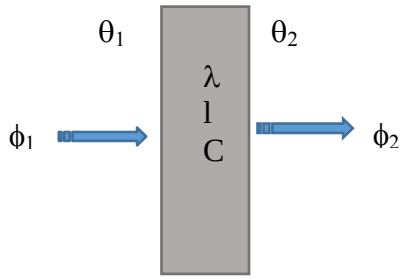

Figure 1. One-Dimensional Heat Flux through a Concrete Element

With these step responses, one can calculate Δϕ and Σϕ from Σθ and □□□as the following:

$$\sum\phi(t) = \frac{2\lambda}{l}\Delta\theta(\mathrm{t})\left[1+2\sum_{k=1}^{\infty}Exp(-4k^2z)\right] \quad (2)$$

$$\Delta\phi(t) = \frac{4\lambda}{l}\Sigma\theta(\mathrm{t})\left[\sum_{k=1}^{\infty}Exp-(2k+1)^2z\right] \quad (3)$$

where

$$\tau = \frac{RC}{\pi^2}, z = \frac{t}{\tau} \quad (4)$$

with Σϕ, Σθ, Δϕ, Δθ are sum and difference of the initial magnitudes ϕ_1, ϕ_2, θ_1, θ_2 respectively . t represents time (s), R is the resistance of the wall and C is specific capacity.

Then the flux on each side of the element can be calculated via the following relations:

$$\phi_{1sim} = \frac{\Sigma\phi + \Delta\phi}{2} \quad \phi_{2sim} = \frac{\Sigma\phi - \Delta\phi}{2} \quad (5)$$

Instrumentation

In the proposed approach, heat flux and temperature are determined in the same plane using ‘‘tangential gradient’’ flux measuring sensors [4-6]. The major advantage of the system lies in the fact that the surface sensors do not cause any disturbance to the measuring material. The thermal flux sensor was specially made to produce a positive or negative voltage, depending on the direction of the thermal flux for a measurement corresponding to a thermal balance. The signal is generated by the heat flux, and the sensor does not require an electrical supply. Its thickness is of the order of 300 mm. The sensitivity is of the order of 3 mV/W/cm^2 for a 1 cm^2 sensor area. The low inertia of the sensor allows a response time on the order of 150 ms.

In this investigation the elements used for mortar testing were 0.20x0.20x0.25 m^3. This can result in surfaces "observations" of 0.16 m and 0.21 m. Thereby, they offer a sufficient space for the establishment of active surfaces of 0.05 x 0.05 m² (Fig. 2). For concrete testing, in order to have good representation of the test medium, the dimensions of the column were increased to 0.40mx0.25mx0.61m^3.

The "observation" surfaces were 0.2 m and 0.4 m aside appear sufficient to implement the four flux sensors that were regularly distributed over the height of the mold with the four sets of sensors facing each other. The flux sensors were covered with a plastic film to protect them from the concrete.

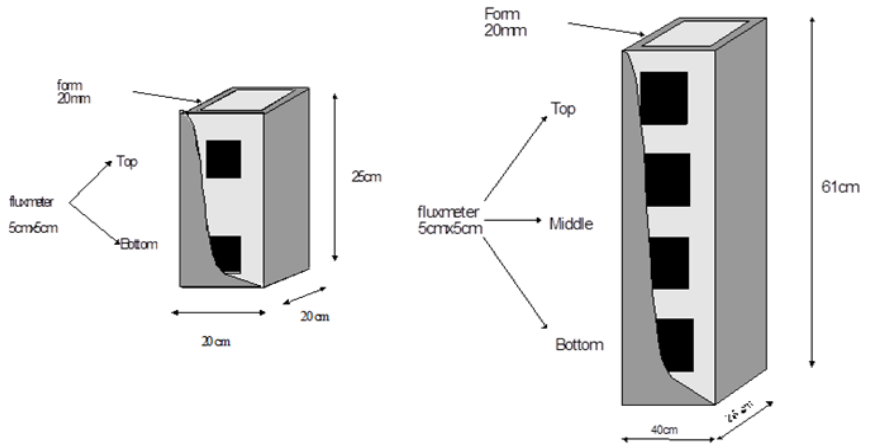

Figure 2. Experimental devices

Experimental investigation

In laboratory

The first phase of this work involved mortar testing to establish the feasibility of the proposed technique in the laboratory under controlled ambient temperature conditions.

The study was performed on mortar, composed of one tier of cement and two tier sand. The W/C ratio is varied from 0.4 to 0.7, which can affect the stability of the mixture, and hence segregation and bleeding.

A Type GU Canadian cement, equivalent to Type I ASTM cement, was used. A siliceous sand with of gradation between 0 and 4 mm and a fineness modulus of 2.4 was used. The absorption of the sand is 1.2%. Table 1 gathers the mixture compositions of the investigated mortars.

Table I. Constituents of mortars [kg/m^3]

W/C	0.4	0.55	0.7
Cement	536	495	461
Sand	1607	1487	1384
Mixing water	214	272	323
Slump (mm)	140	220	320

Five other mortar mixtures were prepared with different concentrations of superplasticizer to evaluate the sensitivity of the proposed flux sensors attached to the 'skin' of the mold to determine heat flux and evaluate the period corresponding to setting. Four mortar mixtures were prepared with superplasticizer dosages varying between 0.2% and 0.5%, by mass of cement. The superplasticizer dosage corresponds to the active mass of the admixture, which was 42% by mass of the admixture solution. A fifth mortar was prepared with 8% silica fume substitution and a superplasticizer dosage of 0.6%, as indicated in Table II.

Table. II. Constituents of mortar prepared with superplasticizer [kg/m^3]

Percentage of RWR, by mass of cement	0	0.2	0.4	0.5	0.6
Cement	536	536	536	536	453
Silica fume					40
Sand	1607	1607	1607	1607	1607
Mixing water	214	212	211	209	207
PNS-based HRWR	0	2.55	5.1	6.37	7.65
Spread (mm)	140	180	280	320	288

In Situ conditions

A series of experiments on three concrete mixtures was conducted. In order to simulate in-situ conditions, the test were conducted outside laboratory in non-controlled ambient. A conventional concrete BO, a self-consolidating concrete BAP, and a segregating concrete BO2 was prepared. The studied elements were made using the mixture compositions highlighted in Table. III.

Table. III. Formulation chosen for concrete

Materials	BO	BAP	BO2
Cement CEM I52.5	350	350	350
Filler		150	
Sand 0/4	828	833	828
Aggregates 4/12.5	662	742	662
Aggregates 11.2/22.4	293	-	293
Water	182	200	200
Superplasticizer (polycarboxilate)	0.5%	4%	1.5%
Slump/flow (mm)	130	660	160

Test results and discussion

In Laboratory

Effect of W/C

The objective of the mortar test was to check the effectiveness of flux laboratory measurements to describe the reaction of the hydration of cement. The evolution of the temperature and the heat flux during the first 24 hours for the mortar with the W/C from 0.4 to 0.7 are presented in Figures 3 and 4. Figure 5 depicts the evolution of the heat flux of mortar made with W/C 0. 7 during the first 10 hours.

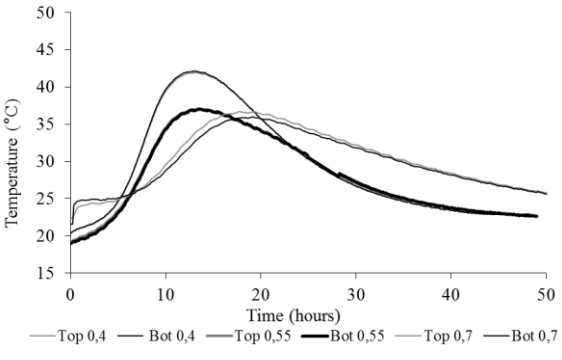

Figure 3. Temperature evolution of mortars

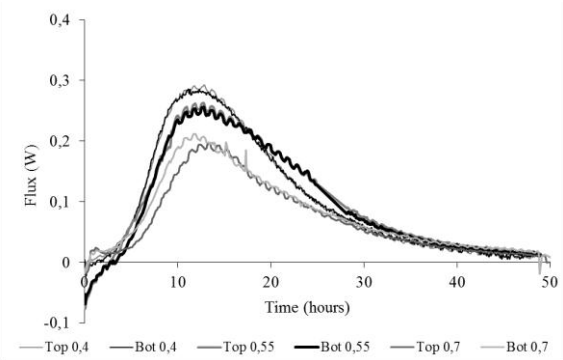

Figure 4. Evolution of heat flux of mortars

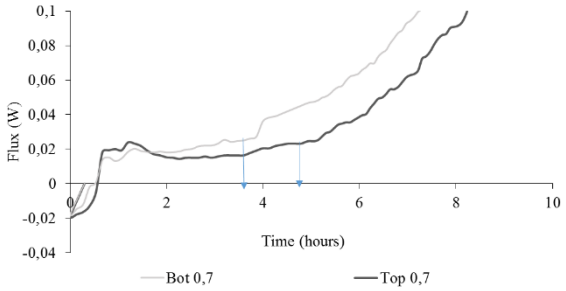

Figure 5. Heat flux of mortar made with W/C 0.7 during the first 10 hours

For the mortars made with W/C of 0.40 and 0.55, the flux and temperatures remain very close during the testing. These mortars can, therefore, be considered to exhibit a good vertical stability. For the mortar with the high W/C of 0.7, a difference between the upper and lower heat flux signals can be noticed. This was especially the case at the beginning of the hydration reaction, which was delayed by nearly an hour and a half (Figure. 5). This delay is not detected when merely measuring the temperature (Figure 3).

The results presented show the interest of using heat flux surface sensors to detect a non-vertical homogeneity that affects setting. In a system in thermal disequilibrium, flux variations can be observable before a significant change in temperature could be detected. In order to obtain a temperature change, the heat flux must integrated. From a purely qualitative and practical point of view, the evolution of the temperature would always "softened" and smoothed compared to flux's changes.

Effect of superplasticizer dosage on hydration kinetics and setting

Figures 6 and 7 present the temperatures and heat flux for the four mortar mixtures prepared with superplasticizer dosages varying between 0.2% and 0.5%.

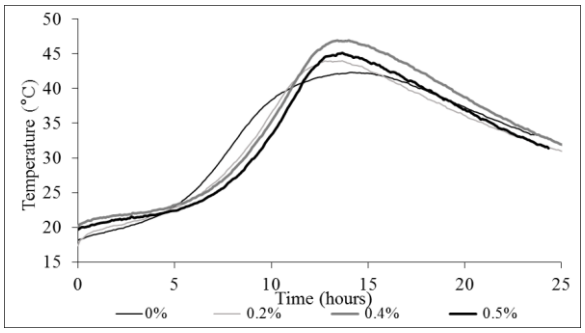

Figure 6. Temperatures of mortars made with different superplasticizer dosages

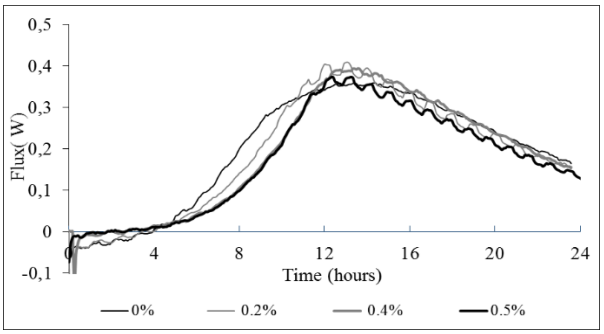

Figure 7. Heat flux of mortars made with different superplasticizer dosages

The hydration kinetics are strongly modified by the presence of the superplasticizer in the mortar. It can be noted that depending on the dosage of the superplasticizer, the start of the reaction is delayed. This delay was of the order of 3 hours for the reference mortar without any superplasticizer, 3.5 hours for the mortar at 0.2% superplasticizer, and 5 hours for the mortars with 0.4% and 0.5% superplasticizer. The peak of heat flux was reached around 13 hours. The peak value was greater for the mortars made with superplasticizer, it is 0.33 Watt for the mortar at 0.2% superplasticizer and 0.28, 0.31, and 0.32 watt for the mortars with 0, 0.4%, and 0.5% superplasticizer, respectively.

Figures 8 and 9 shows the comparison of temperatures and heat flux between the mortar without superplasticizer and additions and the mortar with 8% silica fume substitution and 0.6%.of superplasticizer .

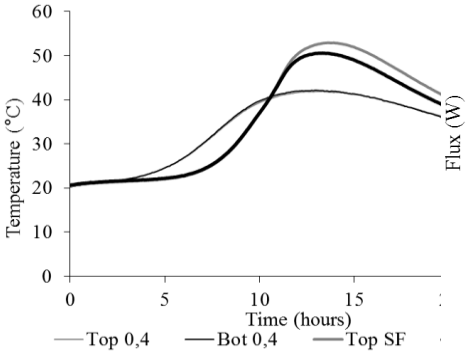

Figure 8. Temperatures of mortars made with and without silica fume

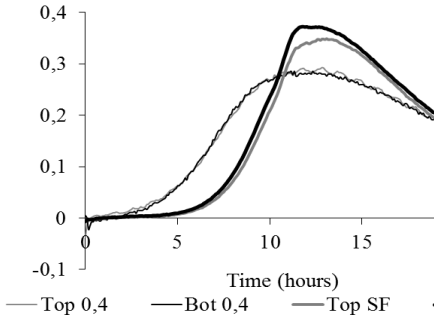

Figure 9. Heat flux of mortars

made with and without silica fume

For the mortar with silica fume and 0.6% superplasticizer (Figures 8 and 9), the beginning of hydration reaction is delayed by 6 hours, and the high level of adjuvantation causes a significant delay in the setting. The peak of the reaction remained around 13 hours, but it is greatly increased with the introduction of silica fume from 0.28 watt to 0.38 watt.

These tests showed that the instrumentation flux an essential is a necessary complement to the measurement of the temperature for a more reliable analysis.

In-situ heat flux measurement for the concrete

Figures 10 - 15 show temperature and flux changes for three concrete, namely BO, BO2 and BAP. For each test, we presented the average temperature and flux of the faces on a same level. Note that the reference temperature, characterize the evolution of the external atmosphere and Cyclical developments day-night appear.

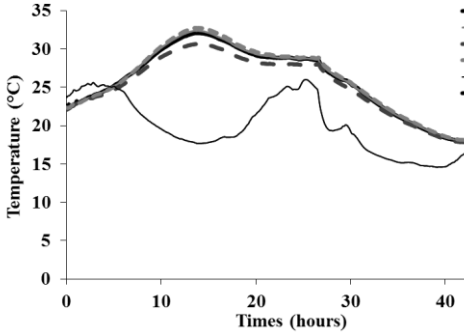

Figure 10. Temperature concrete BO

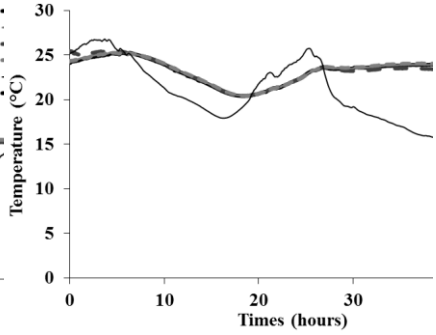

Figure 11. Temperature concrete BAP

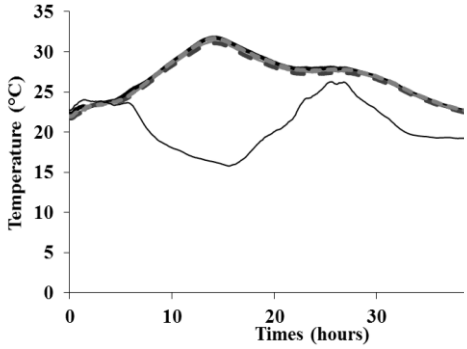

Figure 12. Temperature concrete BO2

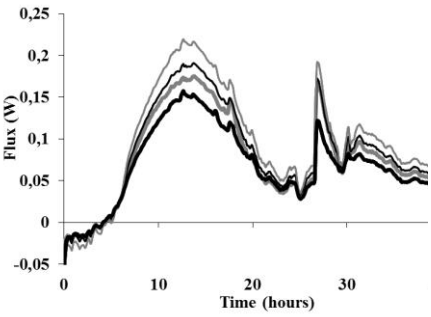

Figure 13. BO concrete flows

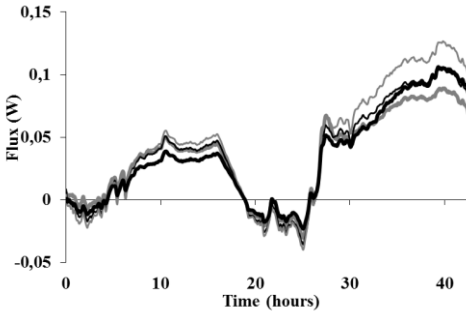

Figure 14. Evolution of BAP concrete flows

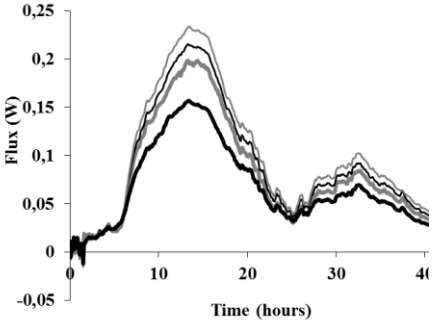

Figure 15. Evolution of flows of concrete BO2

As stated above (paragraph 2), the measured fluxes are a combination of external stresses and the hydration flux. The convolution product allows for the evolution from of sensitive flux from measurements of temperatures at each sensor.

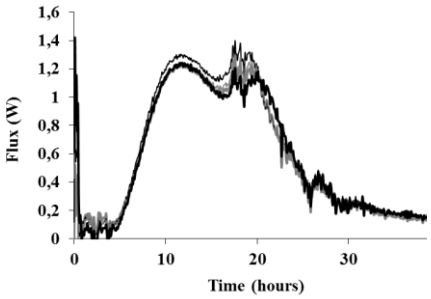

Figure 16. Evolution of reaction of the BO flows

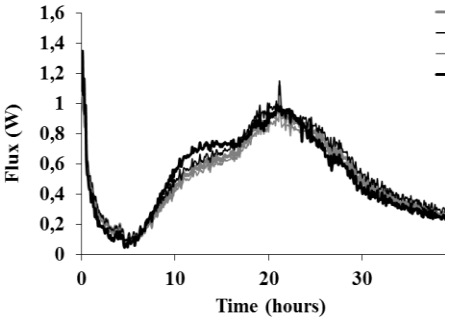

Figure 17. Evolution of reaction of the BAP flows

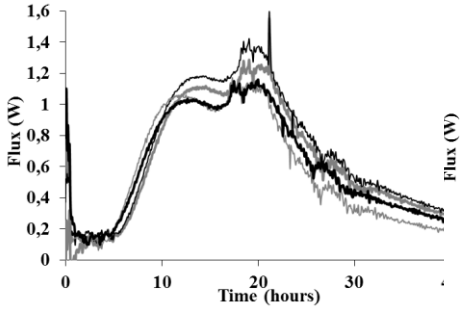

Figure 18. Evolution of reaction of the BO2 flows

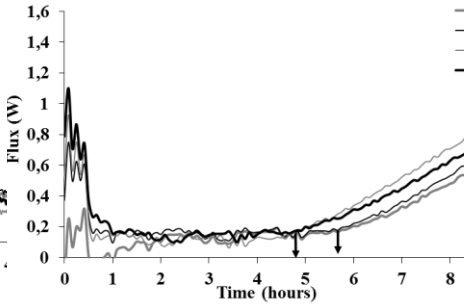

Figure 19. streams of reaction of concrete BO2 on 10 hours

In general, the reaction flux curves (Figures 17 to 18) well describe a hydration reaction of concrete. There are several phases.

- A 'latent' period where the flux changes are very small during the different tests. When looking closely at the first hours of the evolutions of reaction flux, the duration length of this period can be measured and varies from 4 hours for BO concrete to 5 hours for BAP. Whereas for Bole initial setting was 5 hours for the low fluxmeters, whereas it is 6 hours for high the fluxmeters. This can be explained by the water migrating upwards and therefore delaying the hydration reaction.
- A period of acceleration resulting in a rapid increase in the flux and corresponding to the formation of more hydrates compared to the previous period. This leads to a first peak flux around 13 to 15 hours, and then to an acceleration that gives rise to a second peak between 19 and 21 hours. For concrete BO and BO2 the slow hydration reaction results in a specific shape of flow curves which shows very large flow peaks

For the concrete BO and BAP the reaction fluxes are very similar. While fluxes for the BO2 concrete remain two by tow. It can be noted that the reaction is delayed about 1 hour between the bottom and the top. The higher flux peaks are more important, which may reflect not just water migration but more cement laitance

Conclusions

The results presented in this study the show importance of fluxmetric measurements to detect and monitor in-situ the concrete setting. In a system in thermal imbalance, significant flux variations are observed before detecting a significant variations in temperature. In order to obtain a temperature change, it is necessary to integrate heat flux. From a purely qualitative and practical point of view, the evolution of temperatures are always "softened" and smoothed compared

to changes in flux. The detection of the initial setting is facilitated by the measurement of thermal flux. It would be extremely difficult to obtain the similar results as those in the laboratory.
The kinetics of reaction can be properly observed and the order of magnitude of the heat of hydration can be reached. In order to precisely measure the heat of hydration, it is necessary that the heat of hydration is much larger than the heat exchange with the environment. During very cold weather, the heat of hydration will be difficult to detect.

References

[1] Kahouadji A., Clastres P., Debicki G., (1997), Early-age compressive strength prediction of concrete. Construction and Building Materials, n°11 pp 431-436.
[2] Yikici T A., Chen H L., (2015) Use of maturity method to estimate compressive of mass concrete. Construction and Building Materials, n°95 , pp802-812
[3] Zhang J., Cusson D., Monteiro P., Harvey J, (2008): New perspectives on maturity an approach for high performance concrete applications. Cement and Concrete Research, n°38, pp1438-1446
[4] Thery.P., Duthoit. B. (1991),: New heat flow sensors for the thermal nondestructive testing of wall section in their naturel environment, In:IMEKO TC7, International Symposium on AIMAC, Kyoto, Japan
[5] Defer.D., Antczak. E., Duthoit.B. (1998), The characterisation of thermophysical properties through thermal impedance under random solicitation taking sensor-induced disturbance into account», Meas SCi Technol, 3-6 Mars pp 496-504
[6] Kada H., Wirquin E, DUTHOIT B, (2000), Determination of apparent activation energy of concrete by isothermal calorimetry,Cement and Concrete Research, n° 30, pp. 301-305.

Theme 4: Rheology and Workability

3D Printing Methods and Structural Build-up of Cement-Based Materials

Arnaud Perrot[1], Damien Rangeard[2] and Alexandre Pierre[3]

[1]LIMATB, Université de Bretagne Sud, Lorient, France
[2]LGCGM, INSA de Rennes, Rennes, France
[3]L2MGC, Université de Cergy-Pontoinse, Cergy-Pontoise, France

Abstract Additive manufacturing and digital fabrication bring new horizons to concrete and cement-based material construction. 3D printing inspired construction techniques that have recently been developed at laboratory scale for cement-based materials. This study aims to investigate the role of the structural build-up properties of cement-based materials in such a layer by layer construction technique. As construction progresses, the cement-based materials become harder with time. The mechanical strength of the cement-based materials must be sufficient to sustain the weight of the layers subsequently deposited. It follows that the comparison of the mechanical strength, which evolves with time (i.e. structural build-up), with the loading due to layers subsequently deposited, can be expected to provide the optimal rate of layer by layer construction. A theoretical framework has been developed to propose a method of optimization of the building rate, which is experimentally validated in a layer-wise built column.

Keywords: *Additive manufacturing, Cement-based materials, Yield stress, Structural build-up.*

Introduction

Additive manufacturing and digital fabrication bring new horizons to concrete construction. The possibility to build concrete structures without formwork is a major advantage in terms of production rate, architectural freedom and cost reduction; as noted in [1], formwork represents 35 to 60 percent of the overall costs of concrete structures. Moreover, it allows human labour to be replaced by digitally controlled robots and furthermore allows the implementation of these new techniques in highly polluted environments and in spatial applications [2]. Various techniques have been developped in recent years; for example, Smart Dynamic Casting is a result of a combination of slipforming and digital fabrication

techniques [1, 3]. Another family of concrete digital manufacturing has been inspired by the 3D printing technique [4]. This technique is commonly called 'additive manufacturing' and consists of joining materials to produce objects, layer upon layer, from 3D model data. Examples of such techniques belonging to this family of digital-aided construction are the "Concrete printing" process developed at Longhborough University [5-9] and the "Contour Crafting" method [10, 11] developed at the University of Southern California. One way of additive manufacturing in construction of concrete is to combine concrete extrusion with digital fabrication techniques. As noted in [1], the objective is a scaling-up of a desktop 3D printer to the size of a building site. At this time such techniques are not sufficiently developed for industrial application but have succeeded in producing wall elements under laboratory conditions [7, 8, 10]. Nevertheless, additive manufacturing extrusion technique can be developed into a very efficient and robust construction technique at an industrial scale. To achieve this end and optimize the process, two major constraints need to be overcome [1]: Firstly the bonding between the layers which is a weakness in the printed structure. It is worth noting that the bonding strength decreases with the time gap between layers [8]. The second constraint is the monitoring of the material hardening over time: The material must be hard enough to sustain the weight of the subsequently deposited layers. This constraint may lead to a prolonged production time. The juxtaposition of these two constraints confronts us with a paradox concerning the production rate of this process. The time gap between two deposited layers must be sufficiently long to provide adequate mechanical strength capable of sustaining the weight of the subsequently deposited layers and also short enough to ensure both optimized bonding strength and building rate. It therefore appears that the optimized time gap between layers should be the shortest that allows the stability of the structure during construction. Such optimized time gap brings the highest bonding strength and building rate compatible with a stable structure of deposited fresh concrete.

The ability of the deposited layers to sustain its own weight is linked to its rheology and more particularly to its yield stress [3, 7]. During the layer by layer building of a wall, the first deposited layer undergoes the heaviest load. In order to ensure the wall stability during the process, the yield stress must be sufficient to sustain this load. At this point, a new paradox appears: the paste must be sufficiently fluid for extrusion purpose [12] but sufficiently firm for the structure mechanical stability. A way around this paradox is to use the structural build-up of the concrete to ensure both,sufficient fluidity during extrusion and stability after deposit. The yield stress of cement-based materials increases over time at rest [13-19]; this reversible behaviour is due to the nucleation of cement grains at their contact point by CSH formation during the dormant period before the setting time [20]. This yield stress increase is commonly modelled using a linear relationship with resting time [15] during the first hour of rest. Recently, Perrot et al. have proposed an exponential relationship that describes the yield stress increase up to the setting time [21]. It has been shown that the structural build-up properties of cement-based materials can be used to predict or optimize concrete production. For

instance, formwork pressure reduction or distinct-layer casting issues can be predicted using the structural build-up rate of self-compacting concrete [21-24]. In the present case, structural build-up is used to describe and model the competition between the load increase, linked to the building rate, and the mechanical strength of the first deposited layer of the structure which is linked to the cement-based material yield stress. The aim of this paper is to propose a model that predicts the structure failure (or stability) during the additive manufacturing process of a concrete structure. This model is potentially a tool for optimizing the building rate of concrete in 3D printing.

In the first part of the paper, a theoretical framework is developed for structural build-up of cement-based materials and load due to 3D printing is proposed. Experimental tests are then carried out on a firm paste to simulate the loading due to the printing of a concrete column. Finally, the comparison between both the theoretical framework and the experimental results highlights the finding that structural build-up must be taken into account in additive manufacturing extrusion technique in order to find the highest acceptable building rate.

Theoretical Framework

Many studies on digital fabrication techniques have shown that the building rate of the structure influences the success of the process [1, 3, 7]. For additive manufacturing exturion technique, Le et al. [7] defines an open time (linked to the Vicat setting time), to describe the change of the concrete workability with time. This parameter is likely to affect what the authors called "buildability," which consists of quantifying the number of filament layers that could be built up without noticeable deformation of lower layers. The idea of this theoretical framework is to compare the mechanical strength of the bottom first deposited layer with the mechanical load due to the weight of the above-deposited layers, and then to model the so-called "buildability" defined in [7]. It is then necessary to model both the evolution of the mechanical strength of the cement-based material before hydration (which is governed by the material yield stress) and the evolution in time of the mechanical load due to the building of the structure. The developed theory must be able to indicate if the layered structure is able to sustain its own weight and able to predict the failure time when the structure is going to collapse. In case of a wall or a column construction, the vertical stress acting on the first deposited layer increases in time with the built height of the structure. Even if the vertical stress increases step by step as new layers are deposited, an average rate of construction can be computed over the construction time. Initially, it would appear natural to choose a constant rate of vertical construction. This rate of construction is designated by R. Then, the vertical stress σ_v acting on the first layer can be written as follows:

$$\sigma_V = \rho g h(t) = \rho g R t \tag{1}$$

where ρ is the specific weight of the concrete, t is the age of the first deposited layer (which starts with its deposition) and h is the height of the vertical structure located above the first deposited layer. The stability of the first layer can be tested by comparing the vertical stress given by eq. (1) with a critic failure stress, which is linearly linked to the yield stress of the first deposited material:

$$\sigma_c(t) = \alpha_{geom}.\tau_0(t) \tag{2}$$

where τ_0 is the yield stress of the first deposited material and α_{geom} is a geometric factor which depends of the form of the built structure. The increase in yield stress is commonly considered to be linear during the dormant period prior to setting [13 14]. Roussel [14, 15] has defined the structuration rate A_{thix} as the constant rate of increase in yield stress over the time at rest:

$$\tau_0(t) = \tau_{0,0} + A_{thix}t \tag{3}$$

Where $\tau_{0,0}$ is the yield stress of the material with no time at rest. The concrete structural build-up is due to complex and coupled phenomena: flocculation due to colloidal interactions and CSH nucleation at the contact points between cement grains [16, 20]. After a linear increase period which lasts up to 60 minutes, the rate of yield stress increase speeds up [21, 25, 26]. It would therefore appear that there is a non-negligible linear increase of the solid volume fraction which leads to an exponential increase in yield stress. Perrot et al. [17] have proposed an exponential yield stress evolution that describes a smooth transition from the initial linear increase to the exponential evolution and asymptotically tends to the Roussel model as t_t tends to zero:

$$\tau_0(t) = A_{thix}t_c\left(e^{t_{rest}/t_c} - 1\right) + \tau_{0,0} \tag{4}$$

Where t_c is a characteristic time, the value of which is adjusted to obtain the best fit with experimental values. The geometric parameter α_{geom} depends on the form of the built structure. In a straight vertical construction, the horizontal cross section and the height of a deposited layer are the parameters that are used to compute α_{geom}. For example, for circular column of diameter D, α_{geom} can be computed from the theory of squeeze flow of plastic material [27, 28]. To make an analogy between squeeze flow and 3D printing extrusion technique, it can be considered that the first deposited layer is confined between two plates, the ground and the bottom surface of the layer deposited above. In this first approach, the surfaces of these two plates are assumed to be rough in order to comply with the adherent hypothesis for the wall conditions. Thus, using the expression given in [27, 28], the α_{geom} parameter can be expressed as:

$$\alpha_{geom} = 2\left(1 + \frac{D}{2\sqrt{3}h}\right) \tag{5}$$

It should be noted that other form of α_{geom} parameters are required for other types of construction such as a wall. They can be found by a static analysis or by empirical fitting.

Materials and Methods

To validate our theory, we simulate the load acting on a cylindrical sample (i.e. the first deposited layer) due to the layer by layer construction of a cylindrical column. The cylindrical sample was 35 mm high and has a diameter of 60 mm. The initial material yield stress was 4 kPa and was sufficient to provide adequate strength to overcome the gravitational effect; consequently, the fresh sample could sustain its own weight. The material yield stress was higher than those found in studies carried out at Longhborough University [5-9] (which were of the order of 1 kPa) but appeared to be in the range of material yield stress used for contour crafting [10, 11] developed in University of Southern California. To achieve this yield stress value, cement paste containing cement, kaolin and limestone filler were used. The dry binder content, expressed as a weight, was 50 % cement, 25% limestone filler and 25% kaolin. The water/cement mass ratio was 0.41 and a polycarboxylate-type polymer powder SP was added to the mix (SP/cement mass ratio being 0.3%). The mixes were prepared by mixing the dry powder-constituents together for 2 minutes at 60 rpm and water was then mixed with cement in a planetary Hobart mixer. The mixing phase consisted of two steps: 2 minutes at 140 rpm and 3 minutes at 280 rpm. In order to simulate the loading to layer by layer construction, the sample which corresponded to the first deposited layer, was placed between two parallel plates. The upper plate was then loaded in 1.5 N increments. The time gap between each loading increment allowed monitoring of the average building rate. Time gap ranging from 11 to 60s allows the simulation of column 3D printing with an average building rate ranging from 1.1 to 6 $m.h^{-1}$. When the critical stress is exceeded, the sample could be expected to Plastically deform. To detect this plastic failure, the upper plate displacement was recorded with respect to time using a LVDT-type displacement transducer; simultaneously, fractures onset at the surface of the sample is monitored during the test. Each time gap was tested at least twice to check the test repeatability. After mixing, measurements were carried out over a 90 minute period. In this way, the evolution of the yield stress of the cement-based material with respect to time at rest was characterised as described by Perrot et al. [29]. This method is similar to the undisturbed vane test measurement presented in Khayat et al. [30]. In this study, stress growth measurements were performed approximately every 10 minutes at a constant shear rate of $0.001s^{-1}$ as described by Mahaut et al. [31]. For the studied material, the evolution of the yield stress with time at rest is shown on figure 1. Perrot et al. and Roussel models [15, 21] are also plotted . Figure 1 clearly shows that the yield stress evolution, of the tested cement paste, with time can be considered as linear during the first 40 minutes. It follows that the Roussel linear model [15] can be used to describe the yield stress evolution for construction

process lasting less than this critical time. For longer processing, the Perrot et al. model better describes the yield stress increase [21].

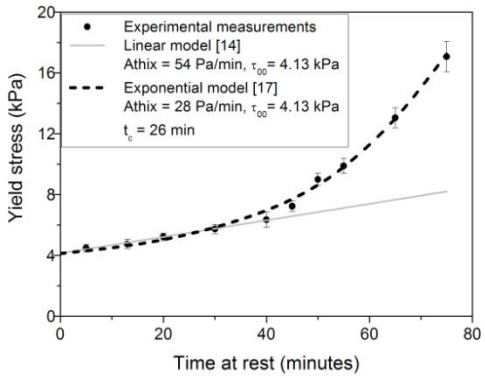

Figure1. Yield stress evolution with time. Comparison of the experimental results with a curve fit to the Perrot et al. [21] and Roussel models [15].

Results and Discussion

The first issue to be discussed relates to sample failure detection. The combination of monitoring fracture onset with the recording of upper plate displacement provides collaborating evidence of sample plastification. Figure 2 shows the recorded displacement of the upper plate for time gap between each layer deposit of 11, 17, 22 and 34 s. For each time gap, the moment when fractures appear on the sample surface is reported (as shown in figure 2). It is considered that sample failure is reached when both phenomena have occurred: fracture onset at the surface and increase in the displacement rate. This detection of failure is supported by squeeze flow of semi-solid paste which undergoes fracture at the sample periphery [27, 28, 32, 33]. It can be seen in figure 2 that the increase of the slope of the displacement curves occurs quasi-simultaneously with fracture occurrence**.** Finally, we have chosen the fracture onset time as a failure indicator because it always occurred simultaneously with a change of the slope of the displacement, time curve. The only sample that remains intact after the test is obtained for the smallest building rate R = 1.1 m/h. For higher building rate, all samples collapsed because of insufficient mechanical strength. In such cases, the material has not had time to become sufficiently stiff to sustain the weight of above deposited layers.

To go a step further, it would be interesting to predict the failure occurrence and time. As proposed in the theoretical framework, the comparison of the vertical stress with the critical stress, which is linked to the material strength, is expected to lead to a failure prediction. By plotting the evolution of both the vertical stress and the critical stress with time, as shown in figure 3, the time when the sample is going to plastically deform is easily identified. In this figure, the predicted time of failure is given by the intersection of the evolution of the vertical stress with the

evolution of the critical stress. It is worth noting that the predicted failure time is in agreement with the experimentally observed failure time which is shown as solid circles in figure 3. Moreover, figure 3 shows that the critical stress is always higher than the vertical stress for a building rate of 1.1 m/h. This is in agreement with the experimental result which shows that the sample sustains the loading for this value of building rate. It therefore appears that the proposed theoretical framework is able to predict the success of the layerwise process of additive manufacturing. The framework provides an efficient tool to determine and optimise the building rate and therefore the bond strength between layers with the assurance of the structure stability. It is of interest to see if an analytical prediction of the failure can be made. Using the linear evolution of the yield stress provided by Roussel [15], a critical failure time t_f can be easily expressed as follows:

$$t_f = \frac{\tau_{0,0}}{\rho g R / \alpha_{geom} - A_{thix}} \tag{6}$$

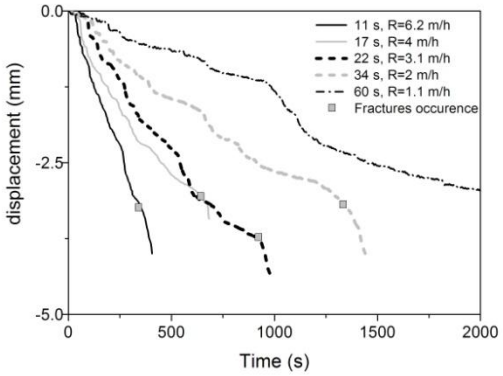

Figure 2. Displacement of the upper plate versus time. The grey squares indicate the instant when fractures are observed on the surface of the samples for time gap ranging from 11 to 60s.

The computed failure time t_f is shown on figure 3 by diagonal crosses. It can be seen that the t_f values are in agreement with experimental results except for those with the smallest building rates. This discrepancy in failure time is due to the fact that for the smallest building rate, the linear description of the yield stress evolution is no longer valid for process time higher than 1500 s (i.e. 25 minutes). Equation (6) is valid only for failure time lower than the critical time t_c , which is given by eq. (4) and predicts the time at which the linear model becomes inaccurate. If t_f , calculated by eq. (6), is greater than t_c, the plot of the evolution of σ_v and σ_c with respect to time remains an effective solution to check structure stability. Furthermore, if the computed value of t_f is of the order of the setting time of the concrete, the structure is expected to remains stable during additive manufacturing extrusion technique.

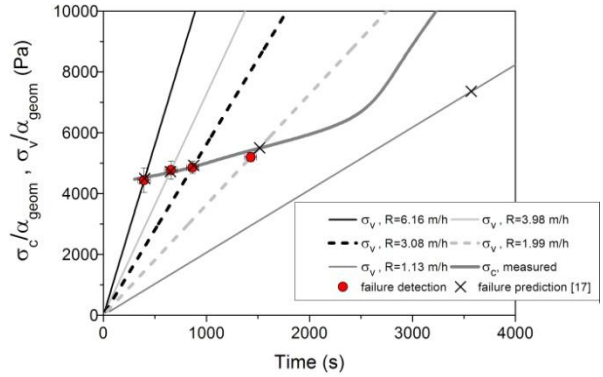

Figure 3. Comparison of the evolution of critical stress σ_c and vertical stress σ_v for building rate ranging from 1.1 to 6.2 m/h. The solid circles indicate the experimental failure time and the diagonal crosses indicate failure time derived from a linear evolution of the yield stress.

Conclusions

In this study we have proposed a theoretical framework to find the highest building rate for layerwise concrete additive manufacturing extrusion technique inspired by 3D printing technologies. This theoretical framework is based on the comparison of the vertical stress acting on the first deposited layer with the critical stress related to plastic deformation that is linked to the material yield stress. Both stresses are time-dependent: the vertical stress depends on the building rate while the critical stress depends on the structural build-up of the concrete at rest. The developed framework consists of ensuring that the vertical stress does not exceed the critical stress. The theoretical framework is validated by simulating the loading due to the additive manufacturing of a 70 mm diameter column. The predicted failure times of the sample are in agreement with the experimentally observed ones for all tested building rates (ranging from 1.1 m/h to 6.2 m/h).

References

[1] Lloret, E. Shahab, A.R. Linus, M. Flatt, R.J. Gramazio, F. Kohler, M. Langenberg, S. (2014) Complex concrete structures: Merging existing casting techniques with digital fabrication, *Computer-Aided Design*, in press.

[2] Cesaretti, G. Dini, E. De Kestelier, X. Colla, V. Pambaguian, L. (2014) Building components for an outpost on the Lunar soil by means of a novel 3D printing technology, *Acta Astronautica*, Vol. 93, p. 430-450.

[3] Shahab, A.R. Lloret, E. Fischer, Gramazio, P. F. Kohler, M. Flatt, R.J. (2013) Smart dynamic casting or how to exploit the liquid to solid transition in

cementitious materials, in: *Proceedings CD od the 1st international conference on rheology and processing of construction materials and of the 7th international conference on self-compacting concrete*, Paris, France.
[4] Pegna, J. (1997) Exploratory investigation of solid freeform construction, Automation in Construction, Vol. 5, p. 427-437.
[5] Buswell, R.A. Soar, R.C. Gibb, A.G.F. Thorpe, A. (2007) Freeform Construction: Mega-scale Rapid Manufacturing for construction, *Automation in Construction*, Vol. 16, p. 224-231.
[6] Buswell, R.A. Thorpe, A. Soar, R.C. Gibb, A.G.F. (2008) Design, data and process issues for mega-scale rapid manufacturing machines used for construction, *Automation in Construction*, Vol. 17, p. 923-929.
[7] Le, T.T. Austin, S.A. Lim, S. Buswell, R.A. Gibb, A.G.F. Thorpe, T. (2012) Mix design and fresh properties for high-performance printing concrete, *Materials and Structures*, Vol. 45, p. 1221-1232.
[8] Le, T.T. Austin, S.A. Lim, S. Buswell, R.A. Law, R. Gibb, A.G.F. Thorpe, T. (2012) Hardened properties of high-performance printing concrete, *Cement and Concrete Research*, Vol. 42, p. 558-566.
[9] Lim, S. Buswell, R.A. Le, T.T. Austin, S.A. Gibb, A.G.F, Thorpe, T. (2012) Developments in construction-scale additive manufacturing processes, *Automation in Construction*, Vol. 21, p. 262-268.
[10] Koshnevis, B. Hwang, D. Yao, K.T. Yeh, Z. (2006) Mega-scale fabrication by Contour Crafting, *International Journal of Industrial and Systems Engineering*, Vol. 1, p. 301-320.
[11] Zhang, J. Khoshnevis, B. (2013) Optimal machine operation planning for construction by Contour Crafting, *Automation in Construction*, Vol. 29, p. 50-67.
[12] Perrot, A. Mélinge, Y. Rangeard, D. Micaelli, F. Estellé, P. Lanos, C. (2012) Use of ram extruder as a combined rheo-tribometer to study the behaviour of high yield stress fluids at low strain rate, *Rheologica Acta*, Vol. 51, p. 743-754.
[13] Josserand, L. Coussy, O. de Larrard, F. (2006) Bleeding of concrete as an ageing consolidation process, *Cement and Concrete Research*, Vol. 36, p. 1603-1608.
[14] Roussel, N. (2006) A thixotropy model for fresh fluid concretes: Theory, validation and applications. *Cem Concr Res*, Vol. 36, p. 1797 – 1806.
[15] Roussel, N. (2005) Steady and transient flow behaviour of fresh cement pastes. *Cem Concr Res*, Vol. 35, p. 1656 – 1664.
[16] Wallevik, J.E. (2009) Rheological properties of cement paste: Thixotropic behavior and structural breakdown. *Cem Concr Res*, Vol. 39, p. 14 – 29.
[17] Billberg, P.H. (2003) Form pressure generated by self-compacting concrete in: *3rd international RILEM symposium on Self-Compacting Concrete*, Reykjavik, Island, p. 271-280.
[18] Lowke, D. Kränkel, T. Ghelen, C. Schiessl, P. (2010) Effect of Cement Type and Superplasticizer Adsorption on Static Yield Stress, Thixotropy and

Segregation Resistance. , *in: K. Khayat, D. Feys (Eds.) Design, Production and Placement of Self-Consolidating Concrete*, Springer, Heidelberg.
[19] Ferron, R.P. Greogori, A. Sun, Z. Shah, S.P. (2007) Rheological Method to Evaluate Structural Buildup in Self-Consolidating Concrete Cement Pastes, *ACI Material Journal*, Vol. 104, p. 242-250.
[20] Roussel, N. Ovarlez, G. Garrault, S. Brumaud, C. (2012) The origins of thixotropy of fresh cement pastes. *Cem Concr Res*, Vol. 42, p. 148 – 157.
[21] Perrot, A. Pierre, A. Vitaloni, S. Picandet, V. (2015) Prediction of lateral form pressure exerted by concrete at low casting rates. *Mater Struct*, Vol. 48, p. 2315–2322.
[22] Billberg, P.H. Roussel, N. Amziane, S. Et al. (2014) Field validation of models for predicting lateral form pressure exerted by SCC, *Cement and Concrete Composites*, Vol 54, p. 70–79.
[23] Ovarlez, G. and Roussel, N. (2006) A Physical Model for the Prediction of Lateral Stress Exerted by Self-Compacting Concrete on Formwork, *Materials and Structures*, Vol. 39, p. 269–279.
[24] Roussel, N. Cussigh, F. (2008) Distinct-layer casting of SCC: The mechanical consequences of thixotropy. *Cem Concr Res*, Vol. 38, p. 624–632.
[25] Lootens, D. Jousset, P. Martinie, L . et al. (2009) Yield stress during setting of cement pastes from penetration tests. *Cem Concr Res*, Vol. 39, p. 401 – 408.
[26] Subramaniam, K.V. Wang, X. (2010) An investigation of microstructure evolution in cement paste through setting using ultrasonic and rheological measurements. *Cem Concr Res*, Vol. 40, p. 33–44.
[27] Roussel, N. Lanos,C. (2003) Plastic Fluid Flow Parameters Identification Using a Simple Squeezing Test, *Applied Rheology*, Vol. 13, p. 132-141.
[28] Engmann, J. Servais, C. Burbidge, A.S. (2005) Squeeze flow theory and applications to rheometry: A review, *Journal of Non-Newtonian Fluid Mechanics*, Vol. 132, p. 1-27.
[29] Perrot, A. Lecompte, T. Estellé, P. Amziane, S. (2013) Structural build-up of rigid fiber reinforced cement-based materials, *Materials and Structures*, Vol. 46, p. 1561-1568.
[30] Khayat K.H., Omran, A.F. Naji, S. Billberg, P. Yahia, A. (2012) Field-oriented test methods to evaluate structural build-up at rest of flowable mortar and concrete, *Materials and Structures*, Vol. 45, p. 1547-1564.
[31] Mahaut, F. Mokéddem, S. Chateau, X. et al. (2008) Effect of coarse particle volume fraction on the yield stress and thixotropy of cementitious materials. *Cem Concr Res* Vol. 38, p. 1276–1285.
[32] Estellé, P. Lanos, C. Perrot, A. Servais, C. (2006) Slipping zone location in squeeze flow, *Rheologica Acta*, Vol. 45, p. 444-448.
[33] Toutou, Z. Roussel, N. Lanos, C. (2005) The squeezing test: a tool to identify firm cement-based material's rheological behaviour and evaluate their extrusion ability, *Cement and Concrete Research*, Vol. 35, p. 1891-1899.

Non-Linear Modeling of Yield Stress Increase Due to SCC Structural Build-Up at Rest

Thibaut Lecompte and Arnaud Perrot

Univ. Bretagne-Sud, EA4250, LIMATB F, 56100 Lorient, France

Abstract It is commonly considered that the yield stress of SCC linearly increases at rest. This increase is due to the SCC structural build-up. This behavior can be explained by the cement particles nucleation at the contact points. During the first tens of minutes, the cement particles nucleation induces a linear increase of the yield stress in time (for instance, see the work developed by Ovarlez and Roussel). However, recent studies have shown that the trend of the yield stress increase becomes non-linear when considering longer time at rest (before the setting time). This work aims to provide a theoretical frame to describe this non-linear increase. The proposed model tends toward the linear model during the first tens of minutes and follows the observed exponential law for longer resting time. We also try to provide some physical explanations about the observed increase. The discrepancy with the linear model is explained by both phenomena: an increase in the solid volume fraction and a decrease in the packing fraction due to cement particles nucleation.

Keywords: *SCC, Yield stress, Structural build-up, Thixotropy.*

Introduction

The rheology of SCC evolves in time due to different physical phenomena acting at different timescale. This evolution is induced by both reversible structural build-up (which is also called thixotropy) and irreversible hydration of the cement grain which is responsible for the concrete workability loss.

Among the rheological properties of cement pastes, the yield stress is involved in lots of forming processes or concrete characteristics such as aggregates stability [1], pressure exerted on formwork by SCC , multi-layer casting [2–5], 3D printing [6]. It is also directly linked to the slump or spread flow values and then to the concrete consistency [7]. It is therefore important to understand and predict the evolution of yield stress over time, especially when the concrete is left at rest.

The yield stress of cement-based materials increases over time at rest [8–11]; this reversible behaviour is due to the nucleation of cement grains at their contact point by CSH formation during the dormant period before the setting time [11]. This yield stress increase is commonly modelled using a linear relationship with resting time during the first hour of rest [8, 9].

Recently, Perrot et al. have proposed an exponential relationship that describes the yield stress increase up to the setting time [5]. This function describes a smooth transition from the initial linear increase to the exponential evolution and asymptotically tends to the Roussel model for time of rest of few tens of minutes. In this model, Perrot et al. used a critical time which is not based on physical arguments but chosen to obtain the best fit with experimental values.

This exponential trend, observed in several studies [5, 6, 10, 12, 13], has been explained with an increase of the solid volume content within the cement paste due to the creation of the CSH gel [13]. This paper aims to provide a physically-based model that is able to predict the evolution of yield stress with time of rest during few hours after the contact cement/water. In a first part, we have performed a state of the art of the modelling of yield stress increase with time of rest. Then we have proposed a new model that uses both, the structural build-up rate defined by Roussel and the hydration degree. Finally, our model is compared with experimental values and other models provided in the literature.

State of the art on structural build-up modelling

The increase in yield stress is commonly considered to be linear during the dormant period prior to setting. Roussel [8, 9] has defined the structuration rate A_{thix} as the constant rate of increase in yield stress τ_0 over the time at rest t_{rest}:

$$\tau_0(t_{rest}) = \tau_{0,0} + A_{thix} t_{rest} \tag{1}$$

Where $\tau_{0,0}$ is the yield stress of the material with no time at rest. The associated dimensionless yield stress is:

$$\tau_0^*(t_{rest}) = \frac{\tau_0(t_{rest})}{\tau_{0,0}} = 1 + \frac{A_{thix}}{\tau_{0,0}} t_{rest} \tag{2}$$

The concrete structural build-up is due to complex and coupled phenomena: flocculation due to colloidal interactions and CSH nucleation at the contact points between cement grains [11]. These two factors are also identified by Wallevik [14] as being responsible for reversible and permanent bridges between cement grains. According to Roussel et al. [11], the flocculation process lasts only several tens of seconds. After flocculation, at a timescale of several tens of minutes, the structural build-up is due to the formation of CSH bridges between cement grains at the

pseudo contact-points. The authors assumed that the rate of formation of CSH bridges is constant because the heat of hydration is constant during the so-called "dormant" period. Therefore, they conclude that the increase of yield stress with time (or the elastic modulus) must be linear. This correlates well with the measurements of yield stress increase between 10 to 60 minutes after mixing.

Much experimental data has shown that the evolution of the yield stress of cement-based materials is highly non-linear between one hour after placing and before the setting time [5, 6, 10, 13]. It would therefore appear that there is a non-negligible increase of the solid volume fraction which leads to an exponential yield stress increase (up to 2% at 2 hours for a W/C ratio equal to 0.4) [13].

It is worth noting that the Taylor series of the exponential function e^t at $t = 0$ is $1+t$ which relates to the linear form of yield stress time evolution assumed by Roussel [8, 9]. Consequently, an exponential-based function introduced in eq. (2), as a first-order Taylor series at $t_{rest} = 0$, represents a quasi-linear evolution during the first hour. This function describes a smooth transition from the initial linear increase to the exponential evolution and asymptotically tends to the Roussel model as t_{rest} tends to zero:

$$\tau_0^*(t_{rest}) = \frac{A_{thix}}{\tau_{0,0}} t_c \left(e^{t_{rest}/t_c} - 1\right) + 1 \tag{3}$$

Where t_c is a characteristic time, the value of which is adjusted to obtain the best fit with experimental values.

Theoretical Framework of the Proposed Model

The yield stress of unstructured cement suspensions (with no resting time) is commonly modelled using the yield stress model "YODEL" defined by Flatt and Bowen [15, 16]. This model defines the yield stress as a function of both the amplitude of Van Der Waals interaction between two cement particles at the contact point and the solid volume fraction of the paste. This model writes:

$$\tau_{0,0} \cong m \frac{A_0 a^*}{d^2 H^2} \frac{\phi^2 \left(\phi - \phi_{perc}\right)}{\phi_m \left(\phi_m - \phi\right)} \tag{4}$$

where m is a pre-factor, which depends on the particle size distribution, a^* is the radius of curvature of the "contact" points, H is the surface to surface separation distance at "contact" points, A_0 is the non retarded Hamaker constant, ϕ is the grains solid volume fraction, ϕ_m is the maximum solid volume fraction, ϕ_{perc} is the percolation volume fraction and d is the average diameter of the spherical particles.

In equation (4), $m\frac{A_0 a^*}{d^2 H^2}$ represents the magnitude of interaction forces between two particles and the other part $\frac{\phi^2(\phi-\phi_{perc})}{\phi_m(\phi_m-\phi)}$ is linked to the spatial congestion within the particle network.

The basic idea of our model is to add the effect of reversible nucleation of cement grains using Roussel model [8, 9] with the effect of irreversible solid volume increase due to cement hydration using eq. (4) with increasing solid volume fraction (linked to the hydration degree α). In this case, equation (1) can be rewritten as follows:

$$\tau_0(t,t_{rest}) = \tau_{0,0}(t) + A_{thix} t_{rest} \tag{5}$$

Where t is different from t_{rest} and is defined as the paste age which starts with the contact between the cement particles and the water. It is important to keep in mind that at very early age (before 30 minutes), the yield stress only grows up with resting time t_{rest}, while more later $\tau_{0,0}$ will increase with hydration time t, starting with the first contact between cement particles and liquid water, during mixing.

The key of this model is the definition of the evolution of the solid volume fraction over the very early age of the paste. A literature survey shows us that it is possible to link this solid volume fraction increase to the hydration degree $\alpha(t)$ as proposed by many researchers.

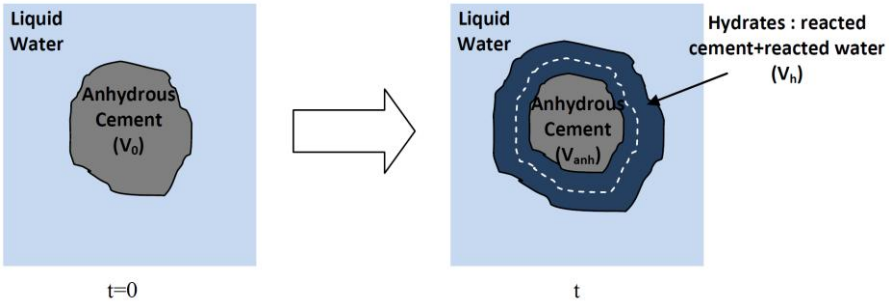

Figure 1. Solid volume growth of a grain during hardening

As seen on Fig. 1, it is well known that anhydrous cement creates hydrates in contact with water. The hydration kinetics can be expressed thanks to an hydration, or maturation degree $\alpha(t)$:

$$V_{anh} = \left(1 - \alpha(t)\right)V_0 \qquad \text{or} \qquad V_c = \alpha(t)V_0 \tag{6}$$

In a first approach, we assume that the hydration increases the radius of the initial cement particles. This is a strong assumption as the hydrates can create very fibrous structures. However, our study focuses on very early age when hydration degree is less than few percent. Therefore, we think it is reasonably acceptable that the hydrates volume increase can be modeled by a simple radius increase of the initial "spherical" particle.

Several functions $\alpha(t)$ have been expressed and confronted to experiments in literature [17–19]. Khawam and Flanagan [20] have made a review of the mathematical models for solid-state reaction kinetics. Taylor [21], has studied the kinetics of C3S consumption at different time scales. At early age, the kinetic corresponds to a germination process, corresponding to different periods: the initial reaction period; the induction period and the acceleratory period [21]. This early age behavior can be expressed by a sigmoid, corresponding to the Brown [17], or Avrami-Erofeyev reaction modelling [22, 23]:

$$\alpha(t) = \beta\left(1 - \exp(-k_n t^n)\right) \tag{7}$$

Where β, k_N are constants and n can take values ranging from 1 to 4 depending on the studies.

Let's compute the hydrates volume, by taking the terms of Powers and Brownyard [24] and Brouwers [25]:

$$V_h = v_c c + v_n w_n \tag{8}$$

Where v_c and v_n are the specific volumes of cement and water into the hydration product. c is the mass of reacted cement and w_n is the mass of reacted water. The ratio (w_n/c) is constant for a given type of cement. For a CEMI cement type, Brouwers [25] provides the values of 0.32g/cm^3 for v_c, 0.62g/cm^3 for v_n, and a value of 0.199 for (w_n/c).

The supplementary volume due to hydration corresponds to the volume of linked water in the producted hydrates:

$$V_w = v_n w_n \tag{9}$$

Furthermore, the reacted cement mass c can be deduced from Eq.6:

$$c = V_c / v_c = \alpha(t)V_0 / v_c \tag{10}$$

w_n can then be calculated from Eq.8, 9 and 10:

$$w_n = \alpha(t)\frac{v_n}{v_c}\left(\frac{w_n}{c}\right) \tag{11}$$

And the supplementary "solid"volume due to the reaction V_w writes:

$$V_w = \alpha(t)\left(\frac{4\pi r_0^{\,3}}{3}\right)\frac{v_n}{v_c}\left(\frac{w_n}{c}\right) = \frac{4}{3}\pi\left(r(t)^3 - r_0^{\,3}\right) \tag{12}$$

It is then possible to express the radius evolution of a particle of cement during hydration:

$$r(t) = r_0\sqrt[3]{1+\frac{v_n w_n}{v_c w_c}\alpha(t)} \tag{13}$$

The evolution of radius with time allows to write the evolution of the cement particles diameter and the solid volume fraction of particles.

$$d(t) = d_0\sqrt[3]{1+\frac{v_n w_n}{v_c w_c}\alpha(t)} \tag{14}$$

$$\phi(t) = \phi_0\left(1+\frac{v_n w_n}{v_c w_c}\alpha(t)\right) \tag{15}$$

Eqs (14) and (15) can be used in the eq. (5) to obtain the evolution of yield stress over hydration time and time of rest:

$$\tau_0 = m\frac{A_0 a^*}{d_0^{\,2}H^2}\frac{\phi_0^{\,2}\left(1+\frac{v_n w_n}{v_c w_c}\alpha(t)\right)^{4/3}\left(\phi_0\left(1+\frac{v_n w_n}{v_c w_c}\alpha(t)\right)-\phi_{perc}\right)}{\phi_m\left(\phi_m-\phi_0\left(1+\frac{v_n w_n}{v_c w_c}\alpha(t)\right)\right)} + A_{thix}t_{rest} \tag{16}$$

With $\alpha(t)$ defined in eq. (7) and depending on constant parameters k_n, β and n. It is worth noting that the developed model assumes that ϕ_m, m, A_0, a^* and H remain constant and are not affected (or in a negligible way) by both the early hydration and the nucleation of the cement grains. In this work, we consider that this is acceptable for cement paste age lower than the setting time.

It is interesting to note that when t tends to 0, eq. (16) tends toward the Roussel linear model. For t_{rest} = 0, the model is able to predict the workability loss brought by cement hydration as reversible bonds created by cement grains nucleations are broken.

Experimental Validation

The experimental validation was carried out on a mortar containing a river sand volume fraction of 0.6. The cement paste have a W/C ratio of 0.32 (cement volume fraction of 0.49) and the cement used is the CEM I 52.5 used in a previous work of Perrot et al [26]. No admixture

It is important to note that we perform the validation in a dimensionless way (i.e. $\tau_0(t)/\tau_{0,0}$). As a result and as proposed by Mahaut et al. [27], the dimensionless yield stress evolutions of the mortar and cement paste are the same.

In their studies, Perrot et al. provide the values of parameters A_0 =1.6x10^{-20} J, H=2x10^{-9} m, d_0 = 10x10^{-6} m, a^*= 300x10^{-9}m, ϕ_m = 0.6 and ϕ_{perc} = 0.36 for the studied cement pastes with no admixture [26]. For a CEMI cement type, Brouwers [25] provides the values of 0.32g/cm^3 for v_c , 0.62g/cm^3 for v_n, and a value of 0.199 for the ratio w_n/c.

The parameter values of the hydration and coagulation kinetics (i.e. β, k_n, n and A_{thix}) are adjusted to obtain the best fit between our model and experimental measurements. The obtained values of k_n =5x10^{-10} and n = 2.54 are in agreement with the values provided in the literature. The value of β is found at 0.43 and the $A_{thix}/\tau_{0,0}$ is equal to 7.2x10^{-4} s^{-1}. This value is close to the value of $A_{thix}/\tau_{0,0}$ computed using eq. (2) with the Roussel linear modelling which is equal to 9x10^{-4} s^{-1}.

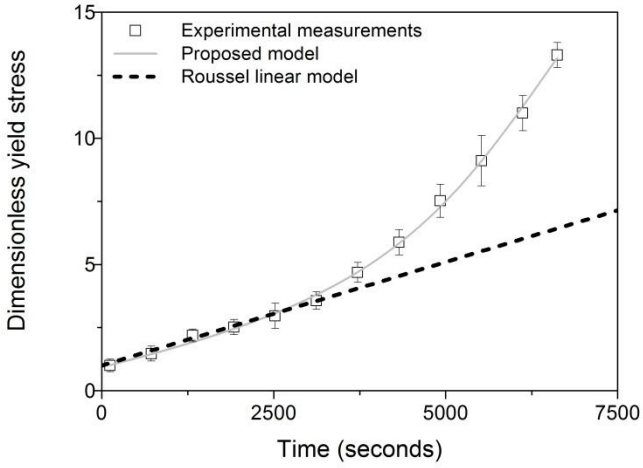

Figure 2. Comparison of the developed model with experimental measurements of yield stress with time.

This model seems to be able to predict the evolution of the yield stress of the concrete before the setting time. This model extends the Roussel linear model for longer time and is able to take into account both the effect of rest and the effect of hydration.

It can be seen on figure 2 that when the resting time is sufficiently short (i.e. for $t <$ 2000 s), the proposed model is equivalent to the Roussel linear model. After this period, the predicted increase rate of the yield stress rises following the experimental trend.

It is important to note that during thie studied, the hydration degree remains under 0.5%. Therefore, the volume increase is small and the assumption of the sphericity of the particle appears valid.

Conclusions

In this study, we have proposed a model that predicts the evolution of the yield stress of cement-based materials in function of both the time of rest and the age of the paste. This model takes into account the nucleation rate of cement grains using the A_{thix} parameter and the growth of the cement grains due to beginning of the hydration reaction using the hydration degree α. Our proposed model provides a good description of the yield stress increase toward the material setting as shown by the performed experimental validation.

This model, based on physical basis, provides an improvement of the Roussel linear model as it can be used for longer time and can be used to predict the workability loss and structural build-up of concrete and cement-based materials.

References

[1] Roussel, N. (2006) A Theoretical Frame to Study Stability of Fresh Concrete. *Mater Struct*, Vol. 39, p. 81–91.

[2] Ovarlez, G. Roussel, N. (2006) A Physical Model for the Prediction of Lateral Stress Exerted by Self-Compacting Concrete on Formwork. *Mater Struct*, Vol.39, p.269–279.

[3] Perrot, A. Amziane, S. Ovarlez, G. Roussel, N. (2009) SCC formwork pressure: Influence of steel rebars. *Cem Concr Res*, Vol. 39, p. 524 – 528.

[4] Roussel, N. Cussigh, F. (2008) Distinct-layer casting of SCC: The mechanical consequences of thixotropy. *Cem Concr Res*, Vol. 38, p. 624–632.

[5] Perrot, A. Pierre, A. Vitaloni, S. Picandet, V. (2015) Prediction of lateral form pressure exerted by concrete at low casting rates. *Mater Struct*, Vol. 48, p. 2315–2322.

[6] Perrot, A. Rangeard, D. Pierre, A. (2015) Structural built-up of cement-based materials used for 3D-printing extrusion techniques. *Mater Struct*, In press, doi: 10.1617/s11527-015-0571-0

[7] Roussel, N. Coussot, P. (2005) "Fifty-cent rheometer" for yield stress measurements: From slump to spreading flow. *J Rheol*, Vol. 49, p. 705–718.

[8] Roussel, N. (2006) A thixotropy model for fresh fluid concretes: Theory, validation and applications. *Cem Concr Res*, Vol. 36, p. 1797 – 1806.

[9] Roussel, N. (2005) Steady and transient flow behaviour of fresh cement pastes. *Cem Concr Res*, Vol. 35, p. 1656 – 1664.

[10] Lootens, D. Jousset, P. Martinie, L . et al. (2009) Yield stress during setting of cement pastes from penetration tests. *Cem Concr Res*, Vol. 39, p. 401 – 408.

[11] Roussel, N. Ovarlez, G. Garrault, S. Brumaud, C. (2012) The origins of thixotropy of fresh cement pastes. *Cem Concr Res*, Vol. 42, p. 148 – 157.

[12] Sleiman, H. Perrot, A. Amziane, S. (2010) A new look at the measurement of cementitious paste setting by Vicat test. *Cem Concr Res*, Cem Concr Res, Vol. 40, p. 681 – 686.

[13] Subramaniam, K.V. Wang, X. (2010) An investigation of microstructure evolution in cement paste through setting using ultrasonic and rheological measurements. *Cem Concr Res*, Vol. 40, p. 33–44.

[14] Wallevik, J.E. (2009) Rheological properties of cement paste: Thixotropic behavior and structural breakdown. *Cem Concr Res*, Vol. 39, p. 14 – 29.

[15] Flatt, R.J. Bowen, P. (2007) Yield stress of multimodal powder suspensions: an extension of the YODEL (Yield Stress mODEL). *J Am Ceram Soc*, Vol. 90, p. 1038–1044.

[16] Flatt, R.J. Bowen, P. (2006) Yodel: a yield stress model for suspensions. *J Am Ceram* Soc, Vol. 89, p. 1244–1256.
[17] Brown, P.W. Liberman, L.O. Frohnsdorff, G. (1984) Kinetics of the Early Hydration of Tricalcium Aluminate in Solutions Containing Calcium Sulfate. *J Am Ceram Soc*, Vol. 67, p. 793–795.
[18] Scrivener, K.L. Juilland, P. Monteiro, P.J.M. (2015) Advances in understanding hydration of Portland cement. *Cem Concr Res*, Vol. 78, Part A, p. 38–56.
[19] Buffo-Lacarrière, L. Sellier, A. Escadeillas, G. Turatsinze, A. (2007) Multiphasic finite element modeling of concrete hydration. *Cem Concr Res*, Vol. 37, p. 131–138.
[20] Khawam, A. Flanagan, D.R. (2006) Solid-State Kinetic Models: Basics and Mathematical Fundamentals. *J Phys Chem B* Vol. 110, p.17315–17328.
[21] Taylor, H.F.W. (1997) *Cement Chemistry* (2nd edition). Thomas Telford Publishing, London
[22] Avrami, M. (1940) Kinetics of Phase Change. II Transformation-Time Relations for Random Distribution of Nuclei. *J Chem Phys*, Vol. 8, p. 212–224.
[23] Avrami, M. (1939) Kinetics of Phase Change. I General Theory. *J Chem Phys* Vol. 7, p. 1103–1112.
[24] Brouwers, H.J.H. (2005) The work of Powers and Brownyard revisited: Part 2. *Cem Concr Res*, Vol. 35, p. 1922–1936.
[25] Brouwers, H.J.H. (2004), The work of Powers and Brownyard revisited: Part 1. *Cem Concr Res*, Vol. 34, p. 1697–1716.
[26] Perrot, A. Lecompte, T. Khelifi, H. et al. (2012) Yield stress and bleeding of fresh cement pastes. *Cem Concr Res*, Vol. 42, p. 937 – 944.
[27] Mahaut, F. Mokéddem, S. Chateau, X. et al. (2008) Effect of coarse particle volume fraction on the yield stress and thixotropy of cementitious materials. *Cem Concr Res* Vol. 38, p. 1276–1285.

Influence of Hydrodynamic Pressure in a 4-Blades Vane Rheometer

Jon E. Wallevik[1]

[1]ICI Rheocenter, Innovation Center Iceland, Arleynir 2-8, IS-112 Reykjavik.

Abstract Vane rheometers are often used to obtain rheological flow parameters in the cement based research and development branch of the concrete industry. In this work, an analysis of the flow phenomenon inside such device is made using the finite volume method. In particular, the shaft torque is calculated at different angular velocities and the effect of hydrodynamic pressure is analyzed separately and compared to the effect generated by viscous stress. The outcome of the overall analysis is that the effect of hydrodynamic pressure constitutes more than 80% of the shaft torque, leaving less than 20% of the torque to viscous stress.

Keywords: *Vane rheometer, Hydrodynamic pressure, Finite volume, Cement paste.*

Introduction

The vane rheometer consists of an impeller rotating in a baffles-cylinder geometry. The one of the objective of this geometrical configuration is to eliminate slip between the sample and the solid boundaries of the rheometer [1,2]. However, with rotation, the impeller's vane blades will both push and drag the fluid, resulting in non-uniform hydrodynamic pressure exerted on the blades. Thus, in addition to the viscous shear stress, this pressure will influence the measured torque registered by the rheometer (i.e. influence the shaft torque). As such, the main question becomes: *How significant is this influence*? Is there a direct relationship between the output of the vane rheometer and the fluid apparent viscosity η, or will the effect of hydrodynamic pressure distorts or damage this relationship? Or more to the point, can the results of the vane rheometer be trusted to give accurate information about the fluid apparent viscosity?

The objective of the current work is to analyze the complex flow phenomenon inside an arbitrary vane rheometer with a special focus on the hydrodynamic

pressure and its effect on the shaft torque. With this aim, the CFD software used is the OpenFOAM. It is licensed under the GNU General Public License (GNU GPL) and is available at www.openfoam.org, without charge or annual fee of any kind. The benefits of having a GNU GPL licensed code over a closed commercial code, is that the user has always a full access to the source code, without any restriction, either to understand, correct, modify or enhance the software. OpenFOAM is written in C++. As such, an object-oriented programming approach is used in the creation of data types (fields) that closely mimics those of mathematical field theory [3]. For the code parallelization and communication between processors, the domain decomposition method is used with the Message Passing Interface (MPI) [4].

A modified version of the simpleFoam solver was programmed in this work. The modifications were done so it could handle a so-called single rotating reference frame approach [5] (SRF). In this solver, the three dimensional momentum equation as well as the continuity equation are solved in parallel to obtain the velocity and hydrodynamic pressure profiles throughout the geometry. More precisely, the pressure velocity coupling is handled with a Semi-Implicit Method for Pressure-Linked Equations (SIMPLE) procedure [6] using a modified Rhie-Chow interpolation for cell centered data storage [7].

Material Model

In this work, the Herschel-Bulkley model is applied (the effect of Newtonian- and Bingham model is well reported elsewhere [1]). With this, the constitutive equation used consists of the Generalized Newtonian Model [8] or in short GNM. The GNM is given by $\mathbf{T} = 2\,\eta\,\dot{\boldsymbol{\varepsilon}}$, where the terms $\mathbf{T}$ and η are the extra stress tensor and the apparent viscosity, respectively [9]. The term $\dot{\boldsymbol{\varepsilon}} = (\nabla \mathbf{U} + (\nabla \mathbf{U})^T)/2$ is known as the rate-of-deformation tensor and $\mathbf{U}$ represents the velocity [10,11].

Oldroy [12] used a von Mises yield criterion for flow to describe the Bingham fluid. Using such approach (with the above mentioned GNM), the flow behavior of the Herschel-Bulkley model can be described with

$$\mathbf{T} = 2\eta\dot{\boldsymbol{\varepsilon}} \qquad \text{for} \qquad \frac{\mathbf{T}:\mathbf{T}}{2} \geq \tau_0^2 \tag{1}$$

$$\dot{\boldsymbol{\varepsilon}} = 0 \qquad \text{for} \qquad \frac{\mathbf{T}:\mathbf{T}}{2} < \tau_0^2 \tag{2}$$

where the apparent viscosity (or equally, the shear viscosity) is given by

$$\eta = \frac{\tau_0}{\sqrt{2\dot{\boldsymbol{\varepsilon}} : \dot{\boldsymbol{\varepsilon}}}} + k\left(\sqrt{2\dot{\boldsymbol{\varepsilon}} : \dot{\boldsymbol{\varepsilon}}}\right)^{n-1} \tag{3}$$

For incompressible, three dimensional flow, where the GNM is valid, it can been shown [1] that **T**:**T**/2 is the shear stress in the second power τ^2, while $2\dot{\boldsymbol{\varepsilon}} : \dot{\boldsymbol{\varepsilon}}$ is the shear rate in the second power. The term τ_0 is the yield stress [Pa], k is the consistency index [Pa·s^n], while n is the power-law exponent (unit less).

Because of the nonlinearities in the governing equation and because of the inherent discontinuity in the constitutive equation, a computer simulation of Herschel-Bulkley flow is difficult. As the yield surface is approached, the presence of $2\dot{\boldsymbol{\varepsilon}} : \dot{\boldsymbol{\varepsilon}}$ in the denominator of Eq. (3) makes the extra stress tensor **T** unbounded. Furthermore, while simulating the velocity field **U**, the location of the yield surface is unknown prior to calculation. To overcome these difficulties, a regularized version of the Herschel-Bulkley model Eqs. (1) and (2) is used in this work [1].

Experimental

The vane rheometer used in this work is shown in Fig. 1. Its rotating geometry consists of a shaft (i.e. a rod) connected to four blades. The stationary part consists of a cub that contains the test material.

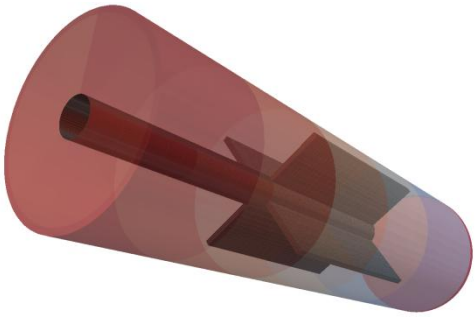

Figure 1. The vane rheometer under consideration.

The thickness of each blade is 1.0 mm. The edge-to-edge diameter of the blades (including the shaft diameter) is 28.0 mm. The diameter of the shaft is 6.0 mm. The diameter of the cub is 30.0 mm. The height of the (rotating) blades is 40.0 mm, while the height of the cub is 110.0 mm. The clearing at the bottom is 30.0 mm.

The number of cells used in generating the vane rheometer is 201,396. The mesh is generated with a native OpenFOAM mesh utility called blockMesh, and the mesh quality is checked with another OpenFOAM utility, named checkMesh. More than 98% of the cells are hexahedra, while the rest consist of prisms. The no-slip

boundary condition (i.e. the Dirichlet boundary condition) is used at all wall boundaries. However, at the top of the rheometer (i.e. at/near the boundary between atmosphere and liquid), the boundary condition consists of $\partial\mathbf{U}/\partial z = 0$ (i.e. the Neumann boundary condition).

In this work, the yield stress $\tau_0 = 0.1$ Pa, while the power-law exponent n is equal to 0.5 (i.e. shear thinning fluid) and the density is set equal to $\rho = 990$ kg/m^3. The difference between experimental cases rests only in difference in the consistency index k, set equal to 0.1, 1 and 10 Pa·s^n. During a single rheological test, the impeller angular velocity ω range from 0.1 to 0.6 rps (i.e. from 0.6 to 3.8 rad/s), while the cub is stationary.

Calculation of Torque

To calculate the shaft torque, the stress acting on the impeller system has to be obtained. This is done by calculating the traction vector [10,11] applied to the shaft and the four blades connected to it, given by $\mathbf{t} = \mathbf{n}\cdot\boldsymbol{\sigma} = \mathbf{n}\cdot(-p\mathbf{I} + \mathbf{T})$. The terms $\boldsymbol{\sigma}$, p and $\mathbf{I}$ are the total stress tensor, hydrodynamic pressure and the unit dyadic, respectively [10,11].

Here, the traction vector $\mathbf{t}$ is split into two components, namely one for the viscous stress $\mathbf{t}_\eta = \mathbf{n}\cdot\mathbf{T}$ and the other for the hydrodynamic pressure $\mathbf{t}_p = \mathbf{n}\cdot(-p\mathbf{I})$, the sum being of course the total traction $\mathbf{t} = \mathbf{t}_\eta + \mathbf{t}_p$. The term $\mathbf{n}$ is the unit normal vector pointing outward from the solid boundary of the impeller system (i.e. pointing into the fluid). After obtaining the viscous traction vector $\mathbf{t}_\eta$, the torque by viscous stress can be calculated with [1]

$$\mathbf{T}_\eta = \int_{\text{imp}} \mathbf{r} \times \mathbf{t}_\eta \, dA \tag{4}$$

The integration is over the impeller system, namely the shaft and the four vane blades connected to it. The term $\mathbf{r}$ is the vector location of the solid boundary of the impeller system and the integrand dA is in terms of surface area. The torque in the axis of the shaft is calculated by $T_\eta = \mathbf{T}_\eta \cdot \mathbf{i}_z$, in which $\mathbf{i}_z$ is the unit vector in the axis of the shaft (i.e. here the z-axis).

In the same manner as above, the torque by hydrodynamic pressure is calculated with [1]

$$\mathbf{T}_p = \int_{\text{imp}} \mathbf{r} \times \mathbf{t}_p \, dA \tag{5}$$

The torque in the axis of the shaft is $T_p = \mathbf{T}_p \cdot \mathbf{i}_z$, and the computed total shaft torque is then $T = T_\eta + T_p$. The computed total shaft torque T is the same as the measured torque [1]. Here, the total shaft torque T will also be designated as *total torque* for

simplicity. For the same reason, the shaft torque by hydrodynamic pressure T_p will be designated as *pressure-torque* and the shaft torque by viscous stress T_η as *viscous-torque*.

Results

The aim of the current work is to calculate the shaft torque at different angular velocities ω and compare the effect of hydrodynamic pressure p to the effect of apparent viscosity η. With this specific objective, one should keep in mind that there is a direct relationship between the apparent viscosity η and the viscous-torque T_η by Eq. (4) (see [1] for more detail). There is also a direct relationship between the hydrodynamic pressure p and the pressure-torque T_p by Eq. (5).

Case 1: k = 10 Pa·s^n

Figure 2 shows the computed shaft torque as a function of angular velocity ω when the consistency index is k = 10 Pa·s^n, yield stress is τ_0 = 0.1 Pa, power-law exponent is n = 0.5 and density is ρ = 990 kg/m^3. Two torque values are shown in this figure. One is the total torque $T = T_\eta + T_p$, while the other torque value is the viscous-torque T_η. The difference between the total torque T and the viscous-torque T_η is of course the contribution by hydrodynamic pressure T_p. This is clearly indicated in the figure.

From Fig. 2, it is clear that the majority of the total torque T originates from the effect of hydrodynamic pressure p, reflected in relatively high T_p. That is, the effect of hydrodynamic pressure constitutes more than 80% of the overall torque T registered by the rheometer. This highlights the importance of understanding what influence the hydrodynamic pressure p during a measurement.

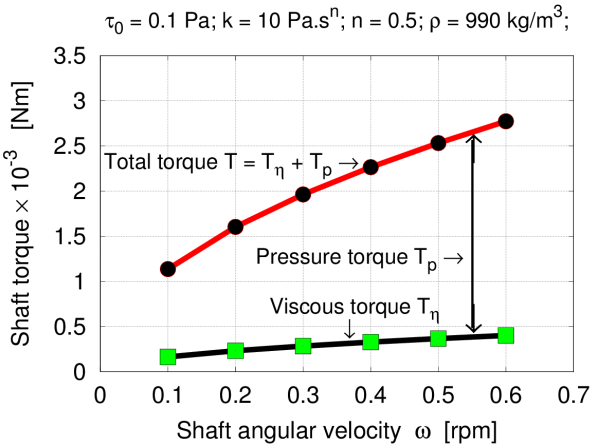

Figure 2. Shaft torque values T_η and $T = T_\eta + T_p$ as a function of ω.

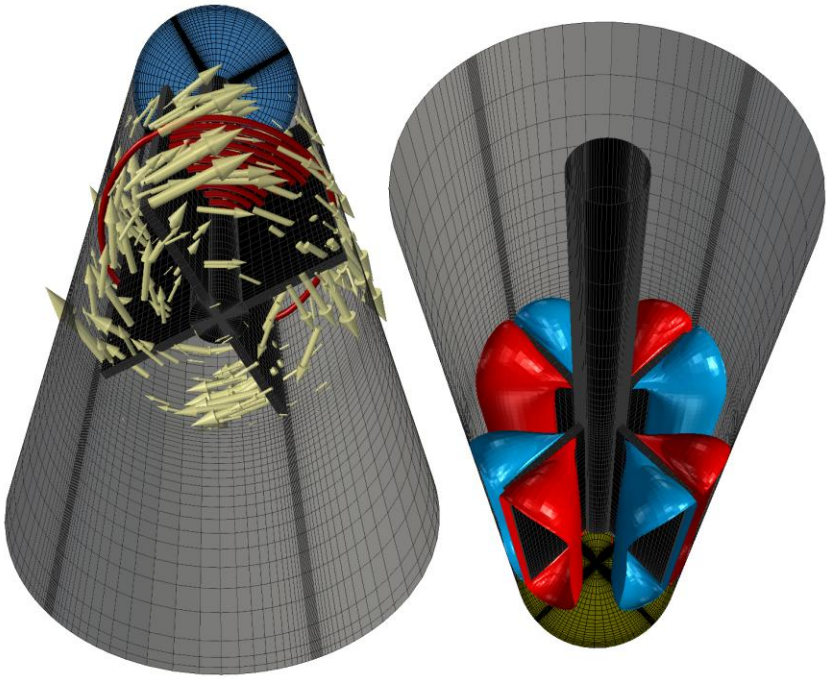

Figure 3. An example of a simulation result for the case shown in Fig. 2.

As an example of a single simulation result from the case of Fig. 2, then in Fig. 3 is a result that applies at $\omega = 0.5$ rps. The left illustration demonstrates velocity vectors **U**, including streamlines at the height $z = 50$ mm (relative to the bottom of the cylinder). The right illustration shows iso-plots of the hydrodynamic pressure. For this last-mentioned illustration, the red surface represents 20 Pa gage, while the blue surface represents –20 Pa gage. In this work, the hydrodynamic pressure is calculated in terms of gage pressure (also gauge pressure) and not in terms of absolute pressure.

Case 2: k = 1 Pa·s^n

Figure 4 shows the same type of result as for Fig. 2, in which now the consistency index is $k = 1$ Pa·s^n. Other material parameters are the same as in Fig. 2 (i.e. Case 1). Compared to the previous case (Fig. 2), the effect of the hydrodynamic pressure p (represented with T_p) is about the same, relatively speaking. That is, the effect of hydrodynamic pressure constitutes more than 80% of the overall torque T registered by the rheometer.

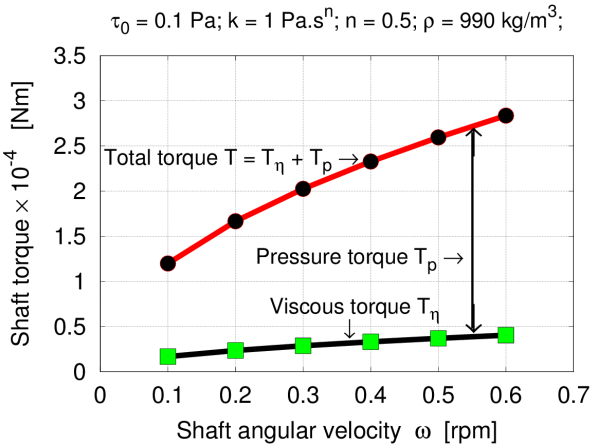

Figure 4. Shaft torque values T_η and $T = T_\eta + T_p$ as a function of ω.

Case 3: k = 0.1 Pa·s^n

Figure 5 shows the same type of result as for Figs. 2 and 4, in which now the consistency index is k = 0.1 Pa·s^n. Other material parameters are the same as in Figs. 2 and 4. Compared to the previous cases, the effect of the hydrodynamic pressure p (represented with T_p) is now even higher in generating the total torque T. That is, the effect of hydrodynamic pressure now constitutes close to 90% of the torque T registered by the rheometer. The reason for this increased effect of hydrodynamic pressure p for such low viscous case (i.e. k = 0.1 Pa·s^n) is well explained elsewhere [1].

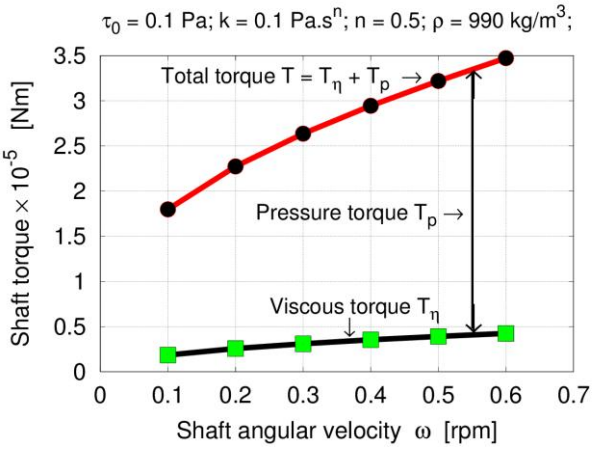

Figure 5. Shaft torque values T_η and $T = T_\eta + T_p$ as a function of ω.

Conclusions

The majority of the total torque T from the vane rheometer originates from the effect of hydrodynamic pressure p and not directly from the apparent viscosity η.

As the apparent viscosity η decreases (here, by the reduction in consistency index k), the effect of hydrodynamic pressure p increases. A physical explanation of this peculiar behavior is available elsewhere [1].

Acknowledgements

This work has been funded by The Icelandic Centre for Research (RANNIS) - Grant Number 110028021 - *Computational Material Modeling*.

Reference:

[1] Wallevik, J.E. (2014), Effect of the hydrodynamic pressure on shaft torque for a 4-blades vane rheometer, *Int. Journal of Heat and Fluid Flow*, 50, 95 - 102.
[2] Nazari B., Moghaddam R.H., and Bousfield D. (2013), A three dimensional model of a vane rheometer, *Int. Journal of Heat and Fluid Flow*, 42, 289 - 295.
[3] Weller H.G., Tabor G., Jasak H., and Fureby C. (1998), A tensorial approach to computational continuum mechanics using object-oriented techniques, *Comput. Phys.*, 12, 620 - 631.
[4] Berberovic E. (2010), Investigation of Free-surface Flow Associated with Drop Impact: Numerical Simulations and Theoretical Modeling, Ph.D. thesis, Technische Universitat Darmstadt, Germany.
[5] ANSYS FLUENT 6.3 User's Guide (2006), ANSYS Inc., USA.
[6] Versteeg H.K., and Malalasekera W. (2007), *An Introduction to Computational Fluid Dynamics - the Finite Volume Method* (2nd ed.), Pearson Education Limited, England.
[7] Karrholm F.P. (2006), *Rhie-Chow Interpolation in OpenFOAM*, Department of Applied Mechanics, Chalmers Univesity of Technology, Sweden.
[8] Tanner, R.I. and Walters, K. (1998), *Rheology: An Historical Perspective*, Elsevier Science, Netherlands.
[9] Barnes H.A., Hutton J.F., and Walters K. (1989), *An Introduction to Rheology*, Elsevier Science, Netherlands.
[10] Malvern, L.E. (1969), *Introduction to the Mechanics of Continuous Medium*, Prentice-Hall Inc., USA.
[11] Mase, G.E. (1970), *Schaums Outline Series: Theory and Problems of Continuum Mechanics*, McGraw-Hill Inc., USA.
[12] Oldroyd, J.G. (1947), A Rational Formulation of the Equations of Plastic Flow for a Bingham Solid, *Proc. Camb. Philos. Soc.*, 43, 100 - 105.

Influence of Carbon Nanotubes on SCC Flowability

Mahyar Ramezani, Young Hoon Kim, Bashir Hasanzadeh and Zhihui Sun

Department of Civil and Environmental Engineering, University of Louisville, KY, USA

Abstract Carbon Nanotubes (CNTs) are considered as one of the most promising nano particles for strengthening concrete structures. Most researches are focused on its contribution to the mechanical properties of concrete, e.g. tensile strength and toughness. Very few studies have been conducted to investigate its influence on the flowability of concrete, especially the relationships among water-to-cement (*w/c*) ratio, superplasticizer (SP) dosage, and CNTs concentration. This paper studies the effect of Multi Walled Carbon Nanotubes (MWCNTs) addition on the workability of Self Consolidating Concrete (SCC) pastes and mortars. Samples with three *w/c* ratios of 0.35, 0.45 and 0.6 have been studied. And for each specific *w/c* ratio, different dosages of superplasticizer were used. The flowability of the SCC pastes and mortars are represented by viscosity, yield stress, and flow diameter obtained from the rheological and flow table tests. The research found that the addition of CNTs in pastes had significant impacts on the pastes' rheological properties. And the SP/CNTs ratio also had a remarkable influence on the shear thickening behavior of the material. However, being different from the SCC pastes, the SCC mortars' flowability was less sensitive to the variations of CNTs content and SP/CNTs ratio.

Keywords: *Carbon nanotubes, SCC paste, SCC mortar, Viscosity, Yield stress, Flow diameter*

Introduction

The superior mechanical properties of Carbon Nanotubes (CNTs) make them one of the most promising nano particles for strengthening concrete structures. Their average Young's modulus value was found to be 1.28 TPa [1] with tensile strength in the range of 11-63 GPa [2]. Most researchers [3, 4] focused on CNTs contribution to the mechanical properties of concrete, e.g. tensile strength and toughness. Abu Al-Rub et al. [3] found addition of 0.2% Multi Walled Carbon Nanotubes (MWCNTs) based on weight of cement, increased flexural strength and

ductility up to about 270% and 80% compared to plain cement pastes, respectively. Konsta-Gdoutos et al. [4] reported that the flexural strength and the modulus of elasticity increased by 25% and 45% by adding MWCNTs concentration of 0.08% based on the weight of cement powder (c-wt%), respectively. This study focuses on the quantification of the influence of CNTs on the rheological properties of fresh concrete. This work primarily investigated the application of CNTs in Self Consolidating Concrete (SCC) pastes and mortars.

Constructability of concrete is affected by its fresh state performance. Therefore, it is essential to determine rheological properties i.e. viscosity and yield stress. These parameters also govern the stability of the material to prevent segregation or bleeding, etc. Rheological properties are affected by particle dispersion in concrete. In a paste containing CNTs, to prevent the agglomeration caused by the van der Waals forces, surfactants are normally used to help disperse CNTs uniformly in the material, in combination with ultrasonic energy [3, 4]. Polycarboxylate based superplasticizer (SP) was shown to be one of the most effective surfactants for CNTs dispersion [4]. However, the optimization of dosage is critical. If too less is used, the solid particles may flocculate and reagglomerate; and if too much is used, the cement paste may start to bleed to lose the material integrity. Therefore, the optimization of the ratio of SP to MWCNTs (herein, SP/CNTs ratio) is an important parameter. Konsta-Gdoutos et al. [4] found an optimum ratio of SP to MWCNTs equal to 4 in their study, beyond which the flexural strength of the composites deteriorated.

In this study, the influence of solid concentration and SP/CNTs ratio on the workability of SCC pastes and mortars was investigated. In the case of SCC pastes, both the Bingham and the Herschel-Bulkley models [5, 6] were used to obtain the plastic viscosity, yield stress, and to identify shear thinning/thickening behavior.

Materials and Experimental Program

Materials and mix proportions

Type I ordinary Portland cement was used for this study. The Blaine surface area of this cement was 400.8 m^2/kg. A polycarboxylate based SP with density approximately 1.1 kg/L was used to achieve the proper dispersion of CNTs and SCC flowability. COOH functionalized MWCNTs were used and their physical properties are given in Table I. In SCC mortars, 20-30 silica sand in accordance with ASTM C778, *Standard Specification for Standard Sand* [7] was used as aggregate.

For the SCC pastes, three different *w/c* ratios of 0.35, 0.45 and 0.6 were employed and for each *w/c* ratio, four different SP dosages were used to study the influences of solid concentration and SP/CNTs ratios on the rheological properties of SCC

pastes. CNTs concentration for all the SCC paste batches were 0.1 c-wt%. Mix proportions of the SCC pastes are listed in Table II.

Table I. Properties of MWCNTs (Reported by Manufacturer)

Length [μm]	Outside diameter [nm]	Inside diameter [nm]	Purity [%]	Surface area [m^2/g]
10-30	< 8	2-5	>95	>500

Table II. SCC paste mix proportions

Batch #	*w/c* ratio	SP [c-wt%]	CNTs [c-wt%]	SP/CNTs ratio
C1	0.35	0.3	0.1	3
C2		0.4		4
C3		0.6		6
C4		0.9		9
C5*		0.3	-	-
C6	0.45	0.3	0.1	3
C7		0.4		4
C8		0.5		5
C9		0.6		6
C10*		0.3	-	-
C11	0.6	0.1	0.1	1
C12		0.2		2
C13		0.3		3
C14		0.4		4
C15*		0.3	-	-

Note: * indicates the control mix in each *w/c* ratio.

Table III. SCC Mortar mix proportions

Batch #	Water:Cement:Sand [ratio by volume]	SP [c-wt%]	CNTs [c-wt%]	SP/CNTs ratio
M1	0.35:1:2.6	0.6	-	-
M2	0.35:1:2.6	0.6	0.05	12
M3	0.35:1:2.6	0.6	0.1	6
M4	0.35:1:2.6	0.7	0.05	14

For the SCC Mortars, the *w/c* ratio of 0.35 was used with two different contents of SP and CNTs. Table III presents the mortars mix proportions. CNTs concentration of 0.05 and 0.1 c-wt% were used for mortars. SP/CNTs ratio varied from 6 to 14

depending on the CNTs content. For all of the listed proportions, the volume of silica sand was fixed at 60% of the total volume.

Sample preparation

For the control pastes (C5, C10 and C15), mixture of water and SP was gradually added to the cement over the first minute of mixing and then continued to mix for 2 additional minutes at a speed of 136 rpm. The sample was then allowed to rest for 2 minutes, which was followed by a mixing of another 3 minutes at high speed of 195 rpm.

For the samples with CNTs, water and SP were mixed first. Then, CNTs were added to the solution and sonicated for 25 minutes at room temperature with 75% of the maximum amplitude of a tip horn sonicator. The tip used for ultrasonication had the maximum amplitude of 60 μm. The sonication was done at cycle intervals of 25 seconds in order to prevent overheating of CNTs. After sonication, the temperature of the solution (with CNTs) gradually decreased to reach the ambient room temperature of 25°C by using water circulator prior to mixing with cement. The cement and sonicated solution were mixed with the same procedure of control mixes.

For mortar samples, first, cement and the first half of the silica sand were mixed. Then, water (or the sonicated solutions) and the rest of silica sand were gradually added to the mixture over the first minute of mixing, followed by the same mixing procedure as of SCC pastes. For each mix proportion, two batches were prepared. All of the tests were conducted at the room temperature of 25°C.

Test Procedure and Rheological Models

Flow test

The mini-cone slump tests were conducted for all of the paste samples to measure the flow diameter. The average of the flow diameter in two perpendicular directions was used to represent the flow diameter. For the mortar samples, flow table test in accordance with ASTM C1437, *Standard Test Method for Flow of Hydraulic Cement Mortar* [8], was used to calculate the flow diameter of the mortars. Flow table tests were conducted 10 minutes after starting of mixing.

Rheological tests and models

The rheometer (Model: Anton Paar MCR 502) with a co-cylindrical cup configuration (gap size of 1.6 mm) was used to measure the rheological properties of SCC pastes. During the tests, the SCC pastes were pre-sheared at shear rate of 600 s^{-1} for 10 seconds and then let rest for 3 minutes. After that, samples were sheared at 7 different shear rates (600, 500, 400, 300, 200, 100, and 10 s^{-1}). Each

shear rate was maintained for 10 seconds. Rheological test and mini-cone slump test were simultaneously conducted 14 minutes after starting of mixing.

Both Bingham and Herschel-Bulkley models are used to determine rheological properties. Bingham model (Eqn. (1)) uses linear regression to find yield stress and plastic viscosity [9, 10]. Hershchel-Bulkley model, on the other side, uses nonlinear regression (Eqn. (2)). The flow index (n) in Herschel-Bulkley model is used as an indication of the shear behavior of the SCC pastes. When flow index is larger than 1, the material exhibits shear thickening behavior, and a shear thinning behavior corresponds to a flow index smaller than 1 [10, 11].

$$\tau = \tau_0 + \mu_P.\dot{\gamma} \tag{1}$$

$$\tau = \tau_0 + K.\dot{\gamma}^n \tag{2}$$

where τ = shear stress (Pa), τ_0 = yield stress (Pa), μ_p = plastic viscosity (Pa.s), $\dot{\gamma}$ = shear rate (s^{-1}), K = consistency ($Pa.s^n$), and n = flow index

Results and Discussion

SCC pastes mini-cone slump test

Figure 1 compares the flow diameters for those pastes with SP/CNTs ratio of 3. By comparing the numbers with those of the control samples, it is evident that adding CNTs would reduce the flow diameter of the paste. Also, as *w/c* ratio increases, the flow diameter increases for both controls and SCC pastes with CNTs. Figure 2 shows the influence of SP dosage on the flow diameter of SCC pastes. Increasing the SP/CNTs ratio from 3 to 4, caused the flow diameter to increase by 23%, 17% and 6% for *w/c* ratios of 0.35, 0.45 and 0.6, respectively, and it continued to increase by keep adding more SP. However, as the SP dosage increases, the potential of bleeding could increase.

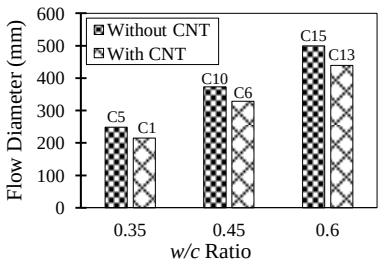

Figure 1. CNTs effect on flowability

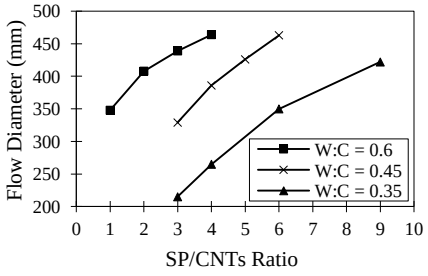

Figure 2. SP effect on flowability

Figure 3 shows pictures of two SCC pastes with *w/c* ratio of 0.6 and SP/CNTs = 3. Figure 3(a) shows the control (Mix C15) and Figure 3(b) shows the specimen with incorporation of CNTs (Mix C13) on the flow table after 30 minutes of the mini-cone slump test. Bleeding issue was observed for the plain SCC paste. However, a clear layer of water was not seen for SCC paste incorporating CNTs, which must be related to the change in its rheological properties.

(a) Without CNTs (Mix C15) (b) With CNTs (Mix C13)

Figure 3. SCC pastes after 30 minutes on flow table test

Table IV. SCC paste test results

Batch #	Flow diameter [mm]	Bingham		Herschel-Bulkley		
		Yield stress [Pa]	Viscosity [Pa.s]	Yield stress[Pa]	Viscosity [Pa.s]	Flow index
C1	215	-1.447	0.429	14.040	0.076	1.267
C2	265	-14.005	0.391	6.823	0.022	1.447
C3	350	-15.622	0.306	3.707	0.008	1.573
C4	422	-14.118	0.270	2.186	0.009	1.534
C5*	249	-14.547	0.440	9.343	0.023	1.458
C6	329	0.586	0.072	2.101	0.029	1.142
C7	386	-0.790	0.066	0.882	0.021	1.174
C8	426	-1.046	0.056	0.677	0.014	1.218
C9	463	-1.101	0.054	0.642	0.012	1.233
C10*	373	-1.205	0.075	1.232	0.017	1.234
C11	348	5.556	0.023	4.193	0.130	0.738
C12	408	0.892	0.018	0.962	0.016	1.023
C13	439	0.181	0.016	0.236	0.014	1.020
C14	464	0.015	0.015	0.059	0.013	1.018
C15*	500	-0.050	0.015	0.172	0.008	1.098

SCC pastes rheology test

Table IV summarizes flow diameters of mini-cone slump and rheology tests for SCC pastes. The yield stress and the viscosity of each mix were obtained from two rheological models. There was substantial difference in yield stresses and

viscosities between two rheological models. As it is clear from Table IV, SP dosage has an influence on the shear behavior of the material. C5, C10 and C15 are control samples with SP amount of 0.3 c-wt% and *w/c* ratios of 0.35, 0.45 and 0.6, respectively. It is clearly shown that the higher the *w/c* ratio, the lower the effect of SP on shear behavior of the material is. It can also be seen that flow index value for all the batches is greater than 1 which represents the shear thickening behavior, except for the batch C11 which has a flow index value of 0.738. This can be attributed to the mix proportion of batch C11: the highest *w/c* ratio and the lowest SP content (0.1 c-wt%). In this case, SP dosage is not high enough causing the paste behaves in a shear thickening manner.

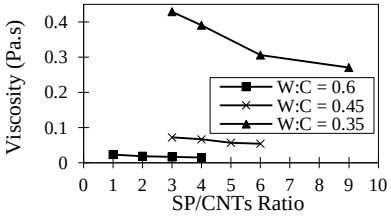

Figure 4. Viscosity vs. SP/CNTs ratio

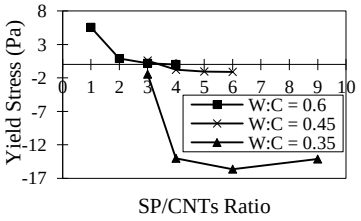

Figure 5. Yield stress vs. SP/CNTs ratio

Figures 4 and 5 show plastic viscosity and yield stress versus SP/CNTs ratio obtained from Bingham model, respectively. It can be seen that the plastic viscosity decreases by increasing the SP/CNTs ratio for all the *w/c* ratios. And for a given SP/CNTs ratio, the higher the *w/c* ratio, the lower the plastic viscosity is. Yield stresses obtained from Bingham model are negative in most cases (except for *w/c* ratio of 0.6) that are practically infeasible. It should also be noticed that by increasing the *w/c* ratio, the yield stress is unexpectedly increasing for a given SP/CNTs ratio. This could be an indication of the non-linear behavior of the material flow. Bingham model probably is not a good indication for the pastes with the *w/c* ratios of 0.35 and 0.45. Other researchers also reported SCC shows shear thickening behavior which causes the Bingham yield stress to become negative [12, 13]. Therefore, the Herschel-Bulkley model was utilized in this research to rationally quantify the rheological properties of the pastes.

Figure 6 shows the flow index values versus *w/c* ratios obtained from Herschel-Bulkley model for SCC pastes with and without CNTs. SP and CNTs contents are constant for all the *w/c* ratios. It is evident that using CNTs in the SCC pastes decreases the flow index for all the *w/c* ratios. Therefore, CNTs effectively decrease the shear thickening behavior of SCC pastes which is beneficial to high shear rate applications such as high speed mixing and pumping. By increasing the SP/CNTs ratio from 1 to 2 for *w/c* of 0.6, the flow index increases by approximately 40% (See Figure 7). However, once this threshold is passed, adding more SP has no significant effect on SCC pastes shear behavior for *w/c* ratio of 0.6.

The same trend is observed for other *w/c* ratios. Therefore, it is evident that after a certain SP/CNTs ratio for each specific *w/c* ratio, adding more SP has minimum effect on SCC pastes' shear behavior. These threshold SP/CNTs ratios are found to be 2, 5 and 6 for *w/c* ratios of 0.6, 0.45 and 0.35, respectively. The higher the *w/c* ratio, the less sensitivity of the material's shear behavior to the SP/CNTs ratio. This is the observation in the range of SP/CNTs ratio between 3 to 4.

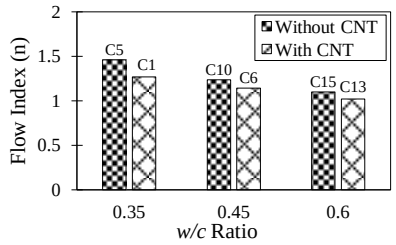

Figure 6. Flow index vs. *w/c* ratio

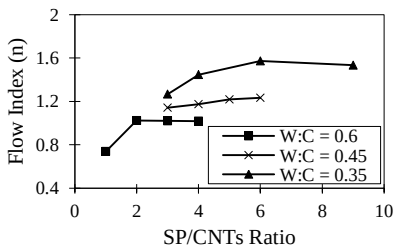

Figure 7. Flow index vs. SP/CNTs ratio

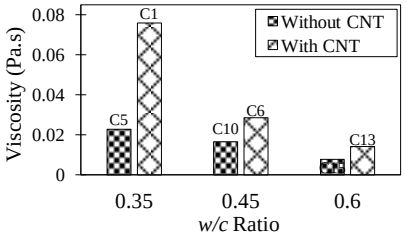

Figure 8. Viscosity vs. *w/c* ratio

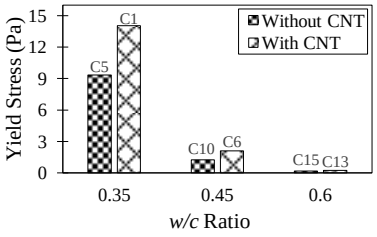

Figure 9. Yield stress vs. *w/c* ratio

Figures 8 and 9 show viscosity and yield stress obtained from Herschel-Bulkley model, respectively, of SCC pastes with and without CNTs with respect to *w/c* ratios. The SP/CNTs ratio is kept constant for all mixes in order to investigate the influence of CNTs addition on SCC pastes' rheological properties. It is clear that CNTs can increase viscosity greatly compared to plain SCC pastes. Using 0.1 c-wt% of CNTs in SCC pastes increased the viscosity by about 230%, 75% and 85% for *w/c* ratios of 0.35, 0.45, and 0.6, respectively. CNTs addition also increased yield stress. By incorporating of 0.1 c-wt% of CNTs, yield stress increased by 50%, 70% and 35% compared to plain SCC pastes for *w/c* ratios of 0.35, 0.45 and 0.6, respectively. The increased viscosity and yield stress in SCC pastes containing CNTs also clearly tied with the observation of bleeding in SCC pastes (See Fig. 3).

SCC mortars flow table test

Because SP/CNTs ratios significantly influenced flowability in the lowest *w/c* ratio in SCC pastes, the *w/c* ratio of 0.35 was selected to investigate flow diameter in

SCC mortars. Table V shows the results of flow table test for SCC mortars. As it is clear, adding 0.05 c-wt% of CNTs reduced the flow diameter by 10%. In SCC mortars with 0.05 c-wt% of CNTs, increasing SP/CNTs ratio from 12 (Mix M2) to 14 (Mix M4), is not effective in increasing the flow diameter. From the table, it can also be seen that by increasing the CNTs concentration from 0.05 to 0.1 c-wt%, and keeping the same amount of SP (M2 and M3), flow diameter did not change significantly. This indicates that being different to SCC paste; the SCC mortar is less sensitive to the SP/CNTs ratio and CNTs content with regard to flowability. Different trends in flowability of SCC pastes and mortars concerning aforementioned parameters is currently under investigation and can be attributed to the larger particle size of sand compared to cement powder which hinders the proper dispersion of CNTs in the case of SCC mortars. Also, by increasing CNTs content, more SP is adsorbed on their surface, and the remaining SP in the mix is not effective on getting higher level of flowability.

Table V. SCC mortars flow table test

Batch #	SP [c-wt%]	CNT [c-wt%]	SP/CNTs ratio	Flow diameter-Test 1 [mm]	Flow diameter-Test 2 [mm]
M1	0.6	-	-	171	-
M2	0.6	0.05	12	153	153
M3	0.6	0.1	6	154	155
M4	0.7	0.05	14	153	154

Conclusions

Flowability and rheological properties are closely related to the construction and early-age behaviors of SCC. From the test results obtained in this study, the following conclusions can be made:

1. For SCC pastes, addition of 0.1% CNTs based on weight of cement can significantly increase the yield stress and viscosity compared to the plain SCC pastes. These improvements in rheological parameters may help to reduce the bleeding issue in SCC pastes.

2. Most of the studied SCC pastes indicate shear thickening behaviors. And the SP/CNTs ratio was found to be critical. Threshold values of SP/CNTs ratio of 2, 5, and 6 were found for SCC pastes with *w/c* ratios of 0.6, 0.45, and 0.35, respectively. Once this threshold value is surpassed, the flow behaviors of the material are not influenced by the SP/CNTs ratio that much.

3. The superplasticizer dosage has very different influences on SCC paste and SCC mortar behaviors. For SCC pastes, adding more superplasticizer will decrease the viscosity and the yield stress (for a given *w/c* ratio). However, for the studied mortar, the flow diameter would remain constant when changing the CNTs content and the SP/CNTs ratio.

Acknowledgements

The authors acknowledge the financial supports from the Speed School of Engineering, Department of Civil and Environmental Engineering, and Intramural Research Incentive Grant (IRIG) No. 50916 at the University of Louisville.

References

[1] Wong, E.W., Sheehan, P.E. and Lieber, C.M. (1997), *Science*, vol. 277, n. 5334, p. 1971-1975

[2] Yu, M.F., Lourie O., Dyer M.J., Moloni K., Kelly T.F. and Ruoff R.S. (2000), *Science*, vol. 287, n. 5453, pp. 637-640

[3] Abu Al-Rub, R.K., Ashour, A.I. and Tyson, B.M. (2012), *Constr. Build. Mater.* vol. 35, pp. 647-655

[4] Konsta-Gdoutos, M.S., Metaxa, Z.S. and Shah, S.P. (2010), *Cement Concrete Res.*, vol. 40, n. 7, pp. 1052-1059

[5] Vikan, H., Justnes, H., Winnefeld, F. and Figi, R. (2007), *Cement Concrete Res*., vol. 37, n. 11, pp. 1502-1511

[6] Yahia, A. and Khayat, K.H. (2001), *Cement Concrete Res*., vol. 31, n. 5, pp. 731-738

[7] *ASTM Standard C778*, (2013), Standard Specification for Standard Sand, ASTM International, West Conshohocken, PA, 2013, DOI: 10.1520/C0778, www.astm.org

[8] *ASTM Standard C1437*, (2013), Standard Test Method for Flow of Hydraulic Cement Mortar, ASTM International, West Conshohocken, PA, 2013, DOI: 10.1520/C1437, www.astm.org

[9] Tattershall, G.H. and Banfill, P.F.G. (1983), *Pitman Advanced Publishing Program*, New York

[10] Ferraris, C.F. (1999), *J. Res. Natl. Inst. Stand. Technol.*, vol. 104, n. 5, pp. 461-478

[11] Yahia, A. and Khayat, K.H. (2003), *Materials and Structures*, vol. 36, n. 6, pp. 402-412

[12] Feys, D., Verhoeven, R. and Schutter, G.D. (2008), *Cement Concrete Res.*, vol. 38, n. 7, pp. 920-929

[13] Cyr, M., Legrand, C. and Mouret, M. (2000), *Cement Concrete Res.*, vol. 30, n. 9, pp. 1477-14.

Effect of Cement Type and Solid Concentration on Kinetics of Structural Build-up of Cement Suspensions

Ahmed M. Mostafa[1] and Ammar Yahia[2]

[1] Ph.D. Candidate, Department of Civil Engineering, Université de Sherbrooke, Quebec, Canada
[2] Associate Professor, Department of Civil Engineering, Université de Sherbrooke, Quebec, Canada

Abstract Build-up of cement-based suspensions is a complex phenomenon, affected by the type of cement, solid concentration, temperature, shear history, and measurement method. Recently, there has been an increasing interest in using general use limestone cement (GUL) to reduce greenhouse gas emissions. Previous studies have highlighted the beneficial effects of GUL on improving workability and pumpability of self-consolidating concrete. However, its effect on the build-up of fresh cement-based materials is not well known. This study aims to evaluate the structural build-up at rest of cement suspensions made with two different types of cement (GU and GUL) and various water-to-cement ratios (*w/c*). Two different testing approaches were used to assess build-up. The first approach consists in determining the rate of increase in static yield stress at rest ($A_{thix.}$), while the second approach consists in monitoring the evolution of storage modulus and phase angle using small amplitude oscillatory shear (SAOS). Test results revealed that for a given *w/c*, the use of GUL resulted in higher kinetics of build-up of cement suspension compared to GU. The faster rate of structuration may be attributed to greater interactions between fine particles. On the other hand, the higher rigidification may be due to the higher fineness and more available nucleation sites provided by the limestone particles.

Keywords: *Cement suspension, General use limestone cement, Solid concentration, Storage modulus, Structural build-up.*

Introduction

Cement-based suspensions are known to behave as thixotropic materials [1]. Thixotropy can be defined as the breaking down of suspensions with time under flow and the subsequent build-up at rest [2]. The structural build-up of cement-

based materials grasps great attention because of its importance from a practical point of view [3, 4]. For example, in the case of multi-layer casting, higher kinetics of structural build-up will reduce the bond strength between cast layers, hence resulting in a poor mechanical performance of the cast element [4]. However, in the case of cast-in-place applications, such as tall panels, higher build-up kinetics can result in a higher decay rate of the lateral pressure, hence lowering formwork costs and improving productivity [3].

The structural build-up of cement-based suspensions is a physico-chemical phenomenon. It originates from the colloidal flocculation due to inter-particles attractive interactions and the chemical bridging resulting from cement hydration [5]. Furthermore, the kinetics of build-up of cement suspensions are highly affected by their ingredients such as content and type of cement as well as the presence of mineral and chemical admixtures [6-8]. Recently, the use of general use limestone cement (GUL), containing up to 15% limestone, has been recommended as an alternative for general use on (GU) due to its environmental and economic benefits. As reported in literature, the use of GUL cement can result in less CO_2 emissions and embodied energy compared to GU. In addition, it can lead to similar durability and mechanical performance of cement-based materials [9, 10]. Several studies investigated the influence of limestone particles on the workability of cement suspensions and reported results seems to be contradictory. A lower water demand was needed for GUL mixtures to achieve a similar consistency of corresponding mixtures made with GU. This was related to the better packing of fine limestone particles which can result in less inter-particle spaces [11]. On the other hand, a slump loss was observed in some SCC mixtures when limestone was used as a filler [12]. Generally, it is agreed that the impact of limestone on rheology of cement suspensions depends on its content, particle size distribution, and fineness.

So far, little is known about the influence of GUL cement on the build-up performance of cement suspensions. The main objective of this study is to evaluate the kinetics of build-up of GUL mixtures proportioned at various cement contents and then, compare them to those determined for corresponding GU mixtures. The structuration at rest was determined using growth of static yield stress as well as the non-destructive dynamic measurements.

Background on Dynamic Rheology

Dynamic rheology is an important part of rheology, which is the science that consists in studying how materials deform and recover after the application of stress. In dynamic rheology, an oscillating stress or strain is applied to the material and the strain or stress response is then determined. On the other hand, the frequency measures how rapidly the oscillatory stress or strain is applied and released. The basic fundamental parameters used in dynamic rheology are: the shear storage modulus (G') and shear loss modulus (G"). The two moduli are used

to define the complex modulus as follow: G* = G' + iG". For an ideal solid material, there is no loss because the material is perfectly elastic and G" = 0, so G* = G'. On the other hand, for an ideal liquid, there is no rigidity and G' = 0, so G* = G". The damping factor (or loss factor) is calculated as the ratio of the lost and stored deformation energy (tan δ = G"/G'). The damping factor indicates the viscous and the elastic portion of the viscoelastic deformation behavior. Its value equals 0° (or tan δ = 0) for an ideal elastic material and = 90° (or tan δ = ∞) for an ideal viscous material, i.e. G" completely dominate G' [13].

Experimental Program

Materials, Mixture Proportions, and Mixing Sequence

A CSA A3001 general use (GU) and general use limestone (GUL) cements were used in this study. The chemical characteristics of used cements are summarized in Table I. The grain size distributions and physical properties of GU and GUL cements are presented in Figure 1. The investigated cement suspensions were prepared at different water-to-cement ratios (*w/c*) of 0.35, 0.40, and 0.45. The prepared mixtures were mixed using a high-shear mixer according to the procedure described in ASTM C1738M. The temperature of mixing water was controlled and cooled (8 ± 1°C) to compensate for heat generation. Following the end of mixing, all mixtures had a constant temperature of 23 ± 1°C. The mixing sequence consisted of introducing the binder gradually over 1 min while the mixer is turned on. After a rest period of 150 seconds, the mixing was presumed for a total mixing time of 4 minutes and 30 seconds. Immediately after mixing, samples were conserved in a sealed container at 23 ± 1ºC for an additional 15 minutes to ensure that early hydration reactions have occurred. The rheological measurements were carried out after 20 minutes from the initial contact between mixing water and cement.

Table I. Chemical characteristics of used cements

	Chemical composition (%)							
	CaO	SiO_2	Al_2O_3	Fe_2O_3	SO_3	MgO	K_2O	Na_2O
GU	63.73	19.89	3.54	2.73	3.79	1.97	0.78	0.19
GUL	63.39	19.27	3.37	2.43	3.18	2.01	0.76	0.21

Testing Methods

The rheological measurements were performed using a coaxial cylinders rheometer. The rheometer is equipped with a profiled bob having 26.660 mm diameter and a cup of 28.911 mm diameter. The effective height of tested sample is 40 mm. The test procedure consists in pre-shearing the sample at 20 s^{-1} for 30

seconds to ensure a homogeneous distribution of the tested sample in the gap [13]. The sample was then subjected to a rest period of 30 seconds to allow temperature equilibrium before starting the structural build-up measurements. The temperature of tested samples was controlled by the rheometer and kept at 23 ± 1ºC.

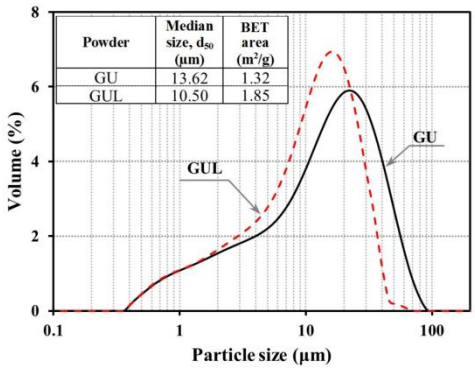

Figure 1. Particle size distributions of GU and GUL cements

Strain sweep measurements were first carried out to establish the linear viscoelastic domain (LVED) and critical shear strain [13]. In the strain sweep test, mixtures were subjected to an increasing shear strain amplitude from 0.0001% to 20% at a constant angular frequency of 10 rad/s.

Two intervals procedure was used to quantify the structural build-up at rest of the investigated mixtures. The first interval is the disruptive shear interval in which an initial dispersed state is obtained. The second interval corresponds to the structuration interval where the structural build-up is monitored. Recently, the authors have shown that the dispersing performance of traditionally applied rotational shear can be enhanced by applying a large amplitude oscillatory shear (LAOS) at high frequency [14]. A shear strain corresponding to the highest liquid state in the strain sweep test performed at a high angular frequency of 100 rad/s was recommended to obtain an effective dispersion. Accordingly, the disruptive interval used in this study consisted of applying a rotational shear rate of 200 s^{-1} for 90 seconds, followed by a LAOS at a shear strain of 6% and an angular frequency of 100 rad/s for 10 seconds. One second after the disruptive interval, the build-up was quantified during 20 minutes of rest using two different approaches, including time sweep and static yield stress measurements. For the time sweep measurements, a small amplitude oscillatory shear (SAOS) was applied at a constant angular frequency of 10 rad/s and shear strain value within the linear viscoelastic domain (LVED). In SAOS regime, the storage (G') and loss (G") moduli were monitored and then the phase angle (δ) was calculated. The evolutions of G' and δ at rest were used to quantify the build-up of GU and GUL cement suspensions. In the second approach, the evolution of static yield stress with rest

time was determined at different resting periods of 5, 10, 15, and 20 minutes after the pre-shear interval. For each resting period, the static yield stress was determined at a constant shear rate of 0.01 s^{-1}. The slope of measured static yield stresses with rest was determined and referred to $A_{thix.}$.

Test Results and Discussions

LVED and Critical Strain

The variation of storage (G') and loss (G") moduli determined from strain sweep measurements carried out on mixtures made with GU and GUL cements are presented in Figure 2. As can be observed, 0.35 and 0.45 *w/c* suspensions exhibited a linear viscoelastic behavior (LVED) characterized by constant G' and G" moduli below a critical shear strain of 0.003%. The critical strain was taken as the shear strain where G'-curve starts declining noticeably from the LVED plateau [13]. At shear strain values lower than the critical strain, the particles can recover elastically and the suspension acts as a solid structure (i.e. undisturbed) [13]. Increasing the shear strain above this critical strain results in destroying the structural network, reflected by a decrease in the elastic modulus. The build-up measurements carried out in this study was performed at a shear strain of 0.001% (lower than the critical strain of 0.003%) to ensure a non-destructive regime.

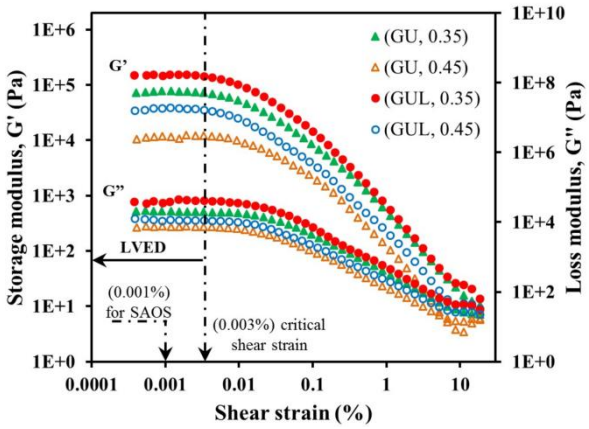

Figure 2. Strain sweep measurements carried out between 0.0001% and 20% strain and an angular frequency of 10 rad/s

Structural Build-up

The evolutions of storage modulus (G') and phase angle (δ) with rest time of GU and GUL cement suspensions proportioned with different *w/c* of 0.35, 0.40, and

0.45 are shown in Figure 3. As can be observed, at zero rest time (i.e. immediately after disruption), the mixtures exhibited almost zero G' and a value of δ higher than 45°, reflecting the negligible rigidity and the liquid-like state of suspension's structure. During the 20 minutes resting period, a continuous increase in G' was observed. This indicates an increase in the rigidity (i.e. stress-bearing capacity) of the network. Simultaneously, the evolution of δ showed a decreasing trend until reaching a steady state, reflecting a transition from the liquid-like state to a solid-like state. For a given cement type, the decrease in *w/c* resulted in a higher evolution rate of G', denoting higher rate of gaining rigidity of the formed network. On the other hand, the decrease in *w/c* caused a greater decay rate in δ at rest, reflecting a faster formation of the elastic percolated network. Furthermore, for a given *w/c*, cement mixtures made with GUL showed faster rates of recovering their stress-bearing capacity and structural connectivity compared to those made with GU type.

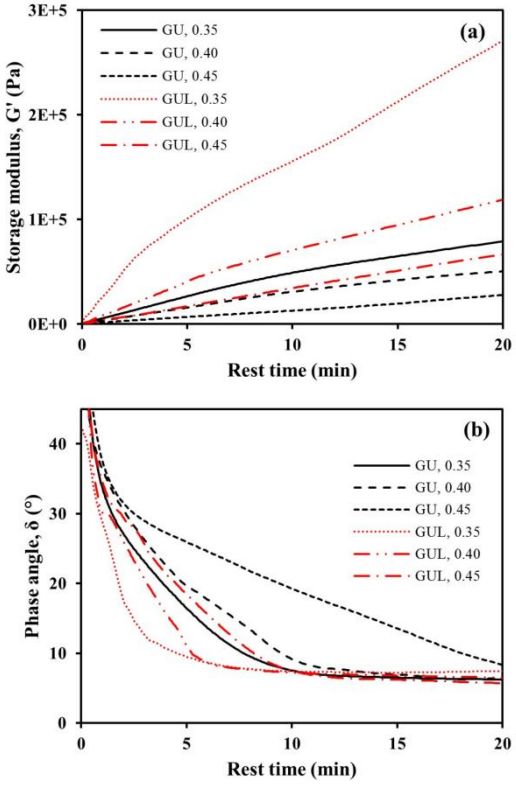

Figure 3. Evolutions of a) Storage modulus and b) Phase angle at a shear strain of 0.001% and an angular frequency of 10 rad/s for various suspensions proportioned with different *w/c*

Percolation Time, Rigidification Rate, and Growth of Static Yield Stress

Two independent indices were recently proposed to describe the physico-chemical kinetics of build-up of cement suspensions [15]. The first one is the percolation time ($t_{perc.}$) which represents the rest time needed to form the colloidal percolated network. This corresponds to the time where δ reaches its lowest and steady value. While the second index is the rigidification rate ($G_{rigid.}$) which describes the linear increase in G' after the percolation time and it expresses the chemical stiffening of the formed structure. The build-up indices $t_{perc.}$ and $G_{rigid.}$ were identified from the monitored evolutions of G' and δ shown in Figure 3 and then plotted as a function of the *w/c* (Figure 4). As can be observed, the increase in *w/c* from 0.35 to 0.45 resulted in increasing $t_{perc.}$ from 10 to 23 minutes and from 5 to 11 minutes for mixtures made with GU and GUL, respectively. Indeed, the decrease in *w/c* results in higher cement fraction in a given volume of cement paste, which can enhance the rate of particles' collisions and allows faster network formation. The shorter $t_{perc.}$ observed for GUL compared to GU can be attributed to the smaller inter-particle distances and the higher number of solid particles. In fact, the GUL cement used in this study showed lower median size and higher BET surface area compared to GU type as shown in Figure 1.

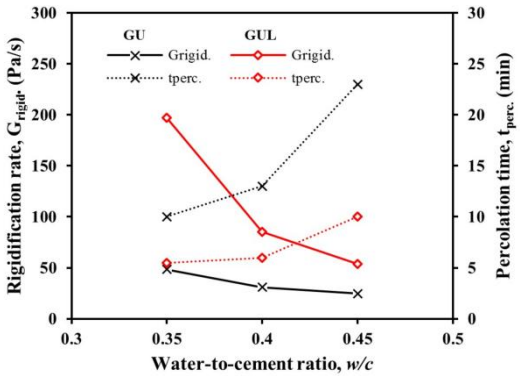

Figure 4. Evolutions of a) Storage modulus and b) Phase angle at a shear strain of 0.001% and an angular frequency of 10 rad/s for suspensions proportioned with various *w/c*

Furthermore, the decrease in *w/c* led to increasing $G_{rigid.}$ by almost two and four times for GU and GUL cement types, respectively. The increase in $G_{rigid.}$ with cement content can be related to the development of a more densified network. On the other hand, at a fixed *w/c*, the higher rigidification observed for GUL may be associated to the increase in both nucleation intensity and sites. Indeed, the limestone particles in GUL can work as nucleation sites [9]. The hydration intensity of GU and GUL cements were examined by performing further

calorimetric measurements on suspensions proportioned with a *w/c* of 0.45. The obtained heat flow due to hydration was recorded per gram of paste (Figure 5). As can be observed, suspension made with GUL exhibited a slightly greater heat flow within the dormant period and at the second peak. This could be an indication of the higher nucleation intensity of GUL cement compared to GU. This higher nucleation intensity leads to a more volume of formed hydrates at the pseudo contact points, hence, promoting the chemical rigidification (higher $G_{rigid.}$).

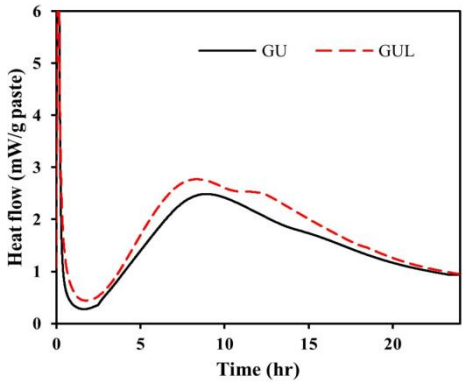

Figure 5. Heat flow curves during hydration for 0.45 *w/c* suspensions proportioned with GU and GUL cement types

In addition to describing build-up via $t_{perc.}$ and $G_{rigid.}$, the growth rates of static yield stress ($A_{thix.}$) of GU and GUL mixtures were estimated and presented in Figure 6. As can be seen, GUL cement resulted in higher value $A_{thix.}$ compared to GU at a given *w/c*, which is in good agreement with the determined oscillatory indices.

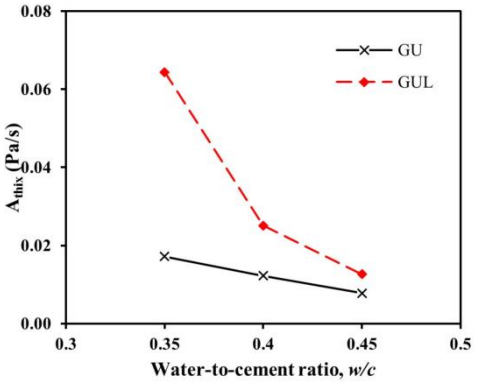

Figure 6. Variations of $A_{thix.}$ determined for GU and GUL suspensions proportioned with various *w/c*

Conclusions

The physico-chemical kinetics of structural build-up of cement suspensions proportioned with various *w/c* and two different cement types (GU and GUL) were investigated. Time sweep measurements were used to monitor the evolution of the storage modulus (G') and the phase angle (δ) after disruption. Based on the obtained results, the following conclusions can be pointed out:

- The percolation time ($t_{perc.}$) and rigidification rate ($G_{rigid.}$) indices were successfully used to quantify the structural build-up of the investigated mixtures.
- The decrease in *w/c* resulted in shorter $t_{perc.}$ and higher $G_{rigid.}$, regardless of the cement type. These higher kinetics of build-up can be attributed to the increase in cement fraction and densified network.
- The GUL cement type showed higher structuration kinetics compared to GU. This was reflected by higher $G_{rigid.}$ and shorter $t_{perc.}$. This finding can be due to the higher fineness of GUL compared to GU, hence resulting in more nucleation sites and higher chemical hydration.

References

[1] Wallevik, J.E. (2009), *Cem. Concr. Res.*, vol. 39, n. 1, pp. 14-29.
[2] Barnes, H.A. (1997), *J. Non-Newtonian Fluid*, vol. 70, pp. 1-33.
[3] Khayat, K.H. and Omran, A.F. (2011), *Concr. Int.*, vol. 33, n. 6, pp. 33-39.
[4] Roussel, N. and Cussigh, F. (2008), *Cem. Concr. Res.*, vol. 38, n. 5, pp. 624-632.
[5] Roussel, N. (2012), *Understanding the rheology of concrete*, 1st ed., Woodhead Publishing, Cambridge.
[6] Assaad, J.J. and Khayat, K.H. (2004), *ACI Mater. J.*, vol. 101, n. 5, pp. 400-408.
[7] Assaad, J.J. and Khayat, K.H. (2006), *ACI Mater. J.*, vol. 103, n. 4, pp. 280-287.
[8] Khayat, K.H. and Assaad, J.J. (2006), *ACI Mater. J.*, vol. 103, n. 3, pp. 186-193.
[9] Barrett, T. and Sun, H. and Weiss, W.J. (2013), *Performance of Portland Limestone Cements: Cements Designed to Be More Sustainable That Include up to 15% Limestone Addition*, pp. 64, Department of Transportation and Purdue University, West Lafayette, Indiana.
[10] Hawkins, P. and Tennis, P.D. and Detwiler, R.J. (2003), *The use of limestone in Portland cement: a state-of-the-art review*, pp. 41, Portland Cement Association.
[11] Tsivilis, S. and Chaniotakis, E. and Badogiannis, E. and Pahoulas, G. and Ilias, A. (1999), *Cem. Concr. Compos.*, vol. 21, n. 2, pp. 107-116.
[12] Ghezal, A. and Khayat, K.H. (2002), *Mater. J.*, vol. 99, n. 3, pp. 264-272.

[13] Mezger, T.G. (2011), *The Rheology Handbook: For Users of Rotational and Oscillatory Rheometers*, 3rd ed., Vincentz Network, Hanover, Germany.
[14] Mostafa, A.M. and Yahia, A. (2015), *Appl. Rheol.*, vol. 25, n. 3, pp. 34337.
[15] Mostafa, A.M. and Yahia, A. (2016), *Cem. Concr. Res.*, under revision.

Time-Dependent Evolution of Rheological Performance and Distinct-Layer Casting of Self-Compacting Concrete

Xiaojian Gao[1,2] and Huan Ye[2]

[1]Key Lab of Structures Dynamic Behavior and Control (Harbin Institute of Technology), Ministry of Education, 150090 Harbin, China
[2]School of Civil Engineering, Harbin Institute of Technology, Harbin 150006, China

Abstract In this paper, the time-dependent evolution of rheological behavior was carried out by a rheometer for self-compacting concretes (SCC) with different mixing proportions. The influence of distinct-layer casting with different delays on mechanical property of concrete specimens was experimentally evaluated by a specific method. The results show that the addition of fly ash or a higher w/b ratio reduces the static yield stress of SCC, the low addition of GGBS increases but the high addition of GGBS decreases the static yield stress of SCC. Both the addition of fly ash, GGBS or retarder and the higher w/b leads to the slower time-dependent increase of static yield stress. The more addition of fly ash, retarder and the higher w/b ratio result in the lower loss of mechanical strength of distinct-layer casting specimens. Finally, the relationship between rheological performance and distinct-layer casting effect for different SCC were discussed.

Keywords: *self-compacting concrete, Rheological performance, Distinct-layer casting, Time-dependent evolution.*

Introduction

Self-compacting concrete (SCC) has been applied in more and more structures in recent years. Due to its ability of filling formworks without vibration, SCC not only reduces the time and difficulty of construction, but also improves the quality of concrete construction. The performance of fresh SCC is generally evaluated by its filling ability, passing ability and stability which are related to rheological performance. The rheological behavior of SCC is usually described by the

Bingham model as Eq.(1) [1-2] and modified Bingham model as Eq.(2) [3-4]. It can be found that the thixotropy of fresh SCC is not considered in conventional tests and the Bingham model.

$$\tau=\tau_0+\mu\cdot\partial\gamma/\partial t \quad (1)$$

$$\tau=\tau_0+\mu\cdot\partial\gamma/\partial t+c\cdot(\partial\gamma/\partial t)^2 \quad (2)$$

where: τ = shear stress (Pa), τ_0 = yield stress (Pa), μ = plastic viscosity (Pa·s), $\partial\gamma/\partial t$ = shear rate (1/s), c = the second order parameter ($Pa\cdot s^2$).

SCC is considered to be thixotropic as it has a high flocculation rate at rest and a high de-flocculation rate when applied a shear rate, the flocculation rate of thixotropic SCC is between 0.1 and 0.5 Pa/s. Roussel proposed the classification of SCC according to their flocculation rate: when the flocculation rate is less than 0.1 Pa/s then it is called non-thixotropic SCC; and higher than 0.5 Pa/s then is called highly thixotropic SCC [5]. The effects caused by thixotropy on fresh SCC can be correlated to the applied shear rate and flow history of SCC, the static yield stress of fresh SCC increases with the rest time before test while a pre-shear before test can reduce the static yield stress. The thixotropic loop is also used to determine the thixotropy in some publsihed documents. Thixotropy can be explained by the potential energy of particle. When the energy given to the particle is lower than a characteristic energy, then the material shows an elastic solid behavior; when it is higher than the characteristic energy then it may overcome the potential energy "wall" and flow, the characteristic energy increases with rest time and can be partial restore by a given shear rate [6]. It has beeen proved that, in short timescales thixotropy is mainly controlled by flocculation and de-flocculation; in longer timescales the dominant affecting factor is hydration process [7].

The static yield stress and its increase rate at rest are related to the formwork pressure, the stability and distinct-layer casting, it has been proved that a low thixotropic SCC has a better distinct-layer casting quality and there is a time after which the two layers cannot mix [8]. There is a short time for SCC to rest before the second layer is cast above it, if the thixotropy of SCC is too serious its static yield stress may increase too much and impede the mix of two layers [9]. There is a critical value of static yield stress above which the two layers can not mix well and result in a weak interface in the final structure. And the weak interface may decrease the mechanical strength and impermeability of concrete structures. The thixotropy of the first layer SCC decides the rest time for SCC to reach the critical static yield stress, while the rheological performance and thickness of the second layer SCC is related to the value of critical static yield stress. Furthermore, the height and pattern of casting may also affect the quality of distinct-layer casting SCC.

In this paper, the rheological behaviors of SCC with different mixing proportions were studied, and several of SCC mixes were selected for experimental measurement of distinct-layer casting by a new method. The relationship between the rheological behaviors and distinct-layer casting performance of SCC was discussed. Accordng to the results, some methods on the basis of controlling rheological behaviors can be found to improve the distinct-layer casting quality of SCC.

Experimental Details

Raw Materials

The cement used is ordinary Portland cement with strength grade of 42.5 according to Chinese standard GB 175-2007. A Class Ⅰ fly ash (FA) was used with a water requirement ratio of 97% according to Chinese Standard GB1596-2005. And the ground granulated blast-furnace slag (GGBS) has a specific surface area of 400m^2/kg (Blaine). Crushed granite gravel was used as coarse aggregate, which had a maximum particle diameter of 25-mm and crushed index of 4.8%. River sand was used as fine aggregate, which was a medium size sand with a fineness modulus of 2.75. A polycarboxylate-based superplasticizer (SP) in liquid state was used which has a solid content of 40% and specific density of 1.07. A sodium gluconate-based retard was used to control the setting time of concrete.

The mixture proportions of SCC are showed in Table 1. All SCC mixtures in this study can meet the requirement of a slump flow between 620 mm and 700 mm and a V-funnel flow time between 10 s and 15 s.

Table I. Mixing proportion of SCC (kg/m^3)

No.	Cement	Water	FA	GGBS	Sand	Gravel	SP	Retarder
C1	530	180	0	0	800	880	4.24	0.53
F1	477	180	53	0	800	880	4.24	0.53
F2	424	180	106	0	800	880	4.24	0.53
F3	371	180	159	0	800	880	4.24	0.53
G1	477	180	0	53	800	880	4.24	0.53
G2	424	180	0	106	800	880	4.24	0.53
G3	371	180	0	159	800	880	4.24	0.53
W1	530	191	0	0	800	880	4.24	0.53
R1	530	180	0	0	800	880	4.24	1.06

Tesing Methods and Process

A RCAD400 rheometer, made in France, was used to measure the rheological parameters of fresh SCC mixtures as showed in Figure 1. As it has been proved that the thixotropy of SCC is mainly attributable to cement paste, the mortars formulated from SCC mixtures were used to determine the rheological perormance for each mixture in this study. The preparation procedure of mortar sample is as follow: mix all dry components for 20 s in a planetary mixer, then add the weighed water and chemical admixture into the dry mixture and blend the wet mixture for another 4 min.

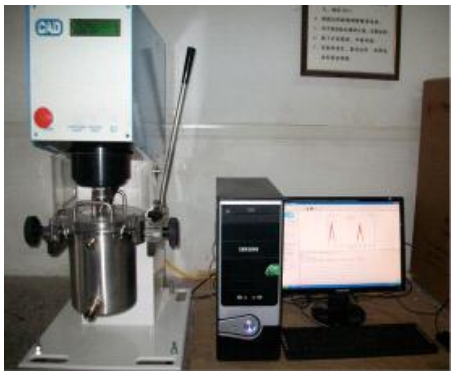

Figure 1. The RCAD400 rheometer used in this study

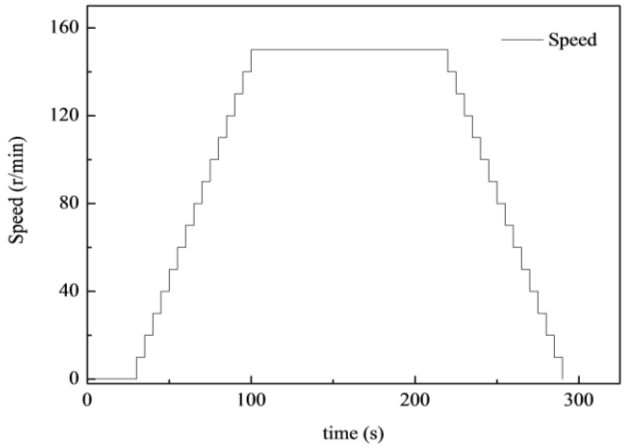

Figure 2. The rotational speed of rheometer

To measure the rheological parameters of mortar, the rotational speed of rheometer was set in an optimum way: at a low speed of 0.1 rev/min for 30 s (step 1) to measure the static yield stress, stepwisely increased to 150 rev/min in 75 s by 15 steps (step 2), then kept at 150 rev/min for 120 s (step 3) to preshear and de-flocculate, and finally gradually decreased to 0 rev/min in 75 s by 15 steps (step 4). On these stages, every step of the increasing and decreasing process lasted 5 s, as showed in Figure 2. To study the influence of rest time the mortar sample was tested again after each 20 min of rest, all samples were prepared to test 4 times. However, some mortars lost the flowability too fast during rest time to finish all tests. The shear stresses at the same shear rate during increasing and decreasing process are different because of the thixotropy of mortar, which is called "thixotropy loop". Although "thixotropy loop" was proved to be not very accurate because it was very depended on test apparatus and procedure, it can be used as a reference of thixotropy. The shear stress during decreasing process can be used to deduce the yield stress of mortar sample. The static yield stress can be seen as the lowest stress needed for a resting SCC to flow and is related to the performance of SCC placed by distinct-layer casting.

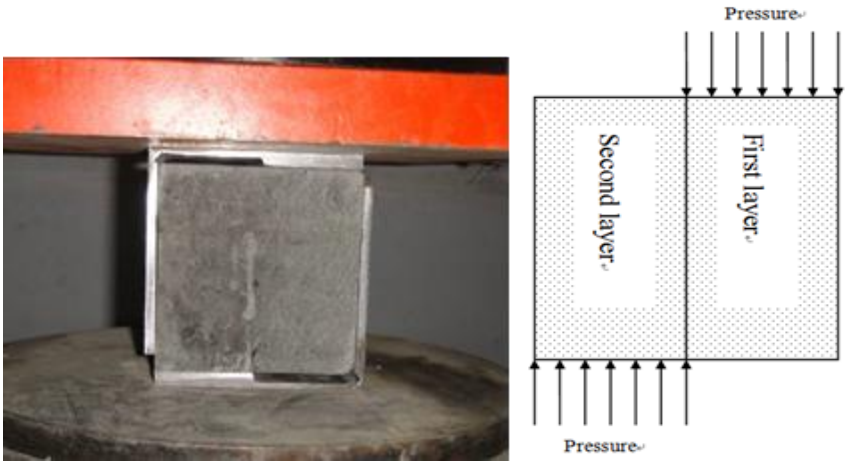

Figure 3. The shear strength measurement of two-layers casting specimen

Distinct-layer casting experiments were carried out for selected concrete mixtures from Table 1. Cubic specimens with size of 100mm×100mm×100mm were prepared in two layers for various times of delay (20 min, 40 min, 60 min) between the first and second casting. The specimens casted without any delay (0 min)were also prepared as control samples for each mixture. After the finish of casting, the specimens were covered with a plastic film for an initial curing of 24 hours at room

temperature, then the specimens were demolded and stored in a foggy room at a temperature of 20±2°C.

After 3, 7 and 28 days of curing, the mechanical strength were carried out on such specimens. To evaluate the influence of distinct-layer casting on mechanical performance of SCC, the shear strength of the interface between two layers was tested by installing a simple metal frame on the specimen and applying a compression load (as shown in Fig. 3). The ultimate pressure upon specimen being broken was recorded for every sample and three specimens were measured for each mixture with the same delay of distinct-layer casting.

Results and Discussion

Rheological Performances of fresh mixtures

The static yield stress was studied under a low shear rate as the mortar started to flow after a specified rest time, and the test result of static yield stress for every mixture after different rest times are shown in Table 2. The thixotropy loop area, the appear viscosity and yield stress extrapolated by the modified Bingham model for every mixture are presented in Table 3.

It can be found that the addition of 10% and 20% fly ash (F1, F2) only reduced the initial static yield stress of fresh mortar from 4.1 Pa to 3.3 Pa and 3.4 Pa, and the addition of 30% fly ash (F3) presented the reduced static yield stress of 2.4 Pa. For all mixtures, the static yield stress increases with rest time, but this increasing tendency is reduced with the more addition of fly ash. The area of thixotropy loop and the apparent viscosity of fresh mortars was decreased by the addition of 20% and 30% fly ash, while the addition of 10% fly ash increased the yield stress a little. The lower static yield stress and apparent viscosity of fly ash mortars could be attributed to the higher stacking density of particles and more free water [10-11], and the sphere particle effect of fly ash. The replacement of fly ash reduced the amount of cement particle, and the activity of fly ash is much lower than cement particle, resulting in a lower influence of rest time. The result showed that the addition of fly ash reduces the static yield stress of fresh mortar at all rest times, and the thixotropy decreases with the increasing addition of fly ash.

The influence of GGBS addition on the rheological parameters was irregular, the addition of 10% GGBS (G1) increased the static yield stress and apparent viscosity of fresh mortar while the addition of 20% and 30% of GGBS (G2, G3) showed an opposite influence. With the addition of GGBS, the area of thixotropy loop and the yield stress extrapolated by the modified Bingham model increased markedly. This

could be attributed to the multangular shape of GGBS particles which may enhance the movement friction among particles.

Table II. Sstatic yield stress at different rest time (Pa)

Time(min)	C1	F1	F2	F3	G1	G2	G3	W1	R1
0	4.1	3.3	3.4	2.4	12.7	1.7	3.0	2.8	4.1
20	158.9	69.6	47.9	60.5	130.7	81.7	71.7	45.6	20.8
40	710.5	102.6	107.5	100.5	392.7	146.9	117.1	187.5	40.8
60	/	170.8	125.2	123.9	/	265.2	140.3	483.1	90.8

The increase of w/b ratio from 0.34 (C1) to 0.36 (W1) decreased all the tested parameter obviously. This can be explained by the higher content of free water which resulted in an increased distance and decreased friction among particles in the mortar. The lower increasing rate of static yield stress with rest time should be beneficial to distinct-layer casting SCC, but the increase of w/b ratio may reduce the final mechanical strength of concrete. The increased addition of retarder had no influence on the initial rheological parameters, but led to the markedly reduced increasing rate of static yield stress with rest time.

Table III. The rheological parameters based on the modified Bingham model

Parameter	C1	F1	F2	F3	G1	G2	G3	W1	R1
Thixotropy loop (Pa/s)	776	897	698	644	1245	1322	1277	634	786
Apparent viscosity (Pa.s)	8.8	9.2	6.2	5.8	20.3	7.8	7.6	5.9	8.7
Yield stress (Pa)	0.4	0.7	0.3	0.2	5.1	1.9	1.2	0.2	0.4

Influence of Distinct-layer Casting on Mechanical Strength

The mixtures of C1, F1, F2, W1 and R1 were selected for the distinct-layer casting experiment. Fig.4 presents the fracture stress of distinct-layer casting SCC specimens with different delays. It can found that the fractrue stress for two-layers casting specimens decreased with the increasing rest time, showing that the defect caused by distinct-layer casting increased. This could be contributed to the development of rheological parameters with time. The disadvantagous effect of distinct-layer casting on fractrue stress could not be eliminated by the increasing curing from 3 days to 28 days. This phenomen of distinct-layer casting can be contributed to the growth of static yield stress and apparent viscosity of the first layer mixtures of SCC, being caused by structuration. When the shear stress caused by the weight of the second layer SCC was not able to break through the resistance of first layer SCC, a weak interface transition area between these two layers

concrete will forms and the coarse particle of the upper layer SCC is not able to enter the bottom layer SCC.

For the specimens without any influence of distinct-layer casting (delay time=0 min), the C1 concrete presented the highest fracture stress and the addition of fly ash or a higher w/b ratio led to a decreased strength as expected. But for the distinct-layer casting with delay of more than 20 min, the fracture stress of C1 was decreased to similar or lower than other mixture specimens. This is related to the higher growth rate of static yield stress with time and severer thixotropy of C1 mixture than other mixtures as mentioned above. According to the experimental results at 3 days curing, about 10% fracture stress loss was measured for the distinct-layer casting specimen of C1 mixture when the delay time was 20 min, while other samples had a loss less than 3%. The loss of fracture stress increased with the increasing delay time of distinct-layer casting, and it could be noticed that for most of the mixtures, there was a critical time beyond which the loss of fracture stress increased significantly. For C1, F1 and F2 the critical time was between 20

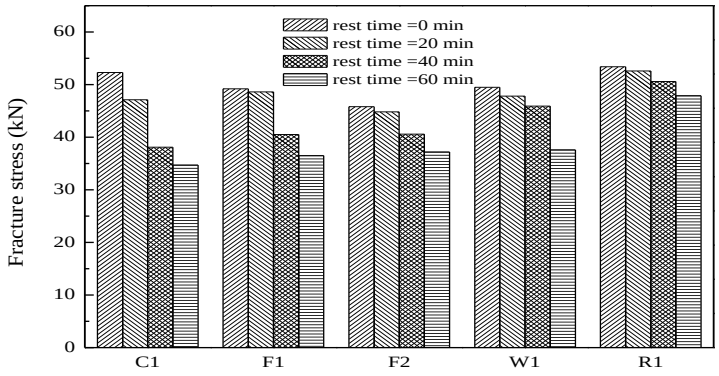

(a) 3 days

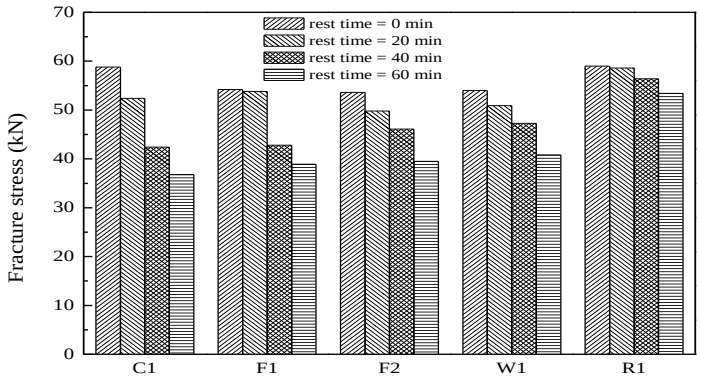

(b) 7days

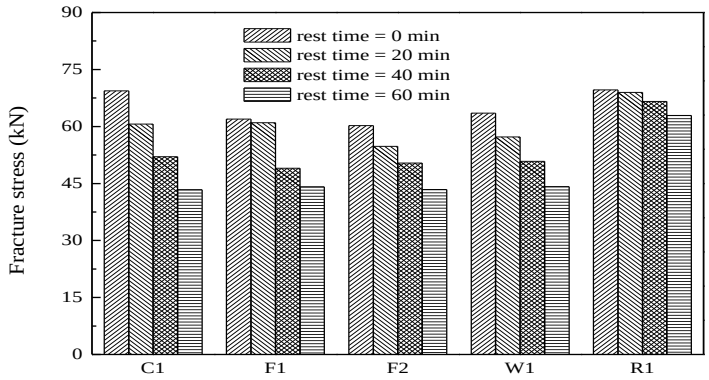

(c) 28 days

Figure 4. The fracture stress of two-layers casting specimen of SCC

and 40 min while for W1 the critical time was between 40 and 60 min and R1 has no such a critical time among 60 min.

From the testing results of specimens at curing age of 7 days and 28 days, it could be found that most of SCC mixtures behaved a higher loss of fracture stress than those at curing age of 3 days when the delay of distinct-layer casting was longer than 40 min. This might be attributed to the slower development with curing age of the degraded interface between two layers. Combining the fracture stress and evolution of rheological parameters with rest time, the concrete mixture with a lower static yield stress and apparent viscosity could have a less loss of fracture stress due to distinct-layer casting.

Conclusions

1) The addition of fly ash reduces the initial static yield stress and its growth with rest time. The addition of 10% fly ash increases the apparent viscosity of SCC mixture while a higher addition of fly ash reduces the apparent viscosity. The addition of fly ash reduces the mechanical strength of concrete while the loss of fracture stress caused by distinct-layer casting is improved.

2) The addition of 10% GGBS increases the apparent viscosity of SCC mixture severely, but the addition of 20% and 30% of GGBS reduces the apparent viscosity of SCC.

3) A higher w/b ratio leads to a lower static yield stress and apparent viscosity, the thixotropy of mortars decreased as the w/b ratio increased. Although the static yield stress was higher than the mortar addition fly ash, the higher w/b ratio has a better result on distinct-layer casting, this could be caused by the more content of free water.

4) A increased dosage of retarder has little influence on the initial rheological parameters of SCC mixture, but decreases the growth of static yield stress with rest time. Therefore, the increased dosage of retarder improves the mechanical strength of distinct-layer casting SCC.

5) For most of SCC mixtures, there is a critical delay time beyond which the loss rate of fracture stress of distinct-layer casting specimens increased markedly, and the critical time is related to the mixing proportion of SCC.

Acknowledgements

This work is funded by the National Natural Science Foundation of China (No. 51578192) and the Program for New Century Excellent Talents in University under Grant (No. NCET-12-0157).

References

[1] Tattersall G.H. (1973), *Mag. Concrete Res.*, vol. 25, n. 84, p.169-172.
[2] Wallevik J. E. (2003), *Rheology of particle suspensions: fresh concrete, mortar and cement paste with various types of lignosulfonates, Norwegian University of Science and Technology*.
[3] Feys D., Verhoeven R., Schutter G. D. (2008), *Cem. Concr. Res.*, vol. 38, n. 7, p. 920-929.
[4] Yahia A., Khayat K.H. (2001), *Cem. Concr. Res.*, vol. 31, n. 5, p. 731-738.
[5] Roussel N. (2006), *Cem. Concr. Res.*, vol. 36, n. 10, p. 1797-1806.
[6] Saak A.W., Jennings H.M., Shah S P. (2001), *Cem. Concr. Res.*, vol. 31, n. 2, p. 205-212.

[7] Jarny S., Roussel N., Rodts S., Bertrand F., Roy R. L. (2005), *Cem. Concr. Res.*, vol. 35, n. 10, p. 1873-1881.
[8] Roussel N. (2005) , *Mater. Struct.*, vol. 39, n. 1, p. 81-91.
[9] Roussel N. and Cussigh F.(2008), *Cem. Concr. Res.*, vol. 38, n. 5, p. 624-632.
[10] Mehdipour I., Razzagh M.S., Amini K., Shekarchi M. (2013), *Constr. Build. Mater.*, vol. 40 n. 3, p. 1029-1037.
[11] Rahman M.K., Baluch M.H. and Malik M.A. (2014), *Constr. Build. Mater.*, vol. 50, n. 1, p. 710-717.

Rheological Behaviour Study of Semi Flowable SCC during CFA Pile-Driving Operations

Mariam Mohaman Dairou[1,2], Yannick Vanhove[1], Chafika Djelal[1], Hassina Kada[1] and Philippe Gotteland[3]

[1] Univ. Artois, EA 4515, Laboratoire de Génie Civil et géo-Environnement (LGCgE), Béthune, F-62400, France
[2] Structure et Réhabilitation, 36 Avenue du Général de Gaulle, Tour Gallieni II, 93170 Bagnolet
[3] Fédération Nationale des Travaux Publics, DTR, Paris, France

Abstract This study is mainly concerned with a concrete placement problem encountered on pile driving jobs using hollow stem augers, namely: the difficulty of introducing a reinforcement cage into fresh concrete. To the best of our knowledge, no current test or recommendation serves to guarantee an appropriate casting technique for lowering a pile without blocking the reinforcement cage from entering into the fresh concrete. At the request of France's National Federation of Public Works (FNTP), a test has been developed to assess the capability of introducing reinforcements into concrete. Moreover, studies have been conducted to determine both the reinforcement embedment capacity vs. pile casting time and the rheological behavior of concrete used to produce the particular pile. This type of concrete is cast without applying vibration, thus offering a highly fluid consistency (SF SCC). The restructuring of concrete, and in particular its thixotropy and loss of workability, alter the capacity of reinforcement to embed into the material, as evidenced by a decrease in such capacity throughout the study (for the given duration and concrete mixes under study). It thus becomes possible to predict ultimate impediments when the extent of concrete restructuring and the sequence for lowering reinforcement cages at the jobsite are both known.

Keywords: *Piles, Fresh concrete, Reinforcements, Thixotropy, Loss of workability, Penetration.*

Introduction

The disorders related to an inadequate load-bearing base of a structure may lead to significant cost overruns or even to a complete structural loss. Consequently,

special attention is paid to building the foundations. The most widespread process in France consists of casting piles bored using a hollow stem auger (CFA piles), which offers an easily implemented and economical solution on a ground cleared of obstacles. This casting protocol encompasses:

- boring, which entails screwing the auger, along with recording progress parameters through the use of sensors;
- concreting of the pile shaft by injecting concrete via the auger's hollow axis while simultaneously raising the auger;
- setting of the reinforcement cage into the fresh concrete by means of gravitation or vibratory pile driving, depending on specific needs.

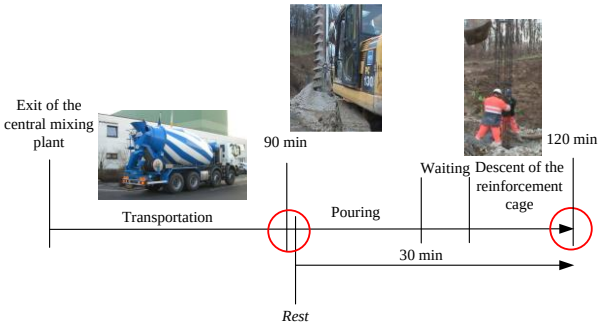

Figure 1. Concrete's life cycle on site.

In 15% of all jobs involving CFA piles, contractors face difficulties when lowering the reinforcement cage. Such was the case at the deep foundation construction site awarded to *Franki Foundations* at the Lille-Fives site (France) : while executing an 8-m high pile, embedment difficulties appeared over the final 3 meters.

These difficulties are correlated in part with the rheological behavior of the concrete as well as with the bleeding phenomenon, both of which pertain to concrete mix design problems. Concrete pile foundations are designed to be pumped and offer a highly fluid consistency (slump average between 16 and 21 cm). Given their level of fluidity, they are quite similar to SF-SCC mix designs developed for slip form paving construction [1].

Fresh concrete undergoes various *in situ* phases during pile casting (cf. Figure 1): transport of the concrete from the mixing plant to the site by means of a truck-mixer; then concreting of the pile shaft by either pumping or gravity flow. During these two phases, the concrete is subjected to a high shear rate (on the order of 10 to 40 s^{-1}), which maintains the material in a disaggregated state. A concrete rest phase begins inside the boring cavity once concreting has been initiated; this phase lasts 30 minutes or longer, extending until the reinforcement cage has been completely lowered, during which time the concrete becomes restructured. The rest period will exert a direct impact on the ease of reinforcement cage placement.

More specifically, studies carried out on yield stress fluids, like concrete (cement pastes, Carbopol solutions, emulsions), reveal a correlation between object displacements in these fluids and their actual yield stresses [2-4]. The goal of this study is thus to evaluate the influence of concrete rheology during the setting of reinforcement cages. It comprises two parts:

- an investigation of concrete rheological behavior: in relying on a widespread pile concrete mix design (B_{0SA0}), employed by the contractor *Franki Foundations* across France's Nord-Pas de Calais region, the influence of admixtures can be effectively examined. In fact admixtures act on concrete yield stress, viscosity, loss of rheology and thixotropy within time.
- An effective characterization of reinforcement embedment into fresh concrete using a technique based on the principles of penetrometry: in addition to the first part, the development of a test device was necessary to compute reinforcement embedment.

Concrete Mix Designs

Table I summarizes the mix designs studied in the laboratory; they all meet the requirements stipulated in Standards NF EN 1536 "Execution of special bored piles for geotechnical works" and NF EN 206/CN "Concrete - Specifications, performance, production and compliance - National complement to Standard NF EN 206". The foundation concretes exhibit the following specific properties:

- the type of cement used is a CEM III A 42.5 N CE CP1 NF, especially well adapted to foundation works;
- C30/37 strength category, equivalent to a minimum characteristic strength of 30 MPa on cylinders and 37 MPa on cubes;
- the targeted consistency is a slump of between 16 and 21 cm;
- the maximum aggregate diameter D_{max} = 20 mm.

The tested mix designs contain 2 sands: the 0/4 Gand sand (siliceous, rolled and washed, extremely clean, containing a high concentration of fines), and the 0/4 TPPL sand (alluvial, screened and washed). Their characteristics (content of clayey fines, coefficient of water absorption, etc.) were measured in the laboratory.

The admixtures introduced were two plasticizers-water reducers (P-WR), both of which were based on lignosulfonate, plus a superplasticizer - high-range water reducer (or SP-HWR) made from polycarboxylate-polyacrylate. The P-WR, just like the SP-HWR, feature very long macromolecular chains that make it possible to deflocculate the grains in contact with water by acting through combined electrostatic and steric effects. The consequence of this set-up is to decrease intergranular friction, in lowering the concrete yield point, thus resulting in a higher slump value. Adding SP-HWR then not only improves the workability of the concrete but extends its period of workability as well [5].

Table I. Concrete mixtures

Proportion (kg/m^3) / Designation	B_{0SA0}	B_{0SA1}	$B_{0SA20.2}$	$B_{0SA20.4}$	Density (kg/m^3)	Absorption (%)
CEM III/A 42,5	350	350	350	350	2 950	-
0/4 Gand	415	415	415	415	2 650	0.2
0/4 TPPL	410	410	410	410	2 570	0.5
6/12 Gaurain	300	300	300	300	2 750	0.5
6/20 Gaurain	590	590	590	590	2 780	0.5
Admixture	0.8%	0.8%	0.2%	0.4%	-	-
E/C	0.54	0.54	0.54	0.54	-	-

B_{0SA0}: Reference formulation, Use of P/WR Pozzolith 399 N. Dry extract=40.7%
B_{0SA1} : Use of P/WR Master Pozzolith 399 N. Dry extract=40%
$B_{0SA20.2}$: Use of SP/HWR Sika Viscocrete Tempo 12. Dry extract=29.5%
SP/HWR proportion =0.2%
$B_{0SA20.4}$: Use of SP/HWR Sika Viscocrete Tempo 12. Dry extract=29.5%
SP/HWR proportion =0.4%

The concrete specimens were produced in strict compliance with Standard NF P18-404 (1981-12-01) entitled: "Concretes - Testing of design, suitability and control - Specimen preparation and storage". In the laboratory, 80-liter mixes were generated according to the procedure described in Figure 2, with the 15-minute idle time proving sufficient for the aggregates to absorb all the water.

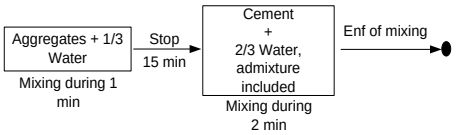

Figure 2. Mixing process.

Laboratory Characterization of Concrete Rheological Behavior

The rheological properties of concrete are characterized over the resting period (30-minute interval) through the use of two tools: the Abrams cone, and the ICAR concrete rheometer.

Abrams cone slump

Abrams cone slump, or more commonly referred to as the "slump test", is the most frequently conducted *in situ* test. It offers an effective measurement of concrete consistency in accordance with the standard NF EN 12350-2. In order to

characterize this consistency within the scope of pile installation, the slump at various concrete ages is measured in the laboratory:

- upon exiting the mixer (t_0): measurement of concrete control with respect to the S4 requirement (slump greater than 18±3 cm) for pile casting;
- after a 30-minute resting time (t_{30}): measurement indicating actual concrete consistency in the pile.

To differentiate reversible concrete restructuring (thixotropy) from irreversible restructuring (aging / loss of workability), a measurement is recorded on the concrete remixed after 30 minutes of resting time (t_{30*}).

As illustrated in Table II, the slump measurement is not applicable to concrete while at rest for 30 minutes (t_{30}) (sliding of the concrete). This measurement does however make it possible to quantify the loss of concrete workability by determining the decrease in slump value from t_0 to t_{30*}. Steadier rheological properties are observed compared to the reference mix design.

Table II. Assessment of concrete workability

	Slump (cm)		
	t_0	**t_{30*}**	**t_{30}**
B_{0SA0}	23±1	19±2	
B_{0SA1}	23±1	22±1	
$B_{0SA20.2}$	17±1	15±1	
$B_{0SA20.4}$	21±2	19±2	

A slump measurement on its own does not provide a characterization of the rheological behavior of a concrete [6]. A rheometer outputting a direct measurement of the intrinsic properties of the concrete specimen has thus been introduced.

The ICAR rheometer

The concrete behaves like a yield stress fluid (i.e. existence of a yield stress above which the material begins to flow) with a given viscosity. A portable vane-type concrete rheometer (ICAR rheometer) was used for this determination (cf. Figure 3.a), by virtue of operating at an imposed shear velocity [7]. Under the same test conditions and analogous to slump measurements, the static yield stress of the concrete τ_S is recorded, in accordance with the protocol described in Figure 3b, along with the dynamic yield stress τ_0. A 0.5 rps pre-shear is applied (i.e. maximum ICAR rheometer speed) so as to both erase the stress history on the specimen and improve test repeatability.

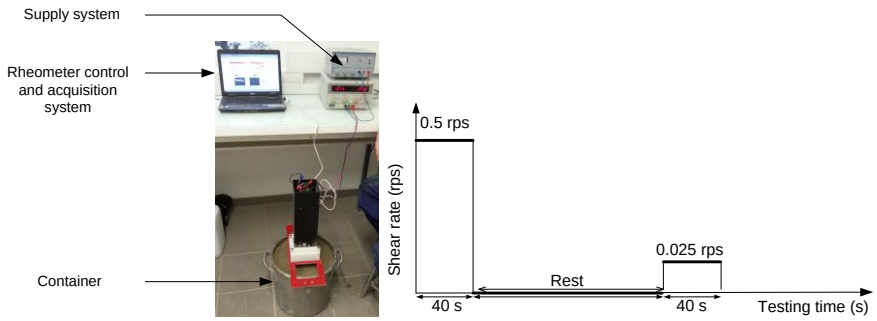

(a) (b)

Figure 3. The ICAR rheometer test: (a) Test set up (b) Static yield stress measurement

As illustrated in Figure 4, whenever the concrete is placed at rest for 30 minutes, it becomes restructured. This transformation is reflected by an increase in its yield stress from t_0 (end of the mixing period) to t_{30} (after 30 minutes of rest): AB. The measurement conducted on the remixed concrete after the 30-minute rest period (t_{30*}) reveals the increases due to both a loss of concrete rheology (C'C) and the concrete thixotropy on its own (CB).

The results obtained from this investigation are listed in Table III.

As mentioned above, admixtures affect the concrete yield stress as well as its period of workability. The plasticizer-water reducer (P-WR) A_1 and superplasticizer-water reducer (SP-HWR) A_2 ensure the concrete maintains its rheological properties (i.e. they limit the loss in reference concrete workability by at least 60%) (cf. Tableau III). Moreover, depending on admixture performance, the initial yield stress of the concrete will vary in magnitude: in using SP-HWR A_2, which is less active than the P-WR A_0 and A_1, the concrete yield stress rises. Beyond the 30 minutes of permanent rest, this time allowance for the concrete to become restructured (i.e. when the duration required for the initial yield stress to double has elapsed) is used to identify its level of thixotropy [8]. A ranking of concretes, from most thixotropic to least, can then be performed (B_{0SA0}, $B_{0SA20.4}$, B_{0SA1} and $B_{0SA20.2}$). The full array of factors can be incorporated during this step (namely yield stress, loss of workability and thixotropy), so as to study their influence on reinforcement embedment.

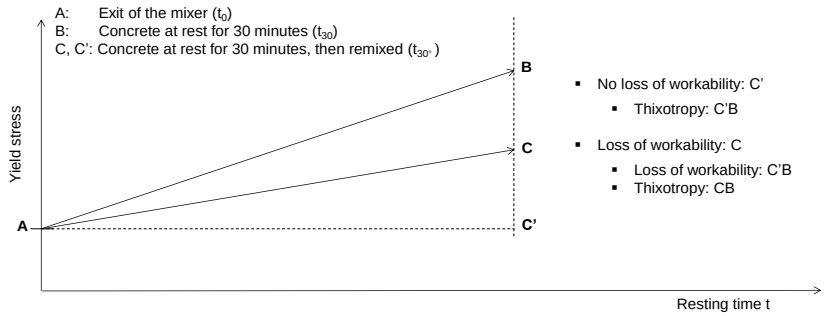

Figure 4. Kinetic of concrete structural buildup at rest

Table III. Rheological characterization of concrete mixtures

	Yield stress t_0 (Pa)	**Loss of workability** t_{30}-t_{30*} (Pa)	**Thixotropy** t_{30*}-t_0 (Pa)
B_{0SA0}	156.1	182.5	474.0
B_{0SA1}	115.3	58.3	255.8
$B_{0SA20.2}$	354.1	18.4	400.4
$B_{0SA20.4}$	188.2	40.5	548.3

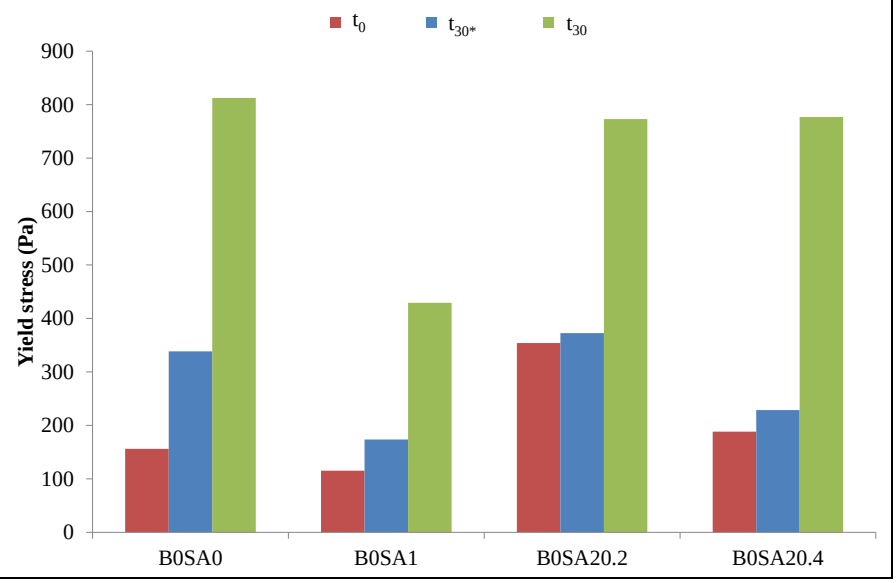

Characterization of the Capacity to Embed Reinforcements into Concrete

A technique for characterizing the embedment of a reinforcement cage into the reference concrete B_{0SA0} has been developed herein. This technique enables determining the embedment capacity of a typical pile reinforcement cage (circular) within the studied concretes.

The test set-up (cf. Figure 5) serves to reproduce a 45-cm diameter pile in the laboratory. Edge effects have been taken into account, in indicating that the 14-cm cage coating exceeds 5 x Dmax = 10 cm. The reinforcement cage guide explains how to avoid committing errors during cage centering or introducing a slant during its lowering.

The heights of both the concrete ($h_{concrete}$) and cage embedment (h) are measured at t_0, t_{30*} and t_{30}, analogously to the previous rheological measurements.

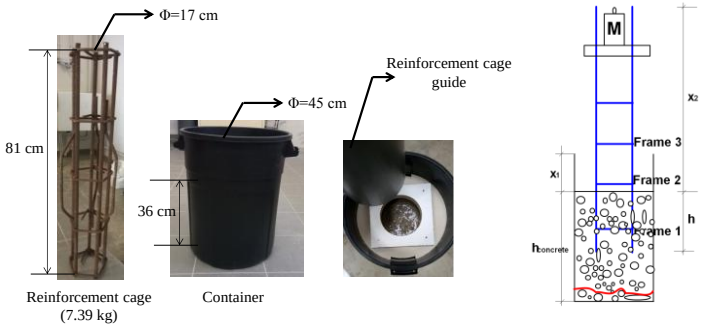

Figure 5. Measurement of reinforcement cage penetration in fresh concrete

From one test to the next, the concrete height varies slightly (from 33.5 cm to 35.3 cm). It is now possible to define the cage embedment rate E, i.e. the ratio of cage embedment height (h) to concrete height ($h_{concrete}$) expressed as a percentage.

The relationship of reinforcement embedment rate vs. yield stress (both static and dynamic) of the concrete (cf. Figure 6) proves the existence of yield stress values above which a rejection of reinforcement cage embedment can be observed: τ_s > 780 Pa (for the case of concretes still at rest after 30 minutes, t_{30}), and τ_0 > 220 Pa (for the case of concretes upon exiting the mixer at times t_0 and t_{30*}). This same trend relative to slump values also displays embedment rejection for a slump < 18 cm.

Subsequent to this laboratory study, testing was conducted at 2 jobsites. The concretes used for the tested pile casting were B_{C1} (BPS NF EN 206/CN XF1-

XC3-XC4-XD1 (F) C30/37 Dmax 20 S4 Cl 0,65) and B_{C2} (BPS NF EN 206/CN XF1 (F) C30/37 Dmax 20 S3 Cl 0,65).

For the first mix design B_{C1}, the τ_0 value of the concrete at t_0 (i.e. removal from the truck-mixer) lies very close to the yield stress value defined previously. Upon implementing the test device, the embedment of a reinforcement cage is seen to be rejected at t_0. Around the pile, a major difficulty was experienced over the final 3 meters in lowering an 8-m long cage. For the B_{C2} design, with a similar τ_0 value, this difficulty was only observed over the final 0.80 m when lowering 13-m long cages. Such a difference can be explained by the reliance on pumping to cast the concrete. Given the high rate of shear being exerted, the τ_0 value of concrete at the pump outlet is less than that measured at the time of removal from the truck-mixer.

It should be pointed out that mix design B_{0SA1} does not follow the general trend (possible reinforcement cage embedment into the concrete for a yield stress = 400 Pa). It would be necessary to combine this yield stress measurement with other concrete properties (e.g. stability, viscosity) to explain this kind of singularity.

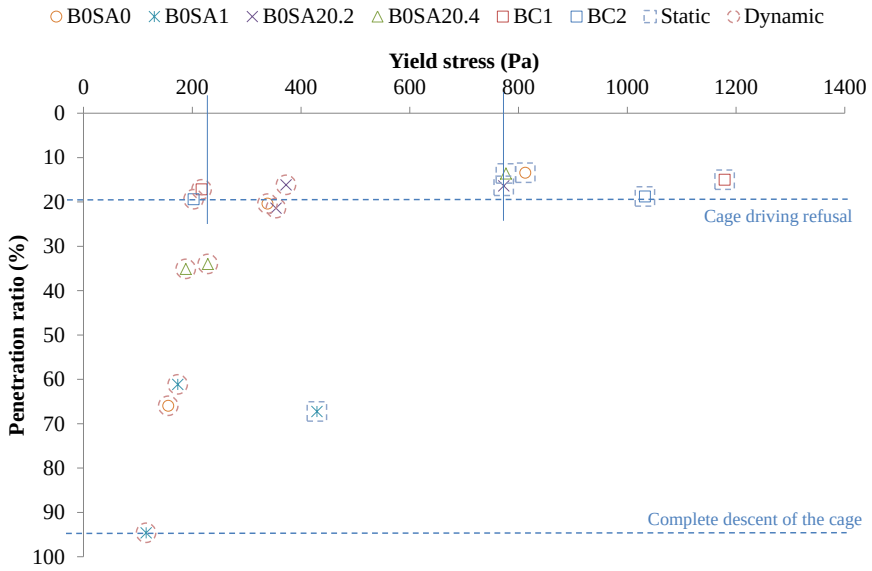

Figure 6. Evolution in reinforcement cage penetration ratio vs. concrete yield stress

Conclusion and Outlook

The efficiency of CFA pile casting is directly correlated with the injected concrete properties. In addition to proposing a tool for the *in situ* characterization of concrete at rest, based on the principles of penetrometry, this study has highlighted

the influence of pile concrete rheological properties on the reinforcement embedment capacity. The restructuring of concrete at rest involves its loss of workability along with thixotropy, which in turn is reflected by a higher yield stress. Through the use of admixtures, the strong rheological behavior of these concretes can be guaranteed. Hence, the increase in yield stress is due to the thixotropy of the concrete alone. It is essential for this thixotropy not to reach excessive values, i.e. a rise in the concrete yield stress, both static and dynamic, up to approx. 200 Pa when lowering the reinforcement cage. Otherwise, depending on cage dimensions, the rejection of reinforcement becomes a real risk. Two preconditions must therefore be adopted for foundation concretes:

- recommended yield stress values (and slump values, if possible) at t_0 that must remain quite low: less than 200 Pa (i.e. a category resembling SF SCC, which typically feature a yield stress varying from 100 to 200 Pa);
- thixotropy threshold values that over time remain low as well.

References

[1] Kejin Wang, Surendra P. Shah, Jim Grove, Peter Taylor, Paul Wiegand, Bob Steffes, Gilson Lomboy, Zhuojun Quanji, Lu Gang, and Nathan Tregger (2011) *Self-Consolidating Concrete—Applications for Slip-Form Paving: Phase II*, Technical report, pp 6,30.

[2] D. Lootens, P. Jousset, L. Martinie, N. Roussel, R.J. Flatt (2009) *Yield stress during setting of cement pastes from penetration* test, Cement and Concrete Research 39 (2009) 401–408.

[3] P.H.T. Uhlherr, J. Guo, T.-N. Fang and C. Tiu (2002) Static measurement of yield stress using a cylindrical penetrometer, Korea-Australia Rheology Journal Vol. 14, No. 1, pp. 17-23.

[4] Jalila Boujlel (2012) *Déplacement d'un objet à travers un fluide à seuil : Couche Limite, Contrainte Seuil et Mouillage*, Thèse de Doctorat de l'Université Paris–Est.

[5] Laeticia Patural (2011) Modes d'action des ethers de cellulose sur la rétention d'eau des mortiers à l'état frais, Thèse de Doctorat de l'Ecole Nationale Supérieure des Mines de Saint-Etienne.

[6] Hu Chong (1995) *Rhéologie des bétons fluides,* Thèse de Doctorat de l'Ecole Nationale des Ponts et Chaussées.

[7] Koehler E. P. and Fowler D. W. (2004) *Development of a portable rheometer for fresh portland cement concrete*, Research report International Center of Aggregates Research –105–3F.

[8] Nicolas Roussel (2006) A theorical frame to study stability of fresh concrete, Materials and structures DO1 10.1617/S11527-005-9036-1.

Influence of Shape, Size, and Solid Concentration of Particles on Rheological Properties of Self-Consolidating Mortar

Kabagire K Daddy [1], Paco Diederich [1], Ammar Yahia [1] and Mohamed Chekired [2]

[1]Université de Sherbrooke, 2500, Boulevard de l'Université, Sherbrooke (QC), J1K 2R1, Canada,

[2]Institut de Recherche d'Hydro-Québec, Varennes, QC J3X 1S1, Canada.

Abstract The rheology of particles suspensions depend on the volume fraction, shape of particles, the rheology of suspending medium (liquid phase), and the maximum packing density of particles. Although the effect of solid fraction on the viscosity of suspensions can be estimated using empirical model, such as the Krieger-Dougherty model, the influence of grading and shape of particles is not taken into consideration. The objective of this investigation is to evaluate the effect of the size, volume fraction, and the shape of particles on rheological properties of self-consolidating mortar (SCM). Different types of aggregates, including glass beads and crushed limestone sand with maximum size ranging between 0.6 and 3.0 mm were evaluated. The suspending phase is proportioned using limestone filler and a constant solid fraction (water-to-powder ratio, w/p) of 0.30. The suspending phase was optimized to achieve a given range of rheological properties. The test results showed that the yield stress of the suspension is mainly influenced by the volume fraction, shape, and mean diameters of the suspended coarse particles, while the viscosity is mainly influenced by the volume fraction, gradation, and the shape of particles. Furthermore, the excess paste thickness is shown to affect rheology of suspension. For a given aggregate size, gradation, and shape, the excess paste thickness should be adjusted to achieve a certain rheology of suspension.

Keywords: *Cement suspension, Excess paste theory, Particle shape, rheology, Self-consolidating concrete.*

Introduction

The rheology of self-consolidating concrete (SCC) is essentially controlled by the rheology of its corresponding mortar, coarse aggregate content, and packing

density of solid particles. SCC can be regarded as a biphasic materials where solid particles are suspended in mortar. As SCC becomes more widely used, and given the complexity to achieve targeted rheological properties, efforts are needed to better understand the factors governing rheology of the suspending phase, i.e. mortar. For a given aggregate size and grading, the rheology of mortar should be tailored to ensure adequate flow and stability performances of SCC. Controlling the rheology of mortar can then facilitate SCC mixture optimization, material selection, and testing production issues, such as aggregate size and grading, etc., without the need to prepare concrete mixtures. Such an approach can reduce time, effort, and cost needed to develop and control complex flowable materials such as SCC [1].

Many studies attempted to estimate the rheological parameters of concrete by assuming that it's a suspension in which solids are dispersed into a fluid phase. The complexity in studying SCC as a biphasic material is due to the broad size range of solid particles. To overcome this complexity, flow properties of SCC can be estimated using the suspended phase, such as mortar, sieve mortar, or micro-mortar [2] [3]. A number of theoretical and empirical models have been developed to predict the viscosity of concentrated suspensions [4] [5] [6]. Most of them express the fact that viscosity increases with the solid concentration of the suspension, and tends towards infinity when the concentration is close to the maximum packing value.

The effects of size, shape, and grading of solid particles on rheological properties of concrete, mortar or cement paste are well documented in literature [7] [8], and attempts have been made to predict rheological behavior of suspension taking into account the mechanical contribution of non-colloid inclusions [5] [4]. Various models predicting rheological properties of suspension are available in literature [9]. One of the most useful model is the semi-empirical equation of Krieger and Dougherty for monodisperse suspensions [4]. This model has been used to predict the relative viscosity of granular materials [10]. It has been also used for cement paste [7]. Although the theoretical Φ_m value of monodisperse spheres is 0.74 (in a face-centered cubic configuration, FCC array), experimental observations have shown that loose random packing is close to 0.60, and that dense random packing (or random close packing, RCP) is close to 0.64. For higher volume fraction (Φ greater than 20%), non-spherical particles, a most efficient model developed by Irvin Krieger and Thomas Dougherty [4] is suitable to predict relative viscosity by taking into account particle volume fraction and intrinsic viscosity which is itself a function of grading and shape of particle.

The yield stress of cement-based materials originates from the attractive inter-particles forces in flocculated systems. It is affected by the volume fraction of solids, particle sizes and their distribution, and the presence of admixtures. Mahaut et al. [8] conducted an experimental study to evaluate the mechanical contribution of mono-disperses particles to yield stress and concluded that the relative yield

stress value can be predicted using Chateau – Ovarlez – Trung model [5]. They reported a packing density of mono-disperse spherical particle of 0.57 [3] for isotropic dispersion, while G. Ovarlez et al. found 0.605 for anisotropic dispersion [11].

Although these models provided alternative tool for evaluating the relationship between rheological properties of a suspension between its fluid phase and particles properties, their applicability is mostly limited to mono-size dispersed particles. The study presented herein aims at understanding the effect of aggregate size and distribution and shape of particles on rheology of self-consolidating mortar (SCM). The experimental investigation on which are based the predicting models will be assess.

Materials, Mix Proportioning, and Testing Procedures

The suspending phase is simulated by an inert limestone filler suspension. The limestone filler has a specific density of 2.70, and a finesse similar to a general use (GU) cement. The obtained limestone suspension showed a non-thixotropic behavior a low yield stress. A polycarboxylate based High-Range Water-Reducing Agent (HRWRA) was used to ensure a well dispersed suspension and self-consolidating properties. The HRWRA has a specific density of 1.07 and solid fraction of 40%. On the other hand, two different types of particles are evaluated, including spherical glass beads and a crushed limestone aggregate. Three different sizes of glass beads corresponding to 1, 2, and 3 mm [Figure 1, (a) and (b)] are evaluated. These three mono-size beads are then combined in 33% of each in order to simulate a spherical grading curve. On the other hand, three different fraction of crushed limestone corresponding to 0.60-2.50 mm, 1.25-2.50 mm, and 0.60-1.25 mm [figure 1 (c) to (e)] were evaluated. The crushed limestone particles were washed to remove the fine powder dust before their use. For each aggregate type and size, the packing density values were determined using a cyclic gyratory compacting method [13]. The packing density of glass beads was measured using a shaking table.

(a) (b) (c) (d) (e)

Figure 1. Glass beads : (a) 2 mm (b) 3 mm and crushed limestone aggregate : (c) 1.25-2.5 mm (d) 0.6-2.5 mm (e) 0.6 – 1.25 mm

The limestone suspension were proportioned using a fixed water-to-powder ratio (W/P) by mass, of 0.30 and a HRWRA dosage of 0.64%, by mass of powder. The mixing sequence consisted in introducing first the mixing water and HRWRA. Then, all the powder is introduced and mixed for 120 s at low speed. After a rest period of 90 s, and after scraping the remaining paste on the bowl edges, a final

mix of 180 s is applied at high speed before performing rheological measurements of paste. Finally, mortar mixture is obtained by adding beads or crushed limestone sand particles considering the volume of paste given the volume fraction of solid particles. Once the mortar introduced into the bowl of the rheometer, the mixture received a manual mixing for 30 sec to ensure uniform distribution inside the gap. Five volume fractions of solid particles ($\Phi = V_p /(V_p+V_{fp})$ (where, V_p is particle volume fraction and Vfp is the filler volume fraction)) ranging between 0.1 and 0.5 are studied (Table 1). The values on table are for beads with density 2.50, and for sand particle the density of 2.65 have to be considered.

Table I. Beads/sand + filler paste mixture for rheological measurement

Beads/Sand + paste proportion					
Volume of sample (mL)	Beads/sand volume fraction	Paste volume fraction	*Bead/sand* mass (g)	Paste mass (g)	Total proportion volume
920	0.0	1.0	0/0	1701	1
920	0.1	0.9	233/249	1531	1
920	0.2	0.8	466/500	1361	1
920	0.3	0.7	699/748	1191	1
920	0.4	0.6	931/998	1021	1
920	0.5	0.5	1164/1247	850	1

For each mixture, the rheological properties of paste is determined using coaxial cylinders rheometers. At the same time, rheological properties of mortar suspensions is determine using a same time of rheometer. The shear protocol for paste and paste + particle mixtures is given on Figure 2(a) and (b) respectively.

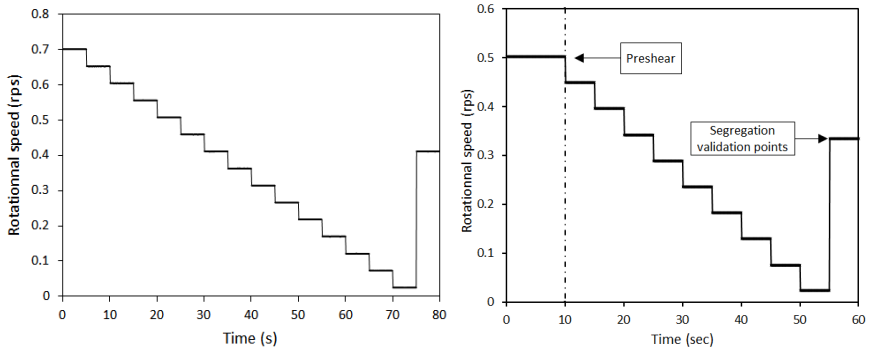

(a) (b)

Figure 2. Shear protocol used to assess rheology of (a) paste and (b) self-consolidating mortar

Determination of the relative excess paste thickness and packing density

The excess paste is defined as the volume of paste which is not used to fill the voids between the compacted aggregate (packing density) [14] [2]. This paste can separate and increase the distance between solid particles and, therefore, contribute in reducing the inter-particle friction between solid particles. On the other hand, the excess paste thickness (e_p) corresponds to the excess paste volume divided by the specific surface of the solid particles. The relative excess paste thickness can be defined as follow:

$$\Gamma_{e_p} = \frac{e_p}{P_d} \tag{1}$$

Were, Γ_{e_p} is the relative excess paste thickness, e_p is the excess paste and P_d is the particle mean diameter. The relationship yield to the following equation:

$$e_p = \Gamma_{e_p} \times P_d \tag{2}$$

For an aggregate with a diameter x, the excess paste volume can be calculated as follow:

$$Ve_{px} = e_{px} \times s_x \tag{3}$$

Where S_x is the specific surface of particle of diameter x. For n particles of a diameter x, the total volume can be determined as follow:

$$Ve_{px} = n_x \times Ve_{px} \tag{4}$$

$$Ve_{px} = n_x \times \Gamma_{e_p} \times P_{dx} \times s_x \tag{5}$$

This volume can be generalized for different series of grading as follow:

$$Ve_p = \Gamma \sum_i^n n_i s_i P_{di} \tag{6}$$

The relative excess paste thickness can then be determined as follow:

$$\Gamma = \frac{Ve_p}{\Gamma \sum_i^n n_i s_i P_{di}} \tag{7}$$

Results and Discussion

Effect of Size and Volume Fraction of Solid Particles on Rheological Properties

The relative viscosity of suspension (i.e. mortar) as a function of the solid fraction of glass bead and crushed limestone particles are summarized in Figures 3 (a) and (b), respectively. The measured viscosity values of mortar were modeled using the Krieger Dougherty model given by the following equation: $\frac{\eta\Phi}{\eta_s} = \left(1 - \frac{\Phi}{\Phi_m}\right)^{-[\eta]\Phi_m}$, where, Φ_m is the maximum packing fraction of particles, η_Φ is the apparent

viscosity of the suspension, η_s is the apparent viscosity of the interstitial phase, Φ the solid volume fraction, Φ_m is the maximum volume concentration of particle, and $[\eta]$ is the intrinsic viscosity, which is a measure of the effect of individual particle on viscosity suspension. As particle concentration approaches the maximum packing of particles (Φ_m), the relative viscosity of the mixtures tend to diverge and converge to infinite value.

As can be observed in Figures 3 and 4, the relative viscosity and relative yield stress increase with solid volume fraction, regardless of the type and size of suspending particles. However, the use of spherical glass particles resulted in lower relative viscosity than those obtained with crushed limestone particles. In the case of spherical glass particles, the size of beads (from 1 to 3 mm) did not showed a significant effect on the relative viscosity of suspensions, regardless of the packing density of spherical particles. In the case of crushed limestone particles, a substantial increase in the relative viscosity beyond a certain solid fraction, regardless of the size of particles. This suggests that the shape and grading of particles have an important effect on the relative viscosity of suspensions. Also, the limestone particle of size comprised between 0.6-1.25 mm has a greater effect on relative viscosity than particle of size between 0.6-2.50 mm, which is probably due to the packing density of the materials (Table. 2).

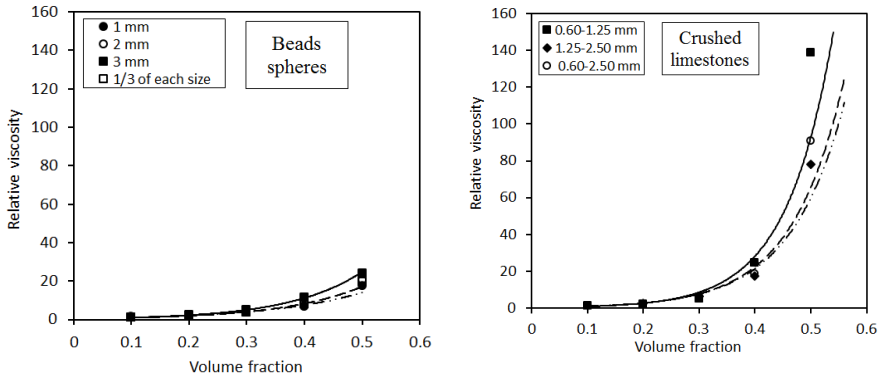

(a) (b)

Figure 3. Variation of the relative viscosity of glass beads (a) and crushed limestone particles (b) suspension with volume fraction

In the case of relative yield stress, the use of both aggregate types (spherical particles vs. crushed limestone) showed a substantial increase in yield stress with solid fraction. Also, the test results revealed the increase in yield stress is more important in the case of particles with higher value of maximum size, especially in the case of spherical glass particles. This might possibly due to reduction in inter-particles distance, thus resulting in higher inter-particles friction and collisions.

These results did not allowed to identify the effect of shape and packing density of suspended particles on the relative yield stress values.

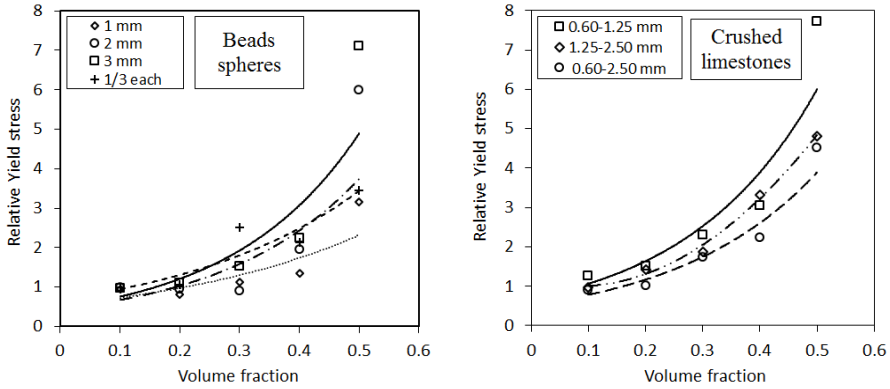

(b) (b)

Figure 4. Variation of the relative yield stress of glass beads (a) and crushed limestone particles (b) suspension with volume fraction

Effect of shape of particles on rheological properties

In order to take into consideration the shape, size, and the grading on flow properties, the excess paste theory is exploited. This approach was shown to be useful in studying the relationship between SCC and its Concrete Equivalent Mortar (CEM) [2]. Test results presented in Figure. 5 showed that the maximum size of solid particles affect both plastic viscosity and yield stress of mortar. For a given particle size and grading, the increase in excess paste thickness reduced the rheological parameters. On the other hand, for a given excess paste thickness, the plastic viscosity and yield stress values increased with the size of particles. This increase is less important when the excess paste thickness is over a certain value (approximately an excess paste thickness of 1 mm).

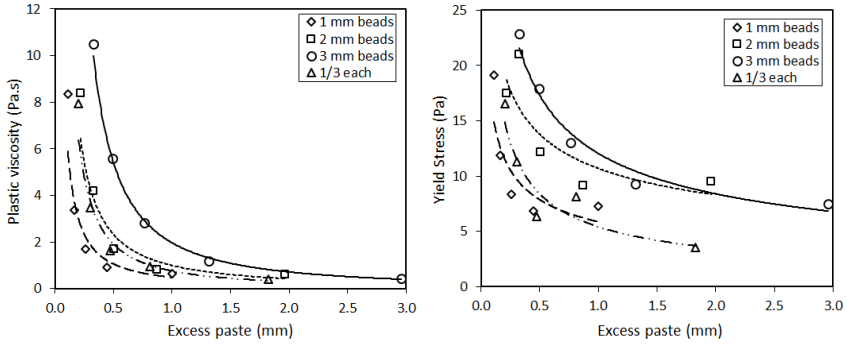

Figure 5. Relationship between excess paste thickness and rheological properties of beads

In the case of crushed limestone sand particles, the grading is shown to have a slight effect on the rheological parameters. The three grades showed comparable rheological parameters. However, it is observed that the increase in plastic viscosity is less important in the case of particle having wide graded distribution.

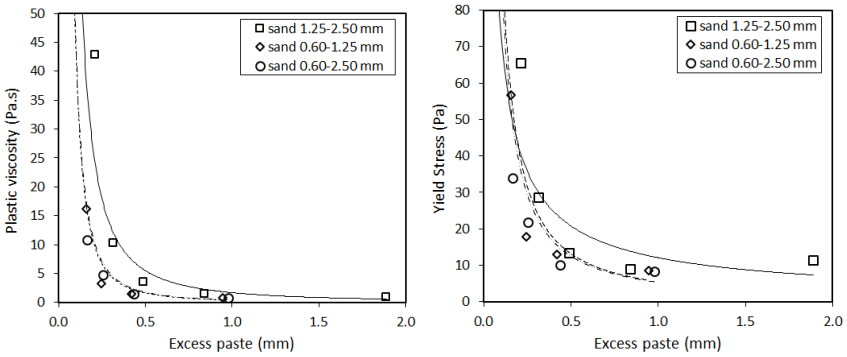

(a) (b)

Figure 6. Relationship between excess paste thickness and rheological properties of crushed limestone sand

Prediction of rheological properties as function of the shape of particles

The effect of shape among both spherical and crushed limestone sand particle can be estimated using the excess paste theory and considering the rheology of the suspending phase. As shown in fig. 7, the rheological parameters (i.e. plastic viscosity and yield stress) of both particles types (spherical vs. crushed) decrease with the excess paste thickness. On the other hand, the difference between the rheological parameter values obtained with spherical and crushed particles is mainly due to their shape. As can be observed, good relationship were proposed to predict the plastic viscosity and yield stress as function of the relative excess paste thickness for each particle shape. In general, the shape of particles did not have a significant effect beyond a certain value of the relative excess paste thickness.

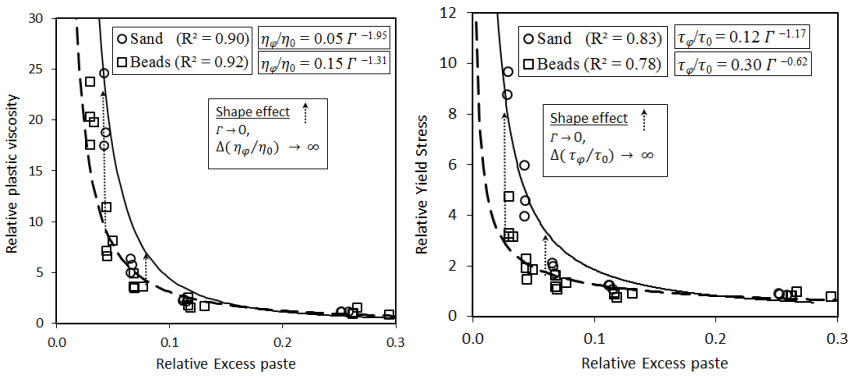

(a) (b)

Figure 7. Relative plastic viscosity (a) and relative yield stress (b) in term of relative paste thickness

Conclusions

The effect of content, size, and shape of particles on the rheological parameters of self-consolidating mortar was evaluated. Based on the test results presented in this paper, the following conclusion can point out:

1. The plastic viscosity and yield stress of self-consolidating concrete increase with solid particles fraction.
2. The use of spherical glass particles resulted in lower relative viscosity than those obtained with crushed limestone particles. Then, the size of spherical beads (from 1 to 3 mm) did not showed a significant effect on the relative viscosity of suspensions.
3. In the case of crushed limestone particles, a substantial increase in the relative viscosity beyond a certain solid fraction can be observed, regardless of the size of particles.
4. The increase in solid fraction resulted in substantial increase in yield stress, regardless of the shape of particles (spherical vs. crushed limestone). Also, the increase in yield stress is more important in the case of particles with higher maximum size, especially in the case of spherical glass particles.
5. Good correlations to predict the yield stress of suspensions are proposed for both shapes of particles. These correlations showed that the rheological parameters (i.e. plastic viscosity and yield stress) decrease with the excess paste thickness.

References

[1] A. C. I. C. 237R, “Self-Consolidating Concrete ,” American Concrete Institute, Farmington Hills, MI, 2007.

[2] D. Kabagire, P. Diederich, and A. Yahia, “New insight into the equivalent concrete mortar approach for self-consolidating concrete,” *J. Sustain. Cem. Mater.*, pp. 1–10, Mar. 2015.

[3] F. Mahaut, S. Mokéddem, X. Chateau, N. Roussel, and G. Ovarlez, “Effect of coarse particle volume fraction on the yield stress and thixotropy of cementitious materials,” *Cem. Concr. Res.*, vol. 38, no. 11, pp. 1276–1285, Nov. 2008.

[4] I. M. Krieger and T. J. Dougherty, “A mechanism for non-Newtonian flow in suspensions of rigid spheres,” *Trans. Soc. Rheol.*, vol. 3, no. 1, pp. 137–152, 1959.

[5] X. Chateau, G. Ovarlez, and K. L. Trung, “Homogenization approach to the behavior of suspensions of noncolloidal particles in yield stress fluids,” *J. Rheol. (N. Y. N. Y).*, vol. 52, no. 2, p. 489, Mar. 2008.

[6] Z. Toutou and N. Roussel, “Multi Scale Experimental Study of Concrete Rheology: From Water Scale to Gravel Scale,” *Mater. Struct.*, vol. 39, no. 2, pp. 189–199, Mar. 2007.

[7] L. Struble and G.-K. Sun, “Viscosity of Portland cement paste as a function of concentration,” *Adv. Cem. Based Mater.*, vol. 2, no. 2, pp. 62–69, 1995.

[8] F. MAHAUT, “Suspension de particules dans un fluide à seuil: approche expérimentale,” *... Congrès Français ...*, 2007.

[9] P. F. G. Banfill, “RHEOLOGY OF FRESH CEMENT AND CONCRETE,” vol. 2006, pp. 61–130, 2006.

[10] M. R. GEIKER, M. BRANDL, L. N. THRANE, and L. F. NIELSEN, “On the effect of coarse aggregate fraction and shape on the rheological properties of self-compacting concrete,” *Cem. Concr. aggregates*, vol. 24, no. 1, pp. 3–6.

[11] G. Ovarlez, F. Bertrand, P. Coussot, and X. Chateau, “Shear-induced sedimentation in yield stress fluids,” *J. Nonnewton. Fluid Mech.*, vol. 177–178, pp. 19–28, Jun. 2012.

[12] R. Hunter, “Foundations of colloid science,” 2001.

[13] Nordtest, “Nordtest Method (NT BUILD 427) for Fresh Concrete: Compactibility with IC-tester,” *Nord. Scand. Inst.*, no. Espoo, pp. 1–4, 1994.

[14] C. Kennedy, “The Design of Concrete Mixes *,” *Concrete*, vol. 36, no. 373, 1940.

A Diphasic Approach to Evaluate the Rheological Properties of Self-consolidating Concrete

Kabagire K Daddy [1], Paco Diederich [1], Ammar Yahia [1] and Mohamed Chekired [2]

[1] Université de Sherbrooke, 2500, Boulevard de l'Université, Sherbrooke QC, J1K 2R1, Canada
[2] Institut de Recherche d'Hydro-Québec, Varennes QC J3X 1S1, Canada

Abstract A diphasic approach was evaluated to predict the rheological parameters of self-consolidating concrete (SCC). SCC is considered as a diphasic material in which coarse particles are suspended in the matrix. The suspending phase was simulated at two different scales corresponding to paste and mortar (particles less than 5 mm). On the other hand, two different types of mortar were considered: sieved mortar and theoretical mortar. Various SCC mixtures were proportioned with different water-to-binder ratios (w/b) and coarse aggregate contents. This approach allowed to evaluate the contribution of coarse aggregate content on rheological properties of SCC. The excess paste theory was also used to highlight the effect of inter-particle distance on yield stress. Test results showed the possibility to predict the rheological parameters of SCC from those of its corresponding mortar.

Keywords: *Flow performance, Rheology, Fine particles, Excess paste, Self-consolidating concrete.*

Introduction

Self-consolidating concrete (SCC) can spread into place, fill the formwork, and encapsulate the reinforcing steel without any mechanical consolidation [1]. The rheological properties of SCC have marked effect on its structural performance, including bond and durability. SCC becomes an attractive solution for civil engineering construction to enhance productivity, reduce construction duration, and improve performance and surface quality. Such performance depends on the rheology of suspending medium and mixture composition. In addition to the rheology of suspending phase, the particle size distribution, or gradation, of the aggregate fraction is one of the most influential factor affecting flow performance

of SCC. Indeed, the volume and shape of aggregate control the interaction forces between solid particles, including frictional and collisional forces. Studies conducted to evaluate the effect of coarse aggregate shape and volume fraction reported that the aspect ratio, the angularity, and surface texture of solid particles affect both the viscosity and yield stress [2][3]. For a given aggregate grading, the ability of concrete to flow is related to the volume of suspending phase (paste or mortar) to fill the void volume among the aggregate as well as coat the aggregate particles to reduce the inter-particles friction.

Achieving highly flowable and non-segregating SCC depends on many parameters such as the mix design, casting methods, intricacy of the element to cast, and the density of reinforcement. Because of the various influencing parameters, many attempts have been evaluated to proportion SCC following a scientific approach rather than an empirical one. For example, statistical design plans were developed to optimize SCC mixtures with adequate flow and stability performance [4] [5]. The concrete equivalent mortar (CEM) approach [6] has been used to highlight the existing relationship between the SCC and its CEM [7] [2]. This approach showed limited success because many parameters vary at the same time, which may not allow a good appreciation of the sole effect of each parameter [10]. Multi-scales approaches have also been used to predict fresh properties of SCC given the rheology of matrix (cement paste or mortar) and solid inclusions (sand and/or coarse aggregate) [3] [8] [9]. For example, a diphasic approach has been used to predict the properties of SCC. The appropriate selection of the matrix phase that can better predict the concrete properties is a very important step in using the diphasic approach to predict the properties of SCC. The matrix can include cement paste, sand, and fines particles from the coarse aggregate (less than 5 mm). Although these methods are shown to be effective in evaluating the effect of different mixture parameters on flow performance of SCC, they are limited to a given set of materials and range of properties. The objective of this study is to evaluate the applicability of a diphasic approach to predict the rheological properties of SCC. Various SCC mixtures were proportioned with different water-to-binder ratios (W/B), aggregate volumes, and sand volume-to-paste volume ratios (SV/PV).

Experimental Program

The experimental program undertaken in this study consisted of two phases. Phase 1 consisted of proportioning various SCC mixtures that cover a wide range of coarse aggregate content and W/B ratios. All the investigated mixtures were prepared with ~~a~~ W/B of 0.30, 0.35, and 0.45 and a sand-to-total aggregate ratio ranging between 0.44 and 0.59. The coarse aggregate volume varied between 27 and 34%, and between 0.87 and 1.1 for the paste-to-sand volume ratio. For each SCC mixture, the required HRWR dosage to achieve the targeted slump flow of 700 ± 100 mm was determined. The mixtures proportioning of investigated SCC mixtures are summarized in Table I. For each mixture, its corresponding paste and

mortar matrix was prepared and characterized in Phase 2 of this study. In addition to the theoretical mortar, the sieved mortar was also obtained by sieving the concrete right after mixing on a 5-mm sieve.

Table I. Mixture proportioning of investigated SCC mixtures VS/VP = 1

SCC mixtures*	W/B	Coarse A. (kg)	Sand (kg)	Binder (kg)	Water (kg)	SP (% by mass of binder)
0.30-26-1	0.30	707	981	536	160	0.42
0.30-30-1		815	928	505	152	
0.30-34-1		924	875	474	142	
0.35-26-1	0.35	707	981	499	175	0.28
0.35-30-1		815	928	471	165	
0.35-34-1		924	875	442	155	
0.45-26-1	0.45	707	981	438	197	0.22
0.45-30-1		815	928	413	186	
0.45-34-1		924	875	388	174	
0.30-26-1.1	0.30	707	1030	503	151	0.42
0.30-34-0.87		924	818	503	151	
0.35-26-1.10	0.35	707	1026	471	165	0.28
0.35-34-0.87		924	814	471	165	
0.45-26-1.10	0.45	707	1027	413	186	0.22
0.45-34-0.87		924	815	413	186	

*Mix ID: W/B-CA (%)-SV/PV

Materials and test methods

The investigated mixtures were proportioned using a ternary binder containing 70 % of a general use cement (GU), 25 % of fly ash, and 5 % of silica fume. The binder is complying with ASTM C150 specifications. A crushed limestone aggregate with a maximum size of 14 mm and a water absorption of 0.40% and a siliceous 5-mm sand having a water absorption of 0.9% were employed. A polycarboxylate based high-range water-reducing agent (HRWRA) with a solid content of 40% and a density of 1.08 was incorporated to secure self-consolidating properties. The concrete was mixed in 60-liters batches using a drum rotating blades. The mixing sequence consisted in mixing first the coarse aggregates, sand, and half of total mixing water for 60 seconds. Then the binder is added and mixed for 30 seconds. The remaining water along with HRWRA is then added and the concrete is mixed for an additional 150 seconds. After a rest period of 120 seconds, the mixing was resumed for 180 seconds before sieving the mortar. Immediately at the end of mixing, the temperature, unit weight, slump flow, V-funnel, L-box and rheological properties are determined. In parallel to concrete testing, the rheological properties of sieved mortar were determined.

For each SCC mixture, the corresponding theoretical mortar was also obtained by removing the coarse aggregate greater than 5 mm. On the other hand, the paste matrix was obtained from mortar mixture by removing sand particles. The mortar mixtures were prepared in 2-L batches using a Hobart mixer. The mixing sequence was similar to that for SCC. The paste mixtures were mixed in 1-L batches using the same mixer used for mortar. The mixing sequence consisted in premixing the HRWRA and water for 30 sec before introducing the binder during 30 sec while the mixer is turning at low speed. After 30 seconds of rest, the mixing was resumed at high speed for 60 seconds. The rheological properties were determined immediately after mixing using coaxial cylinders rheometers for paste, mortar, and concrete. The shear protocol used for determining rheological parameters for concrete and mortar is given on Figure 1(a), while for paste is shown in Figure 1 (b*)*. The Bingham model were considered to determine rheological parameters.

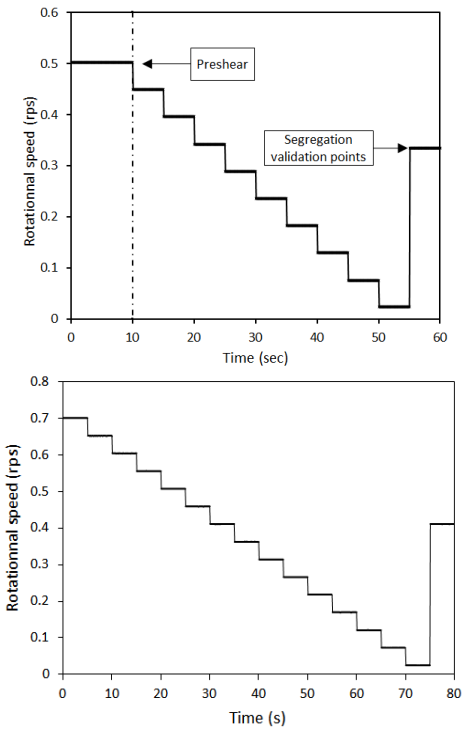

(a) (b)

Figure 1. Shear protocol for (a) mortar and concrete (b) paste

Test results and Discussions

The properties of investigated SCC and corresponding mortar mixtures are summarized in Table II. On the other hand, the rheological parameters of SCC mixtures are presented in Figure 2. As can be observed, all the investigated SCC

mixtures achieved slump flow and T50 values within the recommended range [1]. In general, SCC with a T50 less than 2 seconds are considered as low viscosity mixture. SCC mixtures proportioned with a W/B of 0.45 can be considered as low viscosity mixtures and probably higher risk of segregation (VSI 2) can be expected with these mixtures. Furthermore, mixtures proportioned with 34% of coarse aggregate and less superplasticizer dosage failed to satisfy the L-box criteria of 80% due to blockage of concrete during flow.

In terms of rheological parameters, in general all the investigated SCC mixtures are within the rheological diagram zone suggested in reference [10]. However, the SCC mixtures made with relatively higher W/B and coarse aggregate volume content are outside the recommended zone (Figure 2). These mixtures showed either a low viscosity and high yield stress or high viscosity and low yield stress values, hence resulting in higher segregation and blocking ratio during flow. Although all the mixtures achieved a relatively high slump flow, an important change in yield stress values is observed. This suggests that slump flow is not sufficient to evaluate the flow performance of SCC. All corresponding sieved and theoretical mortar mixtures provided self-consolidating material with values of slump flow between 200 and 300 mm.

Table II. Properties of investigated SCC, sieved, and theoretical mortar mixtures

	SCC					Sieved mortar	Theoretical mortar
Mixtures ID	Slump flow (mm)	T50 (s)	L-box (%)	V-Funnel (s)	VSI	Slump flow (mm)	
0.30-26-1	820	3.10	93	14.94	1	290	270
0.30-30-1	740	3.10	88	24.19	1	285	270
0.30-34-1	650	6.50	20	53.09	1	240	270
0.35-26-1	685	3.06	80	8.28	1	220	240
0.35-30-1	710	1.53	73	9.35	1	250	240
0.35-34-1	580	5.91	54	19.07	1	220	240
0.45-26-1	700	1.12	47	3.47	1	225	270
0.45-30-1	700	1.30	59	3.66	2	225	270
0.45-34-1	620	2.09	29	20.19	3	235	270
0.30-26-1.10	800	2.66	89	10.81	1	280	205
0.30-34-0.87	880	1.32	87	8.70	1	310	240
0.35-26-1.10	640	4.18	73	9.90	1	190	180
0.35-34-0.87	740	2.44	98	6.87	1	275	240
0.45-26-1.10	695	1.78	94	3.00	1	246	210
0.45-34-0.87	740	0.75	56	6.91	2	250	265

Mix ID: W/B-CA (%)-SV/PV

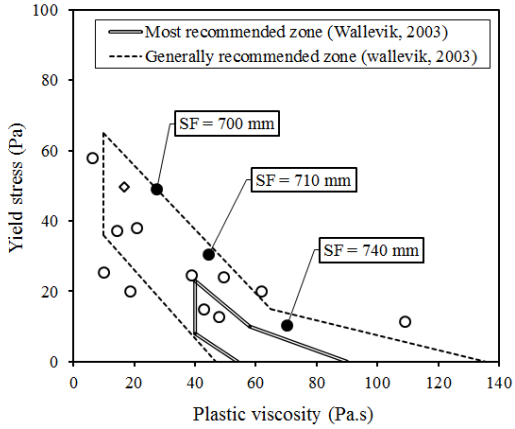

Figure 2. Rheological diagram of the investigated mixtures

Relationship between SCC and its Mortar Matrix

The relationship between slump flow values of SCC and those of the corresponding mortar matrix is presented in Figure 3.

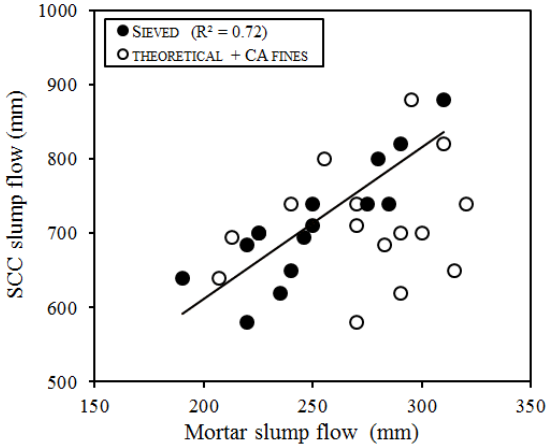

Figure 3. Relationship between SCC and mortar slump flow

In general, good correlation is observed between slump flow values of SCC and those of the corresponding mortar matrix. The sieved mortar seems to provide better correlation with SCC than the theoretical mortar. An attempt of taking into account the fines particles contained in coarse aggregate in designing theoretical mortar (Theoretical + CA fines) did not result in any improvement of the correlation.

The comparison between theoretical and sieved mortar (Figure 4 (a)) revealed that the theoretical mortar containing fines particles of coarse aggregate is better correlated with sieved mortar when considering plastic viscosity. However, a poor correlation was observed in the case of yield stress. On the other hand, the results showed that the ratio SV/PV is an important parameter that should be taken into account for comparing plastic viscosity. Indeed, better correlation between theoretical and sieved mortar is observed for a fixed value of SV/PV of 1 (figure 4(b)). In such case, the effect of fines particles from coarse aggregate is not significant. This suggests the importance of either fixing the SV/PV or including the fine particles from coarse aggregate to design the theoretical mortar. In addition to the extra fines particles of coarse aggregate, the discrepancy between sieved and theoretical mortar can also be attributed to mixing energy and shear regime of SCC due to the presence of CA (sieved mortar). In the case where SV/VP is not constant, sieved mortar can be used as a suspending phase to understand the contribution of coarse aggregate on plastic viscosity and yield stress values of SCC.

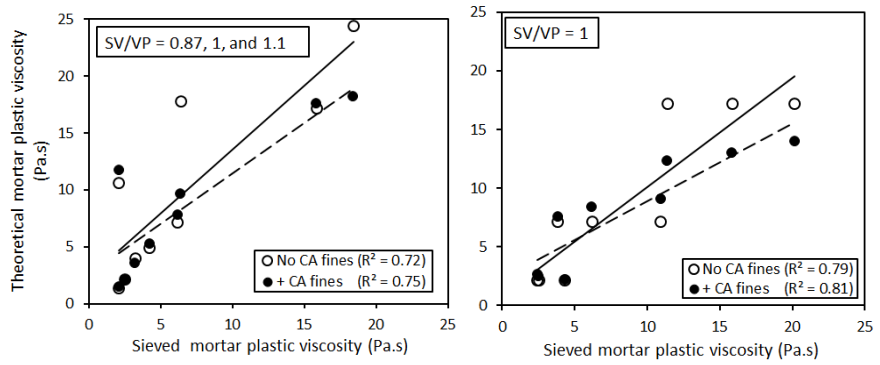

(a) (b)

Figure 4. Relationship between plastic viscosity of theoretical and sieved mortar mixtures (a) SV/ PV = 0.87, 1, and 1.1 (b) SV/VP = 1

As can be observed in Figure 5, for a constant SV/PV of 1, the plastic viscosity of SCC is well correlated with the viscosity of mortar.

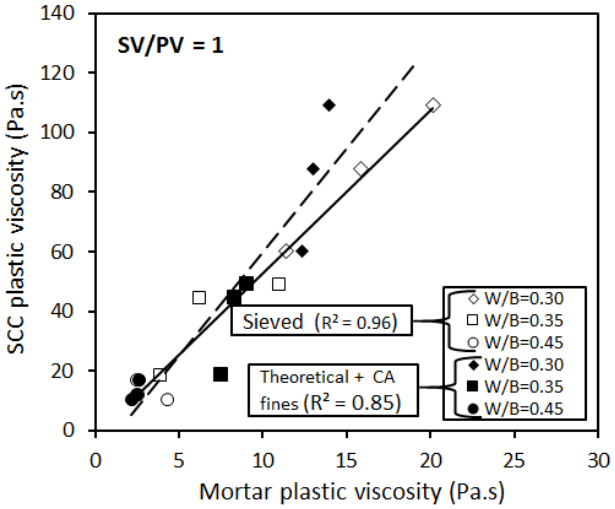

Figure 5. Correlation between plastic viscosity of SCC and mortar

Prediction of the Viscosity of SCC

The Krieger Dougherty model was used to predict the viscosity of SCC (using the paste and mortar matrix as suspending phases. This model is given by the following equation: $\frac{\eta(\Phi)}{\eta_s} = \left(1 - \frac{\Phi}{\Phi_m}\right)^{-[\eta]\Phi_m}$, where Φ is sand volume (between 48-54%) or coarse aggregate content (between 63-67%). In our approach, we primarily assumed that the interstitial phase corresponds to the paste. First, the paste was used to predict the plastic viscosity of the corresponding mortar (Figure 6(a)). The mortar was then used to predict the viscosity of SCC (Figure 6(b)).

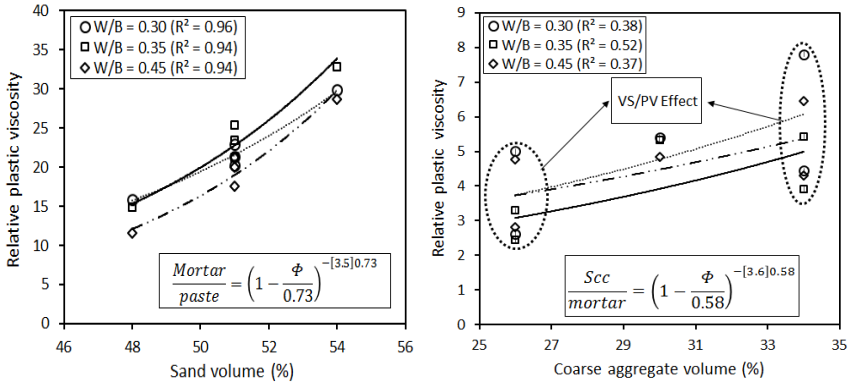

(a) (b)

Figure 6. Prediction of the viscosity of a) mortar and b) SCC

As can be observed, the paste phase can be used to predict the viscosity of mortar using the Krieger-Dougherty model. Besides, the viscosity of SCC can be estimated using the mortar as suspending phase. As expected, the viscosity of suspension increased with solid concentration. It is worthy to mention that the use of paste or mortar as suspending phases did not allowed to accurately predicting the viscosity of SCC. This complexity might be due to the number of variables, including the SV/PV, the packing density of the paste (different W/B), difference in shear regime from SCC to paste (presence of coarse aggregate in the case of SCC), variation in packing density of sand and coarse aggregate, etc. Indeed, as can be observed in Fig. 7, for a constant SV/PV, viscosity of SCC can be accurately estimated from its corresponding mortar using Krieger-Dougherty model.

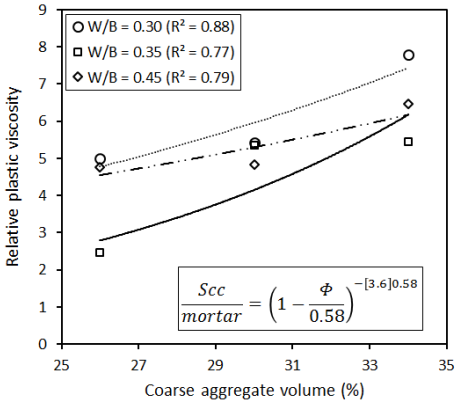

Figure 7. Prediction of SCC relative plastic viscosity for SV/PV = 1

Prediction of the Yield stress of SCC

As mentioned in previous section, the SV/PV showed a tremendous effect on viscosity of SCC, but did not showed any effect on yield stress. Furthermore, the test results showed that there is no direct relationship between the yield stress of SCC and its corresponding matrix (Figure 8 (a)). Since the yield stress is function of the distance between particles, the exploitation of the excess paste thickness may

be useful in predicting the yield stress of SCC.

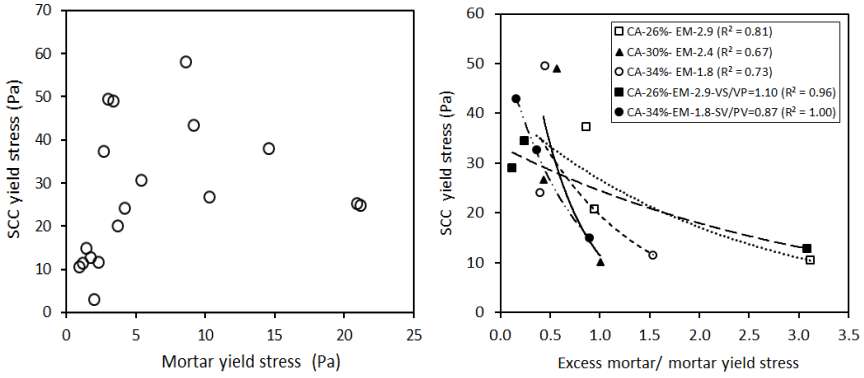

Figure 8. Correlations between a) yield stress of mortar and SCC and b) yield tress of SCC and mortar by taking into account the excess mortar thickness

As can be observed, the yield stress values of SCC are well correlated with those of the corresponding mortar when the excess mortar thickness is taken into account. The excess mortar thickness is determined according to the method proposed in reference [7]. For the investigated mixtures, 3 excess mortar thickness values corresponding to 1.8, 2.4, and 2.9 mm were obtained for coarse aggregate content of 34, 30, and 26%, by volume, respectively. The increase in mortar paste thickness (increase in mortar volume) result in reducing the yield stress of SCC. Moreover, the increase in yield stress of suspending phase (i.e. mortar) increased the yield stress of SCC. This suggests that both the yield stress and the volume of suspending phase should be taken into consideration to achieve targeted yield stress of SCC. In the case of suspending mortar with relatively high yield stress, relatively higher volume of mortar may be required to reduce the yield stress of SCC.

Conclusions

In this study, the relationship between rheological properties of various SCC mixtures and their matrix was investigated. The matrix was studied at different scales (paste and mortar). Based on the results presented in this paper, the following conclusions can be pointed out:

1. Rheological properties of SCC are found to be well correlated with those of its equivalent mortar. In the case of theoretical mortar, it is essential to include the fine particles contained in coarse aggregate.
2. Good correlations between rheological parameters of sieved mortar and theoretical mortar are observed.

3. Sand volume-to-paste volume (SV/PV) play an important effect on the correlation between SCC and its corresponding mortar. Accurate prediction of viscosity of SCC as function of the viscosity of its corresponding mortar is observed when the SV/PV is constant.
4. Krieger Dougherty model is found to be accurate in predicting the viscosity of SCC using the corresponding suspending phase (i.e. mortar). However, the use of paste phase was not successful in predicting viscosity of SCC.
5. Good correlation is proposed to predict yield tress of SCC based on the yield stress of its corresponding mortar. Both the yield stress and the volume of mortar should be taken into consideration. In the case of suspending mortar with relatively high yield stress, relatively higher volume of mortar may be required to reduce the yield stress of SCC.

References

[1] A. C. I. C. 237R, "Self-Consolidating Concrete ," American Concrete Institute, Farmington Hills, MI, 2007.

[2] T. K. Erdem, K. H. Khayat, and A. Yahia, "Correlating rheology of self-consolidating concrete to corresponding concrete-equivalent mortar," *ACI Mater. J.*, vol. 106, no. 2, 2009.

[3] Z. Toutou and N. Roussel, "Multi Scale Experimental Study of Concrete Rheology: From Water Scale to Gravel Scale," *Mater. Struct.*, vol. 39, no. 2, pp. 189–199, Mar. 2007.

[4] A. Ghezal and K. H. Khayat, "Optimizing Self-Consolidating Concrete with Limestone Filler by using Statistical Factorial Design Methods," no. 99, 2003.

[5] "Khayat - Utility of statistical models in proportioning self-consolidating concrete.pdf." .

[6] A. Schwartzentruber and C. Catherine, "La méthode du mortier de béton équivalent (MBE)—Un nouvel outil d'aide à la formulation des bétons adjuvantés," *Mater. Struct.*, vol. 33, no. 8, pp. 475–482, 2000.

[7] D. Kabagire, P. Diederich, and A. Yahia, "New insight into the equivalent concrete mortar approach for self-consolidating concrete," *J. Sustain. Cem. Mater.*, pp. 1–10, Mar. 2015.

[8] C. F. Ferraris, "Measurement of the rheological properties of high performance concrete: State of the art report," *J. Res. Natl. Inst. Stand. Technol.*, vol. 104, no. 5, pp. 461–478, 1999.

[9] F. Mahaut, S. Mokéddem, X. Chateau, N. Roussel, and G. Ovarlez, "Effect of coarse particle volume fraction on the yield stress and thixotropy of cementitious materials," *Cem. Concr. Res.*, vol. 38, no. 11, pp. 1276–1285, Nov. 2008.

[10] O. H. Wallevik, "Rheology—a scientific approach to develop self-compacting concrete," in *Proceedings of the 3rd international RILEM Symposium on Self-Compacting Concrete*, 2003, pp. 23–31.

Influence of Aggregate Shape on Mixing and Rheological Behaviour of Low-Cement Self-Compacting Concrete

Markus Samuel Rebmann[1], Fábio Alonso Cardoso[1], Gustav Hawlitschek[2] and Rafael Giuliano Pileggi[1]

[1] Department of Construction Engineering - Escola Politécnica, University of São Paulo
[2] Department of Mining Engineering - Escola Politécnica, University of São Paulo

Abstract Morphology of aggregates has significant impact on the workability of concretes because it affects particle mobility during flow, and influences aggregate packing as well, which can increase considerably the volume of paste required to promote an adequate rheological behaviour for self-compacting concretes (SCC). Characterization of particle shape using callipers or static image analysis are very time consuming to generate data for statistically reliable results. On the other hand, a recent technique based on Dynamic Image Analysis (DIA) is able to characterize both size and shape of a large number of particles between 0.1-30 mm in a few minutes. The present paper used DIA (Camsizer®) to characterize rounded and lamellar types of fine and coarse aggregates used to produce SCC compositions with low cement content (180 kg/m^3). The effect of the shape of aggregates on fresh properties of SCCs was studied on compositions with the same particle size distribution. Mixing and rheological behaviour were determined by a novel mortar and concrete mixing rheometer (Poli-USP) with planetary configuration. Concretes were also characterized by traditional fresh SCC tests (slump-flow, L-box and V-funnel). Results indicate that the irregular shape of aggregates adversely affected both mixing and flow of concrete, increasing torque levels during the mixing process and shear cycles. This effect was even more significant when the lamellar sand fraction was present. Furthermore, the correlation between shape (sphericity and aspect ratio) and rheological (mixing energy, mixing torques, yield torque and equivalent to plastic viscosity) quantitative parameters can be useful for studying and developing SCC compositions.

Keywords: *Self-compacting concrete. Low cement concrete. Aggregate shape. Dynamic Image Analysis. Mixing rheometer. Rheology.*

Introduction

Several studies have reported the influence of the shape of aggregates on the characteristics of cement-based compositions. In general, spherical shapes are preferred because they promote better packing and have less interference on flow lines pattern. Deviations from the spherical shape increases the porosity of mono-sized particle packing, due to the corners of the grains and the increase of friction between them [1-3]. Experimental evaluation of mortars with different shaped sands (natural and crushed) have shown that the less spherical the particles, the lower the degree of packing of the mixture. In that case, a greater amount of paste becomes necessary to attain the same workability [4]. The worse packing degree of the compositions caused several adverse effects: greater tendency to bleeding, higher plastic shrinkage, absorption and capillarity; and reduction on mechanical strength (compression, tensile, bending) and modulus of elasticity [5].

Despite the recognized importance of particle morphology on fresh and hardened properties of cement-based materials, few studies have assessed quantitatively this physical feature, mainly by the difficulty of carrying out the measurements. The shape is often evaluated only in a visual and subjective comparative way, or the quantitative methods are highly time-consuming and operator dependent, show low reproducibility, and have low statistical significance [5-7].

An attempt to overcome these limitations led to the development of Dynamic Image Analysis (DIA), in which the particles pass in front of a light source and a high-resolution camera captures the projected image at very high frequencies. Particles are feed in a controlled speed so that few particles are captured in each image, preventing the overlapping of projections. Images are quickly evaluated by software that detects each particle and calculates several geometric parameters (size and shape). Easily many thousands or even millions of particles can be considered, extending in an extraordinary way the statistical representativeness of the results. This method only recently became feasible with the development of hardware and software powerful enough to acquire, transmit, analyse and store the large quantity of generated data.

Using DIA several shape parameters can be calculated, such as sphericity, aspect ratio, symmetry and convexity, among which the first two are highlighted (Figure 1). The aspect ratio depicts the elongated format. The smaller this value, the more elongated the particle, whereas, values closer to one denote more equiaxed particles. Sphericity is related to the angularity or macro-roughness of the particle: more angular particles have smaller sphericity, while particles with smoother surface display values closer to one.

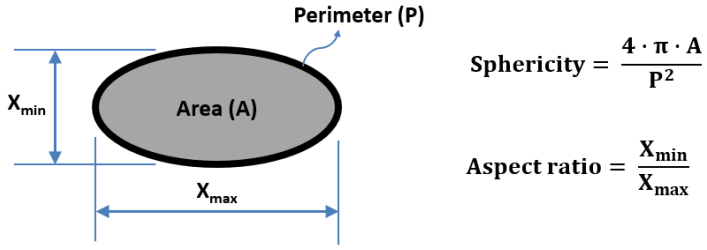

Figure 40. Shape parameters of particles

Objective

The purpose of this article is to assess the influence of morphology of coarse and fine aggregates on the rheology of a self-compacting concrete (SCC) with low cement consumption (more sustainable).

Experimental

Materials

In order to evaluate the effect of the morphology on fresh behaviour of a SCC, crushed aggregates with different morphologies were employed: more rounded coarse (CR) and fine (FR) aggregates and more lamellar coarse (CL) and fine (FL) aggregates. The aggregates were chosen from materials available in the market based only on a comparative and visual analysis. A high early strength Brazilian Portland cement (CPV-ARI) and two calcium carbonate fillers, dispersed by a polycarboxylate superplasticizer, formed the cement paste. The choice of this variety of materials sought to obtain a highly packed composition with low cement consumption. The coarser filler, with particle size distribution close to the cement, was chosen with the aim of replacing the cement, and the finer filler to fill the voids between the cement grains in the paste (micro-filler effect).

For particle size and shape characterization of the aggregates, Dynamic Image Analysis with free fall dispersion was performed by a CAMSIZER-L®, which is able to analyse particles between 30 µm and 30 mm [8]. For the fine particles (fillers and cement) laser diffraction was used for measuring the size distribution. Figure 41 shows the particle size distributions. The fine aggregate is a composition of three sands (coarse, medium and fine). Through selective screening, similar size distributions were produced, despite the different morphologies. The match of the curves shows that this goal was achieved. Densities were measured by helium gas picnometry, obtaining the following values in g/cm^3: aggregate CR (2.70), aggregate CL (2.92), aggregate FR (2.72), aggregate FL (2.87), cement (2.92),

filler (2.65) and microfiller (2.65). The superplasticizer has density of 1.09 g/cm^3 with 30% of solid content.

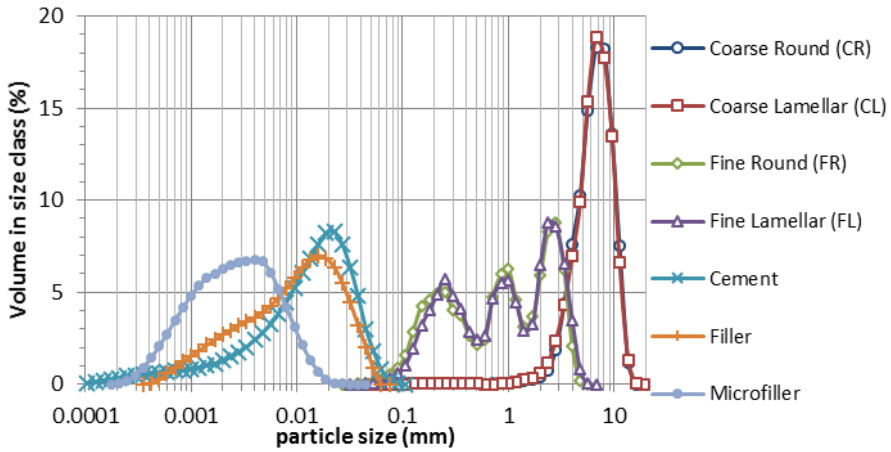

Figure 41. Particle size distribution of the materials

Compositions

The work started with a previously adjusted concrete with self-compacting properties and low cement content, produced with the more rounded aggregates (CR/FR). Then three other concretes were prepared, first replacing by volume only the coarse aggregates (CL/FR), then only the fine aggregates (CR/FL), and finally both aggregates (CL/FL). The compositions are shown in *Table XXVI*. All have the same volumetric water/solids ratio (19,2 %), but the bulk quantities differ slightly from each other due to the different densities of the aggregates and mainly by variations in the air content (measured by gravimetric method).

Table XXVI. Concrete compositions [kg/m^3]

Composition	**CR/FR**	**CL/FR**	**CR/FL**	**CL/FL**
Coarse Rounded (CR)	659	-	694	-
Coarse Lamellar (CL)	-	723	-	758
Fine Rounded (FR)	911	926	-	-
Fine Lamellar (FL)	-	-	1012	1024
Cement CPV-ARI	178	181	188	190
Filler	143	145	150	152
Microfiller	98	100	103	105
Water	140	142	147	149
Air	12.5%	11.2%	7.9%	6.9%
Superplasticizer	0.9% of the mass of the fines (cement + fillers).			

Mixing procedure

Batches of 17 L of concrete were prepared in a novel mortar and concrete mixing rheometer (Poli-USP, Figure 42). Details of the mixing procedure are described in Figure 44.

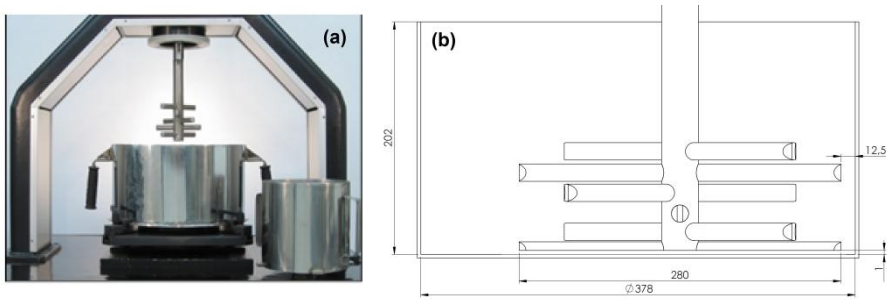

Figure 42. (a) Rotational Rheometer Poli-USP for mortars and concretes; (b) Illustration showing the concrete container and the impeller with six blades in spiral configuration used in planetary setup for mixing and rheological tests

Rheometry and traditional fresh SCC tests

Mixing rheometry: The mixing behaviour of the concretes was assessed with the rheometer by measuring the effort (torque) to maintain the rotation of the impeller constant (126 rpm) along the mixing procedure.
Shear cycles: Immediately after mixing the concrete, a shear cycle was performed to evaluate the rheological behaviour (with the same setup shown in Figure 42). The shear cycle consists of increasing the speed of the impeller (6 to 253 rpm) in 8 steps of 8 s each, and then slowing it down following the same steps.
Traditional fresh SCC tests: Slump-flow, V-funnel and L-box tests.

Results and Discussion

Morphology of the aggregates

Figure 43 shows the shape distribution and median values by DIA. The dashed lines indicate extremes that have been previously observed in aggregates used commercially for the production of concrete in São Paulo state (Brazil). The values of the y-axis represents the percentage by volume of the material that has a shape parameter below that shown in the x-axis. For example, CR has 50% material with sphericity below 0.80. The leftmost the curve, less spherical is the material. The results show that CL has lower parameters (leftmost curve), both close to the limits of the benchmark. FR, approaches the other end, while CR and FL have more

intermediate shapes. It was therefore possible to quantify the morphological differences between the aggregates, selected initially by visual criteria.

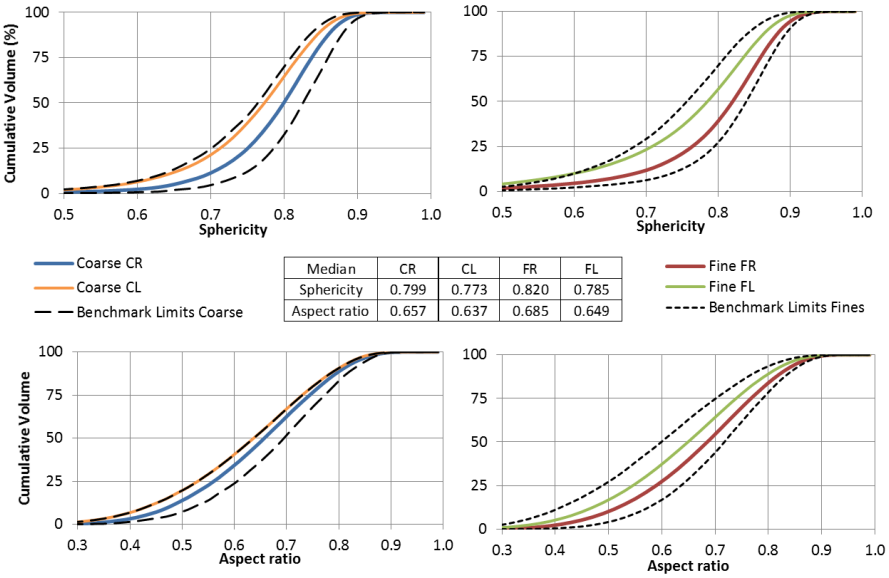

Figure 43. Shape distribution (sphericity and aspect ratio) of aggregates (left coarse, right fine). The dashed lines represent extreme materials found earlier in materials for concrete production. The median values are also indicated

Evaluation of fresh concrete with traditional SCC tests

Table XXVII shows the results of the fresh state tests and indicates the limits usually considered acceptable for self-compacting concrete.

Table XXVII. Characterization of fresh state according to traditional SCC tests

Test	Parameter	Limits	CR/FR	CL/FR	CR/FL	CL/FL
Slump flow	D (cm)	60-80	71	67	53.5	44.5
	t_{50} (s)	2-7	2.5	4.2	7.5	∞
V-Funnel	t_V (s)	6-12	6.0	7.7	22.9	∞
L-Box	t_{20} (s)	0-2	0.6	1.1	9.4	∞
	t_{40} (s)	0-4	2.5	3.7		∞
	h_2/h_1	0.8-1.0	0.8	0.8	0	0

The parameters that measure flow (t_{50}, t_V, t_{20} and t_{40}) increased when replacing the rounded by lamellar coarse aggregate, indicating that there was an increase in the viscosity of the concrete. Despite the small change, in this case it can be considered

that the exchange of coarse aggregate did not influence in an excessive way, keeping the concrete within the limits to be considered SCC. This fact is understandable when one looks at the mortar content, generally high in SCC, in this case close to 66%. With this amount of mortar the coarse aggregates are well apart from each other, reducing the interference. Replacing the fine aggregate caused a more drastic change in behaviour. None of the parameters achieved the established limits. In the extreme case, when both aggregates were lamellar, flow was not possible in the L-box and in the V-funnel the flow stopped before draining all volume. The interference between the grains seemed to be very high. A higher paste volume would be needed to separate the particles and thus reduce the impact of the lamellar morphology.

Mixing behaviour

Figure 44 illustrates the mixing behaviour of the concretes on the rotational rheometer, indicating the variation of torque according to the different steps of the mixing procedure.

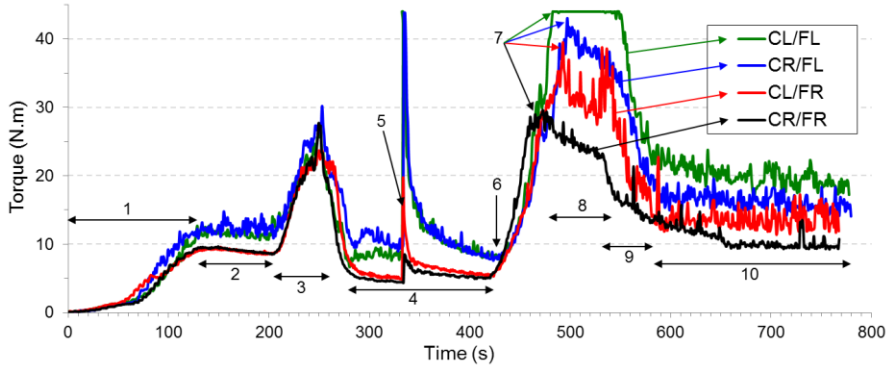

Figure 44. Mixing rheometry at constant rotation (126 rpm) of concretes with different shaped aggregates: (1) introduction of fines and sand; (2) dry mortar homogenization; (3) addition of 90% of water; (4) wet mortar homogenization; (5) stop to scrape container walls; coarse aggregate addition, (6) start and (7) end; (8) concrete homogenization; (9) remaining water addition; (10) final homogenization

Up to the end of step 4, two families of mortars can be observed. The difference of morphology of the fine aggregates have already showed its effects during mixing the dry mortar (step 2). 36% more torque were needed and an increase of noise can be seen when the lamellar aggregate was used. Up to point 6, when the wet mortar was finished, it is observed an increase of 54% in the torque with use of the lamellar aggregate. The energy associated with the mixing process can be calculated by the area under the curve torque vs. time [3]. It is observed an increase

of 50% in the mortar mixing energy (steps 3 + 4).The effects of the introduction of coarse aggregates can be depicted starting on point 6. Torque levels increased and the curves presented greater variations (noise) when the lamellar aggregates were used. Quantification of the area under the curve from the addition of coarse aggregates (starting at point 6) showed that the use of lamellar coarse aggregate increased by 20% the mixing energy in relation to the rounded material. The combined effect of fine and coarse lamellar aggregates was even more significant, increasing the energy in 42%. The final torques are the result of the combined effects of both fine and coarse aggregates. Analysing the end of the mixing procedure it is noted that torque increases 9% to 16% when switching the coarse aggregates from rounded to lamellar. For the sand fraction, the substitution of rounded by lamellar aggregates resulted in increases of 36% to 45%.

Rheological behaviour

According to the results shown in Figure 45, the concretes had Bingham fluid behaviour, i.e., a linear relationship between stress and shear rate (in this case represented by torque and rotation speed, respectively) with yield stress/torque (minimum stress/torque to start the flow).

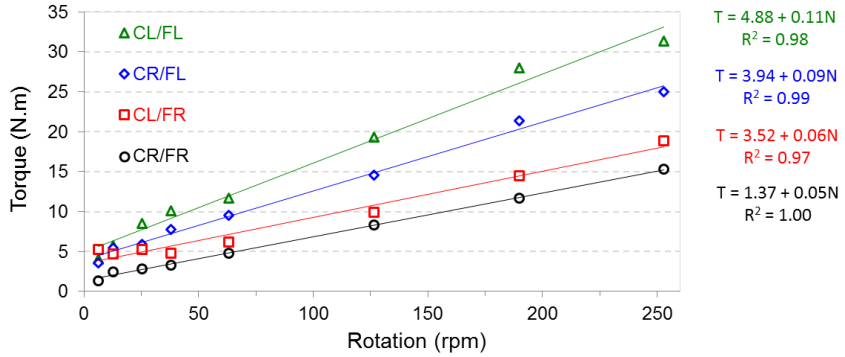

Figure 45. Rheological behavior of concretes. Bingham model: T = g + hN; T = torque, g = yield torque, h = plastic viscosity, N = rotation speed

According to the results, yield torque (g) and equivalent to plastic viscosity (h) seem to be dependent on the morphology of the aggregates. In the concretes with rounded fine aggregates (FR), the main impact of changing the coarse rounded by the lamellar aggregate was on the yield torque, while the plastic viscosity (slope of the line) was influenced only slightly (almost parallel lines). Since viscosity is a measure of the system's power dissipation during flow, the greater distances between the coarse aggregate grains, owing to the high mortar content (close to 66%) of the composition, allowed maintaining the h parameter at similar levels. For the concretes with lamellar fine aggregates, not only g values increased, but

also a significant increase of h occurred. Parameter g increased almost 190% for CR/FL compared to CR/FR, while for CL/FL it was 39% greater than for CL/FR. The plastic viscosity (h) was about 2 times higher in these concretes than in the ones with rounded sand. The effect on both rheological parameters was magnified when both lamellar aggregates were employed.

Rheological behaviour vs quantified morphology

In order to determine the correlations between the morphology of the aggregates with mixing and rheological properties of the concretes, the median parameters for the set coarse+fine aggregates were calculated, pondering the median values of each aggregate by its volumetric proportion in the mixture. Figure 46 shows that both mixing and rheological properties correlate quite well with sphericity and aspect ratio in an inversely proportional linear fashion. The correlations' accuracy is significant, with R^2 values ranging from 0.88 to 0.99. It is worth noting that the variations on the median parameters of the aggregates sets can seem quantitatively low (from 0.64 to 0.68 for aspect ratio and from 0.78 to 0.81 for sphericity), but the influence of these range of variation was very significant on mixing and rheological properties.

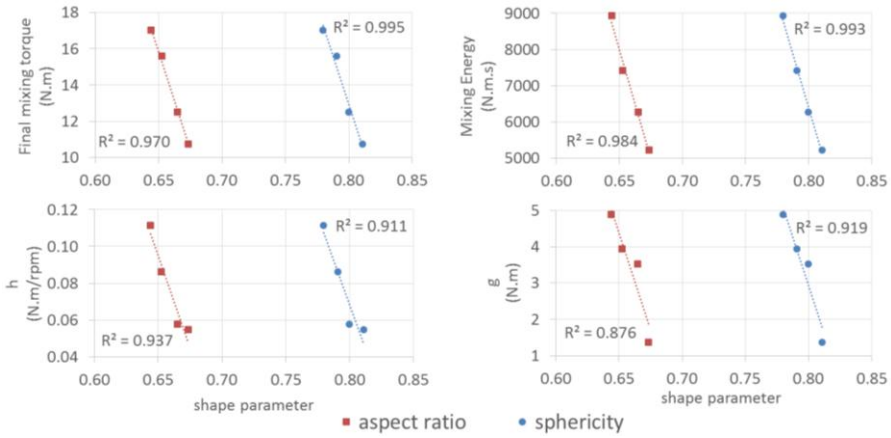

Figure 46. Correlation between the morphological (aspect ratio and sphericity) and rheological parameters (final mixing torque, concrete mixing energy, g and h)

Finally it should be considered that air content (Table I) changed unintentionally, since the presence of aggregates with different morphologies may have affected air incorporation. The concretes with more lamellar sand had significantly lower air contents, resulting in slightly less paste, which, may have contributed to increase

further the rheological parameters. Additional studies, with controlled air content, are needed to truly isolate the morphological effect.

Conclusions

Morphological evaluation by dynamic image analysis (DIA) was able to quantify with good statistical confidence the differences between aggregates with visually different shapes. Four concretes were produced with these different shaped aggregates and their mixing and rheological properties were analysed. Traditional SCC tests identified the effects of substituting rounded by lamellar aggregates. When only the coarse aggregates were changed, the impact was small and the concrete's characteristics remained within limits of SCC. On the other hand, both concretes with lamellar sands failed to present self-compacting characteristics as determined by traditional tests. Through the association of DIA and rotational rheometry it was possible to investigate properly the influence of particle shape on the rheological behaviour of SCC. The mixing process was assessed by a novel rheometer, which was able to separately identify the effects of the morphology of fine and coarse aggregates. The greatest impact was related to the lamellar sand that caused increase of mixing torque, fluctuations (noise in signal) and overall mixing energy. Shear cycles indicated that rheological properties of the concretes were dependent on the morphology of the aggregates, especially on the fine fraction. Yield torque (g) increased more than 3.5 times when both fine and coarse rounded aggregates were substituted by lamellar ones; similarly, the plastic viscosity parameter (h) of the concretes more than doubled with lamellar aggregates. Finally, excellent quantitative correlations between shape parameters with mixing and rheological properties were found. Therefore, DIA appears as a powerful technique to allow for estimating the effects of aggregate replacements, that include shape changes, on rheological properties of cement-based materials.

Acknowledgments

The authors would like to thank FAPESP (The São Paulo Research Foundation) for the financial support through the grant 2012/21134-2.

References

[1] Yu, A. B. and Standish, N. (1993), *Powder. Technol*. vol. 74, n. 3, p. 205-213.
[2] Oliveira, I. R., Studart, A. R., Pileggi, R. G. and Pandolfelli, V. C. (2000). *Dispersão e empacotamento de partículas*, Fazendo Arte Editora, São Paulo.
[3] Pileggi, R. G. (2001). *Doctoral Thesis*. UFSCAR, São Carlos/Brazil.

[4] Cortes, D. D.; Kim, H.-K.; Palomino, A. M.; Santamarina, J. C. (2008), *Cem. Concr. Res*. vol. 38, n. 10, p. 1142-1147.
[5] Tristão, F. A. (2005) *Doctoral Thesis*. UFSC, Florianópolis/Brazil.
[6] ABNT (2008), *NBR 7809*, Rio de Janeiro.
[7] AASHTO (2008), *T304*, Washington DC.
[8] RETSCH (2015), http://www.retsch-technology.com

Influence of Applied Maximum Shear Rate on Rheological Properties of Cement-Paste with SCC Consistency

Azadehalsadat Asghari and Dimitri Feys

Department of Civil, Architectural and Environmental Engineering, Missouri University of Science and Technology, Rolla, MO, United States

Abstract Determining the rheological properties of cement-based materials has enabled significant advancement in different aspects of concrete science, including mix design, fresh properties and placement. In some cases, e.g. intensive mixing and pumping, concrete is subjected to large shear rates. Although it is known that the rheological properties of concrete depend on the shear history, limited research has been performed on the influence of the applied shear rate on values of plastic viscosity and yield stress.

This paper describes the consequences of applying different shear rates, after a rest period, on the rheological properties of cement paste with SCC consistency. Increasing the maximum applied shear rate from 12.5 s^{-1} to 100 s^{-1} has led to significant differences in yield stress and viscosity, which can be attributed to the additional dispersion of cement(-itious) particles when increasing the applied shear rate. In order to enable investigating the influence of mix design factors on the influence of applied shear rate on rheology in the future, two different mathematical models were employed to characterize the changes of yield stress and viscosity with the applied shear rate. The selected logarithmic model appeared most suitable as it did not inhibit repeatability of the results.

Keywords: *Rheology, Cement paste, Pre-shear, Plastic viscosity, Yield stress.*

Introduction

Self-Consolidating Concrete (SCC) is a highly flowable concrete which spreads into place under its own weight, reaches good consolidation without vibration [1, 2], and, at the same time, shows sufficient resistance to segregation. SCC has been invented in Japan in the late 1980s for casting in presence of congested reinforcement or in complex formwork shapes [3]. To assure adequate fresh properties to fulfill the above criteria, rheology, which is the science of deformation of matter, has been applied successfully on cement-based materials

[4, 5].

Typically, cement-based materials obey the Bingham model showing a yield stress and a plastic viscosity. The yield stress (Pa) is the stress which needs to be exceeded to start flow, while the plastic viscosity (Pa s) is the resistance to an increase in flow rate. Equation (1) represents the Bingham model. The values of yield stress and plastic viscosity are useful, e.g. in numerical simulations [6], or to evaluate several key properties of concrete, including formwork filling [7], formwork pressure decay [8], distinct-layer casting [9], shotcreting [10], and pumping [11, 12].

$$\tau = \tau_0 + \mu_p \dot{\gamma} \quad (1)$$

For this equation, τ is the shear stress (Pa), τ_0 is the Bingham yield stress (Pa), μ_p is the plastic viscosity (Pa s) and $\dot{\gamma}$ is the shear rate (s^{-1}).

Due to the complex composition of concrete, its fresh properties depend on the shear history [13]. The influence of pressure and shearing on concrete rheology has studied recently [14–17], showing the influence of the shearing action on the concrete properties. Shear rate values of 30 to 60 s^{-1}, in bulk SCC, have been reported during pumping [18]. The lubrication layer, formed near the pipe wall has significantly lower viscosity and the shear rate in this layer would be several 100 s^{-1}. Rheological properties are thus expected to be largely influenced by pumping or shearing. The objective of this paper is to evaluate the influence of the applied shear rate on the rheological properties of cement pastes with SCC consistency to clarify the behavior observed during pumping. The relationship between plastic viscosity and yield stress subjected to different pre-shear values was investigated and different models have been evaluated.

Experimental Program

Materials

Cement pastes with SCC consistency were prepared with Type I/II Ordinary Portland cement (OPC) according to ASTM C150, and silica fume (SF) and class C fly ash (FA) as cementitious materials. A commercially available polycarboxylate ether (PCE)-based superplasticizer (SP) was used, but no air-entraining agents were employed in this research project. The self-consolidating cement pastes investigated in this research project were derived from standard VMA-type SCC mixtures used North America. The mix proportions for 1.5 liter of cement paste are listed in Table 1. The w/cm was equal to 0.38 and the amount of SP was determined to obtain a mini-slump flow value of 330 ± 10 mm at 7 min after mixing. This mixture was produced 4 times to investigate repeatability of the obtained results.

Table I. Paste mix design. All units are expressed in g for 1.5 liter of paste

Cement	Fly ash	Silica Fume	Water	SP	W/CM
1443.3	499.3	50.4	759.4	7.268	0.38

Rheometer

The Anton Paar MCR 302 Rheometer (Figure 1) is a commercially available rheometer, typically used in polymer science. Based on the many configurations which can be used based, the coaxially rotating cylinders were selected. The inner cylinder rotates at different velocities, while the outer cylinder remains stationary. The resulting torque is registered at the inner cylinder. The sandblasted configuration (to avoid slippage) has the following dimensions: the inner cylinder radius (R_i) measures 13.331 mm, the outer cylinder radius (R_o), 14.561 mm and the height (h) is 40.002 mm. The Bingham model (eq. 1) has been applied and the Reiner-Riwlin equation has been employed to convert the raw data into fundamental rheological properties (yield stress and plastic viscosity).

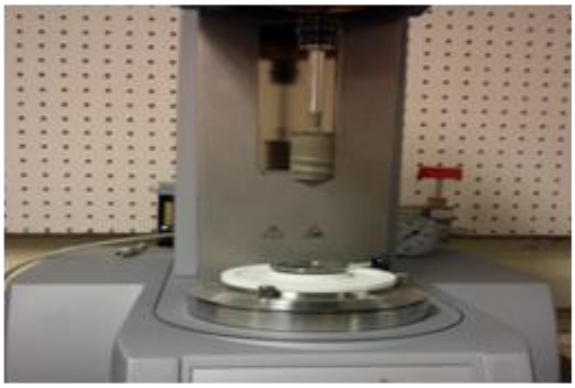

Figure 1. Anton Paar MCR 302, equipped with the sandblasted coaxial cylinders

Testing Procedure

The rheological properties of each cement paste are determined using the following testing procedure. All samples are pre-sheared at 100 s^{-1} at 15 min after contact between cement and water to "reset" the shear history, followed by a 12 min rest period. The static yield stress is determined after the rest period (but not reported in this paper), followed by the following procedure: The cement paste is pre-sheared for 90 s at the maximum shear rate employed during the test, which increases from 12.5 s^{-1} to 25 s^{-1}, 50 s^{-1} and 100 s^{-1}. This time period has been proven to be

sufficient in most cases to eliminate the effect of thixotropy from the results. After each pre-shearing period, the cement paste is subjected to a linear decrease in shear rate from different pre shear (12.5 s^{-1}, 25 s^{-1}, 50 s^{-1} and 100 s^{-1}) to 2 s^{-1} in 30 seconds. The testing procedure is shown in Table 2 and Figure 2.

Table II. Testing Procedure

Step	Pre Shear (s^{-1})	Time	Action
1	*0.0*	*12 min*	*Resting time*
2	*0.005*	*1 min*	*Static yield stress*
3	*12.5 + 12.5 to 2*	*1.5 min + 30 s*	*Flow curve*
4	*25 + 25 to 2*	*1.5 min + 30 s*	*Flow curve*
5	*50 + 50 to 2*	*1.5 min + 30 s*	*Flow curve*
6	*100 + 100 to 2*	*1.5 min + 30 s*	*Flow Curve*

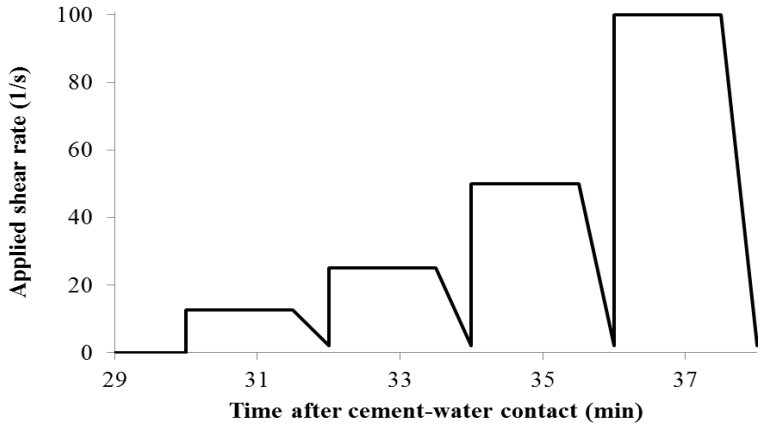

Figure 2. Representation of testing procedure (steps 2 to 6)

Result and Discussions

Observations on Raw Data

The results in Table 3 show that by increasing the maximum applied shear rate, both the plastic viscosity and yield stress decrease. The yield stress value at a pre-shear of 12.5 s^{-1} is approximately 21% larger than the corresponding yield stress value at 100 s^{-1}, while a difference of 34% is observed for the viscosity. The most likely reason for this observation is due to the build-up and breakdown of internal structure. As the sample has been kept at rest during 12 min, thixotropic build-up has connected cement(-itious) particles into a structure. Applying a shear rate re-disperses a number of particles, causing a decrease in rheological properties. Increasing the applied shear rate further increases dispersion, indicating that the

thixotropic structure is built up with different strengths of connections, of which some may not be broken at a lower shear rate, but may be disconnected at a higher shear rate. It is even very likely that some of the connections built up during the resting time cannot be broken down with the 100 s^{-1} shear rate applied.

Table III. Average yield stress and plastic viscosity of four tests at each applied maximum shear rate

Applied pre-shear (s^{-1})	Yield stress (Pa)	Plastic viscosity (Pa s)
12.5	3.926	0.451
25	3.814	0.411
50	3.530	0.384
100	3.245	0.336

In order to be able to quantify the influence of the different pre-shear on the plastic viscosity and yield stress, and to compare the results of different mixtures, it would be useful if the results could be represented by a simple set of parameters. For this process, two types of functions (decreasing exponential and logarithmic) were applied to normalized data. The yield stress and viscosity values were normalized by their extrapolated values at infinite shear rate for the exponential curves, and by the respective value at 100 s^{-1} shear rate for the log curves.

Fit with Infinite Shear Data

Figures 3 and 4 illustrate the correlation between the yield stress and plastic viscosity at each pre-shear applied. Exponential formulae have been used to correlate the yield stress (eq. 2) and plastic viscosity (eq. 3). The values the infinite shear viscosity and yield stress are presented in Table 4.

$$\tau_0 = \tau_{0,\infty}(1 + Ae^{-B\dot{\gamma}}) \qquad (2)$$

$$\mu_p = \mu_{p,\infty}(1 + Ce^{-D\dot{\gamma}}) \qquad (3)$$

where $\tau_{0,\infty}$ (Pa) and $\mu_{p,\infty}$ (Pa s) represent the extrapolated values of yield stress and plastic viscosity to infinite shear rate, and A, B, C and D are fitting parameters.

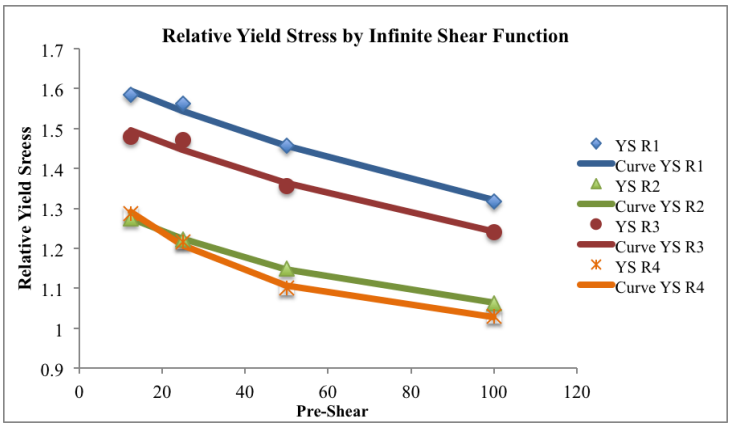

Figure 3. Relative yield stress (compared to yield stress at infinite shear) at 12.5 s^{-1}, 25 s^{-1}, 50 s^{-1} and 100 s^{-1}, modelled with the exponential function for each test

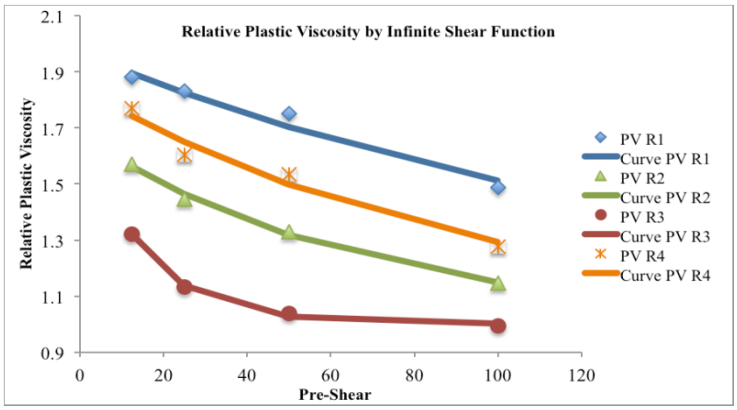

Figure 4. Relative plastic viscosity (compared to plastic viscosity at infinite shear) at 12.5 s^{-1}, 25 s^{-1}, 50 s^{-1} and 100 s^{-1}, modelled with the exponential function for each test

As can be seen in Figures 3 and 4, the exponential function fits the data well. However, the determination of yield stress and plastic viscosity at infinite shear rate appears to reduce repeatability. While the exponential function is theoretically the most correct, it compromises the repeatability of the results and cannot be used. The reason for this anomaly can most likely be attributed to the limited number of data points, making the determination of infinite yield stress and viscosity very sensitive to small errors in the data points.

Table IV. Infinite shear yield stress and viscosity

Sample	infinite shear yield stress (Pa)	infinite shear viscosity (Pa s)
Repeatability 1	1.05	0.237
Repeatability 2	3.02	0.272
Repeatability 3	2.72	0.372
Repeatability 4	2.79	0.243

Fit with Log function

Besides the exponential model, a logarithmic function (equations 4 and 5) has been applied to the set of data of yield stress and plastic viscosity. Figures 5 and 6 show the relationship of yield stress and plastic viscosity with the pre-shear, respectively. In this model, the plastic viscosity and yield stress at 100 s^{-1} pre-shear have been used to normalize the rheological properties. In addition, the number of parameters has reduced to one (A in yield stress and C in plastic viscosity). The values of A and C are presented in Table 5.

$$\tau_0 = \tau_{0,100}(1 + A\log(\dot{\gamma}/100)) \quad (4)$$

$$\mu_p = \mu_{p,100}(1 + C\log(\dot{\gamma}/100)) \quad (5)$$

where $\tau_{0,100}$ (Pa) and $\mu_{p,100}$ (Pa s) represent the yield stress and plastic viscosity values at the applied shear rate of 100 s^{-1}. A and C are fitting parameters.

The logarithmic functions fit the data well (Figures 5 and 6), similarly to the exponential function. However, by taking the rheological value at 100 s^{-1} as reference point, and fitting the curve with one sole parameter, the repeatability of the results is largely maintained, although some variations in the viscosity curves are still observed. The logarithmic curves are more suitable to study the influence of other parameters (e.g. mix design, temperature, etc.) on the behavior of SCC paste subjected to different shear rates.

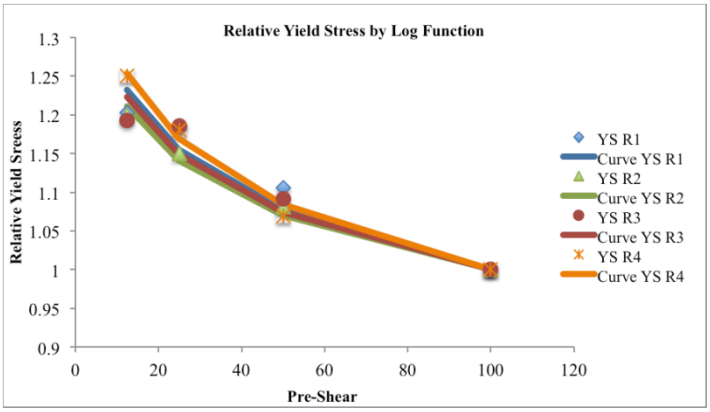

Figure 5. Relative yield stress (compared to the yield stress at 100 s^{-1} pre-shear) at each pre-shear, modelled with the logarithmic function for each test

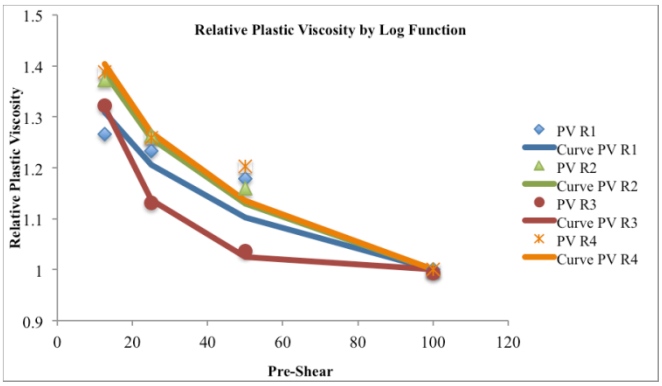

Figure 6. Relative viscosity (compared to the viscosity at 100 s^{-1} pre-shear) at each pre-shear, modelled with the logarithmic function for each test

Table V. A and C parameters for logarithmic function

Sample	A	C
Test 1	0.256	0.342
Test 2	0.233	0.428
Test 3	0.246	0.310
Test 4	0.280	0.446

Conclusions

Rheological tests on cement paste with SCC consistency have revealed that the pre-shear has a significant effect on the rheological properties. From the results and analysis, it can be concluded that:

- The yield stress and plastic viscosity decrease significantly with increasing shear rate applied during the pre-shear period. This can be attributed to the additional dispersion the particles undergo when increasing the applied shear rate.
- Applying a decreasing exponential function, based on infinite shear rheological properties was deemed adequate to fit the data, but hindered the repeatability of the results.
- Logarithmic functions, with the yield stress or viscosity value at a pre-shear of 100 s^{-1} as reference, fit the data well and result in good repeatability.

Acknowledgments

The authors would like to acknowledge the RE-CAST Tier-1 UTC for the financial support and the center for infrastructure of engineering studies (CIES) at Missouri S&T for the technical support of this project.

References

[1] Khayat KH, Manai K, Trudel A (1997), In Situ Mechanical Properties of Wall Elements Cast Using Self-Consolidating Concrete, *ACI Mat. J.*, **94-6**, 491-500.
[2] Okamura H, Ouchi M (2003), Self-compacting concrete, *J. of Advanced Concrete Technology*, **1**, 5-15.
[3] Khayat KH (1999), Workability, Testing, and Performance of Self-Consolidating Concrete, *ACI Mat. J.*, **96-3**, 346-353.
[4] Wallevik OH (2003), Rheology, a scientific approach to develop self-compacting concrete, Proc 3rd Int. RILEM Symp SCC, Reykjavik, pp 23–31
[5] Wallevik JE (2003), Rheology of particle suspensions: fresh concrete, mortar and cement paste with various types of lignosulfonates, Ph-D dissertation, Department of Structural Engineering, The Norwegian University of Science and Technology, Trondheim.
[6] Roussel N, Geiker MR, Dufour F, Thrane LN, Szabo P (2007), Computational modeling of concrete flow: general overview, *Cem. Conc. Res.*, **37**, 1298–1307.

[7] Thrane LN (2007), Form filling with self-compacting concrete. PhD dissertation, Danish Technological Institute, Technical University of Denmark, Copenhagen.
[8] Assaad J, Khayat KH (2004), Assessment of thixotropy of self-consolidating concrete and concrete-equivalent-mortar: effect of binder composition and content, *ACI Mat. J.* **101–5**, 400–408.
[9] Roussel N, Cussigh F (2008), Distinct-layer casting of SCC: the mechanical consequences of thixotropy, *Cem. Conc. Res.*, **38**, 624–632.
[10] Jolin M, Burns D, Bissonnette B, Gagnon F, Bolduc L-S (2009), Understanding the Pumpability of Concrete, Proc. of the 11th Conf. on Shotcrete for Underground Support, Davos
[11] Feys D, De Schutter G, Verhoeven R, Khayat KH (2010), Similarities and differences of pumping conventional and self-consolidating concrete, Proc 6th Int RILEM Symp 4th North-American Conf SCC, Vol. I, Montreal, 153–162.
[12] Kaplan D (2001), Pumping of concretes, PhD dissertation (in French), Laboratoire Central des Ponts et Chaussees, Paris
[13] Wallevik JE (2009), Rheological properties of cement paste: thixotropic behavior and structural breakdown, *Cem. Conc. Res.*, **39**, 14-29.
[14] Ouchi M, Sakue J (2008), Self-compactability of fresh concrete in terms of dispersion and coagulation of particles of cement subject to pumping, Proceedings of the 3rd North-American conference on the design and use of self-consolidating concrete, Chicago
[15] Takahashi K, Bier T (2013), Mechanisms for the changes in fluidity and hydration kinetics of grouts after mixing, Proceedings of the 6th international RILEM conference on self-compacting concrete, Paris
[16] Bier T, Takahashi K (2015), Influence of pumping of fresh concrete properties for SCC, ACI Spring Convention, Kansas-City
[17] Feys D, De Schutter G, Khayat KH, Verhoeven R (2016), Changes in rheology of self-consolidating concrete induced by pumping, *Mat Struct, in press*, doi 10.1617/s11527-016-0815-7.
[18] Feys D, De Schutter G, Verhoeven R (2013), Parameters influencing pressure during pumping of self-compacting concrete, *Mat Struct*, **46**, 533–555.

SCC Flow Curves from Vane Geometry Rheometer

C. Lanos[1] and P. Estellé[1]

[1]LGCGM – UR1, IUT Rennes, 3 rue du clos Courtel, 35704 Rennes Cedex, France

Abstract The objective of the present study is to show how recording the changes in the rotation torque according to the rotation speed can lead to identifying a characteristic flow curve for the tested concrete. The concrete rheometer used for the study is composed of a vane tool. The rotation speed of the tool is imposed and the resulting torques are measured. The experimental rotation protocol used in this study corresponds to a rapid speed increase followed by a steady speed then the rotation speed slows down. The evolution of the torque measured as the rotation speed decrease (restructuring phase) is considered as being a succession of stationary states. By considering the fluid equivalent to a Bingham fluid for which the yield stress has already been identified and by using an analogy with a coaxial-cylinders rheometer, relevant relationships between the rotation speed of the vane and the rate of shearing along the tool are identified. Shear stress and shear rate calculations for each value of torque and rotation speed lead to the complete flow curve of the tested fluid. The data treatment method is adjusted to accurately evaluate the parameter linked to the flow stop in the case of a non-nil shear rate when the yield stress is reached. The comparison of the characteristic rheological parameters of SCC obtained from the rheometer and both spreading and V-Funnel tests indicate very satisfactory correlations.

Keywords: *yield stress, shear stress, shear rate, rheological parameters*

Introduction

The rheological characterisation of concretes still remains a major problem. Based on traditional geometries (coaxial cylinders, vane, and parallel-plates) different concrete rheometers have been developed [1] including two point test [2], the IBB rheometer[3], the ICAR rheometer[4-6], the BML rheometer [7,8] and the BTRHEOM apparatus [9,10] and more recently with vane geometry [11,12]. Such devices are generally characterised by a large sample volume, which complicates the implementation of the test. The rheological characterisation of the concrete

tested using these devices is generally limited to analysing the change to the rotation torque according to the rotation speed. This can be sufficient to make a comparative analysis or to study the effect of a change in concrete composition. But the links between concrete mix proportioning and rheological behaviour is not really identified.
The objective of the present study is to show how recording the changes in the rotation torque of a vane according to the rotation speed can lead to identifying a characteristic flow curve for the tested concrete. The concrete rheometer used for our study was developed by the Laboratory GCGM Rennes, France. But the method is applicable with many other devices. The data treatment method is adjusted to accurately evaluate the parameter linked to the concrete flow stop. The comparison of the characteristic rheological parameters identified on SCC from the rheometer and spreading tests and time for empting the V-Funnel is discussed.

Rheometer, test protocol and recorded data

Rheometer

The concrete rheometer used in our study was previously presented in [11] (figure 1). The device is composed of a vane tool with a 4 blades probe of 15 cm in both height h and diameter D and a cylindrical concrete container of 28 cm in diameter and 35 cm in height. The walls of this container are roughened to avoid any slippage. The vane is plunged into the concrete and level with the surface, as shown in figure 1(right). During a test, the rotation speed of the tool is imposed and the resulting torque is measured using a frictionless sensor. The torque sensor has a capacity of 100 N.m. It is a frictionless sensor that also incorporates a speed sensor to measure the real speed of the tool. The rheometer's motor is monitored by a computer. The maximum rotation speed of the tool is 120 rpm. The acquisition frequency is fixed at 10 Hz. All the experimental data are recorded in real-time and directly displayed in a spreadsheet.

Figure 1. Vane rheometer and data recorder.

Test protocol and representative records

The experimental rotation protocols used in this study are presented in figure 2. A quick and short speed increase is followed by a steady speed then the rotation speed slows down. This first step allows the static yield stress to be estimated that is characteristic of the initial state (more or less structured) of the concrete, then to rapidly de-structure it to reach a stationary state as the rotation speed slows down. This last part will be used to plot the flow curve.

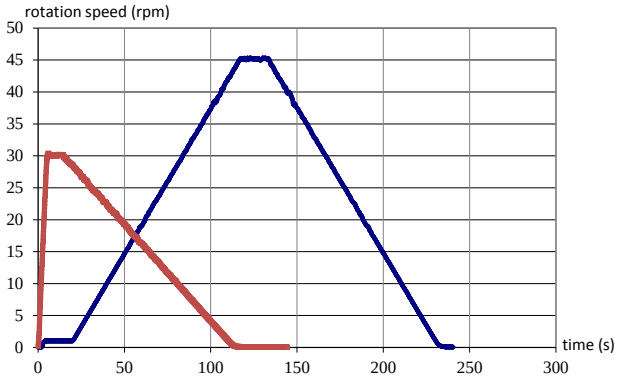

Figure 2. Examples of imposed rotation speed of the vane.

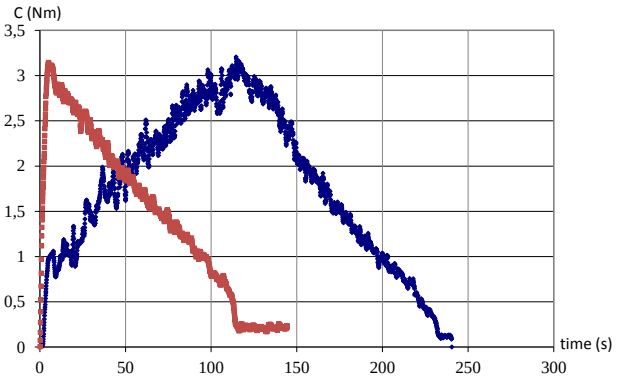

Figure 3. Examples of recorded torque evolution.

Recorded data can be seen in figures 2 and 3. With rapid increase of speed, the maximum torque is obtained in practice before reaching the constant rotation speed (figure 3). The torque reduces significantly during the constant phase (destructuring effect), then the decline is more regular. At the end of the test, we note a rapid decline of the torque as the vane stop (dynamic yield stress). Lastly, the torque may not return to zero at the end of the test (residual torque associated with elastic-plastic effects as the flow stop). Finally, it is observed that experimental data appear noisy probably due to presence of aggregates.

Data treatment methods

Dynamic yield stress and Shear stress

The evolution of the torque measured as the rotation speed decreases (restructuring phase) is considered as being a succession of stationary states. We notice that these curves are quite linear overall and have an intercept with torque axis which directly reflects the existence of a dynamic yield stress at flow stop τ_0. This value, which constitutes the first rheological parameter for the behaviour of concretes, is estimated from intercept torque C_0 tacking into account the bottom effect:

$$\tau_0 = \frac{2C_0}{\pi D^2(h+\frac{D}{6})} \quad (2)$$

In our test configuration, the vane is plunged into the concrete and level with the surface. We therefore overcome the surface shearing effects but the bottom effect are still present. We consider that the torsion flow associated with what occurs under the vane tool contributes to the torque applied to the vane. However, as the distance between the bottom of the tank and the lower surface of the tool is great (20 cm), the contribution of the viscous component of the rheological behaviour on the torque related to this zone under torsion will be ignored. Only the contribution of the yield stress will be considered.

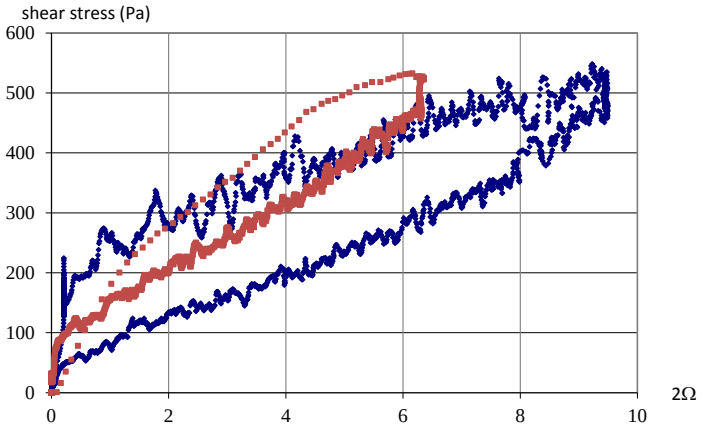

Figure 4. Examples of τ(2Ω) curves obtained for two different SCC.

The shear stress τ applied on cylindrical shearing surface will therefore be estimated taking into account a shear stress equal to τ_0 applied to the surface of the base of the tool:

$$\tau = \frac{2(C-\frac{\pi D^3\tau_0}{12})}{\pi D^2 h} = \frac{2C}{\pi D^2 h} - \frac{D\tau_0}{6h} \quad (3)$$

The figure 4 present the evolution of the shear stress versus 2Ω (Ω is the angular rotation speed) during a test realised on two different SCC and with the two different tests protocols (figure 2 and 3).

Shear rate calculation

A relevant relationship between the rotation speed of the vane and the shear rate induced within the gap is needed. The proposed method developed in [13], appears as a simplification of the data treatment issued from [14] and applied for flow curve identification of several materials from Couette analogy [15]. The main interest of this approach is the identification of the tested fluid flow curve without assumption on the rheological behaviour type. The initial method is based on the evaluation of the local $\tau(2\Omega)$ curve slope as an extension of the method proposed by [16,17] in the case of infinite media. This method produces more accurate flow curves than those produced assuming a homogeneous shear [18] and does not require the rheometer calibration as mentioned by [19]. Data treatment is easier than applying the wavelet-decomposition [20] but is not fully operational for noisy data [21]. So, the outer cylinder is considered equivalent to the inner wall of the rheometer container (radius R_e) while the vane represents the inner cylinder (radius R_i). In this approach, it is assumed that SCC presents a record $\tau(2\Omega)$ mainly linear (figure 4). Two configurations are studied corresponding to fully or not fully sheared gap between cylinders. Considering the fluid equivalent to a Bingham fluid for which the yield stress has already been reached and identified (equation (2)), the plastic viscosity noted μ is estimated for each value of $\tau(\Omega)$. Detail of the calculus are in [13]:

$$\Omega = \int_{Ri}^{r} \frac{d\omega}{dr} dr = \int \frac{\dot{\gamma}}{r} dr = \int \frac{\tau(r) - \tau_0}{\mu r} dr = \frac{\tau - \tau(r)}{2\mu} - \frac{\tau_0}{\mu} \ln\left(\frac{r}{R_i}\right) \tag{4}$$

In the case of a partially sheared gap, with R_p the radius for which $\tau = \tau_0$ (then $\tau < \tau_0.R_e^2/R_i^2.$), the shear rate is obtained with:

$$\dot{\gamma} = \frac{2\Omega}{1 - \frac{\tau_0}{\tau - \tau_0} \ln\left(\frac{\tau}{\tau_0}\right)} \tag{5}$$

In the case of a fully sheared gap ($\tau > \tau_0.R_e^2/R_i^2.$), the shear rate is obtained with:

$$\dot{\gamma} = 2\Omega + \frac{2\tau_0}{\mu} \ln\left(\frac{R_e}{R_i}\right) + \frac{\tau}{\mu}\left(\frac{R_i}{R_e}\right)^2 - \frac{\tau_0}{\mu} \tag{6}$$

Therefore if a is the mean slope of the curve $\tau(2\Omega)$, then :

$$\mu = a\left(1 - \left(\frac{R_i}{R_e}\right)^2\right) \tag{7}$$

In this case, the relationship between a and μ is constant.
Shear stress and shear rate calculations for each value of torque and rotation speed allow a comprehensive flow curve of the tested fluid to be plotted when τ, τ_0, a, R_i

and R_e are known. Proposed relationships appear easy to use in the case of noisy records, such as those obtained with SCC, comparing to relationships proposed in many bibliographical references. Figure 5 shows a comparison of the flow curves obtained by a shearing speed approximated by $\dot{\gamma} = 2\Omega$ [18] and for a shear rate calculated according to the equations (5) and (6). The obtained flow curve differs largely from $\tau(2\Omega)$ curve and from the fit of Reiner- Riwlin equation (straight line). Under the dotted line, the gap is partially sheared and fully sheared above. The flow curve is quite linear and highlights a Bingham rheological behaviour with presence of critical shear rate. The intercept of this curve with shear stress axis differs from the calculated yield stress value (respectively τ_0 = 40 and 70 Pa).

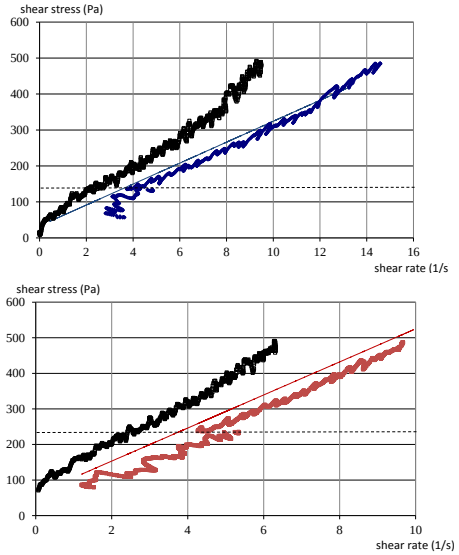

Figure 5. Examples of flow curves without correction of the initial data $\tau=f(2\Omega)$ (black curves) and with correction on the shear rate (colored curve). The straight line corresponds to the fit of "Reiner – Riwlin" equation on data from figure 4.

Method adjustment

We can see in certain cases that the shear stress curve shows a non-nil shear rate when the yield stress is reached, as presented on figure 5. This trend is directly connected to the existence of a critical shear rate beyond which the flow is not stable. An alternative data treatment method is proposed to accurately evaluate the flow curve. The rheological behaviour of the fluid is also assumed as a Bingham fluid. The yield stress is obtain for a critical shear rate value $\dot{\gamma}_c$. Under this value, flow does not occur. The intercept of flow curve with shear stress axis is noted τ_{00}. The yield stress value is estimated according to equation (2) and the plastic viscosity with the equation (7). The equation (4) is then rewritten replacing τ_0 by

τ_{00} and $\tau(r) \geq \tau_0$. Assuming the Newtonian approximation is right when the gap is fully sheared (ie $r = R_e$ and $\tau(r) = \tau_0$) the following equation is obtained:

$$\Omega = \frac{\tau}{2\mu}\left(1-\left(\frac{R_i}{R_e}\right)^2\right) - \frac{\tau_{00}}{\mu}\ln\left(\frac{R_e}{R_i}\right) = \frac{(\dot{\gamma}-\dot{\gamma}_c)}{2}\left(1-\left(\frac{R_i}{R_e}\right)^2\right) \quad (8)$$

Then, the estimation of τ_{00} is given by:

$$\tau_{00}\ln\left(\frac{R_e}{R_i}\right) = \frac{\tau_0}{2}\left(1-\left(\frac{R_i}{R_e}\right)^2\right) \text{ and } \dot{\gamma}_c = \frac{\tau_0-\tau_{00}}{\mu} \quad (8)$$

Shear stress and shear rate calculations for each value of torque and rotation speed lead to the complete flow curve (knowing τ, τ_0, τ_{00}, μ, R_i and R_e). In the case of a partially sheared gap:

$$\dot{\gamma} = \frac{2\Omega + \dot{\gamma}_c}{1-\frac{\tau_{00}}{\tau-\tau_{00}}\ln\left(\frac{\tau}{\tau_0}\right)} \quad (9)$$

In the case of a fully sheared gap, the shear rate is obtained with:

$$\dot{\gamma} = \frac{2\Omega + \frac{2\tau_{00}}{\mu}\ln\left(\frac{R_e}{R_i}\right)}{\left(1-\left(\frac{R_i}{R_e}\right)^2\right)} - \frac{\tau_0}{\mu} + \dot{\gamma}_c \quad (10)$$

Flow curves of SCC

The SCC tested by [13] are produced starting from a reference composition. 25 different SCC compositions deriving from this reference composition (changing content of water, of admixture, of fillers, of cement…) were tested. While composition is changed, all these concrete behaves as Bingham material. So the plastic viscosity of the SCC can estimated from the slope of the flow curves.

In parallel with the rheometer tests, the rheological properties of studied SCC were evaluated at the same time using conventional tests: slump tests (to estimate the dynamic yield stress) and V-Funnel tests (to estimate an equivalent viscosity). In practice, these tests are carried out just before the rheometer test. The slump of fresh concrete is measured using the Abrams cone according to conventional professional rules [22]. The dynamic yield stress can be estimated from the formula proposed by [23]. The flow time is evaluated using a V-Funnel [24] (figure 2) with an opening of 75 mm x 75 mm. Its height is 575 mm and its length at the top is 500 mm. Domone and Jin [25] showed that the flow time of concrete from the V-Funnel is correlated to its viscosity. Based on flow condictions and dimensions of V-Funnel, the viscosity of SCC was calculated from an analogy with the flow of Marsh cone test [26].

The comparison of the characteristic rheological parameters identified from the rheometer and spreading and V-Funnel tests indicate very satisfactory correlations (figure 6). The points in the black circle on figure 6 correspond to tests where segregation of concrete was noticed or for which sample production has been poorly controlled.

The case of a rheological study realized on a fluid concentrated suspension composed with fine coarse aggregates, admixtures and water is used to demonstrate the interest of the revised version of the data treatment method tacking into account the presence of a critical shear rate on the flow curve. The tested fluid is formulated without binder and is used as a reference fluid to compare the results of various apparatus. The flow curves obtained using three reference data treatment method and our two approaches are compared (figure 7). The first reference method consist in the use of infinite media solution [16,17]. The second correspond to the Newtonian approximation and the third is the Couette analogy. Our proposed methods highlight the presence of a critical shear rate expected for the tested fluid. The discrepancy between the obtained flow curves are significant.

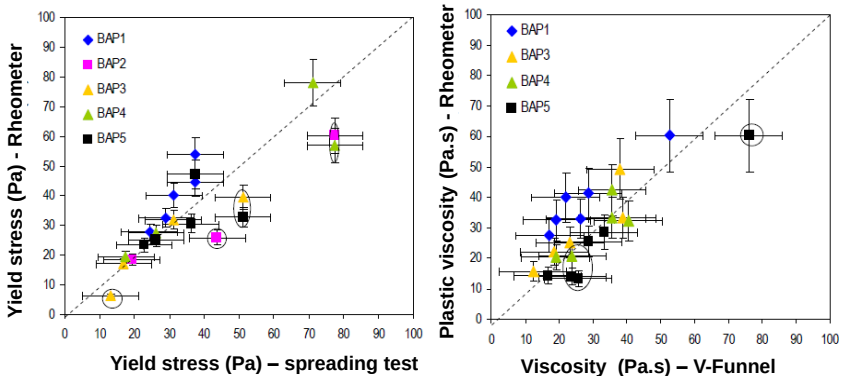

Figure 6. Correlation between the yield stress estimated by slump test and the dynamic yield stress measured using the concrete rheometer and correlation between the apparent viscosity evaluated using the V-Funnel and the plastic viscosity measured using the concrete rheometer [13].

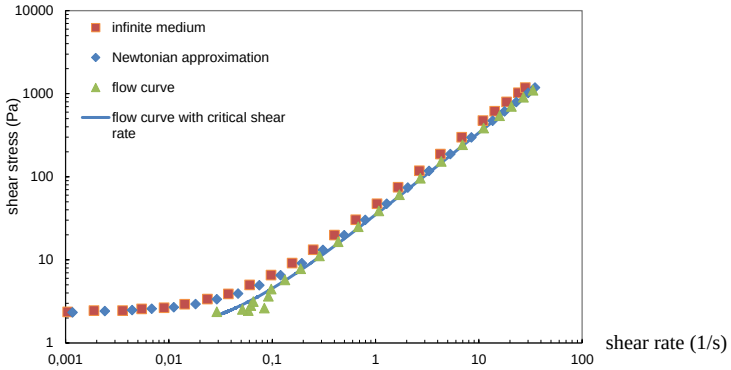

Figure 7. Comparison of flow curves obtained starting from torque measurement on a fluid concentrated suspension and using various data treatment method.

The proposed data treatment method lead to a flow curve very closed to the points obtained with the equation (5) and (6) even if this method do not take into account the presence of critical shear rate. The same type of results obtained with data of a SCC (black dot on figure 4) are presented on figure 8. The estimated critical shear rate value is 0.64 1/s and τ_{oo} = 23 Pa as τ_o = 40 Pa.

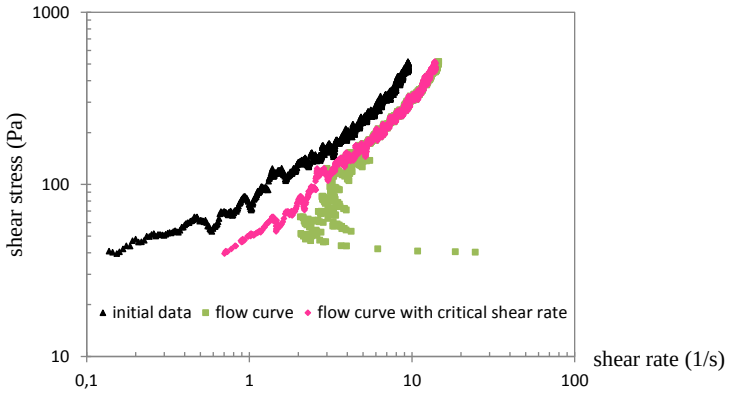

Figure 8. Comparison of flow curves obtained using various data treatment method.

Conclusions

The record analysis method proposed for identifying a characteristic flow curve for the tested fluid in a vane tool rheometer configuration has proved to be highly appropriate. In the case of self-compacting concretes, adjustment of a Bingham-type rheological behaviour on records obtained during shearing under restructuring stage has proved to be acceptable. The comparison of the characteristic rheological parameters identified from the rheometer and spreading tests – slump and time for

empting the V-Funnel – indicate very satisfactory correlations, which allow studies aiming to compare concrete rheometers to be considered from a new point of view. The used data treatment method can highlight, for some concretes, the existence of critical shear rate which constitutes an interesting study perspective.

References

[1] Ferraris C.F. and Brower L.E. editors (2001), *Comparison of concrete rheometers: International tests at LCPC, October, 2000*, NISTI Report 6819.
[2] Domone P.L.J., Xu Y., Banfill P.F.G. (1999), *Magazine of Concrete Research* 51 181-190.
[3] Beaupré, D. *Rheology of High Performance Shotcrete* (1994) Ph D. Thesis Univ. Of British Columbia (Canada).
[4] Koehler, E. P. (2004) *Development of a Portable Rheometer for Portland Cement Concrete*, MS Thesis, The University of Texas at Austin (TX).
[5] Koehler, E. P., Fowler, D. W., Ferraris, C. F., Amziane, S. (2005) *A New Portable Rheometer for Fresh Self-Consolidatinng Concrete*, Proc. of session ACI 2005 (New York).
[6] Koehler, E. P., Fowler D. W. (2004) *Development of a portable rheometer for fresh Portland cement concrete*, Research report ICAR – 105-3F, Univ. of Texas.
[7] Wallevik, O.H. (1990) The rheology of fresh concrete and its application on concrete with and without silica fume, Dr. ing. Thesis, NTH Trondheim (Norway).
[8] Wallevik, O.H., Gjorv, O.E. (1990) *in Proceedings of the Rilem Colloquium*, Chapman & Hall, Hanover, October, 213-214.
[9] De Larrard, F., Szitkar, J.C., Hu, C., Joly, M. (1993) in *RILEM Workshop Special Concretes* Workability and Mixing, 201-208.
[10] De Larrard, F., Sedran, T., Hu, C., Szitkar, J.C., Joly, M., Derkx, F. (1996) in *Rilem International Conference on Production Methods and Workability of Concrete, RILEM Proceedings 32*, Glasgow Scotland, June 3-5, 377-388.
[11] Estellé P. and Lanos C. (2012) *Applied Rheology*, 22 12881.
[12] Soualhi H., Kadri E.H., Ngo T.T., Bouvet A., Cussigh F., Kenai S.(2014), *Appl. Rheol.* 24:2, 22594.
[13] Mokkedem S., Lanos C., Casacliu B. (2013) *Comparison of SCC rheological behavior using laboratory and in situ rheological testing*. In SCC Paris 2013, Paris, France, 2-4 septembre.
[14] Estellé P., Lanos C. (2008) *Chemical Engineering Science*, 63:24, pp. 5887-5890.
[15] Estellé P., Lanos C., Perrot A., Amziane S. (2008) *Applied Rheology*, 18:3, 34037.
[16] Nguyen Q. D. and Boger D. V. (1985) *Journal of Rheology*, 29, pp.335-347.
[17] Nguyen Q.D., Boger D.V., *Rheol. Acta* 26 (1987) 508-515.
[18] Steffe, J.F. (1996) *Rheological methods in food engineering process*, Second Edition, Freeman Press, East Lansing, (USA).
[19] Aït-Kadi A., Marchal P., Choplin L., Chrissemant A.S. and Bousmina M. (2002) *Canadian Journal of Chemical Engineering*, Volume 80, Issue 6, 1166–

1174.
[20] Ancey C. (2005) *Journal of Rheology* 49(2) 441-460.
[21] Estellé P, Perrot A, Mélinge Y, Lanos C, Amziane S (2007) in *5th Int. RILEM Symposium on Self- Compacting Concrete*, Gent 3-5 septembre, vol 1, pp 291-296.
[22] AFNOR (1999), Tests for fresh concrete – Part 2: slump and spreading test, NF EN 12350-2. Technical report.
[23] Roussel N., Coussot P. (2005) *Journal of Rheology*, 49, 705-718.
[24] [8] AFNOR (2010), Test for fresh concrete – Part 9: self-compacting concrete – V-funnel flow test, NF EN 12350-9. Technical report.
[25] Domone P. L. and Jin J. (1999). In *Proceedings of the RILEM Symposium on Self-Compacting Concrete*, pp. 109-120, Stockholm.
[26] Frunz L., Lootens D., Flatt R.J., Wombacher F., and Velten U. (2010). In *RILEM Proceedings, Design, Production and Placement of Self-Consolidating Concrete*, Montreal 2010, Volume 1, Part 2, pp.53-63.

A Correction Procedure to Characterize the Bottom Effect of a Rotational Cylinder during Tribological Measurements of the Lubrication Layer of Highly Workable Concrete

Jan Vosahlik[1], Dimitri Feys[2] and Kyle A. Riding[1]

[1]Department of Civil Engineering, Kansas State University, Manhattan, KS, United States
[2]Department of Civil, Architectural and Environmental Engineering, Missouri University of Science and Technology, Rolla, MO, United States

Abstract The lubrication layer, a thin mortar layer formed at the inner surface of a pipe wall, has been shown to play a key role during concrete pumping. A device called a tribometer has been used to measure the properties of this layer. Various tribometer designs were developed in the past two decades, with a number of them utilizing a steel cylinder to induce shearing on the tested concrete sample placed in a container. During the test, the lubrication layer is formed on the vertical side of the rotating cylinder while the resulting torque is monitored. Unfortunately, measurements performed on a rotary cylinder immersed in concrete are very often biased by the presence of inadvertent flow resistance exerted by the tested concrete sample at the bottom of the cylinder surface. An experimental laboratory program on highly-workable concrete, including self-consolidating concrete was carried out to investigate this effect. Numerous measurements were performed using various filling heights of concrete in the container combined with a set of multiple rotational velocities imposed on examined concrete. Results have shown a very good correlation between measured torque and filling height and consequently, a correction procedure to account for the effect of the bottom surface of the rotary cylinder on tribological measurements of the lubrication layer is suggested.

Keywords: *Self-consolidating concrete, pumping, lubrication layer, tribometer, tribology, bottom effect*

Introduction

The idea of using a hydraulic pump to transport concrete to formwork was introduced over 100 years ago [1]. Since then, concrete pumping became one of the most utilized concrete placement techniques. Concrete pumps make it possible for concrete to be transported significantly faster than using a traditional placement method, such as crane-and-bucket, and therefore help reduce concrete structure construction time. With wide-spread use of concrete pumps around the world, there is a need for a reliable and simple method to characterize and predict concrete pumpability [2]. Recently, a concrete tribometer was proposed as a suitable device to characterize rheological properties of the lubrication layer, a slip layer facilitating the pumping process that is formed on the inner surface of the steel pipe [3]–[6]. A number of tribometer designs were developed using a rotary cylinder that is immersed in concrete during the test, resulting in the formation of the lubrication layer on the vertical wall of the cylinder. Unfortunately, the measured torque is very often distorted by the presence of inadvertent flow resistance exerted by the concrete sample at the bottom of the cylinder surface. In this paper, an experimental study to develop a correction procedure for the bottom effect is described.

Background

Principles of Concrete Flow in Pipe

The flow of fresh concrete in a pipe is a complex fluid mechanics problem arising from the fact that concrete behaves like a non-Newtonian fluid, therefore, any flow characterization requires detailed knowledge of concrete rheological properties. Two distinguishable material zones can be found in the pipeline: the lubrication layer and inner bulk concrete [2]. The flow regime of the inner concrete is a function of shear stress applied to concrete due to pumping pressure and the concrete yield stress. It was shown and experimentally verified that if the shear stress acting on the inner zone is smaller than the concrete yield stress, concrete moves through the pipe as a plug and only the lubrication layer is sheared [3], [7], [8]. When the applied shear stress overcomes the value of concrete yield stress, the outer-part of the bulk concrete is also sheared, as shown in Figure 47 [3], [9]. This is typical for concrete with relatively low values of the yield stress, such as highly-workable concrete (HWC) or self-consolidating concrete (SCC). Nonetheless, in all of these cases, pumping is facilitated by the presence of the lubrication layer.

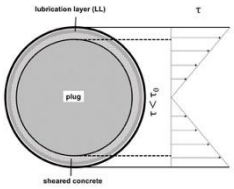

Figure 47: Concrete flow in pipe during pumping

Lubrication Layer

The lubrication layer, also referred to as slippage or the boundary layer, is a material formation adjacent to the pipe surface whose existence was first predicted in the 1930s [10]. This zone reduces friction between the wall of the pipe and concrete and allows the concrete mass to be moved through the pipeline. The layer thickness is estimated to be between 1 and 5 mm, however discussion is still ongoing about the composition of the layer [7], [11], [12]. It was reported that the layer thickness is independent of flow rate, but that it is related to the mix design of concrete and the pipe diameter [12]. Two mutually non-exclusive phenomena have been linked to the process of boundary layer formation. First, the suggestion has been made that large particles migrate towards the center of the pipeline due to a shear rate gradient in the pipeline. Shear rate is maximized at the inner wall surface and is zero in the center of the pipe. Second, the paste content around the pipe wall increases within a zone of thickness equal to half of the maximum aggregate size, as a result of a loose packing of coarse aggregate in close proximity to the pipe wall [13], [14].

The effect of the lubrication layer on pumping pressure and ultimately on pumpability was explained by Kaplan [3]. His experimentally verified analytical model [8], [15] is defined by Eqns. (1) and (2).

$$\Delta p_{tot} = \frac{2L}{R}\left(\frac{Q}{3600\pi R^2 k_r}\eta_{LL} + \tau_{0,LL}\right) \quad \textbf{(1)}$$

$$\Delta p_{tot} = \frac{2L}{R}\left(\frac{\frac{Q}{3600\pi R^2 k_r} - \frac{R}{4\mu_p}\tau_{LL} + \frac{R}{3\mu_p}\tau_0}{1 + \frac{R}{4\mu_p}\eta_{LL}}\eta_{LL} + \tau_{0,LL}\right) \quad \textbf{(2)}$$

where Δp_{tot} is the pressure loss over pipe length (Pa), L is the length of the pipe (m), R is the pipe radius (m), Q is the theoretical flow rate of concrete (m³/h), k_r is the filling coefficient of pump pistons (-) , μ_p is plastic viscosity of concrete (Pa),

τ_0 is the yield stress of concrete (Pa), $\tau_{0,LL}$ is the yield stress of the lubrication layer (Pa) and η_{LL} is the viscous of the lubrication layer (Pa.s.m^{-1}). Eqn. (1) is to be used when the concrete yield stress is lower than the applied shear stress at the wall (plug flow) while Eqn. (2) is valid when the shear stress exceeds the concrete yield stress (concrete is sheared). Both equations are dependent on two parameters of the lubrication layer – yield stress ($\tau_{0,LL}$) and the viscous constant (η_{LL}). As the thickness of the thickness of the lubrication layer is unknown, Kaplan [3] proposed the viscous constant to be used as a viscosity-like parameter of the lubrication layer. The physical meaning of the viscous constant can be explained as a viscosity-to-thickness ratio of the lubrication layer. Both yield stress of the lubrication layer and viscous constant can be measured using a tribometer.

Tribometer

A concrete tribometer is a device based on a similar principle as a regular concentric cylinders rheometer. While concrete rheometers usually have roughened or ribbed surfaces, a tribometer typically consists of a concentric smooth-wall cylinder (inner cylinder) that is immersed in a cylindrical container (outer cylinder) filled with concrete during the test. The outer cylinder remains stationary as the inner cylinder rotates around its axis. The lubrication layer is formed on the wall of the inner cylinder. An essential part of the device is a sensor that is able to register the torque required to maintain a constant rotational velocity of the inner cylinder immersed in the concrete. Several tribometer designs (Figure 48) incorporating different setups of the inner and outer cylinder were previously introduced [3]–[6], [16]. The testing procedure used in tribometers is similar to the procedure applied to concrete rheometers. Tested concrete is pre-sheared for a prolonged amount of time to create the lubrication layer and to avoid any thixotropic behavior. Subsequently, various rotational velocities (in decreasing order) are imposed on the cylinder, holding each velocity level constant for a certain period of time while the resulting torque for each velocity is registered by the device.

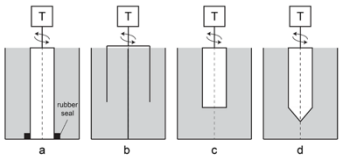

Figure 48: Tribometers by a) Kaplan, b) Chapdelaine, c) Ngo and d) Feys.

Bottom Effect of the Inner Cylinder

All discussed tribometers were found to have issues when used with SCC [6]. In Kaplan's tribometer shown in Figure 2a [3], a complex three-dimensional effect might occur at the interface of the stationary bottom plate and the inner cylinder, in addition to unintentional friction between the rubber seal and the cylinder. In order to eliminate the friction effect at the bottom of the container, Chapdelaine's tribometer shown in Figure 2b [4] uses a hollow open cylinder, resulting in formation of two lubrication layers on the inner and outer wall of the cylinder. Both layers are, however, subjected to different shear rates which may yield to different thixotropic behavior of tested concrete. Furthermore, a third lubrication layer is likely to form at the ribs in the center of the device. Ngo [5] suggested using a two-step procedure to correct for the effect of the bottom of the cylinder in the tribometer shown in Figure 2c. In the first step, the cylinder is placed on the sample so that only its bottom is in contact with the concrete sample, and the test is performed. In the second step, the test is repeated with the whole cylinder immersed in concrete. To obtain the final result, data from the Step 1 are subtracted from the Step 2 measurements. Finally, Feys [6] designed a tribometer to be used with SCC as shown in Figure 2d. In this tribometer, the flat bottom cylinder was replaced with a conical-shaped bottom cylinder to eliminate the 3-D flow phenomena that is typically present at the bottom of the container.

In this paper, a correction procedure to characterize the bottom effect of the inner cylinders developed for Feys' tribometer is introduced. The proposed procedure suggests that the test is performed multiple times, each time with different volume of concrete in the container. By finding the relationship between the filling height of the container and registered torque, one can calculate the level of torque at filling height equal to zero, i.e. the effect of the bottom of the cylinder [17]. However, this procedure did not deliver a successful correction procedure for the bottom of the cylinder, as described in [6]. This is most likely attributed to the lack of cleaning the cylinder and the non-remixing of the concrete in between measurements. Specific attention to these issues has been paid in this experimental study.

Experimental Study

Tribometer

Two concrete tribometers (tribometer M and tribometer K) based on the ICAR portable rheometer were used in this study. The standard four-blade vane for rheological measurements was replaced by an aluminum cylinder in tribometer M and a stainless steel cylinder in tribometer K to perform tribological measurements. Both tribometer cylinders had a conical shaped bottom. Cylinder of tribometer M had radius of 125 mm and height of 201 mm with the conical part height of 62 mm,

and cylinder of tribometer K had radius of 127 mm and height of 203 mm with the conical part height of 51 mm.

Experimental Procedure

Four concrete mixes with different rheological properties were utilized in this investigation. Mix designs are shown in Table . Concrete was mixed in a standard drum mixer, batch volume for each mix was 100 liters.

Table I. Mixture proportionings. WR = Water reducer

ID	*Cement / Fly ash (C) / Silica Fume / Slag (kg/m^3)*	*Coarse Aggregate (kg/m^3)*	*Fine Aggregate (kg/m^3)*	*Water (l/m^3)*	*WR (ml/m^3)*	*w/c (-)*	*Initial slump flow (mm)*
A	***377 / 130 / 13 / 0***	***728***	***960***	***166***	***2500***	***0.32***	***457***
B	***308 / 106 / 11 / 0***	***895***	***854***	***179***	***1000***	***0.42***	***350***
C	***308 / 106 / 11 / 5***	***895***	***854***	***179***	***2000***	***0.42***	***580***

After batching, each concrete was subjected to a procedure to determine the effect of the conical bottom of the cylinder on tribological measurements. The test was run incorporating four filling heights in the tribometer to evaluate the secondary flow effect of the bottom of the rotary cylinder. The four filling heights used were: (1) only the cone tip of the cylinder immersed in concrete, (2) approximately one third of the cone height immersed in concrete, (3) approximately two thirds of the cone height immersed cone, and (4) cone fully immersed in concrete.

The following testing procedure was adopted:

1. Fill the container with concrete to achieve the specific filling height.
2. Insert tribometer into the container.
3. Pre-shear concrete at a constant rotational velocity of 0.6 rps for 30 seconds.
4. Apply a decreasing set of seven rotational velocities from 0.6 rps to 0.030 rps and hold each velocity constant for 5 seconds.
5. Gently remove the tribometer head from the container and record value of the filling height (Figure 49).
6. Remove all material from the cylinder and clean it.
7. Manually remix concrete in the container to homogenize.
8. Repeat steps 1-7 for all filling heights.

***Figure 49*. Filling height measurement**

Results and Discussion

To determine the effect of the bottom of the cylinder, a relationship between the filling height and registered torque was established for each rotational velocity (T-h curve), as shown in Figure 50 and Figure 51 for tribometers M and tribometer K, respectively. These relationships exhibited a linear character in majority of the cases, however, in several instances, a slightly non-linear behavior was observed. This was most likely due to changing rheological properties (i.e. stiffening) of concrete during the test. Additionally, for measurements at low filling heights and/or small rotational velocities, the magnitude of generated friction at the steel/concrete interfaces is typically very low, therefore the registered torque tends to be very small too. As the torque sensor in the measuring device was originally designed for rheological measurements that yield relatively high values of torque, a precision of the measuring device must be taken into account when interpreting the results. For this reason, values obtained at the lowest rotational velocity (0.030 rps) were not considered for further analysis.

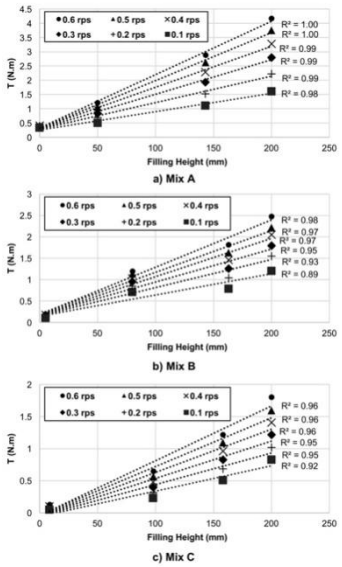

Figure 50. Relationship between torque and filling height – Tribometer M

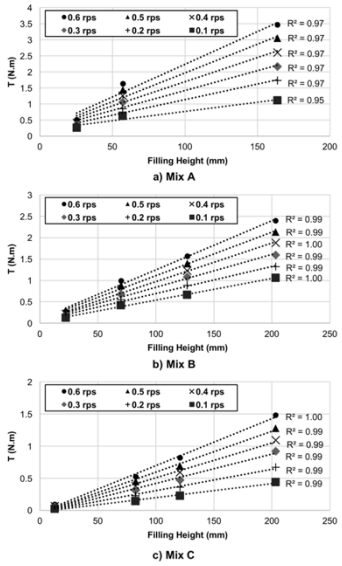

Figure 51. Relationship between torque and filling height – Tribometer K

The recorded data were subjected to a linear extrapolation in order to determine the torque at the theoretical filling height of 0 mm, which corresponds to the situation

when only the conical bottom of the cylinder is immersed in concrete. The contribution of the bottom of the cylinder was expressed as a linear function of the rotational velocity in the form of Eqn. (3):

$$T_{bottom} = aN + b \tag{3}$$

Where T_{bottom} (N.m) is the theoretical torque generated by the bottom of the tribometer cylinder, a and b are correction coefficients and N (rps) is the rotational velocity.

Values of obtained coefficients are shown in Table II, and comprehensive results are presented in Figure 52. Satisfactory results were obtained for all mixtures with the exception of Mix C. For Mix C, negative values of torque representing the effect of the cone were obtained from both tribometers. This would suggest that the bottom of the cylinder did not create any friction at its contact with the tested concrete, which is impossible by the physical nature of the test. Authors believe that the main reason why the correction procedure could not have been successfully applied on Mix C was the fact the rheological properties of this mixture exhibited a fast rate of change over time, resulting in a non-linear relationship between the torque and the filling height. This made it difficult to apply linear extrapolation to characterize the cone effect for that mixture. However, the proposed correction procedure was successfully applied for other two remaining mixes. Based on obtained correction equations, the presence of the cone can be contributed to between 4% and 8% of the friction generated at the steel/concrete interface for the highest rotational velocity (0.6 rps) and between 12% and 16% for the lowest rotational velocity (0.1 rps). As expected, a decrease in the rotational velocity caused an increase in the overall effect of the bottom of the rotatory cylinder.

Table II: Coefficients characterizing the effect of the bottom of cylinder

	Tribometer M			***Tribometer K***		
Coefficient	***Mix A***	***Mix B***	***Mix C***	***Mix A***	***Mix B***	***Mix C***
a (slope)	*0.1307*	*0.0983*	*0.0378*	*0.1315*	*0.1223*	*-0.0301*
b (intercept)	*0.2546*	*0.1387*	*-0.0586*	*0.1252*	*0.0276*	*-0.0226*

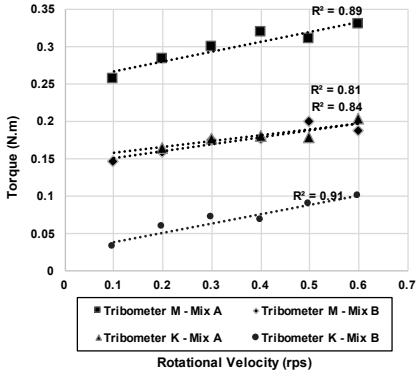

Figure 52. Torque imposed by the bottom of the cylinder as a function of the rotational velocity

Concluding Remarks

A tribometer is an effective device that can be used to determine properties of the lubrication layer, which are fundamental for successful concrete pumping. A correction procedure to characterize the bottom effect of a rotary cylinder during tribological measurements was introduced in this paper. It was shown that the 3-D contribution of the cone can be expressed as a linear function of the rotational velocity imposed on the cylinder and that this procedure can reproducible and independent of used device.

Three concrete mixes were investigated in this study. The correction procedure was successfully applied to two of them and coefficients for the correction equation were obtained. For the case of the unsuccessful attempt, it was determined that the fast rate of change of rheological properties was responsible for a slightly non-linear relationship between the filling height and registered torque, resulting in skewed measurements. Therefore, it is recommended to use a concrete mixture with rheological properties that do not significantly change during tribometer correction procedures.

Acknowledgments

Authors would like to acknowledge the Kansas Department of Transportation for the financial support of this research project.

References

[1] C. A. Cornell and S. E. McKee, "*Concrete Pump,*" US Patent No. 1 093

916, 1914.

[2] M. Choi, C. F. Ferraris, N. S. Martys, D. Lootens, V. K. Bui, and H. R. T. Hamilton, "Metrology Needs for Predicting Concrete Pumpability," *Adv. Mater. Sci. Eng.*, vol. 2015, p. 10, 2015.

[3] D. Kaplan, "*Pompage des bétons*," PhD Dissertation, Laboratoire Central des Ponts et Chausees, Paris, 2001.

[4] F. Chapdelaine, "*Etude Fondamentale et Pratique sur le Pompage du Beton*," PhD Dissertation, University of Laval, 2007.

[5] T. T. Ngo, E. H. Kadri, R. Bennacer, and F. Cussigh, "Use of tribometer to estimate interface friction and concrete boundary layer composition during the fluid concrete pumping," *Constr. Build. Mater.*, vol. 24, no. 7, pp. 1253–1261, Jul. 2010.

[6] D. Feys, K. H. Khayat, A. Perez-Schell, and R. Khatib, "Development of a tribometer to characterize lubrication layer properties of self-consolidating concrete," *Cem. Concr. Compos.*, vol. 54, pp. 40–52, Nov. 2014.

[7] R. Browne and P. Bamforth, "Tests to establish concrete pumpability," *ACI J. Proc.*, no. 74, pp. 193–203, 1977.

[8] D. Feys, K. H. Khayat, A. Perez-Schell, and R. Khatib, "Prediction of pumping pressure by means of new tribometer for highly-workable concrete," *Cem. Concr. Compos.*, vol. 57, pp. 102–115, 2015.

[9] D. Feys, "*Rheological Properties and Pumping of Self-Compacting Concrete*," PhD Dissertation, Ghent University, 2009.

[10] C. F. Ball, "Concrete By Pump And Pipeline," *ACI J. Proc.*, no. 333, pp. 333–349, 1936.

[11] S. Jacobsen, L. Haugan, T. A. Hammer, and E. Kalogiannidis, "Flow conditions of fresh mortar and concrete in different pipes," *Cem. Concr. Res.*, vol. 39, no. 11, pp. 997–1006, Nov. 2009.

[12] M. Choi, N. Roussel, Y. Kim, and J. Kim, "Lubrication layer properties during concrete pumping," *Cem. Concr. Res.*, vol. 45, pp. 69–78, Mar. 2013.

[13] S. Jacobsen, J. H. Mork, S. F. Lee, and L. Haugan, "*Pumping of Concrete and Mortar – State of the Art*," COIN Project Report, p. 46, 2008.

[14] R. Khatib, "*Analysis and Prediction of Pumping Characteristics of High-Strength Self-Consolidating Concrete*," PhD Dissertation, Universite de Sherbrooke, 2013.

[15] D. Kaplan, F. De Larrard, and T. Sedran, "Design of concrete pumping circuit," *ACI Mater. J.*, vol. 102, no. 2, pp. 110 – 117, 2005.

[16] S. Kwon, C. Park, J. Jeong, S. Jo, and S. Lee, "Prediction of Concrete Pumping: Part I—Development of New Tribometer for Analysis of Lubricating Layer," *ACI Mater. J.*, no. 110, pp. 647–656, 2013.

[17] C. W. Macosko, *Rheology: Principles, Measurements, and Applications*, 1st ed. Weinheim: Wiley-VCH, 1994.

Rheological Behavior of Cement Pastes under Large Amplitude Oscillatory Shear

Théau Conte and Mohend Chaouche*

LMT (ENS Cachan, CNRS, Université Paris Saclay). 61, avenue du Président Wilson 94235 Cachan, France
*E-mail address: chaouche@lmt.ens-cachan.fr (Mohend Chaouche)
phone number: +33 147402247

Abstract Cement pastes exhibit virtually all the rheological features of complex fluids. Thus, several rheological methods and setups have been used in the literature to characterize these materials. In the present investigation Large Amplitude Oscillatory Shear (LAOS) is for the first time exploited for cement pastes. LAOS can be used to characterize all the rheological properties within a single procedure. This technique is tested in the case of three different cement mixes: a Portland cement paste, nanoclay blended cement paste and a cement paste containing a hydro-soluble polymer. These mixes were selected in order to get rheological properties that are different both quantitatively and qualitatively. Indeed, addition of a low amount of nanoclay increased significantly the yield stress and the shear-thinning/thixotropic aspects of the cement paste, whereas addition of cellulose ether led to the decrease of yield stress and thixotropy. These non-linear rheological properties are discussed within the framework of LAOS.

Keywords: *Large Amplitude Oscillatory shear (LAOS), cement pastes, thixotropy, aging.*

Introduction

Fresh cement pastes, in particular those containing polymer admixtures, display almost all the properties that can be encountered in rheology: viscoelasticity, yielding, shear-thinning/shear-thickening, thixotropy/rheopexy, irreversible time evolution, etc. [1-4]. In addition, due to their multiphasic aspects, flow induced liquid-solid separation or segregation may take place under certain circumstances [5,6]. This complex rheological behavior may in particular explain the difficulty

and even non-relevance of making comparison among the different results reported in the literature. Beyond the inconsistency of the reported measurements arising from the impact of the rheological setups and the data processing [7], the complexity of the rheological behavior itself, in particular yielding and thixotropy, may lead to non-comparable results [8,9]. Indeed several procedures, leading to different results, can be used to determine yield stress, thixotropy and aging [10]. For instance evolution at rest or aging (due to both hydration and thixotropic recovery) can be characterized using small amplitude oscillatory shear (SAOS) [1,10]. And different protocols can be used to characterize thixotropy: shear cycling, creep after shear [10,11], etc.

Although results for yield stress and flow curves for cement pastes have been reported in the literature, such properties cannot be defined rigorously in the case of evolving materials. Indeed these properties are dependent upon the duration of the measurement and the flow history. In addition steady state at a given stress/strain rate cannot be reached in the case of these materials. Therefore their flow curves cannot be determined. The latter are not then material properties. Cement pastes are also highly sensitive to stress variations. Thus the oscillatory shear protocol for which one has smooth evolution of the stress is the most appropriate. To deal with the non-linear properties, as for example thixotropy or shear-thinning/thickening, the large amplitude oscillatory shear (LAOS) technique seems promising. Indeed, the evolution of the Pipkin diagram, which represents the evolution of non-linear viscoelastic properties at different frequencies and amplitudes [12-16], as a function of the paste age may turn out to be the most appropriate and complete rheological fingerprint of the material. Yet, the physical interpretation of LAOS data in the case of such complex materials is expected to be not straightforward.

In the present investigation the LAOS rheological procedure is tempted for the first in the case of cementitious materials. The objective of the present exploratory study is to determine, even in a qualitative manner, which rheological features can be inferred from the LAOS procedure in the case of cement pastes. To illustrate this investigation three different mixes were considered at the same water/binder ratio: a pure cement paste, clay-blended cement paste and a polymer-blended cement paste.

Materials and Methods

Materials

Portland cement type CEM1 52.5 from Holcim was used in all the mixes. The nanoclay (Acti-Gel®) (designated hereafter as NC) was provided by Active Minerals International (Sparks, MD, USA). It is a highly purified form of attapulgite (palygorskite). It consists of rod-like particles of an average length of

L=1.75 μm and average diameter of D=30 nm. Due to their very high aspect ratio (r=L/D ~ 58), they can form a gel even at very low volume fraction provided they are dispersed into individual particles. However, in practice the particles are more or less flocculated (stacked) depending upon the physicochemical properties of their surface and those of the solvent. Then the actual average aspect ratio should be much smaller. In any case, the fact that the clay particles are rod shaped is very favorable (compared for instance to plate-shaped clays as bentonite [11]) regarding their impact on the rheological properties (in particular the yield stress) when used as rheological modifiers in various materials.

Another type of rheological modifier was used, which is a cellulose ether (CE) based hydro-soluble polymer. We used a commercial grade (WALOCEL™ MW 40000 PFV) from DOW Chemical. The CE is characterized in particular by its viscosity (40000 cp) when dissolved in water at 2% by weight, and as measured using a Brookfield RV viscosimeter at 20 rpm. The value of the viscosity gives an indication of the average molecular weight of the polymer. CE admixtures are generally comb-like polymers consisting of a hydrophilic backbone along which hydrophobic brushes are attached. In aqueous solutions the hydrophobic brushes associate to minimize contact with water making up then physical (reversible) crosslinks. Due in particular to these associative properties, CE based admixtures are characterized by a significant impact on the viscosity of the material [17], even when used in very low amount.

Three different formulations were considered in this study: a pure cement paste, a cement paste blended with 1% bwoc of nanoclay (NC) and a cement paste containing 0.1% bwoc CE. Tap water was used in all the mixes, and the water/powder ratio was fixed to 0.4.

The clay powder was first dispersed in water at 400 rpm during 5 minutes using a blender (IKA Eurostar 40). Then the appropriate amount of cement powder was added to the clay dispersion, and the blended paste is mixed for 2 more minutes. In the case of CE-blended pastes, the cement powder was first dry mixed with the CE by hand for 1 min. Then, it was mixed (also by hand) with water for 2 min.

Rheological Measurements

Measurements

All the rheological measurements were performed with an AR2000EX rheometer from TA instrument. We used the plate-plate geometry with hatched plates in order to minimize wall slip. The gap was set at 1 mm for all the measurements. In order to start with the same flow history, a pre-shear was applied at a rate of 50 s^{-1} for 60 s followed by a period of rest for 60 s. The temperature was kept constant at 20°C ± 0.1°C using a Peltier system.

Since the materials considered are yield stress fluids, it is more appropriate to perform the rheological measurements at controlled stresses. Our rheometer is actually a stress-controlled apparatus. In order to determine the transition from linear (SAOS) to non-linear (LAOS) regimes, an oscillatory stress sweep with amplitude varying from 1 Pa to 100 Pa was performed. For each amplitude step, three cycles are recorded, then data are processed in order to determine LAOS rheological properties. In the present investigation the evolution of the material during the 3 LAOS cycles is ignored. That is, transient effects are not taken into account to determine the LAOS parameters [18,19]. The transient effects in cement pastes include both rebuilding after shear (thixotropy) and change of microstructure due to hydration. These transient phenomena may take place at different time scales. Then, temporal evolution of the LAOS properties as it is considered here corresponds to those taking place at significantly larger time scales than the duration of the LAOS measurement.

Each test was performed three times to check for the repeatability of the measurements.

Data Processing

In the present investigation we consider the stress-controlled oscillatory shear protocol. Contrary to the linear regime, for which there is no difference in viscoelastic properties between stress and strain controlled protocols, in the non-linear regime the two types of solicitations lead to different results [19].

In a LAOStress experiment a sinusoidal stress t is applied at different amplitudes t_0 and frequencies w:

$$t(t) = t_0 \sin(wt) \quad (1)$$

If the stress amplitude is sufficiently small, the output strain g and rate of strain $\dot{\gamma}$ are also sinusoidal and respond with the same frequency, but with generally a phase lag d:

$$g(t) = g_0 sin(wt + d) \quad (2)$$

$$\dot{\gamma}(t) = \omega\gamma_0 cos(\omega t + \delta) \quad (3)$$

Under these circumstances the microstructure of the sample is not significantly modified and this protocol (SAOS) can be used to mechanically probe the material microstructure at rest. Two viscoelastic parameters are enough to describe SAOS behavior, namely J' (storage compliance) and J" (loss compliance) (Equ. 4). In strain-controlled oscillatory shear experiments (SAOStrain) we rather deal with the more familiar viscoelastic properties G' (storage modulus) and G" (loss modulus).

These viscoelastic properties are independent of the stress amplitude within this linear regime. They are defined as:

$$\gamma(t) = \gamma_0 (J' \sin(\omega t) + J'' \cos(\omega t)) \quad (4)$$

The SAOS behavior can be visualized in a stress-strain diagram (Lissajous-Bowditch curves, referred to hereafter as L-B curves) by eliminating the time variable through combination of equations 2 and 4. SAOS behavior is characterized by an elliptic L-B curve. For the extreme case of purely viscous fluid the L-B curve degenerates into a circle, while for a purely elastic solid it degenerates into a straight line.

If the stress amplitude is high enough that the induced change in the material microstructure cannot be ignored anymore, the output strain is no longer sinusoidal, and higher order harmonics come into play. To determine LAOStress viscoelastic parameters, the output strain and rate of strain signals are first decomposed into Fourier series [19] to deal with the higher order harmonics:

$$\gamma(t) = \sum_{n=odd} \gamma_n \sin(n\omega t - \delta_n)$$

Only the odd components of the series are kept due to flow symmetry arguments. Similarly to SAOS (Equ. 4) the strain can be decomposed into two components:

$$\begin{aligned} \gamma(t) &= \tau_0 \sum_{n,odd} \left[J'_n \sin(n\omega t) - J''_n \cos(n\omega t) \right] \\ \dot{\gamma}(t) &= \tau_0 \sum_{n,odd} \left[n\Psi''_n \cos(n\omega t) + n\Psi'_n \sin(n\omega t) \right] \end{aligned} \quad (6)$$

The material properties J'_n and J''_n are the dynamic compliances related to the different harmonics, and Ψ'_n and Ψ''_n are the corresponding dynamic fluidities.

Results and Discussion

Transition between Linear and Nonlinear Regime

Although the oscillatory shear experiments were performed at an input stress, the linear viscoelastic (LVE) properties are discussed in terms of the more familiar storage (G') and loss (G'') moduli, since stress and strain inputs are equivalent in the LVE regime. It is to be noted that the reported values of the moduli beyond the LVE interval are the first order terms of the strain Fourier series.

Fig. 1a illustrates the evolution of G' and G" as a function of stress amplitude in the case of a CE blended cement paste. The moduli display a plateau (delimiting the LVE regime) at low stress amplitudes followed by a significant drop, and then

a moderate decrease. Within the LVE regime (plateau) the output signal (strain) is sinusoidal as the input signal (stress) (Fig. 1b). In addition the output signal is characterized by a constant amplitude and phase lag over cycling. This indicates that the material microstructure is not evolving over the three cycles. On the other hand, for stress amplitudes corresponding to the drop of the moduli, the output signal starts to deviate from a sinusoidal shape (Fig. 1c). Moreover, its amplitude and phase lag evolves slightly over the three cycles, indicating that the material microstructure is being broken by shear (strain amplitude increases for a fixed stress amplitude).

Far beyond the LVE regime (Fig. 1d) the output strain signal deviates significantly from a sinusoidal shape, indicating notable contribution of higher order harmonics (high non-linearities) to the strain. Yet, the evolution of the amplitude and phase lag over a cycle is not significant. This may indicate that the microstructure is almost fully broken and the origin of non-linearity is mainly flow.

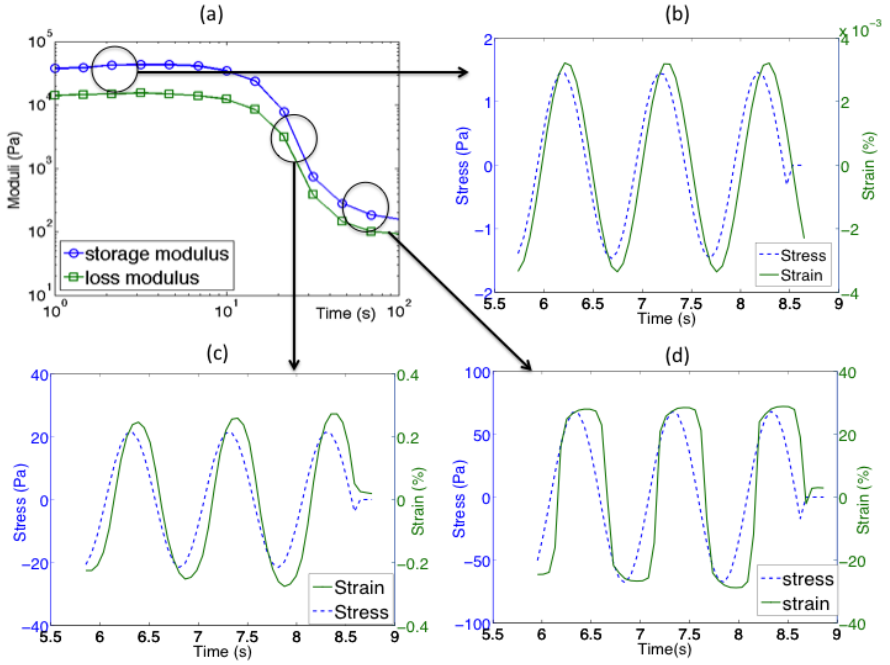

Figure 1. Transition between linear and non-linear viscoelastic regimes. (a) Evolution of the storage and loss moduli as a function of stress amplitude; (b) input stress signal and output strain signal versus time within the linear zone; (c) output signal and input signal versus time under high rate of microstructure breakage conditions; (d) output and input signals versus time under highly non-linear conditions.

Fig. 2 represents the stress sweep results in the case of the three mixes considered. The moduli display a plateau (delimiting the LVE regime) at low stress amplitudes followed by a significant drop and then a moderate decrease. When amplitude increases moduli drop significantly, behavior starts to be non linear. It also means that microstructure is being broken under shear. The material exhibit high elasticity (G' > G") for the three mixes. This is expected for yield stress fluids as long as the stress amplitude is lower than the yield stress. Addition of NC increases both the moduli and the extension of the LVE interval, corresponding therefore to an increase of the yield stress. This is in agreement with the results reported by Kawashima et al [20]. This was attributed to an eventual flocculation of the clay nanoparticles due the high ionic strength of the pore solution. On the other hand, addition of CE leads to the decrease of the LVE moduli and the size of the LVE interval, corresponding to a decrease of the yield stress. This is consistent with the results reported by Cappellari et al [17] for mortars. This may be attributed to an eventual superplasticizing effect of the polymer (due to adsorption of the CE macromolecules on the mineral particles) and air-entrainment.

In the highly non-linear zone (flow) the CE increases the moduli (first harmonic term) due to its viscosifying effect. Finally we can notice that the steepness of the transition from linear to non-linear, which is characteristic of avalanche-type behavior of granular pastes [21], is reduced by addition of CE.

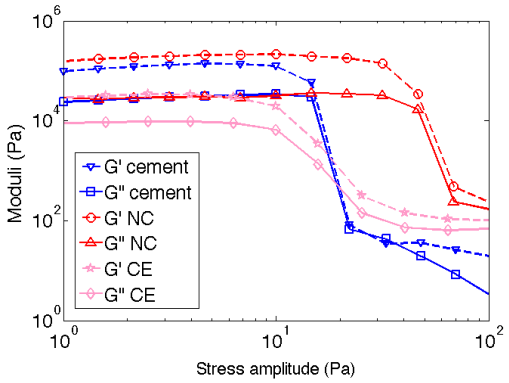

Figure 2. Evolution of the viscoelastic properties over stress sweep in the case of the three mixes considered.

Qualitative Characterization of the LAOS Properties through the L-B Curves

Considering the evolution of the storage modulus versus stress amplitude three different regimes can be delimited as indicated in Fig. 3a : LVE regime, transition regime (or moderately non-linear regime) and highly non-linear regime. Three L-B

curves corresponding to different stress amplitudes are plotted for each regime (Fig. 3b, c, d respectively). The oscillatory tests were performed at the same frequency (1 Hz). As expected the L-B curves for the stress amplitudes located in the LVE interval are ellipse shaped for the three stress amplitudes considered (Fig. 3b). The area embodied by the curves remains sensibly constant over the LVE regime, indicating that the dissipated energy is the same. The rotation of the L-B curves towards the stress axis when increasing the stress amplitude indicates that the material is inter-cycle stress-hardening within the LVE regime. This may be due to inter-cycle thixotropic rebuilding and hydration.

.

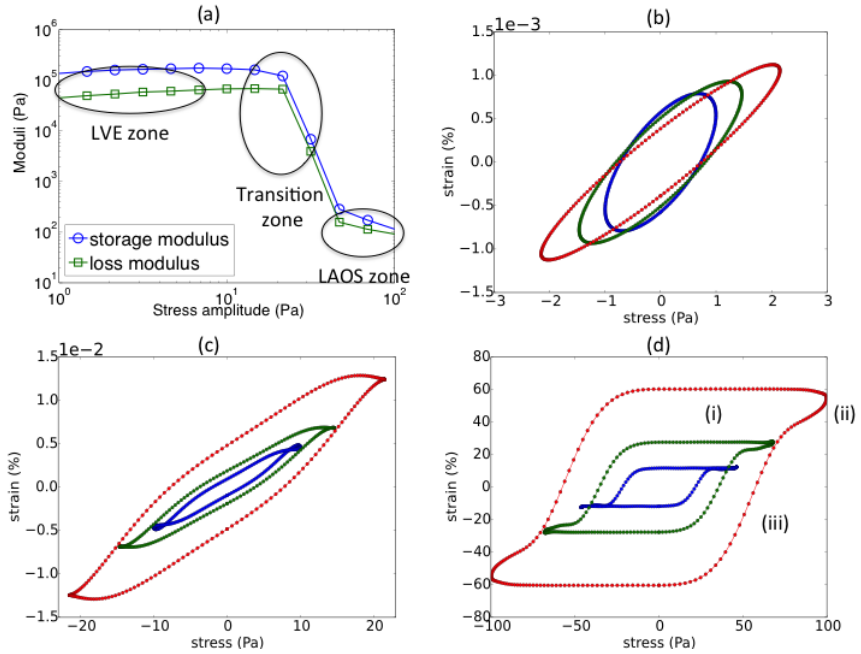

Figure 3. Evolution of the L-B curves in the case of a cement paste over the LVE through the nonlinear regimes. (a) Evolution of the storage and loss moduli as a function of the stress amplitude, and indication of the different regimes; (b) strain versus stress L-B curves for three different stress amplitudes located within the LVE zone; (c) L-B curves within the moderately non-linear (or transition) zone; (d) L-B curves in the highly non linear zone.

The transition to a non-linear response is characterized by a clear deviation of the L-B curves from an ellipse (Fig. 3c). This can be considered as a signature of the transition to non-linearity. The shape of the L-B curves indicates that the material is overall intra-cycle stress-softening. Yet, local stress-stiffening zones can be observed close to stress reversal.

The high non-linearity (Fig. 3d) regime is characterized by a large deviation of the L-B from the elliptical shape. In addition the area delimited by the L-B plot increases indicating that the dissipated energy (due viscous effects) per cycle is becoming higher (flow dominated regime). The L-B plot in the highly non-linear regime is characterized by mainly three features as indicated in Fig. 3d : (i) a vanishingly small evolution of the strain with stress after the stress passes through zero, which corresponds to a highly strain-stiffening intra-cycle behavior, (ii) a second strain-stiffening zone following reversal of stress, and (iii) in between we have an approximately elastic behavior. Within the strain-stiffening intervals it can be considered that buildup kinetics of the material is higher than flow-induced breakage kinetics, while over the quasi-elastic zones the two kinetics are comparable.

Fig. 4 represents the evolution of the L-B plots over the linear to the non-linear intervals in the case of a NC blended cement paste. Due to steepness of the transition from linear to non-linear regimes only a limited number of L-B plots can be captured within the transition zone. Actually the shape of the reported L-B curves in the transition zone (Fig. 4c) remains close to an ellipse indicating that the behavior is still slightly linear and the transition to non-linear behavior is rather brutal. Overall the results are qualitatively similar to those for plain cement pastes. One can however notice that the energy dissipation decreases in presence of NC (Fig. 4d).

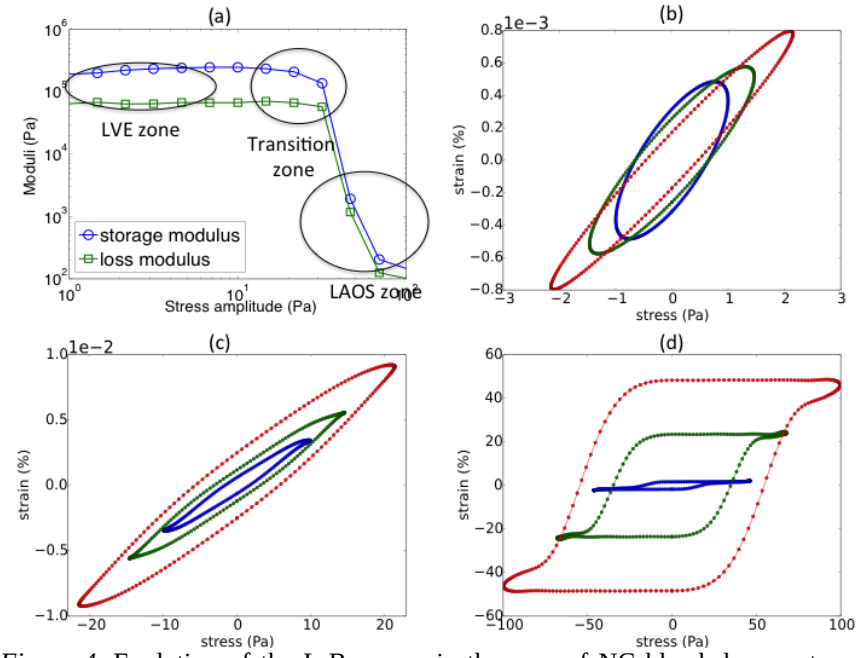

Figure 4. Evolution of the L-B curves in the case of NC blended cement pastes from LVE to nonlinear regimes. (a) Evolution of the storage and loss moduli as a function of stress amplitude; (b) strain versus stress L-B curves within the LVE zone; (c) first non linearities of the L-B curves in the transition zone; (d) L-B curves within the highly non linear zone.

The impact of CE addition on the evolution of L-B plots for different stress amplitudes spanning the linear through the non-linear regimes is reported in Fig. 5. In contrast with the previous mixes, addition of CE does not lead to inter-cycle stress stiffening behavior of the paste within the LVE regime (no significant rotation of the L-B plots) (Fig. 5b). This indicates that the CE slows down inter-cycle rebuilding kinetics (and eventual hydration).

Within the transition zone the L-B curves remain quite close to ellipses (Fig. 5c). And one can notice an inter-cycle rotation of the curves towards the strain axis as the stress amplitude increases. This reflects the inter-cycle stress-softening within this zone due to inter-cycle microstructure breakage. Within the highly non-linear zone, as previously, we observe regions of intra-cycle strain-stiffening upon reversal of the stress.

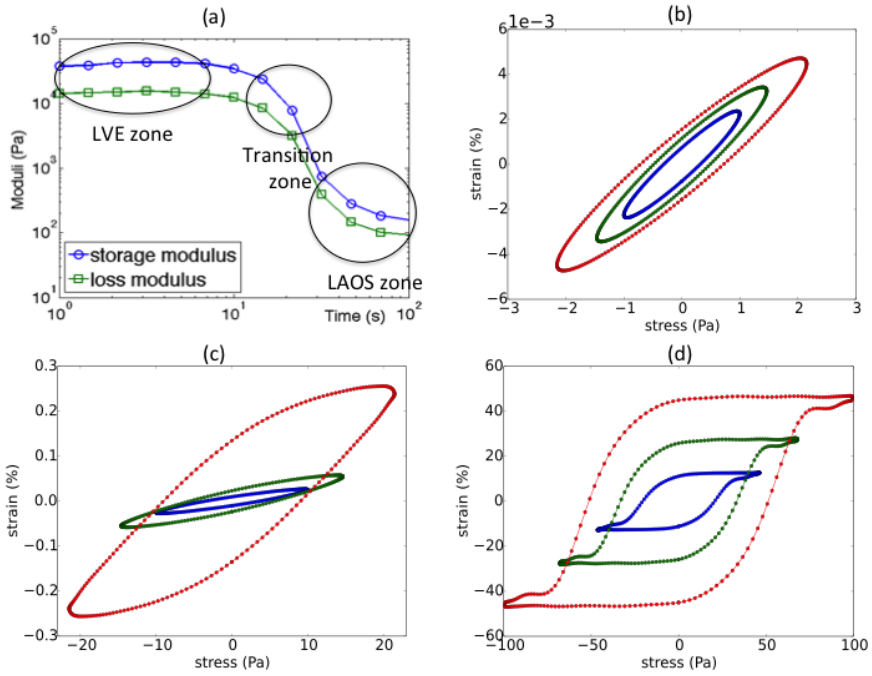

Figure 5. Evolution of the L-B curves of a cement paste blended with CE as a function of stress amplitude. (a) Evolution of the storage and loss moduli as a function of stress amplitude; (b) strain versus stress L-B curves within the LVE zone; (c) emergence of the first non-linearities in the transition zone; (d) L-B curves within the highly non-linear zone.

Conclusions

In the present investigation we exploited for the first time the LAOS protocol in the case of cementitious materials in fresh state. Three cement mixes with qualitatively different rheological properties were considered through their LAOS rheological properties. LAOS tests for cementitious materials seem promising, it allows characterizing intra and inter cycle non-linear properties of the material within a single procedure. Since cement materials behavior is highly dependent on shear history and time, for different set of LAOS parameters (amplitude, frequency), influence of time should be investigated.

References

[1] M.A. Schultz, L.J. Struble, Use of oscillatory shear to study flow behavior of fresh cement paste, Cement and Concrete Research. 23

(1993) 273–282.
[2] O.H. Wallevik, J.E. Wallevik, Rheology as a tool in concrete science: The use of rheographs and workability boxes, Cement and Concrete Research. 41 (2011) 1279–1288.
[3] K.H. Khayat, Viscosity-Enhancing Admixtures for Cement-Based Materials - An Overview, Cement and Concrete Composites. 20 (1998) 171–188.
[4] N. Roussel, G. Ovarlez, S. Garrault, C. Brumaud, The origins of thixotropy of fresh cement pastes, Cement and Concrete Research. 42 (2012) 148–157.
[5] F.A. Cardoso, V.M. John, R.G. Pileggi, P.F.G. Banfill, Characterisation of rendering mortars by squeeze-flow and rotational rheometry, Cement and Concrete Research. 57 (2014) 79–87.
[6] F.A. Cardoso, A.L. Fujii, R.G. Pileggi, M. Chaouche, Parallel-plate rotational rheometry of cement paste: Influence of the squeeze velocity during gap positioning, Cement and Concrete Research. 75 (2015) 66–74.
[7] O.H. Wallevik, D. Feys, J.E. Wallevik, K.H. Khayat, Avoiding inaccurate interpretations of rheological measurements for cement-based materials, Cement and Concrete Research. 78 (2015) 100–109.
[8] A. Saak, S.P. Shah, The influence of wall slip on yield stress and viscoelastic measurements of cement paste, Cement and Concrete Research. 31 (2001) 205–212.
[9] P.C.F. Møller, J. Mewis, D. Bonn, Yield stress and thixotropy: on the difficulty of measuring yield stresses in practice, Soft Matter. 2 (2006) 274.
[10] S. Kawashima, M. Chaouche, D.J. Corr, S.P. Shah, Rate of thixotropic rebuilding of cement pastes modified with highly purified attapulgite clays, Cement and Concrete Research. 53 (2013) 112–118.
[11] A. Kaci, M. Chaouche, P.-A. Andréani, Influence of bentonite clay on the rheological behaviour of fresh mortars, Cement and Concrete Research. 41 (2011) 373–379.
[12] R.H. Ewoldt, A.E. Hosoi, G.H. Mckinley, New measures for characterizing nonlinear viscoelasticity in large amplitude oscillatory shear, J. Rheol. 52 (2008) 1427.
[13] S.A. Rogers, B.M. Erwin, D. Vlassopoulos, M. Cloitre, A sequence of physical processes determined and quantified in LAOS: Application to a yield stress fluid, J. Rheol. 55 (2011) 435.
[14] C.J. Dimitriou, R.H. Ewoldt, G.H. Mckinley, Describing and prescribing the constitutive response of yield stress fluids using large amplitude oscillatory shear stress (LAOStress), J. Rheol. 57 (2013) 27.
[15] K. Hyun, M. Wilhelm, C.O. Klein, K.S. Cho, J.G. Nam, K.H. Ahn, et al., Progress in Polymer Science, Progress in Polymer Science. 36 (2011) 1697–1753.
[16] R.H. Ewoldt, P. Winter, J. Maxey, G.H. Mckinley, Large amplitude

oscillatory shear of pseudoplastic and elastoviscoplastic materials, Cambridge, MA, Self-Published. (2009) 1–46.

[17] M. Cappellari, A. Daubresse, M. Chaouche, Influence of organic thickening admixtures on the rheological properties of mortars: Relationship with water-retention, Construction and Building Materials. 38 (2013) 950–961.

[18] R.H. Ewoldt, Defining nonlinear rheological material functions for oscillatory shear, J. Rheol. 57 (2013) 177–195.

[19] J. Läuger, H. Stettin, Differences between stress and strain control in the non-linear behavior of complex fluids, Rheol Acta. 49 (2010) 909–930.

[20] S. Kawashima, P. Hou, D.J. Corr, S.P. Shah, Modification of cement-based materials with nanoparticles, Cement and Concrete Composites. 36 (2013) 8–15.

[21] P. Coussot, Q.D. Nguyen, H.T. Huynh, D. Bonn, Avalanche Behavior in Yield Stress Fluids, Phys. Rev. Lett. 88 (2002) 175501.

Distinguishing Flocculation and Hydration Effects on the Thixotropy of Cement Pastes

Reiter L.[1], Wangler [1], Roussel N.[2], Flatt R. J.[1]*

[1] Institute for Building Materials, ETH Zürich, Switzerland
[2] Université Paris Est, IFSTTAR, France

Abstract The ability to predict the development of strength of fresh cementitious materials is essential for several questions such as formwork pressure and the building rate in extrusion systems used in digital fabrication, especially with the use of a self-compacting concrete. It has been established, that the reversible formation of a network of colloidal interactions along with the permanent formation of hydrates and their partially reversible connection of cement particles can account for this structuration. A quantitative link to cement hydration is however still missing.
In this study, we examine these two features using oscillation rheometry and isothermal calorimetry and investigate the rate of structural build up in relation to the progress of hydration.
Using sucrose as a set retarder, we show that it is possible to distinguish the contributions of flocculation and hydration to the structuration rates in cement pastes. Sucrose in this study puts the cementitious system to rest, strongly delaying the nucleation and/or growth of hydration products. For this system, we find that at long resting times, the structuration rate is dominated by the formation of hydration products and proportional to the heat rate, while on short time scales it is dominated by flocculation.

Keywords: *Admixtures, cement hydration, structuration, thixotropy*

Introduction

With the development of new processing techniques[1] and the demand for shorter and shorter demoulding times, the assessment of early age strength of concrete is shifting to earlier stages of the material evolution. While the fresh phase in which the material can flow[2], as well as the early age strength are both rather well understood, the transition from a fluid to a solid is not commonly investigated[3][4]. This is also translated in the discrepancy between the many empirical definitions of setting, either from the Vicat test or calorimetry. While it is known that setting occurs in the acceleration period of hydration and that C-S-H and portlandite growth play a key role[5], the contribution of hydration product growth to the structuration of cementitious systems in the transition from a fluid to a solid is not quantitatively reported.

Typically the distinction between the contributions of flocculation and hydration to the structuration of cementitious materials is difficult to measure with simple flow experiments, as both phenomena have a comparable impact on the structuration rate in the timeframe of such experiments. This leads in part to a shear-history-dependent flow behaviour, commonly described as thixotropy. It has been shown in recent years that two distinct critical strains exist at which a fresh cement paste exhibits a drastic change in elastic properties, one on the order of a few % and the other on the order of a few hundreds of % deformation[6]. The former has been associated to the network of colloidal interactions between cement particles, while the latter has been associated to the growth of early hydrates between cement grains respectively.

In the following, the structuration in a resting cement paste is followed using strain oscillation rheometry. Strains are kept well below the critical strain of hydration products bridging cement grains in order to follow the structuration of the studied cement pastes without damaging them.

Using sucrose as a set retarder, the onset of hydration of the cementitious system can be strongly delayed. This allows to study the structuration in cement pastes caused by flocculation separately from the contribution of hydration, without strong modification of the microstructure.

Materials and methods

A commercial portland cement CEM I 52.5R according to the European standard EN 197-1:2000 is used. The specific surface area measured by nitrogen adsorption (BET model) is 1.12 m^2/g following the procedure described elsewhere [7]. Its mineralogical composition is determined by Rietveld analysis of the X-ray diffraction (XRD) patterns and expressed in values normalized to 100% of crystalline phases (see Table 1). D(+)-Sucrose (99.7% for biochemistry - Acros Organics) is used as admixture.

Table I. Mineralogical composition (%w/w) of Portland cement determined by Rietveld analysis of the XRD patterns.

C_3S	C_2S	C_3A	C_4AF	Gypsum	Hemihydrate	Quartz	Calcite
64.6	9.2	5.2	11.6	3.0	5.2	0.3	0.9

Preparation of pastes

The cement pastes are prepared by adding 1000 g of cement to 398.1 g of water (final liquid/solid ratio of 0.4) in a Hobart mixer and mixing for 3 minutes at 139 rpm. Dosages of 0, 0.42 and 0.86 mg of sucrose/g cement (0, 0.42, 0.086 % weight sucrose by cement) are added 20 minutes after initial mixing as a sucrose solution containing 1.9g of water and up to 30% of sucrose by mass and stirred for 2 minutes at 500 rpm with a blade stirrer. The resulting mix is divided in separate containers, sealed and stored at 23°C in a water bath until the measurement.

Methods

Structuration rates of cement paste suspensions using rheometry. Oscillation rheometry measurements is carried out in an Anton Paar MCR 501 rheometer using serrated parallel plate geometry with a diameter of 25mm of the upper plate, a diameter of 50mm of the lower plate and a gap of 1mm. Approximately 5g of paste is deposited on the lower plate and the gap is set. Once the gap distance is reached, the contact quality is assessed visually and the sample is not trimmed. The squeezed out material along with a hood reduce the contribution of drying, while a Peltier temperature control of the hood and lower plate fix the sample temperature to 23°C.

Care is taken to avoid inconsistencies resulting from sedimentation and bleeding in the stored containments and to avoid the presence of agglomerates and air entrapping in the sample deposited on the rheometer plate.

The experiment cycle is divided in two phases. First the sample is pre-sheared until a shear stress of 400 Pa is reached at a shear rate of 50 1/s, a shear rate at which the cement paste has been proven to be shear thinning. Second the pre-shear is stopped and a small shear strain oscillation of 0.0005% is applied at a frequency of 1Hz for 20 minutes. The response of the shear stress is monitored over time at a sampling rate of 2 seconds. It can be noted that the oscillation phase of this experiment is very sensitive to surrounding vibrations.

Isothermal calorimetry. Isothermal calorimetric measurements is carried out in a TAMAIR calorimeter at 23 °C (73 °F) on cement pastes with 5g (+/- 2%) of cement paste sample. This technique is used to monitor the kinetics of the hydration reaction of the cementitious systems under study.

Results

Figure 1 shows a strong delay of hydration caused by the addition of sucrose to the cement paste, delaying the onset of the acceleration phase of hydration by as much as 30 hours and prolonging the induction period. In general, dissolution enthalpies are substantially higher than nucleation ones, thus calorimetry mainly follows the dissolution rate of anhydrous phases. The effects of a possible modification of the initial C3A dissolution due to variable sucrose dosages on the cement paste rheology are reduced by delayed admixture addition in order to create a comparable suspension.

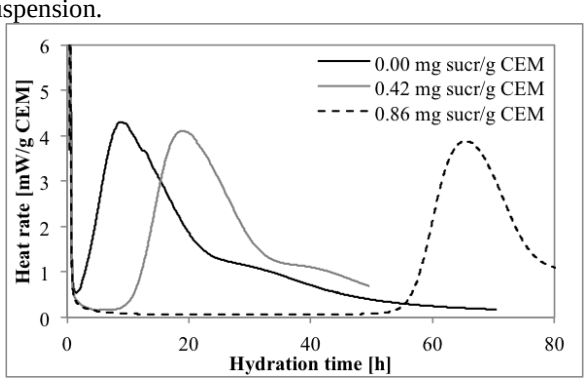

Figure 1. Heat rate of cement pastes as a function of hydration time

Figure 2 shows the evolution of the storage modulus of a non-delayed cement paste for measurements initialized at different times of cement hydration. In the earliest measurement, the cement paste appears to reach a plateau at approximately 500 seconds of resting time. After that, the structuration rate changes inclination and appears to be influenced by another phenomenon. This later contribution to structuration is significantly more pronounced for the later experiments. Thus qualitatively, an interval between 30 and 300 seconds, as well as between 300 and

1200 seconds can be distinguished, in which the structuration rate is dominated by different physical behaviors.

In the last measurement in Figure 2, the preshear event does not seem to be sufficient to completely destroy the built structure and the sample shows a higher initial storage modulus. It should also be noted that the first 20 seconds of the oscillation are dominated by the relaxation of the sample from the pre-shear event and have to be discarded.

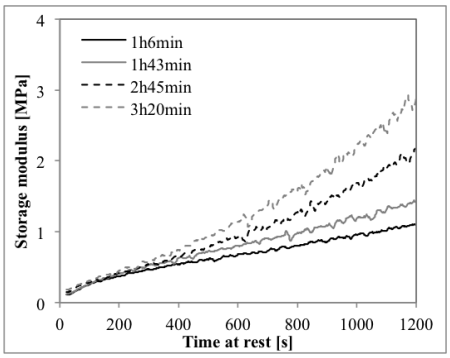

Figure 2. Evolution of storage modulus since the cement paste is resting.

Figure 3 shows the evolution of the storage modulus in the induction period of a strongly delayed cement paste. The structuration appears to level off at a storage modulus plateau value of approximately 500 kPa for all three measurements conducted in a span of more than 20 hours, during which the heat rate was as low as 0.08 mW/g cement.

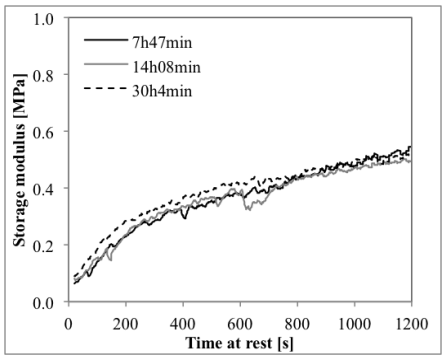

Figure 3. Evolution of storage modulus in the induction period of a delayed cement paste.

Figure 4 shows a comparison between the non-delayed and the delayed cement paste at different times. The early contribution to structuration until approximately

300 seconds is very similar for both compositions, including the strongly hydrating sample without sucrose aged 3h20min. Beyond this time range only the latter exhibits a strong increase in storage modulus.

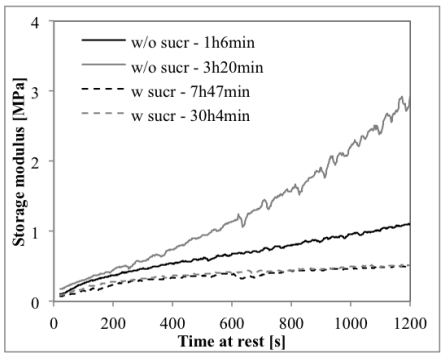

Figure 4. Structuration of cement paste with and without sucrose.

Figure 5 shows a comparison between heat release rates and storage modulus evolution with and without sucrose. Each storage modulus curve represents an individual measurement. The storage modulus increase while the material is at rest, especially the late contribution, is related to the heat release rate. In the acceleration period of hydration, the final storage modulus is substantially increasing. At low heat release rates the final storage modulus tends towards a plateau value.

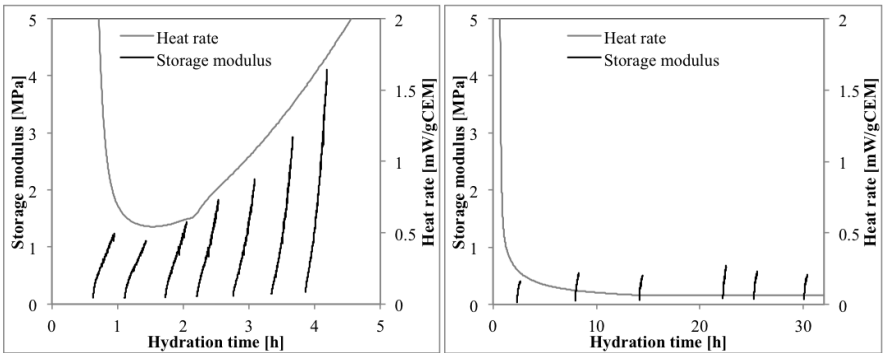

Figure 5. Storage modulus evolution at rest and heat of hydration as a function of hydration time for the cement paste without sucrose (left) and with 0.86mg sucrose/g cement (right).

Figure 6 (left) shows a discretization of the final storage modulus after 20 minutes of rest as a function of hydration time. It is visible that the storage modulus after long resting times is directly related to hydration. A direct proportionality between the final storage modulus and the heat release rate at the time of measurement is

also shown (Figure 6, right). The values in the highlighted grey area are influenced by initial hydration and nucleation of aluminates and can be discarded. It can be suggested that the main contribution to heat release in this time period finds its origin in the on-going dissolution of C3A. The corresponding nucleation of aluminates does not seem to contribute to the increase in storage modulus.

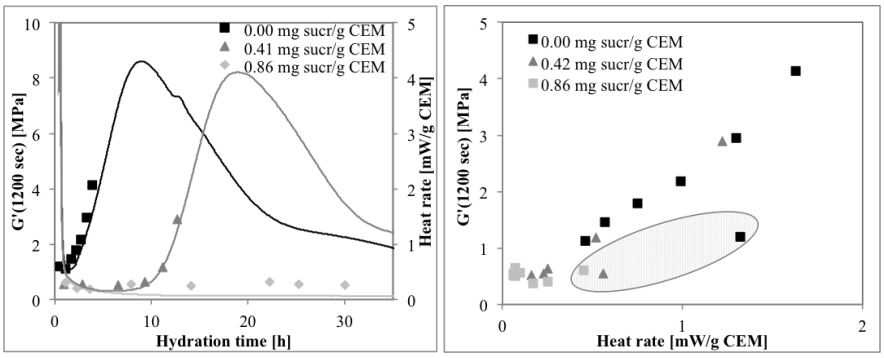

Figure 6. (left) Final storage modulus (G' after 1200 seconds resting time) and heat rate as a function of the hydration time. (right) Final storage modulus as function of the heat rate. The measurement points highlighted in grey are dominated by initial hydration and can be discarded.

Discussion

As shown in figure 1, sucrose mainly delays cement hydration, but does not strongly affect the dissolution rate of C_3S in the acceleration period. Therefore, the silicate peak is not modified substantially, although there seems to be a merge with the sulphate depletion point at high sucrose dosages. Using the delay caused by sucrose, the rheology of a chemically inactive cementitious system can be studied during a prolonged induction period and the contribution of flocculation to structuration of a cement paste can be isolated, assuming no strongly modification of the microstructure or of the nature of colloidal interactions.

The oscillation measurements in figures 2 to 4 clearly show the strong influence of hydration on the structuration rate after a resting time of 5 minutes. In the induction period of hydration, the storage modulus reaches a plateau, which is associated to colloidal interactions between the cement particles building a network. This reflects a pure diffusion/flocculation process, as there is a lack of formation of hydration products in this period. In the acceleration period the storage modulus keeps increasing beyond 5 minutes resting time and this second contribution to storage modulus is incrementally stronger the more C_3S is dissolving as shown in figure 5. This can be explained by and associated to the increased formation and growth of hydration products between the cement grains as a consequence of C_3S reaction. These increasing number of hydration products

strengthen the network of colloidal interactions built during the first minutes of rest.

During the 20 minutes oscillation time interval the contribution of hydration can be considered constant, as the heat rate is not changing substantially. This makes it possible to carry out multiple discretized measurements of a cement paste without the need for modelling hydration contribution during one very long oscillation event of several hours. Using this concept it is possible to directly compare the heat release rate during the oscillation time frame with the structuration rate of the sample (figure 6).

The very good agreement between storage modulus at rest and heat rate of hydration both in the induction period and at the beginning of the acceleration period shows that the structuration rate of cement pastes at rest is quantitatively proportional with the formation and/or growth of hydration products.

Conclusion

Using sucrose as a set retarder, we showed that it is possible to distinguish the contributions of flocculation and hydration to the structuration rates in cement pastes. Following this strategy, we could strongly delay the nucleation of hydration products and in turn show that their formation dominates the structuration in the acceleration phase.

In the induction period the structuration levels off at a certain value of G', indicating that the system's structuration is governed by a diffusion/flocculation process. In contrast, in the acceleration period the storage modulus increases gradually and strongly contributes to the network strength from 5 minutes resting time onwards. This can be associated to the growth of hydration products bridging the cement particles in the flocculated network.

In general, the structuration rate is dominated by the formation of hydration products and proportional to the heat rate at long resting times, while it is dominated by flocculation on short time scales.

Acknowledgements

The authors would like to acknowledge Dr. Michael Plötze for his support in the XRD and Rietveld analysis carried out for this study. This research was supported by the NCCR Digital Fabrication, funded by the Swiss National Science Foundation. (NCCR Digital Fabrication, Agreement # 51NF40-141853) and by an ETH Research Grant ETH-13 12-1 under the name Smart Dynamic Casting (SDC)

References

[1] E. Lloret, A. R. Shahab, M. Linus, R. J. Flatt, F. Gramazio, M. Kohler, and S. Langenberg, "Complex concrete structures: Merging existing casting techniques with digital fabrication," *Comput.-Aided Des.*, no. 0, 2014.

[2] N. Roussel, "11 - Thixotropy: from measurement to casting of concrete," in *Understanding the Rheology of Concrete*, N. Roussel, Ed. Woodhead Publishing, 2012, pp. 286–295.

[3] A. R. Shahab, E. Lloret, P. Fischer, F. Gramazio, M. Kohler, and R. J. Flatt, "Smart dynamic casting or how to exploit the liquid to solid transition in cementitious materials.," *Proc. CD 1st Int. Conf. Rheol. Process. Constr. Mater. 7th Int. Conf. Self-Compact. Concr. Paris Fr.*, 2013.

[4] A. Perrot, D. Rangeard, and A. Pierre, "Structural built-up of cement-based materials used for 3D-printing extrusion techniques," *Mater. Struct.*, pp. 1–8, Feb. 2015.

[5] K. L. Scrivener, P. Juilland, and P. J. M. Monteiro, "Advances in understanding hydration of Portland cement," *Keynote Pap. 14th Int. Congr. Chem. Cem. ICCC 2015*, vol. 78, Part A, pp. 38–56, Dec. 2015.

[6] N. Roussel, G. Ovarlez, S. Garrault, and C. Brumaud, "The origins of thixotropy of fresh cement pastes," *Cem. Concr. Res.*, vol. 42, no. 1, pp. 148–157, Jan. 2012.

[7] S. Mantellato, M. Palacios, and R. J. Flatt, "Reliable specific surface area measurements on anhydrous cements," *Cem. Concr. Res. Accept.*

Coupled Effect of Temperature and Time on Rheology of SCC Used in CRTSIII Slab Ballastless Track

Li Huajian[1,2], Huang Fali[1,2], Tan Yanbin[1,2], Li Linxiang[1,2], Yi Zhonglai[1,2], Xie Yongjiang[1,2]
[1]China Academy of Railway Science, China
[2]State Key Laboratory for Track Technology of High-Speed Railway, China

Abstract As a typical representative of smart concrete, self-compacting concrete (SCC) is used in CRTSIII slab ballastless track with the independent intellectual property rights in China for its high constructability, technique economy and environmental friendliness. However, the SCC has high temperature sensitivity because of high dosage of superplasticizer, low water-binder ratios and multiple powder components. In order to enhance the robustness of SCC, it is important to understand its rheology better. This paper investigates the effect of the temperature (0℃ to 40℃) and the time (5min to 90min) on the rheology of SCC used in CRTSIII slab ballastless track. The results indicate that the initial slump-flow increases with the increase of temperature, while the opposite is true for the T_{500}. The slump-flow loss increases substantially in high temperature and moderately in lower temperature. The higher the concrete temperature, the higher the increase of slump flow loss. There is a clear "return large" phenomenon in 0℃. In opposite to plastic viscosity, yield stress of the concrete increases with elapsed time.

Keywords: *self-compacting concrete*, *rheology*, *temperature*, *elasped time*

Introduction

The achievement of concrete structure's self-filling and self-compacting function by its own intelligent power is a kind of technological revolution which can solve the durability problem caused by construction factors [1-2]. As a typical representative of concrete with special rheological properties——self-compacting concrete which has been applied to foreign prefabricated components factories and CRTSIII slab ballastless track with Chinese independent intellectual property rights because of its high workability, technological economy and environmental friendliness [3-4]. According to preparation technology and powder content, SCC can be divided into three types, powder type SCC (550-650 kg/m^3), combination type SCC (450-550 kg/m^3) and viscosity modifying admixture (VMA) type SCC

(350-450 kg/m^3) [5]. The SCC mix characteristics of high powder content, high superplasticizer content, high sand rate and low water-powder ratio, and characteristic of high flowability (slump flow are larger than 550mm) determine its special sensibility to temperature and time.

Brameshuber and Ubachs pointed out that the slight change of temperature would affect significantly the concrete's workability and durability. It quite has caused difference of concrete's properties between laboratory and field because the mix proportion is usually designed in the condition of room temperature and the effect of climate in field is ignored. The experiment has researched the coupled effect of temperature(0℃~40℃) and time(5min~90min) on the rheological properties with the object of powder-VMA combination type SCC usually used in CRTSIII slab ballastless track, which is expected to provide reference for the design and construction of CRTSIII slab ballastless track.

Experimental

Materials and mixture proportioning

Type P·O 42.5 Portland cement was used. Commercially available fly ash, grinding slag powder and expansive agent were used as the mineral mixture. The ranite dust was filtered through a 0.075mm sieve. The chemical and physical composition of cement, slag and fly ash are shown in Table I. Expansive agent conforms to the requirement of type II expansive agent in GB 23439-2009. The fine aggregate were river sands with the fineness modulus of 2.6. The coarse aggregate were a 5-20mm continuous-grading crushed stone. A polycarboxylate reducer was used to achieve the expected workability. JYQ-3 Air-entraining agent was used to achieve the expected air content. The mix proportions are shown in Table II.

Table I. Physical properties and chemical composition of cement, fly ash and slag powder

Item	Loss of ignition/%	SO_3/%	Cl^-/%	Na_2O+K_2O/%	f-CaO/%	MgO/%	Specific surface /($m^2 \cdot kg^{-1}$)	Density /($g \cdot cm^{-3}$)
Cement	2.97	2.39	0.016	0.63	0.71	3.32	364	3.08
Slag powder	0.18	1.46	0.012	0.44	/	12.72	301	2.86
Fly ash	3.97	0.41	0.006	0.65	0.03	1.65	438	2.21

Table II. Mix proportions of SCC/ (kg·m^{-3})

Cement	Fly ash	Slag powder	Expansive agent	VMA	Coarse aggregate	Sand	Water-powder ratio	Super plasticizer	Air entrainment agent	Water-powder ratio
250	63	142	47	18.3	747	913	0.35	6.25	0.065	0.35

Test methods

Temperature control

In this study, according to the thermal calculation of concrete under the condition of same mix proportion and by controlling each raw material's temperature and inner mixer temperature, mixture temperatures are adjusted at target temperature 0℃, 10℃, 20℃, 30℃, 40℃, respectively. The thermal computation formula shown as Eqn. (1).

$$T_0 = [0.92(T_c M_c + T_s M_s + T_{sa} M_{sa} + T_g M_g) + 4.2T_w(M_w - \omega_{sa} M_{sa} - \omega_g M_g) + c_w(\omega_{sa} M_{sa} T_{sa} + \omega_g M_g T_g) - c_i(\omega_{sa} M_{sa} + \omega_g M_g)]/[4.2M_w + 0.92(M_c + M_s + M_{sa} + M_g)] \quad (1)$$

Where T_0 is the temperature of concrete mixture, ℃; T_s, T_c, T_{sa}, T_g, T_w are temperatures of admixture, cement, sand, gravel, and mix water ,respectively, ℃; M_s, M_c, M_{sa}, M_g, M_w are weights of admixture, cement, sand, gravel, and mix water, respectively, kg; ω_{sa}, ω_g are water content of sand and gravel, %; c_w is specific heat of water, kJ/(kg·K); c_i is heat of solution of ice, kJ/kg.

Testing

The slump-flow test was performed using the Abram's cone. The time was measured for the concrete reaching to the 500mm spread circle (denoted by T_{500}) and the final diameter of the concrete in two perpendicular directions was measured (the average value is the slump-flow in mm). The air content was performed according to "Standard for Test Method of Performance on Ordinary Fresh Concrete" (GB/T 50080-2002). The yield stress and plastic viscosity were determined by means of RHM-3000 ICAR rheometer. The specific test procedures are shown in Table III.

Table III. Rheological experimental test procedures of SCC

Breakdown time/s	Breakdown speed/rps	Number of points	Time per point/s	Initial speed/rps	Final speed/rps
20	0.50	7	5	0.50	0.05

Results

Slump-flow

The evolution of SCC slump-flow under the coupled effect of temperature and time is shown in Figure 1. It can be seen that the initial slump-flow of fresh SCC is increased with increasing temperature. When mixture temperatures are 30℃ and 40℃, slump-flow decreases gradually with time goes by, and slump-flow loss at 90 min are 9% and 14%, respectively. When mixture temperatures are 10℃ and 20℃, slump-flow increases gradually with time goes by, and slump-flow reaches the maximum after 60 min and then decreases. When mixture temperature is 0℃, the mixture shows a obvious phenomenon of "return large". It means that the initial slump-flow of SCC is small but increases significantly after 30 min.

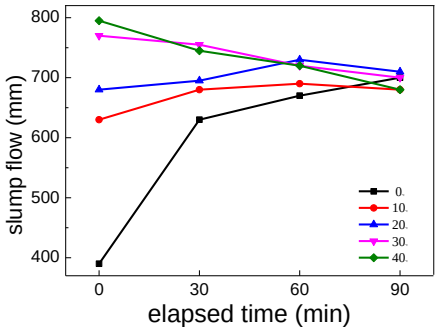

Figure 1. Coupled effects of time and temperature on slump flow of SCC

T_{500}

The flow time, T_{500}, can be tested when mixture temperature is 0℃ because its initial slump-flow is only 390mm. The coupled effect of temperature and time on other mixture's T_{500} is shown in Figure 2. It can be seen that initial T_{500} is decreased with the increase of temperature. When mixture temperatures are 0℃ and 10℃, T_{500} decreases with time passing. When mixture temperature is 20℃, T_{500} decreases with time passing, and the T_{500} of fresh concrete reaches the minimum after 60 min and then increased slightly. The curve of T_{500} fluctuates smoothly and is unchangeable significantly with time passing when mixture temperature is 30℃, while T_{500} increases with time passing when mixture temperature is 40℃.

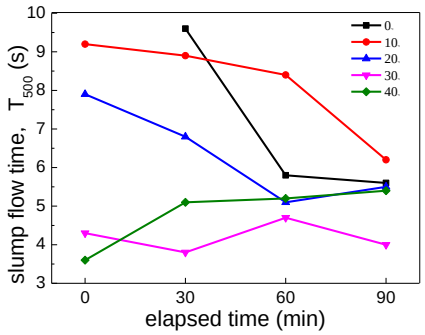

Figure 2. Coupled effects of time and temperature on T_{500} of SCC

Yield stress

The coupled effect of temperature and time on the yield stress of SCC is shown in Figure 3. It can be seen that the initial yield stress is minimum when mixture temperature is 20℃, 10℃ ranks second, initial yield stresses of mixtures at 30℃ and 40℃ are equal, and that initial yield stresses of mixture at 0℃ is largest. Each kind of SCC with different temperature, their yield stresses increase gradually with time passing. The increase of yield stress is largest and the value is 346% when mixture temperature is 20℃. Mixture at 10℃ ranks second and its increasing value of yield stress is 256%. Increasing values of yield stress are 143% and 109% respectively when mixture temperatures are 30℃ and 40℃. The increase of yield stress is smallest and the value is 19% when mixture temperature is 0℃.

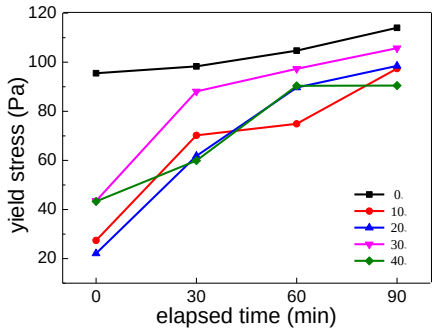

Figure 3. Coupled effects of time and temperature on yield stress of SCC

Plastic viscosity

The coupled effect of temperature and time on plastic viscosity is shown in Figure 4. It indicates that initial plastic viscosity decreases with the increase of mixture temperature. The same research result was concluded by J. Golaszewki *et. al* [6]. Plastic viscosities decrease with time passing when mixture temperatures are 0℃, 10℃, 20℃ and 30℃. The plastic viscosity of mixture at 40℃ decreases at first, reaching to the minimum after 30 min and decreasing subsequently. The plastic viscosity losses of the mixtures at temperatures of 0℃, 10℃, 20℃, 30℃ and 40℃ are 77%, 48%, 42%, 41% and 10% respectively in absolute terms, which means the higher mixture temperature the less plastic viscosity loss.

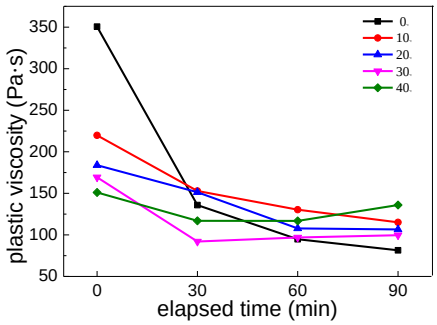

Figure 4. Coupled effects of time and temperature on plastic viscosity of SCC

Discussion

The coupled effect of temperature and time can affect rheological properties of SCC by means of affecting the hydration rate of cement, the adsorption rate of superpalsticizer, the evaporation rate of mix water, the water absorption rate and saturation water absorption of aggregate and other factors. It is known that Arrhenius equation can be used to describe the relationship between hydration rate of cement and temperature [7]. Arrhenius equation as shown in Eqn. (2). Where R is reaction rate constant; A is pre-exponential factor; Ea is activation energy, kJ/mol; T is absolute temperature, K; R is gas constant, kJ/mol·K; e is the Euler's constant.

$$R = A\mathrm{e}^{-E_a/RT} \tag{2}$$

Assumed that Ea (apparent activation energy of cement hydration) is equal to 40kJ/mol, hydration rate will be increased to 184% when the temperature rises from 20℃ to 40℃. In contrary, hydration rate will be decreased by 70% when the temperature drops from 20℃ to 0℃. The increase of hydration rate of cement is the key that slump-flow loss of mixture is quickened at high temperature. Reference

[8] mentioned that the water on concrete's surface can be evaporated fast when temperature rose, resulting in slump-flow loss accelerated in high temperature state. In addition, the research of J. Ortiz *et al* [9]. indicated that the water absorption rate and saturation water absorption of aggregate would be increased when temperature rose, leading to the decrease of effective water-binder ratio, which also made mixture workability loss fast. As for the phenomenon of "return large" that occurs usually at low temperature, it may be the reason that the adsorption rate of superpalsticizer is retarded in cold environment. It still needs to research why slump-flow increases significantly with time passing at low temperature while plastic viscosity increases slowly.

According to above discussions, it can be seen that the SCCs under the condition of same mix proportion and different temperature, their parameter values of initial slump-flow, T_{500}, yield stress and plastic viscosity are different obviously. But the values tend to be equal gradually with time passing. Therefore, the time from mix completed to cast started and the temperature in construction environment should be considered when designing mixture ratio of SCC.

Conclusions

The following conclusions can be obtained by above research results:

(1) The initial workability of SCC can be affected significantly by temperature. The initial slump-flow of mixture increases with the increase of temperature, and the plastic viscosity is just opposite.

(2) The slump-flow loss of SCC is accelerated in state of high temperature. The slump loss resistant property of SCC is better in cold environment. There may be a obvious phenomenon of "return large" in fresh mixture of SCC when temperature is very low.

(3) The SCCs under the condition of same mix proportion and different temperature, their parameter values of initial rheological properties are different greatly, but finally values tend to be equal gradually with time passing

Acknowledgments

The authors are grateful to the financial support of Natural Science Foundation of China (Grant No. 51578545) and the Technological Research and Development Programs of the Ministry of Railways (2015G001-H).

References

[1] Hajime Okamura, Masahiro Ouchi. Self-compacting concrete[J]. Journal of Advanced Concrete Technology, 2003, 1(1): 5-15.
[2] BIBM, CEMBUREAU, ERMCO, EFCA and EFNARC. The European guidelines for self-compacting concrete [S]. 2005
[3] Joseph A. Daczko, Kamal H. Khayat, Claude Bedard, et al. Self-consolidating concrete(ACI 237 R-07)[R]. Farmington Hills, MI, USA: American Concrete Institute, 2007.
[4] LI Huanjian,TAN Yanbin, XIEYongjiang, et al. The characteristics of self-compacting concrete and its application in high speed railway[J]. Railway Engineering, 2012(8): 143-145. (in Chinese)
[5] G.Heiman, L.Vandewalle, D.van Gemert, et al.Time-dependent deformations of limestone powder type self-compacting[J]. Engineering Structures, 2008, 30(10): 2945-2956.
[6] Jacek Golaszewki, Janusz Szwabowski. Influence of superplasticizers on rheological behaviour of fresh cement mortars[J]. Cement and Concrete Research, 2004, 34: 235-248.
[7] Zawde Berhane. The behavior of concrete in hot climates[J]. Materials and Structures, 1992, 25(3): 157-162.
[8] Kenneth C. Hover. Evaporation of water from concrete surfaces[J]. ACI Materials Journal. 2006,103(5): 384-389.
[9] J. Ortiz. Influence of environmental temperature and moisture content of aggregates on the workability of cement mortar[J]. Construction and Building Materials,2009, 23: 1808-1814.

Computational Segregation Analysis during Casting of SCC

Jon E. Wallevik[1], Wassim Mansour[2,3] and Olafur H. Wallevik[1,3]

[1]ICI Rheocenter, Innovation Center Iceland, Arleynir 2-8, IS-112 Reykjavik
[2]Readymix Abu Dhabi, Aldar RM, Redland RM
[3]Reykjavik University, Menntavegi 1, IS-101 Reykjavik

Abstract Variable aggregate distribution can increase the local porosity and thus the permeability of concrete. Varying content of mortar causes heterogeneous shrinkage and creep in a given concrete element. Moreover, high heterogeneity will increase the probability that these phenomenon yields high internal stress gradients and thus cracking. In this work, a status is given about the development of a concrete casting solver within the OpenFOAM framework that can also calculate the coarse aggregate distribution as a function of time. The intention is to predict the overall degree of segregation after casting for a given concrete element. Attempt is being made to include the shear rate induced particle migration into the solver. Example of simulation runs of the current software version is presented.

Keywords: *Simulation, Segregation, Rheology, Casting prediction, OpenFOAM*

Introduction

The load carrying capacity and service life of concrete structure is very much dependent on the quality and success of concrete placement into formwork at jobsite [1,2,3]. In recent years numerical modeling of concrete placement has showed great potentials to become an important tool for optimization of such process [4]. Only recently, researchers from various part of the world have started to work on such casting prediction tools using different CFD softwares [5]. But lot of work is still to be done to understand the large scale behavior of involved flow processes [5], especially in terms of calculating the coarse aggregate concentration as a function of location and time [6]. In particular, variation in aggregate distribution can increase the local porosity and thus the permeability of concrete. This can also cause heterogeneous shrinkage and creep in a given concrete element. Moreover, high heterogeneity will increase the probability that these

phenomenon yields high internal stress gradients and thus cracking with the reduction in load carrying capacity of the concrete structure as a result [3].

The Self Compacting Concrete (SCC) is an extremely fluid concrete and thus was expected to be the answer to casting problems. However, experience has shown even for such type of material, there will always exist a formwork and steel bars configuration in which casting problems may occur [5]. Furthermore, these casting problems may not be fully resolved unless one can calculate the aggregate concentration as a function of time and location and especially its response to different types of obstacles.

The aim of the project is to create a multiphase transient simulator that models the dynamics of multiple fluid phases during casting of concrete. The phases are mortar (or rather fine concrete < 11 mm), coarse aggregates (> 11 mm) and atmospheric air. This is done within the OpenFOAM framework, which uses the finite volume method in cell-centered formulation to solve systems of partial differential equations in three-dimensional unstructured (and structured) mesh.

In the end, the objective of the solver is to simulate operational problems related to uncertainties in casting predictions. This includes the effect of the settlement of aggregates by gravity (i.e. segregation) as well as the effect of shear rate induced particle migration [7,8,9]. Improved prediction accuracy of transient multiphase flow allows for the design of more complex and durable concrete structures.

Short Theoretical Background

The numerical solver encompasses two theories. The first one is the Computational Fluid Dynamics (CFD) of transient viscoplastic fluid with open (free) boundary, thus dividing the system between the atmospheric air and a viscoplastic fluid (e.g. fresh concrete). This is what could be considered as a standard Volume of Fluid approach (VOF) [10] with a non-Newtonian fluid (here, the Bingham fluid). The second theory is the implementation of field equation for particle distribution into the numerical framework to be able to calculate segregation within the viscoplastic fluid (e.g. segregation of concrete), including the shear rate induced particle migration [7,8,9]. The approach used in treating the aggregate segregation is based on the Drift Flux Method (DFM) [11].

The DFM is derived from the so-called two-fluid model [12]. The latter solves the continuity- and momentum equations separately for each phase. However, for the DFM, the continuity equations for each phase are added together to yield a mixture continuum equation and the momentum equation are added to yield a single mixture continuity equation. The use of DFM instead of a two-fluid model, is due to the simplicity in the former (in an already very complex numerical system), as well as increased computational efficiency for large structure simulations.

As already mentioned above, in the current solver, a standard VOF approach is mixed with the theory of DFM (both implemented through the FVM). The former calculates the flow of two fluids that do not generally intermix (immiscible) and thus usually have a clear boundary between them, e.g. concrete and atmospheric air. In this part of the solver, the effect of surface tension is implemented by the Continuous Surface Force (CSF) [13]. For the second part of the solver, where the DFM resides, the phases are always in an intermixed (miscible) state, e.g. coarse aggregates suspended in mortar. It is by the DFM that the effect of slip between the phases is calculated (i.e. the effect of segregation). The surface tension force is not directly calculated in this part, but its effect is indirectly present through the slip velocity. That is, the slip velocity depends (among many other factors) on the adhesion between the phases (i.e. the surface tension between mortar and the coarse aggregates).

With the mixture of the two above mentioned theories, namely the VOF and DFM, then in total, three phases are involved in the solver, in which atmospheric air is the first phase. The viscoplastic fluid (here, the concrete) is divided between a matrix phase and a particle phase, which constitute the second and the third phase. The matrix could for example consist of mortar (or fine concrete), say with aggregate diameter size from 0 to 11 mm. The particle phase (i.e. the coarse aggregate phase) would then consist of coarse aggregates with diameter larger than 11 mm. Final definitions on these two phases is not (and will not be) fixed in the solver and the user can set the definition of the matrix and the dispersed phase as needed for each simulation/testing case. For example, in the specific treatment of mortar, the division could be between the cement paste with aggregate fines (< 0.125 mm) and sand particles above 0.125 mm in diameter.

Here, the term α_i will represent the phase volume (or solid concentration) of component i. Relative to a computational cell, it means the volume of component i inside the cell divided by the cell total volume. Within each computational cell, the volume fraction of concrete is represented with α_1, while the phase volume of atmospheric air is represented with α_2. The two fractions represent the boundary between concrete and air in the sense that $\alpha_1 + \alpha_2 = 1$.

The concrete α_1 will be made of a continuous phase α_m (here the mortar) and a dispersed phase α_d (coarse aggregates), meaning $\alpha_1 = \alpha_m + \alpha_d$. Thus, the amount of mortar is $\alpha_m = \alpha_1 - \alpha_d$.

Results - (Beta) Tests of the Solver

At this stage of the project, the primary aim is to get the solver to actually calculate flow of fresh concrete with coarse aggregate distribution, based on gravity induced segregation as well as by shear rate induced particle migrations. Here, the objective is to see if the solver can run under different conditions as well as to investigate stability problems. As this is a “beta” testing of the solver, arbitrary segregation

functions have been chosen using arbitrary material parameters. As such, the results may be wrong, not by the infrastructure of the solver, but rather because of the incorrect material parameters chosen for the cases.

Casting of a T-beam

As a testing ground for the solver, an existing mesh of T-beam is used [14], shown in Fig.1. Its span is 3 m, height is 0.63 m, top width 0.60 m (flange) and bottom width 0.20 m. The diameter of the two steel reinforcement bars is about 26 mm (near bottom). Note that the dimensions used here are arbitrary. In the top-left part of Fig. 1, is a hose (diameter is 8 cm) in which the concrete is pumped. The number of computational cells used are 287,090, in which 1,620 are prisms, 1,620 are polyhedra and the rest are hexahedra cells.

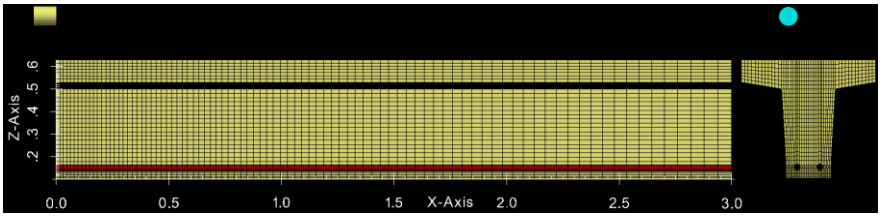

Figure 1. The mesh and dimensions (in meters) of the T-beam used in the test [14].

For analysis of computational outcome, a cross section is used which is located in the center of the T-beam geometry. This cross section (or vertically aligned plane) is shown in Fig. 2. In this figure, the cross sectional plane is mostly colored with blue (but red/yellow is also present at the lower region). The yellow boundary on either side of the plane, demonstrates the surface of the concrete (towards the atmospheric air). The green color represents the two reinforcement bars.

Figure 3 shows the results of the simulations for three different cases, in which all of them apply at 15 seconds after start of pumping. The color bar shown in the top part of Fig. 3, demonstrates the range of solid concentration of coarse aggregates α_d. That is, the dark red color, namely $\alpha_d = 0.4$, represents full compaction (or concentration) of coarse aggregates, while the dark blue color, $\alpha_d = 0$, represents area that is completely absent of coarse aggregates. At such location, only mortar (i.e. here, fine concrete, < 11 mm) remains. In the range of light blue color and light red color, the solid concentration is close to $\alpha_d \approx 0.2$, which means homogeneous concrete, or rather initial state of concentration of coarse aggregates. Finally, the blue color above the concrete, represents the atmospheric air α_2.

The yield stress τ_0 is set equal to 10 Pa, while the plastic viscosity μ is set equal to 50 Pa·s. These values apply when the concrete is homogenous (here, $\alpha_d = 0.2$). However, as the coarse aggregate concentration changes $\alpha_d = \alpha_d(x,y,z,t)$, these two values τ_0 and μ changes accordingly in the simulations. Thus the neither the yield

stress nor the plastic viscosity are constants. It should be noted that a very simple (unrealistic) functions $\tau_0 = \tau_0(\alpha_d)$ and $\mu = \mu(\alpha_d)$ are used in this case. The objective is to investigate how the solver reacts to rheological values that depends on α_d.

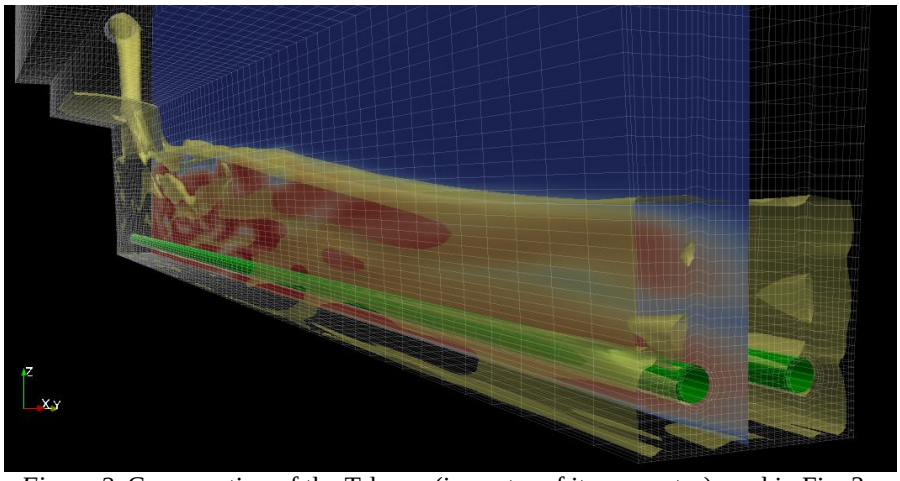

Figure 2. Cross section of the T-beam (in center of its geometry) used in Fig. 3.

In Fig. 3a, neither the segregation by gravity nor the shear rate induced particle migration are active in the simulation. For this case, there is a minor variation in concentration of coarse aggregates $\alpha_d = \alpha_d(x,y,z,t)$, which is due to concentration variation in the discharge from the hose (i.e. there is a lower coarse aggregate concentration at the discharge edge). When this variation hits the formwork wall boundaries, then through advection by its continuity equation, the coarse aggregate variation $\alpha_d(x,y,z,t)$ is smeared out throughout the T-beam. It should be clear that the variation in aggregate concentration is small.

The above-mentioned concentration variation from the hose, is in part a numerical artifact by the VOF. Since computational cells between the atmospheric air and concrete are forced to be in an intermediate state, a reduction in concentration of each phase is imminent at open boundaries. This artifact will however reduce with increased mesh resolution as well as is more or less absent for less volatile flows that does not involve pumping and free fall of concrete. The only computational CFD technique to solve this completely is by Lagrangian mesh deformation techniques, where the phases are clearly separated by mesh boundaries. But such approach is computational expensive and cannot be used for large open boundary deformations (due to severe mesh distortion), like what applies for casting of fresh concrete.

In Fig. 3b, the segregation by gravity is active. The consequence of this is clear when looking at the bottom of the T-beam, in which higher solid concentration of coarse aggregates are present, or up to $\alpha_d \approx 0.4$.

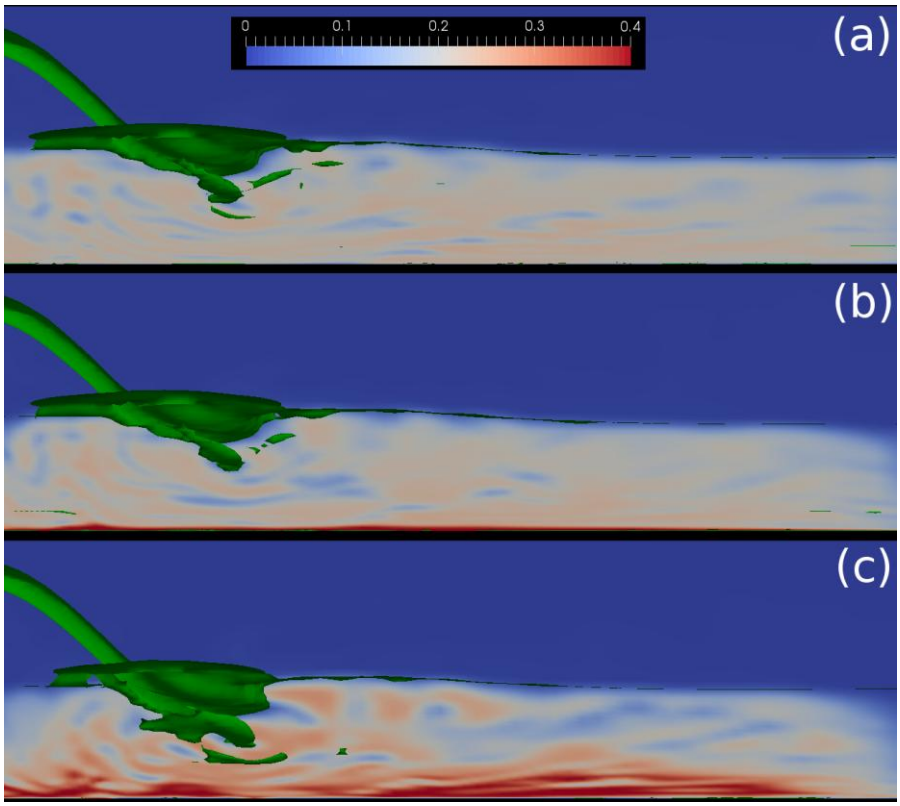

Figure 3. Results of the (prototype) simulations for a T-beam at the time t = 15 s after start of pumping: (a) No segregation is active; (b) Segregation by gravity active (c) Shear induced particle migration and segregation by gravity are active. See also Fig. 2 about the location of current cross section.

For Fig. 3c, the same segregation module by gravity is present as in Fig. 3b. In addition to this, the shear rate induced particle migration is also active, which is generated by Eq. (1) in accordance with [8].

$$\mathbf{q} = -\xi \nabla \dot{\gamma} \tag{1}$$

The vector **q** is the flow of coarse aggregates in m^3/s. Here, the migration function ξ is set as a function of both α_1 and α_d. What is shown in Fig. 3c, is the combined effects of the two segregation processes. The apparently increased aggregate concentration is due to the shear rate gradients at and near the reinforcement bars. That is, the coarse aggregate particles are being pushed away from the reinforcement bars towards (among other directions) the center where the visual plane is, c.f. Fig. 2.

4-Blades Vane Rheometer

One of the design requirements of the new solver is that it must be usable for an entirely different flow setting, for example like in a 4-blades vane rheometer. Using such geometry, the vanes are set as rotating counter clockwise (here, at angular velocity $\omega = 3$ rad/s) and the bucked is set as stationary. Although it is possible to make both segregation modules active in this case, namely both the gravity and shear rate, the former is deactivated in this test. That is, only the shear rate induced particle migration module is activated, by Eq. (1).

Both the diameter and height of the vane blades are 12.7 cm. The bucked diameter is 29.4 cm and its height is 38.5 cm. Thus, the dimensions are such that a fresh concrete can be tested with this rheometer, like the SCC.

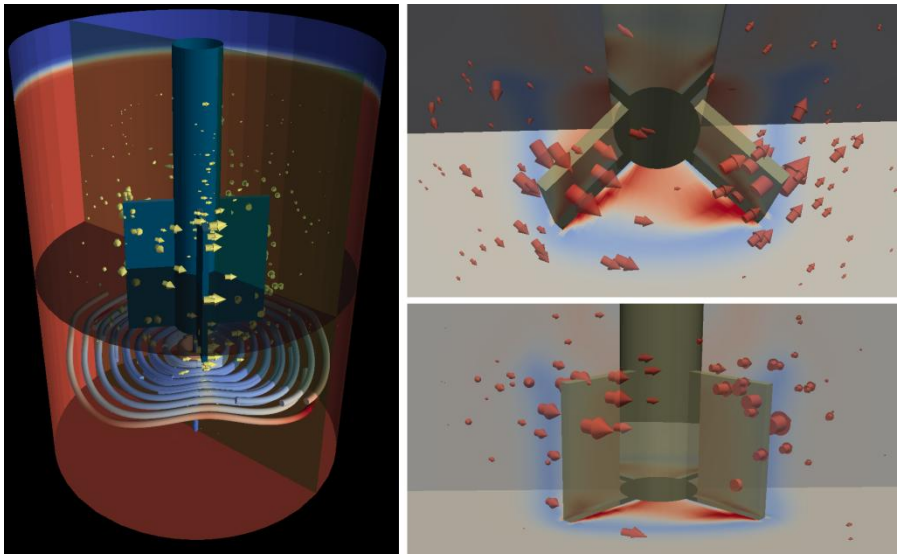

Figure 4. Results of the (prototype) simulation of a vane rheometer at $t = 10$ s.

The yield stress τ_0 and plastic viscosity μ are the same as for the above T-beam case, namely 10 Pa and 50 Pa·s, valid for homogeneous concrete ($\alpha_d = 0.2$). The same functions $\tau_0 = \tau_0(\alpha_d)$ and $\mu = \mu(\alpha_d)$ are also used, meaning that both the yield stress and plastic viscosity will change with varied coarse aggregate concentration α_d, in the same manner as for the T-beam case.

Figure 4 shows the computational result that apply after 10 seconds of rotation at $\omega = 3$ rad/s (i.e. roughly after five revolutions). For analysis of outcome, two cross sectional planes are used that are located in the center of the rheometer, one aligned vertically and the other aligned horizontally. In the two right illustrations are shown the concentration of coarse aggregates $\alpha_d = \alpha_d(x,y,z,t)$, in which dark red

color represents a complete compaction of coarse aggregates ($\alpha_d = 0.4$), while blue color a complete depletion of coarse aggregates ($\alpha_d = 0$). The gray color represents $\alpha_d = 0.2$ or homogenous concrete (i.e. initial state of coarse aggregate distribution). As shown, the most segregated area is in the shearing zone (blue color) of the rheometer and the resulting aggregates are being pushed and compacted in-between the vanes (red color). As mentioned before, the movement of the coarse aggregates is being governed by Eq. (1), in accordance with [8].

Conclusion

The aim of the project has been to create a multiphase transient simulator that can model the segregation of fresh concrete both by gravity (i.e. segregation) as well as by the shear rate induced particle migration. The current aim was to demonstrate "beta" tests of the solver, in which flow of segregating fresh concrete is calculated both in a T-beam as well as in a 4-blades vane rheometer. The two test cases were done to test flexibility of the solver for different flow cases. During this test, very little emphasis has been put on using correct material parameters or correct material behavior/model for such (a future task), but rather to see if the solver can run without major incidence. The solver is still in a developing stage and few complicated issues still need to be resolved, which is too long to explain in a short text like this.

Acknowledgments

This work is funded by The Icelandic Centre for Research (RANNIS) – Simulation of multiphased viscoplastic flow.

Reference:

[1] Tattersall, G.H. and Banfill, P.F.G (1983), *The Rheology of Fresh Concrete*, Pitman Books Limited, Great Britain.

[2] Neville, A.M. (1995.), *Properties of Concrete*, Addison Wesley Longman Limited, Great Britain

[3] Spangenberg, J., Tutum, C., Hattel, J., Roussel, N. and Geiker, M. (2011), Optimization of Casting Process Parameters for Homogeneous Aggregate Distribution in Self-Compacting Concrete: A Feasibility Study, Proceedings of the 6th IEEE Congress on Evolutionary Computation.

[4] Vasilic, K., Roussel, N., Meng, B. and Kuhne, H-C. (2009), Computational Modelling of SCC Flow: Reinforcement Network Modelled as Porous Medium, Proceedings of the 3rd International RILEM Symposium on Rheology of Cement

Suspensions such as Fresh Concrete, August 19-21, 2009, Reykjavik, Iceland, RILEM Publications S.A.R.L., ISBN: 978-2-35158-091-2.

[5] Roussel, N. (2009), Computational Modelling of SCC Flow: Reinforcement Network Modelled as a Porous Medium, Proceedings of the 3rd International RILEM Symposium on Rheology of Cement Suspensions such as Fresh Concrete, August 19-21, 2009, Reykjavik, Iceland, RILEM Publications S.A.R.L., ISBN: 978-2-35158-091-2.

[6] Spangenberg, J. (2012), Numerical Modelling of Form Filling with Self-Compacting Concrete, Ph.D. thesis, Department of Mechanical Engineering, Technical University of Denmark (DTU), Lyngby.

[7] Barnes, H.A., Hutton, J.F. and Walters, K. (1989), *An Introduction to Rheology*, Elsevier Science, Amsterdam.

[8] Wallevik, J.E. (2003), Rheology of Particle Suspensions - Fresh Concrete, Mortar and Cement Paste with Various Types of Lignosulfonates, Ph.D. thesis, Department of Structural Engineering, The Norwegian University of Science and Technology (NTNU), Trondheim, http://www.diva-portal.org/.

[9] Spangenberg, J., Roussel, N., Hattel, J.H., Stang, H., Skocek, J. and Geiker, M.R. (2012), Flow induced particle migration in fresh concrete: Theoretical frame, numerical simulations and experimental results on model fluids, *Cement and Concrete Research*, 42, 633-641.

[10] Hirt, C.W. and Nichols, B.D. (1981), Volume of fluid (VOF) method for the dynamics of free boundaries, *Journal of Computational Physics*, 39, 201-225.

[11] Ishii, M. (1975), Thermo-Fluid Dynamic Theory of Two-Phase Flow, *Eyrolles*.

[12] Brennan, D. (2001), The Numerical Simulation of Two-Phase Flows in Settling Tanks, Ph.D. thesis, Department of Mechanical Engineering, Imperial College of Science, London.

[13] Brackbill, J.U., Kothe, D.B. and Zemach, C. (1992), A continuum method for modeling surface tension, *Journal of Computational Physics*, 100(2), 335 - 354.

[14] Wallevik, J.E. (2013), Computing the Rheological Behavior of Cement Paste, Understanding the Fundamental Properties of Concrete - Celebrating Professor Erik J. Sellevold on his 75th birthday (Workshop Proceedings), 25th - 26th April 2013, Trondheim, Norway, (Eds: Sidney Mindess and Karla Hornbostel), ISBN 82-7482-101-7

Homogeneous Analysis of Self-Consolidating Concrete (SCC) Casting in Reinforced Beam Using Computational Fluid Dynamics (CFD)

Masoud Hosseinpoor[1], Kamal H. Khayat[2], Ammar Yahia[1] and Hahib A. Mesbah[3]

[1]Department of Civil Engineering, Université de Sherbrooke, Canada.
[2]Department of Civil, Architectural and Environmental Engineering, Missouri University of Science and Technology, USA.
[3]Department of Civil Engineering, L.G.C.G.M., INSA of Rennes, University of Rennes 1, France.

Abstract In this study, the casting process of 162 liters of self-consolidating concrete (SCC) in 4.05x0.2x0.2 m reinforced beam was simulated using a computational fluid dynamics (CFD) software. The simulated SCC was cast under gravity using a 1.69-m high vertical funnel. The horizontal part of the L-shaped formwork is reinforced using four 10-mm diameter longitudinal bars. Stirrups with 10-mm diameter are also placed at every 15 cm along the beam. The effect of bar distribution and confinement on flow and passing ability of the SCC is evaluated.
The calculated flow velocity, strain rate, position of flow fronts along the horizontal part, and level of SCC in the vertical funnel, as well as flow rates are presented in 0.1-s time steps during the casting process. The various predicted responses are compared to experimental values determined using three different SCC mixtures cast in the same types of beams. The investigated SCC mixtures had a slump flow of 700 mm and V-funnel flow times ranging between 2.88 and 3.99 s. The simulations are found to be in very good agreements with the experimental results. The numerical simulations are shown to successfully predict the flowability and passing ability of the SCC in vertical and horizontal directions along the cast beams.

Keywords: *Casting, Flowability, Flow Simulation, Homogeneous Analysis, Passing Ability, Rheology, Self-Consolidating Concrete.*

Introduction

Whether on site or in a prefabrication plant, problems related to ensuring complete filling of the formwork are encountered regularly, especially in the case of densely reinforced structural elements and highly restricted sections. SCC is used in the precast and cast-in-place industries to facilitate and speed up casting operations and secure high surface finish. The main functional requirements of SCC are the filling ability, the passing ability, and stability. Passing ability refers to the ability of SCC to flow through tight openings, such as space between reinforcing bars. Filling ability refers to the ability of SCC to flow under own weight and is mostly dealing with non-restricted flow. The filling capacity refers to the ability of the concrete to complete filling of the formwork under own weight. Achieving proper passing ability and filling ability depends on the mixture composition and rheological properties of the concrete, the element characteristics, including the reinforcement detailing and density, as well as the casting conditions [1].

SCC behaves as elasto-viscoplastic material with yield stress [2]. The material behaves as solid for shear stress values lower than the yield stress, and flows when the shear stress overcomes the yield stress. The motion of concrete is eventually arrested when the gravitational forces are in equilibrium with the viscous forces [2-4]. The evolution of flow and the shape of free-surface profile are therefore dependent on the rheological behavior of the concrete. It is essential to develop some numerical techniques for predicting casting operation given a set of properties of concrete, geometry of the element to be cast, and the selected casting process (gravitational, pumping, etc.) [5-8].

In this study, a computational fluid dynamics (CFD) software was employed to simulate casting process of 162 liters of SCC in 4.05 m length reinforced beam. Using rheological properties of SCC as the input parameters for the software, the effect of viscosity on flow properties of SCC was evaluated for a given constant yield stress. The simulations are also found to be in very good agreements with the experimental results in terms of free surface profiles, velocity, strain rate, kinetic energy, and volume flowrate magnitudes for each time step.

Materials and Experimental Program

As summarized in Table I, three SCC mixtures were optimized to achieve an initial slump flow of 700 mm but different V-funnel times. The mixtures were proportioned with a binder content of 450 kg/m^3 (350 kg/m^3 of GU cement and 100 kg/m^3 of Class F fly ash), and three sand-to-total aggregate ratios of 47%, 50% and 56% by mass. The mixtures were proportioned with a water-cementitious material (w/cm) of 0.47 and three high-range water reducer (HRWR) dosages of 3.6, 3.9, and 5.8 L/m^3.

Table I. SCC mixtures proportioning and rheological properties.

Mixture	SCC1	SCC2	SCC3
Cement (kg/m^3)	350	350	350
Fly Ash (kg/m^3)	100	100	100
w/cm	0.47	0.47	0.47
Sand (kg/m^3)	907	823	748
Coarse Aggregate (4-8 mm) (kg/m^3)	144	162	179
Coarse Aggregate (8-12.5 mm) (kg/m^3)	576	650	671
HRWRA (L/m^3)	3.6	3.9	5.8
Slump Flow (mm)	700	700	700
J-Ring (mm)	-	680	680
Filling Capacity (%)	-	95	95
V-Funnel Time (s)	-	2.88	3.99
L-Box Ratio (H_2/H_1)	-	0.58	0.74
Yield Stress (Pa)	60	60	60
Viscosity (Pa.s)	40	30	20
Unit Weight (kg/m^3)	2300	2304	2340

The L-shaped beam that was cast and modeled is shown in Figure 1. It consisted of a vertical section measuring 1.69 m in height and a horizontal section measuring 4.05 m in length with a cross section of 0.2x0.2 m. The sections are separated by a sliding door. The top surface of the first 3 m of the horizontal part is closed by a plexiglass plate to avoid splashing out the concrete during casting.

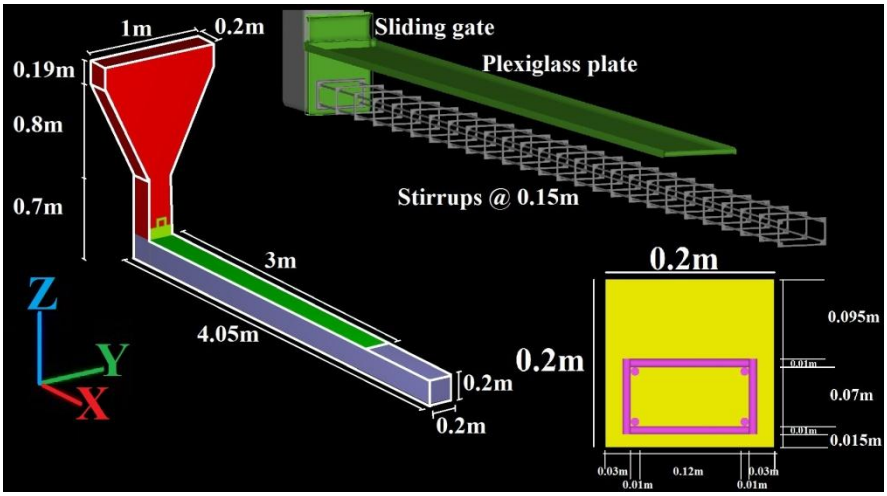

Figure 1. Schematics of the L-shaped beam and reinforcement bars arrangement.

The vertical part is composed of three parts, including the upper rectangular section (1 m width × 0.19 m height), the middle 0.8 m height trapezoid V-funnel part (with 1 m and 0.2 m width at top and bottom, respectively), and the lower rectangular section having 0.7 m height and 0.2 m width. Each of the three sections is 0.2 m in depth. The horizontal part of the formwork is reinforced by four longitudinal 10 mm diameter bars and 26 vertical stirrups of 10 mm diameter equally spaced (0.15 m). This was done to evaluate the effect of bars on the flowability and passing ability of SCC. The schematics of the beam and the reinforcement bars are shown in Figure 1.

The concrete with a total volume of 162 L is cast in the vertical compartment. The sliding door is then opened, and the concrete is gravitationally driven in the horizontal part. In order to evaluate the flowability and passing ability characteristics, the positions of the front of flow surface along the horizontal compartment and the corresponding flow times to reach these positions are recorded till the concrete reaches the end of the beam. In order to do that, several observation gates were fixed throughout the horizontal part of the formwork, and the complete flow process of casting was recorded using a high-speed video camera. As presented in Figure (2), for a given flow time, SCC with lower viscosity is shown to achieve further horizontal motion of the flow front. The experimental results showed also that SCC with higher viscosity would take a longer time to reach the end of beam.

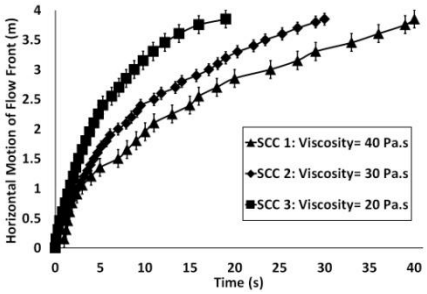

Figure 2. Experimental results of horizontal displacement of flow versus time.

Numerical Simulations and Boundary Conditions

In this paper, a computational fluid dynamics (CFD) software (FLOW3D) was employed to simulate the free surface flow of SCC as a homogeneous Bingham fluid in the reinforced L-shaped beam. The Navier–Stokes equations for incompressible materials are solved by the Volume of Fluid (VOF) method in order to predict free surface profiles and flow properties in terms of velocity, strain rate, and energy magnitudes in each time step. In order to discretize the geometry, solid elements, and the fluid, a total of 36 mesh blocks, resulting in 334,240 cells

with 0.005- to 0.02-m mesh size in the x, y, and z directions were created. The velocity of the concrete flowing at the fixed reinforcing bars, wall boundary, and the rate of raising the dividing gate were set to zero, zero, and 0.05 m/s, respectively. The friction coefficient between fluid and walls of apparatus is fixed at 0.4 [9]. The modelled fluids are implicitly approximated using an elasto-viscoplastic model. Gravitational acceleration and shear elasticity modulus are set to 9.81 m/s^2 and 100 Pa, respectively. The modelled flows are assumed as laminar flow type.

Results and Discussions

The horizontal displacements of the flow fronts for the three mixtures are simulated numerically and compared with the experimental observations, extracted from the recorded videos, as summarized in Figure 3.

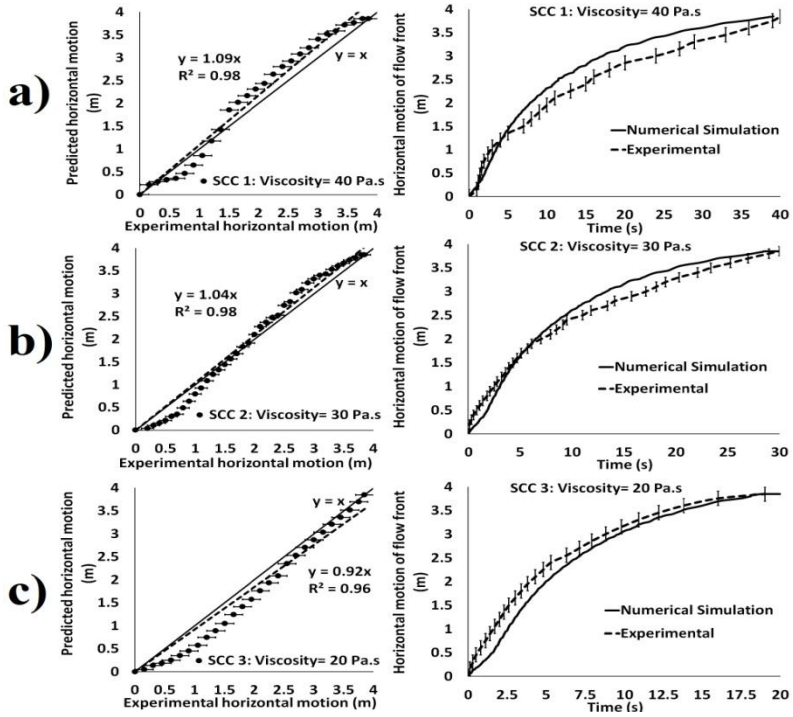

Figure 3. Flow front displacement, a comparison between numerical simulation and experimental results: a) SCC 1, b) SCC 2, and c) SCC 3.

As can be observed, the numerical simulations are shown to be in very good agreements with experimental results with a coefficient of correlation (R^2) greater than 0.96. The predicted-to-experimental profile ratio ranged between 0.92 and

1.09. It shows that the assumptions for boundary conditions, friction coefficient, and mesh settings were selected properly. Moreover, it can be seen that the numerical simulations can predict very well the final time needed for flow front to reach to the end of the beam for all the three mixtures. As can be seen, the minimum R^2 of 0.96 was obtained for the mixture with the minimum plastic viscosity (20 Pa.s corresponding to SCC3). On the other hand, some underestimations by the numerical simulations can be observed in the initial flow times (first 5-7 s) for the three mixtures. These two phenomena could be explained by the inertia effect on flow properties and precision of the numerical models.

In order to evaluate the effect of viscosity on flowability and passing ability of the investigate SCC mixtures, the flow profiles of two additional fluids having a yield stress of 60 Pa and different viscosity values of 15 and 50 Pa.s and density (ρ) of 2300 kg/m^3 are simulated for a maximum 40 s flow period. The simulation results for flow front displacements in the horizontal beam are presented in Figure 4.

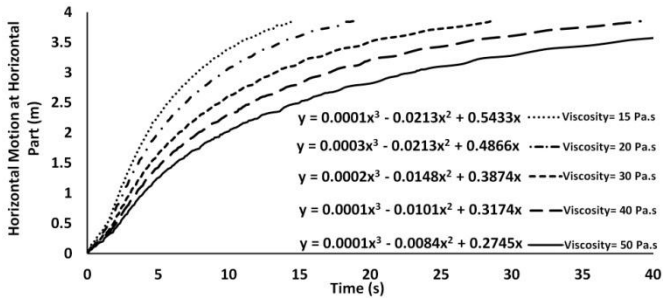

Figure 4. Predicted flow front displacements in horizontal beam versus time.

As can be observed in Figure 4, in a given flow time, the SCC with higher viscosity travels less in the horizontal part of the formwork. Therefore, for a given yield stress, SCC with higher viscosity can exhibit less flow and lower passing ability. Calculating the derivatives of the polynomial correlated functions at time=0 s, the initial velocity of flow front can be estimated for all the mixtures. As can be seen, increasing viscosity from 15 to 50 Pa.s can lead to decrease the estimated initial velocity of flow fronts from V= 0.5433 to 0.2745 m/s. These estimations allow us to compare initial typical inertia stresses ($I=\rho V^2$) for the selected range of plastic viscosity, using a constant density of 2300 kg/m^3. Accordingly, decreasing plastic viscosity from 15 to 50 Pa.s can lead to increase initial inertia stress from 173 to 679 Pa which are much greater than yield stress of the mixtures (60 Pa).

Based on the results of the Figure 4, the front flow velocity magnitudes are calculated in 1-s time steps, while the strain rate and kinetic energy values were simulated. As can be observed in Figures 5a, 6a, and 7a, because of the initial inertia stresses, the flow front velocity, strain rate, and kinetic energy magnitudes increase during the first 3 s of flow time and reach to their maximum values.

Comparing these maximum values, as can be observed in Figures 5b, 6b, and 7b, the use of SCC with higher viscosity resulted in lower flow front velocity, strain rate, and kinetic energy. Furthermore, these properties are well correlated with the viscosity values with R^2 values more than 0.99.

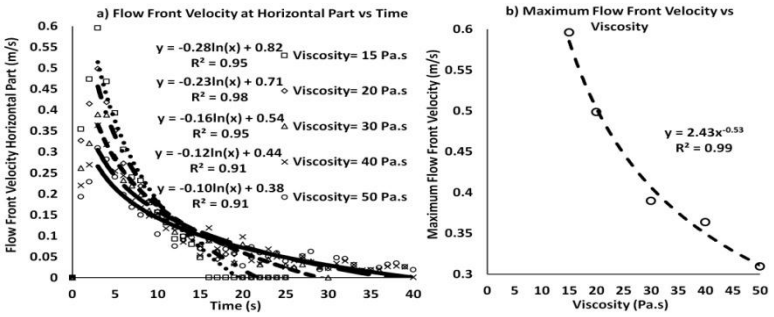

Figure 5. Flow front velocity versus a) time, b) viscosity.

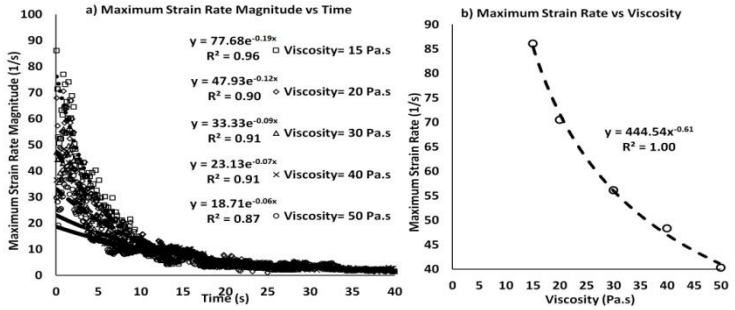

Figure 6. Maximum flow strain rate magnitude versus a) time, b) viscosity.

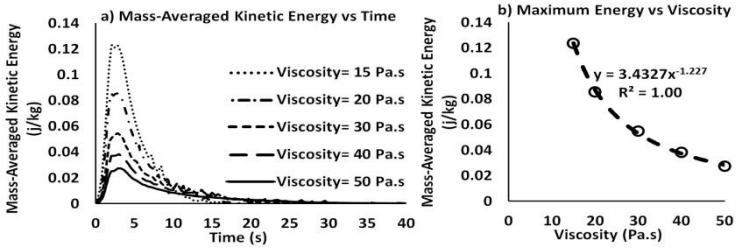

Figure 7. Mass-averaged kinetic energy versus a) time, b) viscosity.

In order to determine in which flow depth there is more deformation that may indicate a risk of dynamic segregation, the correlation of the maximum flow velocity magnitudes with maximum strain rate magnitudes is examined for the total flow period, as presented in Figure (8). From this correlation, critical thickness of segregation ($h_{critical}$) may be approximated as $h_{critical} \cong V / \dot{\gamma}$, where V is the

maximum velocity and $\dot{\gamma}$ is the corresponding maximum shear strain rate magnitude.

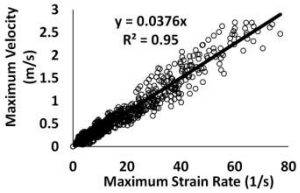

Figure 8. Maximum flow velocity versus maximum strain rate magnitudes.

As can be observed in Figure (8), the $h_{crtical}$ value of 0.0376 m can be estimated. This value refers to the region located above the bottom row of horizontal reinforcing bars.

The effect of viscosity on flowability of concrete in the vertical direction is evaluated by comparing the vertical motion and flow surface velocity magnitudes observed in the vertical compartment of the beam (Figure 9).

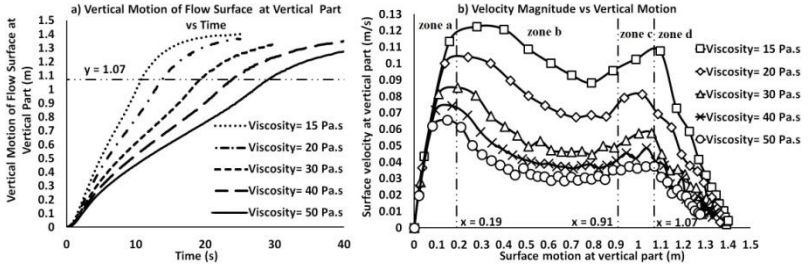

Figure 9. a) Vertical motion of flow surface versus time, b) velocity of flow surface versus vertical motion of flow surface.

As can be observed in Figure 9a, in a given flow time, decreasing the plastic viscosity can lead to an increase in the vertical motion of the flow surface in the vertical section. It can be also seen that the SCC with higher viscosity takes longer time to reach a certain vertical motion. Therefore, increasing the viscosity can lead to a decrease in the velocity of the flow surface in the vertical section. Furthermore, it seems there is some changing in the flow pattern at vertical motion value of 1.07 m, which corresponds to the time that flow surface reached to lower rectangular zone of the vertical section of the formwork. As can be seen in the Figures 9b and more illustrated in Figure 10, different patterns can be observed based on surface flow position at three different parts of the vertical compartment of the beam. As can be observed in Figure 10, fluids with higher viscosity showed lower velocity of surface flow in the vertical compartment. It is also observed that velocity of flow surface can increase in the upper rectangular part (a) compared to the other parts of the vertical section. This can explain by the inertia effect on the

flow velocity in the first moments of the flow. Once the flow surface passes through the V-funnel shaped zone (b), the velocity decreases. In the transition part (c), the flow velocity increased slightly because of the inertia effect created by the change in flow section.

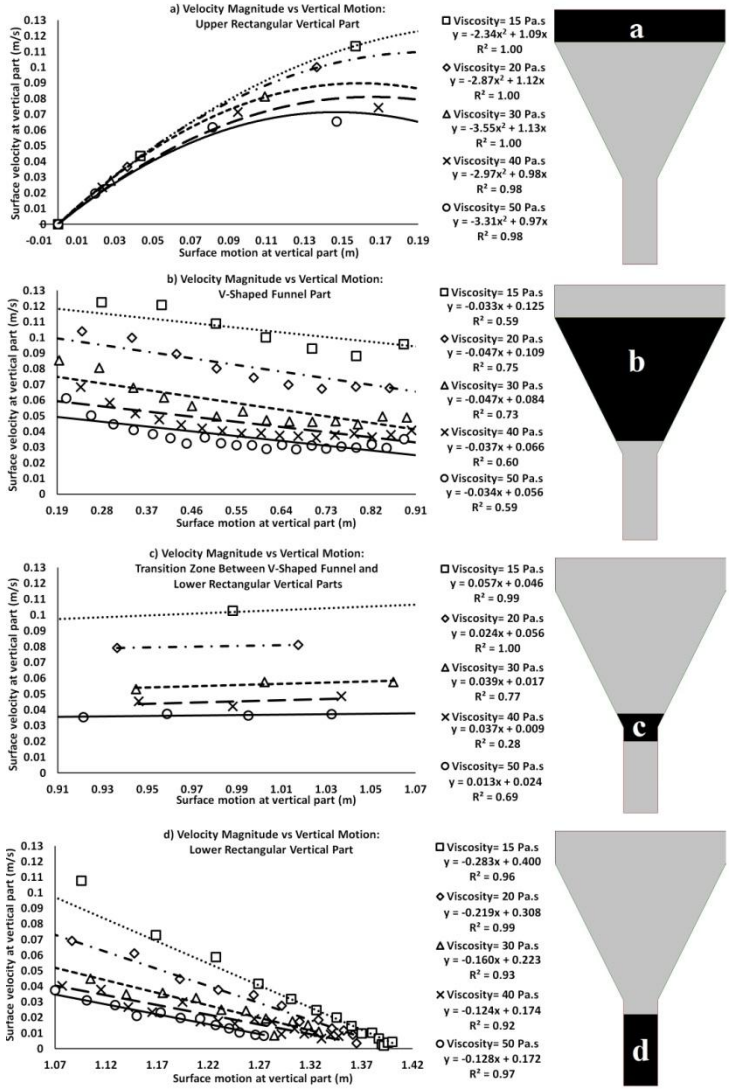

Figure 10. Variation of velocity with surface motion in different parts of the vertical section: a) upper rectangular part, b) V-shaped funnel part, c) transition zone between V-shaped funnel and lower rectangular parts, and d) lower rectangular part.

In the lower rectangular zone (d), velocity losses are almost 3.4 to 8.6 times higher than those observed in the V-shaped funnel zone (b). It is expected, therefore, that SCC mixtures can show higher flowability with less velocity loss in the V-shaped sections than in the rectangular part of the vertical section.

Flow rates of SCC mixtures having different viscosities are calculated (Figure 11) using flow surface velocities in the vertical compartment of the L-beam.

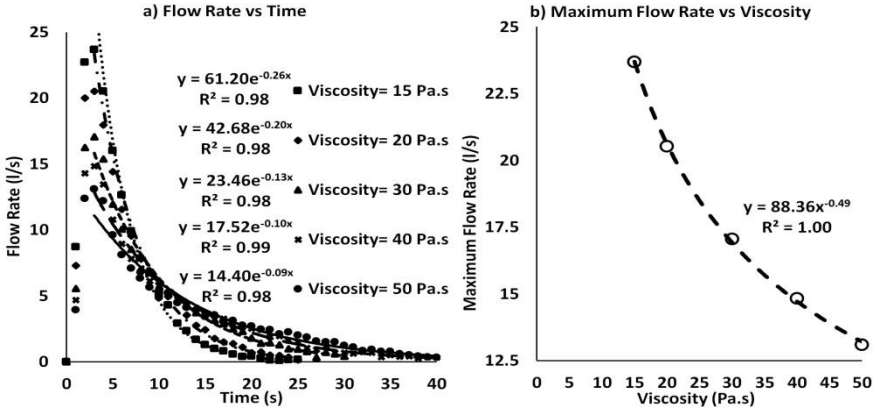

Figure 11. a) Flow rate versus time, and b) maximum flow rate versus viscosity.

As can be observed, the increase in viscosity resulted in decreasing the flow rates following a perfect exponential correlation (R^2 = 1.00). The design of vertical comportment of the beam (three different shapes) provides maximum flow rate values ranging between 13 and 24 l/s. These values are comparable to those encountered in SCC pumping operations [10].

Concluding Remarks

The flowability and passing ability of three SCC mixtures designed with different plastic viscosity levels in a reinforced L-shape beam was evaluated. Test results showed that for a given yield stress value, the maximum flow time is greatly affected by the viscosity of the mixture. Flow simulations were successfully carried out using a commercial CFD software to reproduce the experimental results that were observed in casting these SCC mixtures. The simulations are found to be in very good agreements with the experimental results in terms of free surface profiles, velocity, strain rate, kinetic energy, and volume flowrate magnitudes for each time step.

The effect of viscosity on flow properties of concrete in the L-shape beam was also studied. The simulation shows that for a given yield stress, increasing the viscosity of the SCC can lead to a decrease in flow velocity, strain rate, flow rate, and kinetic

energy. These properties are strongly correlated with the viscosity of mixture. Furthermore, the calculated velocity and shear strain rate values are exploited to calculate the critical flow depth ($h_{critical}$) corresponding to the highest potential of dynamic segregation. This value is estimated to be 38 mm which is located right above the bottom row of horizontal bars in the reinforced cage inside the horizontal leg of the modeled beam.
The simulations of flow surface displacement and flow-ability of SCC in different shaped sections of the vertical compartment of the beam showed that the flow velocity loss in the V-shaped funnel is 3.4 to 8.6 times less than that observed in rectangular part.

References

[1] Khayat, H.K. and Mitchell, D. (2009), *Self-consolidating concrete for precast, prestressed concrete bridge elements*, NCHRP Report 628.
[2] Murata, J. (1984), *Mat. Struct.*, vol. 98, p. 117.
[3] Noguchi, T., and Mori, H. (1998). In: *International Workshop on Self-Compacting Concrete*, pp. 97-110, Kochi, Japan.
[4] Dufour, F. and Pijaudier-Cabot, G. (2005), *Int. J. Numer. Anal. Met.*, vol. 29, n. 4, p. 395.
[5] Roussel, N, and Coussot, P. (2005), *J. Rheol.*, vol. 49, n. 3, p. 705.
[6] Nguyen, T.L.H., Roussel, N., Coussot, P. (2006), *Cem. Concr. Res.*, vol. 36, n. 10, p. 1789.
[7] Roussel, N, Dufor, F., Thrane, L.N. and Szabo, P. (2007), *Cem. Concr. Res.*, vol. 37, n. 9, p. 1298.
[8] Roussel, N, Geiker, M.R., Dufour, F., Thrane, L.N., and Szabo, P. (2007), *Cem. Concr. Res.*, vol. 37, n. 9, p. 1298.
[9] Vanhove, Y., and Djelal, C. (2013), *Int. J. Civil. Eng. Tech. (IJCIET)*, vol. 4, n. 6, p. 67.
[10] Feys, D. and Khayat, K.H. (2015), *Journal of Sustainable Cement-Based Materials*, vol. 4, n. 3, p. 238.

Numerical Simulation of Self-Consolidating Concrete Flow as a Heterogeneous Material in L-Box Set-up

Masoud Hosseinpoor[1], Kamal H. Khayat[2] and Ammar Yahia[1]

[1]Department of Civil Engineering, Université de Sherbrooke, Canada.
[2]Department of Civil, Architectural and Environmental Engineering,
Missouri University of Science and Technology, USA.

Abstract In this paper, a computational fluid dynamics (CFD) software was employed to simulate free surface flow of self-consolidating concrete (SCC) in the L-Box test apparatus. In total, 28 simulations were developed to study the effect of rheological parameters, reinforcing bar spacing, and aggregate content on the flow-ability, dynamic stability, and blocking resistance of SCC. The parameters of the modelling also included that of the suspending fluids made with five plastic viscosity values (10, 17, 25, 38, and 50 Pa.s), three yield stress values (14, 45, and 75 Pa), two fluid densities (2000 and 2500 kg/m^3), and two shear elasticity modulus values (100 and 1000 Pa). In order to study the effect of coarse aggregate content, two values of 20-mm spherical particles were considered (135 and 255). Two bar arrangements (three bars right after gate removal and 18 bars distributed along the horizontal channel) were considered in the numerical simulation.
The paper discusses the results of the numerical simulation in terms of flow velocity, strain rate, flow profiles, and particle distribution throughout the L-box channel. The results of the simulation are found to correlate well with changes in rheological parameters of the surrounding fluid. The most dominant parameter affecting dynamic segregation, blocking resistance, flow velocity, and strain rate is shown to be the plastic viscosity of the surrounding fluid.

Keywords: *Blocking, Dynamic Segregation Flow Simulation, Heterogeneous Analysis, L-Box Test, Rheology, Self-Consolidating Concrete.*

Introduction

Self-consolidating concrete (SCC) has pushed back traditional limits concerning the density of reinforcing bars and the complexity of formwork in concrete construction. Its high fluidity makes it more sensitive to segregation during flow and thereafter at rest [1-4]. Developing numerical techniques to predict the flow

characteristics of SCC during the casting process can lead to better selection of the concrete mixture composition and better planning of the concrete placement to ensure successful filling of the formwork. However, the modeling the flow of concrete presents a great challenge because of the necessity of taking into account the complex interaction between the various solid particles in the system, reinforcing bars, and formwork walls, while simultaneously considering the liquid phase in which they are immersed [5].

The L-box test is often used to evaluate the restricted flow of SCC in the presence of obstacles and evaluate the passing ability of the mixture. The L-box consists of vertical and horizontal compartments that are separated by a sliding door. The concrete is cast in the vertical compartment, and once the sliding door is opened, the concrete is gravitationally driven in the horizontal channel. Recently, limited number of research studies have been conducted to the rheological parameters of SCC and L-box output parameters [6-9].

In this paper, a computational fluid dynamics (CFD) software was employed to simulate free surface flow of SCC in the L-Box test apparatus. The basic equations of the conservation of mass for incompressible materials and the Navier–Stokes equations are solved by the volume of fluid (VOF) method [10]. In total, 28 simulations were developed to study the effect of rheological parameters, reinforcing bar spacing, and aggregate particle content on flowability, passing ability, dynamic stability, and blocking resistance of SCC.

Properties of Modelled Materials

The parameters of the modeling included five plastic viscosity values (10, 17, 25, 38, and 50 Pa.s), three yield stress values (14, 45, and 75 Pa), and two shear elasticity modulus values (100 and 1000 Pa) for the surrounding fluid. In order to study the effect of the difference between the density of particles and surrounding fluid on gravitational segregation of the suspension, two fluid densities of 2000 and 2500 kg/m^3 were used to suspend solid particles with a density of 2500 kg/m^3. Modelled suspensions also included two numbers (135 and 255) of 20-mm spherical particles to study the effect of coarse particle content on flow properties of SCC. The modelled L-Box set-ups also included two bar arrangements after the dividing sliding door of the L-Box in order to evaluate the effect of bar spacing on flow properties. The simulation included three bars of 12 mm in diameter and 200 mm in height located right after the gate separation and 18 bars (six rows of three bars at 100-mm spacing) distributed along the horizontal channel.

Numerical Simulations and Boundary Conditions

A CFD software (FLOW3D) was employed to simulate free surface flow of SCC in the L-Box test apparatus. The basic equations of the conservation of mass for incompressible materials and the Navier–Stokes equations are solved by the Volume of Fluid (VOF) method [10]. In total, 28 simulations were developed for a period of flow of 6.4 s that is the minimum duration of flow time to empty the vertical section of the L-Box for the selected range of plastic viscosity. In order to discretize the geometry, solid elements, and suspension, two mesh blocks of 326,832 cells with 5 -mm size in the x, y, and z directions were created.

The Dirichlet-Neumann boundary condition was imposed to the flow domain based on the geometry of the L-Box; the velocity of the walls and the gate rising rate were set to zero and 0.03 m/s, respectively, as indicated in Figure 1. The friction boundary conditions were assumed between particles, fluid, and the walls of the apparatus with a friction coefficient value of 0.4. The modelled fluids are considered as Non-Newtonian Bingham fluids using an elasto-viscoplastic model with implicit numerical approximation. Gravity stresses are calculated using gravitational acceleration value of 9.81 m/s^2. In order to consider particle-particle and particle-obstacle interactions, a coefficient of restitution of 0.8 was applied for collision physical model. The modelled flow is assumed as laminar flow type.

Sampling Methods and Anticipated Results

In order to evaluate flowability of the modelled suspensions, the results of the simulations are presented in 0.1-s time steps in forms of flow velocity, strain rate magnitudes, and flow profiles. Finally, the modelled mixtures could be classified based on self-leveling and self-consolidating properties using calculated horizontal and vertical motions of the fluid in two perpendicular parts of the L-box apparatus. Dynamic stability and blocking resistance properties of the suspensions are also calculated by measuring the volumetric particle contents in seven different sections through the L-box horizontal channel that are illustrated in Figure 1. In order to do that, the number and position of the particles, as well as the volume of the fluid in each section are calculated at each 0.1-s time step.

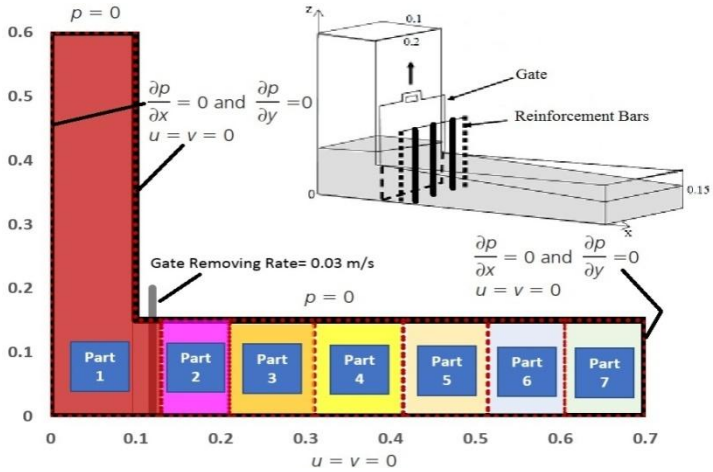

Figure 1. Schematics of L-Box set-up, sampling sections, and boundary conditions.

Results and Discussions

Effect of Viscosity and Yield Stress of the Surrounding Fluid

In this section, the results of the simulations carried out on suspensions with fluid density of 2500 kg/m^3 and shear elasticity modulus of 100 Pa are presented. As expected, for a given viscosity, the increase in yield stress decreases the L-box blocking ratio (H_2/H_1). As shown in Figures 2 and 3, increasing both the viscosity and yield stress of the surrounding fluid resulted in lower L-box blocking ratio (H_2/H_1) and lower displacement of flow front in horizontal part. This resulted also in higher free surface level in the vertical part of the L-Box. The results of the simulation in Figure 4 showed that maximum velocity and strain rate can decrease when the viscosity and yield stress of the surrounding fluid increase; very good correlations were established.

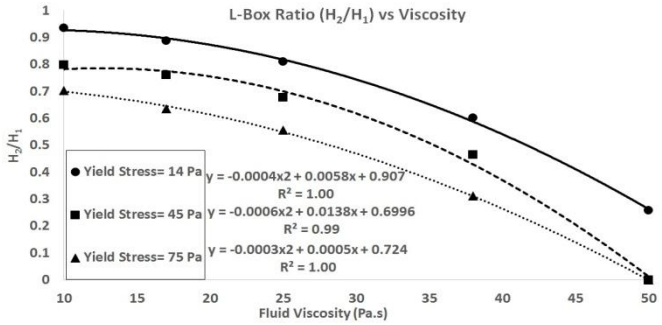

Figure 2. L-Box ratio for different mixtures versus viscosity of surrounding fluid.

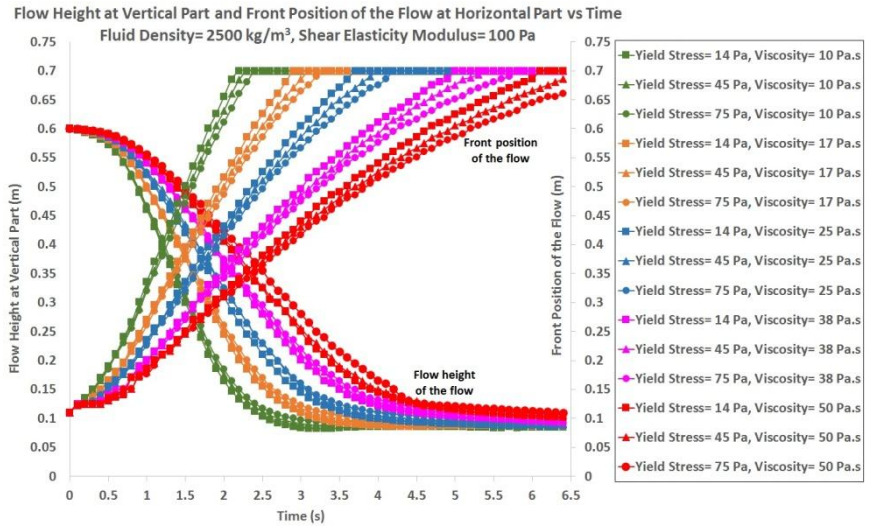

Figure 3. Flow height and front position of the flow at vertical and horizontal parts.

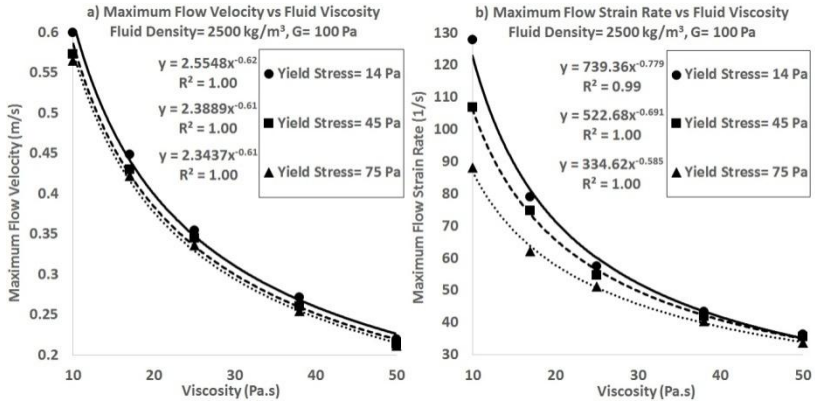

Figure 4. a) Maximum velocity and b) strain rate magnitudes versus viscosity.

Calculating the fluid volume and particle content in each of the seven horizontal sections along the horizontal leg of the L-box, the blocking index (B.I.) can be defined for each 0.1-s time step using Eqn. (1).

$$B.I.(\%) = \frac{Particle\ Content\ @\ Part\ 1 - Particle\ Content\ @\ Part\ 7}{Initial\ Particle\ Content} \times 100\% \quad (1)$$

As shown in Figure 5, increasing the viscosity of the surrounding fluid has more effect on increasing the blocking index of the suspension than yield stress values.

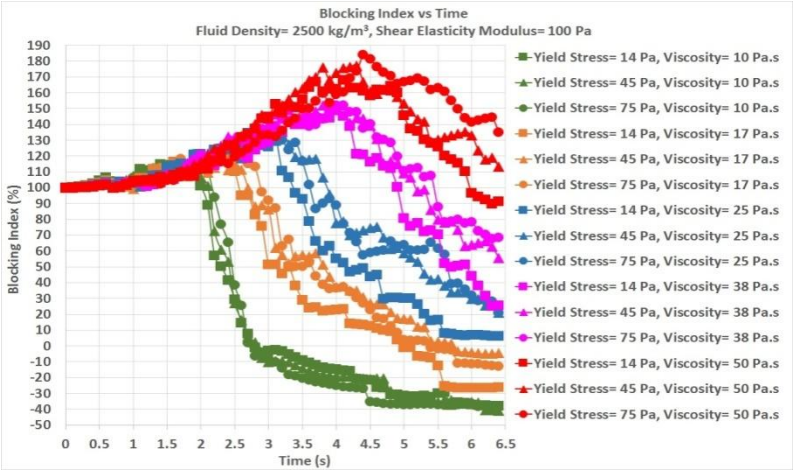

Figure 5. Blocking index versus time.

For each suspension, the maximum B.I. value ($B.I._{max}$) is selected to indicate the risk of blocking (Figure 6). As can be observed, $B.I._{max}$ can increase with viscosity of the surrounding fluid with very high correlation. However, the yield stress showed less effect on $B.I._{max}$ than viscosity.

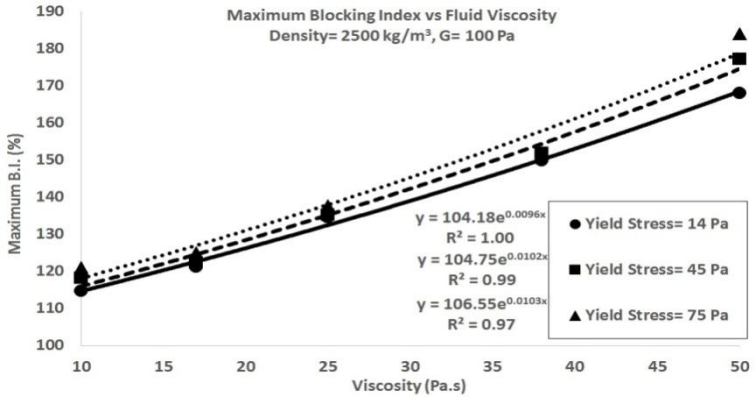

Figure 6. Maximum blocking index versus viscosity.

Effect of Density of the Surrounding Fluid

As seen in the previous section, the maximum $B.I._{max}$ value is obtained with the surrounding fluid that has a yield stress of 75 Pa. The effect of density is studied for this yield stress considering two fluid density values of 2000 and 2500 kg/m^3.

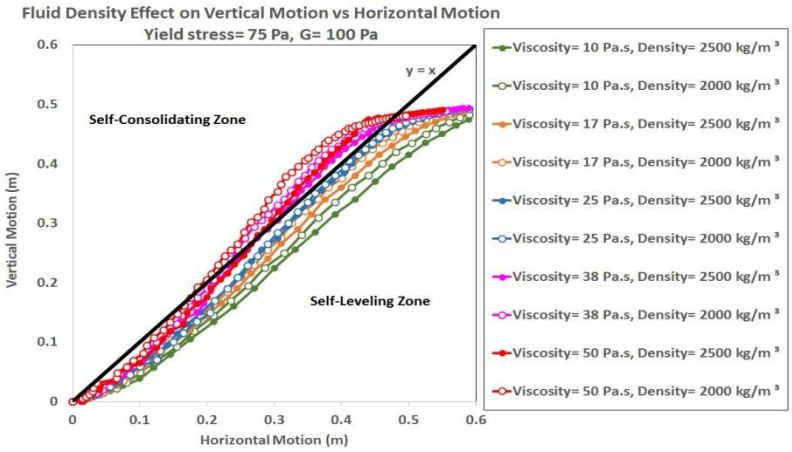

Figure 7. Vertical motion versus horizontal motion.

As can be observed in Figure (7), suspensions with less fluid density exhibit more vertical than horizontal motion and less flowability. This resulted in more self-consolidating behavior than self-levelling properties. It also can be observed in Figure (8) that lower flow velocity and strain rate can be obtained with the lower fluid density because of the reduction in gravitational forces.

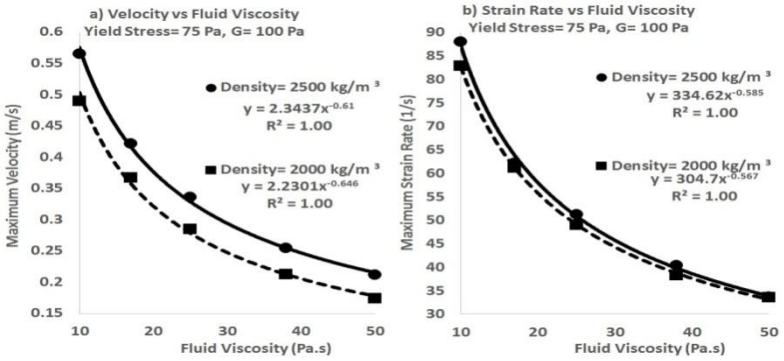

Figure 8. a) Maximum velocity and b) strain rate magnitudes versus viscosity.

As a result of decreasing the fluid density, the relative velocity between the fluid and particles also decrease, which results in decreasing the blocking index and risk of segregation, as shown in Figure 9.

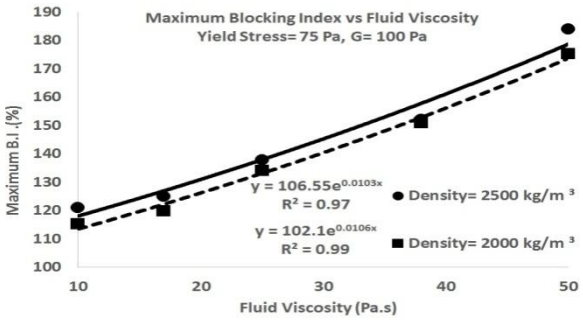

Figure 9. Maximum blocking index versus viscosity.

Effect of Shear Elasticity Modulus of the Surrounding Fluid

In order to evaluate the effect of shear elasticity modulus, the flow behavior of five additional suspensions with shear elasticity modulus value of 1000 Pa and fluid density of 2000 kg/m^3 is modelled. As can be observed in Figure (10), increasing shear elasticity modulus (G) resulted in reducing the maximum flow velocity and strain rate magnitudes. Since G value is only related to elastic state deformation, in a constant gravitational, viscous, and shear stress state (constant density, viscosity, and yield stress) decreasing G value results in higher initial flow energy, velocity, and strain rate magnitudes to initiate plastic state based on Hooke's law. (Eqn. (2))

$$F_1 = K_1\Delta x_1, F_2 = K_2\Delta x_2, F_1 = F_2;\ K_1 \rangle K_2, G \propto K \Rightarrow \Delta x_1 \langle \Delta x_2 \Rightarrow V_1 \langle V_2 \qquad (2)$$

where K is stiffness factor in Hooke`s law and V is the velocity corresponding to displacement of Δx in a constant period of time. Decreasing the flow energy causes less energy applied to transport coarse particles. Therefore, higher blocking indexes are obtained for higher G values, as presented in Figure (11).

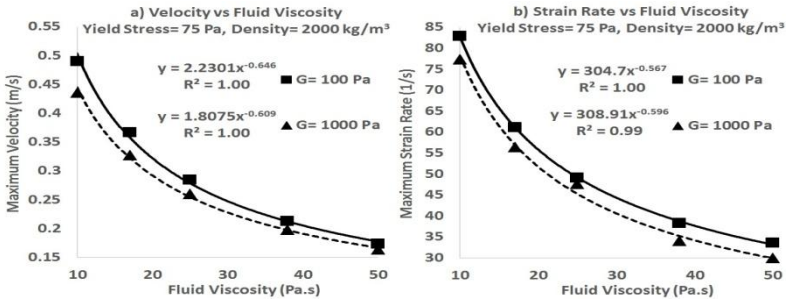

Figure 10. a) Maximum velocity and b) strain rate magnitudes versus viscosity.

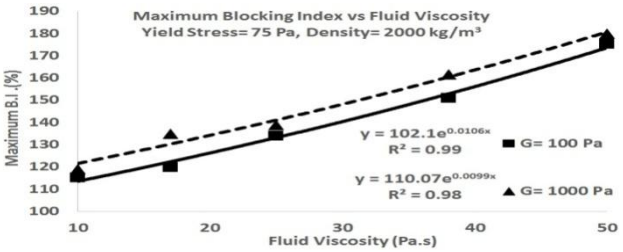

Figure 11. Maximum blocking index versus viscosity.

Bar-Particles Coupled Effect

Bar-particles coupled effect is studied for medium viscosity of 25 Pa.s, the highest yield stress of 75 Pa, a fluid density of 2500 kg/m^3 and shear elasticity modulus of 100 Pa. In order to do that, the flow of two suspensions with 4.6% and 8.7% particle contents are simulated in L-box set-up. Furthermore, two bar arrangements, including three bars right after the gate and 18 bars (six rows of three bars) distributed along the horizontal comportment of the apparatus are considered. As can be observed in Figure (12), suspensions exhibited less horizontal motion and flowability in the case of more congested flows passing through 18 bars after the gate.

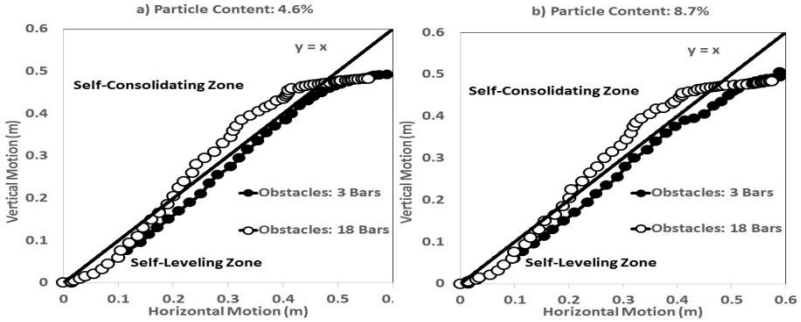

Figure 12. Vertical versus horizontal motion: a) 4.6%, b) 8.7% particle content.

Blocking index (B.I.) (Eqn (1)) and coefficient of variation (COV) of particle contents in seven horizontal sampling sections are also calculated. Then, the bar effects are evaluated by comparing the ratio of B.I. and COV values of 18 bars configuration to the values of three bars configuration for 4.6% and 8.7% particle content suspensions, respectively (Figure 13).

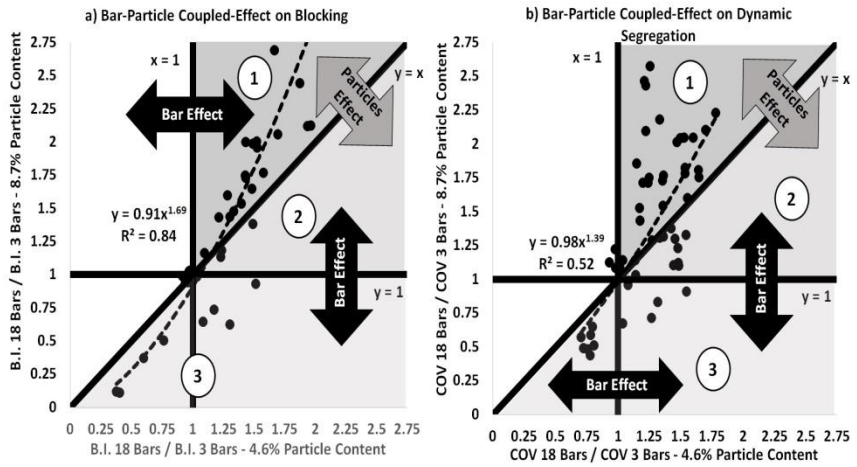

Figure 13. Bar-Particles coupled effect on: a) blocking, b) dynamic segregation.

According to Figure 13, the bar-particles coupled effect can be described in three zones:

1) Bar-particle parallel effect: This zone is limited to the area surrounded by x>1 and y>x. In this part, increasing both the number of bars and initial particle contents can result in greater blocking and dynamic segregation. This can be due to the formation of particle blocking arches behind the bars. In this part, both the presence of bars and particle content have dominant effects.

2) Bar-particle opposite effect: This zone is limited to the area surrounded by y>1 and y>x. In this part, increasing number of bars can result in more blocking and dynamic segregation due to greater risk of blocking and arch formation. On the other hand, increasing the particle content can improve the dynamic stability and passing ability of the suspension. Such more homogeneous behavior can be explained by particle effects on increasing the overall viscosity and yield stress of the suspension, which leads to a lower level of fluid deformation and therefore, less dynamic segregation. In this zone, the presence of bars has more dominant effect.

3) Bar-particle opposite effect: This zone is limited to the area surrounded by y<1 and y>x. In this part, increasing the particle content can decrease the additive effect of bars on blocking and dynamic segregation by increasing the overall viscosity and yield stress of the suspension. In this zone, the particle content has more dominant effect.

Concluding Remarks

In this paper, a CFD software was successfully used to evaluate the flowability, passing ability, and dynamic stability of SCC cast in the L-Box test set-up. The

concluding remarks can be expressed by the effect of rheological parameters, fluid density, reinforcing bar spacing, and aggregate particle content.

The results showed that increasing plastic viscosity, yield stress, and shear elasticity modulus of the surrounding fluid can result in decreasing flowability, dynamic stability, and blocking resistance of the suspension. The simulations showed that the plastic viscosity has more dominant effect on flow properties and shows very good correlation. It also can be concluded that in given viscous and shear stresses, decreasing the fluid density can lead to less flowability, as well as less flow velocity and strain rates. As a result, relative velocity between fluid and solid particles decreases, which results in reducing blocking and dynamic segregation of the suspensions.

A new approach is proposed to explain how particle contents and number of bars can have parallel or opposite effect on dynamic stability and risk of blocking. Increasing both the particle content of the simulated concrete suspension and the number of bars after the gate in the L-box horizontal section can lead to increase the possibility of formation of particle blocking arches. On the other hand, increasing the particle content can lead to an increase the overall viscosity and yield stress values of the suspension and a decrease in the relative velocity between the surrounding fluid and solid particles. This can improve dynamic stability of the mixture.

References

[1] Japan Society of Civil Engineers, (1999), *Recommendations for Self-Compacting Concrete*, Tokyo, 77p.
[2] Khayat, H.K. (1999), *ACI Mat. J.*, vol. 96, n. 3, p. 346.
[3] Khayat, H.K. (1999), *ACI Mat. J.*, vol. 95, n. 2, p. 158.
[4] Noguchi, T., and Mori, H. (1998). In: *International Workshop on Self-Compacting Concrete*, pp. 97-110, Kochi, Japan.
[5] Nguyen, T.L.H., Roussel, N., and Coussot, P. (2006), *Cem. Concr. Res.*, vol. 36, n. 10, p. 1789.
[6] Dufour, F. and Pijaudier-Cabot, G. (2005), *Int. J. Numer. Anal. Met.*, vol. 29, n. 4, p. 395.
[7] Roussel, N, Dufor, F., Thrane, L.N. and Szabo, P. (2007), *Cem. Concr. Res.*, vol. 37, n. 9, p. 1298.
[8] Lashkarbolouk, H, Chamani, M.R., Halabian, A.M. and Pishehvar, A.R. (2013), *Mag. Concr. Res.*, vol. 65, n. 6, p. 365.
[9] Khayat, H.K. and Mitchell, D. (2009), *Self-consolidating concrete for precast, prestressed concrete bridge elements*, NCHRP Report 628.
[10] Hirt, C.W. and Nicholas, B.D. (1981), *J. Comput. Phys.*, vol. 39, n. 1, p. 201.

Effect of Hydration Kinetics on Cement Paste Microstructure Using a Rheological Approach

Willy Mbasha, Rainer Haldenwang and Irina Masalova

Cape Peninsula University of Technology, PO Box 652 Cape Town 8000, South Africa

Abstract The effect of hydration on the fresh properties of four CEM I 52.5 N cement type manufactured at different factories in South Africa was investigated in the presence and absence of a polycarboxylate based superplasticiser. The kinetics of hydration was characterized by following the growth of the dynamic modulus at a constant frequency. A rheokinetic equation of self-acceleration type was used to predict the time dependence of the elastic modulus. The microstructure development was monitored by constructing the flow curves at instant times during cement paste hydration. A rotational rheometer with roughened parallel plates was utilized for this purpose.
It was found that though these cements were of the same type, their rheological behavior was different. The rheokinetic model, as well as the construction of flow curve technics can both be used to study the hydration of cementitious materials. Cements with a high rate of hydration resulted in a rapid yield stress development while cements with low hydration rate resulted in slow yield stress evolution.

Keywords: *hydration; kinetics; yield stress; rheology and microstructure*.

Introduction

Self-compacting concrete and high strength performance concrete are innovative materials that are being used more and more in concrete industries worldwide. The performance of these materials from casting to concrete service life depends strongly on both their fresh properties and hydration kinetics[1, 2].

The understanding of these concrete factors on cement paste scale is very important [3]. Coarse aggregates are considered as inert materials and all hydration products are a function of the interaction of cement paste and admixtures used [4]. Cement paste structures are dynamic and continuously changing as the hydration progresses [5-7].

In previous investigations [8-11], different approaches have been used to show the influence of hydration on the rigidification process of cementitious materials. The heat evolution, the ultrasonic wave method and backscattered image technics have been cited as the most popular ones [9, 10].

Hydration is defined by [11] as the period between when water is added to cement, up to the initial setting. The effect of this process products on the rheological behaviour of cement paste can be found in [13,14].
The kinetic of cement hydration causes the properties of cement paste to evolve from viscous fluid to solid material. The nucleation of calcium silicate hydrate (C-S-H) has been found to be at the origin of this transformation [4].
Nicholas, Roussel in [12] used both physical and chemical approaches to show the connection that exists between the yielding process of C-S-H (that starts a few seconds after the end of mixing) and the development of cement paste yield stress.
The work done by [14] established the main rheological parameters that are involved during setting and associated the yield stress and viscosity to this transformation. Consequently, according to the authors, the yield stress is related to the strength of the interparticle attractive forces responsible for coagulation, while the viscosity is related to the volume of solid particles and their packing density within the paste. It is therefore accepted that the yield stress as well as the viscosity both grow the same time as the hydration develops.

The purpose of this work was to show the influence of the hydration kinetics on the microstructure development of cement paste using a rheological approach. Since the internal network of cement paste particles and its yield stress are both related, the internal changes that take place during hydration were assessed by constructing instantaneous flow curves. These curves gave the evolution of yield stress while a rheokinetic model of self-acceleration type provided coefficients that described the hydration process.

Material and Methodology

The subject of this study was four CEM I 52.5 N cements, supplied by one manufacturer from different factories with differences in their chemical composition and mineralogy compounds as shown in Table 1. The alkali equivalent Na2Oeq of the cements were determined as proposed by [15]. The superplasticiser (SP) used was a polycarboxylate acid based polymers with

characteristics as illustrated in Table 2. The optimum concentration of SP was determined as suggested by [16].

Table I Chemical and phase composition of cements used

Chemical Properties (%)	C1	C2	C3	C4
SiO_2	20.8	21.5	20.9	22.3
Al_2O_3	3.8	4.1	4.0	4.7
Fe_2O_3	2.9	2.8	3.0	3.3
Mn_2O_3	0.1	0.7	0.6	0.4
TiO_2	0.2	0.3	0.3	0.5
CaO	64.0	62.7	62.7	61.3
MgO	1.2	3.3	2.9	2.6
P_2O_5	0.17	0.10	0.03	0.12
SO_3	2.33	2.47	2.81	2.95
Cl	0.00	0.00	0.00	0.00
K_2O	0.66	0.36	0.24	0.25
Na_2O	0.34	0.19	0.15	0.18
$Na_2Oeq.$	0.75	0.41	0.29	0.33
LOI	4.11	1.83	2.83	1.74
Total	100.5	100.3	100.5	100.2
FCaO	1.00	1.30	0.95	1.43
C_3S	59.92	50.80	52.74	54.19
C_2S	13.99	20.43	18.76	17.95
C_3A	3.95	2.75	1.84	2.63
C_3A orthorhombic	3.52	2.59	1.58	2.60
Cubic C_3A	0.13	0.16	0.26	0.03
C_4AF	14.54	18.46	20.49	17.15
lime	0.35	0.41	0.51	0.40
K_2SO_4	1.37	0.78	0.31	1.34
Gypsum	1.62	2.74	2.92	1.29
Blaine (cm^2/g)	3750	3650	4250	3850

Table II Characteristics of superplasticisers used

Characteristics	SP
Consistency	Liquid
Color	Amber
Density according to ISO 758 (g/cm3)	1.07-0.02
Dry content according to EN 480-8 (%)	26-1.3
Chlorides soluble in water according to EN 480-10 (%)	0.1
Alkali content (Na2O equivalent) according to EN 480-12 (%)	2.5

Experimental procedure

The application of shear mode rheology in studying cement paste microstructures has been used by many researchers [18–20]. The construction of flow curve method [20] in shear mode was used to follow the evolution of the yield stress.
The method consists of monitoring the viscosity evolution over time at constant shear rates. A set of kinetic curves are therefore obtained. This provides the shear rate dependency of the apparent viscosity for different periods of setting. Thereafter the Bingham model is fitted to the obtained flow curves and instantaneous yield stress values are obtained.
It was suggested by [21] that the fundamental information concerning the development of the microstructure and the internal forces responsible for the cement paste mechanical properties be investigated in the dynamic mode rheology, since measurement can be done within the linear viscoelasticity domain (LVD) therefore preventing the hydration process from being disturbed.
The hydration kinetics was thus monitored by following the growth of the storage modulus and fitting the rheokinetic model of self-acceleration type [22] as given by Eqn. (1).

$$\frac{d\beta}{dt} = \frac{1}{\theta}(1-\beta)(1+K\beta) \quad (1)$$

With β reflecting the chemical transformation within the paste and thus the ratio of the current storage modulus *G (t)*
to the infinite storage modulus G_∞(the plateau of storage modulus). *K* is a parameter reflecting the rate of self-acceleration and is obtained by determining the position at which the slope of Eqn. (1) is maximum. Two important coefficients can be deduced from Eqn. (1) in order to characterize the evolution of cement paste hydration:

$$T^* \cong \frac{\theta}{1+K}[3+\ln(1+K)] \quad (2)$$

$$R_h = (1-\beta)(1+K\beta) \quad (3)$$

T^* and R_h helps estimating respectively the complete rigidification time of the cement paste and the relative rate of hydration assuming that β=0.95.

Instrumentation and sample preparation

Nehdi and Rahman [17] affirm the challenges that exist in rheometry of cement paste. However, recent work of [23] demonstrates how to avoid all these challenges when studying the rheology of cementitious materials.
Experiments were carried out in a temperature and relative humidity controlled room. Deionized water was used for all the mixes at a constant water cement ratio of 0.45 corresponding to 60.75 g of water in the absence of SP and 60.35 g in the presence of SP with the equivalent solid content.
The energy used during mixing is very important in attempting to homogenize the sample by eliminating or reducing all possible agglomerates, clumps or clusters in order to wet all particle surfaces without structure breakdown [24]. In this research, an intensive mixing method [25] was used for all the cements as suggested by [25,27]. Samples were mixed by hand for 2 minutes in such a way that consistent paste was obtained for all the experiments.
An Anton Paar MCR51 rotational rheometer fitted with a system able to control the temperature set at 25 ^{o}C was used. The test geometry used was a roughened parallel system with a 0.6 mm gap.
For the dynamic mode, oscillatory measurement technique was used:
After mixing the sample was placed immediately at rest for 3 min and thereafter additional mixing was carried out lasting 1.5 min before starting the test. The sample was placed by means of a spatula on the working surface of the rheometer. To ensure that the measurements of moduli were done within the linear viscoelastic domain, the sample was subjected to a strain with constant frequency of 1 Hz and constant amplitude of 0.06% less than the critical strain as determined in a previous amplitude sweep test.
For the shear mode:
After the mixing protocol, samples were pre-sheared at 50 s^{-1} for 10 s. Five different constant shear rate (5 s-1, 10 s-1, 20 s-1, 50 s-1 and 75 s-1) were considered individually and corresponding kinetic viscosity curves were obtained (with 15 s measuring time per point).
For measurement of cement with SP, the admixture was added to the water before the solution was added to the cement and the sequence above was performed.
No sample was used twice. After each experiment, the plates of the rheometer were washed clean and dried with care to avoid any influence of previous sample on the next test.

Results and Discussion

Figures 1 gives the time evolution of yield stress for all four cements in the absence and presence of SP at 0.3%.

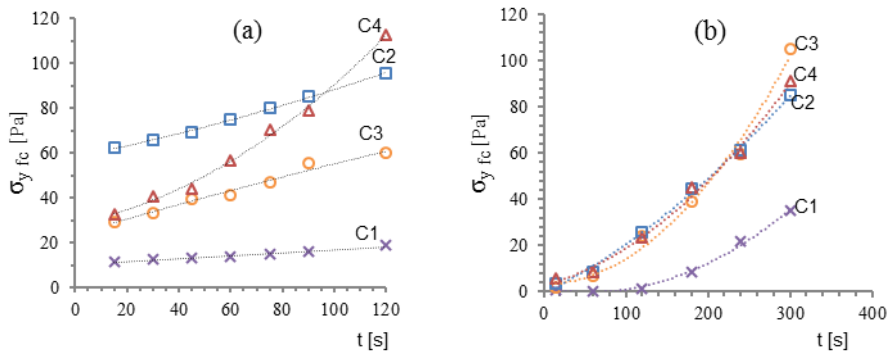

Figure 1 Yield stress values for cements without SP (a) and the same materials with 0.3% SP (b)

It can be seen that cement C1 exhibits the lowest yield stress values with almost a horizontal slope and cement C4 the largest increase. When the SP was added in cements, the picture becomes quite different (Fig. 1b). Firstly, a nearly zero yield stress is observed for all mixes, much slower growth of yield stress in the beginning of the process, and much longer time necessary to reach the same values of the yield stress in comparison with unsuperplasticized cements. Cement C1 remains fluid for a long time and the growth of the yield stress is much less than for other superplasticised cements.
A similar SP-cement interaction was reported by [28, 29] who postulated that the dispersion mechanism of SP on cement particles is dominated mostly by steric forces [29].

The storage modulus (G') of cements were observed over a period of one hour in order to study the effect of hydration kinetics on the rigidification process of cement paste. The kinetics of measured storage modulus for the four cements with and without SP are shown in Fig. 2. The time scale for each sample shown in these figures is the same, to clearly indicate the differences in their rigidification. Figures 2 (b) and (d) present the data on semi-log scale to illustrate the three regions of hydration kinetic of cement paste: retardation, rapid acceleration and the plateau.

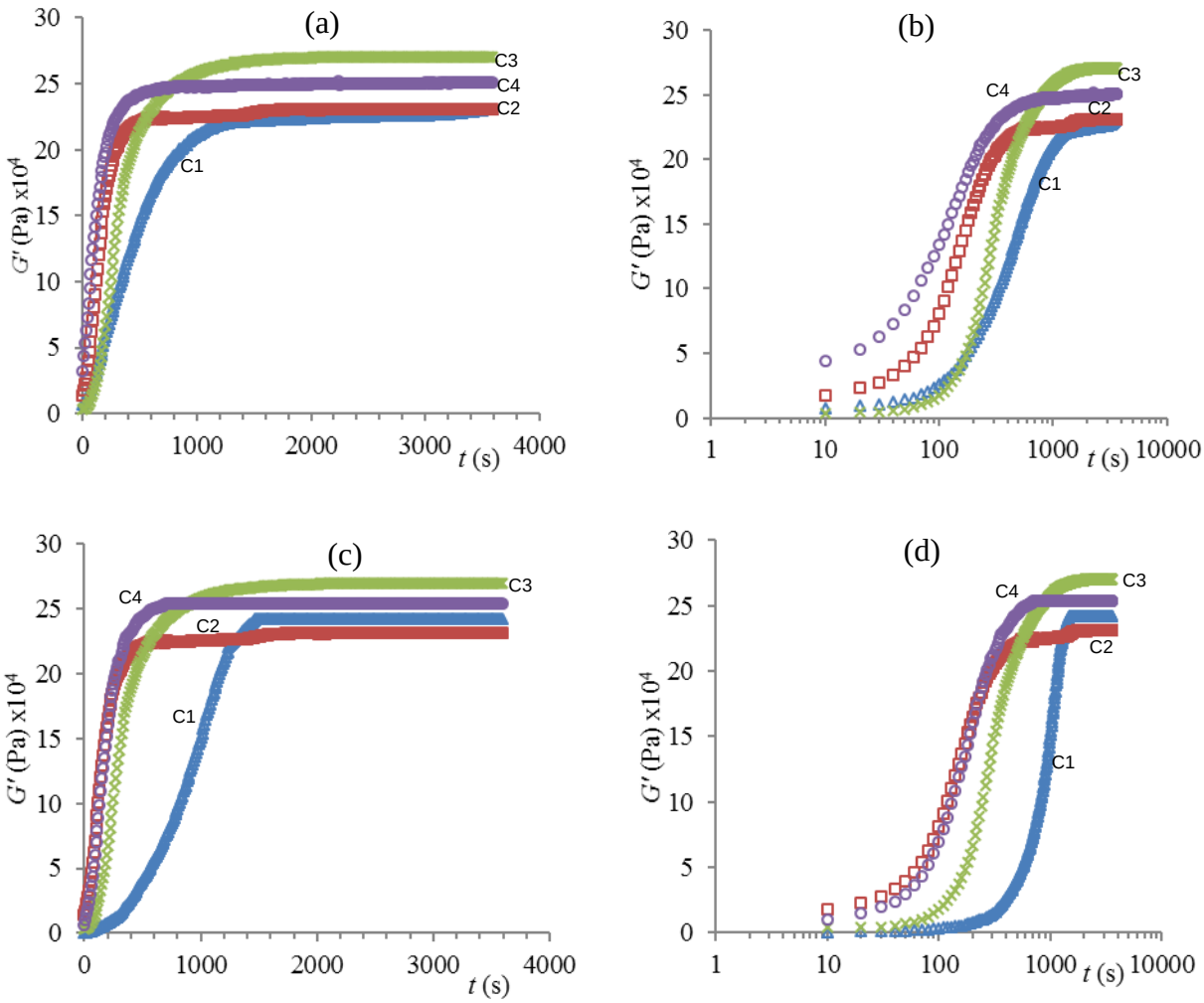

Figure 2 storage modulus evolution for all cements (a); (b) without SP in both linear and semi-log scale, (c); (d) with SP at 0.3% in respectively linear and semi-log scale.

The cements reached the plateau differently in terms of time and value of *G'*. This plateau occurred for Cements C2 and C4, with and without SPs, after an average time of 10 minutes of hydration. However, Cements C1 and C3 without SP reached a plateau after an average time of 20 minutes and the same time was recorded for these cements in the presence of SP.

It is worth noting that this plateau was not a result of 'slip effect' for three reasons: firstly, the roughened plate geometry used minimizes the occurrence of slip; secondly, the fact that the cements reached their plateau differently indicates that this rigidification process was due to the effect of hydration; and finally, the modulus values recorded during experiments were in agreement with those reported in the literature for suspensions [30].

In the absence of SPs, the initial value of *G'* for Cement C3 was the lowest, estimated at 4 kPa, and the highest value was with Cement C4: 44 kPa. However, Cement C3 reached the plateau with the highest value of *G'*, while Cement C1 experienced the lowest *G'* value in the plateau zone.

The hydration kinetics time of cement pastes with and without SP differed, and these hydration times were prolonged with the addition of SP. In all cases, Cement C4 experienced the shortest time of hydration before it reached its plateau, followed by Cement C2 and Cement C3, with Cement C1 experiencing the longest time of hydration.

The addition of SP in the cement pastes resulted in a decrease of the initial values of G' and an increase of hydration time to reach the plateau. For instance, Cement C1 exhibited the longest time of hydration to reach its plateau, followed by Cement C3.

The rigidification time and the relative rates of hydrations of these cement as given in Eqn. (2) and (3) are presented in Figures 3 and 4.

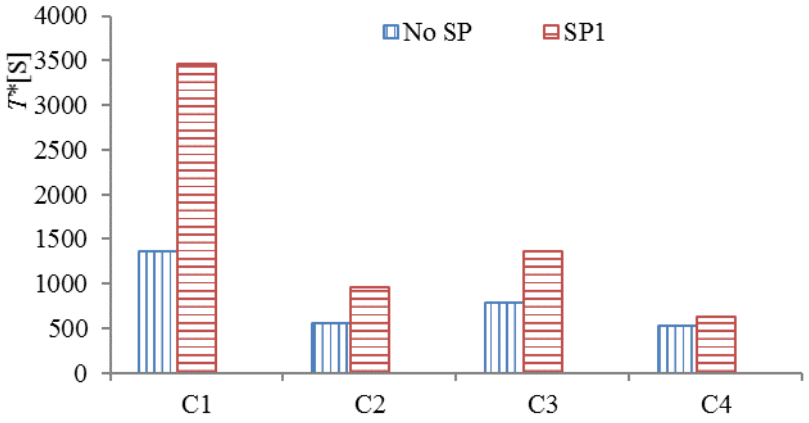

Figure 3 rigidification time *T** for all cements in the absence and presence of SP (0.3%)

It can be seen that cements without SP presented short time values of T^*. This would indicate that cement coagulates very quickly in this case. However, cement C2 exhibited the shortest time of rigidification compared to the other cements.
The addition of SP prolonged these times indicating that the rigidification process of cements was extended. Cement C1 presented the highest value of T^* while C4 the shortest.
In the setting process of cement, it is very important to know the rate of hydration. Looking at Figure 4, the relative rate of hydration for superplasticised and unsuperplasticised cements differed significantly when considering their maxima.

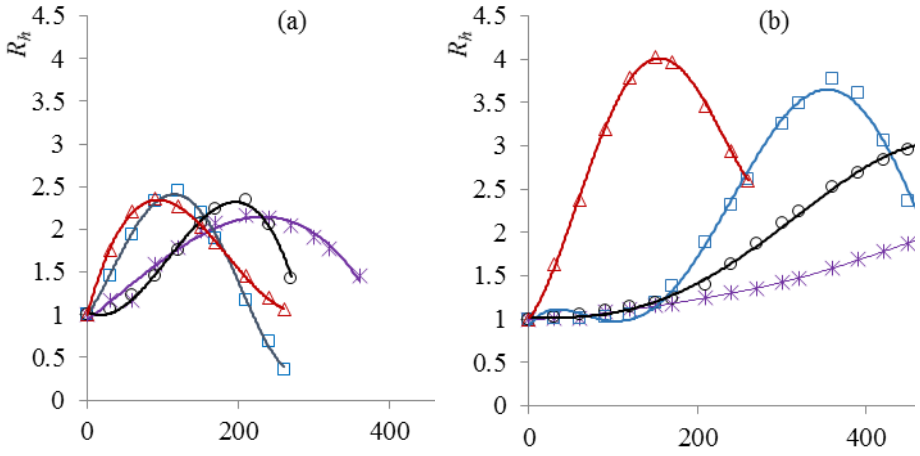

Figure 4 Relative rate of hydration of cement (a) without SP, (b) with SP at 0.3%

It can be seen that the addition of SP Fig.4 (b) increases the values and shifts the maxima of the kinetics curves out in time, thus prolonging the hydration process and slowing down the rate of the hydration within the cement paste. As a general observation of these graphical presentation of R_h, in the absence of SP cements C4 and C2 showed the highest rate of hydration while cements C1 and C3 presented the lowest rate of hydration. With the addition of SP cement C4 performed the highest rate of hydration followed by cement C2, C3 and C1.
The trends that these cement presents considering their rigidification time and rate of hydration interrelate with those obtained in yield stress development of their cement pastes in Figure 1.
Cement with high rate of hydration resulted in a short time of rigidification with a rapid yield stress development. This was observed for cement C2 and C4. Whereas cements with a slow rate of hydration resulted in long time of rigidification process that ended up in a slow yield stress development as for cements C1 and C2. The

introduction of SP in the cement paste prolonged the rheokinetic behaviour and resulted in slowing down the development of yield stress.
Referring to the combined work done by [16], [27], [31], [32] the observed fluctuations in cement rheological behaviour were suspected to be caused by the alkali equivalent Na_2Oeq, C_3A and SO_3 concentrations. In the absence of SP, cements with high alkali equivalent content (for instance C1) had a low rate of hydration resulting in slow yield stress growth. Whereas, those with low alkali content (cement C2 and C4) had great rate of hydration and consequently fast yield stress development. In the presence of SP, the competition between the concentration of C_3A and SO_3 in cement controlled their rheological behaviour. Cements with unbalanced concentration (C1 and C3) of these two compounds exhibited a slow stress evolution, while those with moderate or balanced concentration resulted in a rapid stress growth as for cements C2 and C4.

Conclusions

In summary, it is possible to use the suggested rheological technics: construction of flow curves and the rheokinetics model of self-acceleration type to study the hydration of cementitious materials.
By using this approach, the considerable impact that the hydration kinetics has on the strength development of cement paste microstructure was depicted.
This was proved by a relationship that exists between the relative rates of hydration, the rigidification time of the cement structures and their corresponding yield stress developments. Surprisingly, the influence of SP on the hydration was also detected. The presence of SP in the cement pastes retarded the hydration process by extending the rheokinetic values and consequently slowing down the yield stress evolution. In addition, the interaction between cement-SP was identified.
Subsequently, it was found that, though these cement are commercially sold as the same type (CEM I 52.5 N), they behave differently due to the differences observed in their physical characteristic and chemical compositions.

References

K. L. Scrivener, P. Juilland, and P. J. M. Monteiro, (2015), “Advances in understanding hydration of Portland cement,” *Cem. Concr. Res.*, vol. 78, pp. 38–56,
[2] K. L. Scrivener and A. Nonat, (2011), “Hydration of cementitious materials, present and future,” *Cem. Concr. Res.*, vol. 41, no. 7, pp. 651–665.
[3] H. Figueiras, S. Nunes, J. S. Coutinho, and C. Andrade, (2014), “Linking fresh and durability properties of paste to SCC mortar,” *Cem. Concr. Compos.* vol. 45, pp. 209–226.

[4] J. Hildago, L. Struble, J. Leslies, and C-T.C, (2008), "Correlation between paste and concrete flow behaviour." *Mater. J.*, vol. 105, pp. 281–288.
[5] P. Termkhajornkit, R. Barbarulo, and G. Chanvillard, (2015) "Microstructurally-designed cement pastes: A mimic strategy to determine the relationships between microstructure and properties at any hydration degree," *Cem. Concr. Res.*, vol. 71, pp. 66–77.
[6] Z. Quanji, (2010), "Thixotropic behavior of cement-based materials- effect of clay and cement types." Master of Science, Iowa State University, Iowa.
[7] B.-W. Jo, S. Chakraborty, and Y. S. Lee, (2015) "Hydration study of the polymer modified jute fibre reinforced cement paste using analytical techniques," *Constr. Build. Mater.* vol. 101, pp. 166–173.
[8] T. Lecompte, A. Perrot, V. Picandet, H. Bellegou, and S. Amziane, (2012) "Cement-based mixes: Shearing properties and pore pressure," *Cem. Concr. Res.*, vol. 42, no. 1, pp. 139–147.
[9] Q. L. Yu and H. J. H. Brouwers, (2011) "Microstructure and mechanical properties of β-hemihydrate produced gypsum: An insight from its hydration process," *Constr. Build. Mater.* vol. 25, no. 7, pp. 3149–3157.
[10] T. Danner, H. Justnes, M. Geiker, and R. A. Lauten, (2016) "Early hydration of C3A–gypsum pastes with Ca- and Na-lignosulfonate," *Cem. Concr. Res.*, vol. 79, pp. 333–343.
[11] G. H. Tattersall and P. F. G. Banfill, (1983), *Rheology of Fresh Concrete*. london: Pitman Advanced Publishing Program,.
[12] N. Roussel, G. Ovarlez, S. Garrault, and C. Brumaud, (2012), "The origins of thixotropy of fresh cement pastes," *Cem. Concr. Res.*, vol. 42, no. 1, pp. 148–157.
[13] H. Vikan, (2005), "Rheology and reactivity of cementitious binders with plasticizers," Ph Doctorate, Norwegian University of Science and Technology, Trondheim.
[14] L. J. Struble and L. Wei-Guo, (1995), "rheological change associated with setting time," *Adv. Cem. Based Mater.* vol. 2, no. 6, pp. 224–230.
[15] M. S. Mohammed and M. A. Asmaa, (2010) "The Effect of Alkalis on the Properties of Portland Cement," College of Engineering Al-Mustansiriya University.
[16] L. D. Schwartzentruber, R. Le Roy, and J. Cordin, (2006), "Rheological behaviour of fresh cement pastes formulated from a Self-compacting concrete (SCC)," *Cem. Concr. Res.*, vol. 36, no. 7, pp. 1203–1213.
[17] M. Nehdi and M.-A. Rahman, (2004), "Estimating rheological properties of cement pastes using various rheological models for different test geometry, gap and surface friction," *Cem. Concr. Res.*, vol. 34, no. 11, pp. 1993–2007.
[18] H. Vikan, H. Justnes, F. Winnefeld, and R. Figi, (2007) "Correlating cement characteristics with rheology of paste," *Cem. Concr. Res.*, vol. 37, no. 11, pp. 1502–1511.
[19] V. Fernàndez-Altable and I. Casanova, (2006), "Influence of mixing sequence and superplasticiser dosage on the rheological response of cement pastes at different temperatures," *Cem. Concr. Res.*, vol. 36, no. 7, pp. 1222–1230.

[20] W. Mbasha, I. Masalova, R. Haldenwang, and A. Y. Malkin, (2015), "The yiled stress of cement pastes as obtained by different rheological approaches," *Appl. Rheol.*, vol. 25, no. 5, p. 53517.
[21] L. Nachbaur, J. Mutin, and L. Choplin, (2001), "dynamic mode rheology of cement and tricalcium silicate paste from mixing to setting." *Cem. Concr. Res.*, vol. 31, pp. 183–192.
[22] A. Y. Malkin and S. Kulichikhin, *Rheokinetics: rheological transformations in synthesis and reactions of oligomers and polymers*. .
[23] O. H. Wallevik, D. Feys, J. E. Wallevik, and K. H. Khayat, (2015), "Avoiding inaccurate interpretations of rheological measurements for cement-based materials," *Cem. Concr. Res.*
[24] M. Yang and H. M. Jennings, (1995), "Influences of mixing methods on the microstructure and rheological behavior of cement paste," *Adv. Cem. Based Mater.* vol. 2, no. 2, pp. 70–78.
[25] D. Roy and K. Asaga, (1979), "Rheological properties of cement mixes: iii. The effects of mixing procedures on viscometric properties of mixes containing superplasticizers," *Cem. Concr. Res.*, vol. 9, pp. 731–739.
[26] D. A. Williams, A. W. Saak, and H. M. Jennings, (1999), "The influence of mixing on the rheology of fresh cement paste," *Cem. Concr. Res.*, vol. 29, no. 9, pp. 1491–1496.
[27] A. Zingg, F. Winnefeld, L. Holzer, J. Pakusch, S. Becker, R. Figi, and L. Gauckler, (2009), "Interaction of polycarboxylate-based superplasticizers with cements containing different C_3A amounts," *Cem. Concr. Compos.* vol. 31, no. 3, pp. 153–162.
[28] S. Hanehara and K. Yamada, (1999), "Interaction between cement and chemical admixture from the point of cement hydration, absorption behaviour of admixture, and paste rheology," *Cem. Concr. Res.*, vol. 29, no. 8, pp. 1159–1165.
[29] C. A. Anagnostopoulos, (2014), "Effect of different superplasticisers on the physical and mechanical properties of cement grouts," *Constr. Build. Mater.* vol. 50, pp. 162–168.
[30] G. H. Kirby and J. A. Lewis, (2004), "Comb polymer architecture effects on the rheological property evolution of concentrated cement suspensions," *J. Am. Ceram. Soc.*, vol. 87, no. 9, pp. 1643–1652.
[31] K. Yamada, S. Ogawa, and S. Hanehara, (2001), "Controlling of the adsorption and dispersing force of polycarboxylate-type superplasticizer by sulfate ion concentration in aqueous phase," *Cem. Concr. Res.*, vol. 31, no. 3, pp. 375–383.
[32] A. K. Mukhopadhyay and S. Jang, (2009), "Using Cement Paste Rheology to Predict Concrete Mix Design Problems: Technical Report," Texas Transportation Institute, Texas A & M University System.

Theme 5: Production and Placement of SCC

SCC Under Pressure – Field Validation of Models for Predicting Lateral Form Pressure in Toronto

John Gardner[1], Lloyd Keller[2], Kamal Khayat[3], Ahmad Omran[4], David Lange[5],Stacia Van Zetten[2] and Phil Zacarias[6]

[1]University of Ottawa, [2]EllisDon Construction, [3] University of Missouri S&T, [4]University of Sherbrooke, [5]University of Illinois at Urbana, [6]Canada Building Materials

Abstract Self-consolidating concrete (SCC) has become a material that has endeared the construction community with its ability for ease of placing even in congested reinforcing areas and with the reduction in man-hours to place complex architectural concrete elements with a premium surface finish. A lingering concern continues with predicting the formwork pressure that is transmitted by SCC and with the abilities of engineers and codes committees to develop methods that take into account the plastic properties of the concrete that most affect the formwork pressure. ACI 347 Guide to Formwork for Concrete prescribes a formula to calculate lateral formwork pressure that conservatively assumes full liquid head, and states that this equation "should be used until the effect on formwork pressure is understood by measurement."

In May of 2012, a round robin program of production trials was undertaken in Stockholm, Sweden [1] to enable a core of researchers from Europe, Canada and the USA to measure and predict the formwork pressure based on a series of measured individual plastic performance tests and resulting equations for calculating the formwork pressure based on the plastic parameters. The formwork pressures were measured by load cells attached to tie bars and pressure cells attached flush to the inner formwork surfaces. The placements utilized a series of wall sections that allowed for a varying of the placement rate, thickness of wall and height of wall. The plan of the program was to also alter the rheological properties of the concrete (yield, viscosity and thixotropy) but due to limitations with the ready-mix producer, the mixes did not achieve all of the desired variations.

To build on the results in the Sweden trials, a plan was made to recreate the program in Toronto, Canada with participation from a number of the researchers who also partook in Sweden. The program was carried out over 4 days in August 2014, at a ready-mix producers yard (Canada Building Materials). The concrete was placed in 8 - 6 m highcolumns that had pressure measured by similar pressure

cells as in Sweden. Placement rate, effect of rebar congestion, effect of extraneous vibration, effect of variations in concrete rheological properties and method of pouring were measured and the effects reported. Predicted vs. measured results were produced and shown utilizing each of the researcher's methods of measuring plastic properties and calculating the expected formwork pressure based on these properties.
The planning, methods of placing, measuring pressures and mix properties and prediction results will be described in this paper for the work done in Toronto in a project entitled 'SCC Under Pressure'.

Keywords: *Thixotropy, Formwork Pressure, Self-consolidating Concrete, Rheology, Plastic properties.*

Summary of Planning and Scope of Investigations

During the American Concrete Institute (ACI) Spring Convention in Reno, Nevada in 2014, members of ACI 347 and ACI 237 agreed to plan and schedule a full scale production test program for Toronto in August of 2014.
The initial planning in Reno called for measuring the effect of thixotropy, the effect of minimum section dimension, effect of rebar density and the effect of casting rate using 5 sets of wall pours and 8 sets of column pours. Parameters for walls 6.6m tall with regular rebar density, would be varying the concrete thixotropy from medium to high, the section thickness from 200 to 400mm, and casting rates from 2, 5 or 8m per hour. The columns would also be 6.6m, varying concrete with medium and high thixotropy, sparse and heavy rebar densityand casting rates of 2, 5 and 10m per hour. (see table I).
The final program was modified to include only the 8 columns and maximum element height was 6.0m. Modifications to the various parameters are summarized in table 2 and the effect of pumping from the bottom up was added as an additional parameter..
Other issues that were also of a concern to practitioners that would design the formwork to resist the plastic loads of the concrete being placed were the effects of extraneous vibration from external sources prior to concrete setting, concerns were raised about being able to prescribe, measure and deliver consistent concrete with consistent rheological properties, and a method for placement that would ensure laminar flow during the entire placement process without an impact effect of concrete falling from a point at the top of the column form to the top of the plastic concrete placed at that particular moment in time.

Methodology for Measuring Characteristics

Plastic rheological properties of the concrete were to be measured utilizing apparatus and techniques outlined by the 3 principal research groups:

- Gardner and EllisDon: Slump Flow Loss and DIN Knead Bag Setting time
- Khayat and Omran: Portable Vane test and Inclined Plane Test
- Lange: Pressure decay in a static column Test

Concrete placement pressures were measured using Honeywell AB-HP pressure sensors that were mounted with their sensor face flush with the inside surface of the formwork. A Campbell Scientific 16 channel data logger was used for all gauges of columns 1, 4, 5 and 7 and the sparse reinforcement face gauges at elevations 200, 450, 1000 and 2000mm of column 2. In addition 2, 4 channel National Instruments data acquisition systems (each read by a PC), were used to record pressures for columns 3,6,8 and sparse reinforcement face gauges at elevations 3000 and 3800mm and all dense reinforcement face gauges for column 2. Note that backup systems were planned and described above; a temporary software malfunction with the Campbell Scientific unit eliminated its use for columns 3 and 6.
For laboratory trials and concrete characterization, concrete rheological properties were measured by ASTM C1611 for slump flow, T50 and VSI, by shear vanes for shear stress at time equal to 15 minutes and for rate of shear growth at 30, 45 and 60 minutes. An ICAR rheometer measured static yield stress, plastic viscosity and hysteresis loop properties showing the thixotropic relationship or the degree of structural buildup between the up and down curves of a concrete shear in a rheometer [2].

Concrete Mixture Classification and Development

In order to demonstrate the effects of the concrete mixtures properties it was agreed by all researchers to characterize the mixtures into high, medium and low thixotropy by classifying them by the static yield stress at rest utilizing the portable vane test at 15 minutes (PV $\tau_{0\ \text{rest @ 15 min}}$) [6] . High thixotropy was designated as greater than 1200 Pa, Medium thixotropy as 600 – 700 Pa and low thixotropy as less than 600 Pa.
In order to develop the various mixes needed to produce the ranges of thixotropy, a laboratory and field trial program took place at the laboratory and production plant of CBM in Leaside, Toronto. The program utilized 9 trial mixtures varying the materials properties by water to paste ratio, water to cement ratio, admixture type and combinations of cementing materials including : type GU (General Usage) cement, type GU blended with 8% silica fume, and slag. The final mix designs used in the 4 day trial program are summarized in table III.
During the laboratory trial program,performance differences between various polycarboxylate-based HRWR's became apparent. Our intuitions told us that something within the class of HRWR that we were initially using was giving us a result that was counter intuitive (the rate of shear stress was decreasing with time) see Figure 4 and 5. After sharing the information and consulting with our

admixture supplier, we became aware of the effect that polycarboxylate structure has with respect to both water reducing and slump keeping characteristics [7].

Following our discovery above, we chose to go with a HRWR more specifically designed as a water reducer (with normal, not extended slump keeping performance) and then developed mixes that conformed with the ranges of thixotropy as described above for low, medium and high. To achieve a control for delivery of the properties in production via readymix trucks, we chose to correlate the thixotropic properties to a T50 and slump flow coupled parameter that represented the mixtures rheological properties and would allow for controls for production via the ASTM C1611 slump flow test. See table II for measured concrete parameters.

In order to maintain a uniform consistency with the concrete mixture during our program, we chose to target a maximum temperature at delivery of 20°C. As we were producing in summer months in Toronto with ambient temperatures frequently at or above 30°C we chose to produce all concrete by cooling it using liquid nitrogen. This proved to be very effective and was used throughout the production trials and the actual SCC Under Pressure program in August of 2014.

Program Setup for Field Trials

The program for measuring the concrete lateral pressures was performed over 4 days August 25 – 28th, 2014 at the CBM yard in Leaside (Toronto), Ontario. There were 4 sets of Meva Imperial column forms that were 6.0m high and 24" x 24" in section dimension. These column forms were cycled twice. After the concrete was set and cured on the second day, the forms were stripped and the columns lifted away from the casting deck thus allowing for the formwork to be prepped, reinforcing placed and pressure sensors to be set for casting again on the 3rd day. 8 reinforcing cages were built and placed adjacent to the casting deck so that each could be placed in the formwork in preparation for casting as part of the planned sequence of testing as shown in table I. The dense vertical bars (30M) were spaced at 60mm on center and the sparse bars had only 2 corner 10M bars on the opposite side of the form. To create a cage, 20 - 10 M stirrups were spaced evenly over the 6m height of the column. See attached Figure 1 for casting platform setup.

Three different research groups, Khayat and Omram (Inclined Plane and Portable Vane)[3,6], Lange (static column)[4] and Gardner, EllisDon (Slump flow loss and DIN Knead Bag Setting time) set up at the casting location to sample the plastic concrete and measure rheological properties according to their individual methods for predicting lateral pressure.

Canada Building Materials (CBM) were tasked with the responsibility of batching in 3m^3 batches for each of the 8 individual placements. Quality control and consistency to the prequalified mixtures was tied to a means of relating the rheological properties of the concrete (plastic viscosity, thixotropy, static yield stress) to standard ASTM C1611 Slump Flow test (Slump flow, T50 and VSI see table II). Concrete was cooled and temperature controlled by treating the concrete

with a liquid nitrogen lance broadcast into the freshly batched concrete within the ready-mix concrete truck.
Placing rates were controlled by filling the formwork in 6 incremental steps to match the prescribed casting rates. Concrete was placed by crane and bucket and poured into a receiving hopper on top of the form that was connected to an elephant trunk tremie hose that was extended down to within 500mm of the bottom of the form. The tremie remained in place for the full duration and concrete was allowed to flow through the bottom of the tremie and then through 500mm stepped 150 x 150mm ports cut into the elephant trunk through to the top of the form (Figure 2 and 3).

Results

1. ***Mix Characterization***. Concrete mixes were characterized in lab and production trials by relating slump flow and T50 to rheological properties measured by PV $\tau_{0\ \text{rest @ 15 min}}$ for static yield stress (Figure 6), and rheometer (static yield stress, viscosity and breakdown area from hysteresis curves) see Figure 7. This relationship created a quality control parameter that the ready-mix producer could use to deliver ready-mix concrete to the test placements and achieve the desired uniformity of plastic properties to provide the low, medium and high thixotropy concrete on a consistent basis for the trials.
2. ***Placing Methods.*** Filling the columns by crane and bucket through the hopper/ported elephant trunk tremie in 6 individual partial segments, ensured that fresh concrete (from an agitating ready-mix truck) meeting the plastic rheological properties was always delivered in each of the six lifts (note that a single batch of concrete from one truck was used for each column placement). Previous experience in the Swedish demonstration illustrated the problem with using a concrete pump and a single truck. That being, the extended delays in placing that were necessary to provide a slow rate of pour resulted in the concrete losing a significant amount of workability (slump) while in the static pump line and concrete delivered to the forms was not always within the desired plastic parameters and resulted in some of the placements showing noticeable consolidation deficiencies while formwork pressure cells were at times not measuring a true value of the concrete pressures assuming a surcharge of fresh concrete being continuously applied in the required rate of placements.
3. ***Extraneous Vibration.*** The vibration from freight trains on the railroad track did not cause the concrete to liquefy. Numerous

precautionary comments have been circulated that warn about instability of SCC mixes to the point that it could revert to a liquid state and full hydrostatic head as a consequence of extraneous vibrations or impacts from machinery in the surrounding area. The four day test program inadvertently provided a real time circumstantial proof test as a frequently used rail spur was located within 8mof the test location with rail cars passing on 1hr intervals. The vibration and dynamic effects of the trains could be felt on the test column platforms with no measurable variations in lateral pressure as seen by the pressure sensor data.

4. ***Reinforcement Density***. The results indicate that face reinforcement density does not have a major influence on the lateral pressures experienced by the sheathing (pressure gauges).
5. ***Prediction Models***. Complete details and commentaries will be presented in a soon to be published report about the program. Results show a close correlation between predicted and measured values for formwork pressure. All of the prediction models showed good correlations to measured values. See figure 8 for example of Gardner model tested in the program.
6. ***Pumping from Bottom Up***. Pressure measurements that were taken during the one placement exercise where concrete was placed through a valve and spiggot connector at the bottom portion of the column confirmed previous research [5] suggesting a 1.2 factor x full liquid head be used for predicting formwork pressures in this placing method.

Acknowledgementss

Collaboration and funding support was provided by Meva Formwork Systems, Readymix producer CBM, BASF admixtures group, Gilbert Steel (rebar), Premform and Ontario Formwork Association, Amherst Cranes, Oxford Builders and EllisDon along with researchers from University of Missouri S+T, University of Illinois and the University of Sherbrooke. In addition to the authors, special recognition to EllisDon (Robert Quattrociocchi, Lorena Proietti, Brandon Dale, Adam Makino, Vince Davenport and Mark Gaglione), CBM (Bryan Schultz), Premform (Rob Alonzi), BASF (Joe Daczko, Luis Dos Reis and Shervan Khanna).

References

[1] Billberg P.H.; Roussel N.; Amziane S.; Beitzel; Charitou G.; Freund B.; Gardner N.J.; Grampeix G.; Graubner C.-A.; Keller L.; Khayat K.H.; Lange D.A.; Omran A.F.; Perrot A.; Proske T.; Quattrociocchi R.; Vanhove Y.; "Field Validation of Models for Predicting Lateral Form Pressure Exerted by SCC Concrete." Cement & Concrete Composites, 54(2014), 70-79.

[2] Ferron R.; Gregori A.; Sun Z.; Shah S.P.; "Rheological Method to Evaluate Structural Build-Up at Rest in Self-Consolidating Concrete Cement Pastes." ACI Materials Journal, V.104, No. 3, pp 242-250, May 2007.

[3] Khayat K.H.; Omran A.F.; Pavate T.V.; "Inclined-Plane Test to Evaluate Structural Buildup at Rest of Self-Consolidating Concrete." ACI Materials Journal, V.107,No. 5, pp 515-522

[4] Lange D.A.; Birch B.; Henchen J.; Liu Y-S.; Tejeda-Dominguez F.; Struble L.; "Modelling formwork pressure of SCC." Proceedings of the 3rd North American Conference on the Design and Use of Self-Consolidating Concrete, Ed. S.P. Shah, Chicago, USA, 2008, pp 295-300.

[5] Leeman, A., Hoffmann, C., "Pressure of Self-Consolidating Concrete in Formwork", Proceedings 3rd International Symposium on Self-Compacting Concrete, Reykjavik, Iceland, Ed. Wallevik, O.H., 2003, pp. 288-295.

[6] Omran A.F.; Naji S.; Khayat K.H.; "Portable Vane Test to Assess Structural Buildup at Rest of Self-Consolidating Concrete." ACI Materials Journal, V.108, No. 6, pp 628-636, November- December 2011.

[7] Mäder U., Schober F., Wombacher F., Ludirdja D.; "Polycarboxylate Polymers and Blends in Different Cements"; Cement, Concrete, and Aggregates; Dec 2004, Vol. 26, No. 2; Paper ID CCA 12314

Tables, Photos and Figures

Table I

"SCC Under Pressure" Formwork Pressure Research August 25 - 28 2014

					Tremie Placement				Pumping Bottom Up	Tremie
		20 ft tall - 6.0 M	20 ft tall - 6.0 M	20 ft tall - 6.0 M		20 ft tall - 6.0 M	20 ft tall - 6.0 M	20 ft tall - 6.0 M	20 ft tall - 6.0 M
Casting		Monday	Monday	Tuesday		Wednesday	Wednesday	Thursday	Thursday
		Col #1	Col #2	Col #3	Col #4	Col #5	Col #6	Col #7	Col #8
Concrete thixotropy		High	Med	High	Low	Medium	High	Medium	Medium
Min. section width		24 x 24	24 x 24	24 x 24	24 x 24	24 x 24	24 x 24	24 x 24	24 x 24
		457 x 609	457 x 609	457 x 609	457 x 609	457 x 609	457 x 609	457 x 609	457 x 609
Reinforcing bars		varied	varied	varied	varied	varied	varied	varied	varied
Casting rate (m/hr)		5	5	3	5	10	10	10	3
Anticipated K0 (%)									
Placement Time, hrs.		1.2	1.2	2	0.6	0.6	0.6	0.6	2
Volume (m3)		2.2	2.2	2.2	2.2	2.2	2.2	2.2	2.2
Mass (kg)		5280.0	5280.0	5280.0	5280.0	5351.2	5280.0	5351.2	5351.2
8 lifts - vol per lift		0.275	0.275	0.275	0.275	0.275	0.275		0.275
Time per lift		9	9	15	9	4.5	4.5		15

Testing parameters:

1. Effect of Thixotropy (med and high) High Thixotropy = greater than 1200 Pa Medium Thixotropy = 600 - 700 Pa (values are measured by Pressure Vane
2. Effect of Pumping Bottom Up (med and high) after 15 minutes rest)
3. Effect of rebar density (low, regular and high in columns)
4. Effect of casting rate (3, 5, and 10 m/hr in columns to be done by pouring in lifts or increments of 1/4 height each lift)
5. Benchmark Low thixotropy Base Mix
6. Formwork - Meva 18 x 24 inches

Research Groups

John Gardner and EllisDon	Formwork Pressure Prediction using slump loss measurement
Kamal Khayat and Ahmed Omran (Missouri S&T and University of Sherbrooke)	Formwork Pressure and Prediction using Pressure Vane Method
David Lange (University of Illinois at Urbana)	Formwork Pressure Prediction using Pressure decay from a column.

Notes:

1 Use Noxcrete PCE release agent for all surfaces where pressure cells are located (24"sides). Use Noxcrete Form Release 250 for 18" side of form surfaces.
2 Use 6 - Honeywell Pressure Cells each form face (24"). Located nominal at 250, 450, 1000, 2000, 3000 and 3700 from bottom surface of form support.
3 Concrete batching temperature to be 20 degrees C.

Table II

SCC Under Pressure Lab/Production Trials - Shear Vane, Rheometer, Slump Flow, T50						
Trial #	**Slump Flow (mm)**	**T50 (s)**	**$PV_{t0rest15mins}$**	**Viscosity (Nms)**	**Yield (Nm)**	**Thixotropy**
2	670	1.5	400			
5	640	2.2	633	0.7	0.1	0.09
6	650	5.3	858	1.84	0.67	0.446
7	675	5.1	867	2.79	0.54	0.399
8	620	10.7	1701	4.84	1.24	0.684
9	610	14.2	1167	5.49	1.74	0.811

Table III

SCC Under Pressure Lab/Production Trials - Concrete Mix Designs					
Thixotropy Class			**Low**	**Medium**	**High**
Cementing Materials	Type GU	kg	356		
	Type GUSF	kg		475	525
	Slag	kg	119		
Aggregates	14mm Limestone	kg	865	850	860
	Concrete Sand	kg	868	1015	971
Water		L	184	134	134
Admixtures	HRWR (PC w/o Slump Keeper)	ml/100kg	800	5300	3600
	LRWR	ml/100kg	200	200	200
	Retarder	ml/100kg	220	220	220
	VMA	ml/100kg	150	350	200
w/c Ratio			0.39	0.29	0.26
% Sand			0.5	0.54	0.53

Figure 1

Figure 2

Figure 3

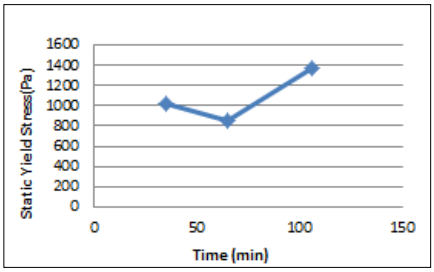

Figure 4

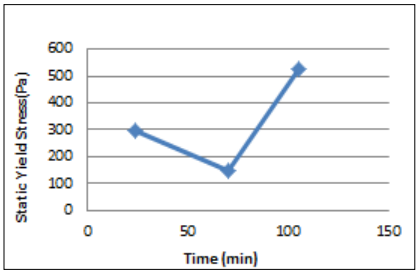

Figure 5

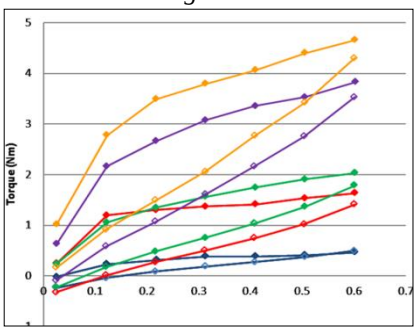

Figure 6

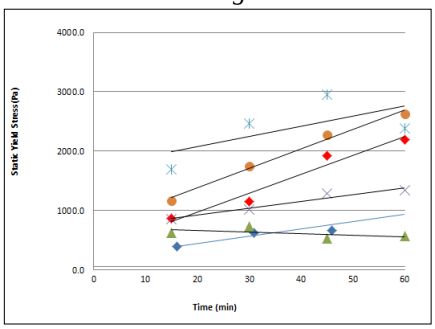

Figure 7

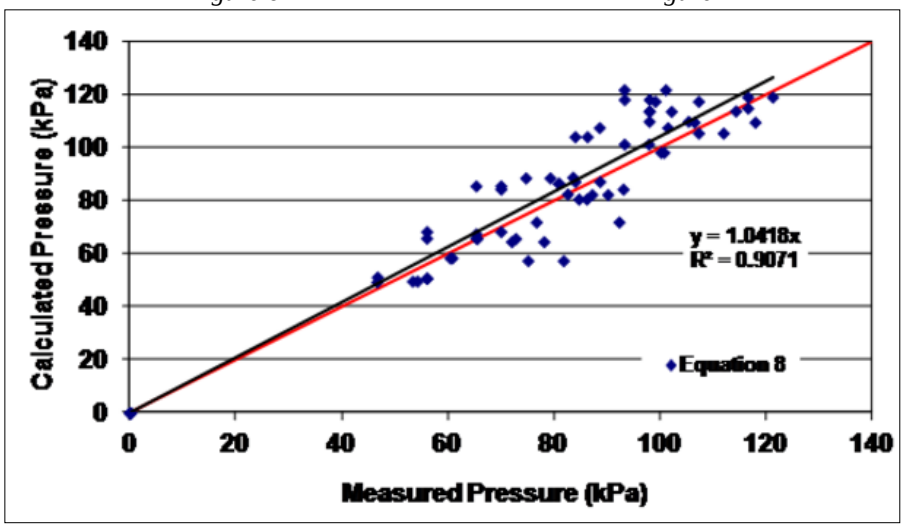

Figure 8

Models to Predict Form Pressure Exerted by SCC – Results of Six Field Campaigns

Ahmed Omran[1] and Kamal Khayat[2]

[1] Research Engineer at Cement and Concrete Research Group in Dept. of Civil Eng. at University of Sherbrooke, Sherbrooke, Canada., and Assistant Professor at University of Minoufiya, Egypt.
Address: 2500 Boul. de l'Université, Sherbrooke (QC) Canada J1K 2R1
Tel. office: +1 819 821 8000 # 62209, Fax: +1 819 821 7212,
A.Omran@USherbrooke.ca
[2] Professor, Missouri University of Science and Technology, Rolla, MO, USA, khayatk@mst.edu

Abstract One of the major obstacles to increased the use of SCC in cast-in-place applications is the uncertainty of lateral pressure exerted on formwork systems. Various prediction models, based on extensive experimental results to evaluate formwork pressure exerted by SCC were established. The proposed models by Khayat and Omran [1] involve the determination of the structural build-up at rest using field-oriented test method (portable vane). The models take also into consideration concrete casting rate and depth, and formwork width. Modification factors related to waiting period between consecutive concrete lifts, maximum-size of aggregate, and vertical steel reinforcement density are also considered. This paper presents the results of six field validation campaigns that were carried out to evaluate formwork pressure characteristics in various types of structural elements. These field sites are (1) eight wall elements at University of Sherbrooke, Canada, (2) eight columns at CTLGroup facility in Skokie IL/USA, (3) an abutment for a highway bridge in Sherbrooke/Canada, (4) eight walls at CBI Stockholm/Sweden, (5) a bridge tower in Ottawa/Canada, and (6) eight columns during "SCC Under Pressure" event in Toronto/Canada. These observations involved the casting of SCC of different mixture proportionings placed at various casting rates in different formwork geometries. Field results are employed to validate the proposed prediction models [1]. The findings confirm that the developed models offer adequate assessment of the maximum formwork pressure exerted by SCC. SCC lateral pressure is should to be significantly controlled by concrete thixotropy, casting rate, and reinforcement density.

Keywords: *Field validation, Prediction model, SCC formwork pressure, Thixotropy.*

Introduction

Despite the obvious benefits of self-consolidating concrete (SCC) involving high flowability and excellent surface finishing, accessibility to heavily reinforced areas, and reduced construction duration and cost [2, 3] compared to the conventional concrete, its widespread use in cast-in-place applications has been hampered by some technical considerations. Provisions of the current ACI Manual of Concrete Practice (i.e. ACI 347R) [4] do not specifically address SCC, but recommend that unless a method based on appropriate experimental data is available, formwork should be designed to withstand the full hydrostatic head of fluid concrete. This guidance generally limits contractors to reduce casting rate of the concrete or strengthen the formwork to sustain hydrostatic pressure. Thus, there is great need for better understanding of the pressures that are actually exerted in the cast-in-place applications in the field. Many researches revealed that SCC lateral pressure can diverge from the hydrostatic pressure [5-11]. In the last decade, a number of prediction models for SCC lateral pressure have been proposed [6-16].
The prediction models proposed by Khayat and Omran in 2009 [1] were modified in [17] by introducing coefficient for the reinforcement density. This paper presents the modified version of the models. SCC mixtures of different proportioning, placed at various casting rates in formwork of different geometries, used in the construction of six field projects are presented in this research. These field results are employed to validate the prediction models of lateral pressure exerted by SCC.

Prediction Model by Khayat and Omran (2009)

Khayat and Omran [1] developed prediction models [Eqn. (1-3)] based on a large number of laboratory tests using a 0.7-m high pressure column [18]. The column is designed to simulate concrete heights of up to 13 m using an air overpressure. From the database involving approximately 800 data points, the authors proposed models to predict the maximum formwork pressure (P_{max}), which takes into consideration the following parameters: casting depth (H), casting rate (R), minimum lateral dimension of formwork (d), and structural build-up at rest of the concrete (thixotropy). The effect of the nominal maximum-size of aggregate (MSA) and waiting period(s) between successive lifts (WP) are also considered using modification factors (f_{MSA} and f_{WP}, respectively). The equations can be used to estimate the lateral pressure at a given casting depth. The prediction models are given along with the ranges of values for which the models were derived.

$$P_{max} = \frac{wh}{100}\,[98\text{-}3.82H\text{+}0.63R\text{+}11D_{min}\text{-}0.021PV\tau_{0rest@15min}]\times f_{MSA}\times f_{WP} \quad (1)$$

$$P_{max} = \frac{wh}{100}\,[95.9\text{-}3.84H\text{+}0.71R\text{+}4.1D_{min}\text{-}0.29PV\tau_{0rest}(t)]\times f_{MSA}\times f_{WP} \quad (2)$$

$$P_{max} = \frac{wh}{100}\,[92.1\text{-}4H\text{+}0.62R\text{+}11D_{min}\text{-}0.00016PV\tau_{0rest@15min}\times PV\tau_{0rest}(t)]\times f_{MSA}\times f_{WP} \quad (3)$$

where

P_{max} : lateral pressure at a given casting depth (kPa), ranges between 0 - 350 kPa

w_c : concrete unit weight (kN/m³), ranges between 18 - 26 kN/m^3

H : mean rate of placement (m), ranges between 1 - 13 m

R : casting rate (m/h), ranges between 2 - 30 m/h

D_{min} : equivalent to minimum formwork dimension (d), ranges between 0.2 - 1.0 m
for $0.2 < d < 0.5$ m, use $D_{min} = d$
for $0.5 < d < 1.0$ m, use $D_{min} = 0.5$ m

f_{MSA} : factor depending on nominal maximum size aggregate (MSA)
for SCC with MSA = 10 mm and ($PV\tau_{0rest@15min@22^oC} \leq 700$ Pa), use $1.0 \leq f_{MSA} \leq 1.10$ for $4 \leq H \leq 13$ m
for SCC with MSA $\geq$ 14 mm and any thixotropic level, use $f_{MSA} = 1.0$ regardless of H
f_{MSA} ranges between 1.0 - 1.1

f_{WP} : factor accounting for delay between successive lifts and varies linearly with the SCC thixotropy:
$f_{wp} = 1.0$ for continuous casting for SCC of any thixotropic levels
$f_{wp} = 1.0 - 0.85$ for SCC with $PV\tau_{0rest@15min} = 50 - 1000$ Pa, respectively, when placement interrupted with a 30-min waiting period in the middle of casting period. f_{wp} ranges between 1.0 - 0.85

$PV\tau_{0rest@15min}$: static yield stress (Pa) measured using PV test at any concrete temperature (Pa). $PV\tau_{0rest@15min}$ ranges between 0 -2000 Pa

$PV\tau_{0rest}(t)$: evolution of static yield stress with resting time (Pa/min) measured using PV test at any concrete temperature (Pa.min). $PV\tau_{0rest}(t)$, ranges between 0 - 125 Pa/min

For the above prediction models, the structural build-up at rest (thixotropy) of SCC is measured using an empirical test method, namely the Portable Vane (PV) test [19]. The thixotropic index can be determined by measuring the static yield stress after 15 min of resting time [$PV\tau_{0rest@15min}$ (in Pa)], the evolution of static yield stress with resting time, slope, [$PV\tau_{0rest}(t)$ (in Pa/min)], or as the coupled effect of the static yield stress at 15 min of rest and the evolution of static yield stress with time [$PV\tau_{0@15min} \times PV\tau_{0rest}(t)$ (in Pa^2/min)]. These three values are used to reflect the structural build-up at rest of concrete in the calculation of P_{max}.
The PV method [19] measures the torque necessary to break the concrete structure by using an immersed four-blade vanes and a torque wrench. The concrete thixotropy was measured at the same temperature of the cast concrete. From this torque value and the vane geometry, the static yield stress (in Pa) at four different rest periods (typically 15, 30, 45, and 60 minutes) of the concrete can be calculated.

Influence of Vertical Reinforcement Density

Recently, Omran and Khayat [17], added to the initial models [17] a coefficient ($f_{\rho sv}$) to account for the reinforcement density of the vertical steel rebars (ρ_{sv}), as given in Eqn. (4). The ρ_{sv} is defined as the ratio between the areas of vertical reinforcing steel rebars (A_{sv}) to the total area of concrete cross section (A_c), and expressed in percent. In addition to ρ_{sv}, Eqn. (4) takes into account the concrete cover (in mm), which is the distance between the reinforcing rebars and the inner formwork face.

$$f_{\rho sv} = 1 - \rho_{sv} \times \left(4.63 + \frac{106.3}{\text{concrete cover}} \right) \quad (4)$$

The modified Equations (1-3), after adding the $f_{\rho sv}$ factor, can be expressed as follows [17]:

$$P_{max} = \frac{wh}{100} [98\text{-}3.82H\text{+}0.63R\text{+}11D_{min}\text{-}0.021PV\tau_{0rest@15min}] \times f_{MSA} \times f_{WP} \times f_{\rho sv} \quad (5)$$

$$P_{max} = \frac{wh}{100} [95.9\text{-}3.84H\text{+}0.71R\text{+}4.1D_{min}\text{-}0.29PV\tau_{0rest}(t)] \times f_{MSA} \times f_{WP} \times f_{\rho sv} \quad (6)$$

$$P_{max} = \frac{wh}{100} [92.1\text{-}4H\text{+}0.62R\text{+}11D_{min}\text{-}0.00016PV\tau_{0rest@15min} \times PV\tau_{0rest}(t)] \times f_{MSA} \times f_{WP} \times f_{\rho sv} \quad (7)$$

Experimental Program

The proposed models [Eqns. (5-7)] are employed to estimate lateral pressure exerted by SCC mixtures on vertical formwork systems in six field projects. The formwork pressure characteristics that were evaluated here involved various types of structural elements, including:

(1) six out of eight wall elements cast with SCC during the construction of an industrial building at the University of Sherbrooke, Canada in 2008,
(2) eight column elements at CTLGroup facility in Skokie IL/USA in 2008,
(3) an abutment column for a highway bridge in Sherbrooke/Canada in 2011,
(4) eight walls at Swedish Institute for Concrete Technology (CBI) Stockholm/Sweden in 2012,
(5) 30-m tall bridge tower in Hunt Club Ottawa/Canada in 2012, and
(6) eight experimental columns cast during the event of SCC Under Pressure in Toronto/Canada in 2014.

The testing parameters considered in each field project are summarized in the following sections. The lateral pressure measurements obtained from the six field projects are collected and used to validate the prediction models Eqns. (5-7). The formwork pressure exerted by concrete was determined using pressure sensors mounted at various casting depths of the formwork using special adaptors. The sensors were set-flushed to the inner formwork surface touching the inner concrete. The pressure data were recorded using data acquisition systems during the concrete casting and thereafter till the pressure cancellation time.

Results and Discussions

The testing parameters and lateral pressure measurements determined from each of the six field projects and their use to validate the prediction models presented in Eqns. (5-7) are discussed below.

(1) Wall Elements, in Industrial Building, University of Sherbrooke, Canada

A summary of the testing program undertaken on the wall elements as well as the fresh and thixotropic properties are given in Table I. These walls were cast at the University of Sherbrooke during the construction of a new research facility of the department of civil engineering. In total, eight wall elements of two different heights were cast: Walls 1-4 measured 3.7 m in height, and Walls 5-8 measured 4.4 m in height (Figure 1). The structural walls are of 0.20 m in width and 5.6 m in length and are reinforced in both directions [20]. The concrete was cast by pumping from top at a rate of rise (R) that was varied between 5 and 15 m/h. Two of the concrete mixtures were conventional vibrated concrete (CVC) and were not used in the validation of the experimental program for SCC mixtures.

Table I. Testing program and thixotropic properties for for wall elements at University of Sherbrooke [20]

	Effect of casting rate				Effect of thixotropy			
Formwork height, m	3.7				4.4			
Wall	1	2	3	4	5	6	7	8
Concrete	CVC	SCC1	SCC1	SCC1	CVC	SCC1	SCC2	SCC3
Slump flow/slump*, mm	120*	650			120*	650		
HRWRA type	--	PCE1			--	PCE1		PNS
Paste vol., l/m^3	--	330			--	330	370	330
Casting rate, m/h	7.5	5	10	15	7.5	10		
w/cm	0.40	0.35			0.40	0.37	0.35	0.42+VMA1
Air content ≤ 2.7%, T = 13-26 ^{o}C, unit weight = 23.81-24.06 kN/m^3, concrete was pumped from top, the walls had minimal rebars (ρ_{sv} is considered = zero), concrete cover = 25 mm								
$PV\tau_{0rest@15min}$, Pa	1815	425	220	325	1905	410	245	505
$PV\tau_{0rest}(t)$, Pa/min	21.5	8.3	6.8	5.9	11.4	6.2	4.2	15

The in-situ P_{max} values were monitored using pressure sensors mounted at different depths along the elements. The data obtained for walls 2, 3, 4, 6, 7, and 8 cast with SCC are compared in Figure 1 to values obtained from the prediction model [Eqn. (4)]. The results indicate excellent correlation between measured and predicted P_{max} values with a slope of the linear regression equals to 1.02 with R^2 equals to 0.99. It has to be noted that the correlation in Figure 1 is different than the one published in [20]

as it includes only the results of the six wall elements at University of Sherbrooke. The correlation in [20] included the results of both the wall elements at the University of Sherbrooke and column elements at CTLGroup.

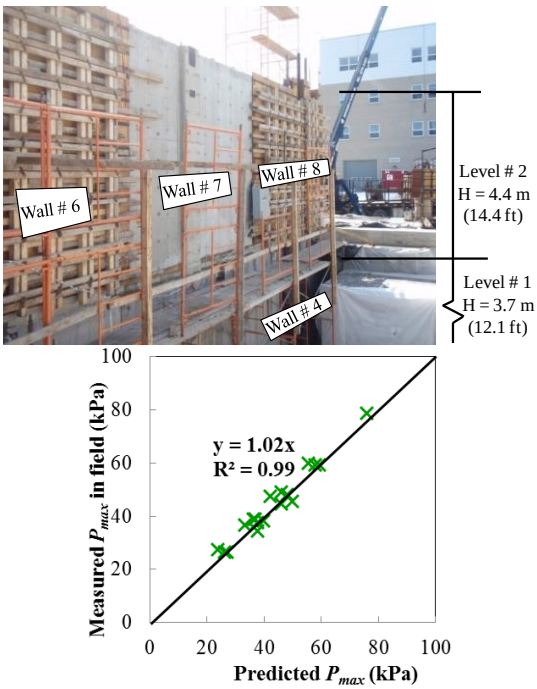

Figure 1. A photo of wall elements at University of Sherbrooke (left) and measured-to-predicted lateral pressure values using Eqn. (5) (right)

(2) Experimental Columns at CTLGroup in Skokie, Illinois USA

Summary of the testing program carried out on column elements cast at the CTLGroup facility in Skokie, Illinois, as well as the thixotropic properties for the investigated mixtures are given in Table II. In total, eight circular columns measuring 3.66 m in height and 0.61 m in diameter were used (Figure 2). Each column was instrumented with two pressure sensors at depths of 2.74 and 3.35 m [20]. SCC mixtures of low, medium, and high thixotropy levels according to the classifications described in [20] (SCC4 through SCC6) were placed at casting rates varying between 2 and 22 m/h. A waiting period (WP) of 20 min was introduced at mid casting of Col. 8 with SCC5. The columns had minimal rebars necessary for transportation and demoulishing purposes (ρ_{sv} is considered = zero) with a concrete cover of 25 mm. The P_{max} values monitored using pressure sensors are compared in Figure 2 to values obtained from an established prediction model [Eqn. (5)].

The results of Cols 3 and 6 were excluded from the correlation due to difference in shear histories of concrete samples used for the determination of structural build-up

at rest and that actually cast in the columns. Indeed, the concrete used in casting the two columns were re-mixed before placement, which resulted in a breakdown of the internal structure of the concrete, leading to lower structural build-up values. However, the concrete sample used for the determination of structural build-up at rest was kept without agitation and had high structural build-up values.
The comparison indicates good agreement between the measured-to-predicted lateral pressure measurements, with a slope of the linear regression equal to 1.01 and R^2 of 0.97.

Table II. Test matrix and thixotropic properties for column elements

Column	Casting rate, m/h	Mixture (thixotropy*), Slump flow in mm	$PV\tau_{0rest@15min}$, Pa	$PV\tau_{0rest}(t)$, Pa/min
1	13	SCC4 (Low), 660 ± 20	345	3.5
2	22			
3	5	SCC6 (High), 610 ± 20	1080	23.1
4	10			
5	2		1220	710
6	15			
7	5	SCC5 (Medium), 610 ± 20	65.2	18.6
8	5 + WP of 20 min			

* low, medium, and high thixotropy levels are defined according to the classifications in [20]

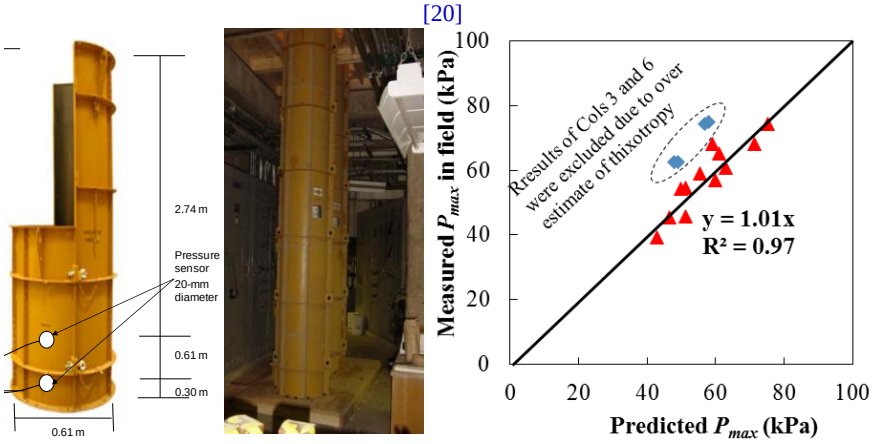

Figure 2. Photos for the CTLGroup columns (left) and measured-to-predicted lateral pressure values using Eqn. (5) (right)

(3) Bridge abutment in Sherbrooke/Canada

During the extension of Highway 410 in Sherbrooke (QC) Canada, a bridge abutment was cast with SCC mixture of low thixotropy level ($PV\tau_{0rest@15min}$ = 390 Pa and $PV\tau_{0rest}(t)$ = 15.46 Pa/min). The concrete unit weight was 22.64 kN/m^3 and

slump flow was 590 mm. The abutment measured 0.90×0.90×6.00 m and was reinforced with vertical reinforcement density of ρ_{sv} = 4.0% (Figure 3). The concrete was placed at a rate of 9.8 m/h. The lateral pressure was measured using pressure sensors mounted at 5.75, 5.25, 4.75, 4.00, and 3.25 m of casting depths.
A photo for bridge abutment during casting and the measured-to-predicted lateral pressure using Eqn. (5) are given in Figure 3. The relationship takes into account the effect of ρ_{sv} (4%) and the formwork lateral dimensions (d = 0.90 m). As indicated, the model is able to predict the measured lateral pressure perfectly with only 5% over estimation (R^2 = *0.98*).

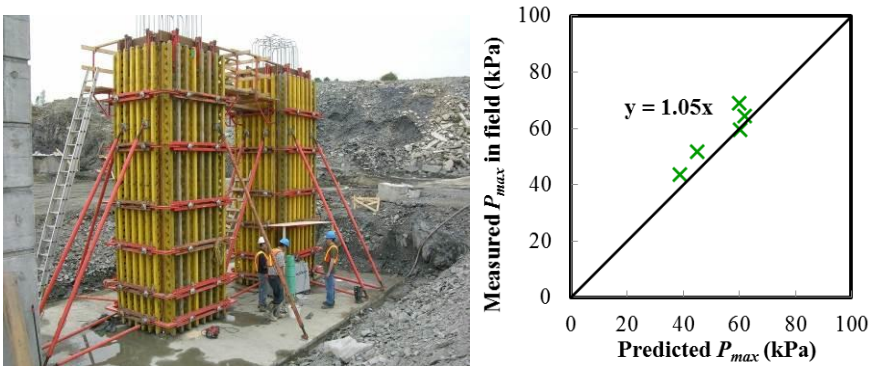

Figure 3. Photo for bridge abutment in highway 410 (left) and measured-to-predicted lateral pressure values using Eqn. (5) (right)

(4) Walls at CBI Stockholm/Sweden

A total of eight experimental wall elements, measuring 4.2 to 6.6 m in height, 2.4 m in length, and 0.2 to 0.4 m in thickness were cast with different SCC mixtures (SCC7 and SCC8) at the Swedish Cement and Concrete Research Institute (CBI) in Stockholm Sweden (Figure 4) [21]. Summary of the testing program undertaken in the wall casting as well as the fresh and thixotropic properties of concrete are given in Table III. It is worth noting that the walls had minimal rebars (ρ_{sv} = zero) with a concrete cover of 25 mm.
The measured lateral pressure results versus those obtained using the prediction model in Eqn. (5) are shown in Figure 4. The results deviate slightly from the 1:1 line with the slope of the linear regression equal to 1.16. The correlation coefficient of the linear regression (R^2) equals to 0.79. It is clear that this model can predict the lateral form pressure satisfactorily. The number of results N = 28.

Table III. Wall geometries, casting rate and fresh concrete properties

Wall No.	1	2	3	4	5	6	7	8
SCC mixture	SCC7	SCC7	SCC8	SCC8	SCC7	SCC7	SCC7	SCC7
Wall height (m)	3.75	4.11	6.58	4.15	5.51	4.2	5.52	4.15
Wall thickness (m)	0.203	0.201	0.198	0.203	0.200	0.202	0.203	0.400
Casting rate (m/h)	3.63	5.13	5.06	2.71	6.44	3.27	5.09	3.19
Concrete density (kN/m³)	22.38	22.64	22.61	23.34	22.38	22.61	23.43	23.11
Slump flow (mm)	610	710	600	630	615	650	710	620
$PV\tau_{0rest@15min}$ (Pa)	410	176	261	215	307	254	319	294
$PV\tau_{0rest}(t)$ (Pa/min)	16.0	5.8	9.9	2.3	11.2	9.6	18.5	9.1

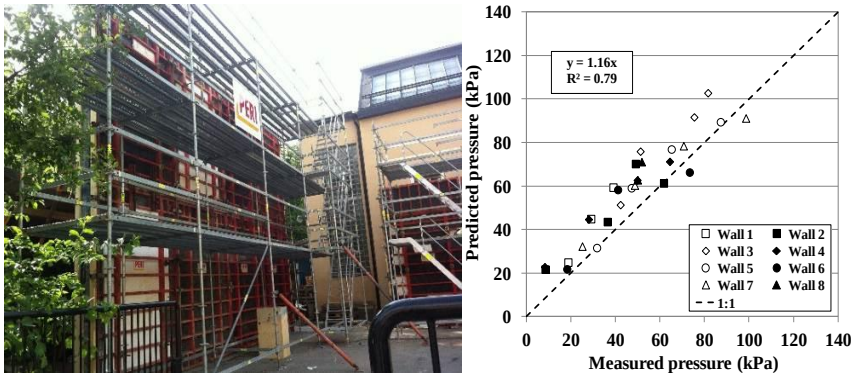

Figure 4. A photo of experimental wall elements in CBI Stockholm (left) and measured pressures vs. predicted values using model in Eqn. (5)

(5) Bridge tower in Hunt Club Ottawa/Canada

It was decided to construct the main tower in the airport parkway pedestrian connection in Hunt Club, Ottawa, Canada using SCC mixture to benefit from its high fluidity to secure excellent filling capacity and good surface finishing, especially since the tower is designed with heavy reinforcement (Figure 5). The tower had two inclined legs at an angle of 71.8º measured from the ground. An SCC mixture with MSA of 13.2 mm, slump flow 710 mm, low thixotropy level ($PV\tau_{0rest@15\ min}$ = 222 Pa and $PV\tau_{0rest}(t)$ = 6.0 Pa/min), and fresh temperature varying between 18.1 and 23.0 ^{O}C was used in the casting. In total, eight pressure sensors were set flush to the concrete surface at various depths of 4.3, 5.3, 7.3, 9.3, 11.3, 12.3, 13.5, and 14.7 m, measured on the inclined surface, to monitor lateral pressure variations with time in the north leg of the tower (Figure 5) during casting

and thereafter. The corresponding vertical casting depths of the pressure sensors (by considering the inclination angle and the main opening in the middle of the twoer) are 2.73, 2.73, 2.73, 2.73, 1.63, 0.33, 2.73, and 2.73 m. The concrete was cast at R of 1.6 m/h. Small windows were cut in the formwork at about 2-m intervals along the height to cast the concrete and observe the concrete level rise. When reaching the window level, they were firmly closed and started pouring new level. The concrete was cast using pump through the window openings.

Because there was no available data about the reinforcement density, a ρ_{sv} of 8% was assumed in the prediction models. The measured lateral pressure values can be fairly predicted using Eqns (5, 6, 7), as indicated in Figures 5A, B, and C, respectively.

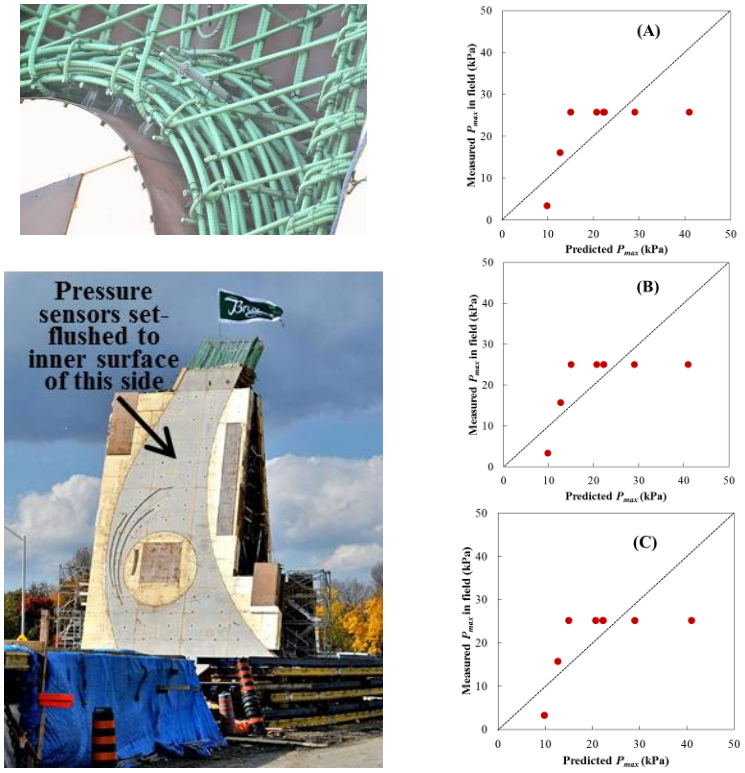

Figure 5. Photo of main tower in airport parkway pedestrian bridge (left) and measured vs. predicted pressures (right) using (A) Eqn (5), (B) Eqn (6), and (C) Eqn (7)

(6) Columns in Toronto/Canada during SCC Under Pressure

In total, eight experimental columns measuring 0.61×0.61×6.00 with ρ_{sv} = 3.42% (9#30M) on one face and no reinforcement on the opposite face were cast with SCC mixtures of different thixotropy levels during the "SCC Under Pressure" event in Toronto Canada organized by EllisDon Construction and St Mary's Cement. The steel rebars were spaced with 50-mm cover from the formwork face. SCC mixtures of low, medium, and high thixotropy levels were placed in at rates varying between 3 and 10 m/h, as indicated in Table IV. The thixotropic properties of the tested column are indicated in the same table. Figure 6 shows two columns that were cast using tremie pipes. The concrete pressure was monitored using pressure cells in the two opposite sides of the formwork (the reinforced and non-reinforced) at different casting depths.
The measured lateral pressure values obtained from these columns versus the predicted ones using Eqns. (5,6,7) are presented in Figure 7. The results indicate that the model based on the $PV\tau_{0rest}(t)$ [Eqn. (6)] and on the couple effect $PV\tau_{0rest@15min} \times PV\tau_{0rest}(t)$ [Eqn. (7)] had better prediction of the lateral pressure than the model based on the initial thixotropic values at 15 min $PV\tau_{0rest@15min}$ [Eqn. (5)].

Table IV. Testing program and concrete properties for "SCC Under Pressure" program

Placement method	Tremie						Pumping from bottom	Tremie
Columns	1	2	3	4	5	6	7	8
Concrete thixotropy	High	Med	Med	High	High	Low	High	Medium
Casting rate (m/hr)	3	5	10	10	5	5	10	3
$PV\tau_{0rest@15min}$, Pa	815	1032	1627	541	2053	2191	1465	1459
$PV\tau_{0rest}(t)$, Pa/min	41.4	40.1	24.3	6.7	50.9	34.6	36.4	17.3

Figure 6. View of "SCC Under Pressure" columns, modified tremie used in concrete placement, and measured-to-predicted lateral pressure

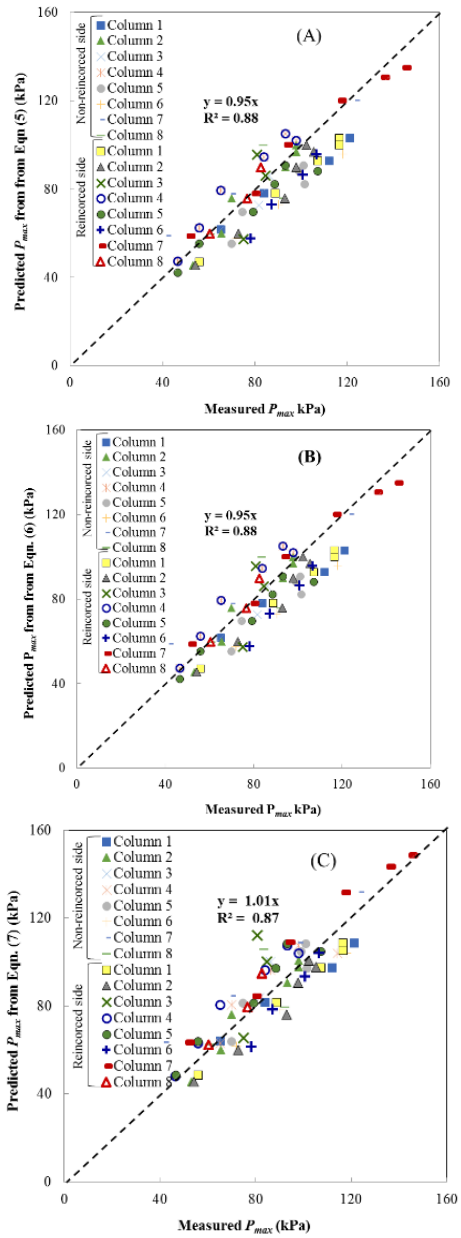

Figure 7. Measured-to-predicted lateral pressure for "SCC Under Pressure" columns: using Eqn (5) in (A), Eqn (6) in (B), and Eqn (7) in (C)

Conclusions

The findings confirm that the proposed models to estimate the maximum pressure of SCC offer adequate assessment of maximum formwork pressure exerted by SCC from full-scale of various structural element castings. The SCC lateral pressure could be significantly controlled by adjusting the concrete thixotropy, casting rate, and also the reinforcement density. The portable vane test can be successfully used to determine the structural build-up at rest of SCC used for lateral pressure prediction. Based on the results of the last project, the two prediction models [Eqn. (6)] (that considers evolution of structural build-up at rest with resting time) and [Eqn. (7)] (that considers coupled effect of both evolution of structural build-up at rest with rest time and initial value at 15 min of resting time) offer the best prediction of the lateral pressure compared to the model [Eqn. (5)] that considers only the value at 15 min.

References:

[1] Khayat KH, Omran AF (Dec. 2009) State-of-the-Art Review of Form Pressure Exerted by Self-Consolidating Concrete. Final Report, Ready-Mix Concrete (RMC) Research and Education Foundation, American Concrete Institute (ACI), and Strategic Development Council (SDC): pp 549. (http://www.concretesdc.org/projects/SCCreport.htm).

[2] De Shutter G, Bartos PJM, Domone P, Gibbs J. Self-compacting concrete. Wittles Publishing, Dunbeath, Scotland, UK, ISBN 978-1904445-30-2, 2008, 296 p.

[3] Daczko JA. Self-consolidating concrete: Applying what we know. Taylor & Francis Group, USA, 2012, 289 p.

[4] ACI Committee 347R-14, "Guide to Formwork for Concrete," American Concrete Institute, Farmington Hills, Michigan, 2004, 32 pp.

[5] Billberg PH, Silfwerbrand J, Österberg T. Form pressures generated by self-consolidating concrete. Journal of Concrete International, Vol. 27, Issue 10, October 2005, pp. 35-42.

[6] Khayat KH, Omran AF. Field monitoring of SCC formwork pressure and validation of prediction models. Journal of Concrete International, Vol. 33, Issue 6, June 2011, pp. 33-39.

[7] Lange DA, Birch B, Henchen J, Liu Y-S, Tejeda-Dominguez F, Struble L. Modeling formwork pressure of SCC. Proceedings of the 3rd North American Conference on the Design and Use of Self-Consolidating Concrete, Ed. S. P. Shah, Chicago, USA, 2008, pp. 295-300.

[8] Ovarlez G, Roussel N. A physical model for the prediction of lateral stress exerted by self-compacting concrete on formwork. RILEM Materials and Structures, Vol. 39, No. 2, 2006, pp. 269-279.

[9] Gardner NJ, Keller L, Quattrociocchi R, Charitou G. Field investigation of formwork pressures using self-consolidating concrete", Concrete International, Vol. 34, No.1, January 2012, pp.41-47.

[10] Graubner C-A, Boska E, Motzko C, Proske T, Dehn F. Formwork pressure induced by highly flowable concrete – Design approach and transfer in practice.

Structural Concrete Journal of the fib, Ernst & Sohn Verlag, 1/2012.
[11] Perrot A, Amziane S, Ovarlez G, Roussel N. SCC formwork pressure: Influence of steel rebars. Cement and Concrete Research, Vol. 39, Issue 6, 2009, pp. 524-528.
[12] Tejeda-Dominguez F. Laboratory and field study of self-consolidating concrete formwork pressure. M.Sc. Thesis, University of Illinois at Urbana-Champaign, 2005.
[13] Proske T. Frischbetondruck bei verwendung von selbstverdichtendem beton – Ein wirklichkeitsnahes modell zu bestimmung der einwirkungen auf schalung und rüstung (Formwork pressure using self-compacting concrete). PhD-thesis, Technische Universität Darmstadt, 2007.
[14] Proske, T., and Graubner, C.-A., "Pressure on Formwork using SCC – Experimental Studies and Modeling", In: Proceedings of the Fifth RILEM International Symposium on Self-Compacting Concrete, Ghent, 2007.
[15] DIN 18218:2010-01. Frischbetondruck auf lotrechte schalungen (Pressure of fresh concrete on vertical formwork). Beuth Verlag, 2010.
[16] Beitzel M. Modeling fresh concrete pressure of normal and self-compacting concrete. Proceedings of SCC2010, the 6th International RILEM Symposium on SCC and the 4th North American Conference on the Design and Use of Self-Consolidating Concrete, Ed. K.H. Khayat and D. Feys, Montreal, Quebec, Canada 2010, pp. 243-254.
[17] Omran, A. F., Khayat, K. H. (2016) Progress in understanding the influence of reinforcement density on SCC lateral pressure, Journal of Materials and Structures, submitted and pending decision.
[18] Omran AF, Khayat KH. Portable pressure device to evaluate formwork pressure exerted by flowable concrete. J Mater Civil Eng 2013;25(6):731–40.
[19] Omran A. F., Naji S., Khayat K. H (2011) "Portable Vane Test to Assess Structural Build-Up at Rest of Self-Consolidating Concrete." ACI Materials Journal, 108(6):628-637.
[20] Khayat KH, Omran AF, D'Ambrosia M (26-29th Sept. 2010) Prediction of SCC Formwork Pressure in Full-Scale Elements. Proceedings of the 6th International RILEM Symposium on Self-Consolidating Concrete, and 4th North American Conference on the Design and Use of SCC (SCC2010), Montreal, Canada, Ed. Springer, RILEM State of the Art Reports, Vol.1(Part 6):231-242.
[21] Billberg PH, Roussel N, Amziane S, Beitzel M, Charitou G, Freund B, Gardner JN, Grampeix G, Graubner C-A, Keller L, Khayat KH, Lange DA, Omran AF, Perrot A, Proske T, Quattrociocchi R, Vanhove Y (2014) Field evaluation of models for predicting lateral form pressure when casting with SCC. Journal of Cement and Concrete Composite (Elsevier), 54:70-79.

Analysis of Friction and Lubrication Conditions of Concrete/Formwork Interfaces

Chafika Djelal, Yannick Vanhove and Laurent Libessart

Univ. Artois, EA 4515, Laboratoire de Génie Civil et géo-Environnement (LGCgE), Béthune, F-62400, France

Abstract Concrete friction plays a fundamental role during various stages of construction and public works operations, including pumping, formwork filling and the production of facings. A tribometer for fluid materials has thus been developed to better study this friction. Tests performed with certain modifications of interface conditions show that friction is governed by interfacial characteristics (e.g. type of demoulding agent, roughness, pressure). The investigation showed that the tribometer is sensitive to obtain a real understanding of the mechanical behavior of the Self-Consolidating Concrete (SCC). The tests and observations made reveal that friction mechanisms depend on the properties of the interface. The interface appears to undergo two types of phenomena which depend of the pressure. The demoulding oil generates a reduction of the friction between the SCC and the formwork. Parameters specific to facing appearance are also addressed in this paper.

Keywords: *SCC, Friction, Formwork, Tribometer, Aesthetics, Release agents.*

Introduction

Since the 1980's, the use of Self-Consolidating Concrete (SCC) has grown considerably in popularity. Many significant structures of varying types have now been built with this material. At present, all key building industry actors take into account the progress provided by this material. SCC is also highly attractive to project owners and architects thanks to its finish in terms of facing quality. The appearance of facings constitutes one of the main SCC advantages. The use of effective demoulding agents helps ensure an impeccable final product. While the oils have already been successfully characterized, our understanding of the thickness of oils applied onto formwork walls before casting is still lacking. Facing quality depends primarily on the concrete skin properties, i.e. the layer of

material in contact with the formwork skin. This would extend to the first tenths of millimeters of concrete, in influencing both color and texture.
Demoulding oils are also used by formwork manufacturers to limit corrosion phenomena. When subjected to repeat concrete pouring, the oil film actually disappears and wear begins to occur as aggregates need to be included in the design of formwork installations capable of withstanding the concrete pressure. Over the past few years, several researchers have begun focusing on friction at the concrete/panel interface, as a means of either determining the lateral pressure of concrete against the formwork [1-2] or conducting phenomenological studies [3-6]. Two plane/plane tribometers have been specially designed for such studies. The underlying principle is identical for both devices, i.e. a metal plate in contact with a movable concrete surface. These devices are capable of reproducing the conditions encountered as concrete is being poured into the formwork.
Several researchers [7] have proposed predictive models for determining the concrete pressure against formwork.
Vanhove et al. [1] and Proske et al. [2] have developed a predictive model based on Janssen's theory in order to evaluate concrete pressure against a formwork. Both these models introduce a coefficient of friction that depends on several parameters. This paper is aimed at studying the influence of these parameters on the coefficient of friction at the concrete/wall interface and, consequently, encompasses their influence on concrete pressure against the formwork as well. The results output concern the behavioral study of a SCC used during the national project ("B@P") held at the Guerville experimental site (France).
In order to better understand the mechanisms taking place at the concrete/wall interface, testing was conducted in the laboratory both with and without demoulding oil [8]. Based on a series of tribometric tests [4], complemented by electrochemical impedance spectroscopy, various phenomenological models could be established to explain the mechanisms in effect at the concrete/oil/formwork interface. A study focusing on facing aesthetics has also been conducted for the purpose of identifying a correlation between the protocol for applying demoulding oil and facing aesthetics.

The Tribometer

The principle adopted herein is to press a sample of concrete against a moving metal surface (see Figure 1). The plate has been cut out from formwork walls by a formwork manufacturer. The sample holders were cylinders 120 mm in diameter fitted with a hatch to feed the concrete, which had been pressurized by the use of pneumatic jacks. A sealant system was installed on the sample holders so as to ensure full containment of the concrete without damaging the oil film applied on the plate. A mobile bottom was also placed at the back of the sample in order to transmit the pressure delivered (N) by the pneumatic jack to the concrete.
This device has already been described in many publications [1,3].

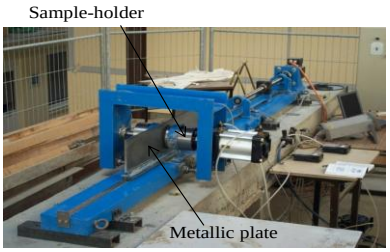

Figure 1. Detailed view of the tribometer

For each test, the tangential force (or frictional force) has been recorded vs. time. This force corresponds to two separate frictional forces, namely:

on the one hand, the resultant force of the interference friction force (Fpar) on the gasket system acting against the metal plate, as well as the resultant force of the tie against the slide;
on the other hand, the resultant force (Fmes) of the tangential friction force of both material samples against the plate, i.e. 2F, if friction is considered to be similar for the two samples tested.

$$\mu = (F_{mes} - F_{par}) / N$$

Properties of Materials and Oils

The metal plate

Previous studies [3,9] carried out on concretes have revealed that surface roughness exerts a significant influence on the coefficient of friction. Roughness measurements of formwork walls were recorded at the Guerville site using a portable roughness meter (R_a = 1 µm, R_t = 9 µm). R_a is the arithmetic mean deviation relative to the average line, while R_t is the distance between the highest maximum and lowest minimum on the roughness profile (Figure 2). For this study, a plate has been cut out from a formwork wall. Machining ridges run in the direction of plate displacement.

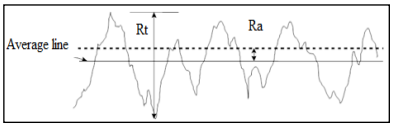

Figure 2. Roughness profile

The concrete studied

This study has focused on the behavior of a SCC that had been used during the national B@P project carried out at the Guerville experimental site. The selected concrete classification is commonly employed for civil engineering structures; this concrete features good rheological characteristics as regards both fluidity and stability. Limestone additives (filler) were introduced into the composition of test specimens as a means of improving facing quality in terms of color uniformity. The concrete composition and characteristics are listed in Table I.
The particle size distribution analysis [10] of the cement, filler, sand and coarse aggregate has served to determine the maximum diameter D_{max} of the grains, as well as the percentage of grain diameters (D) capable of becoming lodged within the plate asperities (Table II).

Table I. Mixture proportions of investigated concrete

Mixture	(kg/m^3)
Cement CEM I 52,5 CP2	365
Limestone filler	255
Sand 0/5	670
Coarse aggregate 3/8	790
Superplasticizer	6.0
Cohesion agent	0.66
Water	206
Water / (Cement+Limestone filler)	0.35
Density	2.3
Slump (cm)	70

Table II. Granulometric analysis of the fine elements of the SCC

	Dmax	D < 80 µm	0.1 µm < D < 10µm
Cement	60 µm	100%	55%
Limestone filler	100 µm	70%	15%
Sand 0/5	5 mm	0%	0%
Gravel 3/8	8 mm	0%	0%

The concrete particle size distribution is very widely spread, extending from roughly a micron for cement grains up to 8 mm for gravel diameter. The cement and filler grains with diameters smaller than 10 µm will potentially become lodged in the tribometer plate asperities.
The term *fine particles* or simply *fines* refers to all cement and filler components whose diameter is less than 80 µm.
Mixing was performed in accordance with the NF P 18-404 Standard entitled "Concretes - Analytical, feasibility and control testing - Specimen manufacturing and preservation". The operating protocol implemented was as follows:

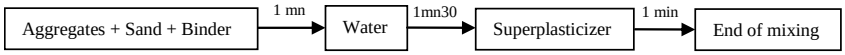

Figure 3. Mixing sequence

The oil used

The oil chosen for this study has a plant-based composition (denoted V for vegetable). It is 95% biodegradable without requiring the use of solvents. It has been used at the Guerville site; all pertinent properties are provided in Table III.

Table III. Vegetable oil properties

Properties	Vegetable based oil (V)
Nature of oil	Liquide
Color	Yellow
Flash point (°C)	> 200°C
Density	0.9
Viscosity at 20°C (mm^2s^{-1})	28

Oil application protocols

Demoulding oils must be applied homogeneously over the entire wall of a formwork. Their application requires the use of a sprayer fitted with an adapted nozzle. Any excess product is removed, as needed, with a scraper. Literature gives a different thickness according to the film. Indeed a 2 µm film can gives a good quality facing, but 10 µm can also gives good aesthetic results [5]. Excess oil however may lead to facing defects (bubbling). The conditions for applying oils on Guerville formworks were replicated in the laboratory. Two cases were examined in detail: application of the oil by spraying using a conical nozzle, followed or not followed by spreading with a rubber scraper.

(a) spraying

(b) spraying followed by scraping

Figure 4. Demoulding oil application protocols

The oil film thickness was measured by means of two distinct methods: weighing, and a technique based on alpha radiation [5]. A sample formwork with a dimension

of 5 x 3 cm was tested for the first method. In knowing the mass density of both the oil and the plate surface, it is simply necessary to weigh the sample in order to determine the oil thickness [5]. These results are given in Table IV. Measurement uncertainty equals +/- 0.15 µm. The oil film thickness measurement principle relies on the possibilities offered by the PIXE device, as well as on the properties of α rays, which are material particles (i.e. nuclei of helium containing 2 protons and 2 neutrons) launched at high speed (with an energy equal to 5.3 MeV). Oil thickness is measured from the maximum fluorescence X of the steel composing the metal plate. The level of steel fluorescence is directly influenced by attenuation of α X-rays in the oil film. From the detection of emitted X protons (given that the film only absorbs a small amount), the number of α particles reaching the wall (through the oil film) can be measured, according to a simple measurement protocol by metric absorption α. Moreover, very strong method sensitivity has been observed.

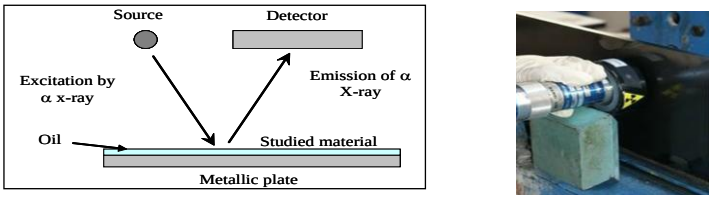

Figure 5. Schematic diagram of the PIXE principle and the Oil film measurement on the tribometer plate

The results are shown in Table IV for both methods. The measurements output by these two methods have yielded practically the same results.

Table IV. Thickness of the oil films

Methods	Weighing	PIXE
Spraying	17 µm	17.5µm
Spraying followed by scraping	0.8µm	0.7µm

Friction tests with and without demoulding oil were then conducted under the casting conditions implemented at the experimental site of the national B@P project. The pressures analyzed, which simulate concrete thrust against the formwork, were defined relative to maximum thrusts recorded at the formwork base ($P = \rho g h$, where ρ is the mass density of the material, g the gravitational acceleration, and H the formwork height). At the Guerville site, 6 concrete walls of 5 and 10 m high were cast. The pressures calculated at the formwork base equaled to 118 (for the 5 meter high wall) and 235 kPa (for the 10 meter high wall). The velocity of the concrete sliding against the tribometer plate were calculated based on the concreting speeds and ground surface area of each formwork; these speeds varied from 1.57 to 12.08 mm/s. A sliding velocity of 5 mm/s was retained.

Influence of contact pressure

The change in the coefficient of friction μ vs. concrete pressure against the plate is without demoulding oil shown in Figure 6 for a speed of 5 mm/s. The variation in this coefficient is not linear.

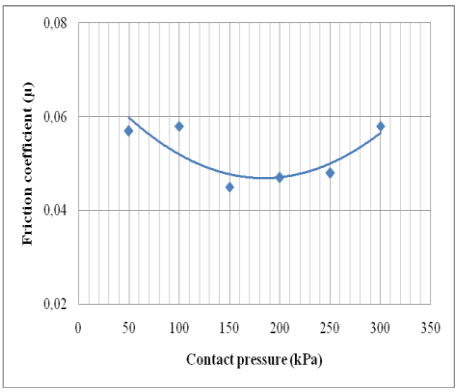

Figure 6. Evolution of coefficient of friction vs. concrete pressure

Two zones can be distinguished, thus reflecting two distinct types of friction. This curve displays a minimum at a pressure of 150 kPa. This same trend can be observed for other concrete mix designs. This critical value is equal to 110 kPa for a conventional concrete [9] [11].
To explain the phenomena taking place at the concrete/wall interface, please refer to the evolution in shear stress (friction) according to contact pressure (Figure 7).

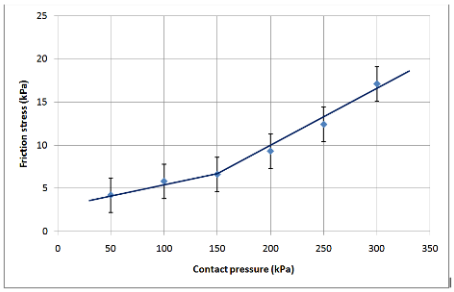

Figure 7. Evolution in shear friction stress according to the contact pressure

The shear stress is lower for pressures applied to concrete of less than 150 kPa. Two distinct types of friction will occur at the concrete/wall interface.
Despite its appearance, fluid concrete is not a continuous medium. The various concrete elements will play very specific roles when friction occurs. The pressure

stress applied to the material is transmitted to the granular phase as well as to the paste formed by the binder (cement + filler). This pressure will then cause a portion of the liquid phase and fines to migrate towards the interface. A lubricating surface *(or boundary*) layer (water + fines) of thickness "e" is thus formed at the interface. Experimentally speaking, the difficulty of highlighting sheared interface phenomena stems from the difficulty of instrumenting the materials in contact and, more specifically, the boundary layer. Owing to the cement particle and filler scales, Schwendenmam [10] and Vanhove et al. [11] used two techniques to develop an understanding of this complex interface. Whether by means of ultrasound [11] or ionizing radiation [10], both methods indicated a decrease in aggregate (sand and gravel) concentration near the wall. At low pressure, the phenomenon at the concrete/wall interface is triggered by the onset of microstructural rearrangement tied to initiating concrete pressurization at the interface. The grains contained in the boundary layer have a number of degrees of freedom, which serves to facilitate shear. As of 150 kPa (critical pressure), a portion of the boundary layer will migrate towards less stressed zones. Based on the conclusions drawn from these two studies, a proposed description of the mechanisms at work can be generated.

The roughness R_t of the plate equals 9 μm, which allows for the possibility that a portion of the cement and filler elements (D < 10 μm) becomes lodged in surface asperities. Shear mainly takes place in this layer (Figure 8a).
For pressures exceeding 150 kPa, a portion of the boundary layer will also migrate towards less stressed zones (Figure 8b). The sand or gravel grains will be placed in direct contact with the asperity tips (i.e. granular friction). The force exerted by these tips during plate displacement will lead to their rotation, thus giving rise to considerable energy dissipation and resulting in a faster increase in both the coefficient of friction and metal surface wear. After a series of tests corresponding to roughly 70 passes of concrete on the plate, the grains added both width and depth to the asperities. An R_a value of 2 μm and an R_t of 26.8 μm were found.

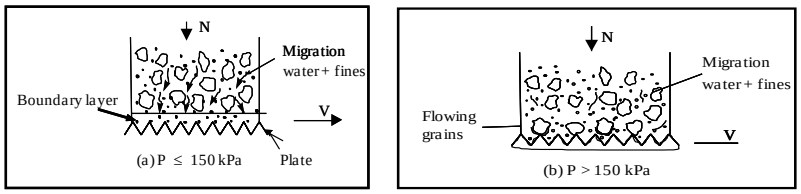

(a) (b)

Figure 8. Schematic representation of a concrete/metal plate interface

Influence of demoulding oil

Figure 9 depicts the evolution in the coefficient of friction vs. pressure for both oil application protocols. A reduction in the coefficient of friction can be observed.

This decrease is more pronounced for the sprayed oil. Like for friction without oil, the critical pressure lies at 150 kPa regardless of the oil application protocol.

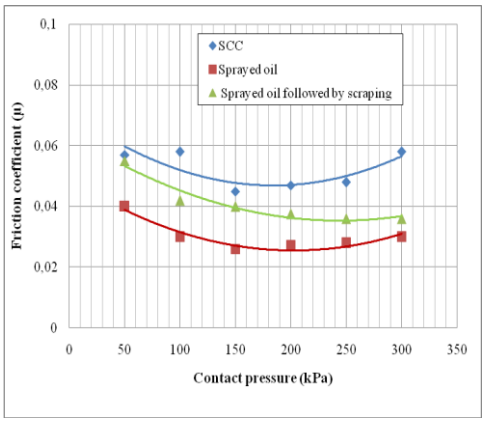

Figure 9. Evolution in the coefficient of friction vs. pressure for both oil application protocols

For high pressures, the effect of oil minimizes granular friction. Libessart et al. [8], in his study intended to better understand oil/concrete/wall interface mechanisms, performed a series of tests on various components of a particular oil mix design. This author studied the percentage of acidifier and solvent in a plant-based oil and moreover demonstrated that the effect of a base alone depends in large part on the thickness being applied. The physical effect takes precedence over the chemical effect (Figure 10a). Conversely, the presence of an acidifier strengthens the chemical effect by creating a greater quantity of soap at the interface (Figure 10b).

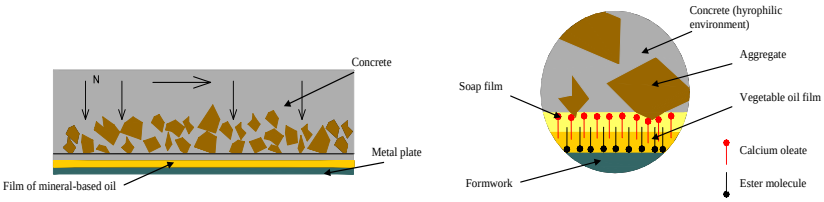

Figure 10. Diagram depicting the sliding of SCC on the oil film

The oil introduced in our study is composed of a vegetable base and devoid of any solvents. In this specific case, the oil film thickness determines friction, which explains the results in Figure 10.

Conclusions

To conclude this paper, a few results are given regarding the aesthetic flaws [12] encountered on concrete facing after formwork removal. The two application protocols described above have been analyzed. Molds sized 30 x 30 x 30 cm were designed by the same formwork manufacturer as the one that built the tribometer plate (Figure 11). Regardless of the application protocol employed, the facings are of high quality and show very little bubbling. No concrete attachment points exist on the wall. On the other hand, extensive fouling and dust accumulation have been observed on the mold surface for oil scraped after spraying.

Figure 11. Facing surface and dirtying of a mould

This study has shown the importance of interface conditions when pouring self-compacting concretes into a formwork.
The originality of this research lies in the fact that very few studies have previously been conducted in this field.

References

[1] Vanhove Y., Djelal C., Magnin A., (2004) *Magazine of Concrete Research*, Vol. 56, n. 1, pp55-62.
[2] Proske T., Graubner C. A., (2007), *Advances in construction materials*, Springer, pp. 463-470.
[3] Djelal C., Vanhove Y., Magnin A., (2004), *Cement and Concrete Research*, Vol. 34, pp. 821-828.
[4] Djelal C., de Caro P., Libessart L., Dubois I., (2008), *Materials and Structures*, Vol. 41,pp. 571-581.
[5] Djelal C., Vanhove Y., Chambellan D., Brisset P., *Materials and Structures*, Vol. 43, n. 5, pp. 687-698.
[6] Bouharoun S., de Caro P., Dubois I., Djelal C., Vanhove Y., (2013) *Construction and Building Materials*, Vol. 47, pp. 1137-1144.
[7] P. H. Bilberg et al., (2014), *Cement & Concrete composites*, Vol. 54, pp. 70-79.
[8] de Caro P., Djelal C., Libessart L., Dubois I., Pebert N., (2007), *Magazine of Concrete Research*, Vol. 59, n. 2, pp.141-149.
[9] Vanhove Y., Djelal C., Magnin A., (2000), Friction behavior of a fluid concrete against a metallic surface, EUROMAT 2000, *Conference on Advances on Mechanical Behaviour, Pasticity and Damage*, Tours, France.
[10] Schwendemann G., (2006), Etude de l'écoulement des bétons autoplaçants dans les coffrages à l'aide de la métrologie des rayonnements ionisants (french), PHD, thesis, University of Artois.

[11] Vanhove Y., Djelal C., Chartier T., (2008), *Journal of Advanced Concrete Technology*, Vol. 6, n. 2, pp. 1-8.
Libessart L., Djelal C., de Caro P., (2014), *Construction and Building Materials*, Vol. 68, pp. 391-104.

Tightness Requirements for SCC Formwork

Thomas Cools[1], Ann Van Gysel[1] and Petra Van Itterbeeck[2]

[1] KU Leuven, Dep. of Civil Engineering, Technology Cluster Construction
[2] Belgian Building Research Institute

Abstract Considerable attention is often dedicated to ensure the tightness of the formwork when placing ready-mixed self-compacting concrete (SCC). These sealing actions lead to additional costs, making the self-compacting concrete solution more expensive than casting traditional vibrated concrete.
This paper presents the results of an experimental research, regarding the required tightness of the joints between formwork panels when using SCC as non-fair faced, structural concrete. First, small scale tests are executed using artificial increase of the pressure exerted onto the tested SCC inside the formwork. In the second phase of this research, experiments are conducted on real scale formwork constructions (up to 6m of concrete height). A wide range of calibrated joint openings between the formwork panels are tested. During casting of the SCC the mortar loss through the gaps is visually observed. After removal of the formwork, the surface and corners of the hardened concrete elements are analysed.
The acceptable gaps between the formwork panels can reach values of up to 7 mm and higher, without leading to honeycombing and/or too widely spread 'infected' zones on the concrete surface.

Keywords: *SCC, Formwork, Joints, Tightness, Mortar loss, Leakage.*

Introduction

The use of ready-mixed self-compacting concrete on construction sites is still limited. In Belgium and most European countries, SCC accounts for 1-2% of the ready-mixed concrete market [1]. Nowadays ready-mixed SCC is mostly used for fair-faced concrete, complex forms or dense reinforced elements. Although 25 years of research performed on physical properties and on structural performance and the availability of guidelines [2-3] and standards, contractors still have a lot of questions concerning the practical aspects of construction using SCC.

To support and enhance on-site applications of SCC, University of Leuven and Belgian Building Research Institute set up a project in collaboration with 18 industrial partners. Besides the material cost of SCC and questions about the lateral pressure exerted by fresh concrete on vertical formwork panels, one of the major concerns of the contractors are the requirements about the tightness of the formwork joints using SCC and the necessity of supplementary sealing actions in comparison to ordinary concrete.

This paper presents the results of an experimental research on the tightness requirements of the formwork by studying the effects of gaps in the joints between formwork panels, when using SCC as non-fair faced, structural concrete.

Experimental program

In order to evaluate the impact of gaps in the joints between the formwork panels, a test program is set up. Calibrated openings are created using small steel sheets. The mortar loss through the gaps during casting of the SCC is visually observed. After stripping the formwork, the concrete surface is examined by detecting honeycombs and structural defects.

Tests on small scale specimens

First, small scale tests are performed on wall elements with a height of 0.9m. Modular formwork is fixed on a concrete baseplate (figure 1). Two series of tests are executed on respectively (i) vertical butt joints with gaps from 1 to 7 mm and (ii) the horizontal connection joint between the panels and the baseplate with gaps from 1 to 9 mm.

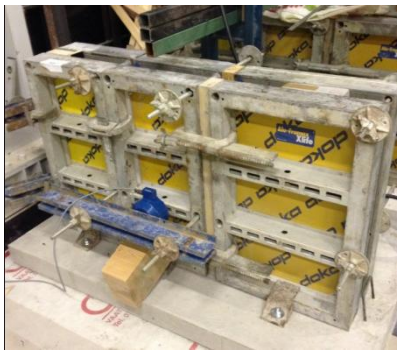

Figure 1. Setup small scale tests.

After filling the formwork with fresh SCC using a bucket, a vertical load is performed on top of the fresh concrete surface to create an artificial increase of the lateral pressure on the formwork, corresponding with a concrete head height of 2.3m. Due to this filling procedure there is a stagnation of the mix in the form before pressure is applied. The load is kept constant for about 10 minutes. The horizontal load on the formwork is measured by a load cell on a form tie.

Three different SCC mixtures are tested. The maximum aggregate size (D_{max}) and the fresh concrete characteristics determined before the filling of the formwork, are given in Table I. For comparison, also tests with vibrated concrete (slump of 130mm) are performed.

Table I. SCC mixture properties small scale tests

	Mixture 1	Mixture 2	Mixture 3
D_{max} [mm]	14	14	14
Slump flow [mm]	690	760	700
V-funnel time [s]	9.2	9.9	4.5
Segregated portion [%]	8	14	11

Full scale tests

To have a more realistic approach of the dynamic pouring process of SCC, full scale tests are performed on columns up to 6m. Five columns with heights varying from 2.4 to 3.3 m are tested. The SCC is produced in the laboratory and the columns are casted with a concrete skip. The vertical casting rate is about 100 m/h. One column of 6m is filled with SCC produced by a concrete supplier, using a concrete pump. (Figure 2). In this test, the rate of vertical rise of the concrete is 36 m/h.

Figure 2. Full scale test setups

Two different types of vertical joints are studied: butt joints and butt corner joints (Figure 3). Calibrated gaps up to 11mm are tested.

Figure 3. Butt joint (left) – Butt corner joint (right)

For each column a specific concrete mixture is used. The maximum aggregate size (D_{max}) is 16 mm for 5 columns and 8 mm for one column. The fresh concrete properties are determined before the filling of the formwork and are given in Table II.

Table II. Concrete properties real scale tests

	Column 1	Column 2	Column 3	Column 4	Column 5	Column 6
D_{max} [mm]	16	16	16	16	8	16
Slump flow [mm]	670	600	700	820	750	650

Results and Discussion

Small scale tests

Leakage during casting

Leakage at the vertical joints is limited for all tested gap sizes and concrete mixtures. Influence of the rheological characteristics of the SCC could not be observed.

At the horizontal joints, moderate mortar leakage is observed. The tests show that a higher fluidity of the SCC (measured by the slump flow) results in more leakage. The influence of the viscosity (by means of the V-funnel time) cannot be determined. Due to leakage at horizontal joints lift-up of the formwork could be a

problem. Therefore is generally advised to fix and seal the formwork to the base [2].

A similar test with ordinary concrete demonstrates that the problem of leakage is bigger for vibrated concrete than for SCC at both horizontal and vertical joints. (Figure 4)

Figure 4. Vibrated concrete – Gap of 7 mm in the vertical joint

Qualitative evaluation of the concrete surface
After removal of the formwork, the concrete surface was visually examined. Although the concrete surface at the joints becomes rougher in case of bigger gaps, this roughness is limited to the joint area and shows no structural defects, nor formation of honeycombs. As stated in the European guidelines [2] leakage of SCC at joints is mostly related to an inadequate concrete composition.

Figures 5,6 and 7 show the results of the vertical joints after demoulding. Figures 8, 9 and 10 show the horizontal joints. Leakage reduces the quality of finish of the concrete surface, but the results are satisfactory for non-fair faced concrete.
However, SCC generally leaks less than concrete that has to be vibrated [2]. For comparison, figure 11 shows the demoulded concrete surface of vibrated concrete. It can be seen that considerable honeycombing occurs.

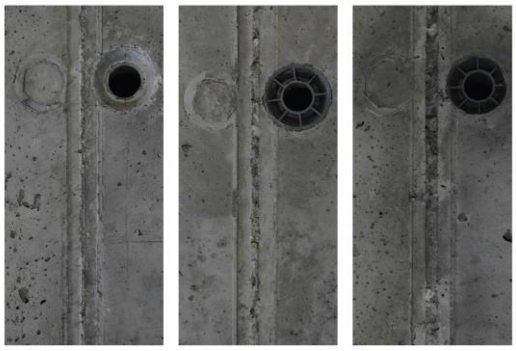

Figure 5. Mixture 1 – Gap of 2 mm – 4 mm – 7 mm (left to right)

Figure 6. Mixture 2 – Gap of 2 mm – 4 mm – 7 mm (left to right)

Figure 7. Mixture 3 – Gap of 2 mm – 4 mm – 7 mm (left to right)

Figure 8. Mixture 1 – Gap of 3 mm – 6 mm – 9 mm (top to bottom)

Figure 9. Mixture 2 - Gap of 3 mm – 6 mm – 9 mm (top to bottom)

Figure 10. Mixture 3 – Gap of 3 mm – 6 mm – 9 mm (top to bottom)

Figure 11. Vibrated concrete – Gap of 9 mm in the horizontal joint

Full scale tests

As described before, the small scale tests are rather static, whereas the full scale tests are performed using conventional dynamic placing methods for concrete, i.e. a concrete skip or pump.

Visual observations and quantification of the defects
In all tests, leakage of the mortar fraction occurs as long as the concrete is placed, but stops directly after casting. Although the amounts of lost material are small, it can be observed that there is increasing leakage with higher fluidity of the SCC. The influence of the maximum aggregate size is not clear.

After stripping the formwork the concrete corners and surface is examined for structural defects. Up to gaps of 4mm, the surface at the joints is rough, from gaps of 5 mm and higher, local honeycombing occurs as coarse aggregates are visible. However, these observations are limited to the joint area.

Figure 12 and 13 show results of the mortar loss during casting and the concrete surface after stripping the formwork, for respectively a corner joint and a butt joint.

Figure 12. Column 2 – Corner joint with a gap of 9 mm

Figure 13. Column 4 – Butt joint with a gap of 9 mm

To have an idea of the impact of the mortar loss on quality of the concrete cover, the depths of the defects in the concrete surface along the joints are measured with a Vernier calliper for columns 1 to 5. For that purpose, the joint length is divided in sections of 300 mm In each section the deepest defect is visually determined and measured. The maximum depth and average of the maximum depths of all sections are summarised in Table III.
As no average depth exceeds 10 mm, which is the defined position tolerance of the reinforcement according to Eurocode 2 [4], it can be concluded that this local honeycombing does not impact the concrete integrity.

Table III. Depth of defects in the concrete surface at the joints

Column number	**1**			**2**			**3**			**4**	**5**		
Column height [m]	3.0			3.3			3.3			2.4	2.7		
Joint type	Corner butt			Corner butt			Corner butt			Butt	Corner butt		
Gap width [mm]	3	5	7	7	9	11	7	7	9	9	2	4	6	8
Maximum depth [mm]	6.3	8.6	8.2	8.8	13.3	11.7	11.9	9.9	13.4	11.6	1.7	7.5	7.0	8.6
Average max. depth [mm]	3.9	4.4	4.6	4.7	6.7	7.1	7.1	5.8	8.6	7.1	0.8	2.9	4.8	5.8

Conclusions

This paper presents the results of an experimental study on tightness requirements of formwork for self-compacting concrete. The objective of this research is to give advice to contractors about the necessity of extra sealing actions in formwork when using SCC for non-fair faced concrete structures. Tests are performed on vertical and horizontal joints in the formwork with different types of concrete mixtures and casting methods. Calibrated gaps up to 11 mm were tested.
The results of this study show that gaps up to 7 mm and even higher don't negatively impact the integrity of the concrete. In general, it is recommended to fix and seal the formwork to the base, especially when uplifting can occur. There is no need for extra sealing of vertical joints for structural reasons. However, it is recommended in order to meet aesthetic requirements of the surface in fair-faced concrete.

Acknowledgements

The authors would like to acknowledge the Flemish Agency for Innovation by Science and Technology (IWT) for funding the research project.

References

[1] ERMCO (2014), Ready-Mixed Concrete Industrial Statistics - Year 2013, European Ready Mixed Concrete Organization, Brussels, Belgium.
[2] BIBM, CEMBUREAU, ERMCO, EFCA & EFNARC (2005), The European Guidelines for Self-Compacting Concrete. Specification, Production and Use. 63 pp.
[3] RILEM Technical Committee (2006), Casting of Self-Compacting Concrete State-of-the-art report. Skarendahl A , Billberg P (eds), RILEM report 35, 2006, 41 pp.
[4] EN 1992-1-1 (2004). Eurocode 2: Design of concrete structures Part 1-1 – General rules and rules for buildings.

Feedback Control of Smart Dynamic Casting through Formwork Friction Measurements

Marc Schultheiss[1], Timothy Wangler[1], Lex Reiter[1], Nicolas Roussel[2] and Robert J. Flatt[1]

[1]ETH Zurich, Institute for Building Materials, Zurich, Switzerland
[2]IFSTTAR, Paris, France

Abstract Smart Dynamic Casting (SDC) explores the well-known construction method of slip forming, in which concrete is poured into an automated short formwork, which moves at a speed set according to the hardening rate of concrete. Formwork translation speed must stay between two critical boundaries. If it is too high, the column collapses, as the material is not stiff enough to leave the form and maintain its shape. If it is too low, the column cracks as the structuring material sticks to the moving form. The most obvious, although time-consuming, method to tailor the speed to the hardening rate of the material is to carry out independent measurements on samples let at rest outside the moving formwork.
The objective of the present work is to retrieve information on the hardening rate of the concrete from the measurement of the friction force needed to move the slip form. This measurement allows for the computation of the friction stress at the interface between the material and the moving formwork. Our results suggest that this interface friction stress is a function of the formwork translation speed whereas the bulk material consistency is only age dependent. This further suggests that friction force measurement allows for avoiding the cracking of the column at low form moving speeds and that a feedback control of SDC is therefore possible. These results also suggest, however, that an additional independent measurement of the bulk consistency is needed to avoid the risk of collapsing.

Keywords: *smart dynamic casting, friction, slipforming.*

Introduction

Smart Dynamic Casting is a novel slipforming technique developed in recent years, which differs from traditional slipforming by shaping the material as it leaves the formwork [1]. This is an application of a set-on-demand admixture control of a

self-compacting mortar, where a large batch of mortar is overdosed with sucrose to produce a long retardation of the onset of hydration, and small accelerated batches are fed into a formwork and shaped at a moment where the material has hydrated to build sufficient structure to support the weight of the material in the formwork above it, but has not stiffened so much that it cannot be shaped. When it has formed too much structure, cracks can result upon deformation of the material. This process window occurs at the very initial stages of the acceleration phase of cement hydration, a point that has been previously examined by other authors [2-3]. This critical time window is seen in a very simplified way in Figure 1.

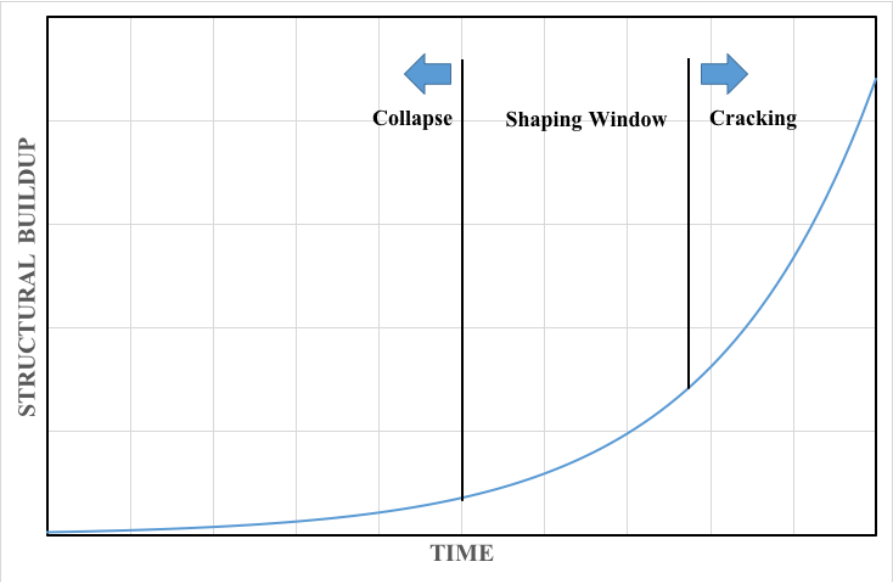

Figure 1. Simplified conceptualization of the process window in Smart Dynamic Casting. Material structuration must be sufficient to support the material above it, but not so stiff that frictional forces lead to cracking.

The translation speed of the formwork must be set so that the material exiting the formwork can remain within this window. Throughout Smart Dynamic Casting, the material that exits the formwork must be within this window to ensure a successful and high quality shaping and finish. While the greatest concern is to prevent the flow and collapse of the material column within the formwork due to a lack of structural build up, the tendency to move the formwork too slow and allow too much structural build up and frictional cracking must also be avoided. In this study, friction measurements are performed during casting to explore the potential for feedback control to avoid this problem in Smart Dynamic Casting.

Materials and Methods

Mix

The SDC mix is a self-compacting mortar made up of (for 1 L mix) 637 g 0-4 mm sand, 845 g CEM I 52.5R ordinary Portland cement, 142 g class F fly ash (Holcim Hydrolent), 80 g silica fume (BASF microsilica Elkem 971U) are mixed with 320 g water, 3.4 g superplasticizer (BASF Glenium ACE 30) and 2.3 g of a 30 wt% solution of sucrose as retarder. The accelerator used is X-Seed 100 (BASF), which is added in a quantity of 51.6 g per liter of retarded concrete.

Robot

The robot, pictured in Figure 2 is a homemade robot with a fixed formwork (ellipse with a=15 cm and b=9cm, and a depth of 40 cm) in a frame that can translate vertically via stepper motor. An additional stepper motor offers control of a turntable at the bottom, allowing rotational deformation. Four load cells were attached to the formwork to measure the force at each corner of the formwork, as indicated in Figure 2. The absolute friction force opposing the slipping is calculated as the sum of the four individual load cell measurements.

Figure 2. Robotic assembly for Smart Dynamic Casting. Rigid formwork translates vertically, while a rotating table underneath allows rotational deformation. Arrows on picture to the right indicate positions of load cells to measure friction force.

Casting Process

Batch acceleration consisted of mixing accelerator with predetermined batch size. The material hardening process was monitored by penetration test with a 2 cm cylindrical head driven at 1 mm/sec on a Zwick Universal Testing Machine. When the plateau force value of 4 N is reached, the slipping process was started. This point was reached typically about 120 minutes following the acceleration.

In initial tests, the formwork was filled with the mortar up to 39 cm and continuously slipped at speeds of 5, 10, and 20 mm/min in three separate tests.

Two more castings were carried out using the actual SDC casting process. One casting was performed at 5 mm/min and the other at 10 mm/min. The process consisted of accelerating individual batches calculated to fill 12.5 cm of the formwork. The batches were divided and intermixed at proportions of 1:3, 1:1, and 3:1 between subsequently accelerated batches, producing individual layers of 5 cm each. Filling was performed manually, and batch acceleration and filling was timed to ensure that material leaving the formwork was the same post-acceleration "age" as much as possible.

Results and Discussion

In Smart Dynamic Casting, there are two major problems to be controlled. The first is the stability of the bulk material, which determines if the material has enough structure to support the material above it. Currently, this is monitored by parallel testing of material, and is not the subject of this study. The other problem is the stability of the zone where material is being deformed, right at the interface of the formwork. At this interface, the rate at which the material is building structure must not be greater than the rate at which it is being destroyed, otherwise cracking could be the result. The material can build up structure from thixotropy as well as hydration; however, as it is continuously sheared at the interface and destroying thixotropy, probably the material stability and the majority of the friction force during slipping is coming from the exponential growth in structure from hydration. This also implies that the greater the "age" of the material post acceleration, the greater the friction force. The results of the three simply slipped columns illustrate this in Figure 3, where the overall friction force increases with decreasing formwork translational speed. In Figure 4, this frictional force is normalized by the filling level of material in contact with the formwork into an average shear stress, and here one can see the exponential growth of the frictional force, which is likely related to the exponential structural build up of the material as it hydrates.

The results of the columns cast via multiple batches using the Smart Dynamic Casting process show similar results. It can be seen in Figures 5 and 6 that within the 5 cm individually placed sections for both speeds of casting, the friction tends to increase towards the top of each one, as the material at the top of the section has been in the formwork for a longer time and therefore has the highest age for that section. One can also see that when one compares these results to the results of Figures 3 and 4, that there tends to be a baseline level of friction regardless of the speed, but that the slower the formwork moves, the longer the material remains in the formwork and the faster the increase in friction. One can also observe in Figures 5 and 6 that as no more material is placed in the formwork at the end of the casting, friction increases overall as there is no new material above it and therefore the average age of all of the material in the formwork is increasing with time.

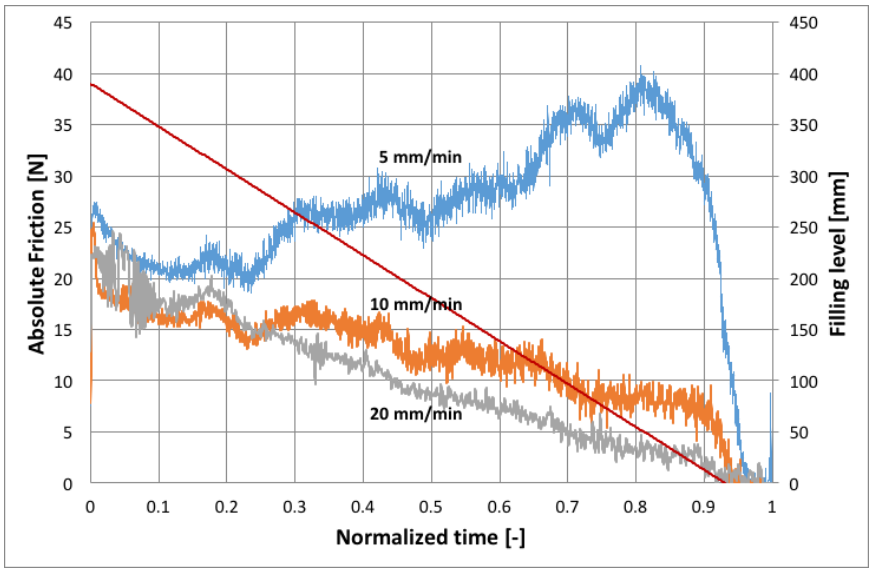

Figure 3. Friction forces measured during slipping of single batch, straight columns (ca. 40 cm total height), at 3 different speeds. Force is the sum of all four load cells attached to the formwork. Straight line is the level of material in the formwork.

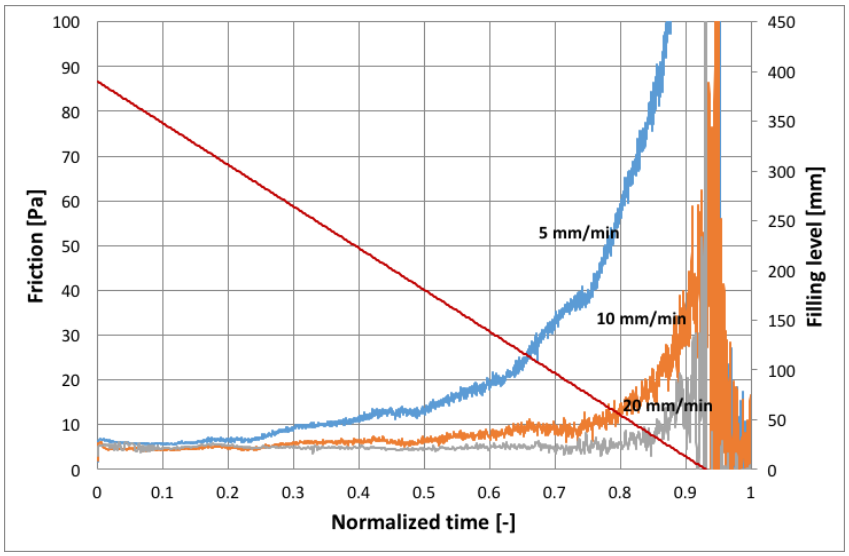

Figure 4. Friction forces measured during slipping of single batch, straight columns (ca. 40 cm total height), at 3 different speeds. Friction force normalized by surface area of material in contact with the formwork. Red level is level of material in the formwork.

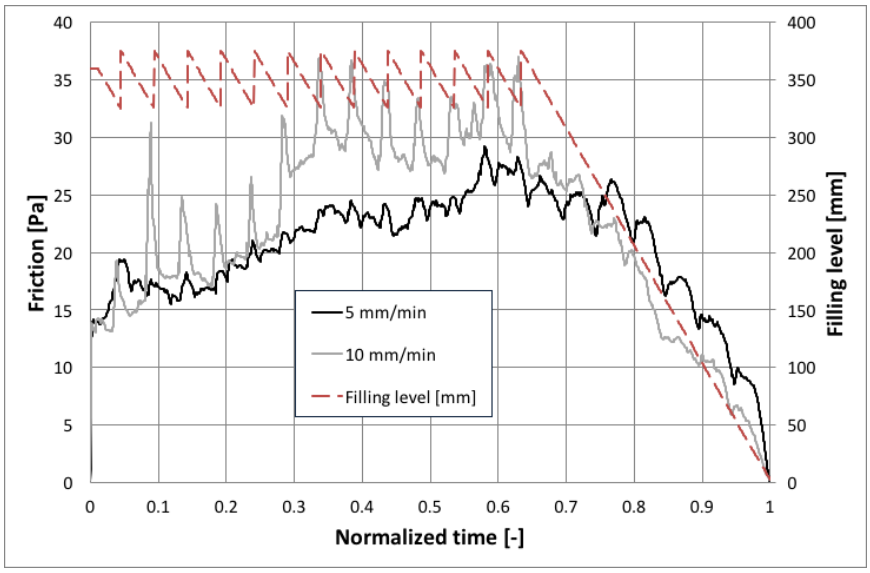

Figure 5. Friction forces measured during slipping of multiple batch, straight columns (ca. 1 m total height), at 2 different speeds. Force is the sum of all four load cells attached to the formwork.

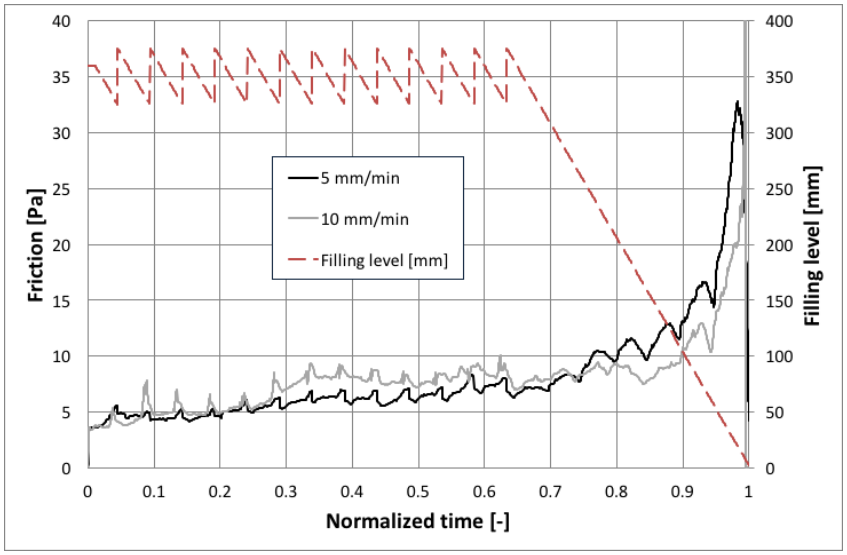

Figure 6. Friction forces measured during slipping of multiple batch, straight columns (ca. 1 m total height), at 2 different speeds. Friction force normalized by surface area of material in contact with formwork.

One failure mode for too much structural build up, besides shear cracking, would be cracking and rip off of the material. In Figure 7, such a failure is shown. This test was similar to the tests of Figures 3 and 4, where the formwork was filled and let at rest until slipping commenced. In this test, the speed was 10 mm/min and slipping began at a longer time after acceleration compared to the tests of Figure 3 and 4. Immediately one can see that the friction force is very high at the outset at 30 N; other experiments rarely reached 30 N. This friction increased to 60 N before it eventually failed by separation of the material in the formwork from the rest of the material at a slipped height of 24 cm. For comparison, the weight of material in the formwork acting against the friction is plotted along the same axis. Beyond the point where the two curves cross, the material at the exit point is in tension and therefore in danger of cracking.

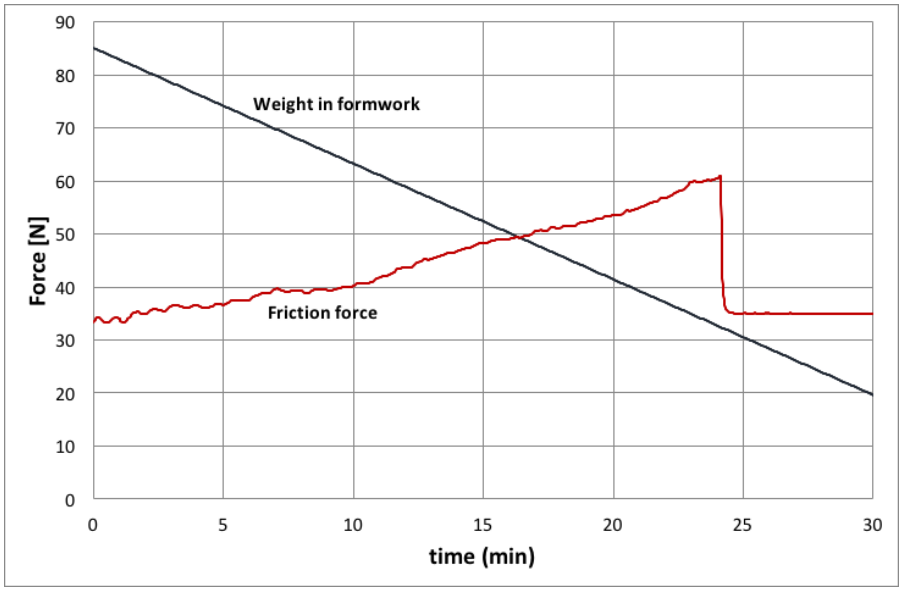

Figure 7. Friction force and weight in formwork against time for a column casting that failed at 24 minutes.

Friction force measurements thus can define a conservative upper limit for friction values based on the filling height by keeping the exit point in compression. In the normal SDC process, however, material is almost never allowed to rest in the formwork for such an extended period of time, and problems of friction can be easily controlled. Of much greater interest for production speed and process control will be determining the maximum slip rate that can be achieved by monitoring the bulk material inline.

Conclusions

In this study, it was demonstrated that friction measurements can be performed during Smart Dynamic Casting, and that the friction during the process increases with increasing material age and increasing material time in the formwork. While it may be possible to use this as a feedback control of the process to prevent cracking at too slow translational speeds, Smart Dynamic Casting would benefit more from inline metrology of the bulk material to indicate that the material has developed enough structure to prevent material collapse.

References

[1] Lloret, E., Shahab, AR., Mettler, L., Flatt, R.J., Gramazio, F., Kohler, M., and S. Langenberg (2015) Complex concrete structures: Merging existing casting techniques with digital fabrication. *Computer Aided Design* **60** 40-49, 2015.

[2] Shahab, A.R., Kristensen, E., Fischer, P., Gramazio, F., Kohler, M., and R.J. Flatt. Smart dynamic casting or how to exploit the liquid to solid transition in cementitious material. Proceedings of 7th RILEM International Conference on Self-Compacting Concrete and 1st RILEM International Conference on Rheology and Processing of Construction Materials, Paris, France, September 2-4, 2013.

[3] Perrot A, Rangeard D, Pierre A (2015) Structural built-up of cement-based materials used for 3D-printing extrusion techniques. *Mater Struct* 1–8. doi: 10.1617/s11527-015-0571-0

Maintaining the Air-Void System during Pumping of Self-Consolidating Concrete: A Challenging Fluid Mechanics Problem!

Dimitri Feys[1], Philip Zacarias[2], Stacia Van Zetten[3], Lloyd Keller[3], Bryan Schulz[2], Kyle Riding[4]

[1]Department of Civil, Architectural and Environmental Engineering, Missouri University of Science and Technology, Rolla, MO, United States
[2]CBM-St-Marys, Toronto, ON, Canada
[3]EllisDon, Toronto, ON, Canada
[4]Department of Civil Engineering, Kansas State University, Manhattan, KS, United States

Abstract Pumping is the fastest and most efficient way to place concrete in formwork. In the last decade, several advances have been made to better understand the pumping process and to predict pumping pressure. Furthermore, guidelines have been developed to minimize the loss of air and to maintain an adequate air-void system after pumping. However, the flow pattern of self-consolidating concrete in a pipe is different compared to normal concrete and its effect on the changes in the air-void system is still unknown.
This paper describes full-scale pumping trials during which different air-entrained self-consolidating concrete mixtures were pumped. Mix design, pumping flow rate and pipeline configuration were varied during the trials. Measurements of slump flow, T_{50}, air content (fresh and hardened) and rheology were performed before and after pumping. The results indicate that one of the most important factors influencing the air-void system was the configuration of the pipeline and the flow rate. Attaching a 75 mm diameter flexible hose at the end of a 125 mm pump line, which is recommended by the industry guidelines to reduce the loss of air, was shown to worsen the air loss and led to the largest increase in spacing factor. Rheological results indicate a more significant decrease in viscosity of the concrete, rendering the air more unstable in SCC. As a consequence, new guidelines for pumping SCC to guarantee air-void stability need to be developed.

Keywords: *Self-Consolidating Concrete, pumping, air-void system, rheology, workability*

Introduction

Pumping is an efficient way to place concrete inside formwork. It gives the contractor more flexibility and it decreases construction time. Although pumping operators have a lot of expertise, the pumping of concrete can still negatively affect concrete properties. One of these problems is the conservation of the air-void system [1]. Practical guidelines have been developed for conventional vibrated concrete (CVC), specifically focusing on the lay-out of the pumping circuit and the vertical drop the concrete undergoes [2]. A vertical drop in the pipeline could lead to negative pressure in the line during the switch of the valve in the pump, resulting in an increase in air-void size due to bubble coalescence. This negative pressure can be practically limited by using a reducer and a smaller hose, a double elbow, or a shut-off valve at the end of the pump line.

For self-consolidating concrete (SCC), the same industry guidelines are used, despite the different composition, rheological behavior and flow pattern in pipes. It is well known that SCC has a significantly lower yield stress compared to CVC, resulting in concrete shearing inside pipes [3,4]. This shearing effect can, theoretically, limit the increase in size of the air bubbles as large bubbles can be broken at high shear rates. On the other hand, Zacarias et al. have recently discovered a positive effect of a more elevated yield stress on the conservation of the air-void system [5]. Based on a limited number of tests on air-entrained SCC, it was concluded that maintaining an appropriate spacing factor was more challenging for SCC with larger slump flows. Furthermore, the Ontario Ministry of Transportation (Canada) currently specifies concrete based on spacing factor, instead of air content, necessitating full control of the air-void system in concrete.

Due to differences in flow behavior, it can thus be questioned whether the practical guidelines are entirely valid for SCC. By means of an experimental program, the influence of different mix design factors and pumping parameters on the change in rheology and air-void system was investigated.

Physical Background for Changes in Air-Void System

In this section, the physical background for changes in the air-void system due to pumping is described. Four phenomena are involved: the effects of pressure, suction, dissolution and reappearance of gas and shearing.

Pressure effects

The influence of pressure on the behavior of a gas can be described by the Universal gas law: $pV = nRT$. For example, assuming n, R and T remain constant, an increase in pressure by a factor of 8 (pumping at 8 bar above atmospheric pressure) will compress the volume of air by a factor of 8, or the radius of the bubbles by a factor 2. Due to the pressure shocks induced by the pumping process,

the air bubbles dynamically respond to compression and expansion. However, the pure pressure effects are not expected to play a major role themselves on the changes in air-void system, but they may amplify the other effects.

Suction effects

Negative pressure relative to atmospheric pressure, suction, will have a similar consequence on the air-void size as applying pressure, but in the opposite sense: air bubbles grow. If air bubbles become larger, it is more likely they will touch or coalesce: two smaller air bubbles forming a larger bubble. Suction has a negative influence on maintaining the air-void system. Suction can occur in two situations during pumping: when drawing the concrete from the hopper and if the end of the boom or hose empties under gravity. The latter effect is avoided when following the practical guidelines of reducing the diameter, installing a double elbow or a shut-off valve at the end of the boom.

Dissolution and reappearance of air

If pressure is applied on a gas bubble in a liquid, the gas in the bubble has a tendency to dissolve in the liquid. The amount of dissolved gas a liquid can carry also depends on the applied pressure. When applying pressure during pumping, a part of the air dissolves into the concrete mixing water. Smaller air bubbles have more tendency to dissolve than larger ones. When the pressure is reduced, near the exit of the pipeline, or due to the pressure shocks, the gas in the water becomes over saturated and will be released. It is most likely to be released into existing air bubbles or other nucleation sites, such as the interface between the liquid and a solid. As a consequence, the dissolved air reappears, but not necessarily at the location where it disappeared. As a consequence, the air-void system is expected to "coarsen" (i.e., increase the spacing factor). There is also some concern as to whether air-entraining agents can still provide sufficient stability to the air bubbles after they are reformed.

Shearing

If a liquid containing gas bubbles is sheared, the bubble can be deformed if the applied shear stress is larger than the surface tension of the gas in the liquid [6]. In the case of concrete, as the yield stress needs to be exceeded to start flow, the shear stress is in the majority of the cases sufficiently high to deform the air bubbles, potentially even leading to break-up of larger air bubbles into smaller specimens. The shearing effect would thus have a positive effect on maintaining the air-void system.

Combination of effects

Suction and dissolution of air are the two effects causing a coarsening of the air-void system, while shearing could counteract this effect. However, the shearing effect is only expected to take place near the end of the pipeline, as the pressure is lower and the air bubbles are larger. An increase in the flow rate would enhance the shearing effect and reduce the suction effect due to emptying of the pipeline. However, it will also increase the applied pressure and enhance the dissolution of the air in the concrete. Which effect is dominant is currently unknown, as the practical guidelines have been established for CVC, in which concrete is not sheared.

Experiments

Pump and pipelines

The pump used was a truck mounted piston pump Schwing 2025 with an S34 X boom. According to published specifications the pump can achieve a maximum flow rate of 136 m^3/h (or 37.5 l/s) or a maximum pressure of 8500 kPa (85 bar). The boom, constructed with 125 mm diameter pipes, can extend to a maximum distance of 34 m vertically. At the end of the boom, a 4 m long, flexible hose with a diameter of 125 mm was installed. During testing, the boom was extended nearly vertically up, and then down into the formwork where the concrete was placed. As a result, the vertical height difference between the pump and the top of the boom, and between the top of the boom and the outlet was between 15 and 17 m (see Figure 1). In some cases, a reducer and a 4 m long flexible hose with a diameter of 75 mm was added to the end of the boom (as is the case in Figure 1).

Testing Program

After batching the concrete at the ready-mix plant, and fine tuning the admixture dosages to obtain the appropriate air content and slump flow, the concrete underwent the following testing procedure before and after pumping:

- Slump flow and T50
- Fresh concrete unit weight and air content
- Rheology by means of the ICAR rheometer
- Casting of cylinders to determine hardened air-void system.

Prior to pumping, the concrete was sampled from the chute of the mixer truck, while after pumping, samples were taken from the concrete containers shown in Figure 1. These containers could hold approximately 0.83 m^3 of concrete, and were filled for a minimum of 80%.

The ICAR rheometer is a coaxial cylinder type apparatus, in which the inner cylinder rotates at a fixed set of rotational velocities, while torque is registered at

the same place. The inner cylinder is a 4-blade vane with an inner radius of 63.5 mm and a height of 127 mm. The radius of the container is 143 mm. During a test, after preshearing during 20 s at 0.5 rps, the rotational velocity is decreased in 7 steps from 0.5 to 0.025 rps, maintaining each step for 5 seconds. Provided the torque is in equilibrium, the average of torque (T) and rotational velocity (N) is calculated for the last 4 seconds of each step. A linear relationship: $T = G + H N$ is fitted to the results, and the Reiner-Riwlin equation [7] is applied to obtain yield stress and plastic viscosity, from G and H respectively. An iterative procedure to correct for plug flow was used if necessary.

Figure 1. Test setup.

SCC mixtures

The SCC mixtures were commercial products from the ready-mix company. The mixtures contained Portland cement and slag as binder, with a w/cm = 0.35. The maximum aggregate size was 14 mm, and the sand-to-total aggregate ratio was 0.54 by mass. In total, 3 batches of SCC were tested. Polycaxboxylate superplasticizer, air-entraining agent, retarder and viscosity modifying agent were used as admixtures. SCC 1 had an initial slump flow of 580 mm, a T50 of 2.0 s and an air content of 7.8%. These values were 690 mm, 1.2 s and 8.2% for SCC 2, and 565 mm, 2.3 s and 7.9% for SCC 3. SCC 1 has been pumped once at an estimated flow rate of 13.5 l/s. SCC 2 was pumped twice, at estimated flow rates of 13.5 and 19.0 l/s. For both SCC 1 and 2, no modifications were applied to the configuration of the pump. SCC 3 was pumped at estimated flow rates of 12.5, 15.0 and 22.0 l/s. At the lowest flow rate, two additional tests were performed using the reducer and 75 mm hose at the end of the pipeline. As SCC 3 was tested for an extended time, additional measurements were performed on samples from the mixer truck to monitor the changes with time. All measurements can be found in Tables 1 and 2.

Table I. Measured properties before and after pumping for SCC 1 and 2.

	SCC 1		SCC 2		
	Before	After	Before	After	After
Slump flow (mm)	585	650	690	690	720
T-50 (s)	2.0	1.8	1.1	1.3	1.0
Fresh air content (%)	7.8	4.6	8.2	3.0	2.8
Yield Stress (Pa)	77	34	51	32	30
Plastic Viscosity (Pas)	25	15	14	16	13
Hardened air cont (%)	9.5	4.2	5.4		2.4
Spacing factor (µm)	220	490	260		630
Estimated Q (l/s)		13.5		13.5	19.0

Table II. Measured properties before and after pumping for SCC 3.

	SCC 3						
	Before	After	Before	After	After	Before	After
End hose diameter (mm)		75		125	75		125
Slump flow (mm)	565	Segre	620	630	615	680	610
T-50 (s)	2.3	gated	2.0	1.8	1.5	1.4	2.5
Fresh air content (%)	7.9	3.0	6.0		3.1	5.1	2.8
Yield Stress (Pa)	46	0	26	19	20	34	23
Plastic Viscosity (Pas)	25	10	22	21	14	30	25
Hardened air cont. (%)	6.7	2.9		2.3	1.8		1.9
Spacing factor (µm)	260	820		530	660		770
Estimated Q (l/s)		12.5		15.5	12.0		22.0

Results and Discussion

For each of the mixtures and most of the tests, the air content decreased, the spacing factor increased and the T_{50} and viscosity decreased after pumping. Furthermore, for all mixtures, pumping caused the air content and the spacing factor to be out of specification, sometimes significantly.

More or less independently from the mix design tested, it appears that the spacing factor increased more when the concrete was pumped at a higher flow rate (black series in Figure 2). It appears thus that the shearing of the concrete, potentially breaking up the air bubbles, is not sufficiently important to prevent the coarsening of the air-void system due to dissolution of the air and potentially the emptying of the pipe under gravity. The results on the effect of the flow rate on the fresh and hardened air content appear inconclusive.

Adding a reducer and a hose with a smaller diameter (75 mm in this case), as is recommended by the industry guidelines for pumping CVC to limit an increase in spacing factor has an opposite effect on SCC (red series in Figure 2). Despite the low flow rate, a significant increase in spacing factor was observed. The main difference between both tests was that in the first test on SCC 3, the hose was horizontal (as in Figure 1), while in the second test with the smaller hose, the hose was vertical (the boom was lifted higher).

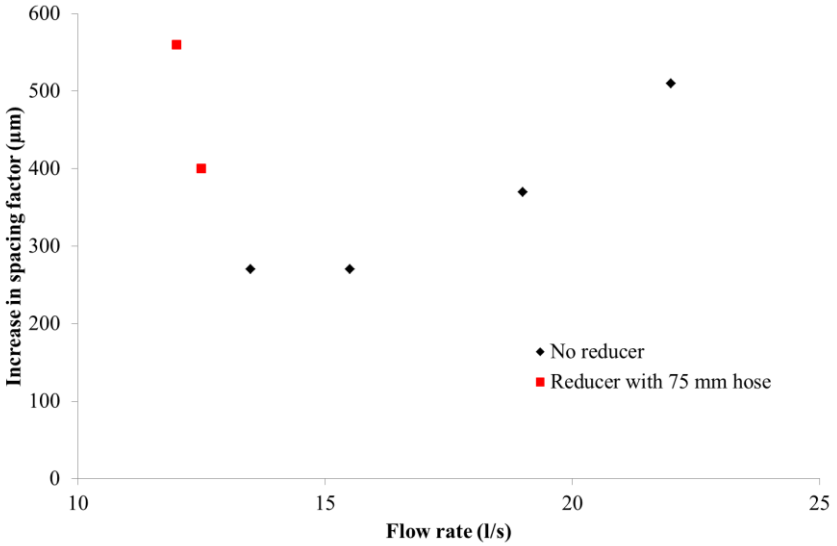

Figure 2. Increase in spacing factor as a function of applied flow rate, with and without reducer and 75 mm hose.

One reason for the increase in spacing factor could be attributed to the reduced viscosity of the mixtures, which led to significant segregation in the first case. Air requires less energy to move or to coalesce (during the preparation of the samples) when the viscosity is lower.

A second reason for the increase in spacing factor could be attributed to a larger pressure due to the presence of the smaller hose, as the pressure loss in the 75 mm hose is estimated to be 4-5 times larger than in the 125 mm hose, which would lead to a 50% increase in pressure in this case. Increasing the flow rate from 13.5 to 15.5 and 22 l/s would approximately increase the pressure by 15% and 60 – 65%, respectively. As mentioned before, an increase in pressure increases the capacity of the water of the mixture to carry dissolved gas, which could lead to more bubble coalescence. The estimates for the increase in pressure (provided the rheology remains approximately the same) can be roughly related to the change in spacing factor.

Summary

Maintaining an adequate air-void system is a challenge when pumping concrete. Practical guidelines for pumping conventional vibrated concrete have been established to minimize the impact of pumping on the spacing factor. However, for SCC, no such guidelines exist.

Dissolution of gas in the water of the concrete due to the applied pressure, and potential suction when the pipeline empties under gravity are the two main causes of bubble coalescence, and consequently, an increase in spacing factor. Theoretically, shearing of concrete can break down larger bubbles into smaller specimens, but evidence of this phenomenon was not observed.

Pumping experiments have been conducted on three air-entrained self-consolidating concrete mixtures. For all tests, a decrease in air content (fresh and hardened) and an increase in spacing factor are attributed to the pumping process. Increasing the flow rate and using a reducer with a smaller hose causes a larger increase in spacing factor, compared to a lower flow rate and no reducer.

Considering that the results indicate a significant reduction in air content and a coarsening of the air-void system, and that the practical guidelines for CVC may be partially inapplicable to SCC, more research on this topic is needed.

Acknowledgments

The authors would like to acknowledge the US Department of Transportation through the RE-CAST Tier 1 UTC for the financial support of this project. Further, the many helping hands from CBM-St-Mary’s and EllisDon to execute this work

are greatly appreciated, and Center for infrastructure of engineering studies at Missouri S&T is thanked for the general assistance in this project.

References

[1] American Concrete Pumping Association (2008), *Concrete 101, A guide to understanding the qualities of concrete and how they affect pumping*, www.concretepumpers.com/files/attachments/concrete_101.pdf.

[2] Pleau R., Pigeon M., Lamontagne A., Lessard M. (1995), In: *Proc. of the TRB Annual Meeting – Session on High Performance Concrete*. Record No. 1478, Washington, pp. 30-36

[3] Feys D, De Schutter G, Verhoeven R (2013), *Mat. Struct.*, 46, pp. 533-555.

[4] Feys D, De Schutter G, Verhoeven R, Khayat K H (2010), In: *Design, Production and Placement of Self-Consolidating Concrete, Proceedings of SCC2010*, Montreal, Springer, pp. 153-162.

[5] Zacarias P, Keller L, Feys D (2015), The Effect of Pumping on the Air Void System of Pumped SCC Mixtures and Methods to Maintain Quality, ACI Spring Convention, Kansas-City.

[6] Rust A C, Manga M (2002), J. *Non-Newt. Fluid Mech.* 104, pp. 53-63.

[7] Reiner M (1949), Deformation and flow. An elementary introduction to theoretical rheology. H.K. Lewis & Co, Limited, Great Britain.

Assessment of Pumpability Quality Control and Performance Parameters of SCC-Type Mixtures

Olga Rio[1], Khanh Nguyen [1], Gonzalo Barluenga[2], Irene Palomar[2], Mercedes Giménez[2], Alberto Sepulcre[3] and Ángel Rodriguez[4]

[1] Institute of Construction Sciences Eduardo Torroja–CSIC, Madrid, (Spain)
[2] Department of Architecture, University of Alcala, Madrid (Spain)
[3] Polytechnic University of Madrid, Madrid (Spain)
[4] AITEMIN, Margarita Salas, 14. 28918 Leganés, Spain

Abstract An experimental program on SCC-type mixtures pumpability was carried out to analyse the material behaviour during pumping, early age and hardened performance. The main goal of this research was to identify the main parameters for pumping quality control related both to the pumping process and the effects of pumping on the material performance at early ages (24 hours after casting) and in the hardened state. The research program was designed in three stages ranging from the mixtures design, the definition of the main flow equations and a laboratory experimental study to identify the main parameters, to the development of QC tools based on both the laboratory and real scale test results assessment. In the present paper the preliminary results of the initial full scale test, recently carried out, are analysed. Results pointed out that also when the cast in place procedure is properly performed, it can affect both the early age performance and the hardened properties of the SCC-type mixtures.

Keywords: *SCC, Pumping, Quality Control, Early age, Hardened*

Introduction

Although it is a recent innovation, SCC is becoming a popular concrete technology worldwide because it speeds up the placement of large volumes of fresh concrete in complex constructions. In such constructions is where SCC shows its enormous advantages and pumping becomes the most commonly technique used [1-3]. SCC can easily flow horizontally for long distances without segregation. Besides, vertical structural members, such as walls and columns, can be pumped from the bottom up as SCC usually pumps very easily and with reduced pumping pressures.

Accordingly, SCC pumping is gaining interest, becoming an area where systematic scientific and technical research is being carried out [4], which would eventually lead to improve the knowledge in SCC rheology and steel-SCC tribology, comprising pumpability predictive tests [5-7].

However, the pressure loss–discharge curve for a SCC does not show a perfectly linear behaviour exhibited by traditional concrete [4, 8]. Some authors have shown that SCC can present a shear thickening or rheopectic behaviour. Hence, neither the traditional tools nor those based on the Bingham approach may be considered further than just a first approximation for SCC mixes. Accordingly, on-site quality control tools and methods for monitoring the pumping process are still needed for SCC pumping [9, 10]. Furthermore, the undesirable effects of the cast in place techniques on the early age parameters and performance of SCC [11] and on the hardened performance [12] must be also controlled.

Due to the large amount of paste, SCC is prone to suffer the adverse cast-in place and environmental effects [13], which could lead to a reduction of the material performance and durability [12]. During early age (EA), SCC would develop a solid-porous microstructure that enables mechanical capacity, due to the cement hydration and pozzolanic reactions of the paste components. Furthermore, the actual EA evolution defines the hardened microstructure and properties.

In the present paper the preliminary results obtained from the initial full scale pumping tests of a SCC-type mixture, recently carried out, are analysed. The pumping parameters and performance are described, the early age monitored parameters are analysed and some hardened non destructive test results are presented.

Materials and Methods

Concrete components, mixing procedures and mixtures

The components and mix compositions used for the sample preparation are summarised in Table 1. A reference mixture (M1) was adjusted in the laboratory to achieve a minimum spread diameter of 600 mm (M2). Afterwards, the mixture was manufactured in an industrial mixer with 3 m^3 of capacity (MR1) that also required a water adjustment (MR2_0). This composition was used in a full scale pumping test carried out the day after, were 10 different batches of the MR2_0 mix (MR2_1 toMR2_10) were pumped. Two samples of batch 3 (MR2_3) were taken for early age (EA) monitoring and hardened properties evaluation: One before pumping and the other after pumping.

Table I. Mixture compositions (kg/m^3).

Batch / Material	Laboratory		Full scale		
	M1	M2	MR1	MR2_0	MR2_3
CEM I 52,5 SR	310	310	310	310	310
Fly Ash	96	96	96	96	96
Sand (0-4)	871	871	871	871	871
Gravel (4-20)	980	980	980	980	980
HRWRA	5.5	7	7	7	7
W/(c+FA)	0.38	0.40	0.40	0.42	0.42

Experimental methods

To verify the feasibility of the approach implemented for determining pumpability indicators [9, 10] a test set up was designed, as shown in Figure1. A standard stationary pump (PM1408D) and a pumping circuit, comprising an horizontal section of 10 m followed by a rubber hose, 3 m long, connected to a waste dump was used. The pump was instrumented with pressure sensors and displacement transducers to monitor the pumping parameters. All sensors were connected to a data logger and a computer, supplying real time data. The real-time experimental results of volumetric flow and the steady state pumping pressure corresponding to that volumetric flow were measured [9].

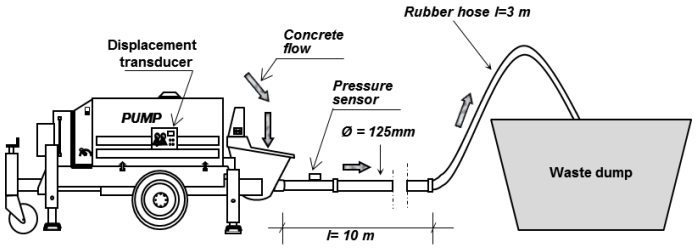

Figure 1. Pumping experimental set-up

The flow ability of the fresh mix was tested with the Slump flow test (According to ASTM C1611) and the environmental conditions (temperature –T- and relative humidity –RH-) were registered. Fresh samples were placed in a plastic mould of 150x100x80 mm were internal temperature, p-wave ultrasonic pulse velocity (UPV) and two capillary pressure sensors were used to monitor them during 8-14 hours [11].

500x100x50 mm samples were also monitored at EA in a shrinkage channel. Free shrinkage was measured on samples placed some under controlled environmental conditions (MR1 and MR2_0) and other tested at the pumping site (MR2 batch 3 Un-pumped –MR2_3U- and Pumped –-MR2_3P-). The samples at the laboratory

were subjected to a 3 m/s airflow in order to amplify the dimensional instability that is related to the microstructure formation and the mechanical capacity development at EA [11].

The samples were air cured and were tested hardened using non-destructive characterization techniques. UPV was measured on 100 mm samples and surface air permeability tests using the Figg method (Porosiscope™) were carried out.

Experimental Results

Pumping parameters and performance

The experimental pumpability results were analysed, relating pumping pressure and volumetric flow of the mix used in the real scale test (MR2_3). The pumping characteristics of this SCC mix were somehow different from that of previously tested conventional vibrated concrete (CVC) [9].

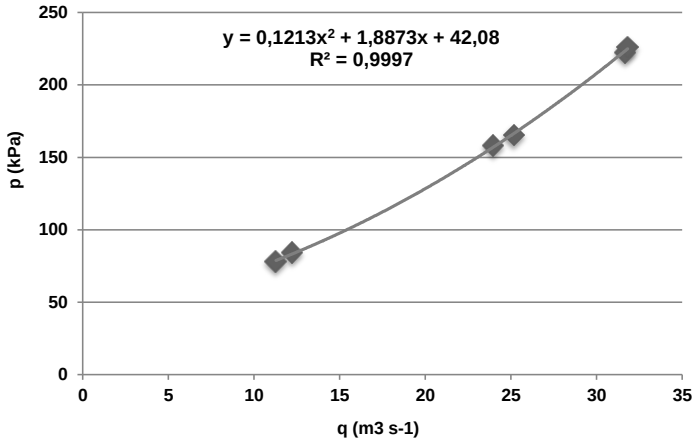

Figure 2. Pressure / flow relationship for a 10m DN125 pipe

While the pressure/flow relationship is usually linear for CVC, of the form $p = k_1 + k_2\, q$ [5], the SCC mix exhibited a rheopectic behaviour, as has been pointed out by some authors [7, 8], expressed sometimes by a potential equation and other by a polynomic pressure/flow relationship. In our case, the best fit was obtained with a 2nd order polynomic equation (Figure 2). Otherwise, pumping pressures were in the normal range for this type of concrete.

Early age performance

This section reports the EA performance of the SCC mixtures under real external conditions: MR2, Un-Pumped and Pumped. The key points of the monitored process were identified [11].

Figure 3 summarises the EA parameters measured on the SCC mix manufactured (MR2_0). The sample was monitored in a room with controlled environmental conditions because the extreme external conditions did not allow a complete monitoring. The temperature in the room was set on 26º C, although the average temperature of the 15 hours was 24.5ºC, the initial temperature was 32ºC and the minimum value was 21ºC. The extremely high initial temperature of the sample (48.7ºC) and the large difference regarding the environmental temperature produced an unusual shape curve for this type of mixtures. Instead, the thermal difference between sample and environment was plotted, because is easier to identify the change in the tendency that corresponds to the beginning of the cement hydration (fairly initial setting time).

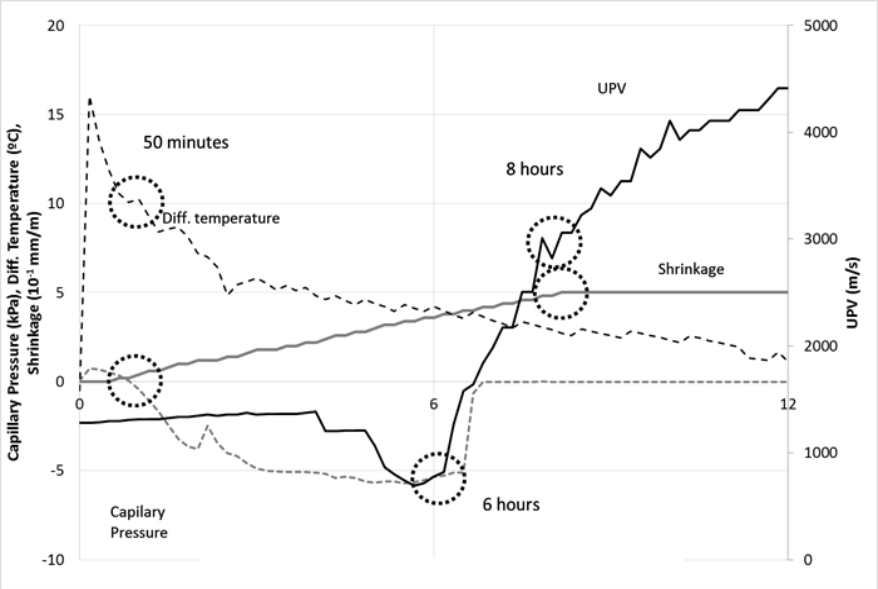

Figure 3. Early age parameters of the SCC mixture MR2_0.

Three key-points could be identified:

- Beginning of the hydration process and solid microstructure formation at 50 minutes, characterized by the change in the cooling tendency of the thermal curve,

the beginning of the dimensional instability and the increase of negative capillary pressure in the pore network;

- SCC stiffening and air entrainment in the pore network at 6 hours, identified by the decrease of negative capillary pressure and the fast increase of UPV;

- End of stiffening process, drainage of water available in the pore network and dimensional stability at 8 hours, related to the slowdown of UPV increase and the end of dimensional change.

The un-pumped sample (MR2_3U) was taken from the concrete after mixing and the experimental results of temperature, capillary pressure and UPV are plotted in Figure 4. Two key-points were identified:

- The beginning of the hydration process and the initial formation of the solid structure was identified at 2 hours, characterized by the temperature stabilization.

- The increase of negative capillary pressure in the sample; SCC stiffening at 6 hours, identified by the fast increase of UPV.

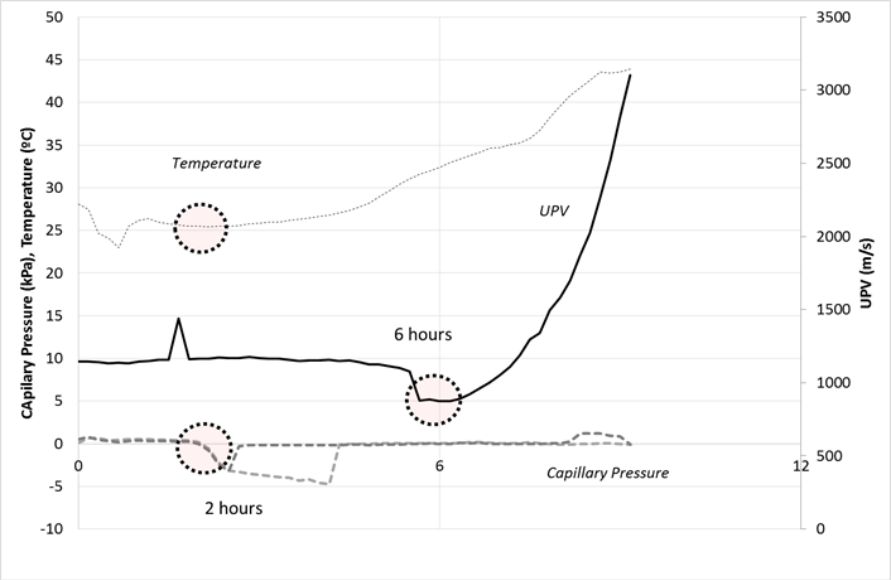

Figure 4. Early age parameters of the MR2_3U SCC mixture.

Figure 5 summarises the experimental results of the EA monitoring of the Pumped sample (MR2_3P). This sample was taken from the same batch as the un-pumped

sample and both samples were submitted to the same conditions. The experimental setup included temperature, capillary pressure, UPV and dimensional stability. Three key-points were identified:

- The dimensional instability and the increase of the negative pressure on one of the capillary sensors were measured at 30 minutes. Those results pointed out that a lack of water in the pore network was occurring locally.

- The beginning of the cement hydration and the solid microstructure formation occurred at 1 hour and 40 minutes after casting. This stage was identified by the thermal stabilization and the increase of the negative capillary pressure on the second pressure sensor. It was observed that the first pressure sensor that previously recorded an increase of negative pressure reduced the measurement and followed the reading of the second sensor. This would confirm that the material did not evolve either microstructurally or mechanically before this second stage, although a dimensional instability was recorded previously.

- SCC stiffening was recorded at 6 hours, corresponding to the dimensional stability and the fast increase of UPV.

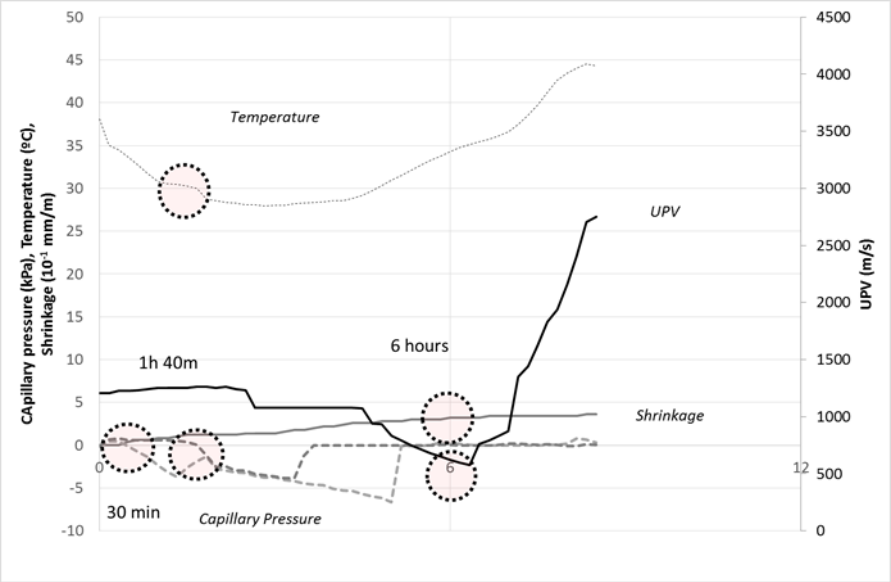

Figure 5. Early age parameters of the MR2_3P SCC mixture.

Hardened performance

The hardened samples were tested using UPV and air permeability non-destructive techniques. The experimental results are reported in Table 2. The UPV values were similar in all the samples, although the increase of water to cement ratio of the compositions leaded to a reduction of the UPV. The same occurred when the sample was pumped.

The air permeability did not follow the same pattern. The loss of flow ability due to the hot conditions observed when the sample was produced at the concrete plant (MR1) compared to that produced at the laboratory (M2) can explain the increase of air permeability associated to the reduction of the Figg time. The adjustment of the mixture to achieve larger flow ability explains the reduction of permeability. It must be highlighted that the samples were not compacted. The samples taken in the full scale initial test pointed a reduction of the Figg time due to the pumping process. The air permeability will be compared to SEM analisys and porosimetry gas adsorption measurements.

Table II. Hardened parameters of SCC samples.

Sample	UPV (m/s)	Air permeability (seg)
M 1	3766	--
M 2	3543	16.3
MR 1	4110	7.4
MR 2_0	3766	29.0
MR2_2U	4018	55.6
MR2_2P	3689	14.3

Discussion and Conclusions

Some preliminary experimental results of the pumping performance of SCC-type mixes and the EA parameters and hardened characterization were presented.

The SCC mix exhibited slightly rheopectic behaviour, which can be expected for SCC. Although in the range of flows considered (up to 50% of the nominal flow of the pump), pumping pressure was within acceptable limits and pressure needed for pumping at higher rates may be unexpectedly high.

The three SCC samples monitored showed a similar behaviour at early age (EA). In all cases, the beginning of the solid microstructure formation (fairly initial setting) followed the thermal stabilization. The material stiffening occurred around 6 hours after casting. Therefore, neither the environmental conditions tested nor the

cast in place procedure (pumped and un-pumped samples) substantially influenced the mechanical capacity development of the material at EA.

However, both the environmental conditions and the cast-in-place procedure influenced the beginning of the hydration process, the dimensional stability and the solid microstructure formation during the first 6 hours. Regarding the temperature, the higher both the temperature of the components or the environment, the faster the hydration process and the solid microstructure formation. Pumping also speeded up the reaction and an increase on the sample temperature was recorded.
Two main effects of pumping were identified: on one hand the temperature increase, which would explain the speed up of the process, and on the other hand the lack of enough water in the pore network which brought forward the beginning of the dimensional instability.

For the compositions considered, the environmental conditions and the casting procedures in this study, it can be said that the beginning of the chemical-physical changes could happened as soon as 40 minutes after casting. The solid microstructure formation could start between 1.5 and 2 hours. Higher temperature of the components or the environment would speed up the process.

The hardened characterization also showed the effect of the environmental conditions and pumping. The samples with lower flow ability showed lower UPV and larger air permeability. When the samples taken from the full scale test were compared, it was observed that the pumped sample had a lower UPV, which is related to a lower concrete stiffness, and the air permeability was larger, which could affect the long term performance of the material.

Acknowledgements

The study, SCC_Pump (BIA2013-48480-C2-2-R and BIA2013-48480-C2-1-R), has been funded by the Spanish Ministry of Economy and Competitiveness. The authors greatly acknowledge the support of the companies OHL, SIKA Spain and BASF construction chemicals España, SL.

References

[1] Kwon, S.H., Park, C.K., Jeong, J.H., Jo, S.D., Lee, S.H. (2013) *ACI Mat J*., vol. 110, n. 6,pp. 657-667.
[2] Roussel, N., Geiker, M.R., Dufour, F., Thrane, L.N., Szabo, P. (2007) *Cem. Concr. Res.*, vol.37, n. 9,pp. 1298-1307.
[3] Roussel N. (2011). In: Proceedings 9th Int.Symp. on HPC. vol. 2 pp. 678-685.
[4] Kaplan, D., Larrard, F. and Sedran, T., (2005), *ACI Mat. J*., vol 102, n. 2, p.110-117

[5] Ngo, T.T., Kadri, E.H., Bennacer, R., Cussigh, F. (2010) *Const. Build. Mat.*, vol. 24, n. 7, pp. 1253-1261.
[6] Choi, M., Roussel, N., Kim, Y., Kim, J. (2013) *Cem. Concr. Res.*, vol. 45, n. 1, pp. 69-78.
[7] Choi, M., Ferraris, C.F., Martys, N.S., Bui, V.K., Hamilton, H.R.T. (2015) *Adv. Mat. Sci. and Eng.* 2015, vol. 2015. N. 456238. pp. 1-10.
[8] Feys D., Schutter G.D., Verhoeven R. and Khayat K.H. (2010). In: *Design, Production and Placement of Self-Consolidating Concrete*, Dordrecht, pp. 153-162.
[9] Río O., Rodriguez A., Nabulsi S. and Álvarez M. (2011), *ACI Mat. J*., 4, pp 97-104
[10] Río O. and A. Rodriguez. (2012), *International Analytical Review*. Vol.2, n. 24, pp 50-61.
[11] Barluenga, G., Puentes and J., Palomar, I. (2015). *Constr. Build. Mat*., vol. 77, p. 66-73.
[12] Barluenga, G., Puentes and J., Palomar, I. (2015). Constr. Build. Mat., vol 94, p 728-736.
[13] Barluenga, G., Puentes J. and Palomar I., Río O. (2015). In: CONCREEP 10. ASCE Proceedings. pp. 1514-1523

Flowability and Stability Performance of Self-Consolidating Concrete in Full-Scale Beam

Habib A. Mesbah[1], Abelkrim Laraba[1,2], Ammar Yahia[3]

[1]Department of Civil Engineering, L.G.C.G.M, Université de Rennes 1, France.
[2]Department of Civil Engineering, LMDC, Université des frères Mentouri, Constantine, Algeria.
[3]Department of Civil Engineering, Université de Sherbrooke, Canada.

Abstract Flowability and stability performance of various self-consolidating concrete (SCC) mixtures in a full-scale reinforced concrete beams were evaluated. The mixtures were cast under gravity using a V-funnel measuring 1.7 in height. The beam is 4 m in length and 0.20 x 0.20 m^2 in cross section. The beam is reinforced with 10-mm diameter longitudinal bars and 10-mm stirrups placed at 150-mm distancel. The effect of mix design and the stability of the SCC on the flowability and passing ability of the concrete cast in the vertical and horizontal directions along the beams is evaluated. The investigated mixtures were made with different water-to-cementitious materials ratio (w/cm) and high-range water-reducing agent (HRWRA) dosage rates. The investigated SCC mixtures had a slump flow of 700 ± 10 mm and V-funnel flow times ranging between 1.75 and 6.75 s. The flowability performance was evaluated in terms of flow velocity of concrete determined at different locations along the beam. The dynamic stability was assessed at the top and bottom zones of different sections along the reinforced beam. Static stability was assessed using a rectangular column measuring 1.5 m in height and 200 x 200 mm in cross section. The variations in ionic concentrations were exploited to derive stability indexes with regards to bleeding and homogeneity of concrete. Derived stability indexes included bleeding coefficient, segregation coefficient, and homogeneity index. Test results showed that the increase in coarse aggregate content could improve the flow performance of SCC. On the other hand, SCC made with relatively higher paste volume of 40% is shown to exhibit lack of static and dynamic stability. The rheology of suspending phase should be then adjusted given the casting conditions and the mixture design.

Keywords: *Rheological properties, Flowability, electrical Conductivity, Static Stability, Dynamic stability, Self-Consolidating Concrete.*

Introduction

Self-consolidating concrete (SCC) is used in the precast and cast-in-place industries to facilitate casting operations and secure good performance and high surface finish [3-4]. These properties are dependent on the mixture composition and the element characteristics, including the reinforcement density, and the casting conditions. The mix design should be tailored to achieve the main functional requirements of SCC, including the filling ability, the passing ability, and stability. The passing ability refers to the ability of SCC to flow through tight space between reinforcing bars. On the other hand, the filling ability refers to the ability of SCC to flow under own weight and is mostly dealing with non-restricted flow, while the filling capacity refers to the ability of concrete to complete filling of the formwork under its own weight.

Achieving proper passing and filling abilities of SCC depends on its dynamic stability. Dynamic segregation is the process in which coarse aggregate separate and settle down when the concrete is flowing. The segregation of coarse aggregate can lead to heterogeneous properties of the hardened concrete with direct impact on mechanical performance, transport properties, and durability [5]. Control of segregation is therefore critical for the material to achieve adequate mechanical properties and structural performance.

The flow performance and the shape of free-surface profile of SCC in formwork are dependent on its rheological properties. Indeed, due to its low yield stress, SCC may present a relatively higher risk of segregation depending on the casting conditions and the reinforcement configuration as well as the geometry of the element. The main objective of this study is to evaluate the flowability and stability performances of various SCC using a 4-m full-scale reinforced beam. The flow performance is evaluated by means of flow velocity at different locations along the beam. On the other hand, the stability is assessed using a non-destructive method based on the electrical conductivity approach. The variations in the ionic concentration of the beam at different vertical and horizontal locations of the beam reflect the dynamic stability of plastic concrete and interpret the material homogeneity in the beam.

Experimental program

The experimental program undertaken in this study aimed at evaluating the flowability and stability performances of various SCC mixtures. In total, nine SCC mixtures were investigated. The mixtures were prepared with a fixed binder content of 450 kg/m^3 (350 kg/m^3 of GU cement and 100 kg/m^3 of Class F fly ash), different water-to-cementitious (w/cm) ratios of 0.40, 0.47, and 0.54, corresponding to 34%, 37%, and 40% of volume paste (Table 1). Three coarse aggregate contents of 27%, 30%, and 33%, by volume, were evaluated. The investigated mixtures were proportioned with a sand-to-total aggregate ratio (S/A)

varying between 0.75 to 1.40, and different HRWR dosage rates in order to secure the targeted slump flow of 700 ± 10 mm.

Materials

The investigated mixtures were proportioned using portland cement (CEM I 52.5 N) combined with a Class F fly ash (binary system). A crushed coarse aggregates with different maximum size aggregate (MSA) of 8 and 12.5, specific gravity of 2.65, and water absorption of 0.5% was used. Well-graded siliceous sand of 0–4 mm was used. The HRWR had a specific gravity of 1.07 and a solid content of 30%.

Table I. SCC mixture proportioning

Mixture	SCC1	SCC2	SCC3	SCC4	SCC5	SCC6	SCC7	SCC8	SCC9
Type CEM I 52.5 Cement, kg/m^3	350	350	350	350	350	350	350	350	350
Fly ash, kg/m^3	100	100	100	100	100	100	100	100	100
Total cementitious materials, kg/m^3	450	450	450	450	450	450	450	450	450
Total water, kg/m^3	182	182	182	212	212	212	242	242	242
w/cm	0.40			0.47			0.54		
Volume paste (%)	34			37			40		
Sand kg/m^3	1010	920	814	907	823	748	850	760	670
Coarse aggregate (4-8 mm) kg/m^3	145	162	178	144	162	179	144	162	180
Coarse aggregate (8-12.5 mm) kg/m^3	580	650	713	576	650	715	576	650	720
Volume of coarse aggregates (%)	27	30	33	27	30	33	27	30	33
Polycarboxylate HRWRA, l/m^3	8.1	8.2	9.4	3.6	3.9	5.6	1.5	1.6	1.8

Test procedures

The investigated mixtures were mixed in batches of 340 L using a laboratory central mixing plant with a capacity of 500 L. The mixing sequence consisted of homogenizing the sand and coarse aggregate for 1 minute before introducing 1/3 of the mixing water. The cementitious materials were then introduced along with the HRWRA diluted in the second 1/3 of the mixing water. The concrete was then mixed for an additional five minutes. The flowability and dynamic stability performances of SCC were evaluated by casting 162 L o concrete in a 4-m reinforced beam (Fig. 1).

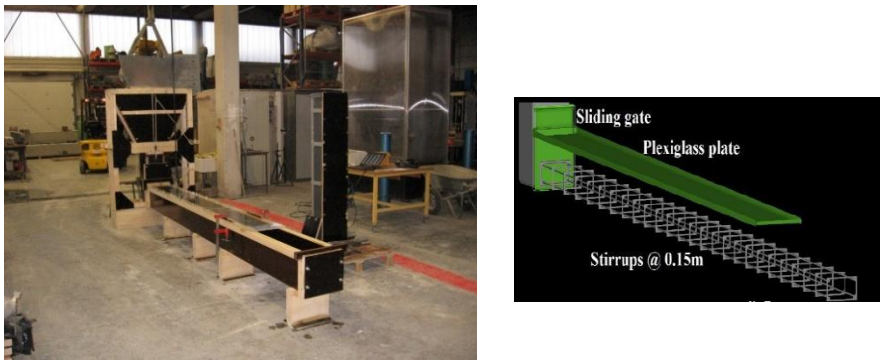

Figure 1. The reinforced beam used to assess flowability of SCC mixtures

Figure 2. Static stability set-up, conductivity probe, and data acquisition system

A 162 L of concrete was cast in the vertical V-funnel measuring 1.79 m in height. This section was composed of three parts, including the upper rectangular section (1 m width × 0.19 m height), the middle trapezoid V-funnel part with 0.8 m height (1 m and 0.2 m width at top and bottom, respectively), and the lower rectangular section having 0.8 m height and 0.2 m width. Each of the three sections had a 0.2 m in depth. Immediately after filling the vertical compartment, the sliding door between the vertical and horizontal compartments was opened, and the concrete flowed under gravity in the horizontal reinforced beam. The beam was reinforced with 4-m longitudinal bars of 10-mm diameter and 26 vertical stirrups of 10 mm diameter equally spaced (0.15 m). The top of the first 3-m of beam was closed with Plexiglas plate to avoid splashing out the concrete during casting. The passing ability was evaluated in terms of the flow time of concrete at different locations and to reach the end of the beam using a high-speed video camera. The electrical conductivity was measured along the depth of the beam at different locations to assess the vertical and horizontal stability resistances, respectively, along the beam. On the other hand, the static stability was determined using a column of 1.5 m in height (Fig. 1). The column was monitored with four electromagnetic sensors using

Time Domain Reflectometry (TDR) technique at different heights of the column. The four sensors were placed as follow: Sensor 1 (at 142 cm), Sensor 2 (at 96 cm), Sensor 3 (at 54 cm), and Sensor 4 (at 8 cm). The test consisted in determining the differences in electrical conductivity measured at different depths of the specimen during 180 minutes. The variations in electrical conductivity throughout the sample as a function of time were used to evaluate the material homogeneity. This method enabled one to evaluate the combined effect of water migration, consolidation, and segregation of cement-based materials during the plastic stage of cement hydration.

Table II. Fresh properties of investigated SCC mixtures

Mixture	SCC1	SCC2	SCC3	SCC4	SCC5	SCC6	SCC7	SCC8	SCC9
Volume paste (%)	34			37			40		
Coarse aggregates content (%)	27	30	33	27	30	33	27	30	33
Unit Weight (kg/m^3)	2300	2310	2320	2300	2300	2340	2360	2360	2360
Slump flow (mm)	700	700	700	700	700	700	700	700	700
T_{50} (seconds)	2.13	0.66	1.23	1.20	2.20	1.03	0.4	0.3	0.25
H2/H1	0.63	0.78	0.58	0.70	0.70	0.70	0.81	0.84	0.75
Time (seconds)	5.47	4.07	4.75	1.20	2.20	1.20	0.40	0.45	0.35
Fill-Box Capacity (%)	91	95	88	86	95	95	93	95	96
V-Funnel (seconds)	6.75	5.06	3.99	3.30	2.88	4.00	1.75	1.80	2.75
Segregation Index **SI**	0.31	0.35	0.41	0.28	0.14	0.42	0.58	0.64	0.58
Bleeding Index **BI**	0.26	0.26	0.36	0.22	0.20	0.54	0.40	0.39	0.48
Homogeneity Index	**0.58**	**0.60**	**0.77**	**0.50**	**0.26**	**0.96**	**0.98**	**0.99**	**1.07**
Dynamic stability Index **SDI-1 (%)**	4.38	0.09	5.41	12.33	0.57	5.98	13.61	7.88	3.92
Dynamic stability Index **SDI-2 (%)**	5.15	0.04	17.17	15.39	8.96	17.21	14.62	7.40	16.32
Mean Dynamic stability Index (%)	**4.80**	**0.07**	**11.30**	**13.85**	**4.80**	**11.60**	**14.10**	**7.65**	**10.15**
Flow time at 2 m (seconds)	26.3	10.6	12.0	10.5	7.0	4.0	2.5	2.0	2.1
Flow time at 4 m (seconds)	**104.6**	**45.0**	**43.0**	**40.0**	**30.0**	**19.0**	**5.2**	**5.8**	**5.4**

Test results and discussions

Effect of coarse aggregate content on passing ability and stability

The variations in the horizontal flow distance with time determined for the SCC mixtures made with paste volumes of 34, 37, and 40% are summarized in Fig. 3.

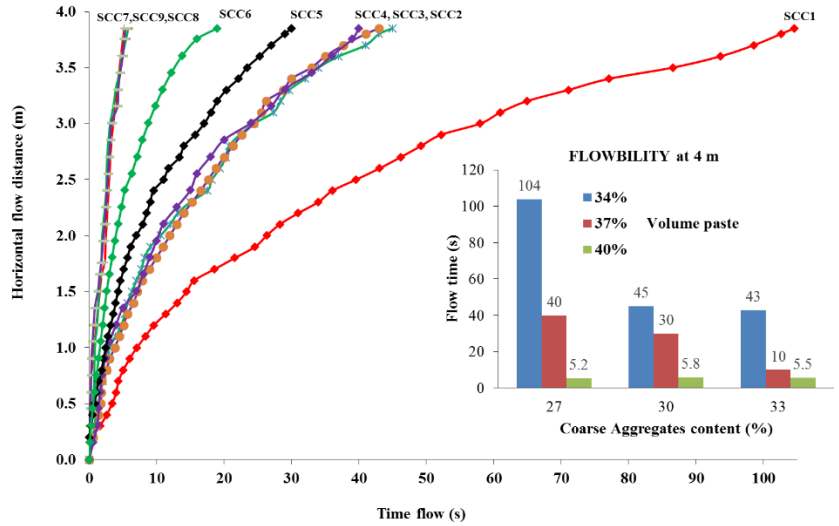

Figure 3. Variations of horizontal flow distance with time of SCC mixtures made with paste volumes of 34%, 37%, and 40%

As can be observed, for the lowest paste volume (i.e. 34%), the increase in coarse aggregate content from 27% to 30%, and 33% resulted in decreasing the flow time from 104 to 45 sec and 42 sec, respectively. Furthermore, in the case of a medium paste volume (37%), the use of high coarse aggregate content (34%) resulted in a significant decrease in flow time. This can be probably due to the higher inertia effect. However, for the highest paste volumes of 40%, the effect of coarse aggregate seems to do not have a significant effect on flowability of SCC (between 5.2 and 5.8 sec). This can be explained by the important excess paste thickness that can contribute in increasing the inter-particles distance, thus reducing the friction and collision between particles.

Effect of coarse aggregate content on dynamic stability

Immediately after casting the reinforced beam, dynamic stability of concrete is determined at every 15 cm along the beam. At each cross section, the test consists in inserting the sensor at two different zones corresponding to 0-12 cm and 8-20 cm from the bottom of the beam. In addition, samples measuring 15x15x15 cm^3 were used to assess the variation of conductivity. The variations of electrical conductivity and dynamic stability indices of various SCC are summarized in Figs. 3.

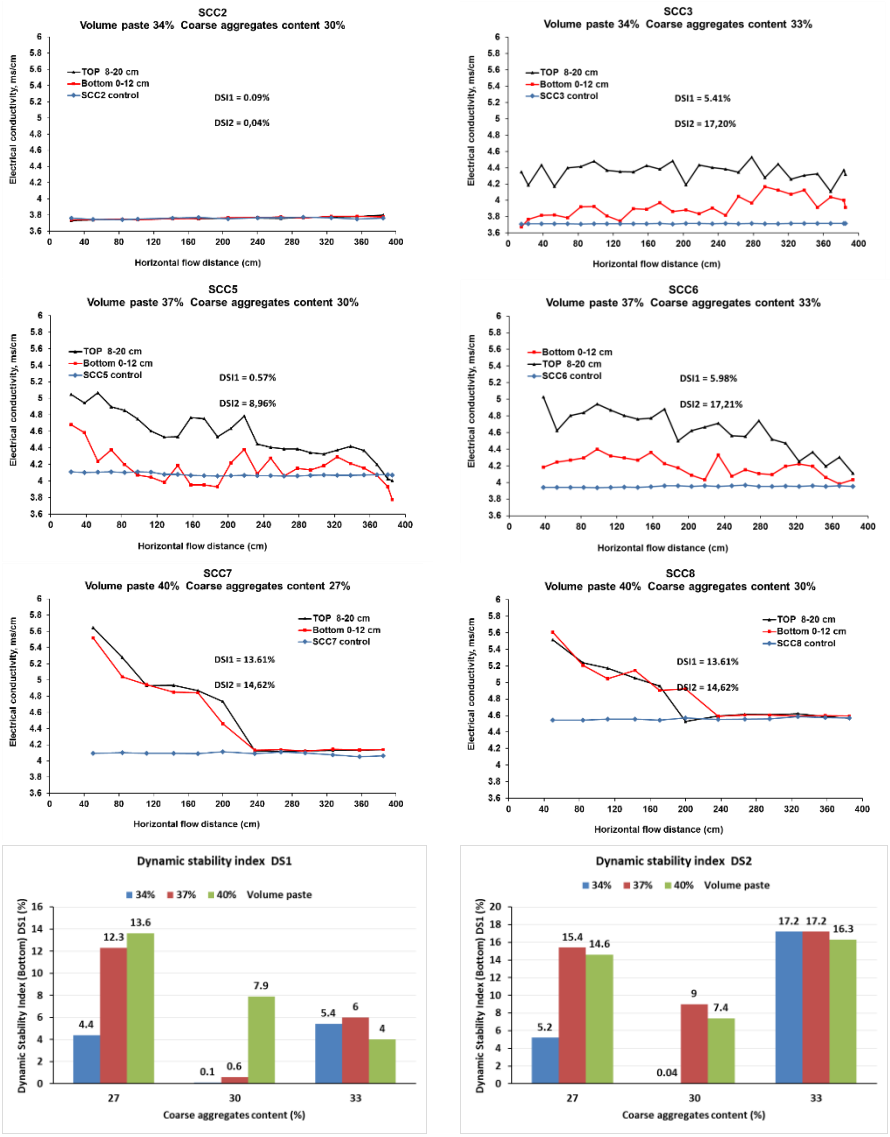

Figure 4. Variations of electrical conductivity and dynamic stability indices of investigated SCC mixtures

Based on the electrical conductivity measurement, two dynamics stability indices (SDI) were defined as follows:

SDI-1 = (average conductivity measured at the top zone along 4 m – Conductivity of control SCC) / (Conductivity of control SCC) x 100

SDI-2 = (average conductivity measured at the bottom zone along 4 m – Conductivity of control SCC) / (Conductivity of control SCC) x 100

In general, the SDI-2 index is higher than the SDI-1 because of the segregation effect that may occur. On the other hand, for a given coarse aggregate content, the dynamic stability increased with the paste volume. A coarse aggregate content corresponding to 30%, by volume, seems to provide an optimum value for dynamic stability, especially in the case of low paste volume of 34%. The differences observed between the electrical conductivity measured at the bottom (0-12 cm) and top (8-20) zones of the beam reflect the dynamic segregation of concrete. The obtained results revealed that SCC mixtures proportioned with coarse content higher than 30%, by volume, showed higher differences between the conductivity values measured at the top and bottom of the beam. This reflects a higher dynamic segregation of concrete. However, in the case of high paste volume (40%) and coarse aggregate of 27 and 30%, by volume, the flow of concrete showed two distinct flow phases (in concordance with reference 2). In the first 2 m of flow, a low aggregate concentration was observed (dominant viscous flow), but a coarse aggregate content equivalent to that of control SCC in the last 2 m of flow distance.

Effect of coarse aggregate content on static stability

The results of static stability measurements are summarized in Table 2. These indices are established using definitions given in Fig. 5 according to reference (2). On the other hand, typical electrical conductivity measurements for SCC mixtures 5 (most stable) and 9 (less stable) are shown in Figs. 6 and 7, respectively.
As can be observed in Table 2, in general, for a given paste volume, SCC mixtures made with higher coarse aggregate content showed less homogeneity that those made with lower coarse aggregate. However, in the case of high paste volume, the effect of aggregate is not significant.

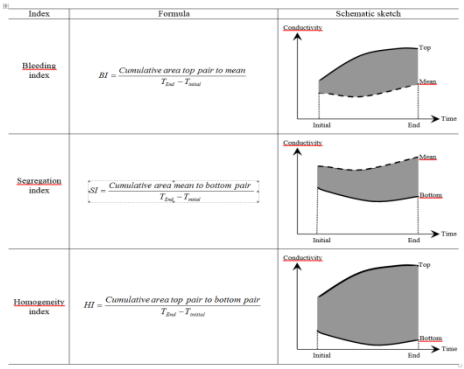

Figure 5. Definition of stability indices [2]

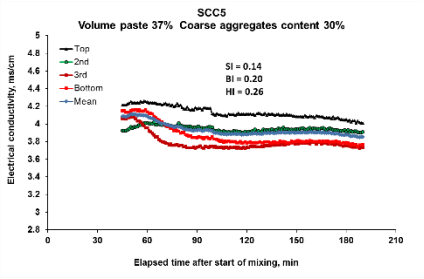

Figure 6. Variation of electrical conductivity of SCC5 mixture (high stability**)**

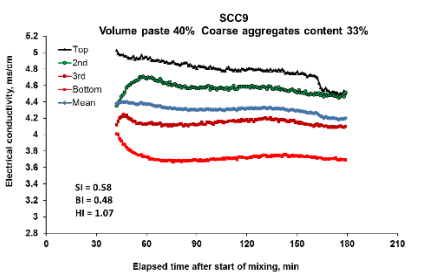

Figure 7. Variation of electrical conductivity of SCC9 mixture (low stability**)**

Correlation between static stability and dynamic stability

Dynamic stability and static stability diagram of the investigated mixtures is presented in Fig. 8. Dynamic stability is calculated as the average of SDI1 and SDI2 indices.

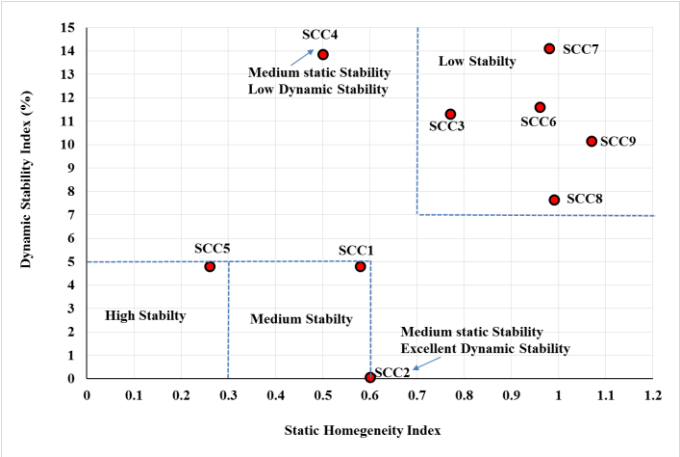

Figure 8. Correlation between static stability and dynamic stability

By comparing workability characteristics of various SCC mixtures, it can be observed that achieving recommended fresh properties, including L-Box, V-funnel, filling capacity, and adequate flow time may not sufficient to ensure good stability performance (i.e., SCC3, and SCC6-9). In the case of SCC mixtures made with 40% paste volume (SCC 7-9), lack of static and dynamic stability is observed, regardless of the coarse aggregate content (27%-33%). Furthermore, SCC made with high coarse aggregate content (33%) showed lack of stability. As expected, there is no relationship between dynamic and static stability of SCC (SCC2 vs. SCC4). For example, SCC2 had a high dynamic stability, but a medium

homogeneity index, while SCC 4 had medium homogeneity index, but low dynamic stability.

Conclusions

The flowability and passing ability of nine SCC mixtures proportioned with different paste volumes and coarse aggregate contents were evaluated in full-scale element casting. Based on the test results, the following conclusions can be drawn:

1. The increase in coarse aggregate content resulted in a significant decrease in flow time (higher velocity) of the SCC, especially in mixtures with relatively low paste volume of 34% and 37%. In the case of SCC with high paste volume of 40%, the coarse aggregate content did not have a significant effect on flow time.
2. A coarse aggregate content corresponding to 30%, by volume, seems to provide an optimum value for static and dynamic stability, especially in the case of low paste volume of 34% and 37%.
3. SCC mixtures made with higher coarse aggregate (33%, by volume) or higher paste volume (40%) can undergo lack of stability. The rheology of suspending phase should be then adjusted given the element to cast and the casting conditions.
4. The flow performance of SCC in full-scale element depends on its stability resistance. The stability performance of SCC should then be selected given the casting direction (vertical vs. horizontal) on hand. A good balance between flowability and stability should be determined by adjusting rheology of suspending phase.

References

[1] H.A. Mesbah, A. Yahia, K.H. Khayat, Electrical conductivity method to assess static stability of self-consolidating concrete, Cement and Concrete Research, Volume 41, Issue 5, May 2011, Pages 451-458

[2] J. Spangenberg, N. Roussel, J.H. Hattel, E.V. Sarmiento, G. Zirgulis, M.R. Geiker,Patterns of gravity induced aggregate migration during casting of fluid concretes, Cement and Concrete Research, Volume 42, Issue 12, December 2012, Pages 1571-1578.

[3] Khayat, K. H. (2005). “Literature Review of Factors Affecting Performance of SCC in Precast Prestressed Applications”, Interim Report NCHRP 18-12, Sherbrooke, Canada.

[4] Khayat, K.H. and Mitchell, D. (2009). “Self-consolidating concrete for precast, prestressed concrete bridge elements.” National Corporative Highway Research Program (NCHRP), Report 628, Transportation Research Board.

[5] Daczko, J. A., and Kurtz, M. A., 2001, “Development of High-Volume Coarse Aggregate Self-Compacting Concrete,” Proceedings of the Second International Symposium on SCC, Oct. 23-25, Tokyo, Japan.

Study on Pumping Pressure Loss of Manufactured Sand Self-Compacting Concrete

Jiang Zhengwu[1], Ren Qiang[1], Chen Qing[1], Yin Jun[1], Tang Haiyan[2]

[1]Key Laboratory of Advanced Civil Engineering Materials of Ministry of Education, Tongji University, Shanghai 201804, China
[2]School of Economics and Management, Tongji University, Shanghai 200092, China

Abstract Due to the angularity, roughness and high-volume stone powder content, manufactured sand(MS) plays a significant role in determining the workability and pumping performance of manufactured sand self-compacting concrete (MSCC). Through utilizing the on-site test of ultra high pumping MSCC, the pumping pressure calculation model (PPCM) of MSCC is established with rheological parameters, including slump *S* and inverted slump cone flow time *T*, based on rheological theory and Kaplan's model in this paper. The effects of manufactured sand characteristics and mix proportion parameters are analyzed on pumping pressure of MSCC with our proposed model. The results show that the higher stone powder content is, the greater the pumping pressure loss becomes; with the increase of fineness modulus, pumping pressure firstly decreases and then increases. Meanwhile, the pumping pressure of MSCC presents a trend of gradual reduction with the increase of water-binder ratio (W/B). The influence of the cementitious material consumption and fly ash (FA) content is similar with those of the fineness modulus of MS. However, the effects are opposite when the sand ratio is considered.

Keywords: *manufactured sand; self-compacting concrete; rheology; pumping pressure; calculation formula.*

Introduction

With the good workability and comprehensive properties, self-compacting concrete (SCC) has been widely used in hydraulic engineering, tunnels, etc. More and more manufactured sand (MS) has been utilized as an alternative in self-compacting concrete (SCC) since the natural sand (NS) resources has been increasingly scarce in the west of China [1~3].

To well predict the onsite pumping behavior of concrete and carry out project construction effectively, many valuable works have been conducted on the calculation of concrete pumping pressure, which aims to find an empirical formula to predict the onsite pumping performance. On the basis of S.Morinaga formula, Zhang SJ [4] proposed that apart from the effects produced by the elbow, tapered tube, hose structures, the cut-off valve, distributing valve and the pump body the resistance from the horizontal, inclined and vertical section of pipes should be also taken into considerations to calculate the total concrete pumping pressure loss. Wu BX etc. [5] validated the formula in [4] was not well suitable for the calculation of pumping pressure loss of high-performance concrete (HPC). Kaplan etc. [6] built up a relationship between the pressure and flow by using the Bingham and Buckingham-Reiner model, and applied the yield stress τ_{0i} and plastic viscosity μ_i of lubrication layer, the yield stress τ_0 and plastic viscosity μ of concrete to calculate the pressure. However, this model is difficult to popularize in the practical engineering, since the complex measurement device and big area space are needed to obtain the required parameters [7, 8].

Compared with the conventional concrete, MSCC presents a different pumping pressure loss phenomenon in the pumping process because of the characteristics, including lower W/B, high-volume stone powder content in MS, large-dosage cementitious materials and mineral admixtures. Very few models can be applied to calculate the pumping pressure loss for MSCC. In this paper, through utilizing the on-site test of ultra high pumping MSCC, the pumping pressure calculation model (PPCM) of MSCC was established with rheological parameters, including slump *S* and inverted slump cone flow time *T*, based on rheological theory and Kaplan's model. And then the effects of manufactured sand characteristics and mix proportion parameters were analyzed on pumping pressure of MSCC with our proposed model in part 3.

Derivation of pumping pressure loss calculation formula of MSCC

Fresh concrete is often regarded as a Bingham fluid. Based on Kaplan's concrete pumping pressure calculation model [6], the pumping pressure loss of concrete can be obtained by Eq. (1):

$$P = \frac{2L}{R}\left(v_g\mu_i + \tau_{0i}\right) = \frac{2L}{R}\left(\frac{\frac{Q_t}{\pi K_r \cdot 3600} - \frac{R}{4\mu}\tau_{0i} + \frac{R}{3\mu}\tau_0}{1 + \frac{R}{4\mu}\mu_i}\mu_i + \tau_{0i}\right)$$

$$= \frac{2L}{R}\left(\frac{\frac{Q_t \cdot \mu_i}{\pi K_r \cdot 3600} + \frac{R}{3\mu}\tau_0 \cdot \mu_i - \left(1 + \frac{R}{4\mu}\mu_i\right)\tau_{0i} + \tau_{0i}}{1 + \frac{R}{4\mu}\mu_i}\right)$$

$$= \frac{2L}{R}\left(\frac{\frac{Q_t \cdot \mu_i}{\pi K_r \cdot 3600} + \frac{R}{3\mu}\tau_0 \cdot \mu_i + \tau_{0i}}{1 + \frac{R}{4\mu}\mu_i}\right) \quad (1)$$

where P is the pumping pressure loss of the concrete (MPa), Q_t is the total flow of the concrete (m^3/h), v_g is the slip rate (m/s), L is the total length of pipes (m), R is the radius of pipe (m), K_r is the filling coefficient, μ is the plastic viscosity of the concrete (Pa·s), τ_0 is the yield stress of the concrete (Pa), μ_i is the plastic viscosity of the lubrication layer (Pa·s), τ_{0i} is the yield stress of the lubrication layer (Pa).

Tanigawa etc. [9] and Ferraris [10] found out there existed a linear relation between the yield stress τ_0 of HPC and slump S in the case S is more than 200mm.

$$\tau_0 = AS + B \quad (2)$$

Hu XF [11] and Wu XL [12] concluded the plastic viscosity μ of the concrete was a function of slump S and inverted slump cone flow time T in the case S is more than 200mm.

$$\mu = ET(S + F) \quad (3)$$

Kaplan [13] and Chapdelaine [14] draw a conclusion that the yield stress τ_{0i} and plastic viscosity μ_i of the lubrication layer increased linearly with the yield stress τ_0 and plastic viscosity μ of the concrete.

$$\tau_{0i} = C'\tau_0 + D' \quad (4)$$

$$\mu_i = G'\mu + H' \quad (5)$$

Although their works may not be general conclusions [9-14], these assumptions are still adopted in our research for simplifications. The verifications in Section 2.2 show that these assumptions are reasonable for our proposed model. Based on equation (2)-(5), the following relations can be reached :

$$\begin{cases} \tau_0 = AS + B \\ \tau_{0i} = CS + D \end{cases} \qquad \begin{cases} \mu = ET(S + F) \\ \mu_i = GT(S + H) \end{cases} \quad (6)$$

where A, B, C, D, E, F, G, H, C', D', G', H' are the constants, S is the slump of MSCC (mm), T is the inverted slump cone flow time of MSCC (s).

By substituting Eq. (6) into (1), Eq. (7) can be derived as below:

$$P = \frac{2L}{R} \cdot \frac{(Q_t aT + b)S^2 + (Q_t cT + d)S + Q_t eT + f}{S + m} \quad (7)$$

It is noted that Eq. (7) calculates the pumping pressure along the way P_{along}. The total pumping pressure P_{total} will be reached by adding the weight $P_{gravity}$ of MSCC, which is expressed as Eq. (8).

$$\begin{aligned} P_{total} &= P_{along} + P_{gravity} \\ &= \frac{4L}{D} \cdot \frac{(Q_t aT + b)S^2 + (Q_t cT + d)S + Q_t eT + f}{S + m} + \rho gH \end{aligned} \quad (8)$$

where a ,b, c, d, e, f, m are the constants, P_{total} is the pumping pressure of MSCC, namely the total pumping pressure loss (MPa), P_{along} is the pumping pressure along the way (MPa), $P_{gravity}$ is the dead weight (MPa), D is the diameter of the pipe (m), ρ is the bulk density (kg/m^3), H is the total height of pumping (m), g is the acceleration of gravity (m/s^2), g=9.8 m/s^2. The parameters Q_t, L, D, S, T, H can be tested in the pumping construction onsite, with which the values of the constants a, b, c, d, e, f, m can be obtained by numerical fitting procedures. Finally, the pumping pressure calculation model (PPCM) of MSCC (Eq. (8)) can be established with the slump S and inverted slump cone flow time T.

Establishment of pumping pressure loss calculation formula of MSCC

Materials and mix proportion

Raw materials at the jobsite of Qingshuihe bridge are as follows: P·O 52.5 Conch cement, Ⅱ FA from Guizhou Qianxi liyuan environmental development co., LTD (water demand ratio of 97%, loss on ignition of 7.4%, fineness of 23.4%), Limestone MS (stone powder content of 11%, fineness modulus of 2.78, MB value of 0.8), Polycarboxylate superplasticizer (PCS). Two types of coarse aggregates are used. The size of large aggregates ranges from 9.5 mm to 26.5 mm and that of small one is from 4.75 mm to 9.5 mm. The construction mix proportion of C50 MSCC was seen in table Ⅰ.

Table I. The construction mix proportion of C50 MSCC

Cementitious materials consumption/ kg/m^3	FA content /%	W/ B	Sand ratio/ %	Large stone: small stone	PCS content /%	Bulk density/ kg/m^3
500	22	0.31	46	8:2	1.2	2500

Establishment of pumping pressure loss calculation formula of MSCC

Eight parameters are tested during the process of pumping at the jobsite, which are respectively *P, Q_t, S, T, L, H, D, ρ*. *P* can be read from the pressure gauge on the pump truck. By recording the volume of concrete tank truck *V* and time difference T_{td} between the starting and ending pumping, Q_t can be calculated with the formula of $Q_t = V/T_{td}$. *L, H, D* can be measured easily. *S, T* can be tested by slump test and inverted slump test by using the concrete from truck during pumping respectively. And among them, *D*=0.125m, *ρ=2450*kg/m^3. Then 20 sets of data of different parameters, as shown in table Ⅱ, were chosen to calculate *a, b, c, d, e, f, m* by using least square method, which were given in table Ⅲ.

Table II. The pumping parameters recorded during pumping

Number	*P* /MPa	Q_t /m^3/h	*S* /mm	*T* /s	*L* /m	*H* /m
1	16.260	25.153	260	2.8	211.4	178.2
2	15.800	24.615	265	3.5	211. 4	178.2
3	16.470	24.406	252	4.4	211. 4	178.2
4	16.530	25.600	255	2.9	211.4	178.2
5	16.200	28.235	255	3.0	217.1	178.0
6	16.600	26.667	260	3.4	217.1	178.0
7	15.207	26.667	255	2.9	217.1	178.0
8	16.041	26.544	250	4.7	217.1	178.0
9	15.774	26.544	260	4.2	217.1	178.0
10	15.300	26.301	260	3.3	217.1	178.0
11	16.730	25.263	240	3.7	223.1	184.0
12	16.555	25.600	265	2.5	223.1	184.0
13	17.578	26.916	255	4.8	223.1	184.0
14	17.833	26.916	250	4.7	223.1	184.0
15	16.370	28.374	255	2.2	229.4	196.2
16	15.278	29.388	265	1.7	229.4	196.2
17	17.663	27.692	250	4.0	229.4	196.2
18	16.685	27.042	265	3.1	229.4	196.2
19	17.481	27.826	260	4.0	229.4	196.2
20	16.789	30.968	260	2.1	229.4	196.2

Table III. The nonlinear fitting results by Matlab

Constants	*a*	*b*	*c*	*d*	*e*	*f*	*m*
Results	0	0	0	3.0	4.1	-384.9	4.264×10^5

With these values, Eq. (8) can be rephrased as

$$P_{total} = \frac{4L}{D} \cdot \frac{3S + 4.1Q_tT - 384.9}{S + 4.264 \times 10^5} + \rho gH \times 10^{-6} \quad (9)$$

Considering the value of slump S is far lower than 4.264×10^5, it can be omitted in the denominator. Therefore, the calculation formula of pumping pressure of MSCC was set up as follows (Eq. (10)):

$$P_{total} = \frac{4L}{D} \times \frac{S \times 3MPa + Q_tT \times 4.1\frac{KPa \bullet h}{m^2 \bullet s} - 384.9MPa \bullet mm}{4.264 \times 10^5 mm} + \rho gH \times 10^{-6} \quad (10)$$

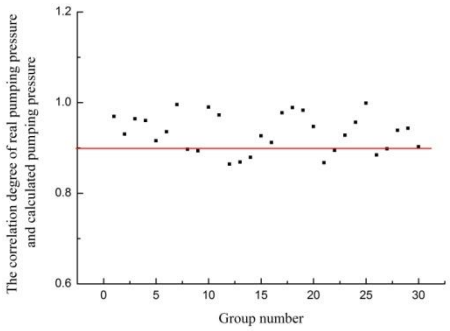

Note: the calculation method of correlation degree: correlation degree =[max(the real pumping pressure, the calculated pressure)-min(the real pumping pressure, the calculated pressure)]/max(the real pumping pressure, the calculated pressure)

Figure 1. The correlation degree of the real and calculated pumping pressure

In order to verify the accuracy of the calculation formula, another 30 sets of the real pumping pressure and calculated pressure were compared, as illustrated in Figure 1. The results demonstrate the correlation degree is larger than 0.90, implying a good agreement. Therefore, it is feasible and reasonable to calculate and predict the pumping pressure loss of MSCC using Eq. (10) quickly.

Effect of manufactured sand characteristics and mixture parameters on the pumping pressure loss of MSCC

Researches show both the aggregate characteristics [15] and mixture parameters [16] have a great effect on the pumpability of concrete. Besides, MS with the different angularity, roughness and stone powder content will generate a different mixture which leads to the different rheological performances of MSCC. Thus, in this section, the raw materials at the jobsite were applied. The reference mix proportion was shown in table Ⅳ. On the foundation of the reference mix

proportion, fix the other parameters except the one which will be discussed, and adjust the superplasticizer content properly. And then, the effects of both MS characteristics (stone powder content and fineness modulus) and mixture parameters (cementitious material consumption, W/B, FA content and sand ratio) on the predictive value of pumping pressure (PVPP) which is calculated by Eq. (10) are studied based on our proposed model.

Table IV. Reference mix proportion and workability of C50 MSCC

Cementitious material consumption/kg/m^3	W/B	FA content/%	Sand ratio/%	Stone powder content/%	PCS content/%	T/ mm	T_d/s
500	0.32	20	50	11	1.106	230	18

For simplification, the values of L, H, D, Q_t, ρ are set to be 100m, 80m, 0.125m, 25m^3/h, 2450kg/m^3, respectively. And the PVPP will be obtained by using the slump S and inverted slump cone flow time T which can be tested in each case.

Effect of manufactured sand characteristics on the pumping pressure loss of MSCC

Stone powder content. Three types of MSCC with different stone powder content (0, 11%, 17%), as exhibited in Table Ⅴ, are utilized to illustrate the effects of stone powder content on the predictive value of pumping pressure (PVPP).

Table V. The effect of MSCC with different stone powder content on the PVPP

Stone powder content /%	PCS content /%	S /mm	T /s	PVPP /MPa
0	1.106	210	11.2	12.414
11	1.106	230	18.0	18.057
17	1.106	220	44.5	38.216
	1.331	230	17.8	17.918

It can be reached that the effect of stone powder content on the pumping pressure of MSCC is of great significance. When superplasticizer content is the same, the higher stone powder content is, the larger the pumping pressure loss becomes. At the same time, the PVPP is reduced significantly by increasing PCS content properly.

Fineness modulus. Different sand fineness modulus (2.45, 2.78, 3.20) are employed to investigate their effects on PVPP, which is showed in table Ⅵ.

Table VI. The effect of MSCC with different fineness modulus on PVPP

Fineness modulus	PCS content /%	*S* /mm	*T* /s	PVPP /MPa
2.45	1.106	220	62.3	51.908
	1.533	255	14.5	15.927
2.78	1.106	230	18.0	18.057
3.20	1.106	225	28.0	25.636

It can be found that the effect of fineness modulus on the pumping pressure loss is also remarkable. Under the same PCS content, the PVPP decreased first and then increased with the increase of fineness modulus. This is because too large fineness modulus will make the gradation of MS unsuitable, resulting in the worse workability of mixture. While fineness modulus is smaller, water demand would be increased. In addition, the pumping pressure loss can be reduced by enlarging the dosage of PCS for the mixture of the lower fineness modulus.

Effect of mixture parameters on the pumping pressure loss of MSCC

Cementitious material consumption

Table VII. The effect of MSCC with varied cementitious material content on PVPP

Cementitious material consumption /kg/m^3	PCS content /%	*S* /mm	*T* /s	PVPP /MPa
480	1.106	220	34.0	30.139
	1.376	210	25.2	23.145
	1.526	225	32.7	29.252
500	1.106	230	18.0	18.057
520	1.106	235	51.9	44.246
	1.386	240	35.0	31.359

Table VII shows the influence of cementitious material consumption(480kg/m^3, 500kg/m^3, 520kg/m^3) on PVPP. It can be obtained that the PVPP decreased firstly and then increased as the cementitious material consumption becomes bigger.

3.2.2 W/B.

Table VIII. The effect of MSCC with different W/B on PVPP

W/B	PCS content /%	*S* /mm	*T* /s	PVPP /MPa
0.31	1.406	210	74.7	61.222
0.32	1.106	230	18.0	18.057
0.34	1.106	255	9.0	11.735

Table VIII shows that PVPP presented a trend of decrease with the increase of W/B. The PVPP are respectively 61.222, 18.057 and 11.735 when the W/B is 0.31,0.32 and 0.34.

FA content. The effect of MSCC with different amounts of FA (20%, 30%, 40%) on the PVPP was studied (table Ⅸ).

Table IX. The effect of MSCC with different FA content on PVPP

FA content/%	PCS content/%	S/mm	T/s	PVPP/MPa
10	1.106	220	25.7	23.755
20	1.106	230	18.0	18.057
30	1.106	245	30.8	28.240
	1.331	230	17.8	17.918

When the PCS content holds the same, the PVPP decreased first and then increased with the increase of FA content. At the very beginning, the rheological performance of mixture becomes better with the increase of FA dosage due to the ball effect. However, once the content reaches a threshold, water demand of mixture becomes larger because of the high ignition loss. In addition, the pumpability of concrete will be improved obviously by enlarging PCS content.

Sand ratio.

Table X. The effect of MSCC with different sand ratios on PVPP

Sand ratio /%	PCS content /%	*S* /mm	*T* /s	PVPP /MPa
50	1.106	230	18.0	18.057
55	1.106	240	65.0	54.436
	1.219	235	28.3	26.092
60	1.106	225	63.0	52.559
	1.406	255	19.0	19.389

From Table Ⅹ, it can observed that different sand ratios (50%, 55%, 60%) also have a notable impact on the pumping pressure of MSCC. When PCS content kept constant, the PVPP increased first and then decreased with the increase of sand ratio. And the PVPP can be reduced obviously by increasing PCS content.

Conclusions

To predict the concrete pumping pressure accurately and reasonably is a key factor to guarantee the normal construction in the progress of pumping concrete. Through utilizing the on-site test of ultra high pumping MSCC, the pumping pressure

calculation model of MSCC was established with rheological parameters, including slump *S* and inverted slump cone flow time *T*, based on rheological theory and Kaplan's model in this paper. The effects of manufactured sand characteristics and mix proportion parameters were analyzed on pumping pressure of MSCC with our proposed model. The work carried out in this project led to the following results.

1. The proposed model is feasible and capable to calculate the pumping pressure loss of MSCC.

2. Manufactured sand characteristics have a significant influence on the pumping pressure loss of MSCC. The higher stone powder content is, the greater the pumping pressure loss becomes; with the increase of fineness modulus, pumping pressure firstly decreases and then increases.

3. Mixture parameters also have a remarkable effect on the pumping pressure loss of MSCC. With the increase of water-binder ratio, the pumping pressure presents a trend of gradual reduction. With the increase of the cementitious material consumption and fly ash content, the pumping pressure firstly decreases and then increases. However, the pumping pressure firstly increases and then decreases with the increase of sand ratio.

Acknowledgments

The authors would like to acknowledge the financial support for this study by the National Natural Science Foundation of China (51478348, 51278360, 51308407), the National Basic Research Program of China (2011CB013805), the National Technology Support Program of China (2014BAL03B02), and the Specialized Research Fund for the Doctoral Program of Higher Education (20130072110047).

References

[1] Jiang ZW, Sun ZP, Wang PM. (2005). *Cement Concrete Res*., vol. 35, n. 8, p. 1539-1545.
[2] Jiang ZW, Pan F, Wu JL, et al. (2011). *China Concrete*, n. 8, p. 66-70.
[3] Jiang ZW, Huang QY, Xiao X, et al.(2013). *China Concrete*, n. 1, p. 35-42.
[4] Zhang SJ, Yang XH. (2010). *Construction Machinery*, n. 3, p. 99-101.
[5] Wu BX, Chen BG, Xu JH, et al.(2011). *Concrete*, n. 01, p. 142-144.
[6] Kaplan D, De Larrard F, Sedran T. (2005). *Aci Mater. J*., vol. 102, n. 2, p. 110-117.
[7] Zheng J. (2009). *Commercial Concrete*, n. 9, p. 43-44.
[8] Feys D, Khayat K H, Perez-Schell A, et al. (2015). *Cement Concrete Comp*., n. 57, p. 102-115.
[9] Tanigawa Y, Mori H, Nagoya. (1998). Journal of University of Jinan (Science and Technology). vol. Z1, p. 43-53.

[10] Ferraris C F, Martys N S. (2003). J. Res. NATL Inst. Stan., vol. 108, n. 3, p. 229-234.
[11] Hu XF, Su ZX. (2006).*Concrete*. n. 8, p. 64-69.
[12] Wu XL. (2013). *The Simulation Analysis of Rheological Properties of Fresh Self-Compacting Concrete Based on V-funnel Test Technology.* Pm.D. Nanhua University, Hunan.
[13] Kaplan D. (2001). *Pumping of Concretes.* Ph.D. Central Laboratory Roads and Bridges, Paris.
[14] Chapdelaine F. (2007). *Fundamental and practical study on pumping of concrete*. Ph.D. Laval University, Laval.
[15] Choi M S, Kim Y J, Kwon S H. (2013). *Cement Concrete Res*., vol. 52, n. 10, p. 216–224.
[16] Mechtcherine V, Nerella V N, Kasten K. (2014). Constr. Build Mater., vol. 53, n. 2, p. 312-323.

Theme 6: Mechanical and Physical Properties of SCC

Modelling the Early Age Drying Shrinkage and Cracking Risk of SCC

Gonzalo Barluenga, Javier Puentes and Irene Palomar

Department of Architecture, University of Alcala, Madrid (Spain)

Abstract Early age water evaporation causes shrinkage on cement based materials that increases cracking risk, which can compromise durability. However, it has been observed that there is not a direct relationship among drying, shrinkage and cracking at early age (EA). The composition of the mixture, the particle size distribution and the type of supplementary cementitious material (SCM) have a strong impact on those EA related parameters. SCC is characterized by the large amount of paste and is prone to EA drying shrinkage, which can increase cracking.
An experimental study was carried out to evaluate the effect of different types and amounts of SCM, as filler or active mineral additions (AMA) on the EA drying shrinkage and cracking risk of SCC pastes and SCC mixtures subjected to intense water evaporation. Several physical parameters related to the role of water on the EA performance of SCC mixtures were monitored for 24 hours: water evaporation rate, capillary pressure, drying free shrinkage, temperature and P- and S- waves' ultrasonic transmission.
Free drying shrinkage was correlated to the composition of the pastes and SCC and to the evaporation rates. The values were compared to a reference SCC paste. Moreover, some equations were established. The effect of the volumetric fraction of cement, filler, AMA and aggregate was also considered.
The cracking risk was assessed on double restrained slabs subjected to intense evaporation. The monitored EA parameters were jointly analysed to identify the stress and the sequence of changes in the solid microstructure. The stress level was calculated with the free shrinkage and the Young modulus obtained from the ultrasonic P- and S- wave transmission velocities. The changes on the material were monitored by the capillary pressure and the ultrasonic measurements. The integrated analysis allowed identifying the most adverse combinations of stress intensity and the sequence of changes of the water related parameters that led to larger EA drying cracking risk.

Keywords: *SCC, Supplementary cementitious Materials, Evaporation, Free shrinkage, Early age cracking.*

Introduction

Self-compacting concrete (SCC) is characterised by its flowability in the fresh state, achieved by the use of larger amounts of paste than in conventional concrete (CC). More paste implies more fine particles and more water in the mixture. Fines can be of many different natures, producing a filler effect and pozzolanic activity in some cases. Some water related problems, as evaporation and shrinkage [1], can also occur leading to increased cracking risk [2, 3], which can seriously compromise durability. Due to its composition, SCC shows some differences during early age (EA) [4, 5]. Nevertheless, SCC has been reported to achieve similar hardened mechanical properties to CC [6].

At EA, main changes on the material take place due to the hydration-related setting and early hardening. The cement hydration and early pozzolanic reactions lead to the formation of both the solid and porous hardened microstructure [7]. Accordingly, the percolation process leads to a solid skeleton which also configures a pore network. The solid skeleton is initiated by the initial solid percolation (grain connection) and followed by the pore filling by the hydration products [8]. Grain connection has been identified to be related to the stiffening of the material while the pore filling is responsible for the strength development due to the thickening of the particle bridging. The characteristics of the pore network is responsible of the capillary pressure development (jointly with the water demand of the cement hydration) and shrinkage (jointly with self-desiccation in the case of autogenous shrinkage or drying due to evaporation).

Many parameters can be monitored at EA to follow the evolution of the material, as calorimetric measurements, transmission techniques [9-11], dimensional stability [2, 4], water related parameters [12] and mechanical direct testing [13], among others. However, a combined simultaneous monitoring of several parameters has been demonstrated to be needed in order to identify the multiple processes that take place in a cement based material during EA [4, 7, 8, 14,]. SCC shrinkage models have been proposed [15], but with poor predictions at EA.

In this paper, the EA drying cracking risk of SCC with different types and amounts of supplementary cementitious materials is evaluated. The experimental results of several EA parameters jointly with the cracking results of double restrained slabs subjected to intense surface drying were measured. The effect of composition and environmental conditions on EA shrinkage was analysed [16]. The theoretical stress demand was calculated and a sequential model to explain when this stress demand would fully apply was proposed.

Materials and Methods

A CEM I 42.5 R cement type, a siliceous aggregate (gravel –G- and sand –S), a limestone filler, condensed microsilica (MS), water dispersed colloidal nanosilica (NS), metakaolin (MK) and a high range water reducing admixture (HRWRA) were used. The reference SCC paste contained only cement, which was replaced by different amounts of SCM: limestone filler and active mineral additions (AMA). The mix designs of the SCC era given in Table 1. SCC pastes were manufactured with an identical relative amount of components as the SCC but without aggregates.

Table I. SCC Mixture compositions (kg/m3). (*) Liquid water added. (**) Water content from sand humidity (6.25 %), HRWRA and nano-silica was also considered.

	HREFG	HCA5	HCA75	HCA10	HCAMS 25	HCAMS 5	HCAMS 10	HCANS 25	HCANS 5	HCAMC 25	HCAMC 5
Cement	700	466	400	350	350	350	350	350	350	350	350
G (4-20)	790	790	790	790	790	790	790	790	790	790	790
S (0-4)	691	691	691	691	691	691	691	691	691	691	691
Filler	-	233	300	350	341	332	315	341	332	341	332
MS	-	-	-	-	8.75	17.5	35	-	-	-	-
NS	-	-	-	-	-	-	-	39.7	79.4	-	-
MK	-	-	-	-	-	-	-	-	-	8.75	17.5
Water (*)	199	202	203	204	204	204	204	173	142	204	204
HRWRA	10.5	7	6	5.25	5.25	5.25	5.25	5.25	5.25	5.25	5.25
W/c (**)	0.36	0.71	0.71	0.71	0.71	0.71	0.71	0.71	0.71	0.71	0.71
W/f (**)	0.36	0.36	0.36	0.36	0.36	0.36	0.36	0.36	0.36	0.36	0.36

SCC pastes (without aggregates) and SCC samples were produced. The samples were cast in molds and monitored during 24 hours after mixture. The EA testing setup included evaporation and free shrinkage measurements of 500x100x50 mm samples subjected to a 3 m/s airflow for 6 hours. Temperature and capillary pressure at 15 and 35 mm depth were measured on 15x10x10 samples and ultrasonic pulse velocity (UPV) of P- and S- waves were measured on 60x100x40 mm samples. A double restrained slab test (400x400x40 mm SCC paste samples and 900x600x50 SCC samples), also submitted to a 3 m/s airflow for 6 hours, was used to evaluate the drying cracking risk of the mixtures at EA. Full descriptions of the experimental setup have been already published [7, 14].

Experimental Results

Table II reports the experimental results of SCC pastes and SCC mixtures of Evaporation rate during 6 hours and EA free drying shrinkage of 500 mm long samples under forced surface desiccation. It also presents the results of cracked area of double restrained slabs also subjected to intense evaporation (4000x400x40 mm for SCC pastes and 900x600x50mm for SCC). The double restraining applied during the first 24 hours and the cracks were measured at 7 days [7].

Table II. Evaporation rate (kg/m^2 h), free shrinkage (mm/m) and early age cracking (mm^2/m^2) of SCC pastes and SCC mixtures at EA.

	HREFG	HCA5	HCA75	HCA10	HCAMS 25	HCAMS 5	HCAMS 10	HCANS 25	HCANS 5	HCAMC 25	HCAMC 5
SCC pastes											
Ev. rate	0,35	0,51	0,57	0,49	0,53	0,55	0,43	0,52	0,43	0,53	0,45
EA Shr.	2,42	2,14	1,96	1,76	2,36	1,94	4,62	2,66	4,36	2,38	4,26
Cr. Area	1075	1412	478	547	2504	2624	721	3771	595	5286	2052
SCC											
Ev. rate	0,38	0,43	0,42	0,54	0,34	0,44	0,45	0,48	0,41	0,45	0,42
EA Shr.	0,58	0,42	0,96	1,38	0,46	0,88	1,6	0,54	1	0,8	1,6
Cr. Area	0	10	74	345	71	365	1271	110	1923	205	536

It was observed that the evaporation rate was very similar for pastes and SCC, because the large amount of paste completely covered the external upper surface which was subjected to forced evaporation [7]. On the other hand, shrinkage and cracking increased with the amount of AMA. However, no linear relation was observed between shrinkage and cracked area.

Temperature evolution of some SCC mixtures has been published elsewhere [7], and follows a conventional three stage pattern (dormant, acceleration and cooling). Temperature increase is due to the cement hydration that is an exothermal reaction. However, every mixture evolves differently regarding time, which makes difficult the direct comparison among the results of different mixtures, as it has been described elsewhere [7]. In order to facilitate the comparison, a reaction degree (R_d) was defined as the ratio of heat released at any moment regarding the total heat released at 24 hours [14]. UPV is related to the microstructure evolution and the mechanical capacity development of the material. P-wave can be measured form the beginning, because it can propagate through water, while S-wave can only propagate through solid and appeared later [8]. P-wave increasing implies the stiffening of the material while the appearance of S-wave reading is related to

strength development. The combination of both waves allowed the calculation of Young modulus (E) and Poisson coefficient (ν).

Early age cracking evaluation

EA cracking of SCC pastes and SCC mixtures was assessed considering three different approaches: The amount of EA drying shrinkage, monitored during 6 hours after casting, that motivates the EA cracking measured in this study; the theoretical stress demand that would apply to the samples, calculated considering the imposed deformation (free shrinkage) and the microstructural evolution (UPV); and the time sequence of stress demand and the development of strength capacity.

Early age Shrinkage correlation model

EA drying shrinkage of any composition can be related to the volumetric fraction of each component of the mixture, both the paste phase and the aggregate. The effectiveness of each paste component would depend on its physical and chemical performance, which can be related primarily to particle size and reactivity respectively. The amount of aggregate will also affect EA shrinkage, according to Pickett model [1]. A third component related to the evaporation rate at EA can also be taken into account. Accordingly, it can be considered that the expected shrinkage of a certain composition ($\varepsilon_{Sh,i}$) will be that of a SCC reference paste only with cement ($\varepsilon_{Sh,r}$) affected by three factors Eq. (1) [15]:

$$\varepsilon_{Sh,i} = k_3 \cdot \varepsilon_{Sh,r} \cdot \frac{\left(\sum V_{comp} \times C_{comp}\right)}{V_{cem_r}} \cdot \left(1 - V_{agg}\right)^n \cdot \left(\frac{Ev_i}{Ev_r}\right)^m \quad (1)$$

Where the first factor is the sum of the volumetric fraction of each component (V_{comp}) multiplied by an effectiveness coefficient (C_{comp}) (coefficient values: C_{cem}=1; C_{filler}=0.55; C_{MS}=25; C_{NS}=C_{MC}=45), divided by the volumetric fraction of cement of the reference mixture ($V_{cem,r}$). The second is the Pickett model of shrinkage, where V_{agg} is the volumetric fraction of the aggregate (zero for the paste samples and the values reported in Table1 for concrete compositions). The third factor is the Evaporation ratio of each mixture (Ev_i) regarding the reference SCC paste (Ev_r). The coefficients used to adjust the estimated to the measured values were: k_3=1.14; n=0.5; m=0.25 (R^2=0.944) [15].

Stress demand evaluation

The stress demand is a second approach that arises when modeling the EA cracking risk. The stress demand can be estimated considering jointly the stiffening of the material during the setting-hardening process and the deformation imposed to the

specimen at EA. The former can be assimilated as the Young Modulus and the later as the free shrinkage.

UPV Young Modulus (E) of the SCC mixtures were calculated form the UPV monitoring tests, according to Eq. (2), after obtaining Poisson coefficient (ν) with Eq. (3) [9]:

$$E = 2 \cdot \rho \cdot v_s^2 (1+\nu) \quad (2)$$

$$\nu = \left(0.5 v_p^2 - v_s^2\right) / \left(v_p^2 - v_s^2\right) \quad (3)$$

Where ρ is the apparent density (g/cm^3) and v_p and v_s are the P- and S-wave velocities (m/s), respectively. Figure 1 plots the evolution of E during the EA. In order to better compare the different mixtures, the reaction degree (R_d) were considered instead of time. R_d was calculated as the fraction of the heat released at any point during the test realted to the total heat released after the first 24 hours [14]. It can be seen that the use of silica-based AMA (MS and NS) accelerated the increase of the SCC Young modulus.

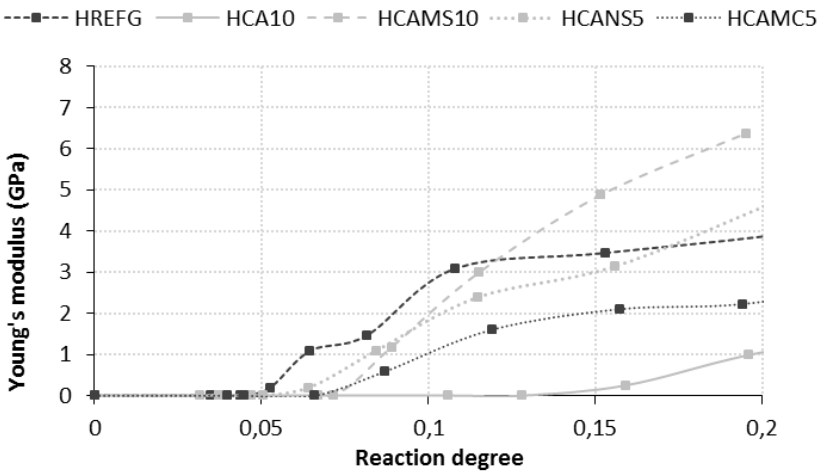

Figure 1. Young modulus of SCC mixtures calculated using p- and s-wave UPV at EA.

The effect of E increase would be the amplified effect of EA shrinkage on stress demand development in the material. The tensional stress demand (σ) was calculated according to Eq. (4):

$$\sigma = E^*(\Delta L/L) \quad (4)$$

Where E is the Young elastic modulus, obtained from transmission velocity of S- and P –waves (Eq. 2), and (ΔL/L) is the free shrinkage of the material during EA. Figure 2 plots the evolution of σ of some SCC mixtures. The SCC with AMA showed the fastest σ evolution at EA, as it was expected from the cracking results reported in Table II.

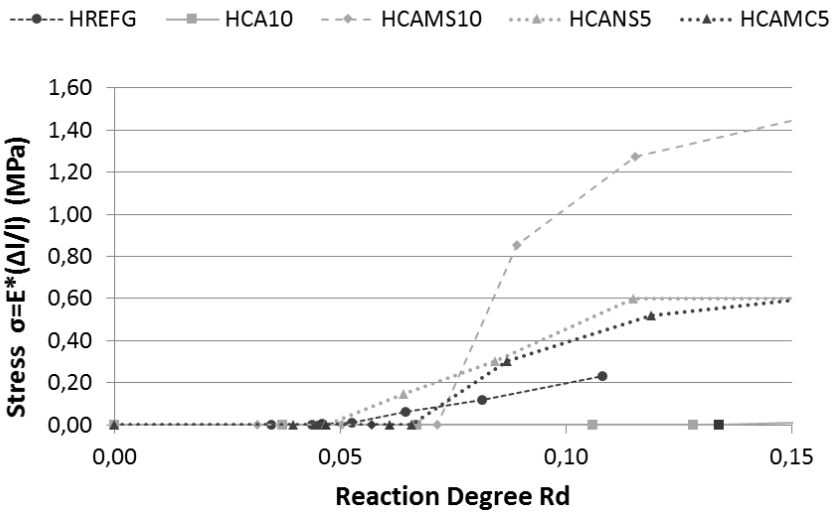

Figure 2. Stress demand of SCC mixtures calculated based on UPV Young modulus and free shrinkage at early age.

Sequential model of SCC EA drying cracking

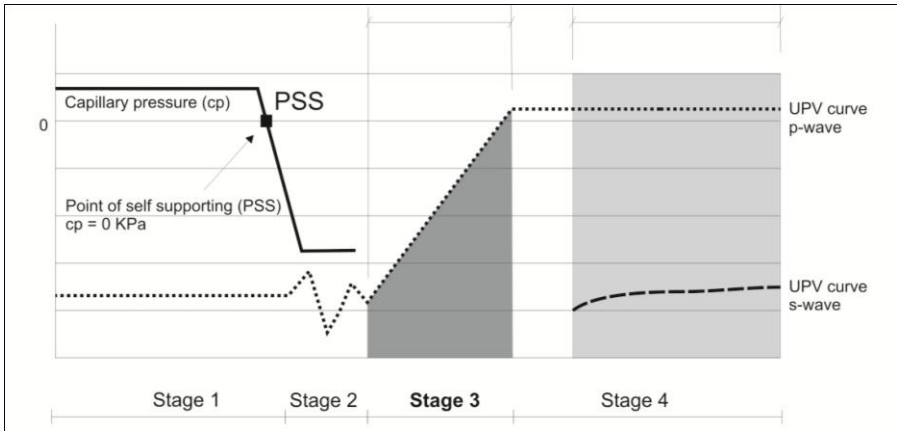

Figure 3. Sketch of the sequence of events related to the 4 stage evolution of p-wave UPV.

The third approach to the evaluation of EA cracking was the analysis of the sequence of events that can be identified by the EA parameters in the setting-hardening process. Figure 3 shows a schematic graph of the capillary pressure and the P- and S- wave UPV simultaneously recorded for each SCC sample. The crossing of the capillary pressure from positive to negative values, point of self-supporting (PSS) [12], indicates the formation of an initial solid percolated skeleton. The fast increase of P-wave UPV is related to the increase of material stiffness, while the appearance of the S-wave reading points out the development of shear capacity of the material. Accordingly, the sequence of events would govern the actual EA drying cracking risk.

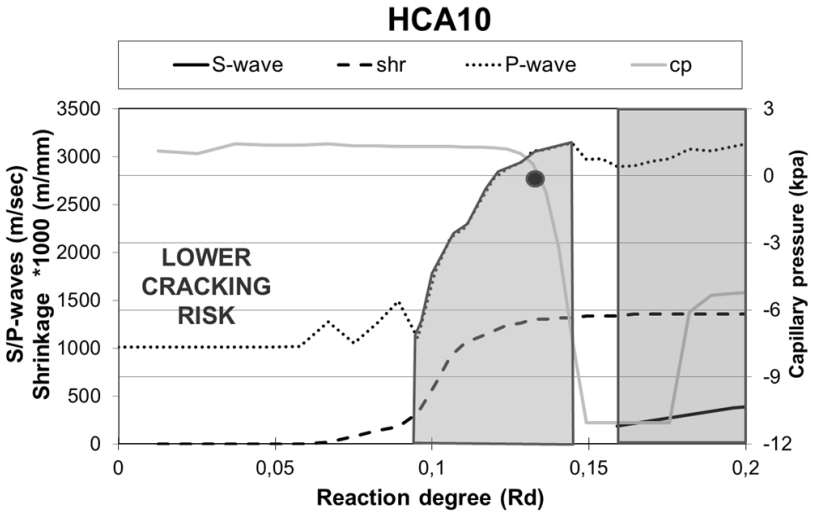

Figure 4. Example of a SCC mixture with a lower risk of cracking at early age.

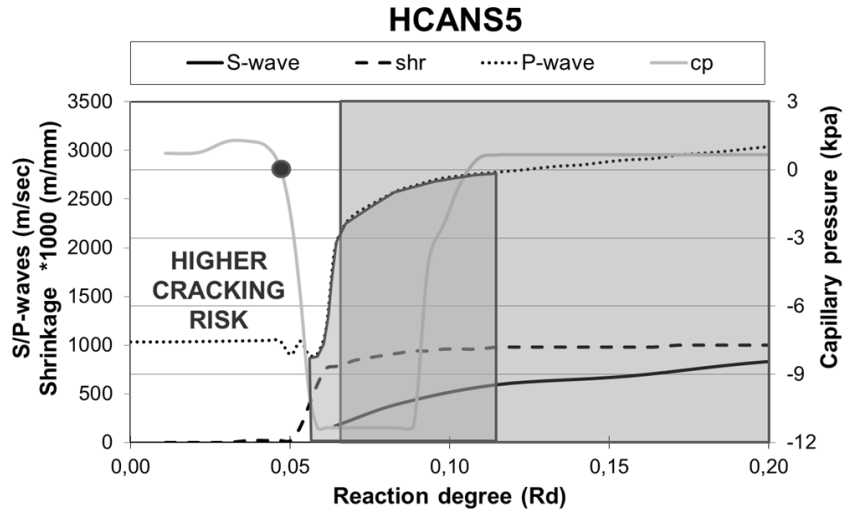

Figure 5. Example of a SCC mixture with a higher risk of cracking at early age.

Figure 4 plots an example of a lower cracking risk mixture (HCA10), characterized by the increase of the P-wave UPV before the PSS. It suggests that the solid percolation occurred after the stiffening process (that occurs simultaneously with free shrinkage). Therefore, the theoretical stress demand (σ) would not affect the unconnected solid skeleton.

Meanwhile, Figure 5 depicts an example of a higher cracking risk mixture (HCANS5), as PSS happened before P-wave increase and shrinkage occurred. In this case, the theoretical σ would be fully applied on the material. In both cases: a) P-wave increase and drying shrinkage occurred simultaneously and b) the mechanical capacity, related to the appearance of S-wave and the development of shear strength, had not happened when the theoretical stress demand applied.

Conclusions

An experimental study on the early age (EA) evolution of SCC pastes and SCC mixtures with different types and amounts of supplementary cementitious materials was presented. Several parameters were simultaneously monitored and the EA drying cracking risk has been assessed considering three different approaches. The first was the development of a phenomenological model that correlated composition and environmental parameters to the EA forced shrinkage of the SCC pastes and SCC mixtures. In a second stage, the theoretical stress demand that applied on some SCC mixtures was evaluated considering the free drying shrinkage jointly with the ultrasonic Young modulus calculated from the p- and s-wave monitoring of the mixtures at EA. It was observed that the active mineral

additions showed larger stress demand, which agreed with the cracking area measurements. Finally, a sequential model of EA drying cracking risk was proposed. The model explains that the sequence of the microstructure development, the stiffening process and the mechanical capacity determines the effective stress demand on the mixture at EA and, therefore, the actual cracking risk.

Acknowledgements

The study has been funded by the Spanish Ministry of Economy and Competitiveness, SCC_Pump Project (Grants BIA2013-48480-C2-2-R and BIA2013-48480-C2-1-R) and the Junta de Comunidades de Castilla la Mancha (Grant PII-2014-022-P). The authors greatly acknowledge the support of the companies BASF construction chemicals Spain SL, OMYA Clariana SL and Cementos Portland Valderrivas.

References

[14] Pickett, G (1956). *Journal of ACI*, vol. 52, pp. 581-590.
[15] Holt, E., Leivo, M. (2004). *Cem Concr Comp*, vol. 26, n. 5, 521-530.
[16] Puentes J, Barluenga G y Palomar I (2014), *Constr Build Mat*. vol. 73. pp. 89-96.
[17] Darquennes, A., Khokhar, M.I.A., Rozière, E., Loukili, A., Grondin, F., Staquet, S. (2011). *Constr Build Mat*. vol. 25, pp. 1836–1847.
[18] Leemann, A., Nygaard, P., Lura, P. (2014). *Cem Concr Comp*, vol. 46, pp. 1–7.
[19] Bonen, D., Shah, S.P. (2005). *Progr. Str. Eng. and Mat.*, vol. 7 (1),pp. 14-26.
[20] Barluenga, G., Puentes and J., Palomar, I. (2015). *Constr. Build. Mat*., vol. 77, p. 66-73.
[21] Boumiz, A.; Vernet, C.; Cohen Tenouj, F., (1996) *Adv. Cem. Bas. Mat*., vol. 3, pp. 94-106.
[22] Birgül R. (2009), *Cem Concr. Res.*, vol. 39, pp. 696-700.
[23] Van Den Abeele K., Desadeleer W., De Schutter G., Wevers M., (2009) *Cem Concr. Res*., vol. 39, pp. 426-432.
[24] Trtnik G, Gams M (2014), *Ultrasonics*, vol. 54, pp. 66-75.
[25] Hammer, T.A.,·Fossa, K.T. (2006). *Mat and Struct.*, vol. 39, pp. 801–808.
[26] Roziere E, Cortas R y Loukili A (2015) *Cem Concr Comp*, vol. 55, pp. 153-161.
[27] Barluenga, G., Puentes and J., Palomar, I. (2013). *Mat and Struct*, vol. 46, pp. 921-941
[28] Leemann, A., Lura, P. and Loser, R. (2011). *Constr. Build. Mat*., vol. 25(5), pp.2283-2289
[29] Barluenga, G., Puentes J. and Palomar I. (2015). In: *CONCREEP 10*. ASCE Proceedings. pp. 1514-1523

Plastic Shrinkage Cracking of Self-Compacting Concrete with Fly ash and Slag

Wang Xuefang[1,3], Zheng Jianlan [2,3], Wang Shengxian[1,3] and Luo Surong[1,2]

[1.] College of Civil Engineering, Fuzhou University, Fuzhou 350116, China
[2.] College of Engineering, Fujian Jiangxia University, Fuzhou 350116, China
[3.] Collaborative Innovation Center for Environmentally Friendly and Energy Saving High Performance Concrete, Fuzhou 350116, China

Abstrac This study is aim to investigate the plastic shrinkage cracking of self-compacting concrete (denoted as SCC) with different proportions of fly ash and granulated blast-furnace slag using the inducing crack method. The plastic shrinkage cracking of the SCC is analyzed by the tests of evaporation capacity and hydration heat of the SCC. The results show that the crack initiation time of SCC specimen is related to the induction period of mortar hydration. Under the same mineral admixtures content, the induction period of mortar hydration and the crack initiation time of SCC specimens are delayed, and the evaporation capacity of SCC is enhanced with proportions of fly ash and granulated blast-furnace slag decreasing. The speed of crack development of the SCC after 12 hours ages is accelerated by increasing the granulated blast-furnace slag content. The influence regular of proportions of fly ash and granulated blast-furnace slag on plastic shrinkage cracking of SCC is related to the total mineral admixtures content.

Keywords: *Self-compacting concrete, Plastic shrinkage cracking, Hydration heat, Evaporation, Compound mineral admixture*.

Introduction

Plastic shrinkage cracking is one of the earliest forms of cracking in concrete as it occurs within the first few hours after the concrete has been cast[1]. Concrete elements with large exposed surfaces are especially vulnerable to plastic shrinkage cracking, e.g. floor slabs or bridge decks. The crack in concrete may provide access for external corrosive substances such as chlorine ion, CO2, etc, and then the concrete structures may be damaged [2,3].The plastic shrinkage cracking of concrete is affected by the mix proportion.

Self-compacting concrete (SCC) can be placed and compacted under its own weight without any vibration effort, which is a challenge to the building industry. In order to achieve the behavior, the paste-aggregate ratio and sand-aggregate ratio of SCC is higher than that of ordinary concrete to obtain the high fluidity and good cohesiveness of the fresh concrete. The more paste means the larger plastic shrinkage of concrete and the more prone to cracking in concrete [4].To reduce plastic shrinkage cracking risk of SCC, there are many measures adopted such as addition fiber or admixture[5,6]. Mineral admixture is an important component of SCC which affect the plastic shrinkage cracking of concrete[7-9]. Fly ash and granulated blast-furnace slag (slag) is the most common mineral admixture. In the paper, the influence of fly ash- slag ratio and mineral admixture content on the plastic shrinkage cracking risk of SCC is investigated.

Experiment Program

Materials

A grade 42.5 ordinary Portland cement according to Chinese Standard GBT175-2007 with density of 3.08g/cm^3, fly ash and slag were used in the experiment. The chemical composition and fineness of the cement, fly ash and slag were presented in TableI Fineness of binder is the volume content of particle size which is greater than 45 micron. The crushed coarse aggregate and natural river sand were used. Fineness modulus and bulk density of sand was 2.2 and 1460 kg/m^3, respectively. The maximum size of coarse aggregate was 20mm, and bulk density and apparent density of coarse aggregate was 1457 kg/m^3 and 2658 kg/m^3, respectively. Polycarboxylate superplasticizer was used.

TableI. Chemical composition and fineness of cement and fly ash and slag (Unit: %)

	CaO	SiO_2	Al_2O_3	Fe_2O_3	SO_3	MgO	K_2O	Others	LoI	Fineness
Cement	59.45	17.64	4.89	3.83	2.99	2.41	0.44	8.35	-	1.88
Fly ash	3.36	62.89	18.61	4.54	0.48	2.53	1.15	7.64	3.88	13.9
Slag	45.17	39.44	8.7	0.96	0.31	2.78	0.42	2.22	1.62	1.4

To investigate the influence of fly ash-slag ratios and mineral admixture content on the plastic shrinkage cracking of SCC, the ratio are 0:1, 3:7, 1:1, 7:3, 1:0 at 30% and 50% total mineral admixture content. The mix proportion of SCC was presented in Table II. In the table, total mineral admixture content of B1~B5 and C1~ C5 is 30% and 50% of binder, respectively. The fresh properties of SCC were tested by slump cone, the segregation resistance and flow properties of fresh SCC are fine as shown in Figure 1 and table II.

Figure 1. Slump test on Self-compacting concrete

Table II. Mixture proportions, fresh properties and compressive strength of SCC

Mix	Mixture proportions [Kg/m^3]							Fresh properties [mm]		Cubic Compressive [Mpa]	
	Cement	Fly ash	Slag	Sand	CA	Water	SP /%	Slump	slump flow	1d	28d
B1	378	162	-	788	888	184	1.00	265	650	12.49	55.9
B2	378	113.4	48.6	788	888	184	0.95	260	600	15..9	59.0
B3	378	81	81	788	888	184	1.00	260	640	13.1	60.6
B4	378	48.6	113.4	788	888	184	1.00	260	610	13.5	62.4
B5	378	-	162	788	888	184	1.05	260	580	7.1	62.8
C1	270	270	-	788	888	184	0.90	265	670	6.8	44.4
C2	270	189	81	788	888	184	1.00	260	690	4.6	53.6
C3	270	135	135	788	888	184	1.00	260	670	2.8	54.2
C4	270	81	189	788	888	184	1.00	265	680	0.8	55.4
C5	270	-	270	788	888	184	1.05	265	640	1.2	58.7

Note: CA and SP are coarse aggregate and superplasticizer, respectiverly.

Test specimens

In the plastic shrinkage cracking test method of ASTM C1579-06, there are two ridges to restrain the concrete and a latter (middle) to localize the plastic shrinkage cracking in the middle of the specimen. However, the thickness of concrete in the middle is only 36.5mm less than other place in which the thickness is 100mm, which may result in uneven distribution of concrete material and the settlement in the middle is also lower than others. And then, the accuracy of test results may be affected.

The inducing crack method was proposed to test plastic shrinkage cracking in concrete (See *Figure 2*) [10]. The concrete was poured into two molds (600mm× 600mm×50 mm) with bolts of 6mm diameter, and a pairs of steel plate. The bolts are mounted uniformly at each two sides of the rigid frame to restrain the concrete. The purpose of the steel plate is to localize and promote the plastic shrinkage cracking. In the specimen, the concrete material distribution and settlement is prepared even. In order to avoid friction between concrete and bottom plate of the restriction steel form, a Teflon sheet is placed at the bottom of the form, and a paraffin paper is placed on it.

After casting, the specimens were stored in a climate chamber at a temperature of 22±3°C and 60±5% of relative humidity. The crack was monitored by cracking observation meter with 40 times of magnification. The specimen was observed every 5 minute until the crack pronged the specimen, and then was observed every 2 hours.

At the same time, SCC was poured to two prisms with width and length of 150mm, height of 60mm to test the water evaporation. The prism was alto exposed to the same environment of plastic shrinkage cracking test. The weight of the prism was weighed per hour by electronic balance weighing with sense of 0.1g until 6h, and then again after every 1.5 h until 12h. The evaporation capacity of the concrete can be calculated with following equation:

$$E_t=(m_t-m_0)/A$$

Where 'm_t' is the weight of the prism specimen at time 't', 'm_0' is the initial weight of the prism specimen, and 'A' is the area of the prism.

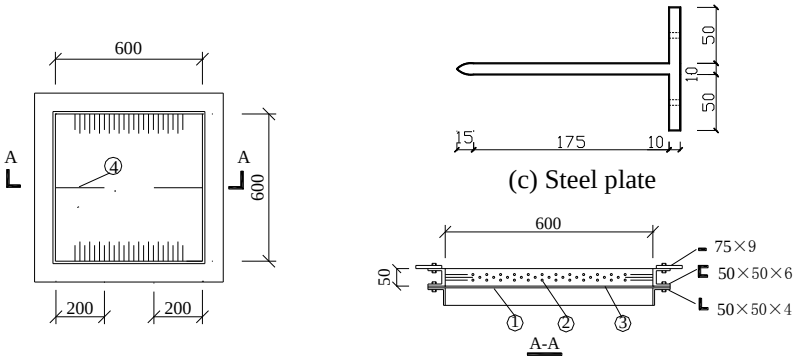

(a) Single partition model (b) Profiles

(c) Steel plate

①—motherboard; ②—ϕ 6 bolt; ③—paraffin paper, teflon paper; ④—steel plate

Figure 2. Details of modified flat-type specimen (Unit: mm)

The hydration heat release characteristics of mortar were tested by TAM Air Microcalorimeter at a temperature of 20°C. The mortar was sieved from fresh SCC by 2.36mm sieve aperture.

Results and Discussion

Hydration heat of mortar

Figure 3 and Figure 4 show the test results of the hydration heat of SCC with 30% and 50% mineral admixtures content, respectively. Under the same mineral admixture content, when the fly ash - slag ratio decrease, the value of hydration heat flow peak is increased, hydration induction period is prolonged, and the appearance of hydration heat flow peak is delayed. The appearance of hydration heat flow peak is delayed 2.5 hours to 10 hours with the fly ash - slag ratio decreasing at 30% mineral admixture content, however, the value at 50% mineral admixture content is about double times of that at 30% mineral admixture content.

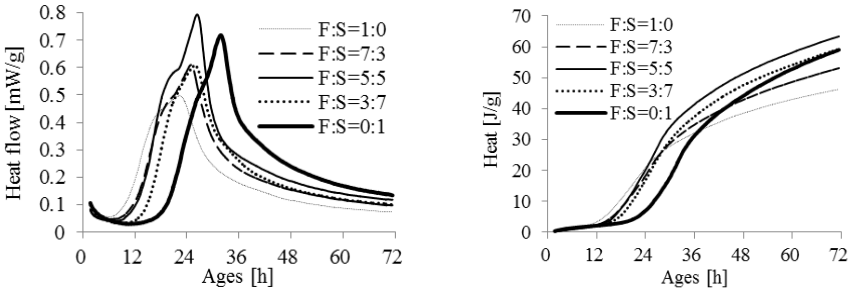

（a）Hydration heat flow （b）Hydration heat

Figure 3. Hydration heat of mortar with 30% mineral admixtures

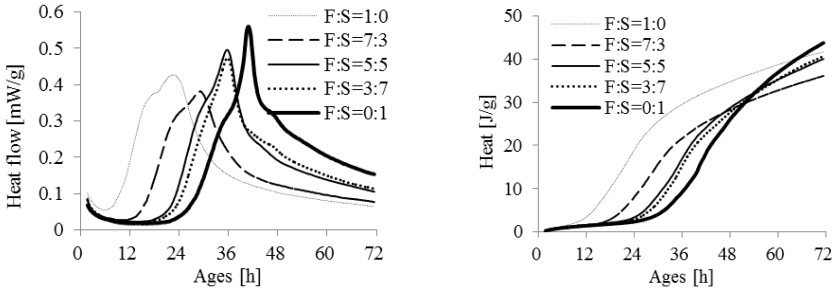

（a）Hydration heat flow （b）Hydration heat

Figure4. Hydration heat of mortar with 50% mineral admixtures

At the same time, the experimental results also show that total hydration heat at 3 days ages is increased with the value of the hydration heat flow peak increasing. When mineral admixture content is 30% of binder, hydration heat flow peak and

total hydration heat of mortar with fly ash-slag ratio of 5:5 is highest, which is about 1.5 times of that only with fly ash. For the mortar with 50% mineral admixture content, due to greatly delay the hydration accelerated period, heat flow of mortar hydration at 3 days ages is higher, thus the total hydration heat curve slope nearly 3 days ages is also steepening with decrease of fly ash-slag ratio.

Evaporation of self-compacting concrete

Figure 5 shows the test results of the evaporation of SCC. As shown in Figure 4, the difference of SCC evaporation is slight when the fly ash-slag ratio is over 1:1. When fly ash-slag ratio is under 1:1, however, the evaporation of SCC is enlarged with decrease of fly ash-slag ratio. The evaporation of SCC with fly ash-slag ratio of 0:1 is about 1.4 times of that with fly ash–slag ratio of 1:0 at 12 hours ages. Increasing mineral admixture content may reduce the evaporation of SCC without changing fly ash-slag ratio. The evaporation difference of SCC between 12 hours and 24 hours ages is slight.

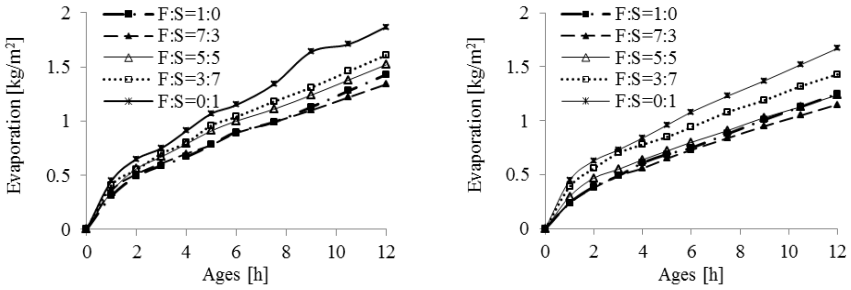

(a) SCC with mineral admixture content of 30%

(b) SCC with mineral admixture content of 50%

Figure 5. Evaporation development of self-compacting concrete

Plastic shrinkage cracking of SCC

Figure 6 shows the test results of the plastic shrinkage cracking of SCC. The cracking initiation time of SCC is delayed by reducing fly ash-slag ratio, the delaying effect is lowered with the increase of mineral admixture content. For SCC with mineral admixture content of 30%, the cracking initiation time is delayed 140 min when fly ash-slag ratio decreased from 1:0 to 0:1. However, For SCC with mineral admixture content of 50%, the cracking initiation time is only delayed 60min.

At the ages of 12 hours, the influence of fly ash-slag ratio on the crack area of SCC specimens with mineral admixture content of 30% is different from that with

mineral admixture content of 50%. When mineral admixture content is 30% of binder, the crack area of SCC specimens there is little difference by the change of the fly ash-slag ratio expect fly ash-slag ratio of 7:3, the crack area of SCC with fly ash-slag ratio of 7:3 is 64% of that only with fly ash at 12 hours ages. When mineral admixture content is 50% of binder, the difference of crack area of SCC is little by replacing fly ash with slag.

Replacing fly ash with slag may magnify the cracking development speed of SCC after 12 hour ages. From 12 hours to 24 hours ages, the increase of crack area of SCC with slag is 2.26-3.82 times of that only with fly ash. As the fly ash-slag ratio is 3:7, the increase is lowest which is 2.3 times of that only with fly ash. On the whole, the magnified amplitude of crack area of SCC is increased with the increase of mineral admixture content. As result of that, the crack area of SCC with slag is higher than that only with fly ash expect SCC with fly ash-slag ratio of 7:3 and with mineral admixture content of 30% at 24 hours ages.

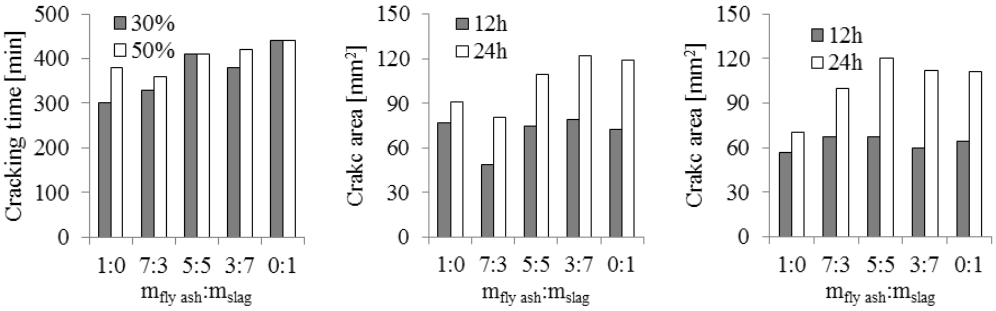

(a) Cracking initiation time (b) Crack area of SCC with mineral admixture content of 30% (c) Crack area of SCC with mineral admixture content of 50%

Figure 6. Comparisons of early-age cracking behavior of SCC with different fly ash-slag ratio

Discussion

Crack may appear in concrete when the restrain tensile stress caused by shrinkage is larger than its tensile strength. The cracking initiation time of the specimen is associated to the setting time of the concrete[11**Error! Bookmark not defined.**]; nd cracking likely occurs in the hydration induction period of concrete, before the main cement hydration started[5]. The effect of slag adsorption superplasticizer is greater than that of fly ash. When the superplasticizer in liquid phase of cement paste is reduced by the hydration of cement, the superplasticizer which is adsorbed by slag is release to the liquid phase to maintain the concentration of superplasticizer. And then, the hydration speed of binder is lowered, and the hydration induction period and SCC is prolonged, the setting time of SCC is

delayed with the fly ash - slag ratio decrease. The test results of hydration heat of mortar (*Figure 3*and *Figure 4*) indicate that the hydration induction period of SCC is prolonged, and the appearance of hydration heat flow peak is delayed when the slag content is increased. As result of that, the cracking initiation time of SCC is delayed with the decrease of fly ash - slag ratio, and cracking occurred in induction period of SCC hydration.

Crack area indicates the balance between the shrinking stress and the tensile strength of the concrete. The tensile strength development of SCC depends on its hydration rate. With the fly ash-slag ratio decreasing, the development of tensile strength and elastic module of SCC is reduced at early age as the result of the prolonged induction period of SCC (*Figure 3* and *Figure 4*). For mineral admixture content of 30%, the end time of induction period of SCC with fly ash-slag ratio of 3:7 is only one hour later than that only with fly ash, which is larger lower than 10 hours for SCC with fly ash-slag ratio of 0:1. When mineral admixture content is 50% of binder, compared to SCC only with fly ash, the end time of induction period of SCC with slag is delayed 6-16 hours. The shrinking stress is enhanced by the increase of plastic shrinkage and elastic module. The plastic shrinkage of concrete maybe enhance with the evaporation increase. The water retention of slag is lower than that of fly ash, and then there are more water is evaporated for SCC with slag. The results show that the evaporation of SCC ((*Figure 5*) is also increasing with the fly ash-slag ratio decrease when fly ash-slag ratio is lower than 1:1. The evaporation of SCC with fly ash-slag ratio of 3:7 is lowest. As result of above, the crack area of SCC with fly ash-slag ratio of 3:7 is lowest for mineral admixture content of 30%, the others is similar at 12 hours ages.

After ages of 12 hours, the hydration of SCC only with fly ash is in acceleration period; however, the hydration of SCC with fly ash-slag ratio under 1:1 is still in induction period (*Figure 3* and *Figure 4*). The hydration degree of SCC is reduced with fly ash-slag ratio increase; the reducing amplitude is enlarged with the mineral admixture content increase. The development of tensile strength of SCC is reduced with the hydration degree. As results, the increase of cracking area of SCC from 12 hours ages to 24 hours ages is increasing with slag incorporated.

Conclusions

1) Slag replaced fly ash prolong the hydration induction period of SCC, delay the appearance of hydration heat flow peak, enlarge the hydration heat flow peak. On the whole, the effect is enhanced with the increase of replacement rate or the increase of mineral admixture content. The hydration induction period end time of mortar is delayed 1-10 hours and 6-16hours when mineral admixture content is 30% and 50% of binder, respectively.

2) As the water retention of slag is lower, the evaporation of SCC is increased with the decrease of fly ash-slag ratio when the fly ash-slag ratio is lower than 1:1. The evaporation of SCC with fly ash-slag ratio of 0:1 is 1.3 times of that with fly ash-slag of 1:0.

3) The cracking of SCC occurs in induction period of SCC hydration. Since the slag replaced fly ash may delay the induction period end time of SCC, the cracking initiation time of SCC is delayed with the decrease of fly ash-slag ratio.
4) The crack area of SCC is affected by the hydration progress and evaporation of SCC. Compared with SCC only mixed with fly ash, when SCC is mixed with mineral admixture content of 30% binder and the fly ash-slag ratio of 7:3, the crack area of which is also lowest, since its hydration progress is only slightly delayed, and its evaporation is a little lower.

At the ages of 12 hours, the crack areas of others SCC with the same mineral admixture content are similar. Between the 12 hours and 24 hours ages, however, the development speed of crack area of SCC is greatly enlarged by replacing fly ash with slag. This may be due to the delay of the acceleration period begin time of SCC hydration by replacing fly ash with slag, which affected the development of tensile strength of SCC.

Acknowledgements

This work was financially supported by the China Natural Science Foundation (51378126) and Fuzhou university science development foundation.

References

[1] Boshoff WP, Combrinck R. (2013). *Modelling the severity of plastic shrinkage cracking in concrete. Cement and Concrete Research*, vol. 48, PP. 34–39
[2] Yoo SW, Kwon SJ, Jung SH. (2012). *Analysis technique for autogenous shrinkage in high performance concrete with mineral and chemical admixtures. Construction and Building Materials*, vol. 34, PP. 1–10
[3] Jang SY, Kim BS, Oh BH. (2011). *Effect of crack width on chloride diffusion coefficients of concrete by steady-state migration tests. Cement and Concrete Research*, vol. 41, PP. 9–19
[4] Almusallam AA, Maslehuddin M, Abdul-Waris M, Khan MM. (1998). *Effect of mix proportions on plastic shrinkage cracking of concrete in hot environments. Construction and Building Materials*, vol. 12, PP. 353-358
[5] Leemann A, Nygaard P, Lura P. (2014). *Impact of admixtures on the plastic shrinkage cracking of self-compacting concrete. Cement & Concrete Composites*, vol. 46, PP. 1–7

[6] Corinaldesi V, Moriconi G. (2011). *Characterization of self-compacting concretes prepared with different fibers and mineral additions*. *Cement & Concrete Composites*,, vol. 33, PP. 596–601
[7] Tongaroonsri S, Tangtermsirikul S. (2009). *Effect of mineral admixtures and curing periods on shrinkage and cracking age under restrained condition. Construction and Building Materials*, vol. 23, PP. 1050–1056
[8] ZHENG JL, WANG XF. (2009). *Influence of fly ash on the early-age cracking behavior of high-flowing concrete. Journal of Central South University of Technology (English Edition)*, vol. 16, n. 2, PP. 312-319
[9] Darquennes A, Staquet S, Delplancke-Ogletree MP, Espion B. (2011). *Effect of autogenous deformation on the cracking risk of slag cement concretes. Cement & Concrete Composites*, vol. 33, PP. 368–379
[10] Zheng JL, Wang XF, Luo SR.(2009). *A New Experimental Method to Fleetly Test Early-Age Cracking behavior of Concrete. Journal of Building Materials*, vol. 12, n. 2, PP. 209-213
[11] Boshoff WP, Combrinck R. (2013) *Modelling the severity of plastic shrinkage cracking in concrete. Cement and Concrete Research*, vol. 48, PP. 34–39

Self-Consolidating Concrete Cracking Sensitivity: Cracking Index and Database

Hamza Samouh[1], Emmanuel Roziere[1] and Ahmed Loukili[1]

[1]Civil engineering and Mechanics Research Institute (GeM), UMR-CNRS 6183, Centrale Nantes, BP 92101, 44321 Nantes, Cedex3, France.

Abstract Since Self-Consolidating Concrete (SCC) does not need any vibration; its use results in better filling of formworks and safer conditions for workers on the construction sites. For these reasons, SCC is taking a more significant market share in France and worldwide. However, some problems associated with vibrated concrete remain, and one of them stands out: shrinkage-induced cracking. Non-structural cracks were observed on thin walls. The occurrence of such cracks is delayed in time, thus repair is more difficult and expensive, especially if the construction phase is completed. Usually, cracks start after several months or/and during the first summer heat waves; thereby linking the problem to the drying phenomena. To assess the cracking sensitivity induced by restrained drying shrinkage, the ring test was chosen and adapted to our case, with smaller dimensions and a one-dimensional drying disposition representing thin walls. The results were gathered to constitute a database of thirty SCC mixtures. To quantify the cracking risk, the ASTM cracking index was adjusted by taking into account our ring dimensions and materials properties. The results allowed us to determine three zones according to a cracking index: cracking and non-cracking zones, in addition to an intermediate zone. This new SCC classification enables us to study the effects of the mix-design parameters on the cracking potential on the one hand, and the relation between the mechanical properties of SCC (strength, Young's modulus, shrinkage, etc.) and the computed cracking index on the other.

Keywords: *Cracking sensitivity, Self-consolidating concrete, Ring test, Cracking index, Database.*

Introduction

SCC technology significantly improves the casting of concrete in reinforced concrete structures as vibration of fresh concrete can be avoided. To meet these needs, the design of SCC mixtures requires higher paste volume and mineral

admixture content. Admixtures were necessary for good flow, such as high-range water-reducing admixture (HRWRA) and viscosity modifying admixture (VMA). Under drying conditions, higher paste volume results in higher drying shrinkage ([1]–[3]). If shrinkage is restrained, tensile stresses are generated in concrete and cracking risk increases. To estimate the cracking sensitivity of concrete, an approach based on the ring test is proposed by ASTM [4]. The steel ring strain and the cracking time are used to calculate two indicators, which classify the potential for cracking in four categories: low, moderate-low, moderate-high and high. Kovler proposed to merge these two indicators parameters in one that he named integrated criterion ([5], [6]). The circumference drying disposition described by ASTM and AASHTO [4] [7] gave a complicated stress distribution which changes shape over time [8]. GeM Laboratory developed rings for restrained shrinkage tests, with adapted dimensions to describe the restraint conditions of structural walls [9]. This ring is used with lateral protection from drying, which provides uniform shrinkage along the radial direction and defined shape of residual stress [4]. This last configuration with difference in dimensions and the drying disposition requests new adapted categories of the potential for cracking. A specific index based on the experimental results from ring tests is adapted to our case and used to classify SCC. A new classification of cracking sensitivity is proposed with a recommended duration for the ring test. The relation between some mix design characteristics or standard mechanical properties and the cracking sensitivity is investigated. It can be shown that some of these parameters have a strong influence on cracking sensitivity but this does not allow a deterministic approach.

Experimental Program

30 mixtures presented in previous studies were used in this paper to determine the key parameter of cracking sensitivity due to the restrained shrinkage. The mechanical parameters of all concretes can be found in these references ([2], [3], [10]–[15]). This database contains one vibrated concrete and 29 self-consolidating concretes and an example of these admixtures can be shown in *Table XXVIII*.

Table XXVIII. Example of concrete mixtures used in this study

	SCC 31%	***SCC 40%***	***SCC 46%***
Gravel (Amphibolite) 10/14 (*G*) (kg/m^3)	*290*	*290*	*290*
Gravel (Amphibolite) 6/10 (*G*) (kg/m^3)	*550*	*550*	*550*
Sand 0/4 (*S*) (kg/m^3)	*780*	*780*	*780*
Cement (*C*) (kg/m^3)	*378*	*330*	*291*
Limestone Filler (*LF*) (kg/m^3)	*170*	*210*	*248*
Addition-*European standard*- (*A*) (kg/m^3)	*126*	*110*	*97*
Superplastizer (kg/m^3)	*3,5*	*2,8*	*2,8*

Water (*W*) (kg/m^3)	*205*	*205*	*205*
V_G/V_S	*0,92*	*0,92*	*0,92*
W/C	*0,54*	*0,62*	*0,70*
W/(C+LF)	*0,37*	*0,38*	*0,38*
W/B_{eq}	*0,50*	*0,57*	*0,65*
LF/(LF+C)	*31%*	*40%*	*46%*
Paste volume (l)	*417*	*415*	*418*
f_{c28} (MPa)	*44,5*	*39,1*	*32,8*

The experimental procedure to measure the time-dependent strains was based on the recommendations of the RILEM Technical report [16]. The cylindrical specimens Ø7x28 cm² were moved immediately after casting to an air-conditioned room for 50% RH at 20±1°C and environmental chamber for 30 %, 70 % RH at the same temperature. The specimens were demolded 16, 24 or 48 hours later. The top and bottom surfaces were covered with an adhesive-backed aluminum foil, to achieve 2-dimension drying (*Figure 53*). The total drying shrinkage was measured on these specimens immediately (within 3 minutes) after removing the molds. LVDT sensors were used to measure the shrinkage strains continuously (one hour interval). The specimens used to measure autogenous shrinkage were carefully protected against drying from the start of testing. Six months later, only an average of 0.03% mass loss was observed on the sealed specimens [14]. The use of a double layer of adhesive-backed aluminum foil is actually more effective than acrylic, latex, or epoxy protection [17]. The drying shrinkage was deduced as the difference between the measured total shrinkage and autogeneous shrinkage [18]. Standard compression and tensile splitting tests were carried out on cylindrical specimens (Ø 11x22 cm²) after 1 day, 2 days and 28 days to determine the strength and the Young's modulus.

The external restraint value R in wall structures varies between 50% and 100% [19]. This value can be estimated by the Eqn. (1) for ring tests. Young's modulus of studied concretes varied between 15 GPa and 40 GPa [14], which results in restraint degrees between 65 and 83 %. Thus the ring test used in this study can be considered as representative of restraint in concrete structures.

$$R = \frac{A_{st}E_{st}}{A_{st}E_{st} + A_cE_c} \quad (1)$$

A_{st} : Cross section of steel ring (m²), A_c : Cross section of concrete (m²), E_c : Young's modulus of concrete (GPa).

The ring test was used to measure restrained shrinkage and to estimate the cracking sensitivity of the concrete. The dimensions of the ring are: a=8.5cm; b=11cm; c=18 cm. a is the inner radius of the inner ring (steel), b is the outer radius of the inner ring (steel), c is the outer radius of the concrete ring (see *Figure 54*). The ring is

chosen with thickness equal to 5 times the maximum aggregate size (70 mm = 5x14 mm).

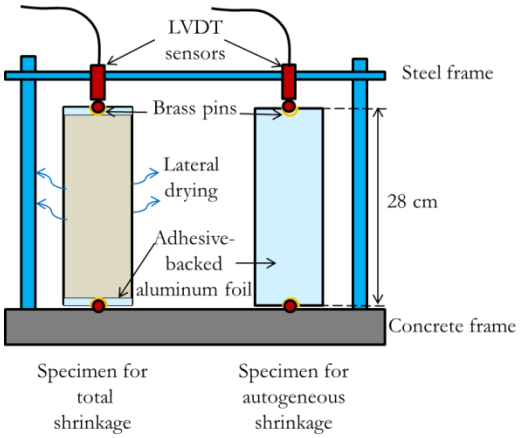

Figure 53. Experimental device for shrinkage tests

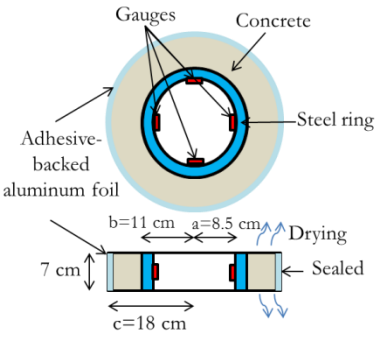

Figure 54. Experimental disposition of the ring test

Results and Discussion

Cracking risk and mix design

The percentage of cracked concrete rings can be plotted as a function of mix-design parameters. Two of them are presented here. The first one is the water/equivalent binder (W/B_{eq}) ratio. The equivalent binder is defined in French and European standards by the Eqn. (2) [20]. The second parameter is the paste volume. An example of these calculated two parameters is exposed in *Table XXVIII*.

$$B_{eq} = \mathrm{C} + \mathrm{K}.\mathrm{A} \qquad (2)$$

C: Cement content (kg/m^3).
A: Mineral admixture content taken into account in equivalent binder (kg/m^3). The maximum value of A is defined by the ratio A/(A + C): The maximum value is given by national annex of European standard [20].
K: Coefficient of activity of a normalized mineral admixture [20].

Figure 55 shows 75% of concrete rings cracked for the values under 0.5. Concrete with a low W/B_{eq} ratio has a high stiffness, which implies that they develop a higher internal stress for the same shrinkage strain. Concrete mixtures with higher W/B_{eq} showed lower cracking sensitivity. 25 % of concretes cracked when this ratio was higher than 0.6. Between 0.5 and 0.6 the percentage of cracking concrete was around 35 %.

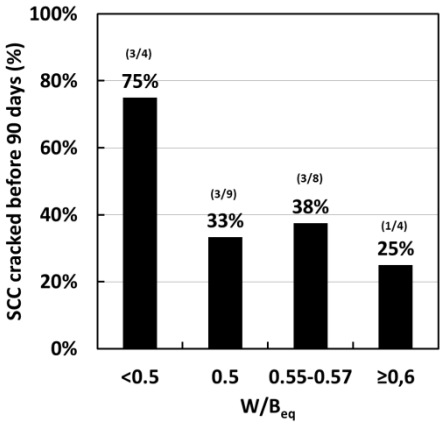

Figure 55. Percentage of concretes cracked before 90 days versus W/B_{eq} ratio

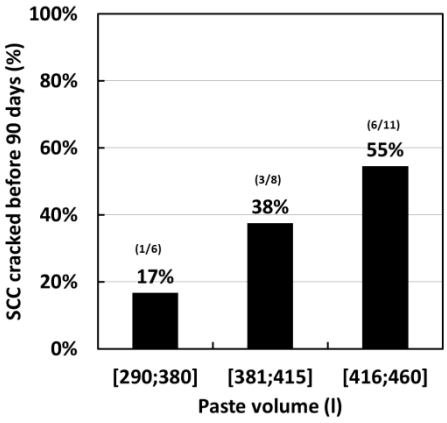

Figure 56. Percentage of concretes cracked before 90 days versus paste volume

The main part of concrete shrinkage is due to the shrinkage of the paste, thus an increase in paste volume induces an increase in concrete shrinkage, which has been observed experimentally in many previous studies ([1] [11] [12]). Rozière et al. also showed an increase in the cracking risk depending on the paste volume [2]. *Figure 56* shows the percentage of cracking concrete varied from 17% when the volume was lower than 380 l to 55% when it was higher than 415 l. To reduce the cracking risk at the mix-design stage, paste volume can be minimized to the minimum volume needed to ensure self-compaction.

The ring test is recommended by ASTM and AASHTO reports ([4], [7]) to estimate the cracking risk. Two criteria were used; the first one is the elapsed time at cracking or elapsed time when the test is stopped. The second one is the average stress rate for the test specimens. In the ASTM approach the two criteria are combined to determine the cracking potential. According to these values the potential for cracking can be classified in one of the four zones: low, moderate-low, moderate high and high [4].

Cracking risk and concrete properties

Compressive strength represents one of the most widely used mechanical parameters determined automatically for concrete intended to scientific or industrial uses. As a consequence it was correlated to the cracking risk.

In *Figure 57*, under the 50 MPa value of compressive strength at 28 days, the percentage of cracked concrete stays constant for the two strength range [25;40] and [40;50]. However, this figure shown also a higher cracking sensitivity of mixtures with the highest strengths (3/4 concretes cracked). This result is

consistent with previous studies showing relatively high cracking sensitivity of high performance concrete [21] [22]. This can be explained by higher stiffness.

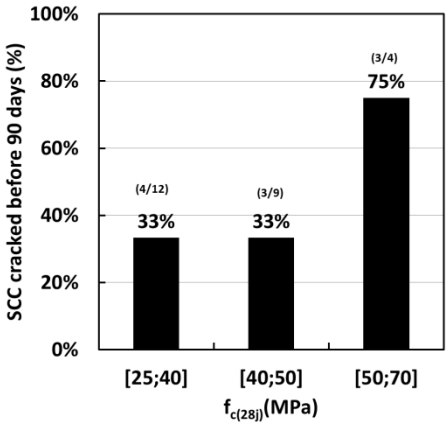

Figure 57. Percentage of concrete cracked before 90 days versus the compressive strength at 28 days

Comparing shrinkage values at a given age of concrete is misleading. [10]. Torben's model [23] can be used to determine long-term drying shrinkage by using the Eqn. (3):

$$\varepsilon_{dry} = \frac{t}{t + N_s}\varepsilon_{\infty} \qquad (3)$$

The two parameters, ε_{∞}, long-term drying shrinkage, and N_s, shrinkage halftime, were determined from the experimental data so as to minimize the mean square error.

Shrinkage magnitude is the second generally used criterion. Experimental results show that the statement "the more concrete shrinks, the more it is susceptible to crack" is not a general rule. *Figure 58* shows the influence of long-term drying shrinkage on the ratio of cracking concretes. When shrinkage was lower than 400 µm/m, no ring cracked, and just one out of 5 cracked when ultimate drying shrinkage was between 400 and 500 µm/m, while 2 concretes out of 2 cracked when this property exceeded the value of 800 µm/m. Finally, no clear trend can be observed for the intermediate interval [500; 800] µm/m.

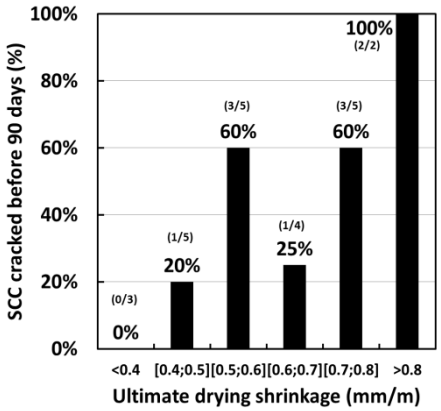

Figure 58. Percentage of cracking concrete before 90 days versus the long-term drying shrinkage

Cracking index

The stress rate in each test specimen at cracking or end time is determined by Eqn. (4):

$$q = \frac{G\alpha}{2\sqrt{t_{cr}}} \tag{4}$$

q : stress rate in each test specimen (MPa/ day),
G : 72.2 GPa ASTM value, for our ring configuration, a 185 MPa value is taken [14] [11],
α : the average strain rate factor for each test specimen (m/m)/day$^{1/2}$,
t_{cr} : elapsed time at cracking or elapsed time at the end of the test (day)
Based on Kovler studies, cracking index i_{cr} can be defined as ratio between the both criteria; S and t_{cr} [5]:

$$i_{cr} = \frac{S}{t_{cr}} \tag{5}$$

Figure 59 shows the dependence of the cracking index on the time of measurement. If the test duration exceeds 90 days without cracking the cracking risk remains low, even for high strain rate factors. 90 days test duration can be suggested for the described experimental conditions. As a consequence Y axes in *Figure 55 Figure 56 Figure 57 Figure 58* correspond to the percentage of cracking concrete before 90 days. Five tests were stopped before this time, thus they were not taken into account in different plots.

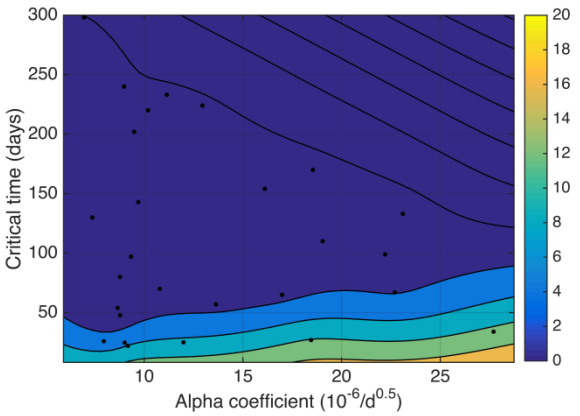

Figure 59. Map of the cracking index versus the alpha coefficient

The database allows plotting, in *Figure 60*, the percentage of the concrete cracked before 90 days versus the cracking index. Three areas immerge: A low risk zone (i_{cr}<1) with no concrete cracking out of 12, a medium risk zone (1<i_{cr}<1) 3 concrete cracking out of 6, and finally a high risk zone (i_{cr}>3) with 7 concrete cracking out of 7. For SCC and similar ring configurations, this new classification can be used to estimate the cracking sensitivity of different concretes.

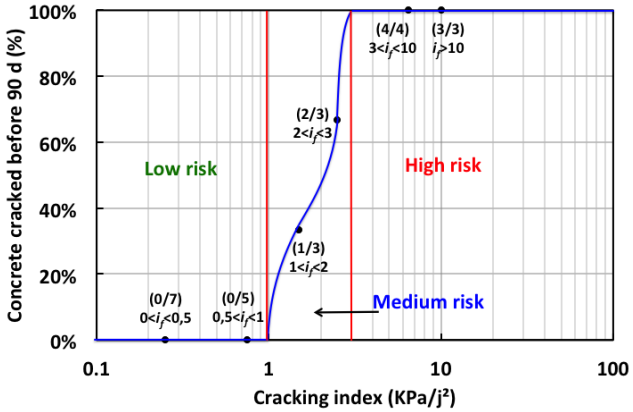

Figure 60. Concrete cracked before 90 days versus the cracking index

Conclusions

A database of 30 concretes including mainly SCC was studied. The cracking sensitivity was assessed experimentally from the ring test results. The proportion of cracked concrete was presented as a function of mix design parameters or mechanical properties. A specific cracking index adapted to our drying disposition

was proposed to estimate the cracking potential from ring tests. Based on a cracking index map, 90 days of the test duration was suggested. Indeed, for our test conditions, no concrete cracked after three months of measurement.
A classification of the proportion of cracked concretes according to this index was given and three zones were observed: low, medium and high cracking sensitivity. For the zone of low risk no concrete cracked, and for high risk zone all concrete cracked. Very few concrete (20%) were in medium cracking zone where some concrete cracked and others did not. In the future, the expanding of the database will increase the accuracy of these boundaries.
As far as mix-design characteristics are concerned, when the ratio W/B_{eq} decreases, the concrete stiffness increases at the same time as the potential of cracking. The percentage of cracking concrete increases with the paste volume. This tendency can be explained by the high value of shrinkage in this case.
For instance, cracking sensitivity was found to be significant for the highest shrinkage magnitudes, and for very low values of shrinkage cracking did not appear. Unfortunately, most of studied mixtures (80%) were in an intermediate interval and no general trend could be obtained. From these results, cracking sensitivity cannot be easily linked to some mechanical properties like drying shrinkage or compressive strength.

References

[1] B. Bissonnette, P. Pierre, and M. Pigeon, "Influence of key parameters on drying shrinkage of cementitious materials," *Cem. Concr. Res.*, vol. 29, no. July, pp. 1655–1662, 1999.

[2] E. Rozière, S. Granger, P. Turcry, and a. Loukili, "Influence of paste volume on shrinkage cracking and fracture properties of self-compacting concrete," *Cem. Concr. Compos.*, vol. 29, no. 8, pp. 626–636, Sep. 2007.

[3] E. Rozière, P. Turcry, A. Loukili, and F. Cussigh, "Influence of paste volume, addition content and addition type on shrinkage cracking of self-compacting concrete," in *SCC 2005 - Second North American Conference on the Design and Use of Self-Consolidating Concrete and Fourth International RILEM Symposium on Self-Compacting Concrete*, 2005, pp. 945–951.

[4] "ASTM C1581-04: Standard Test Method for Determining Age at Cracking and Induced Tensile Stress Characteristics of Mortar and Concrete under Restrained Shrinkage," 2004.

[5] K. Kovler and A. Bentur, "Cracking Sensitivity of Normal- and High-Strength Concretes," *ACI Mater. J.*, no. 106, pp. 537–542, 2009.

[6] S. Zhutovsky, K. Kovler, and A. Bentur, "Effect of hybrid curing on cracking potential of high-performance concrete," *Cem. Concr. Res.*, vol. 54, pp. 36–42, Dec. 2013.

[7] "AASHTO PP34-99: Standard practice for cracking tendency using a ring specimen," 2005.

[8] S. Dean, J.-H. Moon, F. Rajabipour, B. Pease, and J. Weiss, “Quantifying the Influence of Specimen Geometry on the Results of the Restrained Ring Test,” *J. ASTM Int.*, vol. 3, no. 8, p. 100436, 2006.

[9] P. Turcry, A. Loukili, K. Haidar, G. Pijaudier-cabot, and A. Belarbi, “Cracking Tendency of Self-Compacting Concrete Subjected to Restrained Shrinkage : Experimental Study and Modeling,” *J. Mater. Civ. Eng.*, 2006.

[10] H. Samouh, E. Rozière, and A. Loukili, “Interprétation des mesures du retrait de dessiccation des bétons autoplaçants (BAP),” in *XXXe Rencontres AUGC-IBPSA. Chambéry,Savoie, 6au 8 Juin 2012*, 2012.

[11] H. Samouh, “Evaluation de la sensibilité à la fissuration des BAP: Apport de l’analyse du comportement viscoélastique,” in *Prix jeune chercheurs “René Houper”. ISABTP/UPPA, Anglet, 27 au 29 Mai 2015*, 2015.

[12] H. Samouh, A. Soive, E. Rozière, and A. Loukili, “Size effect on long-term drying behavior of self-consolidating concrete: influence of drying depth,” *Mater. Struct.*, pp. 1–20, 2015.

[13] H.Samouh, E.Rozière, and A.Loukili, “Influence of formwork duration on shrinkage, microstructure, and durability of cement based materials,” in *ConCreep 2015*, 2015.

[14] H. Samouh, “Nouvelles approches des relations entre formulation et comportement différé des matériaux cimentaires: application aux bétons autoplaçants.,” Ecole Centrale de Nantes, 2015.

[15] H. Samouh, E. Rozière, A. Loukili, and P. Sigwalt, “Stress relaxation and cracking sensitivity of self- consolidating concrete: effect of limestone filler content,” in *7th RILEM Conference on Self-Compacting Concrete*, 2013.

[16] Z. P. Bazant and S. Baweja, “RILEM Technical committees 107-GCS guidelines for the formulation of creep and shrinkage prediction models,” *Mater. Struct.*, vol. 107, pp. 415–430, 1995.

[17] Z. C. Grasley, D. A. Lange, M. D. D’ambrosia, and S. Villalobos-chapa, “Relative Humidity in Concrete,” *ACI Comm.*, vol. 236, no. October, pp. 51–57, 2006.

[18] V. Baroghel-bouny and J. Godin, “Experimental study on drying shrinkage of ordinary and high-performance cementitious materials,” *RILEM Conf. Shrinkage*, vol. 3, no. 9, pp. 13–22, 2001.

[19] H. T. See, E. K. Attiogbe, and M. A. Miltenberger, “Shrinkage Cracking Characteristics of Concrete Using Ring Specimens,” *ACI Mater. J.*, no. 100, pp. 239–245, 2004.

[20] AFNOR, *Béton: Spécification, performance, production et conformité.NF EN206-1CN*. 2012.

[21] S. Eppers, “Assessing the autogenous shrinkage cracking propensity of concrete by means of the restrained ring test,” Technischen Universität Dresden, 2010.

[22] Q. Nguyen, L. Jiang, and Q. Zhu, "Assessment of early-age cracking of high-performance concrete in restrained ring specimens," *Water Sci. Eng.*, vol. 3, no. 1, pp. 113–120, 2010.

[23] C. Torben, W. Hansen, and A. H. Mattock, "Influence of size and shape of member on the shrinkage and creep of concrete," *J. Am. Concr. Inst.*, vol. 63–10, pp. 267–290, 1966.

Relation between Capillary Pore Pressure, Tensile Strength and Plastic Shrinkage Strain of Self-Consolidating Concrete

Parviz Ghoddousi[1], Ali Akbar Shirzadi javid[2] and Maziar Zareechian[3]

[1] Associate Professor, School of Civil Engineering, Iran University of Science and Technology (IUST)
[2] PhD in Construction and Management Engineering, School of Civil Engineering, Iran University of Science and Technology (IUST)
[3] Master of Construction and Management Engineering,PhD student in Iran University of Science and Technology (IUST)

Abstract An experimental investigation on capillary pore pressure, tensile strength and plastic shrinkage of self-consolidating concrete (SCC) is presented here. The aim of research is to study the relation between capillary pore pressure build up in concretes, early age tensile strength and plastic shrinkage strain. Capillary pore pressure apparatus was created for this research. Test was done in a climate chamber with the constant evaporation rate of 0.7 kg/m²/h.Four types of SCC were tested including SCC without any mineral admixtures and SCC containing of pozzolanic materials such as silica fume andmetakaolin. The results indicated that there is no strong relationship between capillary pore pressure and plastic shrinkage strain and it can be concluded that other parameters such as tensile strength development can play an important role in the plastic state of concrete. The results also showed that early age tensile strength can be effective factor in controlling cracks of concrete. No cracks appeared in the mixtures containing of silica fume and metakaolin because of tensile strength improvement up to 55 and 32 percent respectively, in comparison with the reference mixture. However capillary pore pressure in these mixtures was higher than pressure in the reference mixture.

Keywords: *Self-consolidating concrete, Plastic shrinkage strain, Early age tensile strength, Capillary pore pressure.*

Introduction

Plastic shrinkage occurs in fresh concrete usually within few hours after mixing the concrete and risk of its cracks endangered concrete structuresespecially in the elements with high surface to volume ratio such as slabs or highway pavement. Plastic shrinkage starts to rise when evaporation and hydration begin to consume water of concrete[1]. As a result particles near the surface are not covered by water molecules due to the adhesion of the surface molecules of the water with concrete particles. Therefore meniscus is formed on the surface of the concrete which causes negative pressure in the pores and led to shrinkage in the vertical and horizontal direction. After reaching a certain pressure, meniscus can`t keep concrete particles together and results the air penetration into the pores. This pressure is named as air entry pressure. After this time, the risk of cracking reaches to the highest level. It should be noted that a sudden drop in pressure is not a proof of the occurrence of cracks and tensile stress due to the restrained shrinkage should also overcome early tensile strength of concrete[2].Thus, growth of the negative capillary pore pressure is the main cause of plastic shrinkage cracking[3].

Combrinck et al.[1]suggested that air entry always occurs before or during the initial setting and their results also show that cracks start to develop after this time and its cracking potential decreases at the time of final setting because of growing strength. According to Roziere et al.[4]during the period of the initial setting to the final setting, strain reaches its minimum capacity. The reason for this event is faster growth in the modulus of elasticity than tensile strength.

This cracks is shallow and narrow but over time due to factors such as loading,

The water evaporation rate and amount of bleeding are factors that directly affect plastic shrinkage cracks. Other factors include setting time, construction methods, impact of concrete components including supplementary cementitious materials (SCMs), water-cement ratio, amount of cement paste and using of fibers[1].

A lot of researches have been conducted on the impact of various factors such as concrete components on plastic shrinkage cracking.For instance Almusallam et al. [5]evaluated impact of water-cement ratio on plastic shrinkage cracking and found that the cracks is directly related to water to cement ratio and described this event with lower tensile strength and higher rate of increasing capillary pressure of the samples with higher water to cement ratio. Ghoddousi et al.[6]studied influence of silica fume on plastic shrinkage crackingand found its positive effect on reducing cracking parameters and announced that this improvement was due to the impact of faster growth of tensile strength. Turkry et al. [7]compared self-consolidating concrete (SCC) and conventionally vibrated concrete (CVC) in two evaporation rate. When the evaporation rate is low, plastic shrinkage of SCC was more than CVC due to lack of bleeding while no cracks was observed in both concretes. In higher evaporation rate, amount of plastic shrinkage was approximately similar, however CVC exhibited larger maximum crack width and earlier cracking than the similar SCC mixtures. They expressed that this event may be attributed to the higher tensile strain capacity of SCC.

By reviewing the researches up to now, it can be realized that capillary pore pressure considered as the main reason for plastic shrinkage but other factors that can affect this event such as tensile strength, pore size distribution and relations among parameters were not evaluated.

Also different approaches have been described in conjunction with the risk of cracking. According to ACI Committee 305 [8] evaporation rate is considered as a parameter for the risk of plastic shrinkage cracking and it occurs when the rate of evaporation is over 1 kg/m².h. On the other hand, some researchers found plastic shrinkage as a parameter that can increase the risk of cracking. In the research studied by Holt et al.[9]risk of cracking can be very high in the shrinkage of more than 1000 µm/m, while Turcry et al. [7]declared that this shrinkage is more than 2200 µm/m. The best concept for studying risk of cracking in plastic state may be was proposed by Hammer et al. [10].They described plastic shrinkage cracking with a load and capacity concept where the load is restrained plastic shrinkage and the capacity is the early-age tensile strength of concrete. Thus it can be realized that in order to investigate the factors influencing the cracking in plastic state, all factors that impact load and capacity of concrete should be considered. In studies that have been conducted on factors affecting cracking, direct impact of all these factors on the occurrence of cracks is not addressed yet.

The aim of this study is to study the relation between capillary pore pressure as the main reason of shrinkage and amount of horizontal plastic shrinkage for mixtures.On the other hand, by applying this relationship, evaluate the impact of tensile strength on the plastic shrinkage cracking of concrete in high evaporation rate.

Experimental Program

Materials and mixtures proportioning

*Materials.*In the present research, a locally ordinary Portland cement type II conforming the requirements of ASTM C150[11] was used. The mineral admixtures were limestone powder, silica fume, metakaolin.

Two types of river sand (coarse and fine sand) with a specific gravity of 2440 kg/m3 was also used as fine aggregate. Crushed limestone with maximum size of 19 mm and specific gravity of 2540 kg/m3 was used as coarse aggregate. High-range water reducing admixture (HRWRA) with base of poly-carboxylate was also utilized.

*Mixtures proportioning.*Four types of SCC were prepared as follows:

SCC without any mineral admixtures (SCC-1), SCC containing of metakaolin (SCC-2) and SCC containing of silica fume (SCC-3). Water to cement ratio of SCC-1, SCC-2 and SCC-3 were 0.45. Another SCC without any mineral admixtures but with water to cement ratio of 0.5 were made (SCC-4).

Table XXIX. Mixture proportioning of SCC

Mix		SCC1	SCC2	SCC3	SCC4
Cement, kg/m³		450	360	414	450
Water, kg/m³		202.5	202.5	202.5	225
Metakaolin, kg/m³		0	90	0	0
Silica fume, kg/m³		0	0	36	0
Filler, kg/m³		150	150	150	150
Coarse gravels, kg/m³		358.1	353.3	355	344.1
Fine gravels, kg/m³		238.7	235.6	236.7	229.4
Sand, kg/m³		895.1	883.6	887.5	860.3
W/C		0.45	0.45	0.45	0.5
HRWR (% cement)		0.5	1	0.7	0.3
Slump flow	Spread (mm)	680	630	650	710
	T50 (S)	1.18	3	2.13	1
V-funnel (S)		3.57	11.14	8.84	2.95
Fc-28d, Mpa		45.3	60.3	67.5	41.3

Test procedure

Free plastic shrinkage test

As shown in Figure 2, the device setup for plastic shrinkage test includes two parts: 1) a Plexiglas mold with the inner size of 100 x 150 x 450 mm; and 2) a frame that three linear variable differential transformers (LVDT) were attached it. In order to reduce friction between mold and specimen before casting concrete, mold sides was coated by form release oil and a plastic sheet was placed on coated oil. Element that is intended to measure the settlement is made of aluminum, and its weight can be ignored.

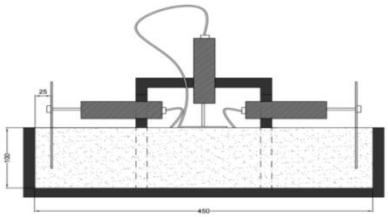

Figure 61. Schematic section view of free plastic shrinkage measurement

Restrained plastic shrinkage test

Test was carried out similar method according to ASTM C 1579[12].A rectangular mold (height 100 mm, length 450 mm and width 150 mm) was used to induce cracking. Five triangular shapes fixed to the bottom of the mold for better restraining. The larger central triangle reduced cross-section and it can induce cracking and four smaller triangles can restrain movement of the concrete as it was shown in figure 3. After about 90 minutes of testing, the sample will be analyzed to determine the starting time of cracking.
As it is stated before, capillary pore pressure is the main cause of shrinkage[3]. Therefore measuring capillary pressure development is essential for realizing shrinkage phenomena.Hencecapillary pressure was measured in the restrained plastic shrinkage molds by using capillary pore pressure apparatus made for this research. Pressure was measured by a pressure transmitter that is connected to the pore system. Device also has a syringe with a conic tip that is filled with degassed water in order to provide a hydraulic connection between the pore water in sample and the pressure sensor. It is placed vertically 45 mm beneath the surface of the sample and data were logged on a computer at 1-minute intervals. In order to avoid the influence of capillary pressure measurement tube on the pattern of cracks (because of pore water pressure connection in the mixture), needle placed 10 cm from the end of the form (figure 3).

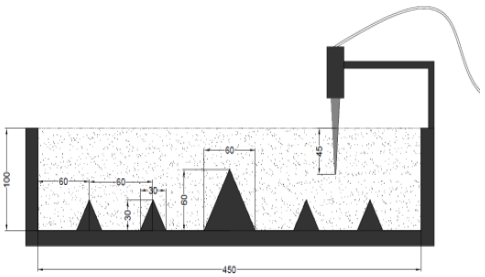

Figure 62. Schematic section view of restrained plastic shrinkage measurement

Early-age tensile strength test

Early-age tensile strength test is based on ASTM C496 [13] using cylindrical samples. Splitting test was done at 24, 48 and 72 hours and their tensile strength was determined.

Exposure condition

The exposure condition for the specimens was controlled in order to simulate hot weather condition. Concrete after mixing was poured into the mold and it was placed in a climate chamber with the temperature of 35±1° C, RH of 35±1% and

the wind speed of 4.2 m/s (15 km/h). This climate results in a constant evaporation rate of 0.7 kg/m².h according to Uno`s equation[14].
It should be noted according to ACI Committee 305 [8] that critical evaporation rate is 1 kg/m².h but some researches shows that plastic shrinkage cracking can occur in lower rate. In order to keep constant the rate of evaporation in concrete, based on the formula provided in ACI Committee 305 [8], concrete was made with a temperature of 27±1° C. For evaluating evaporation rate, a rectangular mold was weighed with an electronic scale every 20 minutes.

Results and Discussion

Capillary pore pressure and plastic shrinkage

The results show that using of pozzolanic materials leads an increase in the slope of the capillary pressure curve growth. Based on figure 4, the highest slope of the pore pressure growth is seen in the mixture containing silica fume (SCC-3). The main reason for this result is the high surface area of silica fume as compared to other materials. Moreover, mixture containing of silica fume has smaller pores and consequently a higher growth sleep than other mixtures [15].On the other hand, the mixture with the water to cement ratio of 0.5 (SCC-4) has the lowest capillary pressure growth slope. This could be ascribed to the increase in the diameter of pores with an increase in the water to cement ratio, which could be explained by the ratio of the reversed radius of curvature with the negative pore pressure [16].

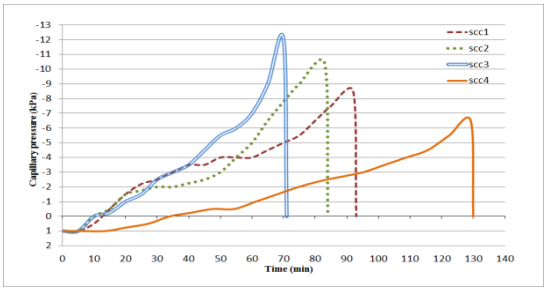

Figure 63. Negative capillary pore pressure

Results regarding the longitudinal plastic shrinkage of SCC mixtures are presented in figure 5. Shortly after the onset of the negative capillary pore pressure, longitudinal shrinkage starts to grow. Meanwhile, the settlement growth rate also decreases gradually. Results show that maximum plastic shrinkage is belonging to the mixture with higher water to cement ratio (SCC-4).The first reason for this behavior may be due to the smaller pores in SCC mixtures contains supplementary

cementitious materials, and its inability of more shrinkage [15]. The second reason for this behavior is the highest growth of tensile strength in theSCC containing limestone powder as filler and metakaolin as mineral admixture, even in early days, due to its nucleation and filling properties, which prevent higher shrinkage[17].

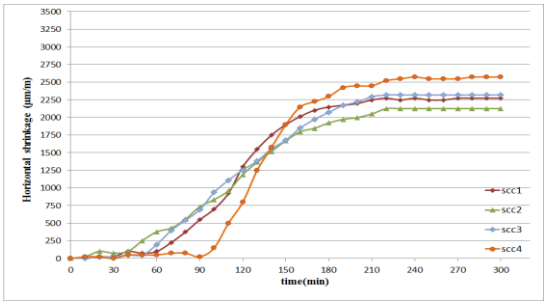

Figure 64. Free plastic shrinkage

These reasons can be proved by examining trend line of capillary pore pressure parameters against slope and maximum plastic shrinkage of each mixture (figure 6). It is clear from figurethat these two parameters are not properly correlated to each other and other factors such as pore size distribution and rate of developing strength in concrete play an important role in shrinkage of the mixtures.
However, it should be mentioned that capillary pressure is the main cause and driving force of concrete shrinkage. As seen in figure 7, the onset of capillary pressure is directly related to the onset of shrinkage, and when the capillary pressure finds the ability to separate the concrete from the mold, shrinkage starts.

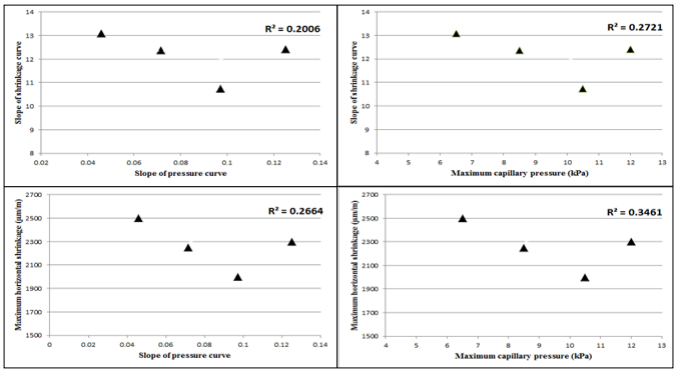

Figure 65. Relation between shrinkage and capillary pressure parameters

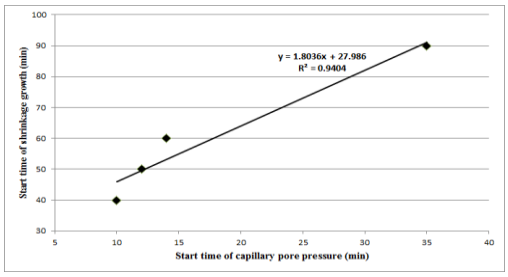

Figure 66. Relation between capillary pressure and shrinkage onset

Early-age tensile strength

Figure 8 presents results of early-age tensile strength at 24, 48, 72 hours. Obtained results show that mixtures with mineral admixtures have more strength due to nucleation effect of fine particles, filler effect and formation of secondary C–S–H by the pozzolanic reaction. Results also show that increasing of water to cement ratio decreases tensile strength. Findings is confirmed by [18].

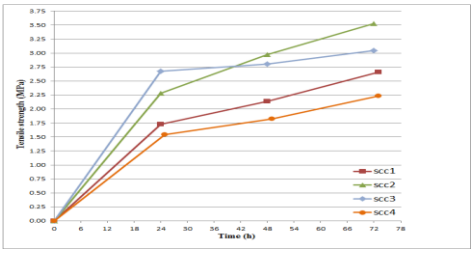

Figure 67. Early age tensile strength of the mixtures

Relation between capillary pore pressure and early-age tensile strength

Relations between tensile strength with the maximum capillary pressure and slope of pressure are illustrated in figure 9. As it can be seen, the slope of the line can be approximately correlated to tensile strength. The reason for this can be found in pore size of the mixtures. According to the Gauss-Laplace's equation the smaller pore size cause the higher rate of capillary pore pressure development. Therefore tensile strength is inversely related to the pore size of the concrete. Results also show that capillary pressure (as the driving factor) and tensile strength (as theshrinkage preventing factor) are directly related. This proportion can be explained by the size of pores. When the capillary pressure is high in the concrete, the tensile

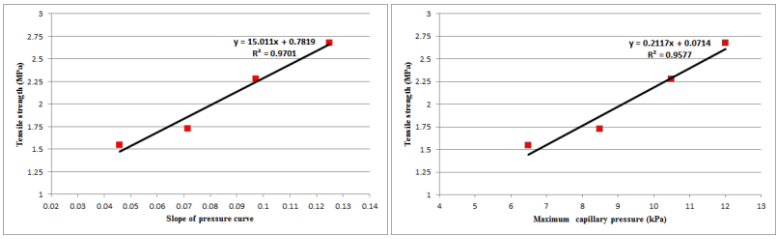

Figure 68. Relation between tensile strength and capillary pressure parameters

strength and size of pores prevent concrete shrinkage. These three parameters influence shrinkage, and cracking does not occur as long as the effect of driving forces fails to dominate all of the resisting forces.

Evaluating the cracks due to restrained shrinkage

Table III presents results of SCC mixture cracking parameters. Significant point according to table is lack of cracking in the SCC containing metakaolin (SCC-2).Two reasons can be explain for this, first is that shrinkage as a cause of stress is less than the others and another reason is better development of early age tensile strength in this mixture.

Table XXX. Crack parameters

Mix	Area (mm²)	Width (mm)	Crack onset (min)
scc1	22.84	0.267	136
scc2	0	0	-
scc3	0	0	-
scc4	63.19	0.601	138

The condition of the SCC containing silica fume (SCC-3) is similar SCC-2 from view point of lack of cracking. However, due to the larger surface area of silica fume, the growth of capillary pressure in the SCC-3 has a higher slope. As a result, shrinkage in SCC-3 (even with its smaller pores and higher growth of its strength) is larger than SCC-2. Therefore the effect of tensile strength is very important in the resistance against cracking. To find a better understanding of this phenomenon, the results of maximum shrinkage, tensile strength during peak shrinkage, and area of cracks are presented in figure10. According to the figure, in the SCC mixture with the water to cement ratio 0f 0.5 (SCC-4), the area of cracks is significantly higher than other mixtures. Another point inferred from this figure is that with an increase in the difference between shrinkage and tensile strength, the areas of cracks also increase. Therefore, it could be concluded that to study the cracks both

sides of the equation, i.e. the load and capacity, should also be examined (here shrinkage level is the driving force and tensile strength is the resisting force). This finding is accordant with the resultsstated by Hammer et al.[10].

.

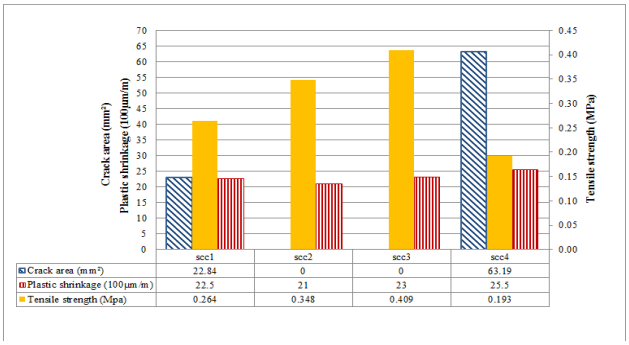

Figure 69. Comparing parameters affecting cracks

Conclusions

Specific findings of this research included the following:

- Capillary pressure is not only factor affecting the shrinkage in concrete, but also tensile strength development and pore size distribution can play an important role.
- Negative capillary pore water pressure is the main factor and driving force of plastic shrinkage and approximately direct relation existed between time of capillary pressure and shrinkage onset.
- Tensile strength can be effective in controlling cracks in concrete. No cracks appeared in the mixtures containing of silica fume and metakaolin because of tensile strength improvement.

References

1. Combrinck, R. and W.P. Boshoff, *Typical plastic shrinkage cracking behaviour of concrete.* Magazine of Concrete Research, 2013. **65**(8): p. 486-493.
2. Slowik, V., M. Schmidt, and R. Fritzsch, *Capillary pressure in fresh cement-based materials and identification of the air entry value.* Cement and Concrete Composites, 2008. **30**(7): p. 557-565.

3. Wittmann, F., *On the action of capillary pressure in fresh concrete.* Cement and Concrete Research, 1976. **6**(1): p. 49-56.
4. Roziere, E., R. Cortas, and A. Loukili ,*Tensile behaviour of early age concrete: New methods of investigation.* Cement and Concrete Composites, 2015. **55**: p. 153-161.
5. Almusallam, A., et al., *Effect of mix proportions on plastic shrinkage cracking of concrete in hot environments.* Constructionand Building Materials, 1998. **12**(6): p. 353-358.
6. Ghoddousi, P., A.M. Raiss ghasemi, and T. Parhizkar, *A comparision between plastic shrinkage of concrete containing silica fume and the normal concrete.* International Journal of Civil Engineering, 2007 :(4)5 .p. 266-273.
7. Turcry, P. and A. Loukili, *Evaluation of plastic shrinkage cracking of self-consolidating concrete.* ACI Materials journal, 2006. **103**(4).
8. ACI, D., *305R-Hot Weather Concreting.* American Concrete Institute International, 1999.
9. Holt ,E., *Contribution of mixture design to chemical and autogenous shrinkage of concrete at early ages.* Cement and Concrete Research, 2005. **35**(3): p. 464-472.
10. Hammer, T., *On the strain capacity and cracking mechanisms of high strength concrete at very early age.* Creep, Shrinkage and Durability Mechanics of Concrete and other Quasi-Brittle materials, 2001.
11. ASTM C 150, Standard Specification for Portland Cement, ASTM International, West Conshohocken, PA, 2007.
12. PCI, *Interim Guidelines for the Use of Self-Consolidating Concrete in PCI Member Plants.* PCI Journal, 2003. **48**(3): p. 14-18.
13. BS Standard 1881, Standard Test Method for Compressive Strength of Cubic Concrete Specimens, Part 116.
14. ASTM C 1579, Standard test method for evaluating plastic shrinkage cracking of restrained fiber reinforced concrete, ASTM International, West Conshohocken, 2006.
15. ASTM C496, Standard test method for splitting tensile strength of cylindrical concrete specimens,ASTM International , vol 04.02, Philadelphia, 1984.
16. Uno, P.J., *Plastic shrinkage cracking and evaporation formulae.* ACI Materials Journal, 1998. **95**(4).
17. Berodier, E. and K. Scrivener, *Impact of filler on hydration kinetics.* 2012.
18. Lafhaj, Z., et al., *Correlation between porosity, permeability and ultrasonic parameters of mortar with variable water/cement ratio and water content.* Cement and Concrete Research, 2006. **36**(4): p .625-633.
19. Stark, J., B. Möser, and F. Bellmann, *Nucleation and growth of CSH phases on mineral admixtures*, in *Advances in Construction Materials 2007*. 2007, Springer. p. 531-538.
20. Tasdemir, M., F. Lydon, and B. Barr, *The tensile strain capacity of concrete.* Magazine of Concrete Research, 1996. **48**(176): p. 211-218

The Effect of Temperature and Humidity on Strength Development of Grouts

A. Farzampour[1] and A. Radlinska[2]

[1, 2] Pennsylvania State University

Abstract Weather at cites with dry or humid, cold or hot, rainy or snowy conditions could be highly variable during any period of time. Grout, compared to other material sources, could be highly sensitive to cold weather conditions, especially when the compressive strength is the matter of concern. Grout as one the substantial residential building material used in retaining walls, rebar fixation, sidewalks is in need of deeper investigation, especially in extreme weather condition. To obtain determined structural performance, in lower temperatures, casting and pouring concrete require special procedures, which should strictly be followed and controlled. Under such cold conditions, special precautions regarding placing, finishing and curing concrete should be warranted.
In this article, compressive strength development of four commercial grouts at three temperatures and two humidity rates are evaluated. This experiment is aimed to better assess grout strength development over time and overall compressive strength when the material is cast at low temperatures. The results show that decreasing the temperature would results in lower ultimate compression strength development capacity in all of the grouts. In addition, the low temperatures could be significantly influential on the behavior of grouts compared to lower humidity rates.

Keywords: *Cold weather Concrete, Compressive strength, Low temperature, Humidity effect.*

Introduction

Due to time and equipment limitation, there is noticeable need to evaluate the concrete behavior on-site without any experimental test. Concrete can be placed in cold weather conditions provided that necessary precautions are taken to reduce the negative effects of low ambient temperatures. Pouring and curing concrete in cold weather require special procedures, which should be strictly followed to achieve determined performance of concrete and structure [1, 2]. Studies accredited by

cement and concrete organizations nationally and internationally have been prepared to address the cold weather concreting procedures [1, 2].

ACI 306 [1] defines cold weather concreting as a period when for more than three consecutive days, either the average daily air temperature is less than 5°C (40°F), or the air temperature is not greater than 10°C (50°F) for more than one-half of any 24 hour period. Under cold temperatures, concrete gains very little strength (or even stops gaining strength) due to decrease in hydration process. At the same time, the forces generated by the expansion of ice compared to water could be highly detrimental to overall strength of concrete [1, 3, 4]. In plastic stage of concrete, if concrete freezes, 50 % of the concrete strength would be reduced and problems associated with durability would be inevitable. In addition, the time of concrete set would be twice by 10°C decrease, leading to longer time of being vulnerable to ambient damage [1, 3, 5]. Therefore, it is important to protect the concrete from cycles of freezing and thawing until it gains minimum strength of 3.5 MPa (500psi).

It is necessary to make sure ACI guide is fully understood and followed prior to and after pouring concrete in cold weather (Figure 1). This paper provides brief overview on cold-weather concreting along with experimental analysis of four commercially available grouts. The significant outcome of this research is to understand the compressive behavior of grouts in cold temperatures as one of the most common materials in constructions and residential buildings as well as to achieve higher safety at a specified time period. The results of this research could be followed in colder months which special concrete practices and appropriate planning are matters of concern, and the loss due to cold temperatures could be irreversible. Generally, it is recommended that higher strength admixture mixes lower water-cementious material ratios, adding non-chloride admixtures, or using type-three cement which is high strength cement to be considered in cold weather.

Figure 70. a) placement of concrete in cold weather [1] b) curing of concrete in cold weather [2]

Another point of concern, especially in cold weather, is that the inner sides of the concrete would have higher temperature due to hydration of the cement with water, while the surface of the member would experience a significantly lower temperature. Significant temperature difference between interior sides and the interface of the concrete member would result in thermal cracks leading to less

compressive strength. Cold weather curing could lead to development of micro-cracks and adversely affects inter-facial zone [6]. In addition, at freezing temperatures, concreting could result in 20% stiffness reduction after 28 days, and the water absorption of hardened concrete would be increased as result of cold-curing leading to increase in vulnerability against cracks [6] (Figure 2). It is noted that concrete which is attained enough strength by appropriate curing conditions, could develop its potential against subsequent cold weather exposures [6, 7].

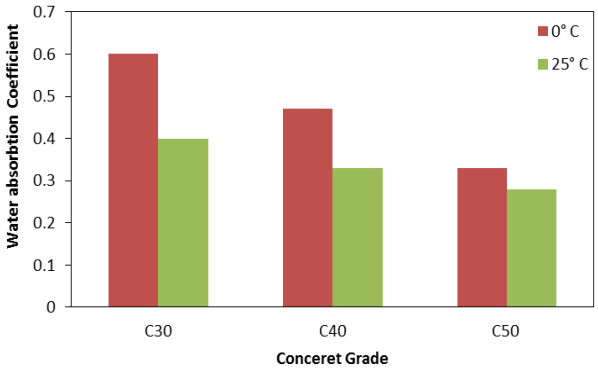

Figure 2. The influence of curing temperature in water absorption for 30, 40, 50 MPA compressive strength samples [8]

Research Significance

This research is conducted to thoroughly investigate the behavior of four commercially available grouts as one the most essential materials used in residential buildings, in extreme weather conditions. Retaining walls, Column-beam rebar fixation, sidewalks are among a number of implementations of this material. The compressive strength development for each grout is indicated and compared, the effect of water cement ratio, temperature, humidity and time are considered.

Materials and Mixing Procedure

To evaluate the behavior of grouts in cold temperature and in humidity index of Pennsylvania, three different temperatures and two humidity indexes were investigated to assess the concrete member curing process in cold weather. Table 1 indicates four different grouts with recommended water cement ratios.

Table I. The water-cement ratio of four investigated grouts

Grout	W/C
BASF	0.12
Dayton	0.12
Five Star	0.18
Quickrete	0.18

Table 2 indicates the testing regime regarding various temperatures, humidity rates and the number of samples. All the grout mixtures are designed based on the recommended cement ratios. The mixing procedure is based on ASTM manual [C109-08, C1437 – 13, C1074-11, C 666-03 and C1611/C1611M − 14]. All samples are placed in molds and consolidated with tamping rod, and then they are immediately covered with wet burlap and plastic for 24 hours. Afterwards, samples are demolded at 24 hours curing and one-day compressive strength is tested according to ASTM C109 [9]. The compressive strength is tested at 3, 7, 14 and 28 days

It should be mentioned that, the samples are kept in the specified temperatures mentioned in Table 2 for a week, and they transported to temperature 23 (º C) rooms with the same humidity rate afterwards. For each grout in each time interval three samples are tested to evaluate compressive strength with higher accuracy.

Table II. Temperature and humidity index plan for each grout

Temperature during the first 7 Days (ºC)	Relative Humidity during the first 7 Days (%)	Temperature after 7 Days (ºC)	Relative Humidity after 7 Days (%)	Number of Cubes (2×2×2in.)	Number of Cylinders (maturity)
23	100%	23	100%	15	1
23	50%		50%	15	1
10				15	1
5				15	1

Discussion of the Results

The strength behavior of four common types of grout in different temperatures and humidity rates are investigated in this section. Figures (3-6) indicate the general behavior of grouts with time.

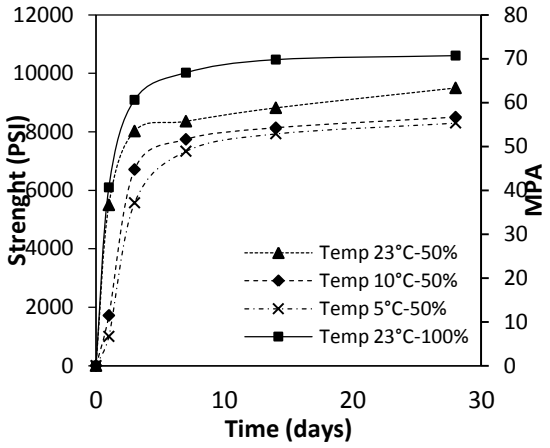

Figure 3. The effect of temperature and humidity on BASF

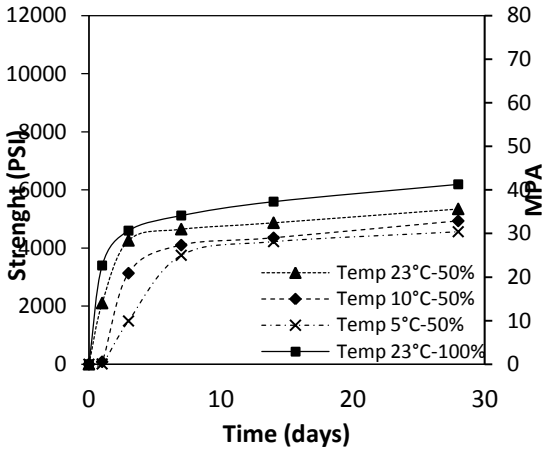

Figure 4. The effect of temperature and humidity on Five Star

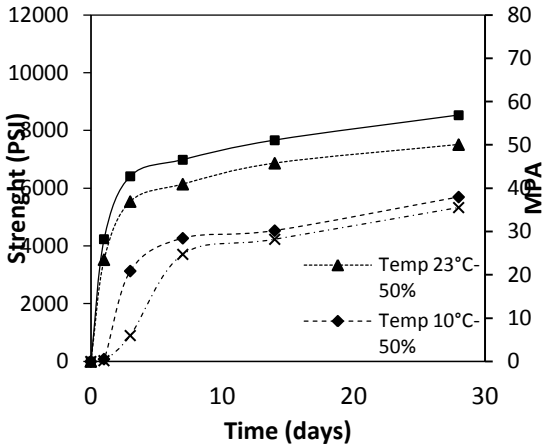

Figure 5. The effect of temperature and humidity on Quickrete

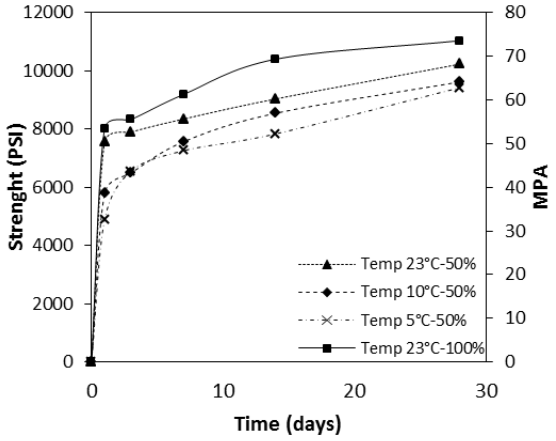

Figure 6. The effect of temperature and humidity on Dayton

According to the strength behaviour, the effect of temperature is significant. Considering the overall strength development of the grouts, reducing the curing temperature as much as 15 degrees could result in more than 20% reduction in ultimate strength; however, decreasing the humidity percentage by 50% could lead to more than 10% reduction in ultimate strength.

Conclusions

The strength development of four commercially available grouts was investigated in three different temperatures and two humidity rates. It is shown that the effect of humidity on curing regime of concrete is noticeable. The effect of temperature on the overall maturity of the concrete is discussed, and it is observed that the concrete cured in lower temperatures could never reach to the strength which the concrete with higher curing temperature could have reached; therefore, curing temperature could be highly essential in strength of the grouts. In addition, the usage of lower water-cement ratios is recommended in cold weather curing, as the water turning to ice, the expanding forces would be increased, and damage would be inevitable; therefore, lower water-cement ratios is strongly recommended, especially in cold weather condition.

References

[1] American Concrete Institute. (2010), *Guide to Cold Weather Concreting*, Committee 306, pp. 1- 18.

[2] Krylov B.A. (2008), *Chapter 14: Cold-Weather Concreting, Design and Control of Concrete Mixtures*, pp 1.18.

[3] Kosmatka S. H. and Wilson M. L., (2011), *Design and Control of Concrete Mixtures*, 15 (Ed.), Portland Cement Association, Skokie, Illinois.

[4] ASTM C94, *Standard Specification for Ready Mixed Concrete*, *PA.*

[5] ASTM C31, *Making and Curing Concrete Specimens in the field, PA.*

[6] Anderson K. W., Uhlmeyer J.S., Kinne C., Pierce L.M. and Muench. S. (2009). *Use of Maturity Method in Accelerated PCC Concrete*, pp.1- 104.

[7] Carino N.J. (2003). *Chapter 5: The Maturity Method*, Handbook on Nondestructive Testing of Concrete, pp. 1-47

[8] Y. Nassif A. and F. Petrou M. (2013). *Influence of cold weather during casting and curing on the stiffness and strength of concrete*, Construction and Building Materials, vol 44, pp. 161-167.

[9] ASTM C109, *Standard Test Method for Compressive Strength of Hydraulic Cement Mortars.*

Self-Roughening Concrete with Enhance Shear-Friction Capacity for Cold Joint Applications

Giovanni Loreto, T. Russell Gentry, Kimberly E. Kurtis and Lawrence F. Kahn

School of Civil and Environmental Engineering
Georgia Institute of Technology, Atlanta, GA

Abstract: The concept of shear friction in the behavior of reinforced concrete and composite structures describes the ability to transmit shear across a given boundary, typically between two separate placements of concrete – sometimes referred as a cold joint. In order to enhance shear capacity across cold joints, a unique self-consolidating concrete (SCC) mixture was developed by incorporating of a small fraction of light-weight coarse aggregate (LWA) so that roughening by raking or other means was not necessary. Fresh and hardened properties such as slump flow, segregation resistance, shrinkage, and strength were evaluated to ensure overall concrete performance. In addition, the roughness of the concrete surfaces was characterized by using a qualitative approach proposed by the International Concrete Repair Institute along with a quantitative approach that complemented the use of existing technology. The test results indicate that the optimized self-consolidating concrete, referred as self-roughening concrete, can successfully increase the shear friction capacity between cold joints showing great potential in real world applications.

Keywords: *Self-Consolidating Concrete (SCC), Light Weight Aggregate (LWA), Cold Joint, Shear Friction, Surface roughness.*

Introduction

Construction joints are necessary in concrete structures when placing concrete in a continuous operation becomes impractical due to unit size, batching and mixing capacity, weather conditions, equipment problems, or the like. When one of these conditions occurs, depending on the time between placements, different surface treatments are used to provide adequate shear capacity between layers of concrete, including manually roughening of the surface.

The concept of shear friction in the behavior of concrete structures describes the ability to transmit shear across a given boundary, typically between two separate placements of concrete – sometimes called a "pour joint" or "cold joint". In conventional reinforced concrete internal reinforcements provides a tension tie that prevents the concrete placements from moving perpendicular to the boundary [1]. The friction of the surface, which is considered by ACI 318 [2] to be a function of the surface roughness, prevents the two placements from moving parallel to the boundary. The normal, clamping force at the interface is provided by the tensile strength of the steel crossing the interface, and the coefficient of friction varies based on the surface roughness, thus "shear friction".

In order to enhance shear friction capacity across as-cast cold joints, a self-consolidating concrete (SCC) mixture was developed by incorporating of a small fraction of light-weight coarse aggregate (LWA), between 5 and 15% by volume of coarse aggregate, so that roughening by raking or other means was not necessary. The purpose of the LWA is to provide an internal source of surface roughening, while still satisfying the requirements for grading (ASTM C33 [3]). Due to its lower specific gravity, the LWA rises to the surface of the concrete shortly after placement.

The attributes of an appropriate SCC mixtures were selected as follows: (1) high spread to facilitate concrete placement in the field without internal vibration, (2) cohesive concrete mixture to prevent segregation of the normal weight aggregates from the cement paste during concrete placement, and (3) low viscosity of the SCC so that the LWA would float. In addition, prior research has demonstrated that high volumes of fly ash, in particular, can be used to produce SCC with reduced drying shrinkage [4]. Therefore, in order to limit shrinkage and heat development associated with cement hydration, improve durability, and to provide the desired self-consolidating behavior [5], the use of relatively high substitution of fly ash (>35%) for cement was included in designing the mixtures.

A SCC mix design that respected all these characteristics was referred as self-roughening concrete (SRC). The following sections discuss the methodology used in designing SRC mixtures: selection of material constituents, optimization of the mixtures, and evaluation of fresh and hardened properties.

Materials and mixture proportioning

Concrete typically contains four main ingredients: coarse aggregate, fine aggregate, cement, and water. Additionally, supplementary cementitious materials (SCM) and chemical admixtures are used to modify the plastic and/or hardened state properties. SCC mixes generally uses a higher volume of fine aggregates and employ super-plasticizers and water-reducers to achieve their increased workability. The SRC mixtures presented in this paper contained coarse and fine aggregates, cement, SCM such as fly ash, water and high-range water reducer as

admixture.

The coarse aggregate was a crushed granite with a maximum size aggregate of 19 mm or #67 (3/4 in.). As a fine aggregate, a blend of 50% manufactured (e.g., fractured granite) sand and 50% alluvial sand was used in order to enhance performances during the fresh state. Gradation curves were generated in accordance to the ASTM C33, which fully respected the upper and lower limits of the ASTM specifications. Density and specific gravity were also determined as per ASTM C29 [6] and ASTM C127 [7], respectively. In addition to the granite, expanded slate aggregate produced using a rotary kiln process was included in the mix design to generate surface roughness.

The cement used for the laboratory mixes was an ASTM C150 [8] Type I/II Portland cement. The only supplementary cementitious material used in combination with cement was fly ash which conformed to ASTM C618 [9] specifications for Class F.

The chemical admixture was a polycarboxylate high range water reducer. For laboratory conditions the recommended dosage was selected between 6 fl. oz. and 8 fl. oz. per 100 lbs. (155-210 ml/100 kg) of cementitious materials. This admixture was added at the end of the batching cycle directly to freshly mixed concrete in the concrete mixer.

Mixture design

All mixes were cast in accordance with ASTM C 192 [10] (standard practice for making and curing concrete test specimens in the laboratory). During the mixing, dry sand was used while coarse aggregates were used in the saturated surface-dry (SSD) condition. LWA were pre-soaked in water for 24 hours and then brought to SSD condition before their use. The design quantities considered in the mix design proportions were:

- Total Cement, kg/m^3 [lb/yd^3]
- Fly Ash, kg/m^3 [lb/yd^3]
- Coarse Aggregate - #67, kg/m^3 [lb/yd^3]
- Coarse LWA - #7 – 5%, 10% and 15% in volume of #67
- Water Cement (w/c) ratio
- Chemical admixtures, ml/m^3 (fl oz/yd^3) (HRWR)

A total of thirty-five trial mixes were cast. Table I reports the quantities for a selected mix that passed the qualification protocol, and also included the mixes with 5%, 10% and 15% of LWA. All trial mixes reported in Table I showed adequate slump flow ranging from 533 – 635 mm (21 in. to 25 in.) and comparable performances using slightly different amount of HRWR.

Table I. Mix design.

Mix Component	*SCC*	*SRC 5%*	*SRC 10%*	*SRC 15%*
Cementitious		*kg/m^3 [lb/yd^3]*		
Cement Type I/II		366.4 [617]		
Fly Ash, Class F		272.3 [459]		
Water		203.6 [343]		
w/cm		*0.318*		
Coarse Aggregates				
# 67	763.2 [1286]	724.0 [1221]	676.0 [1157]	648.4 [1093]
LWA	-	14.4 [24.5]	29.1 [49.0]	44.1 [74.25]
Fine Aggregates				
Natural sand		402.5 [678.5]		
Manufactured sand		402.5 [678.5]		
Admixtures, ml/100 kg [fl oz./cwt]		425 [6.36]		
Flow Slump mm [in.]		585 – 635 [23 – 25]		
T20 (sec)		4 - 5		
"S" groove (0-5)		0 – 0.5		
VSI (0-3)		0		
Compression, MPa [psi]	53.12 [7705]	52.88 [7670]	52.82 [7661]	52.45 [7608]
Std. dev., MPa [psi]	-	807	275	537
Unit weight kg/m^3 [pcf]	2402 [156.3]	2370 [150.4]	2322 [156.3]	2290 [150.4]
CSP Roughness (1-9)	-	7	8	9
S_a, mm^{-1} [in^{-1}]	-	0.018 [0.448]	0.031 [0.789]	0.042 [1.071]

Test Results and Discussion

Fresh properties

Slump flow was used to measure fluidity; the VSI and the “S” groove tests were use to assure filling ability and resistance to segregation.

Slump flow test. To determine the slump flow, an Abrams cone was inverted and placed on a non-absorptive surface and filled with fresh concrete without any tamping. The cone was lifted and the concrete flowed out under its own weight. Two perpendicular measurements of the maximum diameter were taken across the spread of concrete and the average was reported. The final flow time, from cone

removal to flowing completion was recorded, as well as the T50 flow time, which is the time needed by the concrete to spread up to 50 mm (20 in.). Slump flow spread diameter values of 584 ± 51 mm (23 ± 2 in.) were considered satisfactory with test results ranging from 530 mm to 635 mm (21-25 in.). T50 values spanned from 3 sec. to 5 sec., and they were inversely proportionated to the slump flow diameter. Fresh properties are reported in Table I.

"S" groove test. The "S" groove test is a simple and effective method for determining the stability and self-healing ability of fresh SRC. Using a finger or a tamping rod, an "S" is drawn into the concrete on the slump flow board. If the mix is stable, the concrete rapidly fills the 'S' groove and the stability of the concrete is good, otherwise a layer of paste or bleed will fill in the groove, essentially showing the segregation of the coarse aggregate within the mix. An empirical range of values spanning from 0 to 5 was used (0 being highly stable and 5 highly unstable) was associated to the test in order to better characterize the behavior. Numerical data are reported in Table 1.

Visual stability index (VSI) [11]. The VSI test was used in conjunction with the slump flow test. The range of values for the VSI is 0 through 3, with zero being a highly stable mix, and 3 designates a highly unstable mix. The parameters for determining the VSI number of a given mix are mortar halos, bleed, air bubbles, and aggregate pile-up. Table II presents the different criteria for VSI numbers. Mortar halos result from the segregation of the paste from the concrete due to too much water or coarse aggregate in a mix. An unstable mix may contain a mortar halo less than 10 mm (0.4 in.); larger halos result in highly unstable concrete mixes. Slight bleed and few air bubbles surfacing were allowed for stable mixes, but not highly stable. Data are reported in Table I.

Table II. Visual stability index [11].

Rating	**Number**	**Criteria**
Highly Stable	*0*	No evidence of slump segregation
	0.5	Very slight evidence of bleed and air popping
Stable	*1*	No mortar halo No aggregate pile-up
	1.5	Slight bleed and air popping Just noticeable mortar halo and aggregate pile- up
Unstable	*2*	Slight mortar halo, less than 0.4 in. (10mm) Slight aggregate pile-up Noticeable bleed
Highly Unstable	*3*	Large mortar halo greater than 0.4 in. (10mm)

In general, the slump flow tests in conjunction with the visual stability index (VSI) were effective in evaluating the workability of the SRC mixtures. The data collected using these tests appeared to be adequate for quantifying the rheological properties of the SCC. In particular, SRC with a slump flow less than 432 mm (17 in.) did not display self-compacting properties; on the other hand SRC with a slump flow over 660 mm (26 in.) experienced severe segregation and bleeding. The inclusion of LWA into the mix led to the formation of a rough surface as showed in Figure 1.

Figure 1: From left to right, concrete cylinders with 15%, 10%, 5% and no-LWA substitution.

Hardened properties

All specimens were cured following the ASTM C192 requirements: specimens were stored in a fog room with temperature of 23 ± 2 °C (73.5 ± 3.5 °F) and humidity > 95%.

Compressive strength. Compression tests were conducted as per ASTM C39 [12] using 100x200 mm (4x8 in.) cylinders. Five cylinders were cast for every mix, demolded after 24 hours and stored in a fog room for 28 days until testing. Results are reported in Table I along with their standard deviations.

Drying shrinkage. Drying shrinkage tests were performed following the AASHTO T160 [13] and Alabama DOT [14] specifications. Two sets of three specimens per each mix were cast in prism molds (75x75x285 mm - 3x3x11.25 in.), coated in advance with an oil-based form release agent, with gage studs inserted into their ends. Concrete specimens were covered with a polyethylene sheet and wet towels to avoid moisture loss during the first 24 hours. They were demolded after one day; initial length and mass were measured; and then they were stored in the fog room until further testing. Following the Alabama DOT specification, the first set of specimens was cured in these conditions for seven days, whereas the remaining

specimens were cured for 28 days in accordance to AASHTO T160. Upon the end of curing duration, the specimens were moved to an environmental chamber with a temperature of 23 ± 2 °C (73.5 ± 3.5 °F) and relative humidity of 50 ± 4 %. During drying, the length was monitored according to ASTM C 157. The shrinkage measurements were taken at constant intervals from the time the specimens were removed from moist curing. After 54 days, the average shrinkage was equal to 213 με with a standard deviation of 16 με and 207 με with a standard deviation of 17 με for specimen with 7-day and 28-day curing time, respectively. Figure 2 compares the difference between 7-day and 28-day shrinkage where each point represents an average of three repetitions. Average measured drying shrinkage was less than 250 με in both curing times.

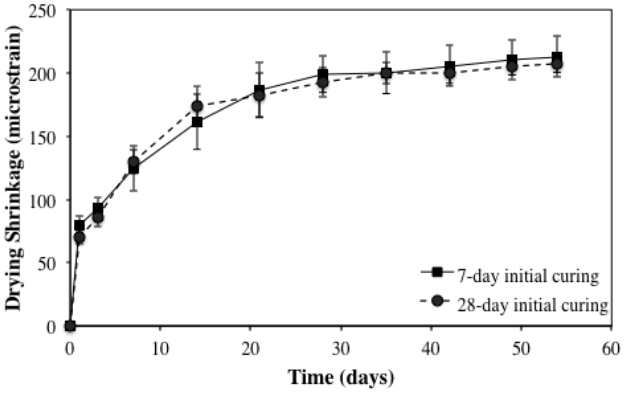

Figure 2: Free Shrinkage test results.

Measurement of surface roughness. One of the main objective in developing the SRC was to generate the appropriate surface roughness essential to facilitate shear interlock between the existing substrate of concrete and the overlay at a cold joint. The ACI 318 shear friction concept is that shear forces are transferred across a joint by friction between the surfaces. The frictional force is a function of the normal force applied and the coefficient of friction, μ, between the surfaces. By incorporating a small fraction of LWA (5%, 10% and 15% in volume,) in the SCC mix designs, the SCC was able to generate a rough surface so that roughening by raking or other means may not be necessary. Surface roughness was measured using two methodologies: (1) International Concrete Repair Institute's (ICRI's) standard concrete surface profiles (CSPs) (qualitative assessment) and (2) a quantitative assessment.

ICRI's CSPs are benchmarks used to establish industry acceptable specifications and represent varying degrees of concrete roughness and texture. Nine rubber profiles represent varying degrees of concrete roughness, with CSP 1 being thought to represent the least rough (smoothest), while CSP 9 being the most rough.

Comparing the concrete surface to the CSPs, a qualitative assessment of the surface roughness was performed by visual inspection.

In addition to the CSP molds, a quantitative assessment of concrete surface condition was also performed. Using 152x559 mm (6x12 in.) concrete cylinders, the amplitude of surface roughness was determined by measuring the distance between the top of the exposed aggregate and its junction with the paste (distance A) using a caliper as shown in Figure 3. A coefficient of surface roughness, S_a, was then calculated considering that roughness is directly proportioned to the number of LWA particles present on the surface and their average amplitude, whereas it is inversely proportional to the surface area. These consideration and the device used for measuring the average amplitude led to the following equation [15]:

$$S_a = \frac{n \times \sum_1^n A_n}{S} \quad (1)$$

where: n is the number of LWA particles present on the surface, A_n represents the average amplitude and S is the nominal surface area of the concrete specimen. Results of both methodologies are reported in the last two rows of Table I.

Figure 3: Roughness quantitative measurements.

Conclusions

1. The SRC mixtures demonstrated slump flows between 530 mm to 635 mm (21-25 in.) which satisfy flow and filling ability for an SCC.

2. The SRC mixes demonstrated cohesive properties, so that the mixtures remained in a consistent state during concrete placement while allowing a controlled segregation of the LWA. This was a particular challenge in the SRC because it is necessary that some small fraction of the lightweight aggregate rise through the

mix (and thus segregate) to form the rough surface, but the remaining portion of the mix, including the normal weight aggregates and fines, should remain cohesive.

3. Because of the high cement fraction in the SRC mixes, early shrinkage of the concrete mix was assessed. High volumes of fly ash used to produce SRC and reduce the early heat of hydration helped to reduce drying shrinkage in the self-roughening SRC mixes with values around 220 με after 54 days.

Acknowledgements

The authors gratefully acknowledge the Department of Energy (DOE) for the support provided to the research under Grant DE-NE0000667NEET and the industrial partner Stalite for the support with the material procurement. Any opinions, findings, conclusions and recommendations expressed in this material are those of the authors and do not represent policies, opinions or conclusions of the sponsor.

Reference

[1] Kahn, L. F. and Mitchell, A. D. (2002), *ACI J. Struct*., vol. 88, n.1, p.98.
[2] ACI Committee 318 (2011) Building Code Requirements for Structural Concrete, American Concrete Institute, Farmington Hills, MI, pp. 503.
[3] ASTM C33/C33M (2013) "Standard Specification for Concrete Aggregates", West Conshohocken, PA.
[4] Kahn, L.F., Kurtis, K.E. and Horta A. (2005) *Report: Research Project 2042*, Georgia Department of Transportation, Atlanta, GA.
[5] Gajda, J. (2007) *Mass Concrete for Buildings and Bridges*, PCA, p. 34
[6] ASTM C29 (2009) *Standard Test Method for Bulk Density (Unit Weight) and Voids in Aggregate***,** West Conshohocken, PA.
[7] ASTM C127 (2012) *Standard Test Method for Density, Relative Density (Specific Gravity), and Absorption of Coarse Aggregate*, West Conshohocken, PA.
[8] ASTM C150 (2012) *Standard Specification for Portland Cement*, West Conshohocken, PA.
[9] ASTM C618 (2008) *Standard Specification for Coal Fly Ash and Raw or Calcined Natural Pozzolan for Use in Concrete*, West Conshohocken, PA.
[10] ASTM C 192 *Standard Practice for Making and Curing Concrete Test Specimens in the Laboratory*, West Conshohocken, PA.
[11] ASTM C 1611/C 1611M – 05 *Standard Test Method for Slump Flow of Self-Consolidating Concrete*, West Conshohocken, PA.
[12] ASTM C39 (2005) *Standard Test Method for Compressive Strength of Cylindrical Concrete Specimens*, West Conshohocken, PA.
[13] AASHTO T160 (1997*) Length Change of Hardened Hydraulic Cement Mortar and Concrete*.
[14] Alabama DOT (2012) *Standard Specification for Highway Construction.*
[15] Leach, R., *Fundamental Principles of Engineering Nanometrology*, Elsevier Science, Amsterdam, 2010, pp. 352.

Shrinkage of Hybrid Fiber Reinforced Self-Consolidating Concrete with Recycled Aggregate

Wu-Jian Long[1] , Jin-Guang Shi[2], Wei-Lun Wang[3] and Xiao-Liang Fang[4]

[1-4] College of Civil Engineering, Shenzhen University, Guangdong Provincial Key Laboratory of Durability for Marine Civil Engineering, China.

Abstract In this paper, the mechanical properties and shrinkage behavior of recycled self-consolidating concrete (SCC) with hybrid basalt-, polyvinyl alcohol (PVA-) and polypropylene fibers were investigated. The experimental results show that the compressive strength and splitting tensile strength decrease, however, the shrinkage strain increases with the incorporation of recycled aggregates. The single incorporation of polypropylene-, PVA- or basalt fiber led to the reduction of shrinkage strain, but the increasing of the splitting tensile strength of recycled SCC. The incorporating of any two kinds of basalt-, polypropylene- and PVA fibers can significantly improve the splitting tensile strength of concrete. The incorporation of 0.63kg/m^3 polypropylene- and 1.2kg/m^3 basalt fibers can largely decrease the shrinkage of the concrete. It is important to note that there is no obvious difference between the incorporation of one, two or three kinds of fibers on mechanical properties and shrinkage behavior of concrete. However, the workability performance decreases remarkably when the three kinds of fibers incorporated in SCC simultaneously.

Keywords: *shrinkage; mechanical properties; self-consolidating concrete; recycled aggregate concrete; hybrid fiber*

Introduction

Used most widely as building material in the field of civil engineering, concrete is cheap and convenient to use with relatively excellent compressive strength. However, some technique issues such as low tensile strength, easiness to shrink and crack arising from damaged brittleness, which have become material technological bottlenecks of using concrete [1].

With rapid development of urbanization, waste concrete has caused serious environmental pollution and waste of resources in the process of demolishing and reconstructing many buildings. Reuse of waste concrete may not only abate great lack of construction resources, but has also fundamentally handled the difficulties in disposing of waste concrete and problems concerning environmental destruction caused by the waste concrete [2-5]. High shrinkage is a fatal defect of recycled concrete, so it will become important to develop and use recycled concrete by studying and improving problems concerning shrinkage of such concrete [1, 6].

Self-Consolidating Concrete (SCC) exhibits great green construability. SCC can consolidate under its own weight without any vibration even in the condition of intensive reinforcement. As a result, it may facilitate construction schedule and improve construction environment [7]. Nevertheless, due to the relatively high cementitious material content and low water to binder ratio (w/b) in SCC, the creep and shrinkage behavior of SCC should be treating carefully [8,9].

With a three-dimensional network structure inside fiber reinforced concrete, fiber supports aggregate, hinders sedimentation of coarse/fine aggregates, reduces water bleeding from the surface of concrete and effectively prevents massive shrinkage resulting from rapid water loss on the surface of concrete [1]. Therefore, monofilament fibers may bear tensile strain generated by concrete shrinkage when many of these fibers are evenly distributed in concrete, to postpone or hinder generation of cracks on concrete. These fibers are effective for inhibiting early plastic shrinkage cracks and improving crack resistance of concrete. In addition, basalt fiber in high elastic modulus, PVA fiber and polypropylene fiber in low elastic modulus may inhibit concrete shrinkage and prevent cracks from presenting their superior performances. Hybrid fibers may complement with each other's advantages, so that they may bring effects of size and performances of both fibers into full play, to finally strengthen crack resistance, toughen the concrete and enhance the effects [10-17].

It is one of effective methods for improving basic mechanical properties, strengthening crack resistance, inhibiting shrinkage deformation and increasing dimensional stability of hybrid fiber reinforced self-consolidating recycled concrete on the premise of guaranteeing excellent construction performances and good social benefits by studying and applying such fiber [14-17]. In this study, the mechanical properties and shrinkage behavior of recycled SCC with hybrid basalt-, polyvinyl alcohol (PVA-) and polypropylene fibers were investigated. The experimental program consisted of different types and contents of fibers, as well as different recycled coarse and fine aggregates replacement ratio.

Experimental Design

Raw materials

In this investigation, P.O 42.5R cement of Guangzhou Zhujiang Cement Co., Ltd and a Class F fly ash were used. The specific gravity of the cement and fly ash are 3.14 and 2.50, respectively, and the Blaine fineness value are 370 and 410 m^2/kg, respectively. Natural coarse aggregates were continuous grading with the maximum size of 20mm, while natural fine aggregates were river sand with a fineness module of 2.84. Recycled aggregates used in this study were chosen as recycled fine (0–5 mm) and coarse aggregates (5–12 and 12–20 mm) of waste broken red bricks, ceramic tiles and concrete. The fineness module of recycled fine aggregate is 3.24. Sika® ViscoCrete high-range water-reducing admixture (HRWRA) was employed.

Three types of fibers, Polypropylene-, PVA-, and basalt-fibers were used. A 6mm long Duline PF5 polypropylene fiber manufactured by Beijing Ronel Engineering Materials Co., Ltd with an equivalent diameter of 26.13μm, a density of $0.91g/cm^3$, a breaking strength of 688MPa, an elongation at break of 37.8% and an initial elastic module of 6681MPa. With an equivalent diameter of 15μm, a density of $1.3g/cm^3$, a breaking strength of over 1, 500MPa, an elongation at break of 6-8% and an initial elastic modulus of more than 35GPa; A 6mm long Duline AV600 PVA fiber was produced by Beijing Ronel Engineering Materials Co., Ltd. BFCS-18-25 chopped basalt fiber was used and manufactured by GBF. The fiber has a monofilament diameter of 18μm, a length of 25mm and a water content of 6%.

Mixing sequence and test methods

The SCC mixtures were prepared in 60-L batches using a drum mixer. The mixing sequence consisted of wetting the sand and coarse aggregate with half of the mixing water, followed by the addition of the binder and fibers. The HRWRA diluted with the remaining mixing water were then introduced over 60 seconds, and the concrete was mixed for 2.5 minutes. The concrete remained at rest in the mixer for 2 minutes for fluidity adjustment and to enable any large air bubbles entrapped during mixing to rise to the surface. The concrete was then remixed for 3 minutes. Fresh concrete properties were measured at 10 minutes after cement and water contact.

Three 75×75×285 mm prism test specimens were cast to monitor drying shrinkage according to ASTMC490. A vertical concrete extensometer was used to determine drying shrinkage. Shrinkage specimens were started at the age of 24 hours and monitored for 3 months at 23 ± 2°C and 50% ± 4% relative humidity.

Mix design

In order to investigate the influence of different mixing contents of basalt-, PVA-, and polypropylene-fibers as well as recycled aggregates on shrinkage behavior of SCC, in this experiment, different fibers and recycled coarse and fine aggregates

are adopted to conduct comparative experiments. The mix design in this experiment includes preliminary experiment and optimal mix design according to the trial batches in the preliminary study.

Preliminary trial batches

Experimental groups and proportion of mixture for initial trial mixing are shown in Tables I and II, respectively.

Table I. Designs of initial trial batches

Mix No.	Fiber content, %	Natural coarse aggregate (863kg/m^3)	Natural fine aggregate (729kg/m^3)	Recycled coarse aggregate replacement %	Recycled fine aggregate replacement %
100	0	100%	100%	0	0
200	0	70%	100%	30%	0
300	0	100%	90%	0	10%
400	0	70%	90%	30%	10%

Table II. Mix proportions of initial trial batches (kg/m^3)

Mix No.	Cement	Fly ash	Natural coarse	Recycled coarse	Natural Fine aggregate	Recycled Fine aggregate	Water	HRWRA	w/cm
100	440	110	863	-	729	-	187	2.20	0.34
200	440	110	604	259	729	-	187	1.65	0.34
300	440	110	863	-	656	73	187	1.65	0.34
400	440	110	604	259	656	73	187	2.30	0.34

Concrete strength test is conducted as per GB/T50081—2002 Chinese Standard for Test Method of Mechanical Properties on Ordinary Concrete. Sample size is 100×100×100mm. Compressive strength is carried out at 7d, 28d and 56d, and splitting tensile strength at 28d. Slump flow and mechanical test results are shown in Table III.

According to the experimental results, Mix No. 400 meets the target slump flow value and exhibits the adequate compressive strength and splitting tensile strength. Therefore, No. 400 is chosen as the basic experimental mix proportion to study the influence of different mixing amounts of fiber on various properties of SCC.

Table III. Slump flow and mechanical properties at different ages

Mix No.	Slump flow mm	Compressive strength, MPa			28d splitting tensile strength
		7d	28d	56d	
100	670	65.5	73.7	77.5	4.22
200	630	56.2	61.8	68.9	3.88
300	600	52.5	61.6	67.5	3.95
400	600	50.5	60.5	66.4	3.77

Optimal mix proportions

Optimal experimental mix design is shown in Tables IV and V.

Table IV. Fiber contents in different concrete mix

Mix No.	Polypropylene fiber (0.9 kg/m^3)	Polyvinyl alcohol fiber (0.9 kg/m^3)	Basalt fiber (4.0 kg/m^3)
411	100%	0	0
412	0	100%	0
413	0	0	100%
421	30%	70%	0
422	70%	30%	0
423	30%	0	70%
424	70%	0	30%
425	0	30%	70%
426	0	70%	30%
431	25%	25%	50%
432	50%	50%	100%

Table V. Mix proportions of tested mixtures (kg/m^3)

Mix No.	Fiber			Coarse aggregate		Fine aggregate		Cement	Fly ash	Water	HRW-RA
	Polypro-pylene	PVA	Basalt	Natural	Recycled	Natural	Recycled				
411	0.9	0	0	604	259	656	73	440	110	187	1.52
412	0	0.9	0	604	259	656	73	440	110	187	1.74
413	0	0	4.0	604	259	656	73	440	110	187	2.16
421	0.27	0.63	0	604	259	656	73	440	110	187	1.54
422	0.63	0.27	0	604	259	656	73	440	110	187	1.60
423	0.27	0	2.8	604	259	656	73	440	110	187	1.92
424	0.63	0	1.2	604	259	656	73	440	110	187	1.52
425	0	0.27	2.8	604	259	656	73	440	110	187	2.40
426	0	0.63	1.2	604	259	656	73	440	110	187	1.76
431	0.225	0.225	2	604	259	656	73	440	110	187	1.72
432	0.45	0.45	4	604	259	656	73	440	110	187	2.94

Test results and analysis

Fresh and mechanical test results are shown in Table VI.

Table VI. Fresh and mechanical properties of concrete at different ages

Mix No.	Slump flow mm	J-Ring mm	L-Box (h_2/h_1)	Filling Capacity, %	Compressive strength, MPa			28d splitting tensile strength
					7d	28d	56d	
411	650	580	0.80	89	47.97	55.9	63.57	4.38
412	640	580	0.82	90	46.06	58.5	61.17	4.47
413	630	560	0.80	88	50.80	59.8	65.80	4.43
421	620	600	0.79	89	40.27	60.0	61.85	4.57
422	600	540	0.78	80	36.80	59.3	63.87	4.24
423	630	580	0.76	83	38.40	60.6	65.07	4.19
424	600	520	0.70	80	37.27	55.9	60.33	4.32
425	620	570	0.80	82	38.70	62.0	65.23	4.13
426	610	560	0.75	82	50.70	58.6	63.90	4.10
431	570	530	0.65	70	46.17	56.5	59.67	4.33
432	550	500	0.60	65	47.57	58.6	63.10	4.45

Influence of fiber on splitting strength

As shown in figure 1, replacement ratio of recycled coarse aggregates and sand was 30% and 10% respectively. Compared with concrete only containing natural sand, splitting strength was weakened by 8.1%, 6.4% and 11% respectively on the 28th day in three concrete groups where the replacement ratio of recycled aggregate and sand was 30% and 10% respectively. It can be concluded that the substitution of recycled aggregates reduce the splitting tensile strength of concrete.

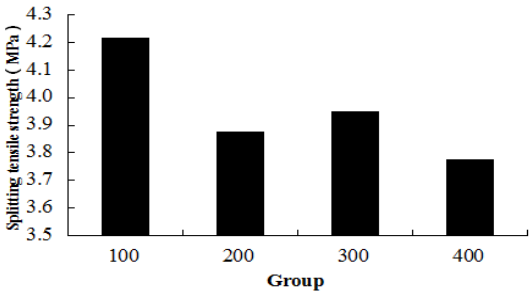

Figure 1. Influence of incorporation of recycled sand and stone on splitting tensile strength

According to figure 2, the splitting tensile strengths of recycled SCCs with polypropylene fiber, PVA fiber and basalt fiber increase by 16.2%, 18.6% and 17.5% respectively, compared with the concrete without fibers. It can be seen from

the comparison between figures. 2 and 1 that the 28d splitting tensile strength of three experimental groups are higher than that of SCC without any recycled aggregate or fiber at the same ages. Thus it can be seen that the incorporation of fiber can effectively improve the splitting tensile strength of concrete and eliminate the reduction of splitting tensile strength caused by incorporating recycled aggregate.

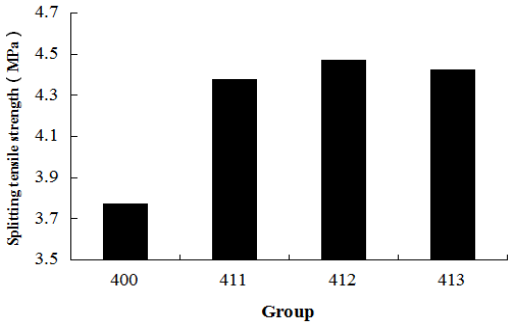

Figure 2. Influence of incorporation of one fiber on recycled concrete splitting tensile strength

By comparing figures. 3 and 4 with figures. 1 and 2, it can be concluded that splitting tensile strength is basically the same for recycled SCC doped with two fibers or three fibers and SCC without recycled aggregates.

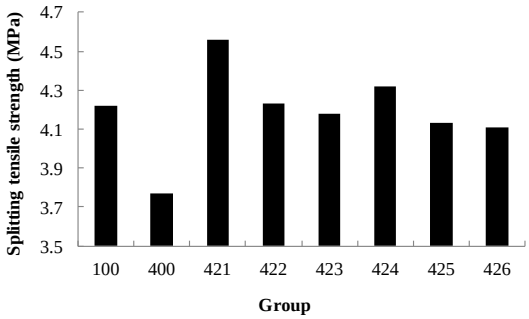

Figure 3. Influence of incorporation of two fibers on splitting tensile strength of recycled SCC

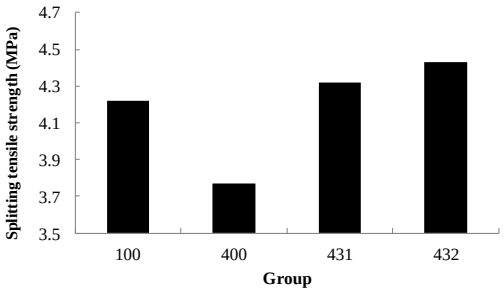

Figure 4. Influence of incorporation of three fibers on splitting tensile strength of recycled SCC

Influence of fiber on shrinkage

Figure 5 shows the influence of doped recycled sand and aggregate on concrete shrinkage. It may be known from the figure 5 that, shrinkage strain of concrete would increase as natural coarse and fine aggregates were replaced by recycled aggregate and sand. The increased shrinkage strain was particularly evident on the 7-day and generally kept unchanged after the 28-day. In No. 400 experimental group, replacement ratio of recycled aggregate and sand increased by 30% and 10% respectively. As compared with mixture No. 400, shrinkage strain of concrete increased by 30.5% in No. 100 without recycled aggregates on the 90-day.

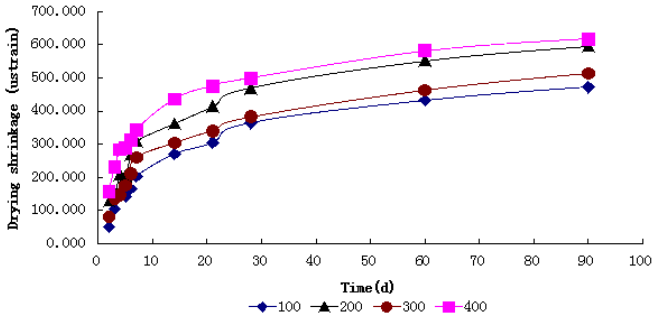

Figure 5. Influence of incorporation of recycled sand and aggregate on concrete shrinkage

Figure 6 shows impacts of single-doped fiber on shrinkage of recycled concrete. Before adding basalt fiber to the experimental group, shrinkage strain at 28-day was nearly the same with the experiment groups without fibers, whereas it was significantly weakened after the 28 days. As concrete was doped with polypropylene fiber and PVA fiber, concrete shrinkage could be weakened from the very beginning. Among these two fibers, polypropylene fiber is more effective for inhibiting shrinkage. Compared with the experimental group with

polypropylene fiber, the shrinkage was weakened by 30.5% on the 90-day in the experimental group without fiber.

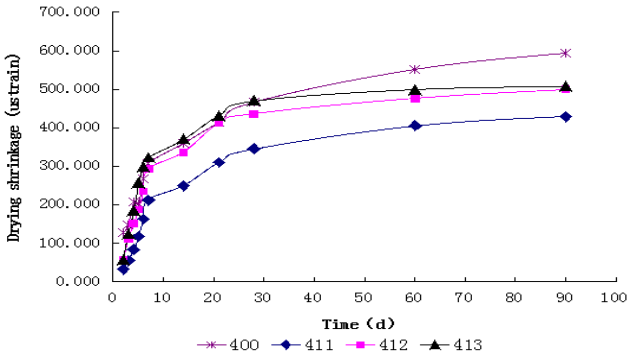

Figure 6. Influence of incorporation of one fiber on recycled concrete shrinkage

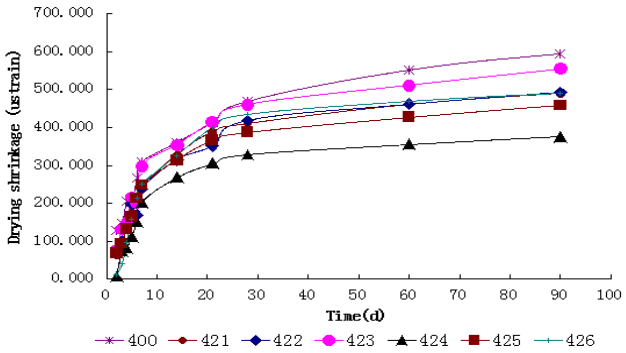

Figure 7. Influence of incorporation of two fibers on recycled concrete shrinkage

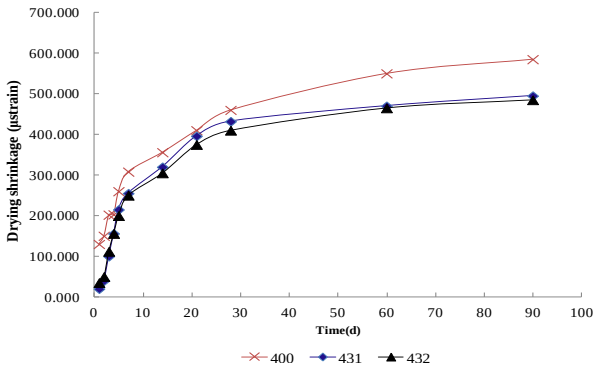

Figure 8. Influence of incorporation of three fibers on recycled concrete shrinkage

Impacts of doped two fibers on shrinkage of recycled concrete are shown in figure 7, from which it may be known that doped fibers are somewhat effective for inhibiting shrinkage of concrete, and the inhibitory effects are the most evident when the concrete is doped with polypropylene fiber at 0.63kg/m^3 and basalt fiber at 1.2kg/m^3. Figure 8 shows impacts of doped three fibers on shrinkage of recycled concrete. By comparing figure 7 with figure 8, there is no obvious difference between the incorporation of three or two kinds of fibers on shrinkage behavior of concrete.

Electron microscope analysis

Figures 9 (a) and (b) are microscopic pictures of interfaces for damaged test samples of concrete. It may be apparently observed from these figures that fibers appeared to form a bridge between broken concrete blocks to prevent these blocks from further fall when they were wrapped by concrete.

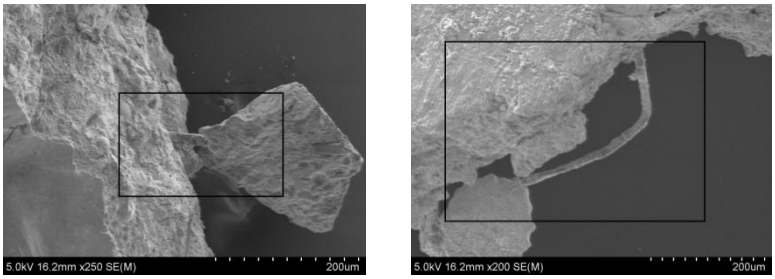

(a) (b)

Figure 9. SEM photos of hybrid fiber recycled SCC

Conclusions

Based on the test results presented in this investigation, the following conclusions can be made:

1. The compressive strength and splitting tensile strength decrease, however, the shrinkage strain increases with the incorporation of recycled aggregates.
2. The incorporating of fibers can significantly improve the splitting tensile strength of SCC prepared with recycled aggregates.
3. The incorporation of 0.63kg/m^3 polypropylene- and 1.2kg/m^3 basalt fibers can largely decrease the shrinkage of the concrete.
4. There is no obvious difference between the incorporation of one, two or three kinds of fibers on mechanical properties and shrinkage behavior of concrete. However, the workability performance decreases remarkably when the three kinds of fibers incorporated in SCC simultaneously.

Acknowledgments

The authors gratefully acknowledge the financial support provided by the National Natural Science Foundation of China (No. 51278306 and 51578341), the Science Industry Trade and Information Technology Commission of Shenzhen Municipality (No. JCYJ20140418095735540).

References

[1] Neville., AM (1996). *Properties of Concrete*, 4th Edition, ISBN: 0-582-23070-5, London, 844 p.
[2] Corominas, AG., Etxeberria, M. (2014), *Constr. Build. Mater.*, vol. 68, n. 15, p. 618-626
[3] Abdulla, NA. (2015), *J. Mater. Civil. Eng.*, vol. 27, n. 10, DOI: 10.1061/(ASCE)MT.1943-5533.0001247
[4] Zhu, LH., Dai, J., Bai, GL., Zhang, FJ. (2015), *Constr. Build. Mater.*, n. 94, p. 620-628
[5] Surya, M., Rao, VVLK., Lakshmy, P. (2015), *ACI. Mater. J.*, vol. 112, n. 5, p. 653-661
[6] Ismail, S., Mahyuddin Ramli. (2014), *Constr. Build. Mater.*, n. 68, p. 726-739
[7] ACI Committee 237R-07, Self-Consolidating Concrete, American Concrete Institute, Michigan, 30 pp.
[8] Long, WJ., Khayat, KH. (2011), *ACI. Mater. J.*, vol. 108, n. 5, p. 476-484
[9] Khayat, KH., Long, WJ. (2010), *ACI. Mater. J.*, vol. 107, n. 3, p. 231-238
[10] Suna, Z., Xu, Q. (2009), *Mater. Sci. Eng. A*, n. 527, p. 198–204
[11] Passuello, A., Moriconi, G., Shah, SP. (2014), *Cem. Concr. Compos.*, vol. 10, n. 31, p. 699-704
[12] Cao, ML., Zhang, C., Lu, HF. (2014), *Constr. Build. Mater.*, n. 57, p. 45-52
[13] Lanzoni, L., Nobili, A., Tarantino, AM. (2012), *Constr. Build. Mater.*, vol. 28 n. 1, p. 798–806
[14] Iqbal, S., Ali, A., Holschemacher, K., Bier, TA. (2015), *Constr. Build. Mater.*, n.98, p. 325-333
[15] Kwon, S., Nishiwaki, T., Kikuta, T., Mihashi, H. (2015), *ACI. Mater. J.*, vol. 111, n. 3, p. 309-318
[16] Uygunoğlu, T., Topçu, B., Çelik, AG. (2014), *J. Clean. Prod.*, In Press, Available online 15 June 2014
Akca, KR., Cakir, O., Ipek, M. (2015), *Constr. Build. Mater*, n. 98, p. 620-630

Crack Resistance of Polypropylene Fiber Reinforced Self-Consolidating Concrete under Restrained Shrinkage Condition

Hani Nassif[1], Zeeshan Ghanchi[2] and Chaekuk Na[3]

[1]Professor, Rutgers University, NJ
[2]Structural Engineer, Bechtel Corporation, VA
[3]Research Associate, Rutgers University, NJ

Abstract The growing demands for Self-Consolidating Concrete (SCC) is attributed to its ability to reduce the cost as well as project period since it eliminates the vibration and reduces labor and equipment needed. However, the major concern of the use of SCC comes with increased shrinkage because of its large volume of cement paste. Enormous efforts have been made to control the volume changes in the concrete matrix by optimizing the mix design or adding various types of fibers, but few study addresses the effect of fibers in fiber-reinforced SCC (FR-SCC) on the shrinkage performance. The objective of this study is to investigate effects of polypropylene fibers (PPE) in SCC mix on the shrinkage properties under restrained condition. Two SCC mixes with PPE with 6.35 mm long at 0.10 and 0.20% by volume were prepared in addition to a control SCC mix. The restrained shrinkage ring specimens were prepared in accordance with AASHTO PP34 but modified to monitor the stress development in the steel ring as well as concrete ring. Results show that when fibers were added up to 0.20% by volume, the free shrinkage strain was decreased by 9% and cracking strain capacity increased by 22%. The use of fibers in SCC increases the initial cracking date by 70% and reduces the averaged cracking area by 33%. The modified restrained ring test enables to provide information on where a crack may form by measuring the strain development in individual segments of the concrete ring.

Keywords: ***s****elf-consolidating concrete, fiber reinforced concrete, flowable concrete, restrained shrinkage, monitoring*

Introduction

Over the past decade, the growing demands for Self-Consolidating Concrete (SCC) is attributed to its ability of filling voids and spaces within formwork without external compaction. SCC is referred to a group of super workable concrete (SWC) that retains a low viscosity without any segregation or bleeding. With the advanced development of chemical admixtures, SCC provides a higher strength and flowability that allows an economical construction since it eliminates the vibration and thus reduces labor and equipment needed. However, similar to conventional concrete or high performance concrete (HPC) with regard to cracking, the major concern of the use of SCC comes with the shrinkage performance because of its large volume of cement paste. To alleviate some of these problems, fibers are a common addition to concrete mixes in an effort to increase its resistance to cracking which refers to a fiber-reinforced SCC or FR-SCC. Among various fibers including steel fiber, glass fiber, polypropylene (PPE), etc., PPE has been widely used in the FR-SCC application because of its relatively low handling effort, low price and flexibility.

When the concrete is cured and hardened, fibers offer additional cracking resistance by bridging the cracks that results in evenly distributed cracks. It was reported that the mechanical properties of concrete increased with the utilization of higher fiber content while modulus of elastic showed somewhat smaller improvements [1]. While an improvement of mechanical property helps the growth of cracks, an improvement of shrinkage performance helps delay the initial formation of cracks. Saje et al. showed that the shrinkage crack could be controlled by increasing the fiber content up to 0.5% by volume, but the effect of over 0.5% fiber volume in the matrix was negligible [2]. While fibers are known to improve the mechanical and shrinkage properties of SCC, the shrinkage performance under restrained condition is more complex. The concrete ring test is a methodology to compare different concrete mixtures by observing the formation of cracks as concrete shrinks around a steel ring. Enormous efforts have been made to control the volume changes in the concrete matrix by optimizing the mix design or adding various types of fibers, but few study addresses the effect of FR-SCC on the restrained shrinkage performance. Therefore, it is important to understand and analyze the shrinkage behavior of FR-SCC under restrained condition.

Experimental Program

Polypropylene fiber (PPE) of a 6.4 mm length was used in this study. When the mix was prepared, various wet concrete properties were observed to determine the effectiveness of the fiber volumes on flowability such as slump flow, T20, visual stability index (VSI), J-Ring, L-Box and air content. Detailed of these tests can be found elsewhere [3]. Various mechanical properties and shrinkage properties such as free and restrained shrinkage, were tested.

Mix Design and Preparation.

SCC mix designs prepared in this study were based on the findings of a research report performed by the Virginia Transportation Research Council (VTRC) [4]. Saje reported that the workability and flowability is proportional to the fiber content and decreases significantly upon reaching 0.25 % fiber volume. Therefore, this study prepared three mixes with various fiber contents by volume, 0.00%, 0.10% and 0.20% while retaining a water-cement ratio of 0.425 and a total cementitious content of 400 kg/m^3. Type I Portland cement and Grade 120 ground granulated blast furnace slag (GGBFS or slag) was used, and slag replaced 35% of cement by weight. Slag is an inexpensive locally sourced cementitious material that provides additional strength at later age while reduces the heat of hydration at early age. Same amount of coarse and fine aggregates was used to maintain the ratio of 1:1 for all mixes. Air entraining agent and high range water reducing admixtures were utilized to achieve desired slump, flow, and air content. The mix designs are summarized in Table XXXI.

Table XXXI. Mix Proportion

Mix ID	PPE0	PPE1	PPE2
Portland Cement, Type I	260 kg/m^3	439 lb/yd^3	439 lb/yd^3
Slag, Grade 120	140 kg/m^3	236 lb/yd^3	236 lb/yd^3
Total Cementitious	400 kg/m^3	675 lb/yd^3	675 lb/yd^3
W/C Ratio	0.425	0.425	0.425
Gravel, #8	852 kg/m^3	1,436 lb/yd^3	1,436 lb/yd^3
Sand	852 kg/m^3	1,436 lb/yd^3	1,436 lb/yd^3
HRWR	3.67 l/m^3	3.67 l/m^3	3.67 l/m^3
Fiber % by volume	0%	0.10%	0.20%
Adjusted Slump Flow	600 mm	585 mm	570 mm
T20	6.1 sec.	5.5 sec.	9.6 sec.
VSI	0	0	1
J-Ring	570 mm	535 mm	430 mm
L-Box	1.2	1.5	2.5
Air Content	7.0%	7.0%	8.0%

Each mix was prepared according to ASTM C192 using an electric revolving-drum mixer. After the concrete has been adequately mixed, various fresh concrete tests in Table I were conducted to assure adequate flowability and minimal segregation. The fresh concrete properties are also summarized in Table II. A total ten 4 by 8 in. cylinders were collected for the compressive strength, splitting tensile strength and modulus of elasticity tests. Three 76 by 76 by 280 mm prisms were cast for

free shrinkage testing and three restrained shrinkage rings were also cast in accordance with AASHTO PP 34. The AASHTO PP 34 ring has an outer diameter of 457 mm, an inner diameter of 305 mm. and a height of 152 mm. Due to the nature of SCC, any vibration or compaction methods including rodding or tapping of samples were not implemented. Instead, concrete was scooped into the respective molds and allowed to settle under its own weight. When an individual mold was filled, a trowel was used to level off the top and a polyethylene sheet or a plastic cylinder lid was used to seal the specimen. Single batch was prepared for each mix for all samples and fresh concrete tests consecutively over the course of 4 hours for the uniformity to minimize the impact of a change in ambient conditions.

Curing Regime

Concrete samples were cured in an environmental chamber for the first 24 hours. The chamber is designed to maintain a steady temperature of 22°C and a relative humidity of 50% to provide a steady environment for shrinkage testing. All shrinkage samples were covered by the polyethylene sheets for 6 hours, and then the polyethylene sheets were removed and wet burlaps were placed over the specimens. The polyethylene sheets were then repositioned over the wet burlaps to minimize moisture loss due to evaporation. After one day of wet curing period, the wet burlap was removed and a coat of paraffin wax was applied on the top surface of the ring. When the paraffin was dried, the ring was demolded and placed on a plexiglass surface. A lining of silicone caulk was spread along the bottom surface of the ring to allow the evaporation from the side surfaces. All cylinders were demolded at 24 hours, and then cured in a curing room for 14 days followed by curing in the environmental chamber until 28 days.

Cylinder Testing

Cylinders were capped using a sulfur mortar according to ASTM C617 for the compressive strength and modulus of elasticity tests at 28 days in accordance with ASTM standards C39 and C469, respectively. Splitting tensile strength test was performed in accordance with ASTM C496 at 28 days. For each test, two samples were tested, and a third sample was used if the variance exceeded 10% between samples.

Shrinkage Testing and Monitoring

Free shrinkage strain measurements were collected at once per week. Stainless steel studs were embedded on each side of the free shrinkage prism to measure the change in length using a length comparator in accordance with ASTM C490. The length change was monitored over a course of 56 days. The restrained shrinkage tests were carried out in accordance with AASHTO PP 34, but a modified testing setup depicted in Figure 71 was used. The ring has four (4) foil strain gauges (FSGs) attached at four equidistant mid-height locations on the ring as per

AASHTO PP 34 to measure the strain applied on the steel ring. In addition to FSGs, six (6) vibrating wire strain gauges (VWSGs) with two ends embedded into the concrete were installed to monitor the strain applied on the concrete ring. Each VWSG was anchored by 76 mm bolts embedded into the concrete at the time of casting forming a closed hexagon loop along the top surface. The advantage of using VWSG is to monitor directly the strain and deformation occurring within the concrete, and therefore, the VWSGs are used to signal the cracking location.

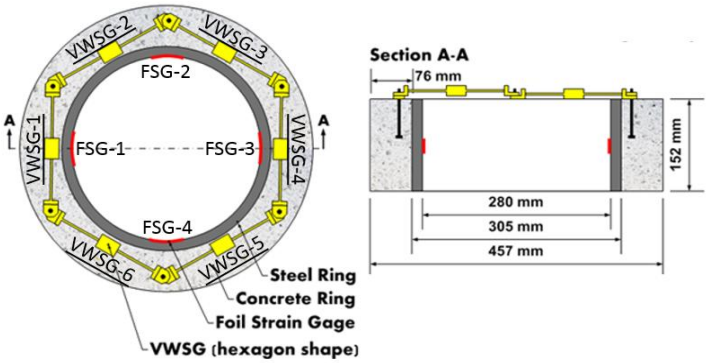

Figure 71. Modified AASHTO PP34 ring test

All sensors were connected to a data acquisition system that collected data from the FSGs and VWSGs once every two (2) minutes. Strain values were checked daily to check for possible indications of possible crack formation in the concrete due to the restrained condition. If cracking was observed or suspected, the surface of the ring was observed using a digital microscope at various ages to see how many and how fast cracks were developing. The crack maps were developed at the end of monitoring at 56 days.

Testing Results and Discussion

Table XXXII summarizes the strength and modulus results at 28 days. The cracking strain that is a capacity to resist cracking is calculated by the splitting tensile strength divided by the modulus of elasticity, or $\varepsilon_c = f_t/E_c$. It was noticed that as fiber content increased, the compressive strength and modulus of elasticity slightly decreased by 7~9%. When the fiber volume increased from 0.0% and 0.2%, the compressive strength reduced by 9% while the modulus of elasticity decreased by a small margin of 7%. The tensile splitting strength, however, shows a slightly more significant change. Tensile strength increased by 14% while compressive strength and modulus of elasticity decreased at the same time. This is because the fibers provide resistance to pull-out force or friction between the cement matrix and the fibers resulting in increased tensile strength. The increase in

tensile strength is a major contributor to the increase in cracking strain and is key to decrease the number of cracks or to distribute the crack density.

Table XXXII. Strength test results at 28 days

Mechanical Property at 28 days	PPE0	PPE1	PPE2
Compressive Strength, MPa	38.8	37.0	35.4
Tensile Strength, MPa	2.5	2.7	2.8
Modulus of Elasticity, GPa	29.6	28.7	27.4
Cracking Strain, με	84	92	103

Free Shrinkage Test Results

Figure 72 shows the free shrinkage strain results of three FR-SCC mixes. It was observed that a decrease in free shrinkage as an increase of fiber content. When PPE was added at 0.20% by volume, free shrinkage decreased by 9%. However, the shrinkage improvement was not as effective as other studies. Saje et al., who performed various shrinkage testing for the mixes of fiber contents up to 0.75% by volume, found that the free shrinkage of fiber-reinforced concrete was about two-third less than that of the control mix [2]. Such small improvement of free shrinkage strain could be resulted from the curing regime, because it was reported that no curing increased the ultimate free shrinkage as well as the shrinkage rate [5]. The fact that the shrinkage specimens were not moisture cured after 1 day may greatly influence the free shrinkage while the effect of fibers was negligible compared with curing regime.

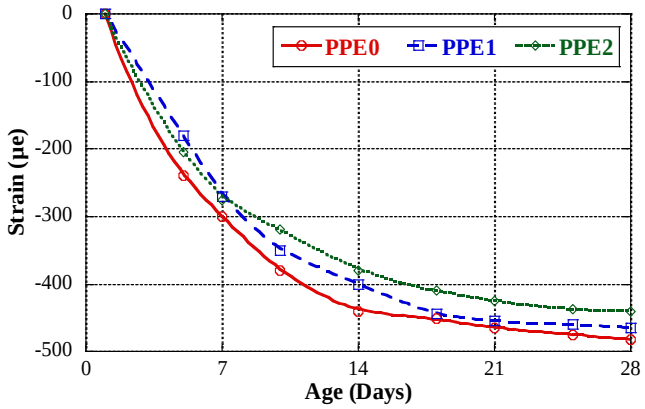

Figure 72. Free shrinkage testing results

Restrained Shrinkage Test Results

A full surface crackmap for each restrained ring was developed up to 28 days. The surface of the ring was checked for cracking as soon as either the FSG or VWSG indicated potential cracking. The observations of the crackmap were compared with the strain data collected by the data acquisition system to determine the age the cracking occurred and the severity of these cracks. The results from three mixes were compared in order to determine whether the addition of fibers provided any improvement in restrained shrinkage cracking resistance.

Figure 73 shows the restrained shrinkage strains in concrete and steel of PPE0 mix, and indicates possible cracking at the section of VWSG-6 and FSG-4. It was noticed that the strain in concrete of VWSG-6 exceeded the cracking capacity of the mix at 13 days after casting. Figure 73 shows that this cracking was corresponded to the strain in the steel (FSG-4). The strain around FSG-4 increased suddenly when the strain measured by VWSG-6 exceeded the cracking strain. Similarly, when VWSG-5 strain exceeded the cracking strain at 17 days, another sudden change in FSG-4 was also observed. Full propagation of the major crack in VWSG=6 occurs at 20 days. After the crack propagated the entire height of the ring, a relaxation was continuously observed throughout all FSGs and the restraint provided by the steel ring was reduced.

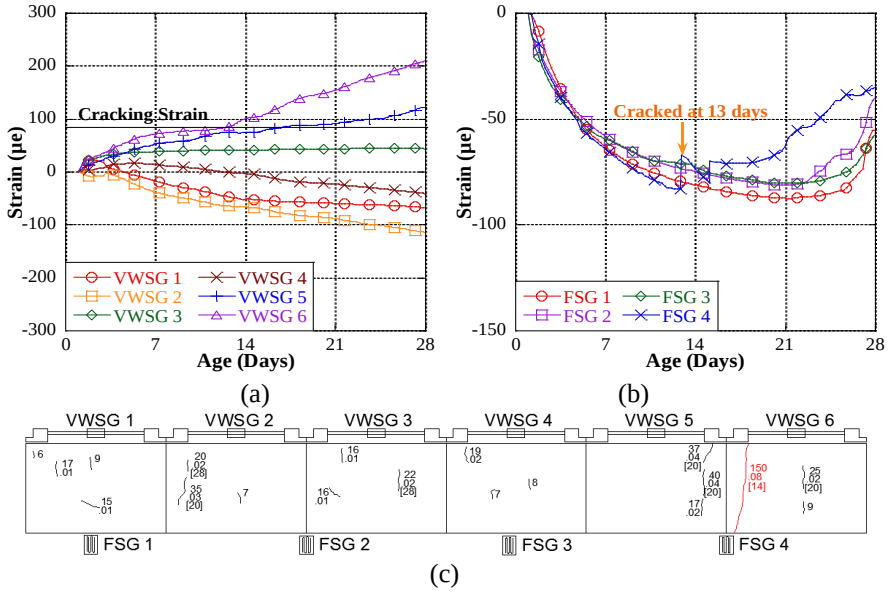

Figure 73. PPE0 restrained ring test results; (a) strain in concrete, (b) strain in steel, and (c) crackmap

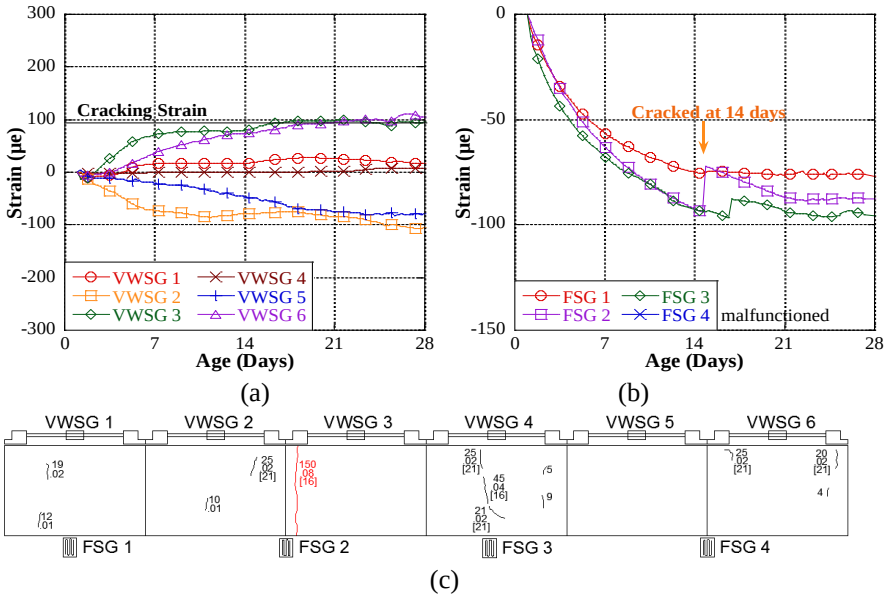

Figure 74. PPE1 restrained ring test results; (a) strain in concrete, (b) strain in steel, and (c) crackmap

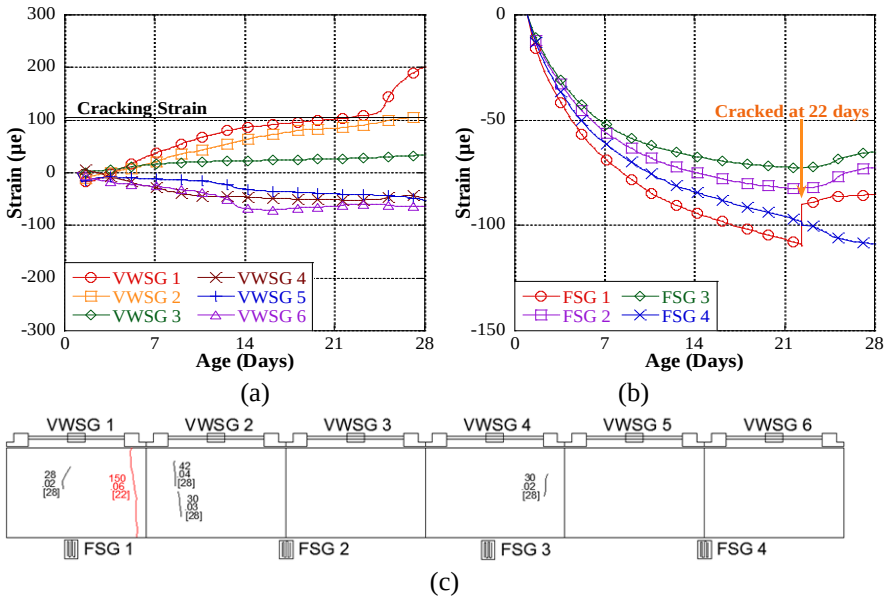

Figure 75. PPE2 restrained ring test results; (a) strain in concrete, (b) strain in steel, and (c) crackmap

The addition of 0.10% polypropylene fibers has a small but noticeable effect on the shrinkage of the concrete. Figure 74 shows the concrete and steel strain measured of PPE1 mix by VWSGs and FSGs, respectively. FSG-2 shows that a crack should have formed at 14 days, however, initial crackmap did not show any crack along the surface. This crack appeared on the concrete surface two days later at 16 days under VWSG-3 region when VWSG-3 had exceeded the cracking strain of 92 με. At the same time, the crack propagated through the depth and height of the concrete ring. Once the crack propagated to its full depth, the strain in the steel leveled off indicating no significant stresses were developed in the ring and no new shrinkage cracks were formed.

The restrained shrinkage test results of PPE2 mix are summarized in Figure 75. It shows that a steady increase of strain in the steel ring (VWSG-1) was observed up to 22 days at which FSG-1 experienced an immediate loss of strain. The crackmap developed on 22 days showed a small crack forming between VWSG-1 and VWSG-2. Figure 75 shows both VWSGs indicated that high tensile stress was occurred when the cracking was observed at 22 days. A large increase in tensile strain was observed on VWSG-1 when cracking likely propagated the entire height of the ring at that time. When most cracks were centered around VWSG-1 and VWSG-2, other regions remained uncracked.

Discussion

Initial Cracking Age. Table XXXIII summarizes the various cracking-age measurements taken during the course of this study. It shows a general trend of increasing cracking age as fiber contents increases. When 0.20% of PPE was utilized, it took 9 days longer to show initial sign of cracking compared with the control mix. The duration of time for the crack to propagate inwards, on the other hand, remained the same for all mixes. While the first crack may be delayed with the use of PPE, the cracks reached the steel ring within 4-6 days after they first appeared, which is typical of all the mixes used in this study.

Table XXXIII. Age of first crack and cracking area summary

Unit: days	PPE0	PPE1	PPE2
Age of Cracking (FSG)	13	14	22
Age of Cracking (VWSG)	13	15	22
First Crack Observed	14	16	22
Complete Propagation	20	22	25
Cracking Area, mm^2	19.1	16.8	12.7

Cracking Area. The results of the cracking area measurements are also summarized in Table XXXIII. It is apparent that the cracking area dropped noticeably with even the smallest addition of fibers tested in this study. The cracking area reduced

by 34% with the small addition of fibers from an average of 19.1 mm^2 to 12.7 mm^2.

Conclusions

This study analyzed the cracking behavior of a set of SCC mixes with various amount of PPE. Based on the results gathered from this study, the following conclusions can be made.

- The inclusion of PPE negatively affects the compressive strength and modulus of elasticity, while it increases the splitting tensile strength. The increase in tensile strength is resulted from the resistance to pull-out forces between the cement matrix and the fibers.

- Free shrinkage strain was reduced as fiber content was increased, and a reduction of 9% was observed for a fiber volume of 0.20%. The shrinkage improvement is small because curing regime governed the free shrinkage performance.

- Shrinkage performance of FR-SCC under restrained shrinkage conditions was also improved as fiber content was increased. Initial cracking was delayed and less cracking area was observed when the fiber content was increased. This implies that FR-SCC can diminish and control the cracking.

- VWSGs were added to the AASHTO ring test to supplement the data being gathered from the FSGs in the steel. It was more effective to use both FSGs and VWSGs to identify cracking and stress development within the concrete.

References

[1] Gencel, O., Ozel, C., Brostow, W. and Martinez-Barrera, G. (2011), *Mat. Res. Inno.*, vol. 15, n. 3, p. 216-225.
[2] Saje, D., Bandeji, B., Sustersic, J., Lopatic, J. and Saje, F. (2011), *J. of Mat. in Civil Eng.*, vol. 23, n. 7, p. 941-952.
[3] El-Khoury, R. (2010), *Creep and shrinkage of self-consolidating concrete*, Doctoral Thesis, Rutgers University.
[4] Brown, M. C., Ozyildirim, C. and Duke, W. (2010), *Investigation of Fiber-Reinforced Self-Consolidating Concrete*, Publication FHWA/VTRC 10-R8, Virginia Transportation Research Council, FHWA.
[5] Na, C.K., Nassif, H. and Johnsen, W.S. (2012), In: *Strength at early age and shrinkage behavior of high performance concrete*, The Transportation Research Board 91st Annual Meeting.

Study on the Creep Behavior Of High-Strength Self-Consolidating Concrete

Peiyu Yan, Zhikai Zhou and Qiang Wang

Department of Civil Engineering, Tsinghua University, Beijing China

Abstract Vertical deformation of concrete structure is one of crucial issues to ensure the veracity of spatial position during the construction of super high-rising buildings. Creep of high-strength self-consolidating concrete (HSSCC) was measured in one year. A prediction of creep coefficient of concrete was done using different models. The results show that the creep coefficient of concrete increases with the decrease of concrete strength at same loading age. The creep coefficient of concrete is greater when the specimens loaded at an earlier age for the same mix proportion. The increasing rate of concrete creep coefficient decreases with the prolongation of loading time. ACI209R model is unsuitable to predict the creep coefficient of high-strength self-consolidating concrete. A good prediction is obtained with the modified B3 model.

Keywords: *high-strength self-consolidating concrete, Creep, Prediction, modified B3 model*

Introduction

Thousands of high-rise buildings have been built in China in recent years. High-strength self-consolidating concrete (HSSCC) is used extensively in these construction projects for performance requirements. The construction of high-rise buildings is with a complex loading condition, which is germane to a high vertical stress. The substructure bears a gradually increasing load during the construction of buildings. Indeed, this process usually lasts for years because of the long duration of civil construction. As a result of structure weight and constructing load, there is a difference between the actual position of floors and the designed place. One of the unavoidable reasons is the deformations of pillars due to concrete creep. It is significant to predict vertical deformation of the concrete structure accurately for the construction of high-rise buildings.

There is different deformablility for HSSCC and conventional concrete due to their variational raw materials and mix proportions. The variety of concrete component and properties complicate the estimating of its creep. Some researchers have observed relatively large creep and shrinkage of precast or prestressed concrete. [1-4] But other researchers showed opponent experimental phenomena. [5] With low water binder ratio, large volume of mineral admixtures, high sand ratio and small nominal maximum size of aggregate, the microstructure of harden cement mortar and the characteristic of interface transition zone in HSSCC is improved particularly. Neville showed that aggregate is the only component in concrete that resists against creep. [6] Therefore, the volume ratio, location and connection condition of cement paste and aggregate effect on concrete creep directly. Several researchers claimed that the large volume of binder paste leads to a greate creep and shrinkage of concrete. [7, 8] In addition, the parameters of loading process matter a lot. When concrete sample is demolded and loaded early, a large creep deformation of concrete is showed. [9, 10]

Currently, some systematic predictive calculation model can be used in estimating the influence of deformation, such as ACI 209R, CEB-FIP, B3, etc. China Academy of Building Research put forward a calculation model in 1986, too. But the application and accuracy of these models to high strength concrete has to be proved. The parameters used in these predictive models and their applicability are statistically diverse. Even to one concrete mix proportion, the accuracy of prediction varies using different calculation models. Some parameters of specific concrete mix proportions may be out of applicability, which brings out a doubtful predictive result.

Ping-an International Financial Centre is one of super high-rising buildings with the height of 660m. It needed amounts of C70 and C60 HSSCC for its construction of steel reinforced concrete pillar and shear wall. This paper investigated the creep characteristics of HSSCC and modified the existing predictive calculation model of concrete creep to get a satisfied prediction of creep for HSSCC.

Experimental

Materials and proportion of concrete mixture

P.II 52.5R Portland cement complying with the Chinese National Standard GB 175 was used. Its 3d compressive strength was 34.2 MPa and 28d compressive strength was 57.6 MPa. Class II fly ash and S95 slag powder complying with the Chinese National Standard GB/T 1596 and GB/T 18046 were used. Crushed granite with a size range of 5mm to 25mm and washed sea sand with a fineness modulus of 2.7 were used as coarse and fine aggregate. A polycarboxylate superplasticizer with the water reducing rate of 28.0% and the solid content of 24% was used.

C60, C70 HSSCC mix proportions used in the project of Ping-an International Financial Centre in Shengzhen, China were used in this study (Table I). The slump flow of fresh C60 and C70 concrete was 780mm and 770mm, respectively. The slump flow loss of fresh concrete was less than 30mm after 2h.

Table I. Mix proportion of concrete (kg/m^3)

	Cement	Fly Ash	Slag	Fine aggregate	Coarse aggregate	Water	Superplasticizer
C60	310	100	80	771	980	153	5.64
C70	370	100	80	743	960	144	6.88

Samples' Preparation and Curing

Two 100mmx100mmx300mm prisms and two 100mmx100mmx515mm prisms were prepared for one sample in creep and dry shrinkage measurement respectively according to the Chinese National Standard GB/T 50082. Concrete mixture was prepared with a countercurrent planetary mixer. The concrete specimens were molded without vibration, which as showed in Figure 1. The concrete specimens after moulding were covered with plastic film and kept in a curing chamber at 20±2℃ and relative humidity higher than 95% for 24h. After demolding, the specimens were cured in the condition of 20±2℃ and 98±2% RH.

The creep and shrinkage measurement began at 7th and 28th day respectively. One day before the test, the surface of specimens was dried and smoothed appropriately. A pair of measuring equipment was installed on the opposite sides of concrete prism. Each measuring equipment contains two fixing bolts, one rod and one dial indicator.

Test Methods

The compressive creep and dry shrinkage measurement of concrete was done in the condition of 20±2℃ and 65±2℃ RH following the Chinese National Standard GB/T 50082. Two kinds of experiment of each concrete mix proportion at each age were done at the same time respectively.

Compressive spring creep apparatus shown in Figure 2 was used. Each apparatus can hold two specimens simultaneously. The constant compressive load of creep test is 40% of axial compressive strength of prism specimen, which is measured by elliptically circular dynamometer. The deformation of specimen is observed periodically from the average reading of dial indicators. A vertical shrinkage measuring frame shown in Figure. 3 was used for dry shrinkage measurement in the condition of 20±2℃ and 65±2℃ RH. The deformation of specimens can be got periodically from the reading of dial indicators installed above the concrete prisms.

According to the required parameters of the predictive models of concrete creep, ACI209R, CEB-FIP, B3 models [11-13] are considered in the contrast.

Figure 1. Fresh concrete

Figure 2. Compressive spring creep apparatus

Figure 3. Vertical shrinkage measuring frame

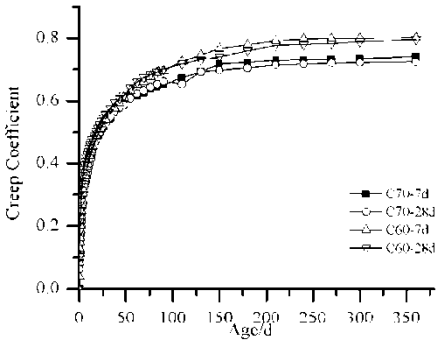

Figure 4. Creep Coefficient of Concrete

Results and discussion

Creep Coefficient of Concrete

Because creep and shrinkage of concrete are not independent phenomena entirely [14, 15], concrete creep is expressed as a difference between the total strain and shrinkage strain measured at same age.[16, 17]

The experimental data of creep coefficient are shown in Figure 4. The age in Figure 4 is counted from the loading time. At the same loading age, the concrete with lower compressive strength show higher creep coefficient. For the same mix proportion, the creep coefficient is greater when the specimens loaded at an earlier age. The increasing rate of concrete creep coefficient decreases with the prolongation of loading time.

Discussion

Comparison of experimental data and the results of predictive models

Figure 5-8 show the measured results of concrete after 7d and 28d curing age and the predicting results based on different models. Most of creep models predictions are very far from experimental data. ACI 209R calculation model gives the largest deviation from the measured results. Thecreep measurement in this paper complies with Chinese standards. Prediction error and inconvenience shall be brought using models following RILEM TC-107 or ASTM C512, due to the difference in material properties, specimen size and curing condition.

ACI 209R calculation model uses a multiplied multi-factor equation to predict the creep coefficient of concrete. It shows a proportional relationship between the creep coefficient of hardened concrete and the slump of fresh concrete. However the creep coefficient of self-consolidating concrete is just 10% to 20% higher than the one of conventional plastic concrete based on a number of experimental results. The CEB-FIP and B3 calculation models based on the hydration degree of binder or the mechanical property of concrete show a better prediction of creep than ACI 209R model.

The actual loading of concrete sample decreases gradually with the prolongation of loading age on account of the spring relaxing caused by concrete deformation and the loading stability of creep apparatus. Thus, a smaller but close deformation observed can be accepted. The prediction of concrete creep based on CEB-FIP or B3 models from 28d loading age is closer to the actually measured results than that from 7d loading age. The difference between the predictive and experimental creep coefficient of concrete from 28d loading age is subtle, while the estimation from 7d loading age is over twice the actually measured results.Binder in HSSCC usually shows a quick hydration in early age. HSSCC gets a sufficiently high early strength for rapid construction. It is controlled by the mix proportion as well as binder composition and the concrete admixture. The hydration of binder is speeded up to form a dense paste microstructure that possesses good deformation-resisting ability. That is the main reason that compressive creep of HSSCC used in high-rise building construction is frequently lower than the expected level, especially at early age. Therefore, the disregard of concrete hydration degree may be the principal cause of error of prediction.

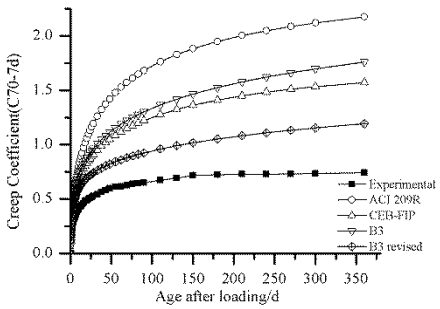

Figure 5. Experimental and predictive creep coefficient (C70; measured from 7d)

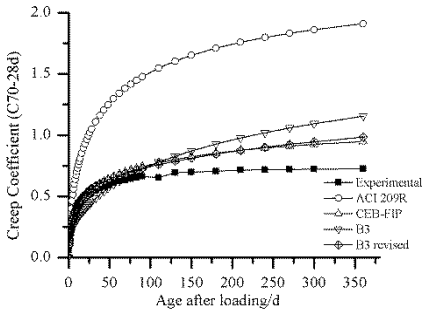

Figure 6. Experimental and predictive creep coefficient (C70; measured from 28d)

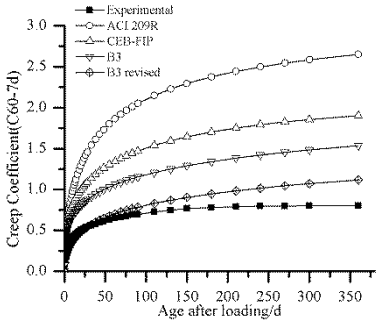

Figure 7. Experimental and predictive creep coefficient (C60; measured from 7d)

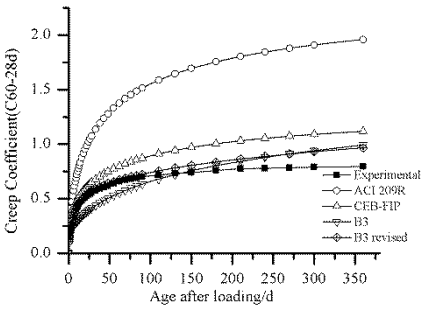

Figure 8. Experimental and predictive creep coefficient (C60; measured from 28d)

A revision to B3 model with experimental data

The micromechanics-based creep model B3 for solidifying material, summarized by Bazant[17], gives the following equations:

$$J(t,t') = \frac{1}{E_0} + \int_0^t \dot{C}(\tau,t')d\tau = \frac{1}{E_0} + \int_0^t \left(\frac{\dot{\Phi}(t-t')}{v(\tau)} + \frac{1}{\eta(\tau)}\right)d\tau \qquad (1)$$

$$\frac{\sigma}{E_0} + \varepsilon^c = J(t,t')\sigma \qquad (2)$$

The following hypothesis is introduced to describe the material properties in these equations:

$$\Phi(t-t') = q_2 \ln(1+\xi^n) \tag{3}$$

$$\xi = \frac{t-t'}{\lambda_0} \tag{4}$$

$$v(t)^{-1} = (\frac{\lambda_0}{t})^m + \alpha \tag{5}$$

$$\eta(t)^{-1} = q_4 t^{-1} \tag{6}$$

There is still large deviation between predicting results based on B3 or CEB-FIP models and the measured results of concrete creep (Figure 5-8). The deviation increases with the prolongation of loading time. It is necessary to modify the existing models to get an acceptable prediction. A new hypothesis is introduced:

$$\Phi(t-t') = p_2'(\xi-t')^k (0<k<1) \tag{7}$$

To avoid misunderstanding, we change the constants q_1, q_3, q_4 and q_5 in B3 model to p_1, p_3, p_4 and p_5 in modified B3 model. Following analogous analysis, the compliance function can be obtained as

$$J(t,t') = p_1 + C_0^{'} + C_d \tag{8}$$

$$C_0^{'} = p_2' P(t,t') + p_3(\xi-t)^k + p_4 \ln(\frac{t}{t'}) \tag{9}$$

$$p_3 = k_3(w/c)^4 p_2 \tag{10}$$

$$p_4 = k_4(a/c)^{-0.7} \tag{11}$$

$$P(t,t') = \frac{p_2'}{\lambda_0^{k-m}} \int_{t'}^{t} \frac{k[\tau-(\lambda_0+1)t']^{k-1}}{\tau^m} d\tau \tag{12}$$

According to experience that indicates the material constants, some boundary values are set:

$$t = 0.1 \quad m = 0.5 \quad \lambda_0 = 1day$$

When $t-t' >> t'$, a good approximate formula has been found as

$$P(t,t') \cong p_2 \exp(\frac{t}{t'}) P_f(t,t') \tag{13}$$

$$P_f(t) = \frac{1}{\sqrt{t'}} \ln(\frac{\sqrt{t}-\sqrt{t'}}{\lambda_0}+1) \tag{14}$$

$$p_2 = k_2 c^{0.5} \overline{f}_c^{-0.9} \tag{15}$$

To simplify the revision of predictive model, it is supposed that the constant of additional compliance function due to simultaneous drying (p_5) is only determined by material properties. Only the constants that are germane to compliance function for basic are considered in the fitting process. Fitting experimental data with Equations 4-15, the value of constants k_2 , k_3 , k_4 can be obtained as

$$k_2 = 101.2 \qquad k_3 = 0.22 \qquad k_4 = 0.06$$

The $C_0^{'}$ can be ascertained with the results above. To test the accuracy of new estimating formula, the modified predicting model is used to calculate the creep coefficient based on the mixture proportions and experimental parameters. A contradistinction between the experimental data and modified predictions is provided from Fig. 4 to Fig. 7. It shows that the prediction of creep coefficient based on the modified B3 model is much more accurate than that based on B3 model and CEB-FIP model.

Conclusions

The creep coefficient of concrete increases with the decrease of concrete strength at same loading age. The creep coefficient of concrete is greater when the specimens loaded at an earlier age for the same mix proportion. The increasing rate of concrete creep coefficient decreases with the prolongation of loading time.

ACI209R model is unsuitable to predict the creep coefficient of high-strength self-consolidating concrete. There is a large deviation between the predictions based on CEB-FIP and B3 models and the measured results of creep coefficient of high strength self-consolidating concrete loaded at an early age. A revision is required to increase the accuracy of estimate, on the basis of Chinese standards.

A new hypothesis is introduced to modify B3 model. A good agreement is obtained with the modified B3 model.

Acknowledgment

Authors would like to acknowledge the support of National Natural Science Foundation of China (No. 51278277).

References

[1] Issa, M., Alhassan, M., Shabila, H., & Krozel, J. (2005). Laboratory performance evaluation of self-consolidating concrete. In *Proceedings of the Second North American Conference on the Design and Use of Self-Consolidating Concrete and the Fourth Int. RILEM Symposium on Self-Consolidating Concrete, Center for Advanced Cement-Based Materials (ACBM), Chicago* (pp. 857-862).

[2] Naito, C. J., Parent, G., & Brunn, G. (2006). Performance of bulb-tee girders made with self-consolidating concrete. *PCI journal*, *51*(6), 72-85.

[3] Schindler, A. K., Barnes, R. W., Roberts, J. B., & Rodriguez, S. (2007). Properties of self-consolidating concrete for prestressed members. *ACI Materials Journal*, *104*(1).

[4] Suksawang, N., Nassif, H., & Najm, H. (2006). Evaluation of mechanical properties for self-consolidating, normal, and high-performance concrete. *Transportation Research Record: Journal of the Transportation Research Board*, (1979), 36-45.

[5] Mazzotti, C., & Ceccoli, C. (2008). Creep and Shrinkage of Self Compacting Concrete: Experimental Behavior and Numerical Model. In *Proc. of the Eighth International Conference on Creep, Shrinkage, and Durability of Concrete and Concrete Structures* (pp. 667-673).

[6] Neville, A. M. (1995). *Properties of concrete*.

[7] Rozière, E., Granger, S., Turcry, P., & Loukili, A. (2007). Influence of paste volume on shrinkage cracking and fracture properties of self-compacting concrete. *Cement and Concrete Composites*, *29*(8), 626-636.

[8] Loser, R., & Leemann, A. (2009). Shrinkage and restrained shrinkage cracking of self-compacting concrete compared to conventionally vibrated concrete. *Materials and structures*, *42*(1), 71-82.

[9] Ito, H., Maruyama, I., Tanimura, M., & Sato, R. (2004). Early age deformation and resultant induced stress in expansive high strength concrete. *Journal of Advanced Concrete Technology*, *2*(2), 155-174.

[10] Østergaard, L., Lange, D. A., Altoubat, S. A., & Stang, H. (2001). Tensile basic creep of early-age concrete under constant load. *Cement and concrete research*, *31*(12), 1895-1899.

[11] Committee 209, ACI (1982). Prediction of creep, shrinkage and temperature effects in concrete structure.

[12] du Béton, CEI. (2010). CEB-FIP model code 2010, first completed draft.

[13] Bazant, Z. P., & Baweja, S. (2000). Creep and shrinkage prediction model for analysis and design of concrete structures: Model B3. *ACI Special Publications*, *194*, 1-84.

[14] Bažant, Z. P., Huet, C., & Müller, H. S. (1994). Comment on recent analysis of concrete creep linearity and applicability of principle of superposition. *Materials and Structures*, *27*(6), 359-361.

[15] Reinhardt, H. W., & Rinder, T. (2006). Tensile creep of high-strength concrete. *Journal of advanced concrete technology*, *4*(2), 277-283.

[16] Leemann, A., Lura, P., & Loser, R. (2011). Shrinkage and creep of SCC–The influence of paste volume and binder composition. *Construction and Building Materials, 25*(5), 2283-2289.
[17] Bazant, Z. P. & Prasannan, S. (1989). Solidification theory for concrete creep. I: formulation. *Journal of Engineering Mechanics, 115*(8), 1691-1703.

Shrinkage Mitigating Strategies for Low Shrinkage Self-Consolidating Concrete

Iman Mehdipour[1] and Kamal H. Khayat[2]

Center for Infrastructure Engineering Studies, Department of Civil, Architectural and Environmental Engineering, Missouri University of Science and Technology, Rolla, MO, USA
[1]Tel.: 573-341-6656; Email: iman.mehdipour@mst.edu
[2]Tel.: 573-341-6223; Email: khayatk@mst.edu

Abstract Statistical factorial design approach was undertaken to evaluate the level of significance of various shrinkage mitigating approaches on autogenous and drying shrinkage, and mechanical properties of self-consolidating cement-based materials. The investigation was carried out using concrete equivalent mortars (CEMs) formulated from environmentally friendly self-consolidating concrete (SCC) mix design proportioned with a low binder content of 315 kg/m^3 and a water-to-binder ratio (w/b) of 0.40. The evaluated shrinkage mitigating materials included the calcium sulfoaluminate EX (CSA-based EX), calcium oxide EX (CaO-based EX), shrinkage reducing admixture (SRA), and use of lightweight sand (LWS). These approaches were compared at various initial moist curing periods (IMCP). Trade-off contour diagrams between investigated parameters and modeled responses were developed. Test results indicate that internal curing provided by LWS can enhance the efficiency of the EX, especially for mixtures subjected to air drying. The synergetic effect of the combination of CaO-based EX with LWS can lead to extended period of expansion. The comparison between EXs shows that the efficiency of the CSA-based EX in reducing shrinkage is more affected by IMCP. Based on the results derived from factorial design, the desirability function approach was used to determine the optimal shrinkage mitigating strategies to secure the targeted properties.

Keywords: *Autogenous shrinkage, drying shrinkage, expansive agent, initial moist curing period, internal curing, statistical models.*

Introduction

The mix design of high-performance concrete (HPC) is typically characterized with relatively high binder content and use of supplementary cementitious materials (SCMs). The incorporation of high binder content can lead to higher water/admixture demand and greater risk of thermal and drying shrinkage. Shrinkage can increase the risk of cracking and reduce durability. Water curing is crucial to enhance cement hydration and pozzolanic reaction, and is necessary for the reduction of porosity and the refinement of the capillary pores, as well as decrease in autogenous and drying shrinkage at early-age. A number of shrinkage mitigating materials can be employed to reduce the early-age shrinkage. These materials include the incorporation of shrinkage reducing admixtures (SRAs) [1,2], expansive agents (EXs) [3,4], lightweight sand (LWS) [5-7]. The combination of shrinkage mitigating materials can be more effective in reducing shrinkage and early-age cracking. Hwang and Khayat [2] investigated the effect of combined use of fiber and SRA on shrinkage cracking potential of high-performance self-consolidating concrete (SCC) designated for repair applications. The results of shrinkage ring test indicated that elapsed time before cracking of SCC made with combination of 0.5% synthetic fiber and 8 L/m^3 SRA was four times longer than that of similar fibrous SCC prepared without any SRA. The effectiveness of incorporating shrinkage mitigating materials is significantly influenced by the wet curing conditions, including the initial moist curing period (IMCP) and internal curing through the use of water-saturated porous aggregate. Collepardi et al. [8] pointed out that the reaction of calcium sulfoaluminate EX (CSA-based EX) with water needs higher moist curing of 5 to 7 days compared to 1 to 2 days for CaO-based EX to complete its hydration and develop its potential expansion.

Therefore, the performance of shrinkage mitigating materials is considerably influenced by water available to hydration of these materials, thus better shrinkage mitigation. The study presented here was undertaken to evaluate the performance of different shrinkage mitigating materials on self-consolidating mortar subjected to various wet curing conditions. The wet curing conditions included the IMCP and the internal curing content provided by using LWS. A statistical factorial design was conducted to assess the level of significance of various materials that can be used to control shrinkage. These materials included SRA, CSA-based and CaO-based EXs, LWS, and changes in IMCP.

Experimental Program

Materials

In order to evaluate the effect of EX type on shrinkage, two types of EX were used, including CSA-based and CaO-based EXs. Continuously graded natural sand with 5 mm nominal maximum size, specific gravity of 2.50, and water absorption of

0.6% was employed. The LWS with 6 mm nominal maximum size and specific gravity of 1.65 was used. The LWS has a 72 hours water absorption of 13% and a desorption capacity of 90% at 94% RH in accordance with ASTM C1761. The LWS was pre-saturated to secure a saturated surface-dry (SSD) condition before batching. A polycarboxylate-based high-range water reducer (HRWR) with a solid content of 23% and a specific density of 1.05 was employed. A commercially available SRA made of propylene glycol ethers was incorporated to mitigate shrinkage. The SRA and EX contents were considered as parts of mixing water and binder materials, respectively, for the mixture proportioning.

Experimental Design and Mixture Proportioning

Factorial design was carried out to evaluate the effect of different shrinkage mitigating approaches on autogenous shrinkage, drying shrinkage, and mechanical properties of CEMs. The modeled parameters (input factors) included the use of CSA-based and CaO-based EXs, SRA, LWS, and changes in IMCP. All of the investigated CEMs were designed based on the environmentally friendly SCC mixtures with a low binder content of 315 kg/m^3 and a water-to-binder ratio (w/b) of 0.40. The quantity of LWS was theoretically estimated based on the internal curing water required to eliminate the self-desiccation proposed by Bentz et al. [5]. The partial replacement of sand by 20% LWS, corresponding to M_{LWS} of 170 kg/m^3, can provide internal curing water of 22 kg/m^3. The factorial design method consisted of three portions; the factorial points (2^n), central points, and points used for validation, where n refers to the number of the modeled parameters. In this study, n corresponded to four parameters; SRA, EX, LWS, and IMCP. The statistical design enables the evaluation of the selected parameters with each evaluated at two distinct levels of −1 and +1 (minimum and maximum levels). In order to separately evaluate the effect of EX type on modeled responses, two different sets of experimental matrixes were designed. Tables 1 and 2 present two different experimental matrixes for CSA-based and CaO-based EXs, respectively. Each experimental design consisted of 16 mixtures (2^4) at two levels for the factorial portion. The significance of variables and their interactions were determined by the analysis of variance (ANOVA) using the least squares fitting technique. Statistical models presented in this study were established by multi-regression analysis.

Test Methods

Autogenous shrinkage was determined in accordance with ASTM C1698. For each mixture, two corrugated samples were prepared using polyethylene tubes. The initial reading (time zero) for the autogenous shrinkage corresponded to the final setting time determined in compliance with ASTM C403. Drying shrinkage was evaluated using a digital type extensometer in the prismatic specimens measuring 25 × 25 × 285 mm in accordance with ASTM C157. In order to evaluate the effect of IMCP on drying shrinkage, the specimens were subjected to initial moist curing

of 0 to 6 days before air drying at 23 ± 1°C and 50% ± 3% RH. It should be pointed out that the term "drying shrinkage" used in this paper refers to ''total shrinkage'' which includes shrinkage induced by drying and autogenous shrinkage. The 7-, 28-, and 91-day compressive strengths of CEMs were determined using 50-mm cube specimens. Cylindrical specimens measuring 100 × 200 mm were cast to evaluate the splitting tensile strength at 28 days. After demolding at 24 hours, specimens were subjected to different IMCP of 0 to 6 days. Following the IMCP, all specimens were exposed to air drying at 23°C and 50% RH until the age of testing.

Table I. Experimental design for mixtures containing CSA-based EX

Type	Mix description	Absolute value			
		SRA (%)	CSA-based EX (%)	LWS (%)	IMCP (day)
Factorial points	C	0	0	0	0
	C-6	0	0	0	6
	L	0	0	20	0
	L-6	0	0	20	6
	S	2	0	0	0
	S-6	2	0	0	6
	S-L	2	0	20	0
	S-L-6	2	0	20	6
	EX1	0	15	0	0
	EX1-6	0	15	0	6
	EX1-L	0	15	20	0
	EX1-L-6	0	15	20	6
	EX1-S	2	15	0	0
	EX1-S-6	2	15	0	6
	EX1-S-L	2	15	20	0
	EX1-S-L-6	2	15	20	6

Notes: C: control mixture, L: lightweight sand, S: shrinkage reducing admixture, EX1: CSA-based expansive agent

Table II. Experimental design for mixtures containing CaO-based EX

Type	Mix description	Absolute value			
		SRA (%)	CaO-based EX (%)	LWS (%)	IMCP (day)
Factorial points	C	0	0	0	0
	C-6	0	0	0	6
	L	0	0	20	0
	L-6	0	0	20	6
	S	2	0	0	0
	S-6	2	0	0	6
	S-L	2	0	20	0
	S-L-6	2	0	20	6
	EX2	0	10	0	0
	EX2-6	0	10	0	6
	EX2-L	0	10	20	0
	EX2-L-6	0	10	20	6

EX2-S	2	10	0	0
EX2-S-6	2	10	0	6
EX2-S-L	2	10	20	0
EX2-S-L-6	2	10	20	6

Notes: EX2: CaO-based expansive agent

Test Results and Discussion

Derived Statistical Models

In this study, P-values less than 0.1 were considered as a significance level. This identifies which variable has a significant influence on the modeled response. Student tests were run to evaluate the significance of the factors and their second-order interactions on a given response. The estimate coefficient of each factor refers to the contribution of that factor to the modeled response. A negative value of estimate coefficient indicates that an increase in the modeled parameters results in a reduction in the response. The derived statistical models of the modeled responses are summarized in Table 3 with variables expressed as actual values. The derived models were arranged in descending order of the factors with the highest effect on the modeled property. The correlation coefficient (R^2) of the derived models ranged between 0.89–0.98. Based on the derived statistical models the findings can be summarized as follows:

Initial moist curing had substantially higher influence on drying shrinkage compared to the LWS replacement.

Unlike the case for CaO-based EX, the SRA concentration was found to have the most significant effect on autogenous and drying shrinkage for mixtures containing CSA-based EX.

Compared to the CaO-based EX system, the IMCP has higher impact on drying shrinkage of mixtures made with CSA-based EX. The second order interaction between IMCP and CSA-based EX or SRA and CSA-based EX has significantly higher influence on drying shrinkage compared to the CSA-based EX alone. However, opposite trend was found for CaO-based EX system. The effectiveness of using LWS to reduce shrinkage was more efficient for mixtures containing CSA-based EX compared to similar mixtures made with CaO-based EX.

The incorporation of CSA-based EX is more efficient to reduce the autogenous shrinkage than the drying shrinkage. Regardless of the IMCP, the use of CaO-based EX was found to be the most efficient way in mitigating shrinkage among the investigated modeled parameters.

Exploitation of Statistical Models

The contour diagram of 28-day autogenous shrinkage in Figure 1 illustrates the trade-off between EX and LWS replacement rate. Regardless of the LWS replacement, the use of CaO-based EX is more effective in mitigating autogenous shrinkage than CSA-based EX system. The increase in LWS replacement can

enable the reduction in EX content to maintain a fixed autogenous shrinkage, especially for CSA-based EX system. This was reflected by larger slope of the contour diagram in Figure 1 (a). For instance, in order to secure an expansion of 50 μstrain, a minimum CSA-based EX content of 12%, by mass of total binder, is required in combination with 16.5% LWS replacement, by volume. However, in the case of CaO-based EX, the use of 2% EX with no LWS can result in the expansion of 50 μstrain.

Table III. Derived statistical models for modelled responses

Experimental design	Modelled response	Age (day)	Derived equation (actual values)
First set for mixtures containing CSA-based EX	Compressive strength (MPa)	7	$39.75-3SRA+0.92IMCP+0.27LWS+0.17EX1$
		91	$51.5-3.75SRA+2.92IMCP+0.64LWS+0.1EX1$
	Autogenous shrinkage (μstrain)	3	$-184.2+40.7SRA+21.6EX1+4.7LWS$
		28	$-251.1+44.8SRA+14.9EX1+7.6LWS$
	Drying shrinkage (μstrain)	3	$-338+47.8IMCP+46.6SRA+5.4LWS$ $+3.8\,(EX1\times IMCP)+0.2EX1$
		28	$-638.6+89SRA+12IMCP+5.3\,(EX1\times SRA)$ $+4.2\,(EX1\times IMCP)+2.2LWS+0.2EX1$
		180	$-771.7+99.2SRA+9.5IMCP+6\,(EX1\times SRA)$ $+4.1\,(EX1\times IMCP)+5.7LWS+0.1EX1$
Second set for mixtures containing CaO-based EX	Compressive strength (MPa)	7	$39.5-2.5SRA+0.92IMCP+0.24LWS+0.1EX2$
		91	$49.6+3.1IMCP-1.4SRA+0.66LWS+0.1EX2$
	Autogenous shrinkage (μstrain)	3	$-191.5+137.6EX2+45.5SRA+15.6\,(SRA\times EX2)$ $+3.2LWS+1.2\,(EX2\times LWS)$
		28	$-260+159.4EX2+39.5SRA+16.8\,(SRA\times EX2)$ $+4.7LWS+1\,(EX2\times LWS)$
	Drying shrinkage (μstrain)	3	$-237.5+30.8IMCP+23.5EX2+19.1\,(EX2\times IMCP)$
		28	$-527.5+61.9EX2+15.3\,(EX2\times IMCP)+10.5IMCP$
		180	$-615.5+73.4EX2+13.9\,(EX2\times IMCP)+8.5IMCP$

The contour diagram of drying shrinkage in Figure 2 shows the trade-off between EX and IMCP for mixtures with no SRA and LWS. The effectiveness of using CSA-based EX to mitigate drying shrinkage at early and later ages is highly affected by the IMCP. In the absence of IMCP, the use of CSA-based EX up to 15% resulted in no significant influence on drying shrinkage. However, opposite trend was found for CaO-based EX, where the use of 10% EX developed an expansion of 100 μstrain after 180 days even without any IMCP. For a given targeted drying shrinkage value, the increase in IMCP can enable the reduction of EX content, especially for the case of CSA-based EX. As illustrated in Figure 2

(b), the increase of IMCP from 4 to 5 days can reduce the CSA-based EX content from 12% to 9%, by mass of total binder, to maintain the drying shrinkage of 550 μstrain after 180 days (points A and B in Figure 2).

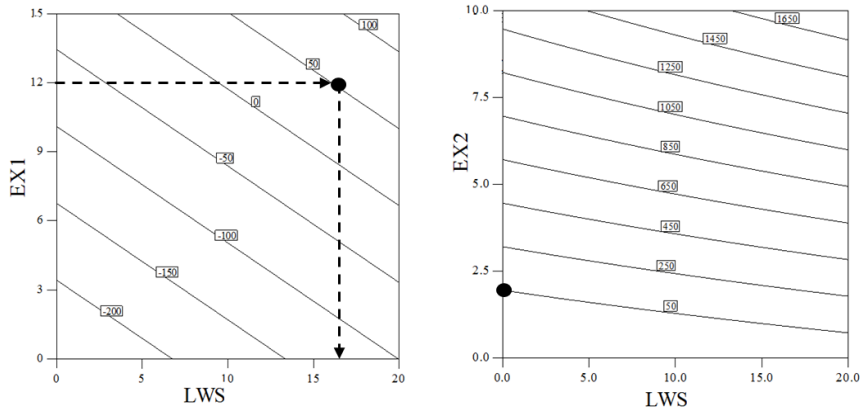

(a) CSA-based EX vs. LWS (b) CaO-based EX vs. LWS

Figure 1. Contour diagram of 28-day autogenous shrinkage (SRA = 0)

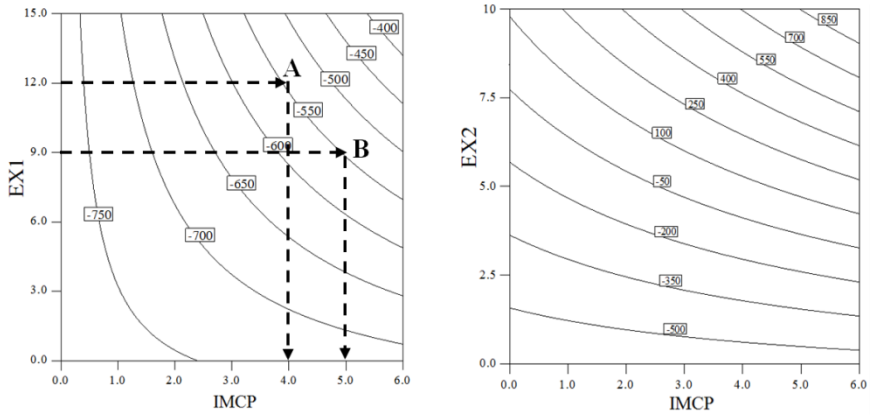

Figure 2. Contour diagram of 180-day drying shrinkage (SRA = 0 and LWS = 0)

The surface response of 180-day drying shrinkage in Figure 3 illustrates the trade-off between EX and SRA for mixtures without any LWS and IMCP. In the absence of IMCP, the combined use of CSA-based EX and SRA was highly effective in mitigating drying shrinkage compared to the CSA-based EX alone. For example, the combination of 15% CSA-based EX and 2% SRA reduced the 180-day drying shrinkage from 780 to 350 μstrain. This is attributed to lower surface tension of pore solution as well as higher degree of saturation of cement paste resulting from

SRA addition [6]. However, no significant improvement in drying shrinkage was found for the combination of SRA and CaO-based EX, as shown in Figure 3 (b).

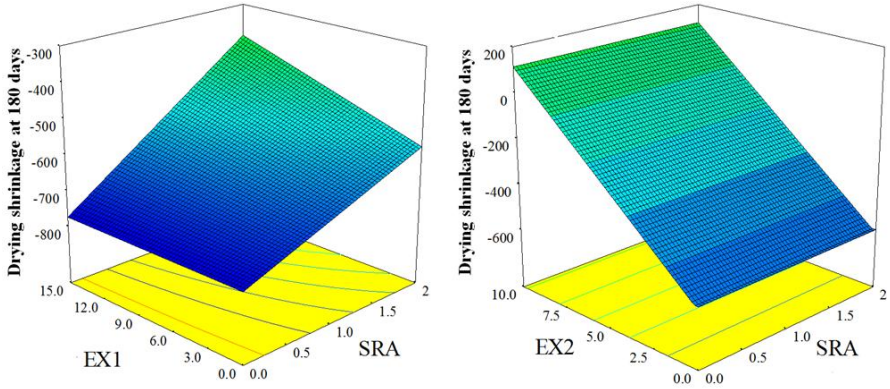

(a) CSA-based EX vs. SRA (b) CaO-based EX vs. SRA

Figure 3. Surface response of 180-day drying shrinkage (LWS = 0 and MCP = 0)

Multi-Objective Numerical Optimization

A multi-objective optimization technique was carried out to determine the optimum combination of EX and IMCP required to achieve the targeted responses. This technique involves satisfying the defined properties without compromising any of the requirements. For the targeted properties, the desirability functions (d_i) are obtained and these functions are simultaneously optimized to determine the best combination. The overall desirability function (D) is expressed as follows:

$$D = (d_1^{r_1} \times d_2^{r_2} \times d_3^{r_3} \times \ldots \times d_n^{r_n})^{1/\sum r_i} = (\prod_{i=1}^{n} d_i^{r_i})^{1/\sum r_i} \quad (1)$$

where n is the number of individual responses in the optimization, and r_i refers to the relative importance of each individual property. The r_i varies from 1 to 5, reflecting the least to most important, respectively. The d_i ranges between 0 (for a completely undesired response) and 1 (for a fully desired response). The D value close to 1 reflects that the optimal combination of variables is able to secure the targeted properties. Table 4 presents the targeted properties defined in this investigation. The autogenous and drying shrinkage were considered to be zero, corresponding to complete elimination of shrinkage. The degree of importance of 3 and 5 were assigned to compressive strength and shrinkage, respectively.

The contour diagram of overall desirability for targeted properties is plotted in Figure 4. For a given targeted properties, mixtures containing CaO-based EX developed higher desirability function of 0.90 compared to 0.65 for CSA-based EX system. The overall desirability for mixtures containing CSA-based EX is

significantly affected by duration of moist curing, in which higher desirability value requires an increase in the IMCP. The optimum combination for mixture containing CaO-based EX corresponds to 6% EX and 1.5 day of IMCP. However, in the case of CSA-based EX, the highest desirability value of 0.65 corresponds to 15% EX and 6 days of IMCP. Therefore, in the case of limited IMCP, the use of CaO-based EX can be more effective to develop low shrinkage concrete proportioned with relatively high w/b.

Table IV. Targeted properties for desirability function

Experimental design	Response	Lower limit	Upper limit	Defined criteria	
				Target >	Importance
First set for mixtures containing CSA-based EX	91-day compressive strength	44	73	50	3
	28-day autogenous shrinkage	-285*	198*	0	5
	180-day drying shrinkage	-768	91	0	5
Second set for mixtures containing CaO-based EX	91-day compressive strength	44	72	50	3
	28-day autogenous shrinkage	-285	2328	0	5
	180-day drying shrinkage	-765	1424	0	5

Note: Positive and negative values refer to expansion and shrinkage, respectively.

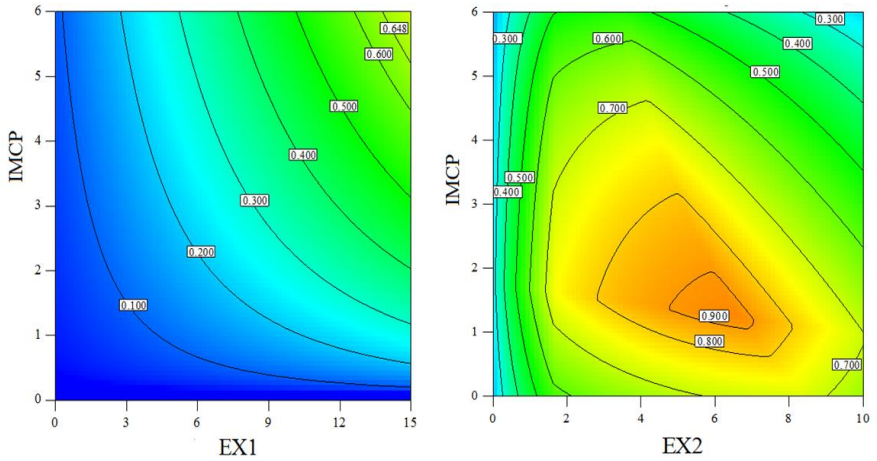

(a) CSA-based EX (b) CaO-based EX

Figure 4. Contour diagram of overall desirability (SRA = 0 and LWS = 0)

Conclusions

The level of influence of various shrinkage mitigating approaches on autogenous and drying shrinkage, and mechanical properties of self-consolidating mortars was evaluated. Based on the results presented herein, the following conclusions can be drawn:

- Regardless of the IMCP and shrinkage mitigating materials, the incorporation of LWS was shown to improve the mechanical properties, especially at later ages.
- The coupled effect of lower self-desiccation and greater degree of saturation of cement resulting from the use of SRA and LWS can enhance the magnitude and duration of expansion supplied by EX, especially for CSA-based EX.
- The second order interaction between IMCP and CSA-based EX or SRA and CSA-based EX has substantially higher influence on drying shrinkage compared to the CSA-based EX alone. However, opposite trend was found for CaO-based EX system.
- For a given targeted drying shrinkage, the increase in IMCP can enable the reduction of EX content, especially for the case of CSA-based EX.
- For a given targeted properties, mixtures containing CaO-based EX developed higher desirability function of 0.90 compared to 0.65 for CSA-based EX system.

References

[1] Weiss, W.J. and Shah, S.P. (2002), Restrained shrinkage cracking: the role of shrinkage reducing admixtures and specimen geometry. *Materials and Structures*, vol. 35, n. 2, pp. 85-91.

[2] Hwang, S.D. and Khayat, K.H. (2008), Effect of mixture composition on restrained shrinkage cracking of self-consolidating concrete used in repair. *ACI Materials journal*, vol. 105, n. 5, pp. 499-509.

[3] Chen, I.A., Hargis, C.W. and Juenger, M.C. (2012), Understanding expansion in calcium sulfoaluminate–belite cements. *Cement and Concrete Research*, vol. 42, n. 1, pp. 51-60.

[4] Mo, L., Deng, M. and Wang, A. (2012), Effects of MgO-based expansive additive on compensating the shrinkage of cement paste under non-wet curing conditions. *Cement and Concrete Composites*, vol. 34, n. 3, pp. 377-83.

[5] Bentz, D.P. Lura, P. and Roberts, J.W. (2005), Mixture proportioning for internal curing. *Concrete International*, vol. 27, n. 2, pp. 35-40.

[6] Lura, P., Pease, B., Mazzotta, G.B., Rajabipour, F. and Weiss, J. (2007), Influence of shrinkage-reducing admixtures on development of plastic shrinkage cracks. *ACI Materials Journal*, vol. 104, n. 2, pp. 187-194.

[7] Hwang, S.D., Khayat, K.H. and Youssef, D. (2013), Effect of moist curing and use of lightweight sand on characteristics of high-performance concrete. *Materials and structures*, vol. 46, n. 1-2, pp. 35-46.

[8] Collepardi, M., Borsoi, A., Collepardi, S., Olagot, J.J. and Troli, R. (2005) Effects of shrinkage reducing admixture in shrinkage compensating concrete under non-wet curing conditions. *Cement and Concrete Composites*, vol. 27, n. 6, pp.704-8

Influences of Rheological Properties on Plastic Shrinkage Cracking in Mortars

Keisuke Takahashi and Suguru Goto

Ube Industries, Ltd., Construction Materials R&D Department

Abstract Plastic shrinkage cracking is a serious problem afflicting cementitious materials with fine powders such as self-consolidating mortars and self-leveling mortars. Previous researchers have investigated the influence of drying shrinkage induced by water evaporation on cracking during the plastic state. However, the mechanism for the generation of plastic shrinkage cracking has not been fully understood. This work examines the dimensional stability, hardening characteristics and oscillatory rheology of cement-based mortars with different amounts of fine powders and identified the importance of rheology for cracking risk. Our results show that plastic cracks were observed only in mortar containing a large amount of fine powders, although there was little difference in the evaporation, shrinkage, or hydration of the mortars. As for the oscillatory rheology of mortars, the storage elastic modulus in the plastic state increases as the mortar comprises a greater amount of fine powders. These findings could be interpreted as follows: increasing the amount of fine powders stiffens the structure in fresh mortars due to the trapping of water within particle aggregates as well as the consumption of superplasticizer molecules in water and subsequently degrades the flexibility of the mortars — hence the frequency of crack initiation increases.

Keywords: *Plastic shrinkage, Cracking, Oscillatory rheology, Capillary pressure, Cement-based mortar*

Introduction

Plastic shrinkage has become of great concern due to recurrent problems with cracking in cement-based mortars with a large amount of fine powders, such as self-consolidating mortars and self-leveling mortars. Plastic shrinkage cracks, which appear soon after casting (until final setting), degrade the durability and the aesthetics of building structures. Slovik and Ju demonstrated that drying induced concrete cracking in the plastic state as menisci were formed in the inter-particle spaces and a capillary contraction force was built up in the water phase because of

water evaporation [1]. In contrast, Shaeles and Hover reported that there was no direct correlation between plastic cracking and evaporation rate, although the use of water-reducing agents had a reducing impact on the plastic cracking [2]. The fluidity and dispersibility of the mortars significantly influence early-age shrinkage as the mobility of water and the microstructure are changed [3]. These previous studies point to plastic shrinkage cracking as being affected by the rheological properties of fresh mortars, but its mechanism has not been fully understood.

In order to identify the dominant factors that influence plastic cracking behaviour and clarify the corresponding mechanisms, our study focused on oscillatory rheology as well as the technological properties of cement-based mortars with different amounts of fine powders: deformation, weight loss, flow value, and setting, as well as hydration kinetics on a laboratory scale and the frequency of crack initiation in field trials.

Experiment

Materials and proportions

The characteristics of ordinary Portland cement (OPC), silicious sand, blast furnace slag and fly ash are listed in Table I. The proportions of the mortar mixes are listed in Table II. Mortars A and B comprised the same type and amount of admixtures such as polycarboxylic superplasticizer (SP), thickener, accelerator, defoamer, and redispersible latex powder. Mortar B contained more fine particles than did mortar A. These mortars are applied to flatten the surface of a concrete foundation. Mortars for field tests and laboratory testing were separately prepared. Prior to the field tests, 25 kg of the dry mortar mixes were pre-mixed and subsequently mixed with 6.5 kg of tap water for 3 min at 750 rpm with a handheld mixer. At the laboratory scale, the dry-mixed mortars were mixed with tap water for 3 min at 650 rpm using a mechanical mixer. Field trials were performed in an outdoor experiment station (18–36 ˚C and 30–85 % relative humidity). All laboratory tests were performed in a 20 ˚C and 65 % relative humidity constant temperature and humidity room. Each test was repeated two or more times under the same conditions.

Table I. Characteristics of OPC, silicious sand and fine powders

	Density (g/cm^3)	Blaine surface area (cm^2/g)	Average particle size (μm)
OPC	3.14	4560	10.7
Sand	2.54	n/a	133.5 (range: 75–300)
Slag	2.85	4300	5.1
Fly ash	2.34	4890	7.4

Table II. Mortar mix proportions (kg/m^3)

Mortars	OPC	Sand	Slag	Fly ash	Admixtures	Water
A	420	1200	300	0	90	260
B	414	788	493	197	89	260

Field tests

In order to build a concrete foundation for our field tests, ordinary concrete (water-cement ratio=55 %, cement-sand ratio=39 % sand-aggregate ratio=48 %, nominal strength=27 N/mm^2) was cast in a 200 cm-long formwork with a rectangular cross section of 60 cm height by 15 cm width. The mix proportion of the concrete used is shown in Table III. 6 h after casting the concrete, mortars A and B (15 cm-thick) were poured on a concrete surface and cured under drying condition without a sealed cover. The period of crack initiation and the number and width of the cracks were monitored for 24 h after casting the mortars. The temperature of mortars A and B after production was 22–24 ˚C.

Table III. Concrete mix proportion (kg/m^3)

OPC	Sand	Gravel	Admixtures	Water
335	846	934	2.68	184

Laboratory testing

Oscillatory rheology. The storage elastic modulus (G') of the fresh mortars, an index of stiffness (consolidation), was tested in a non-destructive way using a physical modular compact rheometer with a concentric-cylinder system. As a suspension has a high G', its structure becomes stiffened and the mobility of water in the suspension becomes restricted. The strain was set at 0.1 %, and the frequency was increased logarithmically from 6 to 100 rad/sec. Mortars were undisturbed in the testing chamber of the rheometer for a maximum of 5 h before the measurement in order to avoid destroying the structure.

Dimensional stability. Horizontal and vertical deformations without a sealed cover were monitored using two contactless laser sensors continually during the 24 h immediately after casting. One sensor was set to monitor the horizontal movement of an end rod embedded in the cast mortar. The other sensor was situated above the specimen with its laser beam directed at the surface of the specimen. The weight change of the mortars was measured using a balance after 4 h and 8 h of casting. The stainless-steel mould depicted in Fig. 1 is 250 mm long and has a rectangular cross-section of 15 mm height by 40 mm width.

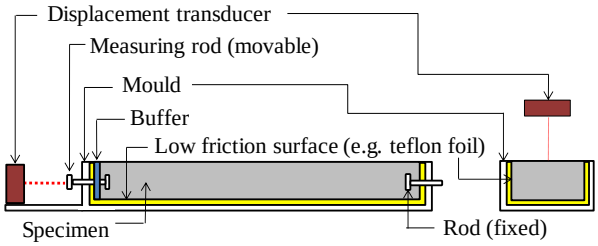

Figure 1. Experiment set-up for measuring dimensional stability

Heat release rate. A calorimetric test used as an index of hydration kinetics was carried out using an isothermal conduction calorimeter. The rate of heat evolution for each mortar samples was monitored for 24 h.

Flow and setting time. The flow was measured immediately after mixing and after 2 h of mixing by using a mini-slump cone 50 mm in diameter and 51 mm in height, based on EN 12706. The setting time was measured based on EN 196.

Results

Field tests

Figure 2 depicts parts of the mortar surfaces cast after 24 h. No cracks were observed in mortar A, although seven cracks with lengths of 1–7 cm and widths of less than 0.3 mm occurred in mortar B. All cracks were generated within 4 h after casting and radiated from a screw. The shrinkage of the concrete foundation (underlayment) with a cover was of almost the same magnitude as that of mortars A and B (overlay) without a cover (about 200 μm/m after 4 h and about 250 μm/m after 24 h. Therefore, shrinkage of the concrete foundation is not considered in this report for analyzing plastic cracks in mortar.

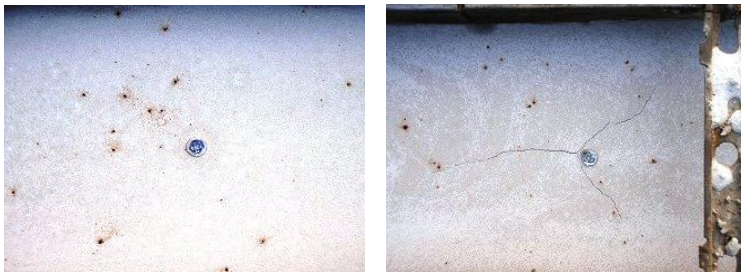

Figure 2. Plastic cracking of mortars A (*left*) and B (*right*)

Laboratory testing

Flow, setting time and weight loss. Table III lists the flow, initial setting (i.s.), final setting (f.s.) and weight loss of mortars A and B. The flow of mortar B immediately after mixing was greater than that of mortar A, but it then decreased drastically. Mortar B, which contained a larger amount of fine powders, set earlier than mortar A, but their weight loss differed slightly.

Table III. Flow, setting time and weight loss of mortars A and B

Mortar	Flow (mm)		Setting time (min)		Weight loss (g/cm^2)	
	0 min	2 h	i.s.	f.s.	4 h	8 h
A	220	90	305	490	0.34	0.64
B	238	50	255	425	0.32	0.60

Oscillatory rheology. Figure 3(a) plots G' for mortars A and B mixed after 30 min and 4 h as a function of the applied angular frequency. The G' curves for each mortar plateaued in the range of the applied frequency. Figure 3(b) plots G' of mortars A and B measured at a constant angular frequency of 10^2 rad/sec as a function of time. Compared to mortar A, G' in mortar B was lower until 30 min had elapsed, although it increased significantly afterwards.

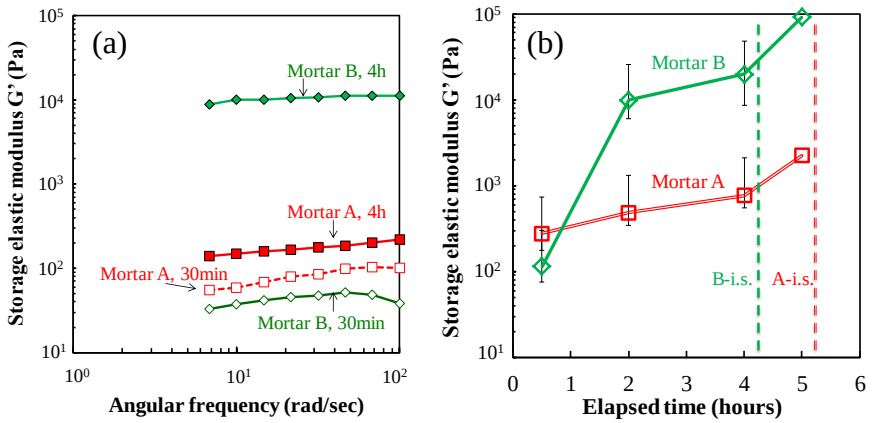

Figure 3. Experimental results for oscillatory rheology; (a) G' of mortars A and B as a function of applied angular frequency and (b) G' of mortars A and B at 10^2 rad/sec as a function of time

Dimensional stability. Figure 4 illustrates the difference between mortars A and B in horizontal and vertical deformation. Horizontal shrinkage of both mortars started after 2 h and increased until final setting. There was little difference between A and B in horizontal shrinkage. Vertical shrinkage increased significantly immediately after casting and then leveled off after about 4 h. The vertical shrinkage of mortar B was smaller than that of mortar A.

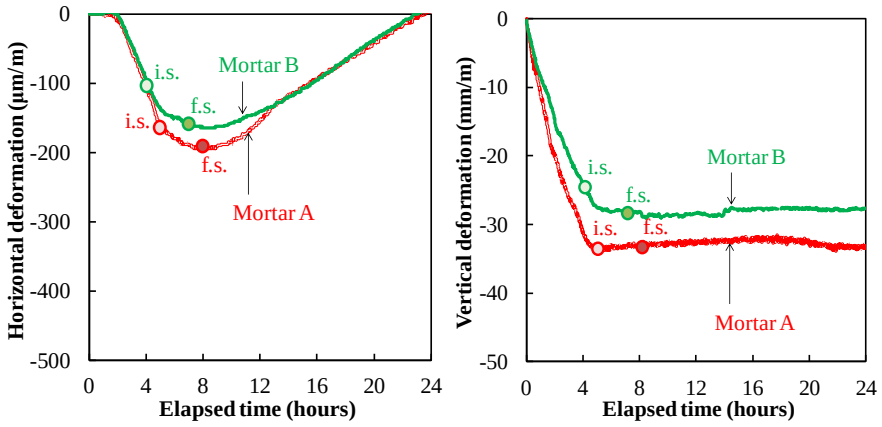

Figure 4. Horizontal (*left*) and vertical (*right*) deformation as a function of time

Heat release rate. Figure 5 plots the heat release rate of mortars A and B as a function of time. The heat release curves did not change with the amount of fine powders in the mortar. Massive hydration started after 4 h, and the second peak of the heat release rate appeared after 11 h.

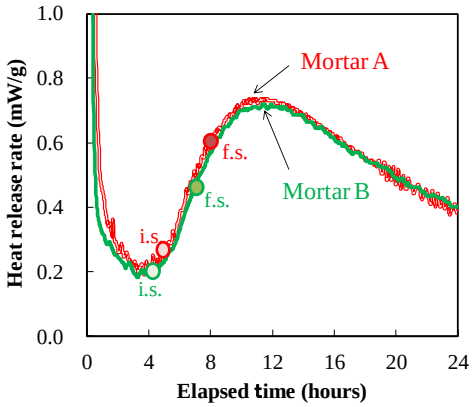

Figure 5. Heat release rate of mortars A and B as a function of time

Discussion

Classical mechanisms of plastic shrinkage

Lura et al. reported that the shrinkage process at early age can be divided into three phases [4] based on the drying model of gels presented by Brinker and Scherer [5]. Figure 6 illustrates the idea of plastic shrinkage that extended the Lura et al. findings. Figure 7 plots the horizontal deformation, vertical deformation, and heat release rate of mortars A and B as a function of time.

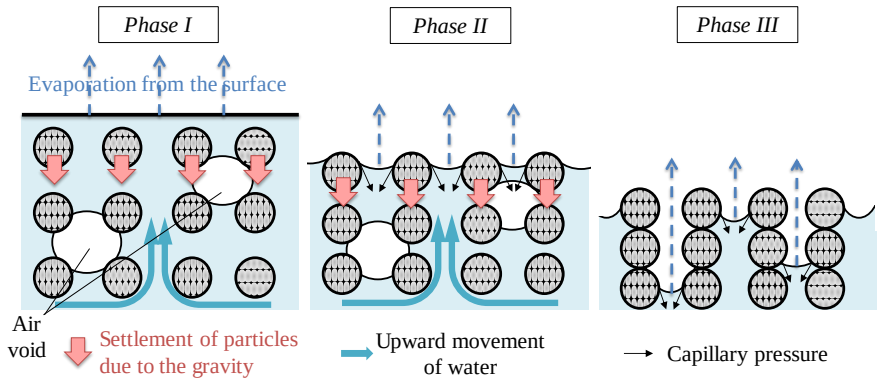

Figure 6. Three phases of plastic shrinkage

Phase I (0–2 h). Initially, gravity leads to settlement of the particles after casting the mortar. Water is pushed out of the space between the particles and accumulates on the mortar surface (i.e., a bleeding layer forms where the water evaporates.) Entrapped air escapes from the cast mortar, and these phenomena lead to the initial increase of vertical shrinkage. As long as water is supplied to the bleeding layer, less capillary pressure is generated as menisci cannot be formed at the mortar surface. Therefore, less horizontal shrinkage occurs in the first two hours.

Phase II (2–4 h). The available water cannot cover the entire mortar surface area any longer, and menisci start to form between the particles at the mortar surface. As a result, capillary pressure builds up due to evaporation from the menisci, and this in turn results in drying shrinkage. The increase in vertical movement slows down in this phase because most of the entrapped air has already escaped, and the structure becomes stiffened.

Phase III (4–24 h). Massive hydration starts. The initial vertical shrinkage provoked by de-airing, water evaporation, and settlement of particles stops. Menisci reach a break-through (minimum possible) radius and recede from the mortar surface into the interior of the mortar [6]. This minimum radius corresponds

to the maximum internal stress caused by capillary tension. The capillary pressure-settlement curve reaches a critical point where cracking is most likely to occur [4].

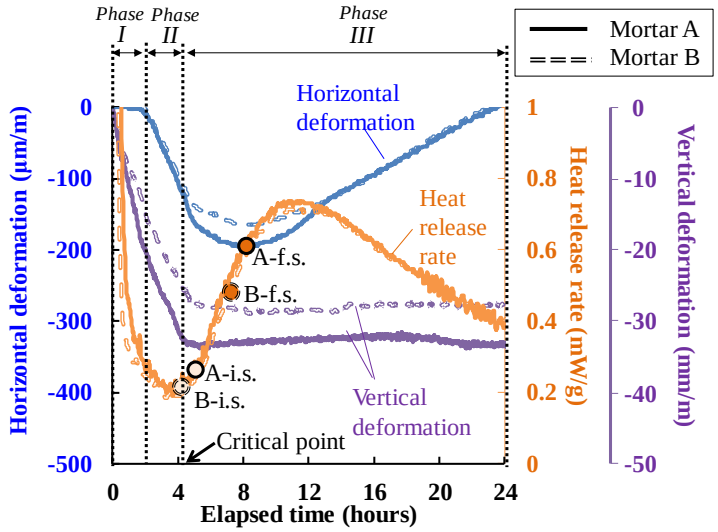

Figure 7. Deformation and heat release rate of mortars A and B

Extended explanation of plastic cracking by accounting for oscillatory rheology

Figure 2 indicates that the risk of plastic shrinkage cracking in mortar B was higher than in mortar A under the same testing condition at a field scale (in the outdoor experiment station), although temperature and humidity were not maintained constant during the field test. In this section several factors influencing the plastic shrinkage cracking are discussed using the results of laboratory tests, which were measured under the constant temperature and humidity condition.

Figures 4–5 and Table III indicate that horizontal shrinkage, hydration kinetics, and water evaporation differed little between mortars A and B, although plastic cracks occurred only in mortar B (Fig. 2). Figure 4 indicates that the early-age shrinkage of mortars A and B was only 200 μm/m. It is suggested that if the early-age shrinkage magnitude exceeds 700 μm/m, there is a high risk of cracking [7]. Based on these results, the classical mechanisms for plastic shrinkage cracking described above need to be extended and/or modified.

In the plastic state, mortars have poorly developed strength against applied stress and/or strain. In order to avoid plastic cracking, fresh mortars need to have a flexible (stress-following) structure. Figure 3(b) indicates that G' of the mortar with a large amount of fine powder increased significantly after 2 h (phase II). A

mortar with a higher G' becomes less flexible with respect to the applied stress, and its cracking risk increases. Therefore, plastic cracks occurred only in mortar B, although there was little difference in the curves of horizontal shrinkage between mortars A and B. The increase in G' in mortar B was provoked not by the hardening of the cement but by structural consolidation, as phase II is the induction period of hydration.

Effects of the addition of fine powders on G'

The difference of G' at phases II and III between mortars A and B (Fig. 3(b)) can be explained by an increase of immobile water in concentrated suspension, such as in mortars and concretes, or by an insufficient SP molecules in the water phase, or by both phenomena occurring together.

As water immobilized between particles and/or particle aggregates is released to their surroundings and as the free-water content subsequently increases, the mortar can flow. If the immobile water increases, the mortar becomes more consolidated and G' of the mortar increases. Fine powders with a smaller particle size and larger Blaine surface area increase the amount of immobile water in concentrated suspension [8]. SP adsorbs onto the particle surfaces and disperses particles (softens the structure). Setting is retarded by the interaction of the SP. As mortars contain a higher amount of fine powder, adsorption sites for SP increase and more SP molecules are consumed (a loss in flow retention occurs, Table III). As a result, setting retardation by the interaction of the SP becomes less pronounced [9]. Table III represents that an increase of the amount of fine powders in mortar (mortar B) shifts the setting to earlier.

Compared to mortar A, mortar B could have more immobile water and inadequate SP molecules than mortar A due to the replacement of coarse grains by fine grains (i.e., sand replaced by slag and fly ash), causing G' of mortar B to be higher than that of mortar A.

Conclusion

In addition to known parameters this study identified importance of rheology of cement-based mortars with different amounts of fine powders for cracking risk.

Plastic shrinkage is generally caused by capillary pressure due to water evaporation and hydration. When the capillary pressure reaches a critical point, cracking is most likely to occur. However, our results indicate that plastic cracks occur only in mortar with a large amount of fine powders, although water evaporation, the hydration process, and shrinkage changed little whether or not some sand was replaced by fine powders.

We extended the understanding of the mechanisms of plastic shrinkage cracking by accounting for oscillatory rheology. Increasing the amount of fine powders added consolidates the structure of fresh mortars and consequently results in an increase in G' (a degradation of flexibility) because of immobilized water within particle aggregates and/or insufficient SP molecules in water — hence the cracking risk increases.

References

[1] Slowik, V. and Ju, J. (2011), In: *Discrete modelling of plastic cement paste subjected to drying*, Cement and Concrete Composites, vol. 33, pp. 925–935.
[2] Shaeles, C. and Hover, K. (1988), In: *Influence of mix proportions and construction operations on plastic shrinkage cracking in thin slabs*, ACI Material Journal, no. 85, pp. 495–504.
[3] Takahashi, K., Bier, T. and Westphal, T. (2011), In: *Effects of mixing energy on technological properties and hydration kinetics of grouting mortars*, Cement and Concrete Research, vol. 41, pp. 1167–1176.
[4] Lura, P., Pease, B, Mazzotta, G., Rajabipour, F. and Weiss, J. (2007), In: *Influence of shrinkage-reducing admixtures on development of plastic shrinkage cracks*, ACI Materials Journal, vol. 104, no. 2, pp. 187–194.
[5] Brinker, J. and Scherer, G. (1990), *Sol-Gel Science*, Academic Press, New York, pp. 407–513.
[6] Wittmann, F. (2011). In: *On the action of capillary pressure in fresh concrete*, Cement and Concrete Research, vol. 15, pp. 218–224.
[7] Slowik, V., Schmidt, M. and Fritzsch, R. (2008), In: *Capillary pressure in fresh cement-based materials and identification of the air entry value*, Cement and Concrete Composite, vol. 30, pp. 557–565.
[8] Goto, S. and Nawa, T. (2011). In: *Prediction for rheological behavior of concentrated and flocculated suspension based on fractal aggregate model considering aggregation and fragmentation*, Cement Science and Concrete Technology, no. 65, pp. 544–551.
[9] Heikal M., Morsy M.S. and I Aiad (2006). In: *Effect of polycarboxylate superplasticizer on hydration characteristics of cement pastes containing silica fume*, Ceramics-Silikaty, 50 (1), 5-14

Performance Comparison of SCC Made with Lightweight Aggregates, Shrinkage-Reducing Admixture, and Expansive Agent

Soo Duck Hwang[1], Étienne Lepesqueux[2] and Kamal H. Khayat[3]

[1] Lead Scientist, Missouri University of Science and Technology, MO, USA
[2] Engineer, Les Services Exp inc., Drummonville, QC, Canada
[3] Professor, Missouri University of Science and Technology, MO, USA

Abstract The first section of the manuscript should be an abstract, where the aims, scope and conclusions of the papers are shortly outlined. A typical length should be between 100 and 250 words. An experimental program was undertaken to determine the effect of the type (expanded shale or slate) and substitution rate of lightweight coarse aggregate (0, 25%, 35%, and 50%, by aggregate volume) and replacement of normal-weight sand by lightweight sand (0 and 20%, by aggregate volume) and on key engineering properties and durability of self-consolidating concrete (SCC) designated for repair applications. Test parameters included the dosage rate of shrinkage-reducing admixture and expansive agent. Test results indicated that the investigated mixtures can exhibit good frost durability with durability factor equal to or greater than 90%, regardless of the substitution rate of lightweight aggregate. The incorporation of 20% lightweight sand and 25% lightweight coarse aggregate led to significant reduction in autogenous and drying shrinkage with limited drop in mechanical properties and durability. This indicates that the contribution of internal curing to reduce autogenous and drying shrinkage is greater than the increase in porosity and decrease in stiffness resulting from the addition of such porous material. The combined use of 20% lightweight sand and 25% lightweight coarse aggregate exhibited the best overall performance compared to other SCC repair materials.

Keywords: *Autogenous shrinkage; expansive agent; lightweight aggregate; restrained shrinkage; shrinkage-reducing admixture.*

Introduction

The use of self-consolidating concrete (SCC) as repair material has been accepted

given the ease of placement into complex sections and areas of limited or restricted access. SCC can flow through narrow spacing without blockage to achieve high passing ability and maintain adequate resistance to segregation, bleeding, and surface settlement during placement and until the onset of hardening. [1] Properly designed and placed SCC can provide higher surface quality compared to the conventional concrete which can include some surface defects, including honeycombs and voids. [2] The mix design of SCC often involves the incorporation of a relatively high content of cement paste and low volume of coarse aggregate, which can lead to high autogenous shrinkage and early-age cracking. This is especially the case when SCC is proposed with low water-to-cementitious materials ratio (*w/cm*). [3, 4]

In particular for repair application, thermal contraction and shrinkage of repair materials can be restrained by existing concrete, reinforcement, and adjacent structural steel, such as steel girders in a composite bridge deck. In the case of SCC made with low *w/cm*, the use of supplementary cementitious materials, such as fly ash, was not sufficient to avoid early-age cracking of concrete due to restrained shrinkage. [5, 6]

Lightweight aggregate (LWA) can provide a dispersed source of water within the mass of the concrete. [7-10] Better cement hydration resulting from internal curing water available from LWA can be obtained leading to lower self-desiccation. LWA has the ability to maintain internal relative humidity (RH) at high level, thus reducing the risk of self-desiccation. [11] At the beginning of hardening, capillary pores in the hydrated cement paste become finer and finer due to the accumulation of the hydrated particles until their diameters fall below those of the LWA that are in contact. The lower pore diameters in the hydrated cement paste compared to those of LWA can cause water to escape from the LWA due to suction caused by self-desiccation in the hydrated cement paste. [11] As a result, large pores of LWA can release water first followed by pores of smaller diameters. This movement of water causes an increase in internal RH in the cement paste in the vicinity of the LWA particles.

The degree of saturation of LWA decreases gradually. It should be noted that there is a limit to which the absorbed water in LWA could be available for reducing shrinkage and providing additional curing water of the cement paste. At approximately 80% RH in the concrete, LWA can release 50% to 95% of the absorbed water, depending on the pore network in the LWA, size of pores, their interconnectivity, and openness to the surface. [7] The efficiency of LWA is primarily dependent on the amount of water in the aggregate, the distance between aggregate particles, and the pore structure (amount and size of capillaries in the aggregate). [12] Akcay and Tasdemir [13] reported that for a given type of LWA, the replacement of normal-weight aggregate by natural LWA with size fractions of 2 to 4 mm is more effective to reduce autogenous deformation than the replacement by LWA with a relatively large fraction of 4 to 8 mm in the case of

concrete made with *w/cm* of 0.28. This can be due to shorter travel distance of internal curing water for the fine LWA. Bentur et al. [8] recommended the use of 25% replacement rate of LWA to effectively reduce autogenous shrinkage in concrete made with 0.33 *w/cm* and 10% silica fume replacement. The authors [8] found that additional curing supplied by LWA tends to decrease the long-term permeability of the concrete, which is associated with the increase in volume of hydration products and segmentation and discontinuity of the capillary pores.

The diffusion coefficient of concrete can also be reduced with the use of LWA, which can reduce the volume of the interfacial transition zone (ITZ) and its pore interconnectivity. [14] LWA can develop better ITZ with the cement paste given the morphology of the aggregate surface, presence of water in the porous structure of the aggregate, and compatibility of the elastic moduli of the LWA and that of the hydrated cement paste. This can reduce the risk of microcracking at the ITZ.

With increasing use of SCC in repair applications, controlling durability, mechanical properties, and shrinkage cracking are essential to secure long service life of the repair material and rehabilitated structure. Compared to that of conventional concrete, the performance of SCC is more sensitive to changes in mix design and properties of constituent materials, such as type and content of aggregate given the highly flowable nature of the concrete.

The use of lightweight coarse aggregate (LWCA) in SCC was found to reduce autogenous shrinkage and provide similar or slightly lower mechanical properties compared to conventional concrete. [15-17] The effect of partial replacement of normal-weight aggregate by lightweight sand (LWS) and LWCA on key engineering properties and durability of SCC designated for repair applications has not fully evaluated.

The experimental program reported here was undertaken to evaluate the effect of the type and replacement rate of LWCA, use of LWS, as well as dosage rates of shrinkage-reducing admixture (SRA) and expansive agent (EA) on workability, key engineering properties, and durability characteristics of SCC designed for repair applications. The investigated properties include compressive strength, modulus of elasticity, splitting tensile strength, air-void system, frost durability, chloride-ion permeability, autogenous and drying shrinkage. The benefit of using LWCA and LWS is compared to that of incorporation of different dosage rates of SRA and EA.

Experimental Program

Materials and mixture composition

All of the investigated mixtures were proportioned with a *w/cm* of 0.38 and with 475 kg/m^3 of CSA Type GUb-F/SF blended cement containing approximately 25% Class F fly ash and 5% silica fume substitutions of binder mass. The sand-to-total aggregate ratio (S/A) was fixed to 0.5, by volume. Continuously graded crushed limestone aggregate with nominal maximum-size aggregate of 10 mm, specific gravity of 2.74, and absorption of 0.38% was used. Similarly, well-graded siliceous sand with specific gravity of 2.67 and absorption of 1.43% was employed. An expanded shale LWS with a specific gravity of 1.82 and water absorption of 21% was used.

Three types of commercially available LWCAs were selected. The specific gravities of LWCA1 (expanded slate), LWCA2 (expanded shale), and LWCA3 (expanded shale) are 1.71, 1.68, and 1.71, respectively. The LWCA1, LWCA2, and LWCA3 had absorption values of 9.2%, 14.2%, and 17.6%, respectively. Before every batch, the LWS and LWCA were pre-saturated by immersing them in water for 24 and 48 hours, respectively.

The mixture compositions of the investigated concrete are presented in Table 1. A monofilament polypropylene synthetic fiber with a circular cross section measuring 50 mm in length and 0.67 mm in diameter was incorporated at 0.25%, by volume, in all mixtures. The LWS was used at the replacement rate of 20% by volume of total aggregate. At the replacement rate of 25%, by volume of total aggregate, three types of LWCAs were used. For a given type of LWCA3, the replacement rate was set at 0, 25%, 35%, and 50%. SRA and EA were also incorporated at different dosage rates to evaluate their influence on SCC performance. For each dosage rate of SRA, a SCC was made with 20% LWS replacement and another SCC was prepared without any LWS to compare the influence of SRA to the use of 20% LWS. In the case of mixtures made with EA, the volume of normal-weight sand was replaced by the volume of EA to maintain the same cement content.

A polycarboxylate-based high-range water reducer (HRWR) and compatible sulfonate-based air-entraining agent (AEA) were used. The dosage rates of the HRWR and AEA were adjusted to secure slump flow of 625 ± 20 mm and air content of 6% to 9%. A glycol ether-based SRA and an oxide calcium-based EA were used. Two dosage rates of the SRA of 0.35% and 0.7%, by mass of binder, corresponding to medium and high dosage rates, respectively, were used. The dosage rates of the EA were set to 5% and 10%, by mass of binder. A viscosity-enhancing admixture (VEA) was used in mixtures made with SRA to enhance stability since such concrete had relatively high segregation and surface settlement compared to similar SCC prepared without SRA.

A simple approach was established to estimate the water content required for the completion of internal curing based on the concept that all of the water loss due to chemical shrinkage during cement hydration would be replaced by water available from internal curing. [7] This is based on ASTM C 1761 (Standard Specification for Lightweight Aggregate for Internal Curing of Concrete) where a typical conservative value for chemical shrinkage of 7% water loss per unit mass of cement or cementitious materials was used for the calculation of internal curing water. The maximum degree of hydration was taken as 1.0 since *w/c* of the investigated mixtures is higher than 0.36.

Test methods

Tests for fresh properties included slump flow, T-50, visual stability index (VSI, ASTM C1611), air volume, J-Ring flow (ASTM C1621), surface settlement, and column segregation (ASTM C1610). Mechanical properties, autogenous and drying shrinkage, frost durability, as well as rapid chloride-ion permeability (RCP) were also determined. The segregation index of the column segregation test (ASTM C 1610) was determined using the relative concentration (coefficient of variation) of coarse aggregate at four sections along the height of the cast column. The monitoring of the surface settlement was investigated using the surface settlement test. [18]

Compressive strength development at 1, 7, 28, 56, and 91 days was determined using cylinders measuring 100 x 200 mm. The modulus of elasticity and splitting tensile strength were determined at 28 and 91 days. After demolding at 1 day, the specimens were stored at 23°C and 100% RH until the age of testing. Autogenous shrinkage was monitored from the day of casting using vibrating wire gauges embedded at the center of prisms measuring 75 x 75 x 350 mm. The prisms were sealed immediately after demolding at 1 day. This was done to eliminate any moisture exchange between concrete and the curing environment (23 ± 2°C and 50% ± 5% RH). Drying shrinkage of each concrete was determined using two cylinders measuring 150 x 300 mm. Mean of three longitudinal measurements were used for shrinkage deformation of each cylinder. After form removal at 1 day and 6 additional days of moist curing, the cylinders were stored at 23°C and 50% RH for one year. Frost durability was determined according to ASTM C666, Procedure A.

Test Results and Discussion

Fresh properties

Table 2 summarizes the fresh properties of the investigated concrete mixtures. All mixtures had similar slump flow and air content values of approximately 625 mm

and 9%, respectively. The mixtures also had similar levels of passing ability (J-Ring flow), regardless of the content of LWCA, SRA, and EA in use. In general, all mixtures exhibited adequate static stability, regardless of the LWCA type. Segregation index and surface settlement values were lower than the maximum limits of 5% and 0.5%, respectively.[18] It should be noted that the LA3-50-LS mixture made with 50% LWCA3 had some signs of segregation. The static segregation of the LA3-50-LS mixture was higher than values of the other mixtures (15% vs. 0.6% to 11%).

Mixtures made with SRA exhibited lower static stability compared to similar concrete prepared without any SRA, despite the incorporation of VEA. In general, mixtures made with SRA developed higher segregation and surface settlement compared to those prepared without any SRA. However, the static segregation and settlement values of the SRA mixtures were still lower than the maximum limits of 15% and 0.5%, respectively. The use of 5% EA, by mass of binder, led to 23% increase in HRWR demand, on the average. The use of EA resulted in a reduction in surface settlement due to its expansion during the testing period.

Mechanical properties

Mechanical properties of the investigated mixtures are presented in Table 3. The total water required for internal curing that corresponds to 0.07 kg water per unit mass (1 kg) of cement or cementitious materials, the maximum water that could potentially be released from LWS and LWCA, and the percentage of released water to total water required for internal curing are summarized in Table 3. According to ASTM C1761, all LWA shall release at least 85% of the absorbed water in the LWA under 94% RH. The water absorption values of the LWCAs and LWS were used then to calculate the maximum water content that can potentially be released from the LWA.

In general, the influence of LWCA replacement on mechanical properties varies with age. On average, the use of 25% LWCA led to 10% decrease in the 28-day compressive strength but resulted in only 3% decrease in 91-day strength for samples subjected to moist-curing at 100% RH until the age of testing. In addition, an increase in LWCA content led to a decrease in compressive strength. For example, the LA3-50-LS made with 50% LWCA3 had 18% lower 91-day compressive strength compared to similar concrete without any LWCA (50 vs. 61 MPa). The increase in LWCA content from 35% to 50% led to 6% and 3% decrease in the 56- and 91-day compressive strength, respectively. As in the case of LWCA, it is important to note that the influence of LWS replacement on compressive strength varies with respect to age of concrete. For example, the use of 20% LWS led to 7% decrease in the 7-day compressive strength but 5% and 8% increase in 56- and 91-day compressive strength, respectively. The slight decrease in the early-age strength is due to the higher porosity of the LWS; however, such

decrease is compensated for by better cement hydration resulting from internal curing at later ages.

It should be noted that the influence of the lightweight materials on compressive strength varies with the water content that could be released from the LWCA and LWS and the content of the LWCA. Mixtures compared in Fig. 1 are prepared with LWS and LWCA and made without any SRA and EA. The 91-day compressive strength values are normalized by the strength of the NA-LS mixture in order to eliminate the effect of LWS replacement on compressive strength. The volume replacement of sand by 20% LWS could provide a maximum of 65% of the water required for internal curing due to the desorption of water from the LWS. The use of 20% LWS resulted in 7% increase in the 91-d compressive strength compared to concrete without LWS (NA-NS), as presented in Fig. 1(a). On the other hand, in the case of LWCA, the increase in LWCA content resulted in considerable reduction in compressive strength due to the increase in porosity of the aggregate, despite the greater chance to enhance internal curing from water available in the LWCA. The LA3-50-LS mixture containing 50% LWCA3 and 20% LWS, which has approximately double the water content compared to that required to compensate for chemical shrinkage, exhibited 13% lower 91-day compressive strength than the NA-LS mixture.

The use of 25% LWCA replacement of normal-weight coarse aggregate (NWCA) led to 9% to 16% reduction in modulus of elasticity at 91 days. This is due to lower elastic modulus of LWCA compared to NWCA. As in the case of the 91-day compressive strength, the elastic moduli at 28 and 91 days decreased with the increase in porosity caused by further addition of LWCA and increase in the amount of water that can be released from LWCA. On the other hand, the use of 20% LWS led to slight increase in the 91-day elastic modulus (Fig. 1(b)). Therefore, the contribution of internal curing by the use of LWS to elastic moduli can overcome a reduction in mechanical properties associated with the increase in volume of the LWS. The modulus reduction by the increase in the LWCA content and in water content available from the LWCA was 50% higher compared to the case of the compressive strength.

It is worthy to point out that the low elastic modulus is beneficial for repair applications due to higher stress relaxation, which can reduce tensile stresses induced by restrained shrinkage. It is necessary to consider the influence of the LWCA on the elastic modulus of concrete for the design of concrete structures.
The mechanical properties of SCC made with SRA and EA are also summarized in Table 3. In general, the incorporation of EA did not have any significant effect on mechanical properties. On the other hand, SCC made with SRA had lower compressive strength and modulus of elasticity compared to similar concrete prepared without any SRA, in particular at high dosage rate. Mixtures containing moderate and high dosage rates of SRA exhibited 30% and 85% lower 1-day compressive strength compared to similar concrete made without any SRA. It

should be noted, however, that strength reduction resulting from the use of SRA significantly decreased with age of concrete. For example, the compressive strength at 91 days of mixtures prepared with moderate dosage of SRA was similar to the reference concrete made without any SRA.

Durability characteristics

All of the investigated mixtures exhibited high frost durability with durability coefficient greater or equal to 90%, regardless of the use of LWS, LWCA, SRA, and EA (Table 3). The investigated mixtures had air-void spacing factors ranging from 230 to 510 μm, which are higher than the recommended limit of 200 μm. [19] The relatively high spacing factor could be in part due to the increase in HRWR demand associated with the incorporation of synthetic fibers used in the investigated SCC mixtures. Such increase in HRWR dosage can lead to a decrease in plastic viscosity of the cement paste, thus reducing stability of the air-void system. Mixtures made with LWS and/or LWCA replacement exhibited higher air-void spacing factor and lower specific volume compared to those prepared without any LWS and LWCA. The incorporation of SRA or EA did not have significant influence on the air-void system. All of the investigated mixtures exhibited low 56-day RCP values of 385 to 665 Coulombs, which is considered to be very low and is mainly due to the type of binder in use.

Effect of LWS, LWCA, SRA, and EA on autogenous shrinkage

In general, the use of LWS and LWCA replacement led to significant decrease in autogenous shrinkage, as presented in Fig. 2. Mixtures made with LWCA and/or LWS exhibited significantly greater expansion during the first day compared to the reference concrete, regardless of the replacement rate of lightweight materials. For example, the NA-LS mixture made with 20% LWS replacement and normal-weight coarse aggregate had approximately 80% lower autogenous shrinkage at 100 days of age compared to that of the reference NA-NS mixture made without any LWS. It is interesting to note that the type of LWCA has significant influence on autogenous shrinkage. For a given replacement rate of 25% by volume, SCC made with LWCA3 had much greater expansion than similar mixtures prepared with LWCA1 and LWCA2. The LA3-25-LS exhibited expansion of 120 μm/m at 100 days. On the other hand, the LA1-25-LS and LA2-25-LS had shrinkage of 50 μm/m and expansion of 15 μm/m at 100 days, respectively. This can be attributed to higher absorption capacity of the LWCA3 compared to the other LWCAs, which results in more water released from the LWCA to the cement matrix. This coincides well with the fact that an increase in LWCA content leads to a significant increase in expansion. An increase in LWCA3 content from 25% to 50% led to approximately 100% increase in expansion. The reduction in autogenous shrinkage is closely related to the amount of water that can be released from the LWS and LWCA. The 20% LWS replacement can release a maximum of 65% of the total

water required for internal curing, which can lead to 240 μm/m decrease in autogenous shrinkage compared to the NA-NS mixture, as presented in Fig. 3. A good correlation was established between the reduction in autogenous shrinkage at 50 days and the maximum water content that can be potentially released resulting from the increase in lightweight materials content (Fig. 3). This indicates that the contribution of internal curing by the use of LWS and LWCA to reduce autogenous shrinkage was greater than any increase in porosity and decrease in stiffness associated with greater use of such porous aggregate. The regression line in Fig. 3 shows that a 100% increase in the percentage of water content that can be released from LWS and LWCA compared to the total water required for internal curing can reduce autogenous shrinkage at 50 days by 240 μm/m.

It should be mentioned that the amount of internal curing water that can be released from LWCAs may vary with their desorption capacity. It is assumed here that all of three LWCAs have similar desorption characteristics; however, the LA1-25-LS and LA2-25-LS mixtures were located below the regression line established between the autogenous shrinkage reduction and the potential water content that can be released compared to the total required water. This may reflect that for a given RH, LWCA1 and LWCA2 can have relatively low desorption rates compared to that of LWCA3.

All SCC mixtures made with 25% LWCA3 and either SRA or EA had no shrinkage and exhibited significant expansion during the first few days, as presented in Fig. 4. In general, SCC mixtures made with EA and 20% LWS replacement had significantly greater expansion compared to those prepared without any EA or LWS. In particular, the LA3-25-LS-HEA made with high dosage (10% by mass of cement) of EA, 25% LWCA3, and 20% LWS replacement exhibited expansion of 800 μm/m at 50 days. An increase in EA dosage also led to a considerable increase in expansion. For instance, the LA3-25-LS-HEA mixture made with high dosage of EA developed 150% higher expansion compared to the LA3-25-LS-MEA mixture made with moderate EA dosage. For a given LWCA replacement of 25%, the increase in expansion at 50 days when using moderate SRA dosage was 130 μm/m for SCC made without any LWS. The expansion increase was 60 μm/m for SCC prepared with 20% LWS.

The influence of SRA and EA dosage rate on autogenous shrinkage at 50 days is presented in Fig. 5. The shrinkage reduction of mixtures containing SRA or EA is compared to that of the LA3-25-NS or LA3-25-LS mixtures to deduct the effect of the LWCA3 and LWS replacement. For a given replacement rate of LWCA and LWS, the incorporation of EA led to greater reduction in autogenous shrinkage (increase in expansion) compared to the use of SRA. For example, mixtures incorporating a high dosage rate of EA exhibited significantly greater shrinkage reduction (710 μm/m) compared to the LA3-25-LS mixture made without any EA. On the other hand, the additional reduction in autogenous shrinkage by using moderate and high contents of SRA was relatively limited compared to the use of

EA (10 to 125 μm/m vs. 170 to 710 μm/m).

The expansion observed during the first 24 hours for mixtures prepared with LWS or LWCA can be due to the formation of ettringite and/or swelling of the gel produced by the hydration products. [20] The mechanism leading to early-age expansion of mixtures made with CaO-based EA used in this study is related to the formation of calcium hydroxide. This results in the expansion of the cement paste and offsets autogenous shrinkage. [21] The use of SRA can increase the degree of saturation of portlandite, which can lead to an increase in crystallization stress resulting in expansion. [22]

In the case of mixtures containing LWS, LWCA, EA, or SRA, volume changes resulting from expansion/shrinkage at early age should be monitored as early as possible due to some expansion that can take place during the first 24 hours. It is important to note that high autogenous expansion of mixtures containing high concentration of EA or SRA may lead to high compressive stress in confined members. The expansion can be, in part, offset by drying and autogenous shrinkage, which should be considered to evaluate the risk of cracking.

Effect of LWS, LWCA, SRA, and EA on drying shrinkage

The use of LWCA replacement led to significant reduction in drying shrinkage. SCC made with 50% LWCA3 (LA3-50-LS) exhibited approximately 70% lower drying shrinkage after 1 year of age compared to similar concrete made without any LWCA (NA-LS), as presented in Fig. 6. In addition, an increase in LWCA content led to a decrease in drying shrinkage. It should be noted that shrinkage reduction when using LWCA is limited up to the replacement rate of 35% since no further reduction in drying shrinkage was observed at 50% LWCA content. As in the case of autogenous shrinkage, the type of LWCA has significant effect on drying shrinkage. For a given LWCA replacement rate of 25%, SCC made with LWCA3 had considerably lower drying shrinkage than similar mixtures prepared with LWCA1 and LWCA2 due to higher volume of absorbed water available in LWCA3.

In general, the use of SRA led to a decrease in drying shrinkage. On average, mixtures made with moderate dosage rate of SRA had 20% lower drying shrinkage at 6 months compared to similar concrete prepared without any SRA, as presented in Fig. 6. The shrinkage reduction resulting from the use of high dosage of SRA was 30% and 27% for mixtures with 20% LWS and without LWS, respectively. On the other hand, the use of 20% LWS replacement led to an average 40% decrease in drying shrinkage. Given the shrinkage results, the use of 20% LWS replacement was shown to be more efficient to reduce drying shrinkage compared to the incorporation of SRA at dosage rates of 0.35% and 0.7%, by mass of binder. This can be due to the fact that LWS replacement reduces autogenous shrinkage as

well as drying shrinkage; whereas the effect of SRA on the shrinkage reduction is more significant in reducing drying shrinkage than autogenous shrinkage.

As in the case of the autogenous shrinkage, a relationship was established between the reduction in the drying shrinkage at 6 months and the maximum water content that can be provided by the LWS and LWCA compared to the water required for internal curing (Fig. 7). The 20% LWS replacement, corresponding to 65% of the total water used for internal curing, led to 170 μm/m decrease in drying shrinkage (NA-NS vs. NA-LS). The regression line in Fig. 7 indicates that 100% increase in the maximum water amount released from LWS and LWCA compared to the total water required for internal curing, can reduce drying shrinkage at 6 months by 430 μm/m. Again, this indicates that the contribution of internal curing by the use of LWS and LWCA to reduce drying shrinkage was greater than the increase in porosity and decrease in stiffness related to the addition of these porous materials.

It is interesting to note that the shrinkage reduction effect by the use of the lightweight materials is negligible beyond 150% of water required for internal curing that can compensate for chemical shrinkage and reduce self-desiccation and drying shrinkage. This is related to the fact that the increase in the volume of LWCA can result in a decrease in stiffness of the concrete due to the high porosity of the lightweight materials.

Conclusions

The influence of LWS and LWCA on compressive strength varies with the water content that could be released from the desorption of LWS and LWCA in use. The 20% volume replacement of NWS by LWS corresponds to maximum of 65% of the total water required for internal curing, which is required to compensate for chemical shrinkage during cement hydration. Such content of LWS can result in 8% increase in the 91-day compressive strength.

The contribution of internal curing by the use of LWS to increase compressive strength and elastic modulus can compensate for the reduction in mechanical properties associated with the use of the porous aggregate. On the other hand, in the case of LWCA, the reduction in mechanical properties due to increase in volume of the porous aggregate was higher than the contribution of internal curing to increase mechanical properties.

The use of LWS and LWCA can lead to significant reduction in autogenous and drying shrinkage, which is related to the amount of water released from the LWS and LWCA and volume of the porous materials. The internal curing water vs. shrinkage reduction relationship could become more accurate when desorption property of the lightweight materials is considered to estimate the maximum water that can be released at a given relative humidity.

The incorporation of 25% LWCA led to some decrease in the modulus of elasticity, autogenous shrinkage, and drying shrinkage without significant reduction in mechanical properties and RCP. The incorporation of LWCA up to 35% replacement rate did not impact workability of the SCC.

The use of 20% LWS replacement did not have any negative effect on the overall performance of the concrete. The combined use of 20% LWS along with 25% LWCA is recommended for SCC mixture designated for repair applications.

Mixtures made with moderate dosage of SRA developed 20% lower drying shrinkage at 6 months compared to similar concrete prepared without any SRA. The use of 20% LWS led to an average 40% reduction in drying shrinkage.

Acknowledgements

The authors wish to thank Béton Provincial, Euclid Canada, Northeast Solite Corp., the Jacques Cartier and Champlain Bridge Inc., the Ministry of Transport of Québec, and the City of Montreal for their support.

References

[1] Khayat, K.H., "Workability, Testing and Performance of Self-Consolidating Concrete." *ACI materials Journal*, V. 96, No. 3, 1999, pp. 346-353.
[2] Khayat, K.H., and Morin, R., "Performance of Self-Consolidating Concrete Used to Repair Parapet Wall in Montreal," *Proceedings* of the 3rd International RILEM Symposium on Self-Compacting Concrete, Iceland, 17-20 August 2003, pp. 913-919.
[3] Holschemacher, K., and Klug, Y., "A Database for the Evaluation of Hardened Properties of SCC," Leipzig Annual Civil Engineering Report No. 7, 2002, pp. 123-134.
[4] Yuan, Y.S., and Marosszeky, M., "Major Factors Influencing the Performance of Structure Repair," *ACI SP-128*, 1991, pp. 819-838.
[5] Lee, H.K., Lee, K.M., and Kim, B.G., "Autogenous Shrinkage of High-Performance Concrete Containing Fly Ash," *Magazine of concrete research*, V. 55, No. 6, 2003, pp. 507-515.
[6] Carette, G., and Malhotra, V.M., "Mechanical Properties, Durability and Drying Shrinkage of Portland Cement Concrete Incorporating Silica Fume," *Cement, Concrete, and Aggregates*, V. 5, No. 5, 1983, pp. 3-13.
[7] Bentz, D.P., Lura, P., and Roberts J.W., "Mixture Proportioning for Internal Curing," *Concrete International*, V. 27, No. 2, 2005, pp. 35-40.

[8] Bentur A., Igarashi, S.-I., and Kovler, K., "Prevention of Autogenous Shrinkage in High-Strength Concrete by Internal Curing Using Wet Lightweight Aggregates," *Cement and Concrete Research*, V. 31, No. 11, 2001, pp. 1587-1591.
[9] Roberts, J.W., "Internal Curing in Pavements, Bridge Decks and Parking Structures, Using Absorptive Aggregates to Provide Water to Hydrate Cement Not Hydrated by Mixing Water," Transportation Research Board, 83rd Annual Meeting, Washington D.C., January 11-15, 2004.
[10] Cusson, D., and Hoogeveen, T., "Internal Curing of High-Performance Concrete with Pre-soaked Fine Lightweight Aggregate for Prevention of Autogenous Shrinkage Cracking," *Cement and Concrete Research*, V. 38, No. 6, 2008, pp. 757-765.
[11] Henkensiefken, R., Bentz, D.P., Nantung, T., and Weiss, J., "Volume Change and Cracking in Internally Cured Mixtures Made with Saturated Lightweight Aggregate under Sealed and Unsealed Conditions," *Cement and Concrete Composites*, V. 31, No. 7, 2009, pp. 427-437.
[12] Hammer, T.A., Bjontegaard, O., and Sellevold, E.J., "Internal Curing Role of Absorbed Water in Aggregates," *ACI SP-218*, 2004, pp. 131-142.
[13] Akcay, B., and Tasdemir, M.A., "Optimization of Using Lightweight Aggregates in Mitigating Autogenous Deformation of Concrete," *Construction and Building Materials*, V. 23, No. 1, 2009, pp. 353-363.
[14] Bentz, D.P., "Influence of Internal Curing Using Lightweight Aggregates on Interfacial Transition Zone Percolation and Chloride Ingress in Mortars," *Cement and Concrete Composites*, V. 31, No. 5, 2009, pp. 285-289.
[15] Kim, Y.J., Choi, Y.W., and Lachemi, M., "Characteristics of Self-Consolidating Concrete Using Two Types of Lightweight Coarse Aggregates," *Construction and Building Materials*, V. 24, No. 1, 2010, pp. 11-16.
[16] Hwang, C.-L., and Hung, M.-F., "Durability Design and Performance of Self-Consolidating Lightweight Concrete," *Construction and Building Materials*, V. 19, No. 8, 2005, pp. 619-626.
[17] Shi, C., and Wu, Y., "Mixture Proportioning and Properties of Self-Consolidating Lightweight Concrete Containing Glass Powder," *ACI Materials Journal*, V. 102, No. 5, 2005, pp. 355-363.
[18] National cooperative highway research program (NCHRP), "Self-Consolidating Concrete for Precast, Prestressed Concrete Bridge Elements," *NCHRP report 628*, Transportation Research Board of the National Academies, 2009.
[19] ACI Committee 201, "Guide to Durable Concrete," *ACI 201.2R-08, ACI Manual of Concrete Practice*, 2008, 41 p.
[20] Bentz, D.P., Sant, G., and Weiss, J., "Early-Age Properties of Cement-Based Materials: I: Influence of Cement Fineness," *Journal of Materials in Civil Engineering*, V. 20, No. 7, 2008, pp. 502-508.
[21] Maltese, C., Pistolesi, C., Lolli, A., Bravo, A., Cerulli, T., and Salvioni, D., "Combined Effect of Expansive and Shrinkage Reducing Admixtures to Obtain Stable and Durable Mortars," *Cement and Concrete Research*, V. 35, No. 12, 2005, pp. 2244-2251.

[22] Sant, G., Lothenbach, B., Juilland, P., Le Saout, G., Weiss, J., and Scrivener, K., "The Origin of Early Age Expansions Induced in Cementitious Materials Containing Shrinkage Reducing Admixtures," *Cement and Concrete Research*, V. 41, No. 3, 2011, pp. 218-229.

Table I. Mixture composition of SCC

Mixture	Binder (kg/m^3)	w/cm	NWCA (kg/m^3)	LWCA type	LWCA (kg/m^3)	NWS (kg/m^3)	LWS (kg/m^3)	Fiber, %	SRA (l/m^3)	EA (l/m^3)	HRWR (l/m^3)	VEA (l/m^3)
NA-NS	475	0.38	774	-	0	743	0	0.25	0	0	3.2	0
NA-LS			774	-	0	594	103 (20%)*	0.25	0	0	2.8	0
LA1-25-LS			580	LWCA1	120 (25%)*	594	103 (20%)	0.25	0	0	2.6	0
LA2-25-LS			580	LWCA2	120 (25%)	594	103 (20%)	0.25	0	0	2.8	0
LA3-25-LS			580	LWCA3	120 (25%)	594	103 (20%)	0.25	0	0	2.8	0
LA3-35-LS			503	LWCA3	169 (35%)	594	103 (20%)	0.25	0	0	2.6	0
LA3-50-LS			387	LWCA3	241 (50%)	594	103 (20%)	0.25	0	0	2.8	0
LA3-25-NS			580	LWCA3	120 (25%)	743	0	0.25	0	0	3.1	0
LA3-25-NS-MSRA			580	LWCA3	120 (25%)	743	0	0.25	1.6	0	8.2	0.42
LA3-25-NS-HSRA			580	LWCA3	120 (25%)	743	0	0.25	3.2	0	12.9	0.57
LA3-25-LS-MSRA			580	LWCA3	120 (25%)	594	103 (20%)	0.25	1.6	0	7	0.45
LA3-25-LS-HSRA			580	LWCA3	120 (25%)	594	103 (20%)	0.25	3.2	0	11.5	0.57
LA3-25-NS-MEA			580	LWCA3	120 (25%)	723	0	0.25	0	23.7	4.3	0
LA3-25-LS-MEA			580	LWCA3	120 (25%)	574	103 (20%)	0.25	0	23.7	4	0
LA3-25-LS-HEA			580	LWCA3	120 (25%)	554	103 (20%)	0.25	0	47.5	5	0

*by volume replacement rate

Table II. Fresh properties of SCC mixtures

	NA-NS	NA-LS	LA1-25-LS	LA2-25-LS	LA3-25-LS	LA3-35-LS	LA3-50-LS	LA3-25-NS	LA3-25-NS-MSRA	LA3-25-NS-HSRA	LA3-25-LS-MSRA	LA3-25-LS-HSRA	LA3-25-NS-MEA	LA3-25-LS-MEA	LA3-25-LS-HEA
Slump flow at 10 min (mm)	625	635	615	625	625	615	625	630	625	630	620	635	625	625	615
J-Ring flow (mm)	560	550	530	545	545	540	540	555	545	555	530	550	560	570	550
T-50 (sec)	1.9	2	2.6	2.2	2.7	2.4	2.6	2.4	2.7	2.2	2.6	2.0	1.8	2.0	2.4
Air content at 10 min (%)	9.0	9.0	8.8	9.0	9.0	9.0	9.0	8.0	9	9	8.8	9.8	9	9.3	9.4
Unit weight (kg/m^3)	2145	2125	2030	2065	2035	2020	1980	2125	2065	2035	2030	2125	2120	2010	2020
VSI	0	0	0	0	0	0	0	0	1	1	1	1	0	0	0
Static segregation (%)	0.6	11	6	3.7	9.4	-	15	4.7	7.4	5.4	11.8	6.6	5.8	5.7	4.6
Segregation index (%)	3.8	2.1	2.4	2.9	1.7	-	3.1	3.8	1.5	1.0	1.7	2.5	2.2	2.3	1.5
Surface settlement (%)	0.36	0.41	0.38	0.38	0.25	0.33	0.33	0.34	0.48	0.43	0.51	0.38	0.19	0.10	0.17

Table III. Mechanical properties and durability aspects of SCC mixture

Mixture	Water for I.C. (kg/m³)	Maximum water from LWS & LWCA / water required for I.C. (%)	Compressive strength (MPa)				Splitting tensile strength (MPa)		Modulus of elasticity (GPa)		Hardened air, %	Spacing factor, μm	ΔL/L, μm/m	Durability factor, %	Mass loss, %	RCP, Coulomb
			1d	7d	28d	56d	28d	91d	28d	91d						
NA-NS	33.3	0.0	20.1	39.5	51.3	57.9	59.7	4.2	4.4	34.0	34.5	6.7	350	240	108	0.4	430
NA-LS		65	19.2	36.5	51.5	61.0	64.4	4.9	5.1	34.5	35.2	4	455	605	105	0.3	385
LA1-25-LS		98	19.0	40.8	47.7	59.3	62.5	5.0	5.1	29.0	29.5	4.1	490	220	104	0.5	390
LA2-25-LS		116	18.7	40.3	46.9	60.4	62.2	4.4	5.0	28.0	31.5	4.1	450	645	101	0.5	390
LA3-25-LS		129	18.3	38.4	48.5	59.6	63.2	4.9	5.0	28.5	32.1	4	510	255	104	0.6	440
LA3-35-LS		155	15.2	37.3	47.2	53.1	57.6	3.8	5.0	27.2	28.0	4.3	400	190	101	0.3	430
LA3-50-LS		193	15.5	36.8	43.4	49.9	56.3	4.8	4.3	26.8	27.8	4.3	500	325	97	1	465
LA3-25-NS		64	20.1	40.1	47.1	60.0	60.4	5.1	5.3	30.0	34.2	4.6	415	195	105	0.4	460
LA3-25-NS-MSRA		64	13.9	38.4	47.0	58.5	60.2	4.2	5.3	31	33	4.1	340	340	102	0.4	550
LA3-25-NS-HSRA		64	3.3	36.1	44.1	54.3	58.8	5.2	6.1	28.5	30.9	5.7	235	155	105	0.2	515
LA3-25-LS-MSRA		129	12.9	37	48.	59.4	63	4.3	5.7	30	33.6	5.6	360	635	90	0.6	495
LA3-25-LS-HSRA		129	2.9	34.4	44.4	54.6	59.8	3.6	5.4	28.5	29.9	3.4	345	195	102	0.3	490
LA3-25-NS-MEA		64	19.2	39.6	48.6	60.4	60	4.7	5.7	31.1	33.3	5.3	375	250	104	0.7	665
LA3-25-LS-MEA		129	20.1	38.9	48.9	59.6	62	4.4	6.1	29.8	32.3	4.6	440	235	101	0.5	570
LA3-25-LS-HEA		129	18.0	37.5	47.6	58.3	60.6	4.6	5.7	28.4	31.9	5.3	375	250	104	0.7	665

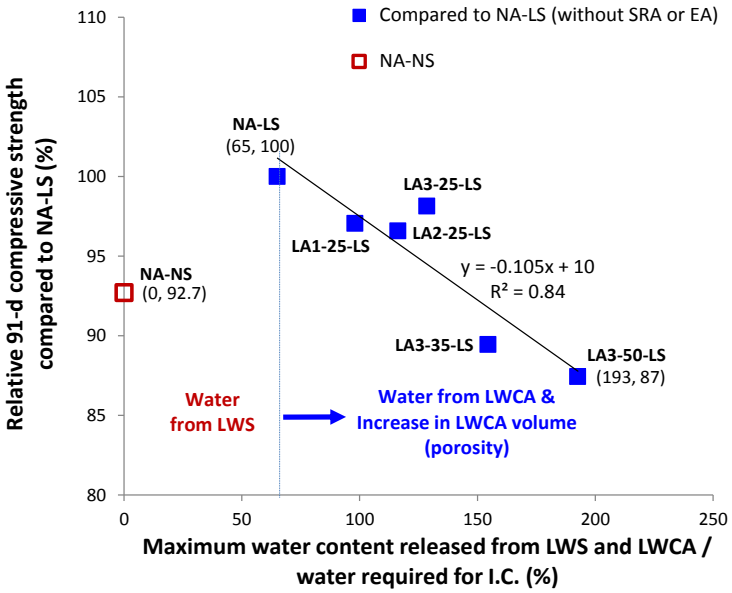

(a) Relative compressive strength to reference concrete without any LWCA

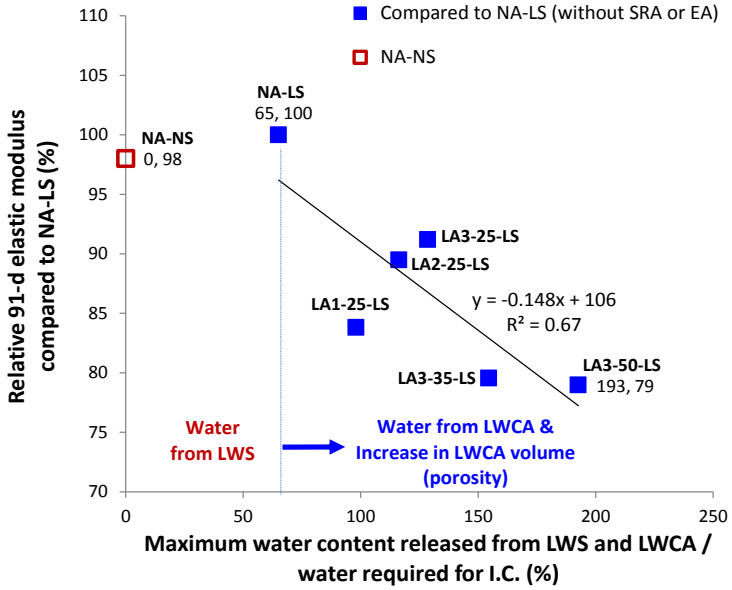

(b) Relative elastic modulus to reference concrete without any LWCA

Figure 1. Changes in mechanical properties at 91 days with water content that can be released from LWS and LWCA associated with increase of LWA

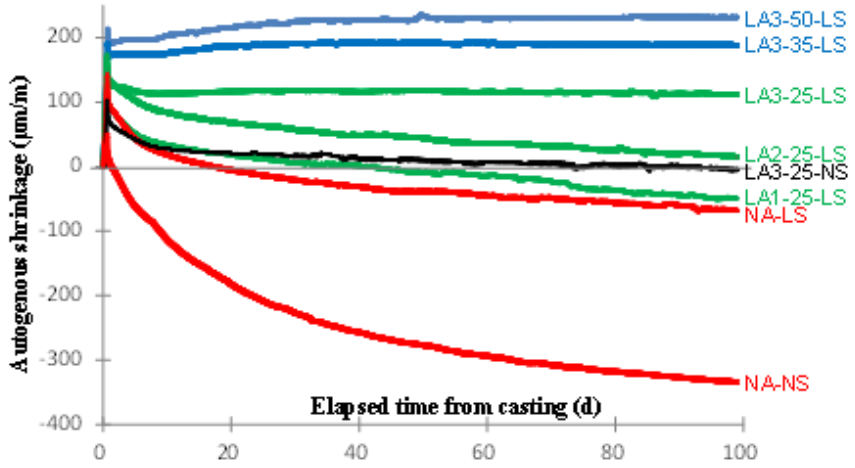

Figure 2. Autogenous shrinkage of SCC made with different types and contents of LWCAs

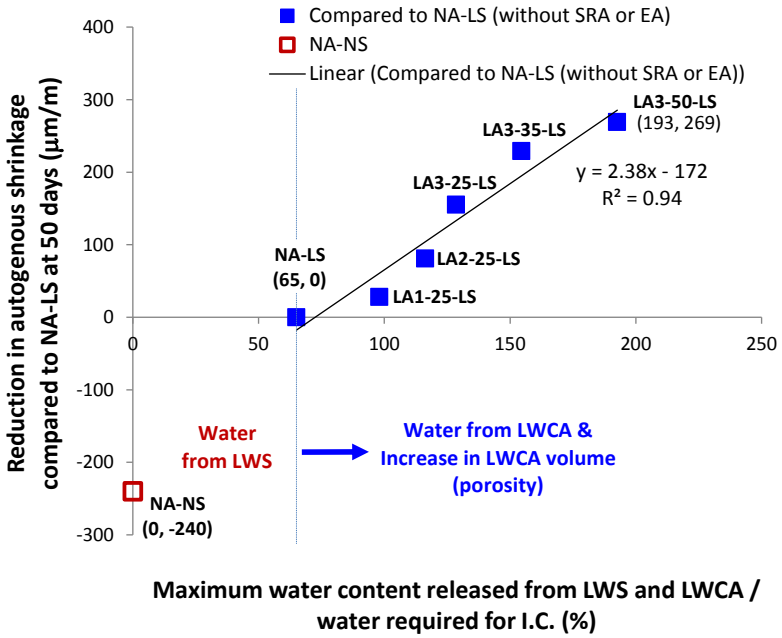

Figure 3. Changes in autogenous shrinkage at 50 days with water content that can be released from LWS and LWCA associated with increase of LWA

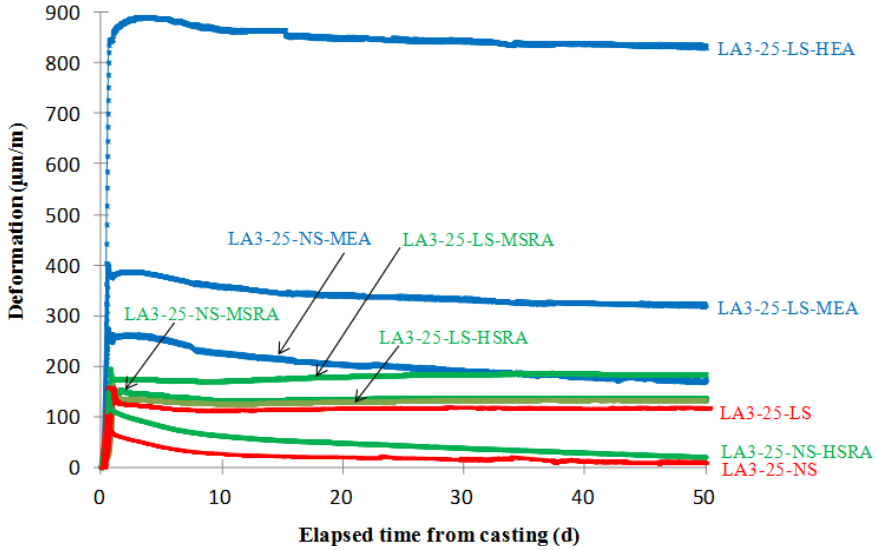

Figure 4. Autogenous shrinkage of SCC made with different dosages of SRA and EA

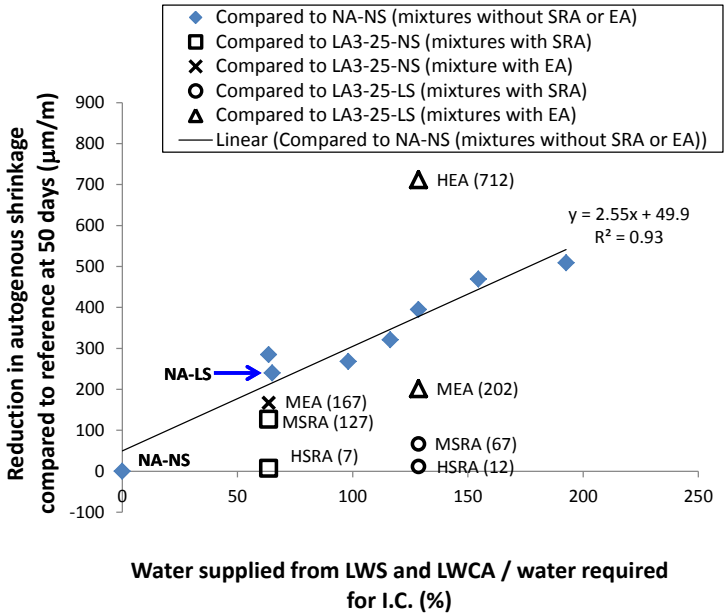

Figure 5. Influence of LWS and LWCA volume on autogenous shrinkage at 50 days and comparison to that of SRA and EA dosage

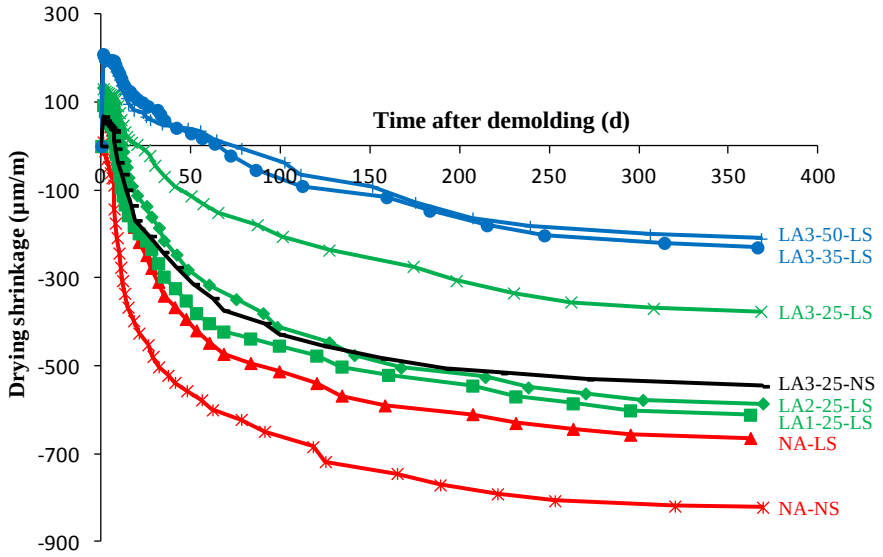

(a) Mixtures without SRA and EA

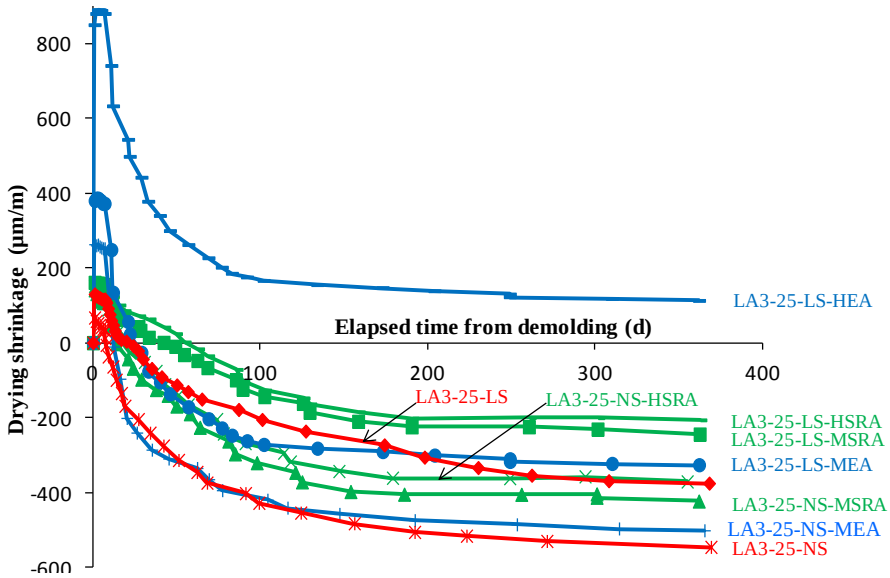

(b) Mixtures with SRA and EA

Figure 6. Drying shrinkage of SCC made with LWS, LWCAs, SRA, and EA

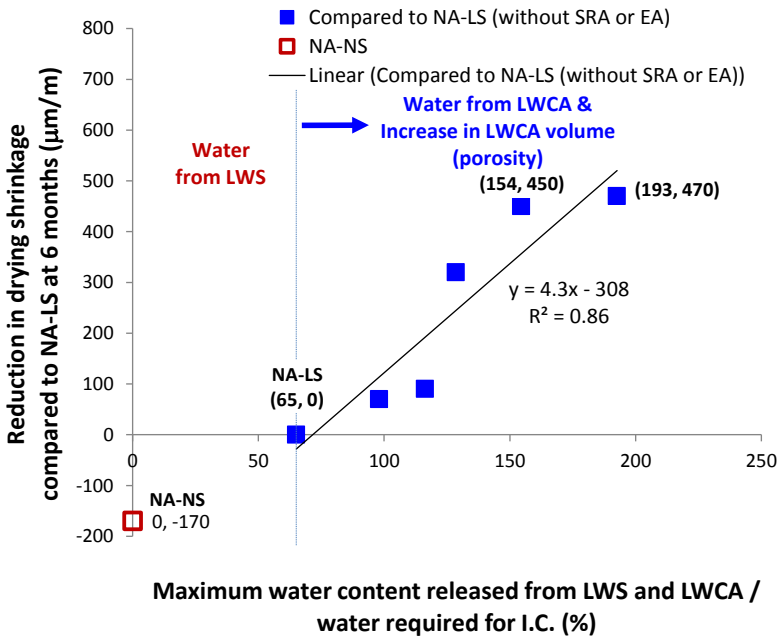

Figure7. Changes in drying shrinkage at 6 months with water content that can be released from LWS and LWCA associated with increase of LWA

Influence of Moist Curing Age and Sample Size on Strength and Drying Shrinkage of Internally Cured Self-Consolidating Concrete

Yudong Dang[1,2], Tao Zhang[3], Zhenghong Yang[3], Zhengwu Jiang[3], Hui Zhang[3], Qingchun Guo[1,4], Xincheng Li[1,2]

[1] Yunnan Institute of Building Research, Kunming 650223, China
[2] Yunnan Key Laboratory of Building Structure and New Materials, Kunming 650223, China
[3] Key Laboratory of Advanced Civil Engineering, Ministry of Education, Tongji University, Shanghai 201804, China
[4] Kunming Key Laboratory of Structure Safety and New Technology, Kunming 650223, China

Abstract To date, internal curing (IC) has been widely accepted as a promising way to mitigate the shrinkage of high-performance concrete, e.g. self-consolidating concrete (SCC). So far, however, there has been little discussion of the influence of IC on the shrinkage and other properties of SCC under insufficient curing conditions. This study mainly investigated the influence of initial moist curing age and sample size on drying shrinkage of internally cured SCC with 0%, 15%, 30% and 50% by the volume of natural sand replaced by a saturated fine lightweight aggregate (LWA). The results revealed that, no matter how long the SCC was initially been moist cured, internally cured SCC exhibited a lower strength and higher drying shrinkage than that of without internal curing. The more the LWA replacement, the greater strength reduction and the higher the drying shrinkage for the internally cured SCC. Besides, the drying shrinkage of internally cured SCC with higher LWA replacement was more sensitive to initial moist curing age, and the longer the initial moist curing age, the less the drying shrinkage. Fortunately, the internally cured SCC specimens with a larger cross-section size exhibited a lower drying shrinkage than that of small specimens without IC, which indicated that the measured drying shrinkage of the internally cured SCC in laboratories might be overestimated, in terms of the real concrete structures with a larger cross-section.

Keywords: *Self-Consolidating Concrete; Drying Shrinkage; Internal Curing; Curing Age; Size Effect.*

Introduction

Compared to conventional vibrated concrete (CVC), the Self-consolidating concrete (SCC) normally exhibits greater total shrinkage due to its higher paste volume, and this phenomenon is more pronounced for high-strength SCC with lower w/b ratios [1-3]. Various methods have been explored to mitigate the risk of excessive shrinkage due to moisture evaporation or internal self-desiccation [4]. One option to avoid this, known as "internal curing", entails the inclusion of pre-saturated lightweight aggregate (LWA) particles or super absorbent polymer (SAP) into the concrete to serve as a water reservoir and to compensate for the water lost by moisture evaporation or self-desiccation [5,6].

Over the years, many studies have investigated the influences and benefits of internal curing on high strength concrete in laboratories [5,6] or fields [7]. A majority of studies have focused on the benefits of internal curing under some effective curing conditions, e.g. sealed condition. However, for real construction fields, drying and moisture evaporation are unavoidable. Thus, it is essential to pay more attention to the effectiveness of internal curing on concrete resistance to shrinkage under insufficient curing conditions.

In most lab studies, it was found that the drying shrinkage and risk of cracking of internally cured concrete remain less severe than traditional concrete without internal curing. However, there are some exceptions as reviewed in [8]. It can be summarized that the efficiency of internal curing on shrinkage reduction depends on w/b ratio [9], duration of early moist curing [10], drying age [11], and so on. It is still unclear how these influential factors impact the efficiency of internal curing on drying shrinkage of concrete. In order to shed more light on this issue and these apparently conflicting results mentioned above, this study aims to investigate the effect of the addition of LWA with different contents on drying shrinkage and other properties of SCC.

Materials and Testing Methods

Materials

The cementitious materials used in this study include a Chinese standard GB 175 Type P·O 42.5 Portland cement (C), a Chinese standard GB 50164 Type FⅡ grade fly ash (FA) and a Chinese GB standard 18064 Type S95 ground granulated blast furnace slag (G). The fine aggregate (S) was a dry natural sand (clean, fineness modulus of 2.8, the maximum size of 4.75 mm, and specific density of 2600kg/m^3). The dry coarse aggregate (CA) was a crashed limestone with a continuous grading and size from 5mm to 25mm. Fine lightweight aggregate (LWA) with a specific density of 1502 kg/m^3 and 24 hours water absorption of 8% was used as internal curing media in concrete. Figure 1 shows the sieve analysis

curves of natural and LWA sand. Note: before the mixing procedure, the LWA was firstly oven dried and air cooled, secondly submerged in water for 24 hours, and then surface dried with paper towel until the saturated and surface dry (SSD) condition was obtained. Thereafter, the SSD LWA was stored in a sealed container until concrete mixing.

For concrete with LWA, the sand replacement fractions were 0%, 15%, 30% and 50% by volume with fine LWA. Note: in order to avoid inhomogeneous LWA was employed in different SCC mixtures, the LWA was also been well blended before adding into the concrete mixer. A liquid polycarboxylate based superplasticizer (PC) was employed to achieve a constant consistency with a spread of 600±20mm for different SCC mixtures with or without LWA. The proportions and properties of fresh and hardened SCC are summarized in Table I and Table II, respectively.

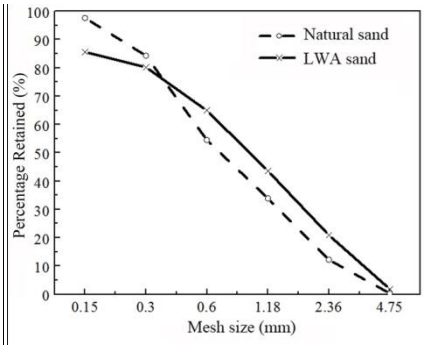

Figure 76 Sieve-analysis curves of natural and LWA sand

Table XXXIV SCC mix proportions (kg/m^3)

Concrete mixture	C	W	GGBS	FA	CA	S	LWA	PC	W_{add} *
0% LWA	430	164	50	70	898	819	0	5.78	0
15% LWA						696	71		5.7
30% LWA						573	142		11.4
50% LWA						410	236		18.9

Note: W_{add} indicates the additional water introduced by LWA into concrete system.

Table XXXV Spread and mechanical properties of SCC

Concrete mixture	Spread of fresh SCC /mm	Compressive strength at 28 days age/MPa (CV)	Young's modulus at 28 days age /GPa (CV)
0% LWA	610	77.3 (6.5%)	41.5 (3.5%)
15% LWA	600	65.4 (2.8%)	39.0 (2.1%)
30% LWA	615	60.8 (5.2%)	34.7 (2.8%)
50% LWA	590	54.0 (2.0%)	33.0 (3.7%)

Testing Methods

(1) SCC mixing - The dry constituents were first mixed automatically for about 60 s. After the addition of water along with the dissolved superplasticizer, the wet mixture was further mixed for 120 s. For the concrete with LWA, the dry constituents, excluding the fine LWA, were first mixed for 60 s, after adding water with the dissolved superplasticizer, the wet mixture was further mixed for 120 s. After that, the fine LWA was added and mixed for another 120 s until a homogeneous mixture obtained. (2) Casting - After mixing, each concrete mixture was cast into different steel molds required by corresponding tests, e.g. 100mm × 100mm × 100mm cubic molds for compressive and splitting tensile strength test, 100mm × 100mm × 515mm or 200mm × 200mm × 515mm prism molds for drying shrinkage test, 150mm × 150mm × 150mm cubic molds for moisture loss test. (3) Mechanical strength test - After concrete casting, the cubic specimens were placed in a moisture room with a temperature of 23±1°C and RH of 100% for 3, 7 and 14 days, after which they were removed from the molds and placed in a room with a temperature of 23±1 °C and RH of 60±5 %. At the age of 28 days and 90d days after casting, the compressive strength and splitting tensile strength were tested.

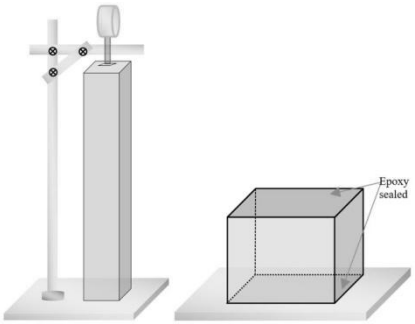

Figure 77 Set-up for drying shrinkage testing (left) and specimen for moisture loss testing (right)

(4) Shrinkage and moisture loss test - For drying shrinkage test, after concrete casting, curing for 1d and demolding , the specimens with size of 100mm × 100mm × 515mm or 200mm × 200mm × 515mm were placed in a moisture room with a temperature of 23±1°C and RH of 100% for 3, 7 and 14 days. Then, the specimens were placed on a set-up illustrated in Figure 2 (left), then dry cured in a room with a temperature of 23±1 °C and RH of 60±5 %. At 0, 1, 3, 5, 7, 10, 14, 21, 28 to 180 days after drying, the readings of the length of two replicate prisms of each concrete mixture were tested, and the shrinkage ratio was calculated. Meanwhile, a cubic specimen with a size of 150mm×150mm×150mm was cured

under the condition same as the drying shrinkage test (Figure 2 right), and weighted at corresponded ages.

Results and Discussion

Effect of moist curing age on compressive strength of SCC

The splitting tensile strength at 28 days age and compressive strength at 28 and 90 days of SCC mixtures are shown in Figure 78.

Generally, because Portland cement is a typical hydraulic binder, the moist curing age can significantly influence the development of microstructure and mechanical properties of concrete, and a longer initial moisture curing will lead to a higher strength. As shown in Figure 78, no matter how much LWC introduced into SCC, it is not surprising that, the longer the initial moist curing age for SCC, the higher the strength gain. For example, in Figure 78b, the 28d compressive strength of SCC that been initially moist cured 3d (50.8MPa) are lower about 10% and 30% than that of 7d cured (56.5MPa) and 14d cured (74.0MPa), respectively. However, it is unexpected that the strength of internally cured SCC is lower than that of without internal curing. As shown in Figure 78a and Figure 78b, the higher the LWA content in concrete mixtures, the lower the strength of SCC.

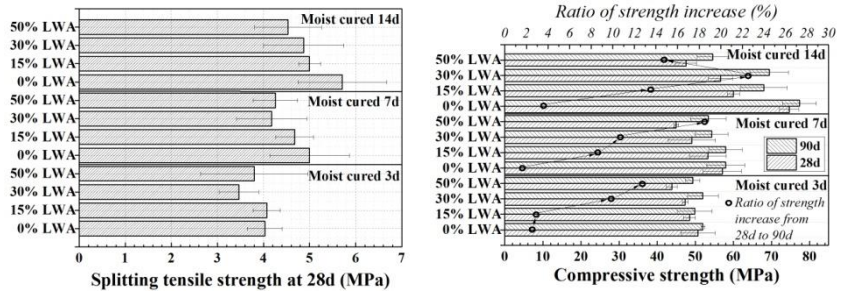

(a) Splitting tensile strength at 28d (b) Compressive strength at 28d and 90d

Figure 78 Effect of moist curing age on strength of SCC

Increase of compressive or flexural strength in comparison with normal concrete, especially at later age, was observed in concrete with LWA [12,13], referring to the influence of additional water introduced by LWA on the achievable final degree of cement hydration[**Error! Bookmark not defined.**]. The onnected points in Figure 78b provide some clues to this mechanism, because the SCCs with higher LWA content mostly exhibit a higher ratio of strength increasing from 28d to 90d.

However, in addition to a higher degree of cement hydration can be expected for internally cured concrete, there are at least three factors that can influence the strength of concrete with IC: (1) One factor is the increased porosity of concrete due to the addition of LWA into concrete. As shown Figure 76, the LWA is a little coarser than natural sand, and the content of particles larger than 2.36mm in LWA is approximately 20%, thus, the negative effect of these large weak particles will significantly offset the positive effect of internal curing on the degree of hydration. (2) The other one is the influence of moisture saturation of concrete. In terms of a comparable situation, higher moisture saturation in concrete may lead to a lower strength [14].

Effect of moist curing age on drying shrinkage of SCC

It has often been reported that internal curing can effectively compensate for the decrease of internal relative humidity [15], reduce the overall shrinkage and crack sensitivity [**Error! Bookmark not defined.**,16]. However, a contradictory esult is gained in this study, as presented in Figure 79. No matter how long the concrete was initially moist cured, all internally cured concretes show higher drying shrinkage than that of the concrete without LWA, and the higher the LWA contents, the more and faster shrinkage the concrete. Similar results have also been reported and reviewed in ref. [8].

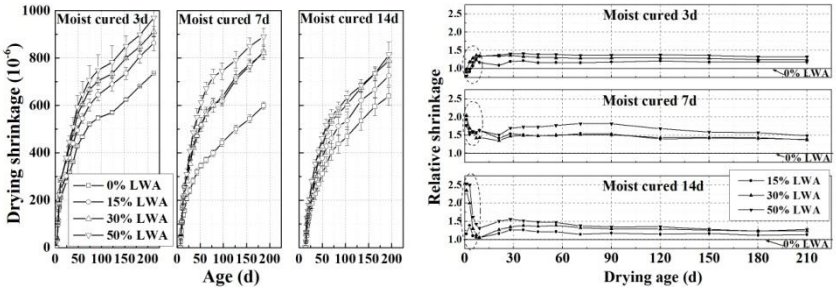

(a) Drying shrinkage *(b) Relative drying shrinkage*

Figure 79. Effect of moist curing age on drying shrinkage of SCC

There may be four mechanisms at work:

(1) the early age volume changes did not include in overall shrinkage curves as shown in Figure 4a. In some publications, a clear volume swelling was often been noticed and measured for the internally cured concrete [17]. On the contrary, due to the existence of autogenous shrinkage, the concrete without internal curing may show a higher total shrinkage than internally cured concrete, even under sufficient moist curing condition[18]. In this work, the shrinkage of concrete was monitored after 3, 7 and 14 days moist curing. The volume changes before 3, 7 and 14 days

were missed, so the measured shrinkage of concrete with and without LWA content might be overestimated and underestimated, respectively. Therefore, if considering the possible volume change of the early ages, the drying shrinkage of the concrete with and without LWA may be comparable; (2) the contribution of autogenous and/or drying shrinkage to total volume change of different ages is different. Since the majority of autogenous or drying shrinkage is often happened at very early ages, and it can be significantly mitigated by the internal curing [19]. For this reason, as shown in Figure 4b, at very early drying ages (before 3 days), for internally cured SCC moist cured for 3 days, its shrinkage is slightly lower than the SCC without LWA. This indicates that the existence of water saturated LWA greatly mitigated the drying and autogenous shrinkage. However, when the SCC was moist cured for 7 or 14 days, the majority of measured shrinkage is highly induced by the moisture loss. The higher free water contents in the internally cured SCC and its loss will lead to more drying shrinkage, which will be further discussed in next section; (3) the LWA particles with low water absorption may lead to an ineffective internal curing [20]. In this study, the 24h water absorption of LWA is only 8%, thus the availability of water for internal curing will be limited. Once the SCC with LWA is suffered from drying, the positive effect of internal curing on shrinkage mitigation will be further offset; (4) Moreover, as shown in Table II, the addition of LWA into SCC directly leads to a lower Young's modulus. The more LWA introduced, the lower the modulus of concrete [**Error! Bookmark not defined.**,21]. Due to this, the concrete with higher WA content will trend to more shrinkage under stresses. This mechanism will probably lead to aggravate the shrinkage of internally cured concrete.

The results and discussions given above suggest that, when evaluating shrinkage behavior of high-strength concrete, due to the existence of autogenous shrinkage, the entire volume change should be monitored from very early ages, even under sufficient curing conditions. Further studies are also needed to investigate the effect of internal curing on shrinkage of SCC using other LWA with higher water absorption.

Effect of moist curing age on moisture loss of SCC

Figure 80 shows the effect of initial moist curing age on moisture loss of SCC with different LWC contents. No matter how long the concrete was initially moist cured, it is clear that the more LWA contents in concrete, the higher the moisture loss, which consists of the previous study in ref. [22], especially for concrete only experienced 3 days moist curing. Meanwhile, as shown in Figure 5, the development and ultimate moisture loss have been significantly reduced by prolonging the initial moist curing. When concrete suffered from an early age drying, the free water in LWA and capillary pores in concrete will be easy to lose, since the cement hydration and microstructure of concrete are far from maturation.

In light of the similar trend of curves in Figure 4a and Figure 5, it is suggested that, the more and faster moisture loss, the greater the drying shrinkage. Thus, the results of moisture loss presented in Figure 5 can be used to well explain the drying shrinkage behavior of SCC in Figure 4a.

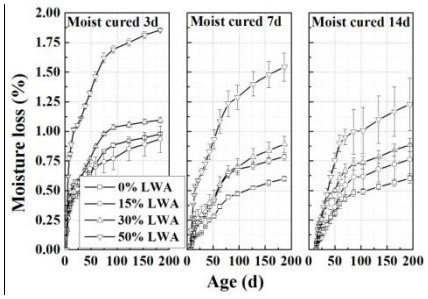

Figure 80. Effect of moist curing age on moisture loss of SCC

In addition to the clear impact of moisture loss on drying shrinkage, the moisture loss at early age can lead to a limited strength and its development as well, this can explain why the SCC after 3 days moist curing exhibited a much lower strength and less strength development from 28d to 90d, as shown in Figure 3.

Effect of specimen size on drying shrinkage of SCC

The experimental results for drying shrinkage of concrete with different size of cross-section of 100mm × 100mm and 200mm × 200mm are presented in Figure 81.

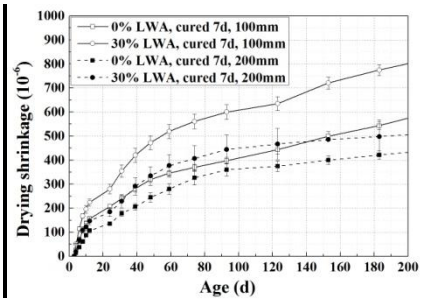

Figure 81. Effect of sample size on drying shrinkage of SCC

As shown in Figure 6, the concrete specimens with a larger cross-section size exhibit lower drying shrinkage compared to that of concrete with small cross-section size. Moreover, when concrete has a larger cross-section size, the difference in drying shrinkage between the concrete without LWA and with 30%

LWA content becomes less obvious, compared to the concrete specimens with a smaller cross-section size. The reason is that the moisture in larger specimens has to transfer long distance from inside to outside area, thus, more free water can contribute to mitigate the concrete from self-desiccation and shrinkage. Breugel et al. reported that the size effect is more pronounced for concrete with LWA than normal concrete [23]. Thus, it could be expected that small size concrete with LWA may exhibit a higher drying shrinkage than normal concrete, but for larger specimens, the difference should be less and less, or even the opposite may be obtained [24]. It is indicated that the drying shrinkage of internally cured SCC might be overestimated for real concrete structures with larger cross-section.

Conclusions

Under the experimental condition of this study, the following conclusions can be drawn: (1) due to the addition of weak LWA particles into the concrete matrix, the overall strength of SCC containing LWA was lower than that of the non-internally cured SCC; (2) the early drying and moisture loss will offset the benefits of internal curing on mitigation of drying shrinkage. And prolonging the duration of initial moist curing can appreciably mitigate the early moisture loss and drying shrinkage of internally cured SCC; (3) the difference in drying shrinkage between SCC with and without internal curing for large specimens is less pronounced than the small specimens. It is indicated that, for real concrete structures with larger cross-section, the laboratory tested shrinkage of internally cured SCC might be overestimated.

Acknowledgements

This work was financially supported by the China National Science Foundation (51302191), National Basic Research Program of China (2011CB013805) and National Key Project of Scientific and Technical Supporting Programs of China (2014BAL03B02). The authors also gratefully acknowledge the financial support received from Yunnan Innovative Research Team of Green Building Materials and Testing.

References

[1] Rozière, E.,Granger, S., Turcry, P., Loukili, A., (2007), *Cem Concr Comp*, vol. 29, n. 8, p. 626-636.
[2] Ghoddousi P, Monir Abbasi A., (2008), In: *(SCC 2008): Challenges and Barriers to Application,* 3rd North American conference on the design and use of self-consolidating concrete, p. 325-330, Shah., S.P. (Ed.), Chicago.
[3] R. Loser, R., Leemann, A., (2009), *Mater Struct*, vol. 42, n. 2, p. 71-82.

[4] Kovler, K., and Zhutovsky, S., (2006), *Mater Struct*, vol. 39, p. 827-847.
[5] Bentz, D., and Snyder, K., (1999), *Cem Concr Res*, vol. 29, n. 11, p. 1863-1867.
[6] Jensen, O. M., and Hansen, P. F., (2001), *Cem Concr Res*, vol. 31, n. 4, p. 647-654.
[7] Delatte, N., Crowl, D., Mack, E., and Cleary, J., (2008), In: *SP-256: Internal curing of concrete paving: laboratory and field experience*, p. 91-104, Mohr, B. J. and Bentz, D. P. (Ed.), American Concrete Institute, Farmington Hill, MI.
[8] Dang, Y., Shi, X., Mery, S., Xie, N., Benson, A., and Yang, Z., (2015), *J Mater Civ Eng*, vol. 27, n. 12, p. 04015037-1-9.
[9] Mechtcherine, V., Dudziak, L., Schulze, J., and Staehr, H., (2006), In: *Proc. RILEM Conf. on Volume Changes of Hardening Concrete: Testing and Mitigation*, RILEM PRO 52, p. 87-96, Jensen, O. M., Lura, P. And Kovler, K. (Ed), RILEM Publ. S.A.R.L., Lyngby.
[10]Kong, X.L., Zhang, Z.L., and Lu, Z.C., (2014), *Mater Struct*, vol. 48, n. 9, p. 2741-2758.
[11] Mönnig, S., Reinhardt, H.-W., Jensen, O., Lura, P., and Kovler, K., (2006), In: *Proc. RILEM Conf. on Volume Changes of Hardening Concrete: Testing and Mitigation*, RILEM PRO 52, p. 67-75, Jensen, O. M., Lura, P. And Kovler, K. (Ed), RILEM Publ. S.A.R.L., Lyngby.
[12] Lura, P., (2003), *Autogenous deformation and internal curing of concrete*, Ph.D. thesis, Delft University of Technology, Delft.
[13] Zhutovsky, S., Kovler, K. and Bentur, A., (2004), *Cem Concr Compos*, vol. 26, n. 5, p. 499-507.
[14] Jensen, O.M., and Hansen, P.F., (2002), *Cem Concr Res*, vol. 85, n. 6, p. 973-978.
[15] Henkensiefken, R., Bentz, D., Nantung, T., and Weiss, J., (2009), *Cem Concr Comp*, vol. 31, n. 7, p. 427-437.
[16] Henkensiefken, R., Briatka, P., Bentz, D., Nantung, T., and Weiss, J., (2010), *Concr Int*, vol. 32, n. 2, p. 49-54.
[17] Sant, G., Lura, P., and Weiss, W., (2006), *Transp Res Rec*, vol 1979, p. 21-29.
[18] Shen, D., Wang, X., Chen, D., Zhang, J., Jiang, G., (2016), *Constr Build Mater*, vol. 106, p. 512-522.
[19] Cusson, D., Hoogeveen, T., (2008), *Cem Concr Res*, vol. 38, n. 6, p. 757-765.
[20] Lura, P. and van Breugel, K., (2000), In: *RILEM Proc. PRO 17, Shrinkage of Concrete - Shrinkage 2000*, p. 533-546, Baroghel-Bouny, V. and Aïtcin, P.-C. (Ed.), RILEM Publ. S.A.R.L., Paris.
[21] Akcay, B. and Tasdemir, A., (2006), In: *Proc. RILEM Conf. on Volume Changes of Hardening Concrete: Testing and Mitigation*, RILEM PRO 52, p. 31-40, Jensen, O. M., Lura, P. and Kovler, K. (Ed), RILEM Publ. S.A.R.L., Lyngby.
[22] Reinhardt, H.W., (2008), *Concr Sci Eng*, vol. 4, n. 14, p. 77-83.
[23] Van Brugel, K., Outwerk, K., De Vries, H., (2000), In: *Proceedings of the International RILEM Workshop on Shrinkage of Concrete*, p. 161–177, Baroghel-Bouny, V. and Aïtcin, P.-C. (Ed.), RILEM Publ. S.A.R.L., Paris.

[24] Lura, P., van Breugel, K. and Maruyama, I., (2003), In: *Proc RILEM Int. Conf. on Early Age Cracking in Cementitious Systems (EAC'01)*, p. 337-344, Kovler, K. and Bentur, A. (Ed.), RILEM Publ. S.A.R.L., Israel.

Theme 7: Durability of SCC

Effect of Alkali Sulfate on Workability, Strength and Volume Stability Related to SCC

Ying Ma and Jueshi Qian

College of Materials Science and Engineering, Chongqing University, Chongqing 400045, China

Abstract: For a self-consolidating concrete (SCC), the workability, strength and volume stability of concrete are much related to the cement paste. High amount of cement is typically used to produce good workability of SCC, but some problems such as high hydration heat, large shrinkage are introduced. The content and type of sulfate phases in Portland cement, especially alkali sulfates including arcanite (K_2SO_4), thenardite (Na_2SO_4), etc., are important factors influencing the workability and volume stability of SCC. This work focused on investigating the impacts of alkali sulfates on the flowability, strength development and volume stability of SCC. The results show that the presence of arcanite, thenardite would promote the increase of fluidity of grout with time-lapse. But, a high content of arcanite and thenardite would result in a great loss of workability, little decrease of 28 d compressive strength and an increase of drying shrinkage. Arcanite and thenardite in cement have great impacts on the performance of SCC associating with other factors related to cement, superplasticizer and other additives, and more attention should be paid.

Keywords: *Alkali sulfate, Workability, Compressive strength, Volume stability, Self-consolidating concrete.*

Introduction

Self-consolidating concrete (SCC) is highly flowable and coherent, providing great spreading and compacting under its own weight without any vibration [1]. SCC can easily fill complex formwork in structural members and provide good pumping through long distances [2].

High content of cement is typically used to produce SCC, and some problems such as high hydration heat, large shrinkage are introduced [3]. Supplementary cementitious materials (SCM) such as fly ash and silica fume are used to partially

replace cement, to enhance the stability of SCC, decrease shrinkage and the amount of CO_2 emission related to the reduced use of cement in concrete [4-6]. However, SCM used in SCC would also weaken the properties of SCC compared to the plain SCC. For instance, silica fume and metakaolin may impair the required workability of fresh concrete. The partial substitutions of cement with silica fume and slag would decrease the plastic viscosity of grout [5, 7]. Assaad [8] reported that binary cement (cement-silica fume), ternary cement (cement-silica fume-fly ash) and quaternary cement (cement-silica fume-fly ash-slag) present lower plastic viscosity values than corresponding plain SCC mixtures.

Based on the high amount of cement in SCC, the performance of SCC would be much attributed to the cement properties such as C_3A content, type and content of sulfate, alkalis content, specific surface area and particle size distribution [9, 10]. The performance of SCC would be primarily and sensitively affected by alkali sulfates in cement, especially associating with other factors, such as C_3A content and specific surface area of cement. However, few studies have been carried out, and the influences of alkali sulfates in cement on the SCC performance were not well known.

The current study aims to the influence of alkali sulfates on the performance of SCC. Alkali sulfates in Portland cement occur as arcanite (K_2SO_4), thenardite (Na_2SO_4), etc. Therefore, arcanite and thenardite, prepared in laboratory, were used in this study. The flowability of grout, the compressive strength of SCC and the volume stability of mortars were investigated to evaluate the impacts of alkali sulfates on the performance of SCC.

Experimental

Materials and mixture proportions

Arcanite and thenardite were used in this investigation. Arcanite(K_2SO_4) was prepared by calcining the reagent grade K_2SO_4 at 1000 ^oC for 2 h. Thenardite (Na_2SO_4) was prepared by calcining the reagent grade Na_2SO_4 at 800 ^oC for 2 h, and then stored in a storage box at room temperature. The X-ray diffractions of arcanite and thenardite are shown in Figure 1. The addition of arcanite and thenardite leads to a high content of Na_2O_{eq} in cement, and the value is 0.6%, 0.8%, 1.0% and 1.2 wt. %.

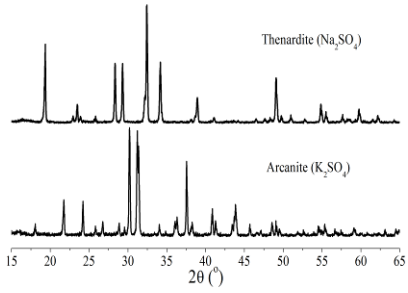

Figure 1. XRD patterns of arcanite and thenardite made in laboratory

Portland cement clinker, with a low content of SO_3, was used to study the impacts of alkali sulfates on the fluidity of grout. The clinker was grounded by grinding mill, and passed through a 75 μm sieve. The Blaine fineness of clinker is 355 m^2/kg. Natural gypsum was used, along with clinker, to prepare cement. The chemical compositions of clinker and gypsum were shown in Table I.

Table I. Chemical composition of clinker, gypsum, cement and fly ash (wt. %)

Oxide	CaO	Al_2O_3	SiO_2	SO_3	Fe_2O_3	MgO	K_2O	Na_2O
Clinker	66.99	3.70	20.91	0.48	3.18	1.74	0.76	0.14
Gypsum	36.44	1.77	7.40	41.30	0.85	3.10	0.84	0.15
Cement	62.40	4.56	22.05	2.60	2.62	1.94	0.72	0.11
Fly ash	5.18	25.76	61.67	0.52	5.17	0.83	2.01	0.74

Three mixes were proportioned to investigate the mechanical properties of SCC specimens. The concrete mix proportions are present in Table Ⅱ. Cement, fly ash and a polycarboxylate ether-based superplasticizer (PCEs) was used to prepare SCC mixtures. And, the chemical compositions of cement and fly ash were shown in Table I. Fine gravel with maximum size of 10 mm and coarse gravel with size of 10-16 mm were used in design of SCC mixtures. The sand was composed by natural and machine-made sand.

Table Ⅱ. Mix proportions of self-consolidating concrete (kg/m^3)

Mix	Water	Arcanite	Thenardite	Cement	Gravel	Sand	PCEs	Fly ash
M1	148	-	-	360	973	804	8.5	145
M2	148	6.06	-	353.94	973	804	8.5	145
M3	148	-	4.95	355.05	973	804	8.5	145

Methods

The paste flow test was performed according to the Chinese standard (GB/T 8077-2012). The grout was prepared at a water/cement (w/c) ratio of 0.29. The PCEs was used in a dosage of 0.4%, 0.6%, 0.8% and 1.0 wt. %. With early addition, PCEs was added to the mixing water, which was then mixed with the cement. The blend was mechanical agitating at a low-speed for 2 min, and at a stop for 15 s, and then at a high-speed for 2 min. Thereafter, the paste was poured into a cone (top diameter 36 mm, bottom diameter 60 mm, height 60 mm). The cone was removed and the diameter of the spread cement paste was measured. The flow value was expressed by a maximum average of two perpendicular spreading diameters. The processes of agitating and measurement would take 5 min and the flow value measured is called the initial or 5 min flow value. Besides, 30 min and 60 min flow values were also measured. After the initial flow test, the cement paste was left in the mixing pot which was coated with a wet towel to prevent water loss. And, before the 30 min or 60 min flow test, the cement paste was agitated and measured, as same as the initial flow test.

The heat release was recorded with an isothermal calorimeter from thermometrics. The ambient temperature was 20 ^{o}C and the measurements were carried out for 24h.

The SCC concrete mixtures were prepared in a standard concrete mixer. In order to characterize the fresh properties of SCC, slump, T_{500}, and spreading diameters were measured in accordance with EN 12350-2. Furthermore, the concrete mixtures were cast on 100 mm*100 mm*100 mm cubic moulds. The specimens were demoulded after 1 day and then cured in the standard curing room (20±2 ^{o}C, RH 95±5%) until the time of test. The tests were performed at the age of 3, 7 and 28 days.

Volume stability of mortars was determined by measuring length changes of 25 mm*25 mm*280 mm prisms. Mortars were cast at a sand-to-cement ratio of 3.0, and water-to-cement ratio was 0.5. The mortar specimens were demoulded after 24 h and cured in the standard curing box (20±2 ^{o}C, RH 95±5%). The values were the average of three test specimens.

Results

Effect of alkali sulfates on the flowability of grout

The effect of arcanite (K_2SO_4) and thenardite (Na_2SO_4) on initial flow values of grout is shown in Figure 2. And, the change of flowability of grout with time-lapse is shown in Figure 3. It can be seen that arcanite favors the initial flow of grout.

With a high content of arcanite (1.2% Na_2O_{eq}), the flow value would not depend on the dosage of PCEs. The initial flowability of grout is more sensitive to the content of thenardite in cement despite of the dosage of PCEs.

It is surprisingly found that both arcanite and thenardite are in favor of the flowability of grout with time-lapse. The spreading diameters of grouts increase with time-lapse. After 60 min, the grouts still have large spreading diameters, especially with the addition of arcanite. Concrete typically needed to be produced in advance in a mixing plant and transported by mixer trucks to the construction site. The development of fluidity with hydration time is expected and beneficial to the transport, pumping and placing of concrete [11].

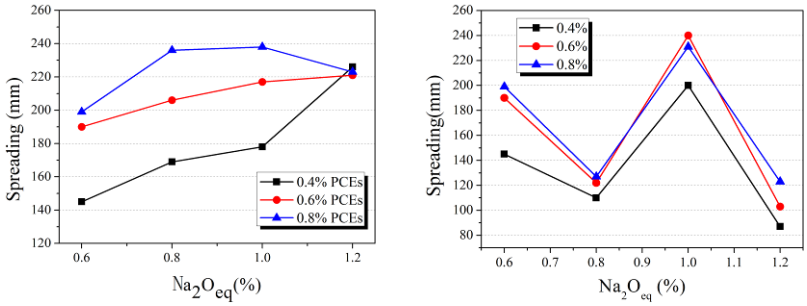

(a) Arcanite (K_2SO_4) (b) Thenardite (Na_2SO_4)

Figure 2. Effect of alkali sulfates on the initial flow value of grout

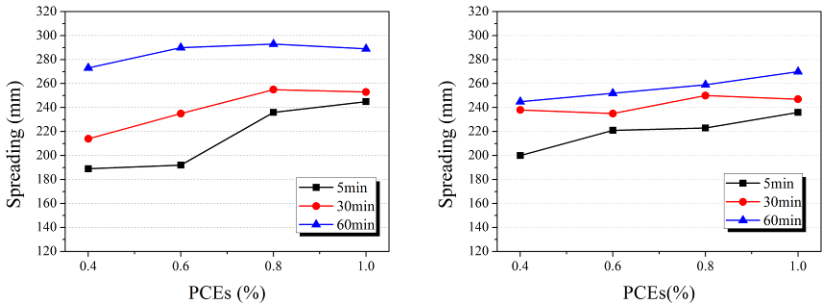

(a) 0.8% Na_2O_{eq} of K_2SO_4 (b) 1.2% Na_2O_{eq} of K_2SO_4

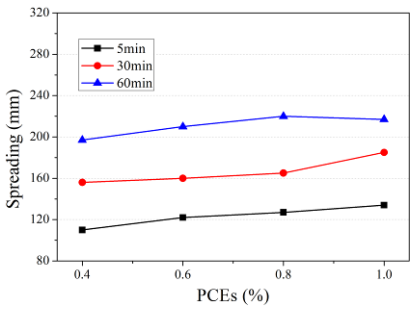

(c) 0.8% Na_2O_{eq} of Na_2SO_4

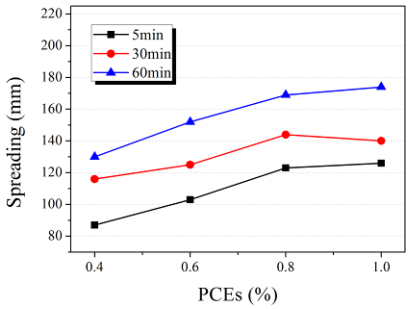

(d) 1.2% Na_2O_{eq} of Na_2SO_4

Figure 3. Change of flow value with time

Effect of alkali sulfates on the compressive strength of SCC

Few studies have been carried out about the influence of alkali sulfates on the properties of SCC. For a preliminary and limited study, the effects of arcanite and thenardite on the fresh properties of SCC mixtures were studied, as shown in Table Ⅲ. And, the impacts on the compressive strength of concretes were shown in Figure 4.

It can be seen from Table Ⅲ that with the addition of arcanite and thenardite, concrete has a great loss of workability. Compared with arcanite, thenardite has a more adverse effect on the workability of fresh concrete. Besides, the addition of arcanite and thenardite could favor early compressive strength of concrete specimens, but much decrease 28 d compressive strength of concrete specimens (Figure 4).

Table Ⅲ. Fresh properties of self-consolidating concrete mixtures

	Ref.	Arcanite	Thenardite
Slump (mm)	240	140	No slump
Spreading (mm)	620	300	-
T_{500} (s)	9	-	-

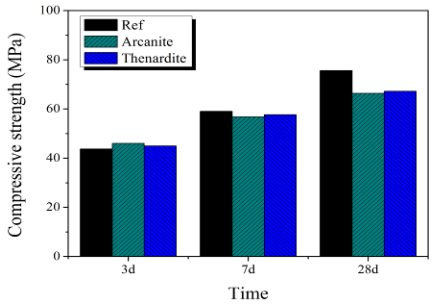

Figure 4. Effect of of alkali sulfates on the compressive strength of concrete

Effect of alkali sulfates on the volume stability related to SCC

High hydration heat and large shrinkage are major problems of SCC [12, 13]. Effect of arcanite and thenardite on the heat flow of cement paste was studied and shown in Figure 5. It can be seen that the addition of thenardite dramatically increases early hydration heat. It indicates that thenardite may result in large early drying shrinkage.

The influences of alkali sulfates on the volume stability, expressed by the linear expansion ratio, were studied. Figure 6 and 7 show the expansion and shrinkage of mortars with water and air curing respectively. High content of arcanite and thenardite would lead to large expansion with water curing and large drying shrinkage with air curing. With addition of thenardite, mortars have large early drying shrinkage, which is in accordance with early heat release.

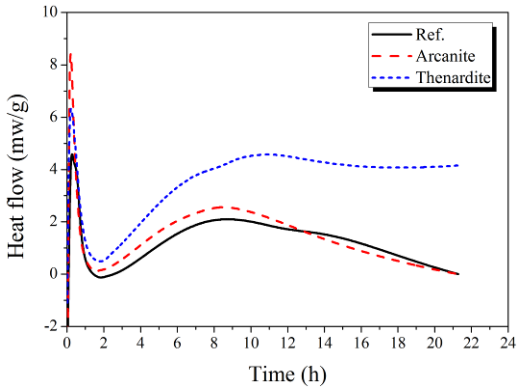

Figure 5. Effect of alkali sulfates on the heat flow of cement paste

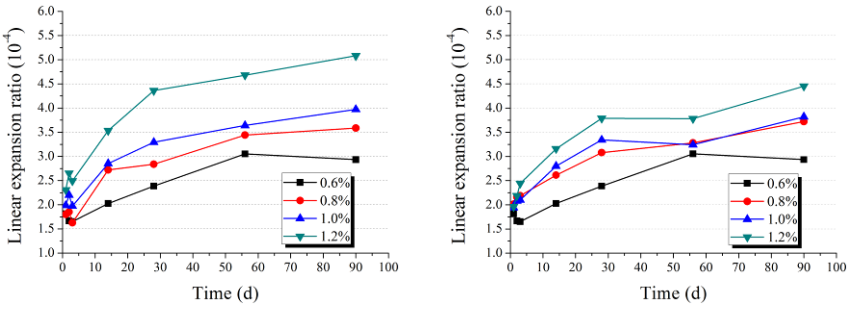

(a) Arcanite (K_2SO_4) (b) Thenardite (Na_2SO_4)

Figure 6. Effect of alkali sulfates on the linear expansion of mortars with water curing

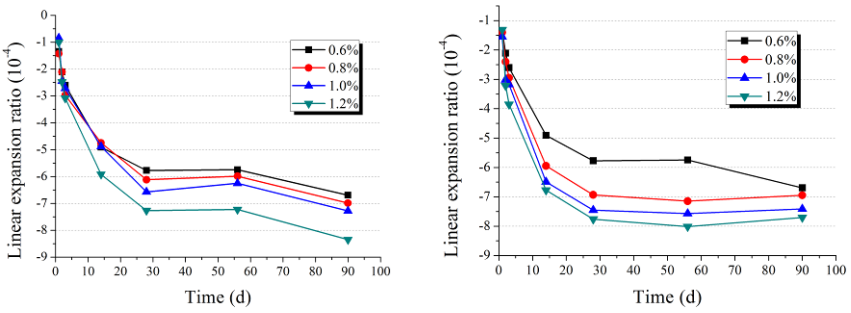

(a) Arcanite (K_2SO_4) (b) Thenardite (Na_2SO_4)

Figure 7. Effect of alkali sulfates on the linear expansion of mortars with air curing

Discussion

From the flow test, arcanite and thenardite in Portland cement are in favor of the flowability of grout with time-lapse. Then, an “appropriate” or “adequate” content of alkali sulfates in cement should be beneficial to the fluidity of SCC [14].

However, with addition of arcanite and thenardite, SCC presents great loss of workability and decrease of 28 d compressive strength. High content of arcanite and thenardite in cement would also lead to high hydration heat and large drying shrinkage to SCC. Limited by the work performed, the distinct results of great loss of workability from the favourable flowability of grout influenced by alkali sulfates could not be well explained. But, the impacts of alkali sulfates in cement on the

fresh and hardened performance of SCC are obvious and should be attracted much attention.

Compared to arcanite, thenardite would have more sensitive impact on the workability, compressive strength and drying shrinkage of SCC. High content of thenardite in cement should be more aware when the cement used to produce SCC. In addition, arcanite in cement is typically much higher than thenardite and, regarded as the major alkali phase [15]. Then, the effect of arcanite in cement on the performance of SCC should be much concerned.

The content of thenardite and arcanite in cement is lower, but the effects on the performance of SCC would be obvious, associating with other factors related to cement, superplasticizer and other additives. Much attention should be paid and further investigation should be required.

Conclusions

Alkali sulfates in cement would have influences on the performance of SCC, but few studies have been carried out. It was found that arcanite and thenardite in cement are in favor of the flowability of grout with time-lapse.

However, it also found that arcanite and thenardite in cement would lead to great loss of workability and decrease 28 d compressive strength of SCC. High addition of arcanite and thenardite would also increase early hydration heat and drying shrinkage of mortars. Compared to arcanite, thenardite has more sensitive impact on the workability, compressive strength and drying shrinkage of SCC. Cement with a lower content of alkali sulfates would be beneficial to the performance of SCC.

The content of thenardite and arcanite in cement is lower, but the effects on the performance of SCC would be obvious, associating with other factors related to cement, superplasticizer and other additives. More investigations about the effect of alkali sulfates on the performance of SCC are required.

Acknowledgements

The authors would like to acknowledge the financial support provided by the Natural Science Foundation Project (Project No. 51132010).

References

[1] Dehestani, M., Nikbin, I.M., Asadollahi, S. (2014), *Constr. Build. Mater.*, vol. 66, p. 685-91.
[2] Lachemi, M., Hossain, K.M.A., Lambros, V., Nkinamubanzi, P.C., and Bouzoubaâ, N. (2004). *Cem. Concr. Res.*, vol. 34, p. 917-26.
[3] Sahmaran, M., Lachemi, M., Erdem, T.K., Yucel, H.E. (2011), *Mater. Struct.*, vol. 44, p. 1193–204.
[4] Khayat, K., Yahia, A., Sayed, (2008), *M. ACI Mater. J.*, vol. 105, p. 585–93.
[5] Khayat, K., Yahia, A., Sayed, M. (2008), *ACI Mater. J.*, vol. 105, p. 585–93.
[6] Vejmelkova, E., Keppert, M., Grzeszczyk, S., Skalinski, B., Cerny, R. (2011), *Constr. Build. Mater.*, vol. 25, p. 1325–31.
[7] Uysal, M., Sumer, M. (2011), *Constr. Build. Mater.*, vol. 25, p. 4112–20.
[8] Assaad, J. (2004), *PhD Thesis*, University of Sherbrooke, Canada: Sherbrooke.
[9] Aydin, S., Aytac, A.H. and Ramyar, K. (2009), *Constr. Build. Mater.*, vol. 23, p. 2402-08.
[10] Petkova, V., Stoyanov, V. and Pelovski, Y. (2012), J. *Therm. Anal. Calorim.*, vol. 109, p. 797-806.
[11] Hwang, S.D., Khayat, K.H., Bonneau, O. (2006), *ACI Mater. J.*, vol. 103, p.121–9.
[12] Madandoust, R., Mousavi, S.Y. (2012), *Constr. Build. Mater.*, vol. 35, p. 752–60 .
[13] Brouwers, H.J.H., Radix, H.J. (2005), *Cem. Concr. Res.*, vol. 35, p. 2116–36.
[14] Jiang, S.P., Kim, B.G. and Aitcin, P.C. (1999), *Cem. Concr. Res.*, vol. 29, p. 71-78.
[15] Qian, J., Ma, Y., Yang, S., Huang, Y. (2015), *J. Chin. Ceram. Soc.*, vol. 43, p. 1441-8.

Investigating Corrosion Problem in Reinforced SCC Members

Ahmed Abdel-Mohti[1], Hui Shen[2], Chelsea Cousins[1] and Edward Duliba[3]

[1]Civil Engineering Department, Ohio Northern University
[2]Mechanical Engineering Department, Ohio Northern University
[3]Department of Chemistry and Biochemistry, Ohio Northern University

Abstract This paper investigates repairing reinforced self-consolidating concrete members that experience rebar corrosion problem. Corrosion is one of the major problems of the durability of reinforced concrete members. A control reinforced concrete member was prepared to have no corrosion problem. Different levels of corrosion in the reinforcing rebars of up to 50% were considered in the current study. Reinforced concrete beams having up to 50% corrosion level were constructed. The beams with corrosion problem were repaired using carbon fiber reinforced polymer sheets. All of the beams constructed in this study were tested under two line loads until failure. The effectiveness of repairing technique was assessed by comparing between the control beam and the repaired beams in terms of load carrying capacity, deflection, and ductility.

Keywords: *SCC, RAP, Corrosion, Load capacity, Deflection.*

Introduction

Self-consolidating concrete (SCC) is defined as the fresh concrete that can flow around reinforcement and consolidate under its self-weight without the need of vibration. SCC should not exhibit any segregation or bleeding. SCC is one of the important products in concrete technology. The performance of SCC has been studied by many researchers [1-8].

The use of fly ash and slag cement is very effective in producing SCC with reasonable fresh and hardened characteristics. Optimization of mixture proportions and the use of new materials in SCC have been examined by many researchers. Since SCC incorporate a large amount of portland cement, that increases the cost of SCC and results in large CO_2 emission. Recycled aggregates invited attention from researchers as they generally come from demolition of roads, returned

concrete, and buildings or structures. The use of recycled aggregates can help to reduce the environmental impact of concrete. Also, it can reduce the consumption of natural resources used in concrete.

Concrete structures are vulnerable to corrosion when concrete structures are exposed to severe environment. Corrosion causes section loss in the reinforcing steel. Therefore, it affects the load capacity of the concrete structure. Corrosion resembles a major threat to hinder the durability and safety of concrete structures. Carbon Fiber Reinforced Polymer (CFRP) is used in strengthening and restoration of concrete structures thus it can be used to restore the capacity of concrete structures with corrosion problem.

Experimental Program

A SCC concrete mixture having both slag and fly ash and 10% recycled asphalt pavement (RAP) was prepared (Table I). The SCC mixture contained cementitious material including ASTM C 150 Type I portland cement, Class C fly ash, and slag cement. The supplementary cementitious materials (SCMs) were incorporated to make SCC more sustainable. Natural sand was used as fine aggregate. Coarse aggregates used are #57 and #8 limestone. A fixed ratio between the amounts of #57 to #8 of 1:1 was used. Water to cementitious material ratio (w/cm) of 0.38 was used. The mixtures included RAP to replace 10% of coarse aggregates in an effort to improve the sustainability further. A viscosity enhancing admixture and a high range water reducer were used to produce SCC. The compressive and tensile strength of SCC mixture were determined at 3, 7, 14, and 28 days of age of concrete to capture the early strength of concrete.

The natural process of corrosion takes a long time, which makes it unrealistic to study various conditions in a reasonable timely manner in the lab. The process is therefore accelerated by chemical means to simulate the real condition. The galvanic cell method was used and the salt water of 25wt% was also used and acted as an electrolyte in this test.

The key equations are the reduction of oxygen:

$$O_2(g) + 2\ H_2O(\ell) + 4\ e^-(aq) \rightarrow 4\ OH^-(aq) \quad (1)$$

and the oxidation of iron:

$$Fe(s) \rightarrow Fe^{2+}(aq) + 2\ e^-(aq) \quad (2)$$

to form iron(III) oxide:

$$4\ Fe^{2+}(aq) + O_2(g) \rightarrow 4Fe^{3+}(aq) + 2\ O^{2-}(aq) \rightarrow Fe_2O_3(s) \quad (3)$$

In the presence of water, a mixture of iron(III) oxide hydrates are formed with Fe_2O_3. Once iron(III) and iron(II) ions have been formed, acid-base chemistry also occurs with water to form $Fe(OH)_2$ and $Fe(OH)_3$:

$$Fe^{2+}(aq) + 2\ H_2O(\ell) \rightarrow Fe(OH)_2(s) + 2\ H^+(aq) \quad (4)$$

$$Fe^{3+}(aq) + 3\ H_2O(\ell) \rightarrow Fe(OH)_3(s) + 3\ H^+(aq) \quad (5)$$

The resulting rust is a complicated and uncontrolled mixture of iron oxide hydrates, based on competing equilibria.

Table I. Concrete mixture proportions

W/C		0.38
Water (kg)		144.0
Cementitious Materials (kg)	Type I portland cement	151.6
	Flyash	113.7
	Slag cement	113.7
Aggregates (kg)	RAP	64.9
	Coarse	584.2
	Fine	625.0

Construction of Samples

A typical beam is 15.24 cm wide, 15.24 cm deep, and 1.828 m long. Distance from one support to another was 1.524 m. A typical beam was also reinforced with two (#5) 15.875 mm diameter deformed rebars. Shear reinforcement was applied by providing three 6.35 mm diameter A36 stirrups at 203.2 mm spacing on each side. The distance from the center of one support to the center of the first stirrup is 50.8 mm. A cover of 25.4 mm was applied all around the reinforcement.

The control beam was reinforced with two rebars, which did not experience any corrosion, whereas, the remaining beams were reinforced with a pair of rebars that contain different corrosion levels. The percentage of corrosion is defined as the amount of weight lost by the rebar due to corrosion. Figure 1 shows an example of corrosion of a rebar. After the reinforcement cage was assembled, chairs were attached to the bottom and sides of the cage to provide the needed cover. The cage was placed in the designed formwork, and then the prepared SCC was poured. SCC was poured only from one side of the beam and was able to completely fill the formwork without the need for any mechanical compaction. The casted beams were allowed to cure for 28 days; afterwards repair and testing were performed.

A number of steps were undertaken to prepare the beam before CFRP was applied as recommended by the manufacturer. The beams were flipped so the bottom is facing up. The CFRP sheets and U-wrap were cut and becoming ready. The beams were sanded and air blasted. A primer layer of epoxy was applied to the beam, where CFRP would be applied. The CFRP that had epoxy already were applied to the designated locations in the beam. Pressure was applied against the fabric to work out any air pockets between the fabric and beam's surface. Another layer of epoxy was applied to the CFRP using a painting roller. A weight was placed on the top of the beam and also a lateral system was placed to hold the U-wrap in place. After epoxy cured, repaired beams were tested. Table II shows the properties of CFRP materials.

Table II. Dry and composites properties of CFRP materials

CFRP Properties	Dry Material Properties	Composite Material Properties
Tensile Strength (GPa)	4.0	0.834
Tensile Modulus (GPa)	230.0	82.0
Ultimate Elongation (%)	1.7	1.0

Results

The concrete mixture achieved a slump flow value above the minimum limits of SCC (Table III). The difference in diameter between that from slump flow and that from J-Ring tests was smaller than 50.8 mm. Moreover, Visual Segregation Index (VSI) score did not exceed 1.

As mentioned before, all of the twelve beams were tested under two line loads until failure using the same test setup. All of the tested beams experienced extensive flexural cracks close to mid-span before failure.

Figure 2 shows comparison between load-deflection relationship of the concrete beam and beams with up to 50% corrosion level. From comparing load-deflection relationships of beams, it can be determined that as the level of corrosion increased, the beam became less stiff. As the corrosion level increased, beams became more ductile except for beam with 40% corrosion as it showed similar stiffness to that with 32% corrosion, but it showed less ductility. Overall, it can be concluded that the cracking load did not changed significantly due to corrosion. It can also be concluded that load capacity decreased as the level of corrosion became higher.

Figure 3 shows testing of non-repaired and repaired beams with 40% corrosion level. For the control beam, the first crack appeared at 9.9 kN in the middle of the

beam. The next crack appeared to the right of the first crack at 28 kN. The third crack appeared to the left of the original crack at 32 kN. A splitting crack occurred at the very end of the test at approximately 55 kN close to the clamped side, where rebars were clamped during the corrosion process. For the beam with 40% corrosion level, the beam showed its first crack at 9 kN. There were extensive flexural cracks close to the mid-span of the beam. Some of the cracks extended to the top of the beam. At 28 kN, a hairline splitting crack developed from under the loading point close to the clamped side and propagated downward. At 30 kN, another hairline splitting crack developed on the other side. At 33 kN, failure took place due to the splitting crack on the unclamped side. There was also crushing of concrete in the top. For the repaired beam with 40% corrosion level, the beam showed its first crack at 2.5 kN. There were extensive flexural cracks close to the mid-span of the beam. Noise indicating debonding in the FRP was first heard at 42 kN in the middle of the beam. A splitting crack occurred close to the unclamped side of the beam at 47 kN. Slight crushing of top concrete also took place. There were signs of debonding in the bottom sheet; however, there were no signs of fracture. Due to 40% corrosion level in rebars, the beam lost about 39% of its load carrying capacity, but when repaired with both CFRP sheet and U-wraps, it recovered about 24% of its load carrying capacity. Beams with 40% corrosion level had smaller stiffness and experienced more ductility than their counterpart control beam, but when repaired, it had stiffness close to the control beam and became even less ductile than the control beam (Figure 4).

Table III. SCC test results

VSI	1
Slump Flow (mm)	749.3
Slump Flow with J-Ring (mm)	698.5
T50 (seconds)	5.0

Figure 1. Sample of rebar corrosion

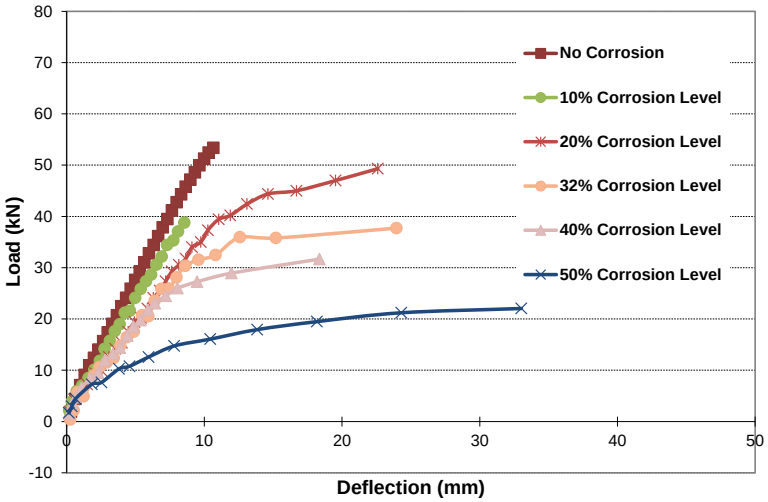

Figure 2. Effect of corrosion level on load carrying capacity

(a)

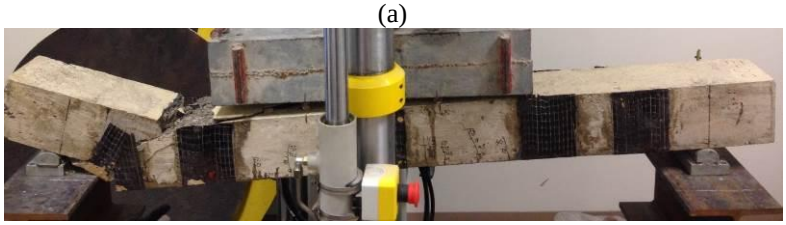

(b)

Figure 3. Testing of beams with 40% corrosion level (a) Not repaired (b) Repaired

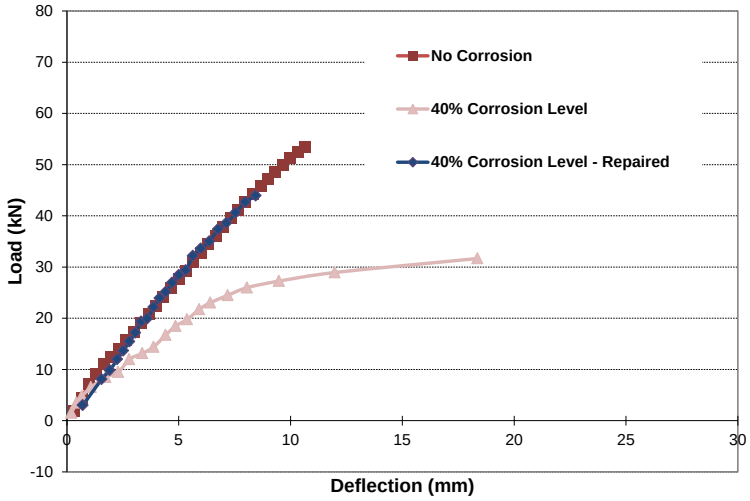

Figure 4. Comparison between load-deflection curves of specimens

Conclusions

This investigation aimed to quantify the effect of corrosion level on the performance of reinforced SCC members. Up to 50% corrosion level was considered and investigated. Also, the effectiveness of repairing RC members using both CFRP sheets and U-wraps was evaluated. The beams were cast using

the SCC concrete mixtures with 10% RAP and tested under two static line loads at the mid-span until failure. The following conclusions are drawn:

- The developed concrete mixture had slump flow values above the minimum limits of SCC.
- Level of corrosion did not seem to affect the cracking load.
- In general, as the corrosion level increases, the RC members become less stiff and load carrying capacity becomes smaller. The relationship between the level of corrosion and load capacity loss is not linear.
- Using both CFRP sheets and U-wraps was found to be an effective method to repair corroded RC members.
- When beam with 40% corrosion level was repaired, it recovered about 24% of its load capacity.

References

[1] Abdel-Mohti, A., Shen, H., and Khodair, Y. (2015), *Characteristics of Self-Consolidating Concrete with RAP and SCM*, Journal of Construction & Building Materials, Elsevier, (under review).

[2] Hossain, K. M. A., and Lachemi, M. (2010), *Fresh, mechanical, and durability characteristics of self-consolidating concrete incorporating volcanic ash*, Journal of Materials in Civil Engineering, 22(7), pp. 651-657.

[3] Khatib, J. M. (2008), Performance of self-compacting concrete containing fly ash, Construction and Building Materials, 22(9), pp. 1963-1971.

[4] Ozawa, K., Maekawa, K., Kunishima, H., and Okamura, H. (1989), *Performance of concrete based on the durability design of concrete structures*, Proceedings of the 2nd East-Asia-Pacific Conference on Structural Engineering and Construction, Vol.1, Chiang Mai, Thailand, pp. 445-456.

[5] Petersson, O. (1998), *Application of self-compacting concrete for bridge castings*, Swedish Cement and Concrete Research Institute, Stockholm, Sweden.

[6] Khayat, K. H., Paultre, P., and Tremblay, S. (2001), *Structural performance and in-place properties of self-consolidating concrete used for casting highly reinforced columns*, ACI Materials, Journal, 98(5), pp. 371-378.

[7] Lachemi, M., Hossain, K.M.A., Lambros, V., and Bouzoubaa, N. (2003), *Development of cost effective self-consolidating concrete incorporating fly ash, slag cement or viscosity modifying admixtures*, ACI Materials Journal, 100(5), pp. 419-425.

[8] Yurugi, M. (1998), *Application of self-compacting concrete in Japan*, Proceedings of the 23rd OWICS conference, CI-Premier, Singapore, pp. 29-42.

The Performance of Self-consolidating Concrete Incorporating Foamed Lightweight Aggregate

Chao-Lung Hwang and Vu-An Tran

Department of Civil and Construction Engineering, National Taiwan University of Science and Technology, Taiwan

Abstract This research examines the effects of foamed lightweight aggregate (FLWA) on the performance of self-consolidating concrete (SCC). Three SCC mixtures were made with three responding types of FLWA produced with/without using foaming agent and surface treatment through cold-boned technique. The slump, fresh unit weight, compressive strength, ultrasonic pulse velocity (UVP), and chloride permeability of SCC specimens were evaluated according to relevant standard. The results showed that fresh SCC mixtures with FLWA exhibit the excellent workability with uniform composition. The fresh unit weight and 56-day compressive strength ranged from 1889 to 2077 kg/m^3 and from 41.0 to 45.4 MPa, respectively. Moreover, the UVP values of all of 28-day SCC specimens exceed 3660 m/s, satisfied durability index of concrete. The chloride permeability of all concrete specimens was either low or very low at 91 days of curing age.

Keywords: *Foamed lightweight aggregate, Cold-bonded lightweight aggregate, Self-consolidating concrete, Chloride permeability, Ultrasonic pulse velocity*.

Introduction

The recent researches have been beginning considerably concern in applications of lightweight concrete (LWC) and self-consolidating concrete (SCC) incorporating cold-bond lightweight aggregate (LWA), meets the needs of construction material in terms of being sustainable and environment friendly, as coarse aggregate. The fresh and oven-dry densities of LWC with cold boned LWA were lower than 2000 kg/m^3 [1]. Using cold-boned LWA with the spherical shape in SCC led to improvement of workability and reduction of superplasticizer (SP) requirement [2]. High performance concrete including cold-boned LWA obtained the compressive strength of 15-38 MPa at 28-day age [3]. Nevertheless, there are a few studies on manufacture of SCC with cold bonded LWA as well as the influences of cold bonded LWA on the performance property of concrete.

This present work concentrated on investigating the properties of SCC incorporating various types of FLWA which produced with/without addition of hydrogen peroxide and surface treatment through cold-bonded technique. The slump and unit weight test were done to assess the behaviors of fresh SCC mixtures. Additionally, the performance of SCC incorporating FLWA were investigated based on the compressive strength, ultrasonic pulse velocity (UPV), and rapid cholride penetration test (RCPT).

Experimental Program

Materials

Hydrogen peroxide was used as the foaming agent for production of FLWA. A combination of sodium silicate and sodium hydroxide was used as the alkaline activator for aggregate production and surface treatment, respectively. Type I cement, Class F fly ash, and ground blast furnace slag (GBFS) used in this study came from local factories, Taiwan. The physical properties of cement, FA and GBFS are as shown in Table I. Moreover, a superplasticizer (SP) was used to control the workability of SCC. In addition, tap water was used as the mixing water. Fine aggregate used to make SCC is crushed sand with density and water absorption of 2650 kg/m^3 and 1.37%, respectively.

Table I. Physical properties of cement, FA and GBFS

Physical properties	Cement	Class F fly ash	GBFS
Fineness (cm^2/g)	3460	3120	4330
Specific Gravity	3.15	2.2	2.86

Preparation of foamed lightweight aggregate

Three types of FLWA were produced with/without addition of hydrogen peroxide and surface treatment through the cold-bonded agglomeration process. A binary mixture of 80% FA + 20% GBFS was used as dry mixtures to produce the FLWA. A procedure of FLWA production was used in previous research [3]. A sprayed solution, occupied 35%-40% total materials by volume and consisted of 50% alkaline solution (molar SiO_2/Na_2O of 1.5) and 50% HP solution, played a role as wetting agent and coagulant to form ball shapes. Fresh particles were maintained at the curing room with a temperature of 23^{0}C and a relative humidity of 60%. On 28-day curing age, sieving process was conducted to select the desired fractions of aggregate in range of 4mm to 10mm as coarse aggregates as shown in Fig. 1. The quality of aggregate H7F8S2-ST was improved by surface treatment which uses alkaline solution with molar SiO_2/Na_2O of 2.5 to pray onto the surface of aggregates. The specific gravity and water absorption of aggregates were determined based on EN 1097-6. Moreover, in this study, particle crushing strength was measured by loading the pellets in a diametrical direction using a CBR testing

machine compliance with suggestion of Li et al. [4]. The properties of different FLWA types were given as Table II.

Table II. Properties of foamed lightweight aggregate

Type of FLWA	Specific gravity	Water absorption (%)	Particle crushing strength (MPa)
H0F8S2	1.46	19.4	5.98
H7F8S2	1.27	25.4	4.81
H7F8S2-ST	1.33	17.5	5.75

Notes: H0: hydrogen peroxide concentration of 0%; H7: hydrogen peroxide concentration of 7%; F8: 80% FA; S2: 20% GBFS; ST: surface treatment.

Manufacturing and tests of self-consolidating concrete

Three SCC mixtures were produced at a water-to-binder ratio (W/B) of 0.3. The densified mixture design algorithm (DMDA) method in which calculates the at least void volume [5] was used to prepare the mix proportions for SCC, given as Table III. SCC mixture was produced based on the mixing procedure suggested in the previous research [3]. Slump and unit weight test of fresh SCC mixtures was done in accordance with EFNARC [6] and ASTM C138, respectively. Furthermore, 100×200mm cylindrical specimens were prepared to evaluate compressive strength under ASTM C39. The UPV and RCPT were measured in accordance with ASTM C597 and ASTM C1202, respectively.

Table III. Mix proportions of self-consolidating FLWA concrete

Mix	Type of FLWA	W/B	Fly ash (Kg/m^3)	Cement (Kg/m^3)	Water (Kg/m^3)	Sand (Kg/m^3)	FLWA (Kg/m^3)	SP (%)
M1	H0F8S2	0.3	158.0	397.0	161.5	787.9	487.3	0.87
M2	H7F8S2		151.4	400.2	160.5	755.1	467.0	0.9
M3	H7F8S2-ST		153.6	399.1	160.8	766.3	473.9	0.86

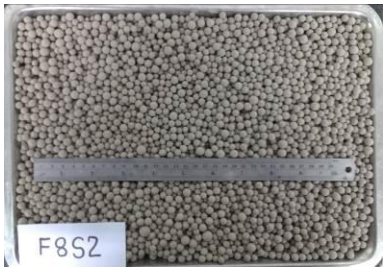

Figure 1. Photographic view of FLWA

Results and discussion

Unit weight and slump test of fresh SCC

The homogenous composition without bleeding and segregation was observed in any fresh mixtures of SCC, as shown in Fig. 2. The result showed that all mixtures of SCC incorporating FLWA indicated the exceptional workability with the slump of 260-280mm and the slump flow of 660-740mm. The best flow between aggregate and paste is offered by the spherical and smooth surface of FLWA [2]. Moreover, the unit weight of fresh SCC mixture ranged from 1889-2077 kg/m^3. The unit weight of the fresh SCC specimen with FLWA that were produced with a foaming agent concentration of 7% (H7F8S2) reduced approximately 9% compared to SCC with FLWA that were produced without a foaming agent.

Figure 2. Slump test of M3

Compressive Strength

The compressive strength of SCC specimens with three different types of FLWA is presented in Fig. 3. As shown, all SCC specimens indicated improved compressive strength with increased time, with the higher long-term compressive strength attributed to the pozzolanic reaction, which affects the paste as well as the aggregate [3]. Compared to 28-day specimens, the 56-day specimens exhibited a increase in compressive strength, in ranged of 5.6-8.6%. As expected, the 56-day compressive strength of SCC specimens produced with H0F8S2, H7F8S2, and H7F8S2-ST were, respectively, 45.4, 41.0, and 44.8 MPa. The SCC specimen M2 incorporating the smallest strength and highest water absorption FLWA had lowest compressive strength. The result reported that it is nearly equal compressive strength between concretes with H7F8S2-ST and concretes with H0F8S2, although the specific gravity of aggregate H0F8S2 was 10.6% heavier than the specific gravity of aggregate H7F8S2-ST. Thus, the water absorption and strength of FLWA are key parameters which affect the strength of SCC. An increase in

compressive strength of SCC was associated with a decrease of water absorption and an increase of strength of FLWA.

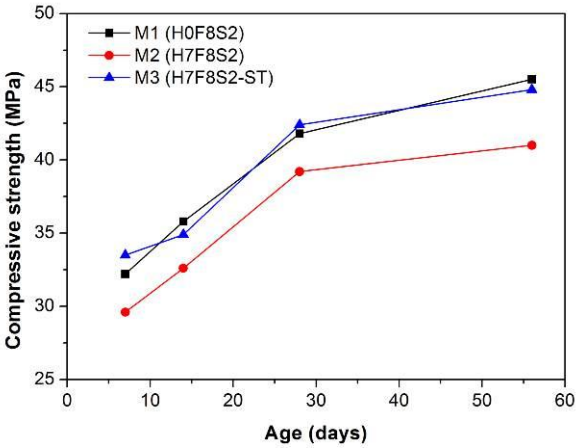

Figure 3. Compressive strength vs curing ages

Ultrasonic Pulse Velocity

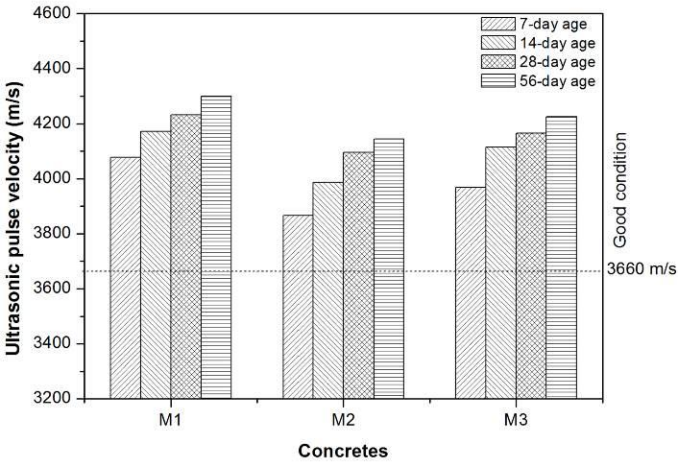

Figure 4. Ultrasonic pulse velocity

According to ASTM C597, pulse velocity method, a nondestructive testing, is done to evaluate uniformity and quality of concrete. Malhotra [7] recommended that concrete are classified as good condition as UPV values ranged of 3660-4575 m/s. The previous research has demonstrated the suitability of using the UPV value to assess the durability of concrete [8-11]. The development of UPV of SCC

specimens is illustrated in Fig. 4. The UPV values of all of the SCC specimens exceeded 3660 m/s by 28 days of age. The UPV values of the 28-day specimens varied from 4095 and 4231.9 m/s. Thus, all specimens were classified as in "good" condition according to Malhotra's proposal. The SCC specimen prepared with aggregate H7F8S2 indicated the lowest UPV value because this aggregate had the highest porosity and water absorption. As expected, The UPV value of the SCC specimens increased with specimen age. Compared to 28-specimens, the UVP values of the 56-day specimens increased in the range of 1.2-1.6%. At long-term age, the denser microstructure of the FLWA and paste due to pozzolanic reaction improves the UPV values.

Chloride Resistivity

The chloride ion penetration is one of key issues concerning the durability of concrete structures. Fig. 5 presents the chloride permeability of SCC specimens with varying FLWA types at 28 and 91 days of curing age. At 28-day age, it was found that charge passed values of SCC specimens ranged from 3522 to 3821 Coulombs (C) which is classified as "moderate" permeability according to ASTM C1202. As expected, the chloride permeability of 91-day specimens deeply decreased due to microstructure improvement of cementitious paste and FLWA. The 91-day passing charges of the SCC specimens made from H0F8S2, H7F8S2, and H7F8S2-ST were, respectively, 1079 C, 1500 C, and 903 C. According ASTM C1203, "low" permeability is classified for SCC mixtures prepared with aggregate H0F8S2 and H7F8S2, while "very low" permeability is classified for SCC specimen produced with aggregate H7F8S2-ST. SCC specimen used surface-treated aggregate H7F8S2-ST was 40% lower than its counterparts with surface-untreated aggregate H7F8S2. The reason for this may be the denser and strong outer shell of FLWA achieved by using surface treatment prevented ion penetration and reduced chloride permeability.

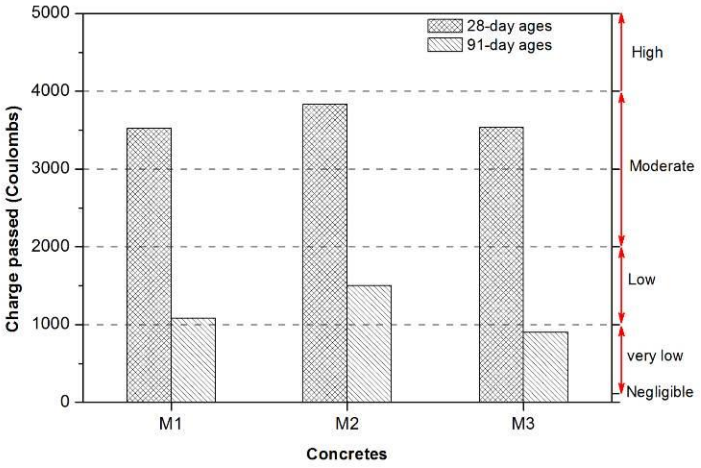

Figure 5. Ultrasonic pulse velocity

Conclusions

The following conclusions can be made based on the findings of this research:
(1) Self-consolidating FLWA concrete indicated the uniform mixtures with various fresh densities in range of 1889-2077 kg/m^3. Additionally, all mixtures of SCC made with three different types of FLWA showed excellent workability with slump, and slump flow in range of 260 to 280 mm, and 660 to 740 mm, respectively.
(2) The 56-day compressive strength of SCC specimens varied from 41.0 to 45.4 MPa. The higher strength of FLWA made the stronger SCC, while an increase of water absorption of FLWA led to reduction of strength of SCC.
(3) The UPV values of the 28-day specimens ranged from 4095 and 4231.9 m/s. A "good" condition was indicated for all of the SCC specimens with FLWA. These mixtures satisfied durability index of concrete.
(4) According to ASTM C1203, all SCC mixtures with FLWA exhibited "moderate" permeability at early age, while the chloride permeability of these specimens revealed the "low" and "very low" rating at later age. Using surface-treated aggegate for SCC mixture showed the improvement of chloride penetration resistivity.

References

[1] Kockal NU, Ozturan T. (2011). *Strength and elastic properties of structural lightweight concretes*. Materials & Design, 32(4):2396-403.
[2] Gesoğlu M, Güneyisi E, Özturan T, Öz HÖ, Asaad DS. (2014). *Self-consolidating characteristics of concrete composites including rounded fine and coarse fly ash lightweight aggregates*. Composites Part B: Engineering, 60(0):757-63.
[3] Bui LA-t, Hwang C-l, Chen C-t, Lin K-l, Hsieh M-y. (2012). *Manufacture and performance of cold bonded lightweight aggregate using alkaline activators for high performance concrete*. Construction and Building Materials, 35(0):1056-62.
[4] Li Y, Wu D, Zhang J, Chang L, Wu D, Fang Z, et al. (2000). *Measurement and statistics of single pellet mechanical strength of differently shaped catalysts*. Powder Technology, 113(1–2):176-84.
[5] Hwang C-L, Hung M-F. (2005). *Durability design and performance of self-consolidating lightweight concrete*. Construction and Building Materials, 19(8):619-26.
[6] EFNARC. (2002). *Specification and guidelines for self-compacting concrete*. http://www.efnarc.org.
[7] Malhotra VM. (1976). *Testing Hardened Concrete: Nondestructive Methods*. American Concrete Institute Monograph Series.
[8] Lafhaj Z, Goueygou M, Djerbi A, Kaczmarek M. (2006). *Correlation between porosity, permeability and ultrasonic parameters of mortar with variable*

water/cement ratio and water content. Cement and Concrete Research, 36(4):625-33.

[9] Hwang C-L, Bui LA-T, Lin K-L, Lo C-T. (2012). *Manufacture and performance of lightweight aggregate from municipal solid waste incinerator fly ash and reservoir sediment for self-consolidating lightweight concrete*. Cement and Concrete Composites, 34(10):1159-66.

[10] Yung WH, Yung LC, Hua LH. (2013). *A study of the durability properties of waste tire rubber applied to self-compacting concrete*. Construction and Building Materials, 41(0):665-72.

[11] Kwan WH, Ramli M, Kam KJ, Sulieman MZ. (2012). *Influence of the amount of recycled coarse aggregate in concrete design and durability properties*. Construction and Building Materials, 26(1):565-73.

Hardening Self-Compacting Mortar Exposed to Gamma Radiation

B. Craeye[1,2], G. De Schutter[3] and I. Gérardy[4]

[1]University of Antwerp, Faculty of Applied Engineering, EMIB Research Group, Antwerp, Belgium
[2]Odisee University College, Industrial Sciences and Technology, DUBiT Research Unit, Aalst, Belgium
[3]Ghent University, Department of Structural Engineering, Magnel Laboratory for Concrete Research, , Ghent, Belgium
[4]ISIB, Engineering Education Institute, Physical an Nuclear Department, Brussels, Belgium

Abstract For the disposal of high level radioactive waste, cementitious barriers are considered worldwide and for various purposes. The Belgian supercontainer concept, for example, considers the use of cylindrical concrete containers: the radwaste is emplaced inside a hardened self-compacting concrete buffer, and for closure of the supercontainer the remaining gap is filled by casting a self-compacting mortar. As a consequence, this cementitious layer is exposed to the radioactive waste and gamma radiation during hardening.
In this research study, small self-compacting mortar samples are irradiated by gamma rays during hardening, and exposed to different doses (Gy) and different dose rates (Gy/h) at different hardening times at first exposure to investigate the cement-waste interactions that might occur during hardening of the cementitious barrier. The effect on the strength and the microstructure is investigated, by means of compressive strength tests, scanning electron microscopy, and nitrogen adsorption tests.
It was found that the observed strength loss due to gamma irradiation increases with an increasing total received dose. Furthermore, the age at which irradiation starts, plays a role in the effect of the gamma irradiation. A link between the strength of the mortar samples and its porosity is found by means of the nitrogen adsorption tests. A higher received dose increases the porosity which leads to a decrease in compressive strength. BET-analysis shows that the specific surface of the pores also increase due to gamma irradiation. Finally, SEM-analysis revealed that gamma irradiation during hardening of cementitious samples affects the microstructure.

Keywords: *Gamma radiation, Self-compacting mortar, Strength, Microstructure.*

Introduction

During fabrication of the supercontainer (Figure 1), the Belgian reference concept, applied for the disposal of vitrified high level waste (HLW) and spent fuel assemblies, the different cementitious layers are exposed to external gamma radiation. Once the buffer is cast and sufficiently hardened out of hot cell and in controlled environment, the radwaste is placed inside the opening of the buffer (construction step performed in radiation blocking hot cell) by means of a waste canister surrounded by a carbon steel overpack, and the remaining gap between this overpack and the concrete buffer is filled by casting a fresh mortar material (the filling: a self-compacting mortar). The self-compacting ability is desired to overcome the difficulty of vibrating the cementitious layer in hot cell, where radiation is present. The composition of the filling is based on the composition of the SCC (self-compacting concrete [1]) used for the buffer [2] and determined using the concrete equivalent mortar method [3]. As a consequence, the filling which is in direct contact with the carbon steel overpack containing the radwaste, will be exposed to gamma radiation during hardening (alpha and beta radiation are blocked by the overpack, the impact of the neutrons can be neglected [4]), with a dose rate inferior to 20 Gy/h [5]. In this paper, two main questions are investigated:

1) What is the effect of gamma radiation on the strength properties of the hardening self-compacting mortar?
2) What mechanisms are responsible for possible strength variations?

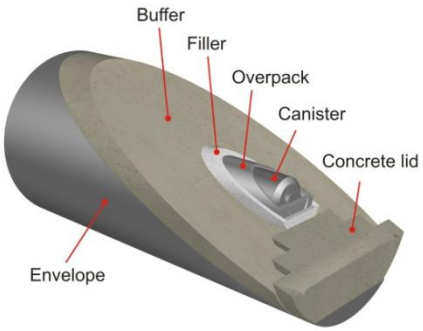

Therefore, a preliminary study is conducted by means of a literature review and a testing program including compressive strength tests, weight loss measurements,

scanning electron microscopy, fluorescence microscopy analysis and nitrogen absorption.

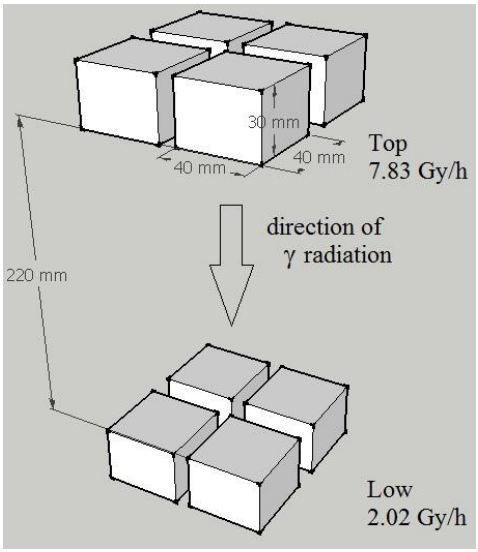

Figure 1 (right). 3D view of the supercontainer for vitrified HLW (C-level waste) [2]

Figure 2 (left). The irradiation test set-up for gamma radiation at the Physical and Nuclear Department of ISIB (dimensions in mm)

Effect of gamma radiation on cementitious materials

Gamma radiation of nuclear safety structures (such as containment buildings, radwaste disposal containers, etc.) can be an important degradation factor of the concrete layers used for these structures. The relevant and available research results concerning the effect of gamma radiation on cementitious materials is rather limited and a summary is given below:

- The most important effect of gamma radiation of concrete is the hydrolysis process (drying process), i.e. the radiolysis of the concrete pore water with a consequential gas production. The reaction product of the water radiolysis, i.e. hydrogen peroxide, can further react with portlandite

present in the cement matrix, forming calcium peroxide. Furthermore, this can lead to a detrimental gas pressure build-up and simultaneous carbonation in the presence of CO_2 present in the air of the pore volume [6].

- Due to gamma irradiation a strength loss of 10 % is found due to changes of the pore structure of the matrix due to carbonation of the hydrated cement paste. Interaction of gamma irradiation with concrete leads to lowering not only its strength, but also its porosity (and other characteristics of pore space)[7].
- Gamma radiation can lead towards altered transport properties and increased carbonation depth [8]. With growing dose (> 1 MGy), enhanced radiolytic dehydration of the samples occurs and formation of microcracks takes place. However, no change of macroscopic properties of the irradiated material is found.
- The use of blast furnace slag cement can lead towards additional ettringite formation [9], and therefore the use of Ordinary Portland Cement is preferred.
- Irradiadition enhanced alkali-aggregate reactions (AAR) and an increase of volume of the aggregates was noticed in case high amounts of SiO_2 aggregates were used [10]. Therefore, the use of limestone is preferred to overcome AAR due to gamma rays [11].
- Gamma irradiation of hydrated cement paste leads to an accelaration of the 'natural' carbonation process driven by diffusion, only taking part in the surface layers of the samples. In addition, also independent radiation-induced carbonation due to gamma rays was found due to gas containing CO_2 which is produced due to gamma irradiation of the hydrated cement paste, and taking part in the entire sample [12]. Due to these two carbonation processes, CO_2 reacts with portlandite with calcite as a product. The arisen crystals of calcite grow through the pores of the hydrated cement paste, decreasing their diameter and hardening the material.

In most cases (except for [7, 11]), the effect of gamma radiation is negligible on behalf of alteration of mechanical properties or was not investigated. It must be mentionned that the total dose rates applied in these studies are rather high (> 200 Gy/h) compared to the estimated dose rate in the supercontainer concept (up to 20 Gy/h [4]). Moreover, these test results and conclusions are based on the radiation of hardened samples: the conrete or mortar samples have an age of 28 days or more at the first time of appliance of gamma irradiation.

Testing procedure

Composition of the self-compacting mortar (the filling)

The experiments are performed on self-compacting mortar samples, where radiation enhanced strength alteration is investigated, with limited size for the sake of homogenous irradiation throughout the whole sample. The mix design of three mortar compositions, with altered W/C-W/P-C/P-ratio, is listed in Table 1. The SCC1 mortar composition is derived from the composition of the self-compacting concrete for the buffer [2] by using the equivalent mortar method (MBE, [3]).

Table 1. Mortar composition of SCC0-SCC1-SCC2 (in kg/m³)

Component	SCC0	SCC1	SCC2
Cement CEM I 42.5N LH LA HSR	512	470	-
Cement CEM III/A 42.5N LA	-	-	470
Limestone filler	146	329	329
Crushed calcareous sand 0/4	1327	1410	1410
Superplasticizer (PCE)	14	4	5
Water	245	353	353
W/C	0.48	0.75	0.75
W/P	0.37	0.44	0.44
C/P	0.78	0.59	0.59

Sample preparation, fresh properties

First the dry components (calcareous sand, limestone filler and cement, in order of appearance) are added to the mixer (type: Hobart) and mixed with a rotational speed of 140 rpm for 30 seconds. Subsequently, the water is added to the blended dry components and the mixing continues for another 60 seconds at 140 rpm. Finally, superplasticizer (polycarboxylic ether PCE) is added, and an additional 60 seconds of mixing time (285 rpm) is supplied, totalizing a mixing time of 150 seconds. For each batch, 1 dm³ of mortar is mixed and the rheology of fresh mortar is characterized by means of the slumpflow value, by using the mini-cone.

Curing conditions and gamma rays exposure

Immediately after casting, the samples are irradiated. Two types of radiation sources are used in this test program:

- Irradiation by means of a ^{60}Co source (Jupiter C, Barzetti), with gamma energy level of 1.17 MeV and 1.33 MeV and an activity of 2 TBq. It generates gamma radiation with a dose rate up to 10 Gy/h. This type of radiation is applied to investigate the effect of cement-waste interactions in case of low dose rates (e.g. for the disposal of radioactive waste).
- Irradiation by means of a ^{137}Cs source, with an energy level of 0.662 MeV and an activity of 25 _ 8.5 TBq which generates gamma radiation with dose rates up to 2000 Gy/h. This type of radiation is applied to investigate the effect of cement-waste interactions in case of high dose rates.

For the low dose irradiation investigation, the samples are placed at two different levels (e.g. Figure 2). To quantify the total applied dose and the applied dose rate, dosimeters with radiochromic film (Gafchromic EBT, thickness of 234 mm) are placed at each level. For the samples at the level closest to the source a dose rate of 7.11-7.83 Gy/h is registered, whereas for the samples at the level underneath, the applied dose rate is 1.75-2.02 Gy/h.

For the high dose irradiation investigation, the samples are placed at one level, with a dose rate of 1360e2000 Gy/h, determined by means of Gammachrome YR dosimeters.

Note that for each batch, a number of samples remain unirradiated as a reference, but conserved at the same environmental conditions, thus with identical temperature and relative humidity as the irradiated samples. The samples have the same maturity and saturation degree, meaning: the gamma radiation dose and dose rate are the only influencing parameter.

Test methods

By means of these low and high dose rate investigation it is studied whether (i) gamma radiation has an effect on the mechanical properties of the mortar, (ii) gamma radiation affects the microstructure of the mortar, (iii) irradiation related parameters (received dose, applied dose rate, radiation time, and mortar age/maturity at first irradiation) alter the obtained results and (iv) mortar related properties (cement type, water-to-cement ratio) have an influence.

After 28 days of hardening, the compressive strength of the samples is determined to evaluate the effect of gamma irradiation on the strength of the hardening self-compacting mortar. Therefore, the samples are placed inside an Amsler compression testing machine. The relative strength loss is expressed in function of total dose of radiation received (expressed in Gy). The relative strength loss D_f of the irradiated samples. This can be found by using Equation (1):

$$D_f = (1-f_{irr}/f_{ref})\cdot 100\% \quad (1)$$

where: f_{irr} is the compressive strength of the irradiated morta sample (MPa), f_{ref} is the compressive strength of the un-irradiated reference mortar samples (MPa).

Also the volumetric weight of the hardened samples is determined to estimate the weight loss and drying of the samples due to gamma ray exposure.

Thin section are made to investigate the effect of gamma radiation on the self-compacting mortar on a microscopic level, using fluorescence microscopy analysis according to the Nordtest Method (1991). Furhermore, scanning electron microscopy is performed by means of a JEOL JSM-5510 with microscope resolution of 3.5 nm and energy level between 0.5-30 kV for visualisation.

By means of nitrogen adsorption porosimetry, the pore size can be determined using the Barrete-Joynere-Halenda (BJH) method which allows the determination of the pore size distribution in mesopore range from the desorption part of the isotherm [13]. A Micromeritics Tristar 3000 equipment has been used in this work to perform the measurements.

Results and Discussion

The uniaxial compressive strength and the density were determined on small samples of both irradiated and un-irradiated samples. Overall, it is found that a strength loss is found, and the strength reduction D_f increases with increasing absorbed dose (Figure 3). The scatter on the results is, however, too wide to establish a reliable predictive model. Nevertheless, 75% of all tests resulted in a strength reduction higher than 5%. Gamma irradiation clearly has a negative effect on the strength of hardening self-compacting mortar. In all cases, except one, the strength reduction D_f is accompanied by a reduction in density between 0.2% and 2.9%, however no correlation was found between strength loss and density reduction.

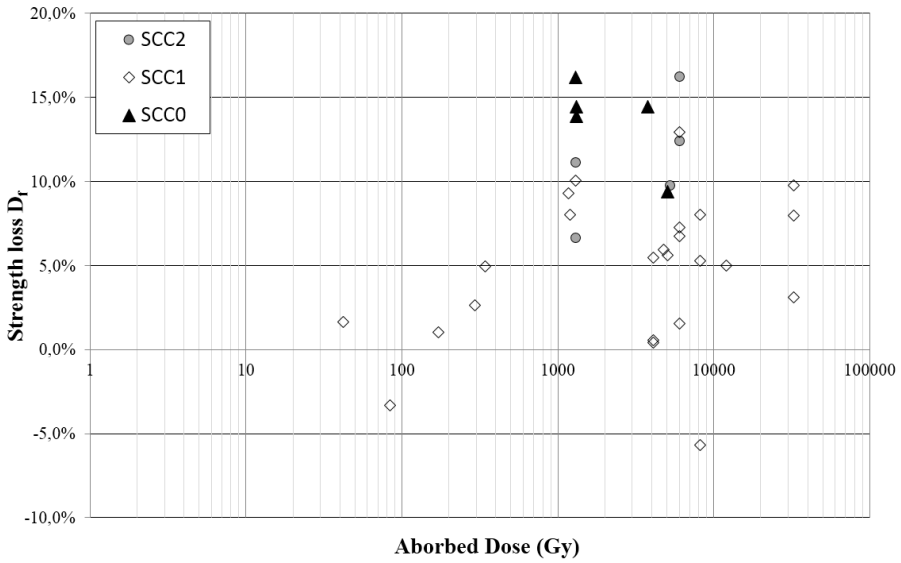

Figure 3. Strength loss vs. Absorbed dose of irradiated samples

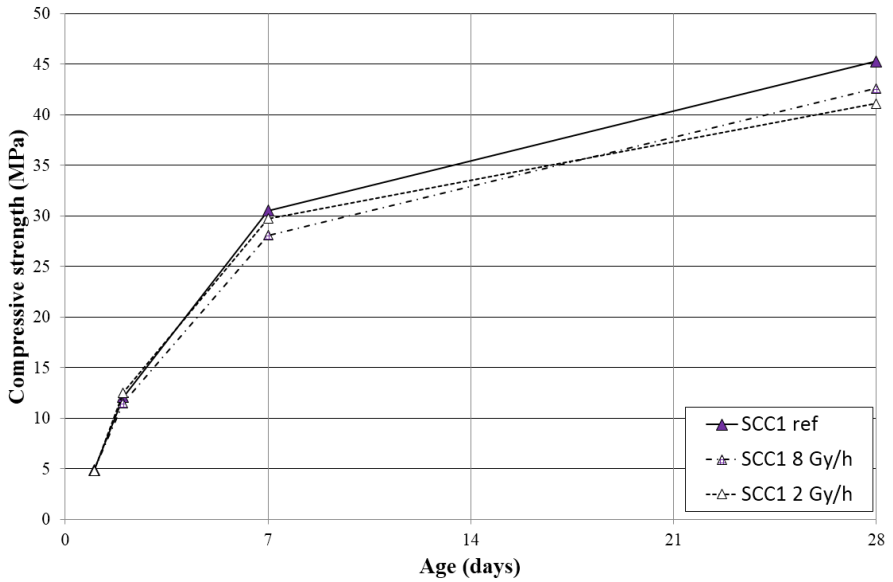

Figure 4. Evolution of compressive strength and effect of radiation

It is found that gamma radiation influences the strength development of the self-compacting mortars (Figure 4): the compressive strength evolves towards a lower 28-day value due to increased dose rates and absorbed doses.

By means of nitrogen absorption tests and fluorescence microscopy analysis the microstructure of irradiated an unirradiated samples is compared. Mainly the desorption pore volume of irradiated samples is higher compared to the reference samples, linked with the applied dose rate (Figure 5). This explained the previously found compressive strength loss and reduction in density.

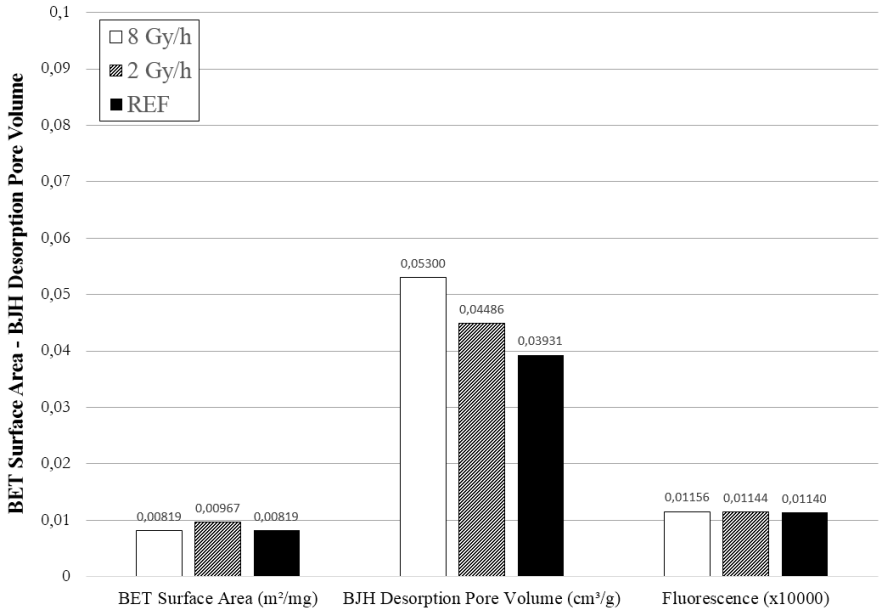

Figure 5. Quantification of the mortar's microstructure (low dose rates)

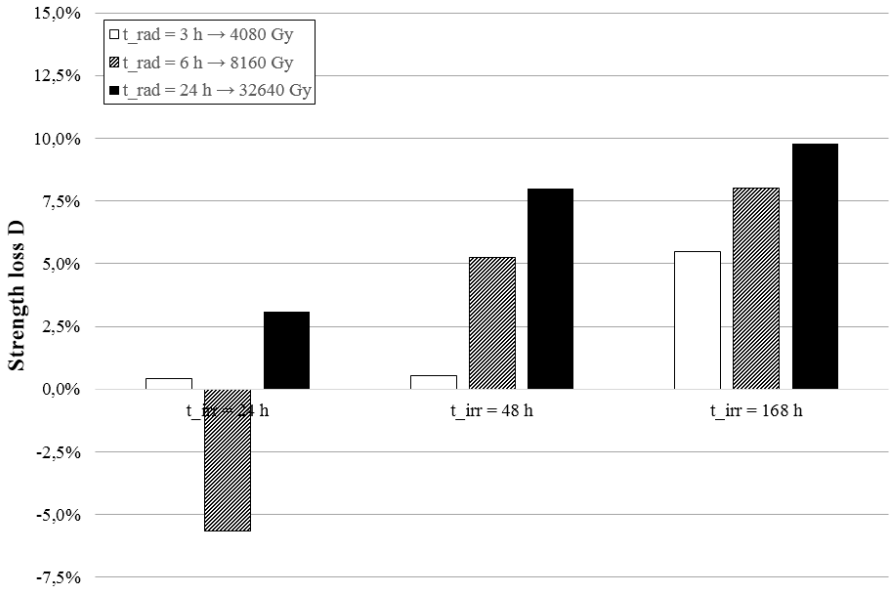

Figure 6. Effect of radiation duration and age ate first radiation (high dose rates)

It was already mentioned that the strength loss due to gamma irradiation increases with increasing the absorbed radiation dose. In case low irradiation dose rates (<10 Gy/h) are applied, the age of the concrete at which irradiation starts does not have a significant effect on D_f. However, in case high dose rates are applied (>1000 Gy/h) a certain trend is found: the older the concrete at which irradiation starts (i.e. higher t_{irr}), the higher the observed strength loss (Figure 6).

Compared to SCC1, the type of cement is changed for SCC2: blast furnace slag cement is used instead of Portland cement. The use of blast furnace slag cement has a significant effect on the strength reduction D_f, especially for medium to high irradiation dose rates. By means of SEM-analysis it was found that due to gamma irradiation, needle formation occurred in the mixes containing blast furnace slag (CEM III/A, Figure 7). These needles are most likely ettringite ones ($C_3A.{}_{3CaSO4}.32H_2O$), in accordance with the findings of [9]. The decrease in strength can be related to the formation of expansive ettringite, which causes internal microcracking within the mortar microstructure.

In case a lower water-to-cement ratio is applied, a higher strength reduction is also found. Fluorescence microscopy analysis indicates that the capillary porosity is not significantly affected. As mentioned by [6] gamma radiation of cementitious materials is linked with radiolysis of the pore water, meaning part of the free water will evaporate and can no longer take place in the hydration process. As a consequence, not enough free water is available to react with all cement, leaving

unhydrated cement particles into the matrix, which can lead to an increase in strength loss.

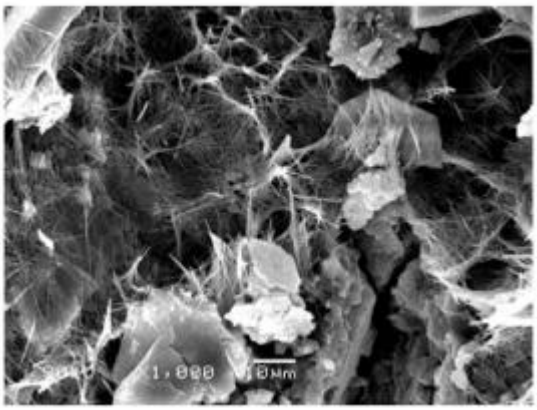

Figure 7. Needle formation after irradiation of samples containing blast furnace slag

Conclusions

Based on an experimental programme, the following conclusions have been obtained:
(1) Gamma radiation during hardening of cementitious materials negatively affects the strength development. The higher the absorbed dose of radiation, the higher the strength decrease will be.
(2) Due to gamma radiation, the porosity (nano, micro and capillary) and pore volume increases. Lowering the water-to-cement ratio and using blast furnace slag cement instead of Portland cement, worsened the above mentioned phenomena.
(4) The total absorbed dose and the age of the concrete at which irradiation starts also influences the strength development.

References

[1] De Schutter, G., Bartos, P., Domone, P., Gibbs, J. (2008), *Self-Compacting Concrete*. Whittles Publishing, Caithness, UK, pp. 296.
[2] Craeye, B. (2010), *Early-age thermo mechanical behavior of concrete Supercontainers for radwaste disposal*. Doctoral thesis, Magnel Laboratory for Concrete Research, Ghent University, Belgium, pp. 376.

[3] Schwartzentruber, A., Catherine, C. (2000), *Method of the concrete equivalent mortar (mortier de béton equivalent, MBE): a new tool to design concrete containing admixture*. Materials and Structure 33(8), p. 475-482.
[4] Wickham, S.M., Bennet, D.G., Galson, D.A. (2005), *Belgian Supercontainer design for HLW and SF disposal: evaluation of the reference design*. Galson Sciences Limited, report no 0460-5, version 1.0, pp. 98.
[5] Poyet, S. (2007), *Design of the ONDRAF/NIRAS Supercontainer concept for vitrified HLW disposal in Belgium: study of the thermo-hydrological behaviour of the concrete buffer*. Rapport CEA, RT DPC/SCCME/07-741-7.
[6] Bouniol P. (2004), *State of knowledge on radiolysis of pore water inside cement medium for waste containment and the approach via simulations*. CEA report (in French), R-6069, pp. 120.
[7] Vodák, F., Trík, K., Sopko, V., Kapicková, O., Demo, P. (2005), *Effect of gamma irradiation on strength of concrete for nuclear-safety structures*. Cement and Concrete Research 35, p. 1447-1451.
[8] Bar-Nes, G., Katz, A., Peled, Y., Zeiri, Y. (2008), *The combined effect of radiation and carbonation on the immobilization of Sr and Cs ions in cementitious pastes*. Materials and Structures 41(9), p. 1563-1570.
[9] Richardson, I.G., Groves, G.W., Wilding, C.R. (1990), *Effect of gamma irradiation on the microstructure and microchemistry of ggbfs/OPC cement blends*. Proceedings of the Materials Research Society Symposium 176, p. 31-37.
[10] Morigani, S. (1997), Preprint East Asia Alkali-Aggregate Reaction Seminar. Tottori, Japan.
[11] Ichikawa, T., Koizumi, H. (2002), *Possibility of radiation-induced degradation of concrete by alkali-silica reaction of aggregates*. Journal of Nuclear Science and Technology 39 (8), p. 880-884.
[12] Vodák, F., Vydra, V., Trík, K., Kapicková, O. (2011), *Effect of gamma irradiation on properties of hardened cement paste*. Materials and Structures 44(1), p. 101-107.
[13] Barrett, E.P., Joyner, L.G., Halenda, P.P. (1951), *The determination of pore volume and area distributions in porous substances*. I. Computations from nitrogen isotherms. J. Am. Chem. Soc. 73 (1), p. 373-380.

Jobsite Experiences from a Tunnel Restoration with Freeze-Thaw-Resistant SCC

Florian V. Mueller[1]

[1]IMP Bautest AG, Hauptstrasse 591, CH-4625 Oberbuchsiten, Switzerland

Abstract Experiences are shared from a jobsite with medium flowable self-consolidating concrete, i.e. class SF2 according to EN 206-9, containing air to ensure freeze-thaw-resistance, and aggregate size up to 16 mm. After difficulties in obtaining a homogenous hardened concrete while focusing on the slump flow value alone, standard fresh concrete tests were performed, revealing the missing balance of flowability (yield stress or slump flow value) and inner resistance against dynamic segregation in terms of plastic viscosity. The application of the rheograph, approximately transformed in terms of standard one-point-rheology results, such as slump flow value, time to reach a spread of 500 mm, or V-funnel flow time, correlated very well with experiences on the jobsite. Here, some mixtures resulted in severely segregated surfaces in hardened concrete, while others did not achieved sufficient self-compactability in the fresh state and the form filling had to be supported. The example reflects the responsibilities the involved parties (i.e. planning engineers, contractors, and concrete producers) have, when SCC is planned to be used at a jobsite.

Keywords: *Self-Consolidating Concrete, Testing, Segregation, Responsibilities.*

Introduction

After self-consolidating concrete (SCC) was developed in the late 1980s [1, 2], the concept has spread around the world by scientists and industry and adapted for local requirements [3, 4, 5]. Tests of fresh concrete properties have been developed [6] and standardized [7, 8]. In Europe, SCC was included in the concrete standard EN 206 as part 9. The countries, in which the European Standards are applied, adapt the European document for national requirements. Thus, the Swiss National Amendment EN 206-9:2009 in Switzerland, where the reported example took place.

In Switzerland, SCC seems to be known by the industry and the engineers in a rather general way, and it is used only as a special concrete in ready mix

applications and the precast industry. Very often, the mix designs are established by admixture companies, not by the concrete producer themselves.

Project Description

The example discussed here pertains to the restoration of a two lane tunnel in Switzerland. The exact place will remain undisclosed. The authors' employing company assisted the construction to test the fresh concrete properties, including the air content, density, water content, and slump flow value (SF). Other tests, typically used for SCC, were not demanded. Within this restoration process, a cover layer of concrete had to be cast with a thickness of approximately seven centimeters. This layer also contained conventional reinforcement bars. The concrete was described according to SN EN 206-9 by: C25/30 (SCC) XC4 (CH) XF2 (CH) XD3 (CH). In order to ensure the moderate enhanced freeze-thaw-resistance required by exposition class XF2, it was decided to use air-entrained concrete, as it is common in Switzerland. A maximum aggregate size of 16 mm had to be used in the concrete. Depending on the stage size, the concrete mold contained one or two filling gaps of about 40 x 5 cm each, located at the top of the mold in about 2 m height, and corresponding openings to release the air ("chimney"). The concrete was released from the concrete truck into a concrete hopper which was mounted on a wheel loader, which was brought to the individual section. Here, the concrete had to fill a mold section of about 6 to 9 m length. For one day's concreting work, one truck was ordered that had to wait at the construction side in order to release batches of concrete as needed. The total emptying of the truck took about one to two hours.

Problem Description

During the execution of the first lane's restoration in the first year, no complications occurred with the concrete. The second year's concrete casting started with the same combination of companies involved, but the concrete differed somewhat yielding four different visual peculiarities (see Fig. 1):

1. Formation of considerable pile figures below the filling spots
2. Formation of severe bleeding marks
3. Formation of foamed mortar layers
4. Formation of sedimentation layers

Figure 1: Example of aggregate pile (middle), bleeding marks (left chimney and bottom)

Case Description

After the molds of the first batching days were opened, the above described visual peculiarities were revealed and the owner questioned the quality of the work. Both the concrete producer and the constructor had no explanation for this remarkable result. The author proposed to extend the testing program beyond the, rather basic, fresh concrete tests originally ordered, and to test the fresh concrete properties that define the suitability of the SCC for the specific application. In the case discussed here, SF was extended by other one-point-standard tests according to SN EN 12350-i, such as flow time T_{500} and V-funnel discharge time. This was done not only as an acceptance test at the beginning of the casting, but the mixture was closely monitored (and measured if necessary) at each time a single batch was released from the truck. Throughout these measures, the contractor was enabled to reject a delivery at any time the major parameters of air and flowability were found to be outside the specified range. In some deliveries for instance, a severe foaming was identified after a few hoppers were released, see Fig. 2. In cores drilled into the construction, the void system visible in the depth of the structure did not meet the expectations one has on the appearance of a self-compacting concrete, see Fig. 3.

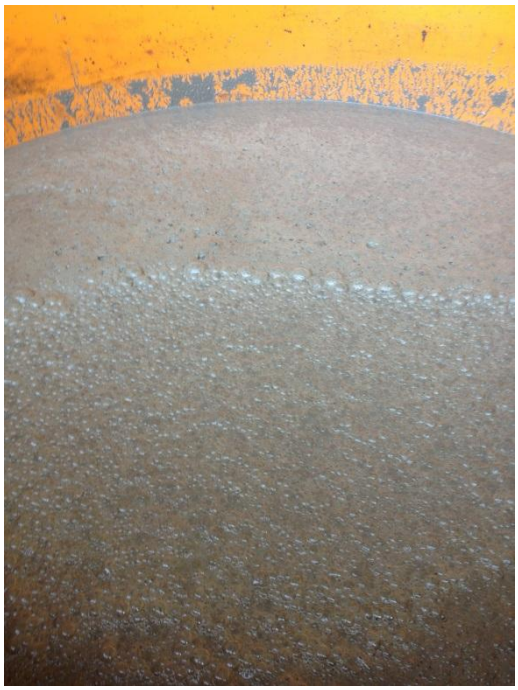

Figure 2: Example of foam formation in batch no. 3 of one truck delivery

Figure 3: Borehole (image turned 90°), with voids inside the structure

Results

The fresh concrete properties of SCC differ considerably to those of conventionally vibrated concrete (CVC). Not only do the number of standard parameters that are relevant for casting increase from two in CVC (w/b and air) to about six (w/b, air, yield stress, plastic viscosity, blocking, static segregation), but it is also different parameters that need to be considered. While the consistency of CVC can be measured with one value only (i.e. slump value, flow value, degree of compaction), the "consistency" of SCC consists of a combination of parameters that describe flowability and inner resistance against deformation. At this point, the comment might be allowed that the use of the word "consistency" in the context with SCC can be easily misleading in practice as, opposed to CVC, SCC cannot be described by one single consistency parameter. In future concrete standards it might be better to differentiate the consistency of CVC and the rheology of SCC. If a measurement of yield stress and plastic viscosity cannot be obtained at the same time in a rheometer device, which is usually the case in practice, these parameters need to be described as best as possible in so called "one-point-tests", which are standardized in EN 12350-i (i= 7-12) for instance, and then their data combined in a useful manner. Here, one is advised to extract as much data as possible from one test. For

instance, by measuring not only the slump flow value, but also the flow time T_{500}, and to apply the visual stability rating systems available, e.g. Visual Stability Index (VSI) according ASTM C 1611, Bui's Penetration test standardized in ASTM C1712-09 [9, 10, 11, 12] or Mueller's Aggregate Surface Appearance Index ASAI [13].

The appearance of the visual peculiarities in this case implied not only a lack of dynamic stability but also a lack of stable air-entrainment. Since for the first properties, the rheology parameters are out of balance, one needs to test both determining rheology parameters, in addition to testing the influencing mixture parameters, i.e. air and w/b. The optimum stable SCC areas in a rheograph [14] (Fig 4) can be approximated [15, 16] into a graph applying SF and a viscosity term, e.g. T_{500} (see Fig. 5).

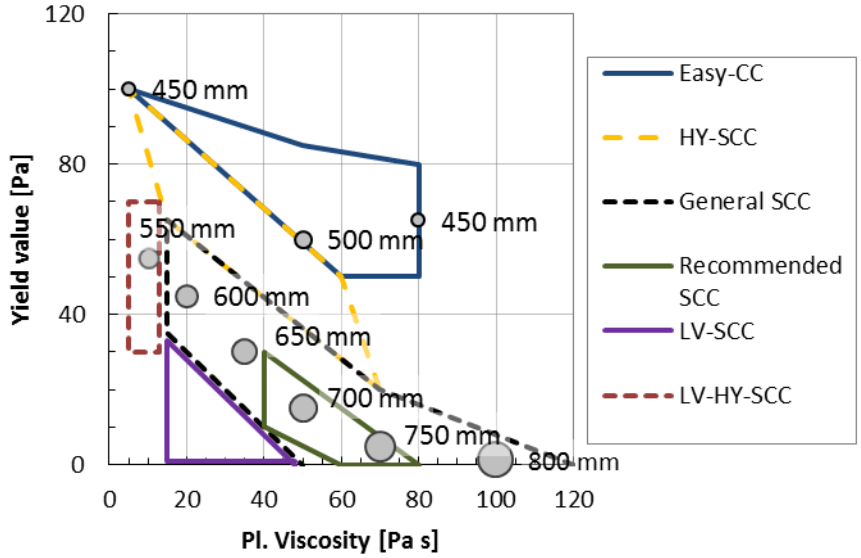

Figure 4: Rheograph, optimized for various SCC and applications [14]; corresponding approximated SF are added by the author according [13, 15]

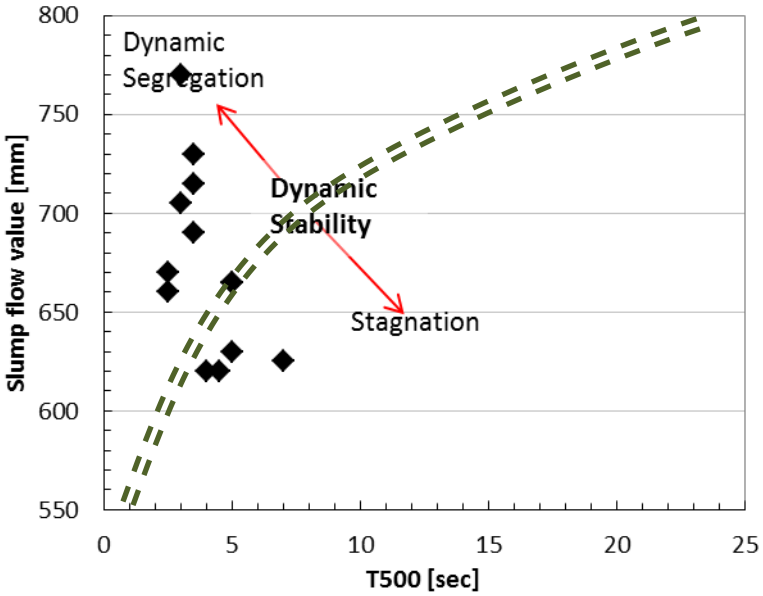

Figure 5: Case data in a, for SF and T_{500}, modified rheograph

To estimate the viscosity of a relatively low-viscous SCC, as was the case and is very common in Switzerland or elsewhere natural round aggregates are used, one should focus on the V-Funnel time (T_V), whole also keeping in mind the impact potential segregation has on the discharge time, see Fig. 6 to Fig. 9. In such case, the time T_{500} establishes too small values in a range where the measurement technique already starts to influence the result. Nevertheless, T_{500} already serves as a reasonable first indication of the viscosity's order of magnitude. Both values T_{500} and T_V have less correlation with the plastic viscosity [17, 18, 15] than SF and yield stress [13, 16], but they are the only values from standardized field test procedures available at the moment. Since both parameters are affected by several aspects of the test procedures, and also by the stability of the mixture, there is only a weak correlation between T_{500} and T_V (Fig. 10).

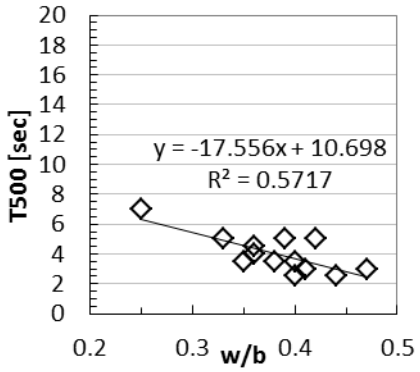

Figure 6: T_{500} versus w/b

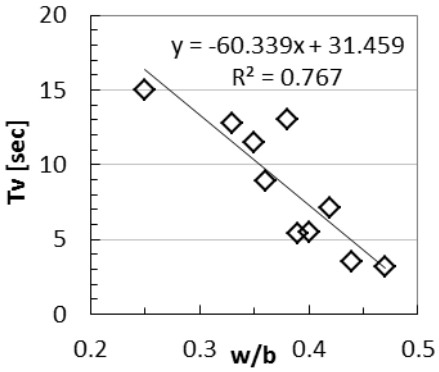

Figure 7: T_V versus w/b

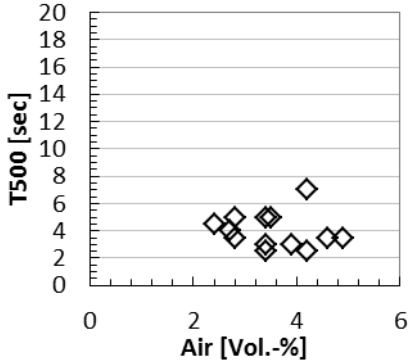

Figure 8: T_{500} versus air content

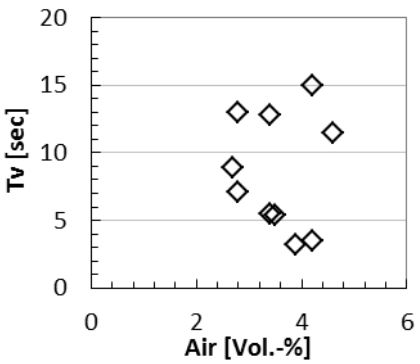

Figure 9: T_V versus air content

The average SF was 674 mm with a standard deviation of 45 mm. The majority of these parameters satisfy the condition of EN 206-9 for class SF 1 (550 to 650 mm) and SF 2 (660 to750 mm). The standard deviation was below the allowed maximum deviation for SF as a target value of less than 50 mm. Since it is actually the relation of rheology parameters that determine a stable flow and self-compacting properties, the application of the standard for each parameter individually, but without connection, contains the risk of failure. Most of the mixtures below class SF2 actually performed well, as long the viscosity was not too high. In contrast, many of the mixtures that satisfied the tendered conditions actually lacked dynamic stability, which could clearly be noticed in the hardened concrete.

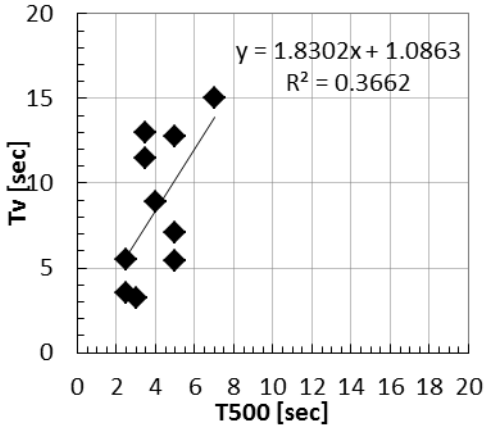

Figure 10: Relation of T_V and corresponding T_{500}

Final Remarks

When SCC is planned to be used, all parties involved need to have a clear understanding of their role and responsibilities, as well as what measures must be taken and what actions have to be prohibited in order to ensure the required hardened concrete properties are met.

The planning engineers are advised to collaborate with the executing constructor in order to not demand concrete parameters in fresh state that negatively affect the placement technique or final result. The successful form filling with a dense concrete depends on both the material parameters (rheology) and the placement technique for a given mold. Opposing parameters should be prevented to be fixed already in the tender documents, unless they are experienced and have already optimized the mix design to meet different requirements, both in the fresh and hardened state.

The constructor is advised to evaluate the concrete mix design considering the effect different design parameters have on rheology [14] and hardened concrete properties. Also, the requirements of the construction process and placement technique have to be considered. Then, the right concrete can be ordered, that fulfills the most critical parameters, which might be different than the engineering properties originally required.

The concrete producer is advised to actually know his concrete and its robustness, as it is suggested in EN 206-9 by chapter 9.5. and its appendix A. This includes a full test scenario in the development phase, including a robustness test where key parameters, such as air, water, admixture content, are altered by purpose and their

effect on fresh and hardened concrete properties are evaluated. In the development phase of a mixture it is important to obtain all rheology parameters necessary to describe the properties of the concrete and its stability. Using only the slump flow value is certainly not an advisable approach. If a customer specifies only a few parameters, such as air content and slump flow value, for instance, there are other intrinsically associated parameters that needs to be tested to ensure static and dynamic stability and a reasonable filling ability. One may not expect the fulfilment of rigid requirements when these are not specifically specified, but control of dynamic and static segregation under simple conditions must always be obtained.

References

[1] Ozawa K., K. Maekawa, M. Kunishima, and H. Okamura (1989), In: Proceedings of the second East-Asia and Pacific Conference on Structural Engineering and Construction (EASEC-2), vol. 1, pp. 445-450
[2] Okamura; H. and Ozawa, K. (1995), Concrete Library of JSCE, vol. 25, pp. 107-120
[3] Japanese Ready-Mix Concrete Association (1998), JRMCA Tokyo
[4] Japanese Society of Civil Engineers JSCE (1999), Translation published as appendix to proceedings of "SCC 2001" in Kochi, Japan
[5] SCC European Project Group (2005)
[6] De Schutter, Geert (2005), Report Growth Contract No. GRD2-2000-30024 "Testing-SCC", 24 p.
[7] SN EN 12350 - 06 to 12: 2010
[8] ASTM C ASTM C1611 /C1611M-09b
[9] Bui, Van K., Montgomery, D., Hinczak, I., and Turner, K. (1998), In: Proceedings of the Fourth CANMET/ACI/JCI International Conference on Recent Advances in Concrete Technology, Tokushima, Japan, ACI SP 179-6, pp.85-103, V.M. Malhotra (Ed.)
[10] Bui, V. K., Montgomery, D., Hinczak, I., and Turner, K. (2002), CemConcRes, vol. 32, n.9, pp. 1489-1496
[11] Bui, V. and Attiogbe E. (2008), In: Proceedings of Third North American Conference on the Design and Use of Self-Consolidating Concrete "SCC 2008", Chicago, Illinois, paper No. 1225, ACBM
[12] ASTM C1712-09
[13] Mueller, F.V. (2012), PhD Thesis, Reykjavik University
[14] Wallevik, O.H. and Wallevik, J.E. (2011), CemConcRes, vol. 41, n. 12, pp. 1279-1288
[15] Mueller, F. V. (2009), MSc Thesis, Reykjavik University
[16] Mueller, F.V., Wallevik, O.H., and Khayat, K.H. (2014) In: Proceedings - of "Eco-Crete", pp. 217-224
[17] Koehler, Eric P. (2007), PhD Thesis, University of Texas, Austin
[18] Esping, Oskar (2007), PhD Thesis, Chalmers University of Technology, Goteborg, Sweden

Effect of Fly Ash on Resistance to Chloride Ion Penetration of SCC under Abrasion

Surong Luo[1,2], Wenda Wu[1,2], Yong Li[1,2] and Jianlan Zheng[1,2]

1College of Civil Engineering, Fuzhou University, Fuzhou, Fujian, 350116 China
2Fujian Province Collaborative Innovation Center for Environmentally Friendly and Energy Saving High Performance Concrete, Fuzhou, Fujian, 350108 China

Abstract The failure mechanism of marine structures such as ports, dams and bridges is more complex than that of ordinary structures due to their long-term exposure to a detrimental chlorine and sulfur environment created by seawater. With reference to the ASTM 1202 standard, electric flux test is carried out to investigate the effect of fly ash addition, curing age and abrasion on the resistance to chloride ion penetration of self-compacting concrete (hereinafter referred to as SCC) under abrasion impact. The results show that the resistance to chloride ion permeability of SCC under abrasion condition is improved with the increased addition of fly ash and the increase of curing age, and the electric flux of SCC decreases with the increase of curing age when abrasion is not applied. It is also found that no matter how long the curing age was (28 or 60 days), the electric flux of SCC increases due to abrasion, and the electric flux of SCC also increases as fly ash content increases.

Keywords: *Self-compacting concrete, Abrasion condition, Fly ash, Age, Turing age, Resistance to chloride ion penetration.*

Intruction

The service life of structures in corrosive coastal environments has always been a great concern [1-3] because of the fact that corrosion damage of concrete structure caused by chloride penetration is among one of the causes of the deterioration of concrete structures around the world.

Statistics show that the loss due to corrosion damage caused by chlorides in the environment in concrete structures has made up 2-4% of the national gross product in some coastal countries [4-6].

A considerable amount of researches concerning the resistance to chloride ion permeability of concrete have been conducted [7-8]. Studies have shown that the coupling of marine environment and chloride ion environment could cause both erosion damage and chlorine ion erosion damage to the protective concrete layer in concrete structures, resulting in the failure of concrete protective layer eventually [9-11].

The mechanism of chloride ion penetration, factors that influence chloride ion penetration in concrete and tested proposals to improve the resistance to chloride ion penetration of SCC are addressed in this paper.

However, certain aspects of the field still need to be ascertained and they are listed as follows:

(1) Numerous researches on the resistance to chloride ion penetration of ordinary concrete have been carried out already, while the corresponding performance of SCC is rarely investigated. In addition, SCC is normally produced with mineral admixtures and superplasticizer depending on the environment conditions and thus different from normal concrete. Therefore, it is necessary to conduct research on the resistance of chloride ion penetration of SCC.

(2) There is no unified method to examine concrete chloride ion penetration hitherto. Current test methods to test chloride ion penetration in concrete are ion diffusion coefficient method (Chloride natural diffusion test and chloride ion migration assay) and electrical parameter method (Method of DC and AC measurement method and a saturated salt concrete conductivity method), and each condition requires a different kind of test method.

It has been discovered that the resistance of chloride ion penetration of concrete is affected by many factors, and for marine concrete structures the curing age of concrete, the mineral admixtures in concrete mix and the abrasion undertook by concrete are three of the most important factors. Therefore, at the beginning of the project, the impact of these three factors on the resistance of chloride ion penetration of SCC is investigated.

Materials used

Cement

Ordinary Portland cement PO 42.5 was used to produce SCC, and the physical properties and chemical composition are presented in Table I.

Fly ash

The fly ash was dry and uncompact powder produced by Houshi coal-fired electric power station with grade II quality according to Chinese standard GB/T 50146-2014. The physical properties and chemical composition are shown in Table I.

Table I. Physical properties and chemical composition of cement and fly ash

Physical properties	Cement	Fly ash
Specific surface (cm^2/g)	3720	2600
Apparent density (kg/m^3)	3080	2230
Degree of fineness (%)	0.6	-
Chemical composition (%)		
CaO	59.45	2.18
SiO_2	17.64	55.61
Al_2O_3	4.89	25.95
Fe_2O_3	3.83	6.69
SO_3	2.99	0.64
MgO	2.41	3.38
K_2O	1	1.02
Na_2O	0.3	1.15
LOSS	7.49	3.38

Aggregate

Coarse aggregate came from crushed granite with maximum size of 20 mm, and natural river sand with fineness modulus of 2.23 and apparent density of 2685 kg/m^3 was adopted as fine aggregate.

Superplasticizer

Polycarboxylate superplasticizer with high water-reducing ration was used in this study.

Experiment

Mixture proportions

Mixture proportions of concrete mixes are shown in Table II, from which it can be observed that the water-binder ratio was 0.34, the amount of cementitious material was 540kg/m3, and the fly ash occupied 0-60% of cementitious material by weight as cement replacement.

Table II. Mix proportions (kg/m^3)

Mix no.	Cement	Fly ash	Water	Sand	Coarse Aggregate	Superplasticizer (%)
SCC-1	540	0	184	788	888	5.4
SCC-2	426	107	182	778	876	5.4
SCC-3	371	159	180	773	871	4.86
SCC-4	316	210	179	767	865	4.32
SCC-5	261	261	178	763	859	4.32
SCC-6	208	312	177	758	854	4.32

Test method

Abrasion

Based on SL352-2001, the test apparatus to carry out the abrasion resistance of concrete was designed (see Figure I) and produced by by Tianjin Gangyuan Test Instrument. To create abrasion on concrete sample which is at the bottom of steel container, steel balls were placed on top of the concrete and then motivated to attack the surface of concrete when the water in the steel container was rotated by the impeller.

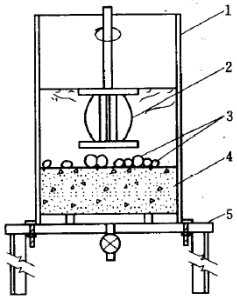

1—steel container,
2—impeller,
3—steel balls,
4—concrete sample,
5—base

(a) The draft of the abrasion testing machine (b) The abrasion testing machine

Figure 1. Test set set-up

The abrasion resistance strength is measured using the mass loss of concrete samples under abrasion condition for 6 h. The formula is given as follows:

$$f_a = \frac{TA}{\Delta M} \quad (1)$$

where f_a (in kg/m^2) is the abrasion resistance strength; T (in h) is the abrasion time; A (in m^2) is the abrasion area of concrete samples, and ΔM (in kg) is the mass loss of concrete samples after T h.

The wear rate is calculated using:

$$L = \frac{M_0 - M_T}{M_0} \quad (2)$$

where L (in %) is wear rate; M_0 (in kg) is the mass of concrete sample before abrasion, and M_T (in kg) is the mass of concrete samples after abrasion.

Resistance to chloride ion penetration

Electric flux method was used to test the resistance to chloride ion penetration of SCC in this experiment, and the equipment consisted of vacuum saturated concrete instrument CABR-BSY (see figure II) and concrete chloride ion diffusion coefficient & electric flux detector CABR-RCMP6 (see figure III). The procedures prescribed in the ASTM C1202 standard were followed to carry out the electric flux test of SCC with curing age of 28 days and 60 days.

Figure 2. Vacuum saturated concrete instrument

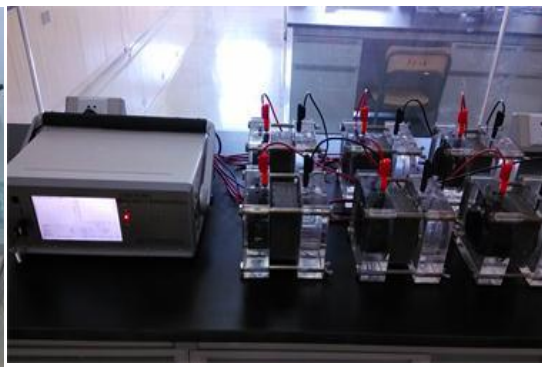

Figure 3. Concrete chloride ion diffusion coefficient & Electric flux detector

Test results and discussion

Effect of fly ash on the abrasion resistance strength of SCC

The electric flux test result of SCC with different curing ages and different abrasion condition is given in table III.

Table III. The electric flux of the SCC for the 28d and 60d (C)

Mix no.	28d no abrasion	28d after 6h abrasion	60d no abrasion	60d after 6h abrasion
SCC-1	3343	3452	2533	2609
SCC-2	2180	2338	1332	1422
SCC-3	1864	2046	1137	1275
SCC-4	1638	1867	1058	1234
SCC-5	1448	1676	795	938
SCC-6	1547	1929	1087	1413

Figure IV shows the effect of fly ash on the abrasion resistance strength of SCC, from which it could be observed that the abrasion resistance strength of SCC with curing age of 28 days decreased significantly with the increase of fly ash addition, and the trend is the same for SCC with curing age of 60 days. For SCC with curing age of 28 days, replacing 20%, 30%, 40%, 50% and 60% of cement with fly ash resulted in 23.30%, 44.56%, 46.26%, 56.80% and 69.56% decrease in the abrasion resistance strength of SCC, respectively. Likewise the decrease was 19.03%, 31.44%, 39.14 %, 53.71% and 63.83% respectively for SCC with curing age of 60 days. Moreover, by comparing the decrease trends of SCC with different curing ages (i.e., 28 d and 60 d), it could be concluded that the increase of curing age tends to alleviate the decrease of abrasion resistance strength of SCC caused by the addition of fly ash.

Fly ash is inherently less active than cement, hence when certain amount of cement was replaced by fly ash the hydration products which formed the bonding between cement matrix and aggregate were reduced, consequently the addition of fly ash resulted in the decrease of abrasion resistance strength of SCC. However, in the case where SCC were cured for 60 days, the pozzolanic effect of fly ash helped improve the situation and consequently showed better performance than that of SCC with curing age of 28 days. Since the incorporation of fly ash decreased the abrasion resistance strength of SCC, it is recommended that the amount of fly ash should be confined depending on the situation.

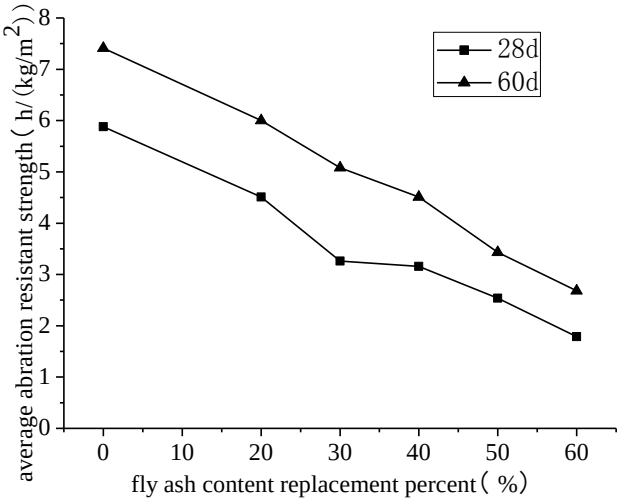

Figure 4. Effect of fly ash content on the abrasion resistance of SCC

***Effect of curing period on the abrasion resistance of** SCC*

Figure V shows the wear rate of SCC after 6 h of abrasion, from which it could be concluded that the addition of fly ash leads to the increase of wear rate of SCC irrespective of curing age. To replace 20-60% of cement with fly ash resulted in 30-243% increase of wear rate for SCC with 28 days of curing, while the increase range was 26-187% for SCC with 60 days of curing. It is noticeable that vast replacement of cement with fly ash could significantly reduce the abrasion resistance performance of SCC.

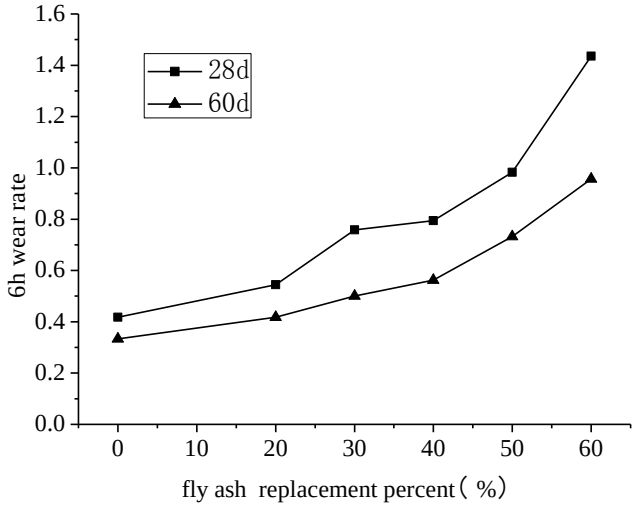

Figure 5. Effect of curing period on the abrasion resistance of self-compacting concrete

Effect of fly ash on electric flux of SCC

The effect of fly ash on electric flux of SCC with curing age of 28 days is shown in Figure VI, from which it could be observed that the electric flux of SCC decreased with the increase of fly ash provided that the replacement rate of fly ash was lower than 50% in the case where no abrasion was applied, while when the replacement rate of fly ash exceeded 50% (i.e., 60%), the decrease trend reversed. To be specific, replacing 20%, 30%, 40%, 50% and 60% of cement with fly ash led to 34.79%, 44.24%, 51.00%, 56.68% and 53.72% decrease of electric flux of SCC with curing age of 28 days, respectively. It is noticeable that when the replacement of cement with fly ash was over 40%, the performance of resistance to penetration of SCC was improved by over 50%.

The relation between electric flux and fly ash addition of SCC under abrasion condition for 6 h was found to be consistent with that of SCC without abrasion with turning point at 50% replacement rate of fly ash. Replacing 20%, 30%, 40%, 50% and 60% of cement with fly ash led to 32.27%, 40.73%, 45.91, 51.45% and 44.12% decrease of electric flux of SCC with curing age of 28 days, respectively. From the curves of Figure VI it could also be concluded that the beneficial effect of electric flux of SCC with abrasion treatment for 6 h caused by the addition of fly ash was smaller than that of SCC without abrasion treatment.This is because the fly ash can reduce the content of the CH in the transition zone and improves the CH alignment. At the same time, CSH gel by hydration produced was able to fill the transition zone pores, improve the performance of the transition zone. After the

second hydration reaction and the incorporation of fly ash, it produced C-S-H gel, more hydrated calcium aluminate and hydrated calcium aluminate. This reacts with Cl- and CH to produce **Friede** salt. In addition, the C-S-H gel has a high surface energy; it can easily get adsorbed into the chloride ions, which could play a solidification role in the chloride ions.

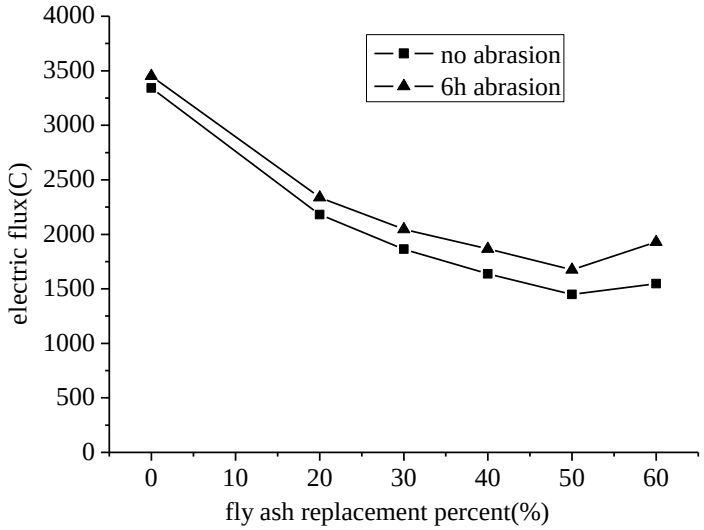

Figure 6. 28d electronic flux with fly ash

Conclusions

According to the experimental research, conclusions could be drawn as follows:

(1) The fly ash addition, curing age and abrasion significantly influenced the resistance to chloride ion penetration of SCC. The performance increased with the increase of curing age fly ash addition, and also a turning point of fly ash addition was found.

(2) In both cases of the curing period being 28d or 60d, the electric flux increased due to the abrasion.

(3) Moreover, the extent of increase of electric flux increases as fly ash content increases. The abrasion resistance strength of SCC increased with curing age and decreased with the increase of addition of fly ash.

Acknowledgments

The authors gratefully acknowledge the financial support provided by the National Natural Science Foundation of China (No. 51378126).

References

[1] (2001), In: *Protection and repair for the Corrosion in Reinforced Concrete*. Fan Y, Cao X.G, Chen H.R. Beijing, China Railway Publishing House. (in Chinese)
[2] Lin J, Jin Z.Q, Zhuang Q.C. (2012), *Corrosion inspection and analysis of coastal bridge concrete structures in marine environment.* Industrial Buildings, vol. 42, n. 7, p. 161-165. (in Chinese)
[3] Wang D.Z, Zhang J.X, Zhang J.H. (2006), *Investigation and analysis of the coastal highway reinforced concrete bridges chloride erosion.* Journal of Beijing University of Technology, vol. 32, n. 2, p. 187-192. (in Chinese)
[4] Boddy, A., Hooton, R. D., Grube, K. A. (2001). *Long-term testing of the chloride penetration resistance of concrete containing high-reactivity metakaolin*. Cement and Concrete Research, vol. 21, n. 5, p. 759–765.
[5] Dhir, R. K., Jones, M. R., Ahmed, H. E. H., Seneviratne, A. M. G. (1990). *Rapid estimation of chloride diffusion in concrete*. Magazine of Concrete Research, vol. 42, n. 152, p. 177–185.
[6] Guo, W., Qin, H. G., Sun, W., Yang, Y. (2010). *Effect of admixture and water to binder ratio on chloride ion permeability of concrete*. Bulletin of the Chinese Ceramic Society, vol. 29, n. 6, p. 1478–1483. (in Chinese).[7] Zhang B.D, Zhang S.L, Chen Z. (2008), *The test and analysis for the old concrete structures of Beicang power station shipment dock loading dock*. Building Construction, vol. 30, n. 8, P. 696-697. (in Chinese)
[8] Wang C.Q, Gu K.P. (2011), *Investigation and Analysis for the durability of the seaport construction of in East China*. Port Engineering Technology, vol. 48, n. 1, p.26-28. (in Chinese)[9] "The application technology specification for the hydraulic concrete "(SL352-2001)
[10] Wee, T. H., Suryavanshi, A. K., Tin, S. S. (2000). *Evaluation of rapid chloride permeability test (RCPT) result for concrete containing mineral admixtures*. ACI Materials Journal, vol. 97, n. 2, p. 221–232.
[11] Yi, C., Guo, T. T., Cheng, T., et al. (2007). *Experimental study on comparing between the NEL and ASTMC1202 testing method for chloride ion permeability in concrete*. Concrete, vol. 10, n. 3, p. 4–6. (in Chinese).

Strength and Durability Properties of Self Cured Self Compacting Mortars (SCSCM)

P Rathish Kumar[1], M Sri Rama Chand[2], P.S.N.R.Giri[2] and G Rajesh Kumar[3]

1 – Associate Professor, Department of Civil Engineering, N. I. T. Warangal
2 - Research Scholar, Department of Civil Engineering, N. I. T. Warangal
3 - Professor, Department of Civil Engineering, N. I. T. Warangal

Abstract Performance of Self Compacting Mortars largely depends on curing, particularly in the initial ages. Due to many different reasons curing is not properly done rendering the repair useless. Self Curing in mortars can achieve this by addition of curing chemicals. Polyethylene Glycol, Liquid Paraffin Wax etc can be very good curing compounds to increase the performance of self compacting mortars. These chemicals internally cure the mortars leading to improved hydration and C-S-H gel formation. In the present work, two self compacting mortars 1:1/0.34 w/c and 1:3/0.5 w/c are investigated with two self curing agents (Polyethylene Glycol 4000 and 200). A comparison was made considering three curing conditions namely wet curing, self-curing and no curing. Different dosages, i.e. 0%, 0.1%, 0.5% and 1.0% were examined with the above two curing agents. Mini-Slump flow and V funnel tests were done to confirm flow properties required as per the specifications. Water retention, compressive strength, sorptivity and acid durability tests were carried out on SCM specimens. A unified factor viz. Acid Durability Loss Factor is introduced to study the influence of acid in terms of loss of strength, stability and weight loss. This factor accommodates both strength and durability performance. It was concluded from the study was that the use of Self curing agents in Self compacting mortars in optimum dosages benefitted self compacting mortars in achieving better strength and durability performance.

Keywords: *Self compacting mortar, Polyethylene glycol, Water retention, Compressive strength, Sorptivity, Acid durability factor.*

Introduction

Self Compacting Mortars have a key role to play in repairs to structures compared to normal mortars [1]. Curing is a major factor important for hydration process to

continue particularly in the initial ages. However, adequate curing is not always possible by conventional curing techniques and it is recommended to make the embedded water available for cuing in order to overcome this problem [2]. The embedded water for curing can be provided using light weight aggregate, super absorbent polymers and hydrophilic materials [3, 4]. Better hydration can be achieved with addition of curing compounds like Polyethylene Glycol (PEG), super absorbent polymers (SAPs), Liquid Paraffin Wax (LPW) etc. The use of Self Curing technique in Self Compacting Mortars hence provides considerable advantage in repair and rehabilitation of structures. The main objective of this work is to identify a suitable self curing compound for Self Compacting Mortars. In the present investigation, the strength and durability characteristics of Self Cured Self Compacting Mortars are evaluated for their suitability in repair works.

Experimental Program

In this study, two SCM mixes i.e. Mix-A (cement: sand 1:1/0.34w/c) and Mix-B (cement: sand 1:3/0.50w/c), two types of hydrophilic compounds (PEG 200 & PEG 4000), four dosages of hydrophilic compounds (0%, 0.1%, 0.5% and 1.0% by weight of cement) and three curing conditions (no curing, curing by conventional water immersion and self/ internal curing) are considered as the parameters of investigation. Mini slump flow test and V funnel tests were carried out to check the flowability as per EFNARC specifications [5]. Mortar Cubes of size 100mm × 100mm × 100mm were cast to determine properties as water retention, sorptivity, compressive strength and resistance to acid attack.

Materials

Ordinary Portland cement was used in the investigation. The fine aggregate confirming to Zone-2 according to IS: 383-1970 [6] was used. Mineral admixture fly ash was used in the study. A polycarboxylate type, new-generation high range water reducing admixture conforming to ASTM C494 [7], was used as super plasticizer for improving the flow or workability of mix with decreased water-cement ratio. Self curing compound Polyethylene Glycols (PEGs) of low molecular (200) and high molecular weights (4000) were used in the study. The chemicals were mixed with water thoroughly prior to mixing of water in concrete.

Tests on Fresh mortar

Mini Slump Cone test and V-funnel tests were conducted to determine the Fresh properties of SCM mixes. The results are shown in Table 1.

Table I. Fresh Properties of SCM with and without PEG

Test	EFNARC Value	Mix	Plain SCM (0% PEG)	SCMs with PEG					
				PEG 4000(H)			PEG 200(L)		
				0.1 %	0.5 %	1.0 %	0.1 %	0.5 %	1.0 %
Slump Flow (mm)	240-260	A B	243 245	241 255	260 250	265 260	252 248	255 252	260 255
V-Funnel (sec)	<11	A B	10.2 9.4	13 11	10 11	11 11	9 10	11 11	11 9

Water Retention test

The resources of water molecules in mortar, particularly when subjected to no curing are extremely important for curing of concrete. The curing compounds added during the mixing time act as internal sealing agents and decrease the self desiccation and progress the hydration of concrete. The retention of water in concrete was monitored by weighing the mortar cubes at regular intervals.

Compressive Strength test

The cube specimens were tested in a standard compression testing machine of capacity 200 Tons as per IS 516-1956 [8]. The maximum load applied on the specimen was recorded to determine the compressive strength.

Sorptivity test

Sorptivity measures the rate of penetration of water into the pores in concrete by capillarity suction. After curing, the specimens the weight of the absorbed water at regular intervals is measured. The test was conducted as per Hall's method [9].

The sorptivity was obtained by using the following expression:

$$\frac{\Delta w}{A*\sqrt{t}} = S \qquad (1)$$

Where, ΔW = the amount of water adsorbed in (kg); A = the cross-section of specimen that was in contact with water (m^2); t = time (min);
S = the sorptivity coefficient of the specimen ($mm/min^{0.5}$).

Results and Discussions

Water Retention

The initial weight of each specimen type was taken as the reference value and the weight loss with respect to time was observed. The difference between the weight at any age and the initial weight (i.e., weight loss) was plotted with respect to the age of the specimen. Table 2 shows the average weight loss of PEG 4000 and PEG 200 in mixes A and B athe the end of 28 days. It was noted physically that the percentage weight loss diminished as the curing progressed. It can be noted from the Table 2 that addition of PEG 200 and PEG 4000 in SCM's resulted in better performance than those specimens which were not cured.

Table II. 28 days Average weight loss and Compressive Strength

PEG Dose (%)	28 days average weight loss in grams						28 days Compressive Strength in MPa							
	AN	AH	AL	BN	BH	BL	AW	AN	AH	AL	BW	BN	BH	BL
0	89	-	-	74	-	-	54	35	-	-	37	22	-	-
0.1	-	64	70	-	51	60	-	-	46	40	-	-	33	25
0.5	-	70	50	-	54	60	-	-	42	45	-	-	30	27
1.0	-	62	68	-	56	58	-	-	51	41	-	-	26	28

Compressive Strength

The average compressive strengths of self compacting mortars (SCM) were determined at the end of 7, 28 and 56 days. The typical 28-day compressive strength results of various mortars are given in Table 2. It can be noted that the use of PEG (both lower and higher molecular weights) benefitted the properties of SCMs. It is also evident that with 0.5% PEG 200 and 1.0% PEG 4000, the 28-day compressive strength is almost equal to the conventional wet curing specimen, with a marginal difference. Hence, it can be concluded that in applications where water curing is not possible, self-curing can be adopted to replenish the loss of moisture for continued hydration process.

Sorptivity test

Sorptivity test indirectly indicates the volume of voids and supports the results obtained by Water Retention test. Sorptivity is found to be more for no cured self compacting mortar specimens than all other specimens. This can be attributed to

the lack of proper hydration of cement particles caused due to the evaporation of water added during mixing, leaving behind most of the un hydrated cement particles. Sorptivity has been found to be less for Self Curing Self Compacting Mortars compared to no cured samples in both A and B categories of mixes.

Fig. 1 shows the sorptivity coefficient values (mm/min$^{0.5}$) obtained for different dosages of PEG compounds. Optimum (minimum) sorptivity coefficients are obtained for Mix-A with 0.5% of PEG 200 (low mol. wt.) & 1.0% of PEG 4000 (higher mol. wt.) and In case of Mix-B 1.0% of PEG 200 (low mol. wt.) & 0.1% of PEG 4000 (higher mol. wt.) was found to be optimum.

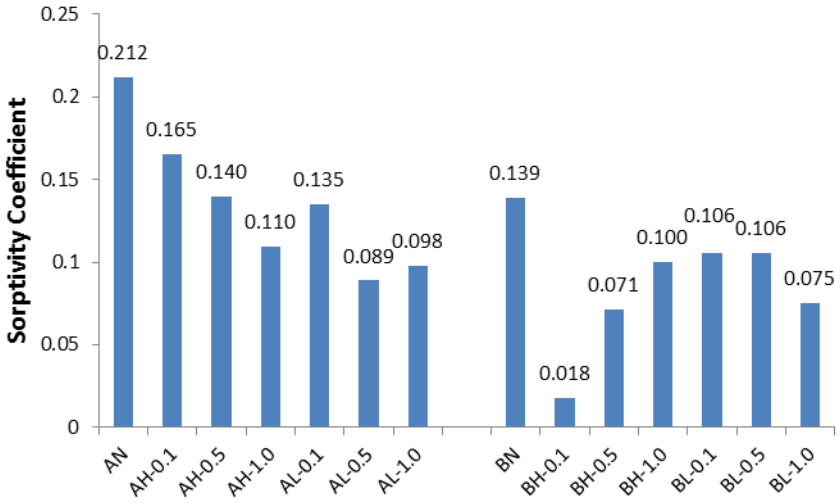

Figure 1. Dosage of Self Curing Compound Vs Sorptivity Coefficient

Acid Durability Studies

After 28 days the chemical resistance of self curing mortars (SCM) was studied through chemical attack by immersing mortar cubes in Hydrochloric acid (HCl) solution. Being alkaline in nature, mortars are susceptible to attack during contact with chlorides. The initial mass, body diagonal dimension values were measured and the specimens were immersed in 5% HCl solution.

The mass, diagonal dimension values were measured at the end of 3, 7, 14, 21, 28 days of immersion. Throughout the immersion period care was taken to maintain constant acid concentration. Compressive strength was measured after 28days of immersion before testing; each specimen is removed from the baths, brushed with a

soft nylon brush and rinsed in tap water. Mass change, reduction in compressive strength values and change in the diagonal dimensions were observed. The results of acid attack on mortars are presented in form of three factors namely, mass loss factor, acid attack factor and acid durability factor, keeping with the philosophy of ASTM C 666-1997 [10].

Acid Mass Loss Factor (AMLF)

The change in mass with age compared to the initial mass of each specimen is defined as Acid Mass Loss Factor. A higher value of AMLF indicates that mass loss is greater, hence less durable.

$$\text{Acid Mass Loss Factor} = \frac{\text{Change in Mass of Specimen}}{\text{Initial Mass}} \times 100 \quad (2)$$

Table III. Acid Mass Loss Factor (Mixes A and B)

Age of Acid attack (Days)	**Acid Mass Loss Factor**						
	AN	**AH 0.1**	**AH 0.5**	**AH 1.0**	**AL 0.1**	**AL 0.5**	**AL 1.0**
7	0.61	0.52	0.57	0.42	0.54	0.44	0.52
14	1.16	0.99	1.10	0.88	1.07	0.99	1.04
21	1.68	1.33	1.62	1.16	1.48	1.28	1.41
28	2.06	1.69	2.02	1.58	1.98	1.73	1.93
Age of Acid attack (Days)	**BN**	**BH 0.1**	**BH 0.5**	**BH 1.0**	**BL 0.1**	**BL 0.5**	**BL 1.0**
7	0.78	0.53	0.61	0.58	0.66	0.56	0.53
14	1.34	0.90	0.98	1.00	1.13	1.03	0.97
21	1.72	1.37	1.45	1.48	1.60	1.49	1.38
28	2.10	1.70	1.96	2.00	2.05	1.91	1.69

Table 3 shows the variation of the Acid Mass Loss Factor for lower and higher molecular weights PEG for Mixes ‘A’ and ‘B’. It can be noted from the Table that in case of both lower and higher molecular weights the mass loss factor is almost same. The optimum being AH-0.1 and AL-0.5 in case of higher and lower molecular weight PEG specimens. A lower acid mass loss factor leads to better durability. The reason for lower mass loss can be attributed to dense formation of matrix leaving minimum pores. This is possible due to the availability of required

moisture for hydration with self curing chemicals only resulting in a dense CSH gel formation.

Acid Attacking Factor (AAF)

The extent of deterioration at each corner of the struck face and the opposite face is measured and the change in the length of diagonal after immersion in the acid for a certain period of time is defined as the acid attack factor (AAF). The extent of loss is determined as

$$\text{AAF} = \frac{\text{Change in dimension of diagonal after immersion in Acid}}{\text{Original diagonal dimension before immersion}} \text{ x } 100 \qquad (3)$$

Table IV. Acid Attacking Factor (Mixes A and B)

Age of Acid Attack (Days)	**Acid Attacking Factor**						
	AN	**AH 0.1**	**AH 0.5**	**AH 1.0**	**AL 0.1**	**AL 0.5**	**AL 1.0**
7	0.93	0.63	0.84	0.53	0.54	0.44	0.52
14	1.69	1.05	1.47	0.95	1.07	0.99	1.04
21	2.25	1.58	2.10	1.37	1.48	1.28	1.41
28	2.67	2.31	2.52	2.00	1.98	1.73	1.93
	BN	**BH 0.1**	**BH 0.5**	**BH 1.0**	**BL 0.1**	**BL 0.5**	**BL 1.0**
7	1.15	0.73	1.04	1.14	1.10	1.04	0.83
14	2.19	1.35	1.76	1.96	2.10	1.76	1.55
21	2.63	1.97	2.38	2.48	2.52	2.28	2.06
28	2.98	2.39	2.59	2.72	2.87	2.80	2.79

Table 4 shows the variation of Acid Attack Factor with age for different mixes with varying dosages and molecular weights. It can be noted that the variation is the same with lower acid attacking factors in AH-1.0 and AL-0.5 in case of Mix 'A' and BH-0.1 and BL-1.0 in case of Mix 'B'. A lower acid attacking factor indicates better durability.

Acid Strength Loss Factor (ASLF)

Acid Strength loss factor (ASLF) represents the relative strength present in concrete specimen after immersing in acid. The relative strengths are always

compared with respect to 28 day compressive strength value. This depends on the period of immersion in Acid.

Acid Strength Loss Factor (ASLF) can be calculated as follows:

$$\text{ASLF} = \text{Sr}\ \frac{\text{N}}{\text{M}} \tag{4}$$

Where, Sr – Relative Strength at N days, (%)

N – Number of days at which the durability factor is needed

M - Number of days at which the exposure is to be terminated

Table 5 shows the variation of Acid Strength Loss Factor (ASLF) for different grades and PEG'S with different molecular weights. With the use of self curing agents, the required amount of hydration was possible resulting in dense microstructure. This indirectly means for optimum proportions of PEG the strength loss has decreased resulting in enhanced durability performance.

Table V. Acid Strength Loss Factor (Mixes A and B)

Age of Acid Attack (Days)	**Acid Strength Loss Factor**						
	AN	**AH0.1**	**AH0.5**	**AH1.0**	**AL0.1**	**AL0.5**	**AL1.0**
7	3.52	0.61	0.86	0.80	1.09	1.45	1.31
14	9.58	3.63	5.02	3.65	4.53	3.91	4.24
21	18.16	7.28	9.68	6.03	11.16	9.75	10.58
28	26.63	12.80	16.68	11.87	17.63	14.49	16.47
Age of Acid Attack (Days)	**BN**	**BH0.1**	**BH0.5**	**BH1.0**	**BL0.1**	**BL0.5**	**BL1.0**
7	4.21	1.29	2.31	2.23	2.14	1.60	1.10
14	11.17	5.45	6.84	8.65	9.24	8.75	6.33
21	21.51	10.85	15.55	17.50	15.98	16.26	13.07
28	39.38	21.87	29.26	28.63	24.09	24.55	21.37

To combine the effect of different factors like weight loss, strength loss and dimension loss, a single unified factor termed "Acid Durability Loss Factor (ADLF)" is introduced combining the loss due of acid. ADLF can be calculated as shown below.

$$\text{Acid Durability Loss Factor (ADLF)} = \text{AMLF} \times \text{AAF} \times \text{ASLF} \tag{5}$$

Durability Loss Factor for different grades of concrete with self-curing agents is calculated and the comparison for different mixes is shown in Table 6. Increased

ADLF results in poor durability performance. ADLF values give an idea about the overall performance of PEG's at their optimum dosages and molecular weights. It can be noted that the overall performance of SCM's have increased at every age for both the mortar grades (A & B).

Table VI. Acid Durability Loss Factor (Mixes A and B)

Age of Acid Attack (Days)	**Acid Durability Loss Factor**						
	AN	**AH0.1**	**AH0.5**	**AH1.0**	**AL0.1**	**AL0.5**	**AL1.0**
7	1.97	0.20	0.41	0.18	0.49	0.41	0.49
14	18.80	3.79	8.09	3.05	7.07	4.05	6.33
21	68.60	15.21	32.93	9.55	34.26	18.39	30.76
28	146.18	49.94	84.76	37.40	87.11	52.55	78.56
Age of Acid Attack (Days)	**BN**	**BH0.1**	**BH0.5**	**BH1.0**	**BL0.1**	**BL0.5**	**BL1.0**
7	3.8	0.5	1.5	1.5	1.5	0.9	0.5
14	32.7	6.6	11.8	17.0	21.9	15.8	9.5
21	97.1	29.3	53.6	64.3	64.3	55.2	37.2
28	246.2	89.1	148.4	155.8	141.7	131.2	100.6

Conclusions

The conclusions drawn from the study are:

1. The loss of moisture content in self compacting mortars was minimised due to the use of PEG as self curing agents. The optimum dosages for PEG 200 and PEG 4000 are arrived.
2. Self cured self compacting mortar specimens attained compressive strength values nearly equal to wet cured specimens. In Mix A, the self compacting mortar specimens with 0.5% of PEG 200 & 1.0% of PEG 4000 have shown 45.2% & 27.8% more compressive strength than no cured specimens. In Mix B, 1.0% of PEG 200 & 0.1% of PEG 4000 have shown an increase in compressive strength of 49.5% and 28.9% compared to no cured specimens.
3. There is a decrease in the sorptivity values in self cured self compacting mortars compared to no cured self compacting mortars. The optimum dosages are the same as that which resulted in minimising the weight loss also.
4. ADLF which accommodates losses due to mass, dimension and strength was calculated and it was proved that higher ADLF indicate poor performance.

5. The present experimental study has confirmed that from the strength and durability point of view the optimum dosages of PEG 200 and PEG 4000 were 0.5% & 1.0% and 1.0% & 0.1% in respect of Mixes A and B respectively.

References

[1] Felekoglu B, Tosun K, Baradan B, Altun A, Uyulgan B, 'The effect of fly ash and limestone fillers on the viscosity and compressive strength of self-compacting repair mortars', Cement & Concrete Research, 36(2006),1719-26.

[2] Bentz DP and W. Jason Weiss, 'Internal Curing: A 2010 State-of-the-Art Review', U.S. Department of Commerce, NISTIR 7765, February 2011.

[3] Jiajun Y, Shuguang H, Fazhou W, Yufei Z and Zhichao L, 'Effect of pre-wetted lightweight aggregate on internal relative humidity and autogenous shrinkage of concrete', Journal of Wuhan University of Technology – Materials Science Edition, 21(2006), 134–137.

[4] Zhutovsky S, Kovler K & Bentur A (2002), 'Efficiency of Lightweight Aggregates for Internal Curing of High Strength Concrete to Eliminate Autogenous Shrinkage', Materials and Structures, Vol. 35, pp. 97-101.

[5] EFNARC, Specification and guidelines for self-compacting concrete, May 2005.

[6] Indian Standards: 383-1970 'Specification for coarse and fine aggregates from natural sources for concrete', Bureau of Indian Standards, New Delhi, India.

[7] ASTM C494, 'Standard Specification for Chemical Admixtures for Concrete', ASTM, Philadelphia, USA, 2005.

[8] Indian Standards: 516 -1956 (Reaffirmed 1999) 'Indian Standard Methods of Tests for Strength of Concrete', Bureau of Indian Standards, New Delhi, India.

[9] C Hall, 'Water sorptivity of mortars and concretes: a review', Magazine of concrete research, 41 (1989), 51-61.

[10] ASTM C 666-97, Standard Test Method for resistance of concrete to raid freezing and thawing, ASTM International, West Conshohocken, PA, USA.

Long Term Durability Performance of Self-Compacting Concretes using Ladle Furnace Slag (LFS) Filler

Kosmas Sideris[1], Alexandros Chatzopoulos[1], Christos Tassos[1] and Panagiota Manita[1]

[1]Laboratory of Building Materials, Democritus University of Thrace P.O. Box 252, Xanthi 67100 GREECE
[*]Corresponding author, email: kksider@civil.duth.gr

Abstract Ladle furnace slag (LFS) is a by-product of the steel making process. In this paper ladle furnace slag was used as filler material for the production of self-compacting concrete mixtures of different strength classes. Different contents of ladle furnace slag filler, ranging from 45 to 90 kg/m3 were incorporated. The different mixtures were tested in the fresh state for fluidity, passing ability and resistance to segregation and in the hardened state for compressive strength, carbonation, chloride penetration resistance, freeze thaw resistance and long term volume stability. The test results indicated that ladle furnace slag can be used as filler for producing self-compacting concretes. All durability indicators examined were increased.

Keywords: *Ladle furnace slag, Sustainability, Long term volume stability, Carbonation, Chlorides, Freeze thaw resistance.*

Introduction

Self-compacting concrete (SCC) is a novel cement based composite which has the potential to improve the quality of structural elements as well as the quality of the construction procedures. It is widely used in different applications such as ready-mixed concrete and the precast industry because of its many advantages. It can spread into place under its own weight and fill restricted sections without the need of mechanical consolidation, improving this way the working environment (reduction of noise in urban environments, reduction of "white finger" syndrome), reducing the manpower need for casting and increasing the speed of construction and the quality of cast structures [1-3]. The basic properties of SCC are the filling ability, the segregation resistance and the passing ability. Rheology of the cement paste is the crucial factor in order to fulfill the above requirements. Self

compactibility is strongly connected with the dosage of fine materials. All materials passing the 0.125mm sieve are considered as fine materials. According to the European Guidelines for Self Compacting Concrete [4], the quantity of fine materials per cubic meter of concrete should be in the range of 380- 600 Kg.

The most widely used filler is limestone powder. In Greece, research has shown that industrial by-products have a potential to be used in SCC mixtures replacing either cement or lime filler or both [5-7]. Replacing limestone filler in Greece is rather vital since the production of this material is limited in only two quarries nationally and its high cost makes it unattractive to engineers and contractors.

The present study focuses on the use of ladle furnace slag (LFS), a by-product of the steel production process, as a means for increasing the total powder content in SCC. LFS is a fine material that shows some weak pozzolanic and latent hydraulic properties [8].

Experimental Program.

Seven different self-compacting concrete mixtures were produced. The mixtures belonged in the strength classes C25/30, C30/37 and C35/45 according to EN206-1 [9]. All concretes were prepared using a Blended Portland Cement, of the type CEM II A-M/42.5N according to European standard EN 197-1 (Table I).

Table I. Chemical characteristics of the materials used

Percentage (%)	CEMII(A-M)42.5N	Limestone filler	Ladle furnace slag
SiO_2	22.71	17.79	18
CaO	58.87	44.24	56
Al_2O_3	6.06	1.57	1.28
Fe_2O_3	3.43	1.62	1.60
K_2O	1.18	0.00	0.31
Na_2O	0.43	0.00	0.46
TiO_2	0.28	0.02	0.01
P_2O_5	0.09	0.01	0.01

Table II. Mix design characteristics of self-compacting mixtures prepared

Mix design kg/m^3	Mixture name	Coarse aggr.	Limstone sand	Limstone filler	Slag	CEM II 42,5N	Water	w/c	Sup/er	Retarder	Air content %	Slump (mm)	V-Funnel (sec)	L-Box (H_1/H_2)
SCC 25/30	SCC1	800	910,5	120	0	300	180	0,60	6,7	0,452	2,5	78	6,4	1
SCC 25/30 LFS 15%	SCC2	800	975,5	0	45	300	180	0,60	4,04	0,452	2,6	69,5	7,5	0,9
SCC 25/30 LFS 25%	SCC3	800	949,3	0	75	300	180	0,60	4,71	0,452	2,5	73,5	7,1	0,84
SCC 25/30 LFS1 15%	SCC4	800	1053,4	0	40,5	270	162	0,60	3,55	0,407	2,8	70	10,8	0,89
SCC 30/37	SCC5	800	901,4	50	0	370	170,2	0,45	6,39	0,556	2,6	71	7,9	0,84
SCC 30/37 LFS 15%	SCC6	800	891,5	0	55,5	370	170,2	0,45	7,02	0,556	2,5	71,5	10,4	0,89
SCC 30/37 LFS 25%	SCC7	800	851,6	0	92,5	370	170,2	0,45	9,36	0,556	2,3	74	9,1	0,89
SCC 30/37 LFS1 15%	SCC8	800	938,8	0	49,95	333	166,5	0,50	6,25	0,502	2,3	72	11,5	0,87
SCC 35/45	SCC9	800	933	0	0	430	180,6	0,42	9,46	0,648	2,5	71,5	8,4	0,85

SCCs were prepared and tested in fresh condition according to the specifications of EFNARC [8]. The coarse aggregates consisted of crushed granite with maximum size of 16mm. The fine aggregates used was crushed limestone sand. Limestone filler was used as additional filler materials for the production of reference SCC mixtures of the strength grades C25/30 and C30/37 (SCC25/30-LF and SCC30/37-LF respectively). Ladle furnace slag was used as an alternative filler material replacing aggregates in four SCC mixtures at percentages of 15% and 25% per weight of cement. In order to further improve the environmental footprint of the concretes cement content was also reduced at percentages of 10% in two more mixtures. In these cases LFS was added at percentage of 15% per weight of the reduced cement (Table II).Ladle furnace slag is a fine material with 100% passing the 96 μm sieve and 95% passing the 45 μm sieve. High range water reducing carboxylic ether polymer admixture was added at different dosages in order to achieve self compactibility in the case of SCCs. The proportions as well as the properties of fresh mixtures are presented for all concretes in Table II. Self-compacting concretes were prepared and tested according to EFNARC [4]. Segregation resistance was also evaluated using the visual analysis of the slump cone test.

The specimens prepared were 150 mm (edge) cubes, 60x100 mm and 100X200 cylinders. All specimens were cured for 28 days in a curing chamber (T=20º C, RH>98%). The 150 mm cubes were used for measuring the compressive strength at different ages. Carbonation resistance was measured on 60X100 cylindrical specimens. These small cylinders were initially cured for 3 days in the above mentioned curing chamber. From this age onwards they were placed in the laboratory air environment (relative humidity = 50-60% and temperature =20±2 °C). At the age of 28 days they were moved into the accelerated carbonation chamber (T=20º C, RH=55%, CO2=1%). Specimens remained in this chamber for 60 days. A second series of specimens was exposed after the age of 3 days in outdoor conditions and remained in unsheltered exposure conditions for 24 months.

Chloride induced resistance of concretes was assessed on cylindrical specimens with a diameter of 100mm and a height of 50 mm formed from the 100X200 cylinders. These specimens were cured as above till the age of 28 days. The chloride diffusion coefficient De was then estimated according to the procedure described in NT Built 492 [10].

Resistance to freeze-thaw attack was assessed according to the procedure described in EN 12390-9 –CDF standard. A concrete segment (100x100x50 mm) was sawed from a 100mm cube specimen cured in the curing chamber for 28 days. From this age onward the segment was immersed in a 3%NaCl solution for 7 more days. At the age of 35 days all specimens (segments) were partially immersed in a plastic tank containing 10 mm of 3% NaCl solution. The weight loss of all specimens after fifteen freezing-down to -18^{o}C- and thawing – up to 20^{o}C- cycles was measured.

Referring to the accelerated aging method proposed in the ASTM D-4792 standard [15],three 100mm edge cube specimens from each mixture were completely dipped (below 5 cm) in a thermostatic tub containing 70 ºC water and properly covered (to limit evaporation) for a total duration of 32 days. After this age all specimens were tested in compression and the residual compressing strength of all mixtures compared with the compressive strength measured at the age of 28 days before the accelerated test.

Experimental Results and Discussion

Influence on the rheological properties of fresh mixtures

Addition of LFS improved the fresh properties of C25/30 SCC mixtures resulting this way to reduction of the superplasticizer amount needed for their production. Segregation resistance of all mixtures was assessed by using the Visual Stability Index (VSI) as described in ASTM-C1611. All mixtures were ranked as VSI=0 and VSI=1 according to this standard, indicating that addition of LFS did not affected negatively the segregation resistance of self-compacting mixtures.

Compressive strength

Compressive strength was measured for all mixtures at the ages of 2, 7, 28 and 90 days. These values are presented in Table III.

Table III: Compressive strength of self-compacting concretes (MPa)

(MPa)	SCC1	SCC2	SCC3	SCC4	SCC5	SCC6	SCC7	SCC8	SCC9
fc_2	26.8	23.6	25.7	24.0	33.0	33.3	34.9	33.2	39.3
fc_7	32.7	29.0	37.7	30.1	44.3	44.3	46.1	42.9	45.1
fc_{28}	44.6	44.8	46.9	41.6	54.1	55.8	57.5	52.4	60.0
fc_{90}	46.0	46.2	49.4	43.3	55.6	57.8	61.8	53.8	63.1

Compressive strength of all SCC mixtures prepared with LFS addition was increased as compared with the one of reference SCC mixtures of the same grade. C25/30 SCC mixtures produced with 25%LFS performed an increase in 28 days compressive strength of 2.3 MPa (5.1% of the strength measured on reference SCC produced with limestone filler). The strength difference was slightly increased up to 3.4 MPa (7.4%) at the age of 90 days. Setien et al [8] also reported that ladle furnace slag performs cementitious hydraulic properties. Anastasiou et al [11] concluded that LFS had a positive effect on strength development concerning 28-days and 120-days compressive strength. The researchers produced self-compacting concretes with addition of ladle furnace slag between 60 and 120 Kg/m3. In this research ladle furnace slag was added at smaller dosages in

SCC25/30 mixtures, thus the strength gain was smaller. Strength gain percentage was higher (6.3% and 11.15% at the ages of 28 and 90 days respectively) in SCC7 mixture where ladle furnace slag dosage was increased up to 92.5 Kg/m^3. It is also noticeable that in this case compressive strength started to increase from the age of 2 days while the value measured at the age of 28 days was very close to the one of the SCC35/45 mixture, enabling this way this mixture to be graded as a C35/45 concrete. Mixtures SCC4 and SCC8 produced with lower cement content performed lower strength values as compared with reference mixtures. However this reduction was quite low and had no negative effect on the strength category of concretes.

Carbonation depth

Carbonation depth was measured by spraying the fresh broken surfaces of concretes with a phenolopthalein indicator, according to the procedure described in EN 14630 Standard [12]. The carbonation depth of all mixtures is presented in Table IV.

Table IV. Carbonation depth of self-compacting concretes prepared

Carbonation (mm)	SCC1	SCC2	SCC3	SCC4	SCC5	SCC6	SCC7	SCC8	SCC9
Natural (24months)	4.8	3.7	2.9	4.0	2.4	1.9	1.6	2.4	1.6
Accelerated	10.6	10	7.9	9.5	3.9	3.4	3	4.1	2.6

Addition of ladle furnace slag increased the carbonation resistance of all SCC mixtures prepared since the carbonation depths were decreased both in natural and accelerated exposed specimens. It was pointed out [13] that carbonation resistance of self-compacting concretes is strictly depending on the type and dosage of the material used as filler. Papayianni and Anastasiou [14] reported that mixtures produced with ladle furnace slag as binders and EAF slag as aggregates are impermeable with improved microstructure and low porosity. These findings were verified in this research since addition of LFS decreased the carbonation depth of SCC mixtures by 25% (SCC25/30 concretes) and 28% (SCC30/37 concretes) as compared with reference SCC mixtures produced with limestone filler. It is also essential to notice that when LFS was used in high dosage -25% of the weight of the cement- the carbonation depth of naturally exposed specimens after 24 months was reduced down to the value measured on higher strength reference SCC mixtures. Further on carbonation depth of mixtures SCC4 and SCC8 was lower than or equal to the one of reference mixtures, irrespective the fact that lower cement content was used. Research is still in progress in order to evaluate the influence of LFS on the carbonation coefficient of SCC mixtures and finally on the service life of reinforced concrete structures produced with LFS containing concretes.

Chloride diffusion coefficient

The Chloride diffusion coefficient values De measured according to NT Built 492 are presented for all mixtures in Table V.

Table V. Chloride diffusion coefficients De (10–12 m^2/s) of self-compacting concretes prepared.

Chloride diffusion coefficients	SCC1	SCC2	SCC3	SCC4	SCC5	SC 6	SCC7	SCC8	SCC9
De ($x10^{-12} m^2/s$	19.5	15.5	15.1	20.1	8.7	7	5.9	9.3	6

Chloride induced corrosion resistance was also improved when SCC mixtures were produced with LFS instead of limestone filler. Chloride diffusion coefficients De of self-compacting concretes prepared was reduced for SCCs containing LFS (Table IV). It is once again noticeable that SCC30/37 LFS25% mixture performs De value equal to the one measured on SCC35/45 specimens. Papayianni and Anastasiou [14] also reported that chloride induced corrosion of LFS produced concretes was improved.

Freezing and thawing resistance

Weight loss of all specimens after completion of fifteen freezing and thawing cycles is presented in Table VI.

Table VI. Weight loss of concrete mixtures after fifteen freezing and thawing cycles

	SCC1	SCC2	SCC3	SCC4	SCC5	SCC6	SCC7	SCC8	SCC9
Weight loss (%)	51.9	39.4	38.1	56.5	3.8	3.2	2.3	4.1	2.0

Addition of LFS improved the resistance of concrete mixtures against freezing and thawing cycles (Figure 1). Addition of LFS reduced the weight loss by 26% (SCC 3) and 39% (SCC 7). SCC mixtures produced with lower cement content (SCC 4 and SCC 8) performed increased weight loss by 8.8% and 7.8% respectively as compared with reference SCC concretes. Once again the performance of SCC 7 was comparable with the one of SCC35/45 (SCC9).

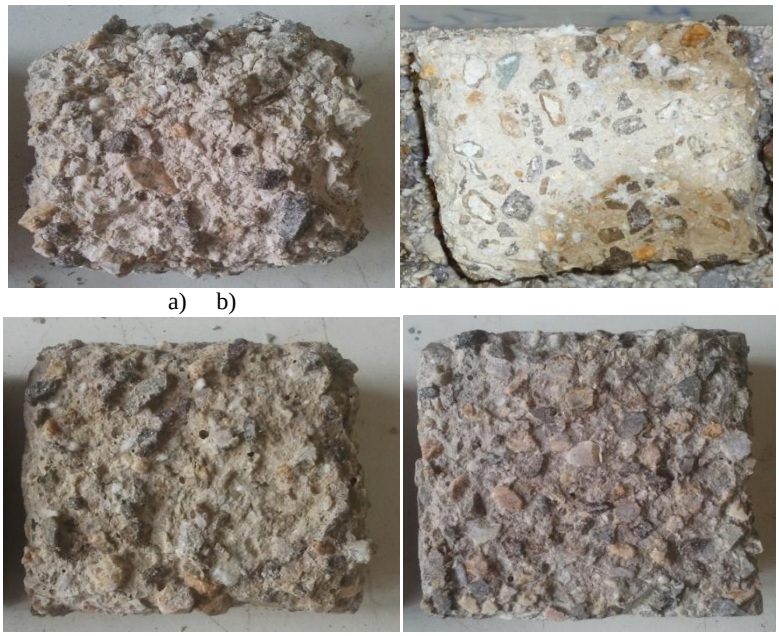

a) b)

c) d)

Figure 1. SCC mixtures after completion of freezing and thawing test: a) SCC1, b) SCC3, c) SCC5, d)SCC7

Long term volume stability.

Reduction in the compressive strength of all mixtures after accelerating aging according to ASTM D-4792 is plotted in Figure 2.

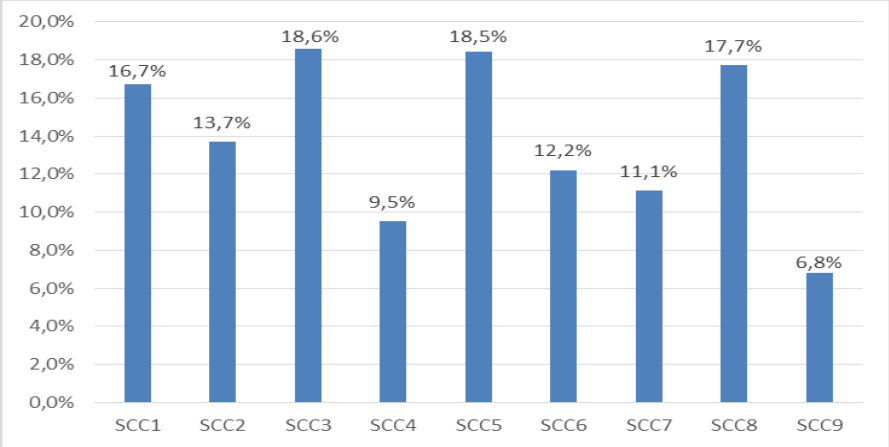

Figure 2. Reduction in compressive strength of all mixtures after completion of accelerating test

Addition of LFS improved the strength loss of the mixtures in most cases. Residual compressive strength of LFS produced SCCs was higher and the strength loss was reduced by up to 43.1% and 40% as compared with reference mixtures (SCC4 and SCC7 compared with SCC1 and SCC5 respectively). Residual compressive strength of mixture SCC3 was slightly lower than the one of reference concrete SCC1. SCC8 performed residual compressive strength almost equal to the value measured on reference concrete SCC5. This mixture was produced with lower cement content. Pelegrino et al [16] reported that concrete mixtures produced with high levels of fine EAF slag aggregates performed lower residual compressive strength as compared with traditional concrete with no recycled aggregates.

Conclusions

Ladle furnace slag may be used as filler material for the production of self-compacting concretes. Addition of LFS improved the fresh properties of SCC mixtures resulting this way to reduction of the superplasticizer amount needed in C25/30 SCC mixtures.

Compressive strength of SCC25/30 mixtures was slightly increased at later ages when LFS was used. The effect on strength increase was more significant in SCC30/37 mixtures where higher dosages of LFS were added. In this case LFS produced mixtures performed higher compressive strength than reference SCC even from the age of 2 days while the 28-day strength of SCC mixture produced with 25% LFS makes possible its classification in an upper strength class.

Durability properties of LFS SCCs were improved especially in mixtures produced with higher amount of LFS and lower w/c ratio. Carbonation, chloride resistance as well as resistance against freezing and thawing were increased. This increase was more essential in SCC30/37 mixture produced with 25%LFS where these durability indicators found to be equal with the values measured on SCC35/45 mixture. Long term volume stability of concrete mixtures was also improved when LFS was added

SCC mixtures produced with lower cement content performed lower compressive strength in all tested ages. However this strength reduction was very small and mixtures still remained in the same strength category with the reference concretes. Durabilty indiacators of these mixtures were in most cases almost equal with those measured in the reference concretes.

Further research is now in progress in order to quantify the effect of LFS on the durability of SCC as well as the long term performance and stability of the produced mixtures. The results will further demonstrate the possibility to use LFS for the production of high performance durable and environmentally friendly self-compacting concrete mixtures.

Acknowledgments

The financial support provided by the 11_SYN_5_344 research project, implemented within the framework of the "Competitiveness and Entrepreneurship" (EPAN II)' and co-financed by the European Development Regional Fund and Greek National Funds, is greatly acknowledged.

Cement and chemical admixtures used in this study were provided by TITAN Cement Industry and Sika Hellas S.A. respectively. Their support is greatly acknowledged.

References

[1] Skarendhal, Å. (2003) In: *The present-the future*, Proceedings of the 3rd International Symposium on SCC, pp. 6-14,Wallenik, O. and Nielsson, I. (Eds.), RILEM, Reykjavik, Iceland.

[2] Assie, S., Escadeillas, G. and Waller, V. (2007), *Construction and Building Materials*, Vol. 21, n.10, pp. 1909–1917.

[3] Boel, V., Audenaert, K., De Schutter, G., Heirman, G., Vandewalle, G., Desmer, L. and Bantomme, BJ. (2007), *Materials and Structures*,Vol. 40, n.5, pp. 507-516.

[4] BIBM, CEMBUREAU, EFCA, EFNARC, ERMCO, (2005)*Self Compacting Concrete Production and Use*, downlodable from www.efnarc.org

[5] Anagnostopoulos, N., Sideris, K.K. and Georgiadis, A. (2009), *Materials and Structures*, Vol. 42, n.10, pp.1393-1405.

[6] Georgiadis, A., Anagnostopoulos, N and Sideris, K.K. (2007), In: *Mechanical Characteristics of Self-Compacting Concretes produced with different filler materials*, Proceedings of the 5th International RILEM Symposium on Self Compacting Concrete, pp. 611-618, G. De Schutter and V. Boel (Eds.), Ghent, Belgium,.

[7] Sideris, K.K. (2009) In: *Self-compacting concrete in Greek reality. Present condition and future perspectives*, Proceedings of the 16th Greek Concrete Conference, Pafos, Cyprus.

[8] Setjin,J., Hernαndez, D. and Gonzαlez, JJ. (2009), *Constr Build Mater*, Vol.23, n.5, pp. 1788–94.

[9] Comite Européenne de Normalisation , (2000)*Concrete - Part 1: Specification, Performance, Production and Conformity*. EN 206-1.

[10] NT Built 492, (1999), *Concrete, Mortar and Cement-based Repair Materials. Chloride Migration Coefficient from Non-Steady Migration Experiments*, NTBuild.

[11] Anastasiou, E.K, Papayianni, I. and Papachristoforou, M. (2014),*Materials & Design*, Vol. 59, pp. 454-460.

[12] Comité Européenne de Normalisation(2006),*Products and systems for the*

protection and repair of concrete structures — Test methods — Determination of carbonation depth in hardened concrete by the phenolphthalein method.

[13] RILEM TC205 (2007),*Durability of self-compacting concrete*, State of the Art Report, RILEM Publications S.A.R.L., Report 38, ISBN978-2-35158-048-6.

[14] Papayianni, I. and Anastasiou, E. (2010),*Construction & Building Materials*, Vol. 24, n. 8, pp. 1412-1417.

[15] ASTM D4792-00: Standard test method for potential expansion of aggregatesfrom hydration reactions. USA: American Society for Testing and Materials;2006.

[16] Pelegrino C., Cavagnis P., Faleschini F. and Brunelli K. (2013), Cement and Concrete Composites , Vol. 37, n. 1, pp. 232-240.

Theme 8: Fiber-Reinforced SCC

Effect of Type of Fibers and Fiber Volume on Flexural Performance of Super-Workable Concrete

Ahmed Abdelrazik[1] and Kamal H. Khayat[2]

[1] Ph.D. candidate, Missouri University of Science and Technology, 202 ERL, 500 W. 16St., Rolla, MO 65409-0710 atarm9@mst.edu
[2] Professor, Missouri University of Science & Technology khayatk@mst.edu

Abstract This paper compares the enhancement of the mechanical properties and the crack resistance of super-workable concrete (SWC) and fiber-reinforced super-workable (FR-SWC). The mechanical properties and crack resistance enhancement measures included the use of fibers at two different fiber volumes 0.5% and 0.75%. In total, 10 SWC mixtures were developed; one plain SWC and nine fiber-reinforced SWCs. Six different types of fibers were investigated with SWC at a fixed fiber volume of 0.5%. Four types of hooked steel fibers (ST1, 3D, 4D, and 5D), a hybrid of crimpled Steel fiber and polypropylene multifilament fiber (STPL), and a combination of micro and macro steel fibers (STST). Only three types of fibers were used with SWC at a fiber volume of 0.75% (ST1, STST, and 5D). Test results revealed that Test results revealed that the FR-SCC containing hybrid fibers (92% steel and 8% polypropylene fibers) of low fiber factor (L/D) of 34 exhibit lower flow ability and passing ability than similar mixtures made with ST1 fibers of higher fiber factor of 80. The SWC made with the 5D steel fibers at 0.75% had the highest compressive strength. The SWC made with the ST1 steel fibers with fiber volume of 0.75% showed the highest splitting tensile strength. The combination of micro and macro steel fibers yielded better flexural strength and flexural toughness compared to those of the macro steel fibers. The 5D steel fibers were better than the 3D, the 4D and the ST1 in terms of flexural strength and flexural toughness. The 5D steel fibers were better than the 3D, the 4D, ST1 and even the micro macro steel fibers (STST) in terms of peak stress and residual stress.

Keywords: *Expansive agent, Cracking resistance, Fibers, Flowable concrete.*

Introduction

Super workable concrete (SWC) is a type of flowable concrete with workability less that SWC contains lower content of binders and needs some compaction during pouring of concrete in order to fill the form work correctly. Super workable concrete is characterized by the high workability in terms of flowability, passing ability as well as stability. Super workable concrete concrete gains its high workability mainly due to high to moderate volume of paste and high w/c resulting in high tendency of shrinkage and plastic cracking. Adding of fibers to SWC helps a lot in reducing of the drying shrinkage and resisting of the plastic cracking. One side effect of adding fibers to SWC is the decrease in workability mainly in terms of flow ability and passing ability. Flow ability change can be adjusted by adjusting of the mixture composition after adding the fibers but still the passing ability of fiber reinforced super workable concrete (FR-SWC) never reach the passing ability of plain SWC. One major advantage of adding fibers to SWC is to enhance the mechanical properties specially, tensile strength, toughness and cracking resistance. Fibers can totally change the behavior of SWC from a brittle material to a ductile material. This paper compares the flexural behavior of FR-SWC with different fiber types and volumes in terms of the toughness and cracking resistance.

Experimental Program

In total, eleven SWC mixtures were investigated. One plain SWC mixture was made without any fibers and without any FA. The remaining SWC mixtures were made with different types of fibers. Fresh properties were determined for all of the investigated mixtures, however, only stable mixtures were tested for mechanical properties and cracking resistance.

Materials and mixture proportioning

Ten mixtures were made with ASTM Type I/II cement and 30% Class C FA replacement, by mass of total binder. One reference SWC was prepared with Type I/II cement only without any FA. Continuously graded natural sand with a fineness modulus of 2.6 and crushed limestone aggregate with a nominal maximum aggregate size of 12 mm (0.5 in.) were used. The coarse aggregate and sand had specific gravities of 2.54 and 2.63, respectively, and water absorption values of 3.81% and 0.62%, respectively. Polycarboxylate-based HRWRA, synthetic resin-type air-entraining admixture (AEA), and polysaccharide viscosity-modifying admixture (VMA) were also used. Four fiber types, including propylene syntactic fiber (PLP), hooked steel fiber (ST1), hybrid of crimpled steel fiber and polypropylene multifilament fiber (STPL), and micro-macro steel fibers (STST) were incorporated at a fiber volume of 0.5% and 0.75%. Table 1 presents the

characteristics of the fibers. The w/c was kept constant at 0.42 for all of the investigated mixtures. Only one types of expansive agents, which is Type G expansive agent (EA) at 4% of mass of total binder was used.

Table I. Characteristics of fibers

	ST1	STST		PLP	STPL		3D	4D	5D	CA
Material	Macro Steel	80% Macro Steel	20% Micro Steel	Pro-pylene	8% Poly-propylene	Steel	Steel	Steel	Steel	Carbon
Shape [(1)]	Hook 	Hook 	Straight 	Mono-flament 	Multifilament Crimped 		Hook 	Hook 	Hook 	Straight 
Color	Golden	Golden	Golden	Transp.	Transp.	Grey	Grey	Grey	Grey	Black
Cross section	Cir.	Cir.	Cir.	Rec.	Cir.	Rec.	Cir.	Cir.	Cir.	Cir.
Specific gravity	7.85	7.85	7.85	0.92	0.91	7.85	7.85	7.85	7.85	7.85
Length (mm)	30	30	13	40	5-15 [(2)]	50	60	60	60	102
Equiv. diameter (mm)	0.55	0.55	0.2	0.44	0.05	0.9	0.92	0.92	0.92	3.18
Aspect Ratio	55	55	65	91	100-300	56	65	65	65	32
Modulus of elasticity (Gpa)	200	200	200	9.5	N.A.	7.16	210	210	210	242
Tensile strength (Mpa)	1100-1300	1100-1300	1100-1300	620	Neglected	413	1160	1160	1160	4137

Mixture proportioning

Khayat et al., (2014) [2] proposed a mixture-proportioning method proposed for shrinkage control in proportioning fiber-reinforced self-consolidating concrete (FR-SCC). They considered the multi-aspect concept proposed by Voigt [3] for calculating the thickness of mortar covering the coarse aggregates and the fibers. The mixture-proportioning method proposed by Khayat et al. (2014) [2] includes reducing the volume of coarse aggregate with the addition of fibers to maintain a fixed thickness of a mortar layer t_{cm} over the fibers and coarse aggregates. The procedure was used to adjust the mixture proportioning of SWC when adding the fibers to SWC to produce a FR-SWC that has similar fresh properties to those of SWC. The reference SWC mixture proportioning is given in Table 2 and named R1, this mixture proportioning was also followed by Khayat et al., (2014) [2] but the amount of binders was reduced from 475 kg/m^3 to 380 kg/m^3.

Table II. Mixture proportions SWC and FR-SWC

	Fiber type	V_f (%)	Water kg/m^3	Cement Type I/II kg/m^3	Fly Ash kg/m^3	Expansive Agent		Sand kg/m^3	Coarse Agg. kg/m^3	VMA	HRWR	AEA
						Type	kg/m^3			ml/m^3	ml/m^3	ml/m^3
R1	-	0	157	380	0	-	-	851	850	2500	1730	45.5
1	ST1	0.5	157	255.4	109.4	G-Type	19	942	727	2500	1730	50
2	3D	0.5	157	255.4	109.4	G-Type	19	872	800	2500	1410	54.5
3	4D	0.5	157	255.4	109.4	G-Type	19	872	800	2500	1545	50
4	5D	0.5	157	255.4	109.4	G-Type	19	872	800	2500	1820	50
5	STPL	0.5	157	255.4	109.4	G-Type	19	864	809	2500	2045	47.7
6	STST	0.5	157	255.4	109.4	G-Type	19	921	752	2500	1820	40.9
7	PLP	0.5	157	255.4	109.4	G-Type	19	924	746	2500	2500	36.4
C1	ST1	0.75	157	255.4	109.4	G-Type	19	972	690	3727	2430	40.9
C2	STST	0.75	157	255.4	109.4	G-Type	19	945	721	3727	2275	43.2
C3	5D	0.75	157	255.4	109.4	G-Type	19	872	800	3727	2320	43.2

Test methods

All the 11 mixtures were tested for slump flow and visual stability index. Fresh testing included; early slump flow (after 10 minutes of first adding water to cement), late slump flow (after 10 minutes of first adding water to cement), J-ring, modified J-ring, bleeding, air content, specific gravity, surface settlement was performed only for mixtures that showed acceptable workability. Slump flow was measured after 10 min and 70 min of first adding cement to water. Sampling of 20 cylinders for both compressive strength and splitting tensile strength, four small beams (7.5cm* 7.5cm* 40cm) for both flexural strength (ASTM C78) and flexural toughness (ASTM C1609) and four big-notched beams (15cm*15cm*55cm) for crack resistance (RILEM TC-162) were done only for mixtures that showed acceptable workability. The mechanical properties of the acceptable SCC mixtures included compressive strength, splitting tensile strength, flexural strength (ASTM C78), flexural toughness (ASTM C1609) and crack resistance (RILEM TC-162) were performed after 28 days and 56 days.

Experimental Results and Discussion

Fresh performance.

Table 3 shows the fresh properties of SWC as well as FR-SWC mixtures. AEA was added to all the mixtures and its dosage was adjusted in order to obtain air volume of a value 7.5 ± 1.5%. Fibers with more specific surface areas as propylene fibers (PLP) fibers or the hybrid fibers of polypropylene and steel (STPL) entrained more air than fibers with less specific surface area like ST1 and STST fibers do. Generally, fibers decrease the workability of SCC specially the passing ability property and fibers with higher fiber factor (Vf Lf/ df) decreases the passing ability of FR-SWC more than those of less fiber factor. Figure 1 shows the relation between the fiber factor and the modified J-Ring ratio, the *D*/*a* passing ability index decreases with the increase in fiber factor, and this is regardless the fiber type, this relation is very close to what obtain by Khayat et al., (2014) [2].

Mechanical properties of FR-SWC

Table 4 shows the compressive strength, splitting tensile strength, flexural strength, toughness and crack resistance of SWC and FR-SWC. Incorruption of fibers to SWC generally enhance the mechanical strength specially the toughness and the crack resistance. Hooked end steel fibers can increase the 56 days' compressive strength of SWC about 8% in case of the 30 mm hooked end steel fibers (ST1) at fiber volume (V_f) 0.5% and by 18% at 0.75% V_f, while combination between 30 mm hooked end steel fibers and micro steel fibers (STST) can increase the compressive strength about 12% at 0.5% V_f and by 20% at 0.75% V_f. 5D fibers at 0.5% V_f increase the compressive strength by 13% and by 18% at V_f of 0.75%. Hooked end steel fibers can increase the 56 days' splitting tensile strength of SWC about 58% in case of the 30 mm hooked end steel fibers (ST1) at fiber volume (V_f) 0.5% and by 113% at 0.75% V_f, while combination between 30 mm hooked end steel fibers and micro steel fibers (STST) can increase the splitting tensile strength about 66% at 0.5% V_f and by 92% at 0.75% V_f. 5D fibers at 0.5% V_f increase the splitting tensile strength by 87% and by 108% at V_f of 0.75%. In case of the hybrid of 50 mm crimpled steel fibers and polypropylene fibers (STPL) at V_f of 0.5% increase the splitting tensile strength of SWC by 20%. Hooked end steel fibers can increase the 56 days' flexural strength of SWC about 6% in case of the 30 mm hooked end steel fibers (ST1) at fiber volume (V_f) 0.5% and by 15% at 0.75% V_f, while combination between 30 mm hooked end steel fibers and micro steel fibers (STST) can increase the flexural strength about 24% at 0.5% V_f and by 35% at 0.75% V_f. 5D fibers at 0.5% V_f increase the flexural strength by 11% and by 114% at V_f of 0.75%. In case of the 4D steel fibers at V_f of 0.5% can increase the flexural strength of SWC by 10%.

Table III. Fresh properties of SWC and FR-SWC mixtures

No	Fiber type	V_f (%)	Unit weight kg/m^3	Air (%)	Slump flow mm 10 min 60 min	J-Ring mm	Modified J-Ring D/a mm/mm	Visual Stability Index	Bleeding (%)	Surface Settlement (%)
R1	-	-	2130	7.8	570 255*	530	565/26	0	0	0.16
1	ST1	0.5	2254	8.8	505 205*	390	470/32	0	0	0.28
2	3D	0.5	2206	9	580 180*	380	450/30	0	0	0.14
3	4D	0.5	2280	8	540 175*	380	430/29	0	0	0.22
4	5D	0.5	2238	8.7	510 165*	380	400/27	0	0	0.13
5	STPL	0.5	2206	9	525 205*	380	430/31	0	0	0.20
6	STST	0.5	2268	7.5	540 230*	420	440/29	0	0	0.39
7	PLP	0.5	-	-	490 -	-	-	2	-	-
C1	ST1	0.75	2314	6.9	550 255*	500	540/45	0	0	0.36
C2	STST	0.75	2280	7.5	540 115*	400	430/37	0	0	0.32
C3	5D	0.75	2278	8	560 125*	-	500/45	0	0	0.19

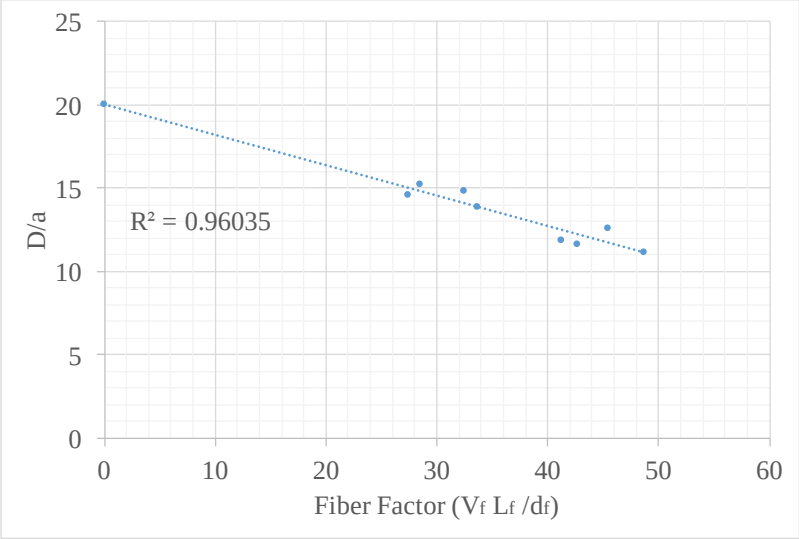

Figure 1. Effect of the fiber factor on the passing ability of FR-SWC

Table IV. Hardened properties of FR-SWC

No	Fiber Type	V_f (%)	Compressive strength (Psi)		Splitting tensile strength (Psi)		Flexural strength (Psi)		Toughness (lb.in)		First Crack stress (Psi)		Residual stress (Psi)	
			28 d	56 d	28 d	56 d	28 d	56 d	28 d	56 d	28 d	56 d	28 d	56 d
R1	-	-	5500	6425	400	415	629	680	6.1	6.7	397	430	0	0
1	ST1	0.5	5350	6940	520	655	670	720	108	117	546	590	505	545
2	3D	0.5	4515	5150	405	575	613	660	95	105	697	750	557	599
3	4D	0.5	5585	6895	605	710	703	750	100	109	835	900	600	645
4	5D	0.5	6060	7250	740	775	703	755	107	115	1392	1501	931	999
5	STPL	0.5	4910	6295	470	495	616	660	24	26	468	505	66	72
6	STST	0.5	6050	7170	620	690	785	840	131	142	909	980	682	735
7	PLP	0.5	-	-	-	-	-	-	-	-	-	-	-	-
C1	ST1	0.75	6660	7585	860	885	729	780	114	120	857	925	461	496
C2	STST	0.75	7460	7680	790	795	849	920	134	146	900	970	496	535
C3	5D	0.75	6595	7250	845	865	1339	1455	189	202	938	1010	674	725

Toughness of FR-SWC

Fibers have great impact on the ductility of SWC. Figure 2 shows the load deflection curves of (7.5cm* 7.5cm* 40cm) Beams of different FR-SWCs loaded at the first and the second thirds of the span with two point loads. The 56 days' toughness of SWC can be increased to 17 times in case of addition 0.5% fiber volume of steel fibers (ST1). While combination between 30 mm hooked end steel fibers and micro steel fibers (STST) can increase the toughness about 21 times at 0.5% V_f and by 20 at 0.75% V_f. 5D fibers at 0.5% V_f increase the toughness of SWC 17 times and by 30 times at V_f of 0.75%. In case of the 4D and 3D steel fibers at V_f of 0.5% the toughness of SWC can increase 16 times and by 4 times in case of 0.5% V_f of STPL.

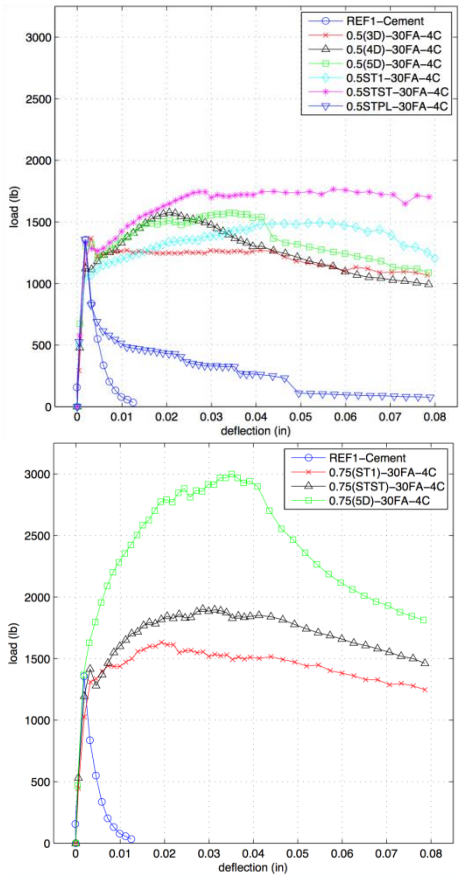

Figure 2. 56-days Flexural strength and flexural Toughness for different SWCs and FR-SWCs

Crack resistance of FR-SWC

Concrete is a brittle material that can not resist cracks. Figure 3 shows the load Vs the crack mouth opening displacement (CMOD) curves of (15cm*15cm*55cm) notched Beams of different FR-SWCs loaded at the mid span with a single point load. Fibers can change completely the flexural behavior of concrete, where FR-SCC can sustain cracking up to 0.14-inch crack width and more. In case of 0.5% fiber volume of 30 mm steel fibers (ST1) with 4% Type-G EA the residual stresses at 0.14-inch crack width were 545 Psi which is 92% of the peak stresses, while at 0.75% V_f the residual stresses were 54%. In case of 5D fibers at 0.5% V_f the residual stresses were 999 Psi which is 67% of the peak stresses and were 725 Psi which is 74%. In case of STPL fibers at 0.5% the residual stresses were 72 Psi which is 14% of the peak stresses. In case of 4D fibers at 0.5% the residual stresses

were 645 Psi which is 72% of the peak stresses and the stresses were 699 Psi which is 80% of the peak stresses in case of 0.5% of 3D steel fibers.

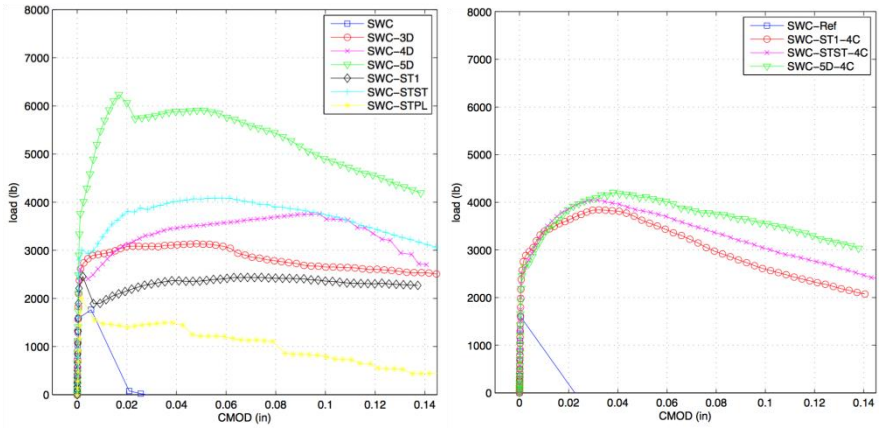

Figure 3. 56-days Flexural crack resistance for different SWCs and FR-SWCs

Conclusions

1. *D*/*a* passing ability index of FR-SWC is inversely proportional to the fiber factor (Vf Lf/ df) a linear relation ship between them was obtained by the author which is very closed to what obtained by Khayat et al., (2014) [2].
2. Hooked end steel fibers can increase the 56 days' splitting tensile strength of SWC about 58% in case of the 30 mm hooked end steel fibers (ST1) at fiber volume (V_f) 0.5% and by 113% at 0.75% V_f, while combination between 30 mm hooked end steel fibers and micro steel fibers (STST) can increase the splitting tensile strength about 66% at 0.5% V_f and by 92% at 0.75% V_f. 5D fibers at 0.5% V_f increase the splitting tensile strength by 87% and by 108% at V_f of 0.75%.
3. Hooked end steel fibers can increase the 56 days' flexural strength of SWC about 6% in case of the 30 mm hooked end steel fibers (ST1) at fiber volume (V_f) 0.5% and by 15% at 0.75% V_f, while combination between 30 mm hooked end steel fibers and micro steel fibers (STST) can increase the flexural strength about 24% at 0.5% V_f and by 35% at 0.75% V_f. 5D fibers at 0.5% V_f increase the flexural strength by 11% and by 114% at V_f of 0.75%.
4. The 56 days' toughness of SWC can be increased to 17 times in case of addition 0.5% fiber volume of steel fibers (ST1). While combination between 30 mm hooked end steel fibers and micro steel fibers (STST) can

increase the toughness about 21 times at 0.5% V_f and by 20 at 0.75% V_f. 5D fibers at 0.5% V_f increase the toughness of SWC 17 times and by 30 times at V_f of 0.75%.

5. In case of 0.5% fiber volume of 30 mm steel fibers (ST1) with 4% Type-G EA the residual stresses at 0.14-inch crack width were 545 Psi which is 92% of the peak stresses, while at 0.75% V_f the residual stresses were 54%. In case of 5D fibers at 0.5% V_f the residual stresses were 999 Psi which is 67% of the peak stresses and were 725 Psi which is 74%.

References

[1] Khayat, K. (1999), *ACI MATERIALS JOURNAL*, vol. 43, n. 96, p. 346.
[2] Khayat, K., Kassimi, F. and Ghoddousi, P. (2014), *ACI MATERIALS JOURNAL*, vol. 13, n. 111, p. 113.
[3] Voigt, T., Bui, V. and Shah, S. (2014), *ACI MATERIALS JOURNAL*, vol. 26, n. 101, p. 233.

Nanoscale Fiber Reinforced SCC: Impact of MWCNTs on the Fresh Properties and Mechanical Properties

M.K. Katotriotou[1], Ch.A. Argyriou[1], P.A. Danoglidis[1], M.G. Falara[1], G.D. Panagiotakis[1] and M.S. Konsta-Gdoutos[2]

[1] PhD Candidate, Department of Civil Engineering, Democritus University of Thrace,12 Vas. Sofias, Xanthi 67100, Greece,
mkatotri@civil.duth.gr,cargyrio@civil.duth.gr, mfalara@civil.duth.gr, pdanogli@civil.duth.gr, panagiotakiscivil@gmail.com
[2] Professor, Department of Civil Engineering, Democritus University of Thrace, 12 Vas. Sofias, Xanthi 67131, Greece,
mkonsta@civil.duth.gr

Abstract Carbon fibers at the nanoscale, thanks to their exceptional properties and high surface-to-volume ratio, are known to improve the pore structure of concrete, accelerate the C-S-H gel formation, increase strength, stiffness and toughness, and provide the electrical conductivity necessary for real time monitoring of the material's stress distribution. In this work, a method in producing nano-reinforced self-compacting concrete using multiwall carbon nanotubes (MWCNTs) at exceedingly small volume fractions is described. Specifically, we focus on two areas: (i) the technical challenges associated with the effective dispersion and utilization of the MWCNTs in SCC and; (ii) the effect of MWCNTs on the flowability, filling and passing ability, hardened properties and fracture characteristics of nanoengineered self-compacting concrete.

Keywords: *Self-compacting concrete (SCC), Multiwall carbon nanotubes (MWCNTs), Strength, Stiffness, Toughness, Fresh properties.*

Introduction

Nanotechnology has immense potentials and abilities to control the materials world including cement based materials. By the nanomodification of the material utilizing nanoparticles and nanoscale fibers new multifunctional, high performance cementitious nanocomposites that could be used in a variety of applications [1, 2] can be developed. The introduction of nanoparticles has been found to improve the pore structure of conventional concrete, reduce the materials' porosity, accelerate

the rate of hydration, and enhance the mechanical properties as well as the durability of the cementitious nanocomposites [3]. In the same way, the incorporation of highly dispersed carbon nanotubes (CNTs) and/or nanofibers (CNFs) at low concentrations has been shown to effectively arrest the cracks at the nanoscale, imposing significant improvements in the fracture properties and the durability of the cementitious matrix [1, 2, 4-8]. These exciting developments however, have not yet found considerable application in the research of self-compacting concrete. SCC is formulated to achieve four main attributes: deformability, flowing ability, resistance to segregation and passing ability [9]. The addition of nanoparticles generally has been shown to increase the viscosity, improve the cohesiveness and reduce the bleeding and the segregation of self compacting concrete [10-12]. Moreover, nanoengineered self-compacting concrete, using any type of nanoparticles such as nanosilica and nanoclay, presents greatly improved mechanical performance [13-15]. To the authors' knowledge no other research group has yet published research on nanomodified SCC concrete using MWCNTs.

The objective of this study is to investigate the fresh and mechanical properties of MWCNT reinforced SCC. SCC nanocomposites reinforced with well dispersed MWCNTs at an amount of 0.1 wt% of cement were fabricated. In most of the studies dispersion of nanoparticles consists of simply stirring the nanoparticles at high speed in water with superplasticizer before mixing [16-17]. In this work, for the effective dispersion of MWCNTs the revolutionary method developed by Konsta-Gdoutos et al. was followed [18-19]. An investigation on the effect of the nanoscale fibers on the fresh properties of the concrete matrix was performed by conducting slump flow test and J-Ring test. The mechanical properties were studied by conducting four-point bending tests. Results compared with similarly processed reference SCC without the nano reinforcement are clearly showing that the incorporation of MWCNTs in the concrete matrix significantly improves the mechanical and fracture properties of the concrete matrix.

Experimental Program

Materials

The material investigated, in this study, was a nanomodified SCC with MWCNTs. The characteristic properties of MWCNTs are shown in Table I. The mixtures were prepared with commercially available Type I ordinary Portland cement (OPC) and standard sand according to EN 196-1. Limestone powder was added as filler to optimize the particle packing and flow behavior of cementitious mixtures. Graded crushed granite with a maximum nominal size of 16mm and minimum nominal size of 4mm was used as coarse aggregates. A commercially available polycarboxylate based surfactant was employed for two purposes: to enhance workability and; to contribute to the effective dispersion of carbon fibers at the nanoscale. To allow homogenous dispersion of the nanoscale fibers in the mixing

water, MWCNTs suspensions including surfactant were prepared and the resulting aqueous suspensions were sonicated at room temperature following the method described by Konsta-Gdoutos et.al. [18-19]. Based on the authors` work, a surfactant to nanofibers weight ratio of 4.0 was found to achieve effective dispersion [1, 7]. The amount of cementitious materials was kept constant at 380 kg/m^3. All the mixtures were proportioned with a fixed water/cement ratio (w/c) of 0.51. The proportions of the designed mixture are shown in Table II.

Table I. Properties of MWCNTs

Fiber Type	Diameter [nm]	Length [μm]	Purity [%]	Surface area [m^2/gr]	Bulk density [gr/cm^3]	Aspect ratio
MWCNTs	20-45	≥10	>98	>100	≤0.18	307

Table II. Mix design proportions of SCC and MWCNTs/SCC

Material	Control SCC [kg/m^3]	MWCNTs/SCC [kg/m^3]
Cement	380	380
Limestone filler	100	100
Sand 0-2	1000	1000
Aggregates 4-16	700	700
Water	194	194
SP	6.1	7.6
MWCNTs	-	0.38
SP amount (%wt of cement)	1.6	2.0
MWCNTs amount (%wt of cement)	-	0.1

Mix proportions and specimen preparation

Mixing of the materials was performed according to procedure outlined by ASTM C192 into batches of ¼ volume. Cementitious materials and fine aggregates were firstly mixed using a standard robust mixer without addition of any aqueous solution until they are thoroughly blended. Water or MWCNTs aqueous solution, in case of nanomodified SCC, was then added to the mixture and the mass was mixed until the mortar was homogeneous in appearance and had the desired consistency. Finally, coarse aggregates were added and the entire batch was manually mixed in parallel with the quantity of superplasticizer until the coarse aggregates were uniformly distributed throughout the mixture (Figure 1). Subsequently, the fresh properties of SCC mixture were determined and the concrete was then placed in prismatic 7×8×38 cm oiled molds and kept for one day

at room temperature covered with a plastic membrane to minimize evaporation. Following demolding, the specimens were cured in saturated-lime water until the age of testing.

Figure 1. Mixing procedure of SCC

Fresh properties

Fresh properties tests were performed to determine the rheological properties of SCC mixtures. According to the EFNARC [20], a concrete mixture can only be classified as SCC if the requirements for filling, passing and segregation resistivity characteristics are fulfilled. The workability of SCC mixtures was evaluated by standard test methods. To quantify the flowability and passing ability of SCC, slump flow tests and J-ring tests were conducted according to ASTM C1611 and ASTM C1621, respectively.

The slump flow value represented by the mean diameter (D, measured in two perpendicular directions) was calculated. The time required (t_{50}) for the SCC mixtures to reach a slump flow diameter of 50cm is within 2–5s for both mixtures. The results are in full compliance with the corresponding limits proposed by EFNARC guidelines (Table II). The passing ability determined by J-ring test was successfully achieved. Specifically, t_{50J} [sec] was measured; maximum spread in J-ring (D_J) and J-ring blocking step (B_J) were calculated and indicated to be within the acceptable range. At this point it should be mentioned that no segregation was observed visually (Figure 2).

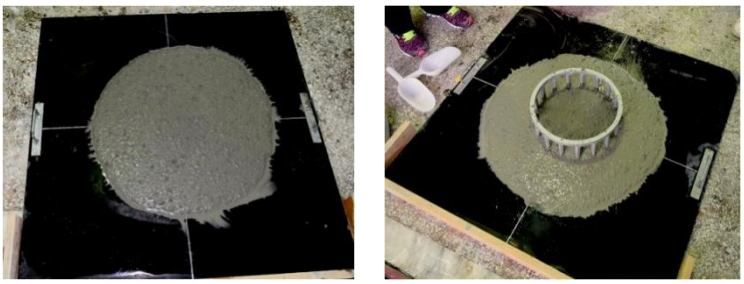

Figure 2. Fresh SCC properties testing

Table III. Fresh SCC Properties and acceptance criteria according to EFNARC 2002.

	Control SCC	MWCNTs SCC	EFNARC 2002 Typical Range of Values	
			min	max
Slump flow D [cm]	73.6	69.5	65	80
t_{50} [sec]	2.0	2.5	2	5
J-ring flow D_J [cm]	72.0	67.0	-	-
t_{50J} [sec]	2.0	2.5	-	-
J-ring blocking step B_J [cm]	0.95	0.975	0	1

Mechanical properties

Mechanical properties of SCC nanocomposites were evaluated by four point bending tests on prismatic 7x8x38 cm beams at the age of 28 days, using a 25 kN MTS servo-hydraulic, closed-loop testing machine under displacement control (Figure 3). The rate of displacement was kept at 0.1 mm/min. The ASTM C293 was followed to determine the average values of the flexural strength and Young's modulus. After four point bending experiments the two halves of each prism were tested by compression test following the ASTM C39.

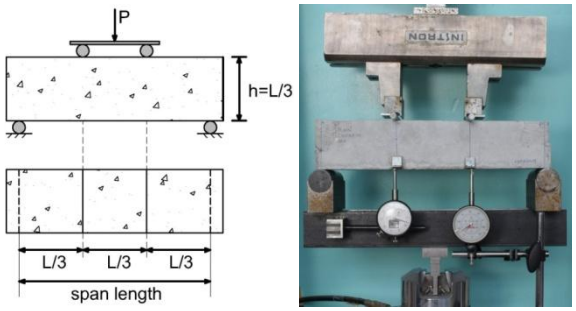

Figure 3. Experimental setup of 4 point bending

Results and Discussion

The fresh state properties of 28 days 0.1%wt MWCNTs nanomodified SCC were experimentally investigated and compared with similarly processed reference SCC without the nanoscale fiber reinforcement (Table III). As discussed earlier, both

SCC mixtures exhibited acceptable filling and passing ability results and resistance against segregation. The incorporation of well dispersed MWCNTs in SCC matrix resulted in significant reduction of workability, as indicated from preliminary experiments due to the adsorption of water from the nanofibers` surface area. Specifically, the calculated flow values were lower than the minimum acceptable values recommended by EFNARC. Therefore, as it is shown in Table II, the SCC nanoreinforced mixtures demanded a larger amount of surfactant than this needed for the reference mix in order to achieve no substantial difference in rheological performance. All of the SCC mixtures exhibited satisfactory slump flow of 73.6 cm diameter for control SCC and 69.5 cm for nanomodified SCC (Table III), which is indicative of sufficient workability.

The four point bending tests results of the flexural strength, Young`s modulus and flexural toughness of 28 days SCC and SCC nanocomposites reinforced with MWCNTs at an amount of 0.1wt% are presented in Table IV. To the authors` knowledge, it is the first time that nanomodified SCC with well dispersed MWCNTs were produced. 0.1wt% MWCNTs/SCC nanocomposites outperformed the conventional SCCs exhibiting exceptional increase in all three mechanical properties: 53% in flexural strength; 68% in Young`s modulus; and 60% in flexural toughness. Figure 4 presents the flexural strength of 28 day SCC and nanomodified SCC. The markers in the graph indicate the low and high values in the determination of flexural strength. These significant increases of mechanical properties are an effect of an enhanced crack arresting at the nanoscale, which leads to a controlled coalescing process of cracking at the nano- and micro scale and allows the material to greatly improve its toughness and mechanical performance. At this point, it should be mentioned that the quality and degree of dispersion is the key for the successful enhancement of the mechanical properties of SCC matrix. Besides dispersion method, several parameters are considered to improve strength, stiffness and toughness of SCC nanocomposites. These parameters include diameter and length of carbon fibers at the nanoscale and the strength of MWCNT/SCC matrix interfacial characteristics [21-22]. To further support the effect of nanoscale fibers, besides the experimental values of strength, stiffness and toughness, load-deflection curves of 28 days SCC and MWCNTs/SCC nanocomposites are presented in Figure 5. Comparing the SCC and 0.1 wt% MWCNT SCC nanocomposites, a higher load is required to achieve the same deflection. As reflected in the curves the MWCNT incorporation effectively increases fracture load; initial compliance of load-deflection curve and the area under the curve implying enhanced strength, stiffness and energy absorption ability of the nanocomposites, respectively. Compressive strength of 28 days SCC and 0.1wt% MWCNTs SCC are presented in Table IV. Nanoreinforced SCC exhibits approximately 1.2 times higher compressive strength over the reference mixture but unlike the four point bending results the nanofibers incorporation leads in lower improvement of compressive strength (13%).

Table IV. Mechanical properties of 28 days SCC and 0.1 wt% MWCNTs nanomodified SCC

	Flexural strength (MPa)	Young`s modulus (GPa)	Flexural toughness (N×mm)	Compressive strength (MPa)
SCC	5.9	23.4	232	37.0
SCC+MWCNTs 0.1wt%	9.0	39.4	372	41.7

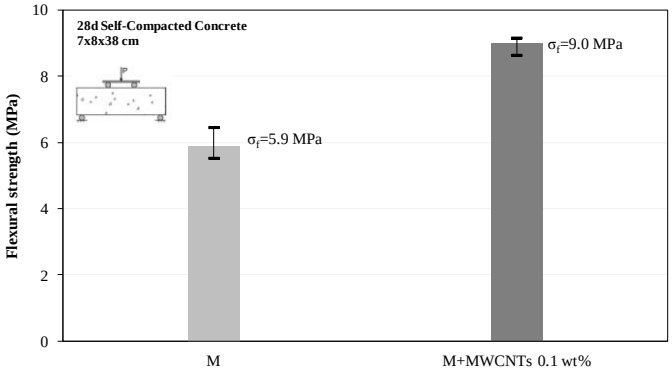

Figure 4. Flexural strength of 28 days SCC and SCC reinforced with MWCNTs at an amount of 0.1 wt%

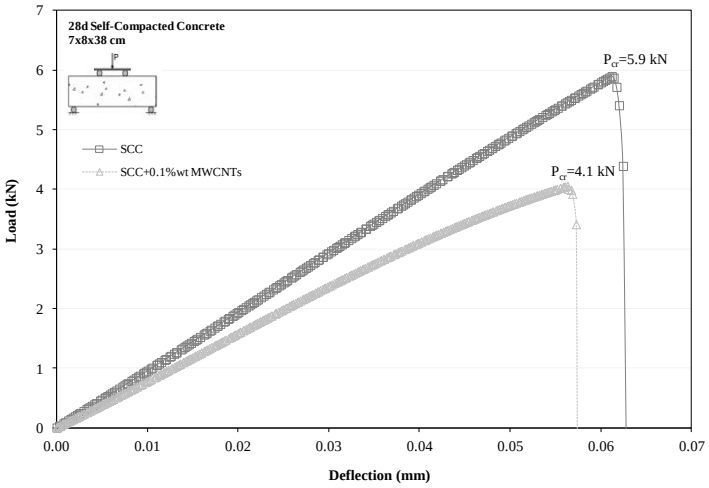

Figure 5. Load-deflection curves for 28 days SCC and SCC reinforced with MWCNTs at an amount of 0.1 wt%

Conclusions

An in depth investigation of the fresh and mechanical properties of SCC reinforced with well dispersed MWCNTs was performed**.** The results of slump flow, t_{50}, J-ring flow, t_{50J} and J-ring block are in full compliance with the corresponding limits proposed by the EFNARC 2002. Flexural strength, Young`s modulus, flexural toughness and compressive strength were investigated and compared with similarly processed reference SCC mixes without the nano-reinforcement. The excellent reinforcing capability of MWCNTs is demonstrated by an exceptional improvement in flexural strength (53%), Young`s modulus (68%), and flexural toughness (60% for MWCNTs).

References

[1] Konsta-Gdoutos, M.S.; Metaxa, Z.S.; Shah, S.P. (2010), *Cement and Concrete Research*, V. 40, pp. 1052-1059.
[2] Konsta-Gdoutos, M.S.; Metaxa, Z.S.; Shah, S.P. (2010), *Cement and Concrete Composites*, V. 32, pp. 110-115.
[3] Sanchez, F.; Sobolev, K. (2010), *Construction and Building Materials*, V. 24, pp. 2060-2071.
[4] Metaxa, Z.S.; Konsta-Gdoutos, M.S.; Shah, S.P. (2010) *Transportation Research Record*, V. 2142, pp. 114-118.
[5] Metaxa, Z.S.; Seo, J.-W.T.; Konsta-Gdoutos, M.S.; Hersam, M.C.; Shah, S.P. (2012) *Cement and Concrete Composites*, V.34, pp. 612-617.
[6] Metaxa, Z.S.; Konsta-Gdoutos, M.S.; Shah, S.P. (2012), *Cement and Concrete Composites*, doi.org/10.1016/j.bbr.2011.03.031.
[7] Metaxa, Z.S.; Konsta-Gdoutos, M.S.; Shah, S.P. (2009), *ACI Special Publication*, V. 267, pp. 11-20.
[8] Metaxa, Z.S.; Konsta-Gdoutos, M.S.; Shah, S.P. (2010), *ACI Special Publication*, V. 270 SP, pp. 115-126.
[9] ACI Committee 237, "Self –Consolidating Concrete (ACI 237R-04), American Concrete Institute Farmington Hills, MI., 2007.
[10] Tregger, N. A.; Pakula, M.; Shah, SP. (2010), *Cement and Concrete Research*, V. 40, pp. 384-391.
[11] Tregger, N. A.; Pakula, M.; Shah, S. P. (2010), *Transportation Research Record*, V. 2141, pp. 68-74.
[12] Kawashima, S.; Kim, JK.; Coor, D.J.; Shah, SP. (2012), V. 36, pp.749-757.
[13] Morsy, M. S.; Alsayed, S. H.; Aqel, M. (2010), *International Journal of Civil & Environmental Engineering*, Vol. 10, pp. 23-27.
[14] Jalal, M.; Mansouri, E.; Sharifipour, M.; Pouladkhan, A.R. (2012), *Materials and Design*, V. 34, pp. 389-400.
[15] Nazari, A.; Riahi, S. (2011), *Composites: Part B*, V. 42, pp. 570-578.
[16] Nazari, A.; Riahi, S. (2010) *Materials Science and Engineering: A*, V. 527, pp. 7663-7672.

[17] Madandoust, R.; Ranjbar, M.M.; Mousavi, S.Y. (2011), *Construction and Building Materials*, V 25, pp. 3721-3731.
[18] Shah S.P., Konsta-Gdoutos M.S., Metaxa Z.S. (2009), *US Patent and Trademark Office*, United States Patent Application 20090229494, Publication number WO/2009/099640.
[19] Hersam M.C., Seo J.-W.T., Shah S.P., Konsta-Gdoutos M.S., Metaxa Z.S. (2014) Publication number US8865107 B2 and US20120042806 A1.

[20] Specification and Guidelines for Self-Compacting Concrete. EFNARC. February 2002.
[21] Chen, Y.L., Liu, B., He, X.Q., Huang, Y., Hwang, K.C. (2010), *Composites Science and Technology*; 70 (9):1360-1367.
[22] Chen, Y., Wang, S., Liu, B., Zhang, J. (2015), *Composite Structures*, 122:496-506.

Effect of Type of Fibers on Flexural Performance of Self-Consolidating Concrete

Ahmed Abdelrazik [1] Kamal H. Khayat [2] and Soo-Duck Hwang [3]

[1] Ph.D. candidate, Missouri University of Science and Technology, 202 ERL, 500 W. 16th St., Rolla, MO 65409-0710 atarm9@mst.edu

[2] Professor, Missouri University of Science & Technology khayatk@mst.edu

[3] Lead scientist, Missouri University of Science and Technology hwangso@mst.edu

Abstract This paper compares the performance enhancement in mechanical properties and cracking resistance that can be achieved when incorporating different types and combinations of synthetic fibers and steel fibers in self-compacting concrete (SCC). Two types of expansive agents (EA), including Type G and K EA were used in order to reduce shrinkage. Four types of fibers, including propylene syntactic fiber (PLP), hooked steel fiber (ST1), hybrid of crimpled steel and polypropylene multifilament fiber (STPL), and micro-macro steel fibers (STST) were incorporated at 0.5%. For SCC mixture made with the ST1 hooked steel fiber, two types of EAs were used as well as one more mixture without EA, while the Type G EA was used for the remaining fiber-reinforced self-compacting concrete (FR-SCC) mixtures. The incorporation of steel fibers is shown to provide greater peak stress and residual strength compared to that of the synthetic fibers and hybrid fibers. Test results revealed that the FR-SCC containing hybrid fibers (92% steel and 8% polypropylene fibers) of low fiber factor (L/D) of 34 exhibited lower flowability and passing ability than similar mixtures made with ST1 fibers of higher fiber factor of 80. The FR-SCC made with the combination of the micro and macro steel fibers (STST) showed the highest mechanical properties 0.5% fiber volume. The combination of the micro and macro steel fibers (STST) also resulted in greater flexural strength and flexural toughness compared to the macro steel fibers. EA may greatly reduce shrinkage and resist cracking from restrained shrinkage, while regarding the mechanical properties and the flexural crack resistance it had no significant effect.

Keywords: *Expansive agent, cracking resistance, fibers, self-compacting concrete.*

Introduction

The workability requirements for successful placement of self-compacting concrete (SCC) necessitate that the concrete exhibits excellent deformability and proper stability to flow under its own weight through closely spaced reinforcement without segregation and blockage [1]. SCC gains its high workability mainly due to high volume of paste and high water-to-cement ratio (w/c) resulting in high shrinkage and cracking. The incorporation of fibers to SCC helps in reducing shrinkage. Possible side effect of adding fibers is the decrease in workability mainly in terms of flowability, passing ability and filling capacity. Flowability change can be adjusted by modifying the mixture composition, however passing ability of fiber reinforced self-consolidating concrete (FR-SCC) never reach the same level of passing ability of SCC [2]. One major advantage of the use of fibers to SCC is to enhance mechanical properties especially, tensile strength, toughness, and cracking resistance. Fibers can totally change the behavior of SCC from a brittle material to a ductile material. This paper compares the flexural behavior of FR-SCC made with different fiber types in terms of the toughness and cracking resistance.

Experimental program

In total, ten SCC mixtures were investigated. Two plain SCC mixtures were made without any fibers; one SCC with Class C fly ash (FA) and the other without any FA. The remaining mixtures were made with different types and combinations of fibers, which included seven FR-SCC mixtures with EA and one without any EA. Fresh properties were determined for all of the investigated mixtures and mixtures established high stability were tested for mechanical properties and cracking resistance. ASTM C39 test was performed in order to evaluate the compressive stress of the cylinder specimens made from SCC and FR-SCC. ASTM C39 and ASTM C496 tests were performed in order to evaluate the compressive stress and the splitting tensile strength of the cylinder specimens made from SCC and FR-SCC, while ASTM C78 and ASTM C1609 tests were followed in order to compute the flexural strength and the toughness of the small scale beams made from SCC and FR-SCC. RILEM TC 162 test was performed in order to estimate flexural crack resistance of FR-SCC.

Materials and mixture proportioning

Nine SCC mixtures were made with ASTM Type I/II cement and 30% Class C FA replacement, by mass of total binder. One reference SCC was prepared with only Type I/II cement without any FA. Continuously graded natural sand with a fineness modulus of 2.6 and crushed limestone aggregate with a nominal maximum

aggregate size of 10 mm (0.39 in.) were used. The coarse aggregate and sand had specific gravities of 2.54 and 2.63, respectively, and water absorption values of 3.06% and 0.62%, respectively. Polycarboxylate-based high-range water-reducer (HRWR), synthetic resin-type air-entraining admixture (AEA), and polysaccharide viscosity-modifying admixture (VMA) were also used. Four fiber types, including propylene syntactic fiber (PLP), hooked steel fiber (ST1), hybrid of crimpled steel fiber, and polypropylene multifilament fiber (STPL), and micro-macro steel fibers (STST) were incorporated at a fixed fiber volume of 0.5%. Table 1 presents the characteristics of the fibers. The w/c was kept constant at 0.42. Two types of expansive agents (EA), including Type G and K at 4% and 8% by mass of total binder, respectively, were used in order to reduce shrinkage and investigate their effect on mechanical properties.

Table I. Characteristics of fibers

	ST1	STST		PLP	STPL		3D	CA
Material	Macro Steel	80% Macro Steel	20% Micro Steel	Propylene	8% Poly-propylene	92% Steel	Steel	Carbon
Shape [1]	Hook	Hook	Straight	Mono-flament	Multiflament	Crimped	Hook	Straight
					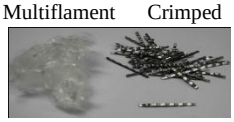			
Color	Golden	Golden	Golden	Transparent	Transparent	Grey	Grey	Black
Cross section	Circular	Circular	Circular	Rectangular	Circular	Rectangular	Circular	Circular
Specific gravity	7.85	7.85	7.85	0.92	0.91	7.85	7.85	7.85
Length (mm)	30	30	13	40	5-15 [2]	50	60	102
Equivalent diameter (mm)	0.55	0.55	0.2	0.44	0.05	0.9	0.92	3.18
Aspect Ratio	55	55	65	91	100-300	56	65	32
Modulus of elasticity (GPa)	200	200	200	9.5	N.A.	7.16	210	242
Tensile strength (MPa)	1100-1300	1100-1300	1100-1300	620	Neglected	413	1160	4137

Mixture proportioning

Khayat et al. (2014) [2] proposed a mixture-proportioning method for FR-SCC. They considered the multi-aspect concept proposed by Voigt [3] for calculating the thickness of mortar covering the coarse aggregate and the fibers. The method recommends reducing the volume of coarse aggregate with the addition of fibers to maintain a fixed thickness of a mortar layer (t_{cm}) over the fibers and coarse aggregate. This procedure was used to adjust the mixture proportioning of SCC

when adding fibers to produce a FR-SCC that has fresh properties similar to those of SCC without fibers. The reference SCC mixture proportioning is given in Table 2 and is referred to as R1. The mixture employed as a reference SCC in [2]. The average mortar thickness method was used to design the rest of the mixtures (R2 and 1 to 7). While R3 is the same as R1 except for the incorporation of 30% FA. The AEA was added to all mixtures to secure air volume of a value 7.5% ± 1.5%.

Table II. Mixture proportions SCC and FR-SCC

	Fiber type	V_f (%)	Water kg/m^3	Cement Type I/II kg/m^3	Fly Ash kg/m^3	Expansive Agent		Sand kg/ m^3	Coarse Agg. kg/m^3	VMA ml/m^3	HRWR ml/m^3	AEA ml/m^3
						Type	kg/ m^3					
R1	-	0	193	475	0	-	-	746	747	4167	1083	104.2
R2	ST1	0.5	193	319.2	136.8	-	-	780	681	4286	1429	104.5
R3	-	0	193	332.5	142.5	-	-	746	747	4182	1545	104.5
1	ST1	0.5	193	305.9	131.1	K-Type	38	728	734	4167	2083	104.2
2	ST1	0.5	193	319.2	136.8	G-Type	19	728	734	4167	1458	104.2
3	PLP	0.5	193	319.2	136.8	G-Type	19	731	731	4167	1875	104.2
4	3D	0.5	193	319.2	136.8	G-Type	19	723	739	4167	1500	104.2
5	STPL	0.5	193	319.2	136.8	G-Type	19	721	740	4167	1803	104.2
6	STST	0.5	193	319.2	136.8	G-Type	19	733	732	4167	1875	104.2
7	CA	0.5	193	319.2	136.8	G-Type	19	717	745	4167	1500	104.2

Test methods

All of the 10 investigated mixtures were tested for slump flow and visual stability index. Fresh property testing included slump flow, J-Ring, modified J-Ring [2], bleeding, air content, specific gravity, and surface settlement. The modified J-Ring was carried out for the FR-SCC and consists of a ring with eight bars compared to 16 bars in the standard test (ASTMC1621). The J-Ring, the modified J-Ring, the bleeding, air content, specific gravity and the settlement tests were performed only for mixtures that showed acceptable workability. Slump flow was measured after 10 and 70 min. Sampling of (100x200 mm) cylinders to determine compressive and splitting tensile strengths, four beams (75x75x40 mm) for flexural strength (ASTM C78) and flexural toughness (ASTM C1609) and four notched beams (150x150x550 mm) for crack resistance (RILEM TC-162) was done only for eight out of 10 mixtures that showed acceptable workability.

Experimental results and discussion

Fresh properties

Table 3 summarizes the fresh properties of the investigated mixtures. The AEA demand for propylene fibers (PLP) fibers and hybrid fibers of polypropylene and steel (STPL) was lower than that of ST1 and STST. Generally, fibers decreased the

workability of SCC, especially the passing ability. The increase in fiber factor (V_f L_f/ d_f) decreased the passing ability of FR-SCC. Fig. 1 shows the relationship between the fiber factor and the modified J-Ring ratio, the ratio between the diameter of spread to the average height (D/a) is referred to as passing ability index and is shown to decrease with the increase in fiber factor regardless of the fiber type. Similar relationship was reported in [2]. Type K EA had significant effect in reducing slump flow of FR-SCC with time, especially with the moderate w/c of 0.42 in use. The decrease in fluidity resulted in enhancement of stability compared to others with Type G EA or without any EA. Type G EA is shown to increase the passing ability of FR-SCC, but it can decrease slightly stability.

Table III. Fresh properties of SCC and FR-SCC mixtures

No	Fiber type	V_f (%)	EA Type	Unit weight (kg/m^3)	Air (%)	Slump flow (mm) 10 min / 60 min	J-Ring (mm)	Modified J-Ring D/a (mm/mm)	Visual Stability Index	Bleeding (%)	Surface Settlement (%)
R1	-	0	-	2152	6.5	680/640	590	650/29	0	0.61	0.57
R2	ST1	0.5	-	2149	8	660/520	520	580/43	0	0.3	0.35
R3	-	0	-	2155	8	670/530	590	660/30	0	0.33	0.20
1	ST1	0.5	K-Type	2205	7	700/350	575	630/47	0	0	0.31
2	ST1	0.5	G-Type	2184	6.8	690/640	565	605/45	0	0	0.64
3	PLP	0.5	G-Type	2090	8.5	670/500	500	550/44	1	0.47	0.53
4	3D	0.5	G-Type	-	-	660/-	-	-	3	-	-
5	STPL	0.5	G-Type	2102	9	690/520	600	620/43	0	0.38	0.65
6	STST	0.5	G-Type	2144	8	700/535	480	600/40	0	0.41	0.34
7	CA	0.5	G-Type	-	-	660/-	-	-	3	-	-

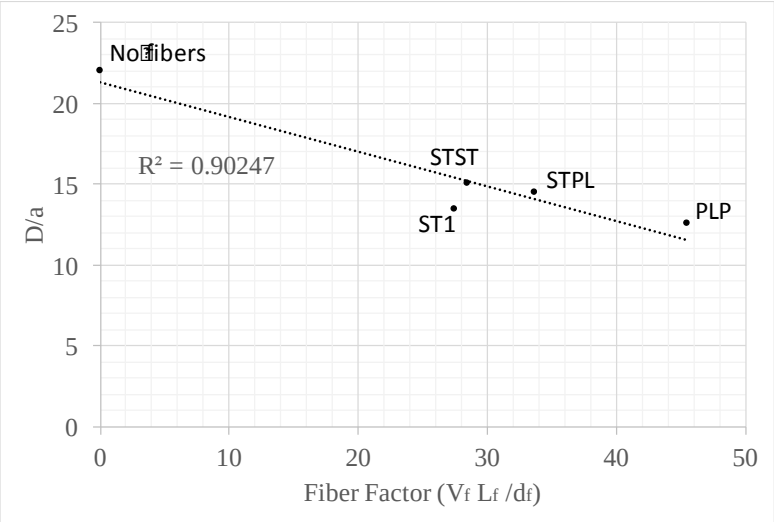

Figure 1. Effect of the fiber factor on the passing ability of FR-SCC

Mechanical properties of FR-SCC

Table 4 shows the compressive strength, splitting tensile strength, flexural strength, toughness, and crack resistance of SCC and FR-SCC. The incorporation of Hooked end steel fibers (ST1) increased the 56-day compressive strength of SCC by 8% and 17% in mixtures containing 4% and 8% G-type and K-type, respectively. On the other hand, the combination between 30 mm hooked end steel fibers and micro steel fibers (STST) increased compressive strength by 30%. The use of 0.5% ST1 increased the 56-day splitting tensile strength by 43% and 56% in mixtures containing 4% and 8% G-type and K-type, respectively. The use of the combined micro-macro steel fibers (STST) increased the splitting tensile strength by 68%. A hybrid of 50 mm crimpled steel fibers and micro polypropylene fibers (STPL) increased the 56-day splitting tensile strength by 12%. Propylene fibers (PLP) increased the 56-day splitting tensile strength of SCC by 11% in the case of the 40 mm Propylene fibers (PLP) with 4% G-type EA. The 56-days flexural strength with the use of 0.5% ST1 increased by 17% and 5% in mixtures containing 4% and 8% G-type and K-type, respectively. The combination between 30 mm hooked end steel fibers and micro steel fibers (STST) increased the 56-day flexural strength by 32%.

Table IV. Hardened properties of FR-SCC

No	Fiber type	V_f (%)	EA Type	Compressive strength (psi)		Splitting tensile strength (psi)		Flexural strength (psi)		Toughness (lb.in)		First Crack stress (psi)		Residual stress (psi)	
				28 d	56 d	28 d	56 d	28 d	56 d	28 d	56 d	28 d	56 d	28 d	56 d
R1	-	0	-	4540	4780	325	360	381	410	4.75	5.13	425	459	0	0
R2	ST1	0.5	-	4560	4780	420	465	676	729	106	114	456	493	323	349
R3	-	0	-	4350	4470	315	340	465	500	4.42	4.78	-	-	-	-
1	ST1	0.5	K-Type	5100	5110	500	530	490	526	72	78	495	535	459	488
2	ST1	0.5	G-Type	4700	5080	440	485	540	585	88	95	545	590	236	246
3	PLP	0.5	G-Type	4020	4230	365	380	360	388	30	33	369	399	151	166
4	3D	0.5	G-Type	-	-	-	-	-	-	-	-	-	-	-	-
5	STPL	0.5	G-Type	3840	5000	365	380	453	482	30	34	485	523	234	260
6	STST	0.5	G-Type	5090	5900	490	570	612	668	95	110	535	562	354	385
7	CA	0.5	G-Type	-	-	-	-	-	-	-	-	-	-	-	-

Toughness of FR-SCC

The incorporation of fibers had a considerable impact on ductility of SCC as shown in Fig. 2 the load deflection curves of beams made with different FR-SCCs. The incorporation of Hooked end steel fibers (ST1) increased the 56-day toughness of SCC by 20 and 16 times in mixtures containing 4% and 8% G-type and K-type, respectively. The combination of 30 mm hooked end steel fibers and micro steel fibers (STST) increased the toughness by 23 times. The 0.5% fiber volume of propylene fibers (PLP) increased the toughness of the FR-SCC by six times, while the use of STPL fibers increased the 56-day toughness by 7 times.

Some of the FR-SCC was shown to exhibit strain softening after concrete cracking such as the case for the STPL and PLP, which results in lower toughness compared to other FR-SCC mixtures made with ST1 and STST that had strain hardening. The incorporation of EA did not have a significant effect on ductility of FR-SCC.

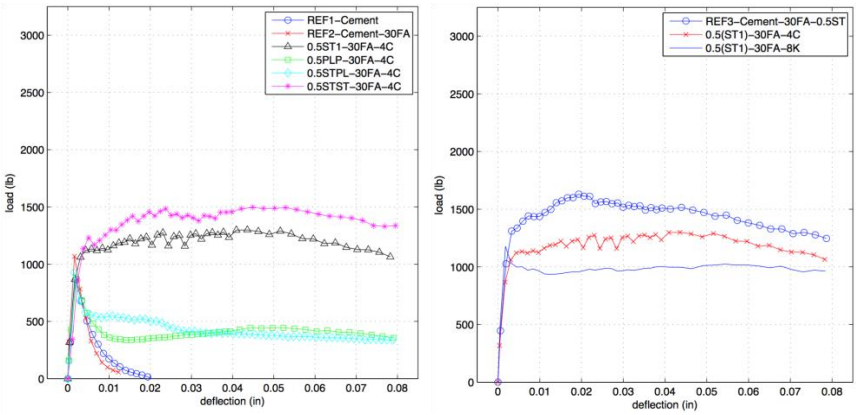

Figure 2. 56-day flexural strength and flexural toughness for SCCs and FR-SCCs

Crack resistance of FR-SCC

Fig. 3 shows the load vs. crack mouth opening displacement (CMOD) of the notched beams made with different FR-SCCs loaded at mid span with a single point loading. In the case of 0.5% fiber volume of 30 mm steel fibers (ST1) with 4% Type-G EA, the residual stress at 0.14-in. crack width was 246 psi, which is 42% of the peak stress. On the other hand, the use of 8% Type-K EA increased the residual stresses at 0.14-inch crack width to 488 psi, which is 91% of the peak stress. The combination of 30 mm hooked end steel fibers and micro steel fibers (STS) resulted in residual stresses of 385 psi, which is 67% of the peak stress. In the case of the 40 mm propylene fibers (PLP) with 4% G-type EA, the residual stress was 166 psi, which is 42% of the peak stress. In the case of hybrid of 50 mm crimpled steel fibers and polypropylene fibers (STPL) with 4% G-type EA, the residual stress was 166 psi, which is 50% of the peak stresses.

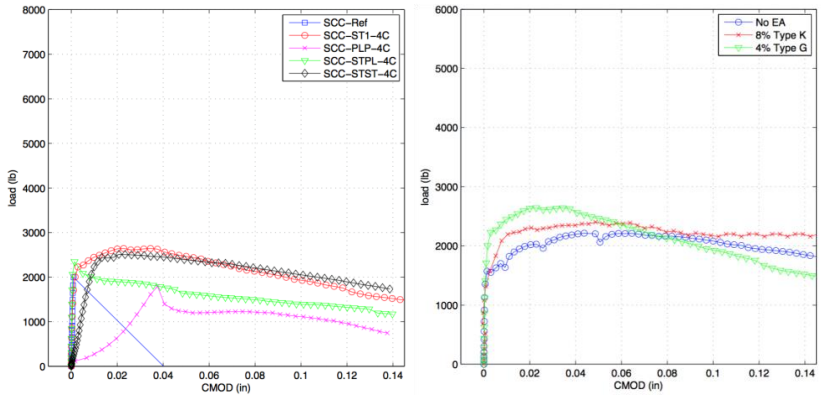

Figure 3. 56-day flexural crack resistance for different SCCs and FR-SCCs

Conclusions

Based on the results presented in this paper, the following conclusions can be warranted:

1. The passing ability index (*D*/*a)* decreases with the increase in fiber factor, regardless of the fiber type.
2. The use of type G EA increases the passing ability of FR-SCC, but it can decrease slightly stability.
3. The use of type K EA resulted in considerable loss of filling ability with time of FR-SCC dropping by 350 mm in 60 min. This decrease in fluidity

results in enhancement of stability compared to others with Type G EA or without any EA

4. The use of Hooked end steel fibers (ST1) increases the 56-day compressive strength of SCC by 8% and 17% in mixtures containing 4% and 8% G-type and K-type, respectively. On the other hand, the combination between 30 mm hooked end steel fibers and micro steel fibers (STST) increases compressive strength by 30%
5. The use of 0.5% ST1 increased the 56-day splitting tensile strength by 43% and 56% in mixtures containing 4% and 8% G-type and K-type, respectively.
6. The use of the combined micro-macro steel fibers (STST) increases the splitting tensile strength by 68%.
7. The combination between 30 mm hooked end steel fibers and micro steel fibers (STST) increases the 56-day flexural strength of FR-SCC by 32%.
8. The incorporation of Hooked end steel fibers (ST1) increases the 56-day toughness of SCC by 20 and 16 times in mixtures containing 4% and 8% G-type and K-type, respectively.
9. The use of 0.5% fiber volume of propylene fibers (PLP) can increase the 56-day toughness of SCC beams to six times while in case of STPL fibers the toughness can increase to seven times.
10. Some of the FR-SCC exhibit strain softening after concrete cracking such as the case for the STPL and PLP, which results in lower toughness compared to other FR-SCC mixtures made with ST1 and STST that exhibit strain hardening. Toughness increases by 20 and 23 times in mixtures containing 0.5% fiber volume of ST1 and STST, respectively.
11. The use of 0.5% fiber volume of 30 mm steel fibers (ST1) with 8% Type-K EA results in the residual stress at 0.14-in. crack width of 488 psi which is 91% of the peak stresses, while in the case of combination of 30 mm hooked end steel fibers and micro steel fibers (STST) the residual stress at 0.14-in. crack width was 385 psi which is 67% of the peak stress.
12. The use of 0.5% fiber volume of 40 mm propylene fibers (PLP) with 4% G-type EA results in residual stress of FR-SCC beams at 0.14-in. crack width of 166 psi which is 42% of the peak stresses. In the case of hybrid of 50 mm crimpled steel fibers and polypropylene fibers (STPL) with 4% G-type EA the residual stress at 0.14-in. crack width is 166 psi which is 50% of the peak stress.

References

[1] Khayat, K. (1999), *ACI MATERIALS JOURNAL*, vol. 43, n. 96, p. 346.
[2] Khayat, K., Kassimi, F. and Ghoddousi, P. (2014), *ACI MATERIALS JOURNAL*, vol. 13, n. 111, p. 113.
[3] Voigt, T., Bui, V. and Shah, S. (2014), *ACI MATERIALS JOURNAL*, vol. 26, n. 101, p. 233.

Workability and Mechanical Properties of Expansive Self-Consolidating Concrete Reinforced with Hybrid Fibers

Qi Cao[1], Yinliang Cheng[2]

[1] Assistant Professor, State Key Laboratory of Coastal and Offshore Engineering, Dalian University of Technology, Dalian, China 116024.
[2] Master Student, State Key Laboratory of Coastal and Offshore Engineering, Dalian University of Technology, Dalian, China 116024.

Abstract The aim of this research is to study the effects of fibers on properties of expansive self-consolidating concrete (ESCC). Hooked end steel fibers and monofilament polypropylene fibers are used in the tests. A series of tests are conducted to investigate workability of fresh concrete and mechanical properties of hardened concrete. Slump flow and V funnel tests are carried out to evaluate the filling ability and passing ability of the fresh concrete. Mechanical properties including compressive strength, splitting tensile strength and flexural strength of hardened concrete are studied. Test results indicate that workability of fresh concrete decreases with increase of volume fraction of fiber. Combined addition of expansive admixture and fibers reduces the concrete strength of SCC at 7 days, while it does not influence the 28 days strength noticeably. It also indicates that steel fibers SCC beam shows deflection hardening behavior.

Keywords: *fibers; expansive SCC; workability; mechanical properties; deflection hardening behavior*

Introduction

Self-consolidating concrete (SCC) is a highly flowable, non segregating concrete that can spread into place, fill the formwork, and encapsulate the reinforcement without any mechanical consolidation [1]. It has excellent properties and has been widely used in engineering field. Since high content of cementitious materials are used in the design, self-consolidating concrete is prone to shrinkage cracks, seriously affecting the service life of self-consolidating concrete-made elements and structures. One way to decrease the shrinkage of SCC is adding expansive agent into self-consolidating concrete [2- 4]. It could compensate shrinkage of self-consolidating concrete and improve the cracking resistance of SCC [5]. Meng [2] reported that the shrinkage of SCC decreases with the increase of expansive agent dosage as well as increasing concrete age within a certain range. It also shows that curing time plays a significant role on the shrinkage of SCC with expansive agent indicating that the shrinkage is smaller when curing time is longer [3]. It was also found that, within a certain range, expansive agent can enhance the compressive strength, flexural strength and elastic modulus of the SCC [4, 5]. Thus, the incorporation of expansive agent in concrete can change the properties of the matrix.

Self-consolidating concrete reinforced by fibers (FRSCC) has gained a lot of attention and extensive research has been conducted. FRSCC possesses properties of both SCC and fiber. F.Aslani [6]'s study indicated that fibers can slightly reduce the creep of SCC，but increases the shrinkage of SCC in early stage. However when the age of SCC is more than 28 days, the creep and shrinkage of FRSCC are close to normal SCC. Although fibers cannot effectively restraint the shrinkage of self-consolidating concrete, they can control the early cracking of SCC, reducing the number and length of shrinkage cracks [7, 8]. As well known, incorporation of fibers in SCC decreases workability of the fresh SCC, and the reduction is getting larger as fiber content increases [9, 10]. Fibers could increase

early strength of concrete especially for steel fibers [11, 12]. Fibers have lower effect on modulus of elasticity of concrete in compression [11], but they can enhance the modulus of elasticity in tension [13]. There is no doubt that steel fibers can improve the tensile strength of SCC[11, 13], most of the reports show that propylene fibers also can improve the tensile strength of SCC. Flexural performance of beams can be improved by steel and hybrid fibers when the steel fiber volume content exceeds 0.50%, and the post-peak load capacity can be increased [12- 14].

Although the effect of expansive agent and fibers on properties of SCC has been studied respectively, the combined effect of both has not been investigated. In this paper, fiber reinforced expansive concrete is proposed. And the aim of this study is to study the effects of fibers on properties of expansive self-consolidating concrete (ESCC) and expansive highly flowable concrete (EHFC). The calcium oxide-sulphoaluminate type expansive agent was used to make expansive concrete with targeted high expansion rate. Then fibers (single steel fiber, hybrid steel and PP fiber) are adopted to optimize ESCC and the effect of fiber on workability and mechanical properties is studied

Experimental program

Materials

The materials used in the self-consolidating concrete composition are P.O42.5R ordinary Portland cement which meets the national standard of China with a density of 3.1 g/cm^3, Type I fly ash with density of 2.3 g/cm^3, calcium oxide-sulphoaluminate expansive admixture with expansion rate of (15-18) × 10^{-4} and dosage of expansive admixture is 8% in mass, river sand with fineness modulus of 2.72 and density of 2.65 g/cm^3; coarse aggregate with 5-10 mm gravel full grade with density of 2.7 g/cm^3, glycolic acid-based white powder superplasticizer (HRWRA). The properties of steel fiber (SF) and polypropylene (PP) fibers are shown in Table I.

Table I. Properties of fibers

Fiber type	Shape	Length L /mm	Diameter d /mm	Aspect ratio L /d	Tensile strength /Mpa	Elastic Modulus /GPa	Specific gravity/ g•cm^{-3}
ST	Hooked	35	0.55	64	>1150	200	7.85
PP	Straight	19	0.07	271	568	4.35	0.91

Specimen production

Expansive self-consolidating concrete was first made with target workability performance according to EFNARC[15]. Then steel fibers and hybrid steel and polypropylene fibers were added respectively into the mix to make fiber reinforced expansive self-consolidating concrete. Compressive strength and splitting tensile strength test specimens are 150 × 150 × 150 mm cubes according to GB / TS0081-2002 [16]. Flexural strength test use specimens with 100 × 100 × 400 mm according to ASTM C1609 [17]. All specimens were demolded 24 h after casting and cured in a standard curing room (temperature: 23 ± 2 °C [73 ± 3 °F], humidity ≥95%) until the age of testing at 28 days.

Table II shows the test matrix. Please note that "SCC" represents control self-consolidating concrete group, ESCC represents self-consolidating concrete with 8% expansive agent which is the optimized dosage. And EHFC represents high-flowing concrete with 8% expansive agent which is the optimized dosage. For SF0.25PP0.10, SF represents steel fibers, followed by the volume fraction of steel fibers which was 0.25%, PP represents polypropylene fiber, followed by fiber volume content of PP which was 0.10%. In this study, all of the fiber-reinforced self-consolidating concrete is mixed with 8% of the expansive agent as the ESCC are all labeled at the end.

Table II. Mixture proportion

Mixture code	Exp. adm.	Cement	FA	Sand	Coarse aggregate	Water	HRWRA	w/c
SCC	-	398	170	795	770	200	1.865	0.35
ESCC	45	366	157	795	770	200	1.840	0.35

NOTE: All component units are：kg•m^{-3}。

Test methods

Fresh properties

Workability is the basis for other performance. Thus, in this study, referring to Eurocodes EFNARC [15], two tests including slump flow and V-funnel were conducted. Three indexes consisting of slump flow, T_{50} and V-funnel time (T_V) were chosen to evaluate flowability and passing ability of tested mixtures.

Mechanical properties

The mechanical properties consist of compressive strength, splitting tensile strength and flexural properties of SCC. In accordance with specification [16], 3 specimens were tested for each mixture at 7 days and 28 days for compressive strength respectively. Flexural properties test were conducted in accordance with test method ASTM C1609 Specification [17]. By using third-point loading setup, specimens were turned over 90° from casting top surface. LVDTs were installed on both sides symmetrically at mid-span of beams to monitor middle-span deflection. Three specimens were tested and test results were averaged.

Table III. Workability of tested mixtures

Mixture code	Slump flow		V-funnel
	D /mm	T_{50} /s	T_v /s
SCC	750	3.1	12.2
ESCC	760	2.3	7.4
SF0.25-ESCC	730	3.1	9.8
SF0.50-ESCC	700	3.5	13.9
SF0.75-EHFC	670	4.8	blocking
SF0.25PP0.10-EHFC	620	4.4	33.1

Results and discussion

Working performance

In general, incorporation and increase of fiber content to SCC have negative impact on flowability and passing ability of SCC [9, 10]. It can be derived from Table III that, flowability of all 6 mixtures meet the criteria of 600mm and higher. And the time of T_{50} is from 2.3 s to 4.8 s. The data in Table III shows that the slump flow ranges between 620 and 760mm, in which SF0.25PP0.10-EHFC exhibit the lowest values. The matrixes meet the EFNARC specification for viscosity (V-funnel) and have good passing ability except for SF0.75-EHFC and SF0.25PP0.10-EHFC. However it should be noticeable that these limits suggested by EFNARC are for plain SCC.

Table IV. Mechanical properties of hardened concrete

Property	SCC	ESCC	SF0.25-ESCC	SF0.50-ESCC	SF0.75-EHFC	SF0.25PP0.10-EHFC
$f_{c,7}$ (MPa)	38.50	42.34	36.60	35.54	35.12	34.72
$f_{c,28}$ (MPa)	51.98	52.08	53.93	52.73	52.45	49.92
f_{st} (MPa)	3.64	3.54	3.65	4.10	4.61	3.90

Compressive Strength

As can be seen from Table IV, compressive strength of ESCC and EHFC is 10% higher than that of SCC at 7 days and it does not shown significant difference at 28 days. It can be seen that, the incorporation of fibers reduces the compressive strength from 42.3 MPa to 35.6 MPa at 18.8% or so at 7 days. While F.Aslani [11] and Ding [12]'s test data indicated that the fiber improved the regular SCC 7 d compressive strength. This suggests that fibers do not improve compressive strength of expansive SCC at early age of 7 days. For 28 days compressive strength, f_c of singular steel fiber reinforced ESCC fluctuated around 52MPa which does not show significant difference with ESCC.

Splitting tensile strength

It can be seen from Table IV that steel fiber can improve splitting tensile strength of ESCC and EHFC with increasing volume fraction of fiber, as expected. Though f_{st} reduces from 3.64 to 3.54 MPa with expansive admixture added, when SF content is 0.25%, f_{st} of SF0.25-ESCC is almost the same with f_{st} of SCC group. It is also indicated that PP can increase f_{st} at 0.10 percentage dosage.

Beam bending test

Figure 1 shows load-deflection curves for each mix under third-point bending test. It compares SCC and ESCC as well as ESCC beams under different fiber reinforcement scenarios. Table V lists the test results of all the tested beams. Similarly as found by other researchers [9,12,14], it can be seen from the figure that, load drops to 0 after it reaches "first-peak load" for SCC and ESCC beams without fiber reinforcement. And it shows ductile behavior for fiber reinforced SCC beams. Compared to SCC beam, ESCC beam shows lower cracking load and mid-span deflection. It is also expected that the descent section of ESCC are steeper than that of SCC as the expansion of concrete reduces the bond between concrete matrix. ESCC beam shows more brittle behavior after cracking than SCC beam. From Figure 1 (b), fiber reinforced beams show linear load-deflection relationship before cracking and the cracking load and deflections are increasing with increase of fiber content. Rambo [13] also drew the similar conclusion and curve was divided into "linear portion" and "proportionality portion". It also found that, the beam shows load-deflection hardening behavior after cracking and the peak load is greater than the cracking load when the steel fibers content reaches at 0.50% and 0.75% (40kg and 60kg in mass). While in Ding's [18] study, steel fiber reinforced beam (40kg mass content) did not show deflection-hardening behavior. It is speculated that addition of fiber limits the free expansion of concrete, causing the concrete to produce a self-stressing and strengthening the bond between steel fibers and concrete matrix. The deflection at peak load for SF0.75-EHFC and SF0.50-ESCC are 0.83mm and 0.66mm respectively. It increases about 25.8% for 0.25% increase of fiber content. Compared to single SF reinforced beam, hybrid

polypropylene-steel fiber reinforced ESCC beams show lower cracking load and higher deflection at cracking as well as improved deformability. That is to say that the load drop of SF0.25PP0.10-EHFC is smaller than that of SF0.25-ESCC and the load-deflection curve of SF0.25PP0.10-EHFC is above that of SF0.25-ESCC after cracking.

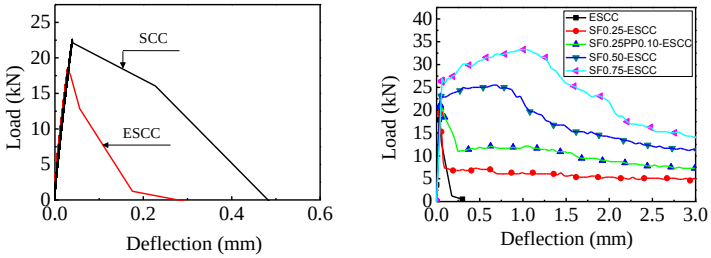

(a) SCC and ESCC (b) Fiber reinforced SCC beams with ESCC

Figure 1. Flexure load-deflection curves of beam test

Table V. Average results of flexural beam test

Mixture code	P_p /kN	δ_p /mm	f_p /MPa	f_{600} /Mpa	f_{150} /Mpa	T_{150} /J	$R_{T,150}$
SCC	22.83	0.04	6.85	-	-	-	-
ESCC	19.66	0.03	5.90	-	-	-	-
SF0.25-ESCC	20.40	0.04	6.12	2.50	1.85	15.75	0.381
SF0.50-ESCC	23.73	0.05	7.12	7.12	3.69	37.06	0.779
SF0.75-EHFC	26.96	0.06	8.09	8.72	6.07	51.97	0.947
SF0.25PP0.10-EHFC	18.38	0.05	5.51	3.67	2.33	22.16	0.606

It shows in Table V that, the residual flexural strength of fiber reinforced concrete beams increases with increase of fiber content. As can be seen, as fiber content increases, T_{150} increases. Specimen with 0.50% SF content presents 135% increase of T_{150} compared with specimen of 0.25% SF. Similarly, specimen with 0.75% SF content presents 230% and 40% increase of T_{150} compared with specimen of 0.25% and 0.50% SF respectively.

Conclusions

From the experiments and analysis conducted above, the following conclusions can be drawn:

1. In compressive strength test, it does not show significant difference between ESCC and EHFC and SCC at 28 days. But the compressive strength of SCC is improved at 7 days. Combined addition of expansive admixture and fibers reduces the concrete strength at 7 days, while it does not influence the 28 days strength noticeably.

2. Flexural results show that flexural stiffness of concrete beam specimens reduces compared with SCC. The incorporation of fiber can enhances the cracking load of ESCC beams. Self prestress generated in fiber reinforced concrete enables deflection hardening of 0.50% SF reinforced ESCC beam specimens. With the increase of fiber content, the deformation and flexural capacity of beams improves.

3. In general, the incorporation of fibers into expansive SCC could improve splitting tensile strength and flexural properties significantly. In a word, both fibers and expansive agent can be used to achieve desired mechanical properties.

References

[1] ACI 237 (2007), *Self-Consolidating Concrete*, American Concrete Institute, Farmington Hills, MI.
[2] Z.L.Meng, J.Zhou, X.W. Ma, Y.S. Xue, G.Y. Li, (2013), *Conc.*, vol.8, pp. 79-82.
[3] N. Li, Y.H.Ye, Y.J.Du, T.M.Zhu, (2011), *Arch. Tec.*, vol.42, pp.1114-1117.
[4] T.S.He, X.F. Song, M.Z. Zhan, (2003), *Jou. of Chang'an Uni.* (*Nat. Sci. Edit.*), vol.23, pp.19-22.
[5] Z.L.Meng, G.Y. Li, X.W. Ma, Y.S. Xue, J. Zhou, (2013), *Conc.*, vol.5, pp.89-92.
[6] F.Aslani, S.Nejadi, (2003), *Jou. of Adv. Conc. Tech.*, vol.11, pp.251-265.

[7] S.R.Luo, H.Li, (2010), *Jou. of Guangxi Uni.: Nat Sci Ed*, vol.35, pp. 901-907.
[8] S.G.Liu, Y.N.Ding, (2008), *Jou. Of Buil. Mat*., vol.11, pp.8-13.
[9] B. Akcay, M.A.Tasdemir, (2012), *Cons. and Buil. Mat.*, vol.28, pp. 287–293.
[10] K.H.Khayat, F.Kassimi, P.Ghoddousi, (2014), *ACI Mat. Jou.*, vol.111, pp.143-151.
[11] F.Aslani, S.Nejadi, (2013), *Comp.: Part B* , vol.53, pp. 121–133.
[12] Y.N.Ding, X.J.Dong, Y.H. Wang, (2005), *Jour. of Buil. Mat*., vol.8, pp.294-298.
[13] D.A.S.Rambo, F.d.A.Silva, R.D.T.Filho, (2014), *Mat. and Des.*, vol.54, pp.32-42.
[14] M.Pajak, T.Ponikiewski, (2013), *Cons. and Buil. Mat.*, vol.47, pp.397–408.
[15] EFNARC(2002): *Specification and guidelines for self-compacting concrete*, European Federation for Specialist Construction Chemicals and Concrete Systems, Norfolk, UK.
[16] GB/TS0081-2002 (2003). *Standard for test method of mechanical properties on ordinary con- crete*[S]. Beijing: China Architecture & Building Press. （In chinese）
[17] ASTM C1609/C1609M- 12 (2013), *Standard Test Method for Flexural Performance of Fiber-Reinforced Concrete (Using Beam With Third-Point Loading)*, ASTM International, West Conshohocken, PA.
[18] Y.N.Ding, X.J.Dong, Y.H. Wang, (2005), *Jou. of Buil. Mat*., vol.8, pp. 660-664.

Case Study of Mechanical Properties of Carbon Fiber Reinforced Self-Consolidating Concrete

M. Yakhlaf[1], Md. Safiuddin[2], K.A. Soudki[3], A. El baden[4]

[1]Research Assistance (Tripoli), Email:mohammed_yekhlif@yahoo.com
[2]Professor Assistance (Canada)
[3]Professors and Canada Research Chair (Canada)
[4]Professor Assistance, Civil Engineering (Libya)

Abstract This paper presents the mechanical properties of ten different carbon fibre reinforced self-consolidating concrete (CFRSCC) mixtures. Two different water/binder (w/b) ratios were used in this project. Concrete with each w/b ratio included five carbon fibres content.High-range water reducer was used to enhance the workability of the concrete mixtures. The fresh properties for all mixtures were examined and successfully fulfilled the requirements of self-consolidating concrete (SCC). The compressive strength, splitting tensile strength, modulus of rapture, and toughness of hardened concretes were evaluated. The test results revealed that the compressive strength of CFRSCC mixtures decreased as the carbon fibre content increased. However, the splitting tensile strength of CFRSCC mixtures increased with the increase in carbon fibre content. The modulus of rapture and toughness of the CFRSCC mixtures with 0.35 w/b ratio also increased as the carbon fibre content increased. Nevertheless, the modulus of rupture and toughness of the CFRSCC mixtures with 0.4 w/b ratio showed random trends where the results frequently changed from higher value to lower value with the increase in fibre content. Scanning electron micrographs (SEM) of the fracture surface for all SCC mixtures was taken to observe the fibres distribution.A scanning electron microscope was used toproduce the magnified images of the fracture surface.

Keywords: *Carbon fibres; Self consolidating concrete; Compressive strength; Tensile strength; Modulus of rupture; Fracture energy.*

Introduction

Self-consolidating or self-compacting concrete (SCC) is arelatively new concrete that flows under its own weight without the use of vibrator [1]. SCC has the ability to fill all the gaps completely in the formwork and go around the congested

reinforcement without segregation and bleeding [2]. In order for the concrete to be classified as self-consolidating concrete, the concrete has to fulfill the keys fresh properties of SCC; such as filling ability, passing ability, and segregation resistance [3,4]. SCC has been described as "the most revolutionary development in concrete" in construction over the last three decades [4]. The advantages of SCC include the following:faster construction, reduction of site workers, better and easy finishing, easy placing, good durability, reducing of noise level, and reduction of pollution [5]. SCC has been developed to compensate for the shortage of skilled labour in concrete industry.

Thus, it has been rendered efficient and beneficial from both technological and economical standpoints. SCC can be used in all kinds of applications. For example, SCC can be used in big or small structures, simple or complicated buildings, horizontal or vertical structural members, precast or cast-in-place concrete components. In the United States, approximately 40% of precast production uses SCC, while approximately 2-4% of cast-in-place production uses SCC [5]. Recently, SCC has been used as a repair material in Canada and Switzerland since it has the capability to flow and fill in the restricted areas [3,4]. However, CFRSCC has been used limitedly in real applications (real world).

Adding fibres to SCC decreases its workability and thereforeit becomes progressively difficult to achieve SCC capacity [2]. For example, carbon fibres can affect negatively the SCC fresh properties such as filling ability and passing ability [6,7]. Carbon fibres may also restrictand prevent coarse aggregate from moving uniformly, thus causing segregation [8].Despite effect on workability, adding fibresto SCC may improve themechanical properties of concrete [9]. Generally, concrete is a brittle material that fractures under tensile load. The addition of randomly dispersed fibres to SCC will reduce the crack opening at the loading stage and create a crack bridging, which can alter the behavior of the concrete at failure [10]. Therefore, if self-consolidation is achieved in concrete the fibreswill play a very important role in improving the mechanical properties.

Many studies were carried out to investigate the mechanical properties of SCC including steel, polypropylene, glass, and naturalfibres [11-13]. The addition of carbon fibresto concrete offers significant improvement to the mechanical properties such as flexural strength and toughness. In addition, impact resistance and fatigue resistance can be improved if the appropriate amount of carbon fibresis added to the concrete. Carbon fibresare attractive to engineers due to their low density and thermal conductivity [14,15].

Carbon fibrescan be used to eliminate or reduce the drying shrinkage problems as well as reduce cracking width. Since 1970s many studies have been conducted to investigate the effectiveness of carbon fibreson the various properties of concrete [16,17]. Carbon fibrereinforced concrete (CFRC) has been used in many projects because of its good thermal conductivity, lightweight, and high modulus of

elasticity.It has been also used to produce curtain walls, partition panel, and formwork for walls [18]. The incorporation of carbon fibreswith self-consolidating concrete showed an improving in mechanical properties and electrical resistivity [19]. The addition of carbon fibresto concrete offers significant improvement to the mechanical properties such as flexural strength and toughness[8,19-20].

Research Significance

It is important to note that carbon fibrereinforced concrete has been well researched. Also, self-consolidating concrete (SCC) incorporating steel and polymer fibreshas been significantly studied. However, the use of carbon fibresin SCC has not been investigated comprehensively.Incorporatingcarbon fibresin SCC can produce ahigh quality special concrete known as carbon fibrereinforced self-consolidating concrete (CFRSCC). CFRSCC offers the benefits of both carbon fibresand SCC. The main objective of this studywas to investigate the effect of pitch-based carbon fibreson the mechanical properties (compressive strength, splitting tensile strength, flexural strength, and toughness) of SCC. The research can be useful to produce CFRSCC commercially for use in new on rehabilitated / repaired concrete structures.

Experimental Investigation

Constituent Materials of Concretes

Normal (Type I) portland cement, crushed limestone (coarse aggregate, CA), manufactured sand (fine aggregate, FA), silica fume (SF), high-range water reducer (HRWR), pitch-based carbon fibres (CFs) and normal tap water (W) were used in this study. The manufactured sand conformed with the specification OPSS 1002 [21]. Table I shows the details of concrete mixture proportions. Figure 1 shows some pitch-based carbon fibres.

Table I. Details of concrete mixture proportions

Concrete mixture	w/b ratio	CA [kg]	FA [kg]	Binder (B)		CFs		W [kg]	HRWR [% B]
				C [kg]	SF [kg]	[vol.%]	[kg]		
M1	0.35	784.2	958.5	432.7	48.1	0.00	0.0	189.8	1.50
M2	0.35	778.4	951.4	432.7	48.1	0.25	4.7	189.8	2.00
M3	0.35	767.1	937.6	432.7	48.1	0.50	9.5	189.8	3.50
M4	0.35	746.4	912.3	432.7	48.1	0.75	14.2	189.8	6.70
M5	0.35	736.2	899.8	432.7	48.1	1.00	18.9	189.8	8.00
M6	0.40	811.9	992.3	378.6	42.1	0.00	0.0	189.8	1.00

M7	0.40	806.7	985.9	378.6	42.1	0.25	4.7	189.8	1.45
M8	0.40	802.2	980.5	378.6	42.1	0.50	9.5	189.8	1.75
M9	0.40	783.5	957.6	378.6	42.1	0.75	14.2	189.8	5.00
M10	0.40	770.8	942.1	378.6	42.1	1.00	18.9	189.8	7.00

Notation: CA= coarse aggregate, FA= fine aggregate, C= cement, CFs = carbon fibres content, SF= silica fume, W= water, HRWR= high range water reducer.

Figure 1. Pitch-based carbon fibres

Test Procedures

Fresh concrete mixtures were tested for filling ability, passing ability, and segregation resistance. ASTM standards were followed to determine the slump flow (filling ability) and J-ring slump flow (passing ability) of concrete. All the fresh properties were tested from the same batch concreteand compressive strength, tensile strength, and fracture energy for hardened properties [22-28]. The segregation resistance of fresh concrete was determined following the procedure proposed by Nagataki and Fujiwara [29]. The details of fresh concrete test procedures have been described in a published paper of the authors [30].

Twelve concrete cylinders (100 mmdiameter × 200 mm height) for the compression test, six concrete cylinders (100 mmdiameter × 200 mm height) for the splitting tension test, and three prisms (100 mm wide × 100 mm deep × 350 mm long) for the fracture energy test (modulus of rupture and toughness) were cast immediately after testing fresh properties. The compressive strength of concrete was determined according to ASTM C39/C39M–09a [26]. The compressiontest

was carried out at the concrete ages of 3, 7, 14, 28 days. The results obtained from three test cylinders were averaged to determine the compressive strength of concrete. The splitting tensile strength of concretes was measured in accordance to ASTM C496/C496M–04 (2004) [27]. The splitting tension test was performed at the concrete ages of 14 and 28 days.The flexural strength (modulus of rupture) of concretes was determined by conducting the fracture energy test under third-point loadingaccording to ASTM C1609/C1609M–10 (2010) [28]. The toughness of concretes was also determined from the fracture energy test.

Scanning electron microscopy was taken to observe the distribution of carbon fibres in hardened concretes. This test was carried out using the prism specimens tested for flexural strength and toughness. The specimens for this test were preparedfrom the fractured prism specimens by cutting them into 20 × 20 mm size(without affecting the fracture surface). The test specimens were cleaned and dried; then the fractured surface was coated with a thin gold coating(conductive material)in order to be properly scanned. These images are known asscanning electron micrographs (SEMs).

Test Results and Discussion

The slump flow, J-ring slump flow, and segregation index were measured simultaneously for each SCC mixture to determine filling ability, passing ability, and segregation resistance, respectively. The compressive strength, splitting tensile strength, and flexural strength (modulus of rupture), and toughness were also determined for all concretes.

Fresh Properties

Table 2 summarizes the results for the properties (filling ability, passing ability, and segregation resistance) of fresh concretes. The filling ability was measured with respect to slump flow. As shown in Table 2, the slump flow value for the mixtures varied from 550 mm to 745 mm. The slump flow for SCC typically ranges from 550 mm to 850 mm [31-33].Carbon fibres greatly affected the slump flow of SCC. This is because, as the fibre volume increases, the interaction between carbon fibres can restrict the filling ability in SCC[9]. However,increased HRWR dosage enhanced the deformability of concrete to achieve the target filling ability[3].

Table II. Properties of fresh concretes

Concrete mixture	w/b ratio	CFs [%]	Slump flow [mm]	J-ring slump flow [mm]	Segregation index [%]
M1	0.35	0.00	720	705	12
M2	0.35	0.25	745	730	11.9
M3	0.35	0.50	700	625	9
M4	0.35	0.75	685	665	11
M5	0.35	1.00	720	715	10
M6	0.40	0.00	660	635	5
M7	0.40	0.25	634	625	7.8
M8	0.40	0.50	700	685	7
M9	0.40	0.75	560	530	3.4
M10	0.40	1.00	550	478	6.7

The J-ring slump flow for different SCC mixtures was in the range of 480-750 mm. The difference between slump flow and J-ring slump flow was 0-50mm; this is within the range specified in ASTM C 1621/C1621M-09b (2009) [23]. The incorporation of carbon fibres decreased the J-ring slump flowof SCC. This is because the presence of fibres restricted the concrete mixture from moving through spacing between obstacles (re-bars).

The segregation index varied from 9% to 12% for concrete mixtures with the w/b ratio of 0.35. On the other hand, the segregation index was between3.4% and 7.8% for concrete mixtures with the w/b ratio of 0.4. All SCC mixtures had their segregation index below the maximum limit of 18% reported by Perez et al. [34]. SCC is more prone to segregation due to higher fluidity [3]. This segregation tendency is reduced in the presence of fibres [3]. Thus, the increased volume of carbon fibres greatly increased the segregation resistance of SCC. Nevertheless, it should be mentioned that HRWR dosage also affected the segregation index of concretes produced in the present study.

Hardened Properties

Table III summarizes the results for the properties (compressive strength, spliting tensile strength, Modulus of Rupture, Toughness and Scanning electron micrographs).

Table III. Properties of fresh concretes

Concrete Mixture	Compressive Strength f_c' [MPa]	Splitting Tensile Strength f_t [MPa]	Modulus of Rupture f_r [MPa]	Toughness [N-mm]
M1	95	4.3	7.7	2475
M2	64	4.33	7.98	3500
M3	64	4.46	7.6	3245
M4	60.2	4.75	8	3250
M5	62	5	8.05	3255
M6	80	4.2	8.29	3000
M7	67	4.54	8.4	3480
M8	68.6	4.6	6.68	2840
M9	39.4	4.65	8.15	3420
M10	48	4.75	7.87	3250

Compressive strength results, the compressive strength test results for different concretes are summarized in table III. Mixture M1 achieved a compressive strength of 95 MPaafter 28 days, which was the highest compressive strength value while mixture M4 had a compressive strength of 60.2 MPa after 28 days, which is the lowest compressive strength in the case of series 1 SCC mixtures. Furthermore, the highest compressive strength was 80MPa for mixture M6 and the lowest compressive strength was 39MPa for mixture M9 in the case of series 2 SCC mixtures. The compressive strength of SCC at both w/b ratios (0.35 and 0.40) generally decreased as the carbon fibres content increased as it can be seen from table III. This is because the carbon fibresreplaced some of the coarse and fine aggregates. The amount of coarse aggregate affects the compressive strength of the concrete mixtures [34].As the coarse aggregates decreased, the compressive strength decreased.

The water/ binder ratio (w/b) significantly affected the compressive strength of concrete. It is clear from Figure 4 that the compressive strength increased as the w/b ratio decreased. The maximum compressive strength at thew/b ratio of 0.35 was 95 MPa while the maximum compressive strength at the w/b ratio of 0.40 was 80 MPa. The compressive strength increased by 15% as the w/b ratio decreased from 0.40 to 0.35. This is mostly related to the cement content of concrete. At the lower w/b ratio, the cement content of concrete was higher as given in Table 1. As stated by Safiuddin et al. the increased of cement content enhanced the binding of

aggregates by increasing theamount of calcium silicate hydrate (C–S–H) that led to a higher compressive strength[14].

However, carbon fibres affected the compressive strength of concretes. Mixture M1 achieved a compressive strength of 95 MPaafter 28 days, which was the highest compressive strength value while mixture M4 had a compressive strength of 60.2 MPa after 28 days, which is the lowest compressive strength in the case of series 1 SCC mixtures as can be seen from table III. Moreover, the highest compressive strength was 80 MPa for mixture M6 and the lowest compressive strength was 39 MPa for mixture M9 in the case of series 2 SCC mixtures. The compressive strength of SCC at both w/b ratios (0.35 and 0.40) generally decreased as the carbon fibres content increased as it can be seen from table III. This is because the carbon fibres replaced some of the coarse and fine aggregates. The amount of coarse aggregate affects the compressive strength of the concrete mixtures [34].

Splitting Tensile Strength Results, the splitting tensile strength for different SCC mixtures is presented in table III. The splitting tensile strength of SCC at both w/b ratios increased as the carbon fibres content increased. Mixture M1 (0% fibres content and 0.35 w/b ratio) had a tensile strength of 4.20 MPa while mixture M5 (1% fibres content and 0.35 w/b ratio) had a tensile strength of 4.80 MPa, as presented in Figure. 5. The splitting tensile strength for mixture M6 (0% fibres content and 0.40 w/b ratio) was 4.10 MPa and the splitting tensile strength for mixture M10 (1% fibres content and 0.40 w/b ratio) was 4.70 MPa as presented in table III. The splitting tensile strength increased up to about 12% at 1% of carbon fibres content.

The w/b ratio had no significant effect on the splitting tensile strength of concrete as evident from table III. As the w/b ratio increased, the splitting tensile strength slightly decreased. The differences in tensile strength between the mixtures with 0.35 w/b ratio and the mixtures with 0.40 w/b ratio were 0.10-0.20 MPa.

Howevre, the effect of carbon fibres on the splitting tensile strength of concrete can be seen from table III.The increased carbon fibres increased the splitting tensile strength. For example, thesplitting tensile strengthfor mixtures M1 (0% fibres content), M2 (0.25% fibres content), and M5 (1% fibres content) was 4.40 MPa, 4.45 MPa, and 4.80 MPa, respectively. This increase in splitting tensile strength was because the increased percentage of carbon fibres reduced the crack growth and thus led to higher failure load. Once the load was applied, the cracks started to appear and the concrete cylinder started to split in two parts. The fibres created a bridge through the split portions of the cylinder and prevented the two parts from splitting.

Modulus of Rupture, the modulus of rapture results for all concretes was are summarized in table III. As it can be seen from table III, the modulus of rupture for

the concrete mixtures with 0.35 w/b ratio ranged from 7.60MPato 8.05MPa. Mixture M5 (1% fibres content and 0.35 w/b ratio) had the highest modulus of rupture, while mixture M3 (0.5% fibres content and 0.35 w/b ratio) had the lowest modulus of rupture. Increase in carbon fibres content increased the modulus of rupture of the SCC compare to the control mixture M1 (0% fibres content).It is evident that a carbon fibres content of 1% and 0.25% gave the optimum modulus of rupture for the SCC mixtures with the w/b ratio of 0.35. Fibres are able to reduce the crack opening. The increased number of fibresthat cross the crack surface also increases the modulus of rupture. Therefore, for SCC mixtures with 0.40 w/b ratio, the modulus of rupture ranged from 6.68MPa to 8.40MPa. Mixture M7 (0.25% fibres content and 0.40 w/b ratio) had the highest modulus of rupture, while mixture M8 (0.5% fibres content and 0.40 w/b ratio) had the lowest modulus of rupture. The modulus of rapture of CFRSCC mixes with 0.4 W/B ratio were close to each other and it seems that fibreshad no clear effect on modulus of rapture values. As it can be seen from table III that the fibers were lower than all other mixtures in the fracture surface that might have led to reduction in the modulus of rapture. The air content values for these mixes were high and this results in decreasing the modulus of rapture. Also, the reduction in workability can affect the modulus of rapture [12].

Toughness, the toughness values for different SCC mixtures are presented in table III. The toughness of the SCC mixtures with 0.35 w/b ratio ranged from 3500 N-mm to 2475 N-mm. The carbon fibres increased the toughness. The carbon fibreshelped the concrete mixtures to absorb more energy and therefore the mixtures with carbon fibreshad improved toughness. Mixture M2 (0.25% fibrescontent) had the highest toughness of 3500 N-mm, while mixture M1 (0%fibrescontent) had the lowest toughness of 2475 N-mm. Mixture M3 to M5 with carbon fibrescontent of 0.5% to 1% had similar toughness regardless of fibrescontent. The toughness achieved by these mixtures was 31% higher than the control mixture (with no fibers), but 20% lower than the mix with 0.25% fibers. These results suggest that the optimum fibrecontent is 0.25%. The number of fibresthat cross the crack surface is one of the main reasons to increase the

On the other hand, the toughness value for theSCC mixtures with 0.40 w/b ratio ranged from 3750 N-mm to 2710 N-mm as can be seen from Fig. 13. However, an opposite trend was observed compared to the mixtures with w/b of 0.35. Mixture M7 (0.25% fibrescontent) had the highest toughness, while mixture M10 (1%fibrescontent) had the lowest toughness. Mixture M9 (0.75% fibrescontent) had a toughness of 3400 N-mm. This value was close to the toughness value of mixture M6. In general, the carbon fibres content higher than 0.25 %did not improve the toughness. It could be because of the high amount of aggregates in the mixture with 0.40 w/b ratio that might cause the fibresto break during the mixing process, thus reducing the embedded length of the fibresat the crack surface. Also, the inappropriate orientation of the carbon fibres can be another reason of these unexpected results.

Scanning electron micrographs, the scanning electron micrographs (SEMs) of the fracture surface for different SCC mixtures are shown in Figures 2 and 3. These micrographs exhibited that the carbon fibres were well distributed in each concrete mixture. The fibre failure mechanism was also noticed in these micrographs.Two types of fibresfailure (pullout and breakage) as shown in Figure 4 were observed. A similar observation was made in other research.Akihama et al. observed that the pitch-based fibresafter the peak load were pulled out or broken. Also, Nishioka et al. confirmed these two types of failure [35].

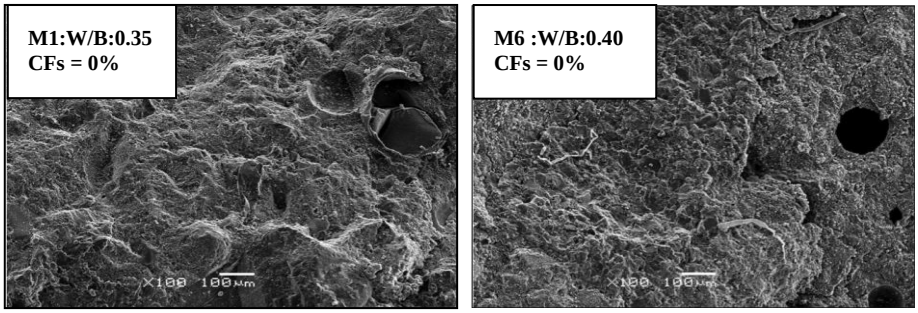

Figure 2. M1 and M6: SEM of fracture surface, no fibres

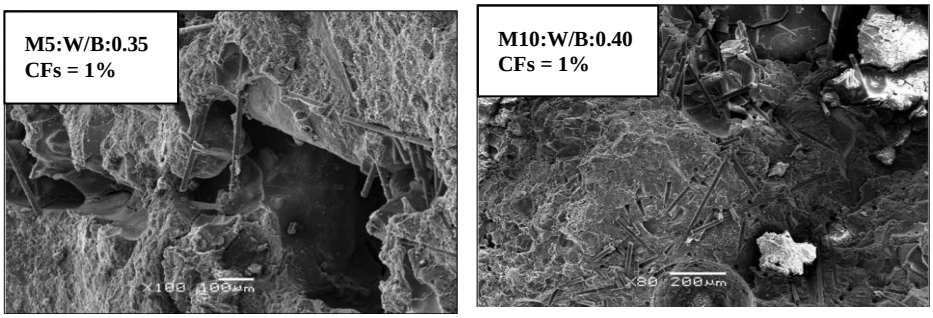

Figure 3. M5 and M10: SEM of fracture surface, well distribution of fibres

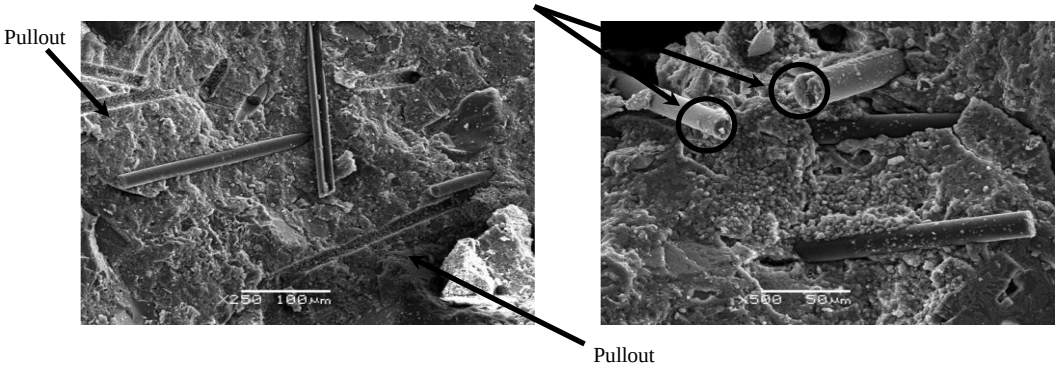

Figure 4. Failure modes of fibres

Conclusions

Based on the test results of this study on carbon fibre reinforced self-consolidating concrete (CFRSCC), the following conclusions can be made:

- Carbon fibres affected the filling ability and passing ability of SCC mixtures. However, These fibres improved the segregation resistance of SCC concrete mixtures with carbon fibres content up to 0.75%satisfactory pass the requirements of an SCC mixture.
- Compressive strength of SCC mixtures decreased as the carbon fibres increased and the splitting tensile strength increased as the carbon fibres increased. The reduction of compressive strength might be because of the reduction of coarse aggregates.
- The flexural strength for the mixtures with w/b ratio of 0.35 increased with the increase of fibers. However, the flexural strength for the mixtures with w/b ratio of 0.40 showed that the flexural strength did not increase with the increase of carbon fibres.
- The toughness or the fracture energy of the mixtures with 0.35 w/b ratio increased when the fibres were added.
- Two types of fibres failure (pullout and breakage) were observed in this study from SEMs. The two types of fibers failure existed in all mixtures.

Acknowledgement

The authorssincerely acknowledge the financial support from the HigherEducation Ministry of Libya. The authors also express their gratitude to BASF Construction Chemicals Canada Ltd. for supplying chemical admixtures and to Mitsubishi Company in USA for supplying carbon fibres.

References

[1] Goodier C. (2003). *Development of self-compacting concrete*. In: Structures and Buildings 156: Proceeding of the institution of civil engineers. London (UK), SB4, pp. 405-414.

[2] El-Dieb A, Reda TM. (2012). *Flow characteristics and acceptance criteria of fiber-reinforced self-compacted concrete (FR-SCC)*. Construction and Building Materials, vol. 27, n 1, pp. 585-596.

[3] EFNARC. Specification and guidelines for self-compacting concrete. Surrey, UK: European Federation of Suppliers of Specialist Construction Chemicals (EFNARC); 2002.

[4] ACI Committee 237R-07. Self-consolidating concrete. Detroit. (USA): American Concrete Institute; 2007.

[5] Daczko J. Self-consolidating concrete: ch. 4 hardened properties of SCC. New York, USA; 2012.

[6] Yin J, Wu ZS. Structural performance of short steel-fiber reinforced concrete beams with externally bonded FRP sheets. Construction and Building Materials 2003; 17(6-7): 463-70.
[7] Cunha V, Barros J, Sena-Cruz J. Tensile behavior of steel fiber-reinforced self-compacting concrete. In: Fiber-reinforced self-consolidating concrete: Research and Applications (ACI SP-274). Detroit, USA: American Concrete Institute; 2010. p. 51-68.
[8] Chang C, Ho M, Song G, Mo L, Li H. Improvement of electrical conductivity in carbon fiber-concrete composites using self-consolidating technology. In: Proceedings of the 12th International Conference on Engineering, Science, Construction, and Operation in Challenging Environments. Honolulu (USA); 2010. p. 3553-8.
[9] Nehdi M,Ladanchuk J. Fibresynergy in fiber-reinforced self-consolidating concrete. ACI Materials Journal2004; 101(6). 508-17.
[10] Forgeron D. and Omer A. Flow characteristics of macro-synthetic fiber-reinforced self-consolidating concrete. In: Fiber reinforced self-consolidating concrete: research and applications (ACI SP-274-1). Detroit (USA): American Concrete Institute; 2010. p. 1-14.
[11] Mobasher B, Destrée X. Design and Construction Aspects of Steel Fiber-Reinforced concrete Elevated Slabs.In: Fiber-reinforced self-consolidating concrete: Research and Applications (ACI SP-274-5),Detroit(USA): American Concrete Institute; 2010. p. 95-108.
[12] Brown M,Ozyildirim C, Duke W. Investigation of steel and polymer fiber-reinforced self-consolidating concrete.In: Fiber-reinforced self-consolidating concrete: Research and Applications(ACI SP-274-5),Detroit(USA): American Concrete Institute; 2010. p. 69-78.
[13] Barluenga G, Hernández-Olivares F. Cracking control modified with short AR-glass fibers at early age. Experimental results on standard concrete and SCC. Cement and Concrete Research. 2007; 37(12): 1624-38.
[14] Safiuddin Md. High Performance Mortar with Carbon Fibers: Properties and Optimization. Saarbrücken, Germany: Lambert Academic Publishing; 2010.
[15] Gao D, Mo L, Peng L. Electrical resistance of self-consolidating concrete containing carbon nanofibers. Journal of Sichuan University (Engineering Science Edition) 2011; 43(5): 52-58.
[16] Ali A, Majumdar J, Rayment L. Carbon fiber reinforcement of cement. Cement and Concrete Research 1972; 2(2): 201-12.
[17] Waller A. Carbon Fiber Cement Composites. In: Fibre reinforced concrete: research and applications (ACI SP-44). Detroit (USA): American Concrete Institute; 1974. p. 143-61.
[18] Carlswärd J, Emborg M. Prediction of stress development and cracking in steel fiber-reinforced self-compacting concrete overlays due to restrained shrinkage. In: Fiber-reinforced self-consolidating concrete: Research and Applications (ACI SP-274). Detroit, USA: American Concrete Institute; 2010. p. 31-50.
[19] Gao D, Mo L, Peng L. Mechanical and electrical properties of carbon-nanofibreself-consolidating concrete. In: Proceedings of the 12th International

Conference on Engineering, Science, Construction, and Operation in Challenging Environments. Honolulu (USA); 2010. p. 2577-85.
[20] Chang C, Ho M, Song G, Mo L, Li H. Improvement of electrical conductivity in carbon fiber-concrete composites using self-consolidating technology. In: Proceedings of the 12th International Conference on Engineering, Science, Construction, and Operation in Challenging Environments. Honolulu (USA); 2010. p. 3553-8.
[21] OPSS 1002. Material specification for aggregates – concrete. Toronto, Canada: Ministry of Transportation of Ontario; 2011.
[22] ASTM C1611/C1611M-09b. Standard test method for slump flow of self-consolidating concrete. Annual Book of ASTM Standards, vol.04.02. Philadelphia (USA): American Society for Testing and Materials; 2009.
[23] ASTM C1621/C1621M-09b. Standard test method for passing ability of self-consolidating concrete by J-ring. Annual Book of ASTM Standards, vol.04.02. Philadelphia, USA: American Society for Testing and Materials; 2009.
[24] ASTM C231/C231M-09b. Standard test method for air content of freshly mixed concrete by the pressure method. Annual Book of ASTM Standards, vol.04.02. Philadelphia (USA): American Society for Testing and Materials; 2010.
[25] ASTM C138/C138M-10b. Standard test methods for density (unit weight), yield, and air content (gravimetric) of concrete. Annual Book of ASTM Standards, vol.04.02. , Philadelphia (USA): American Society for Testing and Materials; 2010.
[26] ASTM C39/C39M-09a. Standard test method for compressive strength of cylindrical concrete specimens. Annual Book of ASTM Standards, vol.04.02. , Philadelphia (USA): American Society for Testing and Materials; 2010.
[27] ASTM C496/C496M-04. Standard test method for splitting tensile strength of cylindrical concrete specimens. Annual Book of ASTM Standards, vol.04.02. , Philadelphia (USA): American Society for Testing and Materials; 2004.
[28] ASTM C1609/C1609M-10. Standard test method for flexural performance of fiber-reinforced concrete (using beam with third-point loading). Annual Book of ASTM Standards, vol.04.02. , Philadelphia (USA): American Society for Testing and Materials; 2010.
[29] Nagataki S, Fujiwara H. Self-compacting property of high flowable concrete. In: Proceedings of the Second CANMET/ACI International Symposium on Advances in Concrete Technology (ACI SP-154). Detroit (USA): American Concrete Institute; 1995. p. 301-14.
[30] Yakhlaf M, Saffiudin M, Soudki KA. Properties of freshly mixed carbon fibre reinforced self-consolidating concrete. Construction and Building Materials, in press. 2013.
[31] Ferraris CF, Brower L, Ozyildirim C, Daczko J. Workability of self-compacting concrete. In: Proceeding of the PCI/FHWA/FIB International Symposium on High Performance Concrete. Chicago, USA: Precast/Prestressed Concrete Institute; 2000. p. 398-407.

[32] Grünewald S, Walraven J, Emborg M, Carlswärd J, Hedin C. Summary Report of Work Package 3.1: Test Methods for Filling Ability of SCC. Netherlands: Delft University of Technology and Betongindustri; 2004.
[33] De Schutter G. Guidelines for Testing Fresh Self-Compacting Concrete. European Research Project: Measurement of Properties of Fresh Self-compacting Concrete., UK, Europe: University of Paisley; 2005.
[34] Aydin A. Self compactability of high volume hybrid fiber reinforced concrete. Construction and Building Materials 2007; 21(6): 1149-54.
[35] Kucharska, L, Brandt, AM. Pitch-based carbon fiber reinforced cement composites-a review. Archives of Civil Engineering 1997; 43(2): 165-86.

Theme 9: Structural Performance of SCC

Effect of Crumb Rubber Content on Structural Behaviour of Self-consolidating Concrete

Mohamed K. Ismail[1] and Assem A. A. Hassan[1]

[1]Department of Civil Engineering, Memorial University of Newfoundland, Canada

Abstract This investigation aimed to evaluate the applicability of self-consolidating rubberized concrete (SCRC) mixtures for structural applications using full-scale steel reinforced beams. Recycled crumb rubber (CR) particles were used as a partial replacement for fine aggregate with percentage ranging from 0% to 15% (by volume of sand). The performance of the tested beams was investigated based on load-deflection response, first crack load, ultimate load, ductility, and toughness. The results showed that increasing the CR content decreased the mechanical properties, first crack load, and self-weight of all SCRC beams. However, using up to 15% CR improved the deformation capacity, ductility and toughness of tested beams without affecting the flexural capacity, significantly.

Keywords: *Self-consolidating rubberized concrete, Reinforced concrete beams, Flexural capacity, Deflection characteristics.*

Introduction

Utilization of waste rubber in construction industry has become increasingly popular over the past 20 years, contributing to recycling millions of scrap tyres that are wasted worldwide [1]. For this reason, many studies have been conducted to investigate the effect of using waste rubber as a replacement for fine and/or coarse aggregates on the properties of concrete. Many studies have observed that adding rubber to concrete could improve its ductility, toughness, dynamic properties and reduced the unit weight [1-3]. On the other hand, the mechanical properties generally decreased as the rubber content increased [1, 4].

Most of the available research focuses on investigating the behaviour of rubberized concrete mixtures using small-scale samples, but there is a dearth of data available regarding the structural behaviour of large-scale rubberized concrete elements, especially when self-consolidating rubberized concrete (SCRC) is used. The main objective of this research was to study the infulence of crumb rubber (CR) on

structural performance of full-scale reinforced under flexural load. The investigation included evaluations of the effect of CR on the first crack load, flexural capacity, load-deflection response, ductility, and toughness of the tested beams.

Experimental Program

Materials

Type GU Canadian Portland cement similar to ASTM C618 [5] Type F was used. Natural sand and 10 mm crushed stone aggregate were used as fine and coarse aggregates, respectively. Both aggregates have a specific gravity of 2.6 and absorption of 1%. A crumb rubber aggregate with a specific gravity of 0.95, maximum aggregate size 4.75 mm, and negligible absorption was used as a partial replacement of the fine aggregate in SCRC mixtures. Glenium 7700 high-range water-reducer admixture (HRWRA), similar to ASTM C494 Type F [6], was used to adjust the flowability and cohesiveness of SCRC and VRC mixtures, respectively.

Concrete Mixtures

The concrete mixtures in this investigation were selected based on a previous study by the authors [7] aimed at developing a number of SCRC mixtures containing maximum percentages of CR (by volume of fine aggregate) and minimum reductions in strength and stability. In order to develop preliminary acceptable fresh properties for all tested SCRC mixtures, a trial mixtures stage was performed to determine the minimum water-to-binder (w/b) ratio and the minimum total binder content that can achieve acceptable SCRC flowability without overdosing the HRWRA. The results of the trial mixtures stage indicated that at least 0.4 w/b ratio and 500 kg/m^3 as a total binder content should be used to obtain SCRC having acceptable slump flow with no visual sign of segregation. Therefore, a w/b ratio of 0.4 and a minimum total binder content of 500 kg/m^3 were used in all tested mixtures (Table I). Also, a constant coarse-to-fine aggregate (C/F) ratio of 0.7 was chosen for all tested mixtures. This ratio was chosen based on previous research [8-9] carried out on SCC with different C/F aggregate ratios. The selected mixtures contained three SCRC mixtures with CR replacement of 0%–15%. All tested mixtures were designated by total binder content, and percentage of CR. For example, a beam containing a 500 kg/m^3 binder content, and 5% CR would be labelled as 500C-5CR.

Fresh and Mechanical Properties Tests

The fresh properties of all tested mixtures were conducted as per the European Guidelines for Self-Compacting Concrete [10]. The fresh properties tests included slump flow, V-funnel, and L-box tests. The percentage of entrained air in the fresh

SCC mixtures was measured by following a procedure given in ASTM C231[11]. The compressive strength and splitting tensile strength (STS) tests were determined according to ASTM C39/C39M [12] and C496/C496M [13], respectively. The results of the fresh properties and compressive strength of the tested mixtures are presented in Table II.

Flexure Test Setup,Iinstrumentation, and Loading Procedure

All beams contained shear and flexural reinforcements and were designed to fail in flexure with a ductile behaviour. Figure 1 shows the test setup used for all 4 concrete beams during testing. The load was applied through a hydraulic jack (with capacity of 500-kN) at a single point and then distributed into two-point loads acting on the beam surface. A linear variable differential transformer (LVDT) and two strain gauges were used to measure the mid-span deflection and reinforcement strain, respectively. The strain gauges were installed at the bottom of the longitudinal reinforcement at mid-span (maximum flexural moment location). The beams were loaded gradually, with a constant loading rate until failure. The overall behaviour of the beams, including the development of cracks, crack patterns, crack widths, crack heights, and failure modes, was observed and sketched for all beams (see Figure 2). The results obtained from the flexure testing of the four tested beams are presented in Table III.

Table I. Mix design for tested mixtures

Beam #	Beam-I.D	Cement (kg/m^3)	C. A. (kg/m^3)	F. A. (kg/m^3)	CR (kg/m^3)	HRWRA (kg/m^3)
B1	500C-0CR	500	686.5	980.8	0.0	2.37
B2	500C-5CR	500	686.5	931.7	17.9	2.37
B3	500C-10CR	500	686.5	882.7	35.8	2.37
B4	500C-15CR	500	686.5	833.7	53.8	2.37

Note: All mixtures have a 0.4 w/b ratio; C. A. = Coarse aggregates; F. A. = Fine aggregates; and CR = Crumb rubber.

Table II. Fresh and mechanical properties of tested mixtures

Mixture of Beam #	Slump flow		L-box H2/H1	V-funnel	Air %	28-Day f'_c	28-Day STS
	D_s mm	T_{50} sec		T_0 sec			
B1	700	1.2	0.89	6.39	1.5	50.2	3.87
B2	690	1.5	0.83	6.95	2.00	43.0	3.23
B3	687	1.7	0.79	7.57	2.3	41.8	2.94
B4	675	2.0	0.75	8.75	4.3	35.3	2.67

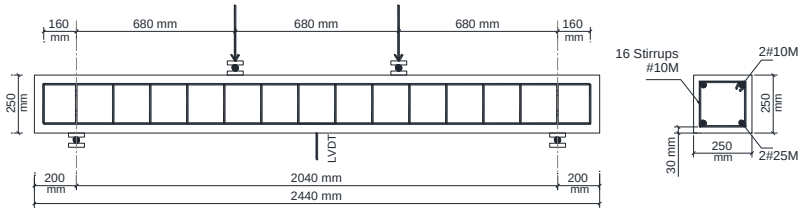

Figure 1. Dimensions and reinforcement of tested beams

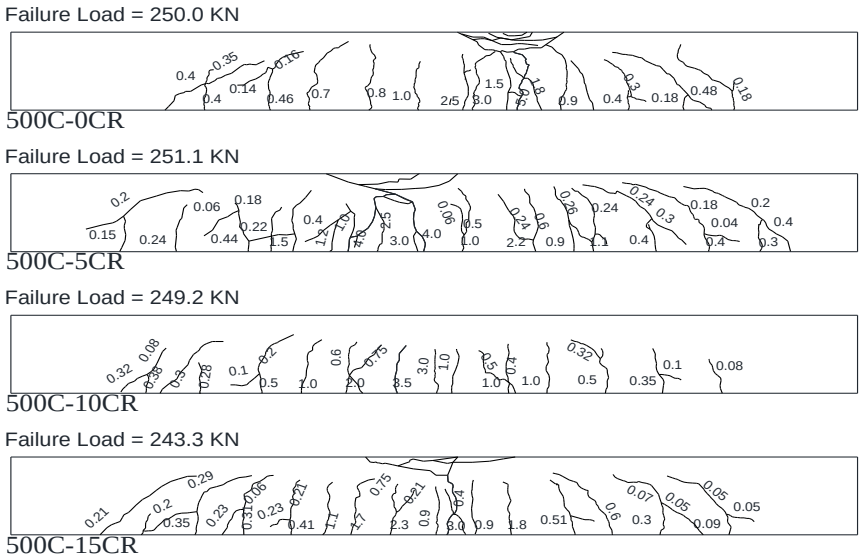

Figure 2. Crack patterns of tested beams at failure (crack width in mm)

Discussion of Test Results

Compressive and Splitting Tensile Strength

Table II shows the 28-day compressive strength and STS of the tested mixtures. Increasing the percentage of CR showed a general reduction in both compressive strength and STS. Increasing the CR from 0% to 15% decreased the 28-day compressive strength and STS by 29.6% and 31%, respectively. The reduction of the mechanical properties with increased percentages of CR may be attributed to the poor strength of the interface between the rubber particles and surrounding mortar, as reported by many researchers [14-15]. In addition, the considerable difference between the modulus of elasticity of the rubber aggregate compared to the surrounding mortar can contribute to decreasing the mechanical properties as

the CR increased. Moreover, increasing the percentage of CR increased the air content (Table II), which may also have contributed to the reduction of the mechanical properties of the mixtures.

Load-deflection Characteristics and Failure Behaviour

Figure 3 presents the load deflection responses of the tested beams at mid span. The first flexural cracking load was detected visually and confirmed by the first step or slope change in the load-central deflection response (Figure 3) and by the load-longitudinal bar strain curves at mid-span. Looking closely at Figure 3, it can be observed that up to the first crack load, the curves appear to be linear with higher stiffness, and then the curves deviate from linearity, showing a reduction in their slopes that indicates lower stiffness due to formation of micro-cracks. After additional application of load, the longitudinal steels started to yield. During the lifetime between the first crack load and the load that caused steel yielding, the slope of the load-deflection curves changed many times due to multiple cracking. Further increasing the applied load finally caused the concrete crushed in the compression zone and beams to fail. All plots present a typical ductile mode of failure, normally called tension failure, in which the steel bars in tension side yielded before the failure occurrence (as confirmed from the steel strain gauges). From Table III and Figure 3, it can be observed that increasing the CR content from 0% to 15% improved the deformation capacity of the tested beams; the maximum deflection increased from 27 to 30.8 mm.

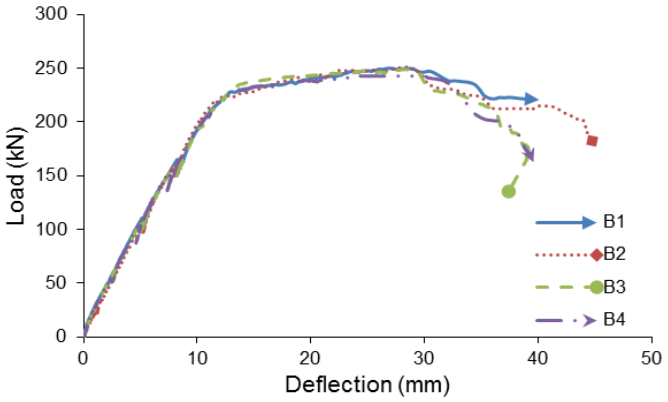

Figure 3. Experimental load-mid-span deflection responses

Ductility and Toughness

Displacement ductility was also investigated in this study. Figure 4 presents the ductility ratio (μ) of the tested beams, which was expressed in terms of $\mu = \delta_u / \delta_y$, where δ_u is the experimental deflection value at peak failure load and δ_y is the experimental deflection at steel yielding. In general, increasing the ductility ratio of the structural member indicates its ability to experience large deflections before failure, and thus provide ample warning to the occurrence of failure. The results showed that increasing the CR content improved the ductility of concrete; as the percentage of CR increased from 0% to 15% (B1 compared to B4), the μ ratio increased by 29.4%. Replacing the conventional aggregate with rubber aggregate, which has lower stiffness, can greatly enhance the flexibility and energy absorption of rubber-cement composite, and thus increase the ductility of beams.

Since the use of CR contributed to enhancing the ductility of the tested beams, it was expected that this improvement can directly affect the beam's toughness. Toughness is the property that can express the capacity of a material to absorb energy up to failure. To compare the toughness of tested beams, the ultimate deformation energy was determined by measuring the area under the load-deflection curve up to the failure load. Figure 4 shows the calculated toughness for all tested beams. Examining the load-deflection curves of the tested beams (B1–B4), it can be seen that the area enclosed by the load-deflection curve increased as the CR increased, which indicates an improved toughness of rubberized concrete. Increasing the percentage of CR from 0% to 15% raised the toughness by 14.9%. The reason for this increase could be attributed to low stiffness of the CR particles that impart relatively high flexibility and, hence, absorb considerably more energy than could be absorbed by conventional concrete.

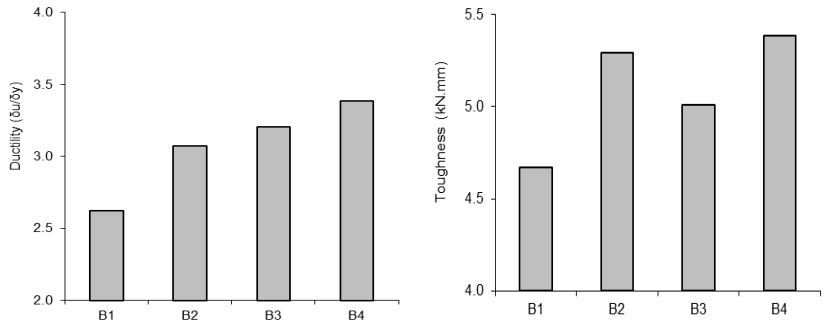

Figure 4. Effect of CR content on the ductility and toughness

General Cracking and Failure Behaviour

Figure 2 shows the crack patterns of all tested beams at the failure stage. During early stages of loading, fine vertical flexural cracks appeared around the mid-span of all beams, as expected. With the increase in load, these flexural cracks extended

and other new flexural cracks were formed along the loaded span. With further increase in load (exceeding 50% of theoretical failure load), the flexural cracks that were formed away from the mid-span started to propagate diagonally towards the loading points, and other new diagonal cracks began to form separately in locations farther away from the mid-span along the beam.

Figure 2 and Table III show the crack pattern and crack widths/numbers of all tested beams, respectively. The beam without CR (B1) appeared to have a larger crack width at failure compared to rubberized concrete beams (B2–B4). This may be attributed to the higher energy absorption capacity of rubber particles. On the other hand, the failure pattern of rubberized concrete beams (B2–B4) was characterized by having slightly more cracks than B1. Such results could be related to increasing the mid-span deflection (beam's curvature) as the CR content increased (Table III), which resulted in the development of more cracks before failure.

Table III. Results of the flexure test

Beam #	First crack load (kN)	Failure crack load (kN)	Deflection (mm)		Failure type	At Failure	
			At yeild	At ultimate		Number of cracks	Maximum crack cidth (mm)
B1	32.8	250.0	10.3	27.0	Flexure	16	5.0
B2	25.3	251.1	9.3	28.5	Flexure	18	4.0
B3	22.8	249.2	8.8	28.2	Flexure	17	3.5
B4	21.4	243.3	9.1	30.8	Flexure	19	3.0

First Crack Load and Ultimate Load

The first flexural crack load was visually observed and then compared/verified with values associated with the change in slope of the load-deflection and load-longitudinal steel strain curves obtained from the test. Table III presents the loads at first flexural crack and failure loads of all tested beams. The results showed that increasing the CR content generally decreased the first crack load and the ultimate failure load of the tested beams. As shown from Table III, the first crack load was highly affected by increasing the CR content compared to the ultimate failure load, which showed a slight decrease with higher percentages of CR. Increasing the CR content from 0% to 15% reduced the first crack load by 34.76% while the ultimate

failure load showed a reduction of 2.67%. The reduction in first crack load could be attributed to the noticeable reduction in the tensile strength of the concrete as the CR content increased, as shown in the results of STS test.

Conclusions

In this investigation, the effect of CR content on the structural behaviour of full-scale reinforced SCRC beams was investigated. The beam mixtures were developed with CR replecement varied from 0% to 15% by fine aggregate volume. The flexural capacity, cracking behaviour, load-deflection response, ductility, and toughness were studied for all beams. From the results described in this paper, the following conclusions can be drawn:

1. Increasing the CR content in SCRC mixtures showed a reduction in the flowability (T_{50} and V-funnel time), passing ability (H2/H1 of L-box), unit weight, compressive strength, and STS while the air content increased.
2. As the percentage of CR increased from 0% to 15%, the first crack load and failure load decreased. However, the deformability, ductility, and toughness of the tested beams appeared to improve with increases in the CR replacement.
3. Utilizing up to 10% CR can improve the beam's deformation capacity, ductility, and toughness without affecting the ultimate flexural load. However, 10% to 15% CR replacement continued to improve the beam's deformation capacity, ductility, and toughness but with a slight reduction in the ultimate flexural load.
4. The addition of CR in concrete appeared to have a noticeable effect on limiting the crack widths, promoting the concept of long-term durability under different exposure conditions.

References

[1] Najim, K. B. and Hall, M. (2012). *Constr. Build. Mater.*, vol. 27, no. 1, p. 521–530.
[2] Fattuhi, N. I. and Clark, L. A. (1996), *Constr. Build. Mater.*, vol. 10, p. 229–236.
[3] Zheng, L., Sharon, H. X. and Yuan, Y. (2008), *Constr. Build. Mater.*, vol. 22, p. 939–947.
[4] Najim, K. B. and Hall, M. (2010), *Constr. Build. Mater.*, vol. 24, p. 2043–2051.
[5] ASTM C618. (2012). *Standard Specification for Coal Fly Ash and Raw or Calcined Natural Pozzolan for Use in Concrete*, ASTM International, pp. 5, West Conshohocken, Pennsylvania.

[6] ASTM C494 / C494M. (2013). *Standard Specification for Chemical Admixtures for Concrete*, ASTM International, pp.10, West Conshohocken, Pennsylvania.
[7] Ismail, M. K. and Hassan, A. A. A. (2015), *J Mater. Civ. Eng*., http://ascelibrary.org/doi/abs/10.1061/(ASCE)MT.1943-5533.0001338.
[8] Hassan, A. A. A. and Mayo, J. R. (2014), *Mag. Concrete Res.*, vol. 66, n. 20, p. 1–15.
[9] Hassan, A. A. A., Ismail, M. K., and Mayo J. (2015), *J. Build. Eng.*, vol. 4, p.113–126.
[10] EFNARC. (2005). *The European Guidelines for Self-Compacting Concrete Specification, Production and Use*, European Federation for Specialist Construction Chemicals and Concrete Systems, English Edition Norfolk.
[11] ASTM C231 / C231M-14. (2014). *Standard Test Method for Air Content of Freshly Mixed Concrete by the Pressure Method*, ASTM International, pp. 9, West Conshohocken, Pennsylvania.
[12] ASTM C39 / C39M. (2011). *Standard Test Method for Compressive Strength of Cylindrical Concrete Specimens*, ASTM International, pp. 7, West Conshohocken, Pennsylvania.
[13] ASTM C496 / C496M (2001). *Standard Test Method for Splitting Tensile Strength of Cylindrical Concrete Specimens*, ASTM International, pp. 7, West Conshohocken, Pennsylvania.
[14] Emiroglu, M., Kelestemur, M. H. and Yildiz, S. (2007). An investigation on ITZ microstructure of the concrete containing waste vehicle tire, Proceedings of 8th international fracture conference, Istanbul, Turkey.
[15] Najim, K. B. and Hall, M. (2013), *Mater. Strut*, vol. 24, p. 2029–2043.

Experimental Investigation on Bond Strength of Self-Consolidating Rubberized Concrete

Mohamed K. Ismail[1] and Assem A. A. Hassan[1]

[1]Department of Civil Engineering, Memorial University of Newfoundland, Canada

Abstract Waste crumb rubber (CR) particles were used as partial aggregate replacement to develop self-consolidating rubberized concrete (SCRC) and vibrated rubberized concrete (VRC). In this investigation, a total of 12 mixtures was cast and tested to study the effect of partial replacement of fine aggregate by CR on bond performance of SCRC and VRC. The variables were CR percentage (0%–50% by volume of sand), different binder contents (500–550 kg/m^3), inclusion of metakaolin, use of air entrainment, and concrete type. The performance of some design codes (ACI 408, CEP-FIP, and EC2) was evaluated in predicting the bond strength of tested mixtures. Based on the results of this study, the bond strength of deformed bars for both SCRC and VRC was found to be decreased as the CR increased, similar to the trend observed for the compressive and splitting tensile strengths. However, the proposed formulas for predicting the bond strength given by the ACI 408, CEP-FIP, and EC2 codes showed a conservative prediction for all tested SCRC and VRC mixtures.

Keywords: *Self-consolidating rubberized concrete, Crumb rubber, Bond strength, Pullout test.*

Introduction

Bond stress is generally described as the shear stress transferred from the concrete to the reinforcing bar through the concrete-steel interface. Mechanical properties of concrete directly affected the confinement effect on the steel reinforcing bar [1]. On the other hand, the bond strength of concrete is influenced by the mechanical interlocking between the ribs of the deformed bar and the surrounding concrete [2]. Previous research reported that using rubber particles in concrete led to the decrease of the mechanical properties of concrete [3-4]. In addition, the low modulus of elasticity of rubber can negatively affect the mechanical interlocking at the concrete-steel interface. For these reasons, using waste rubber (from scrap

vehicle tyres) in concrete as a partial replecement for coarse or fine aggregate might reduce the bond strength of concrete. The objective of this study is to investigate the influence that replacing natural fine aggregate with recycled CR replacement level has on bond strength with reinforcing steel. The mixtures were developed with variable percentages of CR (0% to 50%) using different binder content, addition of MK, and/or utilizing air entrainment. The experimental program, test results, and analyses for this study are presented in the following discussion.

Experimental Program

Materials

Type GU Canadian Portland cement similar to ASTM C618 [5] Type F, and MK conforming to ASTM C618 [5] Class N were used as cementitious materials for both VRC and SCRC mixtures. Natural sand and 10 mm crushed stone aggregate were used as fine and coarse aggregates, respectively. Both aggregates have a specific gravity of 2.6 and an absorption of 1%. A crumb rubber aggregate with a specific gravity of 0.95, maximum aggregate size 4.75 mm, and negligible absorption was used as a partial replacement of the fine aggregate in SCRC and VRC mixtures. Glenium 7700 high-range water-reducer admixture (HRWRA), similar to ASTM C494 Type F [6], was used to adjust the flowability and cohesiveness of SCRC and VRC mixtures, respectively. An air-entrainment admixture similar to ASTM C260/C260M [7] was used to improve the workability of SCRC mixtures.

Concrete Mixtures

The concrete mixtures in this investigation were selected based on a previous study by the authors [8] aimed at developing a number of SCRC mixtures containing maximum percentages of CR (by volume of fine aggregate) and minimum reductions in strength and rubber particles' stability. The selected mixtures are ten SCRC mixtures with CR replacement of 0%–40% and two VRC mixtures with CR replacement of 40%–50%. The investigated mixtures were divided into two stages. Stage 1 was designed to obtain the maximum percentage of CR in mixtures without SCMs and with 500 kg/m^3 total binder content (mixtures 1–4). In this stage, a maximum successful SCRC mixture with up to 15% CR was developed (mixture 4). Increasing this percentage to 20% in this stage resulted in a significant reduction in the passing ability (H2/H1 of L-box). For this reason, stage 2 was designed to allow higher percentages of CR to be used in SCRC mixtures. Stage 2 also included testing SCRC mixtures with a total binder content of 550 kg/m^3, inclusion of MK as an SCM, and the use of an air-entrainment admixture; stage 2 also included testing two VRC mixtures with maximized percentages of CR for comparison. It can be observed from stage 2 that when a 550 kg/m^3 binder was used the maximum percentage of CR that maintains acceptable fresh properties

increased to 20% (mixture 6). Further increasing the percentage of CR in SCRC mixtures with a 550 kg/m^3 binder (from 20% to 30%) showed a reduction in the stability and passing ability. The use of MK in stage 2 proved to enhance the viscosity of the tested mixtures. The increased viscosity of MK mixtures helped to improve the particle suspension and passing ability, which allowed a higher percentage (up to 30%) of CR to be used safely in SCRC mixtures (mixture 8). Utilizing an air-entrainment admixture in this stage helped to alleviate the decreased flowability that resulted from using CR and MK, and raised the maximum possible percentage of CR in SCRC mixtures to 40% (mixture 10). In light of the type of materials used in this investigation, and because of CR's adverse effect on the fresh properties and stability of SCC mixtures, the authors observed that it was not possible to develop SCRC with a CR content higher than 40%. Since the passing ability and segregation are not factors in VRC mixtures, it was possible to develop VRC mixtures in stage 2 with up to a maximum of 50% CR (mixture 12). Stage 1 included four SCRC mixtures with varied CR percentages from 0% to 15% and a binder content of 500 kg/m^3. Stage 2 included a) two SCRC mixtures with a higher binder content of 550 kg/m^3 having 15% and 20% CR; b) two SCRC mixtures with MK having 20% and 30% CR; c) two SCRC mixtures with MK and air-entrainment admixture (0.2205 kg/m^3) with 30% and 40% CR; and d) two VRC mixtures with 40% and 50% CR (see Table I). All tested mixtures were designated by total binder content, percentage of CR, SCM used, and either the inclusion of micro air (MA) or VRC. For example, a beam containing a 550 kg/m^3 binder, 40% CR, MK, and MA would be labelled as 550C-40CR-MK-MA, and a beam with a 550 kg/m^3 binder, 50% CR, MK, and VRC would be labelled as 550C-50CR- MK-VRC.

Table I. Mix design for tested mixtures

Mix. #	Mixture	Cement (kg/m^3)	MK (kg/m^3)	C. A. (kg/m^3)	F. A. (kg/m^3)	CR (kg/m^3)	HRWRA (kg/m^3)
Stage 1							
1	500C-0CR	500	-	686.5	980.8	0.0	2.37
2	500C-5CR	500	-	686.5	931.7	17.9	2.37
3	500C-10CR	500	-	686.5	882.7	35.8	2.37
4	500C-15CR	500	-	686.5	833.7	53.8	2.37
Stage 2							
5	550C-15CR	550	-	648.1	787.0	50.7	1.84
6	550C-20CR	550	-	648.1	740.7	67.7	1.84
7	550C-20CR-MK	440	110	638.4	729.6	66.7	5.26
8	550C-30CR-MK	440	110	638.4	638.4	100.0	5.26
9	550C-30CR-MK-MA	440	110	638.4	638.4	100.0	5.26
10	550C-40CR-MK-MA	440	110	638.4	547.2	133.3	5.53
11	550C-40CR-MK-VRC	440	110	638.4	547.2	133.3	3.50
12	550C-50CR-MK-VRC	440	110	638.4	456.0	166.6	4.00

Note: All mixtures have a 0.4 w/b ratio; MK = metakaolin; C. A. = Coarse aggregates; F. A. = Fine aggregates; and CR = Crumb rubber.

Fresh and Mechanical Properties Tests

The fresh properties of all tested mixtures were determined according to the European Guidelines for Self-Compacting Concrete [9]. The fresh properties tests included slump flow, V-funnel, L-box, and sieve segregation tests. The percentage of entrained air in the fresh SCC mixtures was measured by following a procedure given in ASTM C231[10]. The compressive strength and splitting tensile strength (STS) tests were conducted according to ASTM C39 [11] and C496 [12], in which each of developed mixtures was tested using three identical 100 mm diameter x 200 mm high concrete cylinders. The results of the fresh and mechanical properties of the tested mixtures are presented in Table II.

Table II. Fresh and mechanical properties of tested mixtures

Mixture #	Slump flow/slump		L-box H2/H1	V-funnel	Air %	28-Day f'_c	28-Day STS
	D_s mm	T_{50} sec		T_0 sec			
Stage 1							
1	700	1.20	0.89	6.39	1.5	50.2	3.87
2	690	1.55	0.83	6.95	2.00	43.0	3.23
3	687	1.74	0.79	7.57	2.3	41.8	2.94
4	675	2.00	0.75	8.75	4.3	35.3	2.67
Stage 2							
5	710	1.32	0.76	5.97	3.5	37.6	2.73
6	700	1.54	0.75	6.65	3.2	32.8	2.49
7	680	2.57	0.86	8.25	3.4	40.8	2.69
8	620	2.86	0.75	13.5	4.20	34.8	2.36
9	705	1.53	0.93	5.89	7.5	30.2	2.27
10	700	1.74	0.84	9.79	8	26.4	1.84
11	95	-	-	-	4.5	28.9	2.22
12	80	-	-	-	6.1	22.4	1.74

Pullout Test Setup

The bond strength was measured by conducting a direct pullout test on reinforcing steel bars embedded in a concrete specimen. Each specimen (measuring 100 mm in diameter and 200 mm in height) had a deformed steel bar measuring 20 mm in diameter located at its centre. The bar was embedded five times the bar diameter (100 mm) into the concrete, as recommended by EN 10080 [13]. Bonding between the steel and concrete within the remaining top and bottom 50 mm was prevented

by using 25 mm diameter plastic sleeves (see Figure 1a). This configuration was designed to make only the middle part (100 mm length) of the steel bar subject to the pullout force, thereby reducing the 'end effect' or stress concentration at the ends. A concrete clear cover was kept constant at 40 mm around the steel bar. All specimens were exposed to a curing condition similar to that of the tested beams. A linear variable differential transformer (LVDT) was placed on top of the exposed rebar to measure bar slip. It was observed that splitting failures occurred in all specimens (Figure 1b) regardless of the compressive strength. This type of failure was expected for the level of concrete cover provided. The bond strength of the 12 tested mixtures is presented in Table III.

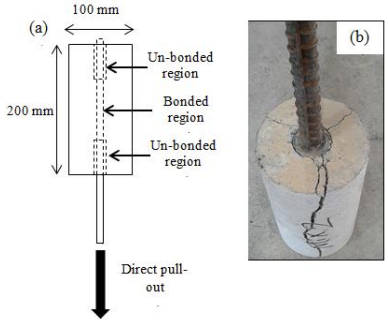

Figure 1. Bond test (a) specimen details, (b) typical failure mode

Table III. Results of bond test for tested mixtures

Mixture	Exp. bond strength τ_{max} (MPa)	Pred. bond strength (MPa)					
		CEB–FIP		ACI 408		EC2	
		Pred.	Exp./pred.	Pred.	Exp./pred.	Pred.	Exp./pred.
Stage 1							
1	13.00	7.09	1.83	7.17	1.81	8.72	1.49
2	11.54	6.56	1.76	6.63	1.74	7.27	1.59
3	10.78	6.47	1.67	6.54	1.65	6.62	1.63
4	9.64	5.94	1.62	6.01	1.60	6.02	1.60
Stage 2							
5	10.18	6.13	1.66	6.20	1.64	6.14	1.66
6	9.47	5.73	1.65	5.79	1.64	5.59	1.69
7	11.02	6.39	1.72	6.46	1.71	6.04	1.82
8	10.22	6.07	1.68	6.14	1.66	5.31	1.92
9	9.13	5.50	1.66	5.56	1.64	5.10	1.79
10	7.97	5.14	1.55	5.20	1.53	4.15	1.92
11	9.35	5.38	1.74	5.44	1.72	4.98	1.88
12	8.12	5.00	1.62	5.05	1.61	3.92	2.07

Discussion of Test Results

Compressive and Splitting Tensile Strengths

The 28-day compressive strength and STS of the tested mixtures are shown in Table II. As seen from mixtures 1–4, increasing the percentage of CR showed a general reduction in both compressive strength and STS. Varying the CR from 0% to 15% reduced the 28-day compressive strength and STS by 29.6% and 31%, respectively. In mixtures 5–6 (mixtures with 550 kg/m^3 binder content), the reduction in the 28-day compressive strength and STS was 12.8% and 13.8%, respectively, as the percentage of CR increased from 15% to 20%. Similar behaviour was also noticed in MK mixtures (mixtures 7–12), in which the compressive strength and the STS reduced as the percentage of CR increased. The reduction of the mechanical properties with increased percentages of CR may be attributed to the poor strength of the interfacial transition zone between the rubber particles and surrounding mortar, as reported by many researchers [14]. In addition, the significant difference between the modulus of elasticity of the rubber aggregate and the surrounding mortar can contribute to decreasing the mechanical properties as the CR increased. Moreover, increasing the percentage of CR increased the air content (Table II), which may also have had a negative effect on the mechanical properties of the mixtures.

Increasing the binder content from 500 to 550 kg/m^3 raised the compressive strength and STS by 6.5% and 2.25%, respectively, as shown in mixture 4 compared to 5. Also, by comparing mixture 6 and 7 it can be seen that the addition of MK showed an enhancement in the mechanical properties; the compressive strength and STS increased by 24.4% and 8%, respectively. Meanwhile, From Table II, using air entrainment helped to develop SCRC with up to 40% CR; however; the 28-day compressive strength and the STS decreased by 13.2% and 3.8%, respectively, with the use of air entrainment as shown in mixtures 8 compared to 9. The results also indicated that the 28-day compressive strength and STS showed some improvement when using VRC compared to SCRC (mixture 11 compared to 10). This can be attributed to the reduction in the air content, as shown in Table II. It should be noted that the use of VRC (mixtures 11 and 12) could benefit from using up to 50% CR, in which a further decrease of the mixtures' self-weight was obtained.

Experimental and Theoretical Analyses of Bond Strength

Table III presents the bond test results for all tested mixtures. The results indicated that the bond strength of concrete decreased as the CR content increased in both stages 1 and 2. For instance, increasing the CR percentage from 0% to 15% in stage 1 (mixtures 1–4) showed a reduction in the bond strength up to 25.8%. This reduction can be attributed to the decreased compressive strength with higher percentages of CR (as shown in Table III), which directly affected the confinement effect on the steel reinforcing bar [1]. Accordingly, improving the compressive strength in stage 2 by using a higher binder content (mixture 5 compared to

mixture 4) or adding MK (mixture 7 compared to mixture 6) improved the bond strength for concrete.

In order to eliminate the effect of the variation of compressive strength in all tested mixtures, the bond stress was normalized by the square root of the compressive strength (Normalized bond strength = $\tau_{max}/ f_c^{'0.5}$). As shown in Figure 2, increasing the CR content led to decreasing the normalized bond strength in both stage 1 and 2. This result showed a considerable effect for CR particles on decaying the bond strength of concrete mixtures, regardless of the concrete compressive strength. The bond strength of concrete is affected by the mechanical interlocking properties of aggregate [2]. Therefore, the low modulus of elasticity for CR particles may have reduced the interlocking at the steel-concrete interface between reinforcing bar and rubber aggregate, contributing to a decreased bond strength. Another reason for the reduced bond strength of the rubberized concrete compared to conventional concrete could relate to the decaying tensile strength of the concrete cover as the CR increased, especially all the tested mixtures failed due to splitting of concrete and no pullout failure was observed (as shown in Figure 1b).

In order to study the effect of CR content on the free end slip of steel bars, the data after the peak bond load were discarded and the curves were refined using trend lines. Figure 3 shows the load-slip curves of the tested specimens in stage 1 (mixture 1–4). Generally, the load-slip curves showed a rapid rise to the peak followed by a sudden drop, exhibiting a brittle behaviour, as expected, for splitting failure mode. From Figure 3 it is worth noting that the initial slope of the load-slip curves (stiffness) decreased as the CR content increased, showing less slip at a given load. As reported by Najim and Hall [3], this finding may be attributed to the fact that the low modulus of elasticity for CR particles can contribute to increasing the energy dissipation along the steel-concrete interface and allowing greater absorption of kinetic energy.

Table III shows the comparison between the experimental and theoretical maximum bond strength proposed in various codes of design such as CEB–FIP [15], ACI 408 [16] , and EC2 [17], as shown in Eqns. 1, 2, and 3, respectively.

$$\tau_{max} = \gamma\ f_c^{'0.5} \quad (1)$$

$$\tau_{max} = 20.23\ f_c^{'0.5}/\phi \quad (2)$$

$$\tau_{max} = 2.25\ f_t \quad (3)$$

where τ_{max} is the maximum bond strength (MPa); γ is a factor suggested based on the confinement and bond condition (γ was taken equal to 1 as recommended for unconfined concrete where splitting of the concrete governs the failure); $f_c^{'}$ is the cylinder compressive strength (MPa); ϕ is the diameter of the steel reinforcing bar (mm); and f_t is the STS (MPa).

Based on the comparison shown in Table III, it can be observed that the ACI 408, EC2, and CEB-FIP safely predicted the bond strength for all the tested mixtures. In fact, the experimental bond strength was 53%–81%, 55%–83%, and 49%–107%

higher than the bond strength predicted using ACI 408, CEB-FIP, and EC2, respectively.

By looking at Tables II and III, it can be seen that as the percentage of CR increased in SCRC mixtures the reduction in the square root of the compressive strengths were lower than the reduction in the bond strengths. When the CR increased from 0%–15% in SCRC mixtures, the square root of the compressive strength decreased by 16.14% compared to the 25.85% decrease in the bond strength. Therefore, increasing the CR content decreased the difference between the predicted values and those obtained from the experiments in both ACI 408 and CEB-FIP codes, resulting in a lower margin of safety. On the other hand, EC2 showed lower predicted/experimental values as the CR increased. This behaviour could be related to the fact that the predicted bond strength in the EC2 equation is directly proportional to the tensile strength of concrete, which was greatly affected by increasing the CR content compared to the bond strength. Increasing the CR content from 0%–15% showed a 31% decrease in the tensile strength compared to a 25.85% decrease in the bond strength (Tables II and III).

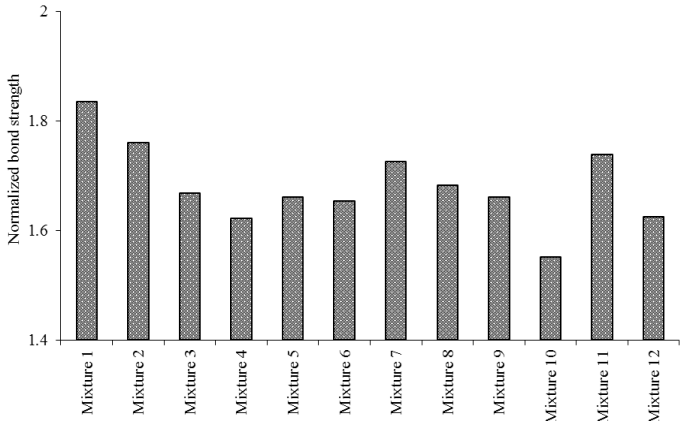

Figure 2. Normalized bond strength of tested mixtures

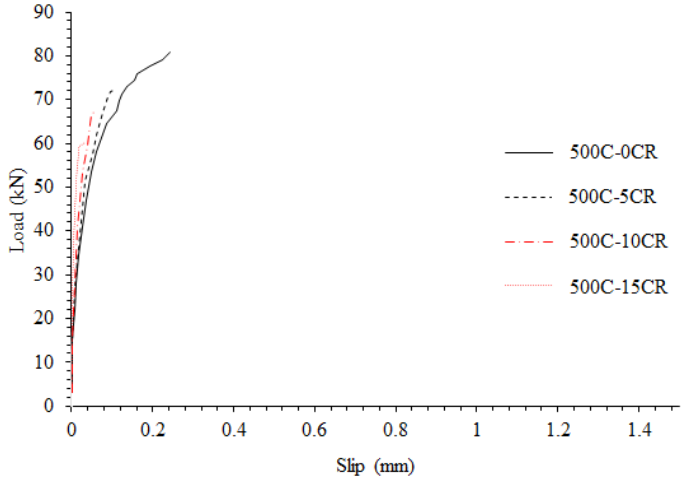

Figure 3. Load-slip curves for mixtures of CR content ranging from 0% to 15%

Conclusions

In this study, the bond strength of small-scale samples made of SCRC and VRC were investigated. SCRC and VRC mixtures were developed with variable percentages of CR using different binder content, addition of MK, and/or use of air entrainment. The following conclusions can be drawn from the results described in this paper:

1. Increasing the percentage of CR in both SCRC and VRC mixtures showed a reduction in the fresh properties and compressive and tensile strengths of the concrete mixtures. For example, the compressive and tensile strengths decreased by 29.7% and 31%, respectively, when developing a successful SCRC mixture with a maximum CR content of 15%.
2. Regardless of the compressive strength of concrete mixtures, increasing the CR content seemed to influence the normalized bond strength: the normalized coefficient of the bond strength decreased as the CR increased. For example, increasing the percentage of CR from 0% to 15% decreased the normalized bond strength by 11.6%.
3. The proposed formulas for predicting the bond strength (given by the ACI 408, CEP-FIP, and EC2 codes) conservatively predicted the strengths of SCRC and VRC mixtures containing up to 50% CR. However, as the percentage of CR increased in SCRC mixtures, both the ACI 408 and CEB-FIP codes' predictions indicated a slight decrease in the margin of safety while the EC2 prediction indicated a slight increase. This behaviour could be related to the fact that the predicted bond strength in the EC2 equation is directly proportional to the tensile strength of concrete, which

was greatly affected by increasing the CR content compared to the bond strength, while the predicted values of both the ACI 408 and CEB-FIP codes were based on the square root of the compressive strengths, which had a lower reduction compared to the experimental bond strengths.

References

[1] Kim, D. Kim, MS. Yun, GY. and Lee YH. (2013), *J. Adhes. Sci. Technol*, vol. 27, n. 5–6, pp. 490–507.
[2] Lachemi, M. Bae, S. Hossain, KMA. and Sahmaran, M. (2009), *Mater. Struct*, vol 42, pp. 1015-1023.
[3] Najim, KB. and Hall, M. (2014), *Construct. Build. Mater*, vol 73, pp. 490–497
[4] Ilker Bekir Topçu. (1995), *Cem. Concr. Res*, vol 25, n. 2, pp. 304-310,
[5] ASTM C618. (2012). Standard specification for coal fly ash and raw or calcined natural pozzolan for use in concrete. ASTM International, West Conshohocken, PA, USA.
[6] ASTM C494 / C494M. (2013). *Standard specification for chemical admixtures for concrete*. ASTM International, West Conshohocken, PA, USA.
[7] ASTM C260. (2010). *Standard specification for air-entraining admixtures for concrete*. ASTM International, West Conshohocken, PA.
[8] Ismail, MK. and Hassan, AAA. (2015), *J. Mater. Civ. Eng*, http://ascelibrary.org/doi/abs/10.1061/(ASCE)MT.1943-5533.0001338.
[9] EFNARC. (2005). *The european guidelines for self-compacting concrete specification, production and use. european federation for specialist construction chemicals and concrete systems*. English ed. Norfolk, UK.
[10] ASTM C231 / C231M-14. (2014). *Standard test method for air content of freshly mixed concrete by the pressure method*. ASTM International, West Conshohocken, PA, USA.
[11] ASTM C39 / C39M. (2011). *Standard test method for compressive strength of cylindrical concrete specimens*. ASTM International, West Conshohocken, PA, USA.
[12] ASTM C496. (2011). *Standard test method for splitting tensile strength of cylindrical concrete specimens*. ASTM International, West Conshohocken, PA.
[13] EN 10080. (2005). *Steel for the reinforcement of concrete – wieldable reinforcing steel–general*. European standard.
[14] Najim, KB. and Hall, M. (2013), *Mater. Struct*, vol 46, pp. 2029–2043.
[15] ACI Committee 408. (2003). *Bond and development of straight reinforcing bars in tension.* ACI 408R–03, American Concrete Institute, Farmington Hills, Mich.
[16] CEB-FIP. (1992). *CEB-FIP Model Code* 1990. Thomas Telford, London.
[17] EN 1992-1-1. (2004). Eurocode 2 – Design of concrete structures – Part 1–1: General rules and rules for buildings.

Concrete Flow on a Steel-Plate Concrete Member Having Congested Studs

Jae Hong Kim[1], Tae Yong Shin[1], Yoon Yi Hwang[3] and Dong Kyu Shin[4]

[1]Ulsan National Institute of Science and Technology, Republic of Korea
[2]Hyundai Heavy Industry, Republic of Korea

Abstract Steel-plate concrete refers a structural member of wall or slab composed of core concrete sandwiched in top and bottom steel plates. Its efficiency on precast construction or production process makes the construction industry and heavy industry consider the sandwiched concrete panel. Its structural integrity is obtained by studs and tie bars between two steel plates. Only when enough numbers of studs and tie bars hold core concrete, the panel shows designed performance on flexural and shear resistance. This presentation discusses concrete flow to cast core concrete through the studs. One of the extreme placings of studs is considered here. Their spacing is less than 50 mm so that the skin plate does not take off from 100 mm-thick core concrete. A small sample of sandwiched concrete panel was devised and an SCC mix was placed on the panel. In addition, simulation of the SCC flow was accomplished to predict a real-scale casting of sandwiched concrete panel.

Keywords: *VOF, Rheology, Studs, Passing, Filling, Panel*

Introduction

Steel-plate concrete is a composite plate or panel composed of outer steel plates and core concrete [1]. Fig. 1 shows its schematic view. The upper and lower steel plates play a role as a formwork and then become reinforcement after core concrete is filled and cured. Studs connecting both steel plates reinforce in-plane shear resistance of the composite. It does not require a construction process of formwork removal, which results in reducing the construction period and labor cost related to formwork. The hardened steel-plate concrete does not require any reinforcement, and its use in a construction field also saves cost and time related to the arrangement of reinforcing bars.

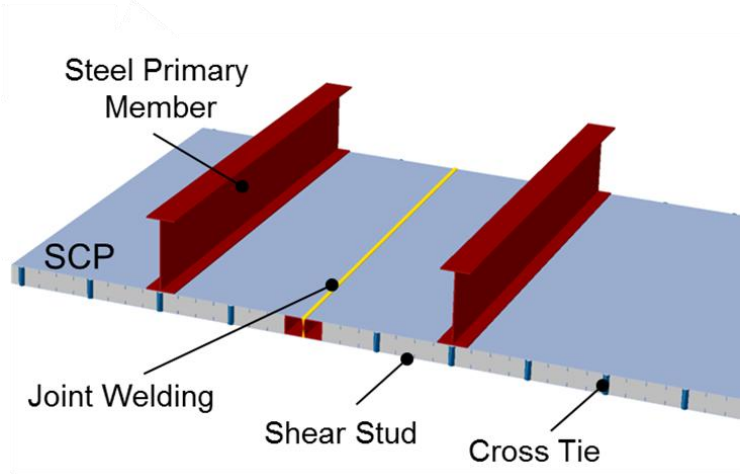

Figure 1. Illustration of steel-plate concrete.

The steel-plate concrete is also called sandwiched concrete panel (SCP) when its thickness is reduced. A thin SCP is possible to be transported, and consequently it can be adopted for precast construction. That would be the third merit enhancing construction efficiency by the use of steel-plate concrete. However, a narrow cross-section of the SCP prohibits access of a vibrator for compacting conventional concrete. Self-consolidating concrete (SCC) is considered for the case. Its filling and passing ability through congested studs distributed on the narrow SCP cross-section need to be evaluated.

In this paper, an L-shape segment test was proposed to evaluate the filling and passing performance of SCC. The viscosity of SCC was measured using a commercialized rheometer, which became a key variable to characterize the property of SCC. Based on the viscosity measurement, a volume-of-fluid (VOF) simulation was accomplished to analyse the L-shape segment test.

Experiments

Materials

Two SCC mixes were used to compare the effect of viscosity on its filling and passing ability. Their mix proportion is identical as reported in Table I, but tailoring the chemical admixture (high-range water-reducing admixture) used for each mix allows to control its viscosity whereas their slump flows are identical. The slump flow, T50, and the rheological properties of both SCC mixes are listed in Table II, where the yield stress and plastic viscosity were measured by using ICAR rheometer (German Instruments).

Table I. Mix proportion of SCC

Label	W/B	S/A	Water	Cement	Expander	Fly ash
C/D	0.41	0.58	175	292	9	43
	GGBFS	Sand	Coarse sand		Gravel	HRWRA
	86	493	488		715	4.35

Table II. Fresh properties of the SCC samples

Label	Slump flow [mm]	T50 [s]	Plastic viscosity [Pa·s]	Yield stress [Pa]
C	620 x 620	11	95	0.9
D	620 x 620	3	60	0.1

L-shape SCP segment test

An SCP segment is designed to measure filling ability of SCC in L-shape SCP. Its configuration is shown in Fig 2. The core concrete is designed to have a thickness of 100 mm. The studs are placed at the interval of 80 mm. Clear distance for concrete flow is then 40 mm.

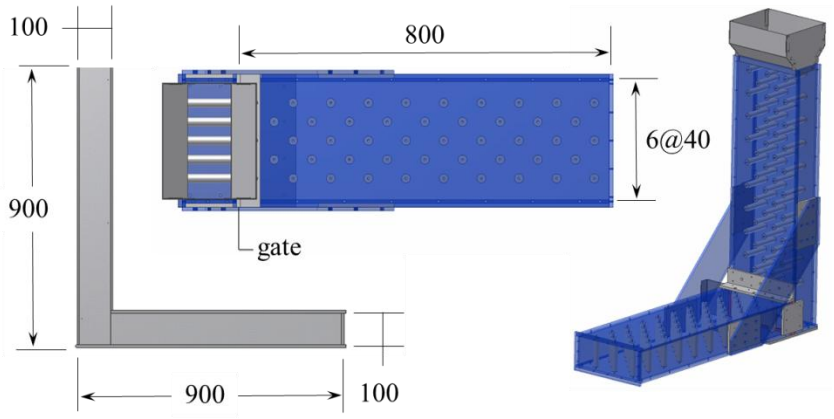

Figure 2. Drawing and pictures of L-shape segment

In order to measure a filling curve for the L-shape SCP segment, (1) the column part of the segment was filled and (2) spread of core concrete is measured after the gate opens. The filling curve, a time-spread curve, was then constructed to describe the core concrete flow on the bottom plate part of the segment. The use of video

camera and tapeline visualized the concrete flow and then provided its quantitative record. Fig. 3 shows the example of the filling test, and Fig. 4 is the filling curve obtained by each mix case.

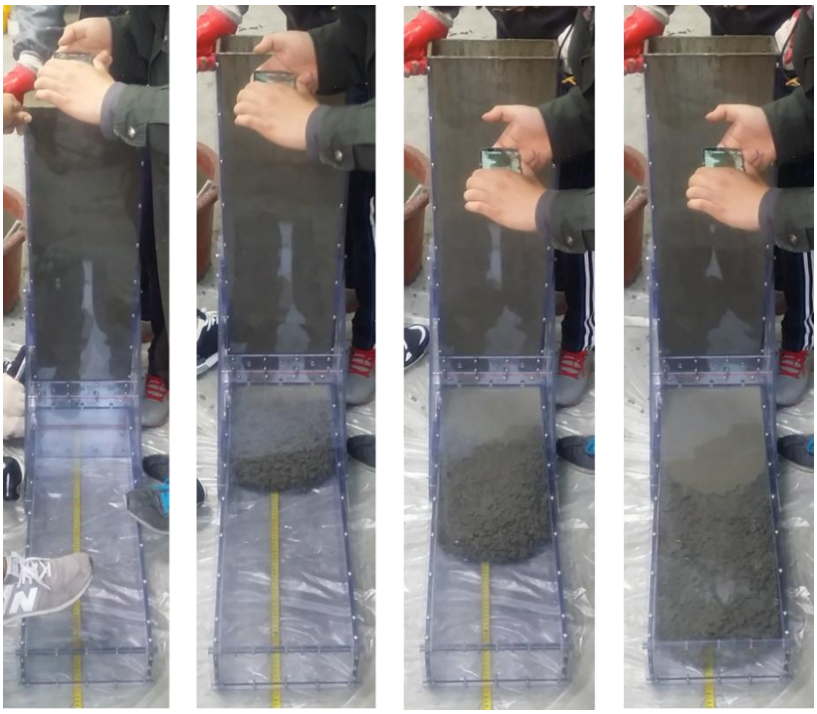

Figure 3. The example of flow test

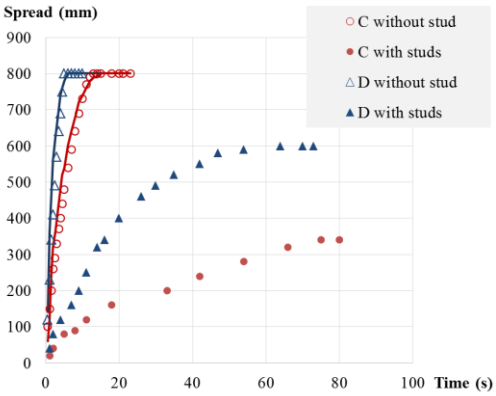

Figure 4. Filling curve of each mix

Simulation

VOF technique

The volume-of-fluid (VOF) technique traces the free surface of a single fluid when it flows, and its application on simulating concrete flow has been widely accepted [2-4]. Assuming a fluid is incompressible simplifies the Navier-Stokes equation governing the field of the fluid flow,

$$-\frac{1}{\rho}+\frac{\mu}{\rho}\nabla^2\vec{v}+\vec{g}=\frac{D\vec{v}}{Dt} \tag{1}$$

where $\boldsymbol{v}$ is the velocity vector field of the fluid and D$\boldsymbol{v}$/Dt indicates its material derivative. In the equation, ρ and μ are the density and shear viscosity of the fluid, respectively. The gravity assigned by its lateral acceleration of g=9.8 m/s^2 initiates the fluid flow. The use of finite element method solves the differentiation equation in a fragmented domain. Each mesh of the domain defines a Eulerian volume fraction of C. If the scalar variable of C is 1.0, the corresponding element is assumed to be filled with the fluid. The void element is represented by C=0, obviously. The Eulerian volume fraction is governed by an advection equation,

$$\frac{\partial \mathrm{C}}{\partial \mathrm{t}}+\vec{\mathrm{v}}\cdot\vec{\nabla}\mathrm{C}=0 \tag{2}$$

The above two equations are coupled in each mesh and the method of weighted residual numerically calculates the velocity vector and the scalar volume fraction at each increment of time. In the result, the scalar volume fraction sometimes indicates an element partially filled on the interface between the fluid and the void space. The discontinuous distribution in the field is released by geometrical reconstruction of the fluid surface. A planer facet for a 3-dimensional model is usually imposed for the fluid surface reconstruction. The sample calculation is successive for each increment of flow time.

Modelling

A total of 3 models were examined to simulate the SCC flow on the L-shape SCP segment. All of them adopted approximately 10 mm mesh size, but they were distinguished by the method of modelling the effect of studs on the concrete flow. Fig. 3 shows distributed, discrete, and effective model of studs embedment, where the numbers of nodes and elements are also listed.

The discrete model was designed to simulate the exact state of concrete flow. Studs in the SCP segment were discretely sketched and occupied void space in the model. A fixed boundary condition was assigned to their surface. SCC flow

through the segment was expected to get resisted by the studs' boundary condition, which is the most promising method to consider the effect of studs. However, modelling studs for a real-scale SCP member is tedious and time-consuming because the total number of studs would be extensive to produce a few meter-scale SCP plate. Moreover, the discrete studs' model need very high cost for analysis time.

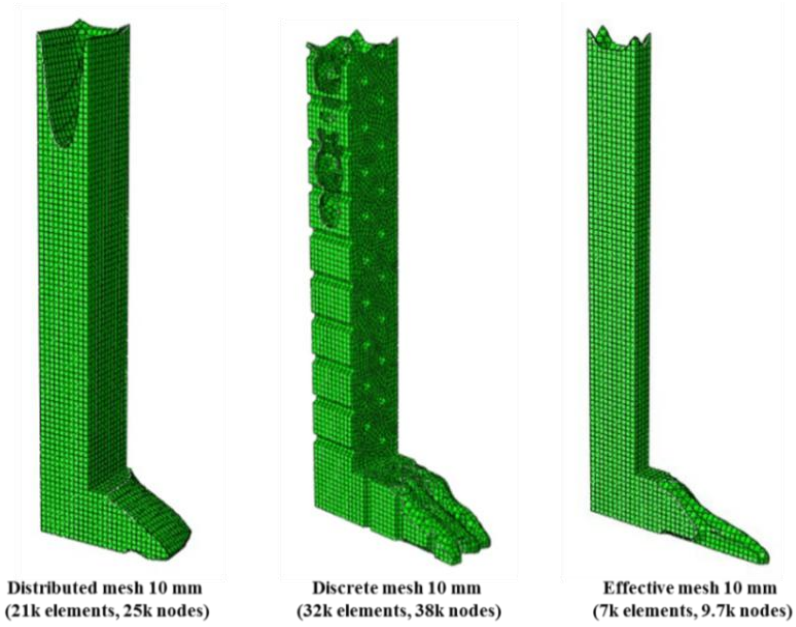

Figure 6. Examples of studs modelling

The distributed model approximates SCC flow resistance by the studs. They were not placed in the model. Instead, the yield stress of SCC was increased to consider the flow resistance even though its yield stress almost vanishes. The model postulates jamming of coarse aggregates through studs, which can be simulated by the increase in the yield stress of SCC.

The effective model is one of an improved version of the distributed model. Jamming of coarse aggregates is localized between two adjacent studs, and the flow resistance between two parallel lines of the studs is symmetric. Taking out the flow path between two studs' lines provided a representative element for an SCP plate-like segment flow. If a segment is wide enough to neglect the edge or side boundary condition, the effective model having the boundary condition specified on the parallel studs' lines is sufficiently accurate.

Verification and yield stress postulation

The SCC samples were assumed as a Newtonian fluid to analyse the flow on the L-shape SCP segment having no stud. The viscosity to show good agreement with the filling curve was determined and listed in Table III. The viscosity of 60 Pa·s was required for precise simulation of the filling curve of the low-viscosity mix D, of which plastic viscosity was 60 Pa·s measured by the ICAR rheometer. The viscosity of 130 Pa·s was good for the high-viscosity mix C. Note that its plastic viscosity was 95 Pa·s as reported in Table II. The ICAR rheometer provided a reasonable measure of the viscosity.

The viscosity was fixed for the flow simulation of the case having arranged studs, but the yield stress was tuned to find an accordance with the measured filling curve. The yield stress for considering the studs' effect was dependent on the modelling method even though the jamming of coarse aggregates between studs is physically inherent. Control of the yield stress postulates to describe the interaction between SCC rheology and drag force by studs. The above three models distinguished by studs' implementation in the VOF model expected to give a different value for the optimal yield stress. A variety of yield stress was examined to match the simulation result with the measured filling curves, and the closest one is plotted in Fig. 7

The simulated filling curve in distributed model has a relatively large difference with the measured filling curve. The postulated yield stress did not represent a shear resistance of studs properly. The wide distance between the boundaries (240 mm) hardly mimicked the resistance by the studs. On the other hand, the effective model shows an acceptable conformity. The distance between the model boundaries was reduced into the distance between studs (40 mm). The flow field between two adjacent studs was more accurately developed in the effective model. The discrete model drew the studs' arrangement as they were, and then the flow resistance initiated from the surface of each stud. The discrete model simulated into detail. For example, the smooth steps on the filling curve were found, which is due to detouring of SCC flow by the studs. The plastic viscosity and the postulated yield stress are listed in Table III.

Table III. Postulated viscosity and yield stress

Label		Viscosity [Pa·s]	Yield stress [Pa]
C	Distributed	130	700
	Discrete		200
	Effective		200
D	Distributed	60	500
	Discrete		50
	Effective		130

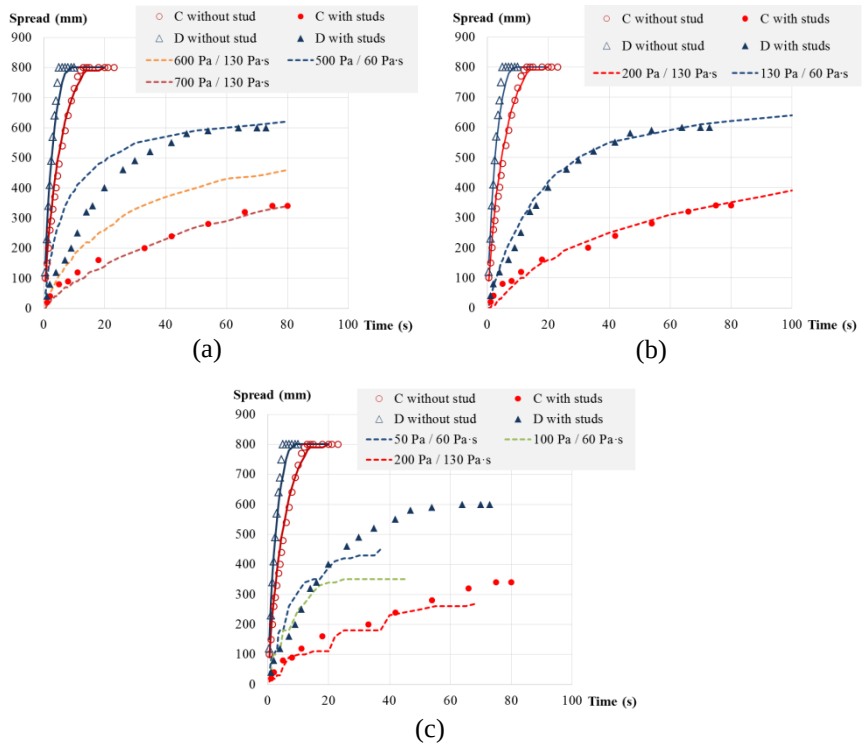

Figure 7. Yield stress postulation in (a) distributed model; (b) effective model; and (c) discrete model

Conclusions

SCC flow through congested studs was simulated and its filling on an SCP segment was evaluated. The arrangement of studs causes shear resistance on the flow. Three models to consider the shear resistance were proposed and their results were compared. The discrete model having the studs as their original shape simulated detailed SCC flow, but it need high cost on modelling and analysis. The effective model concentrated on SCC flow between two adjacent studs. The shear resistance by the studs was mimicked with the fixed boundary condition on two parallel lines following the studs' arrangement. Its result showed reasonable agreement with the measured filling curve of the SCP segment.

Acknowledgements

This research was supported by a grant (13SCIPA02) from Smart Civil Infrastructure Research Program funded by Ministry of Land, Infrastructure and Transport (MOLIT) of Korea government and Korea Agency for Infrastructure Technology Advancement (KAIA).

Reference

[1] Takeuchi, M., Narikawa, M., Matsuo, I., Hara, K. and Usami, S. (1998), Study on a concrete filled structure for nuclear power plants, *Nuclear Engineering and Design*, vol. 179, p. 209-223

[2] Ozaki, M., Akita, S., Osuga, H., Nakayama, T. and Adachi, N. (2004), Study on steel plate reinforced concrete panels subjected to cyclic in-plane shear. *Nuclear Engineering and Design*, vol. 228, n. 13, p. 225–244.

[3] Roussel, N., Geiker, M.R., Dufour, F., Thrane, L.N. and Szabo, P. (2007), Computational modeling of concrete flow: General overview, *Cement and Concrete Research*, vol. 37, n. 9, p. 1298-1307.

[4] Vasilic, K., Meng, B., Kühne, H. C. and Roussel, N. (2011), Flow of fresh concrete through steel bars: A porous medium analogy, *Cement and Concrete Research*, vol. 41, p. 496-503.

[5] Kim, J. H., Jang, H. R. and Yim, H. J. (2015), Sensitivity and accuracy for rheological simulation of cement-based materials, *Computers and Concrete*, vol. 15, n. 6, p. 903-919.

Effects of Dynamic Segregation of Self-Consolidating Concrete on Uniformity and Bond Strength of Pre-Stressed Beams

Aida Margarita Ley Hernández[1], Dimitri Feys[1] and Julie Ann Hartell[2]

[1]Department of Civil, Architectural & Environmental Engineering, Missouri University of Science and Technology, Rolla, MO, United States.
[2]Department of Civil and Environmental Engineering, Oklahoma State University, Stillwater, OK, United States

Abstract Self-Consolidating Concrete (SCC) is a highly flowable concrete that can spread into place under its own weight and achieve good consolidation in the absence of vibration. Due to the high flow capacity of SCC, it is more vulnerable to suffer stability problems compared to conventional vibrated concrete. Static segregation has been studied extensively, but dynamic segregation, which is segregation during flow, has received less attention. Similarly to static segregation, dynamic segregation can negatively affect the homogeneity of the SCC, leading to inferior properties in the hardened stage. In this research project, the effects of dynamic segregation of self-consolidating concrete (SCC) on the uniformity of precast beams, tested by means of ultrasonic pulse velocity (UPV), and the bond strength of pre-stress strands have been investigated. The UPV results show that the SCC stiffness shows the largest variation at the casting point. Bond strength results show that the bond strength of strands imbedded in the top part of the beams are significantly affected by dynamic stability.

Keywords: *self-consolidating concrete; dynamic segregation; rheology; ultrasonic pulse velocity; bond strength.*

Introduction

Segregation is defined as the ability of the coarse aggregate particles to settle in the mortar matrix during production, transporting and placement [2]. It is a common problem observed in self-consolidating concrete (SCC). SCC is a highly flowable concrete that can spread into place and fill the formwork without mechanical vibration and achieve good homogeneity of its constituents. A fresh SCC with poor

segregation resistance may lead to a non-uniform compressive strength and other hardened properties [9]. In addition, it may cause a weaker interface between the aggregate and the cement paste and can adversely affect the bond behavior between steel and concrete. Dynamic segregation is one of the least studied aspects of SCC and refers to the tendency of the coarse aggregates to separate from the mortar while is being transported or placed [3]. A limited number of test methods have been suggested to evaluate the risk of dynamic segregation, none of which is widely accepted. The only current standard method is the visual stability index in ASTM C1611/C1611M [11]. A recent study proposed a new test method (T-box test) to assess dynamic segregation [12].

The objective of this research project is to understand the influence of dynamic segregation of SCC on the structural performance of precast beams in terms of mechanical properties, durability and bond strength of strands. In this paper, the uniformity of the mixture has been evaluated by means of Ultrasonic Pulse Velocity (UPV) and the influence of dynamic segregation on bond strength with pre-stressed strands has been investigated.

Experimental program

Materials and Mix Design

A total of 8 SCC mixtures based on Coreslab Structures' mix design were investigated. Type III Portland cement complying with ASTM C150/C150M-15, with a specific gravity of 3.15 was used. Two types of crushed limestone were employed with a maximum aggregate size of 12.5 mm and 9.5 mm, with absorption of 1.40% and 1.64% respectively. The specific gravity, fineness modulus and absorption of the fine aggregate, which was a natural Kansas river sand were 2.62, 2.53 and 0.4%, respectively. A commercially available polycarboxyl ether-based superplasticizer (SP) with a viscosity modifier incorporated was added to all the mixtures. An air entraining agent (AEA) was also added to improve freeze-thaw-resistance.

The following variations were induced to investigate the effect on dynamic segregation:

- The w/c was changed from 0.36 to 0.4 and 0.45.
- The paste volume was increased 25 l/m^3, or 2.5% of the concrete volume.
- The sand-to-total aggregate ratio was altered from 0.51 (ref) to 0.56.

Mixing procedure

Each SCC mixtures had a volume of about 2.3 m^3 and were prepared in the ready mix plant and transported to the job site in a concrete truck. The mixing sequence was done in accordance to the usual procedure of the company. Slump flow test was done to verify if more SP was needed to achieve the target slump flow. Immediately after the slump flow test each concrete mixture was placed into the formwork.

Pre-stressed beams

Eight pre-stressed beams were produced with the SCC mixtures. Beams 1 to 5 we rectangular beams with a width of 457 mm and a height of 915 mm (Figure 1). Beams 2 and 4 had a total length of 18 m, while beams 1, 3 and 5 were 9 m long. Beams 6 to 8 were MoDOT approved I-beams, each 9 m long, with a bottom flange width of 457 mm, a top flange width of 356 mm and a height of 1143 mm. All beams were pre-stressed with six 12.5mm diameter strands at the bottom and two at the top. Minimum shear reinforcement, using #4 steel bars was installed, spaced 457mm apart in the main section of the beams. All beams were cast while keeping the casting point near one end of the beam.

Figure 82. Left: casting of beam 3. Right: beam 5 with the three sets of prestress strands.

In the 9 m beams, six 12.5 mm diameter pre-stress strands were connected vertically to the shear reinforcement: two near the casting point, two near the end and two in the middle (Figure 1). One of the strands in each pair was imbedded in the first 305 mm of concrete, measured from the top, the other was installed from 305 to 610 mm from the top, while the top portion was covered with a plastic sleeve to avoid bond between the concrete and the strand. The strands will be referred to as installed in the top and in the middle section, respectively. For the 18 m long beams, six sets of two strands were equally installed, spaced 3 m apart.

Testing procedure

Fresh properties

Immediately after the target slump flow was achieved (i.e 700 ± 50 mm), the time needed for the concrete to spread 500 mm (T_{50}) was noted and the visual stability index had to be 0 or 1. For all the eight mixtures the following properties were also measured: V-funnel flow time test, air content, sieve stability, tilting box test. The compressive strength specimens (three 100 x 200 mm cylinders) were cast upon completion of the testing procedure. All specimens were demolded at 24h and kept at the same environmental conditions as those of the beam.

Dynamic segregation resistance

Dynamic segregation was assessed using the tilting box (T-box), developed by Esmaeilkhanian et al [12]. that was modified to evaluate the effect of different formwork dimensions. The T-box consists on a rectangular channel of 1 m, which can tilt from a horizontal to an inclined position. The tilting height of the box is 140 mm. The box width was 400 mm, which can be divided into one section with a width of 100 mm, and one with 200 mm width. Before testing, fresh concrete is placed reaching a height of 80 mm in the tested sections, while the box was maintained in horizontal position. The box is then tilted during 1 second, and brought back to horizontal during another second. Cycle time can be varied during the test, but in this testing program, the cycle time is kept constant at 2 s. The 100 and 200 mm channel widths were used in this work.

At the end of the 60 cycles, which corresponds theoretically to a flow distance of 4.5 m, a sieve-washing technique was used. Samples were taken from the tilt-up and tilt-down sections, from both the 100 and 200 mm width. Standard 100 x 200 mm cylinders were filled with concrete, washed over a #4 sieve (4.75 mm opening), and dried to measure the amount of coarse aggregates in each of the sample sections. The amount of aggregate in each section corresponds directly to dynamic segregation. The Volumetric Index (VI) is defined according to (eq. 1), where V_{td} is the relative coarse aggregate volume in the tilt-down section and V_{tu} is the relative coarse aggregate volume in the tilt-up section.

$$VI(\%) = 100\frac{V_{td} - V_{tu}}{average(V_{td}, V_{tu})} \quad (1)$$

Ultrasonic Pulse Velocity

The velocity of an ultrasonic pulse through a material depends on its density and elastic properties. The ultrasonic pulse velocity test method is often used to assess

the quality and uniformity of concrete. For this study, the ASTM C 597 standard procedure was followed to conduct an ultrasonic through-transmission survey of the beams using 54 KHz compressive wave sensors. The sensors were placed at opposite points of beam side surfaces to measure the wave transit times in micro-seconds (μs) and evaluate changes in wave velocity (m/s) across the beam sections The change in velocity recorded may be indicative of changes in mixture consistency along the beam configuration. The atmospheric conditions at the time of testing were recorded: the temperature was between 32°C and 33°C and relative humidity was between 32% to 35%. The beams moisture content of the beams was considered to be uniform.

One 18 m long beam (Beam 2) was tested with two other beams of 9 m in length (Beams 1 and 5). The width of all beams was 457 mm. Each beam was divided in to different sections, starting from casting point (0 m) up to the end of beam length. Each section was tested at 5 different points, at a distance of 152 mm (6 inches) from each other and from top surface of the beam as shown in Figure 2.

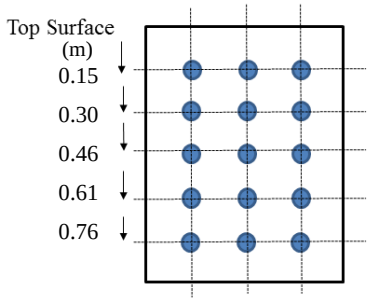

Figure 2. Lay-out of UPV measuring points per measurement section.

Bond Strength

The bond strength between the pre-stress strands and the concrete was performed using the pullout test. The test setup is shown in Figure 3. For each strand, first, a steel plate was placed over the strand, and then the hydraulic jack was collocated, followed by another steel plate, the 445 kN load cell, another steel plate and a pre-stress chuck. The load was increased until a 25 mm slip was measured and the corresponding load was recorded.

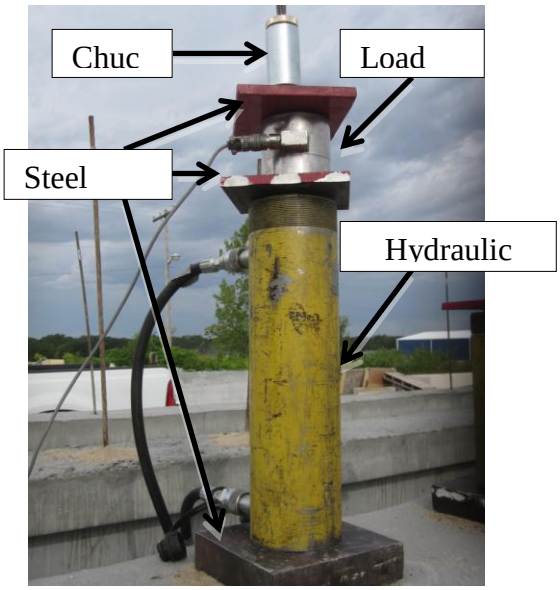

Figure 3. Lay-out of pull-out tests.

Results and Discussion

Fresh properties

Table 1 summarizes workability and dynamic segregation results for the eight mix designs used in this project, the volumetric index values range from 9.9 to 64.7% in the 200 mm channel, while for the 100 mm the values are between 5.1 and 46.2%. V-funnel time ranges from 3.1 to 5.4 seconds and air content values between 3.0 to 14.0 %. Overall, the results show that increasing w/cm from 0.4 to 0.45 has a negligible effect on dynamic segregation, while increasing paste volume may lead to a greater inter-particle spacing and a higher risk of segregation. In addition, a reduction of dynamic segregation was found when increasing sand-to-total aggregate ratio.

Influence of dynamic segregation on ultrasonic pulse velocity

At each horizontal point, three readings were taken in a section and an average velocity was calculated. The average velocities were calculated at 5 points at the distance 6 inches from top surface towards bottom in a section, and longitudinally at different distances from casting point. The results of are presented in Tables 2 to 4:

Table 1. Workability characteristics and dynamic segregation for the SCC tested.

Beam	Mixtures		**Workability** Slump flow (mm)	T 50 (s)	V-Funnel (s)	Air Content (%)	Sieve stability (%)	**Dynamic segregation** VI in 100 mm (%)	VI in 200 mm (%)
Rectangular Beam									
1	Ref		645	0.8	5.4	14.0	5.8	5.1	40.3*
2	w/cm	0.40	725	1.3	4.4	1.5	13.5	8.9	22.5
4		0.45	640	0.9	3.1	3.1	9.9	7.0	16.4
3	Paste Volume	+25 l/m^3	690	0.9	4.3	3.0	5.8	7.8	9.9
5	s/a	56%	675	0.9	2.9	10.0	10.3	10.8	18.1
Type I Beam									
6	Ref		630	1.3	4.0	13.0	16.6	13.9	29.5
7	Paste Volume	+25 l/m^3	680	0.8	4.3	13.0	24.8	46.2	64.7
8	s/a	56%	680	0.8	3.2	12.0	7.5	6.5	12.3

**result is doubted*

Table 2. UPV results, in % relative to the average value of 4130 m/s for beam 1.

		Distance from casting point (m) 0	3	6	9	Sdev horizontal
Distance from top (m)	0.15	96.9	97.8	97.1	99.5	1.2
	0.30	100.0	99.5	98.5	98.5	0.8
	0.46	99.7	100.8	99.2	99.1	0.8
	0.61	101.5	103.2	100.4	100.3	1.3
	0.76	103.3		103.8	101.0	1.5
Sdev vertical		2.4	2.3	2.5	1.0	

Table 3. UPV results, in % relative to the average value of 4602 m/s for beam 2.

		Distance from casting point (m) 0	3	9	12	15	18	Sdev horizontal
Distance from top (m)	0.15	99.0	98.8	99.1	98.8	99.1	99.6	0.3
	0.30	99.5	101.4	99.2	98.4	99.6	100.2	1.0
	0.46	100.6	101.1	100.5	98.5	99.0	99.8	1.0
	0.61	101.2	100.9	99.5	100.3	98.4	99.9	1.0
	0.76	102.1	102.5	102.0	100.8	100.6	99.8	1.1
Sdev vertical		1.3	1.3	1.2	1.1	0.8	0.2	

Table 4. UPV results, in % relative to the average value of 4301 m/s for beam 5.

		Distance from casting point (m)				Sdev
		0	3	6	9	horizontal
Distance from top (m)	0.15	98.1	99.2	98.5	99.3	0.6
	0.30	98.9	99.4	98.9	99.6	0.4
	0.46	100.2	100.0	98.6	98.8	0.8
	0.61	102.0	101.8	99.9	99.5	1.3
	0.76	102.0	103.4	102.2	99.6	1.6
Sdev vertical		1.8	1.8	1.6	0.3	

From the UPV results, it can be concluded that the changes in properties in vertical direction are largest at the casting point (where the concrete has an approximate free-fall of 1 m), and are more homogeneous the further the concrete flows. Also, generally, more variation in horizontal direction is observed at the bottom of the beams. It appears thus that a stiffer concrete can be found at the bottom of the beam, near the casting point, which could be an indication of a larger content of aggregates. However, the magnitude of the variations in pulse velocity does not match the dynamic segregation index (the VI for beam 1 in the 200 mm channel is doubted, as visually, the SCC for beam 1 was most stable). Another explanation for the increased variations in pulse velocity may be a difference in local air content. These properties are currently under investigation, but do not appear to affect the tilting box results.

Influence of dynamic segregation on bond strength

Figures 4 and 5 show the ratio of the load on the strands embedded in the top portion of the beam, relative to the average load applied to the three (9 m beams) or six (18 m beams) strands in the middle section of the beams. The results reflect thus some kind of top-bar effect, although the strands were incorporated vertically. In Figures 4 and 5, it can be observed that with increasing dynamic segregation coefficient, the relative bond strength of the top section decreases.

Beams 3 and 4 have a low VI, leading to bond strengths at the top section of at least 80% of the middle section. Good bond strength is also observed for beam 1, despite the very high VI for this mixture. It is believed that the VI in the 200 mm section of the T-box cannot be entirely trusted, especially as the VI in the 100 mm channel was the lowest, and the mixture appeared visually the most stable of all mixtures used.

Beams 2, 5, 6 and 7 showed the higher VI coefficients, which is in agreement with the lower bond strength results in the top section, compared to the middle section. For beam 8, a relatively low VI is observed, but lower relative bond strengths are obtained. For the beams with lower bond strength, no clear evolution of bond

strength as a function of flow distance can be observed, especially as the observation is opposite for beams 2 and 5.

The research team is currently investigating local concrete properties as a function of the height of the beam and the flow distance, in order to have a better understanding of the influence of dynamic segregation on concrete performance.

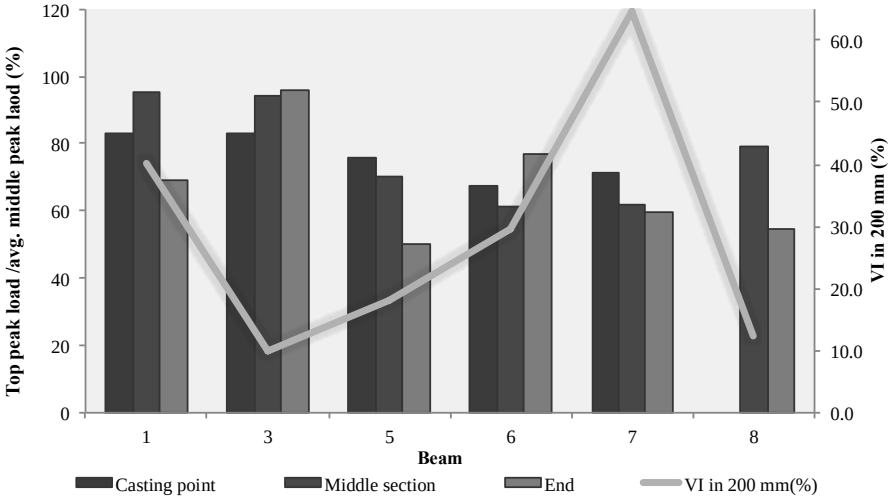

Figure 4. Relationship between bond strength at top and middle and volumetric index for rectangular and "I" sections of 9 m long beams.

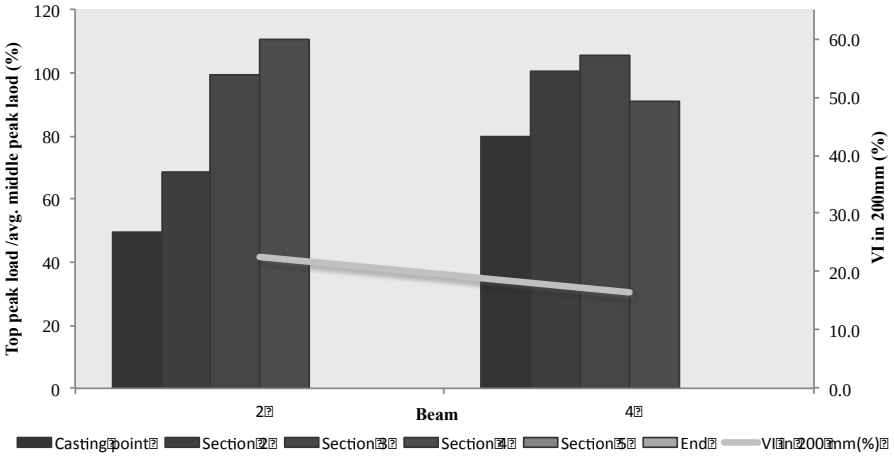

Figure 5. Relationship between bond strength at top and middle and volumetric index for rectangular and "I" sections of 18 m long beams.

Conclusions

Eight beams were cast varying their mixture constituents in order to evaluate the effect of dynamic segregation on homogeneity and bond strength between pre-stress strands and SCC. The following conclusions can be drawn:

- Ultrasonic Pulse Velocity measurements indicate the largest variations in concrete stiffness in vertical direction at the casting point, and in horizontal direction at the bottom of the beam. Stiffer concrete is detected at the bottom of the beam under the casting point.
- No link between dynamic segregation and UPV measurements has been found to date. A possible explanation could be found in variations in air content with the depth and the length of the beam. The research team is currently investigating this assumption.
- The bond strength of bars imbedded at the top section of the beam relative to those embedded in the middle of the beam appears to relate well with the measured dynamic segregation. Higher segregation indices correspond to lower relative bond strengths.

References

8. Panesar, D. K., & Shindman, B. (2012). The effect of segregation on transport and durability properties of self-consolidating concrete. *Cement and Concrete Research*, *42*(2), 252-264.
9. El-Chabib, H., & Nehdi, M. (2006). Effect of mixture design parameters on segregation of self-consolidating concrete. *ACI materials journal*, *103*(5).
10. Shen, L., Jovein, H. B., & Wang, Q. (2015). Correlating Aggregate Properties and Concrete Rheology to Dynamic Segregation of Self-Consolidating Concrete. *Journal of Materials in Civil Engineering*, 04015067.
11. ASTM C1611/C1611M-05, "Standard Test Method for Slump Flow of Self-Consolidating Concrete," ASTM International, West Conshohocken, PA, 2005, 6 pp.
12. Esmaeilkhanian, B., Feys, D., Khayat, K. H., & Yahia, A. (2014). New test method to evaluate dynamic stability of self-consolidating concrete. *ACI Materials Journal*, *111*(3).

Theme 10: Sustainability

Design Considerations and Sustainability of Self-Compacting Concrete

Steffen Grünewald[1,2] and Geert de Schutter[1]

[1] Magnel Laboratory For Concrete Research, Ghent University, Ghent, Belgium
[2] Faculty of Civil Engineering and Geosciences, Delft University of Technology, Delft, The Netherlands

Abstract Self-compacting concrete (SCC) differs from conventional vibrated concrete (CVC) in the rheological behaviour, which is achieved by adequate mix design. The application and production requirements also pose demands on the mix design and workability. Effective production requires adequate strength control. The use of Portland Cement promotes a rapid early age strength development, but it comes with a relative high impact on the environment since decarbonation and a high energy demand accompany cement production. Supplementary cementitious materials have been widely applied to improve the sustainability of concrete but the rate of early age strength development often is compromised. This paper discusses the application of SCC for concrete structures with regard to mix design and its environmental impact. 24 CVCs and SCCs with a variety of mix designs and rheological characteristics were selected from literature. The two objectives of this study were: 1) to determine the environmental impact with regard to the global warming potential and MKI-costs (calculated with the Dutch CUR-tool 'Green Concrete 3.2') and 2) to relate the environmental impact with the compressive strength at 24h and 28d. Quantifying the trade-off between the use of Portland Cement and other mixture components is important information to balance production requirements and to determine the environmental impact of concrete structures produced with SCC.

Keywords: *Self-compacting concrete, Mix design, Rheology, Environmental impact, Sustainability, Relative strength cost*

Introduction

The advantages of concrete are freedom of shape, possibilities to integrate other functions and components, to build structures with limited maintenance costs, ease of use and very high durability. A significant reduction of the environmental impact can convince owners to select concrete rather than other building materials.

Effective production of concrete structures requires adequate control of strength development in order to realize the scheduled production cycles with daily and seasonal changes of temperature. Demoulding of elements can take place only when sufficient strength is gained. The impact of Portland Cement on the global warming potential has been widely discussed in the past years; supplementary cementitious materials can enhance the sustainability of concrete but can come with negative effects on early age strength and decreased durability. Higher replacement levels of Portland Cement often have been compensated for by additional heat curing, an optimization of the granular skeleton and/or the use of a strength accelerator. Wallevik et al. [1] classified concrete with regard to binder content in SCC (Figure 1a) and the carbon footprint of concrete (Figure 1b). Both categories provide a framework for the discussion in this paper.

Category SCC	**Binder: kg/m^3**
Rich	575
Regular powder	515±40
Lean	425±40
Green	355±40
Eco-SCC	≤315
EcoCrete-SCC	≤260
EcoCrete-Xtreme	≤220

Carbon footprint	**kgCO_2/m^3**
Semi-LCC	≤300
LCC250	≤250
LCC200	≤200
LCC150	≤150
EcoCrete	≤125
EcoCrete-Xtreme	≤105

Figure 1: Two classes of categories - a, left) SCC (binder content) and b, right) Concrete carbon footprint (LCC: Low Carbon Concrete Class).

The behaviour of CVC is governed by friction between powders and aggregates, whereas for SCC fluid dynamics are more important. Typically, the paste volume in SCC is higher, the degree to what depends on the mix design, the application, the strength class and the required robustness of a system. In order to obtain a high flowability the paste volume and the viscosity have to be increased and the maximum aggregate size decreased. Five important criteria with regard to the mix design of SCC are:

- 1) For adequate mix design of SCC boundaries with regard to the rheological characteristics yield stress and plastic viscosity have to be respected.
- 2) The required rheological characteristics often depend on the application; use of the full spectrum of rheological characteristics is not always possible or desired.
- 3) Additional restraints are posed with regard to engineering properties, durability demands, production conditions, mixture components and client specification.
- 4) Segregation resistance can be achieved with a high yield value, a high plastic viscosity, thixotropy, stabilizing due to the lattice effect and/or reduction of the ability of liquid/slurry migrating to the shearing zone [2].
- 5) Ecological aspects and sustainability are becoming more important and will provide less freedom for mix design.

A classification of concrete is required for the quantification of sustainability, which needs to be included in the life cycle analysis (LCA) of structures. General

agreement has to be achieved concerning the assessment method of the environmental impact of materials and structures; an example of an impact indicator is the Environmental Product Declaration (EPD). The development of such 'instruments' requires a coordinated and cooperative approach. A discussion of the environmental impact of concrete based on only the mixture composition might seem isolated not taking into account the total life cycle costs of a structure, but it indicates the potential for an optimization on the material level.

Environmental Impact Quantification

According to the Dutch law 'Bouwbesluit' the depletion of raw materials and emission of greenhouse gases has to be determined for new buildings and renovation projects. Worldwide, large differences can be identified with regard to the methods applied for the quantification of the environmental impact in the construction sector and the recognition thereof. In the future, it probably will be common practice to include instruments such as EPD's in tenders and contracts. A LCA has to consider many aspects. In order to compare buildings or concrete structures it is necessary to weight different aspects (i.e. EN 15804 [3] distinguishes seven environmental impact parameters, but does not provide any help with regard to their weighting). In the Netherlands, a national database [4] has been established, which can be applied to quantify the environmental impact of infrastructures. In addition, the CUR-tool 'Green Concrete' [5] was developed to quantify the environmental impact, to weight different environmental aspects, which are then expressed in the same unit (costs in Euro) with the help of conversion factors. Table 1 lists 11 considered parameters and conversion factors.

Table 1: Eleven environmental impact categories and MKI-conversion factors [5].

Nr.	**Impact category**	**Abbre-viation**	**Unit**	**Factor** [Euro/kg]
1	Abiotic Depletion, fuels	ADP1	kg Sb eq	0.16
2	Abiotic Depletion, minerals	ADP2	kg Sb eq	0.16
3	Acidifying Pollutants	AP	kg SO2 eq	4
4	Eutrophication Potential	EP	kg PO4 eq	9
5	Freshwater Aquatic Eco-Toxicity Potential	FAETP	kg 1,4-Dichlorobenzene eq	0.03
6	Global Warming Potential (100 years)	GWP 100 Y	kg CO2 eq	0.05
7	Human Toxicity	HTP	kg 1,4-Dichlorobenzene eq	0.09
8	Marine Aquatic Eco-Toxicity Potential	MAETP	kg 1,4-Dichlorobenzene eq	0.0001
9	Ozone Depletion Potential	ODP	kg CFC11 eq	30
10	Photochemical Ozone Creation Potential	POCP	kg Ethylene eq	2
11	Terrestrial Eco-Toxicity Potential	TETP	kg 1,4-Dichlorobenzene eq	0.06

CO_2-emissions (Global Warming Potential; GWP) have a major influence on the environment; GWP often is referred to as the 'carbon footprint'. The CUR-tool aims at users that want to determine the environmental impact of structures and structural elements made with concrete. It covers: production of components, transport, concrete production, construction phase and demolishing. It is also a tool to optimize concrete and concrete structures with regard to the environmental impact. The user chooses the building materials and processes from a database. With own data, the database can be extended. For the calculation of the environmental cost parameter MKI (Dutch: Milieu-Kosten-Indikator) eleven environmental impact categories from LCA data in a building product EPD are taken into account with conversion factors that reflect their relative effect. The outcome is costs in Euro/unit. The MKI is a factor already taken into account in the Netherlands for the tender of community works as well as for office buildings.

Reference Mixtures

Three reference mixtures (Table 2: R1-R3) were selected with deviating compressive strengths and environmental impact, which represent examples of typical CVCs containing common components applied in the Netherlands. Mixture R1 contains a CEM I 42.5 and might be applied by the prefab-industry; a blast furnace slag cement was used for Mixture R2, which is often the case for in-situ cast concrete structures. The strength class of both mixtures was C35/45. Mixture R3 contains a higher dosage of CEM I 52 R, and as a result, the highest early age strength of all mixtures was obtained (67.7 MPa at 1 day; strength class C67/75). A variety of mix designs for SCC was selected from literature in order to discuss differences and to compare them with CVC; the 21 SCC-mixtures were selected from eight different sources. With regard to the compressive strength, the following was specified as selection criteria: 1) use of cubic moulds with 150 mm size and 2) availability of compressive strength results at 1 day and 28 days (1 day strengths were not determined for S14-S17). No specific requirement was defined for the workability of CVC. Mixtures R1-R3 were 'easy compactable'(Slump > 15 cm); no consistency measurements were carried out. The paste contents of R1, R2 and R3 were 27.8, 27.9 and 29.6 Vol.-% (including air), respectively. The slump flow of the SCCs was at least 630 mm. Not all mixture components could be directly linked with components of the database. The following was assumed:

- the CEM II cement of S3 contains 85% CEM I and 15% GGBS (slag);
- the CEM II of S10&S11 contains 85% CEM I and 15% limestone powder;
- in some cases (S1,S2,S12,S13) the aggregate fraction (i.e. 2-8 mm) did not match the sand 0-4 mm and coarse aggregate 4-12/16 mm grouping of the database, with an assumed distribution these fractions were divided in the available groups.

Table 3 shows the reference database-sets of the Green Concrete tool [5] for the eleven impact parameters and the applied concrete components. The numbers are industry-averages and might be lower or higher for the materials applied. Not all

components are included in the database; the following assumptions were made: 1) granite powder has the same conversion factors as limestone powder and 2) air-entrainer and viscosity agent have the same conversion factors as superplasticizer for the same weight.

Table 2: Mixture composition and characteristics of 3 reference and 21 self-compacting concretes (dosage of components in kg/m^3).

Mixture component	**R1**	**R2**	**R3**	**S1**	**S2**	**S3**	**S4**	**S5**	**S6**	**S7**	**S8**	**S9**
Reference	[6]	[6]	[6]	[7]	[7]	[8]	[9]	[9]	[10]	[10]	[10]	[10]
CEM I 42.5/52.5	300		370	267	368	340		185	600	316	318	386
CEM III B		300					270	184				
GGBS						60						
Limestone powder				248	218	250				202	228	222
Fly ash							273	185		35		43
Silica fume												
Granite powder												
Sand, river	860	856	836	790	722	870	670	662	754	1010	962	719
Crushed aggregates						710			837	541	619	786
Gravel, river	1051	1046	1022	864	873		870	900				
Water	159	159	155	185	150	170	174	177	190	191	184	181
Superplasticizer	0.75	0.45	2.09	6.70	3.04	4.81	2.27	3.14	10.5	10.0	11.8	12.4
Air entrainer					0.02							
Viscosity agent												
Binder content	300	300	370	515	586	650	543	554	600	553	546	651
w/b-ratio [-]	0.53	0.53	0.42	0.36	0.26	0.26	0.32	0.32	0.32	0.35	0.34	0.28
Slump flow [mm]	-	-	-	700	660	740	688	665	>750	>750	>750	>750
$f_{c,cube}$ 1 d [MPa]	10.9	5.5	67.7	18.5	21.4	42.0	4.3	18.5	27.7	12.2	13.5	23.0
$f_{c,cube}$ 28 d [MPa]	51.6	54.1	86.7	45.5	71.6	69.0	36.9	65.0	50.0	33.5	33.7	45.0

Mixture component	**S10**	**S11**	**S12**	**S13**	**S14**	**S15**	**S16**	**S17**	**S18**	**S19**	**S20**	**S21**
Reference	[11]	[11]	[12]	[12]	[13]	[13]	[13]	[13]	[14]	[14]	[14]	[14]
CEM I 42.5/52.5	374	374	379	394	302	218	169	274				300
CEM III B									270	400	270	
GGBS												
Limestone powder	66	186	253					30			243	184
Fly ash	100			263		75	131		216			
Silica fume					12	11		15				
Granite powder												100
Sand, river	1110	1110	896	896	925	922	916	911	710	792	714	807
Crushed aggregates	430	430			909	907	900	895				
Gravel, river			596	596					1078	1094	1074	796
Water	200	200	177	155	204	198	195	203	129	143	133	164
Superplasticizer	4.4	4.4	2.4	2.0	2.25	2.19	1.91	2.03	3.4	2.8	4.1	3.5
Air entrainer												
Viscosity agent										2.4	2.6	
Binder content	540	560	632	657	314	304	300	319	486	400	513	584
w/b-ratio [-]	0.37	0.36	0.28	0.24	0.65	0.65	0.65	0.64	0.27	0.36	0.26	0.28
Slump flow [mm]	800	750	730	780	660	650	630	645	730	665	750	730
$f_{c,cube}$ 1 d [MPa]	17.0	17.0	13.2	8.1	-	-	-	-	6.1	12.1	8.2	22.3
$f_{c,cube}$ 28 d [MPa]	44.0	40.5	54.2	43.2	40.0	40.0	28.9	44.4	50.4	62.5	54.6	57.8

Table 3: Conversion factors for eleven environmental impact categories [5].

Mixture component *Database reference*	ADP 1	ADP 2	GWP	ODP	POCP	AP	EP	HTP	FAE-TP	MAE-TP	TETP
CEM I 42.5/52.5 *SBK CEM-I NL c2*	6.7E-07	5.7E-04	8.2E-01	5.2E-09	2.1E-04	2.7E-03	3.6E-04	5.0E-02	6.9E-04	5.1E+00	6.8E-04
CEM III B *SBK CEM-III NL c2*	6.7E-07	8.5E-04	3.0E-01	5.4E-09	9.0E-05	1.0E-03	1.0E-04	2.7E-02	3.4E-04	8.2E+00	3.6E-04
GGBS *SBK Hoogovensl.*	7.6E-10	1.7E-04	1.9E-02	1.1E-09	1.0E-06	5.8E-06	1.4E-06	3.6E-03	4.6E-06	2.0E+00	2.7E-06
Limestone powder *Kalksteenmeel (DE)*	2.0E-08	2.3E-04	3.2E-02	2.4E-09	1.0E-05	8.5E-05	2.2E-05	7.4E-03	2.1E-04	1.1E+00	8.2E-05
Fly ash *Poederkoolvl. c2*	8.5E-10	2.3E-05	3.3E-03	2.6E-10	1.2E-06	1.5E-05	3.5E-06	6.7E-04	2.1E-05	2.1E-01	7.4E-06
Silica fume *SBK silica fume*	4.8E-09	3.9E-05	5.2E-03	3.9E-10	1.6E-06	1.4E-05	3.3E-06	1.5E-03	3.0E-05	3.2E-01	4.8E-05
Granite powder *Kalksteenmeel (DE)*	2.0E-08	2.3E-04	3.2E-02	2.4E-09	1.0E-05	8.5E-05	2.2E-05	7.4E-03	2.1E-04	1.1E+00	8.2E-05
Sand, river *SBK Betonz. (NL)*	1.3E-09	2.0E-05	2.9E-03	3.1E-10	2.3E-06	1.8E-05	4.2E-05	1.9E-03	3.1E-05	2.0E-01	1.1E-05
Crushed aggregates *Steenslag (BE)*	3.1E-09	4.3E-05	6.2E-03	6.8E-10	7.1E-06	5.7E-05	1.3E-05	1.7E-02	8.9E-05	4.4E-01	1.7E-05
Gravel, river *Grind (DE)*	7.1E-09	2.7E-05	3.8E-03	3.1E-10	2.0E-06	1.6E-05	3.9E-06	2.2E-03	3.3E-05	1.7E-01	1.3E-05
Water *Leidingwater*	2.6E-10	2.7E-06	3.4E-04	1.6E-11	1.1E-07	8.0E-07	1.4E-07	8.3E-05	1.3E-06	2.2E-02	1.5E-06
Superplasticizer *Superplastificeerder*	0.0E+00	8.1E-03	7.2E-01	9.6E-08	1.4E-03	9.7E-03	4.6E-04	8.2E-02	3.0E-02	9.1E+00	3.6E-04
Air entrainer *Superplastificeerder*	0.0E+00	8.1E-03	7.2E-01	9.6E-08	1.4E-03	9.7E-03	4.6E-04	8.2E-02	3.0E-02	9.1E+00	3.6E-04
Viscosity agent *Superplastificeerder*	0.0E+00	8.1E-03	7.2E-01	9.6E-08	1.4E-03	9.7E-03	4.6E-04	8.2E-02	3.0E-02	9.1E+00	3.6E-04

Discussion of the Environmental Impact

Figure 2 shows the GWP of the 3 reference concretes and 21 SCCs.

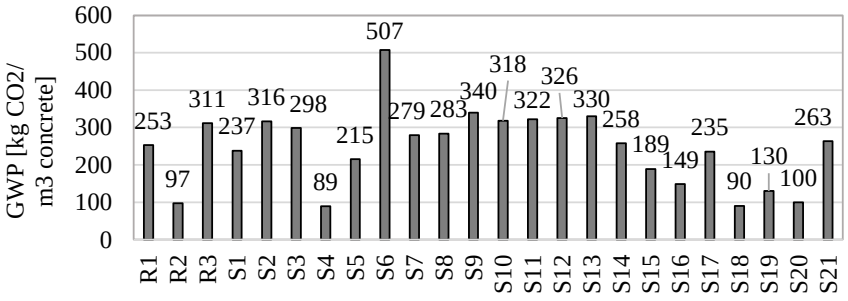

Figure 2: GWP of 3 reference and 21 self-compacting concretes.

Significant differences are obtained, as the range of GWP was from 89-507 $kgCO_2/m^3$ concrete, which is a factor of 5.7. The five mixtures with the lowest GWP all were produced with a blast furnace slag cement (cement only: R2&S19; also with fly ash: S4&S18; also with limestone powder: S20). 300 kg/m^3 of CEM I

contribute 97.2% to the GWP of Mixture R1. A CO_2-reduction often is expressed in literature as a percentage compared to a reference concrete; R1 might be a good choice for a reference concrete, although, the share of applications produced with concrete containing only CEM I as a binder is decreasing. The MKI-costs in Euro/m^3 (contribution of mixture components only) were also calculated and are compared in Figure 3 with the GWP of the 24 mixtures. A good correlation between both parameters is obtained, which reflects the fact that the dosage of Portland clinker is dominant on both numbers.

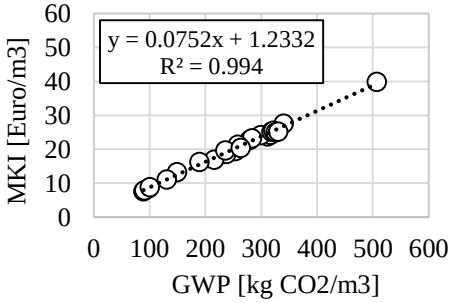

Figure 3: Relation between MKI-costs and GWP for 24 mixtures.

The contribution of the eleven impact parameters to the MKI is shown in Table 4 for Mixtures R1 and S18. The MKI-costs were 19.5 Euro/m^3 for R1 and 7.9 Euro/m^3 for S18, which is a factor of about 2.5. The GWP contribution to the MKI was 64.9% and 57.5% for R1 and S18, respectively. Next highest contributors after the GWP were AP, HTTP and EP (Table 1 lists abbreviations); the contributions of the four highest numbers to the MKI are 98% for R1 and 95% for S18.

Table 4: Contribution of the eleven impact parameters to the MKI for Mixture R1 (19.5 Euro/m^3) and Mixture S18 (7.9 Euro/m^3).

Mix	ADP1	ADP2	GWP	ODP	POCP	AP	EP	HTTP	FAE-TP	MAE-TP	TETP
R1	0.000	0.002	0.649	0.000	0.007	0.174	0.069	0.088	0.000	0.010	0.001
S18	0.000	0.006	0.575	0.000	0.008	0.171	0.073	0.131	0.001	0.033	0.001

The environmental impact of concrete needs to be related to its performance in order compare the real impact and to provide a base for the optimization of the mix design. As a performance criterion, Aïtcin [15] defined the economic efficiency of concrete as cost for 1 MPa or 1 year of service life; Damineli et al. [16] applied the CO_2-intensity indicator and related the CO_2-emission and the compressive strength at an age of 28 days. The CO_2-emissions (production of the concrete components only) divided by the cube compressive strength for different concrete ages was defined in this study as the 'relative strength cost, RSC'; this parameter is time-dependent, since the strength increases more or less in time. The more mature the concrete the relatively lower the RSC becomes. Figure 4 shows the RSC of the 24 mixtures for the age of 28 days. The lowest numbers (1.79-2.41 kgCO_2/m^3

concrete/MPa) are obtained for mixtures R2, S4 and S18-S20. CVC Mixture R2 has a GWP of 97 $kgCO_2/m^3$. The results indicate that similar low values can be achieved also with SCC. A RSC of 2 means that for a compressive strength of 45 MPa only 90 $kgCO_2/m^3$ concrete are emitted, which is a very low number according to Table 1 (class: EcoCrete-Xtreme).

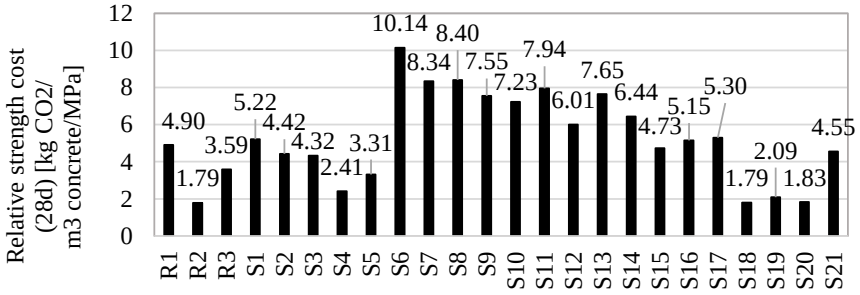

Figure 4: Relative strength costs for GWP at an age of 28 days.

The addition of supplementary cementitious materials enhances the strength beyond 28 days often more compared to concrete with a 100% CEM I binder composition, which further decreases the RSC. However, at an early age CEM I is very effective; early age strengths are especially important for prefabrication and applications, which have high demands with regard to this aspect. Parameters RSC,1d and RSC,28d differ less for mixtures containing only CEM I binder. Figure 5 summarises the RSC-values for 1 day compressive strength results. With the very high early age strength of R3 (67.7 MPa), a very low RSC,1d of 4.6 $kgCO_2/m^3$ concrete/MPa is obtained (RSC,28d: 3.6 $kgCO_2/m^3$ concrete/MPa). The RSC,1d of R1, a more common mixture in the prefab industry, is 23.2 $kgCO_2/m^3$ concrete/MPa which is much higher; lower values were obtained with several SCCs.

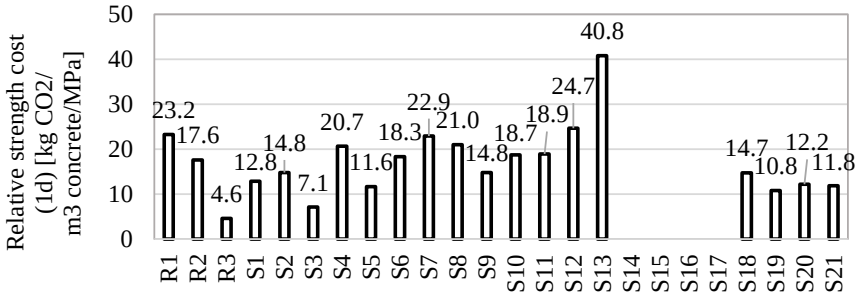

Figure 5: Relative strength costs for GWP at an age of 1 day.

Heat curing usually increases the early age strength. The MKI-approach is very useful for the comparison of different concrete production methods and structural solutions (including heat curing and effect of mixture components). By

accumulating all life cycle steps and environmental impact parameters in a single number (MKI), mix design criteria and sustainability aspects can be balanced. Specific studies with regard to heat curing and the related impact on the environment and MKI need to be executed. Early age strength costs, RSC,28d and other relevant parameters need to be considered for the mix design. With a demoulding strength of 10 MPa at 1 day (curing at 20°C), the RSC,28d (for MKI) of R1 (19.5 Euro/m^3) can be used as a reference to select more sustainable solutions; both criteria are fulfilled for mixtures S1 (97% MKI with regard to R1), S5 (87%) and S19 (57%). Figure 6 compares the RSC,1d and RSC,28d for GWP and MKI. A low RSC,28d is preferred, but dependent on the boundary conditions a low RSC,1d could also be relevant for the selection of the production process and mix design. Figure 6 shows that some SCC can compete with CVC with regard to environmental impact, whereas others are less sustainable. Since the mixture composition of SCC varies widely, a general conclusion should be avoided. The strength of concrete largely depends on the water-cement/binder ratio, which has to be considered for mix design. Mixtures S18-S20 have a relatively low water-binder ratio compared to other SCC's, which makes them competitive with regard to CVC. Consequently, the granular optimization with regard to the water demand is a major key for making concrete more sustainable.

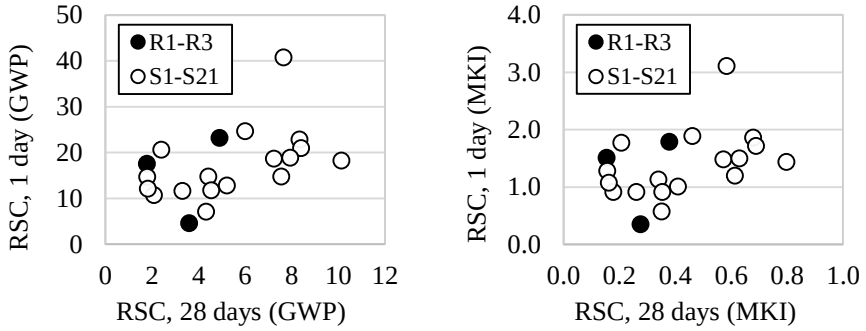

Figure 6: Comparison of relative strength costs for CVC and SCC at an age of 1 day or 28 days (units: GWP; $kgCO_2/m^3$/MPa & MKI: Euro/m^3/MPa).

Conclusions

Sustainability adds an additional but important dimension to the list of requirements for SCC. This paper discussed the relation between mix design and the environmental impact for SCC. The calculations showed that with regard to the relative strength costs SCC can be competitive with CVC. Weighting of different environmental impact parameters was executed with the Dutch CUR-tool and resulted in a single parameter MKI. When only the effect of the mixture composition of the total life cycle is considered, this parameter is correlated with the CO_2-emissions coming mainly from the production of Portland Cement.

References

[1] Wallevik, O.H., Mansour, W.I., Yazbeck, F.H. and Kristjansson, T.I. (2014), *EcoCrete-Xtreme: Extreme performance of a sustainable concrete*, In: Proceedings of the International Symposium on Eco-Crete, Wallevik, O.H. et al. (Eds.), Reykjavik, pp. 3-10.

[2] Wallevik, O.H. (2003), *Rheology - a scientific approach to develop self-compacting concrete*, In: 3rd International Symposium on Self-Compacting Concrete, Wallevik, O.H. and Nielsson, I. (Eds.), Reykjavik, ISBN: 2-912143-42-X, pp. 23-31.

[3] EN 15804+A1 (2013), *Sustainability of construction works - Environmental product declarations – Core rules for the product category of construction products*.

[4] Nationale Milieudatabase (2015), www.milieudatabase.nl, Stichting Bouwkwaliteit.

[5] CUR (2014), Groen Beton (Green Concrete) 3.2, http://www.cur-aanbevelingen.nl/producten/overige-producten/ontwerptool-groen-beton.364344.lynkx.

[6] Grünewald, S. and Köhne. H. (2014), *Ecoconcrete – Balancing environmental and technical aspects of precast concrete*, In: International Symposium on Environmentally Friendly Concrete - Eco-Crete, Wallevik, O.H. et al. (Eds.), Reykjavik, Green Environmental Printing, pp. 197-206.

[7] Gram, H.-E. and Piiparinen, P. (1999), *Properties of SCC – especially early age and long term shrinkage and salt frost resistance*, In: 1st International Symposium on Self-Compacting Concrete, Skarendahl, Å. and Petersson, Ö. (Eds.), Stockholm, ISBN: 2-912143-09-8, pp. 211-225.

[8] Bosiljkov, V.B., Duh, D., Bosiljkov, V. and Zarnic, R. (2010), *Time evolution of properties of SCC mixtures produced using crushed limestone aggregate and high content of limestone filler*, In: Proceedings of SCC2010: Design, production and placement of self-consolidating concrete, Khayat, K.H. and Feys, D. (Eds.), Montreal, ISBN: 978-90-481-9663-0, pp. 317-327.

[9] Grünewald, S., Horeweg, E.M., Mulder, R. and Walraven, J.C. (2001), *Zelfverdichtend beton – CUR-onderzoek B79 Onderdelen: Mengselsamenstelling en mechanische eigenschappen*, Stevinreport 25.5.01-29, TU Delft. (In Dutch)

[10] Felekoglu, B. (2007), Utilisation of high volumes of limestone quarry wastes in concrete industry (self-compacting concrete case), *Resources, Conservation and Recycling*, 51, p. 770-791

[11] Corinaldesi, V. and Moriconi, G. (2011), The role of industrial by-products in self-compacting concrete, *Construction and Building Materials*, 25, p. 3181-3186.

[12] Mňahončáková, E., Pavlíková, M., Grzeszcyk, S., Rovnaníková, P. and Černý, R. (2008), Hydric, thermal and mechanical properties of self-compacting concrete containing different fillers, *Construction and Building Materials*, 22, p. 1594-1600.

[13] Esmaeilkhanian, B., Khayat, K.H. and Wallevik, O.H. (2014), *Ecological self-consolidating concrete: design and performance*, In: International Symposium on Environmentally Friendly Concrete - Eco-Crete, Wallevik, O.H. et al. (Eds.), Reykjavik, Green Environmental Printing, pp. 197-206.

[14] Hunger, M. (2010), *An integral design concept for ecological self-compacting concrete*, PhD thesis, Eindhoven University of Technology, Bouwstenen 146, ISBN: 978-90-6814-628-8.

[15] Aïtcin, P-C. (2000), Cements of yesterday and today: concrete of tomorrow, *Cement and Concrete Research*, 30(9), p. 1349-59.

[16] Damineli, B.L., Kemeid, F.M., Aguiar, P.S. and John, V.M. (2010), Cement and Concrete Composites, 32, p. 555-562.

Development of Eco-Efficient Self Consolidating Concrete (Eco-SCC) with Recycled Concrete Aggregate

Jiong Hu[1], Brian Ledsinger[2] and Yoo-Jae Kim[3]

[1]University of Nebraska-Lincoln
[2,3]Texas State University

Abstract Self-consolidating concrete (SCC) is an innovative type of concrete that requires little to no mechanical vibration, and can be consolidated into formwork under its own weight. While the precast concrete industry has fully adopted SCC because of its tremendous benefits, the overall use of SCC in the U.S. concrete market, particularly in the ready-mixed concrete production is still very limited. One of the main obstacles that prevents the wide use of SCC is the high cost and environmental impact associated with the high cement and cementitious materials content. A new concept of eco-efficient SCC (Eco-SCC), also known as low fines SCC, was recently presented in Europe and Asia, which aims to achieve SCC behaviour with a cement content comparable to conventional concrete. The paper presented a preliminary study of the development of Eco-SCC. Results showed that while the lower amount of cementitious materials and the use of recycled concrete aggregate did affect the fresh and hardened concrete behaviours of SCC, most of the mixtures included in the study showed good flowability, passing ability, stability as well as strength that well satisfied criteria of SCC. The study demonstrated that it is possible to obtain Eco-SCC with lower cement content compared to normal SCC, through the optimization of aggregate gradation and the use of viscosity modifying agent.

Keywords: *Eco-efficient, Cement content, Recycled concrete aggregate, Self-consolidating concrete, Sustainability.*

Introduction

Self-consolidating concrete (SCC), also known as self-compacting concrete, is a highly flowable, non-segregating concrete that can spread into place, fill the formwork and encapsulate the reinforcement without any mechanical consolidation. The use of SCC potentially contributes to increased productivity

(e.g. faster casting operation and with less workers), improved working environment (the elimination of the use of heavy, vibrating and noisy compacting tools), as well as mechanical behaviour and durability. Even with the above-mentioned benefits, the market share of SCC is still generally very low, mainly due to the high cost associate with the high cement and cementitious materials content, as well as the lack of robustness, confidence, and guidelines. As there is no sufficient document to support the savings from the less workers, faster casting, as well as the improved working environment [1], the high material cost due to the high cement and cementitious material content has become an obvious obstacle of the wide application of SCC, particularly in ready-mixed concrete (RMC) production. There is a clear need for the development of SCC with cement and cementitious materials content that compared to conventional concrete.

Eco-efficient SCC (Eco-SCC), also known as Smart Dynamic Concrete or low fines SCC has drawn a lot of attentions in the past decade. The optimization of aggregate gradation and particle packing [6-9], as well as the use of new generations of viscosity modify agent (VMA) [10-13] allows the effective reduction of cement and cementitious materials content, so as to reduce cost as well as to minimize technical issues such as high drying shrinkage. The developed Eco-SCC will realize a host of benefits of economic and ecological, and the technical benefits of traditional SCC [14]. The success of the research will greatly encourage the use of SCC in daily RMC production.

Figure 1 as shown below describes the concept of SCC and Eco-SCC design. In concrete mixture design, to ensure appropriate strength and durability, sufficient paste volume is needed to fill up the voids amount aggregate particles. An excess paste layer of cement paste around aggregates is also needed to achieve a desired workability [2-5]. The excess paste is to cover the aggregate particles and separate them from contacting each other. In SCC mixture design, in order to achieve a higher workability, a larger amount of paste is generally used, so as to increase the thickness of the excess paste layer. Eco-SCC design can be achieved through the optimization of aggregate gradation, i.e., reducing voids among aggregate particles so as to provide higher amount of excess paste. One critical aspect of Eco-SCC design is to have an excess paste layer that is thick enough to maintain sufficient workability yet thin enough to prevent coarse aggregate from segregating. The stability of Eco-SCC is generally achieved through the maximized aggregate packing and/or the application of VMA to increase the viscosity of the paste.

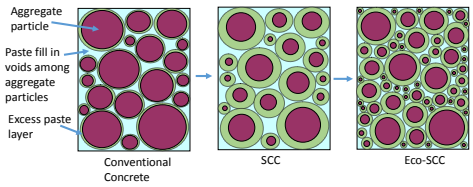

Figure 1. Mechanism of SCC and Eco-SCC mixture design.

Base on the above-mentioned premises, the purpose of this study is to complete a preliminary study to develop an Eco-SCC which has current SCC characteristics but with a cement content that is comparable to conventional concrete. This study intends to justify the feasibility of producing Eco-SCC with a lower amount of fine contents (less than 350 kg/m^3) through the optimization of particle packing and aggregate gradation, as well as the optimum use of chemical admixtures such as high range water reducer (HRWR) and VMA.

Materials and Mixture Design

Cementitious materials

Type I Portland cement that meets ASTM C150 (*Standard Specification for Portland Cement*) [15] and class C fly ash that meets ASTM C618 (*Standard Specification for Coal Fly Ash and Raw or Calcined Natural Pozzolan for Use in Concrete*) [15] were used as cementitious materials in the concrete mix. The chemical compositions and physical properties of cement and fly ash used in the study are reported in Table I.

Table I. Chemical compositions and physical properties of cement and fly ash.

Oxide (%)	SiO_2	Al_2O_3	Fe_2O_3	CaO	MgO	SO_3
Cement	20.4	4.6	4.5	64.4	0.8	3.7
Fly Ash	35.8	20.37	5.54	26.04	4.49	1.52
	Loss in Ignition		Blaine Fineness, m^2/kg			Specific Gravity
Cement	1.8		433			3.15
Fly Ash	0.31		NA			2.60

Aggregate

Crushed dolomite, river sand as shown in Figure 1 were used as aggregate in the concrete mixtures. Recycled concrete aggregate (RCA) with nominal maximum size of 25mm was obtained from a local recycled concrete plant and further crushed with a laboratory jaw crusher with an opening of approximately 15mm.

(a). Natural coarse agg. (b). Natural fine agg. (c). Recycled agg.

Figure 1. Physical appearance of aggregate.

Sieving analyses were performed on all three aggregates used in the study according to ASTM C136 (*Standard Test Method for Sieve Analysis of Fine and Coarse Aggregates*) [15]. Gradation curves of all three different kinds of aggregate are shown in Fig. 2. Fineness modulus of natural coarse aggregate, natural fine aggregate, and RCA were calculated as 6.54, 2.59 and 5.63 respectively.

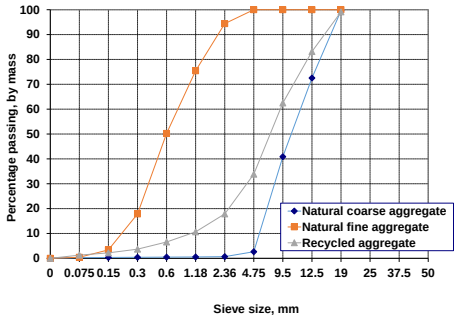

Figure 2. Aggregate gradation curves.

Specific gravities and absorptions of aggregates were measured based on ASTM C127 (*Standard Test Method for Density, Relative Density (Specific Gravity) [15], and Absorption of Coarse Aggregate*) and ASTM C128 (*Standard Test Method for Density, Relative Density (Specific Gravity), and Absorption of Fine Aggregate*) [15] respectively, and the results are shown in Table II. It should be noted that due to the high amount of residual hardened cement paste, RCA has much higher absorption (5.6%) and relatively low specific gravity comparing to the two natural aggregates included in the study.

Table II. Aggregate specific and absorption.

	$G_{sb,\ SSD}$	Absorption
Natural coarse aggregte	2.83	0.7%
Recycled aggregte	2.25	5.6%
Natural fine aggregte	2.64	0.6%

Admixtures

A polycarboxylate-based HRWR (Glenium® 7700) and VMA (Rheomac VMA 362) were used to adjust the workability of SCC mixtures.

Mixture design

A total of six mixes as shown in Table III were included in the study. Mix 1 serves as a reference SCC mix with a total binder content at 386kg/m^3. Mix 2 to 4 were

developed based on Mix 1, but with a gradual decrease of binder contents to 297kg/m^3. The amount of aggregate were increased accordingly. Noted that the water-to-binder ratio (w/b) and the amount of HRWA and VMA were adjusted to compensate the reduced binder content. In order to achieve a comparable workability, a higher amount of HRWR and VMA were used in mixes with lower binder contents. Mix 5 and 6 were developed based on Mix 3, with a replacement of coarse aggregate with 50% and 100% of RCA respectively. Masses of aggregate used in the table were presented in saturated surface dried conditions.

Table III. Concrete mixture design.

Mix ID	1	2	3	4	5	6
Cement (kg/m^3)	309	285	261	237	261	261
Fly Ash (kg/m^3)	78	71	65	59	65	65
Binders (kg/m^3)	386	356	326	297	326	326
Natural Coarse Agg. (kg/m^3)	1011	1036	1060	1084	477	0
Fine Agg. (kg/m^3)	758	775	795	813	794	794
Recycled Agg. (kg/m^3)	0	0	0	0	501	891
Water (kg/m^3)	93	95	86	78	111	116
w/b	0.240	0.266	0.265	0.263	0.339	0.355
HRWR (ml/100kg)	1006	1091	1190	1905	1190	1190
VMA (ml/100kg)	366	397	433	714	433	433

Test Methods

Concrete Mixing

A MP 75 SICOMA Laboratory Mixer was used to mix concrete based on procedure as described in ASTM C192 (*Standard Practice for Making and Curing Concrete Test Specimens in the Laboratory*) [15]. During the mixing, coarse aggregate was first introduced into the mixer and mixed with approximately half of the water for 30 seconds. After that, fine aggregates, cement, fly ash, and approximately half of the remaining water with HRWA and the rest of water with VMA were placed into the mixer and mixed for three minutes. The mixtures were rested in the mixer for three minutes, followed by another two minutes of mixing before the completion of the whole mixing procedure.

Fresh Concrete Properties

After concrete mixed, a slump flow test based on ASTM C1611 (*Standard Test Method for Slump Flow of Self-Consolidating Concrete*) [15] was performed to evaluate the lateral flow and filling potential of different SCC mixtures. The testing apparatus included a standard slump cone and a 900 mm by 900 mm stainless steel plate. With this apparatus, the time for the SCC to spread to 500mm (T_{50}) and the

final slump flow diameters as shown in Fig. 3 can be measured. According to ACI 237R-07 [16], a common range of slump flow and T_{50} for SCC are 450 to 750 mm and 2 to 5 seconds respectively.

J-ring test as shown in Fig. 4 was also performed based on ASTM C1621 (*Standard Test Method for Passing Ability of Self-Consolidating Concrete by J-Ring*) [15]. This test method provides a procedure to determine the passing ability of concrete by using a J-Ring in combination with the slump flow test. The J-Ring is placed outside the slump cone so that the concrete flows through the legs of the ring when the slump cone is lifted. The slump flow with and without the J-Ring is measured.

In additional to slump flow and J-ring test, visual stability index (VSI) test was also used to determine the stability of SCC mixture. The test was performed according to ASTM C1611, which involves the visual examination of the SCC slump flow spread. A VSI number of 0, 1, 2, or 3 (referring to highly stable, stable, unstable, and highly unstable respectively) is usually given to the spread to characterize the stability of the mixture based on the observation of segregation, bleeding and consistence of the spread. Example of mixtures with different VSI rating can be found in Figure 3. A VSI rating of 0 or 1 are indications of stable SCC mixture and a VSI rating of 2 or 3 generally indicate unstable and possible segregation. In order to ensure the consistency and minimize the effect from time elapse, all fresh concrete tests were completed within 15 minutes upon the completion of the mixing.

(a). VSI = 0 (b). VSI = 1 (a). VSI = 2

Figure 3. Examples of SCC with different VSIs.

Hardened Concrete Properties

After all fresh concrete tests, concrete was poured into 75mmx150mm cylinders without any form of consolidating, i.e., action of rodding or vibration. The concrete cylinders were placed in a standard curing room confirmed to ASTM C192 [15] right after casting. All specimens were demolded after 24 hours and cured in the curing room till compressive strength test. The 28 days compressive strength of all

concrete mixtures were tested with a Test Mark CM 400 compression testing machine based on ASTM C39 (*Standard Test Method for Compressive Strength of Cylindrical Concrete Specimens*) [15]. One specimen randomly selected from each of the mix was cut through the middle to examine the coarse aggregate distribution in vertical direction of cross section according to a procedure and criteria similar to AASHTO PP 58-12 [17] yet with a smaller specimen size, which was also used to evaluate the segregation resistance. A hardened visual stability index (HVSI) was used to describe the stability of SCC. Thickness of the mortar layer at the top of the cut plane and variance in size and percent are of coarse aggregate distribution from the top to bottom were used to distinguish the stability of different mixtures. Similar to VSI, a HVSI rating of 0 or 1 are indications of stable SCC mixture and a HVSI rating of 2 or 3 generally indicate unstable and possible segregation.

Results and Discussion

Results of fresh and hardened concrete properties are summarized in Table III.

Table III. Fresh and hardened concrete properties.

Mix ID	1	2	3	4	5	6
Slump flow (mm)	610	635	660	610	610	559
T_{50} (s)	4.5	5.5	3.9	4.5	9.8	6.2
J-ring flow (mm)	508	559	584	508	457	483
VSI	0	0	0	1	0	0
$f'_{c,7}$ (MPa)	50.5	37.8	40.5	40.5	46.7	38.4
HVSI	0	0	0	0	0	0

According to ACI 237R-07 [16], the slump flow spread of SCC typically ranges from 450 to 760 mm. As shown in Table III, all the six mixes included in the study have the spread diameter greater than 550mm in the slump flow test, which indicates good flowability. T_{50}, which is the time for which the concrete reaches the diameter of 500mm measured during execution of slump-flow test, give a relative measure of viscosity. Results show that all the four mixes with only natural aggregates exhibited a T_{50} below or close to 5 seconds. The two RCA mixes (Mix 5 and 6) exhibited a higher T_{50} compared to the 2 to 5 seconds as recommended by ACI 237R-07, which is likely contributed by the higher amount of fine particles and the rougher surface of RCA. Observation of VSI indicated that most of the mixes show good to relatively good stability, with no or very minimum amount of segregation and bleeding observed during the slump flow test. The only mix showing a VSI of 1 was the mix with the lowest binder content (Mix 4), which was expected.

Compressive strengths of all mixtures were measured at the age of 7 days and the results showed that the compressive strength decreases with the decrease of binder

content. However, all mixtures included in this study, including the mix with 100% of RCA replacement, show 7-day compressive strength higher than 35MPa, which is higher than convention concrete at the same age. As the VHSI example shown in Figure 4, no obvious evidence of segregation was observed in any of the mixtures included in the study.

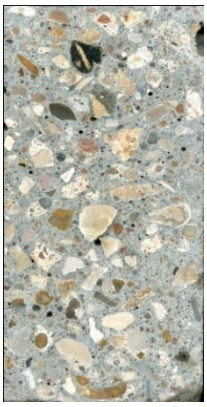

Figure 4. Cross-section of selected specimen from HVSI test.

Results from fresh and hardened concrete tests showed that most mixtures included in this study exhibited good SCC behaviour, i.e., meets SCC criteria. It is interested to note that the two mixtures with RCA both show very promising fresh concrete properties, with high slump flow, and high stability. This phenomenon might result from the higher degree of aggregate packing (lower void ratio) and optimized gradation of aggregate. However, the limited data available through this study was not able to confirm the hypothesis, further investigation is needed to investigate the effect of combined aggregate gradation, particularly the effect of combined aggregate gradation and packing density, on behaviour of SCC with RCA.

Conclusions

The conclusions of this study are summarized as following:

1. The developed Eco-SCC mixtures included in this study, including the two RCA provide concrete with good flowability, passing ability and stability and well satisfy criteria of SCC.
2. The study demonstrated that it is possible to obtain Eco-SCC with lower cement content comparing to conventional SCC, through the optimization of aggregate gradation and the use of viscosity modifying agent.
3. Further study is needed to optimize mix design and to study effect of cement content and VMA in SCC behaviour, both in fresh and hardened concrete stage.

References

[1] Benedict D.E., and Worsfold S.J., (2006), Self-consolidating concrete – economically attractive field applications, *Concrete Construction*, Vol. 1, pp. 106-110.

[2] Kennedy, C., (1940), The design of concrete mixes, *Journal of the American Concrete Institute*, Vol. 36, pp. 373-400.

[3] Hu, J., and Wang, K., (2007), Effects of size and uncompacted voids of aggregate on mortar flow ability, *Journal of Advanced Concrete Technology*, Vol. 5, pp. 75-85.

[4] Koehler, E., and Fowler, D., (2007), Aggregates in self-consolidating concrete, *International Center for Aggregates Research (ICAR)*, Austin, TX.

[5] Fennis S.A.A.M., Walraven J.C., and den Uijl J.A., (2009), The use of particle packing models to design ecological concrete, *HERON*, Vol. 54, No. 2/3, pp. 185-204.

[6] Brouwers H.J.H., and Radix, H.J., (2005), Self-compacting concrete: the role of the particle size distribution, *First International Symposium on Design, Performance and Use of Self-Consolidating Concrete*, SCC'2005-China, May 26-28, 2005, Hunan, China, pp. 109-118.

[7] Wallevik, O.H., Mueller, F. V., Hjartarson, B., and Kubens, S. (2010). The green alternative of self-compacting concrete, Eco-SCC, *35th Conference on Our World in Concrete and Structures*, August 25-27, 2010, Singapore.

[8] Mueller, F. V., and Wallevik, O. H. (2011). Particle packing by gyratory intensive compaction as tool to optimize the aggregate gradation of low binder SCC, Eco-SCC, *36th Conference on Our World in Concrete and Structures*, August 14-16, 2011, Singapore.

[9] Mueller F.V., Wallevik, O.H., Khayat, K.H., (2014), Linking solid particle packing of Eco-SCC to material performance, *Cement & Concrete Composites*, Vol. 54, pp. 117-125.

[10] Kar, N., Seow, K., and Kluegge, J., (2009). A new dimension in self compacting concrete (SCC): Smart dynamic construction, *34th Conference on Our World in Concrete and Structures*, August 16-18, 2009, Singapore.

[11] Jaffer, R., Magarotto, R., and Roncero, J., (2010), Smart dynamic concrete: New approach for the ready-mixed industry, *Advances in Cement-Based Material*, pp. 29-33.

[12] Kar, N., Yamamiya, H., and Sugamata, T., (2013). Challenges in producing low fines self-consolidating concrete in Asia Pacific, *Concrete in Australia*, Vol. 39, No. 4, pp. 29-35.

[13] D'Souza, B., and Yamamiya, H., (2013). Applications of smart dynamic concrete, *Third International Conference on Sustainable Construction Materials and Technologies*, August 18 - 21 2013, Kyoto Research Park, Kyoto, Japan.

[14] Garcia, L., Valcuende, M., Balasch, S., and Fernandez-Lebrez, J., (2013), Study of robustness of self-compacting concretes made with low fines content, *Journal of Materials in Civil Engineering*, April 2013, pp. 497-503.
[15] American Society for Testing and Materials (ASTM), (2015), *Annual Book of ASTM Standards*, West Conshohocken, PA.
[16] American Concrete Institute (ACI), (2007), *Self-consolidating concrete*, *ACI 237R-07*, Farmington Hills, MI.
[17] American Association of State Highway and Transportation Officials (AASHTO), (2012), *Standard Practice of Static Segregation of Hardened Self-Consolidating Concrete (SCC) Cylinders*, AASHTO Designation: PP 58-12, Washington D.C.

Rheology – One Parameter in a Performance Based Design Framework for the Selection of Concretes with Environmental Friendly Binder Systems

Lars Nyholm Thrane[1], Thomas Svensson[1], Oldrich Svec[1] and Claus Pade[1]

[1]Danish Technological Institute, Gregersensvej 4, 2630 Taastrup, DK

Abstract One way of reducing the global environmental impact of the concrete industry is to lower the clinker content of concrete through using supplementary cementitious materials. Within the framework of today's prescriptive norms and standards the use of such alternative binders results in concrete mix designs with significantly reduced water to binder ratios leading to increased viscosity and stickiness, which may be seen as a hindrance to a wide-spread industrial implementation of this green concrete technology. To overcome this challenge transition from prescriptive material specifications to performance based design criteria is needed. As part of an ongoing Danish research project, a performance based design approach was applied for selection of two concrete mixtures for a new road bridge. With the aim of finding alternative low environmental impact paste combinations a parameter study was performed at mortar level assessing the effect of the paste composition on rheological properties, compressive strength and chloride penetration resistance. This paper focuses on the rheological properties measured using a newly developed 4C-mini-Rheometer for paste and mortars. The results revealed a significant effect of the paste composition. Based on the results, a simple procedure was applied to determine the paste composition at which the plastic viscosity of the mortar was equal to or lower than the target value defined by the plastic viscosity of the mortar with the reference paste composition. A similar procedure was applied for strength and durability properties. Two candidate paste compositions fulfilling all requirements were selected for the road bridge as alternatives to a reference paste composition.

Keywords: *Rheology, Environmental friendly binder systems, Sustainability, Performance based design, Prescriptive design.*

Introduction

The demand for environmental friendly concrete structures is increasing. Approximately 5% of the global CO_2-emission is associated with cement production and estimates suggest that in 2050 the amount of concrete produced will be twice that of the present [1].

Already, a lot of research has been carried out on the use of supplementary cementitious materials such as fly ash to reduce the environmental impact of concrete by lowering the amount of cement clinker per unit volume of concrete [2][3][4]. However, the use of alternative binders often results in reduced water to binder ratios leading to concrete with increased viscosity and stickiness, which may be seen as hindrance to a more wider spread industrial implementation of green concrete technology [5][6][7]. Thus, understanding the rheology at paste/mortar level is a key factor for the adaptation of more environmental friendly binder systems e.g. using fly ash and lime stone filler as supplements for cement clinker.

An ongoing Danish research project focuses on the application of green concrete technology using supplementary cementitious materials. In particular, the development and application of alternative binders are being studied under a performance based design framework. A transition from prescriptive material specifications (such as minimum w/c-ratio and minimum cement content) to performance based design criteria in terms of strength, durability and fresh concrete properties may help to promote more environmental friendly paste compositions. Specifically, this approach was applied to select two concretes for the first demonstration project, a road bridge to be constructed in 2016. A parameter study was carried out at mortar level to study the rheological properties, compressive strength and chloride penetration of more than 30 mortars with different binder systems and water to binder ratios. The aim being to select two paste compositions with equivalent or improved performance over a reference paste composition currently approved for Danish civil engineering projects, i.e. the reference concrete is in full compliance with the existing standards and special rules specified by the Danish Road Directorate. This paper presents and analyzes the results of the rheological measurements and discusses the results in relation to the selection of the two candidate paste compositions taking into account also the results on compressive strength and chloride penetration.

Experimental Program

A parameter study was carried out at mortar level to study the effect of paste composition on rheology, strength and durability. In order to obtain as comparable and useful results as possible the volumetric proportions of paste and fine aggregate were kept constant. For all mixtures (except 19 and 20), a constant fine

aggregate content of 580 kg per m^3 of reference concrete was applied corresponding to an excess paste of 350 litres per m^3 of mortar. Mixtures Nos. 19 and 20 were tested to study the effect of reducing the excess of paste to 155 and 228 litres per m^3 of mortar, respectively. In Table 1 the proportions of the investigated mortars are provided as the corresponding constituents' contents in 1 m^3 of concrete.

Three references were included in the study. The main reference (no. 3 in Table 1) is currently used for civil engineering structures by a Danish ready mixed concrete producer. This mix naturally comply with the existing standards and special rules specified by the Danish Road Directorate for civil engineering projects e.g. the cement type is specified, the maximum water to cement ratio is 0.40 and the minimum cement content is 320 kg/m^3. For the sake of comparison, two other references mix designs were included (nos. 1 and 2). These mix designs were based on concretes used back in 2002 as part of a previous national Danish research project on green concrete, however, they do not comply with current standards. In addition, the old mixtures include micro silica (MS), which is not available as a supplementary cementitious material for the current project.

For the parameter study, a range of alternative paste compositions were selected with varying water to cement ratios and contents of supplementary cementitious materials. Only the results obtained with binder combinations of Portland cement, fly ash (FA) and limestone filler (LF) are reported in this paper. Studies with more "exotic" supplementary cementitious materials such as calcined clay are on-going and will be reported at a later stage.

The superplasticiser content was not constant. Due to relative large variations in the water to binder ratio, the superplasticiser content was adjusted for each mix to obtain mortars in the "spread" regime where the flow thickness is much smaller than the radial extent of the sample, thus proving a sound basis for comparing the plastic viscosity measured for the paste compositions, which was the main aim of this rheological study.

Each mortar was prepared following the same batching and mixing procedure. The materials were mixed in a high intensity Eirich RV02 mixer for 6 minutes according to a fixed mixing sequence. The mixed mortar was left to rest for 10 min before it was mixed for 30 seconds at high speed. The rheological properties were then measured using the newly developed 4C-mini-Rheometer (Figure 1). The rheometer is based on numerical analysis of an automatic mini-slump flow test, i.e. the analysis follows the principles of the 4C-Rheometer for concrete [10]. A total of 0.329 litres of mortars is poured into the cone, which is lifted automatically at a constant speed. The flow curve (spread vs. time) is recorded by video image analysis, and by inverse analysis the plastic viscosity is determined. The yield stress is determined following the analytical relation provided by Roussel and Coussot [9].

Table 1. Mixtures compositions

		W/C	W/C Ltd.	W/B	FA/C	LF/C	MS/C	A kg	B kg	C kg	D kg	FA kg	MS kg	LF kg	W kg	0/4 kg
1	Ref1	0,41	0,45	0,36	0,57		0,08	238				135	18		140	580
2	Ref2	0,42	0,42	0,43	0,10		0,06		319			32	18		157	580
3	Ref3	0,37	0,37	0,35	0,15				359			54			143	580
4	A+FA	0,40	0,40	0,35	0,33			305				101		0	142	580
5	A+FA	0,40	0,52	0,30	1,00			209				209		0	125	580
6	A+FA	0,60	0,60	0,53	0,33			243				80		0	170	580
7	A+FA	0,60	0,77	0,45	1,00			171				171		0	154	580
8	A+FA	0,60	1,29	0,38	3,00			90				271		0	136	580
9	A+FA+LF	0,40	0,40	0,31	0,20	0,20		307				61		61	135	580
10	A+FA+LF	0,40	0,40	0,28	0,33	0,33		269				89		89	125	580
11	A+FA+LF	0,40	0,43	0,25	0,50	0,50		231				116		116	116	580
12	A+FA+LF	0,60	0,60	0,47	0,20	0,20		248				50		50	164	580
13	A+FA+LF	0,60	0,64	0,38	0,50	0,50		192				96		96	144	580
14	A+FA+LF	0,60	0,64	0,44	0,50	0,20		208				104		42	156	580
15	A+FA+LF	0,60	0,60	0,39	0,20	0,50		226				45		113	149	580
16	A+FA+LF	0,60	0,77	0,36	1,00	0,50		154				154		77	138	580
17	A+FA+LF	0,40	0,43	0,29	0,50	0,20		255				127		51	127	580
18	A+FA+LF	0,40	0,52	0,24	1,00	0,50		184				184		92	110	580
19	A+FA_H1	0,40	0,40	0,35	0,33			232				77		0	108	755
20	A+FA_H2	0,40	0,40	0,35	0,33			259				86		0	121	690
21	C+FA	0,40	0,40	0,35	0,33					302		100		0	141	580
22	C+FA	0,40	0,52	0,30	1,00					207		207		0	124	580
23	C+FA	0,40	0,40	0,37	0,20					331		66		0	146	580
24	C+FA+LF	0,40	0,40	0,31	0,20	0,20				304		61		61	134	580
25	C+FA+LF	0,40	0,43	0,25	0,50	0,50				230		115		115	115	580
26	C+FA+LF	0,40	0,52	0,24	1,00	0,50				182		182		91	109	580
27	B+FA	0,40	0,40	0,35	0,33				303			100		0	141	580
28	B+FA	0,40	0,52	0,30	1,00				208			208		0	125	580
29	B+FA+LF	0,40	0,43	0,25	0,50	0,50			230			115		115	115	580
30	B+FA+LF	0,40	0,52	0,26	1,00	0,33			191			191		63	114	580
31	D+FA	0,40	0,40	0,35	0,33						302	100		0	141	580

For the calculation of the "W/C" ratio, fly ash has been included with a factor of 0.5. For the "W/C ltd. ratio, fly ash has been included with a factor of 0.5 but only up to a content of 33 % of the cement content according to the Danish standard DS2426. The different cement types are referred to as "A" (CEM I 52,5 N (LA)), "B" (CEM I 42,5 N - SR 5 (EA)), "C" (CEM II/A-LL 52,5 N (LA)) and "D" (CEM II/A-LL 52,5 R (LA)). The mortar volume is fixed at 0.505 m^3 representing the mortar volume of a reference concrete.

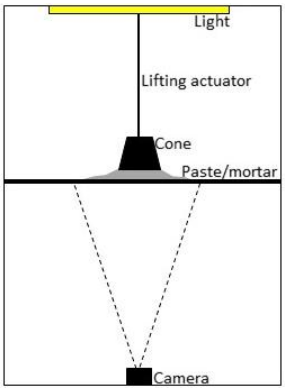

Figure 1. Principal sketch of the 4C-mini-rheometer to measure Bingham rheological parameters of fluid paste and mortar

Results and discussion

Figure 2 shows the measured slump flow for all mixtures including pictures of the two mixtures with the highest and lowest slump flow, respectively. The slump flow varies from approximately 160 mm to 280 mm and most mixtures exhibit slump flows between 200 and 280 mm. All viscosity results are considered to be comparable as the slump flows fall within the required "spread" regime with yield stresses varying from 7 to 90 Pa according to the relation by Roussel and Coussot [9]. In general, it is rather difficult to obtain the same slump flow. Especially, it is challenging to retain a stable mix at high slump flows when the plastic viscosity is low.

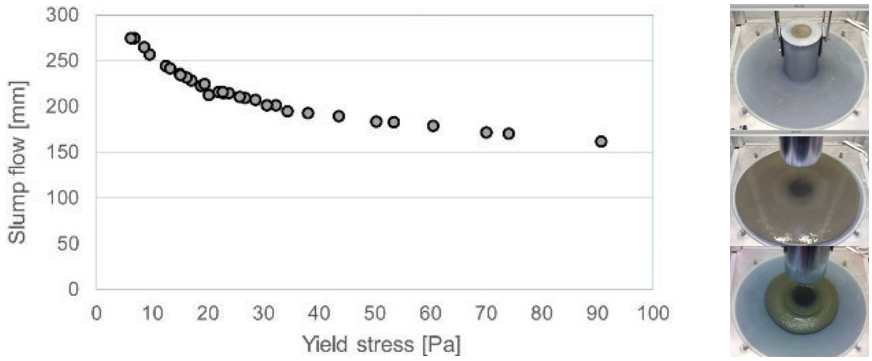

Figure 2. Slump flow measurements and corresponding yield stresses following the relation by Roussel and Coussot [9]. Pictures of the mixtures with the highest and lowest slump flow, respectively

Figure 3 (top graph) shows the plastic viscosity of all mixtures investigated. Significant variation in plastic viscosity is observed ranging between low values of approximately 1.0 Pa·s and high values of approximately 40 Pa·s. The reference mixture (No. 3) has a plastic viscosity of 8.5 Pa·s. The bottom graph highlights mixtures with the same paste proportions but comprising the four different types of Portland cement applied in this study. It is interesting to observe that there is no significant effect on the plastic viscosity between these four cement types despite their physical, chemical and mineralogical differences.

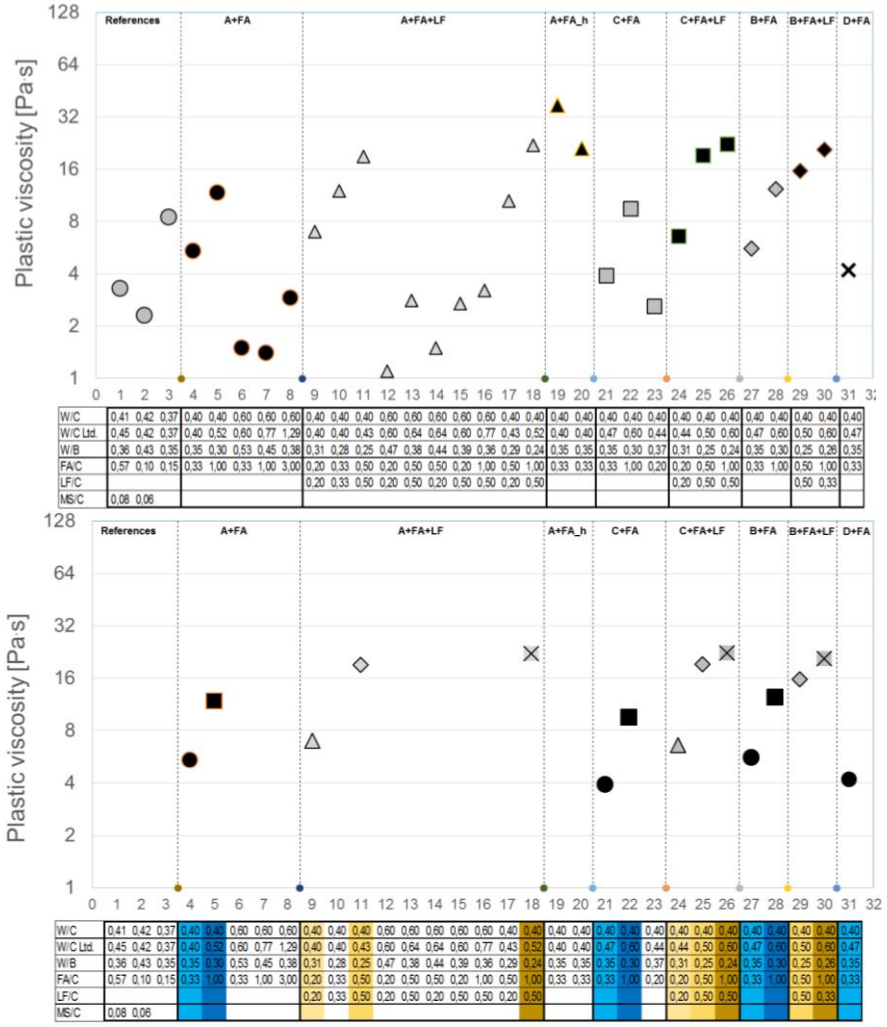

Figure 3. Top: Pl. viscosity of all mixes. Bottom: Pl. viscosity of mixes with the same paste proportions (e.g. the black circles) but different types of Portland cement

All results can also be plotted as shown in Figure 4. It shows the plastic viscosity as a function of the solid volume fraction of the paste i.e. the binder to binder + water ratio (by volume). The results are shown on a linear and a logarithmic scale, respectively. The results show that the plastic viscosity, despite the variation in binder composition, is strongly dependent on solid volume fraction and that the relation seem to be linear on a logarithmic scale for fixed proportions of paste and fine aggregate and for the materials and mixture proportions applied in this parameter study. However, further studies are on-going e.g. to study the effect of other supplementary materials such as calcined clay. The very clear outliers in the diagram (nos. 19 and 20) show the large effect on viscosity of increasing the fine aggregate content, i.e. of reducing the excess paste at mortar level. Mixture No. 19 has the highest viscosity and the lowest excess of paste at mortal level.

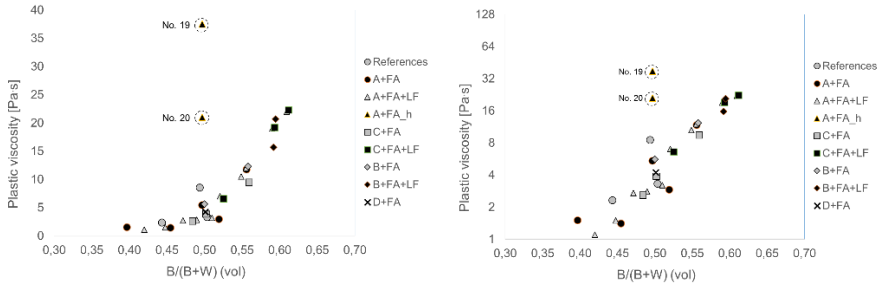

Figure 4. The plastic viscosity as function of the solid volume fraction i.e. the binder to binder + water ratio (vol.). Left: Linear y-axis. Right Logarithmic y-axis

In the context of selecting two alternative low environmental impact binder systems it was decided to use the cement type CEM I 52.5 N (LA) (referred to as "A") for both binder systems. As supplementary cementitious materials, the first binder system should comprise also fly ash and the second binder system should be a combination of cement, fly ash and limestone filler.

To select these two candidate paste compositions limit values in terms of plastic viscosity, compressive strength at 28 maturity days and chloride penetration resistance at 91 maturity days were chosen corresponding to the values obtained for the reference mixture no. 3.

By interpolation, the water to cement ratio was found at which the specified requirements were fulfilled. Figure 5 shows the plastic viscosity for the mixtures

with fixed binder proportions but with different water to cement ratios. For the calculation of the w/c ratio, fly ash has been included with a factor of 0.5. The same procedure was applied for the compressive strength and chloride penetration resistance (not shown here). It turns out that the compressive strength is the limiting parameter for both binder systems.

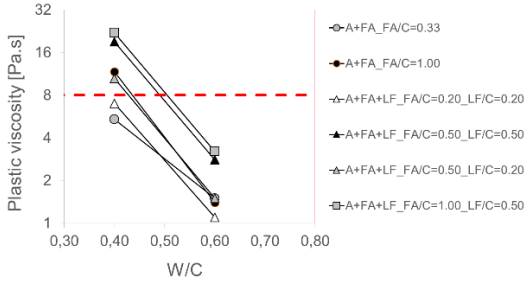

Figure 5. Plastic viscosity as a function of the water to cement ratio. Logarithmic y-axis

For the binder system comprising cement and fly ash it was found that the strength requirement was fulfilled at a w/c ratio of 0.45 and a fly ash to cement ratio of 0.80. The estimated corresponding plastic viscosity (Figure 6) and chloride migration coefficient were 7.0 Pa·s and $1.3 \cdot 10^{-12}$ m^2/s respectively, i.e. both better than the 8.5 Pa·s and $4.9 \cdot 10^{-12}$ m^2/s obtained for the reference mixture. For the second binder system, the strength requirement was fulfilled at a w/c ratio of 0.50 (all fly ash allowed in the calculation, but the limestone filler omitted) at a fly ash to cement ratio of 0.50 and a limestone filler to cement ratio of 0.35. The resulting estimate of plastic viscosity was 6.0 Pa·s, while the chloride migration coefficient was estimated to be $2.3 \cdot 10^{-12}$ m^2/s. Compared to the reference concrete, the CO_2 reduction was 44 % and 42 % with the two alternative paste compositions, respectively.

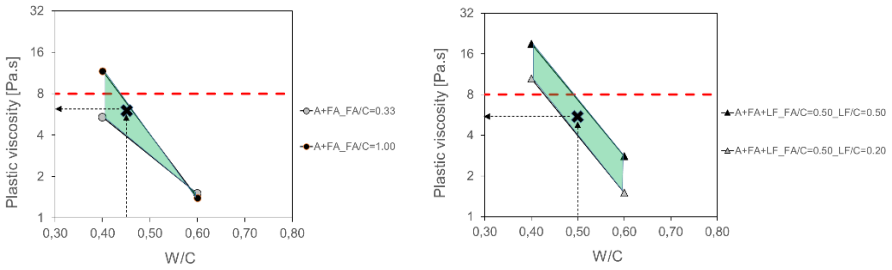

Figure 6. Left: Interpolation to determine plastic viscosity at a fly ash to cement ratio of 0.80. Right: Interpolation to determine plastic viscosity at fly ash to cement ratio of 0.50 and limestone filler to cement ratio of 0.35

Thus, following the described procedure it was possible to select paste compositions with equivalent or better performance with respect to viscosity, compressive strength and chloride penetration resistance to that of the reference mixture. The candidate paste compositions are now being tested and documented at concrete level, and will in early Summer 2016 be used to cast a road bridge between the cities of Herning and Holstebro.

It is worth noticing that if the binder compositions proposed had been selected to fulfil the requirement to maximum w/c ratio of 0.40 as prescribed in the Danish standard (where fly ash contents only up to 33% of the mass of cement is allowed in the calculation), the concrete would not only be less environmentally friendly, but the plastic viscosity would be more than twice as high as that of the reference mixture, which most likely would result in concrete having poor production and execution properties. Such concrete would not receive a favourable evaluation from concrete producers and contractors. The consequence could very well have been negative in terms of promoting the use of environmentally friendly binder systems.

Conclusions

A parameter study comprising 31 mortars with different paste compositions was carried out to measure the plastic viscosity, compressive strength and chloride penetration resistance. A strong effect of the paste composition on the plastic viscosity was observed. For fixed proportions of paste and fine aggregate the plastic viscosity show on a logarithmic scale a linear trend relationship to the solid volume fraction of the paste. Under the framework of a performance based design approach a procedure was developed, from a mortar level parameter study, to determine paste compositions having equivalent or better performance to a reference mixture with respect to the selected performance indicators plastic viscosity, compressive strength and chloride penetration resistance. Following this procedure, two paste compositions comprising relatively large amounts of supplementary cementitious materials (fly ash and fly ash + limestone filler) were selected for the development of environmental friendly concretes to be applied in a new road bridge. The CO_2 reductions were approximately 40 % compared to the reference concrete.

Acknowledgements

The authors would like to thank Innovationsfonden – Denmark for their financial support to the project “Green transition of cement and concrete production”.

References

[1] Imbadi, M. S., Carrigan, C., Mckenna, S. (2012), *Int. J. of Built Environment*, vol. 1, iss. 2, pp. 194-216.

[2] Glavind, M., and Munch-Petersen, C. (2002), In: *Challenges of Concrete Construction*, Proceedings of Int. Congress, pp. 642–650, Dundee, Scotland.

[3] Schneider M., Romer M., Tschudin M., Bolio H. (2011), *Cem. and Conc. Res*., vol. 41, iss. 7, pp. 642-650.

[4] Lothenbach B., Scrivener K., Hooton R. D. (2011), *Cem. and Conc. Res*., vol. 41, iss. 12, pp. 1244-1256.

[5] Ferraris, C. F., Karthik, H.O., Russell, H. (2001), *Cem. and Conc. Res*., vol. 31, pp. 245-255.

[6] Bentz, D., Ferraris, C. F., Galler, M. A., Hansen, A. S., Guynn, J. M. (2012), *Cem. and Conc. Res*., vol. 42, iss. 2, pp. 404–409.

[7] Vance, K., Kumar, A., Santb, G., Neithalatha, N. (2013), Cem. and Conc. Res., vol. 52, pp. 196–207.

[8] Bey, H. B., Hot, J., Baumann, R., Roussel, N. (2014), *Cem. and Conc. Comp*., vol. 54, pp. 17–20.

[9] Roussel, N., and Coussot P. (2005), *J. of Rheo*, 49 (3), pp. 705-718.

[10] Thrane, L. N., Pade, C., Nielsen, C. V. (2010), *J. ASTM Int*., vol. 7.

Self-Consolidating Concrete Prepared with Recycled Asphalt Pavement and High Volume of Supplementary Cementitious Materials

Yasser Khodair[1] and Mahmood Raza[2]

[1] Associate Professor, Department of Civil Engineering and Construction, Bradley University; 1501 West Bradly Avenue, Peoria IL, 61625.
[2] Graduate Research Assistant, Department of Civil Engineering and Construction, Bradley University; 1501 West Bradly Avenue, Peoria IL, 61625.

Abstract This paper studies the fresh and hardened properties of self-consolidating concrete including recycled asphalt pavement (SCCRAP). Constant water to cementitious materials (w/c) ratio of 0.4 was used for all mixtures. RAP was used as a substitution for natural coarse aggregate (NCA) by 0, 15, 30, and 50%. The control mixture for each group was prepared with 100% Portland cement. Moreover, supplementary cementitious materials (SCMs) such as class C fly ash (FA), and granulated blast furnace slag (S) were used by different percentages (75% fly-ash, 75% slag and combination of 37.5% fly-ash and 37.5% slag) as binding materials in addition to Portland cement. The fresh properties of SCCRAP such as: flowability, deformability; filling capacity, resistance to segregation were assessed. Additionally, the hardened properties such as, the compressive strength at different ages (3, 14, and 28 days), and the split tensile strength at 28 days were investigated. All mixtures met the minimum fresh properties requirements for SCC. Furthermore, the use of RAP and SCMs as a partial replacement for NCA, and cement resulted in the decrease of the compressive and tensile strengths of all mixtures.

Keywords: *Self-consolidating concrete, Recycled asphalt pavement (RAP), Fly-ash and slag, Sustainable technologies, Fresh properties, Hardened properties.*

Introduction

Self-Consolidating Concrete (SCC) was primarily used to overcome the problems of concrete flowability. SCC is a high performance concrete that can spread and flow under its own weight without the need for mechanical vibration in congested

spaces without any segregation. These properties of SCC results in reduction of labor cost and construction time [1]. SCC technology allows structural engineers to design economically and environmentally sound structures incorporating smaller highly reinforced concrete members and build them with optimal material use. The first form of SCC developed at the University of Tokyo in the late 1980s, required large amount of cement content and expensive chemical admixtures to obtain highly workable and good compressive strength concrete. However even with this high cost SCC has been used for different important structures and becoming popular day by day [1, 2]. The major obstacle for implementation of SCC technology in construction industry is high material cost which is 25-50% more than conventional concrete [3]. A lot of research has been done in recent years to remove the environmental impacts (same as PCC) and cost issues of SCC so it can be used more in construction industry. The use of recycled construction materials for aggregates and industrial by-products for binding materials are becoming the source to develop new type of Self-consolidating concrete which will be cost effective and environment friendly with the desirable fresh and hardened properties.

Recycled asphalt pavement (RAP) is the pavement material acquired through the removal of old roads during the construction of new asphalt pavements. RAP material consists of well graded aggregates with the coating of asphalt on the surface of these aggregate particles. The asphalt coating on the surface of aggregates usually range from 6 to 9 μm. US highway industry each year produces approximately more than 100 million tons of RAP material from road widening and rehabilitation projects [1, 4, 5, 6]. This paper studies the effect of the use of RAP on the fresh and hardened properties of SCC.

Objectives and Tasks

The objective of this study is to investigate the effect of supplementary cementitious materials (SCMs) such as fly-ash and slag, and recycled asphalt pavement (RAP) on the fresh and hardened properties of SCC. Partial replacement of RAP and SCMs including FA and S for NCA and Portland cement, respectively, in SCC concrete mixtures is utilized. The percentage replacement of NCA by 0%, 15%, 30% and 50% RAP; and cement with 75% FA, 75% S, and 37.5% FA and 37.5% S is adopted in this study.

To achieve the objectives of this research, the following tasks have been performed: 1) a total of 16 mixtures have been prepared. The mixtures were divided into four groups such that for each percentage (0%, 15%, 30%, and 50%) of RAP utilized, the percentage of binding materials were varied: a) 100% Portland cement, b) 25% Portland cement and 75% FA, c) 25% Portland cement and 75% S, d) 25% Portland cement, 37.5% FA, and 37.5% S; 2) An experimental program was conducted to assess the rheological properties of all mixtures using the slump flow, slump flow with J-Ring, T50, and segregation index (SI) tests of the fresh concrete, and the hardened properties including the compressive strength at 3, 14,

and 28 days, and the tensile strength at 28 days. Table I, delineates the mixtures matrix adopted in this study.

Experimental Program

Materials

Crushed limestone aggregate having nominal maximum aggregate size of 19 mm and well-graded sand obtained from local suppliers, were used in the mixtures. Table II, shows the fine and coarse aggregate gradation.

Fresh Properties

Table I. SCC Mixtures Matrix

Mix Description	100% Cement	75% Fly-ash+ 25% cement	75% Slag+ 25% cement	37.5% Fly-ash + 37.5% Slag+ 25% cement
0% RAP-100% NCA	0-0FA-S	0-75FA	0-75S	0-FA-S
15% RAP-85% NCA	15-0FA-S	15-75FA	15-75S	15-FA-S
30% RAP-70% NCA	30-0FA-S	30-75FA	30-75S	30-FA-S
50% RAP-50% NCA	50-0FA-S	50-75FA	50-75S	50-FA-S

Table II. Aggregate Gradation

Fine Aggregate		Coarse Aggregate	
Sieve Size (mm)	**%Passing**	**Sieve Size (mm)**	**%Passing**
9.5	100	25	100
4.75	98	19	97
2.36	84	12.5	30
1.18	68	9.5	10
0.6	54	4.75	3
0.3	21	2.36	0
0.15	5	1.18	0
0.075	1	0.3	0

The flowability, deformability, passing ability, viscosity and segregation resistance of all mixtures prepared was studied. The slump-flow test was conducted according to ASTM C 161 [7], to measure the flowability and deformability. The ability of the prepared mixtures to flow in congested rebar areas and to pass through

obstacles was evaluated using the slump-flow with J-Ring test according to ASTM C 1621 [8].

Table III. Proportions of SCC Mixtures

Mix No.	Slump Flow without J-Ring (mm)	T_{50} without J-Ring (Sec)	Slump Flow with J-Ring (mm)	T_{50} with J-Ring (Sec)	Segregation Index (SI)	HRWRA (ml/m^3)	VMA (ml/m^3)
0-0FA-S	638	4	606	5	0	490	68
0-75FA	658	4	625	5	0	510	72
0-75S	640	3	608	5	0	500	70
0-FA-S	605	5	574	6	0-1	525	75
15-0FA-S	611	3	580	5	0	500	70
15-75FA	622	5	590	6	0	510	70
15-75S	614	3	583	5	0	515	72
15-FA-S	581	4	551	6	0-1	530	75
30-0FA-S	590	3	560	6	0	510	75
30-75FA	601	4	570	6	0	520	77
30-75S	587	3	557	6	0	525	75
30-FA-S	552	4	524	7	1	540	78
50-0FA-S	563	4	534	7	0	520	72
50-75FA	576	4	547	6	0	530	75
50-75S	565	3	536	6	0	540	78
50-FA-S	530	5	503	7	1	550	80

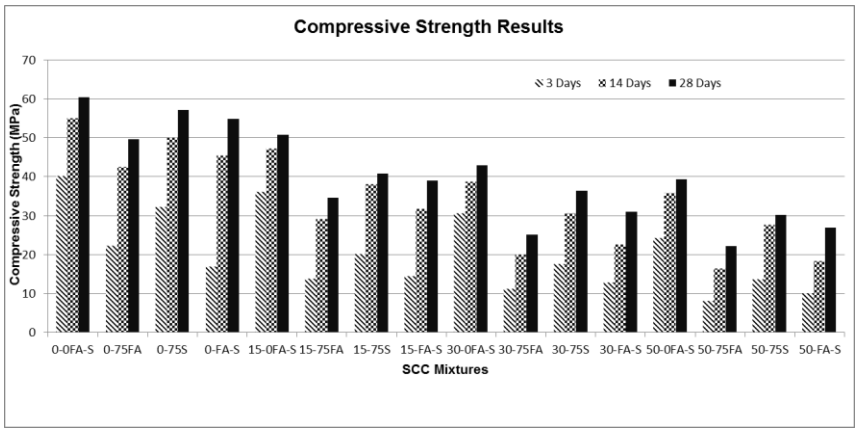

Figure 1. Compressive Strength of all Mixtures

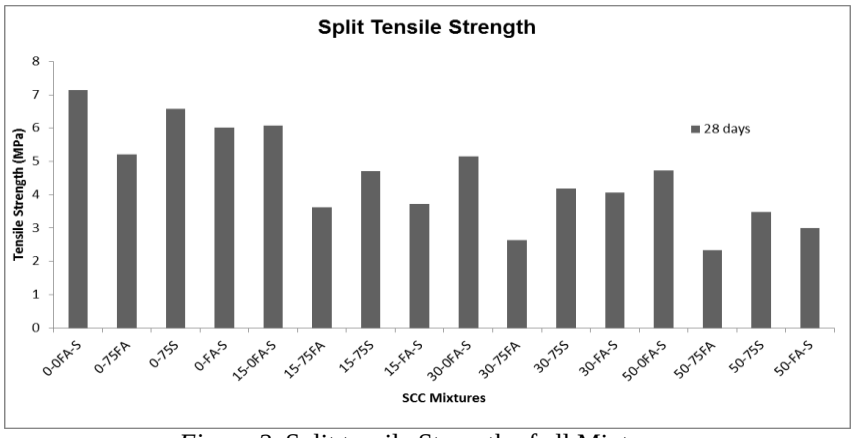

Figure 2. Split tensile Strength of all Mixtures

The viscosity of the mixtures was determined by conducting T50 test with and without J-Ring. Furthermore, segregation of the SCCRAP mixtures was evaluated using segregation index test where the mixtures were visually examined and assigned a *SI* value between 0 and 2, where *SI* = 0, indicates high resistance to segregation, *SI* =1, adequate resistance to segregation, and *SI* = 2, no resistance to segregation. Table II; shows values for the properties of all concrete mixtures at the fresh stage including slump flow with and without J-Ring, T50 with and without J-Ring, and segregation index tests for each mixture.

Hardened Properties

The compressive strength of all mixtures prepared in this study was determined by taking the average results of testing two 100 x 200 mm concrete cylinders at different intervals (3, 14 and 28 days). The concrete cylinders were made and

tested in accordance with ASTM (C39/C39M-09) [9]. Moreover, the split tensile strength of each concrete mixture was determined using a 150 x 300 mm concrete cylinder after 28 days. All SCC specimens were cured in the curing room at a relative humidity of 95% until the day of testing. The split tensile strength was performed in accordance with ASTM (C 496/ C 496M-04) [10]. Figures 1 and 2, show the results of compressive strength and split tensile strength respectively.

Results and Discussion

Effect of SCMs and RAP on the Fresh Properties of SCC Mixtures

Table III, shows the slump flow values with and without J-ring of all mixtures with their corresponding RAP and SCMs constituents. The use of 75% FA has greater effect in increasing the workability when compared to 75% S, and 37.5% FA and 37.5% S if the percentage of RAP remains constant. This indicates that the slump flow values increases with the use of 75% FA, and 75% S used as a partial replacement for cement in all mixtures, when compared with mixtures that contains 100% Portland cement (0-0FA-S, 15-0FA-S, 30-0FA-S, 50-0FA-S). Although the increase in slump flow in case of using FA is significant when compared to mixtures containing 100% Portland cement, the difference is less noticeable in case of using 75% S as partial replacement for cement. The highest slump value was observed in Mix 0-75FA (0% RAP-75% FA) and lowest in Mix 50-FA-S (50% RAP-37.5% FA and 37.5% S). This decrease in slump for ternary mixtures can be due to the different nature of three binding materials being used in these mixtures. Additionally, as the percentage of RAP used in lieu of NCA increases, the values of slump flow decreases for all mixtures.

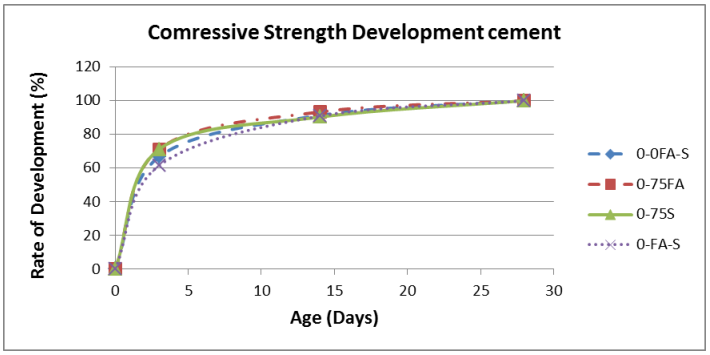

Figure 3(a). Compressive Strength Development Rate in Mixtures with 100% cement

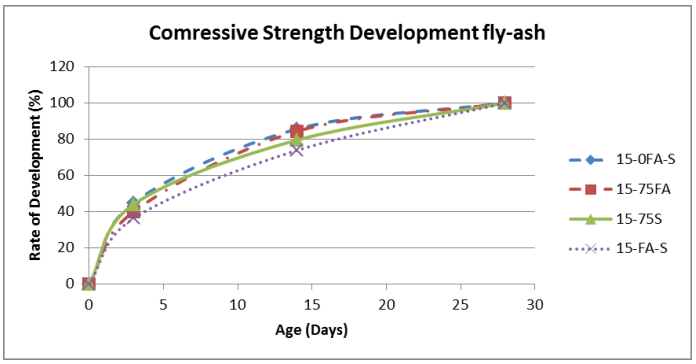

Figure 3(b). Compressive Strength Development Rate in Mixtures with 75% FA

Effect of SCMs and RAP on the Hardened Properties of SCC Mixtures

The compressive strength of all the mixtures measured at 3, 14 and 28 days is shown in Figure 1. The mixtures having 100% Portland cement have the maximum compressive strength, while those containing 75% FA as partial replacement for cement have the lowest strength within each of the four groups with the same RAP percentages. In general, the use of SCMs decreases the compressive strength when compared with mixtures prepared with 100% cement. Furthermore; as the percentage of RAP used as a substitution for NCA increases from 0% to 50%, the compressive strength of all mixtures decreases accordingly with no exception.

Figure 2, shows the split tensile strength for all SCC mixtures, measured at 28 days. The tensile strength decreases with the use of SCMs and RAP content. The maximum tensile strength is 7.14 MPa, corresponding to Mix 0-0FA-S (100% Portland cement and 0% RAP), and the minimum is 2.33 MPa, corresponding to Mix 50-75FA (50% RAP and 75% FA).

The rate of compressive strength development was also studied for all SCC mixtures. Figures 3a-b; show the rate of compressive strength development over 28 days-time period. SCC mixtures with the same binding material were grouped to study the effect of RAP on the compressive strength development. It is observed that the use of 100% Portland cement as a binding material increases the rate of compressive strength development indicated by the small difference between the 14-days compressive strength and 28-days in Figure 3a, as opposed to significant changes in mixtures with SCMs as shown in Figure 3b. The results also show that the inclusion of RAP in replacement of NCA has an adverse effect on the compressive strength development, especially when used in conjunction with SCMs.

Summary and Conclusions

In this study sixteen SCC mixtures containing different proportions of RAP, FA and S were prepared and tested in laboratory. Testing results showed a consistent decrease in the compressive and tensile strength as the SCMs and RAP content

increased in the mixtures. Based on the results obtained in this study, the following conclusions can be made:

- 75% FA and 75% S can be used in concrete mixtures as partial replacement
  for Portland cement to obtain a workable and cost-effective SCC.
- Using RAP as a replacement for coarse aggregate with 15, 30 and 50% in SCC mixtures resulted in the reduction of workability as compared to 0% RAP or 100% coarse aggregate. All mixtures had slump flow exceeding the minimum required for SCC.
- Using 15, 30 and 50% RAP decreased the 28-days compressive strength of SCC mixtures compared with those containing 100% NCA.
- As the percentage of RAP replacing coarse aggregate increased (0-50%), the split tensile strength decreased accordingly.
- The rate of compressive strength development decreased with use of SCMs.

References

[1] Hossain, K. M. A., and Lachemi, M. (2010). "*Fresh, mechanical, and durability characteristics of self-consolidating concrete incorporating volcanic ash*." Journal of Materials in Civil Engineering, 22(7), 651-657.

[2] Ozawa, K., Maekawa, K., Kunishima, H., and Okamura, H. (1989). "*Performance of concrete based on the durability design of concrete structures*." Proceedings of the 2nd East-Asia-Pacific Conference on Structural Engineering and Construction, Vol.1, Chiang Mai, Thailand, 445-456.

[3] El-Chabib, H. and Syed, A. (2013). "*Properties of Self-Consolidating Concrete Made with High Volumes of Supplementary Cementitious Materials*." J. Mater. Civ. Eng., 10.1061/(ASCE)MT.1943-5533.0000733, 1579-1586.

[4] Ibrahim, A., Mahmoud, E., Khodair, Y., Patibandla, V. C. (2013), "*Fresh, Mechanical, and Durability Characterisitics of Self-Consolidating Concrete Incorporating Recycled Asphalt Pavements*," Journal of Materials in Civil Engineering, Vol. 26 (4), pp. 668-675.

[5] Huang, Baoshan, Shu, Xiang, and Li, Guoqiang, (2005), "*Laboratory Investigation of Portland Cement Concrete Containing Recycled Asphalt Pavements*," Cement and Concrete Research, Volume 35, Issue 10, pp. 2008–2013.

[6] Huang, B., Shu, X., and Burdette, E.G. (2006), "*Mechanical properties of concrete containing recycled asphalt pavements*," Magazine of Concrete Research, 58 (5). pp. 313-320.

[7] ASTM C 1611/C 1611 M-09b. (2009). "*Standard test method for slump flow of self-consolidating concrete*." American Society for Testing and Materials, West Conshohocken, PA.

[8] ASTM C 1621/ C 1621M-09b, (2009), "*Standard Test Method for Passing Ability of Self-369 Consolidating Concrete by J-Ring*," American Society for Testing and Materials, Pennsylvania, 370 PA.

[9] ASTM C 39/ C39M-10, (2010), "*Standard Test Method for Compressive Strength of Cylindrical Concrete Specimens*," American Society for Testing and Materials, Pennsylvania, PA.

[10] ASTM C496 / C496M – 11, (2011), "*Standard Test Method for Splitting Tensile Strength of Cylindrical Concrete Specimens*" Cement Concrete & Aggregates Australia - CCAA. *Use of Recycled Aggregates in Construction*. Sydney, Australia: CCAA; 2008 Construction and Building Materials, 22(9), 1963-1971.

Time-Dependent Fresh Behaviour of Self-Compacting Concrete with Recycled Concrete Coarse Aggregate

Iris González-Taboada[1], Belén González-Fonteboa[1], Fernando Martínez-Abella[1], Nicolas Roussel[2] and Sindy Seara-Paz[1]

[1]School of Civil Engineering. Department of Construction Technology, University of A Coruña. Spain
[2]IFSTTAR, Laboratoire Navier – UMR 8205, France

Abstract The present work focuses on the relationship between fresh self-compacting concrete properties obtained with a rheometer (such as yield stress and plastic viscosity) and those measured with empirical tests (slump flow, L-box, V-funnel, J-Ring and sieve segregation). Four types of self-compacting concrete were studied: a reference concrete and three recycled concretes. The replacement percentages of natural with recycled coarse aggregate have been 20%, 50% and 100% (in volume). All mixes were tested over time at 15, 45 and 90 min since the water-cement contact. The tests results show that self-compacting recycled concrete follows the same behaviour as conventional concrete, its specificity lying in the procedure used to compensate water absorption during the mixing protocol.

Keywords: *Self-compacting recycled concrete; Rheology.*

Introduction

It is well known that one of the main differences between a conventional concrete and a recycled concrete is the high absorption of recycled aggregate [1]. This property and the moisture level prior to mixing determine the effective water that influences the final properties of fresh and hardened concrete. This makes the control of recycled concrete dosage difficult and it requires designing specific mixing procedures [2]. Furthermore, the fundamental difference between a vibrated conventional concrete and a self-compacting concrete (SCC) is its fresh behaviour [3]. In the last years, a great number of empirical tests were developed in order to determine the filling ability, the passing ability and the segregation resistance of SCC [4]. Even so, none of them has achieved to characterize all relevant aspects of

rheology of this type of concrete, so the use of different empirical tests combinations to guarantee a suitable workability is required [5]. However, three of the key properties measured with a single rheological test (static yield stress, dynamic yield stress and plastic viscosity) are very useful from a practical point of view, and this test would avoid the need to perform a great number of empirical tests.

Therefore, the combination of these two singularities (the mixing procedure to control the water absorption of recycled aggregate, and the special fresh behaviour of SCC) will have greater influence on self-compacting recycled concrete (SCRC).

Research Significance

Traditionally, to control the high absorption of recycled aggregate, authors proposed two alternative methodologies to produce recycled concrete. In the first one, the recycled aggregate is added dry or with its natural moisture, compensating its absorption with additional water. In the second one, the recycled aggregate is added to the mix after being immersed in water for a pre-established period of time, usually 10 min. Current trends suggest that the first method leads to a better behaviour than the second one. The first objective of the work is to know the influence of the substitution percentage of natural coarse aggregate with recycled aggregate obtained from concrete waste in the workability and rheology of SCRC produced with the extra water addition during the mixing. With this purpose, several empirical and rheological tests were carried out. In this context, this research also studies the time-dependent fresh-state behaviour of SCRC. The originality of the work is to show that rheology of SCRC follows very similar laws to conventional SCC and to demonstrate that the specificity of SCRC is the effective water to cement ratio ((w/c)ef).

Materials and Methods

Materials

The following materials were used in this research (Table XI):
Cement (C) and filler (f): Portland cement, CEM-I 52.5 R (EN 197-1), and a limestone filler were used as powder fraction.
Superplasticiser (s): a modified policarboxylate was used.
Natural aggregates: as fine aggregate (NFA), a siliceous sand with nominal size 0-4 mm and a fineness modulus of 4.19 was used. A crushed granitic coarse aggregate (NCA) with nominal size 4-11 mm and a fineness modulus of 7.14 was also used.

Recycled aggregates: the size fraction used was a 4-11 mm with a fineness modulus of 6.47. This recycled coarse aggregate (RCA) was obtained from real demolition debris of structural concrete. It was made up mainly of concrete and stone. The grading curves were similar for both recycled and natural coarse aggregate.

Table XXXVI. Aggregates properties

Property	NFA	NCA	RCA
Fineness modulus (EN 933-1)	4.19	7.14	6.47
Fines percentage (EN 933-1) (%)	8.40	0.84	3.00
Moisture content (EN 1097-3) (%)	1.18	0.84	5.95
Saturated-surface-dry density (EN 1097-6) (t/m^3)	2.72	2.56	2.34
Absorption (EN 1097-6) (%)	1.00	1.12	6.96
Flakiness index (EN 933-3) (%)	-	5.41	5.33
Shape	Crushed	Crushed	Crushed

Many researchers have studied the influence of aggregates on rheological properties of fresh concrete. Knowledge of the solid volume fraction, the value of the maximum packing fraction (Ømax), the shape and the size distribution of particles is highly important [6]. The Ømax was calculated for different replacement percentages of RCA (Figure 83). The results indicate that Ømax is quite similar in natural and recycled coarse aggregate, although a slight ascending trend can be appreciated.

Water absorption capacity develops over time. Thus, EN 1097-6 establishes that it should be measured after soaking aggregates in water for at least 24 h. In addition to this standard absorption test, a continuous measurement of this property over time was conducted. At the usual reference time of 10 min [7], recycled coarse aggregate absorbs water up to 80% of that at 24 h (Figure 25).

Mixes Design

Four types of self-compacting concrete were studied (

Table ***XII***), a reference concrete and three recycled concretes replacing the natural coarse aggregate with the recycled one, with volume replacements of 20%, 50% and 100% respectively.

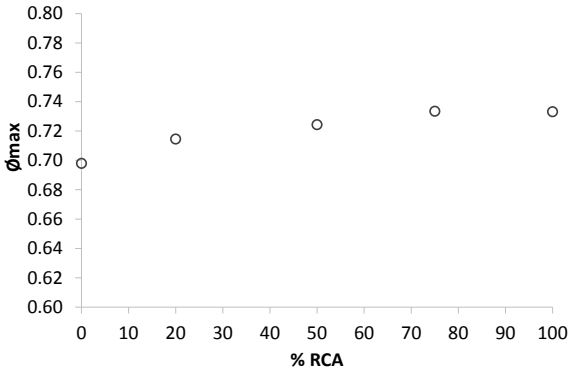

Figure 83. Maximum packing fraction of granular skeleton

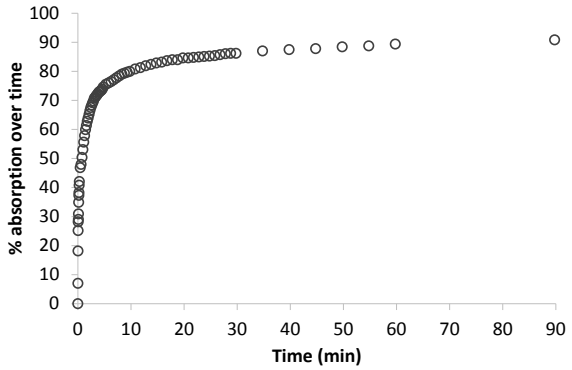

Figure 84. Evolution of recycled aggregate absorption from 0 to 90 min

The reference concrete was designed with a volumetric content of natural coarse aggregate equal to 30%. All recycled concretes were produced adding an extra quantity of water during the mixing. This was calculated to compensate the recycled aggregate absorption at 10 min (i.e. 80% of that at 24 h), which was used in dry-state conditions.

Table XXXVII. Mix proportions (1 m³)

SCRC dosage	**% RCA**			
	0%	**20%**	**50%**	**100%**

SCRC dosage	% RCA			
	0%	20%	50%	100%
Cement, c (kg)	400.00	400.00	400.00	400.00
Filler, f (kg)	180.00	180.00	180.00	180.00
Water, w (kg)	184.00	184.00	184.00	184.00
Natural sand (kg)	865.59	865.59	865.59	865.59
Natural coarse aggregate (kg)	768.00	614.40	384.00	0.00
Recycled coarse aggregate (kg)	0.00	140.40	351.00	702.00
Effective w/c	0.46	0.46	0.46	0.46
Superplasticiser/(c+f) (%)	1.70	1.70	1.70	1.70

Experimental Program

The empirical and rheological tests (Table XIII) were performed at different times: at 15, 45 and 90 min since the contact cement-water (Age). This corresponds to 0, 30 and 45 min resting time (RT) respectively for rheological tests.

In order to use the same material several times, concrete was mixed for 30 s immediately before each empirical test. In the rheological tests, the stress growth test started as soon as the vane was immersed into the concrete. The vane was rotated at a low and constant speed (0.025 rps) and the torque value was acquired. Once the peak torque was reached, the vane was removed and concrete was remixed with a shovel. Then, the vane was reinserted into concrete and the flow curve test started. In this second test, the torques at decreasing speeds after a period of 20 s at a constant speed of 0.50 rps were measured. At the end, the vane was removed and concrete was again remixed with a shovel and left at rest.

Table XXXVIII. Experimental program

Test	Parameter measured	Objective limits
Slump flow	t500 (s)	[2-8]
	Df (mm)	[650-800]
V-funnel	tv (s)	[4-20]
L-box	PL	≥ 0.80
J-Ring	t500J (s)	< 8
	DJF (mm)	> 600
	PJ (mm)	≤ 10
Sieve segregation	SR (%)	$\leq 15\%$
Stress growth test	Static yield stress	–
Flow curve test	Plastic viscosity	–

Results and Discussion

Fresh-State Results with Empirical Tests

Regarding the slump flow test, the objective limits for the parameter t500 were satisfied by SCRC at all ages, except for the mix with 100% of RCA at 90 min age. In the case of the parameter Df, the limits were satisfied by all mixes at 15 min age. The 100% replacement concrete did not reach the minimum limit at 45 min age, and neither did the 50% replacement concrete at 90 min (Figure 85).

The analysis of the V-funnel test results shows that none of the SCRC mixes fulfils the maximum limit time (Figure 86). These results do not correlate well to the ones of other empirical tests. Thus, it would not be recommended for workability control, which has been also stated by other authors [4].

The passing ability (PL, measured with the L-box test) limit was satisfied by all mixes at 15 and 45 min age (Figure 87), whereas at 90 min none of them reached that limit (nor did the reference mix). In the J-Ring test (Figure 88), the highest stability over time took place for low recycled aggregate percentages (20%). Again, at 90 min age, the mixes with substitution percentages of 50% and 100% presented the worst results. Finally, the limit value of 15% fixed for the sieve segregation test was satisfied by all mixes (Figure 89). In this case, the recycled mixes showed a lower tendency to segregation than the conventional SCC.

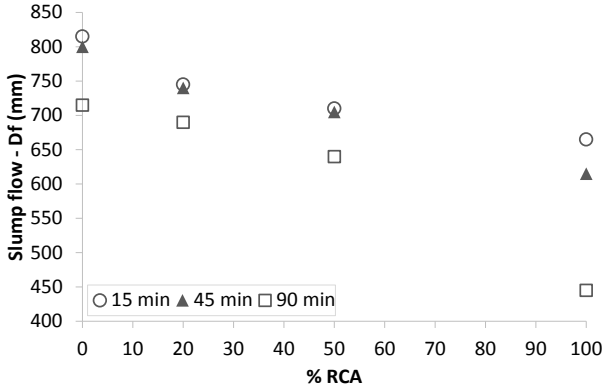

Figure 85. Time-dependent evolution of slump flow diameter

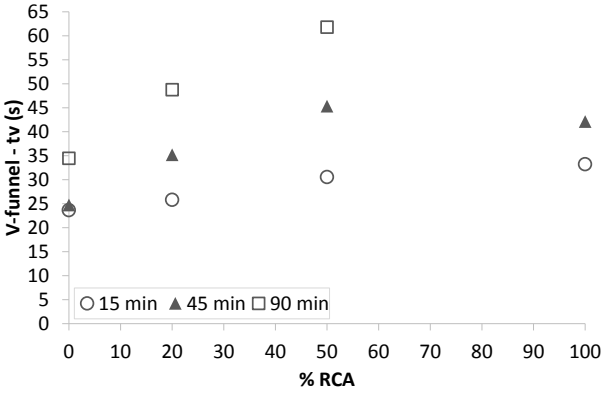

Figure 86. Time-dependent evolution of V-funnel

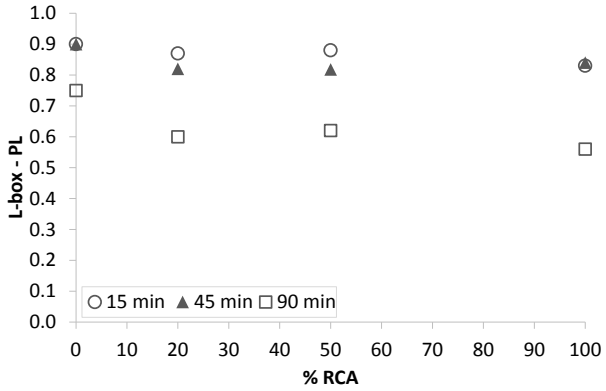

Figure 87. Time-dependent evolution of L-box

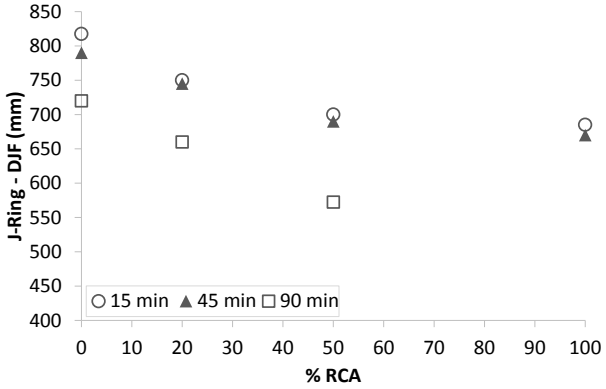

Figure 88. Time-dependent evolution of J-Ring diameter

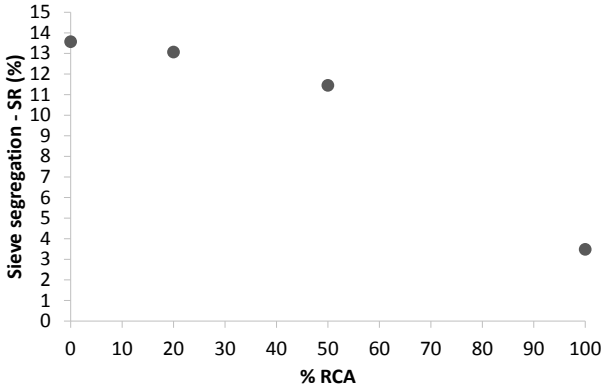

Figure 89. Results of sieve segregation test

Fresh-State Results with Rheological Tests

Figure 90 shows the static yield stress of conventional SCC and SCRC as a function of RCA percentage and age (15, 45 and 90 min). Figure 91 shows the same relationship for plastic viscosity. It is demonstrated that SCRC, up to 20% replacement, will show a rheological performance that satisfies the self-compacting behaviour and that is similar to the reference SCC one. So, the production of recycled concrete adding extra water to compensate the high water absorption of recycled aggregate and using recycled concrete coarse aggregate up to 20% (substitution in volume) guarantees the self-compacting behaviour of concrete (even until a mix age of 90 min).

The analysis of the time-dependent evolution of static yield stress and plastic viscosity allows to conclude that RCA incorporation (20%, 50% and 100%) does not involve significant changes until 45 min age (Figure 90 and Figure 91). However, from 45 min to 90 min, both values are clearly higher in concretes with high replacement ratios (especially in 100% of RCA) than low (up to 50%).

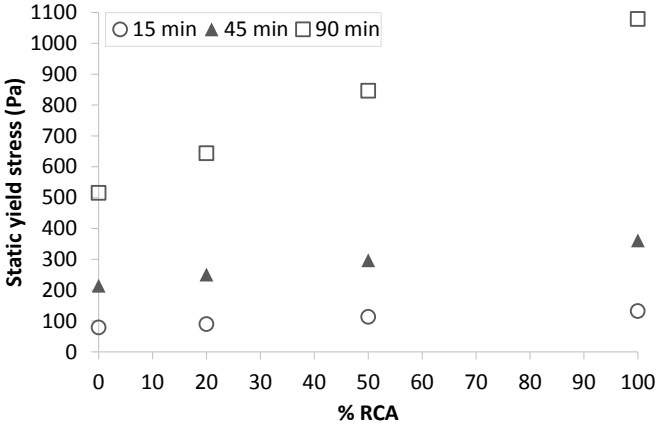

Figure 90. Time-dependent evolution of static yield stress

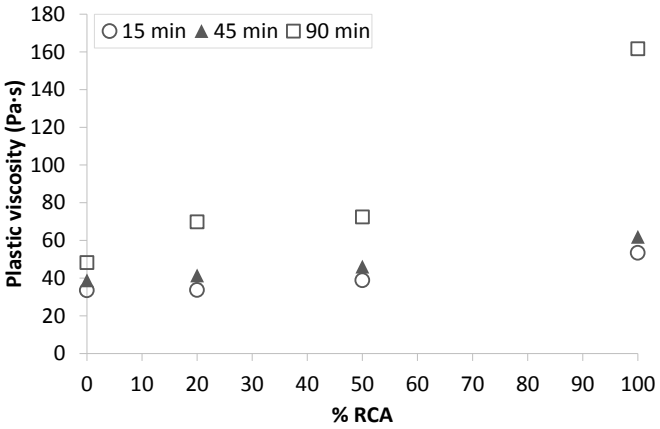

Figure 91. Time-dependent evolution of plastic viscosity

Yield stress and effective water to cement ratio

As it is well accepted, when aggregates are similar (similar Ømax), yield stress of concrete is related to yield stress of mortar [8]. Therefore, in order to observe the

influence of non-compensated water absorption in the SCRC fresh behaviour, different mortars with different w/c ratios were designed. The mini slump flow of these mortars was measured taking into account that it is clearly related to their yield stress [8] (Figure 92). Figure 10 shows two different patterns of behaviour: w/c ratios higher than 0.45 will not imply significant changes in yield stress, whereas w/c ratios lower than 0.45 will lead to important changes. This can be considered a "critical w/c ratio", since a little change in w/c ratio under this critical value will imply a great change in yield stress.

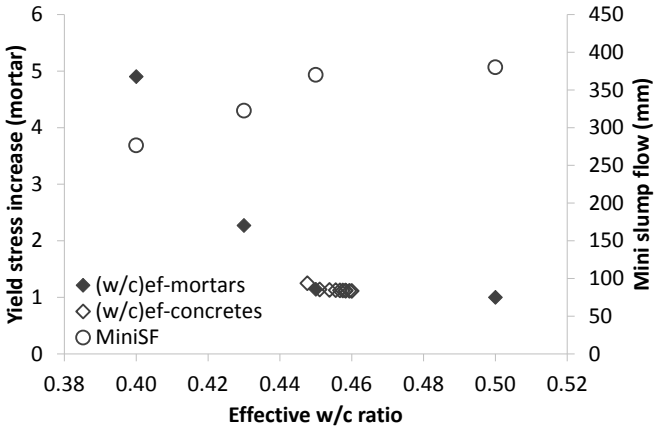

Figure 92. Yield stress increase vs. Effective w/c ratios in mortars and in concretes

Therefore, as the non-compensated water absorption from 10 to 90 min (Figure 25) produces a decrease in the effective w/c ratio, the higher the recycled aggregate percentage, the higher the differences between fresh behaviour of conventional and recycled concretes will be over time. This will be especially significant when the effective w/c ratio decreases under the aforementioned "critical w/c ratio", as it happens for the SCRC with 100% of RCA at 90 min age (Figure 92).

Conclusions

In this research, time-dependent fresh behaviour of self-compacting recycled concrete (SCRC) was studied. Based on the experimental results, the following conclusions can be drawn:

- The production of recycled concrete with additional water to compensate the high water absorption of recycled aggregate and using recycled concrete coarse aggregate up to 20% (substitution in volume) guarantees the self-compacting behaviour of concrete (even until a mix age of 90 min).

- SCRC rheology follows very similar laws as conventional SCC. If the maximum packing fraction of natural and recycled aggregate is similar, the particularity of SCRC is that the effective water to cement (w/c) ratio evolves over time due to the high water absorption of RCA.
- There is a "critical w/c ratio" that depends on the mix proportions. If the evolution of recycled aggregate water absorption generates a non-compensated water that moves the effective w/c ratio down this critical value, great changes in SCRC fresh behaviour will be produced.

Finally, the key step in the SCRC design is to calculate the quantity of extra water necessary to compensate the recycled aggregate absorption during the mixing protocol. This should be selected taking into account the water absorption evolution (that controls the effective w/c ratio) and the final age required to maintain the fresh behaviour.

Acknowledgments

The study is part of two projects: (a) "Industrial Investigation about Concrete for a Sustainable Market" funded by the Innovation Galician Agency; (b) "Robust self-compacting recycled concretes: rheology in fresh state and mechanical properties" funded by MINECO. This work was also made possible by the financial support of INDITEX-UDC 2015 fellowships for international pre-doctoral stays.

References

[8] Silva, R. V.; De Brito, J.; & Dhir, R. K. (2014). Properties and composition of recycled aggregates from construction and demolition waste suitable for concrete production. *Constr. Build. Mater.*, vol. 65, pp. 201-217.

[9] Ferreira, L.; De Brito, J.; & Barra, M. (2011). Influence of the pre-saturation of recycled coarse concrete aggregates on concrete properties. *Mag. Concr. Res.*, vol. 63, n. 8, pp. 617-627.

[10] Billberg, P. (2006). Form Pressure Generated by Self-Compacting Concrete — Influence of Thixotropy and Structural Behaviour at Rest. Doctoral Thesis. School of Architecture and the Built Environment, Division of Concrete Structures Royal Institute of Technology SE-100 44 Stockholm, Sweden.

[11] Khayat, K. H.; Mitchell, D. (2008). Research Description and Findings to Self-Consolidating Concrete for Precast, Prestressed Concrete Bridge Elements. Final Report for NCHRP Project 18-12.

[12] Koehler, E. P.; Fowler, D. W. (2008). In: *Static and dynamic yield stress measurements of SCC*, SCC 2008 Conference Proceedings, Chicago, IL.

[13] Mahaut, F.; Mokéddem, S.; Chateau, X.; Roussel, N.; & Ovarlez, G. (2008). Effect of coarse particle volume fraction on the yield stress and thixotropy of cementitious materials. *Cem. Concr. Res.*, vol. 38, pp. 1276-1285.

[14] González, B.; Martínez, F.; Carro, D.; & Seara, S. (2011). Stress-strain relationship in axial compression for concrete using recycled saturated coarse aggregate. *Constr. Build. Mater.*, vol. 25, n. 5, pp. 2335-2342.
[15] Roussel, N. (2006). Correlation between yield stress and slump: Comparison between numerical simulations and concrete rheometers results. *Mater. Struct.*, vol. 39, pp. 501–509.

Theme 11: Case Studies

SCC Developed for Tunnel End Plugs in a Permanent Nuclear Waste Repository

Tapio Vehmas[1], Markku Leivo[1], Erika Holt[1], Petri Koho[2], and Jari Dunder[2]

[1]VTT Technical Research Centre of Finland Ltd
[2]Posiva Oy

Abstract A unique self-compacting concrete was developed for use in long-term nuclear waste repository tunnel end plugs. The plug's structural design requirements were 50 MPa compressive strength, water tightness under 50mm and durability to withstand a chloride environment in the futures groundwater solutions. For stability of bentonite clay in the repository for thousands of years, the pH of the concrete leachate is required to be below 11. Two applicable mix designs were developed and characterized. A final mix design having a ternary binder composition was selected to be use in a full scale demonstration tunnel end plug at 450 metres underground. Successful demonstration was performed after adjusting the mix design to fulfil the requirements of a batching plant production.

Keywords: *Self-compacting concrete, low-pH concrete, nuclear waste repository, tunnel end plug, mix design development, full-scale demonstration*

Introduction

One of the world first long-term nuclear waste repositories will be constructed into Olkiluoto bedrock in Finland [1]. Concrete plugs are deployed as hydraulic and mechanical barriers in repository tunnel sealing at a depth of approximately 450 metres. The service life of the concrete plug is 100 years, yet the plug is one component of the Engineered Barrier System (EBS) that should protect the environment for hundreds of thousands of years during the storage of spent nuclear fuel. The tunnel end plug is a reinforced concrete structure, having dimensions of approximately 4.5 x 6.5 x 6 metres with a total volume of approximately 150m^3 [2]. The tunnel end plug is cast in two sections due the massive size of the tunnel end plug. Concrete in the plug should be self-compacting because only minimal consolidation is possible during casting. Also the adiabatic temperature rise of the mix design was restricted due the massiveness of the tunnel end plug.

Much of the safety in the long-term nuclear waste repository relies on the stability of bentonite buffer. High pH of traditional concretes endangers the stability of bentonite buffer and therefore the functioning of the total EBS. Low –pH mix designs have been developed to overcome the problem [3].

The materials used in a nuclear waste repository are highly regulated so as to ensure long-term safety [4]. Acceptance of the materials happens through a special procedure that ensures the compatibility of various materials in hundreds thousands years perspective. For example, at Posiva's ONKALO facility, polycarboxylates are forbidden to be used in the repository. From the concrete technology perspective, forbidding polycarboxylates means that today's most common superplasticizers for self-compacting concrete cannot be utilized in the tunnel end plugs. The concrete used in a tunnel end plug should also have low sulphur content.

At least two mix designs for tunnel end plugs exist in the literature, with the primary references being the Swedish tunnel end plug from SKB and the Canadian shaft sealing plug from NWMO [5,6]. A Swedish tunnel end plug has been successfully demonstrated in a vertical EBS, similar to Finland's scenario. The Canadian mix design differs from the Swedish and it has been used for horizontal EBS. The Swedish tunnel end plug mix design utilized a polycarboxylate-based superplasticizer, which is forbidden in Finnish repository. The plasticizer in the Canadian mix design was naphthalene-based, suitable also for a Finnish repository. The Canadian shaft sealing structure differed from the Finnish, making the concrete workability in vertical shaft sealing questionable. However, these two mix designs offered a good starting point for the Finnish tunnel end plug development.

Two potential mix designs for tunnel end plugs were developed. The first one had an identical binder composition of the Swedish tunnel end plug, utilizing Ordinary Portland cement and silica fume. The mix design was labelled as binary mix design, due to its binary binder composition. The other developed mix design was named as ternary mix design due to its three-part binder: Ordinary Portland cement, silica fume and fly ash.

Materials and Methods

Ordinary Portland cement used was CEM I 42.5 MH/SR/LA from Cementa (Anläggningscement, Degerhamn). Silica used was granular Parmix –silica from Finnsementti. Fly ash used was type B4 from Emineral. Limestone filler was purchased from Nordkalk (type SB63). Quartz fillers were from Sibelco Nordic from two quarries, Quartz A from Nilsiä and Quartz B from Kemiö. Aggregates were typical Finnish granitic crushed aggregates (Rudus Oyj), available on-site of the repository. Grading curves of the materials are presented in Figure 1. Laboratory aggregates were also used from VTT's storage to recreate the grading curve of the Swedish tunnel end plug mix design. Superplasticizers used were

polycarboxylate-based Glenium C151 from BASF and naphthalene-based Pantarhit LK(FM) from HaBe. All the materials, except Glenium C151 and limestone, were safety material approved by Posiva Oy.

Mix designs were proportioned according to Compressible Packing Method (CPM) by DeLarrad [7] or the micro-proportioning program developed by Aaro Kohonen Oy in Finland [8]. In the De Larrard's CPM calculation, the desired slump value was set to zero. The beta factor for cement was 0.46, determined according to the procedure described in literature [7]. The Beta value for fillers and aggregates was arbitrary selected for value 0.50. The mix design was calculated with an Excel sheet flow chart according to [7]. The cement content was calculated from the free water volume. Iterative steps of the above described method were performed until the cement content remained constant during the iteration. Laboratory studied mix design was proportioned on the basis of the calculation, expect the binder content was lowered to 200 kg/m^3.

Slump flow was determined according to SFS-EN 12350-5. Plastic viscosity of the concretes was measured with a Contec 5 –viscometer, specially designed for concrete rheology. In the viscosity measurement, large aggregates (16-32 mm) were replaced with 8-16 mm aggregates, because the maximum aggregate size of the measurement was 16 mm. Bleeding and segregation was visually estimated, slight bleeding without aggregate segregation was graded with a +. Bleeding and visual aggregate segregation was graded with ++. If bleeding or segregation was not observed, the mix design was graded as -.

Compression strength, tensile splitting strength and modulus of elasticity were determined according to SFS-EN 12390-3, SFS-EN 12390-6 and SFS 5450, respectively. The standard method SFS-EN 12390-8 was used to determine depth of water penetration. Non-steady state chloride migration coefficient was measured according NT Build 492. The pH-leachate was measured according to method described in SKB R-1202 –report [9]. The medium for pH-leachate measurement was deionized water and simulated Olkiluoto site groundwater.

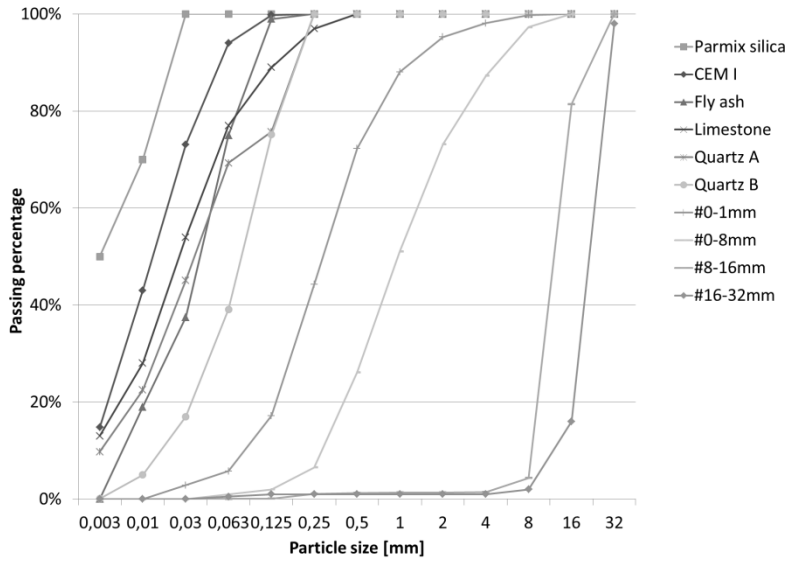

Figure 1. Grading curves of studied materials.

Results

At the beginning in the Finnish development, the Swedish repository concrete described in the literature was repeated with laboratory available aggregates. Concrete flow properties were close to reported, having slump flow 620 mm. Plastic viscosity of the concrete was 65 Pas, measured by the Contec 5 viscometer. Low –pH of the Swedish repository concrete was ensured by the binary composition of ordinary Portland cement and silica fume, using 120 kg/m^3 and 80kg/m^3, respectively.

The next step was to modify the mix design suitable for a Finnish repository. Polycarboxylate-based Glenium C151 –superplasticizer was replaced with naphthalene-based Pantarhit LK(FM). It was observed that equal volumes of 15% Glenium and 40% Pantarhit LK(FM) had roughly equal flow properties. Laboratory available aggregates were replaced with local Olkiluoto on-site available aggregates. The combined grading curve of on-site available aggregates was fitted to the original grading curve with the Excel solver function. In the last phase, limestone filler was replaced with quartz fillers. Quartz fillers were safety material approved for the Finnish repository. Table I summarizes the flow properties of Glenium C151 and Pantarhit plasticized concrete, with laboratory and on-site available aggregates either with limestone or quartz -filler.

Table I. Binary mix design development based on the Swedish recipe.

	SWE	**1**	**2**	**3**
Modification				
Plasticizer exchange	NO	YES	YES	YES
On-site available aggregates	NO	NO	YES	YES
Limestone to quartz filler exchange	NO	NO	NO	YES
Mix design				
CEM I 42,5 MH/SR/LA [kg/m^3]	120	120	120	120
Silica [kg/m^3]	80	80	80	80
Limestone filler [kg/m^3]	370	370	370	-
Quartz filler A [kg/m^3]	-	-	-	260
Quartz filler B [kg/m^3]	-	-	-	110
Laboratory aggregates [kg/m^3]	1600	1600	-	-
#0-1 [kg/m^3]	-	-	500	500
#0-8 [kg/m^3]	-	-	530	530
#8-16 [kg/m^3]	-	-	560	560
Glenium C151 (15%) [kg/m^3]	15	-	-	-
Pantarhit LK(FM) (40%) [kg/m^3]	-	15	15	15
Total water content [kg/m^3]	165	165	165	165
Flow properties				
Slump flow [mm]	620	670	440	500
t50 [s]	10.5	10	-	-
Water/binder -ratio	0.83	0.83	0.83	0.83

Mix design optimization

In order to fulfil the requirements set for repository concrete, mix designs were optimized for the minimum water content. Mix design for the binary binder content was performed with CPM method for zero slump flow. The idea was to obtain optimum fine material grading for concrete which could be further plasticized with plasticizer. It was observed that CPM mix design increased the concrete's workability. After a flowable mix was observed, the coarse aggregate content was maximized with a trial- and error method. Modification was performed by replacing 0-8 mm and 8-16 mm aggregates with 390 kg/m^3 coarse 16-32 mm aggregates. The mix design had high workability with no bleeding or segregation. The next modifications were replacement of limestone filler with quartz filler. After a few modifications, it was observed that single quartz filler was able to replace limestone filler. Only slight water bleeding was observed. At this point the water content was lowered to diminish the water bleeding. It was observed that the total water content 133 kg/m^3 was able to produce a highly workable mix without bleeding. Plastic viscosity of the optimized concrete was 240 Pas, measured by the Contec 5 viscometer. Mix designs are presented in Table II, where mix number 7 presents the final binary mix design composition.

Table II. Binary mix design development based on compressible packing model.

Modification	**CPM**	**4**	**5**	**6**	**7**
Coarsened grading	YES	YES	YES	YES	YES
32mm aggregates	NO	YES	YES	YES	YES
Limestone to quartz filler exchange	NO	YES	YES	YES	YES
Water content reduction	NO	NO	YES	YES	YES
Mix design					
CEM I 42,5 MH/SR/LA [kg/m^3]	120	120	120	120	120
Silica [kg/m^3]	80	80	80	80	80
Limestone filler [kg/m^3]	260	-	-	-	-
Quartz filler A [kg/m^3]	-	185	190	255	256
Quartz filler B [kg/m^3]	-	80	80	-	-
#0-1 [kg/m^3]	240	240	240	225	231
#0-8 [kg/m^3]	740	540	550	520	524
#8-16 [kg/m^3]	720	530	530	500	509
#16-32 [kg/m^3]		390	400	530	541
Glenium C151 (15%) [kg/m^3]	-	-	-	-	-
Pantarhit LK(FM) (40%) [kg/m^3]	15	15	15	15	15
Total water content [kg/m^3]	165	165	155	143	133
Flow properties					
Slump flow [mm]	660	690	670	650	650
Visual segregation and bleeding	-	-	-	+	-
Water/binder -ratio	0.83	0.83	0.76	0.72	0.67

The initial mix design for ternary binder content was received from Aaro Kohonen Oy, related to their work for the plug structural design. It was experimentally observed that the mix design had too low of a water content. In modifications, the binder and water content was increased to include more water into mixture without compromising the water/binder -ratio. It was observed that flowable concrete was not possible to achieve with a constant water/binder -ratio due to the restrictions of the heat development. The next modification was performed to increase the water/ binder -ratio to a maximum tolerable level with maximum binder content. The modification produced a workable concrete. The plasticizer dosage was increased to increase particle dispersion. With increased plasticizer dosage, close to self-compacting concrete flowability was observed. Also only slight water bleeding was observed. Modifications were performed to find the optimum filler content. It was observed that the workability was not affected by increasing the filler and remained fairly constant although the filler content was increased from 88 kg/m^3 to 217 kg/m^3. It was decided that filler content 114 kg/m^2 was sufficient to prevent water bleeding when the plasticizer dosage was slightly lowered. The plasticizer content was further reduced to obtain identical plasticizer dosage as the binary binder mix design. Mix designs are presented in Table III. Mix design 3 was selected for further mechanical- and permeability testing by Posiva Oy.

Table III. Ternary mix design development. Dem = mix design used in tunnel end plug demonstration.

Mix design	0	1	2	3	4	5	Dem
CEM I 42,5 MH/SR/LA [kg/m^3]	91	118	105	105	105	105	107
Silica [kg/m^3]	79	103	91	91	91	91	89
Fly ash B4 [kg/m^3]	73	65	84	84	84	84	85
Limestone filler [kg/m^3]							
Quartz filler A [kg/m^3]			88	114	88	137	114
Quartz filler B [kg/m^3]	200	84					
#0-1 [kg/m^3]	210	207	167	167	167	167	169
#0-8 [kg/m^3]	757	747	785	759	785	736	1026
#8-16 [kg/m^3]	473	467	530	523	530	530	674
#16-32 [kg/m^3]	462	456	392	392	392	392	-
Glenium C151 (15%) [kg/m^3]	-	-	-		-	-	-
Pantarhit LK(FM) (40%) [kg/m^3]	15	15	15	12.6	20	20	23.5
Total water content [kg/m^3]	96	116	135	133	135	135	149
Flow properties							
Slump flow [mm]	-	-	425	550	640	660	600
Visual segregation and bleeding	-	-	-	-	+	-	-
Water/binder -ratio	0.40	0.41	0.48	0.48	0.48	0.48	0.53

Table IV presents the mechanical properties and permeability indicators for the developed mix designs.

Table IV. Mechanical properties, permeability and pH of the developed mix designs, at the age of 91d.

	Binary mix design	Ternary mix design	Target values
Compressive strength [MPa]	91.5	79.5	>50
Splitting tensile strength	5.6	4.5	3.2
Modulus of elasticity [GPa]	37.4	34.2	34
Water tightness [mm]	4.0	5.0	<50
Non-steady state chloride migration coefficient [m^2/s]	$2.1*10^{-12}$	$2.8*10*^{-12}$	(min)
pH leachate in ion exchanged water	11.4	11.4	<11
pH leachate in simulated Olkiluoto groundwater	10.4	10.4	<11

After VTT laboratory mixture development and performance verification, the final binary and ternary recipes were re-produced in the ready-mix suppliers laboratory and then at their batch plant. Three on-site mock-up castings were done at Posiva's ONKALO repository, to verify mix design proportions and construction techniques before the actual plug casting. From these mock-up trials, additional quality control samples were also taken for concrete performance verification of strength,

watertightness and pH leachate. Based on these factory and mock-up demonstrations, the final recipe was selected to be the Ternary mix for casting the 150 m^3 full-scale tunnel end plug. Mix design of the full-scale tunnel end plug with 16mm maximum aggrerates is presented in Table III with label Dem. It was decided that the first 20 m^3 and last 20 m^3 would be cast with a maximum aggregate size of 16 mm, due to the conjected reinforcement around the plug circumference, while the centre section of the plug had maximum 32 mm aggregate.

The full scale concrete tunnel end plug was cast in two sections during July and September 2015. For each casting, there were 20-25 truckloads of 4m^3 each delivered at 45 minute intervals over a 10 hour period to 450 m underground. A total of 172 m^3 low-pH concrete was used, comprised of 78 m^3 in the first plug section and 94 m^3 in the second section. The concrete was placed by pumping at increasing high intervals in the plug. No mechanical vibration was used. The uppermost or last hole in the formwork had concrete pumping or casting with an applied pressure of 0.5 bars maintained for 30 minutes.

The plug sections were instrumented with 67 sensors to measure early age and long-term performance, including temperature measurements. Prior to placement, air content, density and temperature and slump flow were measured at both the factory and on-site to ensure consistency and quality. The formwork pressure was measured during emplacement. Concrete samples were taken for measurements of compressive strength, watertightness and pH leachate at 28, 91 and 365 days after casting. 1 m^3 quality control cubes were also cast underground beside the plug to be used for further quality control sampling for each mix (16 and 32 mm aggregate sizes, for both plug section castings).

The average slump flow during quality control testing underground was 600mm and air content 2.0%. The maximum temperature of the plug after casting was 43°C at approximately 3 days. For the first concrete plug section, the 91 day average results were: compressive strength 85.8 MPa, 3.2 mm watertightness, and pH of 10.8 in groundwater. No problems were encountered during the casting procedure, with very uniform self-compacting concrete achieved having a very low water-content and meeting demanding conditions for casting.

Discussion

Both studied mix designs fulfilled the performance requirements. Compression strengths greatly exceeded the requirements. Water tightness of the mix designs was good. Water tightness was measured for 4-5mm whereas the requirement was <50mm. Non-steady state chloride migration coefficients were 2.1*10-12 – 2.8*10-12 which were tenfold lower than typical values in concrete. In laboratory tests, the pH of concrete leachate did not fulfil the requirements in ion exchanged water to be under 10.5. However, in simulated Olkiluoto groundwater, the pH

values were below 10.5 after 91 days. In demonstration tunnel end plug the pH was 10.8 after 91 days.

Successful full-scale tunnel end plug demonstration was performed at 450 metres deep underground. Before the demonstration, the concrete production in a batching plant was further studied. On the basis of batching plant experiments, the plasticizer content of the mix design was increased. It is typical in concrete technology that changes in the mix design have to be performed when the production system is changed from laboratory to a batching plant. 172 m^3 of self-compacting concrete was then successfully emplaced within two plug sections during summer 2015. Quality control tests have shown that the final product exceeded expectations and fulfilled all requirements for safe tunnel sealing of a spent fuel repository.

Conclusions

Two mix designs were developed for nuclear waste repository tunnel end plugs. The mix designs were developed using two different mix design method. Both mix designs were optimized with laboratory trials and then within factory trials and mock-up castings prior to the full-scale plug emplacement. After the laboratory optimization, the studied mix designs had quite identical particle size distribution, although the material composition varied greatly.

Both developed mix designs fulfilled the performance requirements. The mix design with ternary binder (cement, silica fume and fly ash) was selected on full-scale underground demonstration, using two different maximum aggregate sizes of 16 and 32 mm. The mix design was further adjusted, based on batching plant trials. Full scale tunnel end plug demonstration was performed successfully during July and September 2015, with casting of 172 m^3 of self-compacting low-pH concrete.

The results of this work are being used by Posiva Oy, the radioactive waste management organization of Finland, to demonstrate to the safety regulatory authority their readiness to being operation of a spent fuel repository in the early 2020s. The results were the first full-scale in-situ demonstration of the engineered barrier system (EBS) construction at Olkiluoto. The outcomes of the plug concrete development and construction are used to finalize the tunnel end plug design and construction methodologies for safe and reliable management of nuclear waste for permanent geological disposal.

Acknowledgement

The research leading to these results has received funding from the European Union's European Atomic Energy Community's (Euratom) Seventh Framework

Programme FP7/2007-2013 under Grant agreement no 323273, the DOPAS project.[10]

References

[1] Posiva Oy (2011), *Final disposal of spent nuclear fuel in Olkiluoto*, yleisesite_2011_EN, Posiva Oy Olkiluoto FI-24160 EURAJOKI

[2] Keto, P.(ed), Hassan, M., Karttunen, P., Kiviranta, L., Kumpulainen, S., Korkiala-Tanttu, L., Koskinen, V., Jalonen, T., Koho, P., Sievänen, U. (2012), *Backfill Production Line*, Posiva 2012-18, June 2013

[3] Holt, E., Leivo, M., Vehmas, T. (2014), *Low-pH Concrete Development for Tunnel end plugs used in Nuclear Waste Containment*, Concrete Innovation Conference 2014 (CIC2014), Oslo, June 2014

[4] Posiva Oy. (2014) *Safety Case for the Disposal of Spent Nuclear Fuel at Olkiluoto FEP Screening and Processing*, report 2014-3, Posiva Oy

[5] Vogt, Lagerblad, Wallin, Baldy, Jonasson (2009). *Low pH self-compacting concrete for deposition tunnel plugs*, Svensk Kärnbränslehantering AB, Stockholm, Sweden, SKB report R-09-07

[6] Martino, J., Dixon D., Holowick B., Kim C-S. (2011). *Enhanced Sealing Project (ESP): Seal Construction and Instrumentation Report*, Atomic Energy of Canada Limited, NWMO APM-REP-01601-0003

[7] De Larrard F., (1999). *Concrete mixture proportioning a scientific approach*, *Modern concrete technology 9*, E & FN Spon, 11 New Fetter Lane, London.

[8] Paukku, Meuronen (2013): *The Basis of the ternary mix design of the plug concrete*. Aaro Kohonen FMC group, project number 2001292

[9] Alonso, M., Garcia Calvo, J., Walker, C., Naito, M., Pettersson, S., Puigdomenech, I., Cunado, M., Vuorio, M., Weber, H., Ueda, H., Fujisaki K., (2012): *Development of an accurated pH measurement methodology for the pore fluids of low pH cementitious materials.* SKB R-12-02, Svensk Kärnbräslehantering AB

[10] Hansen J., Holt E. and Palmu M. (2013): *DOPAS - Full scale Demonstrations of Plugs and Seals.* Proceedings of the Euradwaste '13 Conference by the European Commission, Vilnius, Lithuania. 14-16 October 2013, pp. 341-347.

The Use of Self-Consolidating Concrete in the Construction of Precast-Prestressed Beams for the Border Highway West Extension Loop 375 in El Paso Texas

Caroline Talbot Ph.D., P.E.,FACI[1], Martin Aldarette[2] and Adam Mainka[3]

[1] Key Account National Technical Director, The Euclid Chemical Company
[2] Q.C. Manager, Jobe Materials
[3] Director of Operation, Heldenfels Entreprises

Abstract About 80000 yd^3 of Self Consolidation Concrete is being used for the construction of 1300 beams for the extension of the Border Highway in El Paso over the next 3 years. The project started during the summer of 2015. A joint-venture between Heldenfels enterprises and Jobe materials was formed and an optimized mix design with a slump flow target of 25-26 inch diameter and 6000 psi at 14 hrs. was submitted using an admixture system provided by The Euclid Chemical Company. The article will present the mix design, materials properties and quality control measures put in place to ensure performance and proper productivity. Pictures of finished product and video taken during production will be presented.

Keywords: *Self-Consolidating Concrete, Ordinary Concrete, Aggregate gradation, Quality Control*

Introduction

About 80000 yd3 of Self Consolidation Concrete is being used for the construction of 1300 beams for the extension of the Border Highway in El Paso over the next 3 years. The project started during the summer of 2015. A joint-venture between Heldenfels enterprises and Jobe materials was formed and an optimized mix design with a slump flow target of 25-26 inch diameter and 6000 psi at 14 hrs. was submitted using an admixture system proposed by The Euclid Chemical Company.

The article will present the mix design, materials properties and quality control measures put in place to ensure performance and proper productivity. Pictures of finished product and video taken during production will be presented.

Figure 1. Production site

Parties Involved

The following team members collaborated to achieve success on this project.

Texas DOT.: Owner
Heldenfels.:Precast/Prestressed Contractor
Jobe Materials- Concrete Supplier;
The Euclid Chemical Company- Admixture Supplier;
Heldenfels-Jobe– Laboratory/Quality Control

Materials

All materials used had to be tested by the testing laboratory and approved per the established specifications from the Texas DOT before the mix could be developed and approved for used in the beam. A representative from the Texas DOT was

present for the casting of a test beam and approved the mix performance according to specifications. Table 1 and 2 present the Coarse Aggregate blend (top size ¾ and ½") and Sand gradation respectively. The aggregate blend was optimized to give the best particle packing possible with this set of material in order to be able to use the least amount of cementitious material and still meet performance criteria. The moisture content of the aggregates was monitored with probes and by hand (to ensure that the probes are reading well) a few times during every daily pour. Table 3 presents the mix designs used during the construction. Note that the cement used was a Type III manufactured by GCC of America cement plant in New Mexico, and the fly ash was a Type F with 0.21% LOI and a specific gravity of 2.29 as manufactured by Headwaters. Table 3 presents the mix design used.

Table I. Coarse Aggregates (ASTM C33)

	U.S. sieve size	Aggregate ¾"	Aggregate ½"
Specific Gravity		2.696	2.563
Absorption %		0.95	1.05
	1.5 "	100%	100%
	1"	100%	100%
	3/4	99%	100%
	½	98%	99%
	3/8	83%	98%
	#4	13%	73%
	#8	1%	14%
	#16	-	5%
	#30	-	3%
	#50	-	2%
	#100	-	1%

Table II. Fine Aggregate (ASTM C33)

Specific Gravity	2.6
Absorption %	0.7
U.S. sieve size	% Passing
3/8"	96%
#4	85%
#8	76%
#16	66 %
#30	49 %
#50	16%
#100	2%
#200	0%

Table III. Mix Designs and Slump-Flow requirement

	Summer kg/m^3 (lb/yd^3)	Winter kg/m^3 (lb/yd^3)
W/C	0.35	0.33
Water	150 (250)	150 (250)
Type III Cement	315 (530)	335(564)
Flyash	107 (180)	112 (188)
Coarse Aggregate	872 (1470)	830 (1400)
	190 (320)	178 (300)
Sand	789 (1331)	650 (1366)
Plastol SCC HRWR mL/100 kg (oz/cwt)	780-978 (12-15)	978 (15)
Eucon NR Retarder mL/100 kg (oz/cwt)	65-260 (1-4)	Replaced by accelerator 15-30 when needed
Visctrol VMA ml/m^3 (oz/yd^3)	As needed	As needed
Slump or **Flow mm (in)**	600-650 (24-26)	600-650 (24-26)
T50 (20) sec	3-7	3-7
Compressive Strength specified psi (Mpa)	4000-6000 (28-41)	4000-6000 (28-41)

The retarder-water reducer used was a lignin-corn syrup blend, the superplasticizer (HRWR) was a polycarboxylate type and the viscosity enhancing admixture (VMA) was polysaccharide chemistry.

Quality Control Method Used

During production, the first 3 loads delivered were tested for slump flow, J-ring, T50(20), concrete temperature and ambient temperature, and every 5 loads thereafter. The T50 ran around 3.5-4 sec during the summer but during the winter with more cement and lower W/C ratio combined with cold temperature, it went up to 6-6.5 sec. It was hoped not to have to use accelerators but difficulties to meet compressive strengths in time proved otherwise. Tests were run with the use of accelerators instead of a lower W/C and T50 times back to 4 sec were achieved. Compressive strengths were monitored using a Sure-Cure system as shown in fig.2 to make sure the cylinders are curing at the same rate as the temperature generated in the beam. When the required strength is reached, the release and pre-stressing operations are done. Fig.3 shows graphs obtained during the summer versus the winter. It can be observed on the winter graph that a drastic drop in concrete

temperature occurs when the concrete hits the forms and without accelerators the concrete cannot reach the required heat generation and therefore strengths in time on its own. The de-molding operations had to wait 24 hours even if the concrete temperature at delivery was maintained through water and aggregate heating and blankets were used.

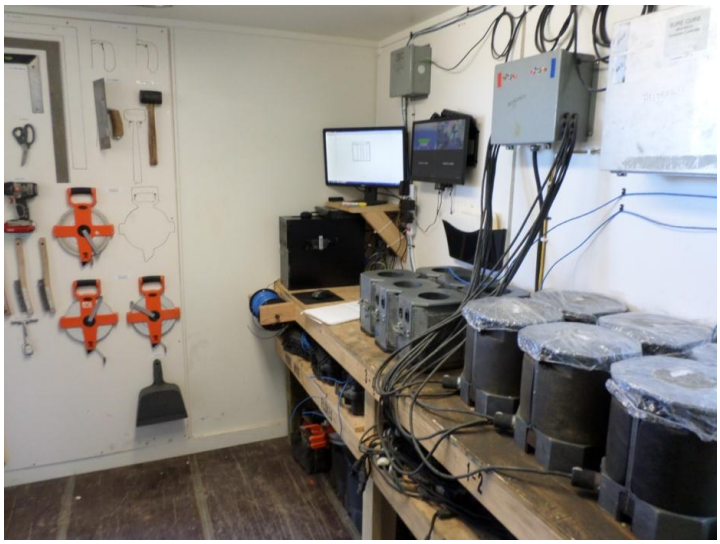

Figure 2. Curing Temperature/Compressive Strength Monitoring System Sure-Cure

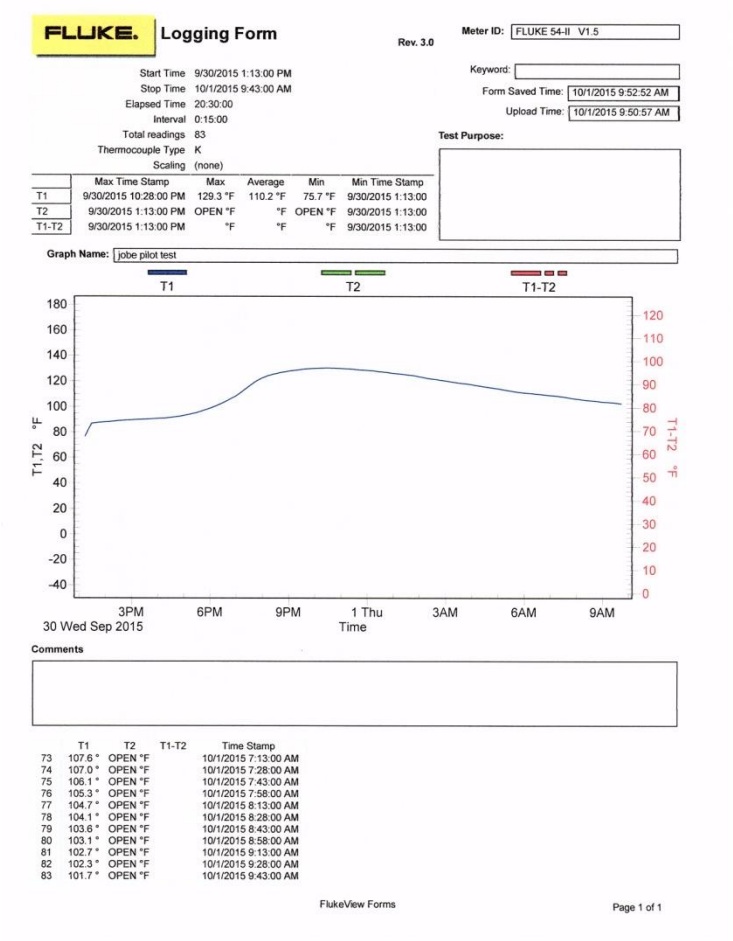

FLUKE. **Logging Form** Rev. 3.0

Meter ID: FLUKE 54-II V1.5

Keyword:

Form Saved Time: 10/1/2015 9:52:52 AM

Upload Time: 10/1/2015 9:50:57 AM

Start Time 9/30/2015 1:13:00 PM
Stop Time 10/1/2015 9:43:00 AM
Elapsed Time 20:30:00
Interval 0:15:00
Total readings 83
Thermocouple Type K
Scaling (none)

Test Purpose:

	Max Time Stamp	Max	Average	Min	Min Time Stamp
T1	9/30/2015 10:28:00 PM	129.3 °F	110.2 °F	75.7 °F	9/30/2015 1:13:00
T2	9/30/2015 1:13:00 PM	OPEN °F	°F	OPEN °F	9/30/2015 1:13:00
T1-T2	9/30/2015 1:13:00 PM	°F	°F	°F	9/30/2015 1:13:00

Graph Name: jobe pilot test

Comments

	T1	T2	T1-T2	Time Stamp
73	107.6 °	OPEN °F		10/1/2015 7:13:00 AM
74	107.0 °	OPEN °F		10/1/2015 7:28:00 AM
75	106.1 °	OPEN °F		10/1/2015 7:43:00 AM
76	105.3 °	OPEN °F		10/1/2015 7:58:00 AM
77	104.7 °	OPEN °F		10/1/2015 8:13:00 AM
78	104.1 °	OPEN °F		10/1/2015 8:28:00 AM
79	103.6 °	OPEN °F		10/1/2015 8:43:00 AM
80	103.1 °	OPEN °F		10/1/2015 8:58:00 AM
81	102.7 °	OPEN °F		10/1/2015 9:13:00 AM
82	102.3 °	OPEN °F		10/1/2015 9:28:00 AM
83	101.7 °	OPEN °F		10/1/2015 9:43:00 AM

FlukeView Forms

Page 1 of 1

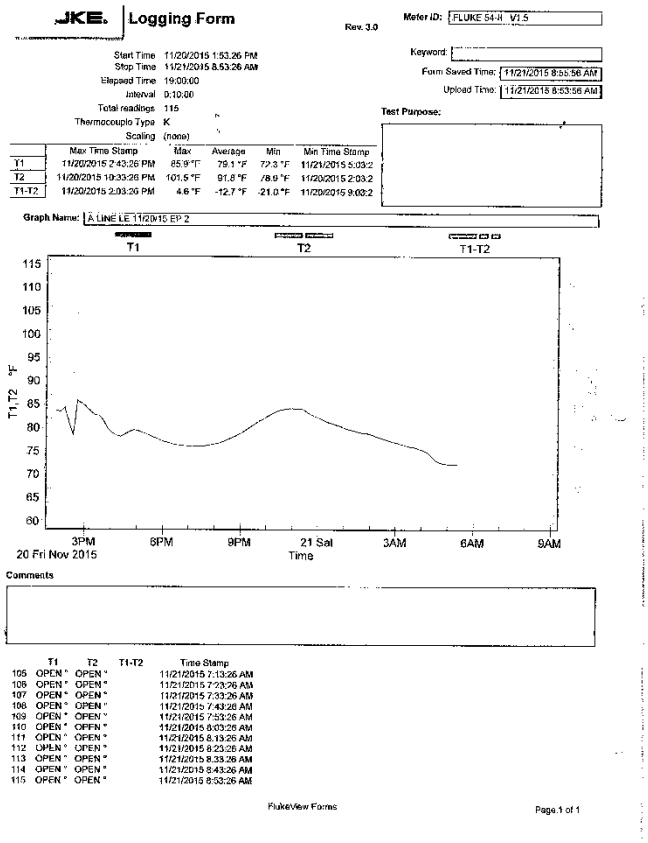

Figure 3. Temperature Monitoring System (Summer versus Winter)

Figure 4. Slump-Flow testing as observed by DOT representative

Figure 5. Casting operation as observed by DOT representative

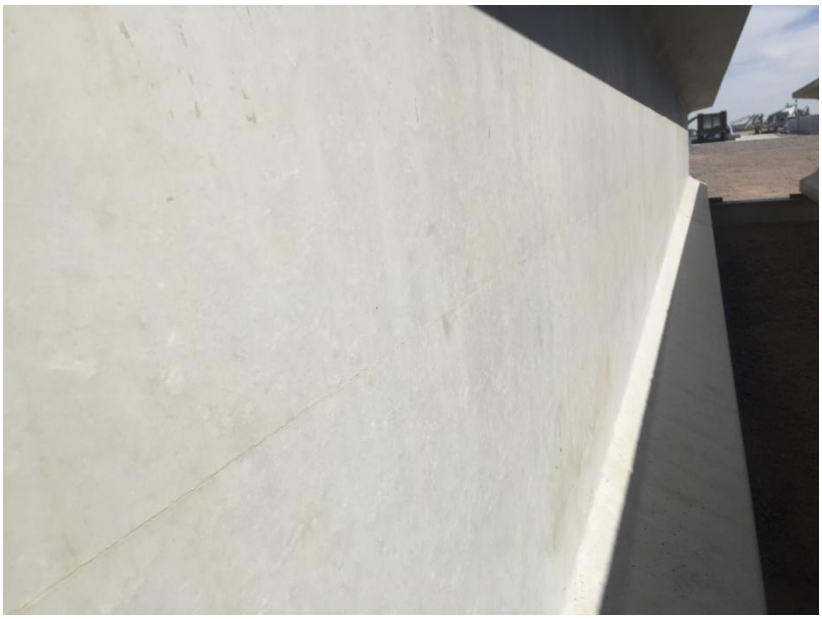

Figure 6. Finished product

Sealed-Space-Filling SCC: A Special Application of SCC in High Speed Rail of China

Yuan Qiang[1], Long guangcheng*[1], Liu Zanqun[1], Ma kunlin[1], Xie Youjun[1], Deng Dehua[1], Huang Hai[1,2]

1. School of Civil Engineering, National Engineering Laboratory for High Speed Railway Construction, Central South University, Changsha 410075, China
2. China Tiesiju Civil Enegineering Group CO.,LTD, Hefei, 230000, China

Abstract Sealed-space-filling self-compacting concrete (SSFSCC) is used in China rail track system (CRTS) III slab track of high speed rail, which has been originally developed in China recently. Millions of cubic meter of SSFSCC for the construction of CRTS III slab track could be consumed in China. SSFSCC layer sits between slab and track bed, and is required to have strong bonding with the upper slab. Compared with normal SCC, SSFSCC presents some prominent characteristics which were addressed in this study. In order to meet the structural requirements of filling layer, the appropriate properties and their testing methods of the fresh SSFSCC were proposed. The construction technology and cases were introduced as well.

Keywords: *CRTS III slab track, High speed rail, self-compacting concrete*

Introduction

High-speed rails (HSR) refer to the rail operated by high-speed trains with much higher speed than conventional trains. According to Chinese definition, newly built lines with speed higher than 250km/h, and upgraded lines with speed higher than 200 km/h can be classified into HSR [1]. This is consistent with European and Japanese definitions [2-4]. China started researches on HSR technology much later than technology leading countries, such as Japan, German and France. The first HSR line (Shengyang- Qinghuangdao) in China with a speed of 200km/h was put into commercial use in 2003, which is 40 years later than the world's first HSR (Tokaido Shinkansen) opened in Japan in 1964. On July 2008, the first HSR line (Beijing–Tianjin) with a running speed of 350 km/h was put into operation, which opens the period of 'rapid HSR development' of China [5]. Since then, Chinese government embarked on an ambitious campaign to build the largest HSR network. The total lines with speed higher than 250km/h in the world, including lines under construction and in operation, are 35708 km. China has the largest HSR networks in the world (19057km), accounting for 53% of the world total [6, 7], and including almost 10000km Passenger- Dedicated Lines with the speed over 300km/h. Through numerous systematic researches and engineering practices, China has become a technology leading country in HSR.

For the past decades, two types of HSR technology have been developed, i.e. wheel-rail technology and Magnetic levitation (Maglev). The former one is most widely used around the world. In the case of Maglev, China was the first country commercialized Maglev. With the technology of German corporations, the Shanghai Maglev Train became the world's first commercially operated high-speed maglev in 2004. Both China and Japan are dedicating to the study of Maglev technology. Japan will build a new line connecting Shinagawa and Nagoya with high-speed Maglev [8, 9], and planned to be open in 2027. China is building a new line with moderate-speed Maglev in Changsha, and planned to be open in 2016 [10]. Track form of HSR based on wheel-rail technology is the subject of this contribution.

Ballastless track has been widely implemented in HSR around the world [11]. Despite of high initial investment and noise problems, it has obvious advantage over ballast track: (1) increase capacity, (2) increase speed, (3) reduce maintenance and life cycle costs, (4) reduce the number of track maintenance operations and thereby increase safety [12]. In order to implement ballastless track wider and better, many countries are developing new ballastless track from [11-14]. For the last decade, China has established China Rail Track System (CRTS):

- CRTS I double-block ballastless track
- CRTS II double-block ballastless track
- CRTS I slab ballastless track
- CRTS II slab ballastless track
- CRTS III slab ballastless track

The first four types of track are developed by Chinese railway companies based on the transferred technology from Germany and Japan. The last one is independent innovative technology by Chinese railway companies. CRTS III slab ballastless track has been implemented in the HSR of circa 900km, including Cheng-guang line, Wuhan metropolitan area intercity line, Panjing-Yingkou line, and Zhengzhou-Xuzhou line [14-17]. Thousands km of HSR lines in planning are going to be built in the near future, and CRTS III slab ballastless track will be implemented in the newly built HSR lines.

CRTS III slab ballastless track

The structure section and layout of CRTS III slab ballastless track is shown in figure 1 [15]. The track form consists of four layers, which are, from top to bottom, prefabricated prestressed-slab, self-compacting concrete layer, isolated geotextile layer, base plate. The SCC layer is cast in-situ, and is required to have strong bonding with the upper prefabricated slab, and thus the two layers function as a composite plate. The loadings of train are transferred to the roadbed by the composite plate. That is to say the interface between upper prefabricated slab and cast-in-place bottom SCC should be strong and durable enough.

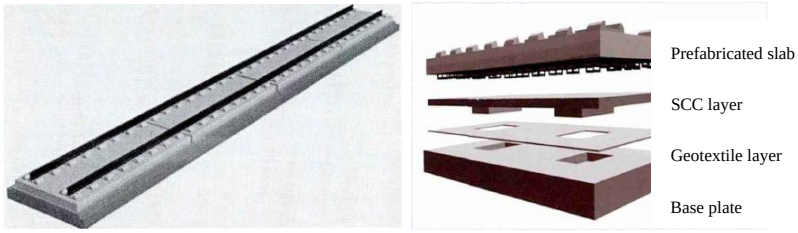

Figure 1. The structure section and layout of CRTS III slab ballastless track [15]

It can be seen from Figure 1 that SSFSCC are cast into the chamber between prefabricated slab and roadbed, which is a sealed space with some exhaust holes. Compared with normal SCC, SSFSCC presents some prominent characteristics:

1) During the construction of CRTS III slab ballastless track, SSFSCC is grouted into a flat, narrow and closed space with the dimension of 90mmx 2500mmx 5600mm. During the process of flowing, filling and resting, bleeding, segregation, surface settlement and instability of air bubble may happen to SSFSCC. With careful design of SCC, bleeding, segregation, surface settlement and instability of air bubble can be reduced to an acceptable level for normal scenario. For a formwork with upper side open to atmosphere, a slight bleeding, surface settlement and air bubble floating of SCC is acceptable. Slight water bleeding and air bubble floating can be covered by finishing. However, in the case of filling a flat, sealed and narrow space, no finishing process is allowed for the upper surface of SSFSCC, and the upper face of SSFSCC is required to have strong bonding with prefabricated slab and those defects of SSFSCC should be minimized to secure good bond (see figure 2).

Figure 2. The weak surface of SSFSCC layer after removing prefabricated slab

2) There is a flexible geotextile layer under the SSFSCC layer. During the casting of SSFSCC, it flows on the geotextile layer. It increases the flow resistance. In addition, geotextile may absorb the water from SSFSCC, and affect the flow of SSFSCC.

3) A HSR line is hundreds of kilometer, and it is usually one time completion. Construction sites along HSR line may extend hundreds of km, and various raw materials will be used, they may show large differences in properties and compositions. It puts forward a challenge to the quality control because of the variation in local raw materials.

Due to the above-mentioned characteristics, SSFSCC for CRTS III slab ballatless track is different from normal SCC, and put forward special requirements for SSFSCC.

Properties requirement

Properties of hardened SSFSCC

The main functions of SSFSCC layer are: 1) position adjustment during construction, 2) work with slab as a composite plate transferring the train loading. The track form implements a concept of "decreasing stiffness from top to down". In order to fulfill its function, the hardened properties of SSFSCC have been proposed [18], as shown in table 1.

Table I. Properties requirement of hardened SSFSCC for CRTS III slab ballastless track (56 days)

Properties	Value
Compressive strength, (MPa)	≥40.0
Flexural strength, (MPa)	≥6.0
Elastic modulus, (GPa)	30-38
6-h charge passed, (c)	≤1000
Spalling under salt solution freezing and thawing test, (g/m^2)	≤1000
Shrinkage, ($\times 10^{-6}$)	450

Properties of fresh SSFSCC

Fresh SSFSCC needs to meet the following requirements:

- There are steel bars in the chamber, and SSFSCC needs to be able to pass steel bar readily.
- The sealed chamber is flat, narrow and closed. SSFSCC needs to have very good filling ability.
- Segregation resistance ability is required.
- Bleeding resistance ability is also required.
- Air stability is required.

Based on the specified conditions of CRTS III slab track, a set of testing methods has been established. In order to specify the parameters of each test, a comprehensive laboratory tests and full scale job-site tests have been carried out. The properties requirements of fresh SSFSCC for CRTS slab ballastless track is proposed in table 2.

Table II. Properties requirement of fresh SSFSCC for CRTS III slab ballastless track

Properties	Value
Slump Flow, (mm)	610-650
Flow rate, $T_{50,}$ (s)	3-7
J-ring, $B_{J,}$ (mm)	≤18
L-box	≥0.9
Bleeding (%)	0
Top surface paste thickness(mm)	≤7
Expansion rate (%)	0-1.0

Construction technology

As stated above, SCC is cast into the sealed space between prefabricated slab and base plate in place. The construction procedure of CRTS III slab track is described in figure 3.

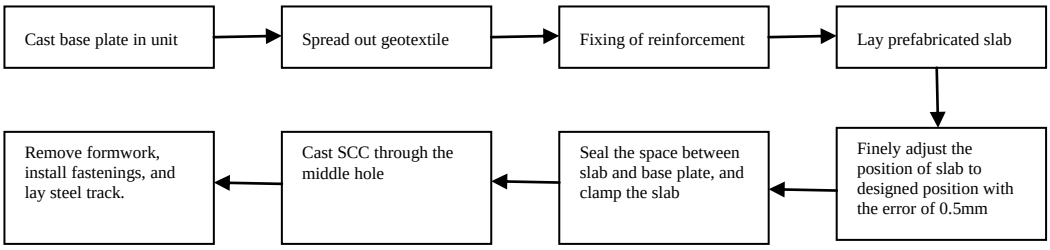

Figure 3. Construction flow chart of CRTS III slab track

With regard to casting SCC, there are several important requirements:

1) Casting speed of SCC. The SCC flows in the sealed space may be in two different ways (see figure 4). Mode 1, the SCC is very flowable or casting speed of SCC is slow. SCC first spread out on the base plate, that is to say the profile of SCC has no contact with upper surface at the beginning. The surface of SCC elevates steadily until fresh SCC has full contact with slab. In this scenario, the air in the sealed space cannot be totally squeezed out, and some big air bubbles are

readily entrapped in the interface between slab and base plate. Mode 2, the SCC is not highly flowable or casting speed of SCC is fast, the profile of SCC has contact with upper and bottom faces during the flowing of SCC. The air in the sealed space can be squeezed out to its largest extent, and no air bubble could be entrapped in the interface. Therefore, mode 2 is used to cast SCC of CRTS III slab track. To strike the balance of flowability and casting speed of SCC is crucial for casting SSFSCC.

a） Mode 1. SCC first spread out, and then elevates the surface until in touch with Slab. In this way, big air bubbles may be entrapped in the interface.

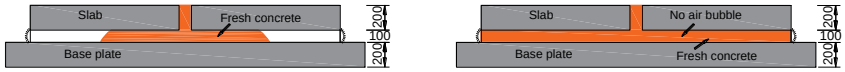

b） Mode 2. SCC has full contact with upper and bottom surfaces to squeeze out air to its largest extent. In this way, almost no air bubbles may be entrapped in the interface.

Figure 4. Two different flow modes of SSFSCC

(2) Do not disturb slab. The slab has been finely adjusted to its design position with high accuracy, and the position has to be maintained during casting SCC. However, in order to cast SCC in mode 2, the SCC height in casting hole has to be high to maintain pressure on SCC. The slab can be lifted up easily. Thus, some clamps are designed to hold slab still, as shown in figure 5. However, if the height in casting hole is too high, a relatively large deformation of the clamp is inevitable, and the position of slab may be changed beyond acceptance. The rheological behavior of SCC, SCC height in casting hole and the clamps collectively affect the position of slab. How to reach the balance is a little tricky. In order to replace all the air in the sealed place with fresh SCC, there are some exhaust holes in the mode. A small amount of SCC is allowed to flow out of the sealed place through exhaust holes, this indicates that air has been totally squeezed out. The quality of SCC in the

sealed place can be judged from the leaking SCC and observation holes, as shown in figure 5.

Figure 5. Full-scale experiment of SSFSCC construction

The quality control of SSFSCC directly affects the quality of CRTS III slab track. Apart from a set of standardized construction procedures, the robustness of SCC to the variation in water content, cement composition and aggregates is of great importance. This involves the compatibility of SP with cement and the application of VEA. The former one is beyond the scope of this paper, and a novel VEA is used to increase the robustness of SCC effectively.

Concluding remarks

SSFSCC is a new application form of SCC and has stricter requirements comparing to normal SCC. This type of concrete will be used in thousands of Km of HSR, and consumes millions of cubic meter concrete. It presents some prominent characteristics.

References

[1] http://www.gov.cn/zwgk/2013-09/06/content_2482594.htm
[2] TSI HS Infrastructure, 2002. Technical Specification for Interoperability

(TSI) Relating to the Infrastructure Subsystem of the Trans-European High-Speed Rail System. EU Commission, Brussels.
[3] Givoni, M., 2006. Development and impact of the modern high-speed train: a review. Transp. Rev. 26 (5), 593–611.
[4] Oskar Froidh, Design speed for new high-speed lines, Journal of Rail Transport Planning & Management 4 (2014) 59–69
[5] Jingjuan Jiao a,b, Jiaoe Wanga,c,, Fengjun Jin a, Michael Dunford. Impacts on accessibility of China's present and future HSR network. Journal of Transport Geography 40 (2014) 123–132.
[6] http://www.uic.org/IMG/pdf/20140901_high_speed_lines_in_the_world.pdf
[7] http://cn.chinagate.cn/economics/2012-12/20/content_27468574_7.htm.
[8] Sato, Y., Briginshaw, D., 2014. Japan: first Hokuriku trains take to the tracks. Int. Railway J. 54 (2), 38-41.
[9] https://en.wikipedia.org/wiki/Shinkansen#Maglev_.28Chuo_Shinkansen.29.
[10] http://www.xxcb.cn/event/changsha/2014-05-06/8917330.html
[11] Pierre-Etienne Gautier. Slab track: Review of existing systems and optimization potentials including very high speed. Construction and Building Materials 92 (2015) 9-15.
[12] Fumey et al., Ballatless tracks: application and experience with ballastless tracks, UIC report, UIC (International Union of Railways); 2008
[13] I. Robertson, C. Masson, T. Sedran, F. Barresi, J. Caillau, C. Keseljevic, J.M. Vanzenberg. Advantages of a new ballastless trackform. Construction and Building Materials 92 (2015) 16-22.
[14] Lu chunfang Jiang Cheng, Wang Jijun et al. Study on the technology of CRTS III slab ballastless track for high speed railway. Research report, China academy of railway science, 2014.9.
[15] Zhao Youming, Ye Yangsheng, Wang Jijun, Jiang Cheng, Wang Meng, The development and application of the independent-innovative of CRTS III slab ballastless track. Railway Technique Innovation. 2015.2, 40-43.
[16] Yan Hua, Li Baoyou, Yang Minghui et al. Technical report of CRTS III slab ballastless track of Chengdu-Dujiangyan rail, Research report, Chengdu, China Railway Eryuan Engineering Group CO. LTD , 2010.
[17] Wei Hedao, Research on the Structure Design of New Unit Slab Ballastless Track on the Zhengzhou-Xuzhou Railway Passenger Dedicated Line. Master thesis, Central South University, 2013.
[18] China Railway Company. Provisional technical requirements for self-compacting concrete for CRTS III slab ballastless track of high speed railway. 2013. 10. Beijing.

Self-Consolidating Concrete Case Study: The Ryman Auditorium, Nashville, TN

Amanda Schweighardt

Irving Materials, Inc.

Abstract Irving Materials, Inc (**imi**) was approached by a local contractor with a request to supply a concrete mix with specific properties suitable for a unique architectural design. The project included an expansion of the Ryman Auditorium incorporating walls with the aesthetics of traditional rough-cut lumber created by the use of ready mix concrete. The requirements included a highly fluid concrete design with the ability to self consolidate. These characteristics accommodated the defined slope and window openings within the walls. Based on the aforementioned design parameters, **imi** utilized local materials to create a durable and visually pleasing concrete mix. The combination of materials yielded a mix capable of reaching 26" to 30" spreads allowing it to flow into the confined spaces and intricate detailing of the lumber throughout the wall forms.

Keywords: *Ryman, SCC, imix, walls, quality*

Figure 1. One of the completed rough-cut lumber formed walls with sign.

HISTORY

Constructed in 1892, the Ryman Auditorium located in Nashville, Tennessee has a rich history filled with musical performances, presidential speeches, and theatrical productions. Famous musicians and performers, including an appearance by President Theodore Roosevelt have graced the stage. Last fall, the Ryman announced a revitalization plan to the main entrance of the auditorium. This decision led to a $14 million expansion and renovation that included restaurant and retail establishments with Nashville-based RC Matthews as the General Contractor.

PROJECT SCOPE

The connection to the auditorium's roots in country music led to the design of exposed concrete walls constructed with form materials that mirrored rough-cut lumber. The desire for detail established a need for concrete that could flow and fill voids while achieving the wood grain appearance. This fact dictated the use of self-consolidating concrete **(SCC).** In addition to textural requirements, black onyx liquid color was specified in order to match the appearance and color scheme of the existing structure.

Not only was the aesthetic value an important consideration in choosing **SCC**, one of the approximate 60' long by 12" wide walls contained six 8' long windows. The

space underneath the windows closest to the original structure began at less than 12" to grade and increased to approximately 4' with spacing between the windows at around 2'. Utilizing traditional means of consolidation was not a feasible alternative for eliminating voids underneath the windows.

THE CONTRACTORS PERSPECTIVE

SCC gave the contractor a vital means to meet the multiple requirements for the exposed concrete walls. "Self Consolidating Concrete **(SCC)** was our only option for such a challenging project, as it was specified by the architect and met the stringent design criteria of the project" said project manager Bob Giese**. "** ***SCC*** *provided us the flexibility to provide a mirrored look to the rough texture of the wooden forms and the random pattern of those forms , giving the onyx colored concrete a rustic feel consistent the Ryman's design."*

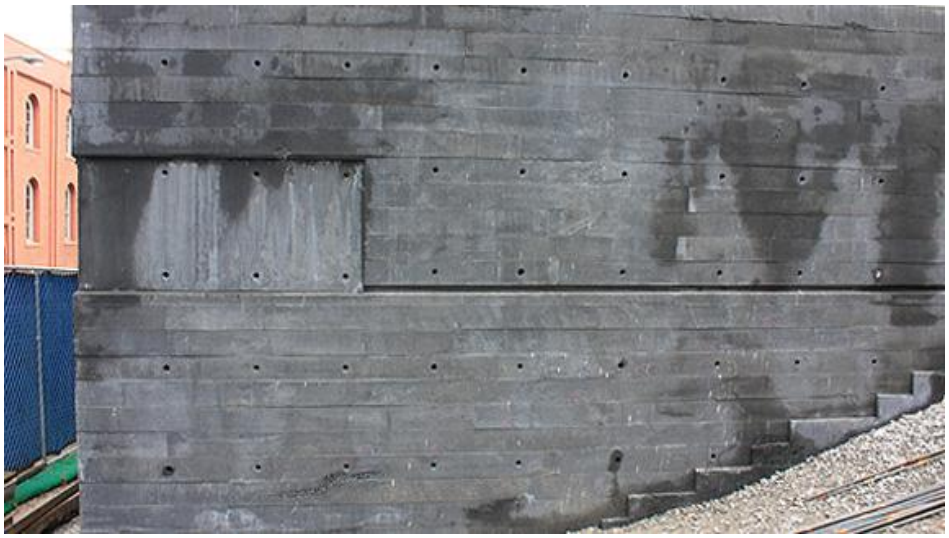

Figure 2. The walls shortly after the removal of form work.

PRODUCT

imi's branded product, **imix 180**, self -consolidating concrete was specifically designed to satisfy the requirements of the project. In order to ensure the voids of the formwork were adequately filled, **imi's** quality control department closely monitored and maintained a 26" to 30" spread for the concrete. In addition, a

moderate air content was maintained to assist with the flow of the concrete. The average of the 28 day strengths exceeded 7000 psi.

Table I. Concrete Test Results

Test Results					
Spread	**Air (%)**	**Concrete Temperature (◦F)**	**Ambient Temperature (◦F)**	**7 Day Compressive Strength (psi)**	**28 Day AVG Compressive Strength (psi)**
30	5.7	81	67	5550	***6540***
29	6	72	81	5070	***7440***
26.5	5.5	75	80	5810	***7850***
27	4.5	83	72	5720	***7090***
29	4	77	65	5680	***7000***

PLACEMENT

The concrete was pumped into the walls, which were placed in lifts. Six placements occurred throughout a five-month period. Upon completion, approximately 100 cubic yards of **SCC** was placed. The entire project was completed by June 2015 making it available for debut during the 2015 County Music Festival.

Figure 3. The SCC flowed underneath and between the windows.

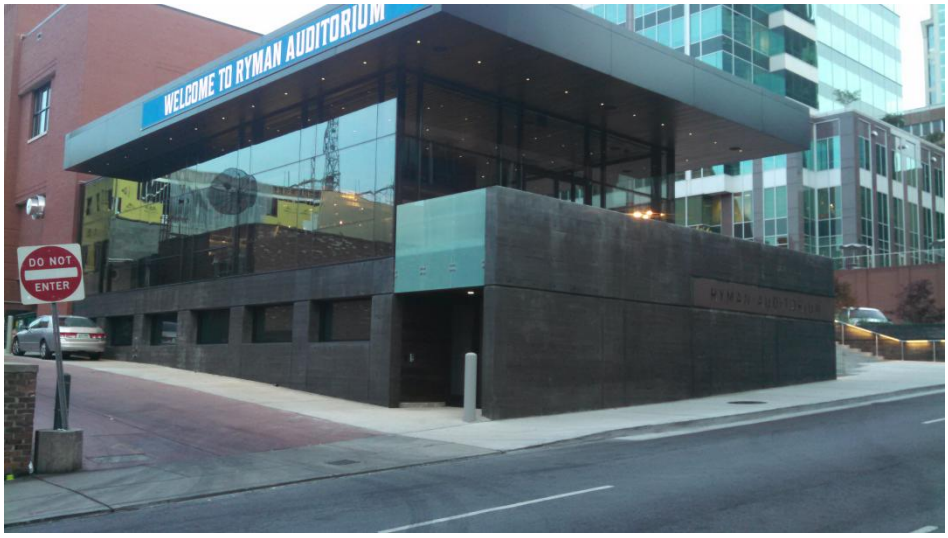

Figure 4. The completed Ryman Auditorium addition.

A Framework to Examine Experimental Material Properties of Self-Consolidating Concrete for Prestressed Bridge Girder Fabrication

Eduardo Torres[1], Junwon Seo, Ph.D., P.E.[2], and Rita E. Lederle, PhD[3]

[1]Graduate Student, Dept. of Civil and Environmental Engineering, South Dakota State Univ., Brookings, SD 57007.
[2]Assistant Professor, Dept. of Civil and Environmental Engineering, South Dakota State Univ., Brookings, SD 57007 (Corresponding Author). E-mail:junwon.seo@sdstate.edu
[3]Structural Design Engineer, Bureau of Structures, Wisconsin Department of Transportation, Madison, WI 53707.

Abstract In the production of self-consolidating concrete (SCC) prestressed bridge girders, precast producers use different material constituents and proportions in their mixes based on state level specifications. However, many precasters have struggled to maintain uniformity in the SCC mixture. This paper presents an experimental framework to effectively examine the fresh and hardened properties of SCC mixtures that exhibit adequate performance for prestressed bridge girder fabrication. The framework was developed through a comprehensive review of associated technical reports and survey inputs from SCC producers in different states in the United States. As part of the framework feasibility check, this framework was applied to two different precast plants that use different aggregates, binders and admixtures. Throughout the framework, multiple SCC mixtures were created and tested to evaluate workability and performance. To maintain the uniformity in the SCC mixture and achieve the desired workability and performance, various mixture parameters were adjusted, including cement type and aggregate size. Preliminary results from this application are included and discussed.

Keywords: *Self-Consolidating Concrete, prestressed concrete girders, workability, performance, fresh properties, strength*

Introduction

SCC was first developed in Japan in the 1980s. Since then, the use of SCC has broadly expanded across Europe and North America [1]. Prestressed industries have experienced several benefits from the use of SCC, including: 1) reducing required labor, 2) shortening of construction time, 3) eliminating vibration and noise hazards, and 4) simplifying the placing process [2]. SCC for use in prestressed bridge girders must meet the required compressive strengths and should be highly workable to easily flow through the reinforcement and fill the formwork without any mechanical vibration [3-4].

SCC workability properties are defined as the combination of flow ability, passing ability, and stability. Desired workability for SCC can be achieved by properly proportioning the constituents and admixtures in a systematic way [5]. The flow ability is the ability to flow through the formwork under its own weight. The passing ability indicates the capability of the mixture to flow through tight openings, such as narrow spacing between reinforcing bars [6]. The stability of SCC, also known as the resistance to segregation, is defined as the distribution of aggregate particles in the concrete that is relatively equivalent at all locations [7]. SCC with a lack of stability can result in settling of the aggregate to the bottom of the paste [7-8]. This phenomenon can adversely affect the workability and performance of SCC. In fact, SCC producers in many states in the United States have struggled to maintain uniformity on SCC in terms of segregations and strengths. Therefore, an experimental framework to efficiently identify SCC mixtures exhibiting optimum workability properties with satisfactory strengths is needed.

Framework

An experimental framework was developed to optimize SCC mixtures for desired workability and strength criteria. Figure 1 illustrates a step-by-step flowchart used to develop optimum SCC mixtures for prestressed bridge girders. The framework has five steps which are discussed in detail as follows.

The first step is to establish testing methods. Testing methods were selected based on previous studies [3-13]. The most commonly used methods to test for each workability property can be divided into flow ability, passing ability and stability, and have been standardized by the American Society for Testing and Materials (ASTM) as the slump flow [14], J-Ring [15], and column segregation [16] tests, respectively. The Prestressed Concrete Institute (PCI) also provides guidelines for SCC mixture proportioning, testing and quality control [3].

The second step relies on the identification of ideal workability for the production of prestressed bridge girders on plants. Table I provides workability criteria with a

range of values recommended for each method. These values were identified according to the information collected by a survey sent to state Departments of Transportation (DOTs) and past publications regarding SCC workability improvement [5, 6, 8-12]. The survey was used to better understand state-level SCC specifications and to reasonably limit the workability criteria to determine optimum SCC mixtures.

The third step involves selecting SCC mixture parameters, including water to cement ratio (w/c), sand to aggregate ratio (S/Agg), and aggregate size, to meet workability criteria established in the preceding step. For example, an appropriate w/c ratio should be selected to meet the required strength and it is recommended to choose an S/Agg value within the range of 0.4-0.6 because it can affect the workability by decreasing plastic viscosity [4]. The influence of these parameters on time-dependent characteristics (e.g. creep and shrinkage) must also be considered because they will affect prestress losses.

The fourth step is to test for the workability of SCC via the aforementioned methods according to ASTM and/or PCI guidelines. If SCC mixtures do not meet the workability criteria shown in Table I, it is necessary to adjust parameters of the SCC mixture design. For instance, by adjusting the dosage of admixtures, viscosity and flow ability of the mixture can be improved. By decreasing the size of the coarse aggregate, the passing ability can be improved and segregation of the mixture will decrease.

Once the workability requirements of tested the SCC mixtures are satisfied, the mixtures can be tested for hardened properties. Thus, the fifth step of the framework is to test for compressive strength of short- and long-term cured SCC mixtures. Compressive strength criteria were also identified based upon the DOT survey where the strength requirements vary across states. Several DOTs, such as Texas and Michigan, have required short-term cured compressive strength (e.g., 14 hours) above 37.92MPa and long-term curved compressive strength (e.g., 28 days) exceeding 48.26MPa. However, for the low w/c ratio used for the mixtures in this study, a higher minimum compressive strength of 46.88MPa at 14 hours was set to determine optimum SCC mixtures based on previous studies with similar parameters [9, 12] and to be consistent with requirements for standard precast bridge girders in Wisconsin.

Finally, the sixth step consists of comparing the results of the mixtures which matched the acceptable range of workability and strength requirements. The mixture closest to the target value will be the optimum mixture. Throughout the framework, optimum SCC mixtures having the most satisfactory workability and compressive strengths at 14 hours will be determined. Note that the framework is not designed for the investigation of time-dependent material characteristics and/or structural performance of SCC mixtures.

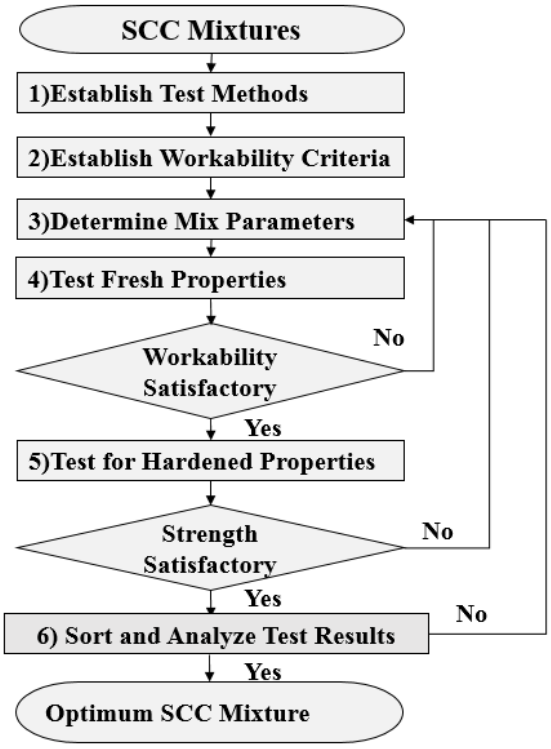

Figure 1. Framework to determine optimum SCC mixture for prestressed bridge girders.

Table I. Target values for specific test methods

Evaluation Table for Fresh Properties		
Fresh Properties Tests	**Acceptable Range**	**Target Value**
Slump Flow	22" - 28 "	25''
J-Ring	max 50.8mm	max 50.8mm
Column Segregation	≤ 15 %	Close to 10 %
T_{50}	3-10 sec	<6 sec
VSI	≤ 1	≤ 1
Hardened Properties Tests	**Accepted Range**	
Compressive Strength	Above 46.88MPa (14 hours)	

Application of Framework to Two Plants

The framework was applied to two different precast plants denoted as Plant A and Plant B. Both plants are located in Wisconsin. Each plant has a unique cement type and geographical source of the aggregates. The coarse aggregate blending was varied, resulting in six mixtures at each plant (see Table II). For instance, mixture 1A will consist of 100% of 9.5mm aggregate, while mixture 2A will have 80% of 9.5mm aggregate and 20% of 19mm aggregate. The rest of mixtures continue with 20% intervals until 100% of 9.5 mm is reached. Blending configurations were applied to the mixture design using a weight method instead of a volume method. The weight method was more suitable for investigating the effects of blending configurations within the mixtures on workability and strength because the 19mm and 9.5mm aggregate blends have the identical material properties for a given plant. Other mixture parameters that were selected for the mixtures are w/c, S/Agg, and cement content with values of 0.35, 0.50, and 362 kg/m^3, respectively.

Table II. SCC mixture composition

Mixture No.	**% 9.5mm Agg.**	**Cement Kg**	**Water Kg**	**Fine Agg. Kg**	**9.5mm Coarse Agg. Kg**	**19mm Coarse Agg. Kg**	**HRWR (oz/cwt)**	**VMA (oz/cwt)**
1A	100	362	127	640	640	0	5	1
2A	80	362	127	640	512	127	5.5	1
3A	60	362	127	640	384	255	6	0
4A	40	362	127	640	255	384	5	1
5A	20	362	127	640	127	512	5.	1
6A	0	362	127	640	0	640	5	2
1B	100	362	127	640	640	0	5	0
2B	80	362	127	640	512	127	6	0
3B	60	362	127	640	384	255	5	0
4B	40	362	127	640	255	384	5	1
5B	20	362	127	640	127	512	5	1.5
6B	0	362	127	640	0	640	5	2

All mixtures for both plants were 100% Portland cement, meaning that no fillers were used to replace cement content. Pozzolans and supplementary cementitious materials were excluded from the project to limit the scope and focus on basic mix design development.

Plant A uses cement Type III with its specific gravity of 3.15. Type III cement is typically used when a high early strength is required [17], which is the case for most products produced at Plant A. The coarse aggregate consists of limestone No 67 (19mm) and No 78 (9.5mm) conforming to the American Association of State Highway and Transportation Officials (AASHTO) M43. The specific gravity of the coarse aggregate was 2.66 and a percent absorption of 1.52%. Fine aggregates had a specific gravity of 2.65 and percent absorption of 0.59%.

Plant B uses a Portland cement Type I/II with a specific gravity of 3.14, as the products this plant produces do not require as high of early strengths as those produced by Plant A. Plant B uses limestone from a different pit than Plant A. The coarse aggregates had a specific gravity of 2.59 and percent absorption of 2.64. The fine aggregates had a specific gravity of 2.65 and percent absorption of 0.69%.

Test Methods: Mixtures of Plant A and B were first tested to determine their workability. Figure 2 shows each test method described in the first step of the framework. Admixture dosages were varied slightly for each mixture to obtain desired criteria as shown in Table I. For the slump flow test, the cone is filled with the SCC mixture (see Figure 2a) and then it is pulled up in approximately 3 seconds, allowing the mixture to flow. Once the concrete stops flowing, the diameter was measured at two different orthogonal directions (see Figure 2b). Also, the time (T_{50}) it takes for the concrete in the cone to reach the 50cm diameter line was measured for each mixture. The VSI is immediately performed after the slump flow. VSI levels are ranged from 0 to 3, indicating the degree of stable to unstable segregation. These levels are determined through visual inspection of the fresh batch after testing the slump flow. VSI also provides a visual image of the distribution of aggregates and the presence of excessive bleeding throughout the mixture [3].VSI is divided in different levels as follows: 1) VSI of 0, meaning mass is homogeneous and no bleeding; 2) VSI of 1, indicating small bleeding observed in the surface; 3) VSI of 2, showing evidence of a mortar halo and water sheen; and 4) VSI of 3, concentration of coarse aggregate at center of concrete mass and presence of a mortar halo[3].

The J-Ring test procedure is similar to that of the slump flow explained previously. The J-Ring is placed around the cone and the SCC passes through the legs of the open circular steel ring as seen in Figure 2c. The average of two orthogonal diameters is recorded and compared to those from slump flow testing.

The column segregation test was performed according to ASTM C 1610 [16]. For this test, the SCC mixture is poured into the cylinder within 2 minutes (see Figure

2e). Then, the SCC in the top and bottom segments of the cylinder are collected and placed in different containers (see Figure 2f). The SCC from the top and bottom segments were washed to discard any particles passing the No. 4 sieve. Then, the weight of the aggregate retained on the No. 4 sieve is recorded for both top and bottom segment, respectively and compared.

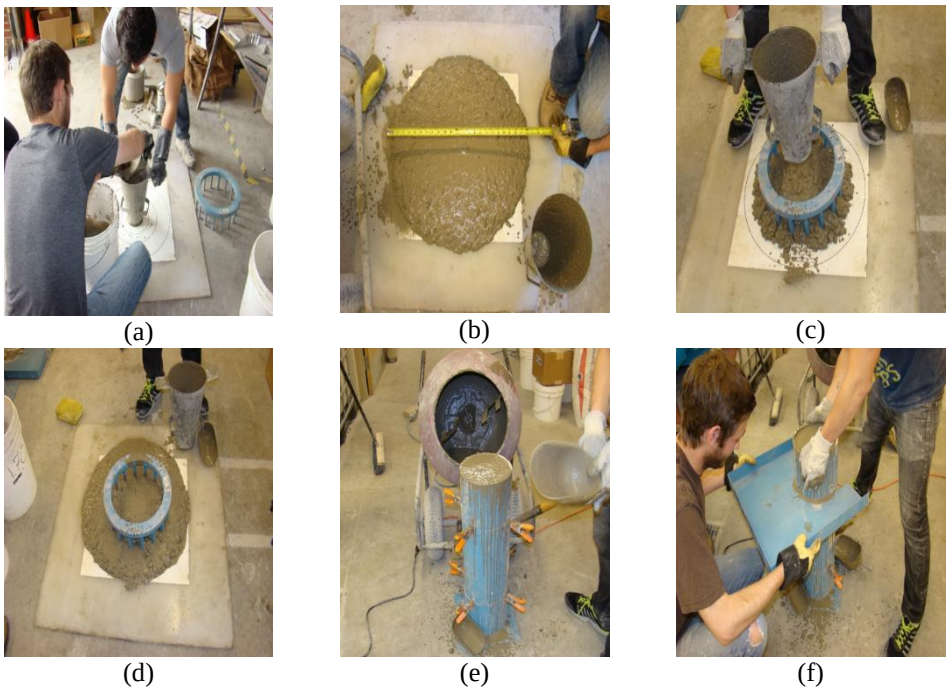

(a) (b) (c)

(d) (e) (f)

Figure 2. Workability test methods: (a) Slump flow setup, (b) Slump spread diameter measurement, (c) J-Ring setup, (d) J-Ring spread diameter measurement, (e) Column segregation set up, (f) Collecting top section of cylinder

To test for compressive strength, curing methods should match the actual curing conditions used at each of the precast plants to ensure representative results. For this study, a water bath was used to simulate steam curing as seen in Figure 3a. SCC cylinders were kept in the water bath at a temperature of 110 F˚ for 14 hours to simulate the curing methods used by both plants. Sulfur caps were then placed at the top and bottom surfaces of 14 hour cylinders to allow uniform distribution of the load applied by the compressive machine as shown in Figure 3b. As specified by ASTM C39, the rate of loading was 0.23 MPa/sec until each of the cylinders reached a complete failure [18] as illustrated in Figure 3c.

(a) (b) (c)

Figure 3. Preparation of cylinders for compressive strength: (a) Water bath curing, (b) Sulfur capping, (c) Cracked concrete cylinder.

Results and Discussion

Workability

The overall workability of the tested SCC mixtures for Plant A and B was determined to be satisfactory because the fresh properties were within target values. Table III lists the workability results and compressive strengths for all SCC mixtures. Note that slight adjustments to the dosage of HRWR and VMA were necessary to meet the minimum requirements for SCC flow ability and passing ability as specified in the in Table I. The flow ability, passing ability and stability for the tested mixtures are further discussed in the following subsections.

Table III. SCC workability results and compressive strengths

Mix No.	**% 9.5mm Agg.**	**T_{50} s**	**VSI**	**Slump Flow Test mm**	**J-Ring Test mm**	**Passing Ability mm**	**Column Segregation %**	**Compressive Strength MPa**
								14 hr
1	100	9.	0	609.6	622.	12.7	2.76	44.4
2	80	7.	0	603.0	609.	6.35	6.32	48.4
3	60	1	0.	622.0	635.	12.7	6.47	46.6
4	40	9.	1	635.0	596.	38.1	8.17	52.8
5	20	1	0	577.0	635.	57.15	9.18	58.1
6	0	7.	0	584.0	622.	38.1	10.10	49.9

1	100	1	0	609.6	571.5	38.1	1.67	36.0
2	80	7	1	660.0	622.3	38.1	3.33	38.1
3	60	9	0	622.3	597.0	25.4	5.15	42.7
4	40	3.	1	641.4	622.3	19.05	8.01	48.2
5	20	4.	0	622.3	596.9	25.4	9.58	40.8
6	0	5.	1	660.4	616.0	44.45	11.80	40.5

Flowing ability: The flowing ability quantified via the slump flow ranged from 557mm to 660mm, which was within the acceptable range for slump flow listed in Table I. The slump flow diameters for the Plant A mixtures have a range from 577mm to 609 mm. The mixtures with a higher percentage of 9.5mm aggregate size showed higher spread diameters than those with a low percentage of 9.5mm aggregate. As shown in *Figure 4a*, for Plant A mixture 4A (40% of 9.5mm aggregate) exhibit the best results in terms of flow ability. The results of Plant B mixtures are illustrated in *Figure 4a,* having better overall flow ability results compared to Plant A, which may be attributable to the different aggregate sources. Spread diameter had a range from 609 mm to 660 mm. Optimum flow ability for Plant B was observed in mixtures 3B, 4B and 5B which had sump diameter values within ± 12 mm from the target value. However, the mixture having 40% of 9.5mm aggregate was the best fit compared to the rest of Plant B mixtures because it was closest to the target value

From the slump flow tests for both Plants A and B, T_{50} values were recorded as seen in Table III to quantify the viscosity of each of the mixtures. Again, T_{50} can be defined as the time it takes to the mortar to reach 50 cm diameter. In Plant B, T_{50} times decrease as the percent of 9.5mm aggregate decreases. Plant A does not follow the linear trend seen for Plant B because the T_{50} times are more inconsistent with a few ups and downs as shown in *Figure 4b.*

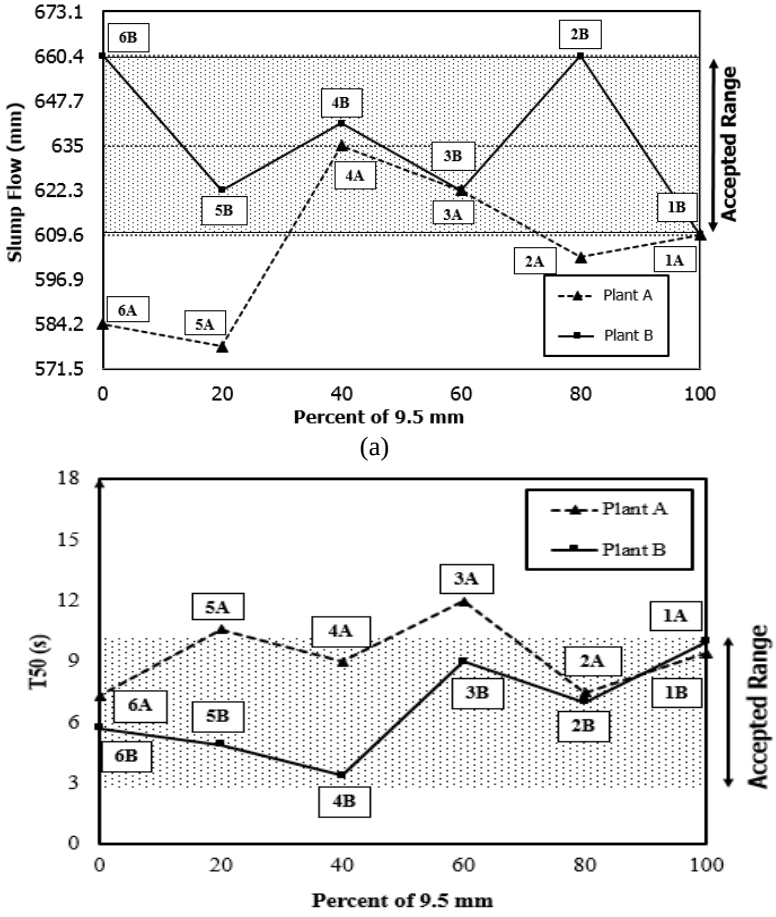

Figure 4. Flowing ability for Plant A and B: (a) Slump flow results, (b) T_{50} results

Passing ability: The difference in diameter between slump flow and J-Ring test methods is called passing ability. As seen in Table I, the difference in diameters should not exceed 50.8mm, though a smaller value is better. *Figure 5* illustrates the passing ability trends for Plant A and B. Passing ability for Plant A ranges from 6.35mm to 57.15mm, and for Plant B ranges from 19.05 to 44.45mm. Plant A shows the best passing ability for mixtures 1A, 2A and 3A having high percentage of 9.5mm coarse aggregate. This trend is expected as less blockage between the J-Ring bars is seen with smaller aggregate size. However, mixtures 4A, 5A and 6A have a noticeable decrease in passing ability where mixture 5A exceeded the 50.8mm established for the optimum workability criteria. Mixture 2A has the overall best results in terms of passing ability and flowing ability with large diameter spreads for slump flow and J-Ring required for SCC to improve the

production of prestress girders. Results from Plant B are within a smaller range compared to the results from Plant A as the percent of 9.5mm aggregate varies. As seen in *Figure 5*, Plant B has the same trend seen in the flowing ability section where the best results were seen in mixtures 3B, 4B and 5B. Mixture 4B has the best passing ability for Plant B with a passing ability value of 19.05mm.

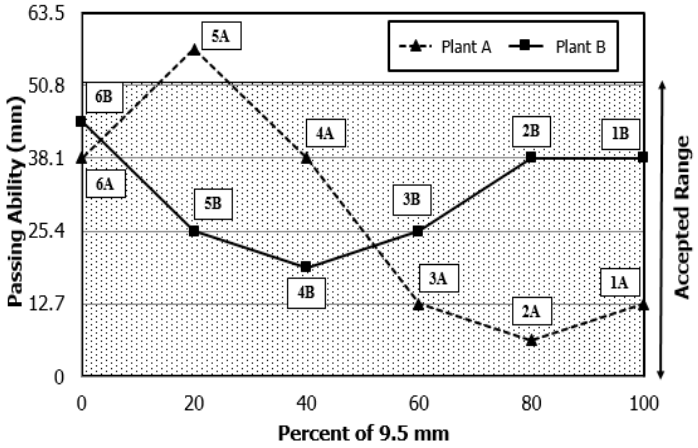

Figure 5. Passing ability for Plant A and B

Segregation: Segregation was measured using the column segregation test. From this test the percent of segregation was calculated as the percent difference of the aggregate weight between the top and bottom sections of the cylinder. Segregation of SCC has negative impact on the structural performance of SCC; therefore a maximum value of 15% segregation was selected, as shown in Table I. Figure 6 illustrates that the percent segregation for both plants are under the maximum percent allowed. Percent segregation for both plants decreases as the percentage of 9.5mm coarse aggregate increases. This trend was expected as the 19mm coarse particles have higher weight causing faster segregation. From the T_{50} values from Plant B, it was also observed that mixtures with higher percentage of 9.5mm aggregate had higher viscosity as a result of less segregation. The cement type does not affect the viscosity of the mixture as similar values were seen for both plants in terms of segregation.

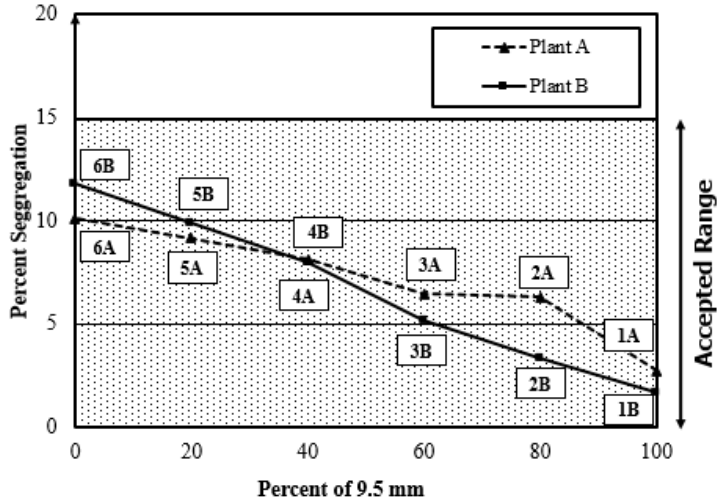

Figure 6. Percent segregation for Plant A and B

Compressive Strength Results

Compressive strengths at 14 hours of all mixtures for Plant A are higher than those from Plant B as expected due to the cement types (recall that Plant A uses type III). *Figure 7* shows the compressive strength results for 14 hours of Plant A and Plant B. As the percent of 9.5mm coarse aggregate decreases the compressive strength of the concrete increases. All mixtures were able to meet segregation criteria, but that does not mean the limit represents optimum segregation to reach the higher level of compressive strength. Compressive strengths of Plant A mixtures range from 44.8MPa to 58.1 MPa where mixture 5A had the higher strength and mixture 1A had the lower value. Plant B values are considerably lower compared to Plant A, which can be attributed to the use of different cement types. These values range from 36MPa to 48.2MPa. Mixture 4B and 1B are the higher and lower compressive strength values, respectively.

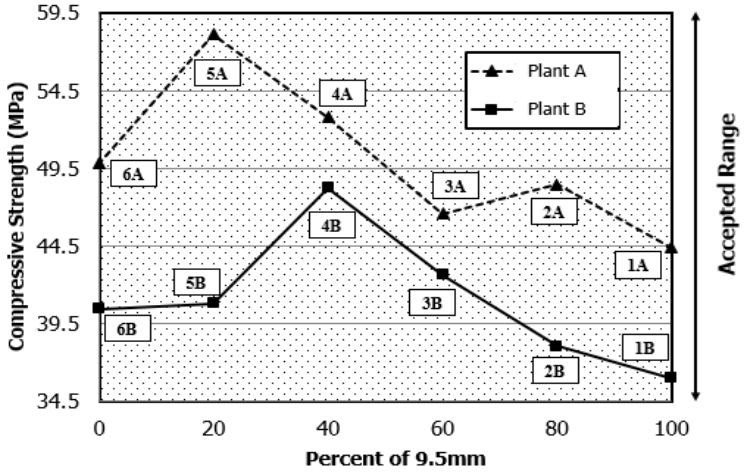

Figure 7. Compressive strength at 14 hours of curing for Plant B and A

Optimum Mixture Selection

The test results obtained from all mixtures following the proposed framework were quantitatively compared with the criteria listed in Table1. Optimum mixtures for each of the plants were identified as those for which test results of the fresh property tests most closely matched workability criteria while still ensuring satisfactory strength.

In Plant A, all mixtures met the required compressive strength and segregation criteria, so the flowing and passing abilities governed the selection. The optimum mixture for Plant A was mix 3A (60% of 9.5 mm aggregate). While mix 4A had a flow ability slightly closer to the optimal value, the mix 3A had much better passing ability and less segregation. Mix 2A had the best passing ability, but its flow ability was outside the accepted range and therefore it could not be considered as a final contender. Following the same process as described for Plant A, the optimum mixture for Plant B was 3B (60% of 9.5mm).

Conclusions

This paper presented an experimental framework to determine the optimum SCC mixtures from two variables of cement type and aggregate size. Specific test methods and result criteria were established aiming to obtain ideal SCC performance for the use in prestressed bridge girder fabrication in terms of workability and strength. This framework was applied to two actual precast plants, denoted as Plants A and B. From this study, the following conclusions can be drawn:

1) SCC mixtures from Plant B using cement type I/II showed better flow ability and passing ability than those from Plant A with cement type III.
2) All flow ability results matched the range of 558.8mm-711.2mm suggested by ASTM C1611 but not the criteria established in the framework of this study. Mixtures of Plant A and B having 40% of 9.5mm aggregate had the best results by meeting the slump flow spread target value of 635mm.
3) Passing ability values of Plant B were satisfactory for all values of the percent of 9.5mm aggregate. For Plant A, the passing ability values were satisfactory from at all levels of 9.5mm aggregate except 20%. The optimum passing ability for Plant A and B occurred at was 80% and 40% of 9.5mm aggregate respectively.
4) Segregation values were satisfactory for all the mixtures of Plants A and B. It was observed that as the percent of 9.5mm aggregate was reduced, the percent of segregation increased due to the higher weight of particles. According to the T_{50} values of Plant B, as the percent of 9.5mm aggregate increased the mixture viscosity was higher.
5) Finally, the optimum blending configuration for Plants A and B was 60% of 9.5mm aggregate and 40% of 19mm. This mixture exhibits excellent workability performance and exceeded compressive strength requirements.

Based on the work presented in this paper, optimal mix designs for SCC were selected for the two plants studied. Before these mixes are implemented, it will be necessary to study the creep and shrinkage characteristics of the mixes to determine how they compare with standard concrete used for precast bridge girders. The framework established in this paper can be used by precast plants to develop additional mixes for testing to explore other mix variations such as the use of supplementary cementitious materials or different admixture or aggregate types.

Disclaimer

The contents of this paper reflect the views of the authors, who are responsible for the facts and the accuracy of the data presented herein. The contents do not necessarily reflect the official views or policies of the Wisconsin Department of Transportation or the Wisconsin Highway Research Program. This paper was not sponsored by the Wisconsin Department of Transportation or the Wisconsin Highway Research Program. This paper does not constitute a standard, specification, or regulation.

References

[1] Okamura, H., and Ouchi, M. (1999). In: *"Self-compacting concrete development, present use and future."* First International Symposium on SCC, RILEM publications PRO 7.

[2] Skarendahl, A. (2003). In: *The present-the future*. Wallevik O, Nielsson I (eds.) Self-Compacting Concrete, Proceedings of 3rd Intern.. RILEM Publications S.A.R.L.

[3] PCI (2003). TR-6-03 Interim Guidelines for the Use of Self-Consolidating Concrete in Precast/Prestressed Concrete Institute Member Plants, 1st Edition. Chicago, IL: Precast/Prestressed Concrete Institute.

[4] Long, W., Khayat, H., Lemiux, G., Hwang, S., and Han, N. (2014). *"Performance-Based Specifications of Workability Characteristics of Prestressed, Precast Self-Consolidating Concrete"*. Journal of Materials, Vol 7, 2474-2489.

[5] Erkmen, S. (2008). *"Self-Compacting Concrete (SCC) for Prestressed Bridge Girders"*. University of Minnesota. Report No MN/RC 2008-51.

[6] Wehbe, N., Sigl A., Gutzmer, Z., and Stripling, C. (2009). *"Structural Performance of Prestressed Self-Consolidating Concrete Bridge Girders Made with Limestone Aggregates"*. Report No MPC-08-196

[7] Turkel, S., and Kandemir, A. (2010). *"Fresh and Hardened Properties of SCC Made with Different Aggregate and Mineral Admixtures".* Journal of Materials in Civil Engineering, Vol 22, 1025-1032.

[8] Bonen, D., and Shah, S. (2004). *"Fresh and Hardened Properties of Self-Consolidating Concrete."* Wiley interscience. Structural Engineering Materials, Vol 7, 14-26.

[9] Burgueno, A., and Bendert, A. (2007). *"Experimental Evaluation and Field Monitoring Of Prestressed Box Beams for SCC Demonstration Bridge."* Michigan State University. RC-1489.

[10] Hamilton, H. and Labonte, T. (2005). *"Figure 10: Testing protocol for establishing an appropriate SCC mixture that can be used for prestressed bridge girders."* Report No 4910 4504 047.

[11] Mata, L. (2004). *"Implementation of Self-Consolidating Concrete (SCC) for Prestressed Concrete Girders".* North Carolina State University. Report No FHWA/NC/2006-30.

[12] Trejo, D. (2008). *"Characterization of Self-consolidating Concrete for Design of Precast, Prestressed Bridge Girders"*. College Station, TX: Texas Transportation Institute. Report No FHWA/TX-09/0-5134-2

[13] Sonebi , M., Grünewald, S., and Walraven, J. (2007). *"Filling Ability and Passing Ability of Self-Consolidating Concrete".* ACI Materials Journal, Vol 104 No2.

[14] ASTM. (2011e). *"Standard Test Method for Slump Flow of Self-Consolidating Concrete"*. ASTM C1611.

[15] ASTM. (2011d). *"Standard Test Method for Passing Ability of Self-Consolidating Concrete by J-Ring".* ASTM C1621.

[16] ASTM. (2011g). *"Standard Test Method for Static Segregation of Self-Consolidating Concrete Using Column Technique"*. ASTM C 1610.

[17] ASTM. (2011g). *"Standard Test Method for Static Segregation of Self-Consolidating Concrete Using Column Technique".* ASTM C 1610.

[18] ASTM. (2011g). *"Standard Test Method for Compressive Strength of Cylindrical Concrete Specimens".* ASTM C 39.

Relationship between Mix Designs and Bleeding for Semi Flowable SCC Applied to Diaphragm Walls

A. Azzi[1,2], C. Djelal[1], Y. Vanhove[1], H. Kada[1], O. Madec[2,3]

[1]Univ. Artois, EA 4515, Laboratory of Civil and Geo-Environment (LGCgE), Béthune, F-62400, France.

[2]Botte Fondations, ZAC du Petit Le Roy, 5 Rue Ernest Flammarion, Chevilly-Larue, 94659 Rungis Cedex, France

[3]Fédération Nationale des Travaux Publics, 3 Rue du Berri, 75008 Paris, France

Abstract Diaphragm walls are used either to support excavation walls on site or prevent water move through the ground. The observations recorded following excavation and planning of diaphragm walls demonstrate that concrete outside the reinforcement cage is of a poorer quality than the one inside the cage. These disorders are mainly chimneys of water upwelling. To prevent their appearance on project sites, the concrete used for the realization of diaphragm walls must meet the requirement of EN-1538 and EN-206/CN. In some case in conformity with standards, companies still have to face problems related to concrete forced bleeding. This study stands on conducted on site and completed in the laboratory. The first part consists of a comparative study which helps us to identify the parameters affecting bleeding phenomenon. The second part highlights the fact that the recommended threshold value for bleeding is inadequate.

Keywords: *Formulation, Concrete, Forced bleeding, Diaphragm wall, channelling.*

Introduction

Diaphragm walls are reinforced concrete foundation elements used as definitive structures in the construction of many types of projects. Anchored into a strong impermeable layer, these walls are intended to absorb thrust forces due to movements of both the ground located in back of the structure and groundwater. Diaphragm walls must perform three functions: support, load-bearing capacity, and

impermeability. **[1]** This technique may be used to build on sites presenting highly varied geotechnical conditions; it allows executing structures of diverse shapes and dimensions extending very deep into the soil, e.g. underground parking lots, platform walls, circular walls for basin projects, cylindrical enclosures, deep load-bearing foundations. The trend in admixtures favouring more efficient products has led to improvements in both the fluidity of concrete foundations and their rheological stability. The mechanical strength of these concretes currently equals 80 MPa, compared with a value of less than 45 MPa a few years ago. The advent of these new concretes has enabled building taller structures featuring complex geometries. Such structures require foundations adapted to their particular shape and weight, as well as to the type of soil. For this reason, diaphragm walls have evolved in adapting to these modern project designs. The thickness of diaphragm wall component panels typically ranges from 0.5 m to 1.5 m, with a maximum height of 70 m; moreover, the diaphragm wall technique is the only foundation process that makes it possible to reach such depth dimensions. These walls are often heavily reinforced in order to resist either the weight of the structure built on the surface or water pressure when the structure is a basin or a parking lot. The execution of a diaphragm wall comprises several phases; Figure 1 depicts the principal phases therein.

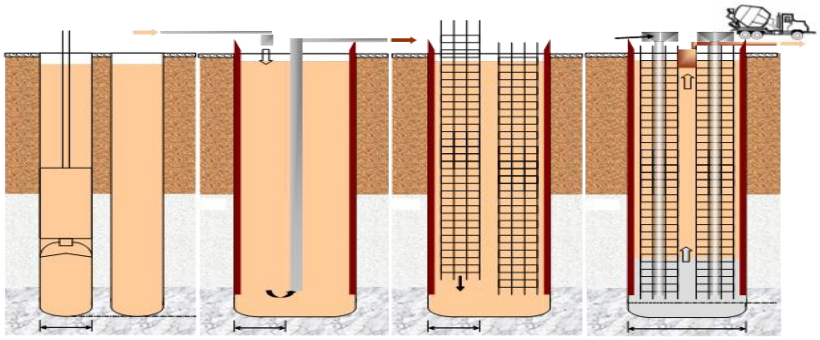

Figure 1. The different phases of the execution of a diaphram wall

Phase (1) - Ground perforation (initial opening) using bentonite sludge with the help of a skip. The drilling sludge or fluid (a bentonite and water-based suspension) is produced by a mixing plant set up on the jobsite. It is continuously poured into the excavation pit as the skip progresses so as to ensure stability of the excavation walls.
Phase (2) - Perforation of the second opening
Phase (3) - Perforation of the bund wall (located between the two openings)
Phase (4) - New sludge introduced into the excavation in order to replace the soil-laden sludge.

Phase (5) - Installation of reinforcement cages and outer formwork fitted with a water-stop joint. These cages are set into place using 12 to 14-meter long elements, or longer ones should conditions warrant.
Phase (6) - Concreting by means of tremie pipes. The concrete delivered onto jobsites, via a truck mixer with a capacity of 7 to 9 m^3, is then injected into the pit by means of one or two tremie pipes or concreting columns (operating continuously) from the bottom of the trench. The tremie pipe is gradually lifted as the pit fills. The sludge is simultaneously extracted by pumping and then recycled.

The execution of diaphragm walls into the ground implies proceeding by concreting the tremie pipe under the sludge, which engenders a number of constraints, namely:

- The concrete must remain extremely fluid (the EN NF206/CN Standard prescribes a slump on the vibrating table equal to 600 ± 30 mm at 20°C) to cast in heavily reinforced zones or relatively inaccessible zones with complex shapes;
- Concrete placement must not require vibration in order to avoid any mixing with earth or groundwater and to prevent breaking the fragile equilibrium of excavation walls held in place by the sludge. Moreover, the concrete must be able to self-compact under its own weight;
- Given the specific mode of installation and casting time of the concrete necessary to build special foundations (several hours), the consistency of the material must be preserved throughout the duration of concreting. A rheological support that extends beyond the concreting time (plus an allowance for uncertainties) is recommended (between 6 and 8 hours);
- The density of reinforcements must not be too high so as to guarantee their effective coating.

Diaphragm walls must satisfy the requirements listed in French Standard NF EN 1538 and European Standard NF EN 206/CN. To ensure its durability, the concrete needs to be produced with a minimum cement content, which depends on maximum aggregate size D_{max}. The Blaine surface area of the cement must exceed 3800 cm^2/g.

The use of CEM II or CEM III type cements is preferred to CEM I cement. A partial replacement of CEM I or CEM II cement by additives, in accordance with NA.5.1.6 (Standard EN NF 206/CN), is indeed feasible. Moreover, this standard requires a minimum content of cement for diaphragm walls according to the maximum size aggregate D_{max}: 350 kg/m^3 for 32 mm, 380 kg/m^3 for 22.4 mm, 385 kg/m^3 for 20 mm and 400 kg/m^3 for 16 mm.

The granular skeleton must be continuous in order to limit segregation as much as possible. The total mass of fine particles ($D \leq 0.125$ mm) in the concrete mix (incorporating the cement and other fines) must lie between 400 and 550 kg/m^3.

Concrete bleeding is to be brought under control. In the event of excessive bleeding, so-called bleeding channels (also called water release paths) may appear. The content of bleeding water is capped at 1%, should it be determined on the basis of European Standard NBN EN 480-4. The American Standard ASTM 232 limits the speed of bleeding to 0.1 m/minute. Australian recommendations are also available ("Recommended Practice Tremie Concrete for Deep Foundations") **[2]** as a supplement to these standards for deep foundations. The quantity of water being bled, as measured by employing Bauer's test at 5 minutes under a pressure of 5 bar, must be less than or equal to 24.4 ml.

Even if all these conditions are being met, many contractors still currently encounter a wide range of problems, tied in large part to bleeding. As a case in point, the observations recorded subsequent to earthworks and planning of walls has revealed that concrete outside the reinforcement cage is of poorer quality than that found inside the cage. These defects may be ascribed to the placement technique, associated with insufficient fluidity and a lapse in maintenance over the placement duration; weak cohesion between layers due to an overly rapid setting; inadequate coating of the reinforcements; a coating concrete fouled by sludge; and a lack of concrete slurry resulting from a loss of workability due to bleeding arising during placement. Less workability can adversely affect the quality of walls both aesthetically and mechanically. The bleed water runs into the concrete (case of an impermeable soil) and create chimneys of water upwelling. These problems represent 90% of the complications observed on jobsites (Fig. 2). For this reason, the present study is primarily focused on such chimneys.

The hydrostatic pressure of fresh concrete in a diaphragm wall rising as high as 70 m may lead to the creation of longitudinal channels along the wall. These channels might tend to follow the tremie pipe alignment in the concrete, which would promote the appearance of water chimneys at the centre of the wall. During its migration, this water may sweep away the concrete fines ("washing-off" of the concrete), thus segregating the concrete granular skeleton. In some cases, honeycombing might also be present.

Figure 2. Chimneys of water upwelling or sandy veins

To the extent that these walls are often performing a definitive function with a projected life cycle of 50 years or longer, it is essential for them not to display any major imperfections. The goal here is not solely to avoid infiltration of the ground and groundwater during and/or prior to excavation of the pit, but also to guarantee that any ultimate defects do not undermine the ability of the concrete to protect the reinforcements.
Before undertaking laboratory tests, a study was conducted on a series of jobsites where diaphragm walls displayed water release paths. This comparative study pertains to four diaphragm wall construction sites overseen by *Botte Fondations* (Vinci) over a 17-month period (from July 2012 through November 2013). Among these sites, three (BF2, BF3, BF4) present, following earthworks and planning, many traces caused by water release paths. No defect was reported for site BF1, which will therefore be taken as the reference site. Information relative to all study sites was taken into account (e.g. surface coverage, technical terms and conditions, concreting conditions, concrete mix designs). Characterization testing (slump, air content) was performed in conjunction with casting of the concrete into the pits. An analysis of test results served to design an experimental campaign in the laboratory. Afterwards, forced bleeding tests were carried out using a press filter developed by the firm Bauer **[2]**.

Comparative study of four diaphragm wall jobsites

Presentation of the jobsites

Tables I and II describe the four study sites and their degrees of pathologies, whose recordings have been strictly limited to water release paths.

Table I. Characteristics of diaphragm walls on jobsites

Name of site	Type of structure	height of the wall	Thickness of the wall
BF1	Station of purification	17 à 19 m	0.8 m
BF2	Building	24 à 26 m	0.8 m
BF3	Pumping station and storage of wastewater	37 à 38 m	1 m
BF4	Railway line	18 m	0.8 m

Table II. Degrees of pathologies of diaphragm walls on site

Name of site	Findings on the wall	Degree of pathology
BF1	No chimneys of water upwelling	nil
BF2	Quelques cheminées de remontées d'eau	+
BF3	A few chimneys of water upwelling	+++
BF4	Many chimneys of water upwelling	++++

No pathology was observed for the (reference) BF1 jobsite. The three other sites all display, after earthworks and planning, many traces caused by these water release paths. The BF4 site exhibited the greatest number of problems.

Concrete mix designs and properties

The following table indicates the various compositions for a 1-m^3 block of concrete. The binder expressed in this table corresponds to the addition of cement and additives (filler, fly ash, slag).

Table III. Composition (kg/m^3) and characteristics of the tested concretes

	BF1	BF2	BF3	BF4
Cement	385	385	400	255
Slag	-	-	-	105
Limestone filler	-	30	-	25
Fly ash	25	-	-	-
Sand 0/1	-	-	-	220
Sand 0/4	820	770	760	660
Gravel 2/10	-	350	-	-
Gravel 6/10	-	-	-	470
Gravel 4/20	840	-	-	-
Gravel 6/20	-	-	980	-
Gravel 11/22	-	580	-	475
Admixture 1	1.3	-	2	4
Admixture 2	0.68	3.32	-	2.89
Set retarding additive	-	-	-	0.96
Effective water	174	190	178	173
Weff/Binder equivalent	0.45	0.49	0.45	0.49
G/S	1.02	1.21	1.29	1.07
Rc28 (MPa)	52	51	60	46
Flow table test	580 ± 40mm	640± 20mm	650± 30mm	610± 40mm
Outside temperature	15.4°C	28.8°C	29.1°C	28.3°C
Concrete temperature	14.8°C	26.7°C	27.5°C	27.8°C
Air content	1.6± 0.6%	1.8± 0.3%	1.9± 0.4%	2.1± 0.3%

Analysis of concrete mix design parameters

Azzi **[3]** demonstrated the influence of mix design parameters on diaphragm wall pathologies. The interactions between these various parameters had received little attention as regards foundation concretes. Table IV lists the pertinent set of parameters.

Table IV. Summary of parameters influencing the water release paths

Composition	BF1	BF2	BF3	BF4
Pathologie	Nil	+	+++	++++
Granulometry curve	continuous	continuous	discontinuous	continuous
Compactness	0.76	0.70	0.74	0.73
Quantity of fines ≤ 125 µm (kg/m^3)	446	427	404	400
Type of cement	CEM III	CEM II	CEM III	CEM II
Quantity of binder (kg/m^3)	385	385	400	356
Blaine area of cement (cm^2/g)	4150	3650	4300	3850
Specific area of aggregates (m^2)	4014.2	3748.5	4457.1	3620.1
Volume of paste (%)	33	33	33	31

A comparative study of all parameters capable of influencing concrete stability has been conducted herein. Based upon relevant standards and a bibliographic search on concretes, a parametric analysis could be carried out:

- The composition of diaphragm wall concretes has been inspired by the composition of pumpable concretes **[4]**. The ACI 304.2R fascicule defines an optimal range for such materials. For our studied jobsites, all concretes lie within this range, and their particle size distribution curves reveal continuity, except for concrete BF3.
- Josserand **[5]** studied the influence of optimal compactness on concrete stability. He showed that for a compactness of around 1, the quantity of bleed water was minimal. In our case, the four concretes feature compactness values varying between 0.70 and 0.76. Since BF1 has a compactness of 0.76 and no pathology, we were able to deduce that this parameter exerts influence on the stability of the studied concretes.
- All cements introduced are compliant with the recommendations issued in Standard EN NF 1538.
- The quantities of fines are all greater than 400 kg/m^3 (Standard EN NF 206/CN).
- The quantity of binder complies with requirements listed in Standard EN NF 206/CN, except for concrete BF4.
- The Blaine surface area of three concretes meets the guidelines accompanying Standard NF EN 1538, while the fourth (BF2) has a slightly smaller Blaine surface area (3,650 vs. 3,800 cm^2/g).

Even though these concretes are compliant with requirements stipulated in Standards NF 1538/ EN and NF 206/CN, three of them still contain rather significant water release paths. It may be assumed that such disorders are

correlated with concrete bleeding. The bleeding study was performed in the laboratory in order to eliminate all jobsite-related uncertainties.

Foundation concrete bleeding study

In the laboratory, the same compositions (Table V) were produced for the four studied concretes. All concrete components used in the laboratory were identical to those found on-site.

Laboratory characterization of the concretes

Despite the fact that the BF2 concrete displays a lower slump value in the laboratory (560 mm) than in the field (640 mm), overall the four concretes reproduced in the laboratory match those delivered to their respective jobsites. This discrepancy for the BF2 sample may be due to site-related uncertainties (e.g. addition of admixtures or water).

Table V. Summary of fresh concrete characterization results from the laboratory

Tests	BF1	BF2	BF3	BF4
flow table test	570 ± 10mm	560 ± 10mm	640 ± 10mm	610 ± 10mm
Temperature exterior	22.4°C	20.6°C	23.6°C	21.2°C
Temperature of concrete	19.8°C	17.2°C	19.5°C	18.8°C
Entrained air	1.3 ± 0.3%	1.1 ± 0.4%	1.4 ± 0.4%	1.8 ± 0.2%

Laboratory analysis of concrete bleeding

For an unstable concrete, the pressure it endures at the bottom of the panel could cause mixing water to migrate towards the surface, in which case the concrete is being subjected to forced bleeding, which constitutes a major problem for fresh concrete stability. This study is carried out using a Bauer press filter, as specified in the Australian recommendations **[2].**

Experimental procedure

The device is composed of a standardized cylinder into which a filter has been introduced on the lower base (Fig. 3).

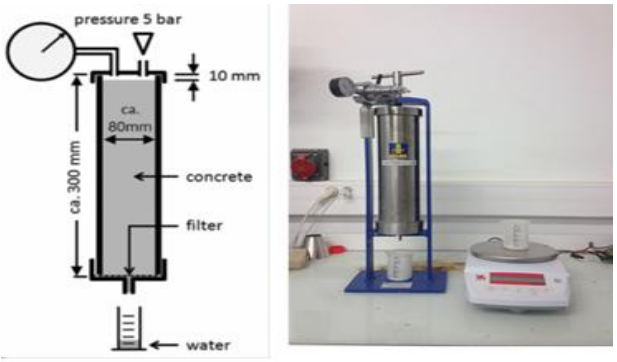

Figure 3. Principle of forced bleeding using a BAUER press filter

The concrete is then inserted into the cylinder in two successive layers, with each layer perforated 25 times in order to de-aerate the concrete. A 5-bar pressure (72.5 psi) **[2]** is applied onto the concrete. The water migrates towards the bottom of the cylinder and crosses the filter before being discharged through the outlet orifice in the direction of a container, where it is continuously weighed. The quantity of bleed water is measured every minute for 45 minutes.

5-bars pressure bleeding study

The quantities of bleed water at a 5-bar pressure for 5 minutes are indicated in Table VI for all four studied concretes.

Table VI. Quantity of bleed water at a pressure of 5 bar for 5 minutes

Concretes	Quantity of water bleed (ml)	Degree of pathology
BF1	11.8	nil
BF2	20.8	+
BF3	18.9	+++
BF4	19.4	++++

The BF1 sample, i.e. the reference concrete, exhibits less bleeding (11.8 ml after 5 min). The quantities of bleed water for the other three specimens all lie close to the recommended threshold (as listed in "Recommended Practice, Tremie Concrete for Deep Foundations"), which equals 24.4 ml. It is impossible to conclude that the degrees of pathologies are strictly due to the quantity of bleed water. The BF2 concrete diaphragm wall actually presents the fewest disorders (+), yet its quantity of bleed water is 20.8 ml. For BF4 on the other hand, despite recording the greatest number of disorders in the field (++++), its bleeding quantity is just 19.4 ml. An additional study would be required to establish a correlation between the degree of diaphragm wall pathology and concrete mix design parameters. Nonetheless, it can still be observed in Table VI that for concretes BF3 and BF4, the further this

quantity is from the threshold value, the fewer the number of water release paths, which is why one solution would be to lower the threshold value of acceptable bleeding water to a quantity of 15 ml.

VALIDATION DE LA VALEUR DU SEUIL ADMISSIBLE ADOPTE

Two jobsites (Fig. 4) were selected to study the influence of the yield value set for the quantity of bleed water. Both sites were underground parking. The diaphragm walls were 22 and 25 m high, respectively, and 0.8 m thick. Azzi **[3]** and de Larrard **[6]** proved that increasing the quantity of fines had the effect of reducing bleed water. The basic mix designs proposed by the concrete manufacturers were modified by taking into account their on-site experience. The particle size distribution of the various mixes was modified in order to have continuous distribution, a gravel/sand ratio lies between 1 and 1.1 and an increasing of the quantity of fines. Table VII lists the modified mix design parameters. Both concretes show a quantity of bleed water less than 15 ml. After earthworks and planning, no water release paths were observed on the walls of the both structures (Fig. 4).

Table VII. Modified mix design parameters

Concrete	BF5 « Paris »		BF6 « Metz »	
	Initial formulation	Modified formulation	Initial formulation	Modified formulation
Quantity of fines	400 kg/m^3	440 kg/m^3	405 kg/m^3	445 kg/m^3
Granulometry curve	Discontinuity	Continuity	Discontinuity	Continuity
G/S	1.14	1.00	1.22	1.08
Quantity of water bleed	17.5 ml	12.8 ml	19.1 ml	13.4 ml

(BF5 « Paris », 2014)

(BF6 « Metz », 2015)

Figure 4. Diaphragm walls of two underground parking

CONCLUSION

The objective of this works program has been to achieve a better understanding of the origins of diaphragm wall pathologies identified following earthworks and

planning, for the purpose of proposing solutions and recommendations aimed at limiting the extent of such pathologies.

The various concrete mix design parameters influencing the disorders encountered have been recorded. A comparison of four concretes stemming from different sites was drawn. A study of the quantity of bleed water, conducted using a press filter (Bauer), served to highlight that the bleed water threshold value of 24.38 ml, as prescribed in the recommendations, is in fact too high. The solution proposed herein is to lower this threshold value to 15 ml.

The basic foundation concrete mix designs of 2 diaphragm walls were consequently modified. The walls visible during earthworks at both these sites revealed no water release paths. A working group (EFFC Concrete Task Group, Munich) has incorporated these results into their modification of existing recommendations.

References

[1] Journal CIMbéton, « *Les coulis et les bétons pour les fondations spéciales* » Routes n°85, september 2003.

[2] Recommended Practice., « *Tremie Concrete for deep foundations* », Recommendation, Concrete Institute of Australia, 2012, pp. 30-33.

[3] AZZI A., « *Influence des paramètres de formulation du béton sur les pathologies des parois moulées* », research report n°02, February 2015, pp. 20-21.

[4] ACI 304.2R., «*Placing Concrete by Pumping Methods*, *ACI Material Journal* », july-august, 1995, pp. 441-464.

[5] JOSSERAND L., « *Ressuage des bétons hydrauliques* », PhD Thesis, Ecole des ponts et chaussées, 2002, pp. 34-41.

[6] DE LARRARD F., « *Structures granulaires et formulation des bétons* », Ecole des ponts et chaussées, 1999, pp. 137-140.

Development of Self Compacting Concrete for a Tremie Application

Egemen Kesler[1], Gülden Keskin[1], Arca Berker[2], Tahir Turgut[2], Yılmaz Akkaya[1]

[1]Istanbul Technical University, Istanbul, Turkey
[2]OYAK Beton RMC, Istanbul, Turkey

Abstract Tremie applications require highly workable fresh concrete properties since no vibration is used for the in-situ compaction of concrete. This type of concrete should be resistant to high wash-out pressures and self leveling, and thus, self compacting concrete (SCC) can be an alternative for such applications. Most of the time, pouring piles and diagraphm walls is a blind process, thus requires strict quality control measures during casting. In order to provide the sufficient workability and stability properties of the SCC, flow, flow retention, passing ability and water retention abilities are needed.

In this study, a self compacting concrete is developed for a tremie application where a minumum 100 years of structural service life is required. The developed SCC satisfied the desired fresh, mechanical and durability properties. Mixture designs, prepared with fly ash and silica fume, or with blast furnace slag were tested for flow, flow retention, passing ability and air content. Properties before and after pumping were also tested. Development of adiabatic heat, compressive, split tensile strength and elasticity modulus were measured at the laboratory. Electrical indication of concrete's ability to resist chloride ion penetration and chloride migration tests were performed on the cores from the structure. Microstructural observations were also performed on the thin sections and plane sections.

Keywords: *self compacting concrete, tremie, permeability, durability, microstructure*

Introduction

Tremie applications for diaphragm walls, require concrete mixtures with passing and flow abilities that can be achieved by using SCC properties. SCC can be defined as a concrete mixture which requires no vibration, flows under its own

weight and fills the formwork properly. Hardened SCC has similar or better mechanical and durability properties compared to conventional concrete mixtures [1]. To define a concrete mixture as SCC, it requires several characteristics such as passing ability, filling ability and segregation resistance [2].

Successful SCC designs require much more attention to factors such as coarse aggregate type, size, volume and grading, binder type and composition, and water/cement ratio compared to conventional concrete. To have proper workability and desired hardened concrete properties, careful selections of material constituents and mixture proportions are necessary [3].

Optimizing self-compacting concrete mixtures for tremie pipe

Powder type SCCs generally have higher amount of fine particles and better flow characteristic compared to conventional concrete mixtures. Improved flow and stability characteristics can be achieved by using low w/c ratio and high-range water reducing admixtures (HRWR) [4]. Due to natural variations in fine material content of natural sand and fillers, and job specific requirements, it is difficult to specify a certain mixture design method during production [5]. Some of the key factors which affect the mixture design and properties of SCC are placement method, formwork shape and size, and amount of reinforcement [6].

Some of the conventional SCC tests for fresh state can be summarized as slump flow, U box, L box, V- flow and J ring. Slump-flow and V funnel tests indicate flowability where, U box and L box tests indicate passing ability of SCC [4,7,8]. It is also important to perform full scale trials on site, before the production to adjust the mixture proportions. Job specifications such as retention of workability, pumpability or setting time, as well as seasonal temperature and humidity conditions, may require final in-situ adjustments.

For achieving a desired construction quality for tremie applications, a proper concrete mixture design, as well as an appropriate casting procedure are important factors. For this reason, a sacrificial buffer between bentonite and concrete is placed in the tremie pipe to prevent mixing and segregation of the concrete and bentonite. Concrete is then poured from the concrete pump into the tremie pipe hopper. During the concreting operation the bottom of the tremie pipes must be kept immersed in the fresh mixture at all times.

Mixture Proportions and Fresh Concrete Test Results

The mixture proportions used in this research are presented in Table I. Mix 1 was produced with CEM I type cement, fly ash, micro silica and high range water reducing admixture (HRWR) that based on polycarboxylic ether. Mix 2 and Mix 3 were both produced with CEM III B type cement and high range water reducing

admixture that based on modified phosphonate. Silica fume content was determined based on electrical indication of chloride penetration test ASTM C1202. 15% fly ash and 5% silica fume addition into Mix 1, resulted in test values below 1000 coulomb, a limit determined by the project designer. Maximum size of the aggregate was 22 mm for Mix1 and Mix 2, and 12,5 mm for Mix 3.

Table I. Mixture proportions (kg/m^3)

	Mix 1	**Mix 2**	**Mix 3**
CEM III B	-	380	380
CEM I	285	-	-
F-type Fly ash	50	-	-
Micro Silica	12	-	-
Water	123	132	149
Eq. w/c	0,38	0,35	0,39
HRWR	3,6	5,7	6,7
Air Entrainer	0,3	0,6	0,3
Natural Sand	426	444	485
Crushed Sand	465	420	397
No 1Aggregate	517	480	909
No 2 Aggregate	481	482	-

Fresh concrete tests such as slump flow (ASTM C 1611), L box (EN12350-10), U box, V flow (EN12350-9) were performed to quantify flowability, filling, passing and segregation properties of concrete mixtures (Table II and Table III). These tests were performed both before and after pumping, to characterize fresh concrete behaviour before casting with tremie. The slump flow values were in SF1 class (550-650 mm) [1]. H_0 measurements in L box test indicate the filling height measurement after the rebars.

Mix 2 and 3 presented similar slump and slump flow values before and after pumping. By elapsing time and pumping; slump, slump flow and flow values of Mix 2 and Mix 3 increased, owing to the chemical properties of the super plasticizer.

Table II. Fresh concrete test results.

Mix No and Testing Time	Air Content [%]	Unit Weight [kg/m^3]	Concrete Temp. [°C]
Mix1@1,5h BP	4,6	2366	20,1
Mix1@3,0h AP	6,8	2282	22,7
Mix2@0,25h	2,7	2424	25,5
Mix2@0,5h BP	3	2387	26,3
Mix2@1h AP	5	2342	27,7
Mix2@1,5h AP	N/A	2319	27,8
Mix3@0,25h	3	2388	21,3
Mix3@1h BP	3,6	2356	21,1
Mix3@1,5h AP	6	2301	21,8
Mix3@2h AP	5	2350	20,4

BP:Before pump, AP:After pump

Mix 1 was a highly workable concrete mixture with a slump value in between 21-24 cm. Mixes 2 and 3 were designed with self compacting characteristics. In SCC characterization tests, due to lower maximum aggregate size, Mix 3 presented better passing ability than Mix 2, although both mixes had similar cementitious material content.

Table III. L box, U box, V funnel test results.

Mix No	Lbox (H_2 / H_0 / H_1) [cm]	Ubox (H2-H1) [cm]	V funnel [s]
Mix2@1h (AP)	1,8 / 7,2 / 40	43,5	-
Mix2@1,5h (AP)	0 / 6,5 /48	15,5	13
Mix3@1,5h (AP)	6 / 10 /23	16	10
Mix3@2h (AP)	6,7 / 10 /18	20	12

Hardening and Hardened Concrete Test Results

Laboratory tests were performed to determine development of compressive and tensile strength (EN 12390-3, EN 12390-6), modulus of elasticity (NT BUILD 205) and adiabatic heat (NT BUILD 388). Tests results are presented in Figure 1. Mix1 presented higher compressive and tensile strengths than Mix 2 and Mix 3 at

early ages. Also, due to use of CEM I type cement, adiabatic heat development of Mix 1 is significantly higher than Mix 2 and Mix 3.

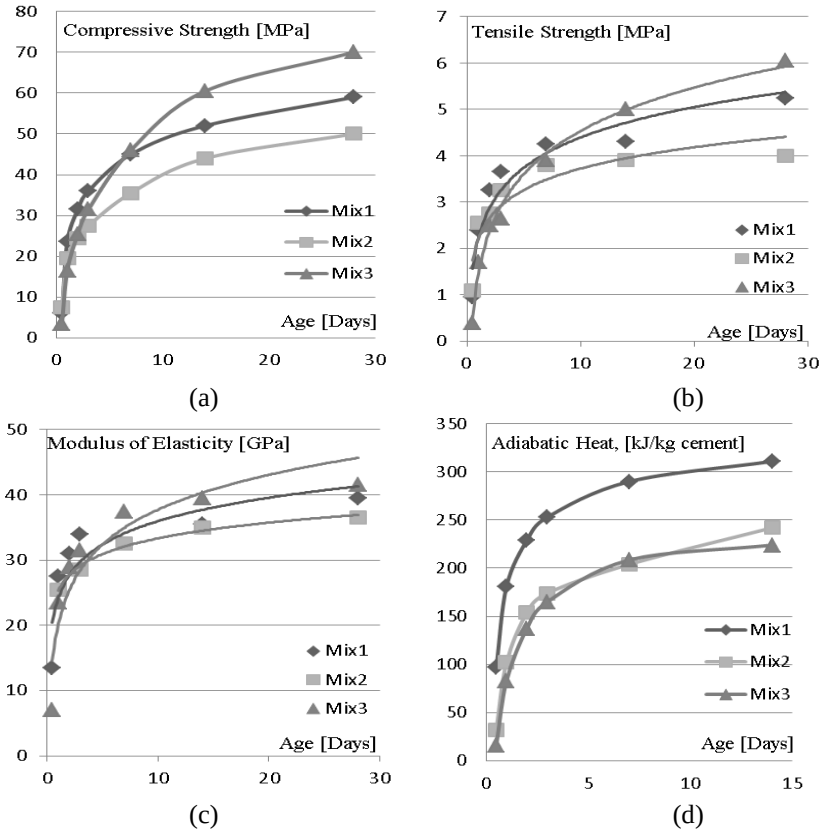

Figure 1. Development of (a) compressive strength, (b) tensile strength, (c) modulus of elasticity, (d) adiabatic heat

Compressive strength developments of the mixtures were measured at different curing temperatures and given in Figure 2. Mix 1 presents faster and higher strength development at 15°C and 25°C curing temperatures. Mixes 2 and 3, with blastfurnace slag, on the other hand, presented a more sensitive behavior to temperature. As the curing temperature increases, the differences with respect to strength development, were less pronounced.

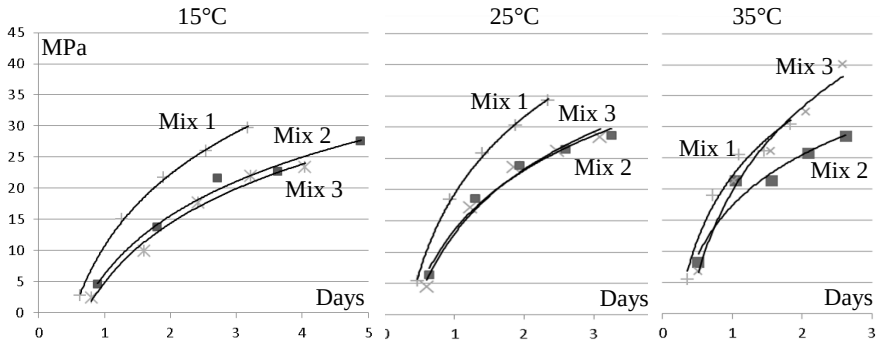

Figure 2. Compressive strength development at different curing conditions.

Site Assessment and Concrete Properties

Full scale diaphragm walls and trial castings were constructed with concrete mixtures 1 and 2 by tremie application. Cast diaphragms were excavated, cleaned and visually inspected (Figure 3). 100x200mm cylinder samples casted and cores with 100 mm diameter were taken from these walls to perform compressive strength and durability tests such as chloride migration (NT BUILD 492) and electrical indication of concrete's ability to resist chloride ion penetration (ASTM C 1202). Compressive test results and durability test results related to cylinder and core samples were given in Tables IV and V.

(a) (b)

Figure 3. Full scale diaphragm walls cast with (a) Mix 1 (b) Mix 2.

In visual inspection it is observed that the diaphragm walls with Mix 1 presented placement problems such as insufficient concrete cover, bentonite contamination and cavities.

All mixtures achieved the designed concrete strength class of C40/50. However, standard deviation of Mix 1 is higher than other mixtures, which might be due to the lesser compactibility of Mix 1.

Table IV. Core compressive strength test results (from $1m^3$ trial).

Mixture	**Age (days)**	**Compressive Strength, [MPa]**	
		Average	St. Dev.
Mix 1	29	42,7	6,6
Mix 2	36	44,2	2,1
Mix 3	29	47,3	1,8

Chloride migration coefficients of Mix 1 and Mix 2 presented similar test results for 100x200mm cylinder samples. Mix 3 presented the lowest chloride migration coefficient. However, cores taken from site casting, indicate that Mix 1 had significantly higher chloride migration coefficient than Mix 2. Also standard deviation of Mix 1 on core test results was higher than Mix 2. All mixtures can be classified as "Very Low" permeability class, according to ASTM C1202. Mix 1 site core samples presented much higher standard deviation value than other samples.

Table V. Permeability test results.

Sample Code / Sample Type	**Chloride Migration Coeff., [10^{-12} x m^2/s]**			**Chloride Ion Penetration, [Coulombs]**		
	Age (days)	Average	St Dev.	Age (days)	Average	St Dev.
Mix 1 / Cylinder	31	5,8	0,3	32	1003	33
Mix 1 / Core	38	5,7	0,3	31	840	15
Mix 1 / Core	168	4,9	2,1	174	666	274
Mix 2 / Cylinder	35	5,4	0,9	35	513	20
Mix 2 / Core	42	1,1	0,2	43	201	5
Mix 3 / Cylinder	29	3,1	0,5	30	783	50
Mix 3 / Core	32	4,8	0,7	34	531	41

Fluorescence impregnated thin sections (30x45 mm) indicated increased capillary porosity around some aggregates for all mixtures. Entrapped air voids and some micro cracks were also observed (Figure 4 and Table VI). Local bleeding zones and air void agglomerations were observed in Mix 2.

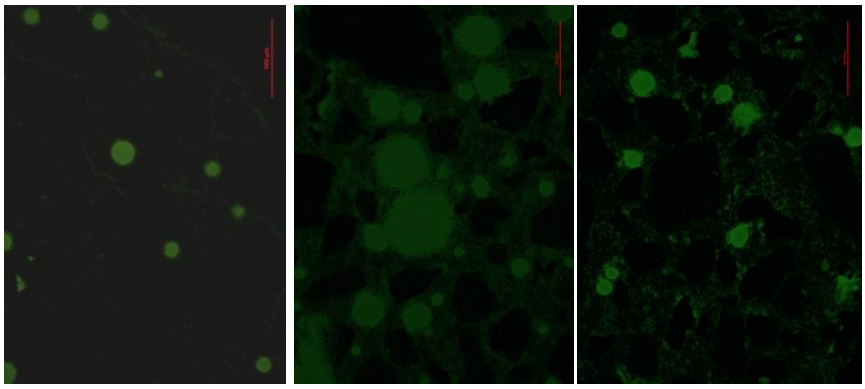

(a) (b) (c)

Figure 4. Thin sections of (a) Mix 1, (b) Mix2 and (c) Mix 3 (x50, UV light,).

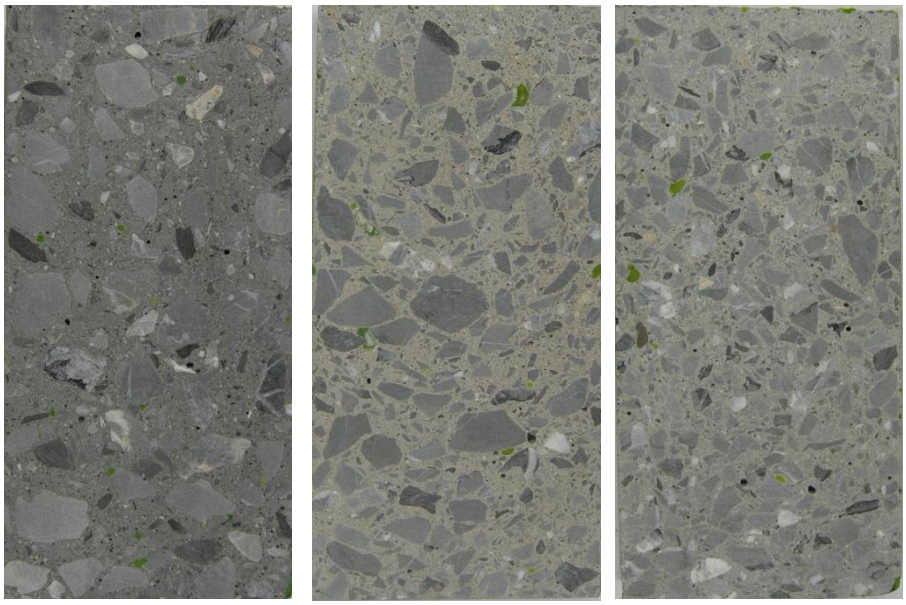

(a) (b) (c)

Figure 5. Plane section views of (a) Mix 1, (b) Mix 2 and (c) Mix3.

Plane section analysis (10 x 20 cm) of Mix 2 and Mix 3 presented better compaction characteristics. No crack was observed in all mixtures (Figure 5 and Table VI). Number of entrapped air voids in Mix 1 presented higher than other mixtures.

Table VI. Thin and Plane Section Analysis Results.

		Mix 1	Mix 2	Mix 3
Number of Entrapped Air Voids	2-5mm	39	17	24
	5-10mm	1	3	4
	>10mm	0	1	1
Micro Paste Cracks [no/mm^2]		0,2	0,1	0,0

Conclusion

Several concrete mixture designs were designed and tested for self compactibility in a tremie application. The results indicate that it is possible to use self compacting concrete in such applications with required durability and permeability characteristics. It is observed that, mixture design modifications, with respect to workability, might be necessary during production. Different types of cement and admixtures, and water-to-cement ratio can be used for mixture design modifications. It is also possible to control the heat development of concrete by selection of cement type. Microstructural observations during the full scale trials, can be a useful tool to verify compaction characteristics of the in situ concrete.

References

[1] The Self-Compacting Concrete European Project Group (2005), "The European Guidelines for Self-Compacting Concrete Specification, Production and Use", p 68.

[2] ACI Committee (2007), *"ACI 237R-07 Self-Consolidating Concrete"*, Emerging Technology Series, Michigan, US, p 34.

[3] Transportation Research Board (2009), "Self-Consolidating Concrete for Precast, Prestressed Concrete Bridge Elements", NCHRP Report 628, Washington, D.C., p 99.

[4] Campion J.M., Jost P. (2000), *"Self-compacting concrete: expanding the possibility of concrete design and placement"*. ACI Conc Int ; Vol 22, no4 pp.31–34.

[5] Naik T.R., Kumar R., Rammeb B.W., Canpolat F. (2012), *"Development of high-strength, economical self-consolidating concrete"*, Construction and Building Materials, Vol. 30, pp. 463–469.

[6] Khayat K.H. (1999), *"Workability, testing and performance of self-consolidating concrete"*, ACI Materials Journal/May-June, pp 346-353.

[7] Ouchi, M. "Self-compacting concrete development, application and investigations",http://www.faggruppeba.no/ikbViewer/Content/738950/doc-23-3.pdf , p. 5.

[8] Yahia A., Aïtcin P.-C. (2015), "Self-consolidating concrete", *Science and Technology of Concrete Admixtures*, Woodhead Publishing, Cambridge, UK, pp 491-502.

Performance of Self-Consolidating Concrete Developed for Iconic and High-Rise Structures in North America

Van Bui

Principal Scientist, BASF Corporation, 23700 Chagrin Blvd., Beachwood, Ohio 44122, USA

Abstract Construction of iconic and high-rise structures require concrete having special properties in fresh state and very high performance in hardened state. Self-Consolidating Concrete (SCC) is an excellent material used in those structures. This paper highlights the performance of SCC developed for various iconic structures and high-rise building in North America. Examples of the iconic and high-rise structures are Trump Tower in Chicago, One World Trade Center and 432 Park Avenue Super-Tall Building in New York and Lorin Park High-Rise Apartment Building in Minnesota. The SCC mixtures typically contained high content of supplementary materials. Laboratory test data, which include flowability, compressive strength, modulus of elasticity, maximum temperature in hardened concrete, and/or drying shrinkage, are presented. The performance data of selected ultra-high performance SCC mixtures with design strength of 138 MPa (20,000 psi) and modulus of elasticity of greater or equal to 55 GPa (8,000 ksi) are also highlighted in the paper.

Keywords: *Compressive Strength, High-Performance, High-Rise Building, Iconic Structure, Modulus of Elasticity, Self-Consolidating Concrete, Ultra-High Performance*

Introduction

Construction of iconic structures and high-rise buildings require high-performance concrete with superior properties. The superior properties typically include high workability, high resistance to segregation, satisfactory pumpability, very high strength, high modulus of elasticity, low heat of hydration and low drying shrinkage. It is usually of great challenge to achieve simultaneously these superior properties. Also, the cast elements of the high-rise buildings typically have high reinforcement level, which could cause the blocking of coarse aggregate particles and insufficient consolidation if conventional concrete were used. The blocking

and insufficient consolidation can lead to poor protection against a corrosion of steel reinforcement, poor formed-surface finish and poor load-carrying capacity of cast elements. High-performance self-consolidating concrete (HP-SCC), which requires none or little vibration, exhibits high flowability, good passing ability and high resistance to segregation. Moreover, properly designed SCC is usually of high pumpability and enhances faster construction speed. Therefore, SCC has been being successfully used in many projects in order to meet the highly challengeable performance requirements.

This paper highlights the performance of SCC developed for various iconic and high-rise structures in North America. Examples of the iconic structures are Trump Tower in Chicago, One World Trade Center and Super-Tall Apartment Building in New York and Lorin Park High-Rise Apartment Building in Minnesota. The SCC mixtures typically contained high content of supplementary materials. Laboratory test data, which include slump flow, compressive strength, modulus of elasticity, maximum temperature in hardened concrete and/or drying shrinkage, are presented. The performance data of selected ultra-high performance SCC mixtures with design strength of 138 MPa (20,000 psi) and modulus of elasticity (hereafter called MOE) of greater or equal to 55 GPa (8,000 ksi) are also presented in the paper.

Holistic Mixture Proportioning Approach

The main properties of fresh SCC include flowability, passing ability, resistance to segregation and formed-surface finishability. In order to achieve these properties of fresh SCC, a proprietary mixture proportioning program with a holistic approach (see *Figure 1*) [1] has been being used successfully in helping concrete suppliers to design SCC mixtures for a number of projects, which include some high profile projects presented in this paper. SCC mixture is modeled as a two-component material with solid and fluid phases. The solid and liquid phase criteria were built. The solid phase criteria ensures that the SCC is of good passing ability, and the fluid phase criteria ensures that the SCC is of excellent flow, good segregation resistance and good formed-surface finish-ability.

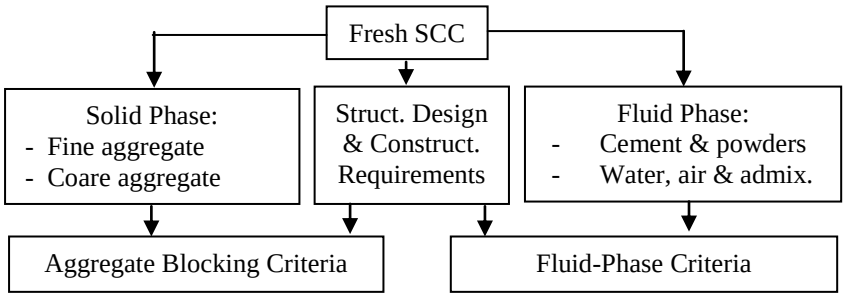

Figure 1. Holistic Mixture Proportioning Approach

Performance of SCC for Iconic and High-Rise Structures

Trump International Hotel and Tower, Chicago, USA

Trump International Hotel and Tower in Chicago is a distinctive 92-level structure with 415-m (1,362 feet) high. Total concrete of 148,325 m^3 (194,000 cubic yards), including 8 unique SCC mixtures formulated exclusively for this project was successfully delivered by Prairie Material Inc. [2]. The 56-day strength from 69 MPa (10,000 psi) and 110 MPa (16,000 psi) and 56-day modulus of elasticity (MOE) of 43 GPa (6,200 ksi) and 50 GPa (7,200 ksi) are required for SCC used in matt foundation and super-structural elements. The SCC temperature was limited to a maximum of 27 ^{O}C (80 ^{O}F) at the time of placement and 77 ^{O}C (170^{O}F). Also, SCC should be able to be pumped to the highest level during construction. While each of the specification requirements for the SCC could be met without much difficulty, their combination and the need for consistency in performance posed a significant challenge.

The mat foundation for this structure measured 60 m (198 feet) in length, 18 m (60 feet) in width and 3 m (10 feet) in depth, and required approximately 3,800 m^3 (5,000 yd^3) to SCC being cast continuously over 24 hours. Concrete producer, Prairie Material Inc. along with their chemical admixture supplier, BASF, collaboratively designed a concrete mixture that adhered to the strict specifications. A trial prior actual pour was conducted with mixing at batching plant and casting at the trial site to learn about the mixing efficiency and place-ability. Testing with actual pours was conducted at the project site. The slump flow of the SCC ranged from 680 – 740 mm (27 to 29 in.), maximum temperature of fresh and hardened status was 22 ^{O}C (72 ^{O}F) and 71 ^{O}C (160 ^{O}F), respectively. An average compressive strength of 63 MPa (9,100 psi) was achieved at 7 days, and the 28-day strength was well over the design 56-day strength of 69 MPa (10,000 psi). Over 30 ready mixed concrete trucks made 600 trips to the Trump Tower site for 23-hour continuous placement with the use of three conveyers. The SCC was conveyed into place and flowed as far as 12 m (40 feet) without segregating as can be seen in *Figure 2*. The mixture was extremely consistent throughout placement.

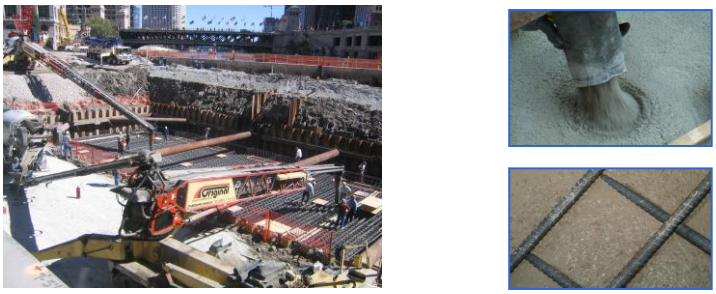

Figure 2. Placement of SCC for Mat Foundation, Trump Tower in Chicago

New World Trade Center, New York City, USA

The core towers at New World Trade Center include One World Trade Center (Tower 1), 2 World Trade Center (Tower 2), 3 World Trade Center (Tower 3), 4 World Trade Center (Tower 4) and 7 World Trade Center (Tower 7) [3]. One World Trade Center (also known as Freedom Tower) is the main building of New World Trade Center in lower Manhattan. At 541 m (1,776 feet) tall, One World Trade Center (hereafter called One WTC) is currently the tallest building in the Western Hemisphere [4, 5].

The performance requirements for One WTC included 56-day strength of 97 MPa (14,000 psi), 83 MPa (12,000 psi), 69 MPA (10,000 psi) and 55 MPa (8,000 psi), and respective 56-day modulus of elasticity (MOE) of 48 GPa (7,000 ksi), 48 GPa (7,000 ksi), 46.9 GPa (6,800 ksi) and 44 GPa (6,400 ksi) [4]. In addition, the SCC should be of satisfactory pumpability and have maximum allowable temperature of 71 ^{o}C (160 ^{o}F) in hardened state.

BASF together with Eastern Concrete Materials, US Concrete group has collaborated in developing Green Sense SCC mixtures in laboratory, field trials at batching plants, and at actual production during construction of New World Trade Center [5]. Similarly to the case of Trump Tower in Chicago, trials at batching plant for Green Sense SCC mixtures and onsite execution were undertaken to make a fine-tune of admixture dosages in order to achieve desired workability and workability retention as well as a good robustness for quality control enhancement. The holistic mixture proportioning approach, thorough laboratory development and field trials had helped to produce and transport successfully SCC mixtures during actual construction.

The 97-MPa (14,000-psi) Green Sense SCC mixture with up to 72% supplementary cementitious materials achieved 56-day compressive strength of approx. 110 MPa (16,000 psi) in laboratory with use of drum mixer and up to 124 MPa (18,000 psi) in field trial and in actual production using a central mixer [5]. This Green Sense SCC exhibited also very high 56-day MOE [55 GPa (7,990 ksi) and 58 GPa (8,350 ksi) for the lab and field trial mixture, respectively], and low maximum temperature [57 ^{o}C (135 ^{o}F) for the laboratory mix and 60 ^{o}F (140 ^{o}F) measured on field trial site] in hardened state. The 97-MPa (14,000-psi) Green Sense SCC mixture also exhibited high flow, excellent flow retention, good segregation resistance and satisfactory passing ability during actual production. The Green Sense SCC with high pumpability were also successfully pumped to 103 stories to the highest elevation in North America at the construction time [5].

Summary of performance of Green Sense SCC developed at BASF laboratory for Tower 4 are shown in *Table I*. As can be seen, all Green Sense SCC at age of 56 days exhibited high compressive strength and MOE, which were higher than the

required target strength and MOE. Those Green Sense SCC, which had high workability retention, were effectively produced at batching plant.

Table I. Performance of Green Sense SCC developed in laboratory for Tower 4

56-day comp. strength (MPa)		56-day MOE (GPa)	
Design	Tested	Design	Tested
83 (12,000 psi)	97 (14,010 psi)	43 (6,250 ksi)	49 (7,140 ksi)
69 (10,000 psi)	93 (13,410 psi)	39 (5,700 ksi)	47 (6,830 ksi)
59 (8,600 psi)	75 (10,940 psi)	36 (5,290 ksi)	41 (5,900 ksi)

Figure 3. New World Trade Center (photo credit of rew-online.com) and typical slump flow of developed SCC mixtures

432 Park Avenue Super-Tall Apartment Building, New York City, USA

The super-tall apartment building at 432 Park Avenue in New York city with a height of just under 425.5 m (1,400 feet) is currently the tallest residential concrete structure in the western hemisphere [6]. Vertically the building is of rectangular shape. The off-white SCC mixtures were used in construction of this building. The SCC mixtures must meet high-performance requirements in fresh and hardened states. They must be of high flow, good segregation resistance, satisfactory passing ability and excellent form-surface finish ability. The SCC mixtures should be also of good colour consistency and pumpable to the highest floor of the building. The design required performance for SCC at age of 56 days

include compressive strength of 97 MPa (14,000 psi) and modulus of elasticity of 51 GPa (7,450 ksi). The maximum allowable temperature of hardened self-consolidating concrete were specified at 71 ^{o}C (160 ^{o}F).

BASF with its customer, Ferrara Bros Building Materials Corp. developed successfully off-white SCC mixtures, which met or exceeded all performance requirements in fresh and hardened states. The SCC mixture, which contained white Portland cement and up to approx. 70% supplementary cementitious materials, including metakaoline, had very high slump flow [up to 760 mm (30 inches)], good segregation resistance, satisfactory passing ability and excellent enhancement for formed-surface finish (see Figure 4). The off-white SCC mixture also had high workability retention and was pumped effectively to the elevation of the highest floor at the speed of 15 to 23 m^3 (20 to 30 cubic yard) per hour [6].

Table II showed the compressive strength, MOE and maximum temperature of the SCC mixture developed in laboratory. As can be seen, the developed SCC exhibited very high performance, which met or exceeded the required design criteria. It was successfully produced and placed thanks to a close collaboration between concrete supplier, Ferrara Bros Building Materials Corp, contractor and admixture supplier, BASF Corporation [6] throughout the process of careful SCC mixture development, field trials and actual production as well as during construction period.

Table II. Laboratory performance of SCC developed for 432 Park Avenue building

56-day comp. strength (MPa)		56-day MOE (GPa)		Max. temperature (^{o}C)	
Design	Tested	Design	Tested	Design	Tested
69 (10,000 psi)	102 (14,760 psi)	43.4 (6,300 ksi)	46.5 (6,747 ksi)	71 (160 ^{o}F)	64 (148 ^{o}F)
83 (12,000 psi)	118 (17,130 psi)	47.6 (6,900 ksi)	51.5 (7,469 ksi)	71 (160 ^{o}F)	64 (147 ^{o}F)
97 (14,000 psi)	126 (18,320 psi)	51.4 (7,450 ksi)	53.9 (7,815 ksi)	71 (160 ^{o}F)	60 (140 ^{o}F)
97 (14,000 psi) (Field)	137 (19,860 psi)	51.4 (7,450 ksi)	53.4 (7,743 ksi)	71 (160 ^{o}F)	-

Figure 4. View of 432 Park Avenue apartment building and formed-surface finish cast with SCC (photo credit of Joe Nasvik [6])

36-Story High-Rise LPM Apartment Tower, Minneapolis, MN

Construction of 36-story high-rise LPM apartment tower requires high-performance concrete having 28-day design compressive strength of 55 MPa (8,000 psi), 69 MPa (10,000 psi) and 83 MPa (12,000 psi) and 28-day modulus of elasticity (MOE) of 35.5 GPa (5,150 ksi), 39.7 GPa (5,760 ksi) and 43.4 GPa (6,300 ksi), respectively. BASF and Cemstone Concrete Products developed and produced high-performance Green Sense Concrete (HP-GSC), which met or exceeded the performance requirements. The HP-GSC with fly ash replacement up to 40%, had a slump flow ranged from 460 mm (18 inches) to 585 mm (23 inches) and high resistance to segregation. It was successfully pumped to the highest elevation of the 36-story tower and easily placed with little vibration. As seen in *Table III*, the performance of the developed HP-GSC, which contained high fly ash content, exceeded the design performance requirements. These good results were achieved without the use of silica fume.

Table III. Laboratory test performance of HP-GSC used in LPM Apartment Tower

28-day compressive strength (MPa)		28-day MOE (GPa)	
Design	Tested	Design	Tested
55 (8,000 psi)	81 – 90 (11,770 – 13,120 psi)	35.5 (5,150 ksi)	38.3 – 41.3 (5,549 – 5,981 ksi)
69 (10,000 psi)	83 – 93 (11,980 – 13,470 psi)	39.7 (5,760 ksi)	40.1 – 41.0 (5,814 – 5,951 ksi)
83 (12,000 psi)	96 – 103 (13,910 – 14,970 psi)	43.4 (6,300 ksi)	47.6 – 49.0 (6,897 – 7,107 ksi)

Figure 4. View of LPM Apartment Tower (photo credit of urbanmsp.com) and typical slump flow of developed HP-GSC

Ultra High-Performance Self-Consolidating Concrete for Future Tall-Structures

BASF, together with its customer, has developed an ultra high-performance self-consolidating concrete (UHP-SCC) with a design 90-day compressive strength of up to 138 MPa (20,000 psi), 90-day MOE of up to 55 GPa (8,000 ksi) and maximum temperature of 71 ^{o}C (160 ^{o}F) in its hardened state. Conventional concrete materials, without fibers, from several sources were used. The developed UHP-SCC mixtures had high slump flow ranging from 660 mm (26 inches) to 760 mm (30 inches) and high segregation resistance (see *Figure 5*). It is expected to be pumpable as their compositions were carefully designed with use of the Holistic Mixture Proportioning Approach mentioned in previous section.

The required strength at 16 hours was 20.7 MPa (3,000 psi). Type I/II cement from two sources (C1 and C2) were used. For mixtures (Mixture A2 and A3) containing cement C2, a low dosage of accelerator was used in order to achieve 16-h strength of 20.7 MPa (3,000 psi), while UHP-SCC mixture (Mixture A1) did not contain any accelerator. The test results of UHP-SCC containing materials are shown in *Table IV*. As can be seen, UHP-SCC exhibited very high performance in both its fresh state and hardened state. 16-h strengths ranged from 31.4 MPa (4,550 psi) to 37.9 MPa (5,500 psi), and 90-day compressive strength ranged from 146 MPa (21,130 psi) to 158 MPa (22,840 psi). The 90-day elastic modulus was ultra-high [ranging from 56 GPa (8,150 ksi) to 61 GPa (8,860 ksi)]. The UHP-SCC also had very low 28-day drying shrinkage (260 μm) and low maximum temperature in its hardened state.

Figure 5. Typical slump flow of developed UHP-GSC

Table IV. Laboratory test performance of selected UHP-SCC

Mix ID/Properties	A1	A2	A3
Slump flow (mm)	725 (28.5 in.)	730 (28.75 in.)	660 (26.00 in.)
Air (%)	1.8	1.8	2.3
Comp. strength (MPa)			
16 hour	34 (4,980 psi)	31 (4,550 psi)	38 (5,500 psi)
7 days	119 (17,250 psi)	118 (17,109 psi)	125 (18,068 psi)
28 days	150 (21,670 psi)	149 (21,540 psi)	140 (20,350 psi)
90 days	154 (22,270 psi)	158 (22,840 psi)	153 (22,133 psi)
90-day MOE (GPa)	57 (8,260 ksi)	61 (8,860 ksi)	56 (8,150 ksi)
Max. temperature (^{o}C)	70 (158 ^{o}F)	59 (139 ^{o}F)	63 (145 ^{o}F)
28-day drying shrinkage *)	-	260 µm	-

*Note: *) Specimens were initially cured in molds for 1 day and under water for 6 days; they were then cured in standard drying conditions for 28 days.*

Summary

Construction of iconic structures and high-rise buildings require concrete with high-performance in its fresh and hardened states. In addition, super-structural elements and/or matt foundation of these structures usually have a high level of reinforcement, which causes a difficulty in achieving sufficient consolidation, if concrete mixture were not properly designed and proportioned. Achieving simultaneously all high-performance requirements of fresh and hardened concrete poses great challenges for concrete producers.

Self-consolidating concrete, which were carefully designed from a holistic mixture proportioning approach, have been developed in laboratory and implemented in field trials, and were successfully produced and used for the iconic structures and high-rise building in North America. The developed SCC had high flowability, good flow retention, excellent segregation resistance and good passing ability, as well as satisfactory pumpability even to very high elevation of the structures. The developed SCC also exhibited very high performance, which met or exceeded extremely high requirements from the aspects of compressive strength, modulus of elasticity, low drying shrinkage and low heat of hydration.

The experience in development and use of SCC in the iconic structures and high-rise buildings in North America shows that, in order to apply successfully high-performance SCC in those structures, it is important that not only holistic mixture proportioning approach should be implemented, but also thorough laboratory investigation, appropriate field trials and good planning before actual construction need to be carried out.

UHP-SCC, which contains conventional concrete materials, without fibers, were successfully developed. The developed UHP-SCC had very high flowability and excellent resistance to segregation. The UHP-SCC exhibited ultra-high strength at early and late ages, ultra-high modulus of elasticity, low heat of hydration and low drying shrinkage.

Acknowledgment

The author would like to thank Mr. Andreas Tselebidis and Mr. Steve Farrington for their collaboration in development and field trials of SCC mixtures for New World Trade Center and 432 Park Avenue Apartment Building in New York city. Special thanks is given to other colleagues from BASF, Prairie Material Inc, Eastern Concrete Materials, Ferrara Bros Building Materials Corp, Cemstone Concrete Products and other BASF's customers for their precious help in the SCC development and application in respective structures.

Special thanks is also given to BASF Technical Center's management team, namely Dr. Tate Coverdale, Dr. Emmanuel Attiogbe, Mr. Paul Seiler and Mr. Steve Schaef for their instruction and support in making a priority during the time of the development and implementation of SCC and UHP-SCC mixtures for the iconic structures and high-rise buildings in North America.

References

[1] Van K. Bui, *Application of Minimum Paste Volume Method in Designing Cost-effective Self-Consolidating Concrete – An Experience in New Zealand*, Proceedings of First North American Conference on the Design and Use of Self-Consolidating Concrete, Chicago, USA, November 12-13, 2002, pp. 127-132.

[2] Http://www.prairie.com/portfolio/trump: *Chicago's Trump Tower Soars with Prairie High-Strength Concrete*

[3] Http://www.wtc.com: *Overview of New World Trade Center*

[4] Casimir Bognacki, *Self-Consolidating Concrete, Tower One, World Trade Center, New York, NY*, Presentation, 2015 World of Concrete, Las Vegas, NV, February 2, 2015.

[5] Gary Graziano, *Standing Strong at Ground Zero*, Concrete Construction, November 2013.

[6] Joe Nasvik, *Constructing a Super Tall Building*, ForConstructionPros.com, Feb. 25, 2014.

Alturki Business Park
Self Consolidating Concrete – A Case Study

Redwan Amin Hameed[1] and Narasimhulu Gary[2]

[1]Saudi Readymix Concrete Company, Saudi Arabia.
[2]Kuppam Engineering College confessions, India.

Abstract Though self-compacting concrete (SCC) is a revolution in concrete technology, until now the use of SCC in the world, in general, and in the Middle East, in particular, has been much less than expected for such high performance concrete.

In order to raise the awareness of the construction community in Saudi Arabia about SCC and to fully benefit from the advantages of this special concrete, Alturki Group decided to build its own headquarters and its business park using SCC for the entire project. Alturki Business Park (ABP) which consists of a 16 story tower and 10 office lofts is a unique project being the first and only building in the region built completely using SCC.

Research and trial mixes commenced before the start of the project. During construction, several challenges were encountered. The toughest challenge was to get a consistent and robust mix with very varying raw materials. This was not an easy task. Other challenges included: hot weather concreting, mix pumpability, controlling the bleeding, high sensitivity of the mixes to any change and the quick loss of flow and slump.

Different chemical admixtures were evaluated. Silica fume and ultrafine fly ash were used. Pumping simulations in the lab and in the field were performed and many trials were conducted to continuously improve the mixes during the course of construction.

The building was completed in 2011. Many lessons and a lot of experience were gained.

This presentation shows our experience in this project, the challenges, the solutions and the lessons learned.

Keywords: *SCC, pumping, quality control, rheology, case study.*

Introduction

Since its development, self-consolidating concrete (SCC) is still considered as a revolution in concrete technology. Despite its many benefits, its usage is still limited worldwide. The two main reasons behind this slow growth and acceptance are: the higher initial cost of SCC compared to conventional concrete and the lack of knowledge about SCC in construction industry. This is true worldwide and the market in Saudi Arabia is no exception.

In 2003; Saudi Readymix Concrete Company took a responsibility to raise the awareness about SCC in Saudi Arabia by sponsoring and conducting many public and private seminars about SCC. Since then, Saudi Readymix managed to pour SCC in several projects throughout the kingdom. However, Alturki Business Park (ABP) was a unique project and, to the best of our knowledge, the only building in the Middle East that was constructed completely using SCC.

SCC history and technology, its properties, advantages and testing methods are well documented in many other papers, guidelines and technical reports. It is not within the scope of this paper to talk about these points. The main objective of this paper is to share the experience and knowledge gained during the construction of ABP and to present the challenges encountered and what could be expected during SCC jobs.

The Project

Alturki business Park project (Figure 1) is located in Dhahran city in the Eastern Province of Saudi Arabia. The project consists of one tower and 10 villas brought together by spacious surroundings, harmonized architectural treatment, serene landscaping, and unified image. The development occupies an area of 34,000 m^2 (365973 ft^2) with a project site area of 8,600 m^2 (92570 ft^2). The villas are three-floor buildings. The tower is 16 floors building with two underground floors parking for 146 cars connecting directly to the building lobby.

The design is based on a 9-meter (29.5 ft) structural grid with a variable cantilever to form a cylindrical building with a 38-meter (125 ft) diameter. The structure is a multiframe system with post-tensioned slabs. The building is fully modern and incorporates all of the latest features of intelligent building design, sophisticated communications, security, computer and other low voltage systems.

The project was designed by Pei Partnership Architects; a New York based design office, and built by a local Saudi contractor.

Construction commenced on June 2008 and last slab was poured on 11/11/2009.

Figure 1. ABP Project at different stages

Why SCC?

Though it was not necessary to use SCC for the whole structure, the decision to build ABP using only SCC hit two birds with one stone.

1. Technical advantages: SCC generally provides better quality concrete for the structure. This was observed in ABP project. Some elements were highly congested with steel reinforcement (Figure 2) and SCC was the right choice to prevent segregation and honeycombing. SCC passed through congested steel and filled the forms without any problem. Moreover, the use of SCC assured a uniform concrete consolidation. Compacting conventional concrete using poker vibrators usually results in non-uniform compaction where one can find well compacted areas, partially compacted areas and areas that were not compacted at all. Placing and finishing SCC was much easier than normal concrete. It was possible to pour concrete for a 7 m high wall continuously in a very short time without any placing difficulties and concrete surface was very smooth.

Figure 2. Congested reinforcement in shear walls

The surface finish was excellent and almost blemish free and there was no need to do any surface repair (Figure 3). The contractor acknowledged that this was one of the best surface finishes they had ever produced.

Figure 3. Excellent surface finish was obtained using SCC

2. Raising the construction industry awareness. This was done by giving a real full scale live example about the constructability and many advantages of SCC. As a matter of fact, many interested engineers, consultants, students and university faculty members visited the site during construction to see SCC being placed and learn from this experience. Technical leaflets were published about the project and distributed to potential clients, engineers, designers and consultants.

Materials

It was very necessary to select raw materials with a good and consistent quality for this project. Selection of these materials and laboratory trial mixes were completed on an early stage before starting the construction.
Local ordinary Portland cement (type I) confirming to ASTM C-150 was used in all mixes. An ultrafine fly ash, with a mean particle size of 5 micron and a surface

area of 13000 cm^2/g was used as a supplementary cementitious material and filler. Dosage of ultrafine fly ash was initially 10% by weight of cement. In a later stage silica fume confirming to ASTM C-618 was used instead of ultrafine fly ash. The initial dosage of silica fume was 7% by weight of cement.

Crushed limestone aggregates of 20 mm, 10 mm and 5 mm sizes were used. The fine aggregate was local fine dune sand. Typical gradation results are shown in Figure 4.

The high-range water reducer was a polycarboxylate based admixture.

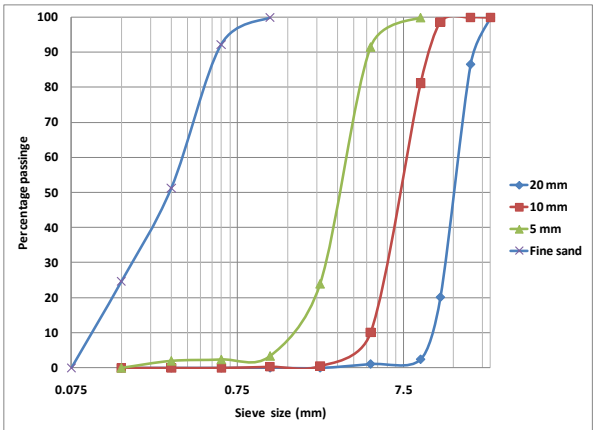

Figure 4. Typical gradation of aggregates

Project Specifications

- Compressive strength for vertical elements: 60 MPa (8700 psi)
- Compressive strength for other elements: 45 MPa (6525 psi)
- Max concrete temperature at the point of discharge: 32^o C (89.6^o F)
- Workability - Acceptance criteria: As per Table I.

Table I. Project Acceptance Criteria

Test	Unit	Limits	
		Min	Max
Slump flow	mm (inch)	650 (25.6)	750 (29.53)
T50	Sec	2	5
J-Ring(flow difference)	mm (inch)	0 (0)	50 (1.97)
L-Box	h_2/h_1	0.8	1.0
V-funnel	Sec	6	12

The Mix

During the bidding stage, SCC mixes were designed and lab trials were commenced and proportioning of mixes was adjusted until reaching, what we thought, "the final mixes". However, when construction activities began and actual concrete supply and pouring started, more adjustments and changes were made to come up with as robust mixes as possible to suite the encountered challenges.
The main adjustments that took place included increasing paste content, decreasing w/b ratio, optimizing mix gradations, optimizing the HRWR dosage, replacing ultrafine fly ash with silica fume and changing the dosage of these additives. Table II presents the typical mixes used in the project.

Table II. Project Mixtures

Design Strength MPa	Cement Kg	Silica Fume Kg	Total Powder Kg	Water Kg	W/B	PC Admix L	Paste %	Slump Flow mm	T50 sec	J Ring mm	V Funnel Sec	L Box	28 day Cylinder Str. MPa
45	490	17	507	150	0.3	4	31.66	720	3.8	685	6	0.92	69
60	520	23	543	150	0.28	3.7	32.86	730	3.6	680	10	0.94	82

Testing and Quality Control

Due to its nature and sensitivity, SCC required a stricter quality control program than conventional concrete. This was taken into consideration from the first day and a testing and inspection plan was put in place.
The following tests were performed on raw materials throughout the project duration:

- Tests on aggregates: gradation, moisture content and absorption, specific gravity, flakiness and elongation, abrasion as well as chemical analysis. Our main concern was the variation in aggregates quality. Water absorption was proven to be the most important to variation.
- Tests on cement: compressive strength and setting time to assure the consistency of cement quality from the same source and from different sources.
- Tests on superplasticizer: Both specific gravity and TDS were determined for each batch of admixtures received. Batches not conforming to the manufacturer's specifications were rejected.

- Marsh cone test was conducted to determine the optimum admixture dosage to be used in the mixes.
- The performance of several polycarboxylate superplasticizers was evaluated in terms of flow and flow retention and the one which gave us the best performance was selected.

The following tests were performed on fresh concrete:

- Slump flow test (spread and T50), J-ring test, L-box test and the V-funnel test. Typical results of different mixes are presented in Table II. Only the mixes that satisfied the acceptance criteria were used.
- Concrete temperature and air content were measured.
- Resistance to segregation was monitored by checking the visual stability index (VSI) (see Figure A1 in the appendix). Though there was no specification in this regard, we were accepting mixtures with VSI of only 1 or 0 (Figure 5).
- Fresh samples were collected in standard 150 x 300 mm (6x12 inch) cylindrical molds to determine the compressive strength of concrete.

Figure 5. SCC slump flow

Pumpability of SCC

Pumping high strength SCC to high rise building is a challenge. Though SCC is flowable, pumping this type of concrete requires more pressure [1] and more care and attention. SCC is very sensitive and may exhibit segregation and slump flow loss due to the change in pumping pressure or discharge rate.

In order to get information about pumpability of the designed mixes, Saudi Readymix sat up a pumping simulation system consisting of a Putzmeister 2110 HPD stationary pump and a 230 m (755 ft) long pipeline including 14 U-shape bends and 4 meters (13 ft) rise pipe (Figure 6). Pumping trials were conducted in cooperation with a Putzmeister team.

Figure 6. Saudi Readymix pumping simulation setup

Different mixes were tested in the laboratory with a special rheometer developed by Mr. K. Kasten from Putzmeister (Figure 7). The results obtained from the rheometer were checked against the results obtained later from the pumping simulation. A good correlation was observed (Figure 8). Using this simple rheometer in lab helped in saving time and effort to select appropriate mixes before running field trials. Based on these results it was determined whether the mixes were pumpable or not. In this case, mix C60_L3b gave better results than mix C60_L3a in terms of pressure and discharge rate

Figure 7. Rheological testing of concrete in the lab

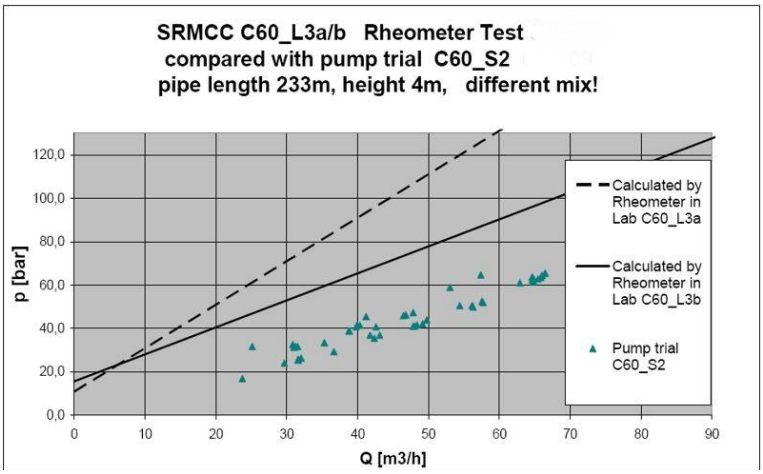

Figure 8. Comparison between Rheometer and pump trial results

Pump hydraulic pressure and concrete pressure in the pipeline were measured at two points. One concrete pressure sensor was installed directly after the hopper (Figure 9); the other sensor was installed after 120m (393 ft).

Figure 9. Concrete pressure sensor after hopper

During pouring, pumping pressure vs. discharge rate was monitored and recorded (Figure 10). Actual results were close to that obtained in the lab from the rheometer. The pressure was quite low even when concrete was pumped to the 14th floor.

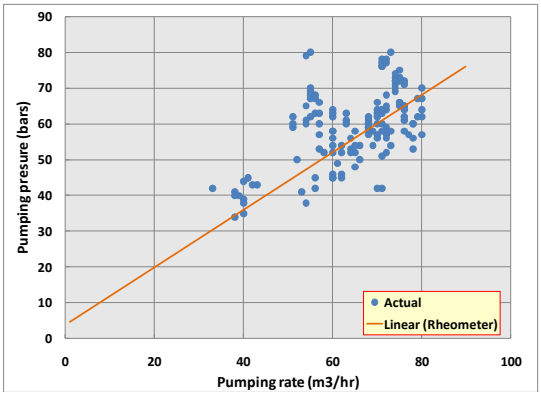

Figure 10. Pumping pressure vs. pumping rate

Challenges and Obstacles

Production and supply of SCC is not a breeze. Producing 0.05 m^3 (0.065 yd^3) of SCC in a lab trial under controlled conditions using uniform and consistent raw materials is very easy. Unfortunately, this is not the case when it comes to actual production and supply. One should be prepared for surprises, challenges and obstacles. The main challenges encountered during this project were:

- Lack of awareness and knowledge about SCC among most parties involved in the project. They started to deal with SCC with skepticism and considered it as "guilty until proven otherwise". The benefits of using SCC were not so sure and clear to them. With time and progress of work, the knowledge increased and some benefits started to be visualized.
- Resistance to change. This was expected and it was a direct result of the previous point.
- Inconsistency of raw materials. SCC is very sensitive to changes in raw materials. Through the course of the project the quality of the aggregates and cement kept changing and the performance of SCC was affected accordingly. It was a challenge to produce a consistent SCC with the required rheological properties. In many cases, it was hard to control the quality of mixtures and each batch had to be adjusted. Dosage of admixtures and mixtures ingredients had to be changed and tweaked with the variation of aggregates quality, especially absorption and moisture condition. There was a shortage in good quality aggregates and it was not possible to maintain the same quality of raw materials. The same problem was observed with cement whose quality was oscillating and difficult to predict.
- Loss of flow. This was confronted several times and in some cases it was necessary to use vibrators to compact the concrete. One reason behind this drop in flow was pumping. It is known that pumping is affecting the rheological properties of SCC

and that was causing the drop in flow from 700 ± 50 mm (27.6 ± 2 in) before pumping to about 575 ± 25 mm (22.6 ± 2 in) after pumping. Pumping affects the viscosity and the yield stress, and hence flowability, of SCC concrete due to structural breakdown and an increase in the air content. Both factors decrease the viscosity. However, yield stress increases due to structural break down and increases due to an increase in air content [1]. In ABP project we measured the air content and found it to increase from about 1.6% before pumping to about 2.5% after pumping.

- Loss of flow was also caused by the delay of trucks on site and due to the high ambient temperature and drying of concrete.
- Bleeding. Though it was not observed in lab trials and on station during production, in some pours, bleeding water was also clearly noticed on the top of concrete after pouring. In one case, a paste layer of about 2.5 cm (1 in) thick was formed on the top of the slab and had to be removed. In those cases, the mix was adjusted immediately. In other cases, ultrafine fly ash caused an unpleasant stained surface on some columns due to its floatation to the surface with the bleeding water. As a result, we stopped using ultrafine fly ash and replaced it with silica fume. This adjustment gave more robust mixes and the stains were never noticed again.
- At early age of the project and upon striking of the forms, pour lines were observed in the soffit of one slab. However, further inspection and investigation proved that these pour lines were superficial and did not have any adverse results on the structure.

Benefits

The benefits obtained from using SCC for the ABP project may be summarized as follows:

- More understanding of SCC behavior, production, transporting and placing. The project provided important learning topics.
- Increased awareness and knowledge as well as satisfaction of all parties involved in the project about SCC.
- Uniform concrete consolidation.
- Reduction in manpower and equipment
- Reduction in noise, since poker vibrators were not needed.
- Excellent, smooth surface finish
- Easier placing and finishing of concrete.
- Accelerated project schedule
- Reduction in equipment wear

Concluding Remarks and Recommendations

As a ready mixed concrete supplier, we learned a lot from this project. The main learning points are:

- Education and awareness about SCC is very essential. It is important to train and educate all personnel involved in the design, production, quality control, and placing of SCC before starting the project.
- Pre-pour meetings are important to plan for successful pouring and to assign the roles. In the ABP project case, a meeting between technical and production team would be held a day before the pour to put a detailed plan and to assign tasks for the team members in order to make sure that the job would go smoothly.
- Conduct necessary trials and mock ups ahead of time and get good knowledge about the behavior of SCC using different raw materials.
- Modify, adjust and optimize the mix as necessary during the course of the project.
- SCC is sensitive to variation. Try to keep the raw materials uniform and consistent and from a single source, if possible.
- Select the most proper and suitable admixture. Different admixtures will perform differently.
- Working with SCC requires stricter and closer quality control.
- Coordination between the teams at plant and site is very necessary.
- Interval between trucks should be planned carefully.
- Rate of placing SCC should not be fast to allow for entrapped air to escape
- Pump SCC using low pressure and continuous constant flow.
- When working with SCC, we have to expect and be ready to encounter different challenges.
- Since SCC does not bleed, plastic shrinkage cracks are more likely to occur during hot weather concreting and necessary preventive precautions need to be taken.
- There is still a lot of work to be done to optimize SCC mixes and reduce its cost.
- Both academia and industry should cooperate to reach to a better understanding and utilization of SCC technology.
- Finally, remember the six P's " Proper Prior Planning Prevents Poor Performance"

References

[1] Feys, D., De Schutter, G. and Verhoeven, R., "Rheology and Pumping of Self-Compacting Concrete", Proceedings of the tenth ACI international conference on recent advances in concrete technology and sustainability issues, Seville, Spain,2009.

Appendix

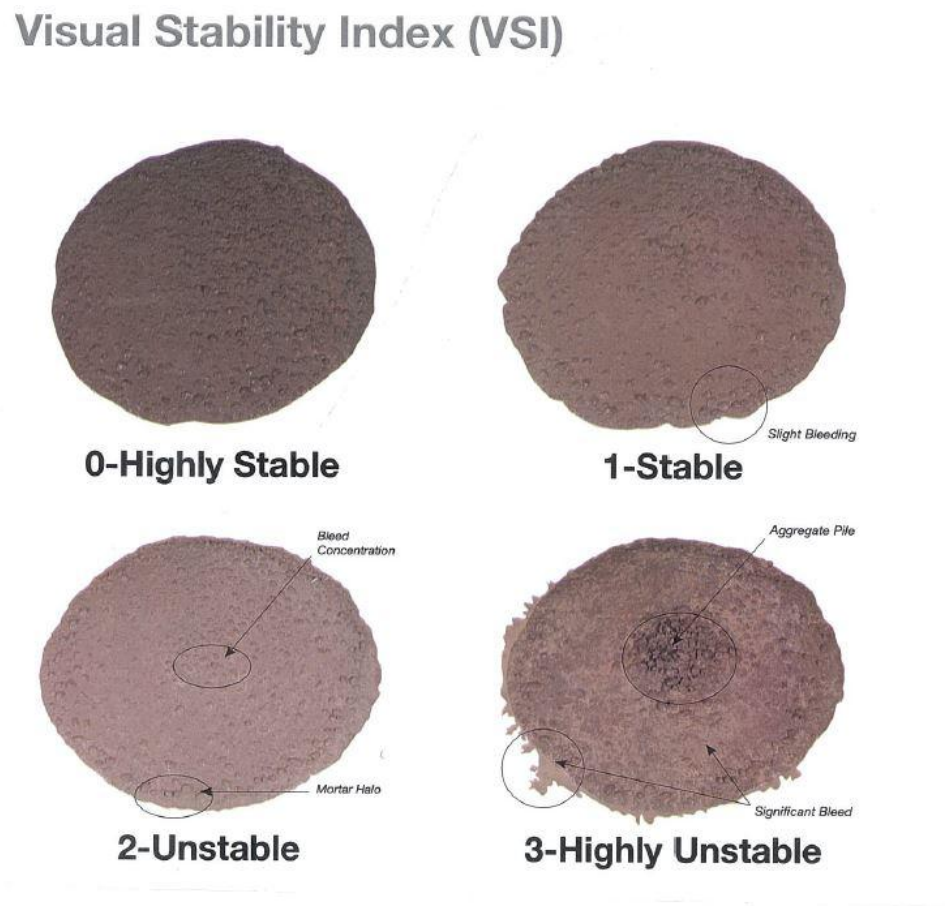

Fig. A.1. Visual Stability Index

Successful Self-Consolidating Concrete in North America

William S. Phelan

The Euclid Chemical Company

Self-Consolidating Concrete (SCC) is increasing at a rapid rate in North America. Structural Engineers are specifying it in their formed members. It is often the only solution for structural repairs. Many concrete contractors now know that its cost in place for reinforced, formed concrete is lower and the end product is superior compared to continuously placed and vibrated concrete.

Savings of $30 dollars per cy. for columns has been reported by one Concrete Contractor. Many contractors report that SCC is more economic than conventional vibrated concrete. A New York Contractor compared the conventional vs. SCC costs on a 35 ft. long 8 ft. high and 1' - 4" thick wall placement. The costs were $2,376.00 for SCC and $2,861.60 for conventional concrete.

SCC usage certainly has increased with the "Vibration White Finger" law in New York and other states. Europe has had White Finger Laws for many years. They clearly outline the limb damage done by vibrating concrete on a regular basis. The shrinkage of the concrete industry work force is also a significant factor in choosing SCC.

Many people today are choosing to live in a major city. Easy access to work, theatre and other entertainment and their friends is very appealing. The only solution in many cities is vertical construction. Tall buildings are being designed and built at a rapid rate throughout North America.

Maximizing rentable or suitable space is a primary requirement. Hence tall building with heavily reinforced columns and shear walls are the norm. High strength SCC is the answer. Proper vibration is often impossible. 12,000 psi SCC mixes @ 56 days is achievable everywhere in North America.

The choice today for tall buildings for engineers and contractors is whether to use flowing concrete (7½" - 10" slump) or SCC with 20" - 30" slump flow) for reinforced members and mass concrete. Flowing concrete requires vibration in accordance with ACI 309.1R, "Report on Behavior of Fresh Concrete during Vibration".

A 10" slump has a slump flow of 17" +/-. If a "flowing mix" is agreed upon an SCC backup mix is required. Many tall buildings have started with "flowing" concrete and switched to SCC because
of difficulty in achieving proper consolidation. The SCC mix should also increase the cementitious efficiency (psi/lb. of cementitious). Tower One in New York City is a good example. The 14,000 psi mix averaged 16,160 psi @ 56 days with a cementitious content of 873 lbs/cy and a w/cm of 0.29. The cementitious efficiency was 18.5 psi/lb. It has 105 floors of concrete. The 14,000 psi mix at 56 days was used for the lower double core for the first 30 floors of the Tower.

	Tower One New York City	**220 Central Park South New York City**	**10 Hudson Yards (52 Stories) New York City**	**Metropolis Phase 2B R3IT Los Angeles**
Cement	300 lbs.	400 lbs.	425 lbs.	715 lbs.
Fly Ash	65 lbs.	120 lbs.	----	180 lbs.
Slag	483 lbs.	600 lbs.	575 lbs.	----
Silica Fume	25 lbs.	50 lbs.	40 lbs.	----
Sand	1160 lbs.	1430 lbs.	1000 lbs.	1430 lbs.
Coarse Aggregate	1646 lbs. (#67 & #8)	1630 lbs. (#57)	1450 lbs. (#67) 450 lbs. (#8)	1442 lbs. (3/4")
Water	220 lbs.	283 lbs.	262 lbs.	283.2 lbs.
Water Reducer, Type A	30 oz.	----		
Type D Stabilizer				9 oz Eucon DS
HRWR Admixture	65 oz.	102 oz. Plastol 5000	135.2 oz. Plastol Series	63.5 oz. Plastol Series
Hydration Control Admixture	----	40 oz.	50 oz.	----
Viscosity Modifying Admixture	----	40 oz. Visctrol	-----	5 oz.
Air Detaining Admixture	----	4 oz. Eucon Air Out	-----	-----
Air Content	< 2%	2% +/-	< 2%	2% +/-
Slump (Spread)	----	26” +/- 2"	25" +/- 1"	27" +/- 2"
Unit Weight	----	151.8		150.0
W/cm	0.25	0.24	0.27	0.32
Compressive Strength, f'c	14,000 psi @ 56 days 16,160 psi Actual	14, 000 psi @ 28 days	12,000 psi @ 56 days 15,150 psi Actual	10,000 @ 56 days

All high performance concrete projects require a pre-concrete conference with a proper agenda and accurate minutes. They should be held 60 days +/- prior to the concrete placement. A successful test placement onsite is mandatory. Often a second placement is required.

The concrete producer should also provide a high range water reducer redosage chart to ensure that unexpected delays do not require concrete placements with spreads below the agreed upon envelope. Hydration control admixtures can maintain the proper spread and workability for several hours. They are always used for projects in major cities.

Additional VMA onsite is also a good idea. It's addition can restore a mildly segregating mix to a homogeneous mixture.

Self Consolidating Concrete for reinforced formed members soon will be as universal as automatic transmissions are in cars.